

Questioning Fundamental Principles of Organic Chemistry

Zhongheng Yu

Institute of Chemistry
Chinese Academy of Sciences
Beijing China

Amazon

Copyright © 2012 Zhongheng Yu

All rights reserved.

ISBN: 9781655790249

To my wife

TABLE OF CONTENTS

PREFACE	XIII
CHAPTER 1 FUNDAMENTAL PRINCIPLES OF ORGANIC CHEMISTRY BEING QUESTIONABLE	
Abstract	1
1.1. Introduction	2
1.1.1. Fundamental Principles of Organic Chemistry	2
1.1.2. Alternation of Conjugation Competition	4
1.2. Experiments and Discussion	6
1.2.1. Synthesis of 2-(N-methylamino)-anthracene	7
1.2.2. Determination of Conjugated-Backbone	8
1.3. Questionable Fundamental Principles	14
1.4. Conclusions	16
1.5. Reference	16
CHAPTER 2 ABNORMAL LARGE TWIST ANGLE OF NBA	
Abstract	19
2.1. Introduction	20
2.1.1. Large Distorted Stilbene-like Species	21
2.1.2. Classic Model and Interpretations	24
2.1.3. Substituent Effect	25
2.2. Experimental Questioning	27
2.2.1. Questioning Role of Non-bonded Interaction	27
2.2.2. Questioning CT-2 Interaction Role	29
2.3. Theoretical Researches	30
2.3.1. NBA-like Species with Five-membered Ring	30
2.3.2. Substituted N-benzylideneanilines	35
2.4. Conclusions	44

2.5. References	46
-----------------	----

CHAPTER 3 CONSTRUCTION OF LFMO BASIS SET

Abstract	52
3.0. Forewords	53
3.1. Introduction	57
3.2. Constructing LFMO Basis Set	59
3.2.1. Fragmentation of a Molecule	59
3.2.2. Sub-LFMO Basis Set for Fragment B	61
3.2.3. Superposition of Sub-basis Sets	70
3.3. Summary	71
3.4. Appendix	71
3.5. References	74

CHAPTER 4 π -DELOCALIZATION DESTABILIZATION

Abstract	79
4.1. Introduction	80
4.1.1. Morokuma Energy Decomposition	80
4.1.2. Natural Energy Decomposition Analysis	84
4.1.3. Our π - σ Energy Decomposition Method	84
4.2. Construction of Localized States	87
4.2.1. Construction of LFMO basis set	87
4.2.2. Construction of DSI State	89
4.2.3. Construction of FUD State	90
4.2.4. Construction of DSI-2 State	91
4.3. Vertical Delocalization Energy	91
4.3.1. N-benzylideneaniline	91
4.3.2. Heterocyclic NBA-like Species	97
4.3.3. Substituted NBAs	99
4.4. Summary	105
4.5. Appendix	106

4.6. References	112
-----------------	-----

CHAPTER 5 ELECTRON DELOCALIZATION DESTABILIZATION

Abstract	115
5.1. NBO Method	116
5.1.1. NBO Basis Set	116
5.1.2. NBO Vertical Delocalization Energy	119
5.1.3. Localization Degree of LMO Basis Set.	120
5.2. π -delocalization Indeed Destabilization	126
5.2.1. Basic Flaws of NBO	127
5.2.2. Deleting Hartree-Fock Exchange	131
5.3. Destabilizing π - σ Interaction	137
5.3.1. N-benzylideneaniline	137
5.3.2. NBA-like Species	141
5.4. Destabilizing Non-bonded σ - σ Interaction	143
5.4.1. Construction of FUL State	144
5.4.2. Reasonable STO-3G Basis Set	145
5.4.3. Construction of PDSI Electronic State	145
5.4.4. Non-bonded σ - σ Interaction	147
5.4.5. σ - σ Interaction Distorting Molecule.	148
5.5. Summary	151
5.6. Appendix	153
5.7. References	159

CHAPTER 6 RESTRICTED GEOMETRY OPTIMIZATION

Abstract	161
6.0. Forewords	162
6.0.1. So-called Evidence of Conjugation Stabilization	162
6.0.2. Benzene and Aromaticity	165
6.1. Our 2007 Method	169
6.1.1. Program of Localizing Geometry	170

6.1.2. A New Type of Additive Energy Effect	174
6.1.3. Extra Stabilization Energy of Benzene	177
6.2. ESEs for Benzene-like Species	180
6.2.1. Aza-1,3,5-Hexatrienes	181
6.2.2. Benzene-like Species	182
6.2.3. Furan-like Species	184
6.3. Substituted Benzenes	189
6.3.1. Extra Stabilization Energy	190
6.3.2. Extra Stabilization Energy of Parent Benzene Ring	194
6.3.3. Pure Conjugation Effect	194
6.3.4. Pure Inductive Effect	195
6.3.5. Conjugation and Inductive Effect	195
6.3.6. Substituent Effect Always Distortive	195
6.4. Conclusions	198
6.5. Appendix	198
6.6. References	203

CHAPTER 7 POLYCYCLIC BENZENOID HYDROCARBONS

Abstract	208
7.0. Forewords	209
7.0.1. Estimation of Resonance Energy	209
7.0.2. Calculation of Electron Delocalization Energy	210
7.0.3. Randić and Plavšić method	212
7.1. Method	215
7.1.1. GL Geometry of Phenanthrene	215
7.1.2. GE-m Geometries of Phenanthrene	215
7.1.3. Substituted 1,1-dibutadienyl-ethylene	218
7.1.4. ESE of Phenanthrene	219
7.1.5. Corrected ESE of Phenanthrene	219
7.2. Acenes	219
7.2.1. Generalized Definition of Fusion Bond	220

7.2.2. Fusion Double Bond	223
7.2.3. ESE and CESE	223
7.2.4. Energy Effect Increments	225
7.3. Position Rule and Energy Rule	230
7.4. Dibenzoacenes	231
7.4.1. Naphtho[2.3-e]pyrene	231
7.4.2. GL Sextet Rule	237
7.5. Conclusions	242
7.6. References	243

CHAPTER 8 NEW METHOD TO LOCALIZE π -ELECTRONS

Abstract	245
8.0. Forewords	246
8.0.1. Historical Roles of Cyclobutadiene	246
8.0.2. $4n+2$ Rule	247
8.0.3. Kollma Method and Jug Method	248
8.0.4. Fundamental Flaws of BLW Method	249
8.1. Introduction	251
8.1.1. Our 2007 Method Needing Improvement	251
8.1.2. π - σ Energy Decomposition	253
8.1.3. Two-electron Exchange Integrals	256
8.1.4. MPn Correlation Energy	257
8.1.5. Evidences for Role of HF-EX	258
8.2. Our 2011 Method	259
8.2.1. Versions of Our 2011 Method	260
8.2.2. Reliable Our 2011 Method	263
8.3. Extra Stabilization Energy of Benzene	267
8.3.1. Hartree-Fock Exchange Effects	267
8.3.2. More Reasonable Our 2011 Method	269
8.4. Vertical Delocalization Energy	273
8.5. Cyclobutadiene	274

8.6. Conclusions	275
8.7. Appendix	275
8.8. References	279

CHAPTER 9 [N]ANNULENES AND PBHS

Abstract	282
9.1. Introduction	283
9.1.1. [4n+2] Rule Not Always a Truth	284
9.1.2 . Driving Force for Distorting Ring	285
9.2. π - σ Energy Decomposition	286
9.2.1. DFT Molecular Energy	286
9.2.2. MPn Molecular Energy	288
9.3. Benzene	289
9.3.1. Three Distortion Models	289
9.3.2. BLE Leading to Minimization of Nuclear Repulsion	291
9.4. [N]Annulenes	294
9.4.1. Meaning of Symbol “[16]-54444”	295
9.4.2. Relationship between Configuration and VDE	296
9.4.3. Possible Configuration Isomers of a [N]Annulene	297
9.4.4. Vertical Delocalization Energies	302
9.4.5. Extra Stabilization Energy	306
9.5. PBHs	311
9.5.1. Phenanthrene	311
9.5.2. Acenes, Triphenylene and Chrysene	314
9.6. Conclusions	317
9.7. References	317

CHAPTER 10 STRAINED-AROMATIC MOLECULES – π -DISTORTIVITY

Abstract	321
10.0. Forewords	322
10.0.1. Mulliken’s Model of Charge Transfer Complex	323

10.0.2. Our Energy Decomposition Methods	323
10.0.3. Thermodynamic Mechanism of Reaction NH ₃ + BH ₃	328
10.1. Introduction	338
10.1.1. Mills-Nixon Effect.	341
10.1.2. Experimental Probe for π -Interaction Role	344
10.2. Eliminating π -Interaction	345
10.2.1. Construction of PLG	345
10.2.2. π -Delocalization Causing BLA	346
10.2.3. Energy Decomposition	348
10.3. Universality of π -Distortion	351
10.3.1. Comparison of Δr (PLG) and Δr (G)	351
10.3.2. $d\Delta r$ (GP) versus ΔE (GP)	353
10.3.3. Large Differences between C ₆ B ₆ H ₆ and C ₆ N ₆ H ₆	357
10.4. Forces Acting on Ring Bonds	360
10.4.1. Endocyclic Bonds	364
10.4.2. Exocyclic Bonds	365
10.5. C ₆ B ₆ and C ₆ N ₃ H ₃	368
10.5.1. Bond Angle	368
10.5.2. Bond Length	369
10.6. Secondary Structural Effects	369
10.7. Conclusions	370
10.8. References	372

CHAPTER 11 STRAINED-AROMATIC MOLECULES – ESE

Abstract	376
11.1. Introduction	377
11.2. Benzotricyclobutadiene	378
11.2.1. ESE of Whole Molecule	380
11.2.2. ESE of Central Ring	384
11.3. Strained-Aromatic Molecules	387
11.3.1. C ₆ X ₆ H ₆ and C ₆ X ₃ H ₃ (X = B, Al, Ga)	387

11.3.2. C ₆ X ₆ H ₆ (X = N, P, As, Si, Ge)	388
11.3.3. C ₆ X ₃ H ₃ (X = N, P, As)	389
11.3.4. C ₆ X ₆ (X = B, N, P, As)	390
11.4. ESE versus Δr(G)	391
11.4.1. Molecules with Δr(G) > 0	391
11.4.2. Molecules with Δr(G) < 0	395
11.5. Conclusions	396
11.6. References	397

CHAPTER 12 LOCALIZED GEOMETRY OPTIMIZATION

Abstract	398
12.1. Introduction	399
12.1.1. Pauling's Resonance Theory	399
12.1.2. Coulson's Method	402
12.1.3. Dewar's Viewpoint of Hybridization	403
12.1.4. Covalent Radii	403
12.1.5. Controversy over Resonance Existence	405
12.1.6. Historical Limitations	406
12.2. Development of Our Method	407
12.2.1. Our 2007 Method	407
12.2.2. Our 2011 Method	411
12.3. Our 2014 Method	413
12.3.1. More Reasonable than Our 2011 Method	413
12.4. Butadiene Derivatives	423
12.4.1. Localized GL Geometries	424
12.4.2. Adjacent Conjugation and Transmission	433
12.5. Conclusions	442
12.6. References	444
INDEX	447

PREFACE

For the structural theory established in the early development of organic chemistry, due to the limitation of understanding in that era, the fundamental principles cannot always be the truth. When the development of organic chemistry reaches a certain level, some chemists will need to use new tools (such as high-performance computers) and new research methods to review the fundamental principles and generally accepted theories.

Fundamental Principles and Basic Causality. Conjugation effect, steric effect and inductive effect are the three basic structural effects in the structural theory of organic chemistry. The conjugation stabilization and the steric hindrance destabilization, as two fundamental principles, have long been used to understand and interpret the relationship between the molecular structure and its properties and to explore and explain the reaction mechanisms. For a conjugated molecule, the conjugation effect and the steric hindrance make the co-planar conformation the most stable and most unstable, respectively. Molecular conformation is the result of a compromise between steric hindrance and conjugation effect, which is the basic causality among molecular conformation, steric hindrance and conjugation effect.

A reasonable and reliable method of localizing geometry (including the localization of the π -molecular orbitals (MOs) and π -electrons) is the prerequisites for the study of the conjugation effect and aromaticity (including the calculation of the conjugation energy, aromatic stabilization energy and anti-aromatic destabilization energy). Our new methods include our 1998 method and its improved version (our 2006 method), and our 2007 method and its improved versions (our 2011 method and our 2014 method). Their establishment and development run through the entire monograph.

Our Questioning Convincing. To convince the reader that our questioning is reasonable, as the first effort, our questioning began with the x-ray crystal structures and with the theoretical results calculated by Gaussian 98 software package. These experimental and calculation results can be verified in any laboratory.

In the literature, so-called experimental evidence of the conjugation stabilization refers to the difference (-3.9 kcal/mol) in the hydrogenation heat between butadiene and two butene-1 (In this book, the values of the stabilizing and destabilizing energies are expressed as negative and positive values, respectively). If the so-called experimental evidence is not rejected, our entire monograph will be worthless. Therefore, as the second effort (Section 6.01), using the same set of hydrogenation heats, we have emphasized that when trans-2-butene, instead of 1-butene, is used as reference molecule, the conjugation energy of butadiene is 1.9 kcal/mol and is destabilizing. The literature reported that, in the hydrogenation reaction of butadiene, the main intermediate (60%) is tras-2-butene. The so-called experimental evidence is the result of artificial selection of experimental data under the guidance of the subjective wishes. In the literature, the existence of conjugation effect in butadiene and the role of the conjugation in determining the distance of CC single bond were once controversial.

Benzene and cyclobutadiene are typical aromatic and anti-aromatic molecules, respectively, and their anti-aromatic energy (55 kcal/mol) and aromatic stabilization energy (-36 kcal/mol) were experimentally determined. The calculations of these two energies have been the hot topics in the literature. Conjugation energy of cyclobutadiene must be destabilizing. Otherwise, the calculation method is definitely not reasonable. Using our methods, as the third effort, the aromatic and anti-aromatic energies for these two typical molecules are, respectively, -36.4 and 54.9 kcal/mol, and are equal to their corresponding experimental values.

Cause of Questioning. As a part of my PhD dissertation, ten compounds, Ar-N(Me)-(CH=CH)_n-CHO (Ar = phenyl, 2-naphthyl, 2-anthryl; n = 0, 1, 2, 3) were synthesized, and their UV absorption frequencies were measured. Using the homologous linear rule and according to the frequency and shape of UV absorption peaks, the following

conclusions can be inferred: for (2-naphthyl)-N(Me)-(CH=CH)_n-CHO, when n = 1, the conjugation between nitrogen electron lone pair and naphthyl group is stronger than when n = 2. According to the principle of the conjugation stabilization, when n = 1, the dihedral angle θ between the methylamino group (-MeN-) and the 2-naphthyl group should be smaller than when n = 2. Out of the expectation, the size order of the experimental twist angle θ is: 33.6° (n = 1) > 31.4° (n = 2). This abnormal size order is further confirmed by the theoretical dihedral angles θ. For a series of molecules (2-naphthyl)-NH-(CH=CH)_n-CHO (n = 1, 2, 3), (a N-methyl group in each of the above molecules is replaced with a hydrogen atom in order to reduce the effect of the steric hindrance on the angle θ), the size order of the theoretical twist angles θ is as follow: 28.0° (n = 0) > 9.6° (n = 1) > 7.3° (n = 2) (Chapter 1). The conjugation between the nitrogen lone pair and the 2-naphthyl group appears to be destabilization and to be a driving force for distorting molecule.

For N-benzylideneaniline (NBA, Ph-N=CH-Ph) and NBA-like species (Ar-NH=CH-Ar') (Chapter 2), as shown by the X-ray crystal structures, the twist angle θ between Ar- and -N=CH-Ar' is abnormally large. For NBA, for example, the experimental twist angle θ is in the region of 36° to 55°. In the literature, it is attributed to the steric hindrance between the hydrogen atom of the -N=CH-Ar' group and the ortho-hydrogen atom of the Ar- group, and to the p-π conjugation between the Ar- group and the nitrogen lone pair. The literature opinions were experimentally and theoretically questioned by us (Chapter 2). Our experiments include the following works: synthesizing eight NBA-like species with five- or six-membered heterocycle rings and four substituted N,2,2-triphenyl-ketenimines, and determining their crystal structures.

For each NBA-like species, the functions, $E_e(\theta) = f(\theta)$, $E_N(\theta) = f(\theta)$ and $E(\theta) = f(\theta)$ ($E(\theta) = E_e(\theta) + E_N(\theta)$, and $E_N(\theta) < |E_e(\theta)|$), describe the changes of the total electronic energy E_e and nuclear repulsion E_N with the increasing of twist angle θ. A relaxed-PES (potential energy surface) scan incrementing twist angle θ shows the following interesting results: $dE_N(\theta)/d\theta > 0$, $dE_e(\theta)/d\theta < 0$, $dE(\theta)/d\theta < 0$, when $0 < \theta < \theta_{exp}$; $d^2E_N(\theta)/d\theta^2 < 0$, $d^2E_e(\theta)/d\theta^2 > 0$ and $d^2E(\theta)/d\theta^2 > 0$ for all twist angle θ. When the angle θ is close to the angle θ_{exp} of the crystal structure, $dE_N(\theta)/d\theta = 0$ (the total nuclear repulsion, as well as the nuclear repulsion between Ar- and -N=CH-Ar', is maximized), $dE_e(\theta)/d\theta = 0$ (total electronic energy is minimized, and is the most stabilizing), and $dE(\theta)/d\theta = 0$ (molecular energy is minimized, and is the most stabilizing). A crowded conformation with a large twist angle is the most stable.

These PES-scan results inevitably lead us to ask the following question: for conjugation and steric hindrance, which effect is the driving force for distorting the molecule from its planar conformation. Due to the presence of the π-σ interaction that may be stabilization or possibly destabilization, it is impossible to determine whether certain types of MO interactions (such as π-π and σ-σ interactions) are destabilization or stabilization, only based on the results of the relaxed PES-scans.

Exploring the structural factors that cause the NBA to be substantially distorted should start with the establishment of a new π-σ energy decomposition method.

Our 2006 Method. As the first feature of our 2006 method (Chapter 3), a multi-step procedure provides a LFMO (absolutely localized fragment molecular orbitals) basis set for a non-planar conjugated molecule such as NBA-like species. In this basis set, π and σ LFMOs are completely separated; the LFMOs are absolutely localized on their respective fragments, and each LFMO has the correct electronic occupancy. Then, the conditional single-point calculations, over the LFMO basis set, give a conjugated molecule the four localized electronic states. Based on the difference in the molecular energy between each pair of the localized electronic states, the following interesting results are obtained (Chapter 4 and Chapter 5): (i) π-π and σ-σ interactions between the fragments Ar- and -N=CH-Ar' are always destabilization, and they are the driving forces for distorting NBA-like species from its planar conformation. (ii) π-σ interaction is also destabilization, and it is resistance to molecular distortion. The conformation with a large twist angle, as well as the maximization of the nuclear repulsion between the Ar- and -N=CH-Ar' groups, is the result of a compromise between the above three destabilization MO interactions.

The π - σ energy decomposition leads us to believe that the fundamental principles and the basic causality are questionable.

Our 2007 Method and Its Improved Versions. In the field of aromaticity, purely theoretical calculation of aromatic stabilization energy has become the goal pursued by theoretical chemists. Our method has achieved this goal (Chapter 6). By conditionally deleting non-diagonal elements of the AO Fock and overlap integral matrices, our 2007 method can provide a full localized GL geometry and a series of the locally delocalized GE-m geometries ($m = 1, \dots, k$). In the optimized GL geometry, all the π MOs are absolutely localized on their respective double bonds. Each optimized GE-geometry arises from the local π interaction between a specific pair of the double bonds in the localized GL geometry. Based on the localized GL geometry and a series of the locally delocalized GE-m geometries, as the biggest feature of our 2007 method, it can provide following two types of π -electron delocalization energies for every conjugated molecule: $\Delta E^A = [E(G) - E(GL)]$ is the molecular difference between the ground state (G) and its localized GL geometry; $\Delta E^{Am} = E(GE-m) - E(GL)$, is the molecular energy difference between a specific GE-m geometry and the GL geometries, and always (or mostly) $\Delta E^{Am} > 0$ (destabilizing).

The greatest success of our 2007 method is the discovery of a new type of additive energy effect, which makes it possible to provide an aromatic molecule with a virtual reference (VR) molecule that has the same configuration and conformation as the aromatic molecule itself.

For a non-aromatic molecule such as polyene and heteroatom-substituted polyene, $\Delta E^A > 0$ (destabilizing), and $\Sigma \Delta E^{Am} \approx \Delta E^A = [E(G) - E(GL)]$, so that energy effects ΔE^{Am} are additive. This discovery ensures that our method can be used to accurately calculate the aromatic stabilization energy of all types of aromatic molecules, without needing the help of any empirical and semi-empirical parameters.

For a typical aromatic hydrocarbon molecule, always $\Delta E^A < 0$ (stabilizing), $\Sigma \Delta E^{Am} > 0$, $|\Delta E^A| > \Sigma \Delta E^{Am}$, and $(\Delta E^A - \Sigma \Delta E^{Am}) < 0$. Due to the additivity, $\Sigma \Delta E^{Am}$ can be considered as the molecular energy difference, $[(E(VR) - E(GL))]$, between the virtual reference (molecule) and localized GL geometry of aromatic molecule itself. In this case, the energy effect difference, $\Delta E^A - \Sigma \Delta E^{Am} = [E(G) - E(GL)] - [E(VR) - E(GL)] = E(G) - E(VR) < 0$ (stabilizing). Therefore, the difference, $\Delta E^A - \Sigma \Delta E^{Am} = E(G) - E(VR)$, can be defined as the extra stabilization energy (ESE) of an aromatic molecule with respect to its virtual reference molecule. For the virtual reference molecule of an aromatic molecule itself, the π -delocalization energy, $\Delta E^A(VR) = [E(VR) - E(GL)] = \Sigma \Delta E^{Am}$, can be calculated using the additivity of the energy effects ΔE^{Am} , without needing to know its detailed structure and molecular energy $E(VR)$. Therefore, $ESE = \Delta E^A - \Sigma \Delta E^{Am} = E(G) - E(VR)$ can also be considered as the difference, in the π -delocalization energy, between an aromatic molecule and its virtual reference molecule, $ESE = \Delta E^A - \Delta E^A(VR)$. For benzene, for example, $\Delta E^A - \Sigma \Delta E^{Am} = E(G) - E(VR) = -39$ kcal/mol (using our 2007 method at B3LYP/6-31G* level). -39 kcal/mol can be defined as the ESE of benzene with respect to its virtual cyclohexatriene, and it is close to the experimental value of -36 kcal/mol.

For benzotricyclobutadiene ($C_{12}H_6$) at B3LYP/6-31G* level (Chapter 11), the central benzene ring, fused to three cyclobutadiene rings, is a real cyclohexatriene ring with alternating single (1.515 Å) and double (1.338 Å) bonds. For this central ring, interestingly, the destabilizing energy effects are as follows (kcal/mol): $\Delta E^A = 38.1$, $\Sigma \Delta E^{Am} = 40.4$, and $\Sigma \Delta E^A \approx \Sigma \Delta E^{Am}$. In the case of cyclohexatriene, the energy effects ΔE^{Am} is indeed additive.

Our 2007 method and its improved versions have been used to reasonably calculate the ESEs of the following various types of aromatic molecules: five- and six-membered ring aromatic molecules, substituted benzenes, polycyclic benzenoid hydrocarbons (PBHs), [N]annulene, and strained aromatic molecules. In the meantime, the substituent effects, including the conjugation and inductive effects, are quantified. Among all the above conjugated molecules except for furan-like species, the ESE/ π of the benzene is the largest.

There are multipole candidates for the GL geometry in the case of PBH. We propose the position rule, energy rule and GL sextet rule in order to choose the GL geometry from its candidates.

However, our 2007 method had to be limited to be used at the B3LYP level of theory (Chapter 8). At the RHF and MP2 levels of theory, for example, the vertical and adiabatic delocalization energies of benzene, obtained from our 2007 method, become destabilizing (at B3LYP level of theory, they are stabilizing).

The improved "our 2007 method" is named "our 2011 method" (Chapter 8). In a localized geometry such as GL, obtained from our 2011 method, the two-electron exchange integrals, $\langle \lambda\rho|\mu\omega \rangle$, between the double bonds have been conditionally deleted, in addition to the Fork and overlap integral matrix elements. For any (planar) conjugated molecule, the electron delocalization energies, including the ESE, vertical delocalization energy (VDE), and adiabatic resonance energy, can be accurately reasonably calculated using our 2011 method at the RHF, DFT and post-SCF levels of theory no matter whether the molecule is non-aromatic, aromatic or anti-aromatic. For benzene at B3LYP/6-31G*, the ESE value is improved from -39 kcal/mol (from our 2007 method) to -36.3 kcal/mol (from our 2011 method). The value of -36.3 kcal/mol is equal to the experimental value of -36 kcal/mol. It is particularly worth emphasizing that when using our 2011 method, the effect of the theoretical level and basis set size on the ESE value of benzene is much smaller than when using our 2007 method. For benzene at (RHF, MP2, LYP, B3LYP, SLATER, BLYP)/(6-31G*, 6-311G**, 6-311G(2d,2p), 6-311G(2df,p), 6-311++G(2df,p) levels, the ranges of the ESE (kcal/mol) are as follows: -34.5 < ESE (our 2014 method) < -39.3, and -31.7 < ESE(2011) < -37.4, and the average values are -35.0 (2011) and -37.0 (2014).

The last version of our method is called our 2014 method. In the GL geometry of benzene optimized using our 2014 method, for example, the MO interaction, the π -electron exchange interaction and the gradients of exchange integrals are all conditionally excluded from the between double bonds. Various energy effects obtained from our 2014 method are more reasonable than from our 2011 method.

π -Distortion. The destabilization feature of π -delocalization determines its performance of distorting molecular geometry.

For 621 pairs of the double bonds in the GL geometries of various types of the aromatic molecules, always $\Delta E^{\text{Am}} > 0$, $\Delta r > 0$, and Δr can be fitted as a polynomial function of ΔE^{Am} . The local conjugation energy ΔE^{Am} between a pair of double bonds in the GL geometry is always destabilization, and the single bond distance between two interacting double bonds in the GE-m geometry is always longer than that of the corresponding single bond in the localized GL geometry.

In the literature including the standard textbook of organic chemistry, the CC bond length alternation in the central benzene ring of strained-aromatic molecule is attributed to the angle strain. In the particular localized geometry (PLG) of benzotricyclobutadiene, the π -interaction and π -exchange have been excluded from between the group A (central benzene ring) and the group B (including three annulated small rings). As a result, the difference, ($\Delta r = r_{\text{endo}} - r_{\text{exo}}$), between the endo- and exocyclic bond lengths decreases from $\Delta r(G) = 0.177 \text{ \AA}$ in the ground state (G) geometry to $\Delta r(\text{PLG}) = -0.002 \text{ \AA}$ in the PLG geometry. It is the π -delocalization (rather than angle strain) to distort the central benzene ring.

For 17 strained-aromatic molecules $C_6X_3H_3$ ($X = B, Al, Ga, P, As$) and $C_6X_6H_6$ ($X = B, Al, Ga, N, P, As$), C_6X_6 ($X = N, P, As$) and $C_6X_6H_6$ ($X = C, Si, Ge$), $d\Delta r$ can be fitted as the polynomial function of ΔE . The molecular energy difference ΔE is the π interaction energy between the central ring and the hetero groups ($X-X$, XH , and $X=X$), and $-82.6 < \Delta E = [E(G) - E(\text{PLG})] \text{ kcal/mol} < 81.7$. Correspondingly, $-0.040 < d\Delta r = [\Delta r(G) - \Delta r(\text{PLG})] \text{ \AA} < 0.180$. The bond length alternation of the central benzene ring should be attributed to π -delocalization.

For the localized GL geometry of benzene, at the moment of electron delocalization, as shown by the energy decomposition (Chapter 9), the CC double bonds are subjected to a pulling force, the double bond length change $dr_a > 0$. In the meantime, the CC single bonds are subjected to a compressive force, the single bond length change $dr_b < 0$. During the deformation of benzene ring from the localized GL geometry to the delocalized ground state geometry(D_{6h}) due to π -electron delocalization, the total electronic energy difference $\Delta E_e = E_e(G) - E_e(\text{GL}) > 0$ (destabilizing), the nuclear repulsion difference $\Delta E_N = E_N(G) - E_N(\text{GL}) < 0$ (stabilizing), and $|\Delta E_N| > \Delta E_e$. The

nuclear repulsion change plays a predominant role in determining the D_{6h} geometry. In particular, when $r_a = r_b$, that is, when all CC bond lengths are equal to each other, the nuclear repulsion is minimized ($d(E_N)/dr = 0$), leading to the formation of D_{6h} geometry of benzene. But the role of the nuclear repulsion is the result of π -electron delocalization. In this case, energy criterion and geometric criterion of the aromaticity are well unified and are mutually causal. This is a new understanding of the essence of aromaticity.

Aromaticity of Furan-like Species. Due to Diels-Alder and 2,5-addition reactions of furan, furan's aromaticity is controversial.

For the furan-like species, the energy difference $ESE = E(G) - E(EG) = \Delta E^A - \Sigma \Delta E^{Am}$, and the size order of ESEs at B3LYP/6-31G* level is as follow (from our 2007 method): -53.1 (2-aza-pyrrole) > -49.4 (pyrrole) > -46.5 (imidazole) > -39.3 (furan) > -39.0 (benzene) = -39.0 (2-aza-furan) > -36.3 (oxazole). In this case, the ESE of benzene is not the largest.

According to the definition of extra stabilization energy, the basic characteristics of an aromatic molecule should be as follows: $\Delta E^A = E(G) - E(GL) < 0$ (stabilizing), $\Sigma \Delta E^{Am} > 0$ (destabilizing), and $ESE = E(GL) - \Sigma \Delta E^{Am} < 0$ (stabilizing). But, for furan-like species, $\Delta E^A > 0$, $\Sigma \Delta E^{Am} > 0$, and $\Delta E^A < \Sigma \Delta E^{Am}$, so that still $(\Delta E^A - \Sigma \Delta E^{Am}) < 0$ (stabilizing). Furan-like species are just a class of the molecule whose electron delocalization energy ΔE^A is less destabilizing than that of its virtual reference molecule. Such type of molecules should not be considered aromatic. There is no comparability between the ESEs of benzene- and furan-like species. In this case, the energy effect difference, ($LDE = \Delta E^A - \Sigma \Delta E^{Am}$), of the furan-like species is best defined as the less destabilization energy (LDE), rather than ESE.

About $4n+2$ Rule and [N]annulene. Whether the $4n+2$ rule is always truth is a controversial topic. In the literature, the $4n+2$ rule was once used as truth to test the rationality of the empirical and semi-empirical calculation methods.

For [N]annulenes, the theoretical level and basis set size have the influences on the size and sign of the energy effects such as ΔE^A and ΔE^{Am} , which is different from the typical aromatic molecules. Therefore, we are only concerned about the effect of the ring size on the aromaticity and anti-aromaticity, rather than the accurate calculation of their ESE value.

For [N]annulenes from $N = 8$ to 26 , the VDE always conforms to the $4n+2$ rule, without exception. When $N = 16$, the destabilizing VDE per π -electron (VDE/ π) for [4n]annulene is quickly becomes constant (about 0.7 kcal/mol \cdot electron). The stabilizing VDE/ π for [4n+2]annulene is slowly approaching the VDE/ π (-0.7 kcal/mol \cdot electron) of [26]annulene.

The CESE for [4n+2]annulene and [4n]annulene is stabilizing and destabilizing, respectively. In terms of electron delocalization energy, all [4n]- and [4n+2]annulenes can be regarded as close to the corresponding polyenes when $N \geq 16$.

Naked CC Single Bond of Butadiene. The experimental distance (1.454 to 1.468 Å) of the CC single bond of butadiene is shorter than that (1.54 Å) of ethane. In the standard textbook of organic chemistry, these two distances are used as the experimental evidences to support the conjugation stabilization. In the literature, however, which structural factor, conjugation or hybridization, determines the distance of the CC single bond of butadiene is controversy.

In the GL geometry of butadiene optimized using our 2014 method, the C(2)-C(3) single bond is called the naked single bond, and its distance $r_{23}(GL)$ (1.451 Å) at B3LYP/6-31G* level is shorter by 0.006 Å than that $r_{23}(G)$ (1.457 Å) in the ground state geometry. Correspondingly, the molecular energy difference $\Delta E = [E(G) - E(GL)]$ between the ground state geometry and the localized GL geometry is 1.4 kcal/mol (destabilizing), and it is close to the difference (1.9 kcal/mol) in the hydrogenation heat between trans-1,3-butadiene and two trans-2-butene.

For 66 molecules including butadiene-like species 18 $X=C(2)-C(3)=Y$ ($X, Y = O, S, Se, NH, PH, AsH$) and 48 substituted butadienes $X_nC=C(2)H-C(3)H=CY_m$ ($n, m = 1, 2; X, Y = BH_2, AlH_2, GaH_2, NH_2, PH_2, AsH_2, F, Cl, Br$), the distance difference $\Delta R_{23} = [r_{23}(G) - r_{23}(GL)]$ can be fitted as the polynomial function of the molecular energy difference ΔE , where $-0.046 \text{ \AA} < \Delta R_{23} < 0.040 \text{ \AA}$, and $-8.1 \text{ kcal/mol} < \Delta E < 13.0 \text{ kcal/mol}$. The conjugation plays an important role in determining the distance $r_{23}(G)$ of the $C(2)-C(3)$ single bond. In the case of the butadiene-like species and substituted butadienes, whether conjugation energy ΔE is stabilizing or destabilizing depends on the electronegativity of the heteroatom of double bond in the butadiene-like species and on the electron occupancy (π electron-sufficient and electron-deficient) of the substituent.

In the GL geometry of substituted butadiene, the conjugation between a CC double bond and its substituent(s) is called the adjacent conjugation (the conjugation adjacent to the $C(2)-C(3)$ single bond). When the substituent is an electron-releasing group such as $-XH_2$ ($X = N, P, As$), the adjacent conjugation has a large influence on the distance $r_{23}(GL)$ of the naked CC single bond through the σ bond(s). But, when the substitute(s) is an electron-withdrawing group such $-XH_2$ ($X = B, Al, Ga$), the adjacent conjugation slightly influences the distance of the naked CC single bond.

Sincere Gratitude to My Graduate Students. My graduate students came from different universities, and they were all undergraduates majoring in organic chemistry. Few of these students had received any training in quantum chemistry. They worked hard and used their own wisdom. Especially worth mentioning is the talent and contribution of Dr. Peng Bao. In 1991, Mr. Bao was admitted to the Department of Chemistry, Tsinghua University. After graduation, he was admitted to the Graduate School of Lanzhou University, and his research interest was organic synthesis. Three years later, he obtained a master's degree. He then worked in the field of organic synthesis for many years. In 2004, Mr. Bao joined my research group as a PhD student. Surprisingly, after only a few months of work, Mr. Bao can read and modify the source code of the Gaussian 98 and PC-GAMESS software packages. It is through Mr. Bao's efforts that my calculation program can be incorporated into the PC-GAMESS program package, which is an important milestone for my research. Therefore, I would like to take this opportunity to express my sincere gratitude to my graduate students.

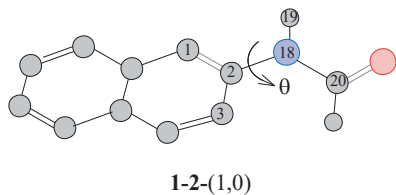
Acknowledgment. This monograph was supported by National Natural Science Foundation of China (Grants: Chemistry 85228, 2880091, 29272070, 29572074, 29872042, 20072041, 20272063 20472088 and 20672119). PC-GAMESS Source code was provided by Professor Alex A. Granovsky, Lomonosov State University, Moscow, Russia. MQAB-80 source code was obtained from Professor Muzhen Liao, Tsinghua University, Beijing.

CHAPTER 1

FUNDAMENTAL PRINCIPLES OF ORGANIC CHEMISTRY BEING QUESTIONABLE

ABSTRACT

The following ten nitrogen-bridge compounds are synthesized: $(Ar)_m-N(Me)-(HC=CH)_n-CHO$ (**1-1-(m,n)**) where $m = 0$ ($Ar = \text{phenyl}$), $n = 0, 1, 2$; $m = 1$ ($Ar = \text{naphthyl}$), $n = 0, 1, 2$; $m = 2$ ($Ar = \text{anthryl}$), $n = 0, 1, 2, 3$. Based on the homologous linear rule, and according to the number, frequencies and shapes of UV absorption peak(s), the nitrogen lone-pair in a specific compound **1-1-(m,n)** can't be conjugated with two branches, $(Ar)_m-$ and $-(HC=CH)_n-CHO$, at the same time. When $n < m$, the nitrogen lone-pair is predominantly conjugated with the aromatic chain; when $n > m$, it is predominantly conjugated with the polyenal chain. With the alternating growth of two branches $(Ar)_m-$ and $-(HC=CH)_n-CHO$, the nitrogen lone pair is alternately conjugated with one of the two branches. Accordingly, the naphthyl group in **1-1-(1,1)** is more ability of competing for nitrogen lone pair than in **1-1-(1,2)**, but the experimental dihedral angle, θ (33.6°), between the naphthyl and amino groups in molecule **1-1-(1,1)** is greater than that (31.4°) in molecule **1-1-(1,2)**. For the three optimized geometries of (2-naphthyl- $N(18)H(19)-HC(20)=CH-(HC=CH)_{n-1}-CHO$ denoted as **1-2-(1,n)** ($n = 0, 1, 2$), the bond distance r_{18-2} between the C(2) and N(18) atoms, and the dihedral angles $\theta = C(20)-N(18)-C(2)-C(3)$, $\alpha = N(18)-C(2)-C(1)-C(3)$ and $\beta = N(18)-C(2)-H(19)-C(20)$, have the following interesting size orders: $r_{18-2}: 1.410 \text{ \AA} (n = 0) > 1.404 \text{ \AA} (n = 1) > 1.401 \text{ \AA} (n = 2)$; $\theta: 28.0^\circ (n = 0) > 9.6^\circ (n = 1) > 7.3^\circ (n = 2)$; $\alpha: -178.4^\circ (n = 0) < 179.4^\circ (n = 1) < -179.5^\circ (n = 2)$; $\beta: 4.3 (n = 0) > 1.2 (n = 1) > 0.9 (n = 2)$. All of the experimental and theoretical data mentioned above imply consistently that the conjugation between the naphthyl and amino groups is destabilization and is a driving force that causes the molecule to deviate from its planar conformation. The conjugation stabilization, as a fundamental principle of organic chemistry, seems questionable. Based on that, for molecule **1-2-(1,0)**, the ground state geometry with $\theta = 28.0^\circ$ is more crowded and stable than the co-planar geometry, the nuclear repulsion (steric hindrance) between the naphthyl group and the formylamino group is resistance to distortion of molecular geometry from the planar geometry.



yuzh@iccas.ac.cn

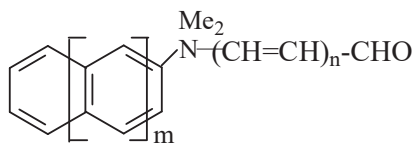
Key words: conjugation destabilization; nitrogen-bridge compounds; alternately competing conjugation; fundamental principles of organic chemistry.

1.1. INTRODUCTION

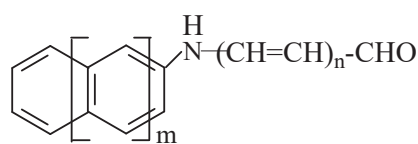
This Chapter can be seen as the preface to this book, and its contents are taken from my PhD dissertation (1982-1985),¹ and this will explain why I had to create a new calculation method that can decompose the molecular energy into π - and σ -parts, and why I use this new method to re-understand and question the fundamental principles of organic chemistry.

In each of nitrogen-bridge conjugated compounds **1-1-(m,n)**,² there are two conjugated branches: aromatic chain and polyenal chain. The purpose of this chapter is to demonstrate that the two branches, $(Ar)_m-$ and $-(CH=CH)_nCHO$, can't be conjugated with the nitrogen lone-pair at the same time. In a specific compound **1-1-(m,n)**, which chain has the competitive advantage depends on the chain lengths m and n . As the chain lengths m and n increases alternately, the nitrogen lone pair is alternately conjugated with one of the two branches,²⁻⁴

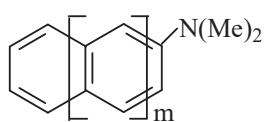
1-1-(m,n) ($m = 0, 1, 2$; $n = 0, 1, 2, 3$)



1-2-(m,n)



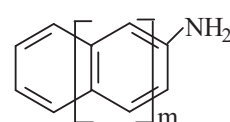
1-3-(m) ($m = 0, 1, 2$)



1-4-(n) ($n = 0, 1, 2, 3$)



1-5-(m) ($m = 0, 1, 2$)



In this Chapter, the following ten compounds, **1-1-(m,n)**, were synthesized: $m = 0, n = 0, 1, 2$; $m = 1, n = 0, 1, 2$; $m = 2, n = 0, 1, 2, 3$. Then based on the homologous linear rule,^{3,4} together with the number, frequency and shape of UV absorption peak(s), the conjugated-backbone structure in a specific molecule is determined, thereby making it possible to get new insight into the relationship between the conjugation effect and the molecular conformation. In **1-1-(1,1)**, for example, the ability of naphthyl group to compete for nitrogen lone pair is stronger than the naphthyl group in **1-1-(1,2)**, but the experimental dihedral angle θ (33.6°) between the naphthyl and amino groups in **1-1-(1,1)** is actually larger than that (31.4°) in **1-1-(1,2)**.^{5,6} Inspired by the unusual size order of the experimental twist angle θ , the geometries of molecules **1-2-(1,n)** are optimized at B3LYP/6-31G* level. Interestingly, for three molecules **1-2-(1,n)** ($n = 0, 1, 2$), as will be pointed out, as the chain length n increases, the changes in the twist angle θ , amino flatness and C(2)-N bond length all do not meet the principle of conjugation stabilization. Based on that, for molecule **1-2-(1,0)**, the ground state geometry with $\theta = 28.0^\circ$ is more crowded and stable than the co-planar geometry, the nuclear repulsion (steric hindrance) between naphthyl group and formyl-amino group is resistance to distortion of molecular geometry from the planar geometry, rather than a driving force.

All the results mentioned above imply that the fundamental principles of organic chemistry are questionable.

1.1.1. Fundamental Principles of Organic Chemistry

On the basis of a large number of experiments, conjugation effect, inductive effect and steric hindrance have been summarized as the basis of organic structure theory.⁷

1.1.1.1. Conjugation and Resonance

The conjugation effect refers to the π molecular orbital (MO) interaction between double bonds, and to the influences of π -interaction on the dynamic and static physical and chemical properties.^{7,8} Such properties include the molecular conformation, bond length and bond angle, molecular dipole moment, molecular stability, substituent's directing effects in electrophilic substitution reaction, and so on. Conjugation effect can also be defined as the effects of π -electron delocalization on molecular properties. Accordingly, the conjugation energy is an energy effect arising from π -electron delocalization, or is an energy effect associated with the π -MO interaction among double bonds. In Chapter 8, it will be detailed that the π -electron delocalization is conceptually different from the π MO delocalization. Therefore, the calculation of conjugation energy is definitely not as simple as imagined. Since 1990, I have been working on the establishment and development of a new method for calculating conjugation energy, which will run through this entire monograph.

The resonance structures refer to the Lewis structures, and the molecule exists as a resonance hybrid, this is called the “resonance”.⁹ The resonance energy is defined as the energy difference between the real molecule and its most stable Lewis structure.¹⁰ The construction of most stable resonance structure is based on the maximization of the MO exchange interaction between each pair of double bonds.¹¹

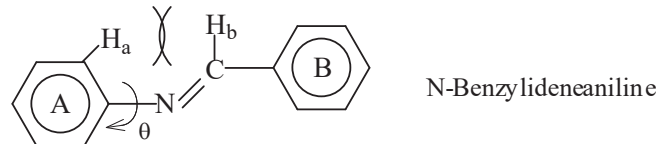
Molecular orbital theory can well describe conjugation, and the resonance theory corresponds to valence bond theory. Based on the fact that the resonance energy of cyclobutadiene, obtained from VB method, is stabilizing,¹¹ as emphasized by Shaik,¹² the molecular orbital theory is more reasonable than valence bond theory. Correspondingly, the conjugation concept should also be better than the resonance concept. Particularly, as will be detailed in Chapter 6 and Chapter 8, the method of constructing localized geometry has successfully been established in our research group, and it is based on the localization of π -electrons. The adiabatic delocalization energy of cyclobutadiene, obtained from our method, is 54.9 kcal/mol, and this destabilization energy is almost equal to the experimental value of 55 kcal/mol¹³ (contrary to the expression of the energy effect value in the literature, in this book, the stabilizing energy effect is expressed as a negative value, and the destabilizing energy effect is written as positive value). In the calculation method and calculation principle and in the calculation result, the conjugation energy (π -electron delocalization energy) and the resonance energy are fundamentally different, the former is more reasonable than the latter.

1.1.1.2. Principle of Conjugation Stabilization

According to the structure theory of organic chemistry, conjugation (resonance) energy (ΔE_R), is always stabilizing, that is, $\Delta E_R < 0$. In butadiene, the distance of CC single bond is 1.47 Å and is shorter than the CC single bond length (1.54 Å) of ethane. The corresponding conjugation energy, i. e., the difference in hydrogenation heat between butadiene and two butene-1, is -3.9 kcal/mol,^{14,15} and it has been used as the basic experimental evidence to support the principle of conjugation stabilization in organic chemistry textbooks.⁸ If this experimental evidence is conclusive and undeniable, then the entire monograph will be meaningless. In fact, as will be detailed in Chapter 6, this so-called experimental evidence is the result of artificially selecting the experimental data (hydrogenation heats of 1-butene-1, trans-2-butene and cis-2-butene) under the guidance of the subjective desire. When trans-2-butene is used as reference instead of 1-butene, the difference in the hydrogenation heat is 1.9 kcal/mol (destabilizing), and it may become the experimental evidence for supporting conjugation destabilization. Probably for this reason, some literature does not agree that the difference in hydrogenation heat between butadiene and two 1-butene is defined as the resonance energy between two double bonds.^{16,17} The debate on the structural factors that determine the distance of the CC single bond of butadiene molecule will be reviewed and discussed in Chapter 12.

1.1.1.3. Basic Causal Relationship

In a planar conformation of conjugated molecule, the steric hindrance between groups is always considered to be the biggest, and meanwhile the conjugation effect becomes the strongest according to the principle of conjugation stabilization. Hence, the steric hindrance is always considered to be a driving force for distorting molecule away from its planar geometry, and the conjugation interaction always tends to planar geometry. The molecular conformation is the result of a compromise between the steric hindrance and the conjugation effect.



According to the principle of conjugation stabilization, for example, the conformation of N-benzylideneaniline (NBA) should be planar. However, as shown by X-ray crystal structure,¹⁸ the twist angle θ , the dihedral angle between the phenyl (A) and N=CH-Ph (B) groups, is large, up to 55° .¹⁹ In the literature, the large twist angle is attributed to the steric hindrance between two nonbonded hydrogen atoms H_a and H_b.¹⁹ With NBA being distorted, the nuclear repulsion energy (E_N) between the fragments A and B reduces, $dE_N(\theta) = E_N(\theta) - E_N(0^\circ) < 0$, where, for example, $E_N(0^\circ)$ is the nuclear repulsion for the $\theta = 0^\circ$ conformation. Following this distortion, the conjugation energy $\Delta E_R(\theta)$, associated with the π interaction between the two fragments, is weakened, $d\Delta E_R(\theta) = \Delta E_R(\theta) - \Delta E_R(0^\circ) > 0$ ($E_R(0^\circ) < 0$). The equilibrium molecular conformation ($\theta = 55^\circ$) is a result of the compromise between $dE_N(\theta)$ and $d\Delta E_R(\theta)$.¹⁹⁻²¹ Accordingly, the weakening of the conjugation effect is the result of molecular deformation caused by steric hindrance, which is the basic causality of organic chemistry.

1.1.1.4. Significance of Questioning Conjugation Stabilization

Conjugation stabilization theory has successfully explained and predicted the stability of carbocation, carbanion and free radical, and has established and developed various theories such as the organic acid-base theory and aromatic theory. It plays an important role in the study of static chemical and physical properties, organic reaction mechanism, molecular configuration and conformation, transition state and reaction products.^{22,23} Hückel molecular orbital theory (HMO) and Dewar's perturbation molecular orbital (PMO) theory²⁴ offer a theoretical basis for the conjugation stabilization principle, greatly promoting the development of organic chemistry theory. On the basis of the HMO and PMO theory, the non-bonded orbital interaction theory,²⁵ frontier molecular orbital theory,²⁶ and the conservation principle of orbital symmetry,^{27,28} are established and developed. As a result, the theories and structural effects related to π -electron almost become the core of structure theory of organic chemistry.²⁹

Therefore, once the principle of "conjugation stabilization" has been negated, as Epiotis pointed out and expected, organic chemists will get rid of the limitations of Hückel's theory and will create new organic structure theory with new research methods and new modes of thinking.³⁰

1.1.2. Alternation of Conjugation Competition

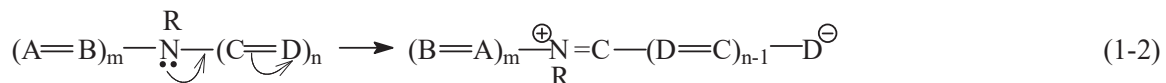
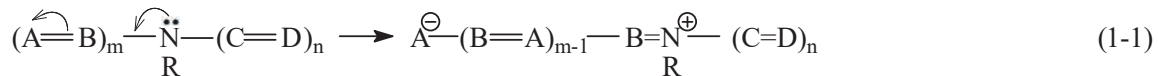
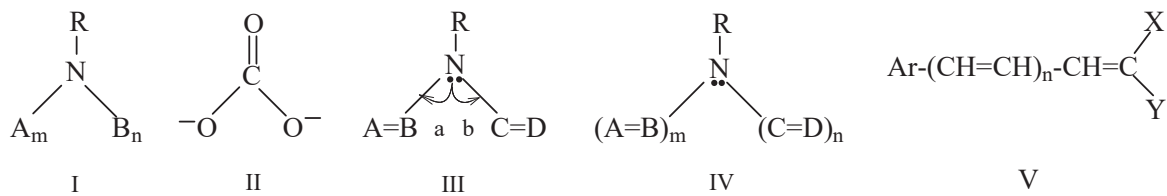
Based on a large number of UV (ultraviolet) spectra, Jiang found "Rule of Homologous Linearity of Organic Compounds".³ On this basis, Jiang has summed up "Combination Law of Conjugated Groups".⁴ That is, in a crossed-conjugated system such as 1-1-(m,n), only one branch can be conjugated with the nitrogen lone-pair. Another one branch only plays a substituent role, and its effect on UV absorption frequency is slight. My PhD dissertation,¹ "Alternation of Conjugation competition in the Nitrogen-bridge Conjugated System", aimed to provide

the experimental evidences for "Combination Law".

The Homologous Linear Rule is a summary of numerous experiments, and it provides a quantitative criterion for the relationship between structure and properties of conjugated molecule and for determining the conjugated-backbone structure of the crossed-conjugated system. The properties (P) of conjugated molecule, such as UV absorption frequency, ionization potential, redox potential, electron affinity, half-wave reduction potential, etc. depend on the energy levels of frontier molecular orbitals. Therefore, as shown by Equation 1-I that was formulated by Jiang, all the properties follow the Homologous Linear Rule:

$$p = a + b (1/\alpha)^{2/N} \quad . \quad (1\text{-I})$$

where a and b are the constant, N is homologous series number, $\alpha = k + 1$, where $k = 1$ for the highest occupied molecular orbital (or the lowest unoccupied molecular orbital), and $k = 2$ for the second highest molecular orbital, etc.



In the conjugated system I, two branched-chains, $-Am$ and $-Bn$, are bonded to a common nitrogen atom, forming a nitrogen bridge conjugated system. Divalent carbonate anion II is a crossed-conjugated system of bridge-type. Experiments show that in a carbonate anion, the negative charge is evenly distributed in the three oxygen atoms, forming a structure with D_{3h} symmetry. This indicates that the two negatively charged oxygen atoms are conjugated equally with a carbonyl group.⁸ For asymmetry crossed-conjugated system III, Ingold believed that there are two opposite directions of conjugation polarization, denoted as a and b .⁷ However, for conjugated system IV, Ingold did not mention how the changes in the chain lengths m and n affect the relative advantage of the two conjugation polarizations. Based on the homologous linear rule, as our demonstrated,^{31,32} in a conjugated system V, only one branch, the X (or Y) group, can be conjugated with polyene chain, forming a conjugated-backbone structure, $Ar-(CH=CH)_n-CH=C-X$ (or Y), another group, Y (or X), only as a substituent group. For the system V, therefore, the homologous series number N in Equation (1-I) is as follow:

$$N = n + 1 + n_1 + n_2 + t$$

where n_2 is the number of double bonds in the Ar - group, n_1 is the number of double bonds in the group X ; t is the substituent equivalent of the group Y , and $0 < |t| < 1$.

However, in conjugated system IV, there may be two conjugated-backbones, denoted as $(A=B)_m-N(R)-$ and $-(R)N-(C=D)_n$, and the two branches compete for the nitrogen lone pair with each other as the chain lengths increase alternately. When the chain length m of the branch $(A=B)_m-$ is long enough, its ability to compete for nitrogen lone pair is greater than the branch $(C=D)_n-$. In this case, the nitrogen lone-pair is predominantly conjugated with the branch $(A=B)_m-$, and the compounds IV polarizes according to Reaction (1-1), leading to the formation of the conjugated-backbone $(A=B)_m-N(R)-$. As for the $-(C=D)_n$ chain, as long as the chain length n is less than the critical value, the influence of the entire branch on the UV absorption frequency is less than that of one chain unit of the conjugated-backbone, that is, $0 < t < 1$. On the contrary, the conjugated system IV polarizes in the direction shown by Reaction (1-2). In this case, the nitrogen atom is at the end of the conjugated-backbone $-RN-(C=D)_n$, still plays the function of a terminal group, and the $(A=B)_m-$ chain becomes a substitute group.

The purpose of my dissertation is to describe the alternation of conjugation competition using UV spectra based on the uniqueness of the homologous linear rule.

1.2. EXPERIMENTS AND DISCUSSION

In order to be able to describe the alternation of conjugation competition, it is very important and critical to rationally design and select the structure of the nitrogen bridge compound $(A_m-N(R)-B_n)$. This type of compound should at least meet the two conditions. First, if $\tilde{\nu} = a_m + b_m (1/2)^{1/N_m}$ and $\tilde{\nu} = a_n + b_n (1/2)^{1/N_n}$ are two linear lines corresponding to the following two series of compounds: $A_m-N(Me)_2$ and $(Me)_2N-B_n$ ($\tilde{\nu}$ is UV absorption frequency, N_m and N_n are their homologous series numbers), then the slopes of two linear function lines, b_m and b_n , should be close to each other. At the same time, the intercepts of two linear lines, a_m and a_n , should also not be much different. Otherwise, if the branched-chain, A_m- , is increased by one chain unit ($dm = 1$), then, in order to ensure that the competitiveness of branched-chain $-B_n$ may become greater than that of the branched-chain A_m- , $-B_n$ must be added more chain units ($dn > 1$). This will definitely increase the difficulty of synthesis.

Theoretically, when the nitrogen lone-pair is conjugated mainly with A_m- , the compound $A_m-N(R)-B_n$ and its corresponding molecule $A_m-N(Me)_2$ (both compounds have the same chain length m) should be similar in the characteristics (the number, frequency and shape of UV absorption peaks) of UV spectrum. Similarly, $(A_m-N(R)-B_n)$ and $N(Me)_2-B_n$ are similar in the characteristics of UV spectrum. Therefore, the second requirement is that the two homologous series of compounds, $A_m-N(Me)_2$ and $(Me)_2N-B_n$, should be significantly different in the characteristics of UV absorption peak(s). In this case, for a specific compound $(A_m-N(R)-B_n)$, based only on the characteristics of the UV spectrum, it can be intuitively determined which branch is predominantly conjugated with the nitrogen lone pair.

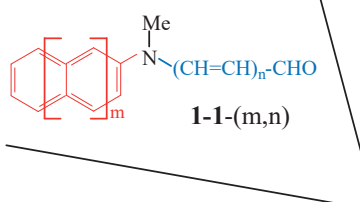
Compounds **1-5-(m)** are the parent compounds of the corresponding molecules **1-3-(m)** [(N,N-dimethyl)-amino-acene]. The former is less stable than the latter and slowly turned black in the air. As shown in the UV spectrum reported by Döller in 1958³³ and by Malhotra in 1960,³⁴ compounds **1-5-(m)** ($m = 0, 1, 2$) are completely different to compounds **1-4-(n)** (ω -dimethylamino-polyenal) in the characteristics of the UV spectrum. In the UV spectrums of **1-5-(m)**, there are three characteristic absorption bands denoted as α , p and β . But there is only a strong absorption K-band in the UV spectrum of **1-4-(n)**.

According to the absorption frequencies reported in the literatures,³³⁻³⁶ the linear relationship between the absorption frequency $\tilde{\nu}$ and the homologous factor $(1/2)^{2/N}$ is as the follows:

$$\tilde{\nu} \cdot 10^{-4} (\text{cm}^{-1}) = 9.464 - 8.46 (1/2)^{2/N} \text{ for } \mathbf{1-3-(m)}$$

$$\tilde{\nu} \cdot 10^{-4} (\text{cm}^{-1}) = 8.825 - 8.47(1/2)^{2/N} \text{ for } \mathbf{1-4-(n)}.$$

Table 1- 1. UV Absorption Wavelengths, λ (Å), of Molecules **1-1-(m,n)**, **1-3-(m)** and **1-4-(n)**.

		$(Me)_2N-(CH=CH)_n-CHO$ 1-4-(n)			
		UV $\lambda = 2040$	2830	3615	4215
		n = 0	n = 1	n = 2	n = 3
	UV λ				
	2970	m = 0	2360 ● ¹	3050 ▲ ²	3780 ▲ ³
	2510		N = m + 3 = 3	N = n + 2 = 3	N = n + 2 = 4
	2000		1-1-(0,0)	1-1-(0,1)	1-1-(0,2)
	3400	m = 1	2780 ● ⁴	3140 ▲ ⁵	3900 ▲ ⁶
	2800		N = m + 3 = 4	N = n + 2 = 3	N = n + 2 = 4
	2400		1-1-(1,0)	1-1-(1,1)	1-1-(1,2)
	4200	m = 2	3400 ● ⁸	3180 ● ⁹	4100 ▲ ¹⁰
	3400		N = m + 3 = 5	N = m + 3 = 5	N = n + 2 = 4
	2680		1-1-(2,0)	1-1-(2,1)	1-1-(2,2)
					3620 ● ¹²
					4480 N = n + 2 = 5
					1-1-(2,3) ▲ ¹¹

The UV absorption Wavelengths for **1-4-(n)** are cited from Malhotra, S. S.; Whiting, M. C. *J. Chem. Soc.*, **1960**, 3812.

Accordingly, the slopes of the two linear lines, 8.46 and 8.47, are almost equal, and the intercept difference, 9.464 – 8.825 = 0.539, between two linear lines is small. Thus, the following two series, a total of 13 compounds, are synthesized and prepared:^{1,2}

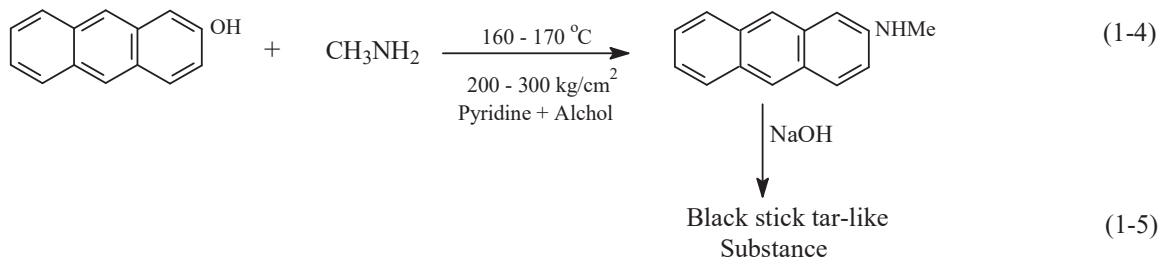
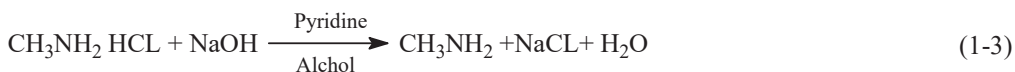
- (i) **1-1-(m, n)**: m = 0, n = 0, 1, 2; m = 1, n = 0, 1, 2; m = 2, n = 0, 1, 2, 3.
- (ii) **1-3-(m)**: m = 0, 1, 2.

Their UV spectrums (Table 1-1), MS (mass spectrometry), IR (infrared), NMR (Nuclear magnetic resonance), and X-ray crystal structures are measured and determined, and their elements are analyzed.²

1.2.1. Synthesis of 2-(N-methylamino)-anthracene

In my dissertation, the synthesis of compounds **1-1-(m,n)** and **1-3-(m)** are detailed.^{1,2} Of them, the synthesis of 2-(methylamino)-anthracene (MAA) is the most interesting and is worth mentioned. MAA is a basic raw material for the synthesis of compounds **1-1-(2,n)** (n = 0, 1, 2, 3). By Imitating the synthesis of (N-methyl,N-2-naphthyl)amine,³⁷ the method of synthesizing MAA is as follows: To 100 ml autoclave, 16 g of sodium hydroxide, 25 g of methylamine hydrochloride, 18 g of 2-hydroxyanthracene, and the amount of the methanol and pyridine mixture (9: 1 by volume) are added. Then, the solution is heated at 160-170 °C for 11 hours under pressure of about 200-300 kg /cm².

However, the product is a black tar-like substance, and it is not MAA. In a few months, such failures



went through many times. One day, when the reaction temperature rose to about 80 °C, power was suddenly interrupted for two days, which actually led to the successful synthesis of the compound MAA.

In dealing with the reaction products, once it was found that in the presence of sodium hydroxide, the product mixture quickly turns into a black tar-like substance (Reaction (1-5)). Therefore, the success, caused by the blackout, let me understand immediately: although the reaction of sodium hydroxide and methylamine hydrochloride is very fast in the solution. However, the solubility of sodium hydroxide in pyridine is limited, and it takes time to dissolve, leading to a slow Reaction (1-3). In the process of Reaction (1-4), the sodium hydroxide is always there. As a result, once MAA is produced, immediately destroyed by the sodium hydroxide. Finally, the product becomes a black tar-like substance. So, the correct procedure should be as follows: (i) a small excess of methylamine hydrochloride; (ii) the reaction solution standing at 100 °C for overnight in order to fully complete Reaction (1-3). Then, the reaction solution is heated at 160 °C and under pressure of 200 kg/cm² for 11 hours (maybe, the reaction time can be shorter), and the product mixture solution shows a nice yellow-green fluorescence. After recrystallization by alcohol, 5 g of MAA is obtained as a yellow-green crystal: m. p. 114-120 °C, MS (m/e⁺) 207 (molecular ion peak, 95%), 178 (30%), 165 (38%).

1.2.2. Determination of Conjugated-Backbone

Before describing alternation of conjugation competition, the uniqueness of homologous linear rule must be used to confirm that the ten compounds **1-1-(m,n)** don't belong to the same homologous series. Then, two methods will be used to verify the existence of the conjugation competition.

According to the definition of homologous linear rule uniqueness, for a homologous series X-An-Y where, for example, electron-releasing group X = (Me)₂N-, electron-withdrawing group Y = -CHO, A_n = -(CH=CH)_n-), there is one and only one homologous linear line $\tilde{\nu} = a + b(1/2)^{2/N}$. The homologous series number, N, is the sum of the numbers of chain units (n) and terminal equivalents. For molecules **1-1-(m,n)**, the terminal equivalent, t, of the benzenoid ring at the end of aromatic chain is 2, t = 1 for amino group, and t = 1 for -CHO. Therefore, if the nitrogen lone-pair is conjugated with two branched-chains, N = m + n + 4. In this case, as shown in Figure 1-1a, all the solid triangle points, $((1/2)^{2/N}, \tilde{\nu})$, are irregularly distributed, and there is no the linear relationship between the UV absorption frequency $\tilde{\nu}$ and the homologous factor $(1/2)^{2/N}$. In each **1-1-(m,n)**, the nitrogen long-pair can't be conjugated with two branches (Ar)_m- and -(CH=CH)_n-CHO at the same time. The ten compounds, **1-1-(m,n)**, don't belong to the same homologous series. Next, need to prove that, for two series of compounds **1-1-(m,1)** (m = 0, 1, 2) and **1-1-(2,n)** (n = 0, 1, 3), each series of compounds don't belong to the same homologous series. For the series of **1-1-(2,n)**, for example, if anthryl group is dealt as a substituent, the homologous number N = n + 2. At this time, as shown by the line in Figure 1-1b, the UV absorption frequency $\tilde{\nu}$ (y) can only be fitted as the following second order polynomial function of $(1/2)^{2/N}$ (x):

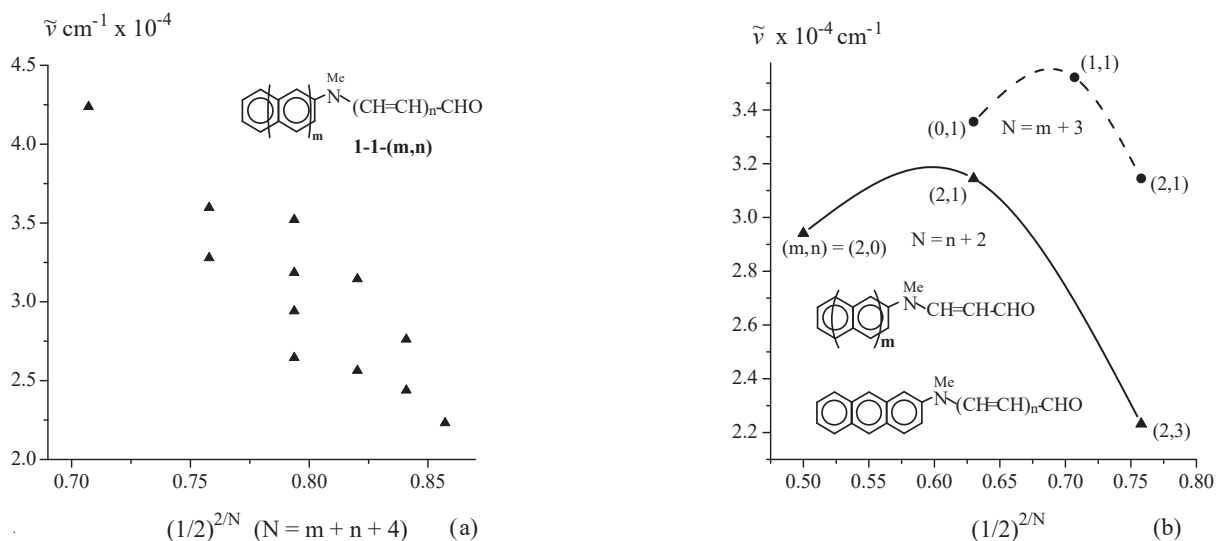


Figure 1-1. Frequency $\tilde{\nu}$ versus $(1/2)^{2/N}$ (a) For molecules **1-1-(m,n)**. (b) For molecules **1-1-(m,n)** ($n=1$) and **1-1-(m,n)** ($m=2$)

$$y = -8.4685 - 39.6876 x - 33.7365 x^2$$

The function line is not linear. Therefore, it can be asserted that, in the ten nitrogen-bridge compounds $(Ar)_m-(Me)N-(CH=CH)_n-CHO$, there are two possible conjugated-backbone structures $(Ar)_m-N(Me)-$ and $-(Me)N-(CH=CH)_n-CHO$. But, in a specific nitrogen-bridge compound, there is only one conjugated-backbone, $(Ar)_m-N(Me)-$ or $-(Me)N-CH=CH)_n-CHO$.

1.2.2.1. UV Spectrum Method

According to the characteristics of UV spectrum, the ten compounds **1-1-(m,n)** can be divided into three groups. In Table 1-1, the four compounds of the first group, **1-1-(m,n)** where $m = 0, 1, 2, n = 0; m = 2, n = 1$ ($m > n, m = n = 0$), are located in the lower left triangle of the Table. The four compounds of the second group, **1-1-(m,n)** where $m = 0, n = 1, 2; m = 1, n = 2; m = 2, n = 3$, are located in the upper right triangle of the Table. The remaining two compounds, **1-1-(1,1)** and **1-1-(2,2)**, are located in the middle of the Table, belong to the third group ($m = n$).

Specifically, as shown by comparison between Figure 1-2a and Figure 1-2b, for each of the first group compounds, the characteristics of the UV spectrum are similar to those of the corresponding compound **1-3-(m)** except for the hypsochromic shift of p- and β -band. But, the λ_p (p-band wavelength) value is still close to the value of the corresponding **1-3-(m)**. For example, compounds **1-1-(1,0)** are similar to **1-3-(1)** in the UV characteristics, their λ_p values are as follows: $\lambda_p = 278$ nm for **1-1-(1,0)** and $\lambda_p = 280$ nm for **1-3-(1)**. The difference in the absorption wavelength between the two molecules is only 2 nm. The difference in the UV characteristics is only that, for **1-1-(1,0)**, the α -band has been replaced by an inflection. This indicates that, in the first group compounds, the nitrogen lone pair is conjugated mainly with the aromatic group to form a conjugated-backbone $(Ar)_m-N(Me)-$, and whole polyenal chain, as a substituent, has a slight influence (about 2 nm) on UV absorption wavelength (λ_p).

For each of the second group compounds, the UV spectrum is similar to the corresponding ω -(dimethylamino)polyenal **1-4-(n)** in the shape and number of absorption peaks, that is, has a K-band of strong absorption (Figure 1-2c), and the value λ_k of K-band absorption wavelength is also close to the value of the corresponding **1-4-(n)** (Table 1-1). For **1-1-(0,1)** and its corresponding compound **1-4-(1)** (ω -(dimethylamino)acrolein), for example, their λ_k values are as follows:

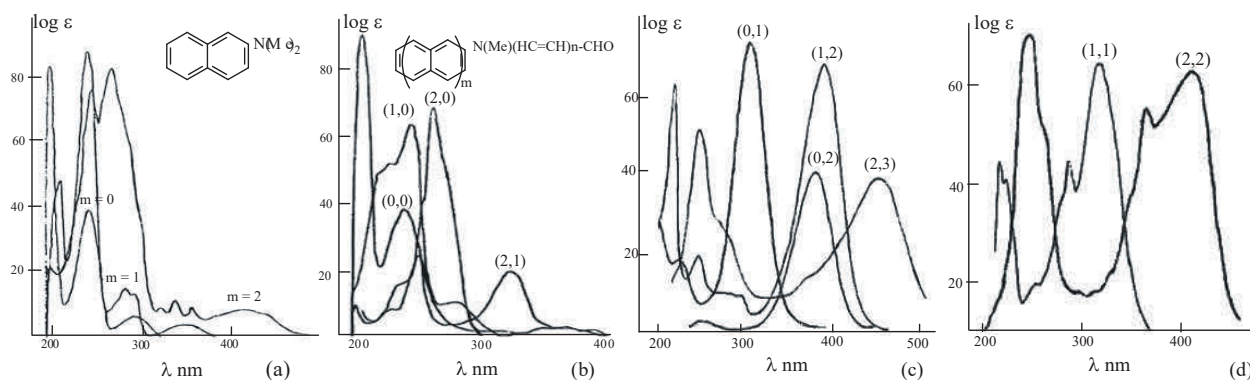


Figure 1-2. UV wavelength λ versus $\log \epsilon$ (a) For **1-3-(m)**. (b) For **1-1-(m,n)** of the first group. (c) For **1-1-(m,n)** of the second group. (d) For the third group of molecules **1-1-(m,n)**.

$$\lambda_k = 283 \text{ nm for } \mathbf{1-4-(1)}, \lambda_k = 305 \text{ nm for } \mathbf{1-1-(0,1)}, \lambda_k = 251 \text{ nm for } \mathbf{1-3-(0)}.$$

The difference in the absorption wavelength between molecules **1-1-(0,1)** and **1-4-(1)** is 22 nm, but the difference between the molecules **1-1-(0,1)** and **1-3-(0)** is large, up to 54 nm. Therefore, in each of the second group compounds, the nitrogen lone-pair is mainly conjugated with polyenal group, forming the conjugated-backbone $-\text{(Me)N}-(\text{CH}=\text{CH})_n-\text{CHO}$.

According to Table 1-1, adding a double bond in each compound **1-4-(n)**, the wavelength λ_k increases by about 80 nm. For the molecule **1-4-(1)**, the replacement of its a methyl group by phenyl leads to the formation of molecules **1-1-(0,1)**, which, theoretically, is equivalent to adding two double bonds (the terminal equivalent $t = 2$ for phenyl ring). However, from 283 nm to 305 nm, the wavelength λ_k increases only by 22nm, which is equivalent to the contribution made by 1/4 chain unit of the polyenal group. Therefore, in molecule **1-1-(0,1)**, phenyl group only plays the function of a substituent group.

The third group of compounds **1-1-(1,1)** and **1-1-(2,2)** ($m = n$) is a transition type of compounds. As far as the characteristics of UV spectrum are concerned, each of the third group compounds is different to the corresponding **1-3-(m)**, also different to the corresponding **1-4-(n)**. In their UV spectra, there is a broad absorption band with characteristic double peaks (Figure 1-2d, Table 1-1). For example, for compound ω -(N,N-naphthylmethylamino)acrolein **1-1-(1,1)**, the absorption wavelengths of the double peaks of a broad absorption band are as follows: $\lambda = 284$ nm for left peak, and $\lambda = 314$ nm for right peak. Two absorption wavelengths are close, respectively, to the absorption wavelength ($\lambda_p = 280$ nm) of compound **1-3-(1)** and to the absorption wavelength ($\lambda_k = 283$ nm) of compound **1-4-(1)**.

1.2.2.2. Homologous Linear Rule Method

In the two figures from Figure 1-3 to Figure 1-4, a dotted red line corresponds to the homologous series **1-3-(m)**, and a solid blue line to **1-4-(n)**. In Figure 1-3a, four solid red circles are very close to the dotted red line, and their vertical coordinates are the UV absorption frequencies of the four compounds of the first group. This, together with the intuitive speculation from UV spectrums (Figure 1-2b), confirms that in each of the compounds belonging to the first group, a nitrogen lone-pair is conjugated mainly with the aromatic branch, and another chain, such as $-\text{CHO}$, $-\text{CH}=\text{CH}-\text{CHO}$, slightly affects the absorption frequency. In Figure 1-3a, four solid blue triangles are close to the solid blue line. This, together with the intuitive speculation from UV spectrums (Figure 1-2c), confirms that in each of the compounds belonging to the second group, the nitrogen lone-pair is predominantly conjugated with the polyenal group $-(\text{CH}=\text{CH})_n-\text{CHO}$.

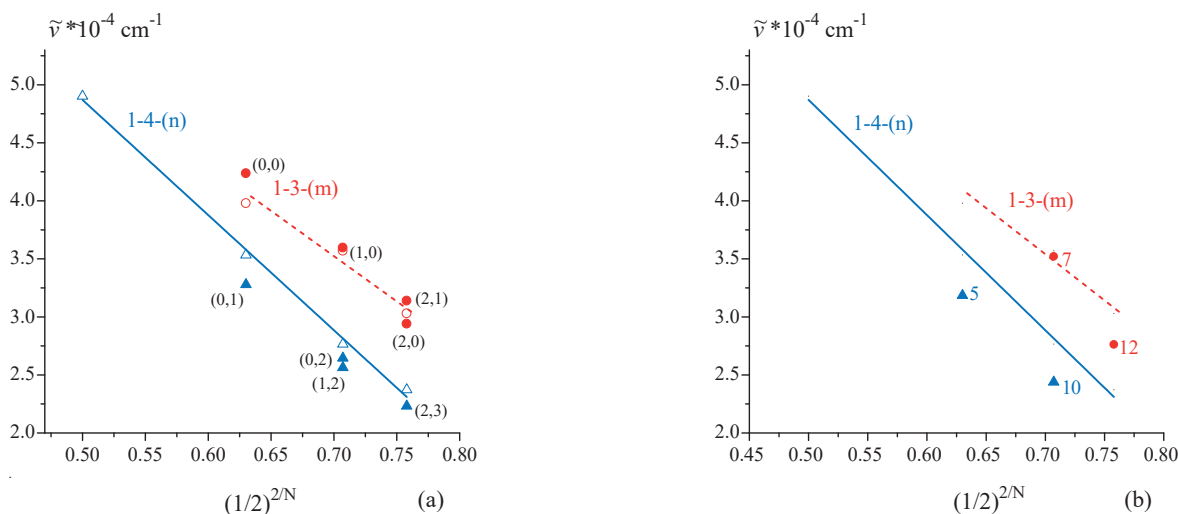


Figure 1-3. (a) Homologous linear lines for **1-4-(n)** and **1-3-(m)**, and the determination of the conjugated-backbones for the first (solid red circles) and second groups (solid blue triangles) of molecules **1-1-(m,n)**. (b) Each pair of points corresponds to the double-peak UV frequencies of a broad absorption band of each molecule in the third group.

In Table 1-1, each pair of points, (solid blue triangle and solid red circle), corresponds to the frequencies of the double-peaks of a broad absorption band for each molecule in the third group. In Figure 1-3b, the solid blue triangles are close to the solid blue line, and the solid red circles are near to the dotted red line. For the molecule **1-1-(1,1)**, for example, the solid blue triangle $\Delta 5$ in Figure 1-3b and Table 1-1 represents the absorption frequency $\tilde{\nu}$ of the right peak of the broad absorption band, the solid red circle, $\bullet 7$, does the absorption frequency $\tilde{\nu}$ of the left peak. In Figure 1-3b, the positions of the 4 points mean that, only in each compound belonging to the third group, the ability of the two branches (Ar_m- and $-\text{CH}=\text{CH}_n\text{-CHO}$) to compete for a nitrogen lone pair is comparable.

1.2.2.3. Alternately Competing for Nitrogen Lone-Pair

In Figure 1-4, a route starts with N,N-dimethylformamide, goes through compounds **1-1-(0,0)**, **1-1-(0,1)**, **1-1-(1,1)**, **1-1-(2,1)**, **1-1-(2,2)**, and finally to **1-1-(2,3)**. As shown in this route, two branches alternately compete for nitrogen lone pair as the two chain lengths, m and n , increase alternately.

In N,N-dimethylformamide (DMF) (**1-4-(0)**), a nitrogen lone-pair can only be conjugated with the carbonyl group. In Figure 1-4, the point $\Delta 0$ (0.5, 4.90), corresponding to DMF, is on the solid linear line for homologous series **1-4-(n)**, and its vertical coordinate ($4.9 \times 10^{-4} \text{ cm}^{-1}$) is the UV absorption frequency $\tilde{\nu}$ of DMF. When a methyl group of DMF is replaced by a phenyl group, compound **1-1-(0,0)** (N,N-phenylmethylformamide) is produced. In Figure 1-4b, the point $\bullet 1$ (0.63, 4.237) corresponds to molecule **1-1-(0,0)** and is close to the homologous linear line (a dotted red line) for **1-3-(m)**.

In Figure 1-4b, the dotted linear red line indicates the relationship between the UV absorption frequency $\tilde{\nu}$ of molecule **1-3-(m)** and the corresponding homologous factor $(1/2)^{2/N}$ ($N = 3 + m$), and it can be fitted as follow linear function ($\text{cc} = 0.889$):

$$\tilde{\nu} \times 10^{-4} = 9.03372 - 7.92576 * (1/2)^{2/N} \quad (1-\text{II})$$

For molecule **1-3-(0)**, the UV absorption frequency is $3.984 \times 10^4 \text{ cm}^{-1}$, and the homologous factor $(1/2)^{2/N} = 0.63$ ($N = 3$). The UV absorption frequency $\tilde{\nu}$ of **1-1-(0,0)** is $4.237 \times 10^4 \text{ cm}^{-1}$. According to Equation (1-II), the homologous number N , corresponding to the UV absorption frequency of $4.237 \times 10^4 \text{ cm}^{-1}$, is 2.7602, and it is defined

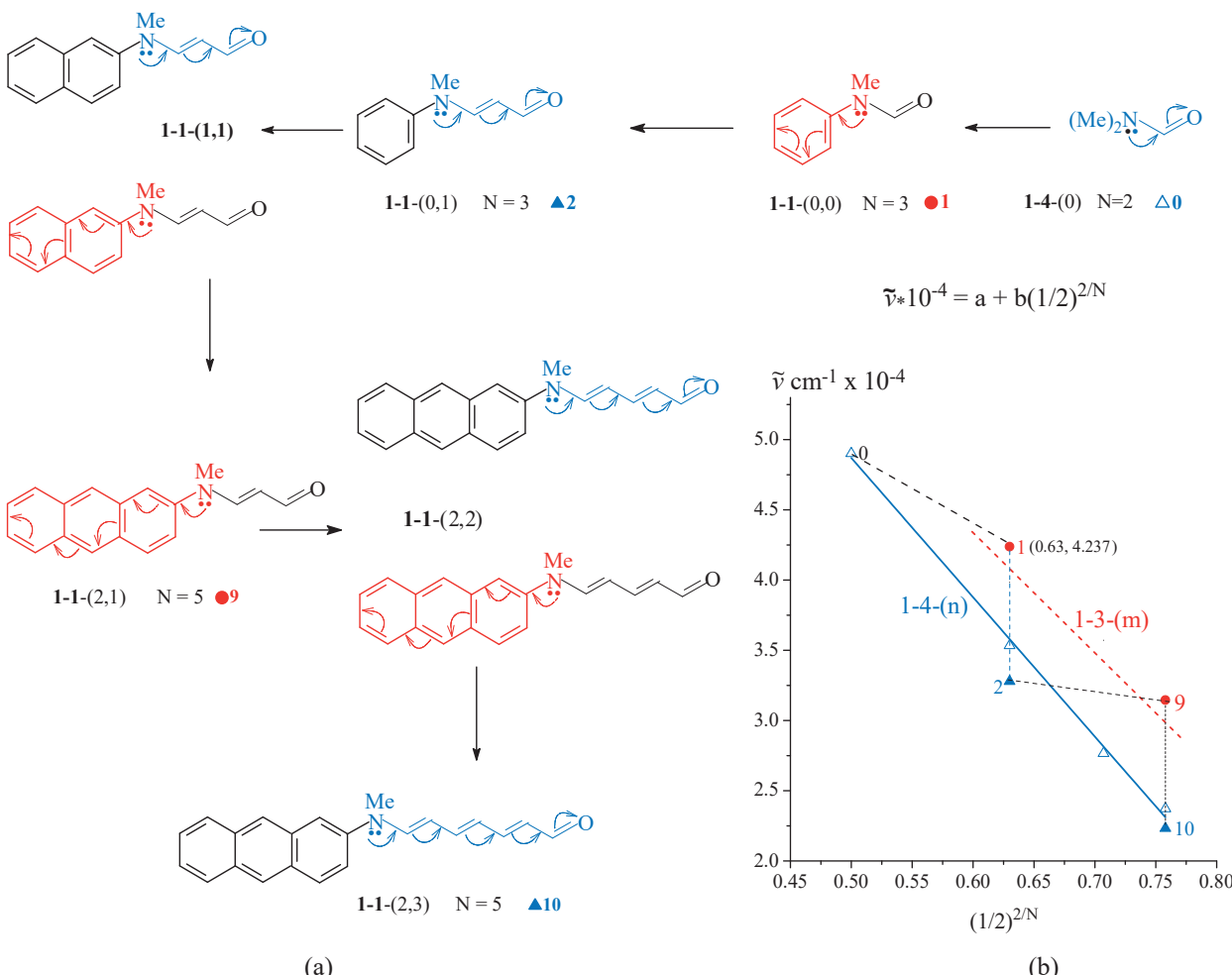


Figure 1-4. Alternating competition for conjugation. From N,N-dimethylamide to (N-methyl-N-formylhexatrienyl)-2-anthramine is a process in which the two branched-chains alternately compete for a nitrogen lone-pair as the chain lengths, m and n, increase alternately.

as the theoretical (actual) homologous number N_T of **1-1-(0,0)**. $\Delta N = N_T - N = -0.24$ is defined as the substitute equivalent of -CHO group. This indicates that, in **1-1-(0,0)**, the nitrogen lone-pair is conjugated mainly with the phenyl ring, forming the conjugated-backbone Ph–N(Me)–. If the frequency ($3.984 \times 10^4 \text{ cm}^{-1}$) of the **1-3-(0)** is regarded as the frequency of the conjugated-backbone Ph–N(Me)–, the frequency ($4.237 \times 10^4 \text{ cm}^{-1}$) of molecule **1-1-(0,0)** means that, in this molecule, the -CHO group makes the UV absorption frequency of conjugated-backbone (Ph–N(Me)–) violet shift. The shift extent is equivalent to the contribution made by -0.24 chain unit of **1-3-(m)**.

In Figure 1-4b, the point $\blacktriangle 2$ (0.63, 3.279) corresponds to the compound **1-1-(0,1)** ω -(N,N-dimethylphenylamino)-acrolein ($N = 3$, $(1/2)^{2/N} = 0.63$), and it is close to the solid linear blue line. For the homologous series **1-4-(n)**, the solid linear blue line indicates the relationship between the frequency $\tilde{\nu}$ of each molecule **1-4(n)** and the corresponding homologous factor $(1/2)^{2/N}$ ($N = 2 + n$), and it can be fitted as the following linear Equation (1-III):

$$\tilde{\nu} \times 10^4 = 9.8472 - 9.9477 (1/2)^{2/N} \quad (\text{cc} = 9.847) \quad (1-\text{III})$$

According to Equation (1-III), the horizontal distance between the point $\blacktriangle 2$ and the solid linear blue line gives $\Delta N =$

$N_T - N = 0.34$. This indicates that, in the compound **1-1-(0,1)**, due to that the competitiveness of formyl vinyl group ($\text{CHO}-\text{CH}=\text{CH}-$) is greater than the phenyl ring, the nitrogen lone-pair has been pulled back by the formyl vinyl group, forming the conjugated-backbone $-(\text{Me})\text{N}-\text{CH}=\text{CH}-\text{CHO}$. As for the phenyl ring, it makes the absorption frequency of the conjugated backbone red shift, but the red shift extent is only equivalent to the contribution made by 0.34 chain unit of **1-4-(n)** although the terminal equivalent of phenyl ring is 2.

Compounds **1-1-(1,1)** (ω -(*N,N*-naphthylmethylamino)-acrolein) belongs to the third group, it results from the replacement of phenyl group of **1-1-(0,1)** by a naphthyl group. Although the naphthyl group's competitiveness is greater than the phenyl ring, its ability is still not large enough to be able to completely take back the lone-pair electrons from the conjugated-backbone $-(\text{Me})\text{N}-\text{CH}=\text{CH}-\text{CHO}$.

As a result of the replacement of the naphthyl of **1-1-(1,1)** by anthryl group, compound **1-1-(2,1)** (ω -(*N,N*-anthrylmethyl-amino)-acrolein) is produced, and the point $(\tilde{\nu}, (1/2)^{2/N})$ in Figure 1-4b is moved from the point $\Delta 2$ (0.63, 3.279) (near to the solid linear blue line) to the point $\bullet 9$ (0.758, 3.145) (close to the dotted linear red line), and $\Delta N = -0.33$ for the point $\bullet 9$. This indicates that in the molecule **1-1-(2,1)**, due to that the anthryl group is more competitive than the formyl vinyl group ($\text{CHO}-\text{CH}=\text{CH}-$), the nitrogen lone-pair is again pulled back to the anthryl group, leading to the formation of conjugated-backbone Anthryl- $\text{N}(\text{Me})-$. In the meantime, the formylvinyl group only causes the UV absorption frequency of the conjugated-backbone Anthryl- $\text{N}(\text{Me})-$ to shift violet, and the violet shift extent corresponds to the contribution made by -0.33 chain unit of **1-3-(m)**.

Finally, as shown by point $\Delta 10$ (0.758, 2.232) in Figure 1-4b, the competitiveness of the formyl-hexatrienyl group is so great that the lone-pair electrons are pulled back by polyenal chain once again. At this time, despite the terminal equivalent $t = 4$ for anthryl group, but its influence (red-shift) on the frequency of $-(\text{Me})\text{N}(\text{CH}=\text{CH})_3\text{CHO}$ is only equivalent to the function of the 0.20 chain unit of **1-4-(n)**.

In Figure 1-4b, the path of the point $(\tilde{\nu}, (1/2)^{2/N})$, moving back and forth between the solid and dotted linear lines, quantitatively and visually, describes the alternating process of competitive conjugation.

1.2.2.4. Competing for π -like Orbital of N-Methyl

In molecule **1-1-(1,0)**, as shown by the Newman projections in Figure 1-5, the two hydrogen atoms, H(20) and H(21), of N-methyl group, are located above and below the plane of the formyl group. In this case, the two 1s atomic orbitals (AO), belonging to H(20) and H(21) hydrogen atoms respectively, and a p_z AO of C(22) carbon atom can be considered to form a π -like molecular orbital.³⁸

The geometries of the three compounds **1-1-(1,n)** ($n = 0, 1, 2$) are fully optimized at B3LYP/6-31G* level and show an interesting phenomenon: as the chain length n increases, the N-methyl group rotates clockwise around the C(22)-N(18) bond, implying that the conjugation competition should include the competition for the π -like MO.

In molecule **1-1-(1,0)**, as shown by the Newman projection in Figure 1-10, the dihedral angles $\alpha = \text{H}(21)-\text{C}(22)-(\text{N}18)-\text{C}(2) = -77.6^\circ$ and $\beta = \text{H}(20)-\text{C}(22)-(\text{N}18)-\text{C}(2) = 43.4^\circ$, that is, the two hydrogen atoms, H(20) and H(21), are facing the naphthyl group. But these two hydrogen atoms are all above the naphthyl plane according to that dihedral angle $\alpha' = \text{H}21-\text{N}18-\text{C}2-\text{C}1 = 0.6^\circ$ and $\beta' = \text{H}20-\text{N}18-\text{C}2-\text{C}1 = 50.5^\circ$. With the increasing of polyenal chain $-(\text{CH}=\text{CH})_n-\text{CHO}$, the two hydrogen atoms, H(19) and H(21), of the N-methyl group change their orientation. From beginning of molecular **1-1-(1,1)**, as shown by the second and third Newman projections and dihedral angle data presented in Figure 1-5, the two hydrogen atoms, H(19) and H(21), becomes facing the polyenal chain. In the meantime, the difference $\gamma - |\delta|$ between the two dihedral angles γ and δ becomes smaller, and the difference are as follows:

$$73.7^\circ (n=0) > 22.3^\circ (n=1) > 18.1^\circ (n=2)$$

Finally, in molecule **1-1-(1,2)**, the dihedral angels, $\delta = \text{H}(19)-\text{C}(22)-(\text{N}18)-\text{C}(23) = -51^\circ$, and $\gamma = \text{H}(21)-\text{C}(22)-$

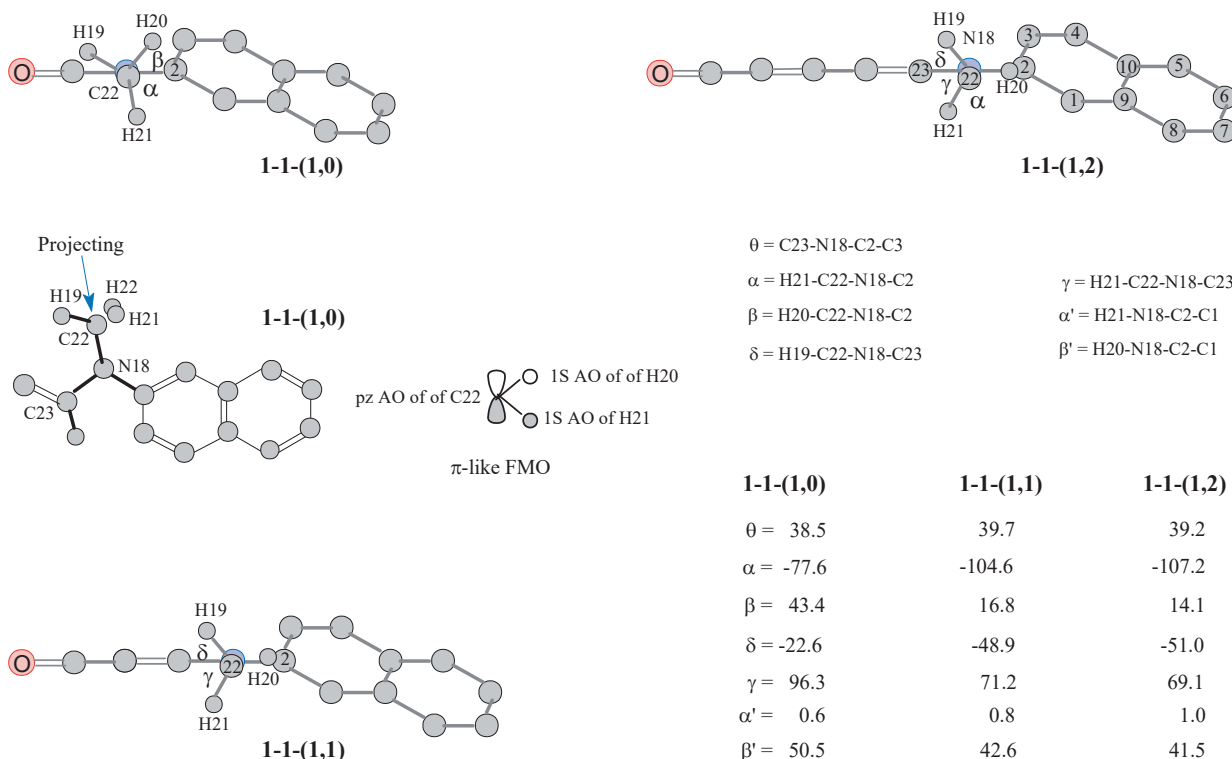


Figure 1-5. For molecules **1-1-(1,n)** ($n=1, 2, 3$) optimized at B3LYP/6-31G* level, the Newman projections along the C(22)-N(18) bond.

$\text{N}(18)\text{-C}(23) = 69^\circ$, and the two hydrogen atoms can be considered symmetrically located above and below the polyenal plane. The 1s AOs of the H(19) and H(21) and the pz AO of C(22) atoms form a typical π -like orbital. The difference, in the difference ($\gamma - |\delta|$), between **1-1-(1,2)** and **1-1-(1,1)** is about 4.2° . The difference is small, but it shows a process of competing for π -like molecular orbital.

The two processes, competing for the lone-pair electrons and for the π -like orbital, are consistent and synchronized.

1.3. QUESTIONABLE FUNDAMENTAL PRINCIPLES

After determining the conjugated backbone of each molecule **1-1-(m,n)**, it becomes possible to discuss the relationship between the twist angle θ of the molecule and the conjugated backbone, that is, the relationship between the conjugation effect and the molecular twist angle θ .

In the molecule **1-1-(1,1)**, the naphthyl ring's ability of competing for lone-pair electrons should be greater than in molecules **1-1-(1,2)**. Then, according to the principle of the conjugation (resonance) stabilization. The following size order can be speculated:

$$\theta(1,1) < \theta(1,2), r_{2-18}(1,1) < r_{2-18}(1,2)$$

where $\theta(1,1)$ represents the dihedral angle between the amino plane C(23)-N(18)-C(2) and the naphthyl plane in

molecule **1-1-(1,1)**, and $r_{2-18}(1,1)$ is the distance (bond length) between two atoms C(2) and N(18) in molecule **1-1-(1,1)**. However, the x-ray crystal structures show the following opposite results:^{5,6}

$$\theta: 33.6^\circ (1,1) > 31.4^\circ (1,2); \\ r_{2-18}: 1.430 \text{ \AA} (1,1) > 1.423 \text{ \AA} (1,2).$$

In the B3LYP/6-31G* optimized geometries of molecules **1-1-(1,n)** ($n = 0, 1, 2$), the size orders of the twist angle θ and C(2)-N(18) bond distance are as follow (Figure 1-10):

$$\theta: 38.5 (1,0) < 39.7 (1,1), \text{ and } 39.7 (1,1) > 39.2 (1,2) \\ r_{2-18}: 1.419 \text{ \AA} (1,0) < 1.421 \text{ \AA} (1,1), \text{ and } 1.421 \text{ \AA} (1,1) > 1.420 \text{ \AA} (1,2)$$

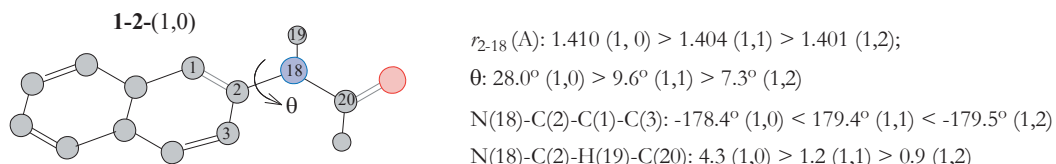
Of the three molecules, the twist angle θ and bond distance r_{2-18} for molecule **1-1(1,1)** are the largest. However, the following size order of the dihedral angle C(2)-N(18)-C(22)-C(23) should also be noteworthy:

$$-174^\circ (1,0) < -175.8^\circ (1,1) < -176.4^\circ (1,2).$$

This dihedral angle indicates the flatness of the amino group. In the molecule **1-1-(1,0)**, it is smaller by 2° than those in the other two molecules, which can be considered as a result of destabilizing π -interaction between the naphthyl group and amino group.

The driving force for causing large twist angle will be discussed in the next chapter. In this chapter, in order to study causal relationship between the conformation and the conjugation intensity, and to exclude the role of the steric hindrance of N-methyl group in determining the molecular conformation as far as possible, three molecules **1-2-(1,n)** ($n = 0, 1, 2$) are optimized at B3LYP/6-31G* level.

The structure difference between molecules **1-1-(1,n)** and its corresponding compounds **1-2-(1,n)** is slight. Therefore, according to the previous discussion, in the compound **1-2-(1,0)**, the nitrogen lone-pair is mainly conjugated with the naphthyl ring, and in **1-2-(1,2)** molecules, the nitrogen lone-pair is mainly conjugated with the polyenyl chain. Then, as shown by the images of the molecules, with the growth of the polyenyl chain, the size orders of the bond length r_{2-18} and dihedral angle θ are as follows:



All the size orders are exactly opposite to the prediction by the classic structure theory. In particular, for molecule **1-2-(1,0)**, the twist angle θ is so large, even up to 28° , and it is about three times the twist angle of the other two molecules. These imply that, in molecule **1-2-(1,0)**, the conjugation between the nitrogen lone pair and the naphthyl ring is destabilization, and the naphthyl ring plane had to rotate about the C(2)-N(18) bond by 28° in order to weaken the destabilizing conjugation. In the molecule **1-2-(1,2)**, due to nitrogen lone has been turn to conjugation with formylbutadienyl group, so the destabilizing interaction between the amino group and the naphthyl ring is weakened. As a result, the twist angle θ is reduced to 7.3° , the bond distance r_{2-18} (\AA) is shortened from 1.410 ($n = 0$) to 1.401 ($n = 2$), and meanwhile the dihedral angle N(18)-C(2)-H(19)-C(20) is reduced from 4.3 in ($n = 0$) to 0.9° ($n = 2$).

For the full optimized geometry ($\theta = 28^\circ$) of **1-2-(1,0)** at B3LYP/6-31G*, the bond length r_{2-18} (1.410 \AA) is longer than that (1.408 \AA) in the co-planar geometry that is restrictedly optimized at B3LYP/6-31G* level. This

seems to support the classical viewpoint of conjugation stabilization. However, it is not only the conjugation effect that determines the molecular conformation, but also the steric hindrance is an important factor. In order to understand the role of the steric hindrance in determining the molecular conformation, two conformations of molecule **1-2-(1,0)**, the ground state geometry with $\theta = 28^\circ$ and the coplanar geometry with $\theta = 0^\circ$, are optimized at B3LYP/6-31G* level. For the ground state geometry, for example, $E^{AB_N}(28^\circ)$ is the nuclear repulsion (hartree) between the naphthyl (A) group and the formylamino (B) group, $E_N(28^\circ)$ is total nuclear repulsion, and $E_e(28^\circ)$ and $E(28^\circ)$ are total electronic energy and molecular energy. For the two conformations of **1-2-(1,0)**, the following size orders are interesting and contrary to the classic view:

$$\begin{aligned} E^{AB_N}(\theta=28^\circ) & (184.23371) > E^{AB_N}(0^\circ) (183.77479); \\ E_N(28^\circ) & (693.53676) > E_N(0^\circ) (693.12936); \\ |E_e(28^\circ) (-1248.12130)| & > |E_e(0^\circ) (-1247.71359)|. \\ |E(28^\circ) (-554.58453)| & > |E(0^\circ) (-554.58423)| \end{aligned}$$

Accordingly, the nuclear repulsion between the two fragments is resistance to molecular distortion, and a preferential geometry ($\theta = 28^\circ$) (the ground state geometry) is a more crowded conformation. Thus, the basic causal relationship in Organic chemistry should also be questioned.

1.4. CONCLUSIONS

For ten nitrogen-bridge compounds **1-1-(m,n)**, when $n < m$, the nitrogen lone-pair is predominantly conjugated with the aromatic chain; when $n > m$, it is predominantly conjugated with the polyenal chain. The determination of conjugated-backbone is to discuss the relationship between the conjugation and molecular confirmation, this is, the relationship between the conjugation effect and the molecular twist angle θ .

For three molecules **1-2-(1,n)**, 2-naphthyl-NH-(HC=CH)_n-CHO ($n = 0, 1, 2$), as the polyenal chain increases from $n = 0$ to $n = 2$, the conjugation state of the nitrogen lone pair is changed from mainly conjugated with naphthyl group to mainly conjugated with polyenal chain, but the corresponding dihedral angle between the naphthyl and amino groups decreases from 28° degree to 7.3° .

Based on the comparison of the two conformations, the planar geometry and the fully optimized geometry, of **1-2-(1,0)**, the nuclear repulsion between naphthyl (A) and formyl amino (B) groups is a resistance to molecular distortion, not the driving force in the classical theory. The fact that total electronic energy of fully optimized geometry is greater in the absolute value than that of planar geometry implies that the conjugation between two fragments A and B is destabilization and A crowded conformation may be energetically preferential.

1.5. REFERENCES

- 1 Yu, Z. H. 1985. *Competition Conjugation Alternating in the Nitrogen-bridge Compounds*. PhD diss., Institute of Chemistry, Chinese Academy of Sciences, Beijing.
- 2 Jiang, M. Q.; Yu, Z. H.; Dai, C. C. 1990. "Alternative Predominance in Competition for Conjugation in Nitrogen Bridge Compound." *Sci. Chin. B.* 33: 409-420
- 3 Chiang, M. C. (Jiang, M. Q.) 1987. *The Rule of Homologous Linearity of Organic Compounds*. Beijing: Science Press.
- 4 Jiang, M. Q. 1987. *The Rule of Conjugated Group Combination*. Beijing: Science Press.

- 5 Bai, C. L.; Yu, Z. H.; Fu, H.; Tan, Y. Q. 1984. "Structure of 3-[(N-methyl, N-2-naphthyl)amino]-acrolein." Chin. J. Struct. Chem., 3: 65-68.
- 6 Bai, C. L.; Yu, Z. H.; Fu, H.; Tan, Y. Q. 1984. "Structure of 5-[(N-methyl,N-2-naphthyl)amino]-penta-2,4-dienal." Chin. J. Struct. Chem., 3: 69-72.
- 7 Ingold, C. K. 1953. *Structure and Mechanism in Organic Chemistry*. New York: Cornell University Press.
- 8 Vollhardt, K. P. C.; Schore, N. E. 1999. *Organic Chemistry*, third Edition. New York: W. H. Freeman and Company.
- 9 Pauling, L. 1932, "Interatomic Distance in Covalent Molecules and Resonance between Two or More Lewis Electronic Structures." Proc. Nat. Acad. Sci., 18: 293-297.
- 10 IUPAC. 1997. *Compendium of Chemical Terminology*, 2nd ed. (the "Gold Book"). Online corrected version: 2006-. "resonance energy".
- 11 Mo, Y.; Schleyer, P. v. R. 2006. "An Energetic Measure of Aromaticity and Antiaromaticity Based on the Pauling-Wheland Resonance Energies." Chem. Eur. J., 12: 2009-2020.
- 12 Shaik, S.; Shurki, A.; Danovich, D.; Hiberty, P. C. 2001. "A Different Story of π -Delocalization – The Distortion of π -Electrons and Its Chemical Manifestations." Chem. Rev., 101: 1501-1539.
- 13 Deniz, A. A.; Peters, K. S.; Snyder, G. J. 1999. "Experimental Determination of the Antiaromaticity of Cyclobutadiene." Science, 286: 1119-1122.
- 14 Conant, J. B.; Kistiakowsky, G. B. 1937. "Energy Changes Involved in the Addition Reactions of Unsaturated Hydrocarbons." Chem. Rev., 20: 181-194.
- 15 Kistiakowsky, G. B.; Ruhoff, J. R.; Smith, H. A.; Vaughan, W. E. 1936. "Heats of Organic Reactions. IV. Hydrogenation of Some Dienes and of Benzene." J. Am. Chem. Soc., 58: 146-153.
- 16 Dewar, M. J. S.; Gleicher, G. J. 1965. "Ground States of Conjugated Molecules. III. Classical Polyenes." J. Am. Chem. Soc., 87: 692-696.
- 17 Altmann, J. A.; Reynolds, W. F. 1977. "Geometry-Optimised *ab Initio* Calculations on 1,3-Butadiene; Evidence Concerning Conjugative Stabilization of Dienes." J. Mol. Struct., 36: 149-153.
- 18 Bally, T.; Haselbach, E.; Lanyiova, S.; Marschne, F.; Rossi, M. 1976. "Concerning the Conformation of Isolated Benzylideneaniline." Helv. Chim. Acta., 59: 486-498.
- 19 Burgi, H. B.; Dunitz, J. D. 1971. "Molecular Conformation of Benzylideneanilines." Helv. Chim. Acta., 54: 1255-1260.
- 20 Choi, C. H.; Kertesz, M. 1997. "Conformational Information from Vibrational Spectra of Styrene, *trans*-Stilbene, and *cis*-Stilbene." J. Phys. Chem. A, 101: 3823-3831.
- 21 Kuze, N.; Ebizuka, M.; Fujiwara, H.; Takeuchi, H.; Egawa, T.; Konaka, S. 1998. "Molecular Structure of *p*-Azoxyanisole, a Mesogen, Determined by Gas-Phase Electron Diffraction Augmented by *ab Initio* Calculations." J. Phys. Chem. A, 102: 2080-2086.
- 22 Gould, E. S. 1960. *Structure and Mechanism in Organic Chemistry*. New York: Holt-Dryden Book-Henry Holt Co..
- 23 March, J. 1992. *Advanced Organic Chemistry*. New York: John Wiley & sons Inc..
- 24 Dewar, M. J. S. 1969. *The PMO Theory of Organic Chemistry*. New York: McGra-Hill.
- 25 Epotis, N. D.; Cherry, W. R.; Shaik, S.; Yates, R.; Bernardi, F. 1977. *Topics in Current Chemistry*; Vol. 70. New York: Springer.
- 26 Fukui, K. 1971. "Recognition of Stereochemical Paths by Orbital Interaction." Acc. Chem. Res., 4: 57-64.
- 27 Woodward, R. B.; Hoffmann, R. 1968. "Conservation of Orbital Symmetry." Acc. Chem. Res., 1: 17–22.
- 28 Woodward, R. B.; Hoffmann, R. 1970. *The Conservation of Orbital Symmetry*. New York: Verlag Chemie and Academic Press.
- 29 Epotis, N. D. 1983. *Lecture Notes in Chemistry*, Vol. 34. New York: Springer-Verlag
- 30 Epotis, N. D. 1996. *Deciphering the Chemical Code*. New York: VCH Publishers Inc..
- 31 Jiang, M. Q.; Yu, Z. H. 1981. "Quantitative Relationship between Molecular Structure and Properties in Forked Conjugative Furyl Polyenic Acid Drivatives (I) Ultraviolet Spetra." J. Struct. Chem., 2: 121-134 (Chinese).

- 32 Jiang, M. Q.; Yu, Z. H. 1982. "Quantitative Relationship between Molecular Structure and Properties in Forked Conjugative Furyl Polyenic Acid Derivatives (I) NMR and IR Spectra." *J. Mole. Sci.*, 65-72.
- 33 Döller, E.; Förster, T.; Renner, H. 1958. "Regelmäßigkeiten in den Absorptionsspektren von Aryl-Alkaliamiden und Anderen Einfach Substituierten Aromaten." *Z. Physik. Chem.*, 15: 34-47.
- 34 Malhotra, S. S.; Whiting, M. C. 1960. "Researches on Polyenes. Part VII. The Preparation and Electronic Absorption Spectra of Homologous Series of Simple Cyanines, Merocyanines, and Oxonols." *J. Chem. Soc.*, 3812-3822.
- 35 Walba, H.; Branch, G. E. K. 1951. "The Absorption Spectra of Some N-Substituted p-Aminotriphenylmethyl Ions." *J. Am. Chem. Soc.*, 73: 3341-3348.
- 36 Steck, E. A.; Ewing, G. W. 1948. "Absorption Spectra of Heterocyclic Compounds. II. Amino-Derivatives of Pyridine, Quinoline and Isoquinoline." *J. Am. Chem. Soc.*, 70: 3397-3406.
- 37 Morgan, G. T.; Evens, F. P. 1919. "C.- β -Naphthylmethylamine." *J. Chem. Soc.*, 115: 1140-1145.
- 38 Houk, K. N.; Domelsmith, L. N.; Stogier, R.; Patterson, R. T. 1978. "Schizophrenic Substituents: The Origin of Anomalous Substituent Effects on Cycloaddition Regioselectivity." *J. Am. Chem. Soc.*, 100: 6531-6533.

CHAPTER 2

ABNORMAL LARGE TWIST ANGLE OF NBA

ABSTRACT

8 substituted N-benzylideneaniline-like species, Ar-N=CH-Ar', with a five- or six-membered heterocyclic ring and 4 substituted triphenylketenimines, Ar-N=C=C(Ar')₂, are synthesized, and their crystal structures are determined by X-ray diffraction. In molecules (p-chlorobenzylidene)-(2-pyridineamine) (**2-22**) to (p-nitro-benzylidene)-(2-pyrimidineamine) (**2-25**), there no hydrogen atom at the ortho-position of N-aromatic ring, but in molecule **2-24** (p-dimethylaminobenzylidene-(2-pyridinamine), the twist angle is still large, up to 35.6°, which seems to question the role of the steric hindrance in distorting molecule. In molecule N-(p-nitrophenyl)-di(p-methoxyphenyl)-ketenimine (**2-32**), the push and pull interaction between the nitro and methoxy groups should enhance the CT-2 interaction between the nitro group and nitrogen lone pair, but its twist angle is only 9.2°. It is so small that the CT-2 role in twisting molecule seems to be questioned. For total electronic energy $E_e(\theta)$ of N-benzylideneaniline (NBA) and 20 NBA-like species, as shown by relaxed PES scan performed using Gaussian 98 package, $d[E_e(\theta)]^2/d^2\theta > 0$; $dE_e(\theta)/d\theta = 0$ when twist angle $\theta = \theta_{\min-e}$, and when $0 < \theta < \theta_{\min-e}$, $dE_e(\theta)/d\theta < 0$, indicating that the electron interaction is a driving force for distorting molecule away from the planar conformation. For nuclear repulsion $E_{N^{PQ}}(\theta)$ between N-aromatic ring (Ar-) and -N=CH-Ar', always $d[E_{N^{PQ}}(\theta)]^2/d^2\theta < 0$, and when distorted angle $\theta = \theta_{\min-N}$, $dE_{N^{PQ}}(\theta)/d\theta = 0$, and when $0 < \theta < \theta_{\min-N}$, $dE_{N^{PQ}}(\theta)/d\theta > 0$, indicating that the nuclear repulsion between the fragments is resistance to the molecular distortion. Exception for the molecules whose ortho-substituents can generate the formation of hydrogen bonds between fragments, the above conclusions are independent of the structure and position of the substituent, and have nothing to do with the theoretical level and with the size of the Gaussian basis set.

yuzh@iccas.ac.cn

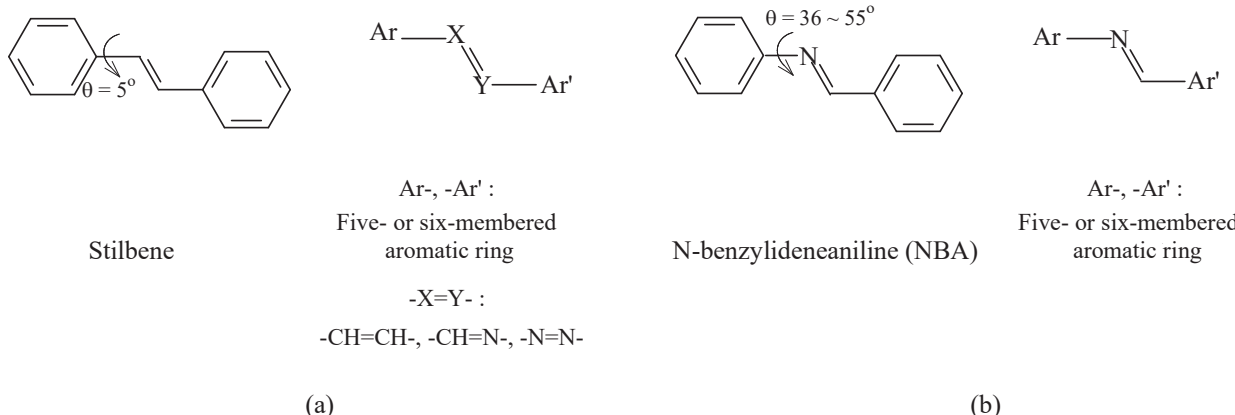
Key words: driving force for distorting molecule; resistance to the molecular distortion; N-benzylideneaniline-like species; substituted triphenylketenimines, large twist angle of NBA.

2.1. INTRODUCTION

From 2-(N,N-methylnaphthyl-amino)acrolein to 2-(N,N-methylnaphthyl-amino)pentadienal, as demonstrated in the first chapter, the changes of the bond length and twist angle are abnormal. This implies that the basic causality, as well as the principle of "conjugation stabilization", is questionable.

In the literature, the challenge to the principle of "conjugation stabilization" can be traced back to Lennard-Jones in 1930s.¹ Since then, the literatures have tried to continue to challenge the principle from both experimental and theoretical aspects. During the period from 1970s to 1980s, the theoretical chemists who questioned the principle of "conjugation stabilization" were undoubtedly Shaik and Epiotis. Shaik said:²⁻⁴ "The delocalized π -electronic component of benzene is unstable toward a localizing distortion", "Therefore, π -bond delocalization must be a byproduct of the constraints applied by the σ -frame which prefers geometries with uniform CC bonds" (By the way, it should be noted that Shaik's "localization" refers to the change in the CC bond lengths, rather than the localization of the molecular orbitals. As the changing of CC bond length, π -electrons are always delocalized. "delocalization" and "localization" are two important concepts. In the following chapters, these two concepts will be strictly defined).

Shaik's viewpoint aroused much controversy.⁵ Epiotis highly and positively commented on Shaik's point of view, and he strongly pointed out that the concept of "conjugation stabilization" should be expelled from the literature.⁶ In fact, back in the early 1980s, Epiotis explicitly put forward the idea of "resonance destabilization", and he also pointed out that the $4n+2$ theory has successfully predicted and explained the stability of aromatic molecules, but it overemphasized the role of π -electrons while ignoring the role of σ -electrons.⁷ In the chapter 9, it will be argue that the aromaticity of benzene, including the aromatic energy and CC bond length equalization, results from the minimization of the nuclear repulsion among the carbon atoms.



Scheme 2-1

However, the controversy on "conjugation destabilization" was mainly confined to the realm of theory and was the lack of a large number of experimental evidences. In the study of conjugation effect and molecular conformation, the interpretation and debate on the distortion of stilbene-like species are worth noting. In the crystal structure of N-Benzylideneaniline (NBA),⁸⁻¹³ for example, the twist angle θ between the phenyl ring and the $-\text{N}=\text{CH}-\text{Ph}$ group is 36° to 55° (Scheme 2-1). The molecular conformation with a large twist angle (usually 10° to 80°) is an experimental fact that can't be explained by the classic structural theory of organic chemistry. By studying the relationship between molecular conformation and related structural factors, it is possible to provide the most direct experimental

evidence for questioning the concept of “conjugation stabilization”.

In this monograph, there are three steps to question the fundamental principles of organic chemistry. In this chapter, as the first step, the theoretical calculations will be performed using Gaussian 98 package, and will lead to the following conclusions:

- (i) Electron interaction is the driving force of molecular distortion.
- (ii) Steric hindrance between the groups is actually resistance to the molecular distortion.
- (iii) A crowded geometry may be energetically preferential.

2.1.1. Large Distorted Stilbene -like Species

In this section, the literatures, about the research and debate on the phenomenon of abnormally large twist angles in the stilbene-like species, will be briefly reviewed in order to argue that the classical theory of organic chemistry can't fully explain this phenomenon. This logically illustrates why we inevitably need to synthesize 8 substituted stilbene-like species and 4 substituted triphenyl ketenimines and to determine their x-ray crystal structures.¹⁴⁻¹⁹

Stilbene-like species refers to stilbene and its iso-electron compounds ($\text{Ar}-\text{X}=\text{Y}-\text{Ar}'$) and related substituted derivatives (Scheme 2-1a), where the groups, $\text{Ar}-$ and $\text{Ar}'-$, are the five- or six-membered aromatic ring such as phenyl, pyridinyl, pyrimidinyl, furyl, et al.; the bridge group $-\text{X}=\text{Y}-$ includes $-\text{CH}=\text{CH}-$, $-\text{N}=\text{CH}-$, $-\text{N}=\text{N}-$. When the bridge group is $-\text{N}=\text{CH}-$, stilbene-like species is called NBA-like (N-benzylideneaniline-like) species (Scheme 2-1b).

N-benzylideneaniline has been used in the fields of polymer material,²⁰⁻²⁴ host-guest complex,²⁵ liquid crystals,²⁶⁻²⁸ nonlinear optics,^{29,30} and medicine³¹. In the meantime, its molecular structure has attracted considerable attention and were widely studied. At an early stage of the studies, Wiegand (1942), Izmailskii (1956), Jaffe (1958) and Ebara (1960 and 1961) found that there is the difference, in UV (ultraviolet) spectrum, between N-benzylideneaniline and its isoelectronic molecules stilbene (STB) and azo-benzene (ABZ).³²⁻³⁶ Stilbene and azobenzene show an intense absorption maximum at $300 \sim 320$ nm. But N-benzylideneaniline shows an intense band at 263 nm, and this absorption band is likely to come from the styrene-type part ($\text{Ph}-\text{CH}=\text{N}-$). This significant difference in the UV absorption wavelength can't be explained by the planar structure of N-benzylideneaniline, which promoted the experimental and theoretical researches, including electronic spectroscopy,³⁷⁻⁴² photoelectron spectroscopy,^{40,43} nuclear magnetic resonance (NMR),⁴⁴⁻⁵⁵ Mass spectroscopy (MS),⁵⁶ infrared (IR),⁵⁷⁻⁶⁰ gas electron diffraction,^{12,61-65} X-ray diffraction,⁶⁶⁻⁷¹ circular dichroism,⁷² and theoretical calculation⁷³⁻⁸⁵. Since then, the significant differences in UV spectra and the abnormally distorted conformation of N-benzylideneaniline have been a hot topic of research and debate.

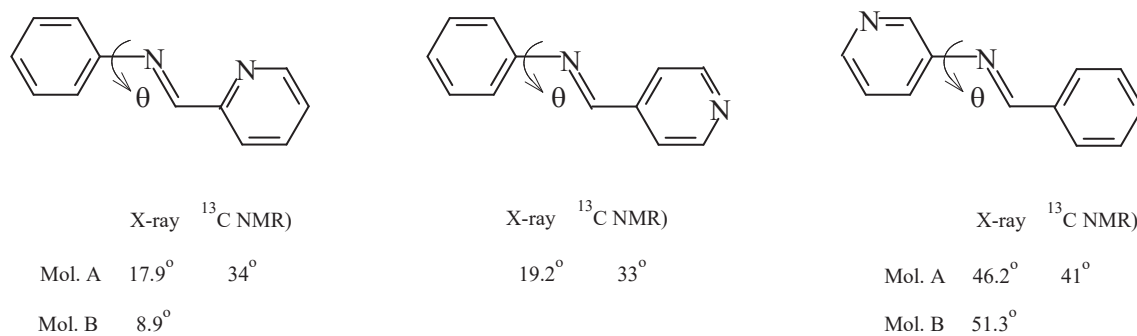


Figure 2-1. For three molecules, the twist angles θ determined by the X-ray diffraction and ^{13}C NMR.

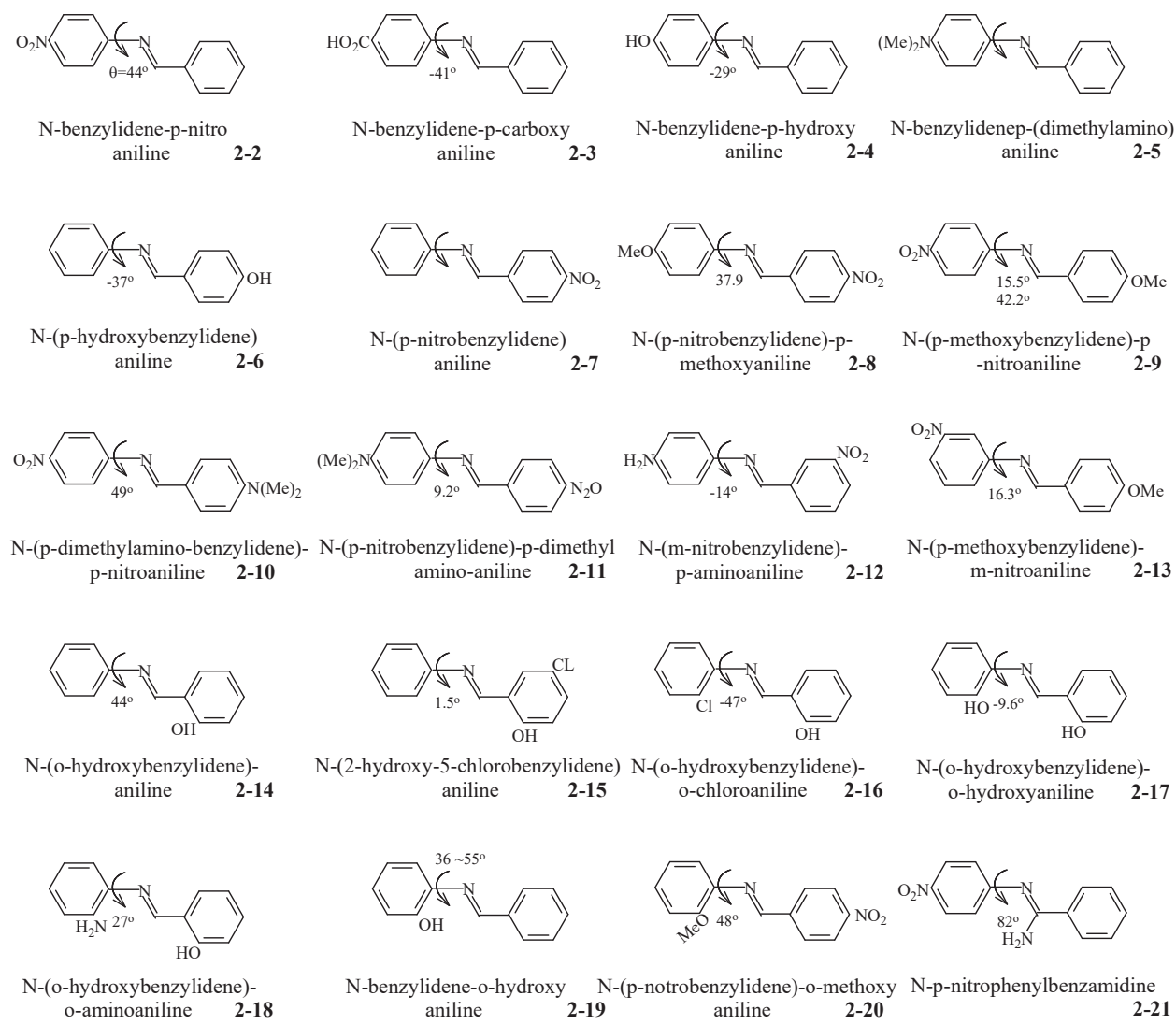
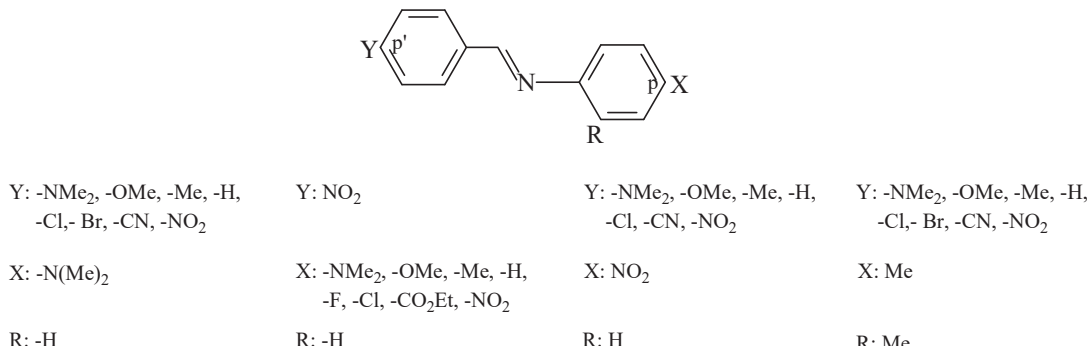


Figure 2-2. For 20 substituted derivatives of N-benzylideneaniline (NBA), and the experimental values of the twist angle θ .

The difference, in UV spectra, between the three molecules seems to be well explained by the conformation difference. In the solid and solution states, the conformation of stilbene and azobenzene is almost planar, the twist angle θ is 5° (x-ray)⁶⁶ and 17° (liquid crystal NMR)⁵² for stilbene; 17° (x-ray)⁶⁷ and planar (¹H NMR)⁵³ for azobenzene. But the conformation of N-benzylideneaniline is non-planar, and its twist angle is roughly the same in the solid (55.2° ,^{9,10} 52.6° and 56.2° ,¹³) gas (36° ,¹¹ 52° ,¹² and 48° ,⁴⁰) and solution state ($30\text{--}35^\circ$,³⁹ and $33\text{--}59^\circ$,⁴⁵).

The phenomenon that there is no obvious difference, in the molecular conformation, between solid, gas and solution states is not common for NBA-like species. For diazastilbenes, such as N-(2-pyridylmethylene)aniline, N-(4-pyridylmethylene)aniline and N-benzylidene-3-pyridinamine (Figure 2-1), for example, their twist angles θ in solution (1982)⁴⁴ are significantly different from in the solid state (1982)⁶⁹. In fact, as Bernstein pointed out in 1978, for this type of flexible molecule, the phenomenon that the conformation in the solid state is not identical with that in solution was found before 1978.⁸⁶⁻⁸⁹ According to such conformation difference and conformational polymorphism, Bernstein (1978),⁷³ Wiebcke and Mootz (1982),⁶⁹ and Ahmet and Silver (1994)⁹⁰ suggested that the crystal force decisively determines the molecular conformation.

It has been estimated that for a carbon-carbon chain, a typical bond stretching of 0.1 Å requires about 15 KJ/mol, a bond-angle deformation of 10°, about 5 KJ/mol, and a distortion of 15°, about 1 KJ/mol. Therefore, as believed by Kitaigoroksdii,⁹¹ the crystal force can't change the bond length and bond angle of organic molecules, but it can cause a group to rotate about a single bond, resulting in a conformation that favors close packing of molecules.



Scheme 2-2

For substituted NBAs, as shown by the values of the twist angle θ in Figure 2-2,⁹²⁻¹⁰⁵ the molecular distortion is a common phenomenon in the crystal structure. It is noteworthy that the type, quantity and position of substituent have a great effect on the twist angle θ . Substituent effects can be roughly summarized as follows:

- (i) As long as an electron-withdrawing group, such as $-\text{COOH}$ and $-\text{NO}_2$, is located at para-position of N-phenyl ring, the twist angle θ is usually within $30^\circ \sim 50^\circ$;
- (ii) When an electron-releasing group, such as MeO- and $(\text{Me})_2\text{N-}$, is located at para-position of N-phenyl ring, the conformation is almost planar, the twist angle θ is about 10° .

In N-(p-dimethylaminobenzylidene)-(p-nitro)aniline (**2-10**)^{71,96}, for example, a nitro group is at para-position of N-phenyl ring, and the twist angle θ is 41.5° to 49° ,⁹⁶ which depends upon the crystallization conditions and polymorphic modifications (for the 5 conformations of molecule **2-10**, the average value of the twist angles is 44.6°). When a dimethylamino group is at para-position of N-phenyl ring, as in N-(p-nitrobenzylidene)-(p-dimethyl)aniline (**2-11**), the twist angle θ is only 9° .⁷¹

In Organic Chemistry, substituent effect belongs to the intra-molecular interaction, and it is via the conjugation effect and inductive effect to influence the conformation and properties of molecule. For the four series of substituted NBAs presented in Scheme 2-2, Akaba and Hirochika (1985)⁴⁵ examined the influence of the interaction between the p-(the para-position of aniline ring) and p'-substituents (p':- the para-position of N-benzylidene group) on the ¹³C chemical shifts of azomethine ($-\text{N}=\text{CH}-$) group, and found that the effects of the p- and p'-substituents on the azomethine carbon chemical shifts are not additive and the direction (down- and up-field) and degree of deviation $\Delta\delta$ from additivity depend upon the electron-withdrawing and electron-releasing ability of the substituents. However, the effect of this type of the interaction on the conformation of a molecule was only based on the molecular conformations (twist angles) reported in the literature. For N-(p'-nitro-benzylidene)(p-nitro)aniline, for example, the interaction between p- and p'-nitro groups causes a slight deviation from the additivity ($\Delta\delta = -0.12$ ppm). For N-(p'-nitro-benzylidene)aniline, thus, the substitution of its p'-hydrogen atom by a nitro group can't obviously change its conformation. In N-(p'-nitro-benzylidene)(p-dimethylamino)aniline (**2-11**), on the contrary, the interaction between the p-dimethylamino and p'-nitro causes a large upfield deviation from additivity ($\Delta\delta = 1.47$ ppm), which corresponds to the change from the mother molecule's (N-(p'-nitrobenzylidene)aniline) conformation

with a large twist angle to the planar conformation (twist angle $\theta = 9.2^\circ$) of molecule **2-11**.

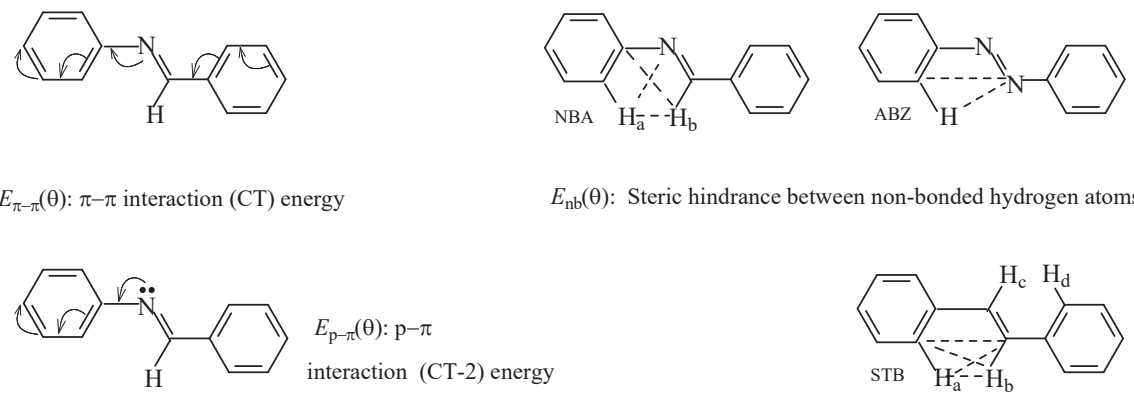
Besides NMR, the UV spectra, the gas electron diffraction, the photoelectron spectra and theoretical calculation have also agreed to exclude the decisive role of the lattice force in determining molecular conformation.

2.1.2. Classic Model and Interpretations

Based on the fundamental principles of organic chemistry and according to HMO (Hückel molecular orbital) calculations, Bürgi and Dunitz designed a simple model (1971) to examine the effects of the interaction energies, ΔE_π , $\Delta E_{p\pi}$, ΔE_{nb} and ΔE_t , on molecular conformation.¹⁰ In the case of N-benzylideneaniline, as concluded by Bürgi and Dunitz, due to the steric hindrance between the non-bonded atoms (Scheme 2-3), the molecule has a tendency to deviate from its planar conformation. Once the deviation from the molecular plane, under the help of p- π interaction, the non-bonded interaction can overcome the resistance arising from π - π interaction and distorts molecule until $\theta = \theta_{min}$. For stilbene, on the contrary, without the help of p- π interaction, the large non-bond interaction alone is not enough to overcome the resistance generated by π - π interaction. For azobenzene, without the non-bonded hydrogen atoms, there is no longer a driving force of distortion. As a result, the twist angle for stilbene and azobenzene is small and is only 5° (Scheme 2-1). Bürgi's interpretation is completely in line with the fundamental principles of organic chemistry and with the basic causal relationship between the conformation and the conjugation effect.

By ab initio calculations, Bernstein (1981) also reached a similar conclusion,⁷⁵ and he concluded that "the most stable conformation of N-benzylideneaniline has been attributed to a compromise between steric interactions and delocalization of the bridge double bond and/or nitrogen lone pair electrons into the conjugated system."

Definitions for $E_\pi(\theta)$ and $E_{nb}(\theta)$



Scheme 2-3

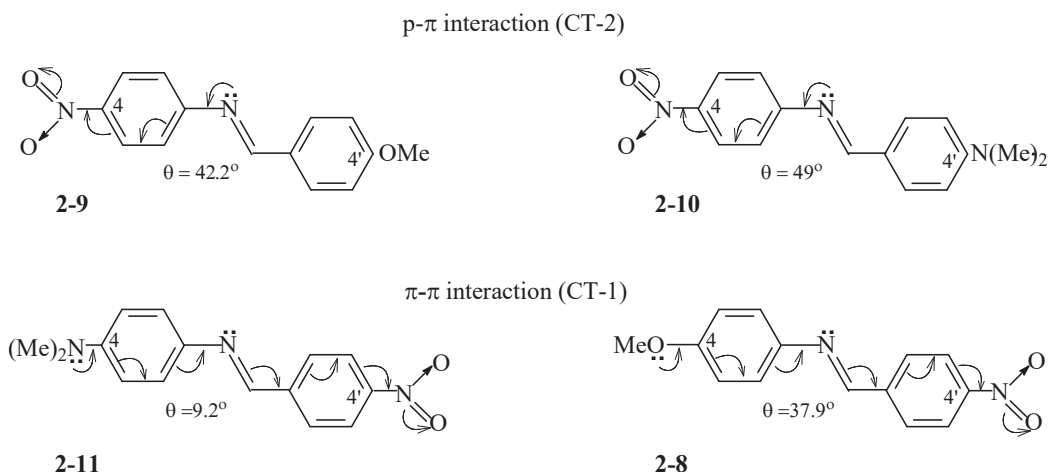
The molecular conformation in the solid state, determined by X-ray diffraction, is related to their environment.⁹⁰ In order to understand the conformation of a free molecule, Traetteberg used gas electron diffraction to determine the conformation of azobenzene (1961)⁶¹, N-benzylideneaniline (1978)¹² and stilbene (1975),⁶² and found that in the gas phase, the twist angle of stilbene and azobenzene is about 30° (their twist angle in the solid is, respectively, 5° and 15°) and that of N-benzylideneaniline is 52° . Traetteberg attributed the non-planarity of gaseous stilbene to the steric hindrance between the two non-bonded hydrogen atoms according to that the average of the distances, between the H_a and H_b and between H_c and H_d , is equal to 2.40 \AA (Scheme 2-3) and is equal to the sum of Van der Waal's radius (1.2 \AA) of hydrogen atom.

For azobenzene, Traetteberg thought that the non-bonded interaction in azobenzene is considerably smaller than in stilbene. Therefore, he attributed the non-planarity of azobenzene to the p- π interaction.

2.1.3. Substituent Effect

The substituent effect is an important effect in organic chemistry, and it includes the π - π and p-p interactions between the conjugated groups, and it also includes the steric hindrance and hydrogen bond between the non-bonded groups. The conjugation interaction between the substituents can be transmitted through the conjugated system between the conjugated groups, and it may also be transmitted through space interaction.

2.1.3.1. Nakai's Interpretation



Scheme 2-4

By measuring the crystal structure of N-(p'-(dimethylamino)benzylidene)-(p-nitro)aniline (**2-10**) and N-(p'-nitrobenzylidene)-(p-dimethylamino)aniline (**2-11**), Nakai found (1976) that the interaction between p- and p'-substituents has a great influence on the molecular conformation.⁷¹ In molecule **2-11**, the nitrogen lone-pair of the electron-releasing group $-\text{N}(\text{Me})_2$ can be transferred, through the entire molecular framework, to the electron-withdrawing group $-\text{NO}_2$ (CT-1 effect) (Scheme 2-4). In the planar conformation, the CT-1 effect is the strongest, so the twist angle θ of molecule **2-11** is small, only 9.2° . In molecule **2-10**, the substituent $-\text{NO}_2$, at the para-position of the N-phenyl group, is a strong electron-withdrawing group. It is possible for the nitrogen lone-pair of the bridge double bond to be transferred, through the N-phenyl ring, to the nitro group (CT-2 interaction in Scheme 2-4). With the increasing of the twist angle θ , the stabilizing energy effect of the CT-2 interaction increases. Therefore, the twist angle θ in molecule **2-10** is larger than in **2-11**, and is approximately 49° .

However, it is not difficult to find the experimental results that are contrary to the Nakai's interpretation. In the solid state of N-(p'-nitro-benzylidene)-(p-methoxy)aniline (**2-8**), for example, the twist angle θ is 37.9° ,⁹⁴ 36° ,¹³ although the MeO- group, as an electron-releasing group, is at para-position of N-phenyl ring, and it is almost equal to that (42.2°)⁹⁵ of N-(p'-methoxybenzylidene)-(p-nitro)aniline (**2-9**) (Scheme 2-4).

It should be Bürgi and Dunitz who first studied the influence of the substituent-substituent interaction on the molecular conformation. In 1971, Bürgi and Dunitz determined the crystal structure of N-benzylideneaniline (**2-1**), N-(p'-methylbenzylidene)-(p-nitro)aniline (MBNA), and N-benzylidene-(p-carboxy)aniline (**2-3**).¹⁰ According to the Nakai's interpretation, the twist angle θ of the molecules MBNA and **2-3** should be greater than that of N-benzylideneaniline. In fact, their experiments gave the following size orders of the twist angle θ :

$$55.2^\circ (\mathbf{2-1}) > 50.2^\circ (\text{MBNA})$$

55.2° (**2-1**) $> 41.1^\circ$ (**2-3**).

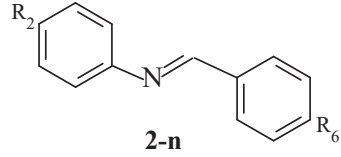
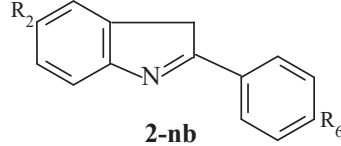
In the case of the optimized geometries at B3LYP/6-311G** level, as shown by the following twist angles,

42.5° (**2-1**) $\approx 45.3^\circ$ (**2-3**)

42.5° (**2-1**) $\approx 45.1^\circ$ (**2-10**)

The p-nitro and p-carboxy groups have a slight effect on the conformation of molecule (**2-1**). At least, the effect is not as big as Nakai thought.

2.1.3.2. Skraba's Experiments

	First group		Second group	
	R2 = H, 2-1: 262	R6 = H 2-1b: 305 nm	R2 = N(Me) ₂ , 2-5: 374	R6 = H 2-5b: 372 nm
	R2 = NO ₂ , 2-2: 295	R6 = H 2-2b: 335 nm	R2 = H, ABAN 342	R6 = N(Me) ₂ 350 nm
	R2 = H, 2-7: 288	R6 = NO ₂ 2-7b: 340, 357 nm	R2 = NO ₂ , 2-10: 382	R6 = N(Me) ₂ 2-10b: 409 nm
			R2 = N(Me) ₂ , 2-11: 438	R6 = NO ₂ 2-11b: 447 nm

Scheme 2-5

To investigate the interaction between the p- and p'-substituents, various methods, such as the UV,^{37,42} ¹³C NMR,⁴⁵ and PES (photoelectronic spectroscopy),⁴⁰ were used. Among these methods, the Skraba's method should be mentioned. In 1975, a year before Nakai's experiments, Skraba et al.³⁷ synthesized nitro- and dimethylamino-substituted NBAs (**2-n**) and the corresponding substituted 3H-indoles (**2-nb**). For 3H-indole and its substituted derivatives, the 3H-indole group is rigid, and the whole molecule is considered planar. According to the UV spectrums reported by Skraba, the seven molecules can be divided in to two groups. The first group includes two nitro-substituted NBAs (**2-2** and **2-7**) (Scheme 2-5). According to the UV spectrums reported by Skraba, the characteristic of these two molecules are as follows:

- (i) The UV absorption wavelength $\Delta\lambda$ between a pair of the molecules **2-n** ($n = 2, 7$) and **2-1** is close to or less than that $\Delta\lambda$ between the corresponding pair of the molecules **2-nb** ($n = 2, 7$) and **2-1b**, and is much smaller than that between the molecule **2-1** and the molecules **2-n** ($n = 5, 10, 11$) belonging to the second group.
- (ii) The difference $\Delta\lambda$ between a pair of the molecules **2-n** ($n = 2, 7$) and **2-nb** is approximately equal to or larger than that $\Delta\lambda$ between a pair of the molecules **2-1** and **2-1b**, and is much larger than that between the pairs of the molecules **2-nb** and **2-n** ($n = 5, 10, 11$) belonging to the second group.

Accordingly, the conformation of the molecules (**2-2** and **2-7**) belonging to the first group must be nonplanar. However, the difference $\Delta\lambda$ between these two nitro-substituted NBAs (**2-2** and **2-7**) is only 7nm. For the mono-nitro substituted NBAs, the effect of the position (p- or p') of the nitro group on the UV absorption wavelength of the parent molecule NBA is very small. In molecule **2-2**, the p-nitro group can help the CT-2 interaction according

to the Bürgi's Model, but why the difference $\Delta\lambda$ (40 nm) between the molecules **2-2** and **2-2b** is less than that (52 nm) between the molecules **2-7** and **2-7b**.

The second group includes molecules **2-5**, (p'-dimethylamino)benzylideneaniline (ABAN), **2-10** and **2-11**. According to Scheme 2-5, as long as there is an electron-releasing group $-N(Me)_2$ in the substituted NBA, the UV spectrum of a substituted NBA is very similar or virtually identical to that of its corresponding substituted 3H-indole, regardless of whether this electron-releasing group is at the p-position or at the p'-position. Unlike the nitro-substituted compounds, the position of the amino group has a great influence on the UV absorption wavelength. For example, the UV absorption wavelength of p-N(Me)₂ substituted NBA (**2-5**) is 374 nm, but that of p'-N(Me)₂ substituted NBA (ABAN) is 342, their difference is 32 nm. No matter how Skraba interpreted the UV spectra of the substituted NBAs, the effect of p- π (CT-2) interaction on the conformation should not be as important as Nakai believed according to the UV spectrums.

Based on the comparison of UV spectrums, the difference $\Delta\lambda$ (87 nm) between the molecules **2-2** and **2-10**, as well as the difference (40 nm) between the molecules ABAN and **2-10**, should be attributed to the π - π interaction between the p-nitro and p'-N(Me)₂ in molecule **2-10**. But the twist angle of molecule **2-10** is still large, up to 49°.

2.2. EXPERIMENTAL QUESTIONING

In the literature, as mentioned above, all explanations for the large twist angle phenomenon are based on the classical theory of organic chemistry. Therefore, questioning the explanations in the literature is equivalent to questioning the fundamental principles of organic chemistry. We do not expect that the substituent effect, found in each crystal structure, is consistent with our viewpoint. However, as long as we can find that the twist angle of a certain compound molecule does not conform to the interpretation of classical theory, we can achieve our goal of questioning classical theory. Of course, in the following chapters, we will establish our new calculation methods and proposed our theories. Our theory should not only be able to explain what the classical theory can explain, but should also be able to explain what the classical theory can't explain.

In 1990's, NBA-like species with a six- (**2-22** to **2-25**) or five-membered (**2-26** ~ **2-28**) heterocyclic ring, as well as substituted ketenimines (**2-30** to **2-33**),¹⁴⁻¹⁹ were synthesized in our research group, and their crystal structures were determined (Scheme 2-6).^{14,16,17} In that time, however, the geometry optimizations of these molecules were performed at the AM1 level of theory.¹⁴ In this chapter, the geometry optimizations are performed again at the B3LYP and MP2 levels of theory.

As indicated in the literature⁹¹ and will be confirmed in this section, the influence of the distortion on the molecular energy is very small, so the discussion on structural effect is, practically, not much sense although it will be mentioned. It is the most important to study the changes, in the nuclear repulsion $E_{N^{PQ}}(\theta)$ and total electron energy $E_e(\theta)$, with the increasing of the twist angle θ , where $E_{N^{PQ}}$ is the nuclear repulsion (steric hindrance) between the fragments P (Ar-N-) and Q (-N=C-Ar'). The space interaction between two non-bonded hydrogen atoms can be considered as a part of steric hindrance between the two fragments P and Q.

2.2.1. Questioning Role of Non-bonded Interaction

On the basis of the crystal structures, 4 molecules, **2-22** to **2-25**, are optimized at B3LYP and MP2 levels of theory. According to Scheme 2-6, the values of the twist angle, obtained from the B3LYP optimization, are usually much smaller than from the MP2/6-31G* optimization, and the basis set size has a slight effect on the twist angle θ at B3LYP level. For a specific molecule, the theoretical values of the twist angle θ are also different from the experimental value determined by X-ray diffraction. For N-(4-dimethylamino-benzylidene)-2-pyridinamine (**2-24**), for example, the twist angle θ in the crystal structure is 35.6°, the B3LYP/6-31G* and MP2/6-31G* values

	2-22	2-23	2-24	2-25
B3LYP/	θ	θ	θ	θ
6-31G*	3.3	4.9	7.6	25.0
6-311G*	5.1	3.8	11.2	25.8
6-311G**	6.6	4.0	9.6	25.9
6-311G(2df,p)	10.1	5.1	9.7	25.9
MP2/6-31G*	21.9	18.9	24.5	35.3
Crystal	15.6	19.6	35.6	25.9
	2-26	2-27	2-28	2-29
B3LYP/	θ	θ	θ	θ
6-311G**	19.1	7.5	1.5	44.1
MP2/6-31G*	33.3	29.5	-26.1	-49.3
Crystal	8.8	4.8	12.0	52.9
	2-30	2-31	2-32	2-33
R1 = R2 = R3 = H	R1 = NO ₂ , R2 = R3 = H	R1 = NO ₂ , R2 = R3 = MeO	R1 = N(Me) ₂ , R2 = R3 = H	
B3LYP/	θ	θ	θ	0
6-311G**	13.2	22.4	24.1	5.5
MP2/6-31G*	11.0	17.3	22.9	6.7
Crystal	0.5	16.1	9.2	5.6

Scheme 2-6

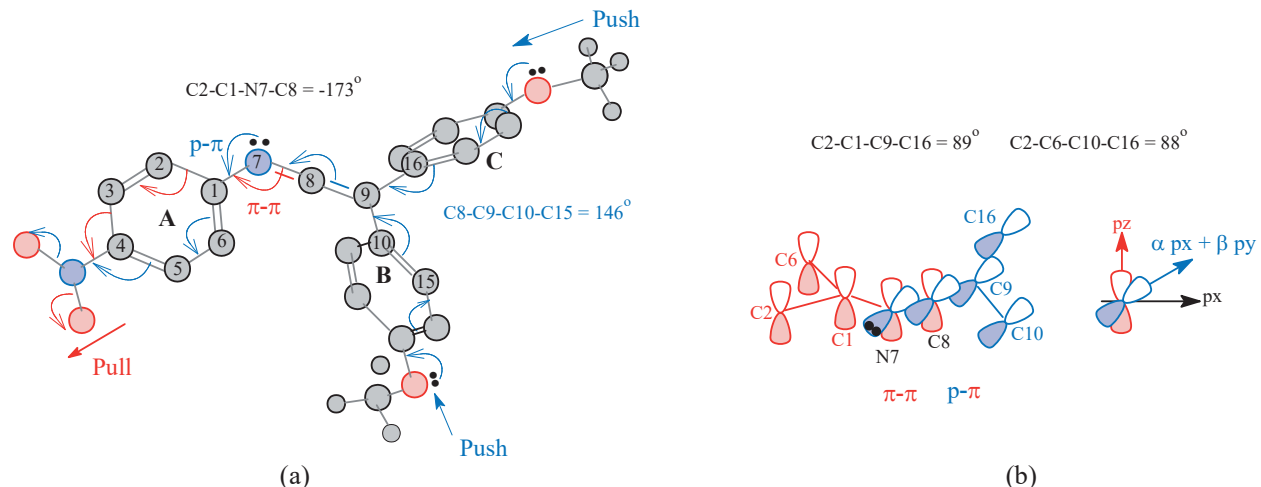
are, respectively, -7.6° and -24.5° . MP2/ 6-31G* value is closer to the experimental value (35.6°) than the B3LYP values. But for N-(4-nitrobenzylidene)-2-pyrimidinamine (**2-25**), the B3LYP/6-31G* values (25.0°) are almost equal to the experimental value (25.9°).

In Molecules **2-22** to **2-25**, N-aromatic group is pyridyl or pyrimidyl ring, there is only one (or no) ortho hydrogen atom (scheme 2-6). In these molecules, therefore, there is no the non-bonded interaction like the interaction between two unbonded hydrogen atoms in NBA. An interesting result is that for N-(4-nitrobenzylidene)-2-pyrimidinamine (**2-25**), the experimental and theoretical values of the twist angle θ are all greater than 25° . In the crystal structures of the four molecules, therefore, the large twist angle, especially the large twist angle of molecules

2-25, should not be attributed to the steric hindrance between the N-aromatic ring and the $-\text{N}=\text{CH-Ar}'$ group.

"The substitution of a CH- group in phenyl ring by a nitrogen atom is equivalent to introducing an electron-withdrawing group $-\text{NO}_2$."¹⁰⁶ Accordingly, the CT-2 interaction in molecule **2-25** should be greater than in molecule **2-23**. This seems able to explain the fact that the experimental and theoretical values of the twist angle θ for molecule **2-25** is greater than those for molecule **2-23**. However, it still can't explain why the experimental value of the twist angle (35.6°) of N-(4-dimethylamino-benzylidene)-(2-pyridin)amine (**2-24**) is greater than those (19.6° and 25.9°) of molecules **2-23** and **2-25**.

2.2.2. Questioning CT-2 Interaction Role.



Scheme 2-7

To further study the influence of the CT-2 interaction on molecular conformation, we synthesized and prepared four ketenimine compounds, and determined their crystal structures.

According to the two dihedral angles $\text{C}(2)\text{-C}(6)\text{-C}(10)\text{-C}(16) = 88^\circ$, $\text{C}(2)\text{-C}(1)\text{-C}(9)\text{-C}(16) = 89^\circ$ in the crystal structure of molecule **2-32**, as shown by Scheme 2-7b, the structure characteristics of the ketenimine bridge ($-\text{N}(7)=\text{C}(8)=\text{C}(9)-$) are as follows:

- (i) the bond angle $\angle \text{N}(7)\text{C}(8)\text{C}(9)$ is 171 to 175° ;
- (ii) the two planes, denoted as $\text{C}(2)\text{-C}(1)\text{-C}(6)$ and $\text{C}(9)\text{-C}(10)\text{-C}(16)$, are approximately perpendicular to each other.

In the ketenimine bridge $\text{N}(7)=\text{C}(8)=\text{C}(9)$, therefore, there are two mutually perpendicular π systems: $\text{N}(7)\text{-C}(8)=\text{C}(9)$ and $\text{N}(7)=\text{C}(8)$ (Scheme 2-7b). The first π system is composed of the blue p atomic orbitals of the $\text{N}(7)$, $\text{C}(8)$ and $\text{C}(9)$ atoms, and it results from the p- π conjugation between the π system of the $\text{C}(8)=\text{C}(9)$ double bond and the nitrogen lone pair of $\text{N}(7)$ atom. The blue π system is on the horizontal plane, i.e. the $\text{N}(7)\text{-C}(8)=\text{C}(9)$ plane (due to the bond angle $\text{N}(7)\text{-C}(8)=\text{C}(9) < 180^\circ$), and it can be conjugated with the π systems of two phenyl rings bonded to the $\text{C}(9)$ atom due to $\text{C}(8)\text{-C}(9)\text{-C}(10)\text{-C}(15) = 146^\circ$. This π system can also be conjugated with the π system of the N-phenyl ring when $\theta > 0^\circ$, which is so called "p- π (CT-2) interaction". The second π system is composed of the red atomic orbitals, and it belongs to the $\text{N}(7)=\text{C}(8)$ double bond. The red π system is perpendicular to the $\text{N}(7)\text{-C}(8)\text{-C}(9)$ plane, and it can be conjugated only with the π system of the N-phenyl ring.

In N-(p-nitrophenyl)-di(p-methoxyphenyl)-ketenimine (**2-32**), there is a -OMe group at the para-position of the ring-B and ring-C, and a -NO_2 group is at the para-position of the ring-A. The methoxy group is an electron-releasing group, and the oxygen lone pair should have an ability to push the nitrogen lone-pair into the ring-A, and meanwhile the strong electron-withdrawing group -NO_2 can pull the nitrogen lone-pair into the ring-A. The synergy of the push and pull actions, as indicated by the red and blue curved arrows in Scheme 2-7a, should greatly benefit the CT-2 interaction. So, the twist angle θ of molecule **2-32** should be much greater than that of **2-30** and **2-31**. In fact, as shown by the experimental data in Scheme 2-6, the twist angle θ (9.2°) of **2-32** is smaller than that (16.1°) of **2-31**. At B3LYP/6-31G level, the twist angle for the former molecule is approximately equal to that for the latter. These two facts seem to mean that the CT-2 interaction may not be a driving force, at least is not as important as the literatures suggested.

2.3. THEORETICAL RESEARCHES

Table 2-1. Theoretical Values of Twist Angle θ (Degree).

Mols	SLATER without HF-EX	B3LYP* with HF-EX	BLYP Without HF-EX	MP2 With HF-EX	LYP with HF-EX	RHF Pure HF-EX
2-26	17.1	19.1	12.4	33.3	33.5	38.1
2-27	7.4	7.5	7.3	29.5	31.5	35.8
2-28	1.5	1.5	1.5	-26.1	1.5	12.6
2-29	-41.1	-44.1	-43.8	-49.3	-38.1	

* For B3LYP, HF-EX is a part of EX (exchange). All the calculations are performed at 6-311G** level except for MP2/6-31G*.

The theoretical calculations include the full geometry optimization of the molecules, and the relaxed potential energy surface scan (PES scan). All these calculations are performed by using Gaussian 98 package at various levels of theory.

2.3.1. NBA-like Species with Five-membered Ring

2-thiazolyl group is an electron-withdrawing group,^{107,108} and its ability to withdraw π electrons is greater than a p-nitro-phenyl group.¹⁰⁹ Accordingly, the CT-2 interaction in molecule **2-27** should be greater than in **2-23**. Out of the expectation, the experimental value of the twist angle (19.6°) for molecule **2-23** is greater than that (4.8°) for molecule **2-27**. For molecules **2-26** to **2-28**, particularly, the experimental values of the twist angle, 4.8° to 12° (Scheme 2-6), are so small that it is, practically, not much sense to discuss the influences of the structural factors on the molecular conformation,

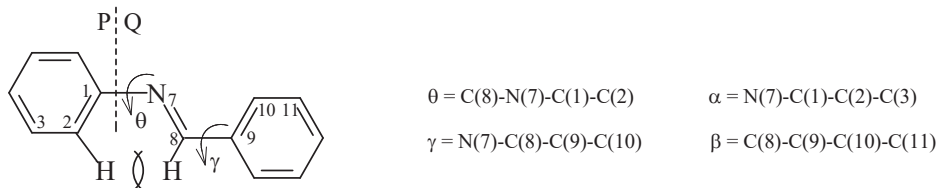
It is worth mentioned that the theoretical value of the twist angle depends upon the level of theory. For molecule **2-26**, for example, the size order of the twist angle θ at 6-311G** level is as follow (Table 2-1):

$$12.4^\circ (\text{BLYP}) < 17.1^\circ (\text{SLATER}) < 19.1^\circ (\text{B3LYP}) < 33.3^\circ (\text{MP2/6-31G}^*) < 33.5^\circ (\text{LYP}) < 38.1^\circ (\text{RHF})$$

According to Table 2-1, the Hartree-Fock exchange term seems to play an important role in determining the twist angle θ . As will be shown in the next section, however, the fact that the value of the twist angle depends on the level of theory is not a critical issue for our questioning. But, the Hartree-Fock exchange term is crucial to the rationality of the calculating π -delocalization energy. This will be discussed in detail in Chapter 8.

2.3.1.1. Relaxed PES Scan

In order to get insight into the driving force and resistance of molecular distortion, it is necessary to study the changes of molecular energy E , total electron energy E_e and nuclear exclusion E_N with the increasing of the twist angle θ , where molecular energy $E = E_e + E_N$. For this reason, the relaxed PES scan is performed using the Gaussian 98 package at the RHF, MP2 and B3LYP levels of theory.



The relaxed PES scan by rotating N-aromatic ring about C(1)–N(7) bond includes two processes. The first process is the sampling of the conformations, and the second one is the conditional optimization of the sampled conformations. For a specific molecule, the conformations are sampled in the following two ways:

- (i) the step size of twist angle θ is 2° within 0° to 12° .
- (ii) the step size of 5° in the region of 12° to 87° .

For a sampled conformation with the twist angle θ° , the molecular energy, total electronic energy, total nuclear repulsion, and the nuclear repulsion between two fragments P and Q are denoted as $E(\theta)$, $E_e(\theta)$, $E_N(\theta)$, and $E_N^{PQ}(\theta)$.

Theoretical optimization and X-ray diffraction have showed that the five- and six-membered aromatic rings in NBA-like species are always not planar. This non-planarity contains two meanings:

- (i) the non-planarity of the aromatic rings (N-Ar and C-Ar') themselves.
- (ii) the N(7) atom is not coplanar with the N-Ar group, and the C(8) atom is not coplanar with the C-Ar' group.

Therefore, each sampled conformation should be conditionally optimized using two different (or one in two) procedures in order to ensure that the π - σ energy partition is feasible. In the first procedure, the restricted conditions for optimizing the conformations of a molecule are as follows:

- (i) All the dihedral angles, except for two twist angles θ and γ , are set equal to 180° or 0° .
- (ii) All the dihedral angles, except for the twist angle γ , are kept unchanged during the geometry optimization.

In the optimized geometry of a sampled conformation, the conditions can ensure:

- (i) Two aromatic rings and the bridge group are planar.
- (ii) The N(7) atom and N-aromatic ring are coplanar.
- (iii) The C(8) atom and C-aromatic ring are coplanar.

This procedure is, hereafter, abbreviated as the SCP (sampled conformation with the two planar aromatic groups) procedure. Each sampled conformation can also be optimized under the following restrictions:

- (i) all the dihedral angles, except for four dihedral angles θ , γ , α and β , are set equal to 180° or 0° .
- (ii) all the dihedral angles, except for the three dihedral angles γ , α and β , are kept unchanged in the process of

the geometry optimization.

In this case, the structure features of the optimized geometry of a sampled conformation are as follows:

- (i) Two aromatic rings and the bridge group are planar.
- (ii) N(7) atom and N-aromatic ring are usually not coplanar.
- (iii) C(8) atom and C-aromatic ring are usually not coplanar.

This procedure is, hereafter, abbreviated as the SCNP (sampled conformation with the two nonplanar groups N-Ar and C-Ar) procedure.

For molecule itself, there are also two corresponding methods of restrictedly optimizing geometry. They are, respectively, called the MP (an optimized molecule with the two planar aromatic groups Ar-N and C-Ar) and MNP (an optimized molecule with the two non-planar groups Ar-N and C-Ar) methods.

For the purpose of geometric optimization, the MP and MNP methods are similar to the corresponding SCP and SCNP procedures. The difference is that the former method optimizes the molecule itself, and the latter method optimizes a specific distorted conformation of the molecule. The twist angle θ , obtained from the MP and MNP methods, is respectively denoted as $\theta_{\text{opt-p}}$ and $\theta_{\text{opt-np}}$.

2.3.1.2. Insight into Driving Force and Resistance.

$\Delta E(\theta) = E(\theta) - E(0^\circ)$ is the molecular energy difference between the conformation with twist angle θ and the $\theta = 0^\circ$ conformation, where, for example, $E(0^\circ)$ is the molecular energy of the $\theta = 0^\circ$ conformation. The phrase “the molecular energy difference $\Delta E(\theta)$ between the two sampled conformations” will be shortened to “molecular energy difference $\Delta E(\theta)$ ”, hereafter. Figure 2-3 shows the change of $\Delta E(\theta)$ with the increasing of the twist angle θ at the RHF, MP2, B3LYP and AM1 levels of theory.

The molecular energy differences $\Delta E(\theta)$ can be locally fitted as the following second order (or third order) polynomial function of twist angle θ :

$$\begin{aligned}\Delta E(\theta) &= a + b * \theta + c * \theta^2. \\ d\Delta E(\theta)/d\theta &= 0 \text{ when } \theta = \theta_{\min}, \\ \theta_{\min} &= -b/2c.\end{aligned}$$

The twist angle θ_{\min} is close to the twist angle $\theta_{\text{opt-p}}$ (or $\theta_{\text{opt-np}}$). For molecule 2-26, for example, the values of the twist angle θ_{\min} at 6-311G** level are as follows (Table 2-2):

37.5° (RHF, SCNP), 11.8° (B3LYP, SCNP), 11.5° (B3LYP, SCP), 31.0° (MP2/6-31G**, SCP).

The difference, $(\theta_{\text{opt-np}} - \theta_{\min})$ or $(\theta_{\text{opt-p}} - \theta_{\min})$ at 6-311G** level, is:

0.9° (RHF, SCNP), -3.5° (B3LYP, SCNP), -3.1° (B3LYP, SCP), 1.4° (MP2/6-31G**, SCP).

Therefore, it is reasonable that the relaxed PES scan is used to get insight into the driving force and resistance of molecular distortion.

In addition, the molecular energy difference, $\Delta E(\theta_{\min}) = E(\theta_{\min}) - E(0^\circ)$, is small. For molecule 2-26, for example, the molecular energy difference $\Delta E(\theta_{\min})$ is only 0.4 kcal/mol at the MP2/6-31G** level although the corresponding difference ($\theta_{\min} - 0^\circ$) of the twist angle is large up to 31°.

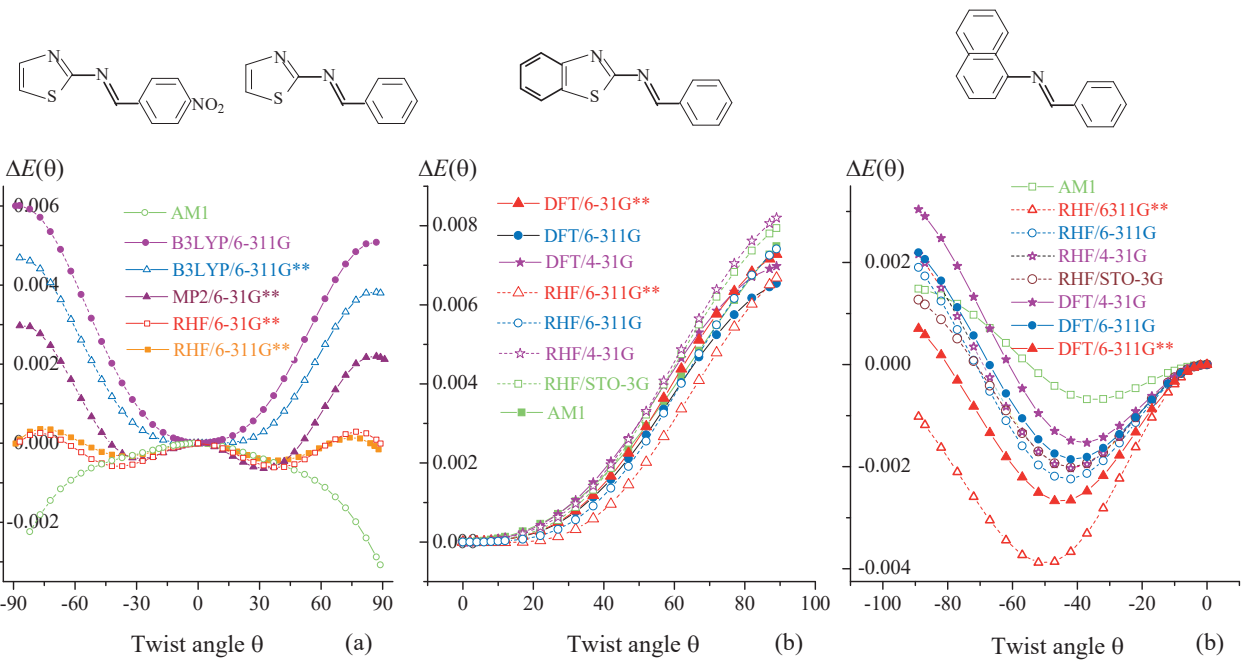


Figure 2-3. Molecular energy difference (hartree) $\Delta E(\theta) = E(\theta) - E(0^\circ)$, and it changes as twist angle θ increases.

2.3.1.3. Features of Functions $E_e(\theta)$ and $E_N(\theta)$

In Figure 2-4, the energy differences, $\Delta E_e(\theta)$ and $\Delta E_N(\theta)$, are obtained from the relaxed PES at various levels of theory, and they can be locally fitted as the polynomial function of the twist angle θ . In the different regions of the twist angle, the features of the locally fitted function are different. In Figure 2-4 and other similar figures, on the left side of the Figure, the twist angle value of the molecule 2-27 is negative, which is only necessary for drawing the function diagram, and has nothing to do with the sign of the twist angle value in the actual calculation.

As shown by Figure 2-4 and Table 2-2, always $d^2E_e(\theta)/d\theta^2 > 0$, $d^2E_N(\theta)/d\theta^2 < 0$, and

$$dE_e(\theta)/d\theta = 0 \text{ when } \theta = \theta_{\min-e}, \theta_{\min-e} \neq \theta_{\min}.$$

$$dE_N(\theta)/d\theta = 0 \text{ when } \theta = \theta_{\min-N};$$

$$\theta_{\min-e} = \theta_{\min-N}, \text{ the value of } \theta_{\min-e} \text{ depends up on the theoretical level.}$$

For molecule 2-26 at MP2/6-31G** (Figure 2-4 and Table 2-2), for example, $\theta_{\min} = 31.0^\circ$, $\theta_{\min-e} = 45^\circ$, $\theta_{\min-N} = 45^\circ$

When $0^\circ < \theta < \theta_{\min-e}$

$$dE_e(\theta)/d\theta < 0,$$

$$d^2E_e(\theta)/d\theta^2 = 2c = 0.00212 \text{ hartree}/\text{deg}^2 > 0,$$

$$dE_N(\theta)/d\theta > 0, 0^\circ < \theta < \theta_{\min}$$

$$d^2E_N(\theta)/d\theta^2 = -0.0012 \text{ hartree}/\text{deg}^2 < 0.$$

$$|dE_e(\theta)/d\theta| > dE_N(\theta)/d\theta$$

In the region of $\theta = 0^\circ$ to $\theta = \theta_{\min-e}$, the electronic interaction is a driving force of molecular distortion. Meanwhile, the nuclear repulsion is resistance to the distortion, and the resistance is less than the driving force.

Table 2-2. For Molecule 2-26, First Order Derivatives, $df(\theta)/d\theta = b + 2c*\theta$, of Total Electronic Energy Difference $\Delta E_e(\theta)$, Nuclear Repulsion Difference $\Delta E_N(\theta)$, and Molecular Energy Difference $\Delta E(\theta)$. These Energies Are Locally Fitted as Second-Order Polynomial Function of Twist Angle θ ($\theta_1 < \theta < \theta_2$).

	SCNP Procedure		SCP Procedure		
	RHF/6-311G**	BLYP/6-311G	B3LYP/6-311G**	B3LYP/6-311G**	MP2/6-31G**
Total electronic energy $dE_e(\theta)/d\theta = b + 2c*\theta$					
b	-0.05077	-0.05023	-0.05687	-0.05966	-0.07565
$c*10^4$	7.2175	7.63238	8.56711	7.93016	8.40762
$\theta_{\min-e}$	35.2	32.9	33.2	37.6	44.9
Nuclear repulsion $dE_N(\theta)/d\theta = b + 2c*\theta$					
b	0.05073	0.05023	0.05684	0.05963	0.08088
$c*10^4$	-7.21184	-7.62227	-8.55688	-7.91871	-9.00541
$\theta_{\min-N}$	35.1	32.9	33.2	37.7	44.9
Molecular energy $dE(\theta)/d\theta = b + 2c*\theta$ (or, $= b + 2c*\theta + 3d*\theta^2$)					
$b*10^5$	-4.11364	-0.385539	-2.36428	-3.94406	-10.2972
$c*10^6$	0.548951	1.00972	0.999662	1.30361	1.65876
θ_{\min}	37.5	2.0	11.8	11.5	31.0
$\theta_{\text{opt-p}}$				8.4	32.4
$\theta_{\text{opt-np}}$	38.4		8.3		

Therefore, it is electron interaction to distort the molecule away from its planar conformation.

when $90^\circ > \theta > \theta_{\min-e}$,

$dE_e(\theta)/d\theta > 0$,

$dE_N(\theta)/d\theta < 0$,

$dE_e(\theta)/d\theta > |dE_N(\theta)/d\theta|$,

$dE(\theta)/d\theta > 0$.

In this region, the electronic interaction becomes a resistance of molecular distortion. In the meantime, the nuclear repulsion becomes the driving force, and the resistance is greater than the driving force.

In particular, the features of these functions are independent of the theoretical level, and the values of the twisted angle $\theta_{\min-e}$, obtained from the relaxation PES scans at various theoretical levels, are not obviously different, although the value of the twisted angle θ_{\min} depends on the theoretical level. For molecule 2-26, for example, the values of the twist angle $\theta_{\min-e}$ are:

35.2 (RHF/6-311G**, SCNP), 32.9 (BLYP/6-311G, SCNP), 33.2 (B3LYP/ 6-311G**, SCNP); 37.6 (B3LYP/6-311G**, SCP), 44.9 (MP2/6-31G**, SCP).

The range of a set of the values of $\theta_{\min-e}$ is 12° and is much smaller than the range (35.2°) of a set of θ_{\min} . Therefore,

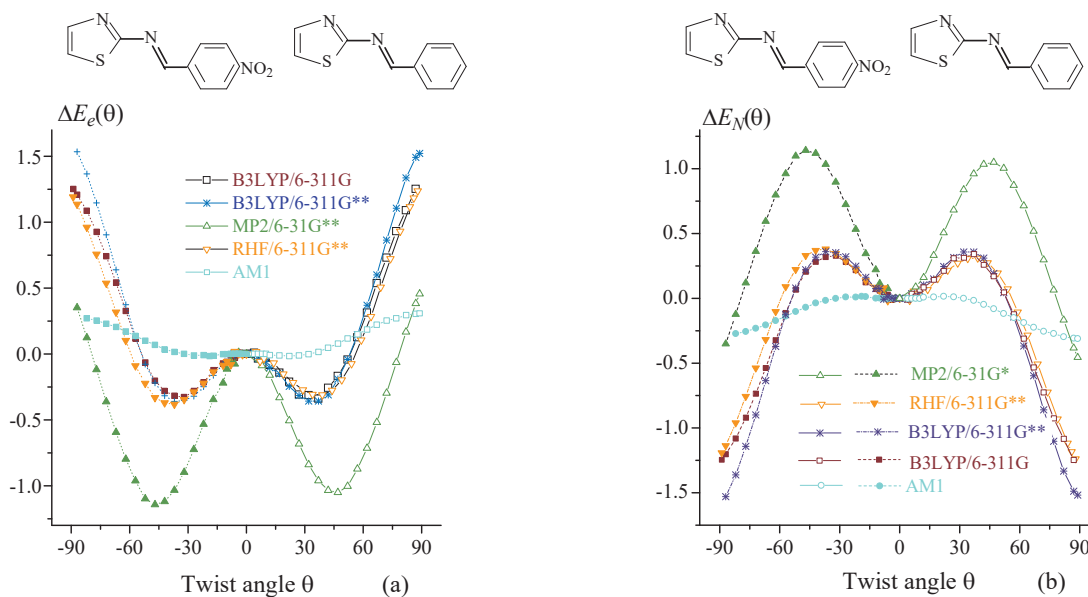


Figure 2-4. For molecules **2-26** and **2-27**: (a) Total electron energy difference (hartree) $\Delta E_e(\theta) = E_e(\theta) - E_e(0^\circ)$. (b) Nuclear repulsion difference (hartree) $\Delta E_N(\theta) = E_N(\theta) - E_N(0^\circ)$, and they change as twist angle θ increases.

the following conclusion can be obtained:

- (i) Electronic interaction is a driving force of molecular distortion, and the nuclear repulsion is a resistance to the distortion.
- (ii) A crowded conformation is energetic preferential.

2.3.2. Substituted N-benzylideneanilines

To further confirm the generality of the conclusions on driving force and resistance of molecular distortion, 21 molecules are selected as typical representatives of NBA-like species, and these compounds refer to N-benzylideneaniline (**2-1**, NBA) and its 20 substituted derivatives **2-2** to **2-21** (Figure 2-2). For each molecule, the geometries of the 20 sampled conformations are optimized using the SCNP procedure.

The molecular energy differences $\Delta E(\theta)$ are locally fitted as the second order polynomial function, $\Delta E(\theta) = a + b * \theta + c * \theta^2$, of the twist angle θ (Figure 2-5a). The coefficients a , b and c , are listed in Table 2-3. As shown by the data in Table 2-3, the twist angle $\theta_{\text{opt}}(\text{RHF})$ of a molecule, obtained from the geometry optimization at RHF/6-311G** level, is generally greater than $\theta_{\text{opt}}(\text{B3LYP})$ obtained from the geometry optimization at B3LYP/6-311G** level. For a specific molecule, which theoretical level is more reasonable seems to be related to the experimental value of its twist angle θ . When $\theta_{\text{exp}} > 30^\circ$, the values of the $\theta_{\text{opt}}(\text{RHF})$ and $\theta_{\text{opt}}(\text{B3LYP})$ both are close to the experimental value. When $\theta_{\text{exp}} < 30^\circ$, $|\theta_{\text{opt}}(\text{B3LYP}) - \theta_{\text{exp}}| < |\theta_{\text{opt}}(\text{RHF}) - \theta_{\text{exp}}|$. For molecule **2-10**, for example, its $\theta_{\text{exp}} = 41.5^\circ > 30^\circ$, the corresponding $\theta_{\text{opt}}(\text{RHF}) = 47.7^\circ$ and $\theta_{\text{opt}}(\text{B3LYP}) = 43.2^\circ$, and these two theoretical values can be considered close to the experimental value. For molecule **2-11** whose $\theta_{\text{exp}} = 9.1^\circ < 30^\circ$, its function curve (red) is at the top of Figure 2-5a, and the absolute value of its $dE(\theta)/d\theta$, $|-0.147 + 0.934*\theta|$, is the smallest of all the data listed in Table 2-3. The curve is so flat that the value of the twist angle is very sensitive to the influence of any structure factor. Therefore, the fact that $|\theta_{\text{opt}}(\text{B3LYP}) - \theta_{\text{exp}}| = 15^\circ < |\theta_{\text{opt}}(\text{RHF}) - \theta_{\text{exp}}| = 25^\circ$ seems mean that at RHF/6-311G** level, the twist angle θ is overestimated.

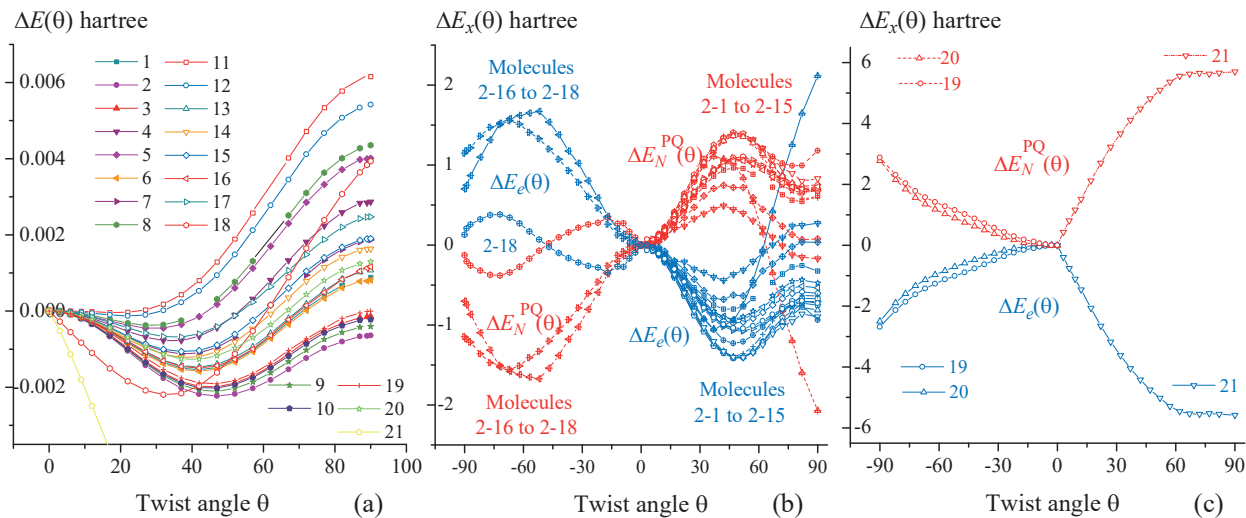


Figure 2-5. For 21 substituted NBA, Energy differences $\Delta E(\theta)$, $\Delta E_e(\theta)$ and $\Delta E_N^{PQ}(\theta)$, and they change as twist angle θ increases at the B3LYP/6-311G** level.

Therefore, the relaxed PES scan will be performed at the B3LYP/6-311G** level.

2.3.2.1. Nuclear Repulsion Between the Fragments.

For molecules **2-26** and **2-27**, as shown by Figure 2-4b, the nuclear repulsion is resistance to molecular distortion. But this nuclear repulsion is the sum of nuclear repulsion between all atoms in the molecule, and it includes the intra- and inter-fragment nuclear repulsions. The intra-molecular steric hindrance should be related to the nuclear repulsion, denoted as E_N^{PQ} , between the fragments P and Q. Therefore, before discussing the resistance and driving force of molecular distortion, the changes of the nuclear repulsions $E_N(\theta)$ and $E_N^{PQ}(\theta)$ with the increasing of the twist angle should be compared.

According to the structure and position of the substituents, together with the characteristics of the total electronic energy function $E_e(\theta)$ (Figure 2-5b and Figure 2-5c), the 21 molecules can be divided into the following four groups (Table 2-3):

- First group, the molecules **2-1** to **2-15**.
- Second group, the molecules **2-16** to **2-18**.
- Third group, the molecules **2-19** to **2-20**.
- Forth group, the molecule **2-21**.

The four molecules **2-1**, **2-16**, **2-19** and **2-21** are the representatives of the four groups. For each representative, the twenty conformations are sampled, and their geometries are optimized using the SCNP procedure at B3LYP/6-311G** level. Then, as shown by the pairs of the curve lines in Figure 2-6, the nuclear repulsion differences, $\Delta E_N(\theta)$ and $\Delta E_N^{PQ}(\theta)$, can be well fitted as the following polynomial functions of the twist angle θ , and the correlation coefficient (cc) is always greater than 0.99: $\Delta E_N(\theta) = a + b*\theta + c*\theta^2 + d*\theta^3$, $\Delta E_N^{PQ}(\theta) = A + B*\theta + C*\theta^2 + D*\theta^3$. For molecule **2-1**, for example,

$$\Delta E_N(\theta) = -0.34463 + 0.04372*\theta - (1.51934E-4)*\theta^2 - (3.31235E-6)*\theta^3$$

$$\Delta E_N^{PQ}(\theta) = -0.37858 + 0.04721*\theta - (2.20709E-4)*\theta^2 - (2.97203E-6)*\theta^3$$

Table 2-3. For 21 Substituted NBAs, Molecular Energy Differences (hartree), $\Delta E(\theta) = E(\theta) - E(0^\circ)$, Are Fitted as $\Delta E(\theta) = a + b * \theta + c * \theta^2$ in Region of $\theta_1 < \theta < \theta_2$. Sampled Conformations Are Optimized Using SCNP Procedure at 6-311G** Level.

Mols	$a * 10^3$	$b * 10^4$	$c * 10^6$	θ_1	θ_2	θ_{opt} RHF	θ_{opt} B3LYP	θ_{\min} B3LYP	θ_{exp}
2-1	2.190	-1.801	2.171	37.00	57.00	-45.43	-42.45	-41.47	-55.2, 52, 36
2-2	2.130	-1.844	1.952	32.00	62.00	47.94	45.08	47.22	
2-3	2.120	-1.815	2.002	27.00	62.00	-47.72	-43.44	-45.31	41.00
2-4	1.270	-1.206	1.773	22.00	42.00	-41.43	-34.35	-34.02	-29.00
2-5	0.988	-0.990	1.695	22.00	37.00	38.43	30.32	29.19	
2-6	2.050	-1.747	2.105	27.00	57.00	-45.54	-40.36	-41.49	-37.00
2-7	1.820	-1.556	2.056	27.00	47.00	43.60	37.88	37.84	
2-8	0.713	-0.784	1.411	17.00	37.00	-38.34	-30.65	-27.77	-37.90
2-9	2.190	-1.867	2.028	27.00	52.00	-47.98	-43.83	-46.02	-42.2, -15.6
2-10	2.180	-1.859	2.057	27.00	57.00	47.68	43.20	45.12	41.5, 49; 50.4, 28.3, 37.1, 43.7, 45.8, 43.1
2-11	0.081	-0.147	0.467	6.00	27.00	34.21	24.17	15.77	9.20
2-12	0.124	-0.218	0.488	9.00	27.00	-36.04	-25.43	-22.32	-14.00
2-13	0.850	-1.030	1.155	12.00	47.00	43.53	40.23	44.58	15.30
2-14	1.430	-1.376	1.793	22.00	47.00	45.17	38.04	38.38	44.00
2-15	0.970	-1.043	1.341	17.00	42.00	44.71	37.18	38.89	1.50
2-16	1.907	-1.664	2.000	27.00	47.00	-48.29	-40.45	-41.60	-47.00
2-17	0.517	-0.645	0.887	12.00	42.00	45.07	35.14	36.36	15.8, -3.9; -9.6
2-18	0.822	-1.836	2.800	17.00	47.00	41.37	32.98	32.79	27.00
2-19	1.990	-1.707	1.875	22.00	67.00	50.44	43.90	47.50	
2-20	1.960	-1.612	2.013	27.00	52.00	-47.85	-39.20	-40.05	-47.00
2-21	-5.530	-1.026	0.764	57.00	82.00	81.26	61.55	67.15	82.00

The experiment twist angles θ_{exp} are determined by X-ray refraction in the literatures. The twist angle $\theta_{\min}(\text{B3LYP})$ refers to the value of the twist angle θ when $dE(\theta)/d\theta = 0$ at B3LYP/6-311G* level

For each pair of the curve lines, a solid line and a dashed line in Figure 2-6, according to the data listed in Table 2-4, the signs of $\Delta E_N^{PQ}(\theta)$ and $d[\Delta E_N^{PQ}(\theta)]/d\theta$ are always consistent with the corresponding signs of $\Delta E_N(\theta)$ and $d[\Delta E_N(\theta)]/d\theta$. In determining the molecular conformation, therefore, the role of the nuclear repulsion $E_N^{PQ}(\theta)$ between fragments is always consistent with the role of total nuclear repulsion $E_N(\theta)$. For molecule **2-1**, for example, the values of $d[\Delta E_N^{PQ}(\theta)]/d\theta$ and $d[\Delta E_N(\theta)]/d\theta$ indicate that the nuclear repulsions $E_N^{PQ}(\theta)$ and $E_N(\theta)$ are the driving force of molecular distortion in the region of $\theta = 0$ to $\theta = \theta_{\min-N}$ ($\theta_{\min-N}$ is between 50° and 60°). The following ratios, $R_n(\theta)$ and $FR_n(\theta)$, and their averages, AR_n and AFR_n , can be used to quantify the relative difference

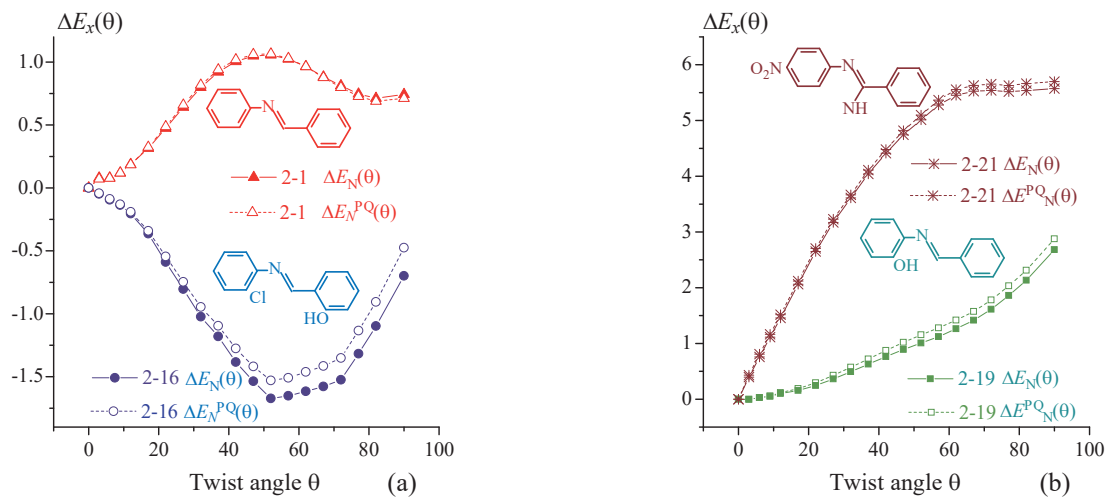


Figure 2-6. The nuclear repulsion differences $\Delta E_N(\theta)$ and $\Delta E_N^{PQ}(\theta)$ at B3LYP/6-311G** level. (a) For molecules **2-1** and **2-16**; (b) For molecules **2-19** and **2-21**, and their change with the increasing of twist angle θ .

between $\Delta E_N(\theta)$ and $\Delta E_N^{PQ}(\theta)$ and the relative difference between $d[\Delta E_N^{PQ}(\theta)]/d\theta$ and $d[\Delta E_N(\theta)]/d\theta$.

$$R_n(\theta) = [\Delta E_N(\theta) - \Delta E_N^{PQ}(\theta)]/\Delta E_N$$

$$AR_n = \Sigma |R_n(\theta)|/n$$

$$FR_n(\theta) = [(d\Delta E_N(\theta)/d\theta) - (d\Delta E_N^{PQ}(\theta)/d\theta)]/(d\Delta E_N(\theta)/d\theta)$$

$$AFR_n = \Sigma |FR_n(\theta)|/n$$

where n is the number of the sampled conformations. For each conformation, as indicated by the data listed in Table 2-4, there is slight difference between the two types of nuclear repulsions, and the values of their $R_n(\theta)$ and $FR_n(\theta)$ are generally less than 10%. For molecule **2-1**, for example, AR_n and AFR_n are, respectively, 2.5% and 7.6 %. Of the four molecules, the AR_n and AFR_n values (14.7 and 13.4%) for molecule **2-19** is the largest.

In fact, whether the signs of $d[\Delta E_N^{PQ}(\theta)]/d\theta$ and $d[\Delta E_N(\theta)]/d\theta$ are consistent or not is crucial. As for the values of $R_n(\theta)$ and $FR_n(\theta)$, it can't change the conclusions on the driving force and resistance of molecular distortion. Instead of $\Delta E_N(\theta)$, the changes, in $\Delta E_N^{PQ}(\theta)$ and $d[\Delta E_N^{PQ}(\theta)]/d\theta$, with the increasing of twist angle θ can be reasonably used to get insight into the molecular distortion.

2.3.2.2. Four Types of Substituted NBA Molecules

For the 15 molecules (**2-1** to **2-15**) belonging to the first group, the structural feature is that there is no substituent at the ortho-position of the N-phenyl ring and at the bridge group. For these molecules, as shown by the curves in the right side of Figure 2-5b, the characteristics of the functions $\Delta E_N^{PQ}(\theta) = f(\theta)$ and $\Delta E_e(\theta) = f(\theta)$ are as follows:

when $0^\circ < \theta < 90^\circ$

$$d^2[\Delta E_N^{PQ}(\theta)]/d\theta^2 < 0$$

$$d^2[\Delta E_e(\theta)]/d\theta^2 > 0.$$

The stationary points, $d[\Delta E_N^{PQ}(\theta)]/d\theta = 0$ and $d\Delta E_e(\theta)/d\theta = 0$, of their nuclear repulsion and total electron energy differences all are around $\theta = 48^\circ$ (Table 2-5).

Table 2-4. For Molecules 2-1, 2-16, 2-19 and 2-21, Nuclear Repulsions, $\Delta E_N(\theta)$ and $\Delta E_N^{PQ}(\theta)$, Their First Order Derivatives, $d\Delta E_N(\theta)/d\theta$ and $d\Delta E_N^{PQ}(\theta)/d\theta$, and Their Relative Differences $R_n(\theta)$ and $FR_n(\theta)$, at B3LYP/6-311G** Level.

		$\theta = 10$	$\theta = 20$	$\theta = 30$	$\theta = 40$	$\theta = 50$	$\theta = 60$	Average
$\Delta E_N(\theta) (\Delta E_N^{PQ}(\theta)) = A + B*\theta + C*\theta^2 + \dots$								
2-1	$\Delta E_N(\theta)$	0.07406	0.44250	0.74080	0.94909	1.04749	1.01614	
2-1	$\Delta E_N^{PQ}(\theta)$	0.06848	0.45356	0.75884	0.96648	1.05864	1.01751	
2-1	$R_n(\theta)$	0.07544	-0.02500	-0.02435	-0.01832	-0.01065	-0.00135	0.025
2-16	$\Delta E_N(\theta)$	-0.16548	-0.48826	-0.93475	1.33977	1.59919	1.66986	
2-16	$\Delta E_N^{PQ}(\theta)$	-0.15575	-0.45156	-0.86283	1.23145	1.45769	1.50024	
2-16	$R_n(\theta)$	0.05881	0.07516	0.07694	0.08086	0.08848	0.10158	0.080
2-19	$\Delta E_N(\theta)$	0.03389	0.23128	0.44921	0.68767	0.94666	1.22619	
2-19	$\Delta E_N^{PQ}(\theta)$	0.03717	0.27460	0.52751	0.79591	1.07979	1.37915	
2-19	$R_n(\theta)$	-0.09699	-0.18729	-0.17430	-0.15739	-0.14062	-0.12475	0.147
2-21	$\Delta E_N(\theta)$	1.17874	2.41704	3.45134	4.28164	4.90794	5.33024	
2-21	$\Delta E_N^{PQ}(\theta)$	1.23575	2.47502	3.51475	4.35493	4.99556	5.43665	
2-21	$R_n(\theta)$	-0.04836	-0.02399	-0.01837	-0.01712	-0.01785	-0.01996	0.024
$d\Delta E_N(\theta)/d\theta (d\Delta E_N^{PQ}(\theta)/d\theta) = B + 2*C*\theta + \dots$								
2-1	$d\Delta E_N(\theta)/d\theta$	0.03969	0.03367	0.02566	0.01567	0.00368	-0.01029	
2-1	$d\Delta E_N^{PQ}(\theta)/d\theta$	0.04190	0.03482	0.02594	0.01529	0.00285	-0.01137	
2-1	$FR_n(\theta)$	-0.05585	-0.03408	-0.01100	0.02416	0.22668	-0.10574	0.076
2-16	$d\Delta E_N(\theta)/d\theta$	-0.01906	-0.04172	-0.04482	-0.03445	-0.01671	0.00228	
2-16	$d\Delta E_N^{PQ}(\theta)/d\theta$	-0.01708	-0.03848	-0.04114	-0.03092	-0.01364	0.00485	
2-16	$FR_n(\theta)$	0.10406	0.07786	0.08204	0.10251	0.18385	1.12308	0.279
2-19	$d\Delta E_N(\theta)/d\theta$	0.01871	0.02077	0.02282	0.02487	0.02693	0.02898	
2-19	$d\Delta E_N^{PQ}(\theta)/d\theta$	0.02297	0.02452	0.02607	0.02761	0.02916	0.03071	
2-19	$FR_n(\theta)$	-0.22740	-0.18061	-0.14224	-0.11021	-0.08306	-0.05976	0.134
2-21	$d\Delta E_N(\theta)/d\theta$	0.13403	0.11363	0.09323	0.07283	0.05243	0.03203	
2-21	$d\Delta E_N^{PQ}(\theta)/d\theta$	0.13391	0.11395	0.09400	0.07404	0.05409	0.03413	
2-21	$FR_n(\theta)$	0.00093	-0.00282	-0.00821	-0.01662	-0.03158	-0.06559	0.021

When $0^\circ < \theta < \theta_{\min-e}$,

$$d[\Delta E_N^{PQ}(\theta)]/d\theta > 0,$$

$$d[\Delta E_e(\theta)]/d\theta < 0,$$

$$|d[\Delta E_e(\theta)]/d\theta| > d[\Delta E_N^{PQ}(\theta)]/d\theta.$$

The electron interaction is the driving force for distorting molecule away from the planar conformation, and the nuclear repulsion between the fragments P and Q is resistance to molecular distortion.

The second group includes three molecules **2-16**, **2-17** and **2-18**. For each of the three molecules, there is a substituent at the ortho-position of each aromatic ring (Figure 2-2). In contrast to the molecules of the first group, as shown by the curves in the left side of Figure 2-5b

$$d^2(\Delta E_N^{PQ}(\theta))/d\theta^2 > 0$$

$$d^2(\Delta E_e(\theta))/d\theta^2 < 0.$$

When $0^\circ < \theta < \theta_{\min-e}$,

$$d\Delta E_N^{PQ}(\theta)/d\theta < 0$$

$$d\Delta E_e(\theta)/d\theta > 0$$

$$|d\Delta E_N^{PQ}(\theta)/d\theta| > d\Delta E_e(\theta)/d\theta$$

In and only in this group of molecules, the nuclear repulsion between the fragments P and Q is the driving force of molecular distortion, and the electronic interaction becomes resistance to distortion. But an exception is found in molecule **2-18**. The energy differences, $\Delta E_e(\theta)$ and $\Delta E_N^{PQ}(\theta)$, for molecule **2-18** can be fitted as the following third order polynomial function of the twist angle θ :

$$\Delta E_e(\theta) = 0.00458 + 0.0366*\theta + 0.00117*\theta^2 + (8.24428E-6)*\theta^3 \text{ (cc = 0.988)}$$

$$d\Delta E_e(\theta)/d\theta = 0.0, \text{ when } \theta = 19.7^\circ \text{, and } \theta = 74.8^\circ.$$

$$\Delta E_N^{PQ}(\theta) = -0.00228 - 0.03625*\theta - 0.00116*\theta^2 - (8.20697E-6)*\theta^3 \text{ (cc = 0.988)}$$

$$d\Delta E_N^{PQ}(\theta)/d\theta = 0.0, \text{ when } \theta = 19.8^\circ \text{, and } \theta = 74.5^\circ.$$

The two stationary points on the function curve $\Delta E_e(\theta) = f(\theta)$ can be considered same as those on the function curve $\Delta E_N^{PQ}(\theta) = f(\theta)$. Accordingly, as shown by the curve lines for **2-18** in Figure 2-5b,

when $0^\circ < \theta < 19.7^\circ$

$$d(\Delta E_e(\theta))/d\theta < 0 \text{ (blue curve line)}$$

$$d(\Delta E_N^{PQ}(\theta))/d\theta > 0 \text{ (red curve line)}$$

which are similar to those for the molecules of the first group.

When $19.7^\circ < \theta < 74.8^\circ$,

$$d(\Delta E_e(\theta))/d\theta > 0 \text{ (blue curve line),}$$

$$d(\Delta E_N^{PQ}(\theta))/d\theta < 0 \text{ (red curve line),}$$

which are similar to those of other two molecules (**2-16** and **2-17**) of the second group. For the second group of molecules, the experimental values of the twist angle are, generally, smaller than those for the molecules of other three groups (Table 2-3).

The third group includes molecules **2-19** and **2-20**. There is a substituent at the ortho-position of N-phenyl ring, and no substituent at the ortho-position of C-aromatic ring (Figure 2-2). Only one molecule (**2-21**) belongs to the

Table 2-5. For Molecules 2-1 to 2-15 of the First Group, Total Electronic Energy Differences Are Locally Fitted as Second Order Polynomial Function of Twist Angle θ , $\Delta E_e(\theta) = a + b * \theta + c * \theta^2$, when $17^\circ < \theta < 75^\circ$. Sampled Conformations Are Optimized Using SCNP Procedure (Energy Unit in hartree).

Mol	Methods	a	b	c x 10 ⁴	$\Delta E_e(\theta_{\min-e})$	$\theta_{\min-e}$
2-1	B3LYP/6-311G**	0.6440	-0.0649	6.272	-1.0349	51.74
2-1	RHF/6-311G**	0.7575	-0.0681	5.906	-1.2056	57.65
2-1	B3LYP/STO-3G	0.8258	-0.0755	7.852	-0.9891	48.08
2-1	RHF/STO-3G	0.8438	-0.0725	7.061	-1.0172	51.34
2-1	AM1	0.1637	-0.0182	2.672	-0.1462	34.06
2-2	B3LYP/6-311G**	1.0137	-0.0957	9.552	-1.3833	50.09
2-3	B3LYP/6-311G**	0.9812	-0.0927	9.085	-1.3835	51.02
2-9	B3LYP/6-311G**	0.9917	-0.0970	9.858	-1.3944	49.20
2-10	B3LYP/6-311G**	0.9849	-0.0971	10.100	-1.3489	48.07
2-4	B3LYP/6-311G**	0.6831	-0.0658	6.586	-0.9604	49.95
2-5	B3LYP/6-311G**	0.6093	-0.0627	6.429	-0.9194	48.76
2-6	B3LYP/6-311G**	0.6572	-0.0665	6.429	-1.0624	51.72
2-7	B3LYP/6-311G**	0.7104	-0.0678	6.535	-1.0481	51.87
2-8	B3LYP/6-311G**	0.7356	-0.0680	7.042	-0.9060	48.28
2-11	B3LYP/6-311G**	0.6212	-0.0612	6.650	-0.7869	46.02
2-12	B3LYP/6-311G**	0.9108	-0.0852	8.606	-1.1979	49.50
2-13	B3LYP/6-311G**	1.3610	-0.1261	16.600	-1.0338	37.98
2-15	B3LYP/6-311G**	0.6361	-0.0595	6.879	-0.6505	43.25
2-14	B3LYP/6-311G**	0.3109	-0.0360	4.645	-0.3866	38.75

fourth group, and one of the two substituents is bonded to the carbon atom of the $-\text{N}=\text{CH}$ bridge group.

For the third and fourth groups of molecules, the curves of $\Delta E_N^{\text{PQ}}(\theta)$ and $\Delta E_e(\theta)$ do not have the stationary point. In the region of $0^\circ < \theta < 90^\circ$, $d[\Delta E_N^{\text{PQ}}(\theta)]/d\theta > 0$ and $d[\Delta E_e(\theta)]/d\theta < 0$ remain unchanged (Figure 2-5c), the nuclear repulsion between the fragments is always resistance to molecular distortion, and the electron interaction is always a driving force.

In particular, it is worth mentioning that in the molecule 2-21, the amino group is located at the $-\text{N}=\text{C}-$ bridge. According to a classic view, the nuclear repulsion between the fragments P and Q should be a driving force of the AS

molecular distortion, and it is a strong driving force. In fact, as shown by the curve in Figure 2-5c and Figure 2-6 and as shown by the values of $d\Delta E_N^{\text{PQ}}(\theta)/d\theta$ listed in Table 2-4, the nuclear repulsion $\Delta E_N^{\text{PQ}}(\theta)$ between the two fragments is the strongest resistance to molecular distortion. When $\theta = 90^\circ$, the value of $\Delta E_N^{\text{PQ}}(\theta)$ is the largest, up to 5.699 hartree, and it is the largest of all the twisted conformations of 21 molecules. Correspondingly, the experimental value of the twist angle for molecule 2-21 is also the largest, up to 82° .

In short, for all the molecules except for the molecules of the second group, the driving force arises from the electronic interaction, and the steric hindrance between the fragments P and Q is resistance to molecular distortion.

2.3.2.3. Intra-molecular Hydrogen Bonds

For the molecules of the second group, the exception to the conclusions about the driving force and the resistance seems able to be attributed to the intra-molecular hydrogen bonds.¹⁰⁴ In the $\theta = 0^\circ$ geometry of molecule **2-17**, as shown by the data presented in Figure 2-7a, the distances, $r_1(0^\circ)$ and $r_2(0^\circ)$, are 2.68 and 1.73 Å, and they are less than (or equal to) the cut-off distance (3.5 Å)¹¹⁰ of hydrogen bond generation. The distance $r_2(\theta)$ (about 1.74 Å) is within the normal range, 1.60 to 2.00 Å¹¹¹, of hydrogen bonds. If there was no hydrogen bond between N(13) and H(27), the dihedron angle H27-O26-C17-C16 might be equal to H(12)-O(11)-C(6)-C(1) (about 180°), and the distance $r_1(0^\circ) = 4.08$ Å. The fact that the dihedron angle H(27)-O(26)-C(17)-C(16) = 0.06° may be due to the formation of the hydrogen bonds between N(13) and H(27) and between O(11) and H(27). According to the distance $r_1(\theta)$, the hydrogen bond O(11).....H(27) in the $\theta = 0^\circ$ conformation is the strongest.

The Mulliken atomic overlap population (MAOP), $M_{i,j}$, between a pair of atoms should be able to be used as a criterion to compare the strength of hydrogen bonds. In Figure 2-7a, for example, the curve line, labeled by "N(13)-H(27)", describes the change in the MAOP difference, $\Delta M_{13-27}(\theta) = M_{13-27}(\theta) - M_{13-27}(0^\circ)$, with the increasing of twist angle θ , where $M_{13-27}(\theta)$ is the Mulliken atomic overlap population between the N(13) and H(12) atoms in the conformation distorted by θ° . The curve line, labeled by "Tot-HB", describes the change, in the sum ($\Sigma \Delta M_{i-j}(\theta)$) of the MAOP difference $\Delta M_{ij}(\theta)$, with the increasing of twist angle, where $\Sigma \Delta M_{i-j}(\theta) = \Delta M_{13-27}(\theta) + \Delta M_{11-27}(\theta)$.

As shown by the curve lines in Figure 2-7a, $M_{11-27}(\theta)$, $M_{13-27}(\theta)$ and $\Sigma \Delta M_{i-j}(\theta)$ can be fitted as the polynomial function of the twist angle θ , and

when $0 < \theta < 80^\circ$

$$d\Delta M_{13-27}(\theta)/d\theta > 0$$

$$d\Delta M_{11-27}(\theta)/d\theta < 0$$

$$d\Sigma \Delta M_{i-j}(\theta)/d\theta < 0$$

For molecule **2-17**, the total hydrogen bond energy is the most stabilizing in the $\theta = 0^\circ$ conformation. Therefore, the hydrogen bond, especially the hydrogen bond between H(27) and O(11) may be an structural factor to cause $d\Delta E_e(\theta)/d\theta > 0$. For molecule **2-18**, the hydrogen bond may generate between the following three pairs of atoms: H(12)-N(14), H(12)-O(27), and N(11)-H(28). The corresponding $\Delta M_{i-j}(\theta)$ and their sum $\Sigma \Delta M_{i-j}(\theta)$ can be well fitted as the following forth order polynomial function of the twist angle θ (cc = 0.999):

$$\Sigma \Delta M_{i-j}(\theta) = 2.13243E-4 - (4.5491E-4)\theta - (1.64889E-5)\theta^2 - (1.77025E-7)\theta^3 - (7.64682E-10)\theta^4.$$

When $\theta_{\min-H} = 20.7^\circ$,

$$d[\Sigma \Delta M_{i-j}(\theta)]/d\theta = 0$$

$$d[\Sigma \Delta M_{i-j}(\theta)]/d\theta > 0, 0 < \theta < \theta_{\min-H}$$

$$d[\Sigma \Delta M_{i-j}(\theta)]/d\theta < 0, \theta_{\min-H} < \theta < 90^\circ$$

Very interestingly, for molecule **2-18**, $\theta_{\min-H} = 20.7^\circ \approx \theta_{\min-e} = 19.7^\circ$. When $\theta = \theta_{\min-H} = 20.7^\circ$, the sum of hydrogen bonds is the strongest (Figure 2-7b), and the corresponding total electronic energy $\Delta E_e(20.7^\circ)$ is about the lowest (Figure 2-5b), which should not be a coincidence.

Figure 2-7a and Figure 2-7b consistently indicate that the hydrogen bonds may play an important role in determining the characters of the function $\Delta E_e(\theta) = f(\theta)$ for the molecules of the second group.

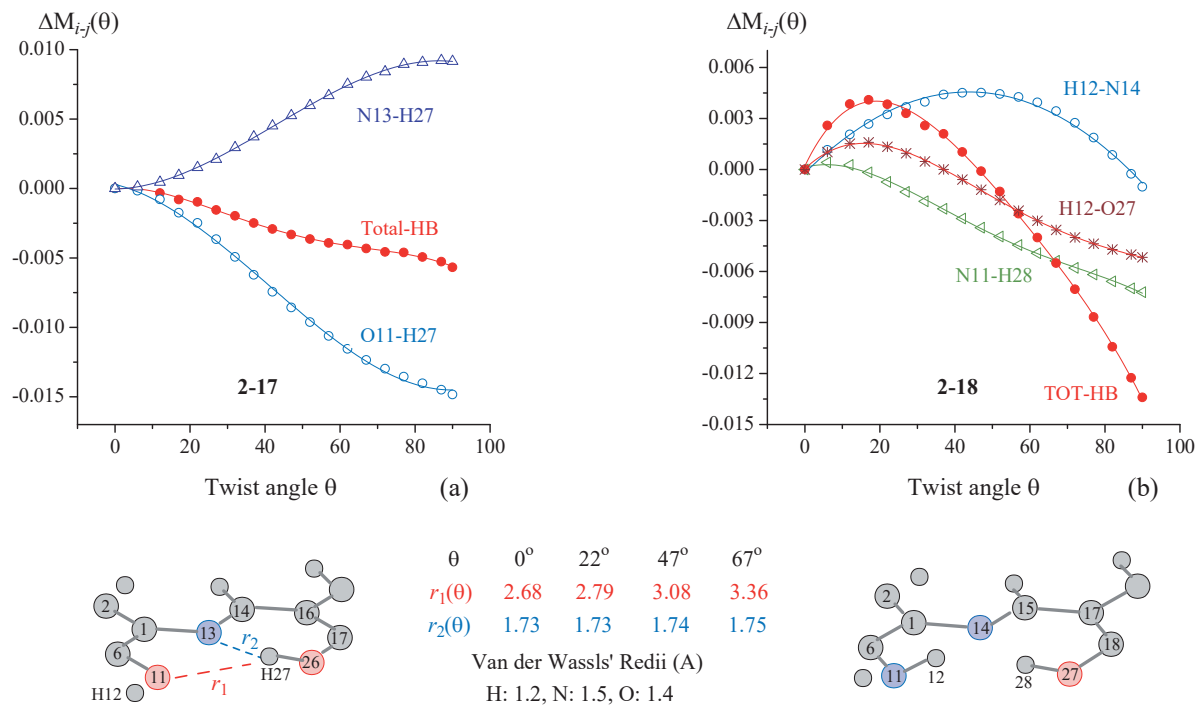


Figure 2-7. Mulliken atomic overlap population M_{ij} between pairs of hydrogen atoms, and their difference $\Delta M_{ij} = M_{ij}(\theta) - M_{ij}(0^\circ)$ changes with the increasing of twist angle θ at B3LYP/6-311G** level.

2.3.2.4. Substituent Effect.

According to Table 2-5, The first group of molecules (**2-2** to **2-15**) are divided into four subgroups. The first sub-group includes four molecules, **2-2**, **2-3**, **2-9** and **2-10**, whose substituent at the para-position of N-phenyl rings is an electron-withdrawing group. In the second order polynomial function $\Delta E_e(\theta) = A + B * \theta + C * \theta^2$, the coefficient c is in the region of $9.552 * 10^{-4}$ to $10.1 * 10^{-4}$, and they are greater than that ($6.272 * 10^{-4}$) for molecule **2-1**. Correspondingly, as shown by the function curves in the right of Figure 2-8a, the curves for these molecules are under the red curve of their mother molecule **2-1** (NBA), and they are almost overlap each other ($0^\circ < \theta < 62^\circ$). The values of their twist angle θ_{\min} , about 45° to 47° , are all greater than that (41°) of NBA (Table 2-3), but the values of the twist angle $\theta_{\min-e}$, about 48° to 52° , are close to that (51.7°) for molecule **2-1**. Thus, an electron withdrawing groups at the p-position of the N-phenyl ring can really increase the twist angle, but the structure and number of the substituent have almost no effect on the $d\Delta E_e(\theta)/d\theta$ and $d^2[\Delta E_e(\theta)]/d\theta^2$.

The six molecules, **2-4** to **2-8** and **2-11**, belong to the second sub-group. In each of these molecules, except for molecule **2-7**, there is an electron-releasing group at the p-position of N-phenyl ring. The coefficients c in the second order polynomial functions are in the region of $6.429 * 10^{-4}$ to $7.042 * 10^{-4}$, and they are close to that for molecule **2-1**. The function curves for these molecules are all above the curve of their mother molecule when $\theta \geq \theta_{\min-e}$, and all the curves are separated from each other (the left side of Figure 2-8a). For a specific molecule, near $\theta = \theta_{\min-e}$, the smaller the vertical distance between the curves of the molecule and **2-1**, the greater the twist angle is. According to the order of the curves from top to bottom, the order of the corresponding molecules is:

2-11 ($p = \text{N}(\text{Me})_2$, $p' = \text{NO}_2$), **2-8** ($p = \text{MeO}$, $p' = \text{NO}_2$), **2-5** ($p = \text{N}(\text{Me})_2$), **2-4** ($p = \text{OH}$), **2-7** ($p' = \text{NO}_2$), and **2-6** ($p' = \text{OH}$).

The corresponding size order of the twist angle θ is as follow:

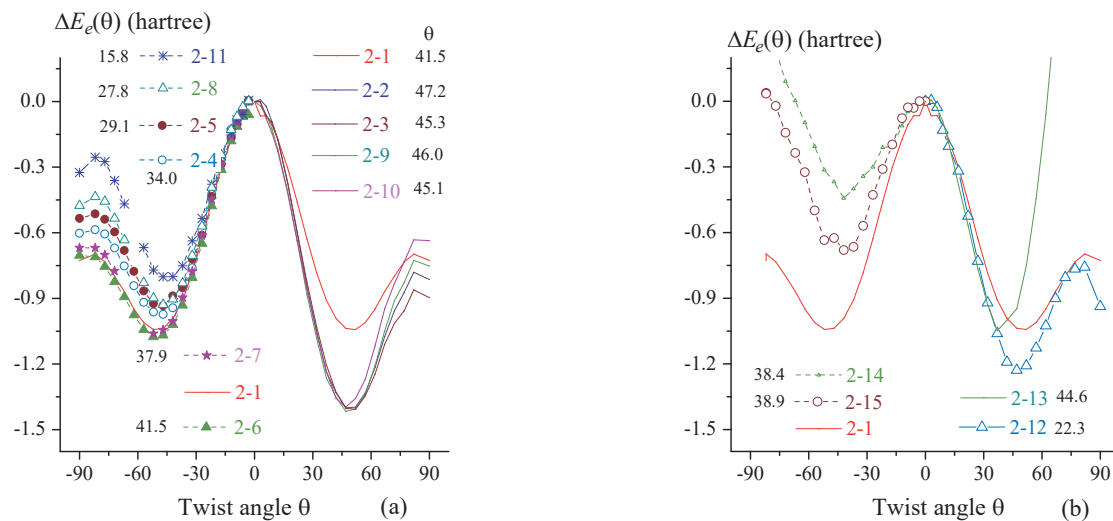
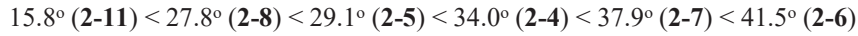


Figure 2-8. At B3LYP/6-311G** level, total electronic energy differences $\Delta E_e(\theta)$ versus twist angle θ , and the twist angle θ_{\min} (black data). (a) For the first and second sub-groups. (b) For the third and fourth sub-groups.



For molecule **2-6** ($R_6 = -OH$), for example, its green curve line is almost overlap with the curve of NBA, and its twist angle θ_{\min} (41.5°) are the greatest among the molecules of the second subgroup, due to that there is no electron-releasing group at the p-position. For molecule **2-11** ($R_2 = -N(Me)_2$, $R_6 = -NO_2$), on the other hand, the vertical distance between the violet and red curve lines is the greatest, and its twist angle θ_{\min} (15.7°) are the smallest, due to that the p- $N(Me)_2$ group has the largest electron-releasing ability with the help of the p'- NO_2 group.

For the molecules of the third and fourth subgroups, their function curves are, respectively, above and below the red curve for NBA, but the relationship between the vertical distance and twist angle θ_{\min} , as discussed in the first and the second groups, is no longer found. However, as previously emphasized, this is not crucial.

In Figure 2-9, the energy differences, $\Delta E_e(\theta)$ and $\Delta E_N(\theta)$, for molecules **2-1**, **2-17**, **2-20** and **2-21** are obtained from the relaxed PES scan at the (RHF and B3LPY)/(STO-3G and 6-311G**) and the AM1 levels, and their function curves show that the characteristics of $d[\Delta E_e(\theta)]/d\theta$ and $d[\Delta E_N(\theta)]/d\theta$ are nothing to do with the theoretical level and basis set size. For N-benzylideneaniline (**2-1**), particularly, the curve lines are almost overlap each other when $0^\circ < \theta < \theta_{\min-e}$.

Therefore, the conclusions about the driving force and resistance, obtained from Figure 2-5 and Figure 2-6, have nothing to do with the theoretical level and Gaussian basis set size.

2.4. CONCLUSIONS

Inspired by an abnormal phenomenon that, for two molecules 2-naphthyl-N(Me)-(HC=CH)_n-CHO ($n = 1, 2$), the stronger conjugation between the naphthyl and amino groups in the molecule ($n = 1$) corresponds to a larger twist angle between the 2-naphthyl and -N(Me)-(HC=CH)_n-CHO groups, the structural factors that cause large twist angles are investigated in this Chapter.

According to the changes, in the total electronic energy $E_e(\theta)$ and nuclear repulsion $E_N^{PQ}(\theta)$ for each NBA-like species, with the increasing of twist angle θ , we have got the following very important and interesting conclusions:

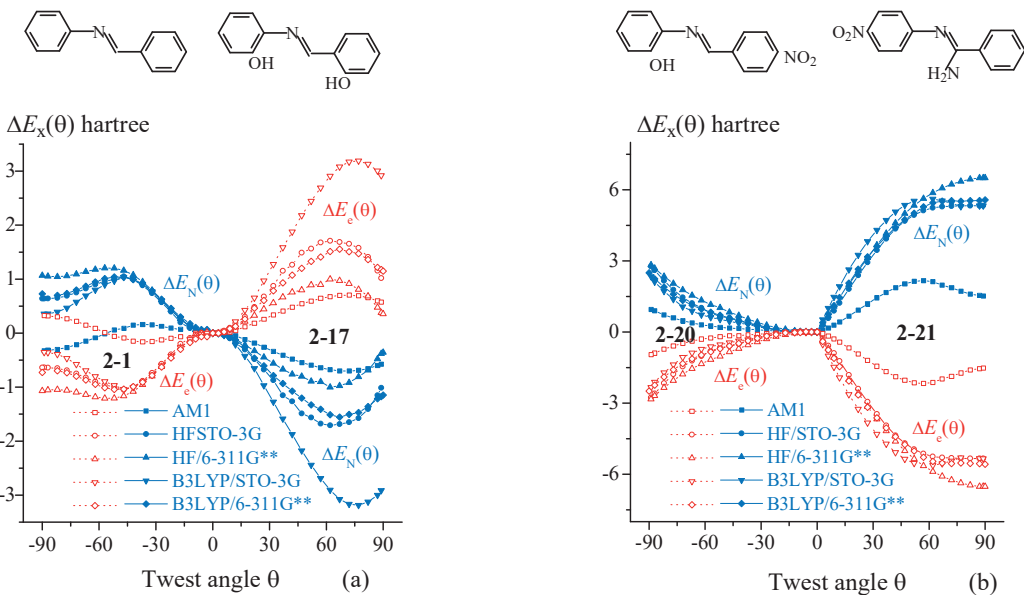


Figure 2-9. Energy differences ($\Delta E_N(\theta)$ and $\Delta E_e(\theta)$) versus twist angle θ . (a) For molecules 2-1 and 2-17. (b) For molecules 2-20 and 2-21.

- (i) always $d[E_N^{PQ}(\theta)]^2/d\theta < 0$.
- (ii) always $d[E_e(\theta)]^2/d\theta > 0$.
- (iii) $dE_N^{PQ}(\theta)/d\theta > 0$, when $0^\circ < \theta < \theta_{\min-N}$.
- (iv) $dE_e(\theta)/d\theta < 0$, when $0^\circ < \theta < \theta_{\min-e}$.
- (v) $dE_N^{PQ}(\theta)/d\theta = 0$ and $dE_e(\theta)/d\theta = 0$, in a preferential geometry with twist angle $\theta_{\min-e}$.

The PES scan calculation results reinforce our confidence in questioning the "principle of conjugation stabilization." The PES scan calculations are only a small part of this monograph. However, logically this part is extremely important, because these calculations that question the fundamental principles and question the driving force of molecular distortion are performed by using the recognized Gaussian 98 software package. Therefore, the PES scan calculations can not only make readers (including the author himself) recognize that our questioning is reliable and credible, but also can make the reader feel that the establishment and development of our subsequent calculation methods are logically unavoidable. If the first chapter is to explain the cause of our questioning, then this chapter is the starting point for our entire monograph.

However, total electron energy includes inter- and intra-fragment electron interaction. Due to the presence of the $\pi-\sigma$ interaction between the N-phenyl ring and the $-N=CH-Ph$ group in the on-planar molecules such as NBA-like species, it can't be asserted that a particular type of MO (molecular orbital) interaction, such as the $\pi-\pi$ and $\sigma-\sigma$ interactions, is destabilization based only on the fact that $dE_e(\theta)/d\theta < 0$ because the following two cases both can cause $dE_e(\theta)/d\theta < 0$ in the region of $0^\circ < \theta < \theta_{\min-e}$:

$$\begin{aligned}\Delta E^{\pi-\pi}(\theta) &> 0 \text{ (destabilizing)} \\ \Delta E^{\sigma-\sigma}(\theta) &> 0 \text{ (destabilizing)} \\ \Delta E^{\pi-\sigma}(\theta) &> 0 \text{ (destabilizing)} \\ \Delta E^{\pi-\pi}(\theta) + \Delta E^{\sigma-\sigma}(\theta) &> \Delta E^{\pi-\sigma}(\theta)\end{aligned}$$

or

- $\Delta E^{\pi\cdot\pi}(\theta) < 0$ (stabilizing)
- $\Delta E^{\sigma\cdot\sigma}(\theta) < 0$ (stabilizing)
- $\Delta E^{\pi\cdot\sigma}(\theta) < 0$ (stabilizing)
- $|\Delta E^{\pi\cdot\pi}(\theta) + \Delta E^{\sigma\cdot\sigma}(\theta)| < |\Delta E^{\pi\cdot\sigma}(\theta)|$

where $\Delta E^{\pi\cdot\pi}(\theta)$, $\Delta E^{\sigma\cdot\sigma}(\theta)$, and $\Delta E^{\pi\cdot\sigma}(\theta)$ are the energy effects associated with the $\pi\cdot\pi$, $\sigma\cdot\sigma$ and $\pi\cdot\sigma$ molecular orbital interactions between the N-(substituted phenyl) ring and the -N=CH-(substituted-Ph) fragments in a specific conformation.

Therefore, it is necessary to develop a method that can decompose the electron interaction energy between the fragments into the π and σ parts.

2.5. REFERENCES

- 1 Lennard-Jones, J. F. 1937. "The Electronic Structure of Some Polyenes and Aromatic Molecules. I. The Nature of the Links by the Method of Molecular Orbitals." Proc. Roy. Soc. London, A158: 280-296.
- 2 Shaik, S.; Shurki, A.; Danovich, D.; Hiberty, P. C. 1997. "A Different Story of Benzene." Theochem, 398-399: 155-167.
- 3 Hiberty, P. C. 1990. "The Distortive Tendencies of Delocalized Π Electronic Systems. Benzene, Cyclobutadiene And Related Heteroannulenes." Top. Curr. Chem., 153: 27-39.
- 4 Shaik, S.; Shurki, A.; Danovich, D.; Hiberty, P. C. 2001. "A Different Story of π -Delocalization – The Distortion of π -Electrons and Its Chemical Manifestations." Chem. Rev., 101: 1501-1540.
- 5 Ichikawa, H.; Kagawa, H. 1995. "Potential-Energy Surfaces Concerning Deformation in Benzene." J. Phys. Chem., 99: 2307-2311.
- 6 Epotis, N. D. 1996. *Deciphering the Chemical Code*. New York: VCH Publishers, Inc.
- 7 Epotis, N. D. 1983. *Lecture Notes in Chemistry*, Vol. 34. New York: Springer-Verlag
- 8 Bürgi, H. B.; Dunitz, J. D.; Züst, C. 1968. "Lattice Parameters and Space Groups of Some Aromatic Schiff Bases." Acta Cryst., 24B: 463-464.
- 9 Bürgi, H. B.; Dunitz, J. D. 1970. "Crystal and Molecular Structures of Benzylideneaniline, Benzylideneaniline-p-carboxylic Acid and p-methylbenzylidene-p-nitroaniline." Helv. Chim. Acta, 53:1747-1764.
- 10 Bürgi, H. B.; Dunitz, J. D. 1971. "Molecular Conformation of Benzylideneanilines." Helv. Chim. Acta, 54: 1255-1260.
- 11 Bally, T.; Haselbach, E.; Lanyiova, S.; Rossi, M.; Marschner, F. 1976. "Concerning the Conformation of Isolated Benzylideneaniline." Helv. Chim. Acta, 59: 486-498.
- 12 Traetteberg, M.; Hilmo, L.; Abraham, R. J.; Ljunggren, S. 1978. "The Molecular Structure Of N-Benzylidene-Aniline." J. Mol. Struct., 48: 395-405.
- 13 (Molecule 2-3, 2-6, 2-8) Harada, J.; Harakawa, M.; Ogawa, K. 2004. "Torsional Vibration and Central Bond Length of N-Benzylideneanilines." Acta Cryst. B, 60: 578-588.
- 14 Yu, Z. H.; Li, L. T.; Fu, W.; and Li, L. P. 1998. "Conformations of Stilbene-Like Species and New Method of Energy Partition." J. Phys. Chem. A, 102: 2016-2028.
- 15 Yu, Z. H.; Peng, X. Q. 2001. "New Insight into the Nature of Electron Delocalization: The Driving Forces for Distorting the Geometry of Stilbene-Like Species." J. Phys. Chem. A, 105: 8541-8553.
- 16 Yu, Z. H.; Xuan, Z. Q.; Guo, Y. S.; Peng, X. Q.; Wang, T. X. 2001. "The Conformation of N-Phenylmethylene-2-thiazoleamine Species and the Driving Forces for Twisting Molecule." Chem. J. Chin. Univ., 22: 122-126 (Chinese).
- 17 Guo, Y. S.; Yu, Z. H.; Jin, X. L. 2002. "The Conformation of N-(phenylmethylene)-1-naphthaleneamine-like

- Species and the π -Driving Force for distorting Geometry”, Acta Chem. Sin., 60: 228-233 (Chinese).
- 18 Xu, H.; Yu, Z. H. 2004. “The Driving Forces for Distorting NBA-Like Species away from Their Planar Geometries.” Theochem, 682: 37-46.
- 19 Xu, H.; Yu, Z. H. 2005. “N-Benzylideneaniline-like Derivatives and Their Conformation.” Chem. J. Chin. Univ., 26: 308-311 (Chinese).
- 20 Natansohn, A.; Rochon, P. 2002. “Photoinduced Motions in Azo-Containing Polymers.” Chem. Rev., 102: 4139-4176.
- 21 Gallant, A. J.; Hui, J. K. H.; Zahariev, F. E.; Wang, Y. A.; MacLachlan, M. J. 2005. “Synthesis, Structure, and Computational Studies of Soluble Conjugated Multidentate Macrocycles.” J. Org. Chem., 70: 7936-7946.
- 22 Duanna, Y. F.; Liua, T. M.; Chenga, K. C.; Sub, W. F. 2004. “Thermal Stability of Some Naphthalene- and Phenyl-Based Epoxy Resins.” Polym. Degrad. Stab., 84: 305-310.
- 23 D'Alelio, G. F. 1969. *Polyazomethines*, in: *Encyclopedia Polymer Science Technology*, vol. 10. New York: Wiley.
- 24 Katon, J. E. 1970. *Organic Semiconducting Polymers*. New York: Marcel Dekker.
- 25 Scott, J.; Asamib, M.; Tanaka, K. 2002. “Novel Chromogenic, Guest-sensitive Host Compounds.” New J. Chem., 26: 1822-1826.
- 26 Liquid Crystal Material, US patents: <http://www.google.com/patents/US4047803>.
- 27 Lee, M.; Yoo, Y. S.; Choi, M. G.; Chang, H. Y. 1998. “Calamitic Smectic Liquid Crystalline Supramolecular Architecture from Octaalkoxy-substituted PdII- η^1 -benzylideneaniline Complexes.” J. Mater. Chem., 8: 277.
- 28 Ichimura, K. 2000. “Photoalignment of Liquid-Crystal Systems.” Chem. Rev., 100: 1847.
- 29 Walree, C. A.; Franseen, O.; Marsman, A. W.; Flipse, M. C.; Jenneskens, L. W. 1997. “Second-Order Nonlinear Optical Properties of Stilbene, Benzylideneaniline and Azobenzene Derivatives. The Effect of π -Bridgenitrogen Insertion on the First Hyperpolarizability.” J. Chem. Soc., Perkin Trans. 2, 799-808.
- 30 Tetsuya, T.; Tetsuya, G.; Keiichi, E.; “Organic Nonlinear Optical Material.” Patent Number: 63113429, 1988-05-18.
- 31 Douglas, G. H.; Nuss, Jr. G. W.; Santora, N. J. US patent 3833606; 3862833; 4047803; 4122026. 1980, April 15.
- 32 Wiegand, C. and Merkel, E. 1942. “Der räumliche Bau des Benzalanilins”. Justus Liebigs Ann. Chem., 550: 175-181.
- 33 Izmailskii, V. A.; Smirnov, E. A. 1956. Zh. Obshch. Khim., 26: 3389-3406.
- 34 Jaffe, H. H.; Yeh, S. J.; Gardner, R. W. 1958. “The Electronic Spectra of Azobenzene Derivatives and Their Conjugate Acids.” J. Mol. Spectr., 2: 120-136.
- 35 Ebara, N. 1960. “Benzylideneaniline. I. Structure and Ultraviolet Absorption Spectrum of Benzylideneaniline.” Bull. Chem. Soc. Jpn., 33: 534-539.
- 36 (Molecule 2-2). Ebara, N. 1961. “Benzylideneaniline. III. Anils of Substituted Benzaldehydes.” Bull. Chem. Soc. Jpn., 34: 1151-1158.
- 37 Skrabal, P.; Steiger, J.; Zollinger, H. 1975 “On the Planarisation of Benzylideneaniline.” Helv. Chim. Acta, 58: 800-814.
- 38 Bernstein, J.; Anderson, T. E.; Eckhard, C. J. 1979. “Conformational Influences on Electronic Spectra and Structure. Polymorphs of N-(p-Chloro-Benzylidene)-p-Chloroaniline.” J. Am. Chem. Soc., 101: 541-545.
- 39 Akaba, R.; Tokumaru, K.; Kobayashi, T. 1980. “Electronic Structures and Conformations of *N*-Benzylideneanilines. I. Electronic Absorption Spectral Study Combined with CNDO/S CI Calculations.” Bull. Chem. Soc. Jpn., 53: 1993-2001.
- 40 Akaba, R.; Tokumaru, K.; Kobayashi, T.; Utsunomiya, C. 1980. “Electronic Structures and Conformations of *N*-Benzylideneanilines. II. Photoelectron Spectral Study.” Bull. Chem. Soc. Jpn., 53: 2002-2006.
- 41 Molina, V.; Merchan, M.; Roos, B. O. 1997. “Theoretical Study of the Electronic Spectrum of *trans*-Stilbene.” J. Phys. Chem. A, 101: 3478-3487.

- 42 Ezumi, K.; Nakai, H.; Sakata, S.; Nishikida, K.; Shiro, M.; Kubota, T. 1974. "The Importance of Intramolecular Change Transfer Effect on the Molecular Conformation of p-nitrobenzylidene-p-dimethylamino-aniline." *Chem. Lett.*, 3: 1393-1398.
- 43 Klasinc, L.; Ruščić, B.; G. Heinrich, G.; Güsten, H. 1977. "Photoelectron Spectroscopy of Substituted N-Benzylideneanilines." *Z. Naturforsch.*, 32B: 1291-1295.
- 44 Denecke, E.; Müller, K.; Bluhm, T. 1982. "¹³C NMR Spectra of Diazastilbenes. II—Torsion Angles of trans-pyridinal-anilines and trans-benzylidene-amino-pyridines." *Org. Magn. Reson.*, 18: 68-70.
- 45 Akaba, R.; Sakuragi, H.; Tokumaru, K. 1985. "Multiple Substituent Effects on ¹³C Chemical Shifts of *N*-Benzylideneanilines. Evidence for Substituent–Substituent Interactions and Their Implications of Conformational Changes with Substituents." *Bull. Chem. Soc. Jpn.*, 58: 1186-1195.
- 46 Koleva, V.; Dudeva, T.; Wawerb, I. 1997. "¹H and ¹³C NMR Study and AM1 Calculations of Some Azobenzenes and N-Benzylidene-anilines: Effect of Substituents on the Molecular Planarity." *J. Mol. Struct.*, 412: 153-159.
- 47 Jovanović, B. Ž.; Mišić-Vuković, M.; Marinković, A. D.; Vajs, V. 1999. "Effect of Substituents on the ¹³C Chemical Shifts of the Azomethine Carbon Atom of N-(Phenyl Substituted) Pyridine-4-aldimines." *J. Mol. Struct.*, 482-483: 375-378.
- 48 Odian, G.; Yang, N. I.; Wei, Y. 1985. "Substituent Effects on ¹H NMR Spectra of 4- and 4'-Substituted trans-N-benzylideneanilines in Acidic Solution." *Magn. Reson. Chem.*, 23: 908-915.
- 49 Ha, S. T.; Win, Y. F. 2010. "Total Assignment of NMR Spectral Lines of, "Schiff Base Derivatives with Pyridine Core." *World Appl. Sci. J.*, 8: 1007-1012.
- 50 Rubeń, M. G.; Armando, A. C. 2003. "Molecular Structure of di-Aryl-Aldimines by Multinuclear Magnetic Resonance and X-Ray Diffraction." *J. Mol. Struct.*, 655: 375-389.
- 51 Curtis, R. D.; Penner, G. H.; Power, W.; Wasylisen, R. E. 1990. "Dipolar-Chemical Shift NMR Spectra of the Carbon-Nitrogen Linkage in Benzylideneaniline: Carbon and Nitrogen Chemical Shielding Anisotropies." *J. Phys. Chem.*, 94: 4000-4006.
- 52 Celebre, G.; De Luca, G.; Di Pietro, M. E. 2012. "Investigated by Liquid Crystal NMR Spectroscopy and Compared with *in Vacuo* Theoretical Predictions." *J. Phys. Chem. B*, 116: 2876-2885.
- 53 Burnell, E. E.; De Lange, C. A. 2003. *NMR of ordered liquids*. Kluwer Academic Publishers, Netherlands.
- 54 Erb, H. P.; Bluhm, T. 1980. "¹³C NMR Spectra of diazastilbenes. I—trans-Styryldiazines." *Org. Magn. Reson.*, 14: 285-289.
- 55 Vikić-Topić, D.; Novak, P.; Meić, Z.; Plavec, J.; Kovaček, D. 1999. "Intrinsic Long Range Deuterium Isotope Effects on ¹³C NMR Chemical Shifts as a Conformational Probe of Benzene Derivatives." *Croat. Chem. Acta*, 72: 967-974.
- 56 Ellas, D. J.; Gillis, R. G. 1969. "The Mass Spectra of Schiff Bases II. Two Deuterated Species." *Aust. J. Chem.*, 22: 2249-2250.
- 57 Choi, C. H.; Kertesz, M. 1997. "Conformational Information from Vibrational Spectra of Styrene, *trans*-Stilbene, and *cis*-Stilbene." *J. Phys. Chem. A*, 101: 3823-3831.
- 58 Meit, Z.; Baranovit, G. 1989. "Vibrational Spectra of trans-N-Benzylideneaniline and Its Isotopomers." *Pure & App. Chem.*, 61: 2129-2138.
- 59 Biswas, N.; Umapathy, S. 1997. "Density Functional Calculations of Structures, Vibrational Frequencies, and Normal Modes of *trans*- and *cis*-Azobenzene." *J. Phys. Chem. A*, 101: 5555-5566.
- 60 Ha, S. T.; Win, Y. F.; Koh, T. M.; Chong, Y. T. 2001. "Synthesis and Characterization of 4-{[(3-cyanophenyl)imino]methyl}-3-hydroxyphenyl octadecanoate." *Aust. J. Basic Appl. Sci.*, 5: 15.
- 61 Traetteberg, M.; Hilmo, I.; Hagen, K. 1997. "A Gas Electron Diffraction Study of the Molecular Structure of *Trans*-azobenzene." *J. Mol. Struct.*, 39: 231-239.
- 62 Traetteberg, M.; Frantsen, E. B. 1975. "A Gas Electron Diffraction Study of the Molecular Structure of *Trans*-stilbene." *J. Mol. Struct.*, 26: 57-68.
- 63 Tsuji, T.; Takashima, H.; Takeuchi, H.; Egawa, T.; Konaka, S. 2001. "Molecular Structure and Torsional

- Potential of *trans*-Azobenzene. A Gas Electron Diffraction Study Molecular Structure and Torsional Potential of *trans*-Azobenzene. A Gas Electron Diffraction Study." J. Phys. Chem. A, 105: 9347-9353.
- 64 Hiroshi, T.; Chihiro, U.; Takemasa, T.; Tooru, E.; Shigehiro, K. 2003. "Molecular Structure of N-Benzylidene-aniline, a Related Compound of Mesogens, as Determined by Gas Electron Diffraction." Nippon Kagakkai Koen Yokoshu, 83: 472.
- 65 Kuze, N.; Ebizuka, M.; Fujiwara, H.; Takeuchi, H.; Egawa, T.; Konaka, S. 1998. "Molecular Structure of *p*-Azoxyanisole, a Mesogen, Determined by Gas-Phase Electron Diffraction Augmented by ab Initio Calculations." J. Phys. Chem. A, 102: 2080-2086.
- 66 Finder, C. J.; Newton, M. G.; Allinger, N. L. 1974. "An Improved Structure of *trans*-stilbene." Acta. Cryst., B30: 411-415.
- 67 Brown, C. J. 1966. "A Refinement of the Crystal Structure of Azobenzene." Acta. Cryst., 21: 146-152.
- 68 Brown, C. J. 1966. "The Crystal Structure of *p*-azotoluene." Acta. Cryst., 21: 153-158.
- 69 Wiebcke, M.; Mootz, D. 1982. "Structures of three Schiff-base diazastilbenes: (I) *trans*-*N*-(2-pyridyl-methylene)aniline, (II) *trans*-*N*-(4-pyridyl-methylene)aniline and (III) *trans*-*N*-benzylidene-3-pyridinamine." Acta. Cryst., B38: 2008-2013.
- 70 Ojala, C. R.; Ojala, W. H.; Gleason, W. B.; Britton, D. 1999. "The Crystal Structures of p-iodo-*n*-(*p*-cyano-cenzylidene)aniline and *p*-cyano-*N*-(*p*- iodobenzylidene)aniline." J. Chem. Cryst., 29: 27-32.
- 71 (Molecules 2-10, 2-11) Nakai, H.; Shiro, M.; Emuzi, K.; Sakata, S.; Kubota, T. 1976. "The Crystal and Molecular Structures of *p*-nitrobenzylidene-*p*-dimethylaminoaniline and *p*-dimethylaminobenzylidene-*p*-nitro-aniline." Acta Cryst., B32: 1827-1833.
- 72 Dudley, R. J.; Mason, S. F.; Peacock, R. D. 1975. "Electronic and Vibrational Linear and Circular Dichroism of Nematic and Cholesteric Systems." J. Chem. Soc. Faraday Trans. 2, 71: 997-1007.
- 73 Bernstein, J.; A. T. Hagler, A. T. 1978. "Conformational Polymorphism. The Influence of Crystal Structure on Molecular Conformation." J. Am. Chem. Soc., 100: 673-681.
- 74 Weiss, K.; Warren, C. H.; Wettermark, G. 1971. "Cis-Trans Isomerization about the Carbon-Nitrogen Double Bond. Structures of the Isomers of N-Benzyliden-Eaniline." J. Am. Chem. Soc., 93: 4658-4663.
- 75 Bernstein, J.; Engel, Y. M.; and Hagler. A. T. 1981. "An ab Initio Study of the Conformational Energetics of N-benzylideneaniline." J. Chem. Phys., 75: 2346.
- 76 Xu, H. Y.; Sohlberg, K.; Wei, Y. 2003. "Conformation of Protonated *trans*-N-Benzylideneaniline: A Revisit.." Theochem, 634: 311-314.
- 77 Proks, V. 2005. "Modeling Substituent Dependence of the Twist and Shielding in a Series of N-[4-(nitro)benzylidene]anilines with an Inclusion of Solvent Effects." THEOCHEM, 725: 69-73.
- 78 Kozhevina, L. I.; Prokopenko, E. B.; Rybachenko, V. I.; Titov, E. V. 1993. "Interpretation of The Vibrational Spectrum of Benzylideneaniline." J. Appl. Spect., 59: 805-809.
- 79 Gaenko, A. V.; Devarajan, A.; Gagliardi, L.; Lindh, R.; Orlandi, G. 2007. "Ab Initio DFT Study of Z-E Isomerization Pathways of N-benzylideneaniline." Theor. Chem. Acc., 118: 271-279.
- 80 Smith, W. F. 1963. "Application of Molecular Orbital Theory to the Electronic Absorption Spectra of Schiff Bases." Tetrahedron: 445-454.
- 81 Wolf, A. 1980. "Non-Empirical Calculations on The Conformational Structure of Azobenzene and Benzylideneaniline." J. Mole. Struct, 67: 89-99.
- 82 Zamir, S.; Bernstein, J.; Ioffe, A.; Brunvoll, J.; Kolonits, M.; Hargittai, I. 1994. "Conformational Studies of the *N*-(3-halo-benzylidene)-3-haloaniline System. Part 2. Molecular Energetics." J. Chem. Soc. Perkin Trans. 2, 895-900.
- 83 Patnaik, L.N.; Das, S. 1985. "Conformation of P-dimethylamino-benzylidene-*p*-Nitroaniline, *p*-nitrobenzylidene-*p*-dimethyl-aminoaniline, their Stilbene and Azobenzene Derivatives." Int. J. Quantum Chem., 27: 135-144.
- 84 Norinder, U. 1987. "Theoretical Investigation of Benzylideneaniline and Salicylideneanile: An AM1 Study." Mol. Cryst. Liq. Cryst., 149: 195.

- 85 Patnaik, L. N.; Das, S. 1987. "conformation of some mono-substituted N-benzylideneanilines." Bull. Chem. Soc. Jpn., 60: 4421-4423.
- 86 Byrn, S. R.; Gruber, C. W.; Midland, S. L. 1976. "Comparison of the Solid and Solution Conformations of Methapyriline, Tripeleannamine, Diphenhydramine, Histamine, and Choline. The Infrared-X-Ray Method for Determination of Solution Conformations." J. Org. Chem., 41: 2283-2288.
- 87 Eckhardt, C. J.; Bernstein, J. 1972. "Molecular Conformation and Electronic Structure. Solid-State Spectrum of a Planar Anil." J. Am. Chem. Soc., 94: 3247-3249
- 88 Tal, R. M.; Engberts, J. B. F. N. 1976. " Folded Conformations. Part VII. Crystal and Molecular Structure of *NN'*-[bis-(α -tosylbenzyl)] Urea Acetone Solvate. Comparison between Solution and Solid-State Conformation" J. Chem. soc., Perkin Trans. 2, 483-488.
- 89 Caillet, J.; Claverie, P.; Pullman, B. 1976. " On the Conformational Varieties of Adrenaline: The Free Molecule and The Molecule in the Crystal." Acta Cryst., B32: 2740-2745.
- 90 Ahmet, M. T.; Silver, J.; Houlton, A. 1994. "Influence of Crystal Environment on Molecular Conformation: *p*-bromo-*N*-(*p*-dimethyl-amino-benzylidene)aniline." Acta Cryst., C50: 1814-1818.
- 91 Kitaigoroksdii, A. I. 1973. *Molecular Crystals and Molecules*. New York and London: Academic Press.
- 92 Molecule **2-4**: Meunier-Piret, J.; Germain, G.; Declercq, J. P.; van Meerssche, M. 1982. "Structure de la N-benzylidene-*p*-hydroxyaniline C₁₃H₁₁N." Bull. Soc. Chim. Belges, 91: 89-90.
- 93 Molecule **2-6**: Meunier-Piret, J.; Germain, G.; Declercq, J. P.; van Meerssche, M. 1982. "Structure de la N-(*p*-hydroxybenzylidene)-aniline C₁₃H₁₁NO." Bull. Soc. Chim. Belges, 91: 93-94.
- 94 Molecule **2-8**: Meunier-Piret, J.; Piret, P.; Germain, G.; Meerssche, M. V. 1972. "Structure Cristalline de la 4-nitro-4'-méthoxy-N-benzylidène-aniline." Bull. Soc. Chim. Belges, 81: 533-538.
- 95 Molecules **2-9** and **2-13**: Clegg, W; Elsegood, M. R. J.; Heath, S. L.; Houlton, A; Shipman, M. A. 1996. "Conformational Flexibility in *N*-benzylideneanilines." Acta Cryst., C52: 2548-2552.
- 96 Molecule **2-10**: Nakai, H.; Ezumi, K.; Shiro, M. 1981. "The Structures of Polymorphs of *N*-(*P*-dimethylamino-benzylidene)-*p*-nitroaniline." Acta Cryst., B37: 193-197.
- 97 Molecule **2-12**: Yang, Q. C.; Tang, Y. Q.; Yang, W. J.; Chen, H. Y. 1998. "N-(3-nitrobenzylidene)-*p*-phenylene-diamine." Acta Cryst., C54: 1532-1534.
- 98 Molecule **2-14**: Destro, R.; Gavezzotti, A.; Simonetta, M. 1978. "Salicylideneaniline." Acta Cryst., B34: 2867-2869.
- 99 Molecule **2-15**: Bregman, J.; Leiserowitz, L.; Schmidt, G. M. J. 1964. "Topochemistry. Part IX. The Crystal and Molecular Structures of *N*-5-chloro-salicylideneaniline Near 90 and 300°K." J. Chem. Soc., 2068-2085.
- 100 Molecule **2-16**: Bregman, J.; Leiserowitz, L.; Osaki, K. 1964. "Topochemistry. Part X. The Crystal and Molecular Structures of 2-chloro-*N*-salicylideneaniline." J. Chem. Soc., 2086-2100.
- 101 Molecule **2-17**: Elerman, Y; Elmali, A; Atakol, O.; Svoboda, I. 1995. "N-(2-Hydroxyphenyl)salicylaldimine." Acta Cryst., C51: 2344-2346.
- 102 Molecule **2-17**: Mukherjee, A. K.; De, R. L.; Banerjee, I.; Samanta, C.; Nayak, N. P. 1999, "6-[*N*-(2-hydroxyphenyl)aminomethylene]cyclo-hexa-2,4-dien-1-one." Acta Cryst., C55: 407-410
- 103 Molecule **2-18**: Kwiatkowski, M.; Kwiatkowski, E.; Olechnowicz, A.; Kosáciuszko-Panek, B.; Ho, D. M. 1994. "Crystal and Molecular Structure of N-salicylidene-1,2-diaminobenzene." Polish. J. Chem., 68: 85.
- 104 Molecule **2-20**: Zhang, D. C. 2002. "The effect of Molecular Planarity on Crystal Non-Centrosymmetry in Benzylideneaniline Derivatives." Acta Cryst., C58: o351-o352.
- 105 Molecule **2-21**: Surma, K.; Jaskólski, M.; Kosturkiewicz, Z.; Oszczapowicz, J. 1988. "Structure of *N*-*p*-nitrophenylbenzamidine." Acta Cryst., C44: 1031-1033.
- 106 Katritzky, A. R.; Ramsden, C. A.; Joule, J. A.; Zhdankin, V. V. 2010. *Handbook of Heterocyclic Chemistry*, Third edition. Amsterdam: Elsevier.
- 107 Lister, J. H. 1996. *The Chemistry of Heterocyclic Compounds, The Purines: Supplement 1 (Chemistry of Heterocyclic Compounds: A Series of Monographs)*, Volume 54. New York: John Wiley & Sons.
- 108 Chen, C. H.; Hsu, Y. C.; Chou, H. H.; Thomas, K. R. J.; Lin, J. T.; Hsu, C. P. 2010. "Dipolar Compounds

- Containing Fluorene and a Heteroaromatic Ring as the Conjugating Bridge for High-Performance Dye-Sensitized Solar Cells." Chem-A Euro. J. 16: 3184-3193.
- 109 Metzger, J. V. 1979. *Thiazole and its derivatives, Part one*. New York: John Wiley & Sons.
- 110 <http://www.nature.com/articles/srep05775/figures/11>
- 111 https://en.wikipedia.org/wiki/Hydrogen_bond#Structural_details

CHAPTER 3

CONSTRUCTION OF LFMO BASIS SET

ABSTRACT

As the first step to construct a LFMO (absolutely localized fragment molecular orbital) basis set, a non-planar molecule such as N-benzylideneaniline should be dissected into three planar fragments: Ph– (A), –N=CH– (B), and Ph– (C). Then our program provides a sub-LFMO basis set $\{\psi_i^P\}$ ($P = A, B, C$) for each fragment. The construction of a sub-LFMO $\{\psi_i^P\}$ is a five-step procedure that includes the Kost's localization and the conditional single-point energy calculation. In the Kost's localization, the singly occupied FMO φ_{k}^{H-s} of a reference hydrogen atom is used as a reference FMO to localize the singly occupied FMO φ_k^{P-s} of a specific fragment P, which ensures the correct electronic occupancy of the singly occupied FMO of a fragment P. The use of reference hydrogen atom simplifies the procedure of Kost's localization, and it ensures the correct direction of singly occupied FMO φ_k^{P-s} in the space. At last, the superposition of three sub-LFMO basis sets leads to the formation of a LFMO basis set $\{\Psi_i\}$. In the LFMO basis set, π and σ FMOs are completely separated out. Each LFMO is absolutely localized on its corresponding fragment, and has a correct electronic occupancy.

yuzh@iccas.ac.cn

Key words: absolutely localized fragment molecular orbital basis set; Kost's localization; conditional single-point energy calculation; singly occupied FMO; separation of π and σ FMOs.

3.0. FOREWORDS

In the second chapter, it has been detailed that the electronic interaction is the driving force for distorting NBA-like species. However, the driving force should refer to the interaction force between the fragments. It should also be emphasized that all NBA-like species are non-planar. In order to further get insight into the role of the electron (or orbital) interaction and to understand the nature of conjugation, therefore, it is necessary to construct a fragment molecular orbital (FMO) basis set in which the π and σ FMOs are absolutely localized and are completely separated. This type of FMO basis set is, hereafter, abbreviated as LFMO basis set.¹⁻²⁰ Before discussing how to build a LFMO basis set, we first briefly review the literature methods of constructing a FMO basis set, and their developments.

In 1959 when the quantum chemistry is over 30 years old, as spoken by Coulson at the conference banquet on June 26, 1959,²¹ theoretical chemists was being split into two parts that were almost alien to each other. For the first part of the quantum chemists, their desire was to calculate exactly, and they were ready to give up all conventional chemical concepts in their calculation results in order to achieve this goal. For the quantum chemists of second part who are called theoretical organic chemists in this section, their representatives argued that organic chemistry is the discipline of experimentally studying the interactions between the functional groups,²²⁻²⁷ and the experimental results are to build a structural theory around fairly elementary concepts. The quantum chemists should understand these concepts and demonstrate the basic characteristics of chemical behaviors, and They should try to relate the calculated data to the following different concepts and theories: resonance, conjugation, hyperconjugation, inductive effect, aromaticity and anti-aromaticity, acid and alkali theory, charge- and electron-transfer, substituent directing effect, reaction mechanisms, etc. For example, quantum chemistry should help the chemists to understand why the UV (ultraviolet) absorption usually shifts to the red when one more vinyl group is added to a conjugated chain. But the molecular orbital (MO) calculations can't provide any valuable information for the interactions between the functional groups. As far as complex wave functions are concerned, the physical picture of chemical bonds cannot inspire the imagination of chemists at all. Therefore, Coulson (1952) appealed to the theoretical chemical community: "give us insight not numbers" in his famous after dinner speech of the conference held in Boulder, Colorado.^{28,29} In the 22nd year after Coulson's speech, Hoffman (1974) also said: "The arrival on the contemporary scene of good molecular orbital calculations, semiempirical and ab initio, on chemically realistic systems has hardly created the heralded millennium of understanding of chemical processes."²⁷

In the 1960s, thus, Chemists are very concerned about the intermolecular cycloaddition reaction and about the explanation of their mechanisms. In the meantime, the spectral behavior and the structure of the excimers of aromatic molecules excited the curiosity of physical chemists and organic chemists. Only based on the resonance interaction between the interacting molecules, as found in the fluorescence of benzene excimers in solution,³⁰ experimental spectral shift is not fully understood, and the orbital overlap needs to be introduced.^{31,32} A direct molecular orbital approach, including all π electrons of the two systems, may be a more adequate method.³² In that time, there was no difficulty, in principle, in extending the Hoffmann's extended Hückel theory to the interaction of two molecules.^{33,34} However, as emphasized by Salem in 1967,³⁵ "the numerical resolution of a large secular equation does not provide any information on the important atom-atom or orbital-orbital interactions, nor on the interaction energy as a function of the various atomic overlaps." In order to develop a theory by which the interaction energy between two conjugated molecules can be explicitly expressed as a function of the various atomic orbital overlaps, Salem (1967) derived the Equations (3-I) and (3-II). In these two Equations, the two-electron stabilization energy ΔE_{ij}^2 and four-electron destabilization energy ΔE_{ij}^4 are expressed as the function of the following variables related to two interacting MOs: MO overlap integral matrix element S_{ij} , one-electron Hamiltonian matrix element H_{ij} , and energy levels, ε_i and ε_j (and their average ε_o), of the two MOs.³⁵

$$\Delta E_{ij}^{(2)} = 2(H_{ij} - \varepsilon_i S_{ij})^2 / (\varepsilon_i - \varepsilon_j) \quad (3\text{-I})$$

$$\Delta E_{ij}^{(4)} = 4(\varepsilon_o S_{ij}^2 - H_{ij} S_{ij}) / (1 - S_{ij}^2) \quad (3-II)$$

The expressions can also take the following forms:

$$\Delta E_{ij}^{(2)} = 2 S_{ij}^2 (k - \varepsilon_i)^2 / (\varepsilon_i - \varepsilon_j), \quad k = -39 \text{ ev} \quad (3-III)$$

$$\Delta E_{ij}^{(4)} = 2 S_{ij}^2 (\varepsilon_o - k) / (1 - S_{ij}^2), \quad \varepsilon_o = (\varepsilon_i + \varepsilon_j) / 2 \quad (3-IV)$$

Since then, the Salem's equations are used in various fields of organic chemistry,³⁶⁻⁴⁵ including cycloaddition reactions.⁴⁶⁻⁴⁸

If the two orbitals contain two or three electrons, as shown by Equation (3-I), the interaction will be stabilization. Of the stabilizing terms, those arising from the interaction between the HOMO of one molecule and the LUMO of the second molecule will dominate energy changes, and their importance is invincibly evident,⁴⁹⁻⁵² since these orbitals are closest in energy. This frontier molecular orbital theory advocated first by Fukui.⁵³ Gradually, the frontier molecular orbital theory was found to be more extensive.⁵⁴⁻⁵⁷ Woodward and Hoffmann independently realized that chemical transformations could be approximately predicted from subtle symmetries and asymmetries in the electron "orbitals" (frontier molecular orbitals) of complex molecules, and developed the Woodward–Hoffmann rules.⁵⁸ This rule is very helpful for understanding and predicting chemical reactions (especially pericyclic reactions) and for predicting different outcomes under the different reaction conditions. For dimerization of cyclobutadiene, for example, examination of secondary orbital interactions, along with the symmetry of HOMO and LUMO, reveals that the *endo* process, leading to the *syn* dimer, should be favored over the *exo* dimerization.^{57,59,60}

However, when explaining the effect of the interaction between groups on molecular properties, the use of frontier MO theory has significant limitation. The conformation and configuration of organic molecules are determined by many structural factors. Usually, they depend on the steric effect. In 1936, based on the experimental fact that the hydrogenation heat (-27.6 kcal/mol) of trans-2-butene is more stable by 1 kcal/mol than that (-28.6 kcal/mol) of cis-2-butene,^{23,61} as concluded by Kistiakowsky, the two methyl groups of 2-butene repel each other.⁶² Afterwards, a large number of experimental facts seem to prove that a crowded structure is not energetically favorable, which has become a fundamental principle of organic chemistry. However, with the development of spectroscopic techniques, it is a common phenomenon that, for 1,2-disubstituted ethylenes XHC=CHY, the cis-configuration is more stable than the trans-configuration.^{63,64} For 1,2-difluoroethylene, for example, the cis-isomer content is 63%.⁶⁵ Hartree-Fock calculations theoretically conformed that the cis-isomer is more stable than trans-isomer, but it cannot interpret why, in 1,2-difluoroethylene, two fluorine atoms are attractive.⁶⁶

Based on Equations (3-I) to (3-IV), Epotis developed the non-bonded interaction theory.⁶⁷ In 1,2-difluoroethylene, for example, the non-bonded interaction between two fluorine atoms may play an important role in determining the cis configuration.^{67,68} Epotis's non-bonded interaction theory can be considered as a great contribution to the development of organic chemistry theory. The Equation (3-I) and Equation (3-II) were also used by Houk to explain the effects of the substituents on the regioselectivity and reactivity in the 1,3-dipolar Cycloaddition reaction of azides and dipolarophile.⁶⁹

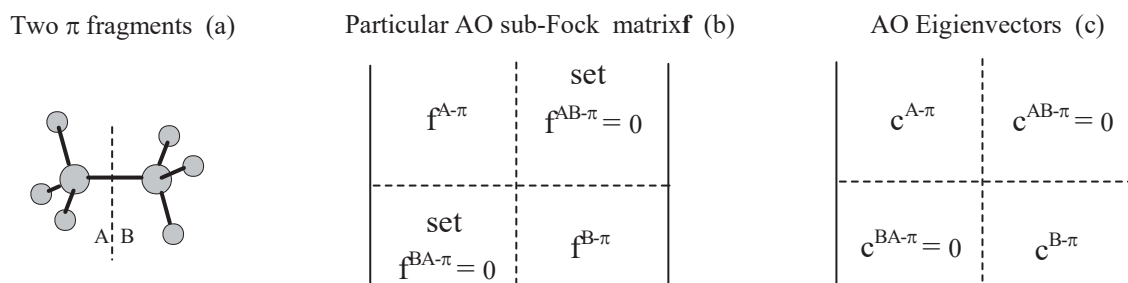
In fact, the establishment of the PMO (Perturbation molecular orbital) method should be attributed to Coulson and Longuet-Higgin (1947-1948).⁷⁰⁻⁷³ With Dewar's efforts, the qualitative PMO theory has been applied to various fields of organic chemistry. As a result, the relationships between the molecular structure and its properties can be described numerically,⁷⁴⁻⁸¹ although these descriptions are still qualitative.

In a series of (CH₃)₂X molecules (X = CH, O, S, C=O, C=CH₂), the molecular conformation depends upon the π - π , σ - σ and π - σ interactions between the groups Me- and MeX-, or between the group X and (Me)₂. In three-dimensional space, only relying on the interactions between two pairs of frontier molecular orbitals can't reveal the structural factors that determine molecular conformation. In order to understand the driving force for distorting the

conjugated molecule, Whangbo, Schlegel, and Wolfe (1977) established the quantitative PMO method, and meanwhile they made an attempt to provide a fragment molecular orbital (FMO) basis set for a conjugated molecule, which is called the WSW procedure.^{82,83} Afterwards, the quantitative PMO procedure is used to calculate the energy effect associated with the $\pi\text{-}\pi$, $\sigma\text{-}\sigma$ and $\pi\text{-}\sigma$ MO interactions between the fragments and to analysis the roles of the sums of two- and four-electron interactions in determining the preferential conformation of a molecule.⁸²⁻⁹⁰

The PMO analysis always begins with a dissection of the molecule into fragments. In order to analysis the roles of the two- and four-electron interactions in determining the preferential rotational geometry of ethane $\text{CH}_3\text{-CH}_3$, for example, the first step of the WSW procedure (Scheme 3-Ia) is to dissect ethane into fragments A (methyl group) and B (methyl group). Then, the MOs and their orbital energies of the fragments A and B are obtained from the single-point energy calculation that is performed on ethane under the conditional settings detailed in Scheme 3-Ib. However, the WSW procedure can only be used to provide a planar conjugated molecule with the following three sub-sets of the closed-shell MOs (i.e. the breaking of the single bond between fragments A and B is not involved):

- (i) two sub-sets of π MOs are localized, absolutely and respectively, on the fragments A and B (Scheme 3-Ic)
- (ii) a sub-set of σ MOs are still delocalized on the whole molecular framework.



Scheme 3-I

The use of Equations (3-I) to Equation (3-IV) is based on that every FMO has a correct electron occupancy. In the case of the opened-shell FMOs (i.e. the breaking of the single bond between two fragments is involved), as indicated by Bernardi and Bottini,^{86,91} the WSW procedure can't ensure that each FMO, absolutely localized on a specific fragment (A or B), has the correct electronic occupancy. In 1981, Bernardi and Bottini improved the WSW procedure.⁸⁶ The improved WSW procedure, i.e. the WSW procedure followed by localization of FMOs, provides each fragment with a set of localized FMOs that are orthogonal and have correct electronic occupancies. In the improved WSW procedure, the Boys' method^{92,93} is used to localize the singly occupied FMOs arising from the breaking of the single bond between the fragments A and B. In the case of non-planar conjugated molecule, however, the improved WSW procedure can't ensure that the π and σ FMOs are completely separated.

NBA-like species are the non-planar molecules. The $\pi\text{-}\pi$, $\sigma\text{-}\sigma$ and $\pi\text{-}\sigma$ orbital interactions should be involved in order to get insight into the driving force of molecular distortion. For a non-planar conjugated molecule, one of the largest computational problems is how to provide a MO basis set in which the π and σ FMOs are localized and separated. (the phrase “a molecular orbital basis set in which the π and σ FMOs are localized and separated” is shortened to the phrase “localized $\pi\text{-}\sigma$ MO basis set”). Keep in mind, LFMO and “localized $\pi\text{-}\sigma$ MO” are two different basis sets. In the LFMO basis set, π and σ FMOs are absolutely localized and completely separated.

At present, only our method¹⁻²⁰ and the NBO method⁹⁴ can provide a localized $\pi\text{-}\sigma$ MO basis set for a conjugated molecule. As discussed in our previous works and will be detailed in this and next chapters, the localization degree of the NBOs is low,^{19,20} and the separation of the π and σ NBOs is incomplete. Therefore, the NBO basis set can't be used to partition the total electronic energy into the π and σ parts. On the contrary, our method can

Table 3-1. Three Occupied π -NBOs (LCAO) for the $\theta = 17^\circ$ Conformation of N-benzylideneaniline at MP2/6-311G Level.

AO	Atoms	^a AOs	3-th NBO	17-th NBO	22-th NBO
			C1-C6	N12-C13	C15-C20
3.6280*					
Fragment A					
5	C1	pz	0.1817	-0.0245	0.0010
9	C1	pz	0.3379	-0.0607	0.0020
13	C1	pz	0.2617	-0.0311	-0.0003
22	C2	pz	-0.0596	0.0033	0.0012
35	C3	pz	0.0001	0.0021	-0.0002
36	C3	s	0.0070	0.0059	-0.0022
48	C4	pz	0.0014	0.0010	0.0000
49	C4	s	0.0014	-0.0021	-0.0003
61	C5	pz	-0.0615	0.0021	0.0000
62	C5	s	0.0053	-0.0022	-0.0009
70	C6	pz	0.1733	0.0024	-0.0004
74	C6	pz	0.3165	0.0035	-0.0004
75	C6	s	-0.0058	0.0242	-0.0008
78	C6	pz	0.2918	-0.0078	0.0013
Fragment B					
98	N12	pz	-0.0260	0.1915	0.0030
99	N12	s	0.0025	-0.0135	-0.0002
102	N12	pz	0.0497	0.3224	0.0066
103	N12	s	0.0122	-0.0053	-0.0017
106	N12	pz	-0.0419	0.3028	-0.0010
111	C13	pz	-0.0005	0.1510	-0.0220
112	C13	s	0.0016	-0.0161	0.0000
115	C13	pz	-0.0001	0.2698	-0.0556
116	C13	s	0.0117	0.0323	-0.0022
119	C13	pz	0.0032	0.2299	-0.0340
Fragment C					
127	C15	pz	0.0005	-0.0205	0.1740
131	C15	pz	0.0010	-0.0511	0.3235
132	C15	s	-0.0050	-0.0167	0.0014
135	C15	pz	-0.0020	-0.0495	0.2683
192	C20	pz	-0.0002	0.0025	0.1625
196	C20	pz	-0.0003	0.0050	0.2925
197	C20	s	-0.0035	-0.0140	0.0021
200	C20	pz	0.0005	-0.0049	0.2750

*Electronic occupancy; All AO coefficients are not equal to zero, and only typical AO coefficients are presented in order to shorten the Table.

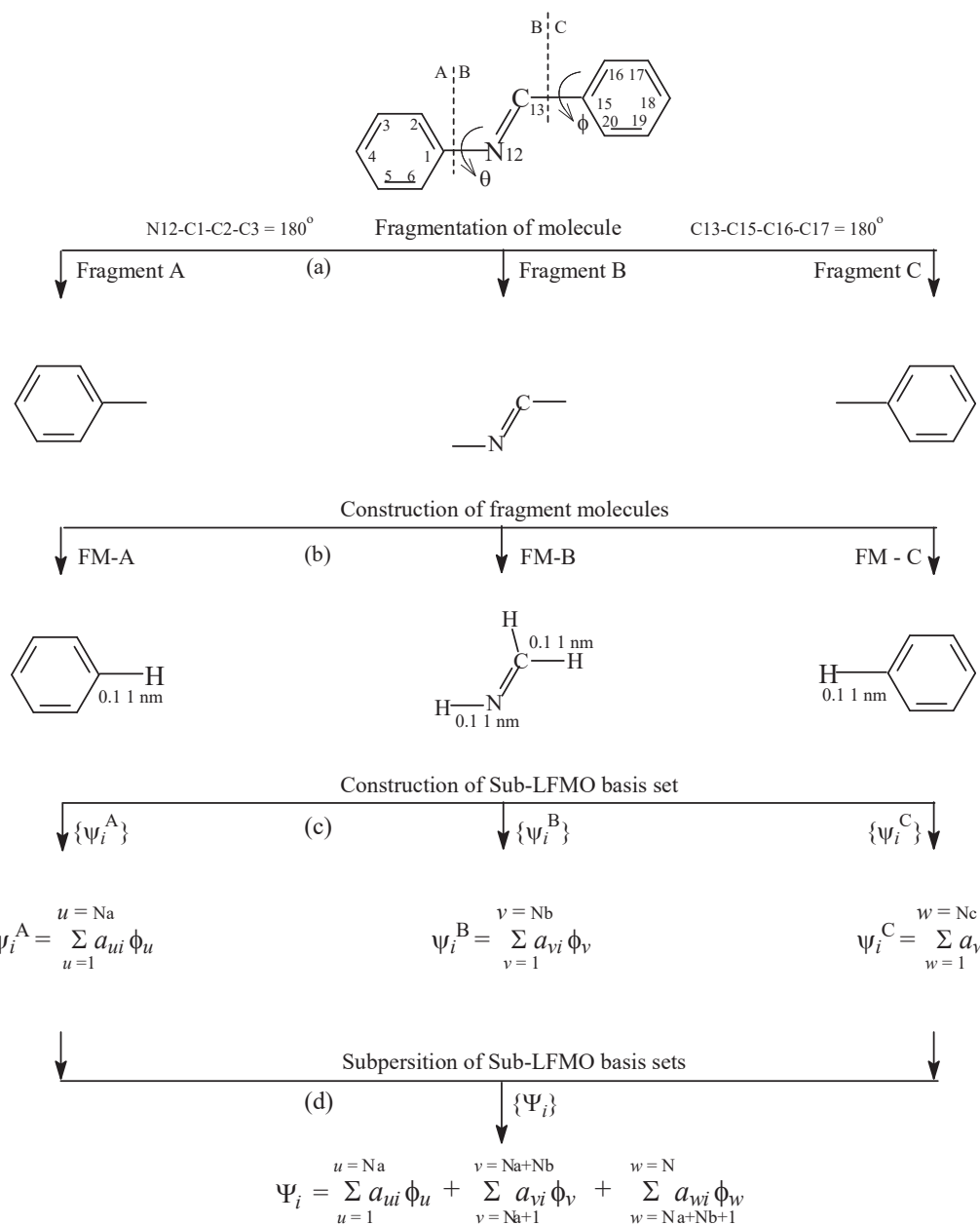


Figure 3-1. A multi-step procedure of constructing LFMO basis set for N-benzylideneaniline

provide a LFMO basis set for a conjugated molecule, no matter whether a conjugated molecule is planar or not.

3.1. INTRODUCTION

The concept of "natural" orbitals was first introduced by Löwdin in 1955,⁹⁵ and the calculation program was established and improved by Frank Weinhold.⁹⁶ NBO 5.0 program has entered the Gaussian-X and Gamess

packages. It is now recognized as the program of localizing molecular orbitals, and has been widely used in many fields of organic chemistry. It's time for the NBO method to be seriously criticized.

NBO can be expressed as a linear combination of atomic orbitals (LCAO), and can also be expressed as a linear combination of natural atomic orbitals (LCNAO). LCNAO can be used to distinguish between the π and σ NBOs. The three NBOs of π -type for the $\theta = 17^\circ$ conformation of N-benzylideneaniline are listed in Table 3-1, and the numbering of atoms is shown in Figure 3-1.

In accordance with the AO coefficients in Table 3-1, three fundamental shortcomings of NBOs can be found. For a NBO, First, the AO coefficients are only concentrated on a specific chemical bond or on a specific atom, and the AO coefficients of all other atoms are not equal to zero. For the 3-th NBO of N-benzylideneaniline, for example, the p_z coefficients of the first and sixth carbon atoms are, respectively, 0.1817, 0.3378 and 0.2617 (C1), and 0.1733, 0.3615 and 0.2918 (C6). All other AO coefficients are less than 0.01, but not equal to zero. Therefore, the third NBO of N-benzylideneaniline can be considered as a π -type NBO of C(1)-C(6) bond whose the coefficients of p_z AOs are concentrated on the C(1)-C(6) bond, but it is not absolutely localized on the C(1)-C(6) bond.

The so-called π and σ MOs refer to the symmetry of molecular orbitals. The π MOs are perpendicular to the framework of the planar fragment. For a π MO, therefore, the s AO coefficients should be equal to zero. In the three π -NBOs listed in Table 3-1, all the s AO coefficients are not equal to zero, and the s AO coefficient of the C(13) atom in the 17th NBO is large, up to 0.0323. As the second shortcoming of NBOs, therefore, it is impossible for π and σ NBOs to be completely separated out in the case of non-planar molecule. Just due to the two shortcomings, as will be detailed in the next chapter, NBO method cannot be used for the π - σ energy decomposition.

In the NBO energy analysis, due to NBOs are orthogonal, only two-electron interaction energy can be calculated and the four-electron interaction energy is always equal to zero, according to Equation (3-I) and Equation (3-II). In addition, as the third shortcoming, the electronic occupancies of NBOs are not correct. For example, the electronic occupancy of the 3th NBO is 1.6280. In this sense, the NBO basis set does not meet the basic requirements of the PMO theory.

Perkins' method (1982) can also be used to localize MOs.⁹⁷ After Pekins' localization, the AO coefficients of the localized MOs are concentrated on their respective bonds, which is similar to the NBO method. But there is a great difference between the NBO and Perkins methods: for the π MOs, the Perkins' localization is invalid.

Before gaining new insight into the nature of electron delocalization, we define the following three energy effects:

$\Delta E^{\pi-\pi}(\theta)$: an energy effects associated with the π - π LFMO interaction between fragments A and (B+C) (Figure 3-1);

$\Delta E^{\sigma-\sigma}(\theta)$: an energy effect associated with the σ - σ LFMO interaction between the two fragments;

$\Delta E^{\pi-\sigma}(\theta)$: an energy effect associated with the MO interaction between the π and σ systems

As indicated in the Chapter 2, due to the presence of the π - σ interaction in the non-planar molecule such as (N-benzylideneaniline (NBA), it can't be asserted that a particular type of MO interaction, such as the π - π and σ - σ interactions, is destabilization only based on that $dE_e(\theta)/d(\theta) < 0$ ($0 < \theta < \theta_{e-min}$). In order to gain new insight into the nature of electron delocalization, it is necessary to construct the following four localized electronic states using the single-point energy calculations that are performed, over the LFMO basis set and under the conditional settings, on the optimized geometry of a specific molecular conformation:

- (i) π electrons (π -MOs) are localized on their respective fragments, and the σ electrons are delocalized over the whole molecular framework. This localized electronic state is denoted as the DSI electronic state.
- (ii) σ electrons (σ -MOs) are localized on their respective fragments, and the π electrons are delocalized over

the whole molecular framework. This electronic state is denoted as the DPI electronic state.

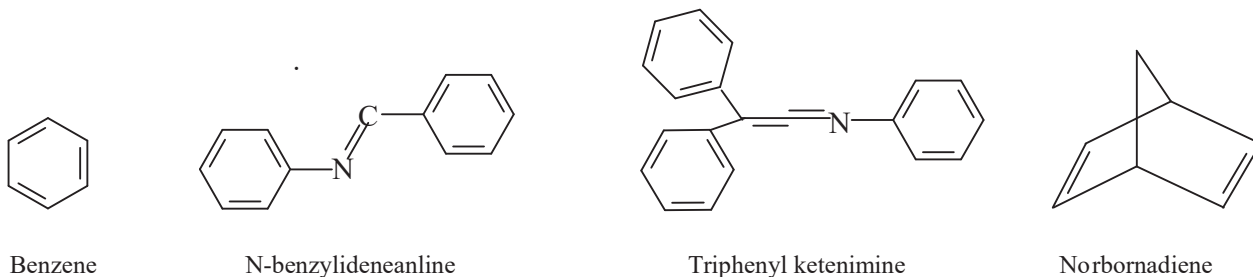
- (iii) π and σ electrons (π - and σ -MOs) are all delocalized over the whole molecular framework, but the FMO interactions between π and σ systems are set equal to zero. This electronic state is denoted as FUD electronic state.
- (iv) π and σ systems both are localized on their respective fragments. This electronic state is denoted as the FUL electronic state.

For a non-planar conjugated molecule, the LFMO basis set must be used to construct the localized electronic states, so the main issue is how to create the LFMO base set.

3.2. CONSTRUCTING LFMO BASIS SET

According to molecular configuration and conformation, conjugated molecules (not including polyenes) can be divided into four categories (Scheme 3-1). The first category is cyclic aromatic compound such as benzene. The second category is the flexible conjugated molecules, such as N-benzylideneaniline, that can be distorted. The third category includes the conjugated molecules having the accumulated double bonds, such as triphenyl ketenimine. The fourth category refers to the rigid non-planar conjugated molecules such as norbornadiene.

The purpose of this chapter is to create a new calculation program. This program is a multi-step calculation procedure (Figure 3-1), and it can provide a LFMO basis set for any conjugated molecule, whether the molecule is planar or non-planar. The first step of the procedure is to dissect a conjugated molecule into several planar fragments. The second step is to construct a sub-LFMO basis set for each fragment. In each sub-LFMO basis set, the π and σ MOs are completely separated. The sub-LFMO basis set of each fragment P (P = A, B, C.....) is denoted as $\{\psi_m^{P-\pi}, \psi_n^{P-\sigma}, \psi_k^{P-s}\}$. The third step is the superposition of the sub-LFMO basis sets to form the LFMO basis set $\{\Psi_m^{P-\pi}, \Psi_n^{P-\sigma}, \Psi_k^{P-s}\}$ of the whole molecule.



Scheme 3-1

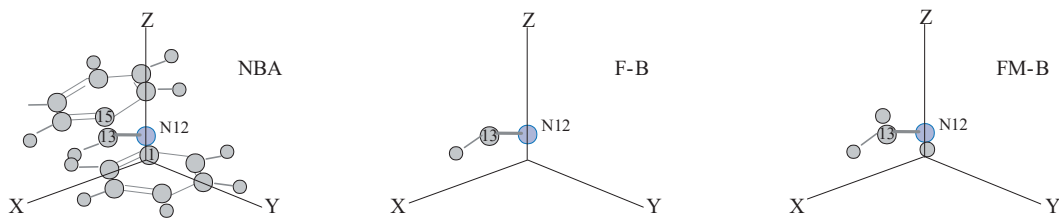
3.2.1. Fragmentation of a Molecule

In the WSW procedure, the conditional SCF-MO calculation (Scheme 3-1b) provides a set of FMOs for a molecule. In this set of FMOs, as shown by Scheme 3-1c, two sub-sets of π FMOs are absolutely localized on their respective fragments A and B. In this case, so called fragments A and B refer to two diagonal blocks of an AO Fock matrix, and do not mean that the molecular framework itself is dissected into two separated fragments (free radicals) A and B.

In a non-planar conjugated molecule such as N-benzylideneaniline twisted by θ , the boys' localization after the

Table 3-2. The Cartesian Coordinates of the Atoms, Respectively, in Fragment B and Fragment Molecule FM-B Are the Same as Those of the Corresponding Atoms in N-benzylideneaniline Twisted By $\theta = 17^\circ$.

Atoms	Molecule			Atom	Fragment B			Fragment molecule FM-B			
	X	Y	Z		X	Y	Z	Atom	X	Y	Z
Fragment A											
C1	0.00000	0.00000	0.00000					H	-.17896	-.25152	.00000
Fragment B											
N12	-0.81669	-1.14779	0.00000	N12	-.81670	-1.14781	.00000	N12	-.81670	-1.14781	.00000
C13	-0.36886	-2.30079	-0.31592	C13	-.36886	-2.30083	-.31592	C13	-.36886	-2.30083	-.31592
H14	0.67606	-2.47270	-0.60669	H14	.67606	-2.47275	-.60670	H14	.67606	-2.47275	-.60670
Fragment C											
C15	-1.21464	-3.49990	-0.31777					H	-1.00290	-3.19974	-.31731



WSW procedure still can't ensure that the π and σ FMOs are completely separated and that the singly occupied FMOs have the correct directions in the space. Therefore, as done in our method, it is necessary for the molecular framework itself, rather than for Fock matrix, to be dissected into several separated fragments. Afterwards, as done by the Kost,⁸⁵ the singly occupied MO of a referential hydrogen atom is used as a referential MO to localize the singly occupied FMO(s) of each molecular fragment. The principle of Kost's localization is as follow.

$$\sum_{l=1}^k (S'_{l,k-s}^2 + S'_{l,i}^2) = \sum_{l=1}^k (S_{l,k-s}^2 + S_{l,i}^2) \quad (3-1)$$

In the subscript of symbol " $S_{l,k-s}$ ", "s" means that $S_{l,k-s}$ is the MO overlap integral matrix element between the singly occupied FMO φ_k^{P-s} of fragment P ($P = A, B, \dots$) and the singly occupied FMO φ_l^{Q-s} of fragment Q ($Q = A, B, \dots, P \neq Q$). Two singly occupied FMO, φ_k^{P-s} and φ_l^{Q-s} , resulted from breaking of the single bond between the molecular fragments P and Q. S_{li} is the overlap integral between the FMOs φ_l^P of fragment P and the singly occupied FMO φ_l^{Q-s} of fragment Q; φ'_k^P and φ'_k^{P-s} are the FMOs of fragment P after localization.

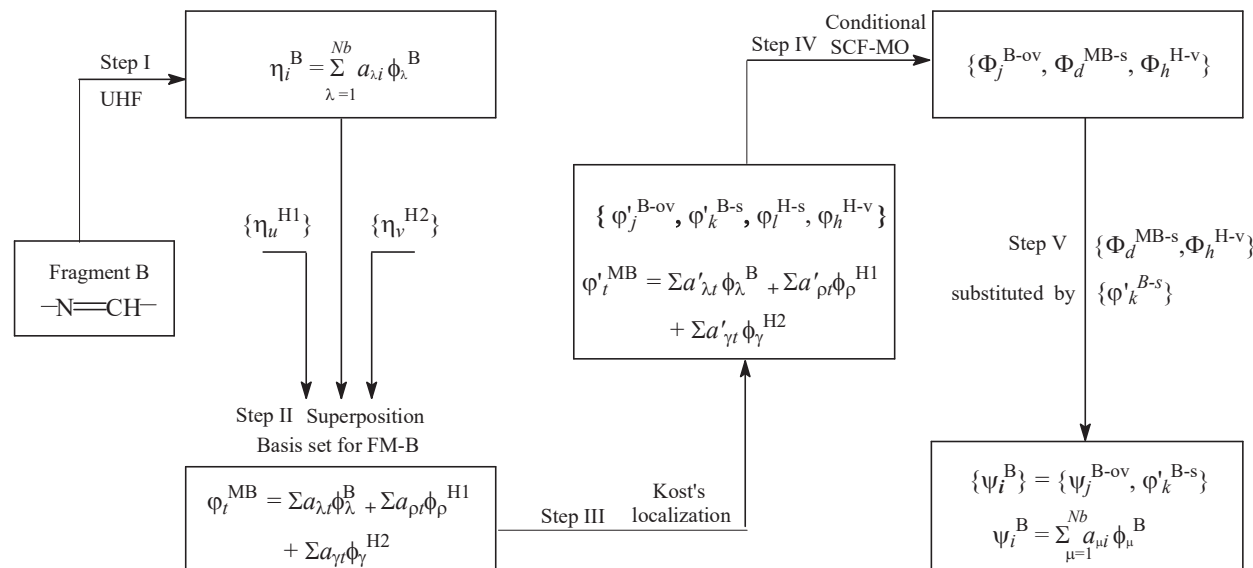
Fragmentation of a conjugated molecule should follow two requirements. First, the fragment way must be able to meet the needs of calculating delocalization energy. In order to understand the role of electron delocalization in determining the conformation of N-benzylideneaniline, for example, the molecule must be dissected into two fragments P and Q ($P = A, Q = (B+C)$) (Figure 3-1a). Second, each fragment must be planar to ensure that the π and σ FMOs can be completely separated. In accordance with Figure 3-1, the A-(B+C) fragmentation way produces the fragments A and (A + B). But the fragment (B+C) is non-planar, so it must be further dissected into two planar

fragments B and C (the A-B-C fragmentation way in Figure 3-1). The related computational programs must ensure:

- (i) The cartesian coordinates of all atoms in the fragments and fragment molecules (except for reference hydrogen atoms H), such as cartesian coordinates of the N(12), C(13) and H(14) atoms in fragment B and fragment molecule FM-B (Table 3-2), are the same as those of the corresponding atoms in the whole molecule.
- (ii) In the fragment molecule, such as FM-B, two referential hydrogen atoms are bonded, respectively, to the N(12) and C(13) atoms, forming two single bonds N(12)-H and C(13)-H. In space, these two bonds must overlap, respectively, with the C(1)-N(12) and C(13)-C(15) bonds in the whole molecule, and their bond lengths are set equal to 0.11 nm (Figure 3-1b).

As will be shown in the next section, the use of the referential hydrogen atoms greatly simplifies the method of localizing molecular orbitals. But the use of Gaussian basis set should be limited as follows: the referential hydrogen atom can only contain s-type atomic orbitals. For example, can only use 6-31G(d), 6-311G(d) basis sets, can't use the basis sets 6-31G(d,p) and 6-311G(d,p), etc.

3.2.2. Sub-LFMO Basis Set for Fragment B



Scheme 3-2

For fragment B ($-N=CH-$) of the $\theta = 17^\circ$ conformation of N-Benzylideneaniline, for example, the construction of its sub-LFMO basis set is a five-step procedure (Scheme 3-2). In this procedure, the single-point energy calculation in Step I and Step IV is performed using the PC GAMESS Version⁹⁸ of GAMESS (US) QC package⁹⁹ that has been improved in our research group. The other steps are performed using our calculation programs.

In order to ensure that the Cartesian coordinates of all atoms in a fragment and fragment molecule are the same as the Cartesian coordinates of the corresponding atoms in the entire molecule, the following points must be kept in mind and are also particularly important:

- (i) In the input data file of PC-Gamess, the coordinates of the atoms must be the cartesian coordinates.
- (ii) During the single-point energy calculation, “symmetry” should be turn off, or should not be called to ensure that the cartesian coordinates of the atoms are kept unchanged.

Table 3-3. For Fragmental Molecule FM-B at MP2/6-31G* Level, Typical MOs, $\phi_m^{B-\pi}$, ϕ_k^{B-s} and ϕ_l^{H-s} before (Regular Font Date) and after (*Italic Font Data*) Kost's Localization.

3.2.2.1. Opened-Shell MOs for Fragment B

At the first step, a set of opened-shell MOs, denoted as $\{\eta_i^B\}$, is obtained from the single-point energy calculation on the fragment B at the theoretical level such as UMP2/6-31G* or UB3LYP/6-31G*, and they can be expressed as following linear combination of AOs ϕ_λ :

$$\eta_i^B = \sum_{\lambda=1}^{Nb} a_{\lambda i} \phi_\lambda \quad (3-2)$$

In a Similar way, a set of opened shell MOs, $\{\eta_j^H\}$, for a reference hydrogen atom is as follow:

$$\eta_j^H = \sum_{\rho=1}^{Nh} a_{\rho j} \phi_\rho \quad (3-3)$$

In the π MOs, $\eta_m^{B-\pi}$, at the UMP2/6-31G* level, as shown by the AO coefficients of 7-th η_i^B (Table 3-3), all the coefficients of s AOs are less than 10^{-10} , and it can be considered to be equal to zero. In $\{\eta_i^B\}$ at UMP2/6-31G* level, therefore, the π and σ MOs are completely separated. At the UB3LYP/6-31G* level, however, the single-point energy computation can't ensure that the π and σ MOs are completely separated. For the π MOs $\eta_m^{B-\pi}$ in Table 3-3-2 (presented in Appendix), for example, their s AO coefficients may be large, up to 3×10^{-6} , and can't be considered equal to zero although the MOs can be considered as the π MOs.

The Fragment B is formed by the breaking of the C(1)-N(12) and C(13)-C(15) bonds. As the literature (1982)^{86,91} pointed out that the breaking of the single bonds will cause the mixture between a newly formed singly occupied MO and the doubly occupied and vacant MOs. As the results, the electronic occupancies of the doubly occupied MOs are less than 2, those of the singly occupied MOs are not equal to 1, and the vacant MOs have non-zero electronic occupancy. Our calculations show that neither MP2 nor B3LYP calculations can ensure that all molecular orbitals have the correct electronic occupancies. At UB3LYP/6-31G* level, for example, the electronic occupancies of two singly occupied MOs are 0.88486 and 0.89621.

In addition, the SCF-MO calculation on fragment also can't ensure that the newly formed singly occupied MOs have the correct orientation in space. These problems can be satisfactorily solved through the localization of the opened-shell MOs.

3.2.2.2. Construction of MO basis set for FM-B

Inspired by Kost-Wolfe method,⁸⁵ we have developed a program of localizing MOs. In the opened-shell MOs, $\{\eta_i^B\}$ of fragment B, the occupied and vacant MOs, η_j^{B-ov} , have been partly mixed into the singly occupied MO η_k^{B-s} . The purpose of localizing MOs is to exclude these compositions from the singly occupied MOs η_k^{B-s} by maximizing the overlap integral between the singly occupied MO of fragment B and the singly occupied MO of a reference hydrogen atom. After localization, there is no need to worry about whether the other MOs of fragment B have the correct electronic occupancies.

In the fragment molecule FM-B, when the singly occupied MO of a reference hydrogen atom is used to localize the singly occupied MO of fragment B, as shown in our practical calculations, the biggest advantage are as follows:

- (i) Greatly simplifying the calculation procedure.
- (ii) In the MOs of the referential hydrogen atom, the AO coefficients are independent on the spatial position of the hydrogen atom. So, after localizing, the singly occupied MOs of fragment B will get the most reasonable

spatial orientation possible.

Before localization, the MOs $\{\eta_i^B\}$ (a $N_b \times N_b$ matrix) of fragment B and the MOs $\{\eta_u^{H1}\}$ and $\{\eta_v^{H2}\}$ ($N_h \times N_h$ matrix) of two reference hydrogen atoms should be superimposed on each other in order to construct the MO basis set, $\{\varphi_i^{\text{MB}}\} = \{\varphi_i^B, \varphi_u^{H1}, \varphi_v^{H2}\}$ [a $(N_b + 2N_h) \times (N_b + 2N_h)$ matrix], of FM-B according to the following three Equations:

$$\varphi_i^B = \sum_{\lambda=1}^{Nb} a_{\lambda i} \phi_{\lambda}^B + \sum_{\rho=Nb+1}^{Nb+Nh} a_{\rho i} \phi_{\rho}^{H1} + \sum_{\gamma=Nb+Nh+1}^N a_{\gamma i} \phi_{\gamma}^{H2} \quad (3-4)$$

where AOs $\phi_{\lambda}^B \in$ fragment B, AOs $\phi_{\rho}^{H1} \in$ first reference H, AOs $\phi_{\gamma}^{H2} \in$ second reference H, and set all $a_{\rho i} = 0$ and all $a_{\gamma i} = 0$, and $a_{\lambda i} = a_{\lambda b}$ in η_b^B (Equation (3-2)).

$$\varphi_u^{H1} = \sum_{\lambda=1}^{Nb} a_{\lambda u} \phi_{\lambda}^B + \sum_{\rho=Nb+1}^{Nb+Nh} a_{\rho u} \phi_{\rho}^{H1} + \sum_{\gamma=Nb+Nh+1}^N a_{\gamma u} \phi_{\gamma}^{H2} \quad (3-5)$$

where set all $a_{\lambda u} = 0$ and all $a_{\gamma u} = 0$, and $a_{\rho u} = a_{\rho h}$ in η_h^H (Equation (3-3)). In this book, there may be the change in the subscript character of the MO symbol. For example, the MO symbols, η_i^B in Equation (3-2) and η_j^H in Equation (3-3), are rewritten as η_b^B and η_h^H in this case. Will keep the subscripts unchanged as much as possible.

$$\varphi_v^{H2} = \sum_{\lambda=1}^{Nb} a_{\lambda v} \phi_{\lambda}^B + \sum_{\rho=Nb+1}^{Nb+Nh} a_{\rho v} \phi_{\rho}^{H1} + \sum_{\gamma=Nb+Nh+1}^N a_{\gamma v} \phi_{\gamma}^{H2} \quad (3-6)$$

where set all $a_{\lambda v} = 0$ and all $a_{\rho v} = 0$, and $a_{\gamma v} = a_{\rho h}$ in η_h^H (Equation (3-3)). In above three Equations, N_b is the number of AOs in fragment B, N_h is the number of AOs in a H atom, N is the number of AOs in the fragment molecule FM-B. The constructed MOs $\{\varphi_i^{\text{MB}}\}$ are localized on their corresponding fragment B and reference hydrogen atoms, respectively. In this constructed basis set, there are six doubly occupied MOs and four singly occupied MOs. The three typical MOs before localizing are listed in Table 3-3.

For the fragment molecule FM-B, Equations (3-7) and (3-8) are used to transform the AO Fock and overlap matrices \mathbf{f} and \mathbf{s} into the MO Fock and overlap matrices, \mathbf{F} and \mathbf{S} .

$$S_{uv} = \sum_{\lambda=1}^N \sum_{\rho=1}^N a_{\lambda u} s_{\lambda \rho} a_{\rho v} \quad (3-7)$$

$$F_{uv} = \sum_{\lambda=1}^N \sum_{\rho=1}^N a_{\lambda u} f_{\lambda \rho} a_{\rho v} \quad (3-8)$$

and the followings must be ensured:

$$S_{uv} = \delta, \varphi_u^{\text{MB}} \text{ and } \varphi_v^{\text{MB}} \in \text{the same fragment P}$$

$$S_{uv} \neq 0.0, \varphi_u^{\text{MB}} \in \text{fragment P}, \varphi_v^{\text{MB}} \in \text{fragment Q}, P \neq Q$$

In Equation (3-7), the AO overlap integral matrix \mathbf{s} is obtained from the single-point energy calculation on the fragment molecule FM-B. In FM-B, however, the MOs φ_i^B are absolutely localized on the fragment B, and are still orthogonal and normalized. This is the reasons why the cartesian coordinates of the atoms in fragment B must be the same as those of the corresponding atoms in FM-B.

In this work, lowercase bold letters, \mathbf{f} , \mathbf{s} and \mathbf{a} (or \mathbf{t}), represent the AO Fock, overlap integral and coefficient

FMO overlap integral matrix for $\{\phi_i^{\text{MB}}\}$ before Kost' localization

	$\phi_j^{\text{B-ov}}$	$\phi_k^{\text{B-s}}$	$\phi_l^{\text{H-s}}$	$\phi_h^{\text{H-v}}$
$\phi_j^{\text{B-ov}}$	$S^{\text{B}} = 1$	0	$S^{\text{B},\text{H-s}} \neq 0$	$S^{\text{B,v}} \neq 0$
$\phi_k^{\text{B-s}}$	0	$S^{\text{B-s}} = 1$	S_{kl-s}	$S^{\text{B-s,v}} \neq 0$
$\phi_l^{\text{H-s}}$	$S^{\text{H-sB}} \neq 0$	S_{lk-s}	$S^{\text{H-s,s}}$	$S^{\text{H-s,v}}$
$\phi_h^{\text{H-v}}$	$S^{\text{v,B}} \neq 0$	$S^{\text{v,B-s}} \neq 0$	$S^{\text{v,H-s}}$	$S^{\text{H-v}}$

$S_{kl-s} = 0.26715, S_{1,2-s} = 0.21104$
 $S_{2,2-s} = 0.42907, S_{2,1-s} = 0.29344$

FMO overlap integral matrix for $\{\phi'_t^{\text{MB}}\}$ after Kost' localization

	$\phi'_j^{\text{B-ov}}$	$\phi'_k^{\text{B-s}}$	$\phi'_l^{\text{H-s}}$	$\phi'_h^{\text{H-v}}$
$\phi'_j^{\text{B-ov}}$	$S^{\text{B}} = 1$	0	0	$S^{\text{B,v}} \neq 0$
$\phi'_k^{\text{B-s}}$	0	$S^{\text{B-s}} = 1$	S'_{kl-s}	$S'^{\text{B-s,v}} \neq 0$
$\phi'_l^{\text{H-s}}$	0	S'_{lk-s}	$S'^{\text{H-s,s}}$	$S^{\text{H-s,v}}$
$\phi'_h^{\text{H-v}}$	$S'^{\text{v,B}} \neq 0$	$S'^{\text{v,B-s}} \neq 0$	$S'^{\text{v,H-s}}$	$S'^{\text{H-v}}$

$S'_{kl-s} = 0.93451, S'_{1,2-s} = 0.07010$
 $S'_{2,2-s} = 0.94151, S'_{2,1-s} = 0.06958$

Scheme 3-3

matrices; uppercase bold letters, \mathbf{F} , \mathbf{S} and \mathbf{T} , represent the MO (or FMO) Fock, overlap integral and coefficient matrices. Before and after Kost's localization, the overlap integrals S_{il} between the pairs of MOs ϕ_i^{B} and $\phi_l^{\text{H-s}}$ are listed in Table 3-4 (presented in Appendix), where $\phi_l^{\text{H-s}}$ is the singly occupied MO of the referential hydrogen atom in FM-B.

3.2.2.3. Kost's Localization

There are multiple ways to distinguish between the π and σ MOs. One is the s AO coefficient method, and another one is the overlap integral method (can only be used before localizing). In the MO basis set $\{\phi_i^{\text{MB}}\} = \{\phi_i^{\text{B}}, \phi_u^{\text{H1}}, \phi_v^{\text{H2}}\} = \{\phi_j^{\text{B-ov}}, \phi_k^{\text{B-s}}, \phi_l^{\text{H-s}}, \phi_h^{\text{H-v}}\}$, the π MOs $\phi_m^{\text{B-}\pi}$ are perpendicular to the fragment plane. In a $\phi_m^{\text{B-}\pi}$, therefore, the s AO coefficients should be small although $\phi_m^{\text{B-}\pi}$ and $\phi_n^{\text{B-}\sigma}$ mixed to some extent. Before the Kost's localization, as shown by the data listed in the Table 3-4 (presented in Appendix), the overlap integrals between $\phi_m^{\text{B-}\pi}$ and $\phi_l^{\text{H-s}}$ are less than 10^{-5} and are greater than 10^{-6} . Therefore, the MOs, $\{\phi_i^{\text{B}}\}$, belonging to the fragment B can be divided into two groups $\{\phi_m^{\text{B-}\pi}\}$ (π MOs) and $\{\phi_n^{\text{B-}\sigma}\}$ (σ MOs) using the s coefficient method and using overlap integral method.

In the sub-basis set $\{\phi_n^{\text{B-}\sigma}\}$ for FM-B, as shown by the regular font data listed in Table 3-3, the two highest occupied σ MOs $\phi_n^{\text{B-}\sigma}$, namely ϕ_i^{B} (or ϕ_i^{MB}) ($n = 6$ and $n = 7$; $i, t = 6$ and $i, t = 8$), are designated as the two singly occupied MOs, and are denoted as “ $\phi_1^{\text{B-s}}$ ” ($k = 1$, the first singly occupied MO $\phi_k^{\text{B-s}}$) and “ $\phi_2^{\text{B-s}}$ ” ($k = 2$, the second singly occupied MO $\phi_k^{\text{B-s}}$). Another two singly occupied MOs ϕ_t^{MB} ($t = 9, 10$) belonging to the two referential hydrogen atoms are denoted as $\phi_1^{\text{H-s}}$ and $\phi_2^{\text{H-s}}$ ($\phi_l^{\text{H-s}}, l = 1, 2$) (Table 3-3 and Scheme 3-3).

Figure 3-2 is a procedure of localizing MOs $\phi_k^{\text{B-s}}$. There are two singly occupied MOs, $\phi_k^{\text{B-s}}$ ($k = 1, 2$), in the fragment B. Therefore, localization should be run in two loops denoted as Loop-A and Loop-B. In each of the two loops, there are two sub-loops. In the calculation program, the four sub-loops, denoted as “Loop-A1”, “Loop-A2”, “Loop-B1” and “Loop-B2”, are alternately and repeatedly run.

In the first loop (“Loop-A”), a singly occupied MO, $\phi_1^{\text{H-s}}$, of the first reference hydrogen atom H bonded to N(13) atom is used to localize the first singly occupied MO, $\phi_1^{\text{B-s}}$, of fragment B. At the beginning, as shown by “Loop-A1” in Figure 3-2, a 2x2 rotation, i. e. Equation (3-9) and Equation (3-10), is repeatedly applied to a set of doubly occupied MOs, $\phi_j^{\text{B-ov}}$, of fragment B until all $|S'_{lj}| < 10^{-10}$ ($j = 1$ to HOMO of the fragment B). For each 2 x 2 rotation, when the value of β is determined by Equation (3-11), the overlap integral, $S'_{1,1-s}$, between $\phi_1^{\text{B-s}}$ and $\phi_1^{\text{H-s}}$ is

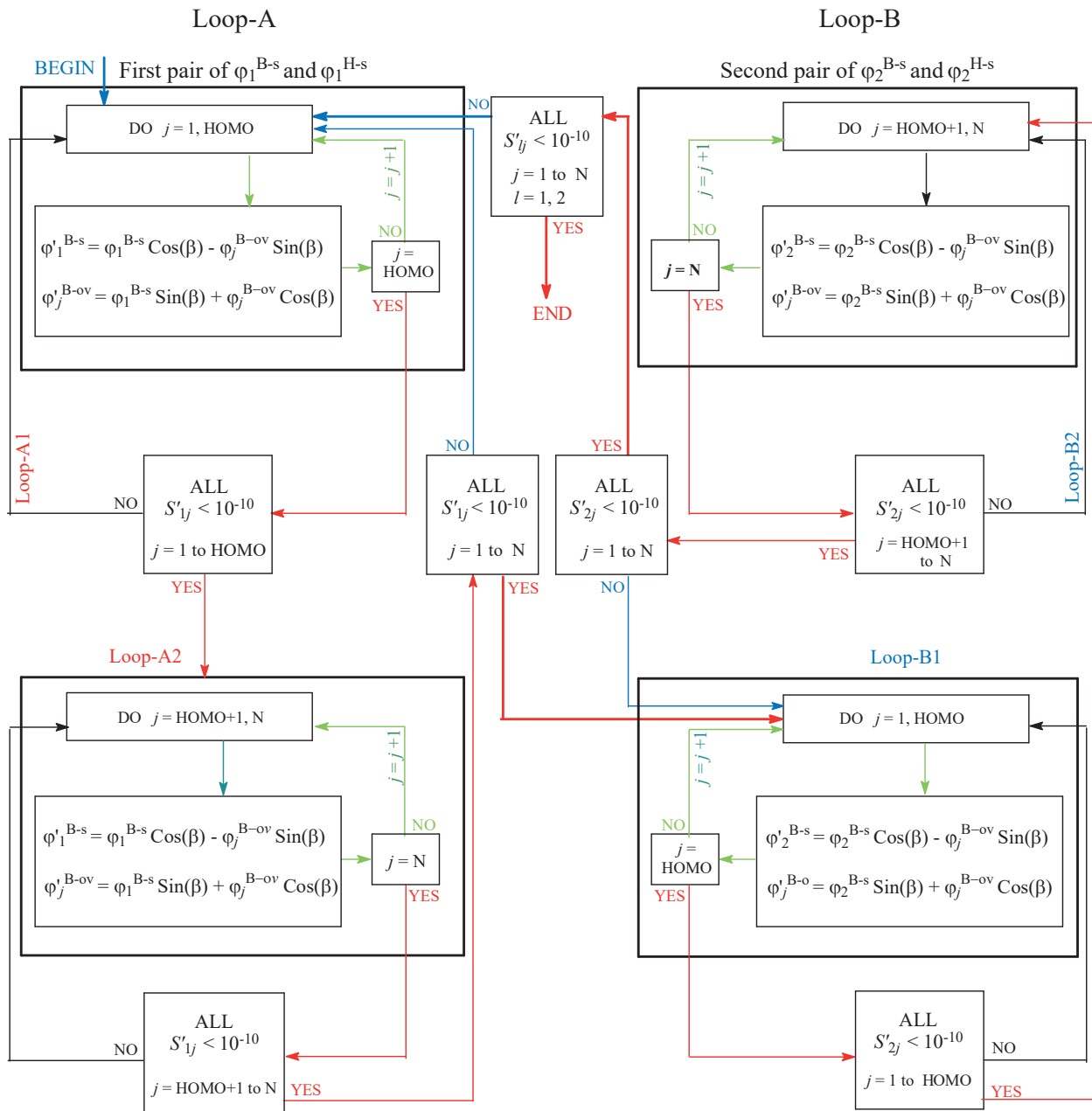


Figure 3-2. Schematic diagram of localizing MOs of fragment B (HOMO: highest occupied molecular orbital).

maximized, and then the new MOs, φ_j^{B-ov} and φ_1^{B-s} , are calculated using Equation (3-12) and Equation (3-13).

$$S'_{lk-s} = S_{lk-s} \cos(\beta) - S_{lj} \sin(\beta) \quad (3-9)$$

$$S'_{lj} = S_{lk-s} \sin(\beta) + S_{lj} \cos(\beta) \quad (3-10)$$

$d(S'^2_{lk-s})/d\beta = 0.0$, (S'^2_{lk-s} is maximized), leading to Equation (3-11)

$$\operatorname{tg}(2\beta) = -2(S_{lk-s} S_{lj}) / \operatorname{abs}(S_{lj}^2 - S_{lk-s}^2)$$

$$\beta = \operatorname{arctg}[-2(S_{lk-s} S_{lj}) / \operatorname{abs}(S_{lj}^2 - S_{lk-s}^2)]/2 \quad (3-11)$$

$$\varphi_k^{B-s} = \varphi_k^{B-s} \cos(\beta) - \varphi_j^{B-ov} \sin(\beta) = \sum_{\lambda=1}^N [a_{\lambda k}^o \cos(\beta) - a_{\lambda j}^o \sin(\beta)] \phi_{\lambda} \quad (3-12)$$

$$\varphi_j^{B-ov} = \varphi_k^{B-s} \sin(\beta) + \varphi_j^{B-ov} \cos(\beta) = \sum_{\lambda=1}^N [a_{\lambda k}^o \sin(\beta) + a_{\lambda j}^o \cos(\beta)] \phi_{\lambda} \quad (3-13)$$

Afterwards, Loop-A2 is started. In this sub-loop, a 2x2 rotation is repeatedly applied to a set of vacant MOs, φ_j^{B-ov} , of fragment B until all $|S_{lj}| < 10^{-10}$ ($j = \text{HOMO}+1$ to N_b). According to Equation (3-12) and to our practical calculations, the change in the value of S_{lj} between φ_1^{H-s} and φ_j^{B-ov} (vacant MOs) can also influence the value of S_{lj} between φ_1^{H-s} and φ_j^{B-ov} (occupied MOs). Therefore, as long as there is one S'_{lj} ($j = 1$ to HOMO) whose absolute value is not less than 10^{-10} , the Loop-A1 should be started again although all $|S'_{lj}| < 10^{-10}$ ($j = \text{HOMO}+1$ to N). Only when all $|S_{lj}| < 10^{-10}$ ($j = 1$ to N), the Loop-B is activated. In the Loop-B, the singly occupied MO, φ_2^{H-s} , of the second reference hydrogen atom bonded to C(13) atom is used to localize the second singly occupied φ_2^{B-s} . Similarly, a 2 x 2 rotation is alternately and repeatedly applied to a set of the occupied φ_j^{B-ov} and to a set of the vacant φ_j^{B-ov} until all $|S_{lj}| < 10^{-10}$ ($j = 1$ to N).

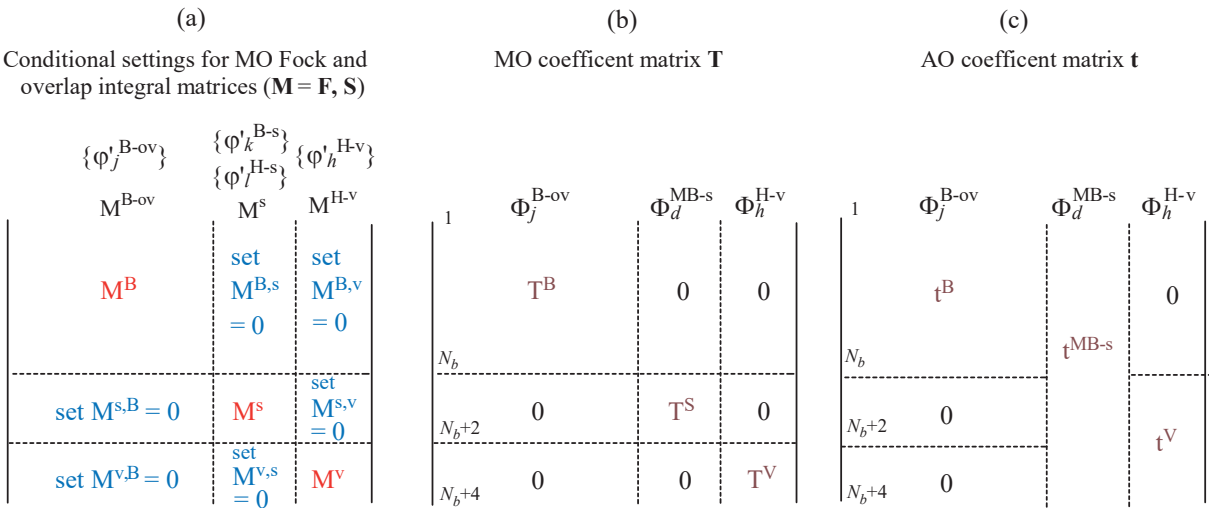
So, as shown by Figure 3-2, two singly occupied MOs, φ_1^{H-s} and φ_2^{H-s} , are repeatedly and alternately used to localize two singly occupied MOs φ_1^{B-s} and φ_2^{B-s} of the fragment B until all $|S_{lj}| < 10^{-10}$ and all $|S_{lj}| < 10^{-10}$ ($j = 1$ to N). At Last, as shown by the Italic font data listed in Table 3-4 (presented in Appendix) and by Scheme 3-3, $S_{1,1-s}$ and $S_{2,2-s}$ are maximized, $S_{1,1-s} = 0.9345169929$, $S_{2,2-s} = 0.9415084220$, and meanwhile all $|S_{lj}| < 10^{-10}$ ($l = 1, 2; j = 1, N$). The maximization of the overlap integrals $S_{1,1-s}$ and $S_{2,2-s}$ ensures that the singly occupied MOs of fragment B have the correct electronic occupancies and reasonable spatial orientation. For the 6th and 8th MOs (two singly occupied MOs of fragment B), as shown by the Italic font data listed in Table 3-4, their AO coefficients have been concentrated, respectively, on the N(12) and C(13) atoms, and their electronic occupancies are, respectively, 1.00037 and 0.99963 after localization. At Last, as shown by Equation (3-14), the Kost's localization provides a set of localized MOs $\{\varphi_t^{MB}\}$ for FM-B:

$$\varphi_t^{MB} = \sum_{\mu=1}^N a'_{\mu t} \phi_{\mu} = \sum_{\lambda=1}^{Nb} a'_{\lambda t} \phi_{\lambda}^B + \sum_{\rho=Nb+1}^{Nb+Nh} a'_{\rho t} \phi_{\rho}^{H1} + \sum_{\gamma=Nb+Nh+1}^N a'_{\gamma t} \phi_{\gamma}^{H2} \quad (3-14)$$

In Equation (3-14), for example, when $\varphi_t^{MB} \in$ fragment B, all $a'_{\rho t} = 0$ and all $a'_{\gamma t} = 0$. The eigenvectors of the referential hydrogen atoms keep unchanged after Kost's localization. For FM-B, the MO basis set can be expressed as $\{\varphi_t^{MB}\} = \{\varphi_i^B, \varphi_i^{H-s}, \varphi_h^{H-v}\} = \{\varphi_j^{B-ov}, \varphi_k^{B-s}, \varphi_l^{H-s}, \varphi_h^{H-v}\} = \{\varphi_m^{B-\pi}, \varphi_n^{B-\sigma}, \varphi_k^{B-s}, \varphi_l^{H-s}, \varphi_h^{H-v}\}$, and the MOs in the sub-MOs set $\{\varphi_i^B\} = \{\varphi_j^{B-ov}, \varphi_k^{B-s}\}$ are still orthogonal and normalized.

3.2.2.4. Conditional SCF-MO Calculation

For the localized π MO $\varphi_m^{B-\pi}$ ($m = 1$; 7th φ_t^{MB}), as shown by a comparison between the regular and italic font data in Table 3-3, the s AO coefficient values are changed from less than 10^{-10} before localization to greater than 10^{-6} after localization. Kost's localization may not be able to guarantee the complete separation of the π and σ MOs. Therefore, after Kost's localization, a conditional single-point energy computation, over the MO basis set $\{\varphi_t^{MB}\}$, on the fragment molecule FM-B should be performed, and it is a multi-step procedure.



Scheme 3-4

Before each SCF (self-consistent field) iteration, as the first step, the AO Fock and overlap integral matrices, \mathbf{s} and \mathbf{f} , should be transformed into the MO Fock and overlap integral matrices \mathbf{S} and \mathbf{F} using Equations (3-7) and Equation (3-8). In this case, the AO coefficient matrix, \mathbf{a} , in the two Equations is the AO coefficient matrix, \mathbf{a}' , of the localized MO basis set $\{\varphi_t^{MB}\}$, and it is obtained from the Kost's localization. During the period of the SCF-MO calculation, the MO overlap integral matrix \mathbf{S} keeps unchanged, but the MO Fock matrix \mathbf{F} should be recalculated using Equation (3-8) before each SCF iteration.

The MO Fock and overlap integral matrices \mathbf{F} and \mathbf{S} can be divided into 9 blocks (Scheme 3-4a). For the non-diagonal block $\mathbf{F}^{B,S}$, for example, it includes the following two types of elements:

- (i) the elements F_{jk} between various pairs of localized MOs $\varphi_j^{B\text{-ov}}$ and $\varphi_k^{B\text{-s}}$,
- (ii) the elements F_{jl} between various pairs of $\varphi_j^{B\text{-ov}}$, $\varphi_l^{H\text{-s}}$.

In the second step, as shown by Scheme 3-4a, all the blue non-diagonal blocks of the MO Fock (and overlap integral) matrix are set equal to zero, forming the particular Fock and overlap integral matrices denoted as \mathbf{F}' and \mathbf{S}' .

After each SCF iteration (the third step), a MO eigenvector matrix \mathbf{T} is obtained, and the obtained MO Φ_i is a linear combination of the localized MOs φ_t^{MB} (Equation (3-15)). In the \mathbf{T} matrix, as shown by Scheme 3-4b, the MO coefficients in the six non-diagonal blocks are all equal to zero. Afterwards, Equation (3-16) should be used to transform the \mathbf{T} matrix into the \mathbf{t} matrix (Scheme 3-4c), i. e. the expression of the MOs should be converted from a linear combination of MOs φ_t^{MB} (Equation 3-15) to a linear combination of AOs ϕ_μ (Equation 3-17), in order to calculate the AO density matrix \mathbf{d} .

$$\Phi_i = \sum_{n=1}^N T_{ti} \varphi_t^{MB} \quad (3-15)$$

$$t_{\mu i} = \sum_{n=1}^N a'_{\mu n} T_{ti} \quad (3-16)$$

$$\Phi_i = \sum_{\mu=1}^N t_{\mu i} \phi_\mu \quad (3-17)$$

In Equation (3-16), T_{it} is the coefficient of t -th MO φ'_t ^{MB} in the i -th MO Φ_i , $a'_{\mu i}$ is the coefficient of the μ -th AO (ϕ_μ) in the t -th localized MO φ'_t ^{MB}. So, $t_{\mu i}$ is the coefficient of the μ -th AO in the i -th MO Φ_i . After transformation, the AO density matrix \mathbf{d} is calculated using Equation (3-18), and then, the AO Fock matrix is renewed

$$d_{\lambda\rho} = \sum_{i=1}^{occ} t_{\lambda i} t_{\rho i} \quad (3-18)$$

Finally, the conditional single-point energy calculation provides a set of MOs $\{\Phi_t^{\text{MB}}\}$ for FM-B:

$$\{\Phi_t^{\text{MB}}\} = \{\Phi_j^{\text{B-ov}}, \Phi_d^{\text{MB-s}}, \Phi_h^{\text{H-v}}\} = \{\Phi_m^{\text{B-}\pi}, \Phi_n^{\text{B-}\sigma}, \Phi_d^{\text{MB-s}}, \Phi_h^{\text{H-v}}\}, \text{ where}$$

$$\Phi_m^{\text{B-}\pi} = \sum_{u=1}^{N\pi} T_{m'm} \varphi_{m'}^{\text{B-}\pi} = \sum_{\lambda=1}^{Nb} t_{\lambda m} \phi_\lambda^B + \sum_{\rho=Nb+1}^{Nb+Nh} t_{\rho m} \phi_\rho^{H1} + \sum_{\gamma=Nb+Nh+1}^N t_{\gamma m} \phi_\gamma^{H2} \quad (3-19)$$

$$\Phi_n^{\text{B-}\sigma} = \sum_{u=1}^{N\pi} T_{n'n} \varphi_{n'}^{\text{B-}\sigma} = \sum_{\lambda=1}^{Nb} t_{\lambda n} \phi_\lambda^B + \sum_{\rho=Nb+1}^{Nb+Nh} t_{\rho n} \phi_\rho^{H1} + \sum_{\gamma=Nb+Nh+1}^N t_{\gamma n} \phi_\gamma^{H2} \quad (3-20)$$

In above two Equations, all $t_{\rho m} = 0$ and all $t_{\gamma m} = 0$, and all $t_{\rho n} = 0$ and all $t_{\gamma n} = 0$.

In MOs $\{\Phi_t^{\text{MB}}\}$, as shown by Equation (3-21), MOs $\Phi_d^{\text{MB-s}}$ are a linear combination of the four singly occupied MOs φ'_k ^{B-s} and $\varphi_t^{\text{H-s}}$. Of all MOs Φ_t^{MB} , as shown by Scheme 3-4c, only four MOs $\Phi_d^{\text{MB-s}}$ are delocalized on the whole molecular framework. The MOs $\Phi_j^{\text{B-ov}}$ are still localized on the fragment B (Table 3-5 presented in Appendix).

$$\Phi_d^{\text{MB-s}} = \sum_{k=1}^2 T_{kd} \varphi_k^{\text{B-s}} + \sum_{l=1}^2 T_{ld} \varphi_l^{\text{H-s}} = \sum_{\lambda=1}^{Nb} t_{\lambda d} \phi_\lambda^B + \sum_{\rho=Nb+1}^{Nb+Nh} t_{\rho d} \phi_\rho^{H1} + \sum_{\gamma=Nb+Nh+1}^N t_{\gamma d} \phi_\gamma^{H2} \quad (3-21)$$

$$\Phi_h^{\text{H-v}} = \sum_{h'=1}^{2Nh-2} T_{h'h} \varphi_{h'}^{\text{H-v}} = \sum_{\lambda=1}^{Nb} t_{\lambda h} \phi_\lambda^B + \sum_{\rho=Nb+1}^{Nb+Nh} t_{\rho h} \phi_\rho^{H1} + \sum_{\gamma=Nb+Nh+1}^N t_{\gamma h} \phi_\gamma^{H2} \quad (3-22)$$

where all $t_{\lambda h} = 0$

According to the comparison of the AO coefficients of φ'_m ^{B- π} and those of $\Phi_m^{\text{B-}\pi}$, the conditional single-point energy calculation, over the localized MO basis set $\{\varphi_t^{\text{MB}}\}$, can adjust the spatial orientation of the π molecular orbitals, but it can't further improve the separation of the π and σ MOs.

3.2.2.5. Formation of Sub-LFMO Basis Set

In the MO basis set $\{\Phi_t^{\text{MB}}\}$ that is a $(Nb+2Nh) \times (Nb+2Nh)$ matrix, as the last step, the two sub-sets of MOs, $\Phi_d^{\text{MB-s}}$ and $\Phi_h^{\text{H-v}}$, are replaced by two singly occupied MO φ'_k ^{B-s}, leading to the formation of the FMOs basis set $\{\psi_i^{\text{B}}\}$ for fragment B. The eigenvectors of MOs $\{\psi_i^{\text{B}}\}$ is a $N_b \times N_b$ matrix

$$\{\psi_i^{\text{B}}\} = \{\psi_j^{\text{B-ov}}, \psi_k^{\text{B-s}}\} = \{\psi_m^{\text{B-}\pi}, \psi_n^{\text{B-}\sigma}, \psi_k^{\text{B-s}}\}$$

For this basis set,

$$S_{uu} = 1 \quad (u = v)$$

$$S_{uv} = 0 \quad (u \neq v), \psi_u^{\text{B}} \text{ and } \psi_v^{\text{B}} \in \{\psi_j^{\text{B-ov}}\}$$

$$S_{uv} \neq 0 \quad (u \neq v), \psi_u^{\text{B}} \in \{\psi_j^{\text{B-ov}}\}, \psi_v^{\text{B}} \in \{\psi_k^{\text{B-s}}\}.$$

3.2.3. Superposition of Sub-basis Sets.

Coefficient matrix of basis set $\{\Psi_i\}$ for N-benzylideneaniline			
	Ψ_i^A	Ψ_i^B	Ψ_i^C
1	a	0	0
N_a	0	b	0
$N_a + N_b$	0	0	c
N			

Scheme 3-5

Overlap integral matrix \mathbf{S} of basis set $\{\Psi_i\}$ for N-benzylideneaniline		
Fragment A	B	C
S^A	$S^{AB} \neq 0$	$S^{AC} \neq 0$
$S^{BA} \neq 0$	S^B	$S^{BC} \neq 0$
$S^{CA} \neq 0$	$S^{CB} \neq 0$	S^C

Scheme 3-6

In a similar way, the sub-LFMO basis sets for fragments A and C can be constructed and are represented as follows:

$$\begin{aligned}\{\psi_i^A\} &= \{\psi_j^{A-\text{ov}}, \psi_k^{A-\text{s}}\} = \{\psi_m^{A-\pi}, \psi_n^{A-\sigma}, \psi_k^{A-\text{s}}\} \quad (k=1) \\ \{\psi_i^C\} &= \{\psi_j^{C-\text{ov}}, \psi_k^{C-\text{s}}\} = \{\psi_m^{C-\pi}, \psi_n^{C-\sigma}, \psi_k^{C-\text{s}}\} \quad (k=1)\end{aligned}$$

Then, according to Equations (3-23), three sub-LFMO basis sets $\{\psi_i^P\}$ ($P = A, B, C$) are superposed on each other, forming a LFMO basis set, $\{\Psi_i\} = \{\Psi_m^{P-\pi}, \Psi_n^{P-\sigma}, \Psi_k^{P-\text{s}}\}$, for N-benzylideneaniline.

$$\Psi_i = \sum_{\lambda=1}^{N_a} a_{\lambda i} \phi_{\lambda}^A + \sum_{\rho=N_a+1}^{N_a+N_b} b_{\rho i} \phi_{\rho}^B + \sum_{\gamma=N_a+N_b+1}^N c_{\gamma i} \phi_{\gamma}^C \quad (3-23)$$

In the above equation, the LFMO Ψ_i is expressed as the linear combination of AOs; the three sum terms belong, respectively, to the fragments A, B and C; N_a and N_b are the numbers of AOs in the fragment A and B, N is the number of AOs in the whole molecule. When $\Psi_i \in$ fragment A, set all $b_{\rho i} = 0$, all $c_{\gamma i} = 0$, and $a_{\lambda i} = t_{\mu i}$ in ψ_i^A (sub-LFMO basis set $\{\psi_i^A\}$ for fragment A); when $\Psi_i \in$ fragment B, set all $a_{\lambda i} = 0$, and all $c_{\gamma i} = 0$, $b_{\rho i} = t_{\mu i}$ in ψ_i^B ; when $\Psi_i \in$ fragment C, set all $a_{\lambda i} = 0$, all $b_{\rho i} = 0$, and $c_{\gamma i} = t_{\mu i}$ in ψ_i^C (Scheme 3-5). In the entire LFMO basis set $\{\Psi_i\}$ for NBA, all LFMOs are absolutely localized on their respective fragments, and have the correct electronic occupancies.

The characteristics of the overlap integrals $S_{ij} = \langle \Psi_i | \Psi_j \rangle$ (Scheme 3-6) are as follows:

- (i) When $P \neq Q$, $S_{ij} \neq 0$. At the MP2/6-31G* level, $\langle \Psi_1^{A-\text{s}} | \Psi_1^{B-\text{s}} \rangle = 0.90731$, and $\langle \Psi_2^{B-\text{s}} | \Psi_1^{C-\text{s}} \rangle = 0.92028$.
- (ii) When $P = Q$, the orthogonality of $\{\Psi_i\}$ is the same as that of the corresponding sub-LFMO basis set $\{\psi_i^P\}$.
- (iii) $[\det(\mathbf{S})]^{2/N} = 0.847$, and $[\det(\mathbf{s})]^{2/N} = 0.144$, where $[\det(\mathbf{S})]$ and $[\det(\mathbf{s})]$ are the values of determinants of the matrices \mathbf{S} and \mathbf{s} . Therefore, LFMO basis set is linearly independent.

In the calculation program, the subscripts i of the LFMOs Ψ_i corresponding to the LFMOs $\Psi_m^{P-\pi}$, $\Psi_n^{P-\sigma}$ and $\Psi_k^{P-\text{s}}$, are, respectively, storied as the data elements in the following three two-dimensional arrays:

$$\pi\text{-LFMO}(L, m) = i, L = 1 \text{ (fragment A)}, 2 \text{ (fragment B)}, 3 \text{ (fragment C)}, \dots; m = 1, 2, \dots, m_p$$

$$\sigma\text{-LFMO}(L, n) = i, L = 1 (\text{A}), 2 (\text{B}), 3 (\text{C}), \dots; n = 1, 2, \dots, n_p$$

$$k\text{-LFMO}(L, k) = i, L = 1 (\text{A}), 2 (\text{B}), 3 (\text{C}), \dots; k = 1, 2, \dots, k_p$$

where m_p , n_p and k_p are the numbers of the π , σ and singly occupied LFMOs in each fragment P.

For fragment B of N-benzylideneaniline, for example, $L = 2$, $k = 1, 2$; $k\text{-LFMO}(2, 1) = 28$, $k\text{-LFMO}(2, 2) = 29$, that is, two singly LFMOs Ψ_k^{B-s} of fragment B are the 28-th and 29-th LFMOs Ψ_i ($i = 28, 29$) in the entire LFMO basis set $\{\Psi_i\}$.

3.3. SUMMARY

Based on the fact that only in a planar molecule, the π and σ MOs can be separated, the dissection of a molecular framework into several planar fragments is a basic mean to construct a LFMO basis set.

The use of the referential hydrogen atom greatly simplifies the procedure for localizing the opened-shell MOs. The Kost's localization can guarantee the correct electron occupancy of the singly occupied MO and its reasonable orientations in the space.

After the Kost's localization, the conditional single-point energy computation is to recovery the orientation of the doubly occupied and vacant MOs in the space. In some case, it can also further improve the separation of the π and σ MOs.

3.4. APPENDIX

Table 3-3-2. Five Typical Opened-Shell MOs, $\eta^B = \sum a_{\lambda,i} \phi_{\lambda}$, Are Obtained from Single-Point Energy Calculation on Fragment B of N-benzylideneaniline at UB3LYP/6-31G* Level.

	AOs	6th	7th	8th	9th	10th
		σ HOMO-1	(π -HOMO)	(σ -HOMO)	(unocc. π MO)	(unocc. σ MO)
1	12N 1s	0.0723539786	-0.0000004142	-0.0026824943	-0.0103422372	-0.0000017410
2	2s	-0.1425848446	0.0000008382	-0.0120825279	0.0079266755	0.0000127310
3	2px	0.4116417319	0.1130436566	0.4176715780	0.1344826667	-0.0409379249
4	2py	-0.2895827467	-0.0804334872	0.2929158994	-0.0188529003	0.0291158587
5	2pz	-0.1538649660	0.4538140864	-0.0521267560	-0.0368420600	-0.1642994233
6	3S	-0.3689736999	0.0000008754	0.0738658440	0.1408983231	0.0000006211
7	3px	0.2165338657	0.0682039478	0.3467233821	0.3193103161	-0.0053522805
8	3py	-0.1179389207	-0.0485288454	0.2054200897	-0.0049278277	0.0037975092
9	3pz	-0.0748414986	0.2738054689	-0.0499618013	-0.0804172909	-0.0215268369
10	4xx	0.0048316550	0.0042596476	-0.0015774454	-0.0076238870	-0.0098486547
11	4yy	0.0227874557	0.0091861624	-0.0082194562	0.0027436243	-0.0178698392
12	4zz	0.0054707987	-0.0134455205	0.0004589783	-0.0093814462	0.0277225850
13	4xy	-0.0248070305	-0.0092034888	-0.0053665709	0.0123188500	0.0185509216
14	4xz	-0.0049750094	0.0079384749	-0.0003690294	0.0018213044	-0.0188388211
15	4yz	0.0102656052	-0.0285470431	-0.0004366990	-0.0006891651	0.0553780697
16	13C 1s	0.0025163785	-0.0000004263	-0.0606198476	0.0940065392	-0.0000002891

17	2s	0.0118255999	0.0000004883	0.1088915452	-0.1770548545	0.0000223324
18	2px	-0.0090776071	0.0940740720	-0.2545858997	-0.4008385902	-0.2403214005
19	2py	0.3727551295	-0.0669394049	-0.3065361275	-0.0033700107	0.1709265292
20	2pz	0.0683340035	0.3776454925	0.0090863861	0.0992548440	-0.9646075355
21	3S	-0.0532122016	0.0000032011	0.4076011956	-1.4608006528	-0.0000371974
22	3px	0.0365229588	0.0560548441	-0.1491707820	-0.9888809567	0.2723094628
23	3py	0.1533309237	-0.0398855036	-0.2542110278	-0.0624333632	-0.1936865263
24	3pz	0.0180812984	0.2250279822	-0.0078982484	0.2352750339	1.0929488911
25	4xx	-0.0159319188	-0.0026947316	-0.0301366099	0.0011369571	0.0061173707
26	4yy	0.0120200383	-0.0068772338	0.0136929168	0.0041313906	0.0085892270
27	4zz	-0.0043488519	0.0095717439	-0.0030418875	0.0022109614	-0.0147019099
28	4xy	0.0091009400	0.0066872287	0.0237137737	-0.0016797520	-0.0094826837
29	4xz	0.0052305267	-0.0048689996	0.0129391442	-0.0000274474	0.0120575721
30	4yz	0.0008798968	0.0214220502	-0.0031524155	0.0008390738	-0.0264668117
31	14H 1s	-0.0834556300	0.0000004362	-0.1917668546	0.0731286971	0.0000053659
32	2s	-0.1018921802	0.0000010913	-0.3161712584	2.0432471539	-0.0000159654

Figure 3-4. The MO Overlap Integrals at MP2/6-31G* Level, S'_{li} ($l = 1, 2$; $i = 1, \dots, 32$), between the pairs of MOs ϕ_i^B and ϕ_l^{H-s} before (Regular Font Data) and after Kost's Localization (Italic Font Data), and the Electronic Occupancies of MOS ϕ_i^B after Kost's Localization at 6-31G* Level.

ϕ_i^B	S_{1i}	S_{2i}	S'_{1i}	S'_{2i}	*Occupancies.	
	(ϕ_1^{H-s})	(ϕ_2^{H-s})	(ϕ_1^{H-s})	(ϕ_2^{H-s})	MP2	B3LYP
1	0.0750910683	0.0110630139	0.0000000000	0.0000000000	1.99254	1.99350
2	0.0142795567	0.0955916410	0.0000000000	0.0000000000	1.98228	1.97990
3	0.4037831545	0.2915165334	0.0000000000	0.0000000000	1.92135	1.94246
4	-0.1801462170	0.4022746141	0.0000000000	0.0000000000	1.94651	1.93782
5	0.4093182769	-0.4105397518	0.0000000000	0.0000000000	1.95763	1.95881
6 ϕ_1^{B-s}	0.2671522092	0.2110422116	0.9345169929	0.0701079174	1.00037	1.00043
7 (π FMO)	0.0000021690	-0.0000016660	0.0000000000	0.0000000000	1.99101	1.98877
8 ϕ_2^{B-s}	0.2934480278	0.4290721053	0.0695873118	0.9415084220	0.99963	0.99957
9	-0.0000015919	-0.0000023351	-0.0000000001	0.0000000000	0.00006	0.00115
10	0.0983180538	0.1179758224	0.0000000000	0.0000000000	0.05142	0.05330
11	-0.2094744920	0.0616544992	0.0000000000	0.0000000000	0.01783	0.01696
12	-0.0105393446	0.4136679291	-0.0000000001	0.0000000000	0.02274	0.02113
13	0.0000008733	-0.0000013663	0.0000000000	0.0000000000	0.00592	0.00598
14	0.2176728844	0.0188606461	0.0000000000	0.0000000000	0.01483	0.00313
15	0.1117517854	0.0762493473	0.0000000000	0.0000000000	0.01004	0.01662
16	0.1456770062	-0.0612390117	0.0000000000	0.0000000000	0.01294	0.02959
17	-0.3979654027	-0.0599785573	0.0000000000	0.0000000000	0.04829	0.00216
18	0.0000020749	0.0000004004	0.0000000001	0.0000000000	0.00151	0.02760
19	-0.0218560815	0.0277890272	0.0000000000	0.0000000000	0.00272	0.00185
20	0.1740682032	-0.0523411967	0.0000000000	0.0000000000	0.00378	0.00345

21	-0.0290929887	0.1417850230	0.0000000000	0.0000000000	0.00482	0.00024
22	-0.0000005309	0.0000008950	0.0000000000	0.0000000000	0.00008	0.00479
23	0.0000012786	0.0000010585	0.0000000000	0.0000000000	0.00045	0.00036
24	0.1289733849	-0.0357348967	0.0000000000	0.0000000000	0.00554	0.00443
25	0.0000013185	-0.0000009758	0.0000000000	0.0000000000	0.00089	0.00129
26	0.0427013881	-0.0562936139	0.0000000000	0.0000000000	0.00129	0.00148
27	0.0053283820	0.0221953062	0.0000000000	0.0000000000	0.00078	0.00073
28	0.0000003766	0.0000002925	0.0000000000	0.0000000000	0.00008	0.00005
29	0.0606013290	0.0418244353	0.0000000001	0.0000000000	0.00209	0.00191
30	0.0025671894	-0.0057268040	0.0000000000	0.0000000000	0.00029	0.00032
31	-0.0050910606	-0.0119917204	0.0000000000	0.0000000001	0.00020	0.00015
32	-0.0047294877	-0.0186890179	0.0000000000	0.0000000000	0.00009	0.00007

Table 3-5. Seven Typical MOs Obtained from Conditional Single-Point Energy Calculation on Fragmental Molecule FM-B at MP2/6-31G* Level.

			Occupied MOs			Vacant MOs	
			$\Psi_1^{\text{MB-s}}$	$\Psi_2^{\text{MB-s}}$	$\Psi_7^{\text{B-}\pi}$	$\Psi_8^{\text{B-}\sigma}$	$\Psi_9^{\text{B-}\pi}$
1	12N	1s	-0.004978	-0.011119	0.000001*	0.085609	0.000000
2	12	2s	-0.016940	-0.039975	-0.000003	-0.261150	0.000000
3	12	2px	-0.017534	-0.006906	0.120935	0.522699	-0.104020
4	12	2py	-0.013576	-0.004707	-0.086047	-0.147447	0.074014
6	12	3s	0.089970	0.218244	-0.000003	-0.278711	0.000001*
7	12	3px	0.124969	0.077779	0.068893	0.412826	-0.119579
8	12	3py	0.165119	0.121265	-0.049015	0.139028	0.085083
9	12	3pz	-0.001864	0.002119	0.276546	-0.078198	-0.480033
10	12	4xx	0.000514	-0.017226	0.014286	0.029084	-0.006425
11	12	4yy	-0.007950	-0.006850	0.007200	-0.011424	0.006894
12	12	4zz	-0.022887	-0.045738	-0.021486	-0.024583	-0.000468
13	12	4xy	0.024595	0.040937	-0.011711	0.013229	-0.002954
14	12	4xz	-0.002385	-0.000901	0.030019	-0.013959	-0.014960
15	12	4yz	-0.003060	-0.002270	-0.021255	0.000015	-0.022408
16	13C	1s	-0.002997	0.006511	0.000000	0.003134	0.000000
17	13	2s	-0.028144	0.037807	0.000001*	-0.030420	0.000001*
18	13	2px	0.001473	0.000531	0.094808	-0.196218	0.116722
19	13	2py	0.002923	0.007208	-0.067458	0.144802	-0.083050
20	13	2pz	0.000151	0.001145	0.380599	0.074541	0.468559
21	13	3s	0.199641	-0.178145	0.000001*	0.104390	0.000001*
22	13	3px	-0.213289	0.028684	0.045448	-0.247315	0.140064
23	13	3py	-0.117195	0.094448	-0.032339	-0.013571	-0.099658
24	13	3pz	0.032359	0.009595	0.182454	0.059200	0.562258
25	13	4xx	0.006533	-0.000585	-0.007333	-0.027924	0.002286
26	13	4yy	0.031054	-0.009765	-0.008910	0.029364	0.011394

27	13	4zz	-0.018707	0.024464	0.016243	-0.009286	-0.013681	0.000000
28	13	4xy	0.030792	-0.037674	0.010243	0.029024	-0.010185	0.000000
29	13	4xz	-0.002048	0.000448	-0.014658	0.011192	0.003332	0.000000
30	13	4yz	0.002689	0.002436	0.027363	0.000192	-0.035716	0.000000
31	14H	1s	0.011522	0.003843	-0.000001*	-0.161825	-0.000001*	0.000000
32	14	2s	0.077841	0.030551	0.000000	-0.034259	-0.000002	0.000000
33	H	1s	0.163896	0.269611	0.000000	0.000000	0.000000	0.769892
34		2s	0.255163	0.419747	0.000000	0.000000	0.000000	-0.703757
35	H	1s	0.241962	-0.177227	0.000000	0.000000	0.000000	0.934388
36		2s	0.376700	-0.275917	0.000000	0.000000	0.000000	-0.854123

3.5. REFERENCES

- 1 Yu, Z. H. 1994. "Quantitative Perturbational Molecular-orbital Analysis of the Conformational Preference of Aniline Molecule and Its Intramolecular Force." *Comput. Chem.*, 18: 95-102.
- 2 Yu, Z. H. 1994. "Quantitative Perturbational Molecular-Orbital Analysis of the Conformational Preference of Aniline Molecule and Its Intramolecular Force.2." *Comput. Chem.*, 18: 363-369.
- 3 Yu, Z. H. 1995. "Localization of Fragment Molecular Orbitals." *Chin. Sci. Bull.*, 40: 2057-2059 (Chinese).
- 4 Yu, Z. H. 1996. "The Localization of the Fragmental Orbital-WSW-like Procedure." *Comput. Appl. Chem.*, 14-19 (Chinese).
- 5 Yu, Z. H.; Li, L. T.; Fu, W.; Li, L. P. 1998. "Conformations of Stilbene-Like Species and New Method of Energy Partition." *J. Phys. Chem. A*, 102: 2016-2028.
- 6 Yu, Z. H.; Peng, X. Q.; Guo, Y. S.; Xuan, Z. Q. 2001. "A Procedure for Constructing a Highly Localized and Symmetrical Bond Orbital Basis set." *Acta Chem. Sin.*, 59: 179-184.
- 7 Yu, Z. H.; Xuan, Z. Q. 1999, "The π -Electron Delocalization Is Destabilizing in N-(phenylethenylidene)-benzeneamine: A Method of Separating out the π and σ Systems in Its Ketenimine Fragment." *Theochem*, 488: 101-112.
- 8 Yu, Z. H.; Xuan, Z. Q.; Wang, T. X.; Yu, H. M. 2000. "A Novel Energy Partition for Gaining New Insight into Aromaticity and Conjugation." *J. Phys. Chem. A*, 104: 1736-1747.
- 9 Yu, Z. H.; Peng, X. Q. 2001. "New Insight into the Nature of Electron Delocalization: The Driving Forces for Distorting the geometry of Stilbene-like Species." *J. Phys. Chem. A*, 105: 8541-8553.
- 10 Yu, Z. H.; Xuan, Z. Q. 2000. "The Destabilization of π -Electron Delocalization in Cyclopentadiene." *Chem. J. Chin Univ.*, 21: 421-426 (Chinese).
- 11 Xu, H.; Yu, Z. H. 2005. "N-Benzylideneaniline-like Derivatives and Their Conformation." *Chem. J. Chin. Univ.*, 26: 308-311 (Chinese).
- 12 Yu, Z. H.; Xuan, Z. Q.; Guo, Y. S.; Peng, X. Q.; Wang, T. X. 2001. "The Conformation of N-Phenylmethylenethiazoleamine Species and the Driving Forces for Twisting Molecule." *Chem. J. Chin. Univ.*, 22:122-126 (Chinese).
- 13 Xu, H.; Yu, Z. H. 2004. "The Driving Forces for Distorting NBA-Like Species away from Their Planar Geometries." *Theochem*, 682: 37-46.
- 14 Yu, Z. H. Dissertation: 1985. "Alternative Predominance in Competition for Conjugation in Nitrogen Bridge Compounds." Institute of Chemistry, Chinese Academy of Sciences.
- 15 Yu, Z. H.; Dai, C. C.; Jiang, M. Q. 1986. "The Conformation and Intramolecular Forces of Nitrogen-bridge

- Cross-Conjugated Molecules." *Acta Chim. Sin.*, 44: 1253-1256 (Chinese)
- 16 Yu, Z. H.; Jiang, M. Q. 1991. "The Conformation of Aniline and its intramolecular Force." *Theochem*, 83: 69-82.
- 17 Yu, Z. H. 1995. "An Atomic Interaction Energy Approach to the Reactivity of the Aromatic Ring toward Electrophilic Attack." *Int. J. Quantum.Chem.*, 55: 485-492.
- 18 Xuan, Z. Q.; Wang, T. X.; Yu, Z. H. 2000. "Automatic Identification of the π FMOs in the Localization Program." *Huaxue Tongbao (Chin.)*, 7: 21-24.
- 19 Bao, P.; Yu, Z. H. 2006. "Theoretical Studies on the Role of π -Electron Delocalization in Determining the Conformation of N-benzylideneaniline with Three Types of LMO Basis Sets." *J. Comput. Chem.*, 27: 809-824.
- 20 Liu, X. W.; Bao, P.; Ma, Y. P.; Yu, Z. H. 2005. "The Difference in the Degree of Localization between the LFMO and NBO Basis Sets, and Its Effects on the Energy Partitions." *Theochem*, 729: 195-201.
- 21 Coulson, C. A. 1960. "Present State of Molecular Structure Calculations." *Rev. Mod. Phys.*, 32: 170-177.
- 22 Ingold, C. K. 1953. *Structure and Mechanism in Organic Chemistry*. New York: Cornell University Press.
- 23 Vollhardt, K. P. C.; Schore, N. E. 1999. *Organic Chemistry*, third Edition. New York: W. H. Freeman and Company.
- 24 Neckers, D. C.; Doyle, M. P. 1977. *Organic Chemistry*. New York: John Wiley & Sons, Inc.
- 25 Gould, E. S. 1960. *Structure and mechanism in Organic Chemistry*. New York: Holt-Dryden Book-Henry Holt Co..
- 26 March, J. 1992. *Advanced Organic Chemistry*. New York: John Wiley & sons Inc..
- 27 Libit, L. Hoffmann, R. 1974. "Toward a Detailed Orbital Theory of Substituent Effects: Charge Transfer, Polarization, and the Methyl Group." *J. Am. Chem. Soc.*, 96: 1370-1383.
- 28 Dykstra, C. E.; Frenking, G.; Kim, K. S.; Scuseria, G. E. 2005. *Theory and Applications of Computational Chemistry: the first Forty years*. Netherlands: Elsevier B. V.
- 29 Frenking G.; Krapp, R. 2007. "Unicorns in the World of Chemical Bonding Models." *J. Comput. Chem.*, 28: 15-24.
- 30 Vala, M. T.; Hillier, I. H.; Rice, S. A.; Jortner, J. 1966. " Theoretical Studies of Transannular Interactions. I. Benzene Excimer Fluorescence and the Singlet States of the Paracyclophanes." *J. Chem. Phys.*, 44: 23-35.
- 31 Murrell, J. N.; Tanaka, J. 1964. " The Theory of The Electronic Spectra of Aromatic Hydrocarbon Dimers." *Mol. Phys.*, 7: 363-380.
- 32 Chestnut, D. B.; Fritchie, C. J.; Simmons, E. 1965. "Extended Hückel Treatment of Excimer Formation." *J. Chem. Phys.*, 42: 1127-1128.
- 33 Hoffmann, R.; Woodward, R. B. 1965. " Selection Rules for Concerted Cycloaddition Reactions." *J. Am. Chem. Soc.*, 87: 2046-2048.
- 34 Herndon, W. C.; Hall, L. H. 1967. "Extended Hückel Theory Applied to Chemical Reactivity." *Theoret. Chim. Acta*, 7: 4-14.
- 35 Salem, L. 1968. "Intermolecular Orbital Theory of the Interaction between Conjugated Systems. I. General Theory." *J. Am. Chem. Soc.*, 90: 543-552.
- 36 Heilbronner, E.; Bock, H. 1970. *Das HOMO-Modell und Seine Anwendung*. Weinheimmergstr: Verlag Chemie, GmbH.
- 37 Dewar, M. J. S. 1969. *The Molecular Orbital Theory of Organic Chemistry*. New York: McGraw-Hill
- 38 Fukui, K. 1970. "Theorie der Orientierung und Stereoselektivitaet." *Fortschr. Chem. Forsch.*, 15: 1
- 39 Klopman, J. Ed. 1974. *Chemical Reactivity and Reaction Paths*. New York: Wiley-Interscience.
- 40 Kepner, R. E.; Winstein, S.; Young, W. G. 1949. "Allylic Rearrangements. XXIV. Abnormal Bimolecular Substitution. The Condensation of Butenyl and Pentenyl Chlorides with Sodium Malonic Ester." *J. Am. Chem. Soc.*, 71: 115-119.
- 41 Stork, G.; White, W. N. 1956. " The Stereochemistry of the SN₂' Reaction. II." *J. Am. Chem. Soc.*, 78: 4609-4619.

- 42 Bach, R. D.; Su, M. D.; Aldabbagh, E.; Andres, J. L.; Schlegel, H. B. 1993. "A theoretical Model for the Orientation of Carbene Insertion into Saturated Hydrocarbons and the Origin of the Activation Barrier." *J. Am. Chem. Soc.*, 115: 10237–10246.
- 43 Bickelhaupt, F. M.; Baerends, E. J.; Nibbering, N. M. M.; Ziegler, T. 1993. "Theoretical Investigation on Base-Induced 1,2-Eliminations in the Model System Fluoride Ion + Fluoroethane. The Role of the Base as A Catalyst." *J. Am. Chem. Soc.*, 115: 9160–9173.
- 44 Nakamura, K.; Osamura, Y. 1993. "Theoretical Study of the Reaction Mechanism and Migratory Aptitude of the Pinacol Rearrangement." *J. Am. Chem. Soc.*, 115: 9112–9120.
- 45 Naito, T.; Nagase, S.; Yamataka, H. 1994. "Theoretical Study of the Structure and Reactivity of Ylides of N, P, As, Sb, and Bi." *J. Am. Chem. Soc.*, 116: 10080–10088.
- 46 Salem, L. 1968. " Intermolecular Orbital Theory of the Interaction between Conjugated Systems. II. Thermal and Photochemical Cycloadditions." *J. Am. Chem. Soc.*, 90: 553–566.
- 47 Devaquet, A.; Salem, L. 1969. " Intermolecular Orbital Theory. 111. Thermal and Photochemical Dimerization of Unsaturated Ketones." *J. Am. Chem. Soc.*, 91: 3793–3800.
- 48 Sustmann, R.; Binsch, G. 1971. "Self-Consistent Perturbation Theory for Interacting Electron Systems H. Semi-Empirical Treatment for Two Closed-Shell Molecules and an Application to the Diels-Alder Reaction" *Mol. Phys.*, 20: 9–29
- 49 Fukui, K. 1966. "An MO-Theoretical Illumination for the Principle of Stereoselection." *Bull. Chem. Soc. Jap.*, 39: 498–503.
- 50 Fukui, K.; Fujimoto, H. 1966. "Sigma-Pi Interaction Accompanied by Stereoselection." *Bull. Chem. Soc. Jap.*, 39: 2116–2126.
- 51 Fukui, K.; Fujimoto, H. 1969. *Mechanisms of Molecular Migrations*, Vol. 2. Thyagarajan, B. S., Ed. New York: Interscience.
- 52 Fukui, K. 1970. *Theory of Orientation and Stereoselection*. Heidelberg: Springer-Verlag.
- 53 Fukui, K. 1982. "Role of Frontier Orbitals in Chemical Reactions." *Science*. 218: 747–754.
- 54 Fukui, K.; Yonezawa, T.; Shingu, H. 1952. "A Molecular Orbital Theory of Reactivity in Aromatic Hydrocarbons." *J. Chem. Phys.*, 20: 722–725.
- 55 Fukui, K.; Yonezawa, T.; Nagata, C.; Shingu, H. 1954. "Molecular Orbital Theory of Orientation in Aromatic, Heteroaromatic, and Other Conjugated Molecules." *J. Chem. Phys.*, 22: 1433–1442.
- 56 Fukui, K. 1964. *Molecular Orbitals in Chemistry, Physics and Biology*. P.-O. Lowdin and B. Pullman, Ed.. New York: Academic Press.
- 57 Fukui, K. 1971. "Recognition of Stereochemical Paths by Orbital Interaction." *Acc. Chem. Res.*, 4: 57–64.
- 58 Woodward, R. B.; Hoffmann, R. 1969. *The Conservation of Orbital Symmetry*. New York: Academic Press.
- 59 Hoffmann, R.; Woodward, R. B. 1965. "Orbital Symmetries and *endo-exo* Relationships in Concerted Cycloaddition Reactions." *J. Am. Chem. Soc.*, 87: 4388–4389.
- 60 Feuer, J.; Herndon, W. C.; Hall, L. H. 1968. " A Perturbational MO Method Applied to Diels-Alder Reactions with Unsymmetrical Dienes and Dienophiles Prediction of the Major Product." *Tetrahedron*, 24: 2575–2582.
- 61 Kistiakowsky, G. B.; Ruhoff, J. R.; Smith, H. A.; Vaughan, W. E. 1935. "Heats of Organic Reactions. II. Hydrogenation of Some Simpler Olefinic Hydrocarbons." *J. Am. Chem. Soc.*, 57: 876–882.
- 62 Kistiakowsky, G. B.; Ruhoff, J. R.; Smith, H. A.; Vaughan, W. E. 1936. "Heats of Organic Reactions III. Hydrogenation of Some Higher Olefins." *J. Am. Chem. Soc.*, 58: 137–145.
- 63 Epotis, N. D.; Bjorkquist, D.; Bjorkquist, L.; Sarkany, S. 1973. "Attractive Nonbonded Interactions in 1-Substituted Propenes. Consequences for Geometric and Conformational Isomerism." *J. Am. Chem. Soc.*, 95: 7558–7562.
- 64 Bernardi, F.; Epotis, N. D.; Yates, R. L.; Schlegel, H. B.. 1976. "Nonbonded Attraction in Methyl Vinyl Ether." *J. Am. Chem. Soc.*, 98: 2385–2390.
- 65 Viehe, H. G. 1960. "Geometrische Isomerenpaare mit bevorzugter *cis*-Struktur." *Chem. Ber.*, 93: 1697–1790.
- 66 M. M. Kreevoy and E. A. Mason, 1957." A Simple Model for Barriers to Internal Rotation. II. Rotational

- Isomers." J. Amer. Chem. Soc., 79: 4851-4854.
- 67 Epiotis, N. D.; WR Cherry, W. R.; Shaik, S.; Bernardi, F. 1977. "Structural Theory of Organic Chemistry." Topics Curr. Chem., vol. 70. Berlin: Springer-Verlag.
- 68 Epiotis, N. D. 1973. "Attractive Nonbonded Interactions in Organic Molecules." J. Am. Chem. Soc., 95: 3087-3096.
- 69 Houk, K. N. 1972. "Regioselectivity and Reactivity in the 1,3-Dipolar Cycloadditions of Diazonium Betaines (Diazoalkanes, Azides, and Nitrous Oxide)." J. Am. Chem. Soc., 94: 8953-8955.
- 70 Coulson, C. A.; and Longuet-Higgins, H. C. 1947. "The Electronic Structure of Conjugated Systems. I. General Theory." Proc. Roy. Soc. Ser. A, 191: 39-60.
- 71 Coulson, C. A.; Longuet-Higgins, H. C. 1947. "The Electronic Structure of Conjugated Systems. II. Unsaturated Hydrocarbons and their Hetero-Derivatives." Proc. Roy. Soc. Ser. A, 192: 16-35.
- 72 Coulson, C. A.; Longuet-Higgins, H. C. 1948. "The Electronic Structure of Conjugated Systems. III. Bond Orders in Unsaturated Molecules; IV. Force Constants and Interaction Constants in Unsaturated Hydrocarbons." Proc. Roy. Soc. Ser. A, 193: 447-464.
- 73 Coulson, C. A.; Longuet-Higgins, H. C. 1948. "The Electronic Structure of Conjugated Systems. V. The Interaction of Two Conjugated Systems." Proc. Roy. Soc. Ser. A, 195: 188-197.
- 74 Dewar, M. J. S.; Dougherty, R. C. 1975. *The PMO theory of Organic Chemistry*. New York and London: Plenum Press,
- 75 Dewar, M. J. S.; Dougherty, R. C. 1969. *The Molecular Orbital Theory of Organic Chemistry*. New York: McGraw-Hill Book Inc..
- 76 Dewar, M. J. S. 1952. "A Molecular Orbital Theory of Organic Chemistry. I. General Principles." J. Am. Chem. Soc., 74: 3341-3345.
- 77 Dewar, M. J. S. 1952. "A Molecular Orbital Theory of Organic Chemistry. II. The Structure of Mesomeric Systems." J. Am. Chem. Soc., 74: 3345-3350.
- 78 Dewar, M. J. S. 1952. "A Molecular Orbital Theory of Organic Chemistry. III. Charge Displacements and Electromeric Substituents." J. Am. Chem. Soc., 74: 3350-3353.
- 79 Dewar, M. J. S. 1952. "A Molecular Orbital Theory of Organic Chemistry. IV. Free Radicals." J. Am. Chem. Soc., 74: 3353-3354.
- 80 Dewar, M. J. S. 1952. "A Molecular Orbital Theory of Organic Chemistry. V.1 Theories of Reactivity and the Relationship between Them." J. Am. Chem. Soc., 74: 3355-3356.
- 81 Dewar, M. J. S. 1952. "A Molecular Orbital Theory of Organic Chemistry. VI.1 Aromatic Substitution and Addition." J. Am. Chem. Soc. 1952, 74: 3357-3363.
- 82 Whangbo, M. H.; Schlegel, H. B.; Wolfe, S. 1977. "Molecular Orbitals from Group Orbitals. 3. Quantitative Perturbational Molecular Orbital Analysis of ab Initio SCF-MO Wave Functions." J. Am. Chem. Soc., 99: 1296-1304.
- 83 Whangbo, M. H. Wolfe, S. 1977. "Molecular Orbitals from Group Orbitals. IV. Quantitative Perturbational Molecular Orbital Analysis of the Methyl Rotational Barriers in $(CH_3)_2X$ Molecules. Effect of The Fragmentation Mode upon the Results of the Analysis." Can. J. Chem. 55: 2778-2787
- 84 Bernardi, F.; Bottoni, A.; Epotis, N. D.; Guerra, M. 1978. "Quantitative Nonempirical Estimates of the Effects of Orbital Interactions. Applications to Difluoroethylenes." J. Am. Chem. Soc. 100: 6018-6022.
- 85 Kost, D.; Schlegel, H. B.; Mitchell, D. J.; Wolfe, S. 1979. "Molecular Orbitals from Group Orbitals. IX. The Problem of Hybrid Lone Pairs." Can. J. Chem., 57: 729-732.
- 86 Bernardi , F.; Bottoni, A. 1981. "Fragment Interaction Analysis of Structural Problems in the Framework of *ab Initio* SCF-MO Computations." Theoret. Chem. Acc., 58: 245-255.
- 87 Wolfe, S.; Mitchell, D. J.; Whangbo, M. H. 1978. "Molecular Orbitals from Group Orbitals. 5. Role of Steric Effects in the Perturbational Molecular Orbital Method of Conformational Analysis." J. Am. Chem. Soc., 100: 1936-1938.
- 88 Whangbo, M. H.; Mitchell, D. J.; Wolfe, S. 1978. "Molecular Orbitals from Group Orbitals. 6. Quantitative

- Evaluation and Nature of the Stabilizing and Destabilizing Orbital Interactions in Difluoroethylenes and Fluoropropenes." J. Am. Chem. Soc., 100: 3698-3706.
- 89 Bernardi, F.; Bottoni, A.; Epotis, N. D. 1978. "Quantitative Nonempirical Analysis of the π -conjugative Effects of Substituents." J. Am. Chem. Soc., 100: 7205-7209.
- 90 Bernardi, F.; Bottoni, A.; Tonachini, G. 1979. "Conformational Preferences in Methylsilane and Disilane. A Quantitative Non-Empirical Analysis of the Importance of the Hyperconjugative Interactions." Theoret Chim. Acta, 52: 37-43.
- 91 Csizmadia, I. G. 1982. *Molecular Structure and Conformation*, Vol. 3. New York: Elsevier Scientific Pub. Comp.
- 92 Boys, S. F. 1960. "Construction of Some Molecular Orbitals to Be Approximately Invariant for Changes from One Molecule to Another." Rev. Mod. Phys., 32: 296-299.
- 93 Foster, J. M.; Boys, S. F. 1960. "Canonical Configurational Interaction Procedure." Rev. Mod. Phys., 32: 300-302.
- 94 http://en.wikipedia.org/wiki/Natural_bond_orbital.
- 95 Weinhold, F.; Landis, C. R. 2001. "Natural Bond Orbitals and Extensions of Localized Bonding Concepts." Chem. Edu. Res. Pract. Eur., 2: 91-104
- 96 Weinhold, F. *NBO 5.0 program Manul*. Wisconsin: Theoretical Chemistry Institute and Department of Chemistry, University of Wisconsin.
- 97 Perkins , P. G; Stewart, J. J. P. 1982. "A New Rapid Method for Orbital Localisation." J. Chem. Soc., Faraday Trans. 2, 78: 285-296
- 98 Granovsky, A. A., <http://classic.chem.msu.su/gran/gamess/index.html>
- 99 Schmidt, M. W.; Baldridge, K. K.; Boatz, J. A.; Elbert, S. T.; Gordon, M, S.; Jensen, J. H.; Koseki, S.; Matsunaga, N.; Nguyen, K. A.; Su, S.; Windus, T. L.; Dupuis, M.; Montgomery, Jr., J. A. 1993. "General atomic and molecular electronic structure system." J. Comput. Chem., 14: 1347-1363.

CHAPTER 4

π -DELOCALIZATION DESTABILIZATION

ABSTRACT

According to the facts that $dE_e(\theta)/d(\theta) < 0$ and $dE_N(\theta)/d(\theta) > 0$ ($0^\circ < \theta < \theta_{e-\min}$), total electronic energy is always the driving force of molecular distortion. Due to the existence of the π - σ interaction, however, the distortivity of total electronic energy does not mean that the electron delocalization is destabilization, and it may be the result of any of the following two opposite natures (stabilization and destabilization) of electron delocalization: (i) stabilizing electron delocalization: the π -electron delocalization energy $\Delta E^{\pi\pi}(\theta) < 0$, $d\Delta E^{\pi\pi}(\theta)/d(\theta) > 0$, the σ -electron delocalization energy $\Delta E_n^{\sigma\sigma}(\theta) < 0$, $d\Delta E_n^{\sigma\sigma}(\theta)/d(\theta) > 0$, and the π - σ interaction energy $\Delta E^{\pi\sigma}(\theta) < 0$, $d\Delta E^{\pi\sigma}(\theta)/d(\theta) < 0$; $|d\Delta E^{\pi\sigma}(\theta)/d(\theta)| > d\Delta E^{\pi\pi}(\theta)/d(\theta) + d\Delta E^{\sigma\sigma}(\theta)/d(\theta)$ (the stabilizing energy is expressed as a negative value); (ii) destabilizing electron delocalization: $\Delta E^{\pi\pi}(\theta) > 0$, $d\Delta E^{\pi\pi}(\theta)/d(\theta) < 0$, $\Delta E_n^{\sigma\sigma}(\theta) > 0$, $d\Delta E_n^{\sigma\sigma}(\theta)/d(\theta) < 0$, $\Delta E^{\pi\sigma}(\theta) > 0$, $d\Delta E^{\pi\sigma}(\theta)/d(\theta) > 0$; $d\Delta E^{\pi\sigma}(\theta)/d(\theta) < |d\Delta E^{\pi\pi}(\theta)/d(\theta) + d\Delta E^{\sigma\sigma}(\theta)/d(\theta)|$ (the destabilizing energy is expressed as a positive value). Based on the construction of the DSI (π -MOs are localized on their respective fragments, and σ -MOs are delocalized on the whole molecular framework) and FUD states (π and σ -MOs are delocalized on the whole molecular framework) for each of NBA-like species, the following results have nothing to do with the theoretical level and basis set size: for the molecular energy of the DSI state: $E^{\text{DSI}}(\theta) < 0$, $d\Delta E^{\text{DSI}}(\theta)/d(\theta) < 0$; for the molecular energy of the FUD state, $E^{\text{FUD}}(\theta) < 0$, $d\Delta E^{\text{FUD}}(\theta)/d(\theta) < 0$. Due to that $|E^{\text{DSI}}(\theta)| > |E^{\text{FUD}}(\theta)|$, always $\Delta E^V(\theta) = [E^{\text{FUD}}(\theta) - E^{\text{DSI}}(\theta)] > 0$, $d[\Delta E^V(\theta)]/d\theta < 0$. Therefore, π -electron delocalization is always destabilization, and it is a driving force for distorting NBA-like species. When the vertical delocalization energy (VRE), $\Delta E^V(\theta)$, of NBA is used as a reference, an electron-releasing group such as -OH makes the VRE to be more destabilizing, and an electron-withdrawing group such as -NO₂ decreases the value of VRE. The ability of electron-withdrawing group is stronger than that of electron-releasing group. For the NBA-like species substituted by -NO₂ and -OH groups, therefore, the VRE is always less than that of NBA.

yuzh@iccas.ac.cn

Key words: destabilizing π -delocalization energy; substituent effect on vertical delocalization energy; π -localized electronic state; π , σ -delocalized electronic state.

4.1. INTRODUCTION

In Chapter 2, it has been shown that, for each type of NBA-like species, whether planar or non-planar, as long as there is no stronger hydrogen bond between the fragments, the total electron energy $E_e(\theta)$ and the nuclear repulsive force $E_N(\theta)$ ($0^\circ < \theta < \theta_{\min-e}$) are characterized as follows: $dE_e(\theta)/d(\theta) < 0$, and $dE_N(\theta)/d(\theta) > 0$ ($0 < \theta < \theta_{e-min}$). Due to the presence of $\pi-\sigma$ interaction in a non-planar conformation, the following two opposing views on the nature of electron delocalization may lead to the same energy change characteristics as described above:

- (i) $\Delta E^{\pi\pi}(\theta) < 0$, $d\Delta E^{\pi\pi}(\theta)/d(\theta) > 0$
 $\Delta E^{\sigma\sigma}(\theta) < 0$, $d\Delta E^{\sigma\sigma}(\theta)/d(\theta) > 0$
 $\Delta E^{\pi\sigma}(\theta) < 0$, $d\Delta E^{\pi\sigma}(\theta)/d(\theta) < 0$
 $|d\Delta E^{\pi\sigma}(\theta)/d(\theta)| > |d\Delta E^{\pi\pi}(\theta)/d(\theta)| + |d\Delta E^{\sigma\sigma}(\theta)/d(\theta)|$
- (ii) $\Delta E^{\pi\pi}(\theta) > 0$, $d\Delta E^{\pi\pi}(\theta)/d(\theta) < 0$
 $\Delta E^{\sigma\sigma}(\theta) > 0$, $d\Delta E^{\sigma\sigma}(\theta)/d(\theta) < 0$
 $\Delta E^{\pi\sigma}(\theta) > 0$, $d\Delta E^{\pi\sigma}(\theta)/d(\theta) > 0$
 $|d\Delta E^{\pi\sigma}(\theta)/d(\theta)| < |d\Delta E^{\pi\pi}(\theta)/d(\theta)| + |d\Delta E^{\sigma\sigma}(\theta)/d(\theta)|$

where $\Delta E^{\pi\pi}(\theta)$ is the π -electron delocalization energy, $\Delta E^{\sigma\sigma}(\theta)$ is the σ -electron delocalization energy, and $\Delta E^{\pi\sigma}(\theta)$ is an energy effect associated with the $\pi-\sigma$ orbital interaction. That is to say, solely based on that $E_e(\theta) < 0$ and $dE_e(\theta)/d(\theta) < 0$ ($0 < \theta < \theta_{e-min}$), it is impossible to be sure that the electronic delocalization must be destabilization. Only by the accurate calculation of the electron delocalization energy such as $\Delta E^{\pi\pi}(\theta)$, can the nature of the electron delocalization be judged. Construction of LFMO (absolutely localized fragment molecular orbital) basis set provides a basic mean for studying the nature of electron delocalization. Next, need to create a suitable energy decomposition method, which is the object of this chapter.

In the literature, several energy decomposition methods have been reported, these methods include Morokuma's energy decomposition (MED),¹⁻⁴ Weinhold's NBO (Natural Bond Orbital)⁵⁻⁷ and NEDA (Natural Energy Decomposition Analysis),⁸⁻¹¹ MO's ODP (Orbital Deletion Procedure) and BLW (block localized wavefunction),¹²⁻¹⁷ Bagus and Bauschlich's CSOV (Constrained Space Orbital Variations),¹⁸ Stevens and Fink's RVS (Reduced Variational Space Self-Consistent-Field),¹⁹ Vaart and Merz's DCDA (Divide and Conquer Decomposition Analysis),²⁰ Dapprich and Frenking's CDA (Charge Distribution Analysis),²¹ Bader's AIM (atoms-in-molecule),^{22,23} Ziegler and Rauk's ETS (Extended Transition State),²⁴ Mayer's CECA (Chemical energy component analysis),²⁵⁻²⁷ Martinov and Cioslowski's REP (Rigorous Energy Partitioning)²⁸.

Our $\pi-\sigma$ energy decomposition (our 1998 and 2006 methods²⁹⁻³⁸) is based on the principle of the Morokuma's energy decomposition.

4.1.1. Morokuma Energy Decomposition

In 1976, a new energy decomposition method within the Hartree-Fock approximation was reported by Morokuma,¹ and it has been installed in the Gaussian and Gamess software packages. In fact, the establishment and development of the Morokuma's method can be traced back to 1971. But this early method is based on AO Fock and overlap integral matrices. Through a perturbation expansion, the interaction energy between the molecules can be decomposed into the electrostatic (ES), polarization (PL), exchange (EX), charge transfer (CT), and dispersion energy terms.³⁹ For this early Morokuma's method, the charge transfer energy can only be calculated as the difference between the total interaction energy and the sum of the remaining three terms (ES, PL and EX). In order

to understand the role of MO charge transfer and exchange interactions between molecules, Morokuma reported a new version of his method in 1976. This new energy decomposition method is based on the MO Fock and overlap integral matrices. Using this method, each of the four terms (ES, PL, EX and CT) can be independently calculated. Since then, as done by our method, it also becomes possible for each energy effects to be decomposed into the π and σ parts.

4.1.1.1. Matrix Transformation and Expansion

In order to decompose the molecular energy E and the energy effect ΔE , as the first step of Morokuma's method, the molecular orbitals, φ^A_u , of the isolated molecule A and the molecular orbitals, φ^B_v , of the isolated molecule B are superimposed according to Equation (4-2):

$$\Psi_i^o = \sum_{\lambda=1, \lambda \in A}^{Na} a_{\lambda i}^o \phi_{\lambda} + \sum_{\rho=Na+1, \rho \in B}^{Na+Nb} b_{\rho i}^o \phi_{\rho} = \sum_{\mu=1}^{Na+Nb} t_{\mu i}^o \phi_{\mu} \quad (4-1)$$

In Equation (4-1), when MO $\psi_i^o \in$ molecule A, set all AO coefficients $b_{\rho i}^o = 0$; MO $\psi_i^o \in$ molecule B, set all AO coefficients $a_{\lambda i}^o = 0$. For the planar molecules A and B, the π and σ ψ_i^o can be separated out, $\{\psi_i^o\} = \{\psi_m^{P-\pi}, \psi_n^{P-\sigma}\}$ ($P = A, B$).

Then, the MO basis set, $\{\psi_i^o\}$, is used to transform the AO Fock and overlap integral matrices, \mathbf{f} and \mathbf{s} , of the complex (A+B) into the MO Fock and overlap integral matrices, \mathbf{F} and \mathbf{S} (a capitalized bold letter represents a MO matrix, and a capitalized letter with two subscripts, such as F_{ij} , represents an element of the MO matrix such as \mathbf{F}), using the following two Equations:

$$F_{ij} = \sum_{\lambda=1}^N \sum_{\rho=1}^N a_{\lambda i} f_{\lambda \rho} a_{\rho j} \quad (4-2)$$

$$S_{ij} = \sum_{\lambda=1}^N \sum_{\rho=1}^N a_{\lambda i} s_{\lambda \rho} a_{\rho j} \quad (4-3)$$

In Equation (4-2) and Equation (4-3), $f_{\lambda \rho}$ and $s_{\lambda \rho}$ are the elements of the AO Fock and overlap integral matrices, \mathbf{f} and \mathbf{s} , of the complex A+B, $a_{\lambda i}$ is the coefficient of the λ -th AO in the i -th MO ψ_i^o , and $a_{\rho j}$ is the coefficient of the ρ -th AO in the j -th MO ψ_j^o .

4.1.1.2. Energy Decomposition

At the Hartree-Fock level, total electron energy E_e can be written as follow:

$$E_e = \sum_i^N \sum_j^N (F_{ij} + H_{ij}) D_{ij} = \sum_P \sum_Q (\sum_{i \in P} \sum_{j \in Q} E_{e-ij}) = \sum_P \sum_Q E_e^{PQ} \quad (4-4)$$

where \mathbf{D} is the MO density matrix. Due to the different belongings of MOs ψ_i and ψ_j , total electronic energy can be partitioned into the following four parts:

$$\sum_P \sum_Q E_e^{PQ} = E_e^{AA} + E_e^{AB} + E_e^{BA} + E_e^{BB} \quad (4-5)$$

According to the Morokuma's definitions, each item in Equation (4-5) can be further partitioned into the following four items:

$$E_e^{PQ} = \left(\sum_{i \in P} \sum_{j \in Q} E_{e-ij} \right) = E_e^{PQ-oo} + E_e^{PQ-ov} + E_e^{PQ-v0} + E_e^{PQ-vv} \quad (4-6)$$

$$E_e^{PQ-oo} = \left(\sum_{i \in P}^{\text{occ}} \sum_{j \in Q}^{\text{occ}} E_{e-ij} \right)$$

$$E_e^{PQ-ov} = \left(\sum_{i \in P}^{\text{occ}} \sum_{j \in Q}^{\text{vac}} E_{e-ij} \right)$$

$$E_e^{PQ-v0} = \left(\sum_{i \in P}^{\text{vac}} \sum_{j \in Q}^{\text{occ}} E_{e-ij} \right)$$

$$E_e^{PQ-vv} = \left(\sum_{i \in P}^{\text{vac}} \sum_{j \in Q}^{\text{vac}} E_{e-ij} \right)$$

Therefore, four types of MO interactions are defined by Morokuma as follows:

- (i) Electrostatic (ES): the classical electrostatic interaction, $E^{\text{PP-oo}}$, between the occupied MOs belonging to the same fragment, and it does not cause any mixing of MOs.
- (ii) Polarization (PL): the interaction which causes the mixing between the occupied and vacant MOs belonging to the same molecule.
- (iii) Exchange (EX): the interaction between occupied MOs belonging to difference molecules, which causes electron exchange and delocalization between molecules.
- (iv) Charge Transfer (CT): the interaction between the occupied MOs of one molecule and the vacant MOs of the other and vice versa, which causes electron delocalization.

Each item E_e^{PQ} in Equation (4-5) can also be partitioned into the following four parts:

$$E_e^{PQ} = \left(\sum_{i \in P} \sum_{j \in Q} E_{e-ij} \right) = E_e^{PQ-\pi\pi} + E_e^{PQ-\pi\sigma} + E_e^{PQ-\sigma\pi} + E_e^{PQ-\sigma\sigma} \quad (4-7)$$

4.1.1.3. Construction of Electronic State

The MO Fock matrix \mathbf{F} and the MO overlap integral matrix \mathbf{S} can also be divided into 16 blocks (Scheme 4-1a). The block $\mathbf{F}^{\text{AB-ov}}$, for instance, includes all the inter-molecular interactions between the occupied MOs of molecule A and the vacant MOs of molecule B. In order to construction an electronic state (denoted as CT+ESX) and to calculate the charge transfer (CT) energy, as shown by Scheme 4-1b, all the non-diagonal blocks (blue block) are deleted, producing a particular MO Fock matrix (Scheme 4-1b). At last, the particular MO Fock matrix is iteratively diagonalized. The molecular energy of the (CT+ESX) state is denoted as $E_{\text{CT+ESX}}$. The energy difference, $(E_{\text{CT+ESX}} - E_{\text{ESX}})$ is an energy effect associated with the CT interaction between two isolated molecules A and B.

When conditionally deleting the non-diagonal blocks of the MO Fock matrix, should avoid the influences of the higher order perturbation on energy decomposition. According to the PMO theory,⁴⁰

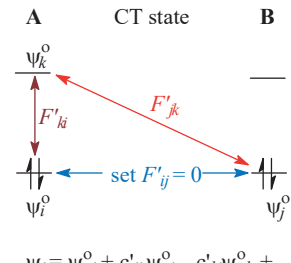
FMO Fock matrix (a)			
A, Occ	A, Vac	B, Occ	B, Vac
$F^{AA\text{-oo}}$	$F^{AA\text{-ov}}$	$F^{AB\text{-oo}}$	$F^{AB\text{-ov}}$
$F^{AA\text{-vo}}$	$F^{AA\text{-vv}}$	$F^{AB\text{-vo}}$	$F^{AB\text{-vv}}$
$F^{BA\text{-oo}}$	$F^{BA\text{-ov}}$	$F^{BB\text{-oo}}$	$F^{BB\text{-ov}}$
$F^{BA\text{-vo}}$	$F^{BA\text{-vv}}$	$F^{BB\text{-vo}}$	$F^{BB\text{-vv}}$

Scheme 4-1

Particular FMO Fock matrix (b)			
A, Occ	A, Vac	B, Occ	B, Vac
$F^{AA\text{-oo}}$	set 0	set 0	$F^{AB\text{-ov}}$
set 0	$F^{AA\text{-vv}}$	$F^{AB\text{-vo}}$	set 0
set 0	$F^{BA\text{-ov}}$	$F^{BB\text{-oo}}$	set 0
$F^{BA\text{-vo}}$	set 0	set 0	$F^{BB\text{-vv}}$

Scheme 4-2

Higher order perturbation

set $F'_{ki} = 0, S'_{ki} = 0$, leading to $c'_{ki} = 0$

$$\psi_i = \psi_i^o + \sum_{j \neq i} c'_{ji} \psi_j^o = \psi_i^o + \sum_{j \neq i}^A c'_{ji} \psi_j^o + \sum_v^B c'_{ki} \psi_k^o \quad (4-8)$$

In Equation (4-8), ψ_i^o , ψ_j^o and ψ_k^o are the unperturbed MOs, and ψ_i is a perturbed MO; the mixing coefficient c'_{ji} , calculated by Equation (4-9), is the contribution of j -th unperturbed MO ψ_j^o to the i -th perturbed MO ψ_i , and c'_{ki} , calculated by Equation (4-10), is the contribution of k -th unperturbed MO ψ_k^o to the i -th perturbed MO ψ_i .

$$c'_{ji} = (H'_{ji} - E_i^o S'_{ji}) / (E_i^o - E_j^o) \quad (4-9)$$

$$c'_{ki} = (H'_{ki} - E_i^o S'_{ki}) / (E_i^o - E_k^o) \quad (4-10)$$

In the CT state, the EX blocks have been set equal to zero. In the Scheme 4-2, therefore, $c'_{ji} = 0$ due to that set $F'_{ji} = 0$. In this case, if the PL interaction between the vacant MO ψ_k and occupied MO ψ_i of molecule A are not set equal to zero ($F'_{ki} \neq 0$ in Scheme 4-2), according to Equation (4-11), the higher order interaction between the occupied MO ψ_i of molecule A and the occupied MO ψ_j of molecule B can't be ensured to be zero although the EX blocks of the MO Fock matrix have been set equal to zero. Therefore, as shown by Scheme 4-1b, all the PLX blocks (F'_{ki} in Scheme 4-2) should also be set equal to zero in order to ensure that the interaction between the monomers A and B is a pure CT interaction.

$$c''_{ji} = [1/(E_i^o - E_j^o)] \sum_{k \neq i} [(H'_{jk} - E_i^o S'_{jk})(H'_{ki} - E_i^o S'_{ki}) / (E_i^o - E_k^o)] \quad (4-11)$$

As Morokuma indicated out, exchange energy (EX) consists of two contributions. One comes from the intermolecular interactions between the occupied MOs and between the vacant MOs. Second one is due to the retention of the two-electron exchange integrals (spatial exchange interaction) between two molecules A and B. In Morokuma's method, not only the MO exchange interaction between molecules A and B but also the space exchange interaction between molecules A and B is excluded in order to calculate the ES energy.

According to the value of the Fermi correction $F^o(\Omega, \Omega)$ for α electrons contained within a region Ω , there is no long exchange with electrons in the remainder of the system when the α electrons are completely localized within the region Ω .⁴¹⁻⁴³ Therefore, as Bader pointed out, the Pauli exclusion principle also controls spatial delocalization of electrons via electron exchange.⁴¹ The delocalization of molecular orbitals is conceptually different from electron

delocalization In the ESX state, molecular orbitals are indeed localized in their respective monomers A and B. But, the electrons can be considered to be still delocalized on the whole framework of complex A+B due to that the two-electron exchange integrals are retained. In the ESX state, therefore, as have been indicated in our previous work³⁵ and will be detailed in Chapter 8, Bader's viewpoint is important for the calculation of electron delocalization energy.

4.1.2. Natural Energy Decomposition Analysis

In 1994, Glendening and Streitwieser developed natural energy decomposition analysis (NEDA).⁸⁻¹⁰ NEDA has been installed in the Gaussian-9X and Gamess software packages.

For the complex A+B, the interaction energy ΔE is calculated by difference:

$$\Delta E = E(\psi'_{AB}) - E(\psi_A) - E(\psi_B) \quad (4-12)$$

In Equation (4-12), ψ'_{AB} is the wave function of A+B complex, and it is obtained from the single-point energy calculation on the optimized geometry of complex A+B; ψ_A and ψ_B are the wave function of the isolated fragments. NEDA partitions the interaction energy ΔE into charge transfer (CT), electrostatic (ES), deformation (DEF), and basis set superposition error (BSSE). No matter how Reed and Weinhold criticized the Morokuma method, and regardless of how the two authors affirmed that their method is more reasonable than the Morokuma method,¹¹ the flaw of NEDA is still fatal.³³ For the A-B complex, Equation (4-2) is used to transform AO Fock matrix to the LMO (localized molecular orbital) Fock matrix, and a LMO Fock matrix element can be further partitioned into the four items, F_{ij}^{AA} , F_{ij}^{AB} , F_{ij}^{BA} and F_{ij}^{BB} , using Equation (4-13):

$$F_{ij} = F_{ij}^{AA} + F_{ij}^{AB} + F_{ij}^{BA} + F_{ij}^{BB} \quad (4-13)$$

$$F_{ij}^{XY} = \sum_{\lambda}^{N_X} \sum_{\rho}^{N_Y} a_{\lambda i}^X f_{\lambda \rho} b_{\rho j}^Y, \quad X, Y = A, B$$

In the case of LFMO Fock matrix element F_{ij} , only one item is not equal to zero due to that LFMOs are absolutely localized on their respective fragments. For NBO basis set, however, the four items in Equation (4-13) are all not equal to zero according to the characteristic of the NBO coefficient matrix (Table 3-1). Therefore, deleting the NBO Fock matrix elements between two molecules A and B is not equal to deleting the AO Fock matrix elements between the molecules, and it includes the deletion of intramolecular elements, f_{ij}^{AA} and f_{ij}^{BB} , of the AO Fock matrix. As will be shown in the next chapter, each of these four items has a large effect on the energy difference ΔE . The so-called intermolecular interaction energy, obtained from NEDA, should include various types of energy effects, such as CT, EX and PL, associated with intramolecular and intermolecular interactions.

For complex A+B, the NBO basis set is orthogonal and normalized. According to Equation (4-14), there is no four-electron destabilizing interaction (i. e. MO exchange interaction) between molecules.

$$\Delta E_{ij}^{(4)} = 4(\epsilon_o S_{ij}^2 - H_{ij} S_{ij}) / (1 - S_{ij}^2) \quad (4-14)$$

This may be a reason why NEDA does not include the MO exchange interaction between molecules.

4.1.3. Our σ - π Energy Decomposition Method

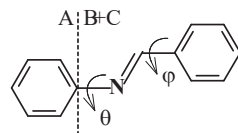
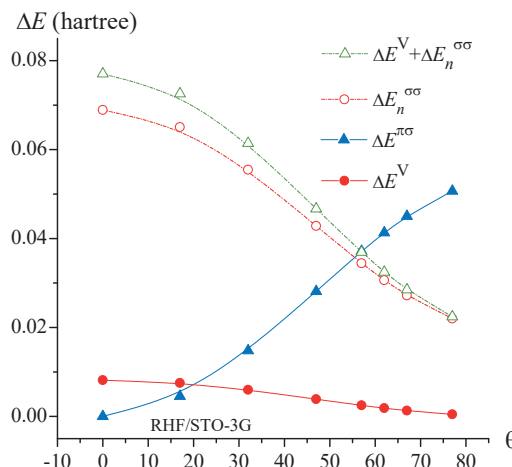


Figure 4-1. Preferential geometry is a compromise between the energy effects associated with the $\pi-\pi$, non-bonded $\sigma-\sigma$, and $\pi-\sigma$ interactions between fragments A and (B+C).

In 1998, inspired by the PMO theory and Morokuma energy decomposition, our $\pi-\sigma$ energy decomposition method (our 1998 method) was developed.²⁹ Our 1998 method is based on the source codes of the easy-to-understand *ab initio* program (Liao-Wu-Liu program) written by Muzhen Liao, Guoshi Wu and Honglin Liu of Tsinghua University.⁴⁴ But, the biggest problem is that the Liao-Wu-Liu program can be run only with the minimal and split basis sets such as STO-3G, 3-21G, 4-31G and 6-31G. In 2005, we got the source codes of PC-Gamess from Dr. Alex Granovsky of Lomonosov State University, Moscow, and our 1998 program is integrated into PC-Gamess. This improved 1998 method is called our 2006 method.³³

Unlike the Morokuma method, we are more concerned with the nature of π - and σ -electron delocalization. For a twisted conformation of every one NBA-like species (N-benzylideneaniline-like species), by using our 2006 method to perform a conditional single-point energy calculation based on LFMO basis set, the following four localized electronic states can be constructed:²⁹⁻³⁸

DSI: (delocalized sigma state), π -MOs are localized on their respective fragments, and σ -MOs (sigma MO) are delocalized on the whole molecular framework, and its molecular energy is denoted as $E^{\text{DSI}}(\theta)$.

PDSI: (partly delocalized sigma state), π -MOs are localized on their respective fragments. σ -MOs are delocalized on the whole molecular framework, but the MO interactions between the singly occupied σ LFMOs and the doubly occupied and vacant σ LFMOs are set equal to zero, and its molecular energy is denoted as $E_n^{\text{DSI}}(\theta)$.

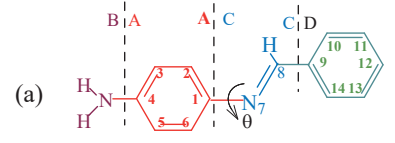
FUD: (fully delocalized state), π and σ -MOs are delocalized on the whole molecular framework, but the MO interactions between the π and σ LFMOs are set equal to zero, and its molecular energy is denoted as $E^{\text{FUD}}(\theta)$.

FUL: (fully localized state), all the MO interactions between the fragments are set equal to zero except for the interaction between the singly occupied LFMOs, and meanwhile the MO interactions between the singly occupied σ LFMOs and the doubly occupied and vacant σ LFMOs are set equal to zero, and its molecular energy is denoted as $E^{\text{FUL}}(\theta)$.

Then, the energy effects, denoted as $\Delta E^V(\theta)$, $\Delta E_n^{\sigma\sigma}(\theta)$ and $\Delta E^{\pi\sigma}(\theta)$, associated with the $\pi-\pi$ interaction, non-bonded $\sigma-\sigma$ interaction, and $\pi-\sigma$ interaction, can be calculated. For NBA-like species, as have been shown in our previous works and will be detailed in this chapter, all the energy effects are destabilizing, and their characters are as follows:

$$\Delta E^V(\theta) > 0, d\Delta E^V(\theta)/d(\theta) < 0$$

	$\Psi_m^{A-\pi}$	$m = 1 \text{ to } 24$	
	$\pi\text{-LFMO}(1,m)$	16 18 19 56 57 60 70 74 77 79 80 83 95 96 98	
		99 100 102 111 112 114 115 116 121	
Fragment A	$\Psi_n^{A-\sigma}$	$n = 1 \text{ to } 74$	
	$\sigma\text{-LFMO}(1,n)$	1 2 3 4 5 6 7 8 9 10 11 12 13 14 15	
		17 20 21 58 59 61 62 63 64 65 66 67 68 69 71	
		72 73 75 76 78 81 82 84 85 86 87 88 89 90 91	
		92 93 94 97 101 103 104 105 106 107 108 109 110 113 117	
		118 119 120 122 123 124 125 126 127 128 129 130 131 132	
	Ψ_k^{A-s}	$k = 1 \text{ to } 2$	
	$s\text{-LFMO}(1,k)$	20 21	
	$\Psi_m^{B-\pi}$	$m = 1 \text{ to } 4$	
	$\pi\text{-LFMO}(2,m)$	25 136 138 143	
Fragment B	$\Psi_n^{B-\sigma}$	$n = 1 \text{ to } 15$	
	$\sigma\text{-LFMO}(2,n)$	22 23 24 26 133 134 135 137 139	
		140 141 142 144 145 146	
Fragment C	Ψ_k^{B-s}	$k = 1$	$\Psi_i = \sum_{\mu=1}^N t_{\mu i} \phi_{\mu}$
	$s\text{-LFMO}(2,k)$	26	
	$\Psi_m^{C-\pi}$	$m = 1 \text{ to } 8$	
	$\pi\text{-LFMO}(3,m)$	31 147 152 155 160 161 163 166	
	$\Psi_n^{C-\sigma}$	$n = 1 \text{ to } 24$	
	$\sigma\text{-LFMO}(3,n)$	27 28 29 30 32 33 34 148 149	
		150 151 153 154 156 157	
		158 159 162 164 165 167 168 169 170	
Fragment D	Ψ_k^{C-s}	$k = 1 \text{ to } 2$	
	$s\text{-LFMO}(3,k)$	33 34	
	$\Psi_m^{D-\pi}$	$m = 1 \text{ to } 24$	
	$\pi\text{-LFMO}(4,m)$	50 53 54 171 172 175 185 189 192 195 196 198 213 215 216	
		217 218 228 229 231 232 233 237 242	
	$\Psi_n^{D-\sigma}$	$n = 1 \text{ to } 76$	
	$\sigma\text{-LFMO}(4,n)$	35 36 37 38 39 40 41 42 43 44 45 46 47 48 49	
		51 52 55 173 174 176 177 178 179 180 181 182 183 184 186	
		187 188 190 191 193 194 197 199 200 201 202 203 204 205 206	
		207 208 209 210 211 212 214 219 220 221 222 223 224 225 226	
		227 230 234 235 236 238 239 240 241 243 244 245 246 247 248	
		249	
	Ψ_k^{D-s}	$k = 1$	
	$s\text{-LFMO}(4,k)$	55	



AO coefficient matrix of the LFMO basis set (b)

Ψ_i^A	Ψ_i^B	Ψ_i^C	Ψ_i^D
t_A	0	0	0
0	t_B	0	0
0	0	t_C	0
0	0	0	t_D

(c)

Figure 4-2. For the $\theta = 17^\circ$ geometry of N-benzylidene-(p-amino)aniline, the LFMO-4 basis set $\{\Psi_i\} = \{\Psi_m^{P-\pi}, \Psi_n^{P-\sigma}, \Psi_k^{P-s}\}$ ($P = A, B, C, D$) at B3LYP/6-31G* level. (a) The A-B-C-D dissection way; (b) The AO coefficient Matrix of the LFMO basis set; (c) The LFMOS in each fragment, and their numberings in the entire LFMO basis set, and m, n and k are the numbers of the π, σ and singly occupied LFMOS in each fragment.

$$\begin{aligned}\Delta E_n^{\sigma\sigma}(\theta) &> 0, d\Delta E^{\sigma\sigma}(\theta)/d(\theta) < 0 \\ \Delta E^{\pi\sigma}(\theta) &> 0, d\Delta E^{\pi\sigma}(\theta)/d(\theta) > 0\end{aligned}$$

Therefore, as indicated by the curves in Figure 4-1, the π - π interaction and non-bonded σ - σ interaction are the driving forces of molecular distortion, and the π - σ interaction is resistance to molecular distortion. In particular, these conclusions have nothing to do with the theory level and basis size. At about $\theta = 57^\circ$ geometry of N-benzylideneaniline (Figure 4-1), interestingly, the total driving force reaches equilibrium with resistance. This twist angle is very close to the twist angle (51.7°) determined by $dE_e(51.7^\circ)/d\theta = 0$.

Contrary to classical views, therefore, the distortion of NBA-like species is not to obtain a higher stability, but it is to make the molecule itself destabilized as small as possible. Thus, “conjugation (resonance) stabilization”, as one of the fundamental principles of organic chemistry, can indeed be questioned.

4.2. CONSTRUCTION OF LOCALIZED STATES

According to the definition,⁴⁵⁻⁴⁷ the vertical delocalization energy is the molecular energy difference, $\Delta E^V(\theta) = E^{\text{FUD}}(\theta) - E^{\text{DSI}}(\theta)$, between the FUD and DSI states. Therefore, the construction of the LFMO basis set is a prerequisite for studying the nature of electron delocalization. In our 2006 method, due to that the two-electron exchange integrals are retained, the conditional deletions of the MO matrix elements can only ensure the localization of the molecular orbitals.

4.2.1. Construction of LFMO basis set

In order to construct a LFMO basis set for a NBA-like species, the number, N_F , of fragments generated by the breaking of single bond(s) should be equal to the number of planar groups that are not coplanar with each other. In a substituted NBA-like species, N_F is usually greater than three. In the $\theta = 17^\circ$ geometry of N-Benzylidene-(4-amino)aniline, for example, there are four planar fragments, N-phenyl ring (fragment A), amino group (B), $-\text{N}=\text{CH}-$ (C), and C-phenyl ring (D). These four planar fragments are not coplanar with each other. Therefore, the molecule should be dissected into four fragments (A, B, C and D) (Figure 4-2a), and the numberings of the LFMOs in each fragment are listed in Figure 4-2c. In the fully optimized geometry of N-benzylidene-(4-amino)aniline, the amino group is tetrahedral. Thus, it should be artificially flattened to separate the π - and σ -LFMOs.

4.2.1.1. LFMO-n Basis Set

Using the method described in Chapter 3, the LFMO-4 basis set for the $\theta = 17^\circ$ conformation of N-Benzylidene-(4-amino)aniline is constructed, and the LFMOs are absolutely localized on their respective fragments (Figure 4-2b). In the calculation program, the values of the subscript variable i of the LFMOs Ψ_i corresponding to $\Psi_m^{\text{P-}\pi}$, $\Psi_n^{\text{P-}\sigma}$ and $\Psi_k^{\text{P-s}}$ are, respectively, stored as the element data in the following three two-dimensional arrays:

$$\begin{aligned}\pi\text{-LFMO(L,m)} &= i, L = 1 (\text{A}), 2 (\text{B}), 3 (\text{C}), \dots; m = 1, 2, \dots, m_p \\ \sigma\text{-LFMO(L,n)} &= i, L = 1 (\text{A}), 2 (\text{B}), 3 (\text{C}), \dots; m = 1, 2, \dots, n_p \\ s\text{-LFMO(L,k)} &= i, L = 1 (\text{A}), 2 (\text{B}), 3 (\text{C}), \dots; m = 1, 2, \dots, k_p\end{aligned}$$

where m_p , n_p and k_p are the numbers of the LFMOs $\Psi_m^{\text{P-}\pi}$, $\Psi_n^{\text{P-}\sigma}$ and $\Psi_k^{\text{P-s}}$ in each fragment P. For example, the array element $\pi\text{-LFMO}(1,3) = 19$, referring to the third red number "19" in Figure 4-2c. Therefore, the 3-th π LFMO

	$\Psi_m^{(A+B)-\pi}$	m = 1 to 28	
	$\pi\text{-LFMO}(1,m)$	16 18 19 56 57 60 70 74 77 79 80 83 95 96 98	
A+B		99 100 102 111 112 114 115 116 121 25 136 138 143	
Fragment A	$\Psi_n^{(A+B)-\sigma}$	n = 1 to 89	
	$\sigma\text{-LFMO}(1,n)$	1 2 3 4 5 6 7 8 9 10 11 12 13 14 15	
		17 20 21 58 59 61 62 63 64 65 66 67 68 69 71	
		72 73 75 76 78 81 82 84 85 86 87 88 89 90 91	
		92 93 94 97 101 103 104 105 106 107 108 109 110 113 117	
		118 119 120 122 123 124 125 126 127 128 129 130 131 132	
		22 23 24 26 133 134 135 137 139 140 141 142 144 145 146	
	$\Psi_k^{(A+B)-s}$	k = 1	
	$s\text{-LFMO}(1,k)$	20	
	$\Psi_i = \sum_{\mu=1}^N t_{\mu i} \phi_{\mu}$		
			(a)
	$\Psi_m^{C-\pi}$	m = 1 to 8	
	$\pi\text{-LFMO}(2,m)$	31 147 152 155 160 161 163 166	
Fragment C	$\Psi_n^{C-\sigma}$	n = 1 to 24	
	$\sigma\text{-LFMO}(2,n)$	27 28 29 30 32 33 34 148 149	
		150 151 153 154 156 157	AO coefficient matrix of
		158 159 162 164 165 167 168 169 170	the LFMO basis set
	Ψ_k^{C-s}	k = 1 to 2	
	$s\text{-LFMO}(2,k)$	33 34	
	$\Psi_m^{D-\pi}$	m = 1 to 24	
Fragment D	$\pi\text{-LFMO}(3,m)$	50 53 54 171 172 175 185 189 192	
		195 196 198 213 215 216	
		217 218 228 229 231 232 233 237 242	
	$\Psi_n^{D-\sigma}$	n = 1 to 76	
	$\sigma\text{-LFMO}(3,n)$	35 36 37 38 39 40 41 42 43 44 45 46 47 48 49	
		51 52 55 173 174 176 177 178 179 180 181 182 183 184 186	
		187 188 190 191 193 194 197 199 200 201 202 203 204 205 206	
		207 208 209 210 211 212 214 219 220 221 222 223 224 225 226	
		227 230 234 235 236 238 239 240 241 243 244 245 246 247 248	
	Ψ_k^{D-s}	k = 1	
	$s\text{-LFMO}(3,k)$	55	(c)

Figure 4-3. The reorganized LFMO-3 basis set $\{\Psi_m^{P-\pi}, \Psi_n^{P-\sigma}, \Psi_k^{P-s}\}$ ($P = A+B, C, D$) for N-Benzylidene-(p-amino)aniline at B3LYP/6-31G* level. (a) The dissection way A-B-C-D. (b) The AO coefficient Matrix of the LFMO basis set. (c) The numberings of LFMOs, and m, n and k are the numbers of the π, σ and singly occupied LFMOs in each fragment.

$\Psi_3^{A-\pi}$ belongs to fragment A, and it is the 19-th LFMO Ψ_i in the entire LFMO basis set $\{\Psi_i\}$. The singly occupied LFMOs are included in the σ -LFMOs $\Psi_n^{P-\sigma}$, and their numberings in the LFMO basis set $\{\Psi_i\}$ are stored in the corresponding elements of the array $\sigma\text{-LFMO}(L,n)$. For example, the 20- and 21-th LFMOs Ψ_i ($i = 20, 21$) are two

singlly occupied LFMOs of fragment A, and their numberings “20” and “21” are storied in the array elements σ -LFMO(1,17) and σ -LFMO(1,18) (the 17- and 18-th red numbers in Figure 4-2c).

4.2.1.2. Reorganization of LFMO-n Basis Set

In order to understand the nature of π -electron delocalization as well as to search for the driving force of distorting NBA-like species, the vertical resonance energy, associated with the π - π orbital interaction between fragments A and (B+C) or between the three fragments A, B and C, should be concerned about. In a localized electronic state such as DSI state, the fragment number should be two or three. Thus, the sub-LFMO basis sets in Figure 4-2c should be reorganized before constructing the DSI state.

In order to distinguish between the original and reorganized LFMO basis sets, the reorganized LFMO basis set is denoted as LFMO-n where n is the number of sub-LFMO basis sets (or fragments) after reorganization. In the LFMO-3 (Figure 4-3c), the first two sub-basis sets (the red and brown numbers) for the fragment Ph- and -NH₂ in the original LFMO basis set have been merged into a single sub-basis set { Ψ_i^{A+B} } (index L = 1). In the first sub-LFMO basis set of the LFMO-3, the number of singly occupied LFMOs has been changed from two (the 20-th and 21-th LFMOs) in the original LFMO basis set to one (the 20-th LFMO) in the LFMO-3, and the numbers of π and σ LFMOs become, respectively, 28 and 89.

In a similar way, the original LFMO basis set can be reorganized into the LFMO-2 that is consisted of two sub-basis sets. In the LFMO-2, the first two sub-basis set in the original LFMO basis set are merged into one sub-base set, and meanwhile the last two sub-basis sets in the original LFMO basis set are also merged into one sub-base set.

In order to facilitate the description, the fragments are represented as A (a substituted aromatic ring), B (a bridge group -N=CH-) and C (a substituted aromatic ring) in the LFMO-3 for a NBA-like species, and the fragments are denoted as A (a substituted aromatic ring), and B (a substituted group -N=CH-Ar) in the LFMO-2.

4.2.2. Construction of DSI State

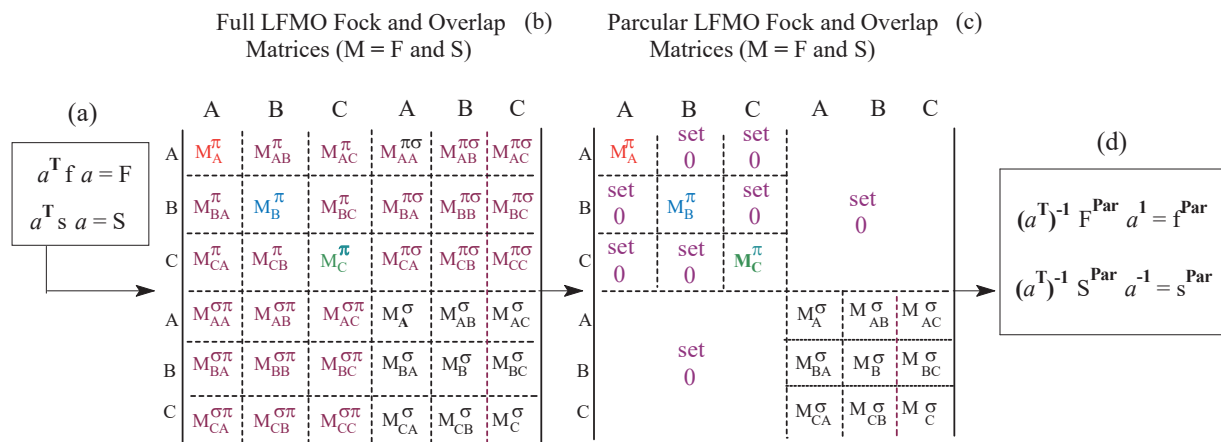


Figure 4-4. For N-benzylideneaniline, a multi-step procedure to construct DSI-3 state, where \mathbf{a} is the coefficient matrix of the LFMO basis set, and \mathbf{a}^{-1} is the inverse of the matrix \mathbf{a} .

Corresponding to the LFMO-n, the DSI state is denoted as DSI-n (n = 2, 3), where n is the number of fragments. For N-benzylideneaniline, the construction of the DSI-n state is a multi-step procedure (Figure 4-4). In this Chapter, the matrix whose elements have been conditionally deleted is called the particular matrix (Figure 4-4c), and the original matrix is called the full matrix.

In each SCF iteration, as the first step of the multi-step procedure, the AO Fock and overlap integral matrices, \mathbf{f} and \mathbf{s} , are transformed into the LFMO Fock and overlap integral matrices, \mathbf{F} and \mathbf{S} according to Figure 4-4a (Equation (4-2) and Equation (4-3)) where the matrix \mathbf{a} is a coefficient matrix of the LFMO basis set, and \mathbf{a}^T is the transpose of the matrix \mathbf{a} . Afterwards, the elements, F_{ij} and S_{ij} , of the LFMO Fock and overlap integral matrices are conditionally deleted according to Figure 4-4c. After the conditional deleting, as the fourth step, the particular LFMO Fock and overlap integral matrices \mathbf{F}^{par} and \mathbf{S}^{par} should be transformed back into their AO matrices according to the two Equations presented in Figure 4-4d. In these two Equations, the matrix \mathbf{a}^{-1} and $(\mathbf{a}^T)^{-1}$ are the inverses of the matrices \mathbf{a} and \mathbf{a}^T .

After step (d), the full and particular matrices both are the AO matrix. Accordingly, inserting our subroutines into the original PC-Gamess package has no effect on the running of PC-Gamess. For some calculation needs, PC-Gamess can also be operated after the step (c). In this case, the coefficient matrix \mathbf{T} of the obtained DSI state is a LFMO matrix, and then the LFMO matrix \mathbf{T} is transformed into the AO coefficient matrix \mathbf{t} in order to calculate the AO density matrix \mathbf{d} .

For the DSI-3 state, at last, the MOs, $\{\Phi_i\} = \{\Phi_i^{P-\pi}, \Phi_j^\sigma\}$, can be expressed as the LC-LFMO MO:

$$\Phi_i^{P-\pi} = \sum_{u=1, u \in A}^{ma} T_{ui} \Psi_u^{A-\pi} + \sum_{v=1, v \in B}^{mb} T_{vi} \Psi_v^{B-\pi} + \sum_{w=1, w \in A}^{mc} T_{wi} \Psi_w^{C-\pi} \quad (4-15)$$

$$\Phi_j^\sigma = \sum_{u=1, u \in A}^{na} T_{uj} \Psi_u^{A-\sigma} + \sum_{v=1, v \in B}^{nb} T_{vj} \Psi_v^{B-\sigma} + \sum_{w=1, w \in C}^{nc} T_{wj} \Psi_w^{C-\sigma} \quad (4-16)$$

and can also be expressed as LC-AO MO:

$$\Phi_i^{P-\pi} = \sum_{\lambda=1}^{Na} t_{\lambda i} \phi_\lambda + \sum_{\rho=Na+1}^{Na+Nb} t_{\rho i} \phi_\rho + \sum_{\gamma=Na+Nb+1}^N t_{\gamma i} \phi_\gamma \quad (4-17)$$

$$\Phi_j^\sigma = \sum_{\lambda=1}^{Na} t_{\lambda j} \phi_\lambda + \sum_{\rho=Na+1}^{Na+Nb} t_{\rho j} \phi_\rho + \sum_{\gamma=Na+Nb+1}^N t_{\gamma j} \phi_\gamma \quad (4-18)$$

When $\Phi_i^{P-\pi} \in$ Fragment A, for example, all the LFMO coefficients T_{vi} and T_{wi} in Equation (4-15) are equal to zero, and all the AO coefficients $t_{\rho i}$ and $t_{\gamma i}$ in Equation (4-17) are equal to zero. In Equation (4-16) and Equation (4-18), the coefficients are (or not) all non-zero. In Equation 4-16, $\{\Psi_n^{P-\sigma}\}$ includes $\{\Psi_n^{P-\pi}\}$ (Figure 4-2c and Figure 4-3c).

At the DSI-3 state of the $\theta = 17^\circ$ geometry of N-benzylideneaniline, as shown by the LFMO coefficients of the LC-LFMO MOs and by the AO coefficients of LC-AO MOs in Table 4-1 (presented in the appendix), the π MOs are absolutely localized on their respective fragments A, B and C, and the σ MOs are delocalized on the entire molecular framework, and meanwhile the π and σ systems are completely separated. For the 37-th LFMO listed in Table 4-1, for example, it is expressed as the linear combination of 24 π LFMOs and as linear combination of π AOs. When the 37-th MO is expressed as the LCAO-MO, the coefficients of all AOs belonging to fragment B and C are equal to zero, and the coefficients of all s AOs are less than 10^{-6} .

4.2.3. Construction of FUD State

The FUD state can be obtained from the single-point energy calculation under the conditional settings detailed by Figure 4-5a. At the FUD state, all the LFMO coefficients in Equation (4-15) and Equation (4-16) and the AO

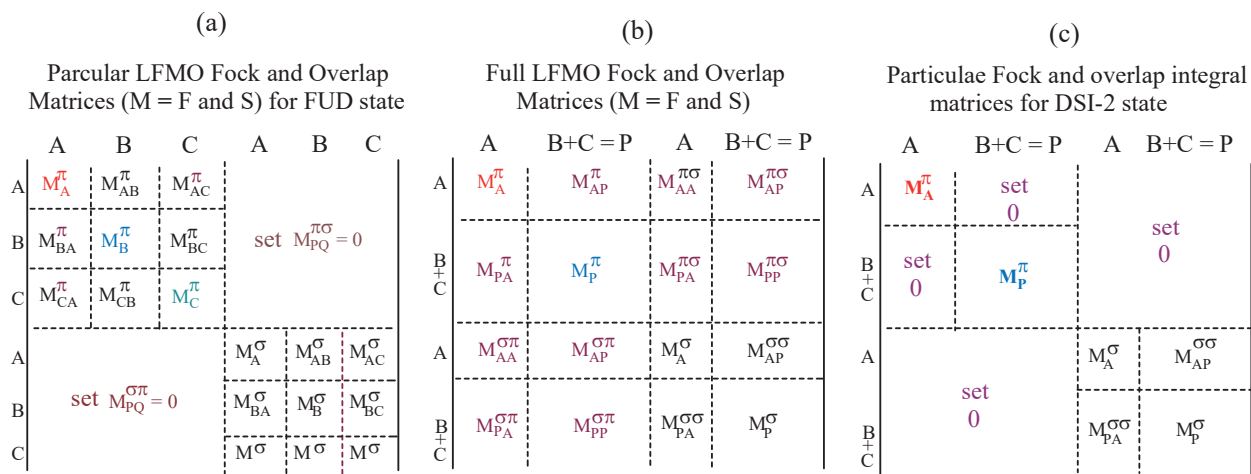


Figure 4-5. For NBA-like species, conditional settings for constructing FUD and DSI-2 states. Fragment A is N-aromatic ring including substituent(s), fragment C is C-aromatic ring including substituent(s).

coefficients in Equation (4-17) and Equation (4-18) are all not zero (but may be not all non-zero). The π and σ MO are separated out, and they are all delocalized on the whole molecular framework, but there is no the π - σ interaction. For example, as indicated by the data listed in Table 4-1 (presented in Appendix), the 37-MO, a π MO, is a result of the interaction among 56 π LFMOs, and it can also be expressed as a linear combination of AOs belonging to three fragments, but the coefficients of all s AOs are less than 10^{-6} .

4.2.4. Construction of DSI-2 State

According to the conditional settings shown by Figure 4-5c, the DSI-2 state can be constructed. In the DSI-2 state, the π MOs are absolutely localized on their respective fragments A and (B+C), and the σ MOs are delocalized on the entire molecular framework. Meanwhile, the inter- and intra-fragment interactions between the π and σ systems have been set equal to zero, which ensure that, in the DSI-2 state, the π and σ systems are completely separated.

In this Chapter, the molecular energy of various electronic states is obtained from the conditional single-point energy calculations, and the molecular conformations are obtained from the relaxed potential energy surface scan (the relaxed PES-scan) at the B3LYP/6-311G** level.

4.3. VERTICAL DELOCALIZATION ENERGY

For N-benzylideneaniline (**2-1**), substituted NBA molecules and NBA-like species, their vertical delocalization energies are calculated at (RHF, B3LYP and MPn) levels of theory with various basis sets. The structures of 20 substituted N-benzylideneanilines (**2-n**) are presented in Figure 2-2, and the structures of the heterocyclic N-benzylideneaniline-like species (NBA-like species) (**2-n**) are shown in Scheme 2-6. N-benzylidene-(3-pyridinyl)amine will be numbered **4-1** (the first one molecule in Chapter 4).

4.3.1. N-benzylideneaniline

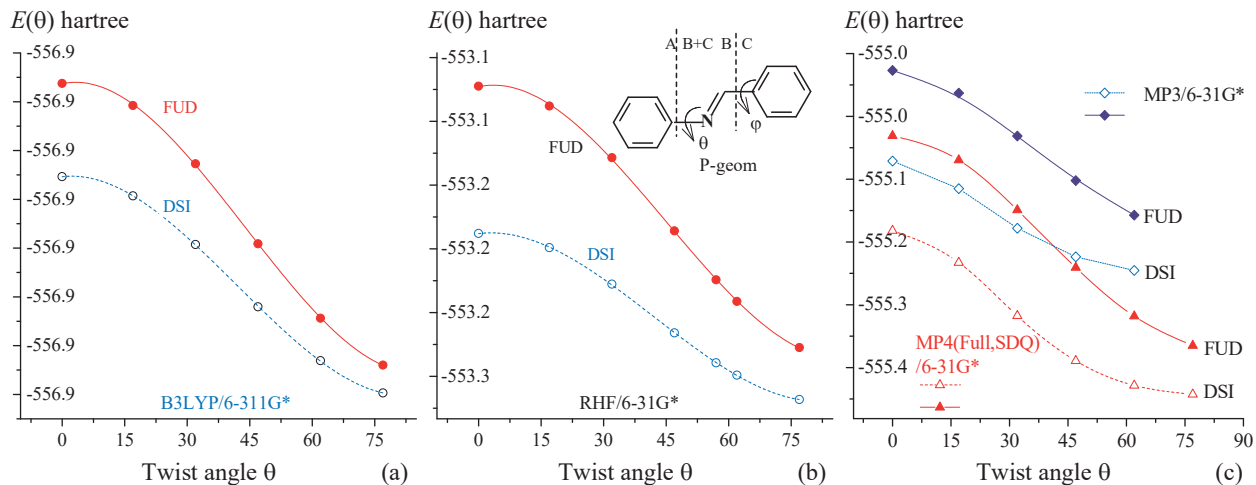


Figure 4-6. Molecular energies, $E^{\text{DSI}}(\theta)$ and $E^{\text{FUD}}(\theta)$, for the DSI (DSI-3) and FUD states of NBA, and their changes with the increasing of twist angle θ .

For a series of the optimized geometries (conformations twisted by 0°) of NBA, the molecular energies, $E^{\text{FUD}}(\theta)$ and $E^{\text{DSI}}(\theta)$, of the DSI (DSI = DSI-3) and FUD states are obtained from the conditional single-point energy calculations at the B3LYP/6-311G* and (RHF and MPn)/6-31G* ($n = 3, 4$) levels (Figure 4-6). The molecular energies $E^{\text{FUD}}(\theta)$ and $E^{\text{DSI}}(\theta)$ can be fitted as the third order polynomial functions of twist angle θ , and the correlation coefficients (cc) are greater than 0.99. At B3LYP/6-311G*, for example, $E^{\text{FUD}}(\theta)$ and $E^{\text{DSI}}(\theta)$ can be fitted as the following functions (cc is 1.0 and 0.9998, respectively):

$$E^{\text{FUD}}(\theta) = -556.8663 + (1.8421 \times 10^{-4})\theta - (2.9152 \times 10^{-5})\theta^2 + (2.2108 \times 10^{-7})\theta^3$$

$$E^{\text{DSI}}(\theta) = -556.8854 + (1.01549 \times 10^{-4})\theta - (2.2591 \times 10^{-5})\theta^2 + (1.7920 \times 10^{-7})\theta^3$$

The function curves in Figure 4-6 unanimously show the following characteristics of molecular energies $E^{\text{FUD}}(\theta)$ and $E^{\text{DSI}}(\theta)$: in the region of from $\theta = 0^\circ$ to $\theta = 90^\circ$

$$E^{\text{FUD}}(\theta) < 0, \text{ and } d[E^{\text{FUD}}(\theta)]/d\theta < 0$$

$$E^{\text{DSI}}(\theta) < 0, \text{ and } d[E^{\text{DSI}}(\theta)]/d\theta < 0$$

Accordingly, the molecular energies, $E^{\text{FUD}}(\theta)$ and $E^{\text{DSI}}(\theta)$, of the FUD and DSI-3 states are the monotonically decreasing function of twist angle θ , and their stationary points, $d(E^{\text{FUD}}(\theta))/d\theta = 0$ and $d(E^{\text{DSI}}(\theta))/d\theta = 0$, should be in the vicinity of the $\theta = 0^\circ$ and $\theta = 90^\circ$. When the twist angle θ is close to 90° , the molecular energies of the FUD and DSI state are the most stabilizing. In particular, in any twisted conformation, always $|E^{\text{DSI}}(\theta)| > |E^{\text{FUD}}(\theta)|$.

For the FUD and DSI-3 states, as shown by actual calculations, all the above energy characteristics are nothing to do with the theoretical level and basis set size, but the theoretical level and basis set size can really affect the magnitude of the $E^{\text{FUD}}(\theta)$ and $E^{\text{DSI}}(\theta)$, and affect the magnitude of the first order derivatives $d[E^{\text{FUD}}(\theta)]/d\theta$ and $d[E^{\text{DSI}}(\theta)]/d\theta$. For NBA, as shown in Figure 4-7 and Table 4-2 and Table 4-3, the vertical delocalization energy is always destabilizing, $\Delta E^V(\theta) = [E^{\text{FUD}}(\theta) - E^{\text{DSI}}(\theta)] > 0$, which is independent on the theoretical level and basis set size.

Figure 4-7a and 4-7b also show that $\Delta E^V(\theta)$ is the monotonically decreasing function of twist angle θ , and $d[\Delta E^V(\theta)]/d\theta < 0$ at the RHF and B3LYP levels of theory. The value of $\Delta E^V(\theta)$ is the largest when the twist angle θ

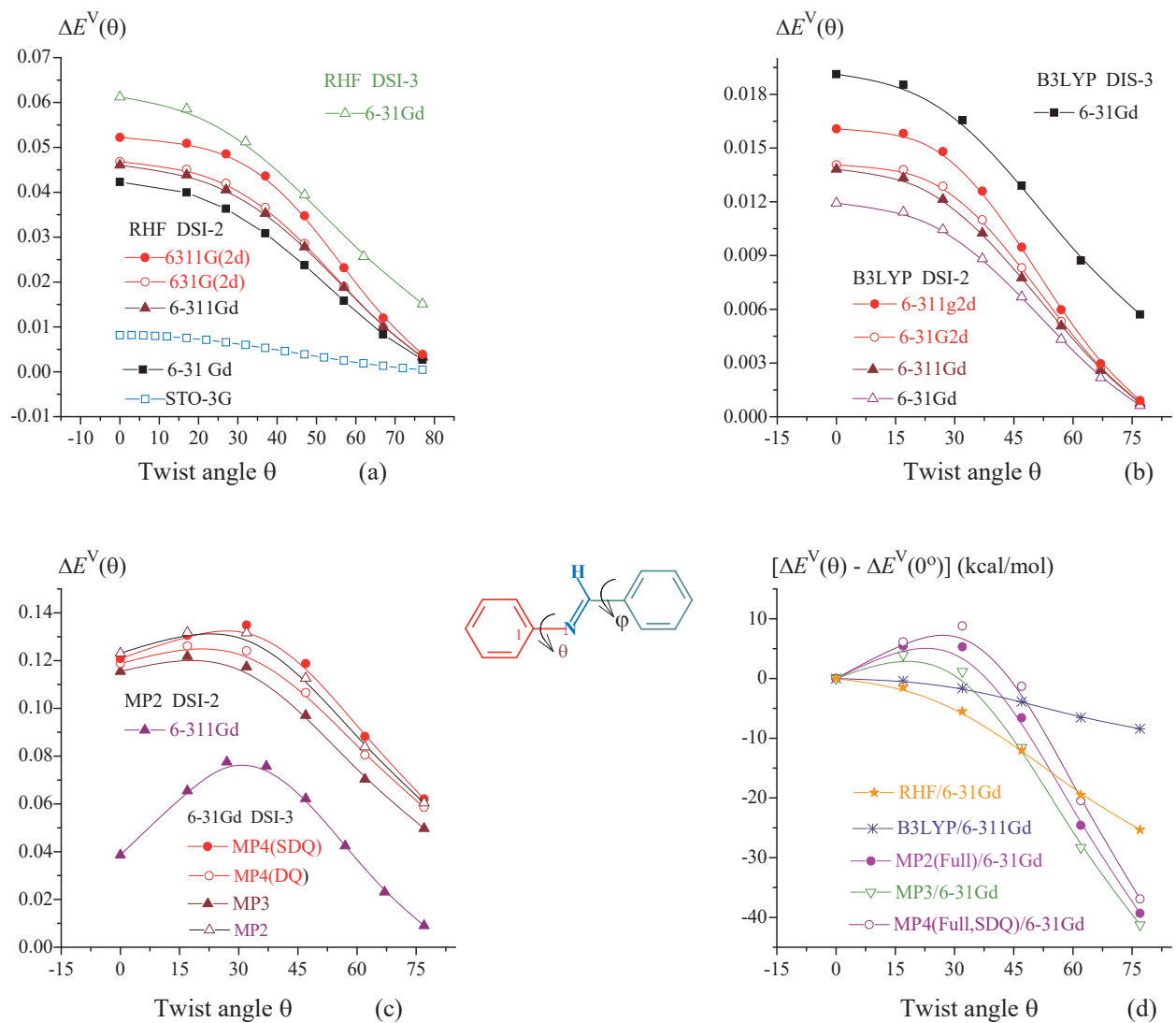


Figure 4-7. For N-benzylideneaniline: (a) to (c) Vertical resonance energy $\Delta E^V(\theta)$ (hartree) at various theory of levels; (d) The difference ($\Delta E^V(\theta) - \Delta E^V(0^\circ)$) (kcal/mol), and their change with increasing of twist angle θ .

is close to 0° . Therefore, π -electron delocalization can be considered as a driving force for distorting NBA molecule. At the B3LYP/6-311G* level (DSI-3), for example, $\Delta E^V(\theta)$ can be fitted as the following third order polynomial function of the twist angle θ (cc = 0.9972):

$$\Delta E^V(\theta) = 0.01905 + (8.28926 \times 10^{-5})\theta - (6.57121 \times 10^{-6})\theta^2 + (4.19706 \times 10^{-8})\theta^3$$

When $\theta = 6.7^\circ$, $d\Delta E^V(\theta)/d\theta = 0$, and the maximum value of $\Delta E^V(\theta)$ is 0.019 hartree. As far as π -electron delocalization is concerned, the molecule should be distorted toward the $\theta = 90^\circ$ conformation as much as possible. Differently, as shown by Figure 4-7c and Table 4-3-1, although the MPn vertical delocalization energy is also destabilizing, but its maximum value is found when θ is about 15° . At MP4(Full,SDQ)/6-31G* levels, for example, $\Delta E^V(\theta)$ (y) can be fitted as the following polynomial functions of twist angle θ (DSI-3) (cc = 0.996):

Table 4-2. For $\theta = 0$ and 17° Geometries of NBA, Vertical Delocalization Energy (hartree) $\Delta E^V(\theta) = [E^{\text{FUD}}(\theta) - E^{\text{DSI}}(\theta)]$ (DSI-3) and Its Various Components.

Entries	Methods	ΔE_H	ΔE_{two}	ΔE_{cou}	ΔE_{ex}	ΔE_{cc} (ΔE_n)	ΔE^V
$\theta = 0^\circ$ Geometry (“P-geom”)							
1	B3LYP/6-31G*	-0.11382	0.12927	0.15320	-0.02301	-0.00091	0.01546
2	B3LYP/6-311G	-0.10349	0.12937	0.15559	-0.02531	-0.00092	0.02587
3	B3LYP/6-311G*	-0.14254	0.16163	0.18826	-0.02564	-0.00100	0.01912
4	RHF/6-311G	-0.15491	0.23335				0.07844
5	RHF/6-311G*	-0.20089	0.27025				0.06936
6	RHF/6-31G*	-0.10796	0.17029				0.06233
7	MP2(Full)/6-31G*					0.06078	0.12312
8	MP3(Full)/6-31G*					-0.00767	0.11545
9	MP4(Full, SDQ)/6-31G*					0.00542	0.12087
10	MP2/6-311G					0.05637	0.13481
11	MP2/6-311G*					0.08928	0.15865
$\theta = 17^\circ$ Geometry (“P-geom”)							
12	B3LYP/6-31G*	-0.10242	0.11737	0.13922	-0.02103	-0.00082	0.01495
13	B3LYP /6-31G(2d)	-0.14247	0.16016	0.18483	-0.02375	-0.00092	0.01769
14	B3LYP /6-311G	-0.10066	0.12506	0.14931	-0.02340	-0.00085	0.02440
15	B3LYP /6-311G*	-0.14270	0.16123	0.18669	-0.02450	-0.00095	0.01853
16	B3LYP/6-311G(2d)	-0.12789	0.15050	0.17669	-0.02520	-0.00099	0.02261
17	RHF/6-311G	-0.12933	0.20376				0.07443
18	RHF/6-311G*	-0.20454	0.27167				0.06712
19	RHF/6-31G*	-0.10560	0.16599				0.05999
20	MP2(Full)/6-31G*					0.07180	0.13179
21	MP3(Full)/6-31G*					-0.01002	0.12176
22	MP4(Full, SDQ)/6-31G*					0.00884	0.13060
23	MP2/6-311G					0.07957	0.15399
24	MP2/6-311G*					0.12006	0.18718

P-Geom: the group N(12)-phenyl ring, as well as the group C(13)-phenyl ring, is planar. ΔE_{two} : the difference in the two-electron interaction energy between the FUD and DSI states. ΔE_{cc} : the difference in the electron correlation between two electronic states.

Table 4-3-1. Vertical Delocalization Energy (hartree) for the Twisted Geometries of NBA (DSI-3, “P-Geom”) at 6-31G* Level.

θ	RHF	MP2(full)	MP3(full)	MP4(full,dq)	MP4(full,sdq)
0.0	0.06233	0.12312	0.11545	0.11877	0.12087
17.0	0.05998	0.13179	0.12176	0.12611	0.13060
32.0	0.05357	0.13157	0.11735	0.12407	0.13488
47.0	0.04322	0.11262	0.09706	0.10659	0.11875
62.0	0.03122	0.08391	0.07036	0.08044	0.08823
77.0	0.02199	0.06043	0.04974	0.05852	0.06203

Table 4-3-2. Vertical Delocalization Energy (hartree) for the Twisted Geometries of NBA at B3LYP Level.

θ	DSI-2 (“Opt-geom”)				DSI-3 (“P-geom”)	
	6-311G(2d)	6-31G(2d)	6-311G(d)	6-31G(d)	θ	6-311Gd
0.0	0.01607	0.01406	0.01382	0.01193	0.0	0.01912
17.0	0.01581	0.01379	0.01333	0.01142	17.0	0.01853
37.0	0.01259	0.01099	0.01025	0.00882	47.0	0.01290
47.0	0.00946	0.00831	0.00776	0.00669	62.0	0.00872
57.0	0.00597	0.00531	0.00507	0.00432	77.0	0.00571
77.0	0.00091	0.00078	0.00076	0.00063		

Opt-Geom: the group including N(12) atom and N-phenyl ring, as well as the group including C(13) atom and C-phenyl ring, is not planar.

$$y = 0.12084 + 2.58587 \times 10^{-5}\theta + 6.32998 \times 10^{-5}\theta^2 - 2.03354 \times 10^{-6}\theta^3 + 1.40047 \times 10^{-8}\theta^4.$$

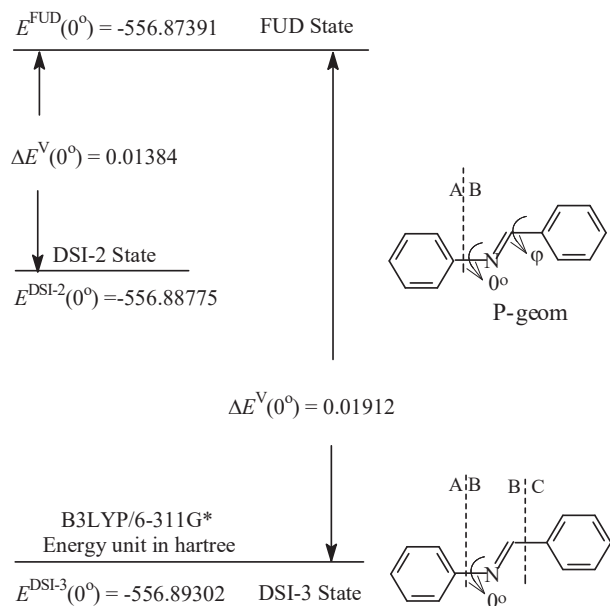
When $\theta = 28^\circ$, $d\Delta E^V(\theta)/d\theta = 0$, and $\Delta E^V(28^\circ) = 0.13516$ hartree.

Table 4-2 shows that the energy difference ΔE_H in the one-electron energy between the FUD and DSI state is always stabilizing, and the difference ΔE_{two} in the two-electron interaction between the two electronic states is always destabilizing. It is the energy difference ΔE_{two} to make the vertical delocalization energy destabilizing. Based on the comparison of the data listed in Table 4-2, the B3LYP ΔE_{two} value is about 2/3 of the corresponding RHF value, and the MPn value of ΔE_{cc} is much larger than the corresponding B3LYP value. At 6-311G* level, for example, the ΔE_{two} and ΔE_{cc} values are:

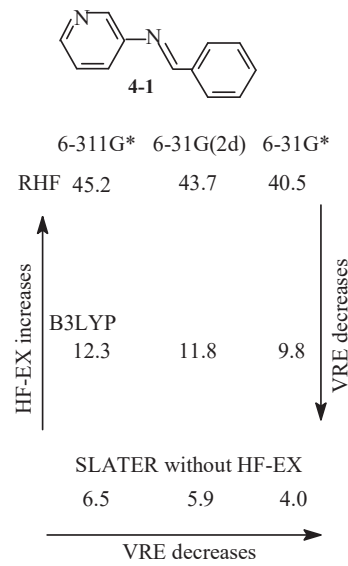
$$\begin{aligned} 0.16163 \text{ (B3LYP)} &< 0.27025 \text{ (RHF)} (\Delta E_{two}) \\ 0.08928 \text{ (MP2)} &>> |-0.00100| \text{ (B3LYP)} (\Delta E_{cc}). \end{aligned}$$

As a result, the MPn and RHF values of vertical delocalization energy are larger than the corresponding B3LYP value. At 6-311G* level, for example, the values of $\Delta E^V(0^\circ)$ are as follows (Table 4-2):

$$0.06936 \text{ (RHF) hartree} > 0.01912 \text{ (B3LYP) hartree}$$



Scheme 4-3



Scheme 4-4

These large differences seem to imply that two-electron exchange integrals between the localized fragments have a larger effect on the vertical localization energy value. In this Chapter and in Chapter 8, we will discuss in detail the role of two-electron exchange integrals in determining the magnitude and sign of the vertical delocalization energy $\Delta E^V(\theta)$, which, actually, have been detailed in our previous works.^{33,35} At that time, we will emphatically point out that the electron localization and molecular orbital localization are two completely different concepts. The Eliminating of Fock matrix elements only ensures localization of the molecular orbitals, but does not ensure electron localization. We will further explain that the RHF and MPn methods are not suitable for constructing localized electronic states just by deleting matrix elements. So, we developed a new energy decomposition program (our 2011 program³⁵) in 2011.

Figure 4-7 and Table 4-3 also show that the larger the basis set, the greater the value of $\Delta E^V(\theta)$. At the $\theta = 0^\circ$ conformation (DSI-2) of N-benzylideneaniline, for example, the size order of the B3LYP and RHF values of $\Delta E^V(\theta)$ (hartree) is as follows (Table 4-3-2):

$$\begin{aligned} 0.01607 \text{ (6-311G2d)} &> 0.01406 \text{ (6-31G2d)} > 0.013817 \text{ (6-311Gd)} > 0.0119 \text{ (6-31Gd)} \text{ (B3LYP)} \\ 0.06936 \text{ (6-311Gd)} &> 0.06233 \text{ (6-31Gd)} \text{ (RHF)} \end{aligned}$$

Due to the electron delocalization destabilization, so at the DS1-n ($n = 2$ and 3) states, the more the number of fragments, the more destabilizing the corresponding vertical delocalization energy is. The molecular energy of the FUD state, $E^{\text{FUD}}(\theta)$, is independent of the number of fragments, but the molecular energy of the DS1 state depends upon the number of its fragments (Scheme 4-3). The DS1-2 state can be considered to be the result of the π - π interaction between two fragments B and C in the DS1-3 state. At the B3LYP/6-311G* level, for example, the molecular energy (hartree) of the DS1 state increases from -556.89302 (DSI-3) to -556.88775 (DSI-2) (Scheme 4-3), and the value (hartree) of $\Delta E^V(0^\circ)$ decreases from 0.01912 (DSI-3) to 0.01384 (DSI-2). Such difference in the vertical delocalization energy shows that our calculations are self-consistent, and it also implies that driving force of distorting NBA mainly arises from the electron delocalization between the fragments A and (B+C). This is probably the reason why the twist angle θ is greater than φ in the ground state geometry.

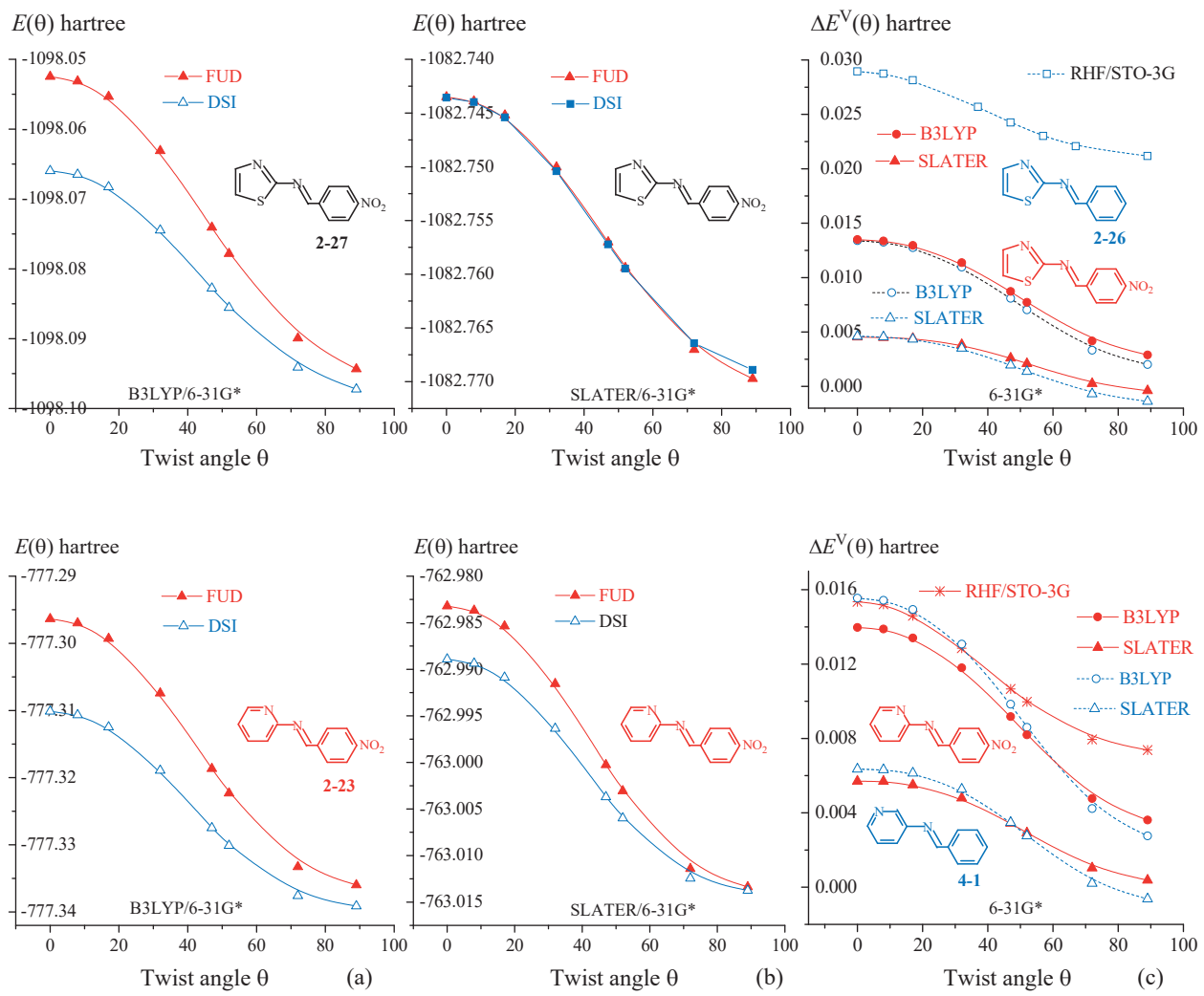


Figure 4-8. Fur NBA-like species: (a) and (b) Molecular energies of the DSI-3 and FUD states; (c) Vertical delocalization energies, and their changes with the increasing of twist angle θ .

4.3.2. Heterocyclic NBA-like Species

For NBA-like species molecules 4-1, 2-23, 2-26 and 2-27, as shown by Figure 4-8 and Table 4-4, the molecular energies, $E^{\text{DSI}}(\theta)$ and $E^{\text{FUD}}(\theta)$, of the DSI and FUD states are the monotonically decreasing function of the twist angle θ , and their characteristics are as follows ($0^\circ < \theta < 90^\circ$):

$$\begin{aligned} E^{\text{FUD}}(\theta) &< 0, \frac{dE^{\text{FUD}}(\theta)}{d\theta} < 0 \\ E^{\text{DSI}}(\theta) &< 0, \frac{dE^{\text{DSI}}(\theta)}{d\theta} < 0, \\ |E^{\text{FUD}}(\theta)| &< |E^{\text{DSI}}(\theta)| \end{aligned}$$

These characteristics are the same as those of NBA. In particular, due to always $|E^{\text{FUD}}(\theta)| < |E^{\text{DSI}}(\theta)|$, as shown by Figure 4-8c, the vertical delocalization energy is always destabilizing, $\Delta E^{\text{VRE}}(\theta) > 0$, and $d[\Delta E^{\text{VRE}}(\theta)]/d\theta < 0$,

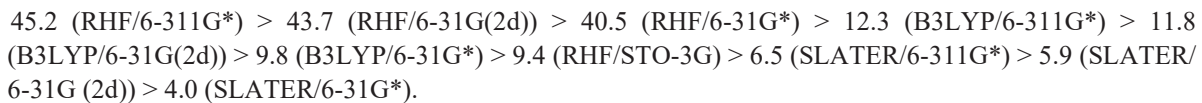
Table 4-4-1. For Two Molecules, Molecular Energies (hartree) of the FUD and DSI-3 States.

Molecule 2-27										Molecule 2-26			
θ	SLATER/6-31G*		B3LYP/6-31G*		SLATER/6-31G*		B3LYP/6-31G*		RHF/STO-3G				
	FUD	DSI-3	FUD	DSI-3	FUD	DSI-3	FUD	DSI-3	FUD	DSI-3			
0	-1082.7391	-1082.7436	-1098.0525	-1098.0660	-881.2238	-881.2284	-893.5532	-893.5666	0	-778.5407	-778.5696		
8	-1082.7395	-1082.7440	-1098.0531	-1098.0665	-881.2243	-881.2288	-893.5539	-893.5671	8	-778.5416	-778.5704		
17	-1082.7410	-1082.7454	-1098.0553	-1098.0683	-881.2259	-881.2302	-893.5562	-893.5689	17	-778.5447	-778.5728		
32	-1082.7466	-1082.7504	-1098.0631	-1098.0745	-881.2316	-881.2351	-893.5640	-893.5750	37	-778.5574	-778.5831		
47	-1082.7546	-1082.7572	-1098.0741	-1098.0828	-881.2398	-881.2418	-893.5751	-893.5832	47	-778.5649	-778.5891		
52	-1082.7574	-1082.7595	-1098.0778	-1098.0856	-881.2426	-881.2440	-893.5789	-893.5859	57	-778.5716	-778.5946		
72	-1082.7662	-1082.7664	-1098.0899	-1098.0941	-881.2516	-881.2509	-893.5911	-893.5945	67	-778.5769	-778.5989		
89	-1082.7693	-1082.7689	-1098.0944	-1098.0972	-881.2546	-881.2532	-893.5955	-893.5975	89	-778.5819	-778.6031		

Table 4-4-2. For Two Molecules at 6-31G* Level, Molecular Energies (hartree) of the FUD and DSI-3 States.

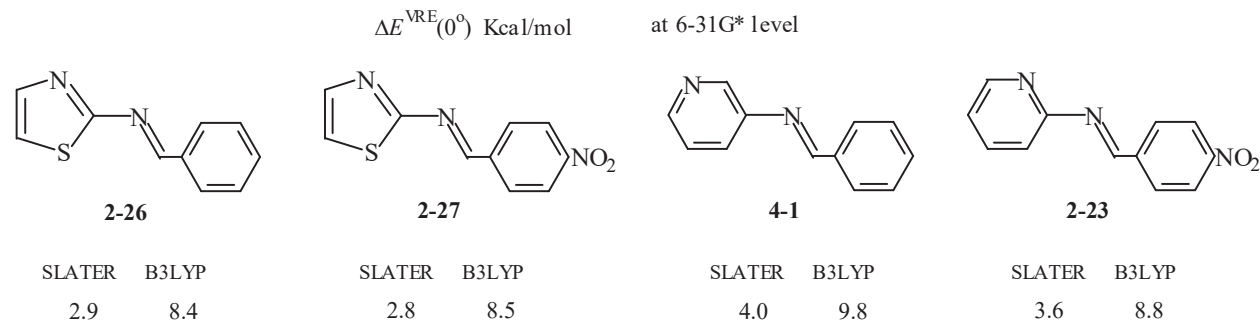
Molecule 4-1								Molecule 2-23			
θ	SLATER		B3LYP		SLATER		B3LYP		RHF/STO-3G		
	FUD	DSI-3	FUD	DSI-3	FUD	DSI-3	FUD	DSI-3	FUD	DSI-3	
0	-561.45721	-561.46356	-572.78604	-572.80158	-762.98321	-762.98891	-777.29635	-777.31031	-762.79539	-762.81075	
8	-561.45786	-561.46418	-572.78687	-572.80229	-762.98367	-762.98937	-777.29698	-777.31086	-762.79636	-762.81157	
17	-561.46015	-561.46628	-572.78979	-572.80472	-762.98536	-762.99087	-777.29929	-777.31269	-762.79953	-762.81413	
32	-561.46818	-561.47345	-572.79982	-572.81289	-762.99155	-762.99635	-777.30742	-777.31921	-762.80886	-762.82171	
47	-561.47968	-561.48316	-572.81411	-572.82395	-763.00026	-763.00370	-777.31867	-777.32784	-762.82041	-762.83108	
52	-561.48353	-561.48629	-572.81893	-572.82753	-763.00306	-763.00598	-777.32231	-777.33050	-762.82405	-762.83403	
72	-561.49516	-561.49536	-572.83375	-572.83797	-763.01141	-763.02030	-777.33329	-777.33805	-762.83465	-762.84260	
89	-561.49842	-561.49778	-572.83802	-572.84078	-763.01337	-763.01375	-777.33598	-777.33959	-762.83719	-762.84456	

although the theoretical levels have a significant effect on the magnitude of the vertical delocalization energy. For the $\theta = 0^\circ$ geometry of molecule 4-1, for example, the values (kcal/mol) of the vertical delocalization energy are as follows (Scheme 4-4):



The range of a set of the above values is large, up to $(45.2 - 4.0) = 41.2$ kcal/mol. For the density functionals, SLATER is a pure exchange functional without Hartree-Fock exchange component,⁴⁸ and B3LYP belongs to Hybrid functional that incorporates a portion of Hartree-Fock exchange.⁴⁹⁵⁰ The above size order means that the Hartree-

Fock exchange interaction (two-electron exchange integrals) plays an important role in determining the value of vertical delocalization energy. The greater the Hartree-Fock component (such as at the RHF level of theory), the greater the vertical delocalization energy. The role of the Hartree-Fock exchange (spatial exchange) interaction is very interesting, and it implies once again that π -molecular orbital localization and π -electron localization are two different concepts. However, when the single-point energy calculation is performed over the LFMO basis set, it is difficult to conditionally delete the LFMO two-electron exchange integrals. That is, the AO two-electron exchange integrals $\langle \lambda\rho|\mu\omega \rangle$ should be transformed into the LFMO two-electron exchange integrals first. The single-point energy calculation at SLATER level can help us to understand the function of two-electron exchange integrals and to confirms the destabilizing character of vertical delocalization energy.



Scheme 4-5

SLATER is a pure exchange density functional without Hartree-Fock exchange (HF-exchange), and B3LYP is a hybrid density functional with a part of HF-exchange. The influences of HF-exchange on the DS1 and FUD states should be different. For the $\theta = 0^\circ$ geometry of molecule **4-1** (Table 4-4-1), for example, $[E^{\text{DSI}}(0^\circ) \text{ (SLATER)} - E^{\text{DSI}}(0^\circ) \text{ (B3LYP)}]$ (15.3224 hartree) $> [E^{\text{FUD}}(0^\circ) \text{ (SLATER)} - E^{\text{FUD}}(0^\circ) \text{ (B3LYP)}]$ (15.3134 hartree). As the results, the SLATER/6-31G* values of vertical delocalization energy are less than the corresponding B3LYP/6-31G* values according to the following comparisons (Scheme 4-5):

- 2.9 (SLATER) < 8.4 (B3LYP) for molecule **2-26**
- 2.8 (SLATER) < 8.5 (B3LYP) for molecule **2-27**.
- 3.6 (SLATER) < 8.8 (B3LYP) for molecule **2-23**
- 4.0 (SLATER) < 9.8 (B3LYP) for molecule **4-1**

But the vertical delocalization energy, calculated at SLATER level, is still destabilizing. Therefore, the reduction or elimination of HF-exchange can increase the molecular energy of the DS1 state. In the case of NBA-like species, however, the increase in the molecular energy $E^{\text{DSI}}(\theta)$ (SLATER) is not larger enough to make the vertical delocalization energy to become stabilizing.

For the $\theta = 89^\circ$ conformation of molecule **2-27** at SLATER/6-31 G* level, as only one exception, $\Delta E^{\text{V}}(89^\circ) = -0.0004$ hartree, and it is stabilizing.

4.3.3. Substituted NBAs

For 11 substituted NBA molecules presented in Figure 4-9f, the substituents $\text{MeO}-$ and $-\text{N}(\text{Me})_2$ have been replaced by planar $-\text{OH}$ and $-\text{NH}_2$ groups, the molecular energy of the FUD and DS1-2 states and the vertical delocalization energies are calculated at (B3LYP, RHF and MP2)/6-311G*.

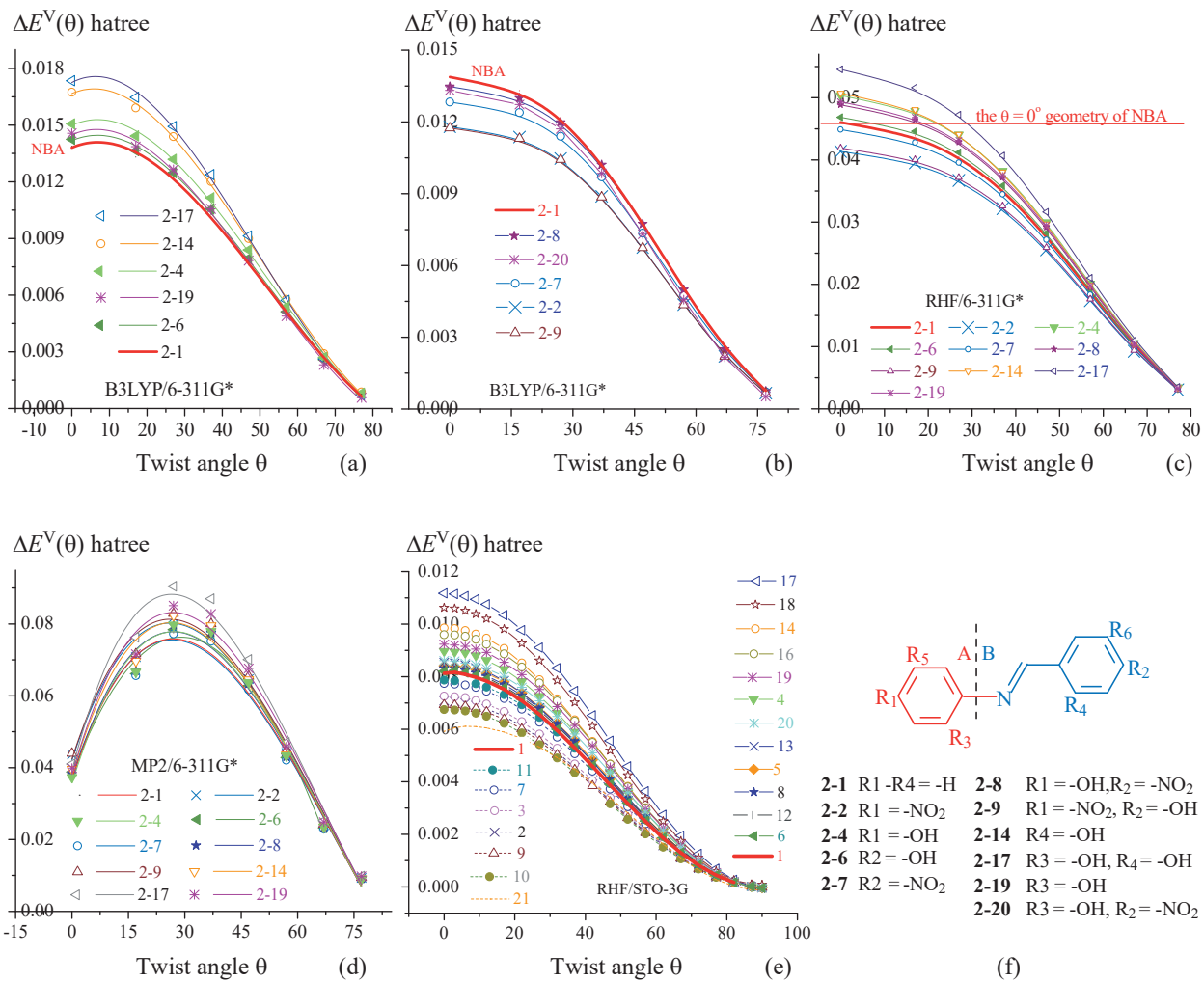


Figure 4-9. (a), (b), (c) and (d) The vertical delocalization energies of 11 substituted NBAs. (e) The vertical delocalization energies of 21 substituted NBAs (see Figure 2-2).

Practical calculations indicate that, for substituted NBAs, the characteristics of the electronic state energies $E^{\text{FUD}}(\theta)$ and $E^{\text{DSI}}(\theta)$ are exactly the same as those of the NBA molecule, and are no longer discussed and described in this section.

The curves in Figures 4-9a to 4-9c show the following characteristics of the vertical delocalization energies for substituted NBAs:

$$\Delta E^V(\theta) > 0, d[\Delta E^V(\theta)]/d\theta < 0 \quad (0 < \theta < 90^\circ), \text{ and } d[\Delta E^V(0^\circ)]/d\theta = 0.$$

These Figures, together Tables 4-4 and 4-5, indicate that, in heterocyclic NBA-like species and substituted NBAs, π -electron delocalization is always destabilization and is a driving force of the molecular distortion. The characteristics of the MP₂ curves in Figure 4-9d are the same as those of the MP_n curves in Figure 4-7c. These abnormal characteristics will be discussed

According to the positions of the curves in Figure 4-9a and Figure 9b, 11 substituted NBAs can be divided into two groups when the red curve of NBA (2-1) is used as the reference, where the symbol “ $\Delta E^{\text{VRE}}(0^\circ, n)$ ” represents the

Table 4-5. Vertical Delocalization Energies (hartree) for 11 Substituted NBAs (DSI-2) at B3LYP/6-311G* Level.

Mols	$\theta = 0^\circ$	17°	27°	37°	47°	57°	67°	77°
2-4	0.01507	0.01443	0.01319	0.01115	0.00839	0.00538	0.00270	0.00081
2-6	0.01425	0.01365	0.01248	0.01055	0.00795	0.00512	0.00258	0.00078
2-14	0.01674	0.01591	0.01439	0.01201	0.00899	0.00577	0.00290	0.00087
2-17	0.01735	0.01647	0.01493	0.01238	0.00913	0.00572	0.00263	0.00072
2-19	0.01457	0.01386	0.01265	0.01057	0.00783	0.00489	0.00231	0.00057
2-1	0.01388	0.01331	0.01219	0.01028	0.00778	0.00501	0.00252	0.00076
2-2	0.01180	0.01137	0.01047	0.00889	0.00675	0.00436	0.00220	0.00066
2-7	0.01283	0.01239	0.01140	0.00970	0.00735	0.00474	0.00239	0.00071
2-8	0.01348	0.01300	0.01199	0.01021	0.00774	0.00499	0.00250	0.00074
2-9	0.01175	0.01131	0.01043	0.00886	0.00674	0.00435	0.00220	0.00066
2-20	0.01332	0.01273	0.01171	0.00985	0.00731	0.00457	0.00216	0.00052

vertical delocalization energy of the $\theta = 0^\circ$ geometry of molecule **2-n**.

4.3.3.1. First Group of Substituted NBAs

The first group includes five molecules **2-4** ($R_1 = -OH$), **2-6** ($R_2 = -OH$), **2-14** ($R_4 = -OH$), **2-17** ($R_3 = -OH$, $R_4 = -OH$) and **2-19** ($R_3 = -OH$) (Table 4-5). In each of these hydroxy-substituted molecules, at least one electron-releasing group -OH is at the p- or o-position of the phenyl ring (including C-phenyl and N-phenyl ring). As will be indicated in other Chapters, the electron-releasing group, such as -OH and -NH₂, may increase the MO exchange interaction energy and decrease the MO charge transfer interaction energy, making the vertical delocalization energy more destabilizing. For the first group of the substituted NBAs, exception for the $\theta > 67^\circ$ conformations of the molecules **2-17** and **2-19**, as a result, all $\Delta E^{VRE}(\theta, n)$ are greater than that for NBA, and the corresponding curves for these molecules are all above the red line for NBA in Figure 4-9a. In the molecule **2-17**, two hydroxyl groups are at o-position of N- and C-phenyl groups, and the values of $\Delta E^{VRE}(\theta, 17)$ are the greatest of the five molecules. Correspondingly, the blue curve line for molecule **2-17** in Figure 3-9a is above the red curve for NBA and is the farthest from the red curve. In molecule **2-6**, there is only one hydroxyl group, and this group is at p-position of C-phenyl ring. The values of vertical delocalization energy are the smallest. The corresponding green curve line for molecule **2-6** is also above the red line, but it is the closest to the red line. For the $\theta = 0^\circ$ conformation at B3LYP/6-311G* level, for example, the size order of the vertical delocalization energies (hartree) is as follow:

0.01735 (**2-17**, $R_3 = -OH$, $R_4 = -OH$) > 0.01674 (**2-14**, $R_4 = -OH$) > 0.01507 (**2-4**, $R_1 = -OH$) > 0.01457 (**2-19**, $R_3 = -OH$) > 0.01425 (**2-6**, $R_2 = -OH$) > 0.01388 (NBA).

When $0^\circ \leq \theta \leq 37^\circ$, the vertical delocalization energies also follow the above order. When $\theta = 47^\circ$ to 77° , the vertical delocalization energy is in the following order:

$$\Delta E^V(\theta, 14) > \Delta E^V(\theta, 4) > \Delta E^V(\theta, 6) > \Delta E^V(\theta, 1).$$

At RHF/6-311G* level, similarly, the vertical delocalization energies (hartree) for this group molecules are all greater than that for NBA. For the $\theta = 0^\circ$ conformations, the size order is the same as the B3LYP one, and it is as follow (hartree):

$$0.05456 (\mathbf{2-17}, R_3 = -OH, R_4 = -OH) > 0.05072 (\mathbf{2-14}, R_4 = -OH) > 0.05036 (\mathbf{2-4}, R_1 = -OH) > 0.04933 (\mathbf{2-19}, R_3 = -OH) > 0.04685 (\mathbf{2-6}, R_2 = -OH) > 0.04605 (\mathbf{2-1}, NBA)$$

For the $\theta = 17^\circ$ conformations at MP2/6-311G* level, the size order is as follow:

$$0.12791 (\mathbf{2-17}, R_3 = -OH, R_4 = -OH) > 0.11845 (\mathbf{2-19}, R_3 = -OH) > 0.11773 (\mathbf{2-14}, R_4 = -OH) > 0.11445 (\mathbf{2-4}, R_1 = -OH) > 0.11075 (\mathbf{2-6}, R_2 = -OH) > 0.10934 (\mathbf{2-1}, NBA)$$

Except for the molecule **2-19**, this size order is consistent with the order at B3LYP/6-311G* level.

For the electron-releasing group $-OH$, therefore, it always makes the vertical delocalization energy more destabilizing, and the position and the number of the $-OH$ group affect the ability of the $-OH$ group. For molecule **2-6** ($R_2 = -OH$), the vertical delocalization energy $\Delta E^V(\theta)$ is the smallest. This indicates that the ability the $-OH$ group at the para-position of the C-aromatic ring is the weakest, and the group at the ortho-position of the C-phenyl ring has the strongest ability. For molecules **2-14** ($R_4 = -OH$) and **2-17** ($R_3 = -OH, R_4 = -OH$), for example, the vertical delocalization energy is the most destabilizing.

The conformation also has the effect on the size order. For molecule **2-19** at B3LYP/6-311G* level, when $\theta \geq 57^\circ$, $\Delta E^V(\theta, 19) < \Delta E^V(\theta, 1)$. The same situation is also found in the size order of the vertical delocalization energies for molecules **2-17** and **2-14**, when $\theta \geq 57^\circ$, $\Delta E^V(\theta, 17) < \Delta E^V(\theta, 14)$.

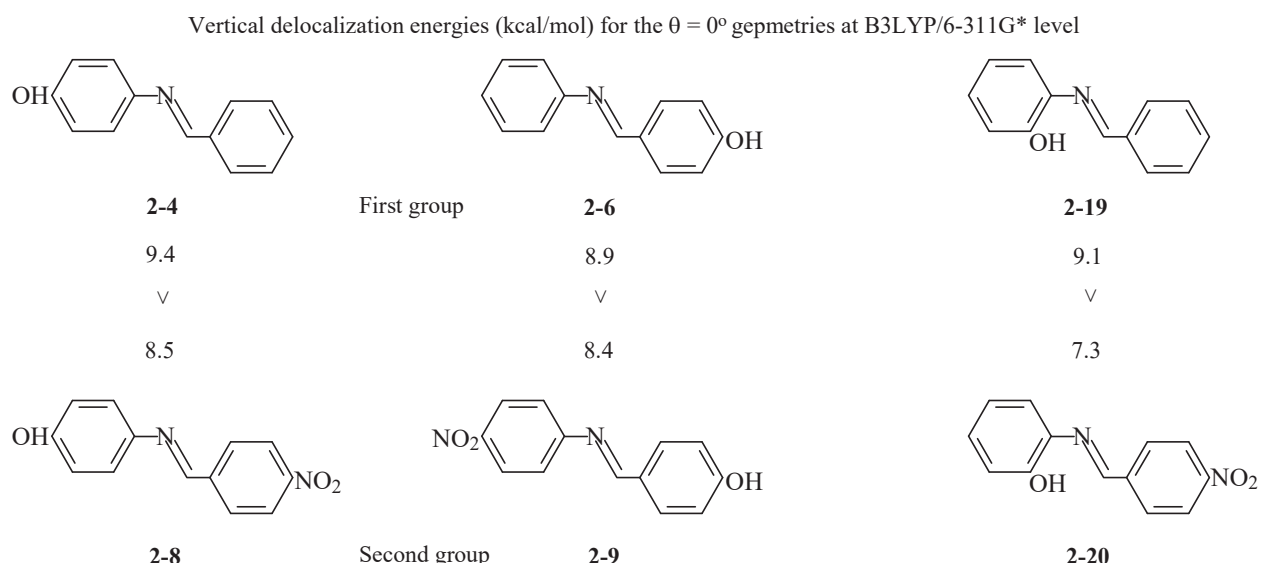
4.3.3.2. Second Group of Substituted NBAs

The second group includes another five molecules **2-2** ($R_1 = -NO_2$), **2-7** ($R_2 = -NO_2$), **2-8** ($R_1 = -OH, R_2 = -NO_2$), **2-9** ($R_1 = -NO_2, R_2 = -OH$), and **2-20** ($R_3 = -OH, R_2 = -NO_2$). In each of these molecules, there is an electron-withdrawing group $-NO_2$, and the vertical delocalization energies for various conformations, $\Delta E^V(\theta, n)$, are always less than the corresponding those for NBA (Table 4-5). In Figure 4-9b, the corresponding curves for these molecules are all below the red curve for NBA. The brown line for molecule **2-9** is the farthest from the red line, and the purple curve for molecule **2-8** is the closest to the red line. Thus, the nitro group ($-NO_2$) in the molecule makes the vertical delocalization energy less destabilizing. For the $\theta = 0^\circ$ conformations of the second group molecules at B3LYP/6-311G* level, the size order of the vertical delocalization energies (hartree) is as follow:

$$0.01388 (NBA) > 0.01348 (\mathbf{2-8}, R_1 = -OH, R_2 = -NO_2) > 0.01332 (\mathbf{2-20}, R_3 = -OH, R_2 = -NO_2) > 0.01239 (\mathbf{2-7}, R_2 = -NO_2) > 0.01180 (\mathbf{2-2}, R_1 = -NO_2) > 0.01175 (\mathbf{2-9}, R_1 = -NO_2, R_2 = -OH).$$

When a $-NO_2$ group is at the para-position of N-phenyl ring, as in molecule **2-2** ($R_1 = -NO_2$), its ability to reduce the vertical delocalization energy is stronger than at the para-position of C-phenyl ring. Therefore, the vertical delocalization (0.01180 hartree) for molecule **2-2** is smaller than that (0.01239 hartree) for molecule **2-7**.

Molecules **2-8** ($R_1 = -OH, R_2 = -NO_2$), **2-9** ($R_1 = -NO_2, R_2 = -OH$) and **2-20** ($R_3 = -OH, R_2 = -NO_2$) can be considered as the NO_2 -substituted derivative of following molecules: **2-4** ($R_1 = -OH$), **2-6** ($R_2 = -OH$) and **2-19** ($R_3 = -OH$). Comparison of the data in Scheme 4-6 shows:

**Scheme 4-6**

$$\Delta E^V(\theta, 4) > \Delta E^V(\theta, 8), \Delta E^V(\theta, 6) > \Delta E^V(\theta, 9), \Delta E^V(\theta, 19) > \Delta E^V(\theta, 20)$$

In the molecules **2-8**, **2-9**, and **2-20**, the nitro group plays a predominant role in determining that their vertical delocalization energies are less than that of NBA.

The molecules, **2-4** ($R_1 = -OH$), **2-6** ($R_2 = -OH$), **2-2** ($R_1 = -NO_2$), **2-7** ($R_2 = -NO_2$), are the para-substituted NBAs. The following differences (hartree) are interesting:

$$|[\Delta E^V(0^\circ, 2) - \Delta E^V(0^\circ, 1)] (-0.00208)| > [\Delta E^V(0^\circ, 4) - \Delta E^V(0^\circ, 1)] (0.00119)$$

$$|[\Delta E^V(0^\circ, 7) - \Delta E^V(0^\circ, 1)] (-0.00149)| > [\Delta E^V(0^\circ, 6) - \Delta E^V(0^\circ, 1)] (0.00037)$$

The ability of the $-OH$ group to increase the vertical delocalization energy is less than that of the $-NO_2$ group to reduce the vertical delocalization energy.

In molecule **2-8** ($R_1 = -OH$, $R_2 = -NO_2$), the $-OH$ group is at the para-position of the N-phenyl ring, and the $-NO_2$ group is at the para-position of the C-phenyl ring. According to the following size order (hartree):

$$\Delta E^V(0^\circ, 4) \text{ (} R_1 = -OH; 0.01507 \text{)} > \Delta E^V(0^\circ, 1) \text{ (} 0.01388 \text{)} > \Delta E^V(0^\circ, 8) \text{ (} R_1 = -OH, R_2 = -NO_2; 0.01348 \text{)} > \Delta E^V(0^\circ, 7) \text{ (} R_2 = -NO_2; 0.01239 \text{)}$$

In molecule **2-8**, the ability of the nitro group seems greater than the ability of the hydroxyl group, and it is weakened by the hydroxyl group. As a result, the vertical delocalization energy of molecule **2-8** is greater than that for molecule **2-7**, but it is still $\Delta E^V(0^\circ, 8) < \Delta E^V(0^\circ, 1)$. In molecule **2-9** ($R_1 = -NO_2$, $R_2 = -OH$), however, the hydroxyl group seems to help the nitro group to reduce the vertical delocalization energy via the push and pull action. As a result, the vertical delocalization energy of molecule **2-9** is the smallest of all the second group molecules, leading to the following size order (hartree):

$$\Delta E^V(0^\circ, 6) \text{ (} R_2 = -OH, 0.01425 \text{)} > \Delta E^V(0^\circ, 1) \text{ (} 0.01388 \text{)} > \Delta E^V(0^\circ, 2) \text{ (} R_1 = -NO_2, 0.01180 \text{)} > \Delta E^V(0^\circ, 9) \text{ (} R_1 = -NO_2, R_2 = -OH, 0.01175 \text{)}$$

Table 4-6. MP2/6-311G* Values of $\Delta E^V(\theta)$ (hartree) for 10 Substituted NBAs (DSI-2).

Mols	$\theta = 0^\circ$	17°	27°	37°	47°	57°	67°
2-4	0.08766	0.11445	0.12381	0.11612	0.09372	0.06339	0.03404
2-6	0.08564	0.11075	0.11960	0.11239	0.09107	0.06188	0.03338
2-14	0.09030	0.11773	0.12645	0.11756	0.09419	0.06343	0.03397
2-17	0.09556	0.12791	0.13774	0.12770	0.10174	0.06801	0.03619
2-19	0.08920	0.11845	0.12824	0.12031	0.09710	0.06559	0.03517
2-1	0.08467	0.10934	0.11806	0.11103	0.09002	0.06121	0.03304
2-2	0.08503	0.11031	0.11850	0.11113	0.09021	0.06149	0.03325
2-7	0.08422	0.10838	0.11678	0.10964	0.08884	0.06041	0.03261
2-8	0.08710	0.11345	0.12254	0.11480	0.09260	0.06262	0.03363
2-9	0.08589	0.11171	0.12008	0.11261	0.09136	0.06223	0.03362

In molecules **2-8** and **2-9**, as shown by the above two size orders, the exchange of the nitro and hydroxyl positions actually allows the hydroxyl group to produce two completely different effects.

Nitro and hydroxyl groups compete with each other (some time help with each other), and weaken each other's abilities. However, the conformation can affect their relative abilities. In molecule **2-20** ($R_3 = -OH$, $R_2 = -NO_2$), for example, a $-OH$ group is at ortho-position of the N-phenyl ring, and its ability to increase the vertical delocalization is weakened when $\theta > 47^\circ$. Thus, total ability of the $-NO_2$ and $-OH$ groups to reduce the vertical delocalization energy has been increased. This may be a reason why $\Delta E^V(\theta, 20) > \Delta E^V(\theta, 7)$ when $\theta < 47^\circ$, but $\Delta E^V(\theta, 20) < \Delta E^V(\theta, 7)$ when $\theta \geq 47^\circ$. However, as shown by the data in Table 4-6, the MP_n values of the vertical delocalization energies do not show the above-mentioned rule. For the second group of molecules, all the vertical delocalization energies, except for those of molecule **2-7**, are still greater than those for NBA.

4.3.3.3. RHF/STO-3G Method

When a fragment, such as $-N=CH-$, has more than one singly occupied LFMO, the method of constructing LFMO basis set can ensure that, only at the RHF/STO-3G level, the singly occupied LFMOs have the correct spatial extension direction. Therefore, the FUL state must be constructed at the RHF/STO-3G level. Before using RHF/STO-3G method to calculate the molecular energy difference between DSI and FUL states, should try to prove the method's rationality in many ways.

At RHF/STO-3G level, as shown by Figure 4-9e, the vertical delocalization energies for 20 substituted NBAs have the same characteristics as those for 11 substituted NBAs at (RHF and B3LYP)/6-311G* level. But the RHF/STO-3G values are always less than the corresponding (B3LYP and RHF)/6-311G* values.

According to the positions of the curve line in Figure 4-9e, the 20 molecules can also be divided into two group. The first group of the molecules includes 12 substituted NBAs. In the 12 molecules except for molecules **2-8** ($R_1 = -OH$, $R_2 = -NO_2$), **2-12** ($R_1 = -NH_2$, $R_6 = -NO_2$), **2-13** ($R_5 = -NO_2$, $R_2 = -OH$) and **2-20** ($R_3 = -OH$, $R_2 = -NO_2$), all the substituents are the electron-releasing groups such as $-OH$, $-NH_2$, and $-CL$. The size order of the vertical

delocalization energies (hartree) for the $\theta = 0^\circ$ geometries of the 12 molecules is as follow (RHF/STO-3G):

NBA (0.00813) < **2-6** (R₂ = -OH, 0.00821) < **2-12** (R₁ = -NH₂, R₆ = -NO₂, 0.00826) < **2-8** (R₁ = -OH, R₂ = -NO₂, 0.00832) < **2-5** (R₁ = -NH₂, 0.00842) < **2-13** (R₅ = -NO₂, R₂ = -OH, 0.00854) < **2-20** (R₃ = -OH, R₂ = -NO₂, 0.00861) < **2-4** (R₁ = -OH, 0.00897) < **2-19** (R₃ = -OH, 0.00924) < **2-16** (R₃ = -CL, R₄ = -OH, 0.00959) < **2-14** (R₄ = -OH, 0.00985) < **2-18** (R₃ = -NH₂, R₄ = -OH, 0.01062) < **2-17** (R₃ = -OH, R₄ = -OH, 0.01117).

Similar to the RHF/6-311G* size order, this size order shows the following three rules: First, for the molecules, such as **2-16**, **2-18**, and **2-17**, with two electron-releasing groups at the o-position of two phenyl rings, the vertical delocalization energies are the most destabilizing. Secondly, Of the mono-substituted molecules such as **2-14**, **2-19**, **2-4**, **2-5** and **2-6**, the vertical delocalization energy for molecule **2-14** with a hydroxyl group at the o-position of C-phenyl ring is the most destabilizing. Except for molecule **2-19**, the size order for these five molecules is consistent with the RHF/6-311G* order. At last, for the di-substituted NBAs, such as **2-12** (R₁ = -NH₂, R₆ = -NO₂) and **2-13** (R₅ = -NO₂, R₂ = -OH), with a -NO₂ group at the m-position, the vertical delocalization energy is still larger than that of NBA.

A comparison of the vertical delocalization energies (0.00854 and 0.00821 hartree) for molecule **2-13** (R₅ = -NO₂, R₂ = -OH) and **2-6** (R₂ = -OH) indicates that the m-NO₂ group of N-phenyl ring can increase the ability of the -OH group at the p-position of C-phenyl ring.

According to grouping of substituted NBAs at B3LYP/6-311G* level, the molecules **2-8** and **2-20** belong to the second group, and its vertical delocalization energies are slightly larger than that of NBA. For the second group of the substituted NBAs, the size order of the vertical delocalization energies is as follow (RHF/STO-3G):

NBA (0.00813) > **2-11** (R₁ = -NH₂, R₂ = -NO₂, 0.00787) > **2-7** (R₂ = -NO₂, 0.00774) > **2-3** (R₁ = -COOH, 0.00726) > **2-2** (R₁ = -NO₂, 0.00708) > **2-9** (R₁ = -NO₂, R₂ = -OH, 0.00693) > **2-10** (R₁ = -NO₂, R₂ = -NH₂, 0.00675) > **2-21** (R₁ = -NO₂, R₇ = -NH₂, 0.00592).

For the molecules **2-7**, **2-2** and **2-9**, the size order of the vertical delocalization energies is consistent with the B3LYP/6-311G* order.

Therefore, although STO-3G is a minimal basis, RHF/STO-3G can also be used to reasonably study the nature of electron delocalization, which will be further confirmed in other section of this Chapter.

4.4. SUMMARY

The facts that $dE_e(\theta)/d(\theta) < 0$ and $dE_N(\theta)/d(\theta) > 0$ means that electron interaction is always the driving force of molecular distortion, regardless of whether the electron delocalization is stabilization.

Based on the constructions of the DSI and FUD states for various types of the NBA-like species including the heterocyclic NBA-like species and substituted NBAs, it has been repeatedly demonstrated that the following results have nothing to do with the theoretical level and basis set size:

$$\begin{aligned} E^{\text{DSI}}(\theta) &< 0, d\Delta E^{\text{DSI}}(\theta)/d(\theta) < 0, \\ E^{\text{FUD}}(\theta) &< 0, d\Delta E^{\text{FUD}}(\theta)/d(\theta) < 0 \\ |E^{\text{DSI}}(\theta)| &> |E^{\text{FUD}}(\theta)|, \\ \Delta E^V(\theta) &> 0, d[\Delta E^V(\theta)]/d\theta < 0 \end{aligned}$$

Therefore, in the case of NBA-like species, π -electron delocalization is always destabilization, and it is a driving force for distorting NBA-like species.

When the vertical delocalization energy (VRE) of NBA is used as a reference, an electron-releasing group such as $-\text{OH}$ makes the VRE more destabilizing, and an electron-withdrawing group such as $-\text{NO}_2$ decreases the VRE. The ability of electron-withdrawing group is stronger than that of electron-releasing group. For NBA-like species substituted by $-\text{NO}_2$ and $-\text{OH}$ groups, therefore, the VRE is always less than that of NBA.

4.5. APPENDIX

Table 4-1. For The $\theta = 17^\circ$ Geometry of N-benzylideneaniline at B3LYP/6-31G* Level, 4 Typical LC-AO MOs and 3 Typical LC-LFMO MOs of the DSI-3 and FUD States.

AO	DSI		FUD		LFMO	DSI		FUD	
	37-th MO (A- π)	38-th MO (σ)	36-th MO (σ)	37-th MO (π)		37-th MO (A- π)	38-th MO (σ)	37-th MO (π)	
1	1C	1s	0.000000	0.017174	-0.003440	0.000000	1	0.000000	0.004029
2	1	2s	0.000000	-0.041839	0.006684	0.000000	2	0.000000	-0.000067
3	1	2px	0.000000	-0.066149	-0.010760	0.000000	3	0.000000	0.000705
4	1	2py	0.000000	-0.059318	0.122617	0.000000	4	0.000000	0.000023
5	1	2pz	0.234021	0.000000	0.000000	0.215733	5	0.000000	-0.000021
6	1	3s	0.000000	-0.010854	0.012420	0.000000	6	0.000000	-0.000041
7	1	3px	0.000000	0.019605	-0.005553	0.000000	7	0.000000	-0.002940
8	1	3py	0.000000	0.040206	0.029893	0.000000	8	0.000000	-0.004554
9	1	3pz	0.156178	0.000000	0.000000	0.116606	9	0.000000	-0.000058
10	1	4xx	0.000000	-0.002320	-0.001351	0.000000	10	0.000000	-0.011964
11	1	4yy	0.000000	0.008430	0.001327	0.000000	11	0.000000	0.020576
12	1	4zz	0.000000	-0.000919	0.000402	0.000000	12	0.000000	0.017504
13	1	4xy	0.000000	0.016247	-0.002488	0.000000	13	0.000000	-0.035892
14	1	4xz	0.003290	0.000000	0.000000	-0.002667	14	0.000000	0.033663
15	1	4yz	0.005492	0.000000	0.000000	-0.004445	15	0.000000	-0.006900
16	2C	1s	0.000000	-0.014295	0.002691	0.000000	16	-0.996265	0.000000
17	2	2s	0.000000	0.034848	-0.002045	0.000000	17	0.000000	-0.942278
18	2	2px	0.000000	0.118198	0.008500	0.000000	18	0.000000	-0.139688
19	2	2py	0.000000	0.192925	0.200300	0.000000	19	0.079675	0.000000
20	2	2pz	0.226672	0.000000	0.000000	0.128263	20	0.009190	0.000000
21	2	3s	0.000000	0.020271	-0.016604	0.000000	21	0.000000	-0.128888
22	2	3px	0.000000	0.068655	0.004387	0.000000	22	0.000000	0.008162
23	2	3py	0.000000	0.055718	0.063129	0.000000	23	0.000000	-0.001562
24	2	3pz	0.121917	0.000000	0.000000	0.074571	24	0.000000	0.090928

25	2	4xx	0.000000	-0.005998	-0.000640	0.000000	25	0.000000	-0.085157	0.000000
26	2	4yy	0.000000	0.000393	-0.004009	0.000000	26	0.000000	0.000000	-0.575032
27	2	4zz	0.000000	-0.000365	0.000746	0.000000	27	0.000000	0.108673	0.000000
28	2	4xy	0.000000	0.007353	0.005629	0.000000	28	0.000000	0.175653	0.000000
29	2	4xz	-0.004447	0.000000	0.000000	-0.005878	29	0.000000	0.021305	0.000000
30	2	4yz	0.008088	0.000000	0.000000	0.002587	30	0.000000	0.000033	0.000000
31	3C	1s	0.000000	0.007002	-0.010647	0.000000	31	0.000000	-0.000560	0.000000
32	3	2s	0.000000	-0.010023	0.021539	0.000000	32	0.000000	0.000261	0.000000
33	3	2px	0.000000	-0.121901	-0.043336	0.000000	33	0.000000	0.000001	0.000000
34	3	2py	0.000000	-0.193718	-0.147087	0.000000	34	0.000000	0.000011	0.000000
35	3	2pz	0.220933	0.000000	0.000000	0.089269	35	0.000000	-0.000001	0.000000
36	3	3s	0.000000	-0.042975	0.045004	0.000000	36	0.000000	0.001488	0.000000
37	3	3px	0.000000	-0.025183	-0.019766	0.000000	37	0.000000	-0.011596	0.000000
38	3	3py	0.000000	-0.059512	-0.035722	0.000000	38	0.000000	-0.002866	0.000000
39	3	3pz	0.129750	0.000000	0.000000	0.045040	39	0.000000	0.028088	0.000000
40	3	4xx	0.000000	-0.012825	-0.000247	0.000000	40	0.000000	-0.001357	0.000000
41	3	4yy	0.000000	0.009331	-0.001326	0.000000	41	0.000000	-0.001413	0.000000
42	3	4zz	0.000000	0.001059	-0.000892	0.000000	42	0.000000	0.063418	0.000000
43	3	4xy	0.000000	0.011875	0.007407	0.000000	43	0.000000	-0.005061	0.000000
44	3	4xz	-0.009739	0.000000	0.000000	-0.004342	44	0.000000	0.027736	0.000000
45	3	4yz	-0.000372	0.000000	0.000000	-0.001319	45	0.000000	0.000000	-0.478132
46	4C	1s	0.000000	0.007033	0.008367	0.000000	46	0.000000	-0.142541	0.000000
47	4	2s	0.000000	-0.024913	-0.018869	0.000000	47	0.000000	0.120456	0.000000
48	4	2px	0.000000	0.191064	-0.031073	0.000000	48	0.000000	0.000000	-0.072227
49	4	2py	0.000000	0.213859	0.108122	0.000000	49	0.000000	0.000000	-0.005370
50	4	2pz	0.218031	0.000000	0.000000	0.075927	50	0.000000	0.011536	0.000000
51	4	3s	0.000000	0.002557	-0.032859	0.000000	51	0.016602	0.000000	-0.026631
52	4	3px	0.000000	0.048687	-0.027146	0.000000	52	0.001816	0.000000	0.003055
53	4	3py	0.000000	0.046217	0.044386	0.000000	53	0.000000	-0.029150	0.000000
54	4	3pz	0.123080	0.000000	0.000000	0.042671	54	0.000000	0.028527	0.000000
55	4	4xx	0.000000	-0.006317	-0.002036	0.000000	55	-0.005721	0.000000	0.009550
56	4	4yy	0.000000	0.016062	0.004353	0.000000	56	0.000000	-0.004276	0.000000
57	4	4zz	0.000000	-0.001121	0.000325	0.000000	57	0.000000	0.009650	0.000000
58	4	4xy	0.000000	0.020263	-0.000001	0.000000	58	0.000000	0.004564	0.000000
59	4	4xz	-0.004723	0.000000	0.000000	-0.001979	59	0.000000	-0.022517	0.000000
60	4	4yz	-0.008267	0.000000	0.000000	-0.003549	60	0.000000	-0.006316	0.000000
61	5C	1s	0.000000	0.004979	0.013340	0.000000	61	0.000000	0.000246	0.000000
62	5	2s	0.000000	-0.009049	-0.029280	0.000000	62	0.000000	0.006520	0.000000

63	5	2px	0.000000	-0.203458	0.030533	0.000000	63	0.000000	-0.013748	0.000000
64	5	2py	0.000000	-0.188147	0.164480	0.000000	64	0.000000	0.003410	0.000000
65	5	2pz	0.215503	0.000000	0.000000	0.086592	65	0.015843	0.000000	0.003352
66	5	3s	0.000000	-0.012288	-0.062567	0.000000	66	0.000000	-0.002998	0.000000
67	5	3px	0.000000	-0.078547	0.018186	0.000000	67	0.000000	0.003348	0.000000
68	5	3py	0.000000	-0.065580	0.062967	0.000000	68	0.000000	-0.007451	0.000000
69	5	3pz	0.127511	0.000000	0.000000	0.045726	69	-0.015970	0.000000	-0.002936
70	5	4xx	0.000000	-0.007606	0.000925	0.000000	70	0.000000	0.001110	0.000000
71	5	4yy	0.000000	0.006284	0.002531	0.000000	71	0.000000	0.002347	0.000000
72	5	4zz	0.000000	0.000476	0.000624	0.000000	72	0.000052	0.000000	0.000831
73	5	4xy	0.000000	0.013428	-0.003269	0.000000	73	0.000000	-0.001946	0.000000
74	5	4xz	0.004626	0.000000	0.000000	0.001011	74	0.000000	-0.000032	0.000000
75	5	4yz	-0.008604	0.000000	0.000000	-0.004474	75	-0.011836	0.000000	0.000622
76	6C	1s	0.000000	-0.008994	-0.003564	0.000000	76	0.001009	0.000000	0.001224
77	6	2s	0.000000	0.026251	0.004917	0.000000	77	0.000000	-0.011865	0.000000
78	6	2px	0.000000	0.178823	-0.064712	0.000000	78	-0.007838	0.000000	0.001455
79	6	2py	0.000000	0.199967	-0.149345	0.000000	79	0.000000	0.001283	0.000000
80	6	2pz	0.218328	0.000000	0.000000	0.124789	80	0.000000	-0.001506	0.000000
81	6	3s	0.000000	-0.014145	0.033495	0.000000	81	0.000000	-0.000381	0.000000
82	6	3px	0.000000	0.025191	-0.008854	0.000000	82	0.000000	-0.000181	0.000000
83	6	3py	0.000000	0.066190	-0.027661	0.000000	83	0.000000	0.002064	0.000000
84	6	3pz	0.112948	0.000000	0.000000	0.066529	84	0.000000	0.003029	0.000000
85	6	4xx	0.000000	-0.013307	0.003145	0.000000	85	0.000000	-0.002326	0.000000
86	6	4yy	0.000000	0.006015	-0.001529	0.000000	86	0.000000	-0.000190	0.000000
87	6	4zz	0.000000	0.000218	-0.000547	0.000000	87	0.000000	-0.000679	0.000000
88	6	4xy	0.000000	0.005693	-0.007278	0.000000	88	0.000000	0.003952	0.000000
89	6	4xz	0.009419	0.000000	0.000000	0.005242	89	0.000000	0.001153	0.000000
90	6	4yz	-0.000022	0.000000	0.000000	-0.003792	90	0.000000	0.002779	0.000000
91	7H	1s	0.000000	-0.059129	-0.103162	0.000000	91	-0.000168	0.000000	-0.000201
92	7	2s	0.000000	-0.071844	-0.082744	0.000000	92	0.000000	0.007267	0.000000
93	8H	1s	0.000000	-0.098575	-0.014212	0.000000	93	0.001113	0.000000	0.005533
94	8	2s	0.000000	-0.101736	-0.014989	0.000000	94	0.000000	-0.000155	0.000000
95	9H	1s	0.000000	0.201001	0.039645	0.000000	95	-0.000274	0.000000	0.003161
96	9	2s	0.000000	0.215850	0.039098	0.000000	96	-0.000025	0.000000	-0.000043
97	10H	1s	0.000000	-0.053616	0.066368	0.000000	97	-0.000502	0.000000	0.003133
98	10	2s	0.000000	-0.053453	0.063774	0.000000	98	-0.000208	0.000000	0.000174
99	11H	1s	0.000000	-0.116459	0.043279	0.000000	99	0.000000	-0.007015	0.000000
100	11	2s	0.000000	-0.121712	0.034605	0.000000	100	0.000000	0.001193	0.000000

101	12N	1s	0.000000	-0.025238	0.018670	0.000001	101	0.000000	-0.001407	0.000000
102	12	2s	0.000000	0.053812	-0.037353	-0.000008	102	0.000000	-0.001274	0.000000
103	12	2px	0.000000	0.011106	0.068064	0.066308	103	0.000000	-0.001444	0.000000
104	12	2py	0.000000	0.124962	-0.107511	-0.047177	104	0.000000	-0.000136	0.000000
105	12	2pz	0.000000	0.019383	-0.036011	0.266155	105	0.000000	-0.000941	0.000000
106	12	3s	0.000000	0.146731	-0.093635	0.000016	106	0.000000	-0.001157	0.000000
107	12	3px	0.000000	0.017637	0.027797	0.038595	107	0.000000	0.000013	0.000000
108	12	3py	0.000000	0.062917	-0.037765	-0.027455	108	-0.000757	0.000000	0.002642
109	12	3pz	0.000000	0.006764	-0.013618	0.154885	109	-0.000086	0.000000	-0.000018
110	12	4xx	0.000000	-0.001117	0.005116	0.006682	110	0.000000	0.000525	0.000000
111	12	4yy	0.000000	-0.005650	-0.001583	0.001221	111	-0.000003	0.000000	-0.000079
112	12	4zz	0.000000	-0.001510	0.001286	-0.007907	112	0.000605	0.000000	-0.001553
113	12	4xy	0.000000	0.004269	-0.012127	-0.003737	113	-0.000156	0.000000	0.000873
114	12	4xz	0.000000	0.000780	-0.003590	0.014352	114	0.000000	-0.002075	0.000000
115	12	4yz	0.000000	-0.002005	0.002674	-0.003171	115	0.000000	0.000207	0.000000
116	13C	1s	0.000000	0.009061	-0.017330	0.000000	116	0.000000	0.002067	0.000000
117	13	2s	0.000000	-0.024786	0.039705	0.000011	117	0.000024	0.000000	-0.000020
118	13	2px	0.000000	0.073070	0.171340	0.055049	118	0.000000	0.001909	0.000000
119	13	2py	0.000000	-0.045873	0.165346	-0.039167	119	0.000000	0.000557	0.000000
120	13	2pz	0.000000	-0.026331	-0.013376	0.220992	120	0.000000	-0.000154	0.000000
121	13	3s	0.000000	-0.025601	0.033290	-0.000027	121	0.000000	-0.000401	0.000000
122	13	3px	0.000000	0.020663	0.064502	0.031768	122	0.000000	-0.000638	0.000000
123	13	3py	0.000000	-0.021094	0.066341	-0.022621	123	0.000000	-0.003227	0.000000
124	13	3pz	0.000000	-0.008889	-0.004311	0.127559	124	0.000000	0.000932	0.000000
125	13	4xx	0.000000	0.002748	0.004847	-0.002877	125	0.000000	-0.000185	0.000000
126	13	4yy	0.000000	0.001852	-0.005017	-0.002300	126	0.000000	-0.000008	0.000000
127	13	4zz	0.000000	0.000759	-0.000935	0.005178	127	0.000000	0.000492	0.000000
128	13	4xy	0.000000	0.000431	-0.007287	0.003049	128	0.000000	0.000023	0.000000
129	13	4xz	0.000000	-0.000536	-0.003203	-0.005925	129	0.000000	-0.001156	0.000000
130	13	4yz	0.000000	0.000147	0.001155	0.006961	130	0.000000	0.000000	-0.011308
131	14H	1s	0.000000	0.035872	0.098621	0.000004	131	0.000000	-0.120460	0.000000
132	14	2s	0.000000	0.031203	0.070007	0.000002	132	0.000000	-0.026142	0.000000
133	15C	1s	0.000000	-0.002599	0.000343	-0.000006	133	0.000000	0.015692	0.000000
134	15	2s	0.000000	0.006470	-0.001150	0.000030	134	0.000000	0.052064	0.000000
135	15	2px	0.000000	0.002787	-0.140923	0.042935	135	0.000000	0.000000	-0.029756
136	15	2py	0.000000	-0.013407	-0.170256	-0.030573	136	0.000000	-0.000327	0.000000
137	15	2pz	0.000000	-0.003085	0.004907	0.172020	137	0.000000	-0.007215	0.000000
138	15	3s	0.000000	-0.006286	0.015657	0.000008	138	0.000000	0.000000	-0.016120

139	15	3px	0.000000	0.013129	-0.027498	0.020544	139	0.000000	-0.020531	0.000000
140	15	3py	0.000000	-0.009345	-0.040607	-0.014663	140	0.000000	-0.002618	0.000000
141	15	3pz	0.000000	-0.004927	-0.000290	0.083796	141	0.000000	0.016170	0.000000
142	15	4xx	0.000000	0.001021	0.001003	0.000491	142	0.000000	-0.011214	0.000000
143	15	4yy	0.000000	-0.002284	-0.000327	-0.000513	143	0.000000	0.000000	-0.003937
144	15	4zz	0.000000	0.000190	0.000233	0.000026	144	0.000000	0.000000	0.001463
145	15	4xy	0.000000	-0.001933	-0.001145	0.000214	145	0.000000	0.019000	0.000000
146	15	4xz	0.000000	-0.000621	-0.000463	0.001129	146	0.000000	0.000000	0.000494
147	15	4yz	0.000000	0.000004	0.000201	0.001654	147	0.000000	0.005945	0.000000
148	16C	1s	0.000000	-0.001170	-0.014303	-0.000008	148	0.000000	-0.000001	0.000000
149	16	2s	0.000000	0.000044	0.030377	-0.000005	149	0.000000	0.009102	0.000000
150	16	2px	0.000000	0.014623	0.083796	0.026562	150	0.000000	0.000000	-0.000239
151	16	2py	0.000000	0.060897	-0.041339	-0.018938	151	0.000000	-0.001068	0.000000
152	16	2pz	0.000000	0.007141	-0.028208	0.106808	152	0.000000	0.003495	0.000000
153	16	3s	0.000000	0.017915	0.071997	-0.000079	153	0.000000	-0.001167	0.000000
154	16	3px	0.000000	0.014909	0.006519	0.015804	154	0.000000	0.000000	-0.013422
155	16	3py	0.000000	0.018555	-0.043045	-0.011370	155	0.000000	0.000000	-0.000600
156	16	3pz	0.000000	-0.000429	-0.009254	0.063969	156	0.000000	0.004106	0.000000
157	16	4xx	0.000000	-0.000559	0.003838	0.002000	157	0.000000	-0.004098	0.000000
158	16	4yy	0.000000	0.002008	-0.007263	0.000790	158	0.000000	0.000000	0.002986
159	16	4zz	0.000000	-0.000133	-0.000449	-0.002808	159	0.000000	-0.001511	0.000000
160	16	4xy	0.000000	-0.003276	-0.004645	-0.001482	160	0.000000	0.001441	0.000000
161	16	4xz	0.000000	-0.000550	-0.002186	0.004271	161	0.000000	-0.002808	0.000000
162	16	4yz	0.000000	0.001320	-0.000145	-0.002318	162	0.000000	0.003393	0.000000
163	17C	1s	0.000000	0.000197	0.015507	0.000011	163	0.000000	0.006525	0.000000
164	17	2s	0.000000	-0.000077	-0.033216	-0.000043	164	0.000000	-0.000247	0.000000
165	17	2px	0.000000	0.000312	-0.084065	0.019306	165	0.000000	-0.001500	0.000000
166	17	2py	0.000000	-0.068242	0.040413	-0.013887	166	0.000000	0.000443	0.000000
167	17	2pz	0.000000	-0.012179	0.028137	0.077881	167	0.000000	-0.001036	0.000000
168	17	3s	0.000000	0.000048	-0.077766	0.000079	168	0.000000	0.000000	0.001651
169	17	3px	0.000000	-0.001554	-0.038878	0.009832	169	0.000000	0.000548	0.000000
170	17	3py	0.000000	-0.021749	-0.014714	-0.007123	170	0.000000	-0.002252	0.000000
171	17	3pz	0.000000	-0.003474	0.007064	0.039213	171	0.000000	0.000546	0.000000
172	17	4xx	0.000000	-0.001012	0.003240	0.001618	172	0.000000	0.000000	-0.000622
173	17	4yy	0.000000	0.000580	0.000105	-0.000243	173	0.000000	-0.000378	0.000000
174	17	4zz	0.000000	0.000259	0.000371	-0.001373	174	0.000000	0.000000	0.000213
175	17	4xy	0.000000	-0.002461	0.007545	-0.000459	175	0.000000	0.000000	-0.000225
176	17	4xz	0.000000	-0.000109	0.000643	0.003545	176	0.000000	-0.000222	0.000000

177	17	4yz	0.000000	0.000705	-0.002027	0.000979	177	0.000000	-0.000825	0.000000
178	18C	1s	0.000000	-0.000908	0.013107	-0.000002	178	0.000000	0.000000	0.001881
179	18	2s	0.000000	0.003665	-0.032797	-0.000005	179	0.000000	0.000000	-0.000375
180	18	2px	0.000000	-0.012014	-0.151102	0.017213	180	0.000000	-0.001648	0.000000
181	18	2py	0.000000	0.060883	-0.173582	-0.012215	181	0.000000	0.000000	0.002438
182	18	2pz	0.000000	0.013779	0.006913	0.069251	182	0.000000	-0.000298	0.000000
183	18	3s	0.000000	-0.002159	-0.044738	-0.000021	183	0.000000	-0.000347	0.000000
184	18	3px	0.000000	-0.012081	-0.047288	0.010235	184	0.000000	-0.000044	0.000000
185	18	3py	0.000000	0.017153	-0.042153	-0.007255	185	0.000000	0.000080	0.000000
186	18	3pz	0.000000	0.006041	0.004264	0.039957	186	0.000000	-0.000149	0.000000
187	18	4xx	0.000000	-0.000766	0.000896	0.000930	187	0.000000	-0.000484	0.000000
188	18	4yy	0.000000	-0.000884	0.005835	-0.000908	188	0.000000	0.000022	0.000000
189	18	4zz	0.000000	0.000401	-0.000476	-0.000029	189	0.000000	0.000327	0.000000
190	18	4xy	0.000000	-0.003738	0.008677	0.000350	190	0.000000	-0.000003	0.000000
191	18	4xz	0.000000	-0.000382	0.001268	0.002137	191	0.000000	-0.000125	0.000000
192	18	4yz	0.000000	0.000707	-0.000953	0.002915	192	0.000000	-0.000623	0.000000
193	19C	1s	0.000000	-0.002799	0.008289	-0.000012	193	0.000000	-0.000252	0.000000
194	19	2s	0.000000	0.003821	-0.018087	0.000036	194	0.000000	0.000001	0.000000
195	19	2px	0.000000	0.013288	0.122613	0.019720	195	0.000000	-0.000544	0.000000
196	19	2py	0.000000	-0.028356	0.011390	-0.013918	196	0.000000	0.000000	-0.003385
197	19	2pz	0.000000	-0.008343	-0.028485	0.078957	197	0.000000	0.000125	0.000000
198	19	3s	0.000000	0.024872	-0.044434	0.000010	198	0.000000	0.000000	0.001364
199	19	3px	0.000000	0.004078	0.015500	0.010186	199	0.000000	0.000000	0.000000
200	19	3py	0.000000	0.001026	-0.014316	-0.007125	200	0.000000	0.000000	-0.002056
201	19	3pz	0.000000	-0.000839	-0.006415	0.040393	201	0.000000	0.000000	-0.000239
202	19	4xx	0.000000	-0.000797	-0.005622	-0.000325	202	0.000000	0.000538	0.000000
203	19	4yy	0.000000	0.001587	0.007845	-0.001164	203	0.000000	-0.000321	0.000000
204	19	4zz	0.000000	-0.000213	-0.000255	0.001486	204	0.000000	0.001006	0.000000
205	19	4xy	0.000000	-0.003378	0.005780	0.001068	205	0.000000	0.000088	0.000000
206	19	4xz	0.000000	-0.000519	0.002730	-0.000507	206	0.000000	0.000144	0.000000
207	19	4yz	0.000000	0.001273	0.000101	0.003641	207	0.000000	-0.000012	0.000000
208	20C	1s	0.000000	0.005683	-0.012111	0.000015	208	0.000000	-0.000826	0.000000
209	20	2s	0.000000	-0.011464	0.027919	0.000018	209	0.000000	-0.000040	0.000000
210	20	2px	0.000000	-0.006752	-0.146269	0.027341	210	0.000000	-0.000037	0.000000
211	20	2py	0.000000	0.018676	-0.010342	-0.019368	211	0.000000	0.000000	-0.001771
212	20	2pz	0.000000	0.004981	0.034599	0.109687	212	0.000000	0.000000	-0.000161
213	20	3s	0.000000	-0.030983	0.048962	-0.000011	213	0.000000	-0.000105	0.000000
214	20	3px	0.000000	0.003819	-0.062343	0.016237	214	0.000000	0.000000	0.000121

215	20	3py	0.000000	0.011209	-0.032277	-0.011304	215	0.000000	0.000000	-0.001205
216	20	3pz	0.000000	0.001032	0.009818	0.064847	216	0.000000	0.000000	0.000298
217	20	4xx	0.000000	-0.001429	-0.005969	-0.001739	217	0.000000	0.000261	0.000000
218	20	4yy	0.000000	0.001447	0.000837	-0.000983	218	0.000000	-0.000139	0.000000
219	20	4zz	0.000000	0.000433	-0.000313	0.002752	219	0.000000	-0.000121	0.000000
220	20	4xy	0.000000	-0.000449	-0.004572	0.001533	220	0.000000	0.000000	0.000030
221	20	4xz	0.000000	0.000472	0.000807	-0.003669	221	0.000000	0.000018	0.000000
222	20	4yz	0.000000	0.000307	0.001379	0.002997	222	0.000000	-0.000397	0.000000
223	21H	1s	0.000000	0.035843	-0.032982	-0.000021	223	0.000000	0.000050	0.000000
224	21	2s	0.000000	0.034895	-0.029493	0.000032	224	0.000000	-0.000069	0.000000
225	22H	1s	0.000000	-0.005276	0.039676	0.000065	225	0.000000	0.000000	0.000009
226	22	2s	0.000000	-0.005600	0.039762	0.000045	226	0.000000	0.000257	0.000000
227	23H	1s	0.000000	-0.031097	0.133565	-0.000025	227	0.000000	-0.000113	0.000000
228	23	2s	0.000000	-0.033996	0.130140	-0.000011	228	0.000000	0.000020	0.000000
229	24H	1s	0.000000	0.027890	0.020635	-0.000027	229	0.000000	-0.000035	0.000000
230	24	2s	0.000000	0.029501	0.020918	-0.000009	230	0.000000	-0.000046	0.000000
231	25H	1s	0.000000	-0.012073	-0.079478	0.000045	231	0.000000	-0.000033	0.000000
232	25	2s	0.000000	-0.008507	-0.065844	-0.000067	232	0.000000	0.000099	0.000000

4.6. REFERENCES

- 1 Kitaura, K.; Morokuma, K. 1976. "A New Energy Decomposition Scheme for Molecular Interactions within the Hartree-Fock Approximation." *Int. J. Quantum Chem.*, 10: 325-340.
- 2 Umeyama, H.; Morokuma, K. 1977. "The Origin of Hydrogen Bonding. An Energy Decomposition Study." *J. Am. Chem. Soc.*, 99: 1316- 1332.
- 3 Morokuma, K. 1977. "Why Do Molecules Interact? The Origin of Electron Donor-Acceptor Complexes, Hydrogen Bonding and Proton Affinity." *Acc. Chem. Res.*, 10: 294-300.
- 4 Kitaura, K.; Morokuma, K. 1981. *Chemical Applications of Atomic and Electrostatic Potentials*. New York: Plenum.
- 5 Foster, J. P.; Weinhold, F. 1980. "Natural Hybrid Orbitals." *J. Am. Chem. Soc.*, 102: 7211-7218.
- 6 Reed, A. E.; Weinstock, R. B.; Weinhold, F. 1985. "Natural Population Analysis." *J. Chem. Phys.*, 83: 735-746.
- 7 Glendening, E. D.; Reed, A. E.; Carpenter, J. E.; Weinhold, F. 1990. "NBO 3.1 program." *QCPE Bull.*, 10: 58.
- 8 Glendening, E. D.; Streitwieser, A. 1994. "Natural Energy Decomposition Analysis: An Energy Partitioning Procedure for Molecular Interactions with Application to Weak Hydrogen Bonding, Strong Ionic, and Moderate Donor–Acceptor Interactions." *J. Chem. Phys.*, 100: 2900-2909.
- 9 Glendening, E. D. 1996. "Natural Energy Decomposition Analysis: Explicit Evaluation of Electrostatic and Polarization Effects with Application to Aqueous Clusters of Alkali Metal Cations and Neutrals." *J. Am. Chem. Soc.*, 118: 2473-2482.
- 10 Schenter, G. K.; Glendening, E. D. 1996. "Natural Energy Decomposition Analysis: The Linear Response

- Electrical Self Energy." *J. Phys. Chem.*, 100: 17152-17156.
- 11 Reed, A. E.; Curtiss, L. A.; Weinhold, F. 1988. "Intermolecular Interactions from a Natural Bond Orbital, Donor-Acceptor Viewpoint." *Chem. Rev.*, 88: 899-926.
- 12 Mo, Y. 2006. "Intramolecular Electron Transfer: Computational Study Based on the Orbital Deletion Procedure (ODP)." *Curr. Org. Chem.*, 10: 779-790.
- 13 Mo, Y.; Peyerimhoff, S. D. 1998. "Theoretical Analysis of Electronic Delocalization." *J. Chem. Phys.*, 109: 1687-1697.
- 14 Mo, Y.; Zhang, Y.; Gao, J. 1999. "A Simple Electrostatic Model for Trisilylamine: Theoretical Examinations of the $n \rightarrow \sigma^*$ Negative Hyperconjugation, $p\pi \rightarrow d\pi$ Bonding, and Stereoelectronic Interaction." *J. Am. Chem. Soc.*, 121: 5737-5742.
- 15 Mo, Y. 2003. "Geometrical Optimization for Strictly Localized Structures." *J. Chem. Phys.*, 119: 1300-1306.
- 16 Mo, Y. 2004. "Resonance Effect in the Allyl Cation and Anion: A Revisit." *J. Org. Chem.*, 69: 5563-5567.
- 17 Mo, Y.; Schleyer, P.v.R. 2006. "An Energetic Measure of Aromaticity and Antiaromaticity Based on the Pauling-Wheland Resonance Energies." *Chem. Eur. J.*, 12: 2009-2020.
- 18 Bagus, P. S.; Hermann, K.; Bauschlicher, C. W., Jr. 1984. "A New Analysis of Charge Transfer and Polarization for Ligand-Metal Bonding: Model Studies of Al₄CO and Al₄NH₃." *J. Chem. Phys.*, 80: 4378-4386.
- 19 Stevens, W. J.; Fink, W. H. 1987. "Frozen Fragment Reduced Variational Space Analysis of Hydrogen Bonding Interactions. Application to the Water Dimer." *Chem. Phys. Lett.*, 139: 15-22.
- 20 Van der Vaart, A.; Merz, K. M. Jr. 1999. "Divide and Conquer Interaction Energy Decomposition." *J. Phys. Chem. A*, 103: 3321-3329.
- 21 Dapprich, S.; Frenking, G. 1995. "Investigation of Donor-Acceptor Interactions: A Charge Decomposition Analysis Using Fragment Molecular Orbitals." *J. Phys. Chem.*, 99: 9352-9362.
- 22 Bader, R. F. W. 1990. *Atoms in Molecules. A Quantum Theory*. Oxford: Oxford University Press.
- 23 Bader, R. F. W. 1998. in *Encyclopedia of Computational Chemistry*, Vol. 1, edited by Schleyer, P. v. R.; Allinger, N. L.; Kollmann, P. A.; Clark, T.; Schaefer, H. F. S.; Gasteiger, J.; Schreiner, P. R. Chichester: Wiley-VCH..
- 24 Ziegler, T.; Rauk, A. 1977. "On the Calculation of Bonding Energies by the Hartree Fock Slater Method." *Theor. Chim. Acta*, 46: 1-10.
- 25 Mayer, I.; Hamza, A. 2001. "Energy Decomposition in the Topological Theory of Atoms in Molecules and in the Linear Combination of Atomic Orbitals Formalism: A Note." *Theor. Chem. Acc.*, 105: 360-364.
- 26 Salvador, P.; Duran, M.; Mayer, I. 2001. "One- and Two-Center Energy Components in the Atoms in Molecules Theory." *J. Chem. Phys.*, 115: 1153-1157.
- 27 Salvador, P.; Mayer, I. 2004. "Energy Partitioning for "Fuzzy" Atoms." *J. Chem. Phys.*, 120: 5046-5052.
- 28 Martinov, M.; Cioslowski, J. 1995. "Rigorous Energy Partitioning Scheme." *Mol. Phys.*, 85: 121-129.
- 29 Yu, Z. H.; Li, L. T.; Fu, W.; Li, L. P. 1998. "Conformations of Stilbene-Like Species and New Method of Energy Partition." *J. Phys. Chem. A*, 102: 2016-2028.
- 30 Yu, Z. H.; Peng, X. Q. 2001. "New Insight Into the Nature of Electron Delocalization: The Driving Forces for Distorting the Geometry of Stilbene-Like Species." *J. Phys. Chem. A*, 105: 8541-8553.
- 31 Xu, H.; Yu, Z. H. 2004. "The Driving Forces for Distorting NBA-Like Species away from Their Planar Geometries." *J. Mol. Struct. (Theochem)*, 682: 37-46.
- 32 Ma, Y.P.; Bao, P.; Yu, Z. H. 2007. "Substituent Effect on N-Benzylideneanilines by DFT Energy Partition." *Chin. J. Chem.*, 25: 300-306.
- 33 Bao, P.; Yu, Z. H. 2006. "Theoretical Studies on the Role of π -Electron Delocalization in Determining the Conformation of N-Benzylideneaniline with Three Types of LMO Basis Sets." *J. Comput. Chem.*, 27: 809-824.
- 34 Bao, P.; Yu, Z. H. 2007. "Restricted Geometry Optimization: A Different Way to Estimate Stabilization Energies for Aromatic Molecules of Various Types." *J. Phys. Chem. A*, 111: 5304-5213.

- 35 Bao, P.; Yu, Z. H. 2011. "New Procedure to Evaluate Aromaticity at the Density Functional Theory, Hartree–Fock, and Post-Self-Consistent Field Levels." *J. Comput. Chem.*, 32: 248-259.
- 36 Bao, P. 2007. "Restricted Geometry Optimization – the New Research Method of Organic Electronic Structure." PhD Dissertation, Institute of Chemistry, ACS, Beijing.
- 37 Xu, H. 2004. "The Driving Forces for Distorting NBA-like Species away from the Planar Geometries and Their Substituent Effect." PhD Dissertation, Institute of Chemistry, ACS, Beijing.
- 38 Ma, Y. P. 2007. "The Nature of the π Electron Delocalization in NBA-like Species and the Substituent Effect." PhD Dissertation, Institute of Chemistry, ACS, Beijing.
- 39 Morokuma, K. 1971. "Molecular Orbital Studies of Hydrogen Bonds. III. COHO Hydrogen Bond in H₂COH₂0 and H 2CO₂H₂0." *J. Chem. Phys.*, 55: 1236-1244.
- 40 Libit, L.; Hoffmann, R. 1974. "Toward a Detailed Orbital Theory of Substituent Effects: Charge Transfer, Polarization, and the Methyl Group." *J. Am. Chem. Soc.*, 96: 1370-1383.
- 41 Bader, R. F. W.; Streitwieser, A.; Neuhaus, A.; Laidig, K. E.; Speers, P. 1996. "Electron Delocalization and the Fermi Hole." *J. Am. Chem. Soc.*, 118: 4959-4965.
- 42 Bader, R. F. W.; S.; Tang, T. H.; Popelier, P. L. A. 1996. "The Electron Pair." *J. Phys. Chem.*, 100: 15398-15415.
- 43 Bader, R. F. W.; Stephens, M. E. 1975. "Spatial Localization of the Electronic Pair and Number Distributions in Molecules." *J. Am. Chem. Soc.*, 97: 7391-7399.
- 44 廖沫真(Mu-Zhen, Liao), 吴国是(Guo-Shi, Wu), 刘洪霖(Hong-Lin, Liu). 1984. 量子化学从头算法, 北京: 清华大学出版社.
- 45 Glendening, E. D.; Faust, R.; Streitwieser, A.; K. Vollhardt, K. P. C.; Frank Weinhold, F. 1993. "The Role of Delocalization in Benzene." *J. Am. Chem. Soc.*, 115: 10952-10957.
- 46 Katritzky, A. R.; Boulton, A. J. 1974. *Advances in Heterocyclic Chemistry*, Vol. 17. New York: Academic Press, INC..
- 47 Hiberty, P.C.; Danovich, D.; Shurki, A.; Shaik, S. 1995. "Why Does Benzene Possess a D_{6h} Symmetry? A Quasiclassical State Approach for Probing π -Bonding and Delocalization Energies." *J. Am. Chem. Soc.*, 117: 7760-7768.
- 48 <http://www.oraxcel.com/cgi-bin/yabb2/YaBB.pl?num=1202391862>
- 49 http://en.wikipedia.org/wiki/Hybrid_functional

CHAPTER 5

ELECTRON DELOCALIZATION DESTABILIZATION

ABSTRACT

Due to the low localization degree of the natural bond orbitals (NBOs) and to the low separation degree of the π and σ NBOs, it is impossible to construct an absolutely localized π -system by conditionally eliminating the NBO-Fock matrix elements. Therefore, the π electron delocalization (energy decomposition analysis) energy, calculated based on the NBO basis set, is unreasonable. In the case of NBA-like species, the π - π interaction (conjugation) between fragments is destabilization and is a driving force of molecular distortion (π - π driving force). The π - σ interaction between fragments is also destabilization, but it is resistance to molecular distortion (π - σ resistance). The π - σ resistance is much greater than the π - π driving force. Therefore, there should be another greater driving force. This greater driving force comes from the non-bonded σ - σ interaction between fragments. If there are no MO interactions between the fragments, due to that the nuclear repulsion between fragments is resistance to the molecular distortion, the molecule, such as NBA and its derivatives, should tend to the planar conformation. Preferential geometry with a large twist angle θ is a compromise between the destabilizing energy effects associated with the π - π , non-bonded σ - σ , and π - σ interactions between fragments, which has nothing to do with the theoretical level and basis set size. It can now be clearly answered that this is the result of the destabilizing electron delocalization, facing the following conclusions obtained from the relaxed PES-scans by Gaussian software package (Chapter 2): $dE_e(\theta)/d(\theta) < 0$ and $dE_N(\theta)/d(\theta) > 0$ ($0 < \theta < \theta_{e-min}$). Contrary to the classical view, the distortion of NBA-like species is not intended to achieve higher stability, but to make the molecule itself to be less destabilized as far as possible. The use of the density functionals without Hartree-Fock exchange (such as PBE96, BLYP, SVWN5 and SLATER), as well as the use of our 2011 method, confirms that Hartree-Fock exchange cannot change the destabilizing feature of these energy effects and cannot change the role of these destabilizing energy effects in determining the conformation of NBA-like species.

yuzh@iccas.ac.cn

Key Words: localization degree of localized molecular orbital; the flaws of the NBO energy decompose analysis; electron delocalization destabilization; destabilizing π - π , σ - σ and π - σ interactions; driving force for distorting NBA.

In Chapter 4, the single-point energy calculation was performed, over the LFMO basis set, using our 2006 method,¹ and it was verified that, in the case of NBA-like species, the π - π interaction between the fragments is destabilization and is a driving force of molecular distortion. In this Chapter, it will be demonstrated that the σ - σ and π - σ interactions are also destabilization. In the literature, the NBO basis set is considered to be a localized basis set. Therefore, as the first objective of this Chapter, the NBO basis set should be used to calculate the vertical delocalization energy to prove that our 2006 method is superior to the NBO method.

5.1. NBO METHOD

The NBO basis set is a recognized and widely used LMO (localized molecular orbital) basis set and has entered Gaussian-X and Gamess software packages. NEDA (NBO energy decompose analysis) has been used in various fields. For example, it was used to study through-bond and through-space electron transfer at RHF/STO-3G level of theory.²

In this chapter, the localization degree of the LMO basis set such as LFMO, NBO and NBO-II basis sets will be defined. Ultimately, it will be proved that the NBO basis set can't be used for Morokuma's energy decomposition due to the low separation degree of the π and σ NBOs and owing to its low localization degree. From then on, we can say with certainty: only the LFMO basis set is a real LMO basis set and our calculation, performed by using our 2006 method, is reasonable.

5.1.1. NBO Basis Set

In this section, two types of NBO basis set will be constructed in order to illustrate the effects of the localization degree of LMO basis set on the energy decomposition. The first type of NBO basis set refers to the standard NBO basis set and is obtained from the density matrix of the ground state (The ground state of a molecule should be an equilibrium geometry and is obtained from the full geometry optimization. In this Chapter, the ground state of a specific geometry twisted by θ refers specifically to the full delocalized electronic state and is obtained from the unconditional single-point energy calculation on a molecular conformation with a specific twist angle θ . In the planar geometry, therefore, the FUD state is the real ground state). The second type of NBO basis set is obtained from the AO density matrix of the DSI-LFMO state and will be denoted as NBO-II, where the DSI-LFMO refers to the DSI state obtained from the conditional single-point energy calculation based on the LFMO basis set.

In this section, in each twisted geometry of N-benzylideneaniline obtained from the relaxed PES-scans, all the dihedron angles, except for the twist angle θ , are set equal to 180° or 0°.

5.1.1.1. Picking out π -Type NBOs

In the case of LC-NAO (linear combination of natural atomic orbitals), as shown by the NAO coefficients listed in Table 5-1 (listed, as an appendix, at the end of Chapter), NBOs are absolutely localized on their respective double bonds (2-center LC-NAO NBOs) or on their respective atoms (1-center LC-NAO NBOs), no matter whether a molecular is planar or non-planar. In terms of the localization, LC-NAO NBO basis set is different from LC-AO (linear combination of atomic orbitals) NBOs and is the same as LFMOs. But, the π and σ LC-NAO NBOs are still not completely separated when a molecule is not planar. For the $\theta = 32^\circ$ geometry of N-benzylideneaniline (NBA), for example, its 17-th LC-NAO NBO is a π NBO and is absolutely localized on the N(12)-C(13) bond. But the s-NAO coefficients of this NBO are as follows (Table 5-1): -0.0359 (N12, 2s), -0.0021 (N12, 3s), -0.0340 (C13, 2s) and -0.0040 (C13, 3s). In our calculation program, therefore, LC-NAO NBOs can be used to identify π -NBO and to

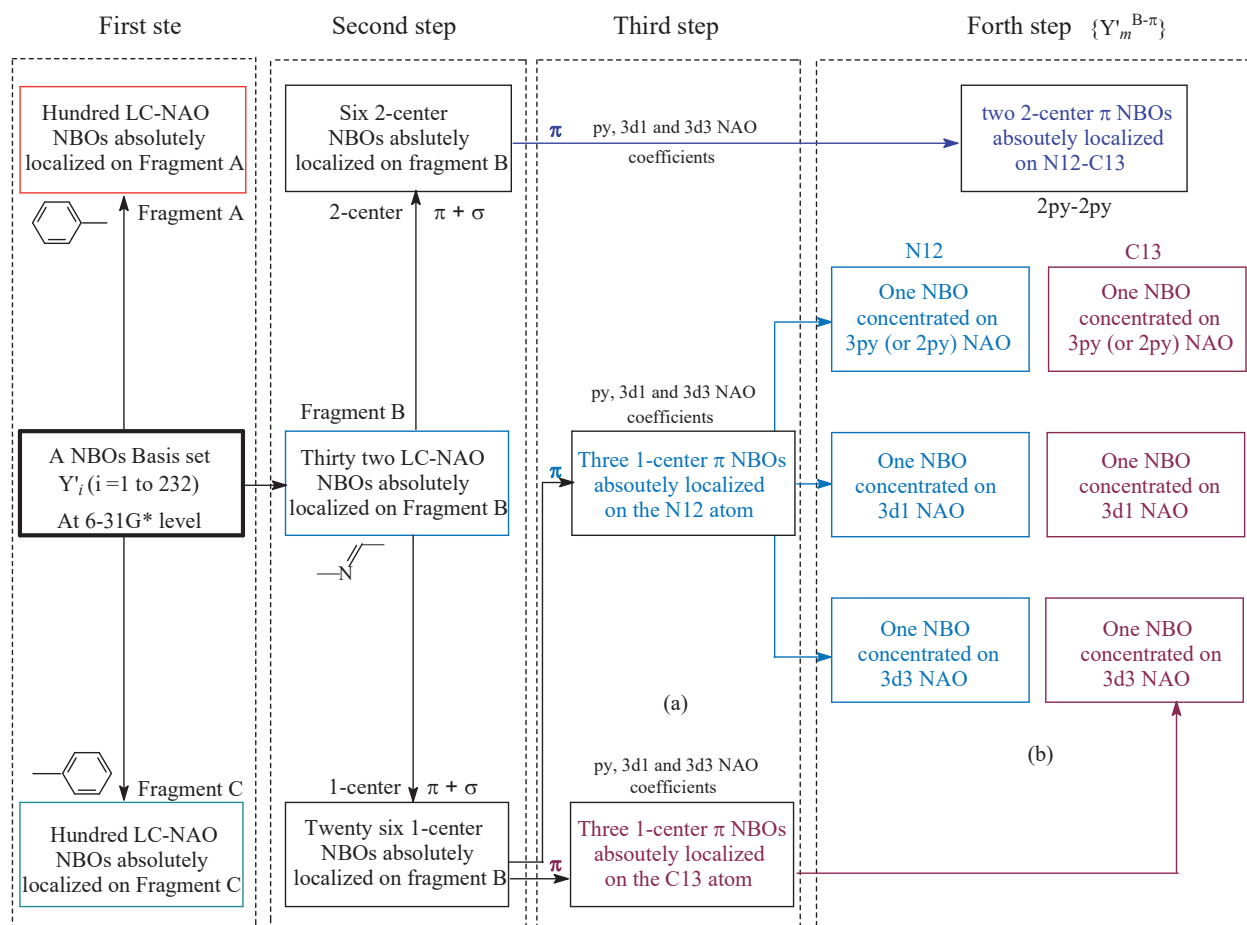


Figure 5-1. A four-step procedure for identifying and selecting the π LC-NAO NBOs belonging to fragment B ($-\text{N}=\text{CH}-$) of N-benzylideneaniline (NBA) according to the NAO coefficients at 6-31G* level.

determine to which fragment a specific NBO belongs, but the coefficient of s-NAO cannot be used to distinguish between π and σ NBOs.

At 6-31G* level, for example, each non-hydrogen atom, such as nitrogen and carbon, has 15 NAOs that include 4 π -type NAOs: 2py, 3py, 3d1, and 3d3 (Table 5-1), when a planar molecule is placed on the XOZ plane of a Cartesian coordinate system. For N-benzylideneaniline at 6-31G* level, total number of NAOs is 232, and the number of π -type NAOs is 56. For fragment B ($-\text{N}=\text{CH}-$), there are two 2-center and six 1-center π LC-NAO NBOs. In the case of planar conformation of N-benzylideneaniline, each 1-center π NBO is expressed as a linear combination of four π -type NAOs (absolutely localized on a specific atom), but its NAO coefficient is concentrated on a specific NAO; 2-center π NBO be done as a linear combination of 8 π -type NAOs. For example, the three 1-center LC-NAO NBO, the 133-th, 127-th and 128-th NBOs listed in Table 5-1, belong to the C(13) atom, and their NAO coefficients are concentrated on 3d3, 3d1 and 3py, respectively. When the molecular geometry is non-planar, the three 1-center LC-NAO NBOs are found to be still absolutely localized on a specific atom. In this case, as shown by the NAO coefficients of 17-th, 116-th, 121-th and 117-th LC-NAO NBOs in Table 5-1, 1-center π NBO results from the linear combination of 15 NAOs including s-type NAOs, and 2-center π NBO consists of 30 NAOs.

Therefore, the procedure for identifying, selecting and grouping π NBOs should be different from the procedure for doing π -LFMOs, and should follow the following characteristics of LC-NAO NBOs (at 6-31G* level):

Table 5-2. For Twisted Geometries of N-benzylideneaniline, Molecular Energies (hartree), $E^{\text{FUD-N}}(\theta)$ and $E^{\text{DSI-N}}(\theta)$ (DS-3), of the FUD- and DSI-NBO States, and the NBO Vertical Delocalization Energies $\Delta E^{\text{V-NBO}}(\theta)$ (kcal/mol) at 6-31G* Level.

		$\theta = 0^\circ$	17	32	42
B3LYP	$E^{\text{FUD-N}}(\theta)$	-556.7505	-556.7421	-556.7297	-556.6836
	$E^{\text{DSI-N}}(\theta)$	-556.6692	-556.6637	-556.6578	-556.6208
	$\Delta E^{\text{V-NBO}}(\theta)$	-51.0	-49.2	-45.1	-39.4
RHF	$E^{\text{FUD-N}}(\theta)$	-553.1342	-553.1274	-553.0948	-553.0710
	$E^{\text{DSI-N}}(\theta)$	-553.0554	-553.0518	-553.0273	-553.0104
	$\Delta E^{\text{V-NBO}}(\theta)$	-49.4	-47.5	-42.3	-38.0
MP2	$E^{\text{FUD-N}}(\theta)$	-555.0009	-554.9848	-554.9353	-554.9065
	$E^{\text{DSI-N}}(\theta)$	-554.9172	-554.9056	-554.8659	-554.8440
	$\Delta E^{\text{V-NBO}}(\theta)$	-52.5	-49.7	-43.5	-39.3
SLATER	$E^{\text{FUD-N}}(\theta)$	-545.5204	-545.5136	-545.4990	-545.4651
	$E^{\text{DSI-N}}(\theta)$	-545.4360	-545.4322	-545.4245	-545.3993
	$\Delta E^{\text{V-NBO}}(\theta)$	-53.0	-51.1	-46.7	-41.3

- (i) LC-NAO NBOs are absolutely localized on their respective fragments.
- (ii) 1-center LC-NAO NBOs are absolutely localized on their respective atoms.
- (iii) NAO coefficients are concentrated on the specific NAO(s) such as 2py, 3py, 3d1 and 3d3 when the twist angle $\theta < 50^\circ$.

Accordingly, as shown by Figure 5-1, our program for the identifying and selecting π NBOs is a four-step procedure. As the first step, 232 LC-NAO NBOs are divided into three groups that are belonged, respectively, to fragment A, B and C, according to the absolute localization features of LC-NAO NBOs. Then 32 LC-NAO NBOs belonging to fragment B are divided into the π and σ sub-groups (second step) according to the coefficients of 4 π -type NAOs 2py, 3py, 3d1, and 3d3. By the third step, at last, eight π -NBOs are identified from 32 LC-NBA NBOs and are divided into two sub-groups of π NBOs: two π -NBO with 2-center, and six π -NBOs with 1-center. At last, two sub-groups, one sub-group of π NBOs and one sub-group of σ NBOs, are combined to a sub-basis set for fragment B.

In the program, the priority is the π -NAO coefficients when identifying π NBOs. Since π and σ NBOs are not completely separated, the program can't ensure that the identification and selection of π -NBOs are reliable when the twist angle θ is greater than 50° .

There is a corresponding relationship, in the numbering of NBOs, between LC-NAO and LC-AO NBOs. For example, the 17th LC-NBA NBO corresponds to the 17-th LC-AO NBO. Based on the coefficients of the π -type NAOs, therefore, the NBOs can be divided into the six groups denoted as $\{\Psi_u^{\text{A-}\pi}, \Psi_v^{\text{B-}\pi}, \Psi_w^{\text{C-}\pi}, \Psi_r^{\text{A-}\sigma}, \Psi_s^{\text{B-}\sigma}, \Psi_t^{\text{C-}\sigma}\}^{\text{G}}$ = $\{\Psi_m^{\text{P-}\pi}, \Psi_n^{\text{P-}\sigma}\}^{\text{G}}$ (P = A, B, C). The superscript "G" means that the NBO basis set, $\{\Psi_i^{\text{P-}\pi}, \Psi_j^{\text{P-}\sigma}\}^{\text{G}}$, is obtained from the AO density matrix of the ground state geometry twist by θ using NBO 5.0 program. In a similar way, the NBO-II basis set is obtained from the AO density matrix of the DSI-LFMO state and is denoted as $\{\Psi_m^{\text{P-}\pi}, \Psi_n^{\text{P-}\sigma}\}^{\text{DSI}}$.

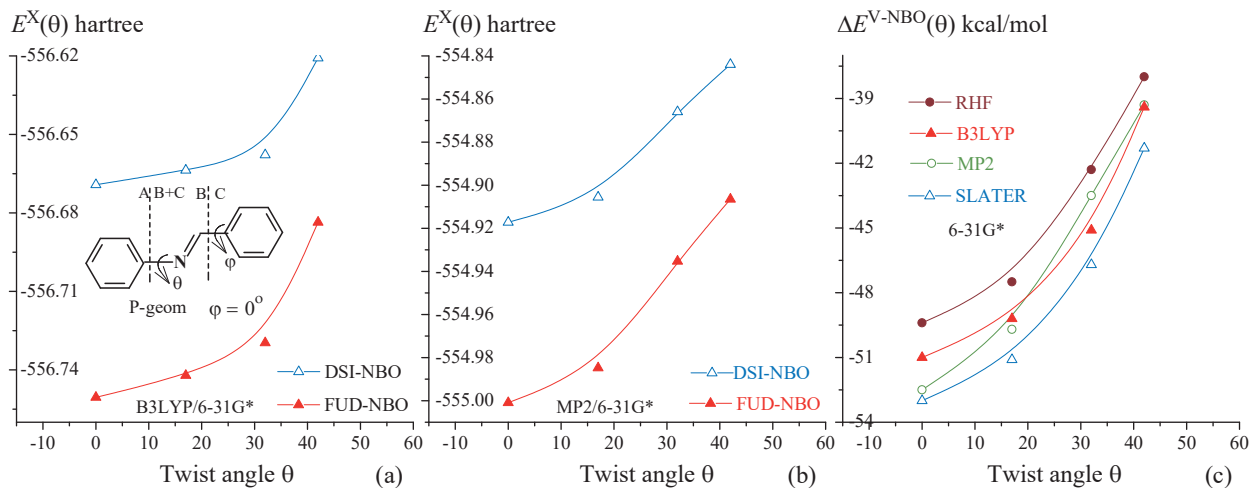


Figure 5-2. (a) and (b) Molecular energies, $E^{\text{FUD-N}}(\theta)$ and $E^{\text{DSI-N}}(\theta)$, of the FUD- and DSI-NBO states for NBA. (c) NBO vertical delocalization energies, and their changes with the increasing of twist angle θ .

The two NBO basis sets, $\{\Psi_i\}^G = \{\Psi_m^{\text{P-}\pi}, \Psi_n^{\text{P-}\sigma}\}^G$ (NBO) and $\{\Psi_i\}^{\text{DSI}} = \{\Psi_m^{\text{P-}\pi}, \Psi_n^{\text{P-}\sigma}\}^{\text{DSI}}$ (NBO-II), will be used to calculate the vertical delocalization energy (VRE).

5.1.2. NBO Vertical Delocalization Energy

After transforming AO Fock and overlap integral matrices into the NBO matrices, under the conditional settings described in Figure 4-4c to Figure 4-5, the single-point energy calculations, over the NBO basis set, provides the FUD and DSI states for a twisted geometry of N-benzylideneaniline. In this case, the FUD and DSI states are denoted as FUD-NBO and DSI-NBO, and their molecular energies are denoted as $E^{\text{FUD-N}}(\theta)$ and $E^{\text{DSI-N}}(\theta)$. The molecular energy difference, $[E^{\text{FUD-N}}(\theta) - E^{\text{DSI-N}}(\theta)]$, between the FUD state and DSI states is specially called the NBO vertical delocalization energy, and it is denoted as $\Delta E^{\text{V-NBO}}(\theta)$.

According to the data listed in Table 5-2 and based on the curves in Figure 5-2, the molecular energies of the FUD-NBO and DSI-NBO (DSI-3) states have the following characteristics:

$$\begin{aligned} & E^{\text{FUD-N}}(\theta) < 0, \text{ and } E^{\text{DSI-N}}(\theta) < 0, \\ & |E^{\text{FUD-N}}(\theta)| > |E^{\text{DSI-N}}(\theta)|. \\ & dE^{\text{FUD-N}}(\theta)/d\theta > 0, \text{ and } dE^{\text{DSI-N}}(\theta)/d\theta > 0, \\ & dE^{\text{FUD-N}}(\theta)/d\theta > dE^{\text{DSI-N}}(\theta)/d\theta. \end{aligned}$$

As the results, as shown by Figure 5-2c, the NBO vertical delocalization energy is always stabilizing (Table 5-2) and has the following features:

$$\begin{aligned} & \Delta E^{\text{V-NBO}}(\theta) < 0 \\ & d[\Delta E^{\text{V-NBO}}(\theta)]/d\theta > 0 \end{aligned}$$

$\Delta E^{\text{V-NBO}}(\theta)$ becomes less stabilizing as twist angle θ increases. In particular, the effect of the theory levels on the value of $\Delta E^{\text{V-NBO}}(\theta)$ is slight and is much smaller than on the value of $\Delta E^{\text{V-LFMO}}(\theta)$. For the $\theta = 0^\circ$ geometry of N-benzylideneaniline at 6-31G* level, for example, the pair of the LFMO (the first data) and NBO (second data)

LMO $\Psi_i^{\text{P-}\pi}$	Fragment A	na	B	$na+nb = nk$	C	N	LMO $\Psi_j^{\text{Q-}\pi}$
$\Psi_{ai} = \sum_{u=1}^{na} a_{ui}^\pi \phi_u$	1 A	$F_{Ai,Aj} = \sum_{u=1}^{na} \sum_{r=1}^{na} a_{ui}^\pi f_{ur} a_{rj}^\pi$	4	$F_{Ai,Bj} = \sum_{u=1}^{na} \sum_{s=n+1}^{nk} a_{ui}^\pi f_{us} b_{sj}^\pi$	5	$F_{Ai,Cj} = \sum_{u=1}^{na} \sum_{t=nk+1}^N a_{ui}^\pi f_{ut} c_{tj}^\pi$	1 A
	na B	$F_{Bi,Aj} = \sum_{v=n+1}^{nk} \sum_{r=1}^{na} b_{vi}^\pi f_{vr} a_{rj}^\pi$	2	$F_{Bi,Bj} = \sum_{v=n+1}^{nk} \sum_{s=n+1}^{nk} b_{vi}^\pi f_{vs} b_{sj}^\pi$	7	$F_{Bi,Cj} = \sum_{v=n+1}^{nk} \sum_{t=nk+1}^N b_{vi}^\pi f_{vt} c_{tj}^\pi$	B
	nk C	$F_{Ci,Aj} = \sum_{w=nk+1}^N \sum_{r=1}^{na} c_{wi}^\pi f_{wr} a_{rj}^\pi$	9	$F_{Ci,Bj} = \sum_{w=nk+1}^N \sum_{s=n+1}^{nk} c_{wi}^\pi f_{ws} b_{sj}^\pi$	3	$F_{Ci,Cj} = \sum_{w=nk+1}^N \sum_{t=nk+1}^N c_{wi}^\pi f_{wt} c_{tj}^\pi$	C
$\Psi_{bj} = \sum_{r=1}^{na} a_{rj}^\pi \phi_r$	na						
	nb						
	N						

(a)

(b)

(c)

Figure 5-3. For the LMO Fock matrix (or Hamiltonian matrix), a π -element $F_{ij}^{\pi\text{-LMO}}$ is expanded into 9 sum terms $F_{Pi,Qj}$ in the case of A-B-C fragmentation.

values (kcal/mol) of the vertical delocalization energy are as follows:

9.7 and -51.0 (B3LYP), 4.1 and -53.0 (SLATER), 39.1 and -49.4 (RHF), 77.3 and -52.5 (MP2)

According to the values of NBO vertical delocalization energy, π -electron delocalization is always stabilization and is resistance to molecular distortion. These conclusions are exactly opposite to the conclusions from the calculations of the LFMO vertical delocalization energy, but they are fully in line with the fundamental principles of organic chemistry. Therefore, it is necessary to prove that the LFMO vertical delocalization energy is reasonable and our calculation programs are reliable from the following four aspects:

- (i) Localization degree of LMO basis set.
- (ii) Localization degree affects the calculation results that determine the conclusions about nature of the delocalization.
- (iii) Comparison between the AO and the LMO vertical delocalization energies.
- (iv) An important role of Hartree-Exchange in determining the value of vertical delocalization energy.

5.1.3. Localization Degree of LMO Basis Set.

In the case of A-B-C fragmentation (Figure 5-2a), the elements of LMO Fock and overlap integral matrices, denoted as F_{ij}^{LMO} (and S_{ij}^{LMO}), between a pair of LMOs Ψ_i and Ψ_j can be expanded into nine sum terms according to Equations (5-1) and (5-2) (Figure 5-3).

$$F_{ij}^{\text{LMO}} = \sum_{\lambda=1}^n \sum_{\rho=1}^n a_{\lambda i} f_{\lambda \rho} a_{\rho j} = \sum_P^A \sum_Q^B F_{Pi,Qj} \quad (5-1)$$

$$S_{ij}^{LMO} = \sum_{\lambda=1}^n \sum_{\rho=1}^n a_{\lambda i} s_{\lambda \rho} a_{\rho j} = \sum_P^{A,B,C} \sum_Q^{A,B,C} S_{Pi,Qj} \quad (5-2)$$

Table 5-3. For the $\theta = 0^\circ$ Geometry of N-benzylideneaniline, Values of Nine Sum Terms (Pi, Qj) = $F_{Pi,Qj}$ ($P, Q = A, B, C$) in Each of Five Typical π -Elements $F_{ij}^{\pi-LFMO}$ of the LFMO Hamiltonian Matrix, and Values of Nine Sum Terms, $S_{Pi,Qj}$ in Each of the Corresponding Elements $S_{ij}^{\pi-LFMO}$ of the LFMO Overlap Integral Matrix (at MP2/6-31G* Level).

$F_{Pi,Qj}$ $S_{Pi,Qj}$	Ki	Lj	Ai,Aj	Ai,Bj	Ai,Cj	Bi,Aj	Bi,Bj	Bi,Cj	Ci,Aj	Ci,Bj	Ci,Cj	$F_{ij}^{\pi-LFMO}$ $S_{ij}^{\pi-LFMO}$
$F_{Ki,Lj}$	A17	A17	-18.43746	0.00000	0.00000	0.00000	0.00000	0.00000	0.00000	0.00000	0.00000	-18.43746
$S_{Ki,Lj}$	A17	A17	1.00000	0.00000	0.00000	0.00000	0.00000	0.00000	0.00000	0.00000	0.00000	1.00000
$F_{Ki,Lj}$	B26	B26	0.00000	0.00000	0.00000	0.00000	-20.77096	0.00000	0.00000	0.00000	0.00000	-20.77096
$S_{Ki,Lj}$	B26	B26	0.00000	0.00000	0.00000	0.00000	1.00000	0.00000	0.00000	0.00000	0.00000	1.00000
$F_{Ki,Lj}$	C46	C46	0.00000	0.00000	0.00000	0.00000	0.00000	0.00000	0.00000	0.00000	-18.36634	-18.36634
$S_{Ki,Lj}$	C46	C46	0.00000	0.00000	0.00000	0.00000	0.00000	0.00000	0.00000	0.00000	1.00000	1.00000
$F_{Ki,Lj}$	A17	B26	0.00000	-1.82824	0.00000	0.00000	0.00000	0.00000	0.00000	0.00000	0.00000	-1.82824
$S_{Ki,Lj}$	A17	B26	0.00000	0.09218	0.00000	0.00000	0.00000	0.00000	0.00000	0.00000	0.00000	0.09218
$F_{Ki,Lj}$	B26	C46	0.00000	0.00000	0.00000	0.00000	0.00000	-1.47260	0.00000	0.00000	0.00000	-1.47260
$S_{Ki,Lj}$	B26	C46	0.00000	0.00000	0.00000	0.00000	0.00000	0.07590	0.00000	0.00000	0.00000	0.07590

Table 5-4. For the $\theta = 0^\circ$ Geometry of N-benzylideneaniline, Values of Nine Sum Terms $F_{Pi,Qj}$ ($P, Q = A, B, C$) in Each of Five Typical Elements $F_{ij}^{\pi-NBO}$ of the NBO Hamiltonian Matrix, and Values of Nine Sum Terms, $S_{Pi,Qj}$, in Each of the Corresponding Elements $S_{ij}^{\pi-NBO}$ of the NBO Overlap Integral Matrix (at MP2/6-31G* Level).

$F_{Pi,Qj}$ $S_{Pi,Qj}$	Ki	Lj	Ai,Aj^*	Ai,Bj	Ai,Cj	Bi,Aj	Bi,Bj	Bi,Cj	Ci,Aj	Ci,Bj	Ci,Cj	$F_{ij}^{\pi-NBO}$ $S_{ij}^{\pi-NBO}$
$F_{Ki,Lj}$	A3	A3	-19.80295	0.33882	0.00004	0.33882	-0.18332	-0.00004	0.00004	-0.00004	-0.00007	-19.30871
$S_{Ki,Lj}$	A3	A3	1.02554	-0.01714	0.00000	-0.01714	0.00873	0.00000	0.00000	0.00000	0.00000	1.00000
$F_{Ki,Lj}$	B17	B17	-0.22850	0.46116	-0.00075	0.46116	-21.67567	0.33138	-0.00075	0.33138	-0.16826	-20.48885
$S_{Ki,Lj}$	B17	B17	0.01133	-0.02331	0.00004	-0.02331	1.06109	-0.01715	0.00004	-0.01715	0.00843	1.00000
$F_{Ki,Lj}$	C22	C22	-0.00027	0.00016	-0.00007	0.00016	-0.18160	0.38528	-0.00007	0.38528	-19.74415	-19.15530
$S_{Ki,Lj}$	C22	C22	0.00001	-0.00001	0.00000	-0.00001	0.00915	-0.02009	0.00000	-0.02009	1.03103	1.00000
$F_{Ki,Lj}$	A3	B17	1.68196	-3.20855	0.00477	-0.04764	1.69520	-0.00758	-0.00001	-0.00106	0.00226	0.11935
$S_{Ki,Lj}$	A3	B17	-0.08422	0.16323	-0.00025	0.00239	-0.08148	0.00039	0.00000	0.00004	-0.00011	0.00000
$F_{Ki,Lj}$	B17	C22	0.00655	-0.01125	0.00534	-0.01084	1.35932	-2.66337	0.00001	-0.04652	1.44076	0.07999
$S_{Ki,Lj}$	B7	C2	-0.00032	0.00060	-0.00028	0.00053	-0.06874	0.13861	0.00000	0.00241	-0.07282	0.00000

AO coefficient matrix t^{LFMO} of
LFMO basis set

	$\Psi_i \in A$	$\Psi_i \in B$	$\Psi_i \in C$
A	t^π_A	0	0
B	0	t^π_B	0
C	0	0	t^π_C

AO coefficient matrix t^{NBO} of
NBO basis set

	$\Psi_i \in A$	$\Psi_i \in B$	$\Psi_i \in C$
A	t^π_A	$t^\pi_A \neq 0$	$t^\pi_A \neq 0$
B	$t^\pi_B \neq 0$	t^π_B	$t^\pi_B \neq 0$
C	$t^\pi_C \neq 0$	$t^\pi_C \neq 0$	t^π_C

Scheme 5-1

Scheme 5-2

When a π LMO $\Psi_i \in$ fragment K, and a π LMO $\Psi_j \in$ fragment L,

$$F_{Ki,Lj} = \sum_{\lambda \in K}^{\text{all } \lambda} \sum_{\rho \in L}^{\text{all } \rho} a_{\lambda i} f_{\lambda \rho} a_{\rho j} \quad (5-3)$$

$$S_{Ki,Lj} = \sum_{\lambda \in K}^{\text{all } \lambda} \sum_{\rho \in L}^{\text{all } \rho} a_{\lambda i} s_{\lambda \rho} a_{\rho j} \quad (5-4)$$

In Equations (5-3) and (5-4), K and L are two particular fragments. In this case, a sum term $F_{Ki,Lj}$ (and $S_{Ki,Lj}$) is called the particular sum term of a π LMO Fock matrix element, $F_{ij}^{\pi\text{-LMO}}$ (and $S_{ij}^{\pi\text{-LMO}}$), between a pair of π -LMOs Ψ_i and Ψ_j . In the practical calculation, the Fock matrix \mathbf{F} is replaced by the one-electron matrix \mathbf{H} in order to simplify the discussion and calculation.

For LFMO basis set, owing to the localization characteristics of the AO coefficient matrix (Scheme 5-1), all the sum terms of a π -element $F_{ij}^{\pi\text{-LFMO}}$ are equal to zero except for its particular sum term $F_{Ki,Lj}$. Certainly, as shown by the data listed in Table 5-3, we have:

$$F_{ij}^{\pi\text{-LFMO}} = F_{Ki,Lj}, \quad F_{Ki,Lj}/F_{ij}^{\pi\text{-LFMO}} = 1; \quad S_{ij}^{\pi\text{-LFMO}} = S_{Ki,Lj}, \quad S_{Ki,Lj}/S_{ij}^{\pi\text{-LFMO}} = 1,$$

where $F_{ij}^{\pi\text{-LFMO}}$ is a π -element of LFMO Hamiltonian (one-electron) matrix. For example, $F_{17,26}^{\pi\text{-LFMO}}$ is a LFMO Hamiltonian matrix element between two π -LFMOs $\Psi_{17}^{A-\pi}$ and $\Psi_{26}^{B-\pi}$, where $\Psi_{17}^{A-\pi}$ is the 17-th LFMO and is absolutely localized in the fragment A; $\Psi_{26}^{B-\pi}$ is the 26-th LFMO and is absolutely localized in the fragment B. In this case, $F_{A17,B26}$ is a particular sum term of the π -element $F_{17,26}^{\pi\text{-LFMO}}$. According to the data listed in the "Ai,Bj" and " $F_{ij}^{\pi\text{-LFMO}}$ " columns of Table 5-3,

$$F_{17,26}^{\pi\text{-LFMO}} = -1.82824, \quad F_{A17,B26} = -1.82824, \quad F_{17,26}^{\pi\text{-LFMO}} = F_{A17,B26}$$

$$S_{17,26}^{\pi\text{-LFMO}} = 0.09218, \quad S_{A17,B26} = 0.09218, \quad S_{17,26}^{\pi\text{-LFMO}} = S_{A17,B26}$$

On the contrary, due to that the LC-AO NBOs are not absolutely localized on their respective fragments (Table 3-1 and Scheme 5-2), as shown by the data listed in Table 5-4, the sum terms $F_{Pi,Qj}$ in a NBO π Hamiltonian matrix

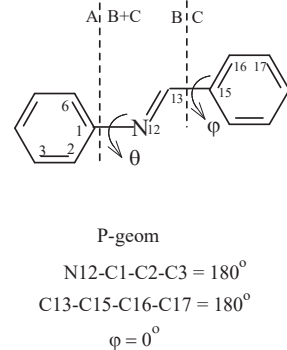


Table 5-5. For Total Electronic Energy $E_e(\theta)$ of the Twisted Geometries of NBA (A-B-C Fragmentation) at RHF/6-31G* Level, the total π Component $E_e^\pi(\theta)$ and the Particular π Component, $E_e^{\pi-KL}(\theta)$, the Difference $E_e^{\pi-KL}(\theta) - E_e^\pi(\theta)$, and the Ratio $E_e^\pi(\theta)/E_e^{\pi-KL}(\theta)$ (Energy Unit in hartree).

θ°	LMO	$E_e^\pi(\theta)$	$E_e^{\pi-KL}(\theta)$	$E_e^{\pi-KL} - E_e^\pi$	$E_e^\pi/E_e^{\pi-KL}$
0	NBO	-130.99258	-136.67374	-5.68116	0.95843
0	NBO-II	-130.99258	-130.99258	0.00000	1.00000
0	LFMO	-130.99258	-130.99258	0.00000	1.00000
17	NBO	-131.08423	-136.77918	-5.69495	0.95837
17	NBO-II	-131.10755	-131.11091	-0.00336	0.99997
17	LFMO	-131.10282	-131.10282	0.00000	1.00000
32	NBO	-131.27425	-137.36171	-6.08746	0.95566
32	NBO-II	-131.32027	-131.33615	-0.01589	0.99988
32	LFMO	-131.35751	-131.35751	0.00000	1.00000
42	NBO	-131.36592	-137.25045	-5.88453	0.95713
42	NBO-II	-131.63830	-132.52905	-0.89075	0.99328
42	LFMO	-131.58103	-131.58103	0.00000	1.00000

element $F_{ij}^{\pi\text{-NBO}}$ are all not equal to zero, so we can find:

$$F_{ij}^{\pi\text{-NBO}} \neq F_{Ki,Lj}.$$

For example, Ψ_3 and Ψ_{17} are two π -NBOs, and they belong, respectively, to fragment A and fragment B, as shown by the data listed in Table 5-4,

$$F_{3,17}^{\pi\text{-NBO}} = 0.11935, F_{A3,B17} = -3.20855, |F_{A3,B17}/F_{3,17}^{\pi\text{-NBO}}| = 26.9.$$

According to Table 5-3 and Table 5-4, the following ratio can be defined as the localization degree of individual LMO:

$$R_{ind} = F_{Ki,Lj} / F_{ij}^{\pi\text{-LMO}}$$

However, R_{ind} can't be used to measure the localization degree of an entire LMO basis set for a molecule such as N-benzylideneaniline, because there are 56 π LMOs at 6-31G* level. Two physical quantities, defined by Equations (5-5) and (5-6), seem to be two possible criteria for the localization degree.

$$R_L(\theta) = E_e^\pi(\theta) / E_e^{\pi-KL}(\theta) \quad (5-5)$$

$$\Delta E_e^{\pi-KL}(\theta) = E_e^{\pi-KL}(\theta) - E_e^\pi(\theta) \quad (5-6)$$

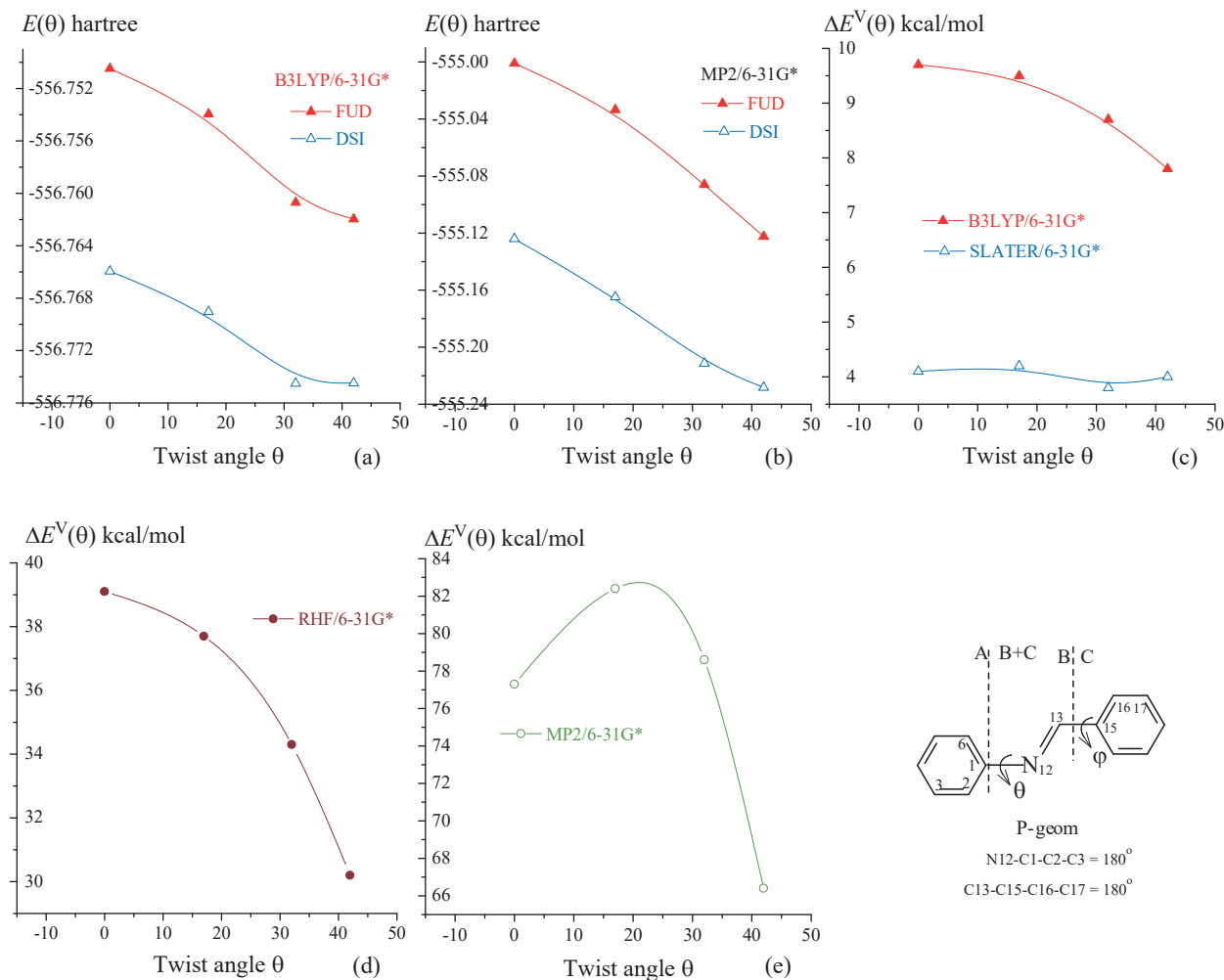


Figure 5-4. For the N-benzylideneaniline: (a) and (b) Molecular energies (hartree) of the FUD- and DSI -NBO-II states. (c) to (e) The NBO-II vertical delocalization energies (kcal/mol).

$$E_e^\pi(\theta) = \sum_i^{all\ \pi} \sum_j^{all\ \pi} [(F_{ij}^{\pi-LMO} + H_{ij}^{\pi-LMO}) D_{ij}^{\pi-LMO}] \quad (5-7)$$

$$E_e^{\pi-KL}(\theta) = \sum_i^{all\ \pi} \sum_j^{all\ \pi} [(F_{Ki,Lj} + H_{Ki,Lj}) D_{ij}^{\pi-LMO}] \quad (5-8)$$

In the equations, $H_{ij}^{\pi-LMO}$, $F_{ij}^{\pi-LMO}$ and D_{ij}^{π} are the LMO one-electron, Fock and density matrix elements, respectively. When LMO = LFMO, as shown by the data in Table 5-5, the ratio $R_L(\theta)$ is always equal to 1.0, and the energy difference, $\Delta E_e^{\pi-KL}(\theta)$, is always equal to zero. When LCM = NBO, always $R_L < 1.0$, and the energy difference $|\Delta E_e^{\pi-KL}(\theta)| > 5$ hartree. Interestingly, the localization degree $R_L(\theta)$ of the NBO-II basis set is very close to that of the LFMO basis set. At RHF/6-31G* level, for example, the values of $R_L(0^\circ)$ and $\Delta E_e^{\pi-KL}(0^\circ)$ (hartree) are as follows:

1.0 and 0.0 (LFMO), 1.0 and 0.0 (NBO-II), 0.95843 and -5.68116 (NBO).

Table 5-6. For Each of Four Twisted Geometries of N-benzylideneaniline, Molecular Energies (hartree), $E^{\text{FUD-NII}}(\theta)$ and $E^{\text{DSI-NII}}(\theta)$, of the FUD- and DSI-NBOII States (DSI-3), and the NBO-II Vertical Delocalization Energy (VRE) (kcal/mol) (at 6-31G* Level).

		0	17	32	42
B3LYP	$E^{\text{FUD-NII}}(\theta)$	-556.75048	-556.75395	-556.76070	-556.76197
	$E^{\text{DSI-NII}}(\theta)$	-556.76594	-556.76903	-556.77451	-556.77448
	VRE	9.7	9.5	8.7	7.8
SLATER	$E^{\text{FUD-NII}}(\theta)$	-545.52042	-545.52295	-545.52832	-545.52772
	$E^{\text{DSI-NII}}(\theta)$	-545.52693	-545.52962	-545.53442	-545.53417
	VRE	4.1	4.2	3.8	4.0
RHF	$E^{\text{FUD-NII}}(\theta)$	-553.13415	-553.14235	-553.15715	-553.15255
	$E^{\text{DSI-NII}}(\theta)$	-553.19648	-553.20246	-553.21184	-553.20065
	VRE	39.1	37.7	34.3	30.2
MP2	$E^{\text{FUD-NII}}(\theta)$	-555.00093	-555.03350	-555.08606	-555.12241
	$E^{\text{DSI-NII}}(\theta)$	-555.12405	-555.16479	-555.21133	-555.22831
	VRE	77.3	82.4	78.6	66.4

In a planar geometry, the localization degrees of the NBO-II and LFMO basis sets are the same. The localization degree of the NBO-II basis set, as well as the separation degree of π and σ NBO-IIs, decreases as the twist angle θ increases, but it is still close to that of the LFMO basis set. For the $\theta = 42^\circ$ geometry, for example, the values of $R_L(42^\circ)$ and $\Delta E_e^{\pi-\text{KL}}(42^\circ)$ (hartree) become as follows:

1.0 and 0.0 (LFMO), 0.99328 and -0.89075 (NBO-II), 0.95713 and -5.88453 (NBO).

Correspondingly, as shown by comparison of Figure 5-4 with Figure 4-6 and Figure 4-7, the FUD-NBO-II and DSI-NBO-II states are similar to the FUD-LFMO and DSI-LFMO states, respectively, in terms of the characteristics of the molecular energy. It is also similar to the LFMO vertical delocalization energy that the NBO-II vertical delocalization energy is always destabilizing and is a driving force of the molecular distortion. For the $\theta = 0^\circ$ geometry of N-benzylideneaniline at 6-31G* level, for example, the following LFMO (Table 4-2) and NBO-II (Table 5-6) vertical delocalization energies (kcal/mol) are the same:

9.7 and 9.7 (B3LYP), 4.1 and 4.1 (SLATER), 39.1 and 39.1 (RHF), 77.3 and 77.3 (MP2).

As the twist angle θ increases, the localization degree of NBO-II basis set slightly decreases. The practical calculations show that, when the twist angle θ of N-benzylideneaniline is larger than 40° , the π NBO-IIs are no longer absolutely localized on their respective fragments and meanwhile the coefficient of the s AOs are also not equal to zero. For the $\theta = 32^\circ$ conformation of N-benzylideneaniline at RHF/6-31G* level, for example, the 24-th

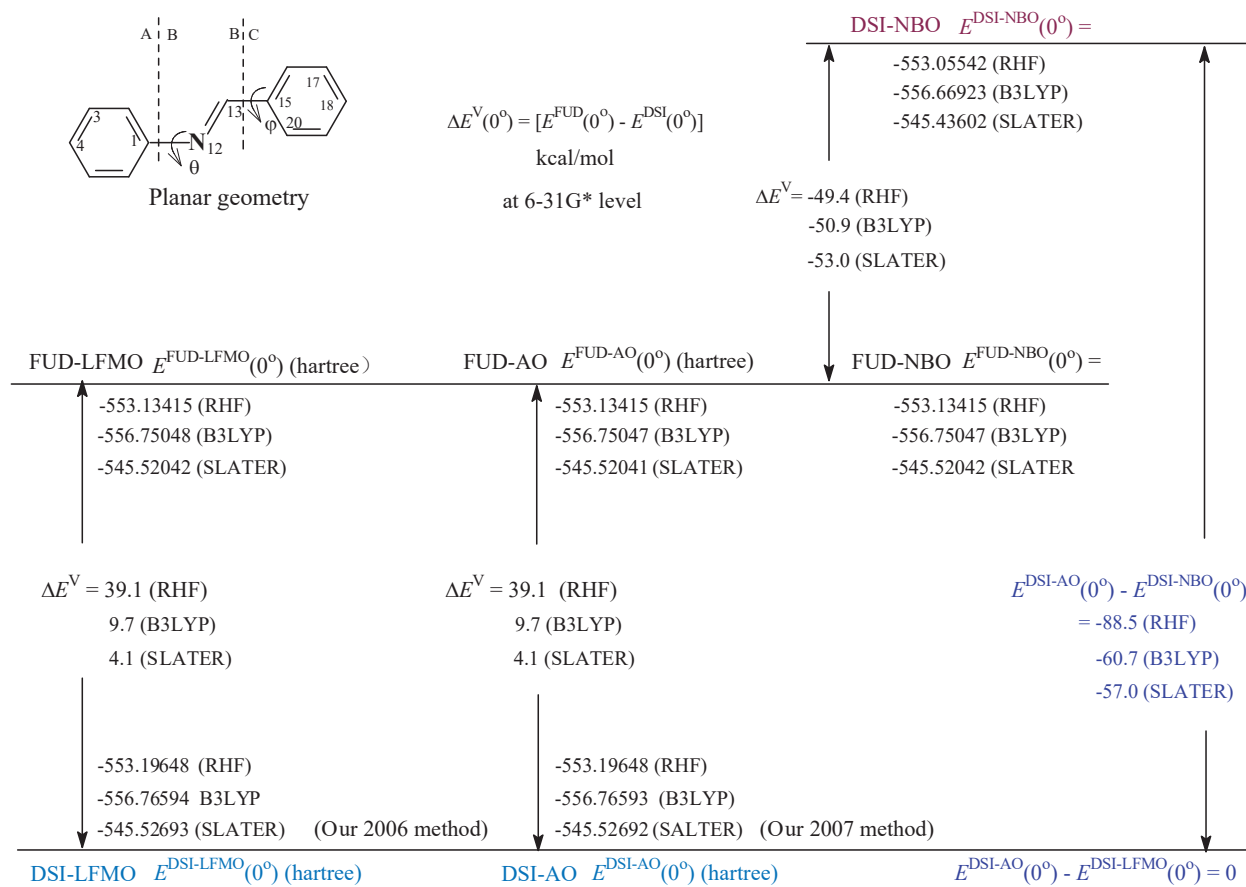


Figure 5-5. For planar geometry of N-benzylideneaniline, the molecular energies (hartree) of the FUD and DSI states, and the vertical delocalization energy (kcal/mol), which are calculated at 6-31G* level using our 2006 method and our 2007 method.

NBO-II is a π NBO belonging to fragment C, the py AO coefficient of the C(13) atom belonging to fragment B is -0.00032, and the s AO coefficient of the 20-th carbon atom belonging to fragment C is -0.00032. As a result, when $\theta = 32^\circ$, the LFMO and NBO-II vertical delocalization energies for NBA become slightly different according to the following values (kcal/mol): 3.5 and 3.8 (SLATER), 33.6 and 34.3 (RHF), 82.6 and 78.6 (MP2).

The stabilizing feature of the NBO vertical delocalization energy may be ascribed to its low degree of localization.

5.2. π -DELOCALIZATION INDEED DESTABILIZATION

The difference in the localization degree merely indicates that the LFMO and NBO are two different types of LMO basis sets, but it cannot be concluded that the LFMO vertical delocalization energy must be more reasonable than the NBO-VRE. In addition, a LFMO basis set is constructed by a complex procedure. In order to confirm that π -delocalization is indeed destabilization, first of all, it is necessary to establish a recognized and reliable method that can be used to prove the reasonability of the LFMO vertical delocalization energy, and meanwhile to confirm the reliability of our calculation program. Then according to that our 2006 method cannot eliminate the Hartree-Fock exchange, our method of 2011 is used in advance to confirm the destabilization of π -electron delocalization.

Table 5-7. For the $\theta = 0^\circ$ Geometry of N-benzylideneaniline, the Values (hartree) of the Nine Sum Terms $F_{ij}^{\text{DSI}_{P_iQ_j}}$ ($P, Q = A, B, C$) for Each of Five Typical Elements $F_{ij}^{\text{DSI-}\pi}$ of the LFMO Hamiltonian Matrix (at RHF/6-31G* Level).

i (P)	j (Q)	Ai, Aj^*	Ai, Bj	Ai, Cj	Bi, Aj	Bi, Bj	Bi, Cj	Ci, Aj	Ci, Bj	Ci, Cj	$F_{ij}^{\text{DSI-}\pi}$
17(A)	17(A)	-18.43746	0.00000	0.00000	0.00000	0.00000	0.00000	0.00000	0.00000	0.00000	-18.43746
26(B)	26(B)	0.00000	0.00000	0.00000	0.00000	-20.77096	0.00000	0.00000	0.00000	0.00000	-20.77096
46(C)	46(C)	0.00000	0.00000	0.00000	0.00000	0.00000	0.00000	0.00000	0.00000	-18.36634	-18.36634
17(A)	26(B)	0.00000	0.00000	0.00000	0.00000	0.00000	0.00000	0.00000	0.00000	0.00000	0.00000
26(B)	46(C)	0.00000	0.00000	0.00000	0.00000	0.00000	0.00000	0.00000	0.00000	0.00000	0.00000

* Ai, Aj : $F_{ij}^{\text{DSI}_{Ai,Aj}}$; 17(A) means that Ψ_{17} belongs to fragment A.

Table 5-8. For the $\theta = 0^\circ$ Geometry of N-benzylideneaniline, Values (Hartree) of the Nine Sum Terms $F_{ij}^{\text{DSI}_{P_iQ_j}}$ ($P, Q = A, B, C$) for Each of Five Typical Elements $F_{ij}^{\text{DSI-}\pi}$ of the NBO Hamiltonian Matrix (at RHF/6-31G* Level).

i (P)	j (Q)	Ai, Aj^*	Ai, Bj	Ai, Cj	Bi, Aj	Bi, Bj	Bi, Cj	Ci, Aj	Ci, Bj	Ci, Cj	$F_{ij}^{\text{DSI-}\pi}$
3(A)	3(A)	-19.80295	0.00000	0.00000	0.00000	-0.18332	0.00000	0.00000	0.00000	-0.00007	-19.98634
17(B)	17(B)	-0.22850	0.00000	0.00000	0.00000	-21.67567	0.00000	0.00000	0.00000	-0.16826	-22.07243
22(C)	22(C)	-0.00027	0.00000	0.00000	0.00000	-0.18160	0.00000	0.00000	0.00000	-19.74415	-19.92602
3(A)	17(B)	1.68196	0.00000	0.00000	0.00000	1.69520	0.00000	0.00000	0.00000	0.00226	3.37942
17(B)	22(C)	0.00655	0.00000	0.00000	0.00000	1.35932	0.00000	0.00000	0.00000	1.44076	2.80663

5.2.1. Basic Flaws of NBO

In fact, instead of discussing the rationality of our calculation method, it is better to discuss the basic flaws of the NBO method first. This discussion will be carried out using several of the following methods recognized in the literature.

5.2.1.1. Eliminating AO Matrix Element Method

In order to achieve the above purposes, a most simple way is to perform the conditional single-point energy calculation over the AO basis set, which is the so-called method for eliminating AO matrix element (EAME). The use of EAME method can be traced back Hückel era. In that era, as summarized by Kollma,³ the EAME method was used to calculate the resonance energy at the level of Huckel theory. Since 1979, the EAME method has been used to calculate the vertical delocalization energy within semi-empirical and non-empirical SCF-MO theory.^{3, 4} In addition, as discussed in Chapter 3, the EAME method (the WSW method) was used to construct a LMO basis set.⁵ In the later chapters, will continue to confirm the rationality and reliability of the EAME method.

For a $\theta = 0^\circ$ conformation of the N-benzylideneaniline, all of the atoms are coplanar. Therefore, the DSI and FUD state, denoted as DSI-AO and FUD-AO, can be constructed by the conditional single-point energy calculation based on the AO basis set (our 2007 method). In this case, the FUD-AO state is the ground state of the $\theta = 0^\circ$ conformation (the ground state of conformation is different from the ground state of molecule). In order to construct

the DSI-AO state, the single-point energy calculation is performed under the following conditional settings.

When π AO $\phi_\lambda \in$ Fragment P, and π AO $\phi_\rho \in$ Fragment Q, and $P \neq Q$

Setting AO Fock matrix elements $f_{\lambda,\rho} = 0$

Setting overlap integral matrix elements $s_{\lambda,\rho} = 0$

The AO Fock matrix whose elements have been deleted according to the above conditions is called the particular AO Fock matrix for the DSI state, and it is denoted as \mathbf{f}^{DSI} . For the DSI-AO state, as shown by the practical calculations, all the π MOs are absolutely localized on their respective fragments, and the σ MOs are delocalized on the entire molecular framework. For the $\theta = 0^\circ$ geometry of N-benzylideneaniline, for example, the RHF/6-31G* values are as follows (Figure 5-5):

$$E^{\text{FUD-AO}}(0^\circ) = E^{\text{FUD-LFMO}}(0^\circ) = E^{\text{FUD-NBO}}(0^\circ) = -553.13415 \text{ hartree}$$

$$[E^{\text{DSI-AO}}(0^\circ) - E^{\text{DSI-LFMO}}(0^\circ)] = 0.0 \text{ kcal/mol}$$

$$[E^{\text{DSI-AO}}(0^\circ) - E^{\text{DSI-NBO}}(0^\circ)] = -88.5 \text{ kcal/mol}$$

Correspondingly, as indicated by the data presented in Figure 5-5, the AO vertical delocalization energy $\Delta E^{\text{V-AO}}(0^\circ)$ is exactly equal to the LFMO vertical delocalization energy $\Delta E^{\text{V-LFMO}}(0^\circ)$, and it is not equal to the NBO vertical delocalization energy $\Delta E^{\text{V-NBO}}(0^\circ)$. At B3LYP/6-31G* level, for example, the values (kcal/mol) of vertical delocalization energy are as follows:

$$\Delta E^{\text{V-AO}}(0^\circ) = 9.7, \Delta E^{\text{V-LFMO}}(0^\circ) = 9.7, \Delta E^{\text{V-NBO}}(0^\circ) = -50.9$$

$$\Delta E^{\text{V-AO}}(0^\circ) = \Delta E^{\text{V-LFMO}}(0^\circ)$$

$$\Delta E^{\text{V-AO}}(0^\circ) \neq \Delta E^{\text{V-NBO}}(0^\circ)$$

Thus, it is confirmed that the LFMO vertical delocalization energy is reasonable, and it is also proved that the entire procedure for constructing the LFMO basis set is reliable.

5.2.1.2. Transformation of Particular AO Fock Matrix

Transforming particular AO Fock matrix \mathbf{f}^{DSI} into the LFMO Fock matrix should also be a method to confirm the rationality of LMO basis set. When the full AO Fock matrix \mathbf{f} in Equation (5-1) is replaced with the particular AO Fock matrix \mathbf{f}^{DSI} , the LMO Fock matrix \mathbf{F}^{DSI} can be obtained, and its π matrix element is denoted as $F_{ij}^{\text{DSI}-\pi}$ and can also be expanded into 9 sum terms $F^{\text{DSI}}_{P_i, Q_j}$. When a π LMO $\Psi_i \in$ fragment K, and a π LMO $\Psi_j \in$ fragment L, the particular sum term $F^{\text{DSI}}_{K_i, L_j}$ of a specific π -element $F_{ij}^{\pi-\text{DSI}}$ can be calculated by using Equation (5-9):

$$F_{K_i, L_j}^{\text{DSI}} = \sum_{\lambda \in K}^n \sum_{\rho \in L}^n a_{\lambda, i} f_{\lambda, \rho}^{\text{DSI}-\pi} a_{\rho, j} \quad (5-9)$$

Based on the features of the AO coefficient Matrix for LFMO basis set (Scheme 5-1) and according to Equation (5-9), the particular sum term $F^{\text{DSI}}_{K_i, L_j} = 0$ when π LFMO $\Psi_i \in$ P, π LFMO $\Psi_j \in$ Q, and $P \neq Q$, due to that the inter-fragment elements $f^{\text{DSI}-\pi}_{\lambda, \rho}$ in Equation (5-9) have been set equal to zero. Other 8 sum terms are also equal to zero (Table 5-7) due to the features of the AO coefficient matrix (Scheme 5-1). As the result, every inter-fragment element $F_{ij}^{\text{DSI}-\pi}$ is equal to zero (Table 5-7). For example, $F_{17, 28}^{\text{DSI}-\pi}$ is a Fock matrix element between a specific pair of LFMOs $\Psi_{17}^{\text{A}-\pi}$ and $\Psi_{28}^{\text{B}-\pi}$, and $\Psi_{17}^{\text{A}-\pi} \in$ fragment A, $\Psi_{28}^{\text{B}-\pi} \in$ fragment B. In this case, as shown by Table 5-7,

nine sum terms $F^{\text{DSI}}_{P17,Q28} = 0$, due to the followings:

- (i) $f_{\lambda\rho}^{\text{DSI}}$ are set equal to 0, when π AO $\phi_\lambda \in$ fragment P, π AO $\phi_\rho \in$ fragment Q, $P \neq Q$, leading to that particular sum term is equal to zero.
- (ii) $a_{\lambda,17} = 0$ (π AO $\phi_\lambda \notin$ fragment A), and $a_{\rho,26} = 0$ (π AO $\phi_\rho \notin$ fragment B), although $f_{\lambda\rho} \neq 0$ when AO ϕ_λ and AO $\phi_\rho \in$ the same fragment P, leading to that other eight sum terms are equal to zero.

For the intra-molecular elements $F_{ij}^{\text{DSI}-\pi}$ ($\Psi_i \in P$, $\Psi_j \in Q$, and $P = Q$), such as $F_{17,17}^{\text{DSI}-\pi}$ in Table 5-7,

$$\begin{aligned} F^{\text{DSI}}_{A17,A17} &= F_{17,17}^{\text{DSI}-\pi} = -18.43746 \text{ hartree} \\ F_{17,17}^{\pi\text{-LFMO}} &= F_{A17,A17} = -18.43746 \text{ hartree} \quad (\text{Tale 5-3}) \end{aligned}$$

and all other sum terms are equal to zero, owing to the matrix element characteristics shown by Scheme 5-1. In the case of planar conformation, when LMO = LFMO, deleting the inter-fragment elements, $f_{\lambda\rho}^{\text{DSI}-\pi}$, of AO Fock matrix is equivalent to deleting the inter-fragment elements $F_{ij}^{\pi\text{-LFMO}}$ of LFMO Fock matrix.

When LMO = NBO, as shown by the data listed in Table 5-8, deleting the inter-fragment elements $f_{\lambda\rho}^{\text{DSI}-\pi}$ can only ensure that the six sum terms $F^{\text{DSI}}_{P_i,Q_j}$ ($P \neq Q$) = 0.0. Other 3 sum terms $F^{\text{DSI}}_{P_i,P_j} \neq 0$ due to that, in Equation 5-9, $a_{\lambda i} \neq 0$, $a_{\rho j} \neq 0$, and $f_{\lambda\rho} \neq 0$ ($\lambda \in P$, $\rho \in Q$, $P = Q$). For the NBO matrix, therefore, the inter-fragment π -elements $F_{ij}^{\text{DSI}-\pi}$ are not equal to zero. In a specific π -element $F_{3,17}^{\text{DSI}-\pi}$, for example, 6 sum terms $F^{\text{DSI}}_{P_3,Q_17}$ ($P \neq Q$) are equal to zero, but other three sum terms $F^{\text{DSI}}_{P_3,P_{17}} \neq 0.0$ ($P = A, B, C$). The values of three pairs of sum terms $F^{\text{DSI}}_{P_3,P_{17}}$ (Table 5-8) and $F_{P_3,P_{17}}$ (Table 5-4) are as follows:

$$\begin{aligned} F^{\text{DSI}}_{A3,A17} &= 1.68196, F_{A3,A17} = 1.68196 \\ F^{\text{DSI}}_{B3,B17} &= 1.69520, F_{B3,B17} = 1.69520 \\ F^{\text{DSI}}_{C3,C17} &= 0.00226, F_{C3,C17} = 0.00226 \end{aligned}$$

As a result, $F_{3,17}^{\text{DSI}-\pi} \neq 0$, and its value (3.37942 hartree) is a sum of its three sum terms $F^{\text{DSI}}_{P_3,P_{17}}$. Therefore, setting the inter-fragment AO elements $f_{\lambda\rho}^{\text{DSI}-\pi} = 0$ does not ensure that the inter-fragment NBO Fock elements are equal to zero. According to Table 5-8, as a result of setting inter-fragment NBO elements $F_{ij}^{\pi\text{-NBO}} = 0.0$, not only the inter-fragment interaction is set equal to zero, but also the intra-fragment interactions are partially set equal to zero. Similarly, as shown by the values of elements $F_{3,17}^{\text{NBO}-\pi}$ and its 9 sum terms listed in Table 5-4, when constructing the DSI state, keeping the intra-fragment elements $F_{ii}^{\pi\text{-NBO}} \neq 0$ means that in the DSI state, the inter-fragment interaction is partially preserved. When LMO = NBO, therefore, deleting the inter-fragment elements, $f_{\lambda\rho}^{\text{DSI}-\pi}$, of AO Fock matrix is not equivalent to deleting the inter-fragment elements $F_{ij}^{\pi\text{-NBO}}$ of NBO Fock matrix.

5.2.1.3. LMO Interactions between Fragments

At RHF level of theory, the energy effects, associated with the CT (charge transfer) and EX (exchange) interactions between the fragments in the FUD state, can be calculated using Equations (5-10) and Equation (5-11).

$$\begin{aligned} E_{CT}^\pi &= \sum_{i \in P}^{\text{all occ } \pi} \sum_{j \in Q, P \neq Q}^{\text{all vac } \pi} (F_{ij}^{\pi\text{-LMO}} + H_{ij}^{\pi\text{-LMO}}) D_{ij}^{\pi\text{-LMO}} \\ &\quad + \sum_{i \in P}^{\text{all vac } \pi} \sum_{j \in Q, P \neq Q}^{\text{all occ } \pi} (F_{ij}^{\pi\text{-LMO}} + H_{ij}^{\pi\text{-LMO}}) D_{ij}^{\pi\text{-LMO}} \end{aligned} \quad (5-10)$$

Table 5-9. For the $\theta = 0^\circ$ Geometry of N-Benzylideneaniline, CT and EX Interaction Energies (kcal/mol) between Fragments P and Q in the FUD state ($P \neq Q$) (at RHF/6-31G* Level).

P	Q	LFMO			NBO	
		E^{π}_{CT}	E^{π}_{EX}	$E^{\pi}_{CT} + E^{\pi}_{EX}$	E^{π}_{CT}	E^{π}_{EX}
A	B	-509.0	532.7	23.6	-12.8	-2.9
A	C	3.2	-3.0	0.2	0.0	-0.2
B	C	-496.9	383.0	-113.9	-5.7	-3.2

$$E_{EX}^{\pi} = \sum_{i \in P}^{all \text{ occ } \pi} \sum_{j \in Q, P \neq Q}^{all \text{ occ } \pi} (F_{ij}^{\pi-LMO} + H_{ij}^{\pi-LMO}) D_{ij}^{\pi-LMO} \\ + \sum_{i \in P}^{all \text{ vac } \pi} \sum_{j \in Q, P \neq Q}^{all \text{ vac } \pi} (F_{ij}^{\pi-LMO} + H_{ij}^{\pi-LMO}) D_{ij}^{\pi-LMO} \quad (5-11)$$

where $H_{ij}^{\pi-LMO}$, $F_{ij}^{\pi-LMO}$ and $D_{ij}^{\pi-LMO}$ are the LMO one-electron, Fock and density matrix elements. According to Table 5-9, the energy effect, associated with the LMO interactions between fragments P and Q, does include the CT and EX interaction energies. Between two bonded fragments such as (A and B) and (B and C), as shown by Table 5-9, the CT interaction energy, E^{π}_{CT} , is always stabilizing, and the EX interaction energy, E^{π}_{EX} , is always destabilizing, when LMO = LFMO. Whether total interaction energy between two bonded fragments, $E^{\pi}_{CT} + E^{\pi}_{EX}$, is destabilizing depends upon which interaction is stronger. For the $\theta = 0^\circ$ geometry of N-benzylideneaniline, for example, total interaction energy (23.6 kcal/mol) between fragments A and B is destabilizing, because $E^{\pi}_{EX} = 532.7 > 0$, $E^{\pi}_{CT} = -509.0 < 0$, and $|E^{\pi}_{EX}| > |E^{\pi}_{CT}|$. Since the fragment $-\text{N}=\text{CH}-$, as a substituent of C-phenyl ring, is an electron-withdrawing group, the CT and EX interactions between fragments B and C are weakened, but the EX interaction is more weakened than the CT interaction is done (Table 5-9). As a result, total LFMO interaction Between the C-phenyl ring and its electron-withdrawing group B is -113.9 kcal/mol, and it is stabilizing.

In the case of NBO basis set, as have been discussed, the interaction between fragments contains the intra-fragment interaction. Therefore, as shown by Table 5-9, the NBO CT and EX interaction energies both are stabilizing, and they are much smaller in the absolute value than the corresponding LFMO CT and EX interaction energies. It should be noted that the stabilizing characteristic of the NBO EX interaction between the bonded fragments does not conform to the destabilizing principle of the four-electron interaction.^{6,7}

5.2.1.4. Conclusions

The two criteria, R_L and $(E_e^{\pi-KL} - E_e^{\pi})$, of localization degree are defined and consistently prove that the localization degree of NBO basis set is low, which causes the inter-fragment and intra-fragment NBO interactions mixed with each other. In other words, it is difficult to distinguish between the NBO intra- and inter-fragment interactions. Eventually, the fundamental flaws of NBA lead to the following results:

- (i) In the NBO-DSI state, only part of the inter-fragment interaction has been excluded, and the intra-fragment NBO interaction is not completely retained.
- (ii) The NBO exchange interaction energy between two bonded fragments may become stabilizing, rather than destabilizing.
- (iii) Vertical delocalization energy is stabilizing.

Therefore, as a localized MO basis set where the π - and σ -NBOs are not completely separated and whose localization degree is low, NBO basis set cannot be used to calculate π -electron delocalization energy and to decompose the molecular energy.

5.2.2. Deleting Hartree-Fock Exchange

For ease of description, the sentence “the values of the vertical delocalization energy at the $\theta = 0^\circ$ geometry of NBA is calculated by our 2011 program”, or the similar phrases, will be shortened into the phrase “the 2011-values”. Other phrases can also be abbreviated in a similar manner, such as the phrase “the 2011-range(L)” that is the abbreviation of the phrase “the range(L) of a set of the values obtained from the 2011 program”.

It has been emphasized that electron localization is conceptually different from the localization of molecular orbitals according to the Bader's viewpoint.^{8,9} For the Morokuma's energy decomposition, the Hartree-Fock (HF) exchange was also concerned and stressed.¹⁰ In order to accurately calculate the extra stabilization energy of aromatic molecules, two versions of the restricted geometry optimization program have been developed in our research group since 2007 and are named our 2007 method and our 2011 method in this book. The principles and applications of our two methods have been reported,^{11,12} and will be detailed in Chapter 6 and Chapter 8.

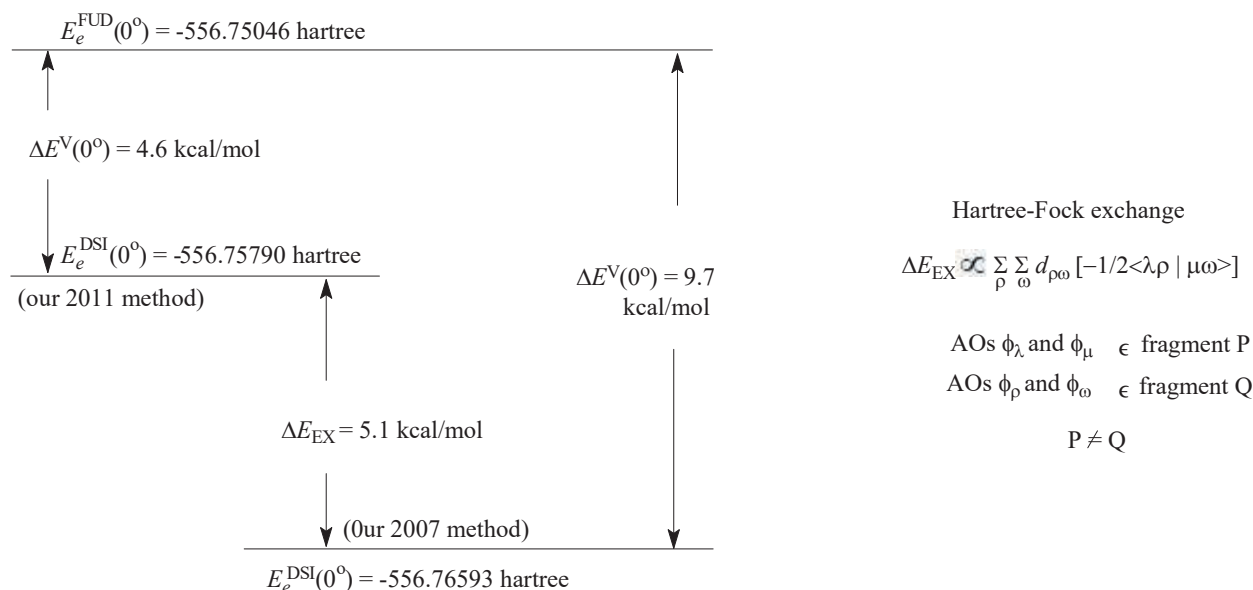
Our 2007 method can only ensure that the π MOs of the localized electronic state such as DSI are localized on their respective fragments by conditionally deleting the elements of the AO Fock and overlap integral matrices. Our 2007 method is the same as our 2006 method in the calculation principles, and it can be used to do geometry optimization or to do single-point energy calculation. But our 2006 method is run over the LFMO basis set, and it can only be used to do conditional single-point energy calculation. In the DSI state constructed using our 2006 method, it is the π MOs, rather than π -electrons, to be absolutely localized in their respective fragments.

In the localized geometry optimized using our 2011 program or in the localized electronic state obtained from our 2011 method, the AO Fock and overlap integral matrix elements and the AO two-electron exchange integrals $\langle \lambda\rho|\mu\omega \rangle$ have been conditionally excluded from between the fragments, so the π -electrons and π -MOs are absolutely localized on their respective fragments at the same time, where π AOs ϕ_λ and $\phi_\mu \in$ fragment P, and π AOs ϕ_ρ and $\phi_\omega \in$ Q, $P \neq Q$ (, which has been detailed in our publication¹² and will be described in Chapter 8). For benzene at RHF level of theory, as will be shown in Chapter 8, when the Hartree-Fock exchange integrals between the π systems of two double bonds are retained, the vertical delocalization energy is destabilizing. But it becomes stabilizing when the two-(π -electron) exchange integrals between two double bonds are conditionally deleted. The important role of HF exchange in determining the size and sign of the vertical delocalization energy makes us feel the need to reconfirm the destabilizing nature of the vertical delocalization energy in the case of NBA-like species.

Our 2007 method and our 2011 method are based on the AO basis set, and can also be used to construct the DSI state of the NBA-like species when the conformation geometry of a NBA-like species is planar. For the planar conformation, as have been indicated in the above section, the DSI state obtained from the conditional single-point energy calculation, over the LFMO basis set, performed by our 2006 program is the same as that obtained from the single-point energy calculation, over the AO basis set, performed by our 2007 program. For the $\theta = 0^\circ$ geometry of NBA, for example, the B3LYP/6-31G* values of vertical delocalization energy (DSI-3), obtained from our 2006 method and our 2007 method, are the same and are equal to 9.7 kcal/mol (Figure 5-5).

In the DSI state obtained from our 2011 program, as shown by Scheme 5-3, due to the additional deletion of the two-electron exchange integrals $\langle \lambda\rho|\mu\omega \rangle$, the molecular energy (hartree) of the DSI state increases from -556.76593 by our 2007 method to -556.75790 by our 2011 method. As a result, the vertical delocalization energy (kcal/mol) decreases from 9.7 to 4.6 and is still destabilizing.

5.2.2.1. Density functionals

**Scheme 5-3**

The Gamess (US) package provides the following four types of density functionals:

- (i) Pure exchange functionals without Hartree-Fock exchange (such as SLATER and XPBE96).
- (ii) Pure correlation functionals with Hartree-Fock exchange (such as CPBE96 and LYP).
- (iii) Exchange-correlation functionals without Hartree-Fock exchange (such as PBE96, SVWN5 and BLYP).
- (iv) Hybrid functionals with part of Hartree-Fock (such as PBE0, X3LYP and B3LYP).

In the density functionals, the exchange term includes the exchange of the density functional itself and the Hartree-Fock exchange (HF-EX). Our 2011 method can only exclude the Hartree-Fock exchange from between the π -systems of fragments. In the second type of density functionals such as CPBE96 and LYP, there is only Hartree-Fock exchange (100%). Therefore, only in the DSI state constructed, at the (CPBE96 and LYP) levels of theory, using our 2011 method, can it be ensured that there is no longer any type of the exchange interaction between fragments. In the first and third types of density functionals, there is no Hartree-Fock Exchange component. As a result, as shown by the corresponding data listed in Table 5-10-1 and Table 5-10-2, the 2011-values are equal to the corresponding 2007-values. The comparison of the calculation results obtained from our 2007 and 2011 methods can well understand the role of Hartree-Fock exchange in determining the value (including the size and sign) of vertical delocalization energy.

It is difficult or seems impossible that, for a non-planar geometry of a NBA-like species, the LFMO two-electron exchange $\langle ik|jl \rangle$ integrals are deleted when the π LFMO Ψ_i and $\Psi_j \in$ Fragment P and the π LFMO Ψ_k and $\Psi_l \in$ Fragment Q, $P \neq Q$. In this section, at first, the vertical delocalization energy of the $\theta = 0^\circ$ geometry will be calculated by using our 2007 and 2011 programs at various levels of theory. After understanding the role of Hartree-Fock exchange, at last, the pure exchange density functionals (such as SLATER) and the exchange-correlation density functionals (such as PBE96, SVWN5 and BLYP) will be used to calculate vertical delocalization energy of the twisted geometries, and the calculation results can confirm the destabilizing nature of the vertical delocalization energy, because there is no Hartree-Fock exchange component in each of these density functionals. In the DSI state constructed by using our 2006 program at the (SLATER, PBE96, SVWN5 and BLYP) levels of theory, the π -electrons can be considered to be localized in their respective fragments although the exchange of density functional

Table 5-10-1. Vertical Delocalization Energy $\Delta E^V(0^\circ)$ (kcal/mol) (DSI-3) for the Planar Geometry of N-Benzylideneaniline Are Obtained from Our 2007 Method.

Basis Sets	Pure EX without HF-		Pure Corr		EX-Corr			Hybrid	
	EX and Corr		with HF-EX		without HF-EX		with HF-EX		
	SLATER	XPBE96	CPBE96	LYP	PBE96	SVWN5	BLYP	PBE0	X3LYP
6-31G*	4.1	3.3	38.7	38.4	2.9	3.2	2.9	11.4	10.4
6-311G(2d,2p)	8.9	7.9	49.1	49.5	7.1	7.8	7.4	16.7	15.9
6-311G(2df,p)	9.9	8.8	51.3	51.6	8.0	8.7	8.3	17.9	17.0
6-311G(2d,p)	8.6	7.7	48.4	48.8	6.8	7.4	7.1	16.4	15.5
6-311G**	6.4	5.4	42.4	42.9	4.6	5.3	5.0	13.6	12.8
Average	7.6	6.6	46.0	46.2	5.9	6.5	6.1	15.2	14.3
Range (L)	5.8	5.5	12.6	13.2	5.1	5.5	5.4	6.5	6.6

Table 5-10-2. Vertical Delocalization Energy $\Delta E^V(0^\circ)$ (kcal/mol) (DSI-3) for the Planar Geometry of N-Benzylideneaniline Are Obtained from Our 2011 Method.

Basis Sets	Pure EX without HF-		Pure Corr		EX-Corr			Hybrid	
	EX and Corr		with HF-EX		without HF-EX		with HF-EX		
	SLATER	XPBE96	CPBE96	LYP	PBE96	SVWN5	BLYP	PBE0	X3LYP
6-31G*	4.1	3.3	8.8	8.9	2.9	3.2	2.9	5.0	4.9
6-311G(2d,2p)	8.9	7.9	9.6	10.2	7.1	7.8	7.4	8.2	8.5
6-311G(2df,p)	9.9	8.8	10.4	10.9	8.0	8.7	8.3	9.1	9.3
6-311G(2d,p)	8.6	7.7	9.4	9.9	6.8	7.4	7.1	7.9	8.2
6-311G**	6.4	5.4	9.1	9.5	4.6	5.3	5.0	6.3	6.5
Average	7.6	6.6	9.5	9.9	5.9	6.5	6.1	7.3	7.5
Range(L)	5.8	5.5	1.6	1.3	5.1	5.5	5.4	4.1	4.4

(PBE96, SVWN5 and BLYP) itself is retained.

The vertical delocalization energies for the $\theta = 0^\circ$ geometries of the molecule such as N-Benzylideneaniline and its substituted derivatives, calculated by our 2007 and 2011 programs, are listed in Table 5-10 to Table 5-12, and they confirm that, for the planar geometry of each substituted NBA, π -electron delocalization is still destabilization, when the MO CT and EX interactions and spatial exchange are excluded from interaction between the fragments.

For density functionals, the exchange interaction (including its own exchange and Hartree-Fock exchange) should increase in the following order:



Correspondingly, as shown by the 6-31G* data listed in Table 5-10-1, the 2007-value (kcal/mol) increases as the

Table 5-11. For the Co-planar Geometry of N-Benzylideneaniline, Vertical Delocalization Energy $\Delta E^V(0^\circ)$ (DSI-3) (kcal/mol) Are Obtained from Our 2011 and 2007 Methods.

Basis sets	6-31G*		6-311G*		6-311G**		6-311G(2d,2p)		6-311G(2df,p)		Range(L)	
	2011	2007	2011	2007	2011	2007	2011	2007	2011	2007	2011	2007
B3LYP	4.7	9.7	6.2	12.0	6.4	12.1	8.3	15.1	9.2	16.2	4.5	6.5
RHF	9.2	39.1	9.7	43.5	9.8	43.7	10.5	50.4	11.2	52.6	2.0	13.5
MP2	1.7	77.3	2.7	99.8	2.6	100.8	7.1	181.4	9.8	199.2	8.7	121.9
Average	5.2	42.0	6.2	51.8	6.3	52.2	8.6	82.3	10.1	89.3		
Range(B)	7.5	66.6	7.0	87.8	7.2	88.7	3.4	166.3	2.0	187.0		

Average: $\Sigma \Delta E^V(\text{basis})/n$ at a specific basis level. Range(B): the difference between the maximum and minimum values in a series of the values of the vertical delocalization energy at a specific basis level. Range(L): the difference between the maximum and minimum values in a series of the values of the vertical delocalization energy at a specific level of theory

Table 5-12. Vertical Delocalization Energies (kcal/mol) $\Delta E^V(0^\circ)$ (DSI-3) for the Planar Geometries of 6 Substituted NBAs Are Obtained from Our 2011 Program (the Positions of Substituents Are Shown in Figure 5-6).

Mols	Rn	Rn'	LYP			RHF		
			6-31G*	6-311G(2df,p)	6-311G**	6-31G*	6-311G(2df,p)	6-311G**
2-4	R1= -OH		9.9	12.1	10.7	10.2	12.4	11.0
2-8	R1= -OH	R2= -NO ₂	9.5	11.5	10.1	9.8	11.9	10.5
2-12	R1= -NH ₂	R6= -NO ₂	10.6	12.7	11.3	10.9	13.1	11.7
2-9	R1= -NO ₂	R2= -OH	8.5	10.6	9.1	8.8	11.0	9.4
2-16	R3= -Cl	R4= -OH	5.6	8.0	6.2	6.0	8.4	6.7
2-21	R1= -NO ₂	R7= -NH ₂	6.6	8.6	7.0	6.9	8.9	7.3

exchange interaction increases:

$$2.9 (\text{BLYP}) < 4.1 (\text{SLATER}) < 10.4 (\text{X3LYP}) < 38.7 (\text{CPBE96})$$

In a series of the 2007-values at 6-31G* level, the range(B) is 38.7 - 2.9 = 35.8 kcal/mol, where the symbol "range(B)" represents the range of a set of values at a specific basis level. In Table 5-10-1, Range (L) is the range of a set of the values at a specific theoretical level and can be used to evaluate the effect of basis set size on the 2007-value at a specific theoretical level, and it increases as the exchange interaction increases:

$$5.4 (\text{BLYP}) < 5.8 (\text{SLATER}) < 6.6 (\text{X3LYP}) < 12.6 (\text{CPBE96})$$

On the contrary, as shown by the data listed in Table 5-10-2, when our 2011 method is used, the effects of the theoretical level and basis set size on the 2011-values become smaller than on the 2007-values. When the DSI-3 state is constructed at CPBE96 level of theory, the range(L) of a set of the 2007 values is 12.6 kcal/mol and is the largest of four types of the ranges, but the range(L) of a set of the 2011 values is only 1.6 kcal/mol and is the smallest of the four types of the ranges, due to that there is no longer any type of the exchange interaction between the fragments when our 2011 method is used. In the meantime, the value of the vertical delocalization energy (kcal/mol) at CPBE96/6-31G* level decreases from 38.7 (the 2007-value) to 8.8 (the 2011-value).

Therefore, in the case of NBA-like species, it is necessary to confirm the destabilizing nature of vertical delocalized energy and the rationality of treating it as a driving force for molecular distortion.

5.2.2.2. Hartree-Fock Exchange Effects

A comparison of the 2007- and 2011-values listed in Table 5-11 shows the smaller effect of the theoretical level on the 2011-values. At 6-31G* level, for example, the 2007-values are as follows:

$$9.7 \text{ (B3LYP)} < 39.1 \text{ (RHF)} < 77.3 \text{ (MP}_2\text{).}$$

For the above three 2007-values at 6-31G* level, the average value and range(B) are 42.0 and 67.6 kcal/mol. The MP₂/6-31G* value (77.3 kcal/mol) is the largest, and it is eight times of the B3LYP/6-31G* value. On the contrary, according to the following values (kcal/mol):

$$1.7 \text{ (MP}_2\text{)} < 4.7 \text{ (B3LYP)} < 9.2 \text{ (RHF)} \text{ (2011-values at 6-31G* level)}$$

The 2011-values are smaller than the corresponding the 2007-values, and the effect of the theory level on the 2011-value is much smaller than on the 2007-value. The average of the 2011-values is 5.2 kcal/mol, and the range(B) of a set of the 2011-values is 7.5 kcal/mol. Particularly, the MP₂/6-31G* value becomes the smallest, and the B3LYP value (4.7 kcal/mol) is close to the average value (5.5 kcal/mol). Similarly, the basis set size has also a small effect on the 2011-value. At the MP₂ level of theory, for example, the 2011-values are as follows:

$$1.7 \text{ (6-31G*)} < 2.7 \text{ (6-311G*)} \approx 2.6 \text{ (6-311G**)} < 7.1 \text{ (6-311G(2d,2p))} < 9.8 \text{ (6-311G(2df,p)).}$$

The range(L) of this set of the 2011-values is 8.1 kcal/mol, and it is only 6.6 % of the 2007-range(L) (121.9 kcal/mol) (Table 5-11). At the MP₂ level of theory, the ratio of the 2007-values to the corresponding 2011-values are as follows:

$$45.5 \text{ (6-31G*)}, 37 \text{ (6-311G*)}, 38.8 \text{ (6.311G**)}, 25.5 \text{ (6-311G (2d,2p))}, 20.3 \text{ (6-311G(2df,p)).}$$

At the B3LYP level of theory, however, the 2011-range(L) (4.5 kcal/mol) is close to the 2007-range(L) (6.5 kcal/mol), and the ratio of the 2007-value to 2011-values are:

$$2.1 \text{ (6-31G*)}, 2.0 \text{ (6-311G*)}, 1.9 \text{ (6.311G**)}, 1.8 \text{ (6-311G (2d,2p))}, 1.8 \text{ (6-311G(2df,p))}.$$

The B3LYP ratio is not only much smaller than the corresponding MP₂ ratio, but also the smallest of the three theoretical levels. In particular, the B3LYP value of this ratio is almost independent of the size of the base set.

According to the above discussion, the differences, in the calculation principles, between the 2011 and 2007 programs have the slight effect on the B3LYP value of the vertical delocalization energy. When using the 2006 method to try to get the calculation results that are equivalent to the 2011 program, the B3LYP should be the most reasonable of the three theoretical levels (RHF, B3LYP, and MP₂).

As discussed above, the exchange interactions, including the density functional exchange and the Hartree-Fock exchange, has an obvious effect on the value of vertical delocalization energy. In the DSI state constructed by our 2011 method at the RHF, CPBE96 and LYP levels of theory, there should be no longer any type of the exchange between fragments. In this case, as shown by the data in Table 5-12, the vertical delocalization energies of the six substituted NBAs are still destabilizing, $\Delta E^V(0^\circ) > 0$. In particular, the theoretical level (RHF and LYP) and basis set size (from 6-31G* to 6-311G(2df,p)) have a slight effect on the 2011-value of the vertical delocalization energy. For molecule **2-4** at 6-311G** level, for example, the RHF value (11.0 kcal/mol) is almost equal to the LYP value (10.7

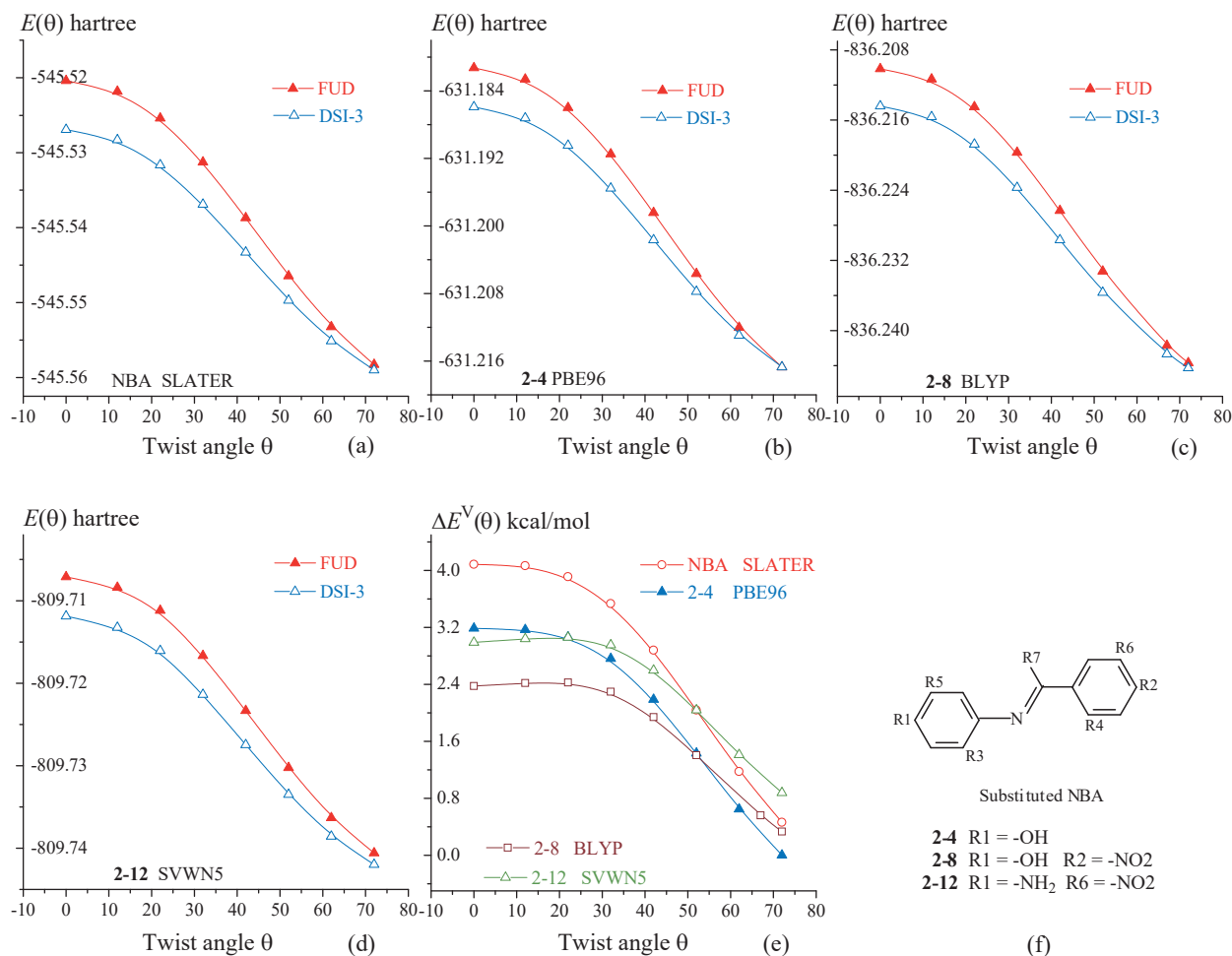


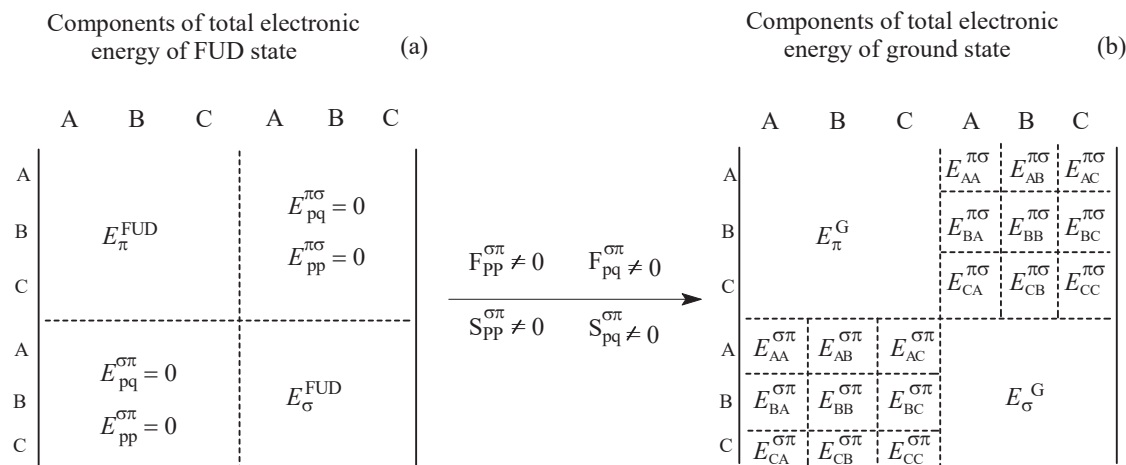
Figure 5-6. For NBA and its three substituted derivatives: (a) to (d) Molecular energies, $E^{\text{FUD}}(\theta)$ and $E^{\text{DSI}}(\theta)$, of the FUD and DSI-3 states. (e) Vertical delocalization energies $\Delta E^V(\theta)$, calculated using our 2006 method at the 6-31G* level.

kcal/mol). For the NBA-like species, the destabilizing nature of the π -electron delocalization is reasonably conformed.

When using the 2006 program, in order to eliminate the effects of the spatial exchange as much as possible, the DSI states of the NBA and three substituted derivatives are constructed at SLATER, PBE96, BLYP and SVWN5 levels of theory, and the corresponding vertical delocalization energies are calculated. As shown by the curves in Figure 5-6, the molecular energies of the FUD and DSI states have the following characteristics in the region of θ from 0° to 90°:

$$\begin{aligned} E^{\text{FUD}}(\theta) &< 0, E^{\text{DSI}}(\theta) < 0, |E^{\text{FUD}}(\theta)| < |E^{\text{DSI}}(\theta)| \\ dE^{\text{FUD}}(\theta)/d\theta &< 0, dE^{\text{DSI}}(\theta)/d\theta < 0, \\ \Delta E^{\text{VRE}}(\theta) &> 0, \text{ and } d\Delta E^{\text{VRE}}(\theta)/d\theta < 0. \end{aligned}$$

When our 2006 method is used to do calculation at the theoretical levels such as the density functionals without Hartree-Fock exchange, the characteristics of the molecular energies and vertical delocalization energies are the same as those of the corresponding energies calculated at the (B3LYP and RHF) levels of theory.

**Scheme 5-4**

5.3. DESTABILIZING π - σ INTERACTION

In the previous section, it has been argued that the π -electron delocalization is destabilization and is the driving force of molecular distortion. In this section, will discuss the characteristics of the π - σ interaction and the effects of the π - σ interaction on molecular conformation. All the conditional single-point-energy calculations are performed using our 2006 method based on the LFMO basis set.

5.3.1. N-benzylideneaniline

The regular (unconditional) single-point energy calculation, over the LFMO basis set or over the AO basis set, can provide a fully delocalized electronic state (specially referred to as the ground (G) state of a conformation twisted by θ) for N-benzylideneaniline. For a twisted conformation (non-planar geometry), the ground state can also be considered as the result of the π - σ interaction between the π and σ systems of the FUD electronic state. The molecular energy difference, $[E^G(\theta) - E^{\text{FUD}}(\theta)]$, between the G and FUD states can be defined as an energy effect, $\Delta E^{\pi\sigma}(\theta)$, associated with the π - σ interaction. As a face to face MO interaction between the σ and π systems, the π - σ interaction, includes the inter- and intra-fragment MO interactions, which is different from the π -MO interaction that is a head to head interaction between the fragments. The inter- and intra-fragment components of the π - σ interaction energy are defined as follows (Scheme 5-4b):

$$\Delta E_{pp}^{\pi\sigma}(\theta) = E_{pp}^{\pi\sigma}(\theta) + E_{pp}^{\sigma\pi}(\theta)$$

$$\Delta E_{pq}^{\pi\sigma}(\theta) = E_{pq}^{\pi\sigma}(\theta) + E_{pq}^{\sigma\pi}(\theta)$$

As two indirect energy effects that arise from the influences of the π - σ interaction on the electronic energies of the π and σ systems of the FUD state itself, the energy differences $\Delta E_{\pi}^{\pi\sigma}(\theta)$ and $\Delta E_{\sigma}^{\pi\sigma}(\theta)$, in the σ and π systems, between the ground state and the FUD state are defined as follows:

Table 5-13. For Each of Twisted Geometries of N-benzylideneaniline, Molecular Energy Difference (hartree), $\Delta E^{\pi\sigma}(\theta) = E^G(\theta) - E^{FUD}(\theta)$, between the G (Ground) and FUD States.

θ	RHF	MP2	MP3	MP4(SDQ)	θ	B3LYP			
	6-31G*					6-31G*	6-311G*	6-31G(2d)	6-311G(2d)
0.0	0.0	0.0	0.0	0.0	0.0	0.0	0.0	0.0	0.0
17.0	0.00775	0.03656	0.02806	0.03018	17.0	0.00323	0.00329	0.00397	0.00396
32.0	0.02853	0.11000	0.08185	0.09260	27.0	0.00867	0.00940	0.01058	0.01110
47.0	0.05914	0.19195	0.13774	0.16533	37.0	0.0168	0.01878	0.02015	0.02181
62.0	0.08966	0.25960	0.18245	0.22782	47.0	0.02677	0.03030	0.03158	0.03478
77.0	0.11018	0.30016	0.20865	0.26628	57.0	0.03678	0.04176	0.04279	0.04755
					77.0	0.05119	0.05799	0.05859	0.06532

Table 5-14. For Six Twisted Geometries of N-benzylideneaniline, Various DFT Values (kcal/mol) of $\Delta E^{\pi\sigma}(\theta)$ at 6-31G* Level.

θ	BLYP	SVWN5	XPBE96	SLATER	PBE96
0.0	0.0	0.0	0.0	0.0	0.0
17.0	1.3	1.4	1.4	1.5	1.4
32.0	5.5	5.7	5.5	5.9	5.7
42.0	9.7	10.2	9.8	10.6	10.0
62.0	19.0	20.1	19.0	20.7	19.6
77.0	23.7	25.2	23.7	26.0	24.5

$$\Delta E_{\pi}^{\pi\sigma}(\theta) = E_{\pi}^G(\theta) - E_{\pi}^{FUD}(\theta)$$

$$\Delta E_{\sigma}^{\pi\sigma}(\theta) = E_{\sigma}^G(\theta) - E_{\sigma}^{FUD}(\theta)$$

For N-benzylideneaniline, always $\Delta E^{\pi\sigma}(\theta) > 0$ according to Table 5-13. and it can be fitted as a fourth order polynomial function $\Delta E^{\pi\sigma}(\theta) = a + b\theta + c\theta^2 + d\theta^3 + e\theta^4$ (Figure 5-7). At the MP2/6-31G* level, for example,

$$\Delta E^{\pi\sigma}(\theta) = 1.36608 \times 10^{-5} - (2.87752 \times 10^{-4})\theta + (1.76686 \times 10^{-4})\theta^2 - (2.0849 \times 10^{-6})\theta^3 + (6.44435 \times 10^{-9})\theta^4.$$

$$d\Delta E^{\pi\sigma}(\theta)/d\theta > 0 (0^\circ < \theta < 88^\circ.)$$

Accordingly, the $\pi\sigma$ interaction is destabilization and is resistance to molecular distortion due to $d\Delta E^{\pi\sigma}(\theta)/d\theta > 0$. Resistance is the greatest at about the $\theta = 90^\circ$ geometry and is the smallest at the $\theta = 0^\circ$ geometry.

The density functionals BLYP, SVWN5, PBE96, XPBE96 and SLATER and (Table 5-14) belong to the pure exchange (or exchange + correction) functional without the HF-EX. In the FUD state constructed by our 2006 method with these density functionals, there is no the spatial HF-EX interaction between the π and σ electrons. Thus, Figure 5-7b confirm the conclusions obtained from Figures 5-7a and 5-7c.

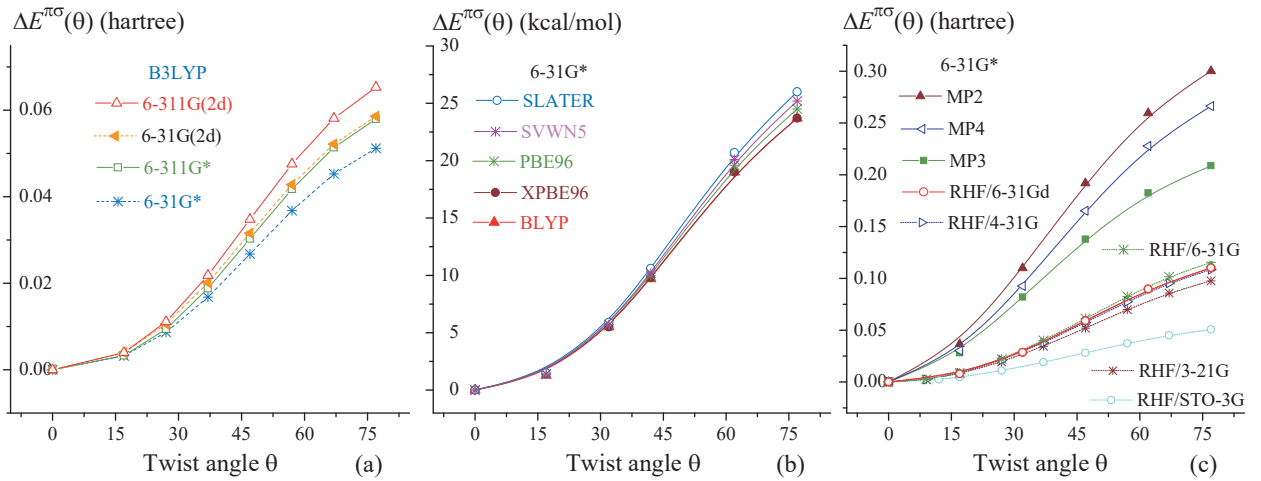


Figure 5-7. For N-benzylideneaniline, the energy effect $\Delta E^{\pi\sigma}(\theta)$ associated with the π - σ interaction, and its change with the increasing of twist angle θ .

5.3.1.1. Decomposition of π - σ Interaction Energy

The interaction between the π and σ systems includes the inter- and intra-fragment π - σ interactions, but the resistance to molecular distortion should arise from the π - σ interaction between fragments A and (B+C). At the RHF level of theory, therefore, the π - σ interaction energy, $\Delta E^{\pi\sigma}(\theta) = \Delta E_e^{\pi\sigma}(\theta)$, should be decomposed into various components. (Figure 5-8 and Scheme 5-4b) according to Equation (5-12) to Equation (5-16):

$$\Delta E^{\pi\sigma} = E^G - E^{FUD} = \left(\sum_p^{\text{all}} \Delta E_{pp}^{\pi\sigma} \right) + \left(\sum_p^{\text{all}} \sum_{q,p \neq q}^{\text{all}} \Delta E_{pq}^{\pi\sigma} \right) + \Delta E_{\pi}^{\pi\sigma} + \Delta E_{\sigma}^{\pi\sigma} \quad (5-12)$$

Where

$$\Delta E_{pq}^{\pi\sigma} = \sum_{i \in p, i \in \pi}^{\text{all}} \sum_{j \in q, j \in \sigma}^{\text{all}} (H_{ij}^{\pi\sigma} + F_{ij}^{\pi\sigma}) D_{ij}^{\pi\sigma} \quad (5-13)$$

$$\Delta E_{pp}^{\pi\sigma} = \left[\sum_{i \in \pi, i \in p}^{\text{all}} \sum_{j \in \sigma, j \in p}^{\text{all}} (H_{ij}^{\pi\sigma} + F_{ij}^{\pi\sigma}) D_{ij}^{\pi\sigma} \right]^G \quad (5-14)$$

$$\Delta E_{\pi}^{\pi\sigma} = \left[\sum_{i \in \pi}^{\text{all}} \sum_{j \in \pi}^{\text{all}} (H_{ij}^{\pi\pi} + F_{ij}^{\pi\pi}) D_{ij}^{\pi\pi} \right]^G - \left[\sum_{i \in \pi}^{\text{all}} \sum_{j \in \pi}^{\text{all}} (H_{ij}^{\pi\pi} + F_{ij}^{\pi\pi}) D_{ij}^{\pi\pi} \right]^{FUD} \quad (5-15)$$

$$\Delta E_{\sigma}^{\pi\sigma} = \left[\sum_{i \in \sigma}^{\text{all}} \sum_{j \in \sigma}^{\text{all}} (H_{ij}^{\sigma\sigma} + F_{ij}^{\sigma\sigma}) D_{ij}^{\sigma\sigma} \right]^G - \left[\sum_{i \in \sigma}^{\text{all}} \sum_{j \in \sigma}^{\text{all}} (H_{ij}^{\sigma\sigma} + F_{ij}^{\sigma\sigma}) D_{ij}^{\sigma\sigma} \right]^{FUD} \quad (5-16)$$

According to the data listed in Table 5-15 and to the curves in Figure 5-9, the strength and weakness of the

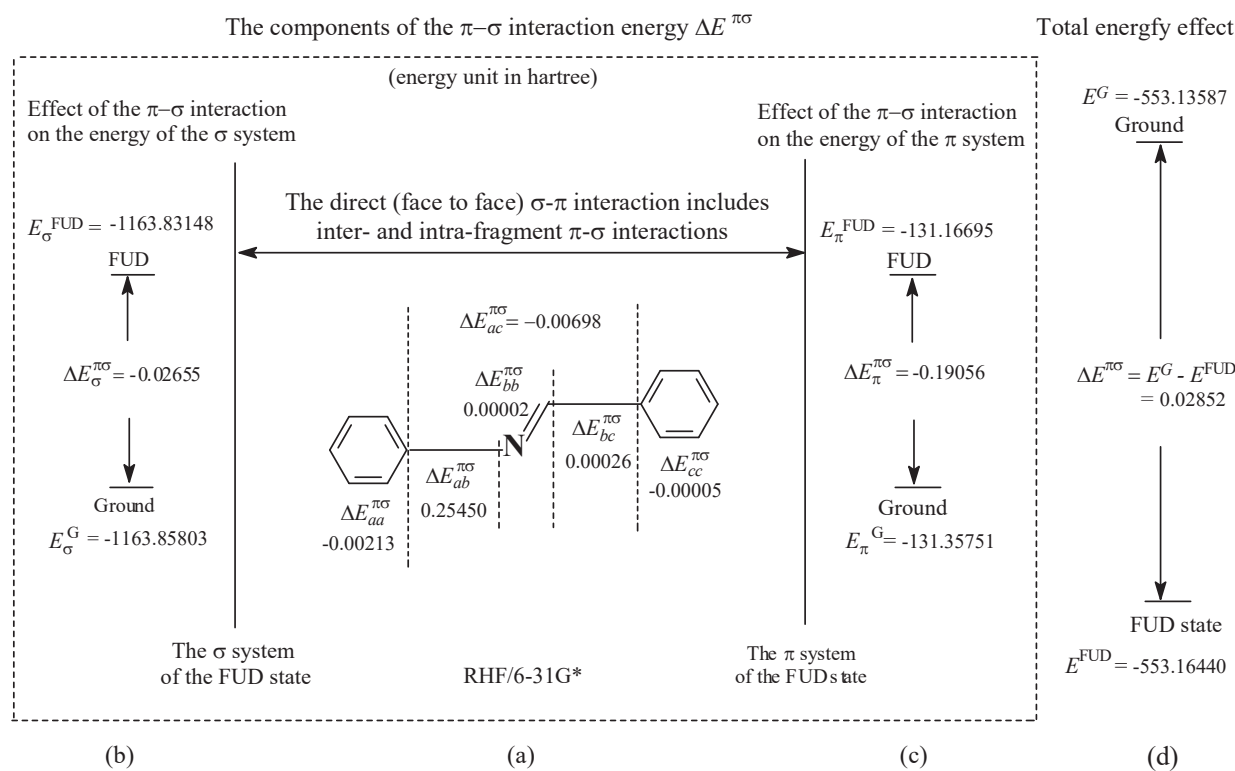


Figure 5-8. For the $\theta = 32^\circ$ geometry of N-benzylideneaniline: (a) The direct inter- and intra-fragment $\pi-\sigma$ interactions. (b) and (c) The effects of $\pi-\sigma$ interactions on the electronic energies of the π and σ systems themselves. (d) Total $\pi-\sigma$ interaction energy. At RHF/6-31G* level (energy unit in hartree).

inter- and intra-fragment interactions are as follows:

$$\Delta E_{ab}^{\pi\sigma} \gg \sum \Delta E_{pp}^{\pi\sigma} \quad (P = A, B, C), \quad \sum \Delta E_{pp}^{\pi\sigma} \text{ is almost a constant (Figure 5-19)}$$

$$\Delta E_{ab}^{\pi\sigma} \approx \sum \Delta E_{pq}^{\pi\sigma} \quad (P \neq Q), \quad d[\Delta E_{ab}^{\pi\sigma}(\theta)/d\theta] \gg d[\sum \Delta E_{pp}^{\pi\sigma}(\theta)]/d\theta > 0$$

The destabilizing characteristics of the $\pi-\sigma$ interaction and its ability to prevent molecular distortion are mainly determined by the destabilizing $\pi-\sigma$ interaction, $\Delta E_{ab}^{\pi\sigma}$, between fragments A and B. In addition, the π and σ systems of the FUD state themselves are stabilized due to the $\pi-\sigma$ interaction, and get more stabilized as the twist angle θ increases. According to the data listed in Table 5-15 and to Figure 5-9,

$$\Delta E_{\pi}^{\pi\sigma}(\theta) < 0, \quad d\Delta E_{\pi}^{\pi\sigma}(\theta)/d\theta < 0$$

$$\Delta E_{\sigma}^{\pi\sigma}(\theta) < 0, \quad d\Delta E_{\sigma}^{\pi\sigma}(\theta)/d\theta < 0$$

$$[\Delta E_{\pi}^{\pi\sigma}(\theta) + \Delta E_{\sigma}^{\pi\sigma}(\theta)] = -1.0418 \cdot 10^{-4} - (7.1891 \cdot 10^{-4})\theta - (7.1603 \cdot 10^{-5})\theta^2 - (5.5228 \cdot 10^{-6})\theta^3 + (5.5827 \cdot 10^{-8})\theta^4 < 0$$

$$d[\Delta E_{\pi}^{\pi\sigma}(\theta) + \Delta E_{\sigma}^{\pi\sigma}(\theta)]/d\theta < 0$$

$$\Delta E_{ab}^{\pi\sigma} = 1.113048 \cdot 10^{-4} + (1.8327 \cdot 10^{-4})\theta + (1.40491 \cdot 10^{-4})\theta^2 + (5.05881 \cdot 10^{-6})\theta - (5.64877 \cdot 10^{-8})\theta^4 > 0$$

$$d[\Delta E_{ab}^{\pi\sigma}]/d\theta > 0$$

$$d[\Delta E_{ab}^{\pi\sigma}]/d\theta > |d[\Delta E_{\pi}^{\pi\sigma}(\theta) + \Delta E_{\sigma}^{\pi\sigma}(\theta)]/d\theta|$$

Therefore, the changes of the original π and σ system themselves are the driving force for distorting geometry, but

Table 5-15. For N-benzylideneaniline, Molecular Energy Difference $\Delta E^{\pi\sigma}$ (hartree) between the Ground and FUD States at RHF/6-31G* Level, and Its Various Components (hartree).

θ°	$\Delta E^{\pi\sigma}$	$\Sigma \Delta E_{pp}^{\pi\sigma}$	${}^*\Delta E_{ab}^{\pi\sigma}$	$\Sigma \Delta E_{pq}^{\pi\sigma}$	$\Delta E_\pi^{\pi\sigma}$	$\Delta E_\sigma^{\pi\sigma}$
0	0.0	0.0	0.0	0.0	0.0	0.0
17	0.00774	-0.00010	0.06467	0.06397	-0.05011	-0.00604
32	0.02852	-0.00216	0.25450	0.24778	-0.19056	-0.02655
42	0.04837	-0.00423	0.45631	0.44620	-0.33696	-0.05665
62	0.08964	-0.00787	0.92201	0.90828	-0.67921	-0.13158
77	0.11016	-0.00858	1.17110	1.15769	-0.87286	-0.16611

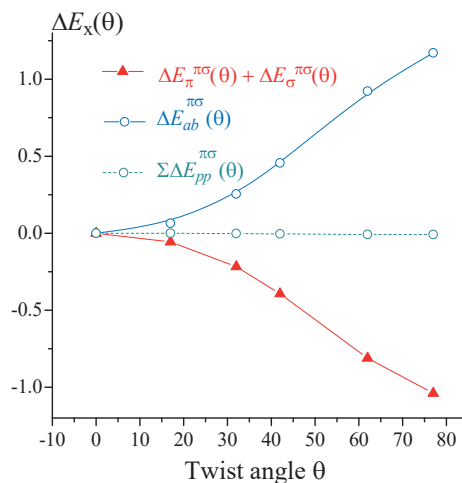


Figure 5-9. The components (hartree), $\Delta E_{ab}^{\pi\sigma}$, $\Sigma \Delta E_{pp}^{\pi\sigma}$ and $(\Delta E_\pi^{\pi\sigma} + \Delta E_\sigma^{\pi\sigma})$, of the $\pi\text{-}\sigma$ interaction energy at RHF/6-31G*, and their changes with the increasing of the twist angle θ .

the sum of these two driving forces is less than the resistance $d[\Delta E_{ab}^{\pi\sigma}(\theta)]/d\theta$. At the $\theta = 32^\circ$ geometry of N-benzylideneaniline (Table 5-15), for example, the components (hartree) are as follows:

$$\begin{aligned} \Delta E_{ab}^{\pi\sigma}(32) &= 0.25450, \\ \Sigma \Delta E_{pp}^{\pi\sigma} &= -0.00216 \\ [\Delta E_\pi^{\pi\sigma}(\theta) + \Delta E_\sigma^{\pi\sigma}(\theta)] &= -0.21711 \\ \Delta E_{ab}^{\pi\sigma}/|\Sigma \Delta E_{pp}^{\pi\sigma}| &= 118 \\ \Delta E_{ab}^{\pi\sigma}(32)/|\Delta E_\pi^{\pi\sigma}(\theta) + \Delta E_\sigma^{\pi\sigma}(\theta)| &= 1.17 \\ \text{Total energy effect } \Delta E^{\pi\sigma}(32^\circ) &= 0.02852 \text{ hartree.} \end{aligned}$$

In the case of N-benzylideneaniline, thus, the $\pi\text{-}\sigma$ interaction is destabilization, and the resistance to molecular distortion mainly comes from the $\pi\text{-}\sigma$ interaction ($\Delta E_{ab}^{\pi\sigma}$) between the fragments A and B.

5.3.2. NBA-like Species

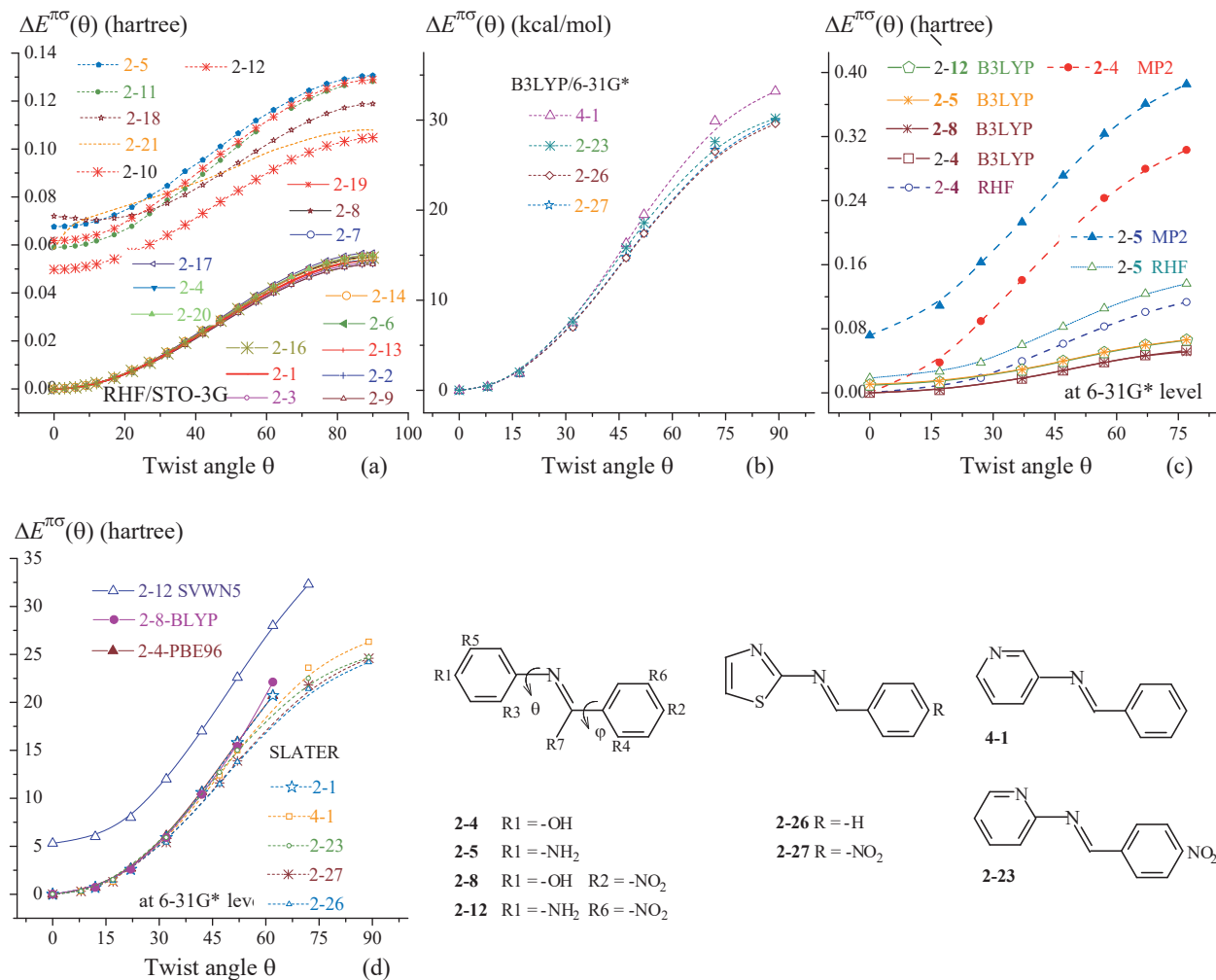


Figure 5-10. The $\pi\text{-}\sigma$ interaction energies, $\Delta E^{\pi\sigma}(\theta)$, for NBA-like species, and their changes with the increasing of twist angle θ . Whether the $\Delta E^{\pi\sigma}(0^\circ)$ value is equal to zero depends on the twist angle ϕ and does on the twist angle of substituents.

In the early days, the $\pi\text{-}\sigma$ interaction energies of 21 substituted NBA molecules were calculated at the RHF/STO-3G level (Figure 5-10a).^{13,14} In the Figure, whether the $\Delta E^{\pi\sigma}(0^\circ)$ value is equal to zero depends on the value of the twist angle ϕ and on the dihedral angle between the phenyl ring and the plane of substituent. In the molecules **2-5** ($R_1 = -\text{NH}_2$), **2-12** ($R_1 = -\text{NH}_2$, $R_6 = -\text{NO}_2$), **2-11** ($R_1 = -\text{NH}_2$, $R_2 = -\text{NO}_2$), **2-18** ($R_3 = -\text{NH}_2$, $R_4 = -\text{OH}$), **2-21** ($R_1 = -\text{NO}_2$, $R_7 = -\text{NH}_2$), and **2-10** ($R_1 = -\text{NO}_2$, $R_2 = -\text{NH}_2$), there is at least an amino group, and the dihedral angle between the phenyl ring and the substituent plane is not equal to 180° or 0° . The corresponding dashed curves in Figure 5-10a are separated from each other, and all the solid curves almost overlap each other. If all the dihedral angles except for the twist angle θ are equal to zero or 180 degrees, all the curves in Figure 5-10a should overlap each other.

In this section, the $\Delta E^{\pi\sigma}(\theta)$ for four substituted NBAs **2-4**, **2-5**, **2-8**, **2-12**, and for four NBA-like species **2-23**, **4-1**, **2-26** and **2-27** are calculated at the RHF, MP2 and various DFT levels of theory with 6-31G* basis set (Figure 5-10, and Table 5-16). A comparison of the sub-Figures in Figure 5-10 shows that the characteristics of the $\Delta E^{\pi\sigma}(\theta)$ and $d\Delta E^{\pi\sigma}(\theta)/d\theta$ at (MP2, RHF and B3LYP)/6-31G* levels are the same as the characteristics at RHF/STO-3G level. At B3LYP/6-31G* level, as shown by Figure 5-10b, the curve lines for four molecules **2-23**, **4-1**, **2-26** and **2-27**

Table 5-16. Energy Effect $\Delta E^{\pi\sigma}$ (kcal/mol) for 8 NBA-like Species at 6-31G* Level.

θ	2-12 SVWN5	2-4 PBE96	NBA SLATER	2-8 BLYP	θ	2-27 B3LYP	2-26 B3LYP	4-1 B3LYP	2-23 B3LYP
0	5.3	0.0	0.0	-0.0	0	0.0	0.0	0.0	0.0
12	6.0	0.7	0.7	0.7	8	0.4	0.4	0.4	0.4
22	8.0	2.7	2.6	2.6	17	1.9	1.9	1.9	2.0
32	12.0	6.1	5.9	5.9	32	7.1	7.0	7.5	7.6
42	17.0	10.7	10.6	10.4	47	14.8	14.7	16.3	15.8
52	22.6	15.9	15.8	15.4	52	17.5	17.4	19.5	18.6
62	28.0	20.7	20.7	22.1	72	26.7	26.5	29.9	27.6
72	32.3				89	29.9	29.6	33.2	30.2

almost overlap each other when $\theta < 45^\circ$.

When the single-point energy calculations are performed with the density functionals such as PBE96, SLATER, and BLYP, the values of the energy effects $\Delta E^{\pi\sigma}(\theta)$ for molecules **2-1**, **2-4** and **2-8** are almost overlap each other in the region of twist angle from $\theta = 0^\circ$ to $\theta = 45^\circ$ (Figure 5-10d). For molecule **2-12**, the dihedral angle $\varphi \neq 180^\circ$ and the dihedral angle between the C-phenyl ring and the planes of substituent groups is not equal to zero. In Table 5-16 and Figure 5-10d, as a result, the SVWN5 value of $\Delta E^{\pi\sigma}(0^\circ)$ for molecule **2-12** is not equal to zero. Importantly, Figure 5-10d demonstrates that even if the DFT used does not contain the Hartree-Fock exchange, it cannot change the destabilizing characteristics of the energy effect $\Delta E^{\pi\sigma}(\theta)$ and cannot change its ability to prevent molecular distortion.

In the case of substituted NBAs and NBA-like species, the π - σ interaction is also destabilization, and it is resistance to molecular distortion.

5.4. DESTABILIZING NON-BONDED σ - σ INTERACTION

In order to study the effect of σ -electron delocalization on molecular properties, a referential electronic state must be constructed, and its σ systems are localized on their respective fragments. There are two possible reference states of this type: FUL state (full localized) in which the π and σ systems are localized on their respective fragments; DPI state in which π -electrons are delocalized and σ -electrons are localized. In this section, only the FUL state is considered. Of course, must also construct an electronic state in which σ -electrons are delocalized on whole molecular framework in order to calculate σ -electron delocalization energy. Two such types of electronic states are called the DSI state and FUL state.

In our earlier work,¹³ the π - σ interaction energies were calculated using our 1998 method at RHF/STO-3G level. Since 2006, our 1998 method has been incorporated into the PC-Gamess package, known as our 2006 method.¹ After that, our 2006 method is no longer limited by theory level and Gaussian basis size. Nonetheless, the FUL state and the PDSI (partly delocalized sigma) state must still be constructed at the RHF/STO-3G level, which cannot be improved so far. In this chapter, a lot of efforts must be made to prove that all the conclusions about the σ - σ interaction, obtained from the calculations at the RHF/STO-3G level, are reasonable. In fact, Figure 4-9 and Figure 5-10 have demonstrated that the destabilizing characteristics of the π - π and π - σ interactions have nothing to do with

the theoretical level and basis set size. In terms of the sign of the $\pi\text{-}\pi$ and $\pi\text{-}\sigma$ interaction energies, the calculation at RHF/STO-3G is reasonable.

5.4.1. Construction of FUL State

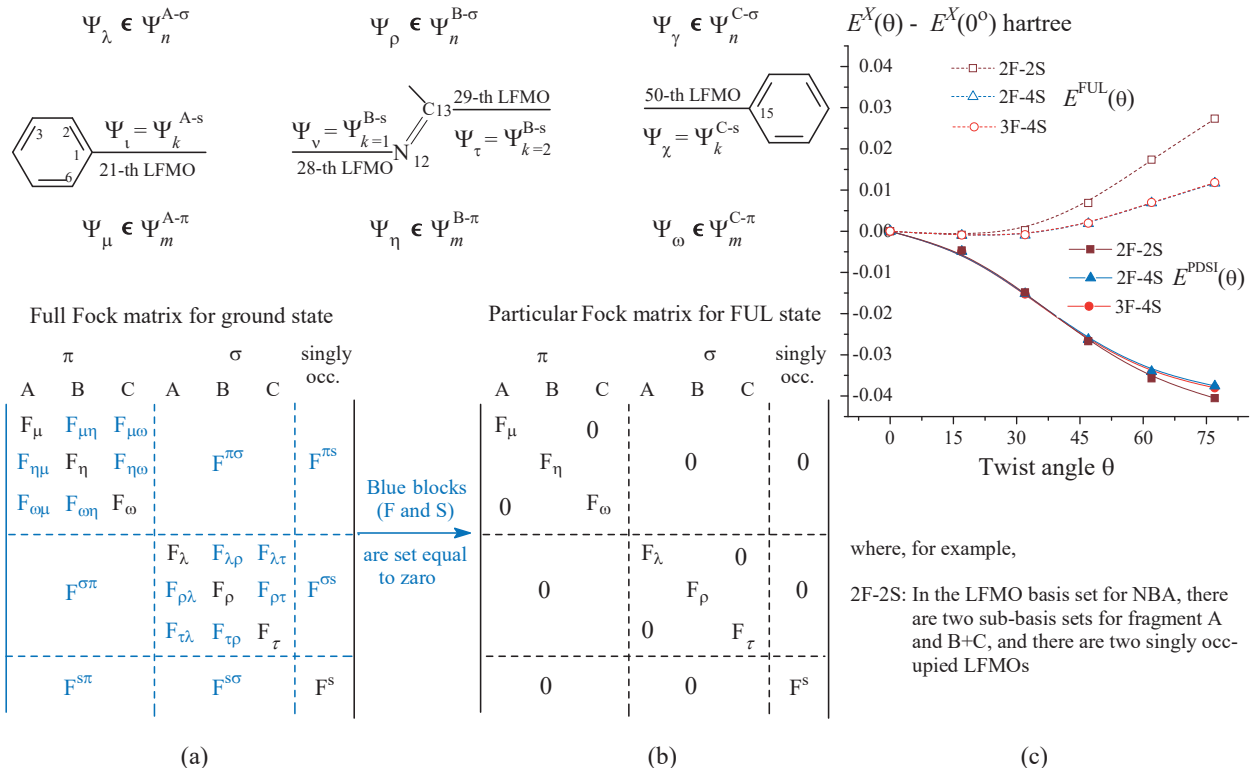


Figure 5-11. (b) The conditional settings for constructing FUL state of NBA at RHF/STO-3G based on the LFMO basis set $\{\Psi_m^{P-\pi}, \Psi_n^{P-\sigma}, \Psi_k^{P-s}\}$. (c) For the FUL and PDSI states of N-benzylideneaniline, the molecular energy differences $[E^{\text{FUL}}(\theta) - E^{\text{FUL}}(0^\circ)]$ and $[E^{\text{PDSI}}(\theta) - E^{\text{PDSI}}(0^\circ)]$, and their changes with the increasing of twist angel θ at RHF/STO-3G level.

For N-benzylideneaniline, its LFMO basis set can be expressed as $\{\Psi_m^{P-\pi}, \Psi_n^{P-\sigma}, \Psi_k^{P-s}\}$ ($P = A, B, C$, or $P = A, B+C$), and the four singly occupied LFMOs generate from the breaking of the C(1)-N(12) and C(13)-C(15) single bonds. In Figure 5-11, the four singly occupied LFMOs Ψ_k^{P-s} are denoted as Ψ_i , Ψ_v , Ψ_τ and Ψ_χ , and they are concentrated, respectively, on the C(1), N(12), C(13) and C(15) atoms. In the LFMO basis set at the RHF/STO-3G level, the numberings of the four singly occupied LFMOs are 21, 28, 29 and 50. In order to construct the FUL state, the single-point energy calculation, over the LFMO basis set, should be performed under the conditional settings described in Figure 5-11b. Accordingly, the FUL-3 state is the result of the interaction between the four singly occupied LFMOs, and its MOs are expressed as $\{\Phi_i\} = \{\Phi_i^{P-\pi}, \Phi_j^{P-\sigma}, \Phi_w^S\}^{\text{FUL}-n}$, where "n" in the superscript "FUL-n" is the number of fragments. In the meantime, two single bonds, C(1)-N(12) and C(13)-C(15), are recovered, and the corresponding LC-LFMO MOs Φ_w^S , as the fourth σ system, can be expressed as the following linear combination of four singly occupied LFMOs:

$$\Phi_w^S = A_{iw} \Psi_i + A_{vw} \Psi_v + A_{tw} \Psi_\tau + A_{\chi w} \Psi_\chi$$

For the FUL-3 state of NBA at RHF/STO-3G level, as shown by Table 5-17 (presented at the end of this Chapter), three σ systems, denoted as $\{\Phi_j^{A-\sigma}\}$, $\{\Phi_j^{B-\sigma}\}$ and $\{\Phi_j^{C-\sigma}\}$, and three π systems, denoted as $\{\Phi_i^{-\pi}\}$, $\{\Phi_i^{B-\pi}\}$ and $\{\Phi_i^{C-\pi}\}$, are still absolutely localized on their respective fragments A, B and C, and meanwhile the π and σ systems are completely separated. The fourth σ system $\{\Phi_w^S\}$ are delocalized on the whole molecular framework, but their AO coefficients are concentrated, respectively, on the C(1)-N(12) and C(13)-C(15) single bonds. According to Figure 5-11c, the molecular energy features of the FUL state are as follows:

$$E^{\text{FUL}}(\theta) < 0, dE^{\text{FUL}}(\theta)/d\theta > 0$$

The change of the molecular energy of FUL state is resistance to molecular distortion. But the first derivative $dE^{\text{FUL}}(\theta)/d\theta$ is small. As the twist angle increases from $\theta = 0^\circ$ to $\theta = 77^\circ$, for example, the corresponding molecular energy (hartree) of FUL-3 state (3F-4S in Figure 5-11c) increases from -545.88932 to -545.87754, the energy difference $dE^{\text{FUL}}(77^\circ) = E^{\text{FUL}}(77^\circ) - E^{\text{FUL}}(0^\circ) = 7.4 \text{ kcal/mol}$. It will be shown that the energy difference $\Delta E^{\text{FUL}}(77^\circ)$ is about 1/3 of $dE^{\text{PDSI}}(77^\circ)$ (PDSI state will be defined in section 5.4.3). In the case of the FUL state, the rotating of the fragment (A+B) about the C(1)-N(12) bond slightly increases the molecular energy $E^{\text{FUL}}(\theta)$.

5.4.2. Reasonable STO-3G Basis Set

The actual calculations show that only STO-3G can be used to construct a reasonable FUL state. The so-called reasonable FUL state refers to an electronic state that meets with the following basic characteristics:

- (i) Of the four MOs Φ_w^S , two MOs are doubly occupied, and other two MOs are vacant.
- (ii) At RHF level of theory, the eigenvalues of all vacant MOs are greater than zero.

However, all Gaussian basis sets, except for STO-3G, can't guarantee the reasonableness of the constructed FUL state. When the FUL state is constructed at the RHF/6-31G level, for example, at least one or two vacant MOs have negative eigenvalue. When the FUL state is constructed at 6-31G* level, three Φ_w^S , rather than two Φ_w^S , are the occupied MOs. Therefore, we must first prove that RHF/STO-3G can be reasonably used to construct the localized electronic state such as FUL.

Substituted NBAs can be divided into 4 groups, as already pointed out in the third chapter, the molecules, **2-1** (NBA), **2-17** ($R_3 = R_4 = -OH$), **2-20** ($R_3 = -OH$, $R_2 = -NO_2$), and **2-21** ($R_1 = -NO_2$, $R_7 = -NH_2$), are the typical representatives of their respective groups. For each of the four substituted NBA molecules, a series of optimized conformations with twist angle θ have been obtained from the relaxed PES-scan at the B3LYP/6-311G** level. At the different theoretical levels (B3LYP, RHF, MP2, BLYP and BVWN) with the different basis sets (6-311G**, 6-31G and STO-3), the single-point energy calculations on the same series of the optimized geometries provide 12 function curves of total electronic energy difference $dE_e(\theta) = [E_e(\theta) - E_e(0^\circ)]$ for each of the four molecules. For each molecule, interestingly, the 12 function curves, $dE_e(\theta) = f(\theta)$, completely overlap each other. This indicates that the characteristics of total electronic energy difference function $dE_e(\theta) = f(\theta)$ not only has nothing to do with the basis set size, but also irrelevant to the theoretical level. Accordingly, the effects of the electron correlation and other factors on the values (magnitude and sign) of $dE_e(\theta)$ are small, and the influence of the basis set size on the total electron energy is almost canceled out, since the energy difference is calculated.

5.4.3. Construction of PDSI Electronic State

For the FUL state, the MOs can be expressed as $\{\Phi_i^{P-\pi}, \Phi_j^{P-\sigma}, \Phi_w^S\}^{\text{FUL}-n}$. The DSI state can be considered to

Particular LFMO Fock (overlap integral) matrix for DSI state			Particular LFMO Fock (overlap integral) matrix for PDSI state			LFMO Coefficient matrix for PDSI state		
$\Psi_m^{P-\pi}$			$\Psi_n^{P-\sigma}$			Ψ_k^{P-s}		
A	B	C	A	B	C	A	B	C
A	F_A	0	0	set	set	A	F_A	0
B	0	F_B	0	0	0	B	0	F_B
C	0	0	F_C	0	0	C	0	F_C
A	set	F_A	F_{AB}	F_{AC}	F_{AK}	A	set	F_A
B	0	F_{BA}	F_B	F_{BC}	F_{BK}	B	0	F_{BA}
C	F_{CA}	F_{CB}	F_C	F_{CK}	0	C	F_{CA}	F_{CB}
	set 0	F_{KA}	F_{KB}	F_{KC}	F_k		set 0	F_k

Scheme 5-5

be such an electronic state: its delocalized σ system is a result of the σ - σ interaction between the four localized σ systems $\{\Phi_j^{P-\sigma}, \Phi_w^S\}$ ($P = A, B, C$) of FUL state. In order to construct the DSI state, the single-point energy calculation is performed, over the LFMO basis set $\{\Psi_m^{P-\pi}, \Psi_n^{P-\sigma}, \Psi_k^S\}$, under conditional settings (including the conditional settings of the LFMO overlap integral matrix) described by Scheme 5-5a. In the DSI state, the σ - σ interaction includes not only the non-bonded σ - σ interaction between three groups of σ LFMOs $\{\Psi_n^{P-\sigma}\}$ ($P = A, B, C$), and also includes the inter- and intra-fragment σ - s interactions between $\{\Psi_n^{P-\sigma}\}$ and $\{\Psi_k^S\}$.

In order to study the effect of the non-bonded σ - σ interaction on molecular conformation, it is necessary to construct an electronic state in which the σ - s interaction between $\{\Psi_n^{P-\sigma}\}$ and $\{\Psi_k^S\}$ is set equal to zero. This electronic state is called PDSI (partially delocalized sigma state). The PDSI state can be constructed by the single-point energy calculation that is performed, over the LFMO basis set, under the conditional settings described by Scheme 5-5b. In the PDSI state, as shown by Scheme 5-5c and Table 5-18 (presented in Appendix), three π systems, $\{\Phi_i^{A-\pi}\}_{\text{PDSI}}$, $\{\Phi_i^{B-\pi}\}_{\text{PDSI}}$ and $\{\Phi_i^{C-\pi}\}_{\text{PDSI}}$, are localized on their respective fragments. In the meantime, two σ systems, $\{\Phi_j^\sigma\}_{\text{PDSI}}$ and $\{\Phi_w^S\}_{\text{PDSI}}$, are delocalized on the whole molecular framework, and their LC-LFMOs can be expressed as the following Equations:

$$\Phi_j^\sigma = \sum_P \sum_n A_{nj} \Psi_n^{P-\sigma}$$

$$\Phi_w^S = \sum_P \sum_k A_{kw} \Psi_k^{P-s}$$

In the 38-th MO that is a σ MO of the PDSI state of NBA, as shown by the data in Table 5-18, the coefficients of the singly occupied LFMOs and the coefficients of π LFMOs are equal to zero. For the FUL and PDSI states, the 15-th MO Φ_t is one of the MOs Φ_w^S , the coefficients of its four singly occupied LFMOs in the FUL state are almost the same as the corresponding coefficients in the PDSI state. As shown by Table 5-17 and Table 5-18, the four LFMO coefficients are: -0.465485 (FUL) and -0.464074 (PDSI), 0.594534 (FUL) and 0.595671 (PDSI), 0.119919 (FUL) and 0.120437 (PDSI), and 0.106495 (FUL) and 0.106795 (PDSI). The PDSI state can be viewed as the result of the non-bonded σ - σ interaction between the three localized σ systems $\{\Phi_m^{P-\sigma}\}_{\text{FUL-3}}$ of the FUL state. For N-benzylideneaniline, as shown by Figure 5-11c, the features of molecular energy for the PDSI state are as follows:

$$E^{\text{PDSI}}(\theta) < 0, dE^{\text{PDSI}}(\theta)/d\theta < 0$$

Table 5-19. For Each of 6 Typical Substituted NBAs (FUL-2), the RHF/STO-3G Values of $\Delta E_n^{\sigma\sigma}(\theta)$ (hartree).

0	2-1 (NBA)	2-2 (R1 = -NO ₂)	2-4 (R1 = -OH)	2-8 (R1 = -OH, R2 = -NO ₂)	2-17 (R3 = -OH, R4 = -OH)	2-19 (R3 = OH)
0	0.06891	0.07044	0.06825	0.06890	0.06579	0.06776
17	0.06504	0.06627	0.06425	0.06484	0.06201	0.06398
27	0.05913	0.06041	0.05844	0.05900	0.05648	0.05838
37	0.05142	0.05270	0.05085	0.05132	0.04917	0.05097
47	0.04282	0.04396	0.04242	0.04273	0.04087	0.04255
57	0.03444	0.03558	0.03406	0.03425	0.03202	0.03422
77	0.02197	0.02326	0.02156	0.02140	0.02003	0.02176
90	0.01897	0.02028	0.01848	0.01826	0.01698	0.01857

$$|dE^{\text{PDSI}}(\theta)/d\theta| > dE^{\text{FUL}}(\theta)/d\theta$$

For the PDSI state of N-benzylideneaniline, as the twist angle θ increases from 0° to 77° , the molecular energy $E^{\text{PDSI}}(\theta)$ decreases from -545.76885 to -545.80689 hartree:

$$\begin{aligned} dE^{\text{PDSI}}(77^\circ) &= E^{\text{PDSI}}(77^\circ) - E^{\text{PDSI}}(0^\circ) = -23.9 \text{ kcal/mol.} \\ dE^{\text{PDSI}}(77^\circ)/dE^{\text{FUL}}(77^\circ) &= 3.2. \end{aligned}$$

For the PDIS state, the distortivity of total electron energy should be attributed to the non-bond σ - σ interaction.

5.4.4. Non-bonded σ - σ Interaction

Due to the non-bonded σ interaction between fragments, an electronic state is changed from the FUL state that favors the planar conformation to the PDSI state that tends to distort the molecular geometry. The molecular energy difference, $\Delta E_n^{\sigma\sigma}(\theta) = [E^{\text{PDSI}}(\theta) - E^{\text{FUL}}(\theta)]$, between the PDSI and FUL states is defined as the non-bonded σ - σ interaction energy. For the 21 substituted NBAs, as shown by the data listed in Table 5-19 and by the curves in Figure 5-12a, always:

$$\Delta E_n^{\sigma\sigma}(\theta) > 0.0, d[\Delta E_n^{\sigma\sigma}(\theta)]/d\theta < 0.$$

The non-bonded σ - σ interaction (σ -electron delocalization) is destabilization and is the driving force of the molecular distortion. Figure 5-12a also show that except the molecules **2-18** (R3 = -NH₂, R4 = -OH) and **2-21** (R1 = -NO₂, R7 = -NH₂), the function curves of all other molecules almost overlap each other, indicating the influence of the substituents on the driving force is small.

In order to confirm the rationality of the use of RHF/STO-3G, the energy effect $\Delta E_n^{\sigma\sigma}(\theta)$ is calculated at the (SLATER, BLYP, B3LYP and CPBE96)/STO-3G levels. CPBE96 is a pure correlation density functional with HF-EX, and the corresponding (blue dashed) curve in Figure 5-12b indicates that the CPBE96 values of $\Delta E_n^{\sigma\sigma}(\theta)$ and $d\Delta E_n^{\sigma\sigma}(\theta)/d\theta$ are greater than the corresponding values obtained from other three density functionals BLYP

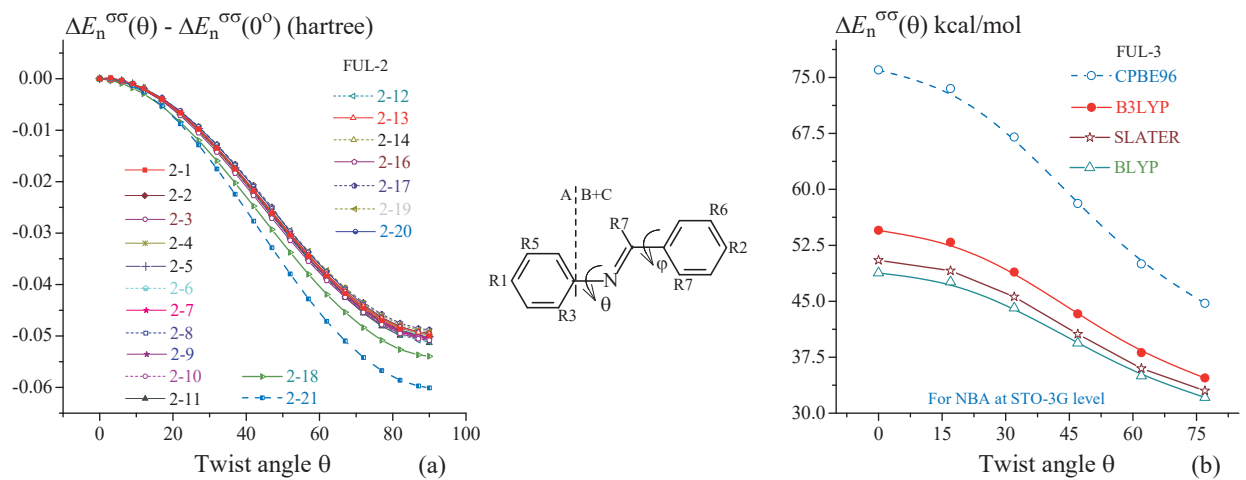
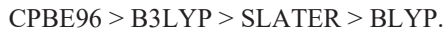


Figure 5-12. (a) Energy effect differences, $[\Delta E_n^{\sigma\sigma}(\theta) - \Delta E_n^{\sigma\sigma}(0^\circ)]$, for the 21 substituted NBAs (**2-n**) at RHF/STO-3G level. (b) For NBA, the energy effect $\Delta E_n^{\sigma\sigma}(\theta)$ at various DFT/STO-3G levels. Their changes as the twist angle θ increases.

and SLATER (without HF-EX) and B3LYP (with part of HF-EX). In the four density functionals, their HF-EX content increases roughly in the following order:



This order is consistent with the top-down order of their corresponding curves in Figure 5-12b. For the $\theta = 0^\circ$ geometry of N-benzylideneaniline, for example, the size order of $\Delta E_n^{\sigma\sigma}(\theta)$ (FUL-3) (kcal/mol) is as follow:

$$76.0 (\text{CPBE96}) \approx 75.6 (\text{RHF}) > 54.5 (\text{B3LYP}) > 50.5 (\text{SLATER}) > 48.8 (\text{BLYP})$$

Therefore, the Hartree-Fock exchange can affect the magnitude of the energy effect $\Delta E_n^{\sigma\sigma}(\theta)$, but it cannot change the destabilizing feature of the energy effect $\Delta E_n^{\sigma\sigma}(\theta)$ and cannot change the ability of $d\Delta E_n^{\sigma\sigma}(\theta)/d\theta$ to distort the molecule.

5.4.5. σ - σ Interaction Distorting Molecule.

The molecules energy difference, $\Delta E^{\sigma\sigma}(\theta) = [E^{\text{DSI}}(\theta) - E^{\text{FUL}}(\theta)]$, between the DSI state and FUL state is defined as σ -electron delocalization energy (or σ - σ interaction energy). The DSI state may also be considered as an electronic state resulting from σ - s interaction between two σ systems, $\{\Phi_j^\sigma\}^{\text{PDSI}}$ and $\{\Phi_w^\sigma\}^{\text{PDSI}}$, of the PDSI state, and the molecular energy difference, $\Delta E^{\sigma s}(\theta) = [E^{\text{DSI}}(\theta) - E^{\text{PDSI}}(\theta)]$, between the DSI state and PDSI state is defined as the σ - s interaction energy. As shown by the data listed in Table 5-20, $\Delta E^{\sigma\sigma}(\theta) < 0.0$, $d\Delta E^{\sigma\sigma}(\theta)/d\theta < 0$. Thus, the σ - σ orbital interaction is stabilization, but it is still a driving force for distorting molecule. According to Equation (5-17), we have Equation (5-18),

$$E^{\text{DSI}}(\theta) - E^{\text{FUL}}(\theta) = [E^{\text{DSI}}(\theta) - E^{\text{PDSI}}(\theta)] + [E^{\text{PDSI}}(\theta) - E^{\text{FUL}}(\theta)] \quad (5-17)$$

$$\Delta E^{\sigma\sigma}(\theta) = \Delta E^{\sigma s}(\theta) + \Delta E_n^{\sigma\sigma}(\theta). \quad (5-18)$$

The energy effects $\Delta E^{\sigma s}(\theta)$ and the $\Delta E_n^{\sigma\sigma}(\theta)$ are two additive components of the $\Delta E^{\sigma\sigma}(\theta)$. For the $\theta = 0^\circ$ geometry of

Table 5-20. The RHF/STO-3G Values (hartree) of $\Delta E^{\sigma\sigma}(\theta)$ for Six Typical Substituted NBAs (FUL-2).

2-1	2-2	4-4	2-8	2-17	2-19
θ	(NBA)	(R1 = -NO ₂ ,)	(R2 = -OH)	(R1 = -OH, R2 = NO ₂)	(R3 = -OH, R4 = OH)
0	-0.35278	-0.35265	-0.34733	-0.34244	-0.32219
17	-0.35622	-0.35593	-0.35168	-0.34736	-0.32737
27	-0.36176	-0.36033	-0.35815	-0.35462	-0.33521
37	-0.36935	-0.36669	-0.36703	-0.36434	-0.34549
47	-0.37843	-0.37478	-0.37754	-0.37637	-0.35728
57	-0.38811	-0.38276	-0.38879	-0.38853	-0.37041
67	-0.39668	-0.38930	-0.39889	-0.40006	-0.38101
77	-0.40304	-0.39418	-0.40653	-0.40872	-0.38929
90	-0.40659	-0.39671	-0.41108	-0.41335	-0.39531

The conditional RHF/STO-3G calculation was performed on the B3LYP/6-311G** “Opt-geom” geometry.

Table 5-21. The RHF/STO-3G Values (hartree) of $\Delta E^{\sigma s}(\theta)$ for Six Typical Substituted NBAs.

2-1	2-2	2-4	2-8	2-17	2-19
θ	(NBA)	(R1 = -NO ₂ ,)	(R1 = -OH)	(R1 = -OH, R2 = NO ₂)	(R3 = -OH, R4 = -OH)
0	-0.42169	-0.42308	-0.41558	-0.41134	-0.38797
9	-0.42152	-0.42288	-0.41547	-0.41169	-0.38818
17	-0.42126	-0.42219	-0.41592	-0.41220	-0.38938
27	-0.42090	-0.42073	-0.41659	-0.41362	-0.39169
37	-0.42077	-0.41939	-0.41788	-0.41565	-0.39465
47	-0.42125	-0.41875	-0.41997	-0.41910	-0.39815
57	-0.42255	-0.41834	-0.42285	-0.42278	-0.40242
67	-0.42387	-0.41778	-0.42572	-0.42694	-0.40610
77	-0.42502	-0.41744	-0.42809	-0.43013	-0.40932
90	-0.42556	-0.41700	-0.42956	-0.43161	-0.41230

The conditional RHF/STO-3G calculation was performed on the “Opt-geom” geometry which is obtained from the relaxed PES-scan at B3LYP/6-311G** level). The brown color data mean that $d\Delta E^{\sigma s}(\theta)/d\theta > 0$, and blue color data do that $d\Delta E^{\sigma s}(\theta)/d\theta < 0$.

NBA at RHF/STO-3G level, for example, the energy effects (hartree) are as follows:

$$\Delta E_n^{\sigma\sigma}(0^\circ) = 0.06891$$

$$\Delta E^{\sigma s}(0^\circ) = -0.42169$$

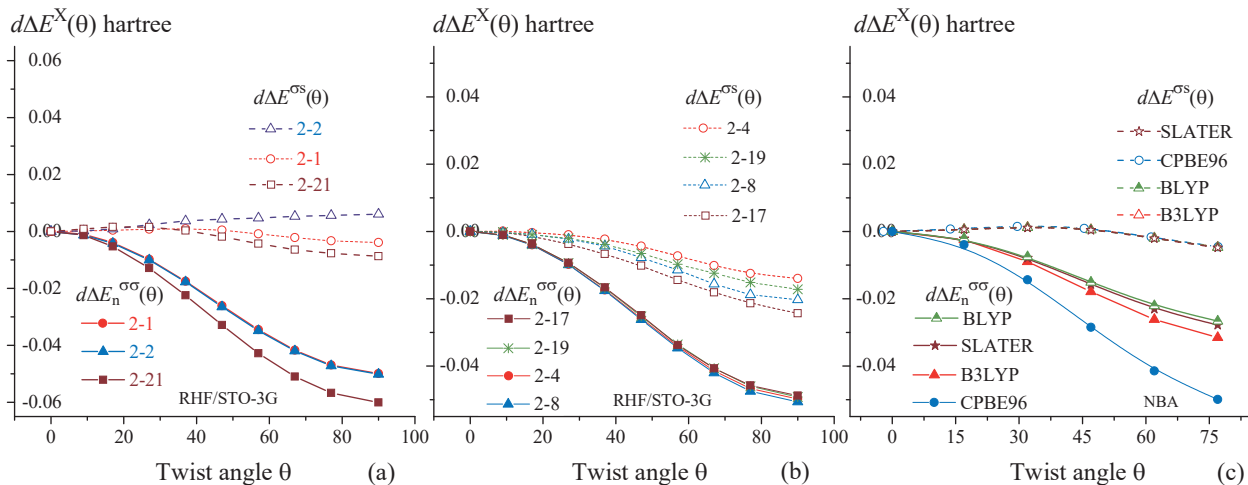


Figure 5-13. Energy effect differences, $d\Delta E_n^{\sigma\sigma}(\theta) = \Delta E_n^{\sigma\sigma}(\theta) - \Delta E_n^{\sigma\sigma}(0^\circ)$, and $d\Delta E^{\sigma s}(\theta) = \Delta E^{\sigma s}(\theta) - \Delta E^{\sigma s}(0^\circ)$, and their changes with the increasing of twist angle θ . (a) and (b) For substituted NBAs at RHF/STO-3G level. (c) For NBA at (CPBE96, B3LYP, BLYP and SLATER)/STO-3G levels

$$\Delta E^{\sigma s}(0^\circ) + \Delta E_n^{\sigma\sigma}(0^\circ) = -0.35278$$

$$\Delta E^{\sigma\sigma}(0^\circ) = -0.35278$$

$$\Delta E^{\sigma\sigma}(0^\circ) = \Delta E^{\sigma s}(0^\circ) + \Delta E_n^{\sigma\sigma}(0^\circ)$$

As a component of the stabilizing energy effect $\Delta E^{\sigma\sigma}(\theta)$, as described in the previous section, the $\Delta E_n^{\sigma\sigma}(\theta)$ is always destabilizing. According to the data listed in Table 5-21, the energy effect $\Delta E^{\sigma s}(\theta)$ is always stabilizing. Based on the comparison of the data listed in Table 5-19 and Table 5-21, $|\Delta E^{\sigma s}(\theta)| > \Delta E_n^{\sigma\sigma}(\theta)$. The $\Delta E^{\sigma s}(\theta)$ controls the sign and magnitude of the $\Delta E^{\sigma\sigma}(\theta)$. For the $\theta = 0^\circ$ geometry of NBA,

$$|\Delta E^{\sigma s}(\theta)|/\Delta E_n^{\sigma\sigma}(\theta) = |-0.42169|/(0.06891) \approx 6$$

$$\Delta E^{\sigma\sigma}(\theta)/\Delta E^{\sigma s}(\theta) = (-0.35278)/(-0.42169) = 0.84.$$

Interestingly, as shown by a comparison of the curves of functions $d\Delta E^{\sigma s}(\theta)$ and $d\Delta E_n^{\sigma\sigma}(\theta)$ in Figure 5-13,

$$|\Delta E^{\sigma s}(\theta) - \Delta E^{\sigma s}(0^\circ)| \ll [\Delta E_n^{\sigma\sigma}(\theta) - \Delta E_n^{\sigma\sigma}(0^\circ)],$$

In the case of molecules **2-1** (NBA), **2-2** ($R_1 = -NO_2$) and **2-21** ($R_1 = -NO_2$, $R_7 = -NH_2$) (Figure 5-13a), particularly, the first order derivative $d[d\Delta E^{\sigma s}(\theta)]/d\theta$ is almost a constant. During the molecular distortion, the effect of the molecular distortion on the molecular energy of the FUL state and the effect on the σ -s interaction are probably so small that $\Delta E^{\sigma s}(\theta)$ is almost a constant, and the σ driving force of molecular distortion mainly arises from the non-bonded σ - σ orbital interaction. For the NBA molecule at RHF/STO-3G, for example, $\Delta E^{\sigma s}(\theta)$ and $\Delta E_n^{\sigma\sigma}(\theta)$ can be fitted as the following polynomial functions:

$$\Delta E^{\sigma s}(\theta) = -0.42168 - (2.52053 \cdot 10^{-5})\theta + (5.06759 \cdot 10^{-6})\theta^2 - (1.31528 \cdot 10^{-7})\theta^3,$$

$$\Delta E_n^{\sigma\sigma}(\theta) = 0.06888 + (7.75005 \cdot 10^{-5})\theta - (2.04071 \cdot 10^{-5})\theta^2 + (1.4881 \cdot 10^{-7})\theta^3.$$

The ratio $|d\Delta E_n^{\sigma\sigma}(\theta)/d\theta|/|d\Delta E^{\sigma s}(\theta)/d\theta|$ are as follows:

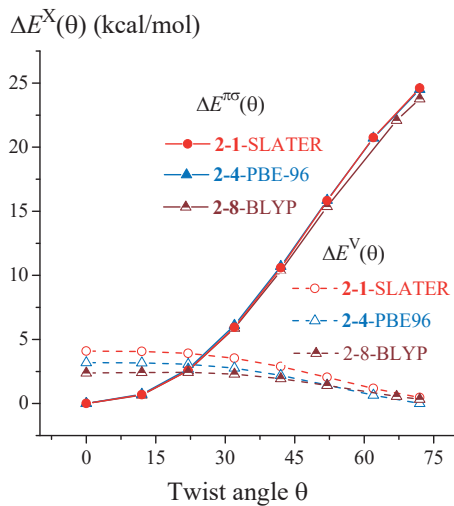


Figure 5-14. For molecules NBA (2-1), 2-4 and 2-8, the energy effects $\Delta E^V(\theta)$ (DSI-3) and $\Delta E^{\pi\sigma}(\theta)$ at 6-31G* level, and their change with increasing twist angle θ .

3.1 (0°), 9.9 (17°), 28.3 (27°), 31.6 (37°), 10.2 (47°), 6.2 (57°), 4.6 (67°).

Based on the comparison of the solid and dashed lines in Figure 5-13c, it is confirmed once again that Hartree-Fock cannot change the destabilizing feature of the energy effect $\Delta E_n^{\sigma\sigma}(\theta)$ although it can change the magnitude of the energy effect. Therefore, $\Delta E_n^{\sigma\sigma}(\theta)$ can be used instead of $\Delta E^{\sigma\sigma}(\theta)$ to describe the role of the σ - σ interaction in distorting molecular geometry.

In Figure 5-14, the energy effects, $\Delta E^{\pi\sigma}(\theta)$ and $\Delta E^V(\theta)$, are calculated at (SLATE, BLYP and PBE96)/6-31G* levels in order to minimize the effect of HF-EX on energy effect characteristics. The Figure shows that the resistance ($\Delta E^{\pi\sigma}(\theta) > 0$, $d\Delta E^{\pi\sigma}(\theta)/d\theta > 0$) to molecular distortion is much greater than the driving force ($\Delta E^V(\theta) > 0$, $d\Delta E^V(\theta)/d\theta < 0$) of molecular distortion. There should be another driving force in the molecule to balance that big resistance. As indicated by Figure 5-13, this other driving force comes from the energy effect $\Delta E_n^{\sigma\sigma}(\theta)$. As a driving force, the energy effect $\Delta E_n^{\sigma\sigma}(\theta)$ must be destabilizing. Therefore, the argument in this section is self-consistent.

5.5. SUMMARY

The five electronic states and the molecular energy difference between each pair of electronic states are summarized in Figure 5-15.

Of all electronic states, the FUL state is a very interesting and very important electronic states, and its molecular orbitals, $\{\Phi_i^{A-\pi}, \Phi_i^{B-\pi}, \Phi_i^{C-\pi}, \Phi_j^{A-\sigma}, \Phi_j^{B-\sigma}, \Phi_j^{C-\sigma}, \Phi_k^S\}^{FUL-3}$ or $\{\Phi_i^{A-\pi}, \Phi_i^{(B+C)-\pi}, \Phi_j^{A-\sigma}, \Phi_j^{(B+C)-\sigma}, \Phi_k^S\}^{FUL-2}$, can also be considered as a secondary LMO basis set. Based on the secondary LMO basis set, the conditional single-point energy calculations can also provide all the electronic states for the geometry of a specific confirmation.

In addition, the FUL state is also a very good reference electronic state. Except for the orbital interaction recovering the C1-N12 and C13-C15 single bonds, all the inter- and intra-fragment LFMO interactions have been set equal to zero, which exclude all the π - π , π - σ , non-bonded σ - σ , and σ -s interactions from between the fragments. Therefore, the change of the energy sum $E_{PQ}^{FUL}(\theta) = [E_e^{FUL}(\theta) + E_{N^{PQ}}(\theta)]$ with the increasing of twist angle θ reflects the change of molecular energy without orbital interaction between fragments, where $E_{N^{PQ}}(\theta)$ is nuclear repulsion between fragments A and (B+C). Except for molecule 2-1 (NBA), as shown by the curves in Figure 5-16a,

always $[E_{PQ}^{FUL}(\theta) - E_{PQ}^{FUL}(0^\circ)] > 0$ (P = A, Q = (B + C)).

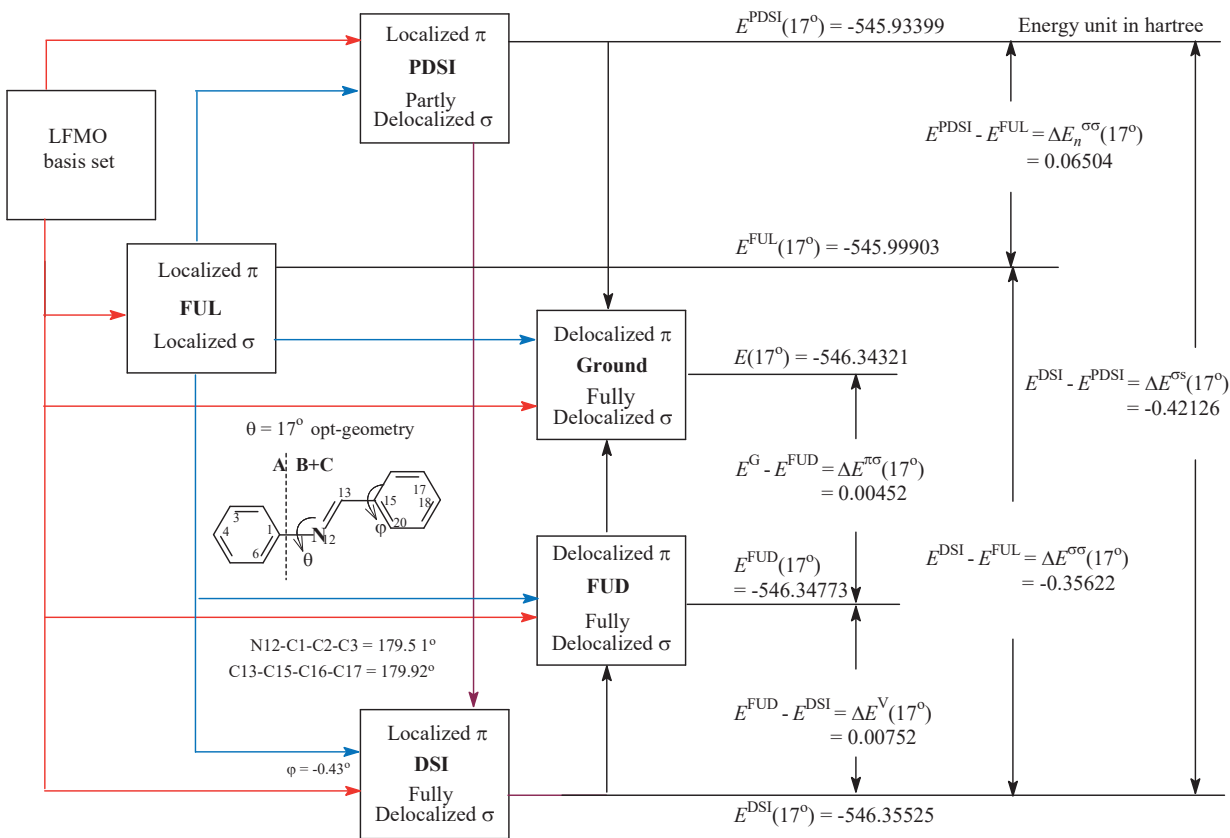


Figure 5-15. Thermodynamic cycle for the LFMO interactions between fragments A and (B+C) for the $\theta = 17^\circ$ geometry of NBA molecule at RHF/STO-3G level (energy unit in hartree).

For the $\theta = 27^\circ$ geometry of NBA at RHF/STO-3G level, for example,

$$([E_e^{FUL}(27^\circ) + E^{NPQ}(27^\circ)] - [E_e^{FUL}(0^\circ) + E^{NPQ}(0^\circ)]) = 0.01705 \text{ hartree} > 0.$$

The corresponding molecular energy difference at RHF/STO-3G level:

$$E(27^\circ) - E(0^\circ) = -556.88654 - 556.88543 = -0.00111 \text{ hartree} < 0.$$

This suggests that if there were no MO interaction between the fragments, due to steric hindrance, i.e. nuclear repulsion, between fragments A and (B + C) (Figure 2-5), the molecule, such as NBA and its derivatives, should tend to planar conformation. It can now be said with certainty that the π - π and σ - σ MO interactions (delocalization) between the fragments is the fundamental reason of the molecular distortion.

Of all the electronic states, only the FUL and PDIS electronic states must be constructed at the RHF/STO-3G level. As have been detailed in this Chapter, the π - π interaction and π - σ interactions are destabilization and these two interactions are, respectively, the driving force and resistance of molecular distortion. Fortunately, the role of these two interactions in molecular deformation has nothing to do with the theoretical level and with the basis set size, which once again confirms that the conclusion of the RHF/STO-3G calculation is reasonable.

Of all orbital interaction types, only the σ - σ interaction is stabilization, but its stabilizing feature is mainly determined by the σ - s interaction. In particular, it is still the driving force of molecular distortion.

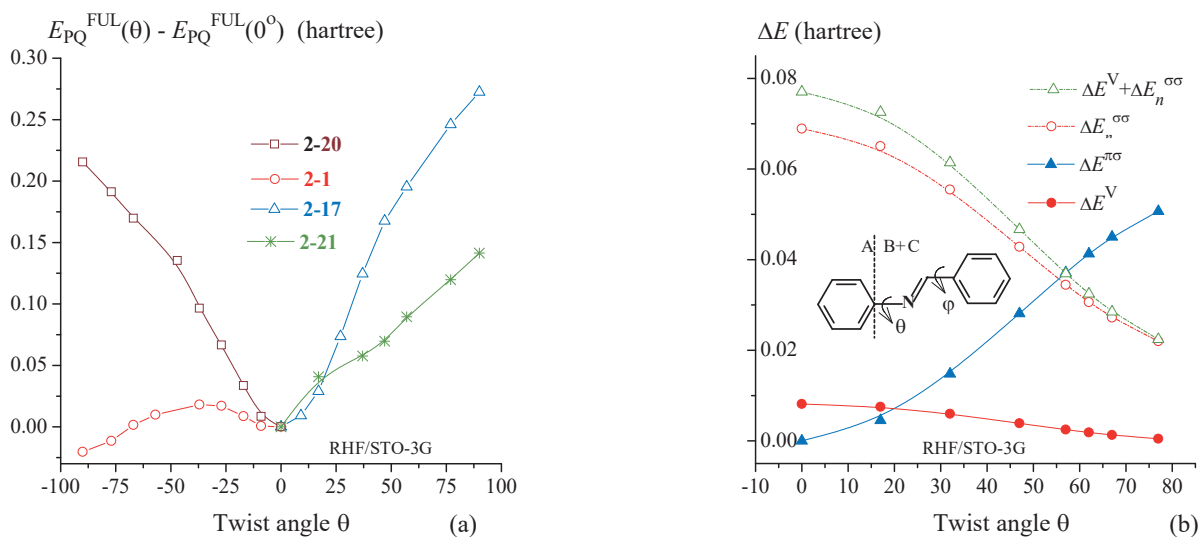


Figure 5-16. (a) For each of 4 typical substituted NBAs, the energy difference (hartree) between two twisted geometries, and its change with the increasing twist of angle θ , where $E_{\text{PQ}}^{\text{FUL}}(\theta) = [E_e^{\text{FUL}}(\theta) + E_{\text{NPO}}(\theta)]$. (b) Preferential geometry with the twist angle $\theta = 51.7^\circ$ is a compromise between the energy effects (hartree) associated with the $\pi\text{-}\pi$, non-bonded $\sigma\text{-}\sigma$, and $\pi\text{-}\sigma$ interactions between fragments A and (B+C).

Although the $\sigma\text{-}s$ interaction energy can determine the magnitude and sign of the $\sigma\text{-}\sigma$ interaction energy, but its first order derivative is so small that the non-bonded $\sigma\text{-}\sigma$ interaction can be used to describe the role of the full $\sigma\text{-}\sigma$ interaction in distorting molecule.

Of the three orbital interaction types, as shown in Figure 5-16b, the capability of the $\pi\text{-}\pi$ interaction to drive molecular distortion is the smallest, the driving force of molecular distortion comes mainly from the non-bonding $\sigma\text{-}\sigma$ interaction. The resistance to distortion comes from the $\pi\text{-}\sigma$ interaction between fragments A and (B+C). At about $\theta = 57^\circ$ geometry, the total driving force reaches equilibrium with resistance. For N-benzylideneaniline at B3LYP/6-311G** level, the total electron energy $E_e(\theta) < 0$, it is a monotonically decreasing function of twist angle, $dE_e(\theta)/d\theta < 0$, the total electron energy is minimum (the absolute value is the greatest) when $\theta = 51.7^\circ$, $dE_e(51.7^\circ)/d\theta = 0$ (Table 2-5), this twist angle is very close to that ($\theta = 57^\circ$) of the conformation that is the result of a compromise between the non-bonded $\sigma\text{-}\sigma$, $\pi\text{-}\pi$ and $\pi\text{-}\sigma$ interactions.

It can now be clearly answered that this is the result of the destabilizing electron delocalization, facing the following conclusions obtained from the relaxed PES-scans by Gaussian software package (Chapter 2):

$$dE_e(\theta)/d\theta < 0, dE_N(\theta)/d\theta > 0$$

Therefore, contrary to the classical view, the distortion of NBA-like species is not intended to achieve higher stability, but to make the molecule itself to be less destabilized as far as possible.

Due to the low localization degree, the NBO basis set cannot be used to calculate the energy effect associated with the MO interaction between the fragments.

5.6. APPENDIX

Table 5-1. For the $\theta = 32^\circ$ and 0° Geometries Of N-benzylideneaniline at B3LYP/6-31G* Level, 8 π -LC-NAO NBOs Belonging to Fragment B.

130	C13(3d5)	-0.0058	0.0000	0.0000	0.0000	0.0000	0.0000	0.0000	0.0000
131	H14(1s)	0.0000	0.0000	0.0000	0.0000	0.0000	0.0000	0.0000	0.0000
132	H14(2s)	0.0000	0.0000	0.0000	0.0000	0.0000	0.0000	0.0000	0.0000
Fragment C									
133	C15(1s)	0.0000	0.0000	0.0000	0.0000	0.0000	0.0000	0.0000	0.0000

Table 5-17. Four typical LC-LFMO MOs and Four typical LC-AO MOs in the FUL-3 State of the $\theta = 17^\circ$ Geometry of NBA at RHF/STO-3G level.

LFMO	7-th Φ_t	15-th Φ_t	26-th Φ_t	43-th Φ_t	AO	7-th Φ_t	15-th Φ_t	26-th Φ_t	43-th Φ_t	
	$\Phi_j^{C-\sigma}$	Φ_w^S	$\Phi_j^{A-\sigma}$	$\Phi_l^{B-\pi}$		$\Phi_j^{C-\sigma}$	Φ_w^S	$\Phi_j^{A-\sigma}$	$\Phi_l^{B-\pi}$	
1	0.000000	0.000000	-0.000011	0.000000	1C	1s	0.000000	-0.038382	0.085036	0.000000
2	0.000000	0.000000	0.000003	0.000000	1	2s	0.000000	0.347817	-0.197117	0.000000
3	0.000000	0.000000	0.000013	0.000000	1	2px	0.000000	-0.259917	-0.244877	0.000000
4	0.000000	0.000000	0.000034	0.000000	1	2py	0.000000	0.000000	0.000000	0.000000
5	0.000000	0.000000	0.000048	0.000000	1	2pz	0.000000	-0.191941	-0.157566	0.000000
6	0.000000	0.000000	-0.000032	0.000000	2C	1s	0.000000	0.000201	-0.010053	0.000000
7	0.000000	0.000000	0.012075	0.000000	2	2s	0.000000	0.006286	0.032827	0.000000
8	0.000000	0.000000	0.003000	0.000000	2	2px	0.000000	0.031959	-0.030473	0.000000
9	0.000000	0.000000	-0.032298	0.000000	2	2py	0.000000	0.000000	0.000000	0.000000
10	0.000000	0.000000	0.001774	0.000000	2	2pz	0.000000	-0.006470	0.265508	0.000000
11	0.000000	0.000000	0.998259	0.000000	3C	1s	0.000000	-0.000038	-0.066717	0.000000
12	0.000000	0.000000	-0.017652	0.000000	3	2s	0.000000	-0.005475	0.207755	0.000000
13	0.000000	0.000000	0.038075	0.000000	3	2px	0.000000	0.004270	-0.143954	0.000000
14	0.000000	0.000000	0.013333	0.000000	3	2py	0.000000	0.000000	0.000000	0.000000
15	0.000000	0.000000	0.005719	0.000000	3	2pz	0.000000	-0.000769	0.159398	0.000000
16 π	0.000000	0.000000	0.000000	0.000000	4C	1s	0.000000	-0.000201	0.070156	0.000000
17	0.000000	0.000000	0.016669	0.000000	4	2s	0.000000	-0.000474	-0.209685	0.000000
18	0.000000	0.000000	-0.000627	0.000000	4	2px	0.000000	-0.002375	0.000831	0.000000
19 π	0.000000	0.000000	0.000000	0.000000	4	2py	0.000000	0.000000	0.000000	0.000000
20 π	0.000000	0.000000	0.000000	0.000000	4	2pz	0.000000	-0.001188	-0.017294	0.000000
21 singly	0.000000	-0.465485	0.000000	0.000000	5C	1s	0.000000	-0.000175	-0.075286	0.000000
22	0.000000	0.000000	0.000000	0.000000	5	2s	0.000000	-0.003632	0.234401	0.000000
23	0.000000	0.000000	0.000000	0.000000	5	2px	0.000000	-0.000175	0.083809	0.000000
24	0.000000	0.000000	0.000000	0.000000	5	2py	0.000000	0.000000	0.000000	0.000000
25	0.000000	0.000000	0.000000	0.000000	5	2pz	0.000000	0.004417	-0.187443	0.000000
26 π	0.000000	0.000000	0.000000	0.999938	6C	1s	0.000000	0.001051	-0.002127	0.000000
27	0.000000	0.000000	0.000000	0.000000	6	2s	0.000000	-0.009419	0.006691	0.000000
28 singly	0.000000	0.594534	0.000000	0.000000	6	2px	0.000000	0.016756	0.209353	0.000000

29 singly	0.000000	0.119919	0.000000	0.000000	6	2py	0.000000	0.000000	0.000000	0.000000
30	0.984632	0.000000	0.000000	0.000000	6	2pz	0.000000	0.024075	-0.142266	0.000000
31	-0.143803	0.000000	0.000000	0.000000	7H	1s	0.000000	0.015881	0.120718	0.000000
32	-0.097995	0.000000	0.000000	0.000000	8H	1s	0.000000	0.001104	0.184926	0.000000
33	0.002690	0.000000	0.000000	0.000000	9H	1s	0.000000	0.001077	-0.092342	0.000000
34	-0.014482	0.000000	0.000000	0.000000	10H	1s	0.000000	0.001137	0.197205	0.000000
35	0.000031	0.000000	0.000000	0.000000	11H	1s	0.000000	0.021536	0.096416	0.000000
36	-0.000014	0.000000	0.000000	0.000000	12N	1s	0.000000	-0.051489	0.000000	0.000000
37	0.000001	0.000000	0.000000	0.000000	12	2s	0.000000	0.434539	0.000000	0.000000
38	-0.000018	0.000000	0.000000	0.000000	12	2px	0.000000	0.341393	0.000000	0.108246
39	-0.000002	0.000000	0.000000	0.000000	12	2py	0.000000	-0.002851	0.000000	0.610703
40	-0.000007	0.000000	0.000000	0.000000	12	2pz	0.000000	0.231468	0.000000	-0.152131
41	-0.000007	0.000000	0.000000	0.000000	13C	1s	0.000000	-0.011967	0.000000	0.000000
42	0.000003	0.000000	0.000000	0.000000	13	2s	0.000000	0.110169	0.000000	0.000000
43	0.000001	0.000000	0.000000	0.000000	13	2px	0.000000	-0.054012	0.000000	0.108122
44	-0.000002	0.000000	0.000000	0.000000	13	2py	0.000000	-0.010982	0.000000	0.610008
45 π	0.000000	0.000000	0.000000	0.000000	13	2pz	0.000000	-0.082516	0.000000	-0.151958
46	0.000001	0.000000	0.000000	0.000000	14H	1s	0.000000	0.029570	0.000000	0.000000
47	-0.000002	0.000000	0.000000	0.000000	15C	1s	0.000716	-0.008806	0.000000	0.000000
48 π	0.000000	0.000000	0.000000	0.000000	15	2s	0.000113	0.079779	0.000000	0.000000
49 π	0.000000	0.000000	0.000000	0.000000	15	2px	0.000095	0.060109	0.000000	0.000000
50 singly	0.000000	0.106495	0.000000	0.000000	15	2py	0.000015	-0.000005	0.000000	0.000000
51 π	0.000000	0.000000	0.000000	0.000000	15	2pz	0.000129	0.042749	0.000000	0.000000
52 π	0.000000	0.000000	0.000000	0.000000	16C	1s	-0.004765	0.000141	0.000000	0.000000
52 π	0.000000	0.000000	0.000000	0.000000	16	1s	-0.004765	0.000141	0.000000	0.000000
53 π	0.000000	0.000000	0.000000	0.000000	16	2s	-0.000070	-0.000116	0.000000	0.000000
54	0.000000	0.000000	-0.001921	0.000000	16	2px	0.000067	-0.007109	0.000000	0.000000
55	0.000000	0.000000	0.000381	0.000000	16	2py	-0.000019	0.001232	0.000000	0.000000
56	0.000000	0.000000	-0.003178	0.000000	16	2pz	-0.000029	-0.000114	0.000000	0.000000
57	0.000000	0.000000	-0.001408	0.000000	17C	1s	0.018292	-0.000023	0.000000	0.000000
58	0.000000	0.000000	0.000517	0.000000	17	2s	-0.006390	-0.001112	0.000000	0.000000
59	0.000000	0.000000	-0.002878	0.000000	17	2px	0.003897	-0.000953	0.000000	0.000000
60	0.000000	0.000000	0.000198	0.000000	17	2py	-0.001157	0.000231	0.000000	0.000000
61	0.000000	0.000000	0.000677	0.000000	17	2pz	-0.001870	0.000247	0.000000	0.000000
62	0.000000	0.000000	-0.000324	0.000000	18C	1s	0.991506	-0.000050	0.000000	0.000000
63	0.000000	0.000000	0.000214	0.000000	18	2s	0.036023	-0.000097	0.000000	0.000000
64	0.000000	0.000000	0.001808	0.000000	18	2px	0.000860	0.000534	0.000000	0.000000
65 π	0.000000	0.000000	0.000000	0.011135	18	2py	-0.000003	-0.000007	0.000000	0.000000
66	0.000000	0.000000	0.000000	0.000000	18	2pz	0.000601	0.000354	0.000000	0.000000

67	0.000000	0.000000	0.000000	0.000000	19C	1s	0.027070	-0.000027	0.000000	0.000000
68 π	0.000000	0.000000	0.000000	0.000000	19	2s	-0.006039	-0.001010	0.000000	0.000000
69 π	0.000000	0.000000	0.000000	0.000000	19	2px	-0.000225	-0.000053	0.000000	0.000000
70 π	0.000000	0.000000	0.000000	0.000000	19	2py	0.001127	-0.000233	0.000000	0.000000
71	0.000006	0.000000	0.000000	0.000000	19	2pz	0.004365	-0.000974	0.000000	0.000000
72	-0.000002	0.000000	0.000000	0.000000	20C	1s	-0.018120	0.000176	0.000000	0.000000
73	-0.000001	0.000000	0.000000	0.000000	20	2s	-0.000624	-0.000856	0.000000	0.000000
74	-0.000018	0.000000	0.000000	0.000000	20	2px	0.000024	-0.003076	0.000000	0.000000
75	0.000001	0.000000	0.000000	0.000000	20	2py	0.000027	-0.000990	0.000000	0.000000
76	-0.000007	0.000000	0.000000	0.000000	20	2pz	0.000123	-0.006165	0.000000	0.000000
77	0.000001	0.000000	0.000000	0.000000	21H	1s	-0.000050	0.004193	0.000000	0.000000
78	-0.000006	0.000000	0.000000	0.000000	22H	1s	-0.000039	0.000268	0.000000	0.000000
79	-0.000006	0.000000	0.000000	0.000000	23H	1s	-0.006820	0.000257	0.000000	0.000000
80	-0.000004	0.000000	0.000000	0.000000	24H	1s	-0.000096	0.000263	0.000000	0.000000
81	0.000006	0.000000	0.000000	0.000000	25H	1s	0.000037	0.004325	0.000000	0.000000

Table 5-18. Four typical LC-LFMO MOs and Four typical LC-AO MOs in the PDSI-3 state of the $\theta = 17^\circ$ Geometry of NBA at RHF/STO-3G level.

LFMO	15-th Φ_t	43-th Φ_t	38-th Φ_t	39-th Φ_t	AO		15-th Φ_t	38-th Φ_t	39-th Φ_t	43-th Φ_t
	Φ_w^S	$\Phi_m^{B-\pi}$	Φ_n^σ	$\Phi_m^{B-\pi}$	1C	1s	Φ_w^S	Φ_n^σ	$\Phi_m^{C-\pi}$	$\Phi_m^{B-\pi}$
1	0.000000	0.000000	0.000000	0.000000	1C	1s	-0.038266	0.021316	0.000000	0.000000
2	0.000000	0.000000	0.000003	0.000000	1	2s	0.346763	-0.020118	0.000000	0.000000
3	0.000000	0.000000	-0.000005	0.000000	1	2px	-0.259129	-0.143216	0.000000	0.000000
4	0.000000	0.000000	-0.000029	0.000000	1	2py	0.000000	0.000000	0.000000	0.000000
5	0.000000	0.000000	0.000069	0.000000	1	2pz	-0.191359	-0.089613	0.000000	0.000000
6	0.000000	0.000000	-0.001041	0.000000	2C	1s	0.000201	-0.013715	0.000000	0.000000
7	0.000000	0.000000	-0.000692	0.000000	2	2s	0.006267	0.040908	0.000000	0.000000
8	0.000000	0.000000	0.001571	0.000000	2	2px	0.031862	0.289356	0.000000	0.000000
9	0.000000	0.000000	-0.001362	0.000000	2	2py	0.000000	0.000000	0.000000	0.000000
10	0.000000	0.000000	0.004306	0.000000	2	2pz	-0.006451	0.152462	0.000000	0.000000
11	0.000000	0.000000	-0.011530	0.000000	3C	1s	-0.000038	0.004693	0.000000	0.000000
12	0.000000	0.000000	0.001621	0.000000	3	2s	-0.005459	-0.023256	0.000000	0.000000
13	0.000000	0.000000	0.002128	0.000000	3	2px	0.004257	-0.302704	0.000000	0.000000
14	0.000000	0.000000	-0.016349	0.000000	3	2py	0.000000	0.000000	0.000000	0.000000
15	0.000000	0.000000	0.014688	0.000000	3	2pz	-0.000767	-0.133002	0.000000	0.000000
16 π	0.000000	0.000000	0.000000	0.000000	4C	1s	-0.000201	0.009725	0.000000	0.000000
17	0.000000	0.000000	0.990929	0.000000	4	2s	-0.000473	-0.022359	0.000000	0.000000
18	0.000000	0.000000	0.083131	0.000000	4	2px	-0.002368	0.306900	0.000000	0.000000
19 π	0.000000	0.000000	0.000000	0.000000	4	2py	0.000000	0.000000	0.000000	0.000000

20 π	0.000000	0.000000	0.000000	0.000000	4	2pz	-0.001185	0.182096	0.000000	0.000000
21 singly	-0.464074	0.000000	0.000000	0.000000	5C	1s	-0.000175	0.004622	0.000000	0.000000
22	0.000000	0.000000	-0.006182	0.000000	5	2s	-0.003621	-0.022579	0.000000	0.000000
23	0.000000	0.000000	-0.000706	0.000000	5	2px	-0.000175	-0.265105	0.000000	0.000000
24	0.000000	0.000000	0.023717	0.000000	5	2py	0.000000	0.000000	0.000000	0.000000
25	0.000000	0.000000	0.074762	0.000000	5	2pz	0.004404	-0.199999	0.000000	0.000000
26 π	0.000000	0.999905	0.000000	0.000000	6C	1s	0.001047	-0.014091	0.000000	0.000000
27	0.000000	0.000000	0.044473	0.000000	6	2s	-0.009390	0.041502	0.000000	0.000000
28 singly	0.595671	0.000000	0.000000	0.000000	6	2px	0.016705	0.273998	0.000000	0.000000
29 singly	0.120437	0.000000	0.000000	0.000000	6	2py	0.000000	0.000000	0.000000	0.000000
30	0.000000	0.000000	0.000000	0.000000	6	2pz	0.024002	0.180271	0.000000	0.000000
31	0.000000	0.000000	0.000003	0.000000	7H	1s	0.015833	-0.152184	0.000000	0.000000
32	0.000000	0.000000	-0.000003	0.000000	8H	1s	0.001101	-0.146719	0.000000	0.000000
33	0.000000	0.000000	0.000098	0.000000	9H	1s	0.001074	0.359332	0.000000	0.000000
34	0.000000	0.000000	-0.000067	0.000000	10H	1s	0.001133	-0.148607	0.000000	0.000000
35	0.000000	0.000000	-0.000028	0.000000	11H	1s	0.021470	-0.154826	0.000000	0.000000
36	0.000000	0.000000	0.000238	0.000000	12N	1s	-0.051587	0.005086	0.000000	0.000000
37	0.000000	0.000000	-0.004571	0.000000	12	2s	0.435370	-0.040651	0.000000	0.000000
38	0.000000	0.000000	-0.000931	0.000000	12	2px	0.342056	0.013918	0.000000	0.108609
39	0.000000	0.000000	-0.012473	0.000000	12	2py	-0.002854	0.011142	0.000000	0.612752
40	0.000000	0.000000	-0.000444	0.000000	12	2pz	0.231926	0.054633	0.000000	-0.152641
41	0.000000	0.000000	0.004871	0.000000	13C	1s	-0.012014	-0.004586	0.000000	0.000000
42	0.000000	0.000000	-0.007471	0.000000	13	2s	0.110598	0.014900	0.000000	0.000000
43	0.000000	0.000000	-0.036740	0.000000	13	2px	-0.054274	-0.011500	0.000000	0.107758
44	0.000000	0.000000	-0.005048	0.000000	13	2py	-0.011004	0.009898	0.000000	0.607954
45 π	0.000000	0.000000	0.000000	0.998989	13	2pz	-0.082791	0.031551	0.000000	-0.151446
46	0.000000	0.000000	0.038998	0.000000	14H	1s	0.029629	0.014792	0.000000	0.000000
47	0.000000	0.000000	0.033121	0.000000	15C	1s	-0.008831	0.001218	0.000000	0.000000
48 π	0.000000	0.000000	0.000000	-0.013882	15	2s	0.080004	-0.001916	0.000000	0.000000
49 π	0.000000	0.000000	0.000000	0.038608	15	2px	0.060278	0.005767	0.060141	0.000000
50 singly	0.106795	0.000000	0.000000	0.000000	15	2py	-0.000005	0.000089	0.339300	0.000000
51 π	0.000000	0.000000	0.000000	0.000000	15	2pz	0.042870	0.004462	-0.084522	0.000000
52 π	0.000000	0.000000	0.000000	0.000000	16C	1s	0.000141	-0.002609	0.000000	0.000000
53 π	0.000000	0.000000	0.000000	0.000000	16	2s	-0.000116	0.009754	0.000000	0.000000
54	0.000000	0.000000	0.000989	0.000000	16	2px	-0.007129	0.006153	0.054629	0.000000
55	0.000000	0.000000	-0.001710	0.000000	16	2py	0.001235	-0.002547	0.308207	0.000000
56	0.000000	0.000000	0.003689	0.000000	16	2pz	-0.000115	-0.005847	-0.076777	0.000000
57	0.000000	0.000000	0.001723	0.000000	17C	1s	-0.000023	0.001277	0.000000	0.000000
58	0.000000	0.000000	0.000757	0.000000	17	2s	-0.001115	-0.005061	0.000000	0.000000
59	0.000000	0.000000	-0.004111	0.000000	17	2px	-0.000956	-0.005445	0.055098	0.000000

60	0.000000	0.000000	0.002189	0.000000	17	2py	0.000231	0.003467	0.310852	0.000000
61	0.000000	0.000000	0.000763	0.000000	17	2pz	0.000248	0.010042	-0.077435	0.000000
62	0.000000	0.000000	-0.000265	0.000000	18C	1s	-0.000050	0.000022	0.000000	0.000000
63	0.000000	0.000000	0.001409	0.000000	18	2s	-0.000097	0.000466	0.000000	0.000000
64	0.000000	0.000000	0.000759	0.000000	18	2px	0.000536	-0.001059	0.055701	0.000000
65 π	0.000000	0.013801	0.000000	0.000000	18	2py	-0.000007	-0.005648	0.314256	0.000000
66	0.000000	0.000000	-0.003734	0.000000	18	2pz	0.000355	-0.023425	-0.078283	0.000000
67	0.000000	0.000000	0.004800	0.000000	19C	1s	-0.000027	-0.000367	0.000000	0.000000
68 π	0.000000	0.000000	0.000000	0.015568	19	2s	-0.001013	0.001308	0.000000	0.000000
69 π	0.000000	0.000000	0.000000	-0.003897	19	2px	-0.000053	0.013629	0.056716	0.000000
70 π	0.000000	0.000000	0.000000	0.008979	19	2py	-0.000234	0.003756	0.319980	0.000000
71	0.000000	0.000000	-0.000442	0.000000	19	2pz	-0.000977	0.024777	-0.079709	0.000000
72	0.000000	0.000000	-0.000080	0.000000	20C	1s	0.000176	0.000474	0.000000	0.000000
73	0.000000	0.000000	-0.000417	0.000000	20	2s	-0.000858	-0.002655	0.000000	0.000000
74	0.000000	0.000000	0.000487	0.000000	20	2px	-0.003085	-0.018816	0.057676	0.000000
75	0.000000	0.000000	0.001760	0.000000	20	2py	-0.000993	-0.001214	0.325399	0.000000
76	0.000000	0.000000	-0.000085	0.000000	20	2pz	-0.006182	-0.018260	-0.081059	0.000000
77	0.000000	0.000000	0.001183	0.000000	21H	1s	0.004205	0.008895	0.000000	0.000000
78	0.000000	0.000000	-0.000977	0.000000	22H	1s	0.000269	-0.013944	0.000000	0.000000
79	0.000000	0.000000	-0.000305	0.000000	23H	1s	0.000257	0.014630	0.000001	0.000000
80	0.000000	0.000000	0.000702	0.000000	24H	1s	0.000263	-0.000141	0.000000	0.000000
81	0.000000	0.000000	0.000141	0.000000	25H	1s	0.004337	-0.017880	0.000000	0.000000

5.7. REFERENCES

- 1 Bao, P.; Yu, Z. H. 2006. "Theoretical Studies on the Role of π -Electron Delocalization in Determining the Conformation of N-benzylideneaniline with Three Types of LMO Basis Sets." *J. Comput. Chem.*, 27: 809-824.
- 2 Paddon-Row, M. N. 1982. "Some Aspects of Orbital Interactions through Bonds: Physical and Chemical Consequences." *Acc. Chem. Res.*, 15: 245-251.
- 3 Kollma, H. 1979. "Direct Calculation of Resonance Energies of Conjugated Hydrocarbons with ab Initio MO Methods." *J. Am. Chem. Soc.*, 101: 4832-4840.
- 4 Behrens, S.; Köster, A. M.; Jug, K. 1994. "Delocalization Energy of π Electrons as an Index for Aromaticity of Polycyclic Hydrocarbons." *J. Org. Chem.*, 59: 2546-2551.
- 5 Whangbo, M. H.; Schlegel, H. B.; Wolfe, S. 1997. "Molecular Orbitals from Group Orbitals. 3. Quantitative Perturbational Molecular Orbital Analysis of ab Initio SCF-MO Wave Functions." *J. Am. Chem. Soc.*, 99: 1296-1304.
- 6 Epiotis, N. D.; Cherry, W. R.; Shaik, S.; Yates, R.; Bernardi, F. 1977. *Topics in Current Chemistry*; Vol. 70. New York: Springer.
- 7 Salem, L. 1968. " Intermolecular Orbital Theory of the Interaction between Conjugated Systems. I. General Theory." *J. Am. Chem. Soc.*, 90: 543-552.

- 8 Bader, R. F. W.; Streitwieser, A.; Neuhaus, A.; Laidig, K. E.; Speers, P. 1996. "Electron Delocalization and the Fermi Hole." *J. Am Chem. Soc.*, 118: 4959-4965.
- 9 Bader, R. F. W.; Stephens, M. E. 1975. "Spatial Localization of the Electronic Pair and Number Distributions in Molecules." *J. Am Chem. Soc.*, 97: 7391-7399.
- 10 Kitaura, K.; Morokuma, K. 1976. "A New Energy Decomposition Scheme for Molecular Interactions within the Hartree-Fock Approximation." *Int. J. Quantum Chem.*, 10: 325-340.
- 11 Bao, P.; Yu, Z. H. 2007. "Restricted Geometry Optimization: A Different Way to Estimate Stabilization Energies for Aromatic Molecules of Various Types." *J. Phys. Chem. A*, 111: 5304-5213
- 12 Bao, P.; Yu, Z. H. 2011. "New Procedure to Evaluate Aromaticity at the Density Functional Theory, Hartree-Fock, and Post-Self-Consistent Field Levels." *J. Comput. Chem.*, 32: 248-259.
- 13 Yu, Z. H.; Li, L. T.; Fu, W.; Li, L. P. 1998. "Conformations of Stilbene-like Species and New Method of Energy Partition." *J. Phys. Chem. A*, 102: 2016-2018.
- 14 Xu, H. 2004. "The Driving Forces for Distorting NBA-like Species away from the Planar Geometries and Their Substituent Effect." PhD Diss., Institute of Chemistry, ACS, Beijing.

CHAPTER 6

RESTRICTED GEOMETRY OPTIMIZATION

ABSTRACT

For a planar conjugated molecule (ground state energy $E(G)$), a localized GL geometry (molecular energy $E(GL)$) and a set of the locally delocalized GE-m geometries ($m = 1, 2, \dots, k$) (molecular energies $E(GE-m)$) are optimized by conditionally deleting the Fock and overlap integral matrix elements between the double bonds (or groups). For acyclic polyene, the adiabatic delocalization energy $\Delta E^A = [E(G) - E(GL)] > 0$ (destabilizing), the energy effects $\Delta E^{Am} = E(GE-m) - E(GL) > 0$ (destabilizing), and $\Delta E^A \approx \sum \Delta E^{Am}$, indicating that ΔE^{Am} are additive. For an aromatic molecule, $\Delta E^A < 0$ (stabilizing), also $\Delta E^{Am} > 0$, and $\Delta E^A \neq \sum \Delta E^{Am}$. Due to the additivity of ΔE^{Am} , the equation, $[E(EG) - E(GL)] = \sum \Delta E^{Am}$, is defined, where $E(EG)$ is the molecular energy of the virtual reference molecule. In the case of aromatic molecule, therefore, $\Delta E^A - \sum \Delta E^{Am} = [E(G) - E(GL)] - [E(EG) - E(GL)] = [E(G) - E(EG)] < 0$ (stabilizing). Accordingly, $[\Delta E^A - \sum \Delta E^{Am}]$ is the molecular energy difference $[E(G) - E(EG)]$ between an aromatic molecule and its virtual reference molecule, and it can be defined as the extra stabilization energy (ESE) (aromatic stabilization energy) of an aromatic molecule. For benzene at B3LYP/6-31G* level, $ESE = \Delta E^A - \sum \Delta E^{Am} = -39.0$ kcal/mol, close to the experimental value of -36 kcal/mol. For furan-like species, however, $\Delta E^A > 0$ (destabilizing), $\Delta E^{Am} > 0$, and $\Delta E^A - \sum \Delta E^{Am} < 0$. In this case, $\Delta E^A - \sum \Delta E^{Am}$ should be defined as the less destabilizing energy (LDE) of a furan-like species. ESE and LDE should be two different physical quantities, and there is no comparability. Furan-like species cannot be considered aromatic. Our 2007 method has been used to calculate the ESEs of the following types of aromatic molecules: benzene-like species, furan-like species, and substituted benzenes. The size orders (kcal/mol) of ESEs are as follows: -39.0 (benzene) > -38.5 (pyridine) > -37.8 (pyrazine) > -37.5 (pyrimidine) > -36.1 (1,3,5-triazine) > -32.6 (pyridazine) > -32.2 (tetrazine); -39.0 (benzene) > -38.3 (fluorobenzene) > -38.1 (phenol) > -38.0 (chloro-benzene) > -37.6 (nitro-benzene) > -37.3 (cyanobenzene) > -35.5 (aniline) (benzene is the most stable); -53.1 (2-aza-pyrrole) > -49.4 (pyrrole) > -46.5 (imidazole) > -39.3 (furan) > -39.0 (benzene) > -39.0 (2-aza-furan) > -36.3 (oxazole). Our 2007 method can also be used to quantitatively distinguish between conjugation effect and inductive effect, and meanwhile it has been demonstrated that conjugation between the substituent and benzene ring is always distortive. In short, using our 2007 method (and our 2001 method and our 2014 method), the aromatic stabilizing energies for various types of aromatic molecules can be theoretically and accurately evaluated without needing for the help of any empirical and semi-empirical parameters.

yuzh@iccas.ac.cn

Key words: restricted geometry optimization; extra stabilization energy of an aromatic molecule; additivity of energy effects; benzene-like species; substituted benzene; furan-like species; conjugation and inductive effects.

6.0. FOREWORDS

In chapter 4 and Chapter 5, the following conclusions have been detailed: in NBA-like species such as substituted NBAs:

- (i) Conjugation interaction between an aromatic ring $-Ar$ and its substituent ($-N=CH-Ar'$) is destabilization, and it is a driving force of molecular distortion.
- (ii) Nuclear repulsion between fragments ($Ar'-CH=N-$) and $-Ar$ is resistance to molecular distortion.

These conclusions strongly question the following two fundamental principles of organic chemistry: "steric hindrance destabilization" and "conjugation stabilization". In the subsequent chapters, using our 2007 method and our 2011 method,¹⁻⁵ will continue to demonstrate that, for a conjugated hydrocarbon molecule, the conjugation between two conjugated groups is destabilization. In a specific molecule such as butadiene substituted with the heteroatom group(s), whether the conjugation energy between the two double bonds is destabilization or stabilization depends on the electron occupancy (electron-rich or electron-deficiency) of the substituent(s).

However, "conjugation stabilization" is one of the fundamental principles of organic chemistry, and it seems to be based on the experimental results. We must first argue that the so-called experimental evidence is questionable in order to prove that our questioning of the basic principles is reasonable and necessary. Otherwise, the discussion and conclusions in this book are meaningless, because reliable experimental facts cannot be denied.

6.0.1. So-called Evidence of Conjugation Stabilization

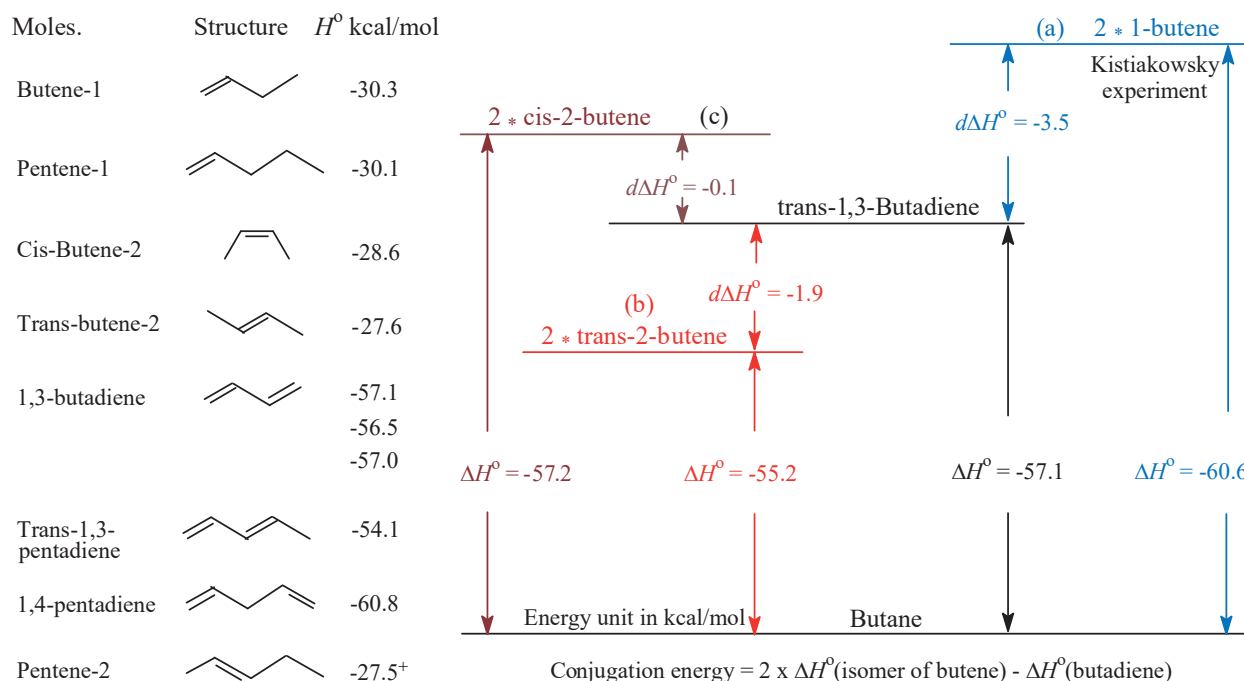


Figure 6-1. For trans-1,3-butadiene, the determination of the conjugation energy depends on the choice of reference molecule: (a) The reference molecule is 1-butene. (b) The reference molecule is trans-2-butene. (c) The reference molecule is cis-2-butene.

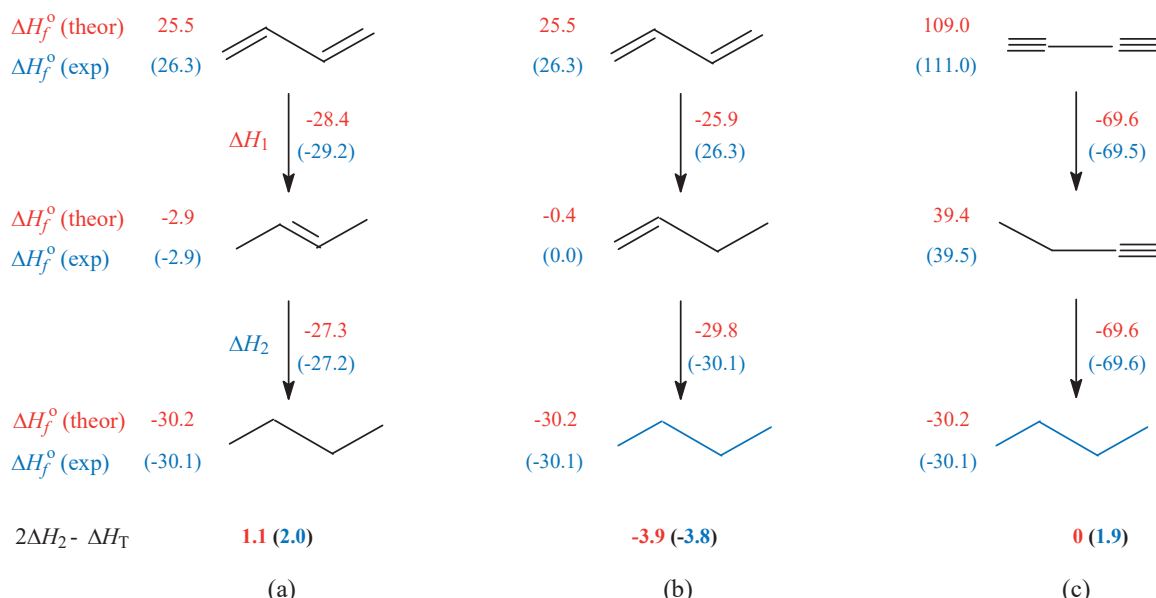


Figure 6-II. The determination of conjugation energy. (a) and (b) The hydrogenation heat difference (kcal/mol), $2\Delta H_2 - \Delta H_T$, between trans-1,3-butadiene and two butenes. (c) Between 1,3-butadiyne and the two butynes, where $\Delta H_T = \Delta H_2 + \Delta H_1$; ΔH_f° (exp) and ΔH_f° (theor) are, respectively, the experimental and theoretical values (kcal/mol) of the formation enthalpies for the molecules at 298 K, and those are cited from. Rogers, D. W. et al. *Org. Lett.* **2003**, 5: 2373-2375.

The following two points will be emphasized in this section:

- (i) Experimental evidence of conjugation stabilization is questionable.
- (ii) 1-Butene was used by Kistiakowsky as a reference for calculating the conjugation energy of butadiene (Figure 6-Ia), which is the result of artificially selecting experimental data.

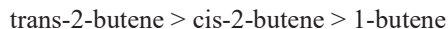
For the experimental basis and controversy of conjugation stabilization of 1,3-butadiene, March⁶ and Wikipedia⁷ have given a brief summary and introduction. For 1,3-butadiene, as the smallest and most basic conjugated molecule, according to the standard text book of organic chemistry,^{8,9} the experimental bases of conjugation stabilization include the following geometrical and energetic evidences:

- (i) The distance (1.47 Å)¹⁰ of the CC single bond between two double bonds is shorter than the distance (1.54 Å)¹¹ of the CC single bond in ethane.
- (ii) Cis- and trans-1,3-butadiene are planar.
- (iii) Hydrogenation heat of one mole of trans-1,3-butadiene is -3.5 kcal/mol less than that of two moles of 1-butene (Figure 6-Ia).^{8,12-16}

In the standard textbooks of organic chemistry, these experimental foundations are still used today to teach students, and seems to tell students that the principle of "conjugation stabilization" is unshakable.

The hydrogenation heat of acyclic polyene is a thermodynamic physical quantity and is independent on the reaction mechanism. However, as implied by Figure 6-II,^{17,18} the choice of a reference molecule can be considered to depend on the understanding of reaction mechanism. When electrophilic addition is carried out on a compound having two conjugated double bonds, the 1,2-addition product is obtained, but in most case, the 1,4-addition product is often found in a large yield.^{6,19} The hydrogenation of 1,3-butadiene may also be a multi-step reaction. the first step

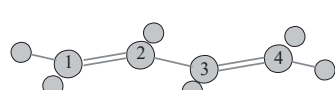
of the hydrogenation reaction may be 1,2-addition or 1,4-addition. After hydrogenation of one double bond, the intermediates of the reaction should be a mixture of 1-butene (1,2-addition), trans-2-butene and cis-2-butene (1,4-addition). In the case of a selected hydrogenation, as emphasized by Silvestre-Albero et al.,²⁰ the main intermediate is trans-2-butene (about 60%) as long as the reaction time is long enough (> 100 min.). According to the intermediate distribution versus reaction time and according to the formation enthalpies of the intermediates presented in Figure 6-I, the order of the thermodynamic stability is as follows:



When 1-butene is used as a reference molecule, as done by Kistiakowsky's method (Figure 6-Ia), conjugation energy = $2 \times (-30.3)$ (1-butene) - 57.1 (butadiene) = -3.5 kcal/mol, and it is stabilizing. This extra stabilization energy of -3.5 kcal/mol is used to break the partial double bond between two C=C double bonds. If cis-2-butene is used as a reference molecule, conjugation energy = $2 \times (-28.6)$ (cis-2-butene) - 57.1 (butadiene) = -0.1 kcal/mol (Figure 6-Ic), and it is so small that the conjugation between two double bonds can be ignored. When the reference is considered to be trans-2-butene, the conjugation energy is 1.9 kcal/mol (Figure 6-Ib), it becomes destabilizing.

Recently, uncatalyzed 1,4-hydrogenation of linear conjugated systems was theoretically studied, finding that the barrier for 1,4-hydrogenation is always substantially lower (by approximately 200 kJ/mol) than that for 1,2-hydrogenation.²¹ Figure 6-IIa and Figure 6-IIb show that the difference in hydrogenation heat between 1,3-butadiene and the two butenes depends upon the reaction mechanism, i.e. depends on the choice of the intermediate (reference). In the mechanisms of 1,4- and 1,2-hydrogenation reactions, total heat (-55.7 kcal/mol) of hydrogenation for 1,3-butadiene is the same, but their intermediates are different. When the different intermediates are used as the references, the so-called conjugation energies, $2\Delta H_2 - \Delta H_T$, are different, they are respectively 1.1 (destabilizing) and -3.9 (stabilizing) kcal/mol.

If the conjugation between two double bonds in butadiene is stabilization, the heat of 1,4-hydrogenation should be less than the hydrogenation heat of trans-2-butene because the super-conjugation should be weaker than the conjugation between two double bonds. In fact, as shown by Figure 6-IIa, the former ($\Delta H_1 = -28.4$ kcal/mol) is greater than the latter ($\Delta H_2 = -27.3$ kcal/mol). For 1,3-butadiene, therefore, whether the conjugation between two double bonds is stabilization or destabilization depends upon the understanding of reaction mechanism. According to the reaction mechanism reported by Silvestre-Albero et al, it is more reasonable that the trans-2-butene is chosen as the reference in the case of 1,3-butadiene.



	r_{3-4}	θ	E	E_e	E_N	
Planar	1.457	180.0°	-156.03850	-259.80321	103.76471	Scheme 6-I
Non-planar	1.456	179.98°	-156.03851	-259.80927	103.77076	

For the optimized planar and non-planar geometries of 1,3-butadiene at B3LYP/6-311G** level, as shown by Scheme 6-I, the difference, in the dihedral angle $\theta = \text{C1-C2-C3-C4}$, between the two geometries is 0.02° and the non-planar geometry is only 0.006 kcal/mol more stable than the planar geometry, but the total electronic energy, E_e , of non-planar geometry is more stable by 3.8 kcal/mol than that of planar geometry, and meanwhile the nuclear repulsion, E_N , of non-planar geometry is larger by 3.796 kcal/mol than that of planar geometry. For 1,3-butadiene, the slight deformation of the geometry seems to be able to confirm that the conjugation between two double bonds is destabilization. Therefore, it is inevitable for the “conjugation stabilization” concept based on such experiments to be questioned.

In fact, as pointed out by March,⁶ “doubt has been cast on the reality of delocalization in butadiene and similar molecules.” Since about 1959, for example, the shortening of the central single bond in 1,3-butadiene has been

explained by hybridization changes,²² inter-molecular van der Waals force,²³ and non-bonded interaction.^{24,25} In the same period, Dewar argued that, for 1,3-butadiene, small value of 4 kcal/mol is not resonance energy but arises from differing energies of bonds of different hybridization.²⁶⁻²⁹ In a word, as reluctantly indicated by Tantillo in 2018,³⁰ all these structure effects obscure the nature of the conjugation between two double in 1,3-butadiene.

In 1,3-diacetylene, there are two mutually perpendicular conjugated systems. The stabilization energy of 1,3-diacetylene should be somewhat greater than that (-3.5 kcal/mol) of butadiene, perhaps it should be two times of the stabilization energy of 1,3-butadiene. For diacetylene, as shown by Figure 6-IIc, the theoretical hydrogenation heats of the two acetylene bonds are equal, both equal to 69.6 kcal/mol, when the two acetylene bonds are hydrogenated into two CC single bonds by a two-step process. Accordingly, Rogers argued that thermodynamic stabilization enthalpy of 1,3-diacetylene is zero.^{17,18}

Another group led by Houk et al. gave the same calculation results as Rogers,³¹ but they suggested that the methods employed by Rogers are inappropriate because that comparisons of hydrogenation heats evaluate not only conjugation effects but also other structural and electronic differences. However, they still had to admit: "The results of Rogers et al. bring to light the limitations in Kistiakowsky's method". That is to say, Houk et al indirectly admitted that it is unreasonable for the Kistiakowsky's results to be considered as the experimental basis for conjugation stabilization.

The controversies of "conjugation stabilization of trans-1,3-butadiene" proved, at least, that it is not impossible and unnecessary to question and shake the so-called experimental bases of "conjugation stabilization". At the same time, the controversy also involves a critical issue: how to choose the reasonable reference system(s).

In this and next chapters, we will detail our method of constructing the new type of reference state, and will argue that in the case of acyclic polyene:¹⁻⁵

- (i) Conjugation effect between two double bonds is destabilization.
- (ii) the destabilizing conjugation between the two conjugated double bonds elongates the sp²-sp² CC single bond, instead of shortening the bond length.

6.0.2. Benzene and Aromaticity

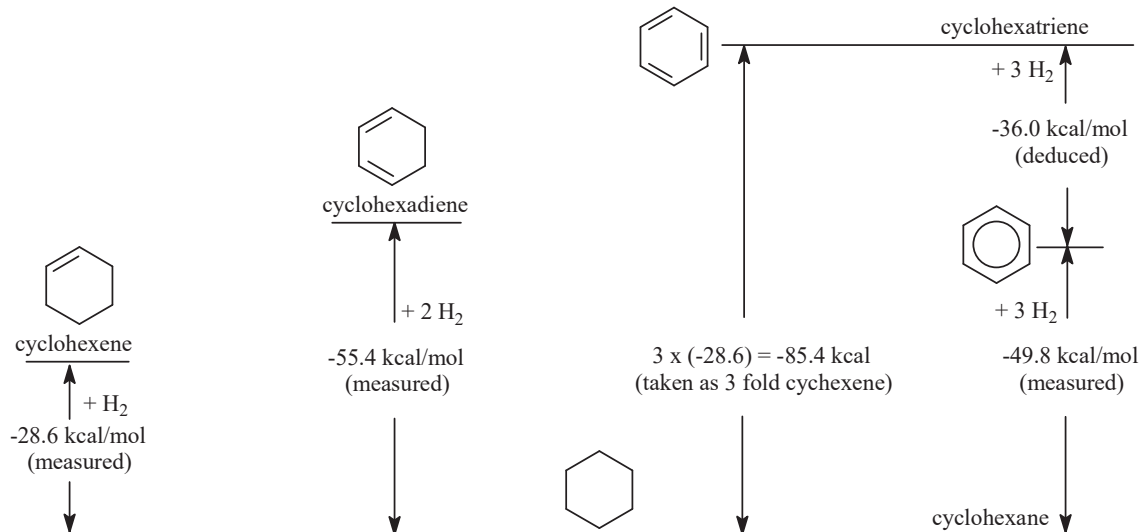


Figure 6-III. Kistiakowsky's procedure for determining the aromatic stabilization energy of benzene by measuring the hydrogenation heats of cyclohexene, cyclohexadiene and benzene.

As mentioned in Chapter 4 and will be detailed in the Chapter 8, π -electron delocalization arises from the CT and EX π -orbital interaction³² and from the spatial exchange interaction³³⁻³⁵ between the double bonds. Therefore, the π -MO localization and the π -electron localization are two different concepts.⁴ Strictly speaking, conjugation effect should be defined as a π -electron delocalization effect.

Therefore, the debate about "conjugation stabilization" is essentially a debate about the nature of electron delocalization. In this book, "the nature of electron delocalization" refers to the effect of electron delocalization on the stability of conjugated molecules, ie, conjugation makes molecule more stable or unstable.

6.0.2.1. Driving Force for Equalization of CC Bond lengths

Since the Kistiakowsky's experiment was reported in 1936 (Figure 6-III),¹² the extra stabilization energy (aromatic stabilizing energy) of -36 kcal/mol of benzene (in the literature, the extra stabilization energy is expressed as a positive value, which is 36 kcal/mol), together with the equalization of the CC bond lengths, has been another experimental basis of " π -electron delocalization stabilization".

Cyclohexene and cyclohexadiene have no structural isomer. Therefore, the determination of the aromatic stabilizing energy of benzene is more reasonable than that of the stabilizing energy of trans-1,3-butadiene when the stabilizing energy is measured by Kistiakowsky's method. So far, the concept of aromaticity is ubiquitous and has become one of the basic concepts of organic chemistry, and is widely used in various fields of organic chemistry. In the meantime, however, the viewpoint that the π -electron delocalization is stabilization is also often questioned. As early as in 1980s, Epiotis unequivocally proposed the viewpoint of "resonance destabilization",^{36,37} and pointed out that, the so-called "stability" of benzene relative to non-aromatic and anti-aromatic compounds is understood to be less instability of the π -conjugated system of benzene, rather than, as emphasized by the HMO (Hückel Molecular Orbital) theory, being more stable.

At the WATOC (World Association of theoretical and Computational Chemists) conference in Jerusalem July 8-12, 1996, Shaik summarized their collaborative research over more than a decade in the following one sentence: "The π -component is, on the one hand, distortive along a localizing mode, and on the other hand, it is stabilized by resonance energy relative to a localized reference".^{38,39} Shaik's researchs rised the controversy over the role of π -system in determining the D_{6h} geometry of benzene. At the same time, it also promoted the development of the π - σ energy decomposition method.⁴⁰⁻⁴⁴

In Chapter 9, we will mathematically demonstrate that the equalization of the CC bond lengths is the result of minimization of the nuclear repulsion of benzene ring. Of course, the driving force for the minimization of nuclear repulsion energy comes from the delocalization of π -electrons in the benzene ring.

In order to avoid confusion of the concepts, a clear definition should be given for the "localization". In this monograph, the localization means that the molecular orbitals (MOs) and electrons (including π and σ electrons) are absolutely localized on their respective bonds or groups (fragments). In the Shaik articles, the so-called localization just refers to a series of geometric structures of benzene with alternating single and double bonds, and it does not involve the localization of π -MOs and π -electrons. In the localized geometry of benzene defined by Shaik, the π -MOs and π -electron are still delocalized on the whole molecular framework.

6.0.2.2. Energetic Criteria.

It should be emphasized that, for the aromaticity, the aromatic stabilization energy and the energetic criterion are two different concepts. Aromatic stabilization energy is defined as "the enhanced chemical stability with respect to a structurally analogous reference system."⁴⁵ It can also be understood as the the difference, in conjugation energy, between an aromatic molecule and its reference molecule. Cretainly, the reference molecule is a non-aromatic but a conjugated molecule.

Aromatic compounds are a large number of compounds with various structures. Except for benzene, it has never been found that all CC bonds are equivalent in the resonance structure(s) of an aromatic molecule. For all of the aromatic molecules except for benzene, therefore, it is almost impossible to attempt to determine the aromatic stabilization energy using the Kistiakowsky method. Thus, various experimental and theoretical methods have been proposed in the literature to determine and compare the aromatic stabilizing energies of various types of aromatic molecules.

Energetic criterion refers to various types of the energy effects associated with the π -interaction between double bonds. The energy effects may be the isomerization energy,⁴⁶ the vertical delocalization energy,⁴⁷ the adiabatic delocalization energy, or it might even be the CT (charge transfer) interaction energy between two double bonds in a conjugated molecule.⁴⁸ Within the frame of molecular orbital theory (MO), the energy criteria may also include the Hückel resonance energy (HRE),⁴⁹ Dewar resonance energy (DRE)⁵⁰ and Hess and Schaad resonance energy (HSRE)⁵¹. These energy effects can be used to compare the aromaticity of aromatic molecules, but can not be considered as the aromatic stabilization energy. The conjugation energy is an energy effect based on the molecular orbital method, and the vertical and adiabatic resonance energies are two energy effects based on the valence bond method. If the source of the energy effect definitions is not concerned, these two energy effect definitions can also be applied to the similar energy effects calculated by the molecular orbital method. In this monograph, therefore, the vertical and adiabatic delocalization energies are used, but their calculations are based on molecular orbital method. Since there is a fundamental difference, in the localization method, between the valence bond method and the molecular orbital method, for a conjugated molecule such as cyclobutadiene, the sign and size of the conjugation energy value depend on the calculation method and may be fundamentally different.

According to the definition of the aromatic stabilization energy, the selection of reasonable reference molecule(s), or the construction of the localized state of an aromatic molecule, is the prerequisite for determining aromatic stabilization energy. In the different literatures, for an aromatic molecule, the values of its aromatic stabilization energy are different, due to using different reference molecules and different parameters. For benzene, for example, the values (kcal/mol) of the aromatic stabilization energy are as follows:

-33.2,⁴⁶ -33.9,⁵² -33.1,⁵³ -36.7,⁵⁴ -21.2,⁵⁰ -48.7,⁵⁵ -32,⁵⁵ -20.9,⁵⁶ -74.7⁵⁷, etc.

The range of this series of values is -53.5 kcal/mol (In the original literatures, the stabilizing energy effects, including aromatic stabilization energy, are always expressed as a positive value. In this book, the values of all of these stabilizing energies have been changed into the negative values. Similarly, the values of all the destabilizing energies are expressed as a positive value in this book).

6.0.2.3. Pauling and Dewar Resonance Energy of Benzene

In the literature method such as Kistiakowsky's method, the heats of combustion and hydrogenation were used to experimentally estimate the energies of π -electron delocalization in the conjugated molecules such as benzene and butadiene (Figure 6-I to Figure 6-III). For an aromatic molecule, the heat of combustion can also be used to calculate the heat of atomization. In 1933, for example, the heat of atomization of benzene, $\Delta H^{\circ a}$, was calculated by Pauling and Sherman using the heat of combustion of benzene, and then it was compared with the sum of bond energies of a hypothetical reference (cyclohexatriene), leading to the following expression for the resonance energy (RE) of benzene:⁵⁸

$$\text{RE} = \Delta H^{\circ a}(\text{benzene}) - [3E(\text{C=C}) + 3E(\text{C-C}) + 6E(\text{C-H})] \quad (6-1)$$

In Equation (6-1), $E(\text{C=C})$ is the energy of the double bond, and it is estimated from the heat of atomization of ethene; $E(\text{C-C})$ is the energy of the C-C single bond, and it is from the heat of atomization of ethane; and $E(\text{C-H})$ is

the energy of the C-H bond and is from the heat of atomization for methane. In the literature,⁴⁵ Pauline's method of calculating resonance energy was called an experimental method for determining the resonance energy of aromatic molecule such as benzene.

Using a formula similar to Equation (6-1),⁴⁵ the Dewar resonance energy (DRE) of a conjugated molecule was defined as the difference in the atomization enthalpies between the conjugated molecule and the hypothetical acyclic polyene in 1969.^{26,50,59} In the case of benzene, the double and single CC bonds in the Equation similar to Equation (6-1) are the formal CC single and double bonds in acyclic polyene, and the bond energies are as follows:⁶⁰ $E_{C-C} = 4.3499$ ev and $E_{C=C} = 5.5378$ ev, and $E_{C-H} = 4.4378$ ev.

The difference, in the definition, between the Pauling's resonance energy and the Dewar's resonance energy lies in the source the bond energies of the CC single and double bonds. In the DRE, the single bonds have the π character, and E_{C-C} includes the contribution of the π character to the bond energy. In the Pauling's resonance energy, $E(C-C)$ are the energy of the C-C single bond in the ethane. In the case of benzene, accordingly, the Pauling's resonance energy should be viewed as the adiabatic resonance energy rather than the aromatic stabilization energy of benzene because there is no conjugation interaction between the double bonds in the reference cyclohexatriene, but its value is exactly equal to -36 kcal/mol. On the other hand, the Dewar resonance's energy of benzene seems to be the aromatic stabilization energy of benzene because there is conjugation interaction between the double bonds in the reference cyclohexatriene, but it is only -22.6 kcal/mol.⁵⁰ In fact, from today's point of view, whether it is the Pauling's resonance energy or the Dewar's resonance energy, it is meaningless to discuss the accuracy of these two resonance energy values. However, as the biggest achievement made by Pauling, Dewar and etc., they found or suggested that the bond energies of acyclic polyene are additive. Then, by the additive nature of the bond energies, the heat of atomization of the reference molecule can be calculated without knowing the geometric parameters and molecular energy of the reference molecule. That is, the reference molecule is virtual and only a nominal borrowing.

Therefore, finding an additive physical quantity that can be accurately calculated is a good way to accurately estimate aromatic stabilization energy.

6.0.2.4. BLW Method

According to the definitions of the vertical delocalization and adiabatic delocalization energies, it is necessary to construct the localized geometry of a conjugated molecule itself. Before the development of our new method (our 2007, our 2011 and our 2014 methods), the BLW (block-localized wave function) method seems to be the only way to be able to optimize the localized geometry where the π MOs are absolutely localized on their respective double bonds.⁵⁴ In order to calculate the aromatic stabilization energy of simple aromatic molecules such as benzene, the BLW method needs to compare the resonance energies of benzene and cyclohexatriene. That is to say, the BLW method is not based on the additivity of energy effects. In particular, the rationality of the calculation principle of the BLW method is questionable, and there are fundamental flaws (seeing Chapter 8).

There are the fundamental differences, in the construction of the localized geometry (resonance structure) of an aromatic molecule, between our method and the BLW method. The difference should be attributed to the difference in understanding of the nature of π -electron delocalization. Essentially, these differences also reveal the fundamental flaws of the covalent bond method. In Chapter 8, the differences will be explained in detail.

Cyclobutadiene is the one of the most basic conjugated molecules, and it is also a well-known anti-aromatic molecule. Therefore, as Shaik emphasized,³⁹ the π -electron delocalization energy for cyclobutadiene can be used to judge the rationality of the calculation method. If the calculated π -electron delocalization energy is stabilizing, the calculation method must be unreasonable. In the localized geometry optimized by the BLW method, only the CT (charge transfer) orbital interaction has been excluded from between the pairs of double bonds, and meanwhile the exchange interaction between the double bonds is maximized.⁶¹ As a result, the π -electron delocalization energy obtained from the BLW method is always stabilizing regardless of whether the conjugated molecule is aromatic or anti-aromatic. For example, the vertical resonance energy and adiabatic resonance energy of cyclobutadiene,

obtained from the BLW method, are -10.9 and -10.3 kcal/mol (the original data are expressed as the positive values) and are all stabilizing (the blue data in Figure 6-IV).⁵⁴ On the contrary, as will be detailed in Chapter 8 and Chapter 9, when the π -electron delocalization energy is obtained from our 2007 and our 2011 methods,¹⁻⁵ it is stabilizing for an aromatic molecule and is destabilizing for an anti-aromatic molecule. For cyclobutadiene, the adiabatic resonance energy, obtained from our 2011 and 2014 methods, is 53.6 and 54.9 kcal/mol (the black data in Figure 6-IV), and it is almost equal to the experimental value of 55 kcal/mol.⁶² Of course, the BLW method has the fundamental flaws in the calculation principle.

Aromaticity is an ancient controversial topic.⁶³ Even so, the new research methods are still constantly being reported. It is strange that the Hückel method can be allowed to be used continuously,⁶⁴ but our current method is not tolerable. In 2008, our 2007 method was criticized rudely and unreasonably.^{65,66} So, in this book, we will have to comment on the BLW method.

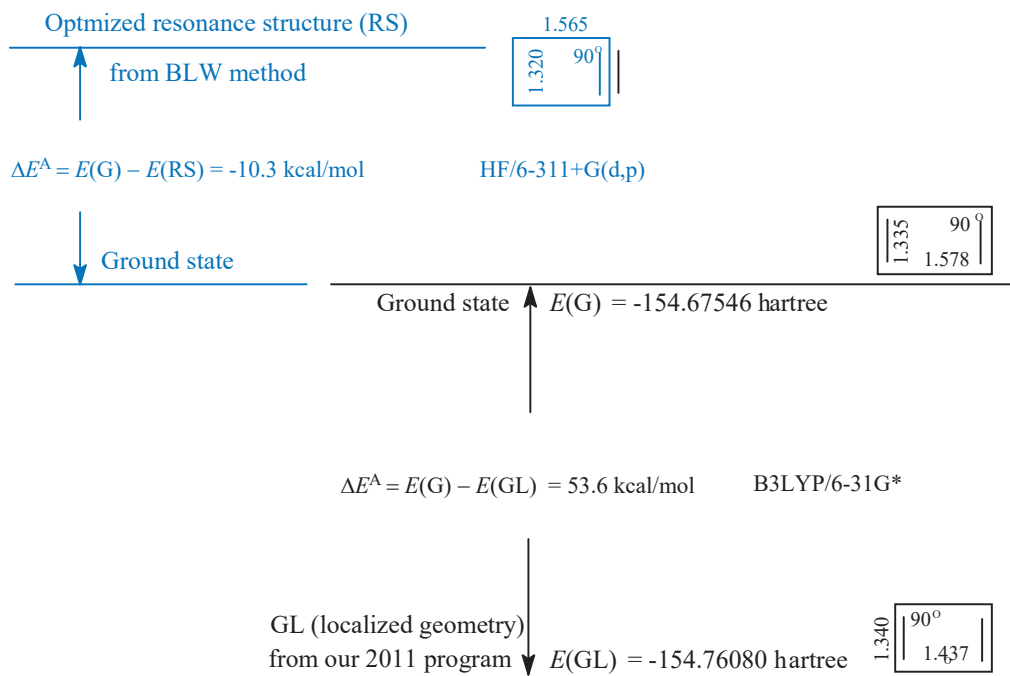


Figure 6-IV. The adiabatic resonance energy ΔE^A of cyclobutadiene shows the fundamental difference between Our 2011 method and the BLW method. The positive value means a destabilizing energy effect.

6.1. OUR 2007 METHOD

In the literature, there are two types of reference molecules, one is virtual, just like the reference molecules used by Pauling and Dewar to calculate resonance energy, and one is real, such as reference molecules involved in the BLW method. The bond energies of a virtual molecule come from the several specific molecules such as methane, ethane and ethene. That is to say, in the Pauling and Dewar methods, the bond energies of several specific molecules were applied to various types of conjugated molecules. The model is so simple that the accuracy of the calculation must be lost. Therefore, the method that can accurately and reasonably calculate the aromatic stabilization energy should be able to calculate the additive energy effects of the aromatic molecule itself, and then use these additive energy effects to obtain the molecular energy of the virtual reference molecule of the aromatic molecule itself.

In order to accurately calculate aromatic stabilization energy, two type of the reference state (geometry), the localized reference state and the virtual reference molecule, should be used. The localized reference state should meet the following requirements:

- (i) Reference structure should be a specific localized state (geometry) of the aromatic molecule itself. This can ensure that, in the structural factors such as the chemical bond type, atomic orbital hybridization, ring tensor, hyperconjugation, and steric hindrance, etc., there are no significant differences between an aromatic molecule and its reference molecule (state).
- (ii) Reference structure should be obtained from geometry optimization. This can ensure that the reference state has the determined structural parameters (such as bond lengths, bond angles, and dihedral angles), and has the exact molecular energy (including the total electron energy and nuclear repulsion energy).
- (iii) A set of energy effects can be found from the reference state(s). For the acyclic polyene, this set of energy effects is additive, but not additive for an aromatic molecule.

The third requirement is the ultimate goal. In order to obtain such a reasonable localized reference state, inspired by the Kistiakowsky method¹² and bond energy additivity,^{45,67} we developed a new method for optimizing localized geometry.¹⁻⁵ Our new method can provide the following two types of the localized reference geometries for every conjugated molecule (a planar molecule):

- (i) A fully localized geometry, and it is denoted as GL.
- (ii) A series of specific localized geometries, denoted as GE-m, m = 1, 2, ……, k.

In the GL geometry of the conjugated molecule, the π systems are absolutely localized on their respective double bonds. The structure of the GL geometry is similar to a resonance structure of the conjugated molecule itself. In each GE-m geometry, only a specific pair of double bonds is conjugated, and all other π systems are localized on their respective double bonds. The symbols, $E(G)$, $E(GL)$ and $E(GE-m)$, represent the molecular energies of the ground state (G), GL and GE-m geometries.

At present, the restricted geometry optimization has three versions. In the first version, the restricted geometry optimization is performed by conditionally deleting the elements, $f_{\lambda,\rho}$ and $s_{\lambda,\rho}$, of the AO Fock and overlap integral matrices. This version is named our 2007 program.² In the second version, the following elements are conditionally deleted before each SCF iteration: AO Fock matrix elements $f_{\lambda,\rho}$, AO overlap integral matrix elements $s_{\lambda,\rho}$, and the two-electron exchange integrals $\langle \lambda\rho | \mu\omega \rangle$. This version is named our 2011 method.⁴ The results, calculated by the two versions, show that the π -MO localization and the π -electron localization are two different concepts. In the last Chapter, will release the third version (our 2014 method) in order to further improve the restricted geometry optimization. In our 2014 method, in addition to the AO matrix elements and two-electron exchange integrals, the gradients, $\partial \langle \lambda\rho | \mu\omega \rangle / \partial a$, of the two-electron exchange integral should be conditionally deleted.

In this chapter, all calculations are performed within the PC-Gamess software package improved in our research group. The source code of PC-Gamess is provided by Professor Alex A. Granovsky, the Moscow State University.⁶⁸ Currently, the restricted geometry optimization is limited to planar molecule.

6.1.1. Program of Localizing Geometry

For trans-1,3,5-hexatriene, for example, the optimization of its GL geometry is a two-step procedure. In the first step (Figure 6-1), one-electron matrix elements are storied in a two-dimension array $h(i,i)$. The two sets of the elements of this array, $h(i,1)$ and $h(kp,ks)$, are used to identify π -AOs (atomic orbitals). In the second step (Figure 6-2), the localized geometry, such as GL and GE geometries, is optimized by conditionally deleting the AO Fock

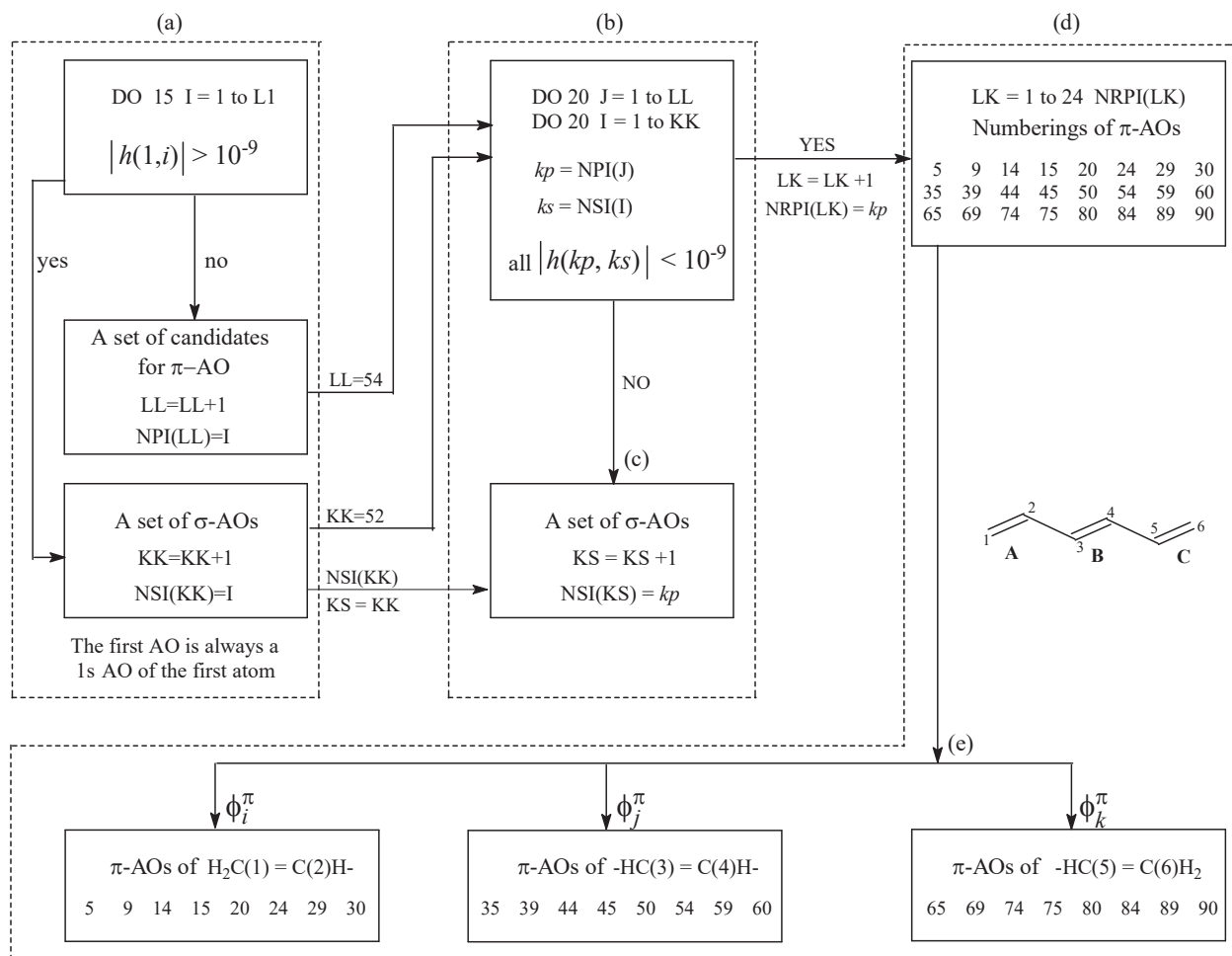


Figure 6-1. A new subroutine "FIXINI1" in the PC-Gamess improved in our research group. (a) Identifying the candidates for the π AO of trans-1,3,5-hexatriene, where $h(i,1)$ is an AO one-electron matrix element between the first AO and the i -th AO, and L1 ($L1 = 106$) is the total number of AOs in trans-1,3,5-hexatriene at the B3LYP/6-31G* level. (b) 24 π -AOs are picked out from the candidates. (e) Assigning 24 π -AOs to their respective double bonds based on their numberings in the whole molecule.

matrix elements and overlap integral matrix elements.

In the literature,⁴⁵ emphatically, polyene is often used as a reference molecule to calculate aromatic stabilization energy of an aromatic molecule. In our method, polyenes are used only to prove that a new type of additive energy effect has been found from the GL and GE-m geometries of each of polyene molecules. From then on, polyene itself is no longer involved in the calculation of the aromatic stabilization energy of aromatic molecules. This is the fundamental difference between our method and the literature methods such as the BLW method. But in the calculation principle of utilizing the additivity of energy effects, our 2007 method is similar to the Pauling and Dewar methods.

6.1.1.1. Identifying of π -Type AOs

For a planar conjugated molecule, π -AO is a type of AO perpendicular to the molecular plane. At 6-31G* level,

for example, π -AOs of a carbon atom include $2p_z$, $3p_z$, $4x_z$ and $4y_z$ when the molecular plane is placed on the X-O-Y plane of Cartesian coordinate. Therefore, every one-electron matrix element $h_{\lambda\rho}$ between the λ -th π -AO (π -type AO) and the ρ -th σ -AO (σ -type AO) is equal to zero. This is the fundamental principle for identifying π -AOs.

In any molecule, the first AO is definitely the $1s$ AO and is a σ -type AO. Therefore, the AO one-electron matrix element, $h(1,i)$, between the first AO and the i -th AO can be used to distinguish between π -AO and σ -AO. When $|h(1,i)| > 10^{-9}$, as shown by Figure 6-1a, the i -th AO is the σ -AO. When $|h(1,i)| < 10^{-9}$, unsure that the i -th AO is definitely a π -AO and can only be regarded as a candidate for π -AO. Fifty-four AOs are identified as the candidates for π -AO after scanning all matrix elements $h(1,i)$ ($i = 1$ to L_1), where L_1 is the total number of AOs in the molecule. At 6-31G* level, however, there are twenty-four π -AOs in 1,3,5-hexatriene. It is necessary to pick the real π -AOs from the candidates using the elements $h(kp,ks)$ (Figure 6-1b), between the kp -AO and the ks -th AO, where the kp -th AO is a j -th candidate for the π -type AO, and the ks -th AO belongs to the σ -type AOs. When $|h(kp,ks)| > 10^{-9}$, the kp -th AO, i.e. j -th candidate stored in the array NPI(J), is definitely a σ -type AO, and it should be excluded from the candidates. When all $|h(kp,ks)| < 10^{-9}$, the j -th candidate whose numbering in the whole molecule is kp can finally be confirmed as a π -type AO. After scanning $KK \times LL$ elements $h(kp,ks)$, twenty four real π -type AOs are picked up from the fifty four candidates.

At last, as shown by Figure 6-1e, twenty-four π -AOs are assigned to their respective double bonds, according to their numberings in the whole molecule.

6.1.1.2. Construction of GL Geometry

In order to obtained the optimized GL geometry of trans-1,3,5-hexatriene, as shown by Figure 6-2e, before each SCF iteration, the following conditional settings should be performed:

```
set AO Fock matrix elements  $f_{\lambda\rho} = 0.0$ 
set AO overlap integral matrix elements  $s_{\lambda\rho} = 0.0$ 
```

when

π -AO $\phi_\lambda \in$ double bond P,
 π -AO $\phi_\rho \in$ double bond Q,
P, Q = A, B, C; P ≠ Q.

For the localized GL geometry, all π MOs are absolutely localized on their respective double bonds (Figure 6-2f), the σ MOs are delocalized on the entire molecule framework. For example, the 20-th, 21-th and 22-th MOs are three occupied π MOs, and they are absolutely localized, respectively, on the C(3)=C(4), C(5)=C(6), and C(1)=C(2) double bond according to their AO coefficients (seeing Table 6-1 presented in appendix). Thus, the C(2)-C(3) bond and C(4)-C(5) bond in the GL state can be regarded as the naked sp^2-sp^2 CC single bond. This leads us to pay great attention to the following interesting results:

- (i) Due to the conjugation interaction between three double bonds originally belonging to the optimized GL geometry, as shown by a comparison of Figure 6-2a with Figure 6-2d, the single bonds C2-C3 and C4-C5 (Å) are slightly lengthened from $r_{2-3}(\text{GL}) = r_{4-5}(\text{GL}) = 1.447$ in the GL geometry into $r_{2-3}(\text{G}) = r_{4-5}(\text{G}) = 1.450$ in the ground state geometry.
- (ii) Correspondingly, the molecular energy (hartree) increases from $E(\text{GL}) = -233.40935$ to $E(\text{G}) = -233.39855$. The adiabatic conjugation energy, $\Delta E^\text{A} = E(\text{G}) - E(\text{GL}) = 6.8$ kcal/mol > 0, and it is destabilizing (Figure 6-2j)

These interesting results tell us that, in trans-1,3,5-hexatriene, conjugation effect is destabilization. The restricted

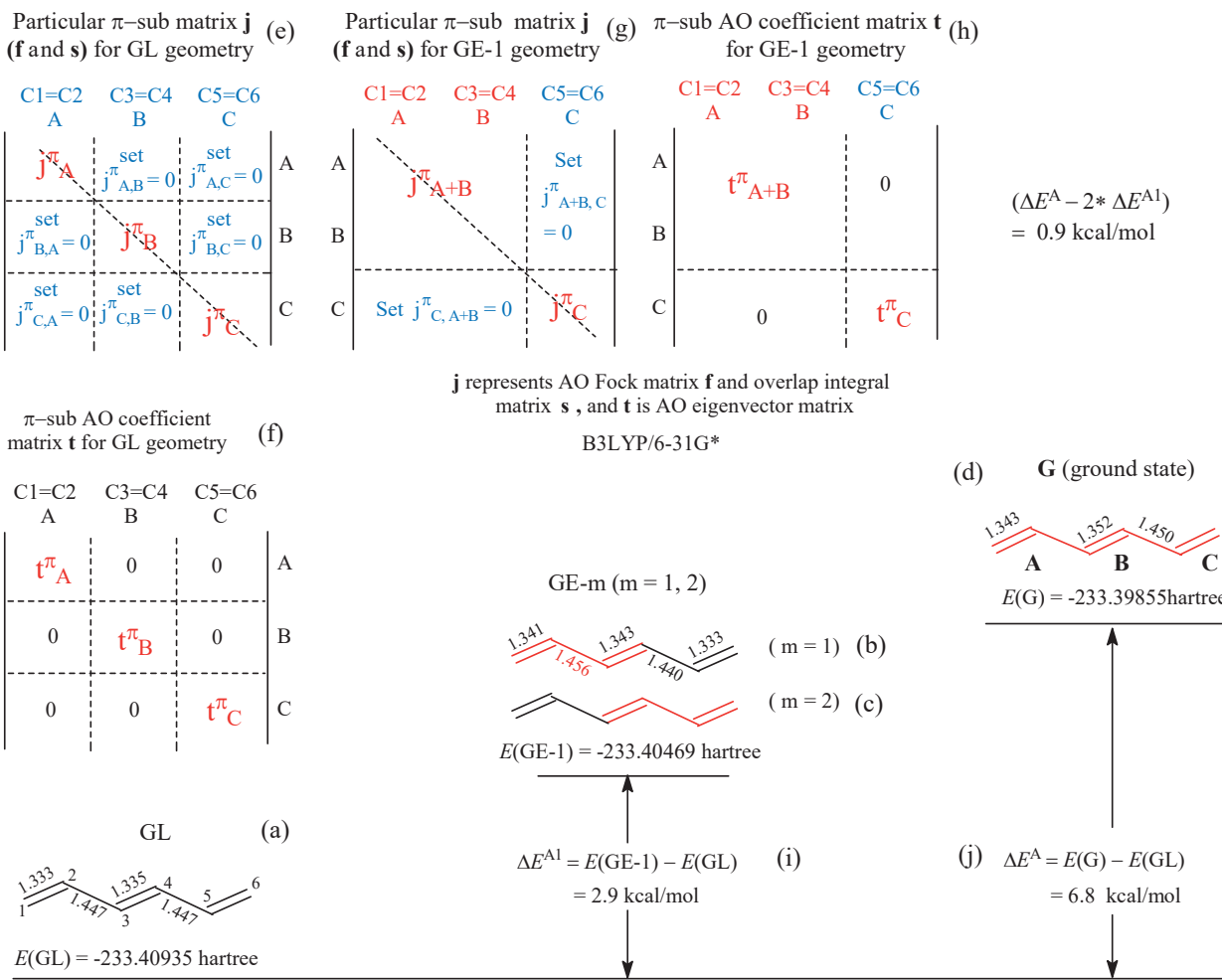


Figure 6-2. (a) to (d) The GL geometry, GE-m geometry and Ground state (G) geometry of trans-1,3,5-hexatriene are obtained from the full and restricted geometry optimizations at the B3LYP/6-31G* level. (e) and (g) The conditional settings for optimizing the GL and GE-1 geometries. (f) and (h) the π blocks of the AO coefficient matrices for GL and GE-1 geometries. In the molecular structures, the red and black lines indicate that, in the optimized geometry, all the π orbital interactions between the double bonds are set equal to zero except for those between the red double bonds.

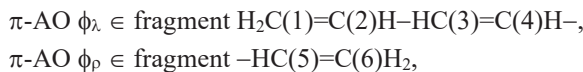
geometry optimization makes it possible to calculate the distance of a naked sp^2-sp^2 CC single bond and to calculate the adiabatic conjugation energy ΔE^A .

6.1.1.3. Construction of GE-m Geometry

For trans-1,3,5-hexatriene, there are two locally delocalized geometries denoted as GE-1 and GE-2 (Figure 6-2b and Figure 6-2c). Due to the C_{2v} symmetry of GL geometry, GE-1 and GE-2 are equivalent. So, in actual calculations, it is sufficient to only optimize the GE-1 geometry. According to the conditional setting shown by Figure 6-2g, the GE-1 geometry can be obtained from the geometry optimization under the following conditional settings: before each SCF iteration,

set AO Fock matrix elements $f_{\rho\rho} = 0.0$

set AO overlap integral matrix elements $s_{\lambda,\rho} = 0.0$
when



In the GE-1 geometry, as shown by Figure 6-2h, two double bonds, C(1)=C(2) and C(3)=C(4) represented by the red lines in Figure 6-2b, are conjugated, and the double bond C(5)=C(6) is kept isolated from the other two double bonds. Correspondingly, as shown by the AO coefficients of 20-th, 21-th and 22-th MOs listed in the right-hand side of Table 6-1, the two π system are localized, respectively, on the fragments H₂C(1)=C(2)H-HC(3)=C(4)H- and -HC(5)=C(6)H₂, and the σ system is delocalized on the entire molecular framework. The 20-th and 22-th π MOs can be considered as the result of the conjugation interaction between the 20-th and 22-th π MOs of the GL geometry.

A comparison of Figure 6-2a and Figure 6-2b shows the following very important results:

- (i) $dr_{2-3}(\text{GE-1}) = [r_{2-3}(\text{GE-1}) - r_{2-3}(\text{GL})] = 0.009 \text{ \AA} > 0.$
- (ii) $\Delta E^{\text{A}1} = E(\text{GE-1}) - E(\text{GL}) = 2.9 \text{ kcal/mol} > 0.$

These results are contrary to what the classic theory expects, and they indicate that the local conjugation between the C(1)=C(2) and C(3)=C(4) double bonds of the GL geometry is destabilization.

In this chapter, will further prove that, for any conjugated hydrocarbon molecule (including aromatic molecule), the energy effect, associated with the local conjugation interaction between a pair of bonded double bonds, is always destabilizing. The optimization of GL and GE-m geometries may provide a new way to explore and understand the nature of π -electron delocalization.

6.1.2. A New Type of Additive Energy Effect

As emphasized in the beginning of this section, the purpose of constructing the localized reference states, such as the GL and GE-m geometries, is to look for a new type of the energy effect that is additive in the case of acyclic polyene.

For trans-polyene H-(CH=CH)_n-H, k is the number of GE-m geometries and depends upon the number n of double bonds. But the number of the GE-m geometries that must be optimized depends upon the symmetry of GL geometry. For trans-1,3,5,7,9-decapentaene (C₁₀H₁₂), for example, it has four GE-m ($m = 1, 2, 3, 4$), but for two pairs of GE-m geometries (GE-1 and GE-4) and (GE-2 and GE-3), each pair of geometries are equivalent (Table 6-2) due to the molecular symmetry. Therefore, the number of the GE-m geometries that must be optimized is 2.

In the case of trans-polyene, as shown by the brown and blue color lines in Figure 6-3, ΔE^{A} and $\Sigma \Delta E^{\text{Am}}$ can be fitted as a linear function of the number n of double bonds:

$$\begin{aligned}\Delta E^{\text{A}}(n) &= 1.83295 + 1.69469n \\ \Sigma \Delta E^{\text{Am}}(n) &= 0.92639 + 1.64003n.\end{aligned}$$

Based on the facts that $\Delta E^{\text{A}}(n) > 0$, $\Sigma \Delta E^{\text{Am}}(n) > 0$ and $\Delta E^{\text{A}}(n) - \Sigma \Delta E^{\text{Am}}(n) > 0$, and the quantity, $[\Delta E^{\text{A}}(n) - \Sigma \Delta E^{\text{Am}}(n)]$, can be defined as the extra destabilization energy (EDE) of trans-polyene. Relative to the functions $\Delta E^{\text{A}} = f(n)$ and $\Sigma \Delta E^{\text{Am}}(n) = f(n)$, as shown by the red color curve in Figure 6-3, the function $[\Delta E^{\text{A}}(n) - \Sigma \Delta E^{\text{Am}}(n)] = f(n)$ is approximately a constant. The values of EDE in Table 6-2 are about 1.2 kcal/mol, and it is small. Therefore, the sum of energy effects, $\Sigma \Delta E^{\text{Am}} = \Sigma [E(\text{GE-}m) - E(\text{GL})]$ ($m = 1, \dots, k$), can be considered to be approximately equal to $\Delta E^{\text{A}}(n)$, $\Delta E^{\text{A}}(n) \approx \Sigma \Delta E^{\text{Am}}$. In the case of acyclic polyene, the energy effects, ΔE^{Am} , can be considered additive.

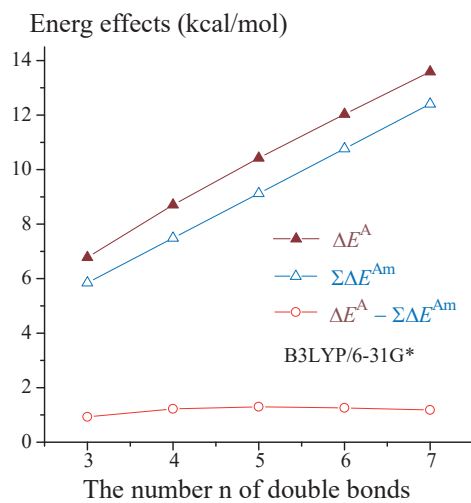


Figure 6-3. For trans-polyenes $H-(CH=CH)_n-H$ at B3LYP/6-31G* level, the energy differences, $(\Delta E^A = E(G) - E(GL))$, $(\Sigma \Delta E^{Am} = \sum [E(GE-m) - E(GL)])$ and $(\Delta E^A - \Sigma \Delta E^{Am})$, and their changes with the increasing of the number n of double bonds.

Table 6-2. For Each of Trans-polyenes $H-(CH=CH)_n-H$, Molecular Energies (hartree), $E(G)$, $E(GL)$ and $E(GE-m)$, of the Ground State (G), GL and GE-m Geometries, and the Energy Effects ΔE^A , $\Sigma \Delta E^{Am}$ and $[\Delta E^A - \Sigma \Delta E^{Am}]$ (kcal/mol), Calculated by Our 2007 Method at B3LYP/6-31G* Level.

Locally conjugated groups in GE-m geometry		C ₆ H ₆ n = 3	C ₈ H ₁₀ n = 4	C ₁₀ H ₁₂ n = 5	C ₁₂ H ₁₄ n = 6	C ₁₄ H ₁₆ n = 7
$E(G)$		-233.39855	-310.80566	-388.21308	-465.62065	-543.02831
$E(GL)$		-233.40935	-310.81953	-388.22969	-465.63983	-543.04997
$E(GE-1)$	C(1)=C(2)-C(3)=C(4)	-233.40469	-310.81492	-388.22510	-465.63526	-543.04540
$E(GE-2)$	C(3)=C(4)-C(5)=C(6)	-233.40469	-310.81684	-388.22700	-465.63716	-543.04731
$E(GE-3)$	C(5)=C(6)-C(7)=C(8)		-310.81684	-388.22700	-465.63715	-543.04730
$E(GE-4)$	C(7)=C(8)-C(9)=C(10)			-388.22510	-465.63716	-543.04730
$E(GE-5)$	C(9)=C(10)-C(11)=C(12)				-465.63526	-543.04731
$E(GE-6)$	C(11)=C(12)-C(13)=C(14)					-543.04540
ΔE^A		6.8	8.7	10.4	12.0	13.6
$\Sigma \Delta E^{Am}$		5.8	7.5	9.1	10.8	12.4
EDE		0.9	1.2	1.3	1.3	1.2

$\Delta E^A = E(G) - E(GL)$, $\Sigma \Delta E^{Am} = \sum [E(GE-m) - E(GL)]$ ($m = 1, 2, \dots, k$), $EDE = \Delta E^A - \Sigma \Delta E^{Am}$

For trans-hexatriene $H-(CH=CH)_3-H$, for example, there are two GE-m geometries. The molecular energy differences are as follows:

$$\Delta E^{A1} = E(GE-1) - E(GL) = \Delta E^{A2} = \sum [E(GE-2) - E(GL)] = 2.9 \text{ kcal/mol},$$

$$\Sigma \Delta E^{Am} = 2 \times \Delta E^{A1} = 5.9 \text{ kcal/mol}.$$

$$\Delta E^A = E(G) - E(GL) = 6.8 \text{ kcal/mol}.$$

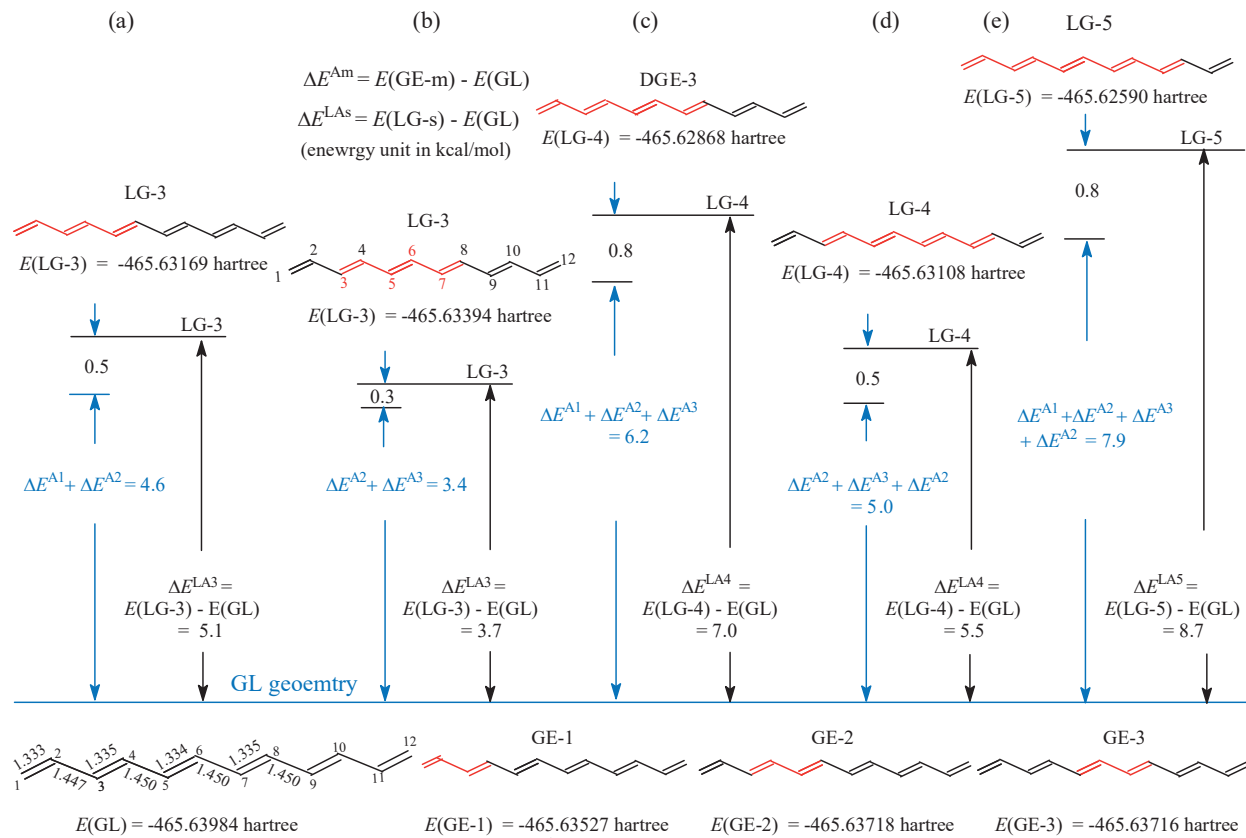


Figure 6-4. For trans-1,3,5,7,9,11-dodecahexaene at B3LYP/6-31G* level, the energy effects ΔE^{Am} are compliances with additivity, $\Delta E^{LAs} \approx \sum \Delta E^{Am}$. In the GE-m and LG-s geometries, the double bonds, represented by the red lines, are conjugated.

$$\Delta E^A - (2 \times \Delta E^{A1}) = 0.9 \text{ kcal/mol.}$$

$$\Delta E^A \approx \sum \Delta E^{Am}.$$

In addition, as shown by Figure 6-4, if the ground state is replaced with a locally delocalized geometry denoted as LG-s, the energy effect $\Delta E^{LAs} = E(LG-s) - E(GL)$. The letter "s" in the symbol "LG-s" is the number of the conjugated double bonds represented by the red lines in the LG-s geometry, and $E(LG-s)$ is the molecular energy of the LG-s geometry. In the case of the LG-4 (s = 4) geometry of trans-1,3,5,7,9,11-dodecahexaene (Figure 6-4d), for example, the following four double bonds are conjugated: $-C(3)=C(4)-$, $-C(5)=C(6)-$, $-C(7)=C(8)-$, and $-C(9)=C(10)-$, and each of two double bonds $C(1)=C(2)-$ and $C(11)=C(12)$ remains isolated from all other five double bonds. Correspondingly, there are three GE-m geometry ($m = 2, 3, 2$). As shown by Figure 6-4d, the energy effects (kcal/mol) are as follows:

$$\Delta E^{LA4} = E(LG-4) - E(GL) = 5.5$$

$$\Delta E^{A2} + \Delta E^{A3} + \Delta E^{A2} = 5.0$$

$$\Delta E^{LA4} \approx (\Delta E^{A2} + \Delta E^{A3} + \Delta E^{A2})$$

In the next Chapter, it will be further demonstrated that, for acyclic polyene, the additivity of the energy effects ΔE^{Am} is independent of molecular configuration.

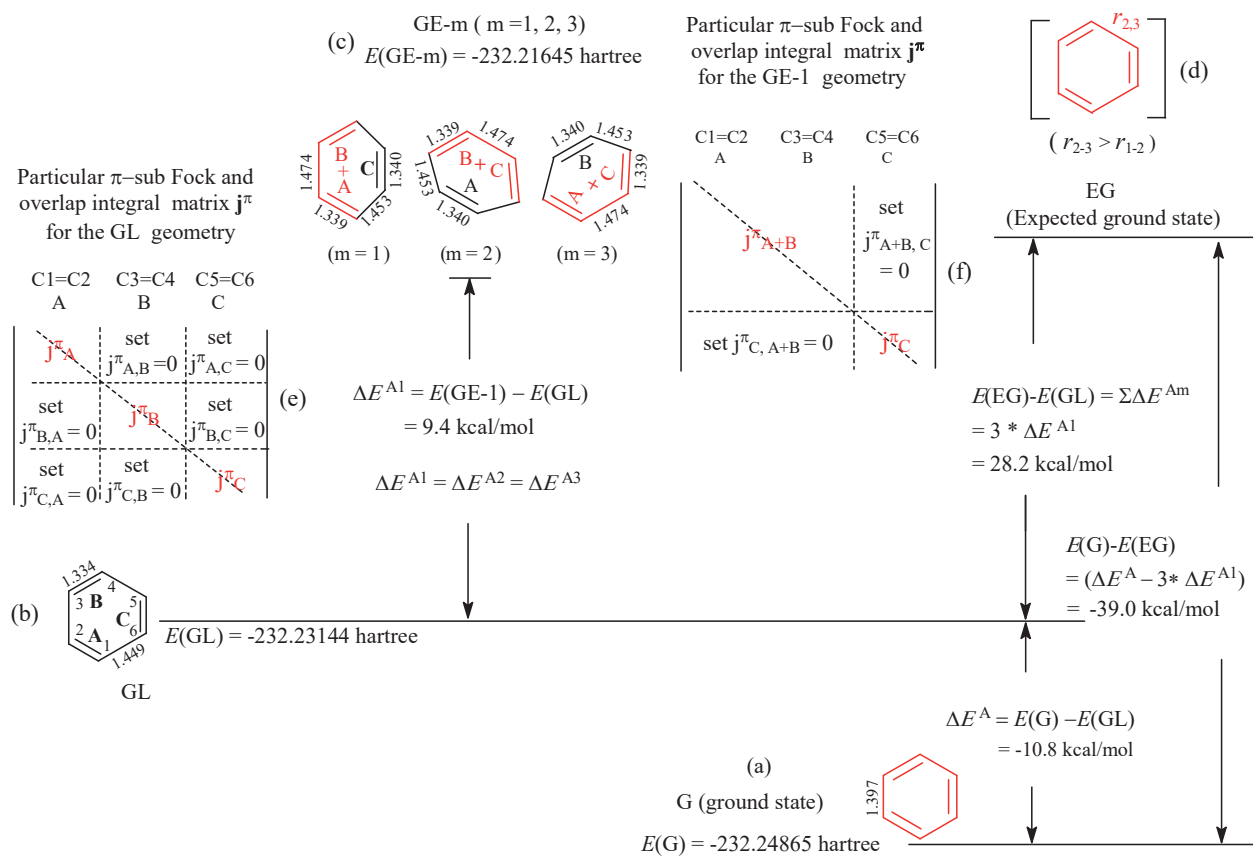


Figure 6-5. The procedure for calculating the extra stabilization energy (ESE) of benzene, and the G, GL and GE-m ($m = 1, 2, 3$) geometries are obtained from the full and restricted geometry optimizations at the B3LYP/6-31G* level. In the molecular structures, the meaning of the red and black lines is the same as those in Figure 6-2.

All these show that, in the case of acyclic polyene, the energy effects ΔE^{Am} , arising from the local conjugation interactions between the corresponding pairs of double bonds, are additive. In particular, the GL and GE-m geometries are the localized geometries of a conjugated molecule itself, and they are obtained from the geometry optimization. The differences between a conjugated molecule and its localized geometries are merely in the distances of the single and double bonds and in the molecular energy. In the chemical bond type, atomic orbital hybridization and conformation, there is no difference between them. Therefore, the additive energy effects are obtained from the localized GL and GE-m geometries of a conjugated molecule itself, rather than from the several specific molecules.

According to the third requirement of a reasonable reference state, it is necessary to further investigate whether the energy effects ΔE^{Am} are not additive in the case of aromatic molecules.

6.1.3. Extra Stabilization Energy of Benzene

For benzene, according to the conditional settings described in Figure 6-5e and Figure 6-5f, the GL geometry and three degenerate GE-m ($m = 1, 2, 3$) geometries can be obtained from the restricted geometry optimization.

In the GL geometry, as indicated by the AO coefficients on the left side of Table 6-3 (presented in Appendix), three π systems are absolutely localized on their respective double bonds. In the GE-1 geometry,

as shown by the AO coefficients listed in the right side of Table 6-3, only the C(1)=C(2) and C(3)=C(4) double bonds, represented by the red lines in Figure 6-5c, are allowed to be conjugated, and the C(5)=C(6) double bond, represented by the black line, is unconjugated with the other two double bonds. In the GE-2 geometry, C(3)=C(4) and C(5)=C(6) are conjugated, and the C(1)=C(2) double bond keeps isolated from other two double bonds. In the GE-3 geometry, the C(5)=C(6) and C(1)=C(2) double bonds are conjugated, and the C(3)=C(4) double bond is localized. The three GE-m geometries are equivalent due to the D_{3h} symmetry of GL geometry.

Similar to trans-hexatriene, $\Delta E^{Am} = [E(GE-m) - E(GL)] > 0$. Correspondingly, the distance of the single bond between two conjugated double bonds in GE-m geometry is longer than that of the corresponding single bond in GL geometry. In the GE-1 geometry, for example, the distance (1.474 Å) of the C(2)-C(3) single bond is 0.025 Å longer than the distance (1.449 Å) of the corresponding single bond in the GL geometry, and meanwhile the corresponding molecular energy difference $\Delta E^{A1} = E(GE-1) - E(GL) = 9.4 \text{ kcal/mol} > 0$ (destabilizing). But it is different from trans-hexatriene that, for benzene, $\Delta E^A = [E(G) - E(GL)] < 0$ (stabilizing).

The following results show that the greater the bond length change dr_{2-3} , the greater the energy change ΔE^{A1} :

- (i) For benzene, $dr_{2-3} = [r_{2-3}(GE-1) - r_{2-3}(GL)] = 0.025 \text{ \AA}$, and for hexatriene, $dr_{2-3} = 0.009 \text{ \AA}$. The dr_{2-3} of the former is 0.016 Å larger than that of the latter.
- (ii) For benzene, $\Delta E^{A1} = [E(GE-1) - E(GL)] = 9.4 \text{ kcal/mol}$, and for hexatriene $\Delta E^{A1} = 2.9 \text{ kcal/mol}$. The ΔE^{A1} of the former is 6.5 kcal/mol greater than that of the latter.

If these three energy effects ΔE^{Am} ($m = 1, 2, 3$) are additive, the molecular energy difference $[E(G) - E(GL)]$ between the ground state and the GL geometry should be approximately equal to $3 \times \Delta E^{A1} = 28.2 \text{ kcal/mol}$. But contrary to expectation,

$$\begin{aligned}\Delta E^A &= E(G) - E(GL) = -10.8 \text{ kcal/mol} < 0 \\ \Delta E^A - 3\Delta E^{Am} &= (-10.8) - (28.2) = -39 \text{ kcal/mol.}\end{aligned}$$

In fact, the conjugated cyclohexatriene is virtual, and its geometry and energy cannot be optimized and calculated. According to the additivity of the energy effects ΔE^{Am} , however, the sum of the energy effects, $3\Delta E^{Am}$, can be considered as the molecular energy difference, $E(EG) - E(GL)$, between an expected ground state (a virtual conjugated cyclohexatriene) of benzene and the GL geometry. Accordingly,

$$(\Delta E^A - 3\Delta E^{Am}) = [E(G) - E(GL)] - [E(EG) - E(GL)] = E(G) - E(EG) = -39 \text{ kcal/mol}$$

-39 kcal/mol is the deviation of the additivity of the energy effect. In our published work,² it is defined as the extra stabilization energy (ESE) of benzene because the molecular energy difference, $E(G) - E(EG)$, between the benzene and its expected ground state (a virtual conjugated cyclohexatriene, or a reference conjugated cyclohexatriene) is in accordance with the definition of aromatic stabilizing energy. That is to say, in the practical calculation of the aromatic stabilization energy of benzene, the conjugated cyclohexatriene, as a virtual reference molecule, is never involved. The entire calculation only borrows the virtual reference molecule nominally, without calculating the molecular energy $E(EG)$ of cyclohexatriene, nor without knowing the detailed geometry of the virtual cyclohexatriene. Our calculation is similar in principle to the calculation of Dewar resonance energy.

When the ESE is calculated at the RHF and MP2 levels of theory, as shown by the data listed in Table 6-4, the ESE values of benzene are big and the energy difference ΔE^A becomes destabilizing, and meanwhile the basis set size has a big effect on the value. At 6-31G* and 6-311G** levels, for example, the ESE and ΔE^A values (kcal/mol) respectively are as follows:

Table 6-4. For Benzene, Extra Stabilizing Energy (ESE) and Energy Effects $\Delta E^{\text{A}1}$ (kcal/mol), and Corresponding Bond Length Change $dr_{2,3} = r_{2,3}(\text{GE-1}) - r_{2,3}(\text{GL})$ (Å), Calculated Using Our 2007 Method.

Optimization methods	$\Delta E^{\text{A}1}$	$dr_{2,3}$	$\Sigma \Delta E^{\text{Am}} = 3 * \Delta E^{\text{A}1}$	ΔE^{A}	$ESE = E^{\text{A}} - \Sigma E^{\text{Am}}$
B3LYP/6-31G*	9.4	0.0248	28.2	-10.8	-39.0
B3LYP/6-311G**	11.2	0.0273	33.6	-6.5	-40.1
B3LYP/6-311G(2df,p)	14.6	0.0536	43.9	2.7	-41.2
MP2(Full)/6-31G*	46.9	0.0749	140.7	89.5	-51.2
MP2(Full)/6-311G**	64.5	0.0860	193.5	136.1	-57.3
RHF/6-31G*	27.8	0.0867	83.5	37.1	-46.5
RHF/6-311G**	31.8	0.0987	95.3	46.7	-48.6

ESE: -39 and -40.1 (B3LYP), -46.5 and -48.6 (RHF), -51.2 and -57.3 (MP2)

ΔE^{A} : -10.8 and -6.5 (B3LYP), 37.1 and 46.7 (RHF), 89.5 and 136.1

Of the values, the B3LYP/6-31G* value of -39.0 kcal/mol is the closest to the experimental value (-36 kcal/mol).¹² Therefore, in this chapter, the ESEs of all conjugated compounds will be calculated at B3LYP/6-31G* level.

For benzene's ESE, the difference between B3LYP/6-31G* value and MP2/6-311G** value is -18 kcal/mol and is 50% of the experimental value (-36 kcal/mol), and is 46% of the B3LYP/6-31G* value (-39.0 kcal/mol). The difference is so big that our 2007 method must be improved. In our second version (our 2011 method), the localized GL and GE-m geometries will be optimized by conditionally deleting matrix elements and two-electron exchange integrals. When using our 2011 method, as will be shown in the Chapter 8 and has been shown in our published work⁴, the theoretical level and basis set size will have less influence on ESE value. When using a further improved version (our 2014 method), the theoretical level and basis set size will have the smallest effect on the ESE value.

In our 2007 method, the reference states of benzene are the localized GL and GE-m geometries of benzene molecule itself, and they are obtained from the restricted geometry optimization. The chemical bond types and configuration of the reference states (GL and GE-m) are exactly the same as those of benzene, and their geometrical difference is merely in the distance of the single and double bonds and in the molecular symmetry. Therefore, the GL and GE-m geometries of the conjugated molecule itself fully meet the requirements of the localized reference state, and particularly meet the third requirement: finding a type of the additive energy effect. The new type of the additive energy effect that we are looking for is the energy difference ΔE^{Am} ($m = 1, 2, \dots, k$). In particular, these additive energy effects are obtained from the localized geometries, GL and GE-m, of an aromatic molecule itself, rather than from several specific molecules that are structurally unrelated to the aromatic molecule. Therefore, our 2007 method makes it possible to accurately calculate the aromatic stabilization energy of aromatic molecules.

The following results are particularly worth reemphasizing: for benzene, the local conjugation interaction between two double bonds of the GL geometry is destabilization although the adiabatic conjugation energy, ΔE^{A} , is stabilizing, and meanwhile the CC single bond distance between two conjugated double bonds in the GE-m geometry is longer than the corresponding CC single bond in the GL geometry.

On the basis of comparison of Figure 6-III and Figure 6-5, can discover: in principle, our theoretical method and the Kistiakowsky experimental method is completely consistent. The only difference is that, in Kistiakowsky method, energy effect is the hydrogenation heat of cyclohexene, while our energy effect is the π -electron

delocalization energy caused by the local conjugation between the pairs of double bonds. It will be shown that the ESE value of benzene, obtained from the 2011 program, is -36.3 kcal/mol.⁴ For benzene, the ESE values of -39.0 and -36.3 kcal/mol are the closest to the experimental value of -36 kcal/mol.

6.2. ESEs FOR BENZENE-LIKE SPECIES

The aromatic stabilization energy of benzene (-36 kcal/mol) was determined by Kirtiakowsky using hydrogenation method in 1936, creating a landmark method for experimental measurement of aromatic stabilizing energy. Since then, as commented by Katritzky, Jug and Oniciu,⁶⁹ “combustion and hydrogenation were among the first methods used to measure aromatic stabilization energies, by direct measurement of ΔH_a values”. The discovery of the bond energy additivity makes it possible to calculate ΔH_a (atomization enthalpy) of a reference structure, and greatly promoted the aromatic research. It can be said that the most of the methods, including the theoretical calculations and experimental measurements, are based on the principle of the bond energy additivity.

More recently, many measurement difficulties in the combustion method have been overcome.⁷⁰⁻⁷³ The enthalpies of formation for heterocycles can be measured very accurately. However, the aromatic stabilization energy of an aromatic molecule is the difference between the experimental atomization energy and the energies calculated by using the bond energies. Therefore, either the experimental determination or the theoretical calculation, the estimation of aromatic stabilization energy always needs to calculate the energy of the reference molecule using the bond energies. In this case, there is a strong contrast between the exact determination of the atomization heat of aromatic compound and the very approximate calculation of the energy of the reference molecule.

Based on the principle of the bond energy additivity, as summarized by Cyrański,⁴⁵ various methods, such as the scheme of Cox and Pilche (bond energy additivity in 1970),⁶⁷ Cohen and Benson method (the group additivity in 1993),⁷⁴ and the harmonic oscillator stabilization energy (HOSE) model of Krygowski (1983)^{75,76} and Bird (1997)⁷⁷ were developed in order to calculate the energy of the reference molecule, and then to estimate the aromatic stabilization energy of an aromatic molecule. In the HOSE method, the reference is the Kekulé structure of an aromatic molecule itself, and the aromatic stabilization energy is defined as the energy necessary to deform the real molecule (such as a heterocyclic aromatic molecule) into its Kekulé structure. In the HOSE method, therefore, the empirical parameters a , b , and F need to be defined in order to calculate the individual bond energy. In a specific Kekulé structure, the distances of the localized single and double bonds are artificially specified, and they are constants. It seems that, in the HOSE method, the calculation of the individual bond energy is more reasonable than the scheme of Cox and Pilcher, and more reasonable than the Kistiakowsky method. The disadvantage of the HOSA model is that a reasonable number of resonance structures needs to be considered.

For the methods mentioned above, as Cyrański has pointed out, there are many structural factors that can affect the rationality of the calculation results. But I think the biggest problem is the limitations of the application of these methods. Or rather, by using a limited type of chemical bonds and using the limited empirical constants, it should be impossible to estimate the aromatic stabilizing energy of various types of aromatic molecules.

In the early structural theory of organic chemistry, the Dewar resonance energy (DRE) and the Hess-Schaad resonance energy⁷⁸⁻⁸¹ were two most common empirical resonance energy. The Dewar approach is often considered as the standard resonance energy, and the DREs for a broad range of systems, including polycyclic and heterocyclic compounds, have been reported. However, the DRE values are significantly less than the values calculated by other methods. For a specific aromatic molecule, the value of the aromatic stabilization energy, calculated by the different methods, is quite different. For the following six-membered heterocyclic aromatic molecules, for example, the size order of the Bird resonance energies (kcal/mol) is as follow (the original data were expressed as positive value):^{45,77}

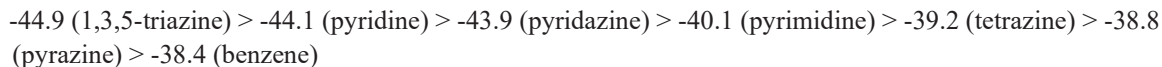
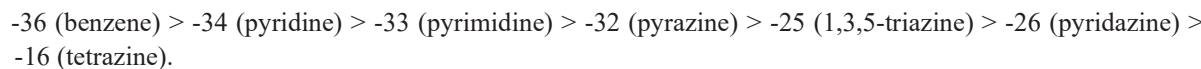


Table 6-5. For Aza-1,3,5-hexatrienes, Energy Effects (kcal/mol) ΔE^A , ΔE^{Am} and EDE = $\Delta E^A - \Sigma \Delta E^{Am}$, and the Corresponding Bond Length Changes dr_{m-n} (Å), Calculated Using Our 2007 Method at B3LYP/6-31G* Level.

Molecules	ΔE^A	ΔE^{A1}	dr_{2-3}	ΔE^{A2}	dr_{4-5}	$\Sigma \Delta E^{Am}$	EDE
NH=CH-CH=CH-CH=CH ₂	4.6	1.4	0.004	3.0	0.008	4.4	0.2
CH ₂ =N-CH=CH-CH=CH ₂	8.4	5.0*	0.012	2.1	0.005	7.0	1.4
CH ₂ =CH-N=CH-CH=CH ₂	6.8	5.2*	0.011	0.8	0.002	6.0	0.9
NH=N-CH=CH-CH=CH ₂	4.7	2.2*	0.000	2.6	0.006	4.5	0.2
NH=CH-N=CH-CH=CH ₂	3.4	3.0	0.010	0.3	0.000	3.2	0.2
NH=CH-CH=N-CH=CH ₂	6.4	1.0	0.002	5.3*	0.011	6.3	0.2
CH ₂ =N-N=CH-CH=CH ₂	9.4	7.8	0.027	0.3	-0.001	8.1	1.3
CH ₂ =N-CH=CH-N=CH ₂	9.9	4.0	0.008	4.0*	0.008	9.9	2.0
NH=CH-N=CH-N=CH ₂	4.7	2.6	0.007	1.4	0.005	4.0	0.7

*The energy effects correspond to the blue solid circle in Figure 6-6a.

Accordingly, the aromatic stabilization energy of the six-membered heterocyclic aromatic molecules are all greater than that (-36 kcal/mol) of benzene. The above size order should be unreasonable. The resonance energies (kcal/mol), determined by the energies of hydrogenation, have the following size order:⁸²



The range of a series of resonance energies described above is 20 kcal/mol, although the resonance energy of benzene is the largest. The above size orders show also a fact that, in the literature, there is no a universal method that can be used to determine the aromatic stabilization energy of aromatic molecules of various types.

Now, we have found a new type of energy effect ΔE^{Am} . In particular, as will be shown in this and subsequent chapters, our 2007 method and our 2011 method can be reasonably applied to all types of conjugated compounds, whether it is aromatic, non-aromatic, or anti-aromatic.

6.2.1. Aza-1,3,5-Hexatrienes

In order to understand the effect of heteroatom(s) on the additivity, the energy effects, ΔE^A and ΔE^{Am} , of aza-1,3,5-hexatrienes are calculated at B3LYP/6-31G* level. According to Table 6-5, always $\Delta E^A > 0$, $\Delta E^{Am} > 0$, and $\Delta E^A \approx \Sigma \Delta E^{Am}$. In the case of aza-1,3,5-hexatriene(s), the energy effects ΔE^{Am} are still additive. For molecule NH=CH-CH=CH-CH=CH₂, for example, the values (kcal/mol) of energy effects are as follows:

$$\Delta E^A = 4.6, \Sigma \Delta E^{Am} = 4.4, \text{ and } \Delta E^A - \Sigma \Delta E^{Am} = 0.2.$$

$$\Delta E^A \approx \Sigma \Delta E^{Am}$$

Table 6-5 also shows that the position of nitrogen atom has a larger influence on the energy effect ΔE^{Am} . Position effects are ranked from strong to weak according to the following order of energy effects ΔE^{Am} (kcal/mol) from large to small:

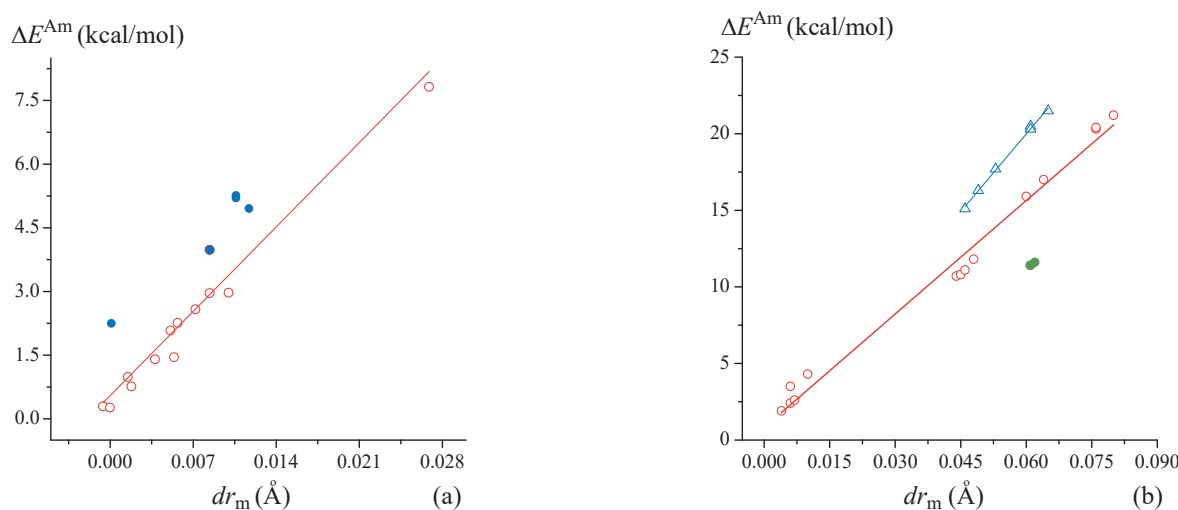


Figure 6-6. (a) For aza-1,3,5-hexatrienes at B3LYP/6-31G*, the energy effect ΔE^{Am} , except for those corresponding to the blue solid circles, can be fitted as a linear function of dr_{m-n} . (b) For substituted divinyl ether-like species containing nitrogen and oxygen atom(s), two groups of energy effects ΔE^{Am} can be fitted as the linear function of dr_{m-n} .

7.8 ($\text{CH}_2=\text{N}-$ and $-\text{N}=\text{CH}-$) > 5.3 ($-\text{CH}=\text{N}-$ and $-\text{CH}=\text{CH}_2$) \approx 5.2 ($\text{CH}_2=\text{CH}-$ and $-\text{N}=\text{CH}-$) \approx 5.0 ($\text{CH}_2=\text{N}-$ and $-\text{CH}=\text{CH}-$) > 3.0 ($\text{NH}=\text{CH}-$ and $-\text{N}=\text{CH}-$) > 1.4 ($\text{NH}=\text{CH}-$ and $-\text{CH}=\text{CH}-$, and $-\text{N}=\text{CH}$ and $-\text{N}=\text{CH}_2$) > 0.8 ($-\text{N}=\text{CH}-$ and $-\text{CH}=\text{CH}_2$) > 0.3 ($-\text{N}=\text{CH}-$ and $\text{CH}=\text{CH}_2$)

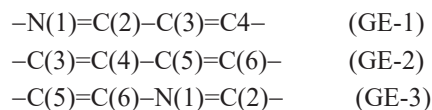
In the case of molecule $\text{NH}=\text{CH}-\text{N}=\text{CH}-\text{CH}=\text{CH}_2$, the energy effect ΔE^{A^2} , associated with the π interaction between the $-\text{N}=\text{CH}-$ and $-\text{CH}=\text{CH}_2$ double bonds, is 0.3 kcal/mol, and it is the smallest of all the energy effects listed in Table 6-5, which may be attributed to the larger charge transfer interaction between the electron-withdrawing group $-\text{N}=\text{CH}-$ and the electron-releasing double bond $-\text{CH}=\text{CH}_2$. For molecule $\text{NH}=\text{CH}-\text{CH}=\text{N}-\text{CH}=\text{CH}_2$, on the contrary, the large energy effect (5.3 kcal/mol), associated with the interaction between the $-\text{CH}=\text{N}-$ and $-\text{CH}=\text{CH}_2$ groups, may attribute to the large exchange interaction between them two.

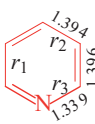
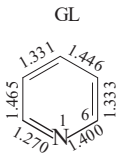
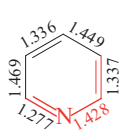
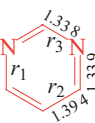
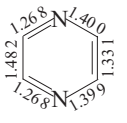
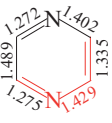
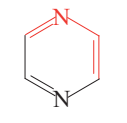
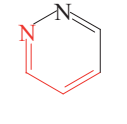
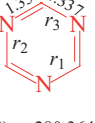
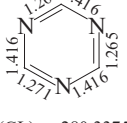
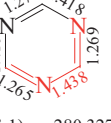
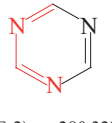
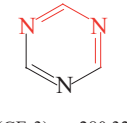
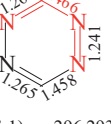
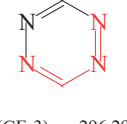
In addition, as shown by Figure 6-6a, the energy effects ΔE^{Am} (y), except for those corresponding to the blue solid circles in the Figure, can be fitted as the following linear function of dr_{m-n} (x):

$$y = 0.54725 + 283.87426x \quad (\text{cc} = 0.93296)$$

6.2.2. Benzene-like Species

For a six-membered heterocyclic aromatic compound (shortened into “benzene-like species”), three GE-m geometries are obtained from the local conjugation interaction between the corresponding pairs of double bonds. For different molecules, the number of GE-m geometries is different due to the difference in the symmetry of GL geometry. For pyridine, for example, the symmetry of the GL geometry is C_s , so its three GE-m geometries are not equivalent, and they all need to be independently optimized. In the three GE-m geometries (Figure 6-7a), the two conjugated double bonds (represented by the red lines) are as follows, respectively:



	Ground	GL	GE-1	GE-2	GE-3	ESE
(a) Pyridine	 $E(G) = -248.28497$ hartree $r_1 = 1.394$, $r_2 = 1.396$, $r_3 = 1.399$	 $E(GL) = -248.26507$ $\Delta E^A = -12.5$	 $E(GE-1) = -248.24862$ $\Delta E^{A1} = 5.6$ $dr_1 = 0.017$	 $E(GE-2) = -248.24862$ $\Delta E^{A2} = 10.3$ $dr_2 = 0.027$	 $E(GE-3) = -248.24898$ $\Delta E^{A3} = 10.1$ $dr_3 = 0.028$	$ESE = -38.5$ kcal/mol
(b) Pyrimidine	 $E(G) = -264.32372$ $r_1 = 1.338$, $r_2 = 1.339$, $r_3 = 1.339$	 $E(GL) = -264.30041$ $\Delta E^A = -14.6$	 $E(GE-1) = -264.28306$ $\Delta E^{A1} = 10.9$ $dr_1 = 0.029$	 $E(GE-2) = -264.29026$ $\Delta E^{A2} = 6.4$ $dr_2 = 0.019$	 $E(GE-3) = -264.29143$ $\Delta E^{A3} = 5.6$ $dr_3 = 0.020$	$ESE = -37.5$
(c) Pyrazine	 $E(G) = -264.31722$ $r_1 = 1.339$, $r_2 = 1.339$, $r_3 = 1.338$	 $E(GL) = -264.29825$ $\Delta E^A = -11.9$	 $E(GE-1) = -264.29213$ $\Delta E^{A1} = 3.8$ $dr_1 = 0.012$	 $E(GE-2) = -264.28067$ $\Delta E^{A2} = 11.0$ $dr_2 = 0.030$	 $E(GE-3) = -264.28067$ $\Delta E^{A3} = 11.0$ $dr_3 = 0.030$	$ESE = -37.8$
(d) Pyradazine	 $E(G) = -264.28759$ $r_1 = 1.336$, $r_2 = 1.336$, $r_3 = 1.384$	 $E(GL) = -264.27060$ $\Delta E^A = -10.7$	 $E(GE-1) = -264.25488$ $\Delta E^{A1} = 9.9$ $dr_1 = 0.040$	 $E(GE-2) = -264.26095$ $\Delta E^{A2} = 6.1$ $dr_2 = 0.017$	 $E(GE-3) = -264.26095$ $\Delta E^{A3} = 6.1$ $dr_3 = 0.017$	$ESE = -32.6$
(e) Triazine	 $E(G) = -280.36477$ $r_1 = 1.337$, $r_2 = 1.337$, $r_3 = 1.337$	 $E(GL) = -280.33753$ $\Delta E^A = -17.1$	 $E(GE-1) = -280.32740$ $\Delta E^{A1} = 6.3$ $dr_1 = 0.022$	 $E(GE-2) = -280.3274$ $\Delta E^{A2} = 6.3$ $dr_2 = 0.022$	 $E(GE-3) = -280.3274$ $\Delta E^{A3} = 6.3$ $dr_3 = 0.022$	$ESE = -36.1$
(f) Tetrazine	 $E(G) = -296.32115$ $r_1 = 1.326$, $r_2 = 1.339$, $r_3 = 1.326$, $r_4 = 1.339$	 $E(GL) = -296.29973$ $\Delta E^A = -13.4$	 $E(GE-1) = -296.29374$ $\Delta E^{A1} = 3.8$ $dr_1 = 0.013$	 $E(GE-2) = -296.28184$ $\Delta E^{A2} = 11.2$ $dr_2 = 0.050$	 $E(GE-3) = -296.29374$ $\Delta E^{A3} = 3.8$ $dr_3 = 0.013$	$ESE = -32.2$

$$ESE = [\Delta E^A - (\Delta E^{A1} + \Delta E^{A2} + \Delta E^{A3})] \text{ (kcal/mol)} \quad \Delta E^A = E(G) - E(GL) \text{ (kcal/mol)} \quad \Delta E^{Am} = E(GL) - E(GE-m) \text{ (kcal/mol)} \quad dr_m = r_m(GE-m) - r_m(GL) \text{ \AA}$$

Figure 6-7. For each six-membered heterocyclic aromatic molecule, the molecular energies, $E(G)$, $E(GL)$ and $E(GE-m)$ (hartree), of the ground state (G), GL and GE-m ($m=1, 2, 3$) geometries, and the extra stabilization energy (ESE) (kcal/mol), calculated using our 2007 method at the B3LYP/6-31G*level. Where $dr_m = [r_m(GE-m) - r_m(GL)]$ (Å) quantifies the effect of the local conjugation between two double bonds represented by the red lines on the single bond distance between them two.

In the case of 1,3,5-triazine, the GL geometry has the C_{3v} symmetry (Figure 6-7e), and its three GE-m geometries are equivalent. For benzene-like species, as shown by the data presented in Figure 6-7, the following energy features are the same as those of benzene and can be considered as the basic features of aromatic molecules:

$$\Delta E^A = [E(G) - E(GL)] < 0$$

$$\Delta E^{Am} = [E(GE-m) - E(GL)] > 0$$

$$ESE = \Delta E^A - \Sigma \Delta E^{Am} < 0$$

For benzene-like species at B3LYP/6-31G* level, the absolute size order of the ESEs (kcal/mol) is as follow:

-39.0 (benzene) > -38.5 (pyridine) > -37.8 (pyrazine) > -37.5 (pyrimidine) > -36.1 (1,3,5-triazine) > -32.6 (pyridazine) > -32.2 (tetrazine)

This size order is basically the same as the order determined by the hydrogenation method. For all of the benzene-like species, the ESEs are less in absolute value than the ESE (-39.0 kcal/mol) of benzene. In the series of the ESE values, the difference between the greatest ESE (-38.5 kcal/mol, pyridine) and the smallest ESE value (-32.2 kcal/mol, tetrazine) is -6.8 kcal/mol. This difference is very close to the range (-6.1 kcal/mol) of the series of the aromatic stabilization energies determined by the Bird method. According to the size order and range, therefore, the ESE values should be reasonable.

The following size order of the energy effects ΔE^{Am} (kcal/mol) is similar to those for aza-1,3,5-hexatrienes:

3.8 (-N=CH- and -CH=N-) < 5.6 (-CH=CH- and -CH=N-) < 6.3 (-CH=N- and -CH=N-) < 10.1 (-CH=CH- and -N=CH-) < 11.2 (-CH=N- and -N=CH)

The smaller value of ΔE^{Am} should correspond to the larger charge transfer interaction between a pair of double bonds, and the larger value results from the larger exchange interaction. Correspondingly, $dr_m = [r_m(GE-m) - r_m(GE-m)] > 0$ without exception, where $r_m(GE-m)$, for example, is the single bond distance between two conjugated double bonds in GE-m geometry.

In the six-membered ring of the benzene-like species, therefore, the local conjugation between a pair of double bonds is always destabilization.

6.2.3. Furan-like Species

The resonance energies of imidazole and pyrrole, determined by the Bird's modification of the HOSE Model, are -34.9 and -31.8 kcal/mol, respectively. The aromatic stabilization energies (kcal/mol) of five-membered heterocyclic aromatic molecules (shortened into "furan-like species"), determined by Cyrański, are as follows (in the original literature, the values are expressed as positive):⁴⁵

-23.7 (2-aza-pyrrole) > -20.6 (pyrrole) > -18.8 (imidazole) > -17.3 (2-aza-furan) > -14.8 (furan) > -12.4 (oxazole).

And the size order (kcal/mol) of DREs is as follow:⁶³

-4.3 (furan) < -5.3 (pyrrole) < 15.4 (imidazole)

Cyrański's size order is basically in line with the following Minkin's rule:⁸³ the greater the electronegativity difference between a hetero atom (the O(1) or N(1) atom) and its bonded atom (the C(5), C(2) or N(2) atom) is, the weaker the aromaticity of a heterocyclic molecule is.

6.2.3.1. Substituted Divinyl Ether-like Species

In benzene and benzene-like species, each double bond participates in the formation of the GE-m geometry



Figure 6-8. For each five-membered heterocyclic aromatic molecule, the ground state (G), and its GL and GE-m ($m = 1, 2, 3$) geometries, and the less destabilization energy (LDE) at the B3LYP/6-31G* level. The meaning of the red lines and symbol dr_m is the same as in Figure 6-7.

twice. In each double bond, each atom has only one chance to participate in the formation of the GE-m geometry through bonding. For a furan-like species such as Furan, as shown by Figure 6-8, the energy effects ΔE^{Am} ($m = 1, 2, 3$) arise, respectively, from the local conjugation interactions between following three pairs of groups:

- C(2)=C(3)- and -C(4)=C(5)- (GE-1)
- O- and -C(2)=C(3)- (GE-2)
- O- and -C(5)=C(4)- (GE-3).

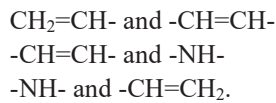
Table 6-6. For Substituted Divinyl Ether-like Species Containing Nitrogen or Oxygen Atom(s), Various Energy Effects (kcal/mol) and the Corresponding Single Bond Length Changes (Å), Obtained from Our 2007 Method at B3LYP/ 6-31G* Level.

	ΔE^A	ΔE^{A1}	dr_{2-3}	ΔE^{A2}	dr_{4-5}	ΔE^{A3}	dr_{5-6}	$\Sigma \Delta E^{Am}$	ESE
<chem>CH2=CH-NH-CH=CH2</chem>	36.0	20.3	0.061	20.3	0.061			40.6	-4.6
<chem>CH2=CH-O-CH=CH2</chem>	37.3	20.3	0.076	20.3	0.076			40.6	-3.3
<chem>CH2=CH-NH-CH=NH</chem>	27.5	21.5	0.065	10.7	0.044			32.2	-4.6
<chem>CH2=CH-O-CH=NH</chem>	29.1	21.2	0.080	11.4	0.061			32.6	-3.4
<chem>NH=CH-NH-CH=NH</chem>	19.4	11.8	0.048	11.8	0.048			23.5	-4.1
<chem>CH2=CH-CH=CH-NH-CH=CH2</chem>	38.5	2.6	0.007	16.3	0.049	20.5	0.061	39.4	-0.9
<chem>CH2=CH-CH=CH-O-CH=CH2</chem>	40.2	1.9	0.004	17.0	0.064	20.4	0.076	39.3	0.9
<chem>CH2=CH-CH=CH-NH-CH=NH</chem>	30.4	2.4	0.006	17.7	0.053	10.8	0.045	30.9	-0.4
<chem>CH2=CH-CH=CH-O-CH=NH</chem>	30.4	2.4	0.006	17.7	0.053	10.8	0.045	30.9	-0.4
<chem>CH2=N-CH=CH-O-CH=NH</chem>	33.1	3.5	0.006	15.9	0.060	11.6	0.062	33.1	2.1
<chem>CH2=N-CH=CH-NH-CH=NH</chem>	31.2	4.3	0.010	15.1	0.046	11.1	0.046	30.5	0.6

The red, blue and green color data correspond to the color lines in Figure 6-6b.

In the two geometries GE-2 and GE-3, the π -electron lone pair (π -lone pair) of oxygen atom is involved in the local conjugation. Therefore, the substituted divinyl ether-like species containing nitrogen or oxygen atom(s) can be used to examine the effect of the local conjugation between the π -lone pair and the double bond on the additivity.

From the left to the right of Table 6-6, the energy effect ΔE^{Am} corresponds to the local conjugation between a pair of bonded groups from left to right of the molecule. For molecule CH2=CH-CH=CH-NH-CH=CH2 (an ethenyl-substituted divinyl ether-like species containing a nitrogen atom), for example, the three energy effects ΔE^{Am} (kcal/mol) are related to the following three pairs of conjugated groups:



and

$$\Sigma \Delta E^{Am} = \Delta E^{A1} + \Delta E^{A2} + \Delta E^{A3} = 39.4, \text{ and } \Delta E^A = 38.5$$

$$\Delta E^A \approx \Sigma \Delta E^{Am}$$

According to Figure 6-6b, the values of the energy effects ΔE^{Am} can be divided into two groups. In Table 6-6 and Figure 6-6b, the first group of the values are shown in red, and the second group of the values are shown in blue. These two groups of the energy effects (y) can be fitted as the following two linear functions of dr_{m-n} (x):

$$y = 0.81433 + 247.04434x \text{ (red, cc = 0.9859)}$$

$$y = -0.27669 + 337.66938x \text{ (blue, cc = 0.9968)}$$

For the first four molecules listed in Table 6-6, always

$\Delta E^A > 0$, $\Sigma \Delta E^{Am} > 0$, and $\Delta E^A < \Sigma \Delta E^{Am}$

$\Delta E^A - \Sigma \Delta E^{Am} < 0$

$|(\Delta E^A - \Sigma \Delta E^{Am})| / \Sigma \Delta E^{Am} \approx 0.1$

For all the molecules listed in Table 6-6, the energy effect ratio, $|(\Delta E^A - \Sigma \Delta E^{Am})| / \Sigma \Delta E^{Am}$, decreases from about 10% to about 2% with the increasing of the numbers of the double bonds and heteroatoms increase. In the case of the substituted divinyl ether-like species, the energy effects $\Sigma \Delta E^{Am}$ can be considered additive.

6.2.3.2. ESE for Furan-like Species

According to Figure 6-8, the fundamental difference between the benzene-like and furan-like species is as follows:

$\Delta E^A > 0$ for furan-like species

$\Delta E^A < 0$ for benzene-like species

The energy effect difference, $\Delta E^A - \Sigma \Delta E^{Am}$, for furan-like species is still stabilizing, and the size order (kcal/mol) of the absolute values is as follow:

-53.1 (2-aza-pyrrole) > -49.4 (pyrrole) > -46.5 (imidazole) > -39.3 (furan) > -39.0 (benzene) > -39.0 (2-aza-furan) > -36.3 (oxazole)

Since the values of the above energy effect differences ($\Delta E^A - \Sigma \Delta E^{Am}$) are more negative than the ESE (-39.0 kcal/mol) of benzene, our 2007 method needs improvement. The following energy effect differences (kcal/mol), ($\Delta E^A - \Sigma \Delta E^{Am}$), are obtained from our 2011 method that is an improved version of the 2007 method (Our 2011 method will be detailed in Chapter 8):

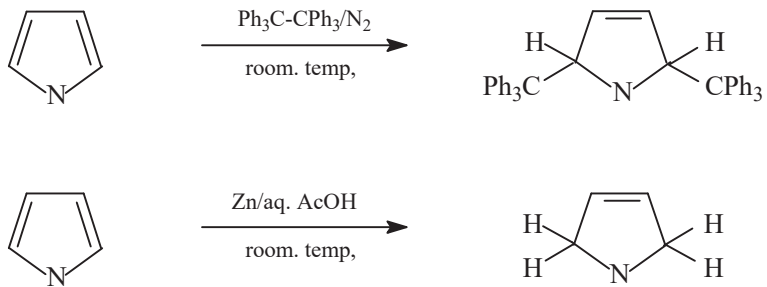
-44.9 (2-aza-pyrrole) > -41.0 (pyrrole) > -38.9 (imidazole) > -36.3 (benzene) > -33.1 (2-aza-furan) > -32.8 (furan) > -30.5 (oxazole)

The above size order is the same as the order determined by Cyrański. When our 2011 method is used, the energy effects ΔE^A for furan-like species are still destabilizing ($\Delta E^A > 0$), but their values are smaller than the corresponding values obtained from our 2007 method. For furan, for example, the values (kcal/mol) of the energy effects ΔE^A decreases from 33.5 (2007) to 18.1 (2011) due to that the two-electron exchange integrals, as well as the Fork matrix and overlap integral matrix elements, are conditionally deleted. But some energy effect differences ($\Delta E^A - \Sigma \Delta E^{Am}$) are still more negative than that of benzene.

In the case of furan-like species, the facts that $\Delta E^A > 0$, $\Sigma \Delta E^{Am} > 0$ and $(\Delta E^A - \Sigma \Delta E^{Am}) < 0$ only mean that the five-membered heterocyclic rings are less destabilized than their corresponding virtual reference molecules, rather than more stabilized, which is fundamentally different from benzene-like species. As far as $\Delta E^A > 0$ is concerned, furan-like species should not be regarded as aromatic although $(\Delta E^A - \Sigma \Delta E^{Am}) < 0$. In other words, for an aromatic molecule, its adiabatic delocalization energy must be stabilizing ($\Delta E^A < 0$), which can be regarded as an important energy criterion for judging the aromaticity of molecules.

Electrophilic substitution reactions of aromatic compounds are usually very much easier than addition reactions. In fact, as shown by the literatures,^{8,84-86} Diels-Alder reactions of furan and like species can be proceed under the appropriate conditions, and the use of furan as a diene in the inter- and intra-molecular Diels-Alder reactions is one of the most common applications in organic synthesis. For the following two reactions, in addition, the main

products are from the 2,5-addition reactions:⁸⁷



6.2.3.3. π -Charge Transfer Energy and Chemical Shifts

According to the Epiotis' interpretation,³⁷ the ring current occurring in aromatic ring should depend upon the π charge transfer (CT).

In Figure 6-9, the red and blue dotted arrows indicate the direction of the CT interaction between the double bonds P and Q, and a solid (green) arrow represents the orientation of the net CT. For pyridine, for example, a blue dotted arrow in the aromatic ring, pointing from the nitrogen atom to the adjacent carbon atom, indicates that the corresponding CT energy effect, associated with charge transfer from the C=N bond to the C=C bond, is -0.9676 hartree (blue value). In benzene-like species, each set of (red or blue) dotted arrows form a closed CT loop around the aromatic ring. In 2000,⁵ we found that there is a polynomial relationship between the experimental chemical shift δ (ppm)⁹ and the theoretical CT energy effect ΔE_{ov}^{pq} . In our 2000 work, the CT energy effects were calculated using our 1998 method at RHF/STO-3G level. In this section, the CT energy effects are recalculated using our 2011 method at RHF/6-31G* level.

Inspection of the orientations of the green solid arrows in Figure 6-9 shows that there are two groups of aromatic compounds. In the first group of compounds, such as pyridine, pyrimidine and triazine, three solid green arrows point in the same direction, clockwise or anti-clockwise. In the second group of compounds such as pyrazine, pyridazine and naphthalene, there are two reverse green arrows pointing to two equivalent atoms.

In the case of benzene-like species, as shown by Figure 6-9b, the chemical shift δ (pp m) (y) can be fitted as a second order polynomial function of ΔE_{ov}^{pq} (x) ($cc = 0.94461$):

$$y = 5.62047 - 4.08556x - 1.01218x^2$$

In this case, the energy effect ΔE_{ov}^{pq} is caused by the CT interaction that directs to the carbon atom bonded to the hydrogen atom, and the chemical shift of the hydrogen atom corresponds to the CT interaction energy. For the hydrogen at o-position of pyridine, for example, the chemical shift is 8.58 ppm, and the corresponding energy effect ΔE_{ov}^{pq} , arising from the charge transfer from C=N bond to C=C bond (dotted blue arrows), is -0.9676 hartree.

In the case of furan-like species, there is no such closed CT loop around the five-membered ring. In furan, for example, the charge transfer between the oxygen atom and the CC double bond is unidirectional. In this molecule, the energy effect, arising from the π charge transfer from oxygen to the CC double bond, is -0.8131 hartree, and the energy effect, arising from the π charge transfers from the CC double bond to oxygen, is 0.0338 hartree. May be due to the unidirectional CT interaction, as shown by the blue triangle points in Figure 6-9b, the chemical shifts (6.42 and 6.07 ppm) of the β -hydrogens for furan and pyrrole are all less than 7.0 ppm, and are close to the chemical shift (6.36 ppm) of cyclobutadiene that is calculated at RHF/6-31G* level using Gaussian 98 program.

According to that the energy effects ($\Delta E^A > 0$, $\Sigma \Delta E^{Am} > 0$), chemical shifts and addition reactions, furan-like species do not appear to be aromatic.

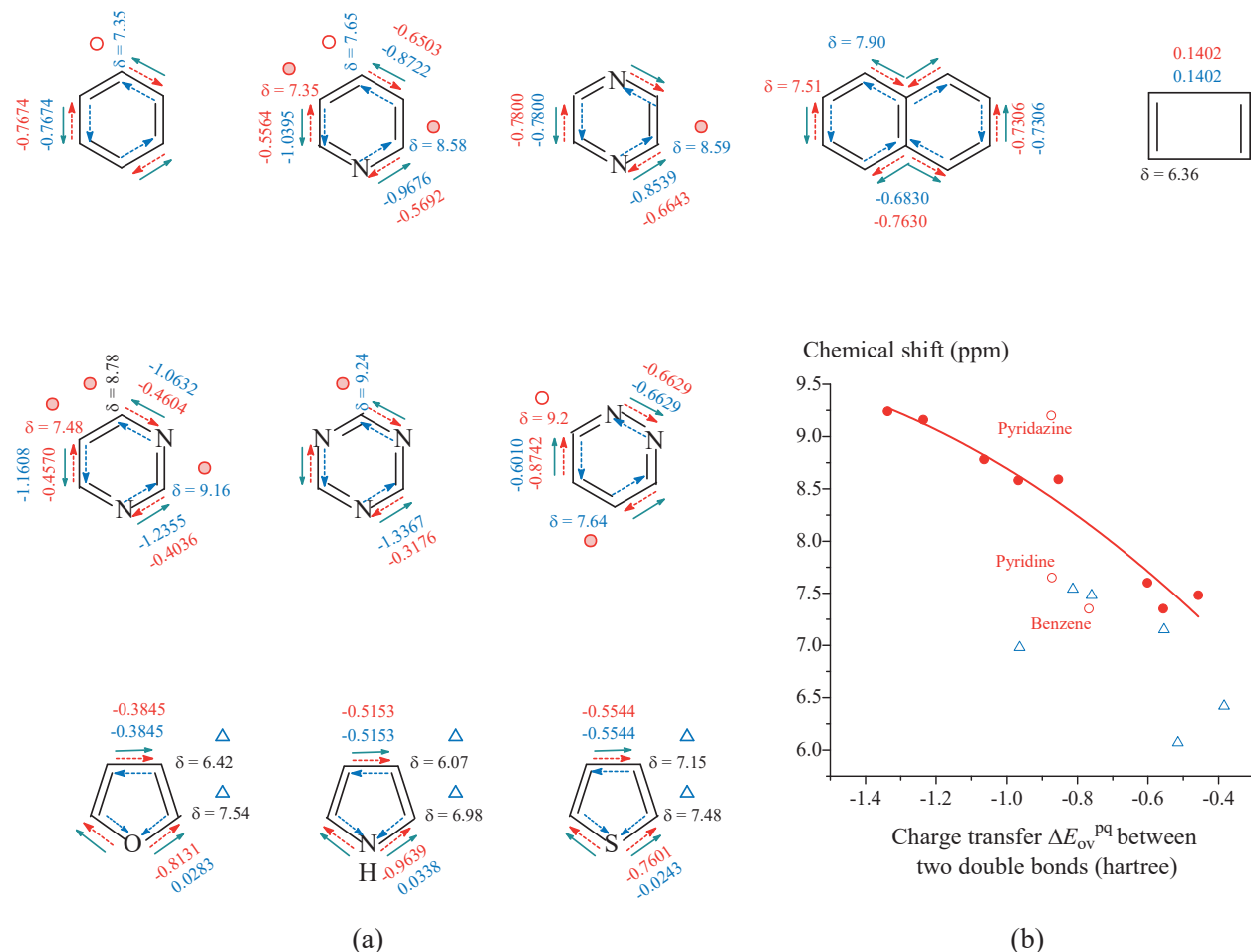


Figure 6-9. (a) The charge transfer (CT) energies, ΔE_{ov}^{PQ} and ΔE_{ov}^{QP} , between the double bonds P and Q, are calculated at RHF/6-31G* level using our 2011 method, and the experimental chemical shift (ppm). The blue and red dotted arrows indicate the directions of the two CT energy components ΔE_{ov}^{PQ} and ΔE_{ov}^{QP} , and the green solid arrows indicate the direction of the net CT ($\Delta E_{ov}^{PQ} - \Delta E_{ov}^{QP}$). Red hollow and solid circles and blue triangles correspond to the points $[\Delta E_{ov}^{PQ}, \delta]$ in Figure 6-9b. (b) Chemical shift versus ΔE_{ov}^{PQ} .

6.3. SUBSTITUTED BENZENES

Substituent effect is one of the most important structural effects, and it affects the chemical, physicochemical, and biochemical properties of organic compounds. The structural theory of organic chemistry is essentially qualitative. However, there exist a number of quantitative relationships between molecular structure and properties. The oldest and most familiar is the Hammett equation. In 1935, Hammett introduced the concept of the substituent constant to quantitatively describe the relationship between the substituent constant and the rate of reaction and between the substituent constant and the equilibrium constant of reaction.⁸⁸

Substituents of benzene ring may be divided into three categories. The substituents of the first category, such as $-NO_2$ and $-CN$, are the electron-withdrawing group. Such substituents attract part of the electron charge from its ortho- and para-positions on benzene ring. Therefore, these substituents deactivate the nucleophilicity of the benzene

ring, and are meta directing. The substituents of the second category, such as $-\text{NH}_2$, are the electron-releasing group. These substituents donate part of electron charge to its ortho- and para-positions on the benzene ring. So, such substituents activate the nucleophilicity of benzene ring, and are ortho and para directing. The substituents of the third category, such as $-\text{Cl}$ and $-\text{F}$, deactivate nucleophilicity of the benzene ring through induction, and are kinetically ortho and para directing through conjugation. In the literature, the Hammett substituent constants are often used to quantify the ability of substituents to release or to withdraw electron charge.

In this section, the restricted geometry optimization will be used to quantitatively distinguish between conjugation and inductive effects. May say so, the restricted geometry optimization provides a new way to quantitatively research substituent effects.

In addition, as will be shown in this section, the π interaction (conjugation) between substituent and phenyl ring is destabilization, so the bond length between substituent and phenyl ring in the localized geometry is shorter than the corresponding bond length in the ground state geometry. This confirms that the π - π interaction is a driving force of molecular distortion.

6.3.1. Extra Stabilization Energy

In the literature, the homodesmotic reactions,⁴⁵ as well as the isomerization reaction,⁴⁶ were used to calculate the aromatic stabilization energies, ASE(n) ($n = 1, 2, 3, 4$), of substituted benzenes. The size orders of ASE(n) (kcal/mol) for five mono-substituted benzene molecules are as follows:

- ASE(1): -34.1 (phenol) > -33.5 (chlorobenzene) > -33.4 (nitro-benzene) > -33.2 (benzene) > -33.2 (aniline) > -33.1 (Fluorobenzene).
- ASE(2): -28.5 (nitrobenzene) > -24.9 (cyano-benzene) > -24.7 (benzene) > -24.6 (aniline) > -22.6 (fluorobenzene) > -22.5 (phenol).
- ASE(3): -31.9 (cyanobenzene) > -31.7 (nitro-benzene) > -30.7 (benzene) > -29.6 (aniline) > -29.3 (fluorobenzene) > -29.2 (phenol).
- ASE(4): -33.3 (aniline) > -32.7 (benzene) > -32.2 (fluorobenzene) > -32.1 (phenol) > -31.6 (cyaobenzene) > -31.3 (nitrobenzene).

For mono-substituted benzenes, the isomerization reactions are not always available. In order to calculate the aromatic stabilization energies, such as ASE(1), by isomerization reactions, therefore, the substituted benzenes must be replaced with the substituted toluenes.

The existence of substituent should always weaken the aromaticity of the benzene ring according to the geometrical criteria. However, as shown by the above size orders of the ASE(n), the aromatic stabilization energy of benzene is not the biggest. In addition, the size orders of ASE(n) ($n = 1, 2, 3, 4$) are different from each other. For the ASE(2), for example, -28.5 (nitrobenzene) > -24.6 (aniline), But for ASE(4), -31.3 (nitrobenzene) < -33.3 (aniline).

In order to calculate the ESE of substituted benzenes, the GL and GE-m ($m = 1, 2, 3$) geometries of substituted benzene are obtained from the restricted geometry optimization using our 2007 method at B3LYP/6-31G* level, and the number of the GE-m geometries that must be optimized depends on the symmetry of the GL geometry. In the GL geometry, as shown by the red groups in Figure 6-10, the substituent(s) should be contained in the double bond group to which it is bonded. In Figure 6-10, the black line between the red groups means that the two red groups are not conjugated. In the GL geometry of 1,2,4-trihydroxy-benzene, for example, three π systems are respectively localized on the following three double bond groups: $-\text{C}(1)(\text{OH})=\text{C}(2)(\text{OH})-$, $-\text{C}(3)=\text{C}(4)(\text{OH})-$, and $-\text{C}(5)=\text{C}(6)-$. In the corresponding three GE-m geometries that need to be optimized, a locally delocalized π system arises from the local conjugation between the corresponding pairs of the localized double bond groups in the GL geometry, and these three π systems are respectively localized on the following groups: $-\text{C}(1)\text{OH}=\text{C}(2)\text{OH}-\text{C}(3)=\text{C}(4)\text{OH}-$ (GE-1), $-\text{C}(3)=\text{C}(4)\text{OH}-\text{C}(5)=\text{C}(6)-$ (GE-2), $-\text{C}(2)\text{OH}=\text{C}(1)\text{OH}-\text{C}(6)=\text{C}(5)-$ (GE-3). For 1,2,4-trihydroxy-benzene,

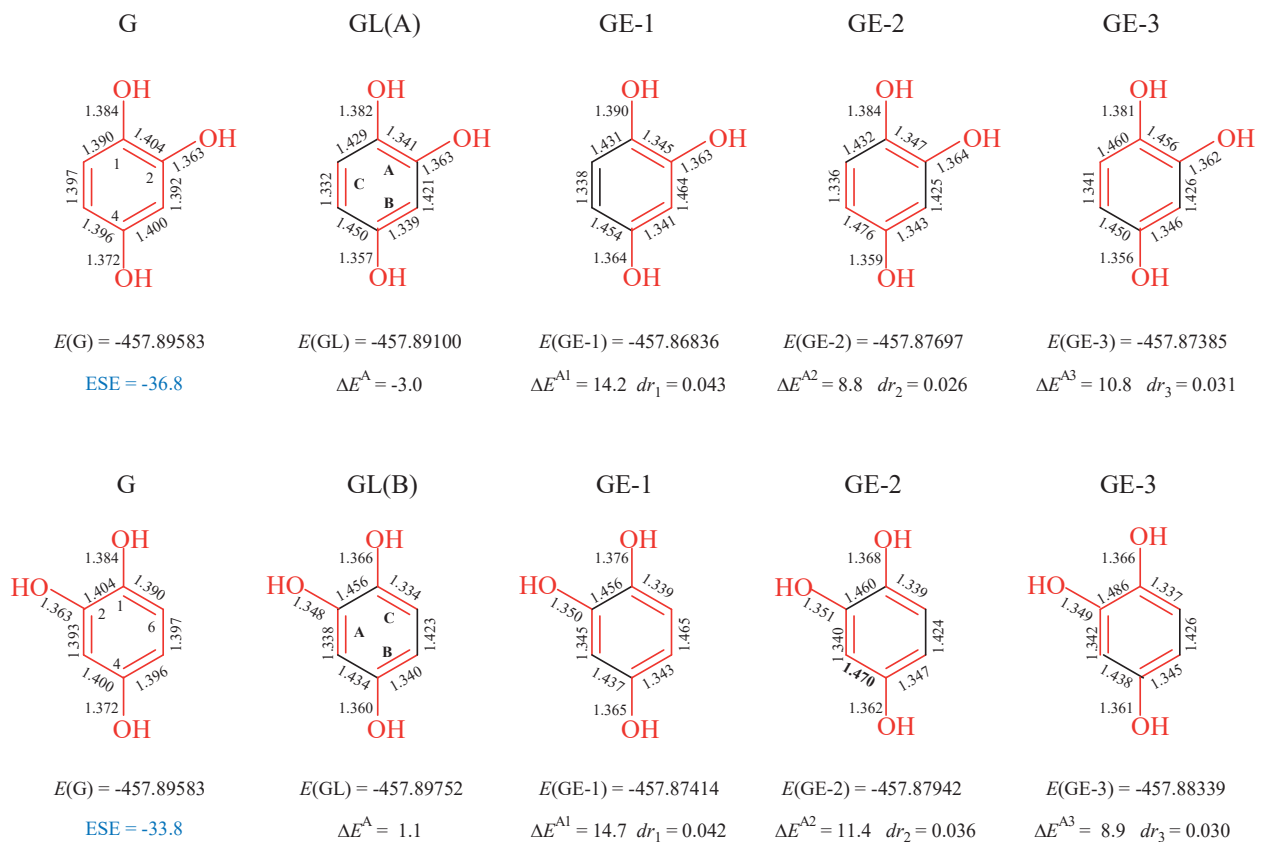


Figure 6-10. For 1,2,4-trihydroxy-benzene, the molecular energy of the ground state (G), GL and GE-m ($m = 1, 2, 3$) geometries, and the extra stabilization energy (ESE) calculated by our 2007 method at the B3LYP/6-31G* level. The meanings of the red lines and symbol dr_m are the same as those in the Figure 6-7.

however, there should be another candidate GL(B) for the GL geometry (Figure 6-10). In the GL(B) geometry, π systems are respectively localized on the following groups: $-C(2)OH=C(3)-$, $-C(4)OH=C(5)-$, and $-C(6)=C(1)OH-$. Based on the two candidates, GL(A) and GL(B), for the GL geometry, the extra stabilization energy (ESE) for 1,2,4-trihydroxy-benzene, defined as $ESE = \Delta E^A - (\Delta E^{A1} + \Delta E^{A2} + \Delta E^{A3})$, is -36.8 and -33.8 kcal/mol, respectively.

According to the CC bond lengths of 1,3,5-trihydroxybenzene, the three CC double bonds in the GL(B) geometry are localized on the three shorter CC bonds of the ground state geometry. Therefore, the candidate GL(B) geometry is considered to be more reasonable than the candidate GL(A) geometry, which is named the position rule for choosing the GL geometry from the candidate geometries. The rationality of the position rules will be discussed in the next chapter. According to the position rule, the ESEs of sixteen substituted benzenes are calculated using our 2007 method at B3LYP/6-31G* level, and are listed in Table 6-7.

For planar mono-substituted benzenes, there is only one candidate for the GL geometry, and the size order of the ESEs(SB) values (kcal/mol) is as follow:

$$\begin{aligned} & -39.0 \text{ (benzene)} > -38.3 \text{ (fluoro-benzene)} > -38.1 \text{ (phenol)} > -38.0 \text{ (chloro-benzene)} > -37.6 \text{ (nitro-benzene)} > \\ & -37.3 \text{ (cyanobenzene)} > -35.5 \text{ (aniline)} \end{aligned}$$

For aniline containing a strong electron-releasing group $-NH_2$, the absolute value of ESE is the smallest. For

Table 6-7. For Sixteen Substituted Benzenes (Planar), Molecule Energy $E(G)$ (hartree), Extra Stabilizing Energies (ESE) and Their Components (kcal/mol) ΔE^A , ΔE^{Am} , and Bond Length Differences dr_m (\AA) Corresponding to Energy Effects ΔE^{Am} , Calculated Using our 2007 Method at B3LYP/6-31G* Level.

R	o-R	m-R	p-R	$E(G)$	ΔE^A	ΔE^{A1}	dr_1	ΔE^{A2}	dr_2	ΔE^{A3}	dr_3	ESE
CN				-324.49222	-11.7	6.9	0.015	9.9	0.031	8.8	0.023	-37.3
NO ₂				-436.75058	-12.3	6.7	0.014	10.0	0.027	8.7	0.023	-37.6
F				-331.48231	-9.2	11.1	0.030	9.0	0.026	9.1	0.023	-38.3
CL				-691.84497	-9.3	9.5	0.025	9.0	0.023	10.0	0.029	-38.0
OH				-307.46487	-8.8	10.6	0.028	9.6	0.029	9.1	0.021	-38.1
NH ₂				-287.59985	-5.9	10.5	0.028	9.6	0.030	9.4	0.024	-35.5
NH ₂			NO ₂	-492.10812	-10.0	3.2	0.002	9.0	0.020	10.1	0.021	-32.2
NH ₂		NO ₂		-492.10373	-8.5	6.7	0.017	9.5	0.024	9.9	0.029	-34.6
OH	OH		OH	-457.89583	1.1	14.7	0.042	11.4	0.036	8.9	0.030	-33.8
NH ₂	NO ₂		NO ₂	-696.61069	-3.2	5.8	0.012	9.3	0.026	6.6	0.020	-25.0
NO ₂	OH		OH	-587.19616	-1.1	5.1	0.013	8.4	0.024	11.7	0.036	-26.3
NO ₂		2NO ₂		-845.73670	-13.1	7.4	0.019	7.4	0.019	7.4	0.019	-35.2
NH ₂		NO ₂	CL	-951.68472	-8.2	6.0	0.015	9.6	0.024	10.9	0.038	-34.7
NH ₂	2-NO ₂	5-NH ₂	4-NO ₂	-751.97371	-5.2	2.6	0.002	9.6	0.035	5.5	0.014	-22.8
NH ₂	6-CL 2-NO ₂	3-CL 5-NH ₂	4-NO ₂	-1671.11638	-1.1	9.6	0.036	3.7	0.009	6.1	0.015	-20.5
OH	2,6-OH	3,5-OH	OH	-683.54295	6.1	13.5	0.045	13.5	0.045	13.5	0.045	-34.3

The GL geometry for the multi-substituted benzene is determined by the position rule. All the substituted benzenes are planar

the substituted benzene containing an electron-withdrawing group, the value of ESE is larger in the absolute value than that for the molecule containing an electron-releasing group. For the three molecules nitrobenzene, cyano-benzene and aniline, the stronger the ability to withdraw electron, the larger the ESE value.

For multiple substituted benzenes, in general, the more the number of substituents, the smaller the ESE value. For the three substituted benzenes containing the different number of substituents, for example, the size order of their ESE values is as follow:



For these three molecules, in addition, the ESEs are the smallest of all the molecules listed in Table 6-7, due

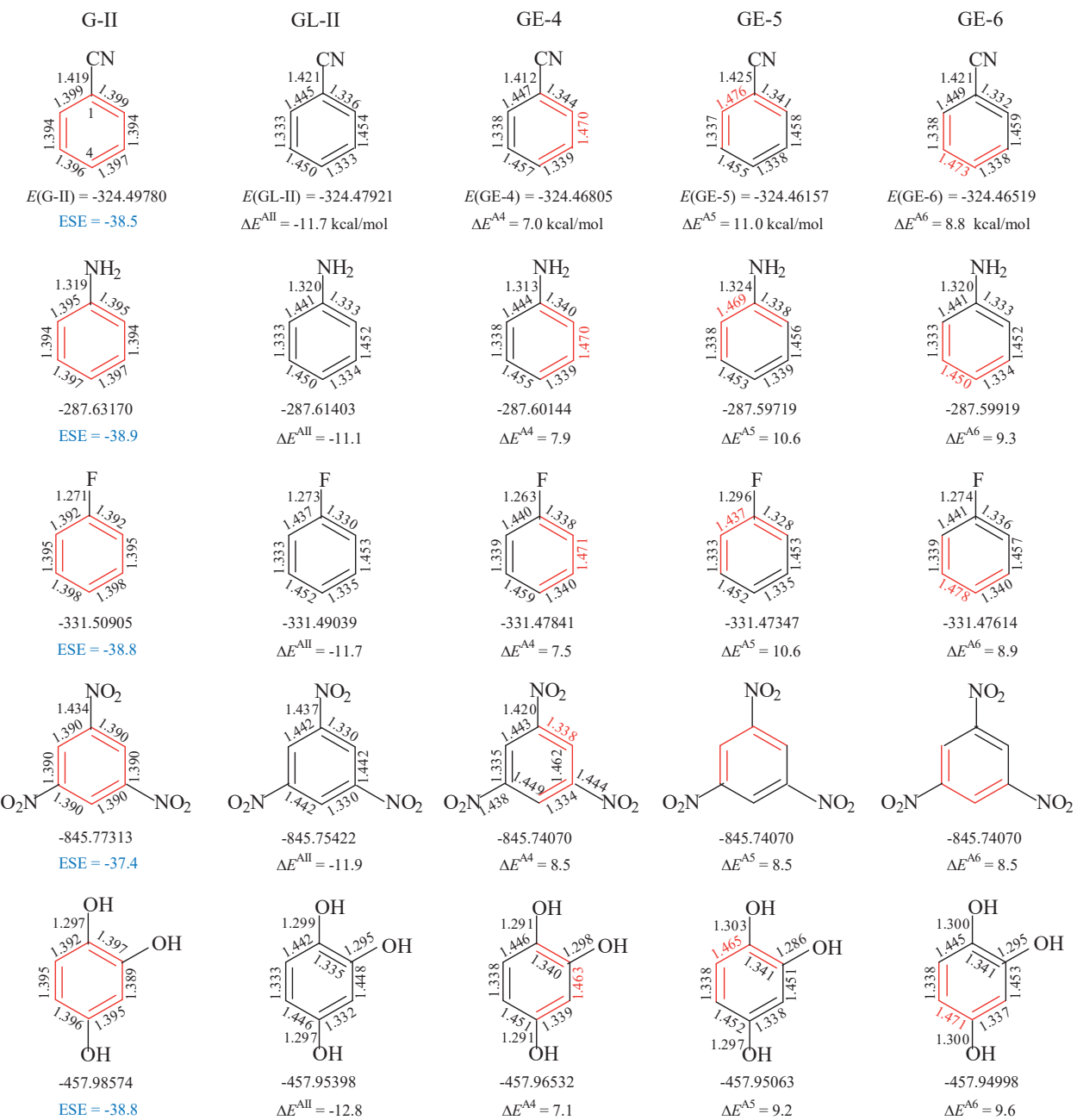


Figure 6-11. For each of five substituted benzenes, the molecular energies (hartree) of the localized geometries denoted as G-II, GL-II and GE-m ($m = 4, 5, 6$), and the extra stabilization energy, ESE(Ph) (kcal/mol), of an isolated phenyl ring, calculated using our 2007 method at the B3LYP/6-31G*level. The meanings of the red and black lines are the same as in Figure 6-7.

to the push-pull interaction between the electron-releasing and electron-withdrawing groups. For 2,4-dinitroaniline, for example, the energy effect ΔE^{A1} arises from the π -interaction between two groups, $\text{NH}_2\text{C}(1)=\text{C}(\text{NO}_2)$ and $\text{C}(3)=\text{C}(4)(\text{NO}_2)$, of the GL geometry. Due to the pull-push interaction between the amino group and the p-nitro group, the CT interaction between the two groups is enhanced, and the corresponding energy effect ΔE^{A1} (5.8

kcal/mol) is less destabilizing than the energy effects for most molecules listed in Table 6-7. Similarly, the energy effect ΔE^{A1} for 2,4-dinotro-3-amino-aniline is 2.6 kcal/mol, and its value is the smallest.

When a substituted benzene containing six hydroxy groups, in particular, the energy effect ΔE^A is 6 kcal/mol and becomes destabilizing, implying that our 2007 method needs to be improved. After improvement of our 2007 method, the energy effect ΔE^A , obtained from our 2011 method, is -5.1 kcal/mol and becomes stabilizing.

6.3.2. Extra Stabilization Energy of Parent Benzene Ring

In order to distinguish between the inductive and conjugation effects of substituent, a possible method is to calculate the ESE of the parent benzene ring of substituted benzene, which needs to construct two localized geometries denoted as G-II and GL-II and to construct three GE-m ($m = 4, 5, 6$) geometries (Figure 6-11). In each of these five optimized geometries, the π interaction between substituent(s) and benzene ring is set equal to zero, and meanwhile the non-bonded conjugation interactions between substituents are also set equal to zero according to the following conditional settings: before each SCF iteration,

- (i) Set $f_{\lambda,\rho} = 0.0$ and $s_{\lambda,\rho} = 0.0$ when the π AO $\phi_\lambda \in$ substituents and the π AO $\phi_\rho \in$ benzene ring.
- (ii) Set $f_{\lambda,\rho} = 0.0$ and $s_{\lambda,\rho} = 0.0$ when the π AO $\phi_\lambda \in P$ -th substituent and the π AO $\phi_\rho \in Q$ -th substituent; $P, Q =$ all substituents, and $P \neq Q$.

For a substituted benzene, thus, the extra stabilization energy of the isolated benzene ring can be defined as $ESE(Ph) = ([E(G-II) - E(GL-II)] - \Sigma [E(GE-m) - E(GL-II)]) = [\Delta E^{AII} - (\Delta E^{A4} + \Delta E^{A5} + \Delta E^{A6})]$. The ESE(ph) (kcal/mol) for eight molecules are almost equal to the ESE (-39.0) of benzene, and are as follows:

-37.4 (1,3,5-trinitro-) < -38.5 (-CN) < -38.7 (-NO₂) < -38.8 (-OH) < -38.8 (-F) < -38.8 (1,2,4-trihydroxy) < -38.9 (-NH₂) < -38.9 (4-nitro-aniline).

6.3.3. Pure Conjugation Effect

Conjugation effect and inductive effect are two important structural effects in organic chemistry. However, it is almost impossible to attempt to quantify and separate these two structural effects although the substituent constants have been determined. The purpose of calculating ESE(Ph) is to calculate the ESE difference, $d(ESE)_C = ESE(SB) - ESE(Ph)$. The subscript “c” in the symbol “ $d(ESE)_C$ ” means that this difference can be used to measure the influence of the conjugation effect of substituent(s) on the extra stabilization energy of substituted benzene, and it can also be used to measure the ability of substituent(s) to release or withdraw electron through conjugation effect. The size order of $d(ESE)_C$ (kcal/mol) is as follow:

6.7 (4-nitro-aniline) > 5.0 (1,2,4-trihydroxyl-benzene) > 3.4 (aniline) > 2.2 (1,3,5-trinitro-benzene) > 1.2 (cyanobenzene) > 1.1 (nitrobenzene) > 0.7 (phenol) > 0.5 (fluorobenzene).

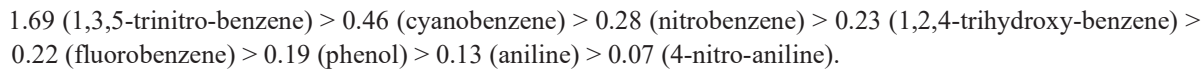
In 4-nitro-anilin, an amino is an electron-releasing group, and its p-nitro is an electron-withdrawing group, due to the push-pull action exerted by the amino and nitro groups, ESE has been weakened the most. As a result, its $d(ESE)_C$ (6.7 kcal/mol) is the greatest. For fluorobenzene, it is recognized that the ability of fluoro group to release electron through conjugation effect is very weak. Its substituent constant $\sigma_p = 0.06$. Correspondingly, its $d(ESE)_C$ (0.5 kcal/mol) is the smallest in the series of the molecules mentioned above.

In addition, the size order confirms that the ability of electron-releasing group to reduce the ESE of substituted

benzene is greater than that of electron-withdrawing group. For example, 1,3,5-trinitro-benzene contains three strong electron-withdrawing groups $-NO_2$, and 1,2,4-trihydroxy-benzene has three electron-releasing groups $-OH$, their $d(ESE)_C$ are respectively 2.1 and 5.0 kcal/mol. For similar reason, the $d(ESE)_C$ (3.4 kcal/mol) of aniline is greater than that (1.1 kcal/mol) of nitrobenzene.

6.3.4. Pure Inductive Effect

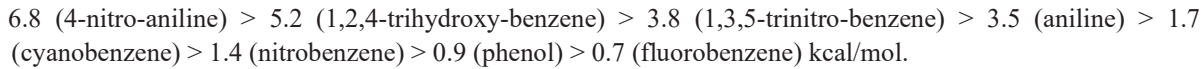
Another ESE difference can also be calculated, and it is defined as $d(ESE)_I = [ESE(Ph) - ESE(benzene)] = [ESE(Ph) - (-39.0)]$. The subscript “I” in the symbol “ $d(ESE)_I$ ” means that this difference can be used to measure the influence of the inductive effect of substituent(s) on the aromatic stabilization energy of phenyl ring, and it can also be used to measure the ability of substituent(s) to release or withdraw electron through pure inductive effect. The size order of $d(ESE)$ (kcal/mol) is as follow:



Except for 1,3,5- trinitro-benzene, the influence of all the substituents, through the inductive effect, on the ESE(Ph) of benzene ring is very weak. For the $-OH$, $-NH_2$, $-F$ substituents, for example, their substituent constants σ_m can be used to measure their ability to withdraw electron through inductive effect. The size order of their substituent constants σ_m is: $0.34 \text{ } (-F) > 0.0 \text{ } (-OH) > -0.16 \text{ } (-NH_2)$.⁸⁹ The sequence of substituent constants σ_m is consistent with the size order of the corresponding $d(ESE)_I$.

6.3.5. Conjugation and Inductive Effect.

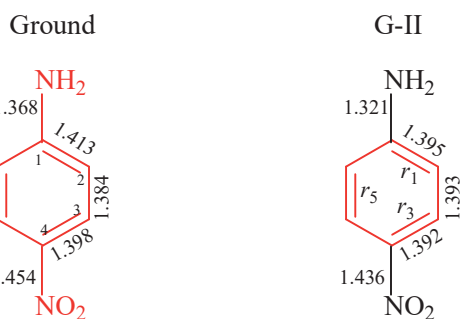
Third ESE difference $d(ESE)_{CI} = [ESE(SB) - ESE(benzene)] = [ESE(SB) - ESE(Ph)] + [ESE(Ph) - ESE(benzene)] = d(ESE)_C + d(ESE)_I$, and it is the comprehensive results of the conjugation effect and inductive effect of substituent(s). The size order of $d(ESE)_{CI}$ (kcal/mol) is as follow:



Except for 1,3,5- trinitrobenzene, the size sequence of $d(ESE)_{CI}$ and the size order of the $d(ESE)_C$ are completely consistent. This shows that the conjugation effect of substituent controls the aromaticity of the benzene ring itself. In 1,3,5-trinitro-benzene, since there are three nitro groups, so their inductive effect ($d(ESE)_I = 1.69$ kcal/mol) is almost equivalent to their conjugation effect ($d(ESE)_C = 2.2$ kcal/mol).

6.3.6. Substituent Effect Always Distortive.

In the localized G-II geometry, as shown by the CC bond distances presented in Figure 6-11, the six CC bond distances of the benzene ring are almost equal. In the G-II geometry of 4-nitro-aniline, for example, the CC bond distances of the benzene ring are almost equal, and are about 1.3935 ± 0.0015 Å, but in the ground state geometry, the distance (1.413 Å) of C(1)-C(2) bond is 0.029 Å longer than the distance (1.384 Å) of C(2)-C(3) bond. It is also interesting that the distance (1.368 Å) of N-C(1) bond in the ground state geometry is 0.047 Å longer than the corresponding distance (1.321 Å) in the G-II geometry. In the substituted benzene, the π -interaction between substituents and benzene ring is a driving force for distorting benzene.



Therefore, the distortivity of the substituent effect includes the effects of the substituent on the following two bond lengths:

- (i) The single bond length r_{B-R} between the phenyl ring and a substituent.
- (ii) The difference in the bond length between two adjacent CC bonds in the phenyl ring.

The difference, $dr_{B-R} = [r_{B-R}(G) - r_{B-R}(G-II)]$ between the ground state geometry (G) and the G-II geometry can be used to measure the effect of the substituent(s) on the single bond distance, r_{B-R} , between the benzene ring and its substituent. The size order of dr_{B-R} (Å) is as follows (Table 6-8):

0.087 (C(1)-O, 1,2,4-trihydroxy-benzene) > 0.080 (fluorobenzene) > 0.073 (phenol) > 0.060 (aniline) > 0.047 (C(1)-N, 4-nitro-aniline) > 0.046 (1,3,5-trinitro-benzene) > 0.039 (nitrobenzene) > 0.017 (C(4)-N, 4-nitro-aniline) > 0.016 (cyanobenzene).

As shown by this size order, always $dr_{B-R} > 0$, and the electron-releasing group has the greater effect on the single bond length (r_{B-R}) than the electron-withdrawing group. For instance, in 1,2,4-trihydroxy-benzene, the difference (0.087 Å) of the C(1)-O single bond length is greater than that (0.046 Å) of the C(1)-N single bond in 1,3,5-trinitrobenzene. In 4-nitro-aniline, especially, the change dr_{B-R} of the C(1)-N bond between the benzene ring and its electron-releasing group -NH₂ is 0.047 Å and is larger than the change (0.018) in the C(4)-N single bond between the benzene ring and its electron-withdrawing group -NO₂.

For the three substituted benzenes containing electron-releasing group, the size order of dr_{B-R} is as follow:

0.073 Å (phenol) > 0.060 Å (aniline) > 0.039 (nitrobenzene)

Correspondingly, the size order of the $d(ESE)_C$ (kcal/mol) for these three molecules is as follow:

Table 6-8. For Substituted Benzenes, Single Bond Distances r_{B-R} (Å) between the Benzene Ring and Its Substituent, and Difference $dr_{B-R} = [r_{B-R}(G) - r_{B-R}(G-II)]$ (Å), Obtained from Our 2007 Method at B3LYP/6-31G* Level.

	CN	NO ₂	NH ₂	OH	F	1,3,5-Tri-NO ₂	1-OH	2-OH	4-OH	1-NH ₂	4-NO ₂
$r_{B-R}(G-II)$	1.419	1.434	1.319	1.296	1.271	1.434	1.297	1.292	1.296	1.321	1.436
$r_{B-R}(G)$	1.435	1.473	1.379	1.369	1.351	1.480	1.384	1.363	1.372	1.368	1.453
dr_{B-R}	0.016	0.039	0.060	0.073	0.080	0.046	0.087	0.071	0.076	0.047	0.017

Table 6-9. For the G and G-II Geometries of Each of the Eight Substituted Benzenes at B3LYP/6-31G* Level, the Geometrical Indexes, dr_{m-n} , r_{av} and dr_{av} , Describing the Fluctuation of the Benzene Ring Bonds.

R	State	dr_{1-2}	$*dr_{2-3}$	dr_{3-4}	dr_{4-5}	dr_{5-6}	dr_{6-1}	r_{av}	dr_{av}	Range (dr_{m-n})
CN	G	0.012	-0.004	0.000	0.004	-0.012	0.000	1.398	0.005	0.024
	G-II	0.005	-0.003	0.001	0.002	-0.005	0.000	1.397	0.003	0/010
NO ₂	G	0.001	-0.005	0.000	0.005	0.000	-0.001	1.395	0.002	0.010
	G-II	-0.002	-0.003	0.000	0.003	0.002	0.000	1.394	0.002	0.006
F	G	-0.006	-0.001	0.000	0.001	0.006	0.000	1.394	0.002	0.012
	G-II	-0.003	-0.003	0.000	0.003	0.003	0.000	1.395	0.002	0.006
OH	G	0.006	-0.005	0.003	-0.001	-0.003	0.000	1.397	0.003	0.011
	G-II	-0.001	-0.004	0.001	0.002	0.000	0.002	1.395	0.002	0.005
NH ₂	G	0.016	-0.005	0.000	0.005	-0.016	0.000	1.399	0.007	0.032
	G-II	0.001	-0.003	0.000	0.003	-0.001	0.000	1.395	0.001	0.006
Tri-OH	G	0.012	-0.008	0.004	-0.001	0.007	-0.014	1.396	0.008	0.026
	G-II	0.008	-0.006	-0.001	0.001	0.003	-0.005	1.394	0.004	0.014
Tri-NO ₂	G	0.000	0.000	0.000	-0.000	0.000	0.000	1.391	0.000	0.000
	G-II	0.000	0.000	0.000	0.000	0.000	0.000	1.390	0.000	0.000
NH ₂ NO ₂	G	0.029	-0.014	0.000	0.014	-0.029	0.000	1.398	0.014	0.058
	G-II	0.002	0.001	0.000	-0.001	-0.002	0.000	1.393	0.001	0.004

3.4 (aniline) > 1.1 (nitrobenzene) > 0.7 (phenol)

The larger conjugation corresponds to the larger change dr_{B-R} in the bond distance between the benzene ring and its substituent. Correspondingly, the molecular energy difference, $E(G) - E(GLL)$, between the ground state (G) geometry and the G-II geometry is always destabilizing

In Table 6-9, the quantities dr_{n-m} and dr_{av} are defined as follows:

$$dr_{n-m} = r_n - r_m$$

$$dr_{av} = \Sigma |dr_{n-m}| / 6$$

where the subscripts n and m are the numberings of CC bonds in benzene ring, for example, r_1 (n = 1) is the distance of the C(1)-C(2) bond (the first CC bond), r_6 (n = 6) is the distance of the C(6)-C(1) bond (the 6-th CC bond). As shown by a comparison of the values of dr_{n-m} and dr_{av} listed in Table 6-9, the average fluctuation of the CC bond distances in the ground state geometry is greater than that in the G-II geometry, and the range of a set of CC bond lengths in the ground state geometry is greater than that in the G-II geometry. The CC bond lengths in the isolated benzene ring are almost equalized. For the ground state geometry (G) and G-II geometry of 4-nitro-aniline, for

example, the CC bond lengths are as follows:

G: 1.413, 1.384, 1.398

G-II: 1.395, 1.393, 1.392

6.4. CONCLUSIONS

Based on the conditional optimization of the GL and GE-m geometries, a new type of additive energy effect is found, and the virtual delocalized reference molecule of an aromatic molecule itself can be defined. Therefore, our 2007 method can be used to reasonably and accurately calculate the extra stabilization energy (ESE) of the following aromatic molecules: benzene, benzene-like and furan-like species, substituted benzenes. According to our definition of extra stabilization energy, the basic characteristics of an aromatic molecule should be as follows: $\Delta E^A = E(G) - E(GL) < 0$ (stabilizing), $\Sigma \Delta E^{Am} = \Sigma [E(GE-m) - E(GL)] > 0$ (destabilizing), and $ESE = E(GL) - \Sigma \Delta E^{Am} < 0$ (stabilizing). For an aromatic molecule, its adiabatic energy ΔE^A must be stabilizing. For furan-like species, $\Delta E^A > 0$, $\Sigma \Delta E^{Am} > 0$, and $ESE = \Delta E^A - \Sigma \Delta E^{Am} < 0$. Therefore, Furan-like species (so-called aromatic molecules) are just a class of the molecules whose electron delocalization energy ΔE^A is less destabilizing than that of its virtual reference molecule. For furan-like species, the energy effect difference ($\Delta E^A - \Sigma \Delta E^{Am}$) is best defined as the less destabilizing energy (LDE), $LDE = \Delta E^A - \Sigma \Delta E^{Am}$, rather than ESE (extra stabilization energy). ESE and LDE should be two different physical quantities, and there is no comparability between the ESEs of benzene-like species and the LDE of furan-like species. LDE should not be able to be used to quantify the aromatic stabilization energy and can only be used as an energy criterion to compare the (so-called) aromaticity of a series of furan-like species.

Substituent always makes benzene ring destabilized and deformed regardless of whether the substituent is electron-releasing or electron-withdrawing. For a substituent, the influences of its conjugation and inductive effects on the extra stabilization energy of the benzene ring can be quantitatively evaluated.

6.5. APPENDIX

Table 6-1. Three Occupied π MOs in the GL and GE-1 Geometries of Trans-1,3,5-hexatriene (B3LYP/6-31G*).

			GL 20-th	GL 21-th	GL 22-th	GE-1 20-th	GE-1 21-th	GE-1 22-th
Eigenvalues		-0.2844	-0.2795	-0.2795	-0.3253	-0.2758	-0.2365	
Fragments		B	C	A	A+B	C	A+B	
1	C1	1s	0.000000	0.000000	0.000000	0.000000	0.000000	0.000000
2	C1	2s	0.000000	0.000000	0.000000	0.000000	0.000000	0.000000
3	C1	2px	0.000000	0.000000	0.000000	0.000000	0.000000	0.000000
4	C1	2py	0.000000	0.000000	0.000000	0.000000	0.000000	0.000000
5	C1	2pz	0.000000	0.000000	0.392905	0.220907	0.000000	0.336112
6	C1	3s	0.000000	0.000000	0.000000	0.000000	0.000000	0.000000
7	C1	3px	0.000000	0.000000	0.000000	0.000000	0.000000	0.000000
8	C1	3py	0.000000	0.000000	0.000000	0.000000	0.000000	0.000000
9	C1	3pz	0.000000	0.000000	0.259654	0.141413	0.000000	0.267771

52	C4	3px	0.000000	0.000000	0.000000	0.000000	0.000000
53	C4	3py	0.000000	0.000000	0.000000	0.000000	0.000000
54	C4	3pz	0.293428	0.000000	0.000000	0.161833	0.000000
55	C4	4xx	0.000000	0.000000	0.000000	0.000000	0.000000
56	C4	4yy	0.000000	0.000000	0.000000	0.000000	0.000000
57	C4	4zz	0.000000	0.000000	0.000000	0.000000	0.000000
58	C4	4xy	0.000000	0.000000	0.000000	0.000000	0.000000
59	C4	4xz	-0.009425	0.000000	0.000000	-0.009169	0.000000
60	C4	4yz	0.009800	0.000000	0.000000	0.006555	0.000000
61	C5	1s	0.000000	0.000000	0.000000	0.000000	0.000000
62	C5	2s	0.000000	0.000000	0.000000	0.000000	0.000000
63	C5	2px	0.000000	0.000000	0.000000	0.000000	0.000000
64	C5	2py	0.000000	0.000000	0.000000	0.000000	0.000000
65	C5	2pz	0.000000	0.400792	0.000000	0.000000	0.399750
66	C5	3s	0.000000	0.000000	0.000000	0.000000	0.000000
67	C5	3px	0.000000	0.000000	0.000000	0.000000	0.000000
68	C5	3py	0.000000	0.000000	0.000000	0.000000	0.000000
69	C5	3pz	0.000000	0.317873	0.000000	0.000000	0.318646
70	C5	4xx	0.000000	0.000000	0.000000	0.000000	0.000000
71	C5	4yy	0.000000	0.000000	0.000000	0.000000	0.000000
72	C5	4zz	0.000000	0.000000	0.000000	0.000000	0.000000
73	C5	4xy	0.000000	0.000000	0.000000	0.000000	0.000000
74	C5	4xz	0.000000	0.009673	0.000000	0.000000	0.009704
75	C5	4yz	0.000000	-0.010882	0.000000	0.000000	-0.010615
76	C6	1s	0.000000	0.000000	0.000000	0.000000	0.000000
77	C6	2s	0.000000	0.000000	0.000000	0.000000	0.000000
78	C6	2px	0.000000	0.000000	0.000000	0.000000	0.000000
79	C6	2py	0.000000	0.000000	0.000000	0.000000	0.000000
80	C6	2pz	0.000000	0.392906	0.000000	0.000000	0.393079
81	C6	3s	0.000000	0.000000	0.000000	0.000000	0.000000
82	C6	3px	0.000000	0.000000	0.000000	0.000000	0.000000
83	C6	3py	0.000000	0.000000	0.000000	0.000000	0.000000
84	C6	3pz	0.000000	0.259654	0.000000	0.000000	0.259713
85	C6	4xx	0.000000	0.000000	0.000000	0.000000	0.000000
86	C6	4yy	0.000000	0.000000	0.000000	0.000000	0.000000
87	C6	4zz	0.000000	0.000000	0.000000	0.000000	0.000000
88	C6	4xy	0.000000	0.000000	0.000000	0.000000	0.000000
89	C6	4xz	0.000000	-0.013802	0.000000	0.000000	-0.013701
90	C6	4yz	0.000000	0.006745	0.000000	0.000000	0.006644
91	H7	1s	0.000000	0.000000	0.000000	0.000000	0.000000
92	H7	2s	0.000000	0.000000	0.000000	0.000000	0.000000
93	H8	1s	0.000000	0.000000	0.000000	0.000000	0.000000

Table 6-3. For the GL and GE-1 Geometries of Benzene, Occupied π MOs At B3LYP/6-31G* Level.

24	C2	3pz	0.000000	0.000000	0.293503	0.184587	0.000000	0.163621
25	C2	4xx	0.000000	0.000000	0.000000	0.000000	0.000000	0.000000
26	C2	4yy	0.000000	0.000000	0.000000	0.000000	0.000000	0.000000
27	C2	4zz	0.000000	0.000000	0.000000	0.000000	0.000000	0.000000
28	C2	4xy	0.000000	0.000000	0.000000	0.000000	0.000000	0.000000
29	C2	4xz	0.000000	0.000000	0.007761	0.010257	0.000000	-0.003805
30	C2	4yz	0.000000	0.000000	0.011734	0.001056	0.000000	0.018852
31	C3	1s	0.000000	0.000000	0.000000	0.000000	0.000000	0.000000
32	C3	2s	0.000000	0.000000	0.000000	0.000000	0.000000	0.000000
33	C3	2px	0.000000	0.000000	0.000000	0.000000	0.000000	0.000000
34	C3	2py	0.000000	0.000000	0.000000	0.000000	0.000000	0.000000
35	C3	2pz	0.000000	0.392704	0.000000	0.315142	0.000000	-0.243179
36	C3	3s	0.000000	0.000000	0.000000	0.000000	0.000000	0.000000
37	C3	3px	0.000000	0.000000	0.000000	0.000000	0.000000	0.000000
38	C3	3py	0.000000	0.000000	0.000000	0.000000	0.000000	0.000000
39	C3	3pz	0.000000	0.293480	0.000000	0.184522	0.000000	-0.163607
40	C3	4xx	0.000000	0.000000	0.000000	0.000000	0.000000	0.000000
41	C3	4yy	0.000000	0.000000	0.000000	0.000000	0.000000	0.000000
42	C3	4zz	0.000000	0.000000	0.000000	0.000000	0.000000	0.000000
43	C3	4xy	0.000000	0.000000	0.000000	0.000000	0.000000	0.000000
44	C3	4xz	0.000000	0.011491	0.000000	0.000779	0.000000	-0.018883
45	C3	4yz	0.000000	0.008058	0.000000	0.010310	0.000000	0.003369
46	C4	1s	0.000000	0.000000	0.000000	0.000000	0.000000	0.000000
47	C4	2s	0.000000	0.000000	0.000000	0.000000	0.000000	0.000000
48	C4	2px	0.000000	0.000000	0.000000	0.000000	0.000000	0.000000
49	C4	2py	0.000000	0.000000	0.000000	0.000000	0.000000	0.000000
50	C4	2pz	0.000000	0.392752	0.000000	0.225987	0.000000	-0.338933
51	C4	3s	0.000000	0.000000	0.000000	0.000000	0.000000	0.000000
52	C4	3px	0.000000	0.000000	0.000000	0.000000	0.000000	0.000000
53	C4	3py	0.000000	0.000000	0.000000	0.000000	0.000000	0.000000
54	C4	3pz	0.000000	0.293540	0.000000	0.171894	0.000000	-0.276257
55	C4	4xx	0.000000	0.000000	0.000000	0.000000	0.000000	0.000000
56	C4	4yy	0.000000	0.000000	0.000000	0.000000	0.000000	0.000000
57	C4	4zz	0.000000	0.000000	0.000000	0.000000	0.000000	0.000000
58	C4	4xy	0.000000	0.000000	0.000000	0.000000	0.000000	0.000000
59	C4	4xz	0.000000	-0.014063	0.000000	-0.012237	0.000000	0.008676
60	C4	4yz	0.000000	0.000876	0.000000	0.001396	0.000000	0.000988
61	C5	1s	0.000000	0.000000	0.000000	0.000000	0.000000	0.000000
62	C5	2s	0.000000	0.000000	0.000000	0.000000	0.000000	0.000000
63	C5	2px	0.000000	0.000000	0.000000	0.000000	0.000000	0.000000
64	C5	2py	0.000000	0.000000	0.000000	0.000000	0.000000	0.000000
65	C5	2pz	0.392803	0.000000	0.000000	0.000000	0.392591	0.000000

66	C5	3s	0.000000	0.000000	0.000000	0.000000	0.000000	0.000000
67	C5	3px	0.000000	0.000000	0.000000	0.000000	0.000000	0.000000
68	C5	3py	0.000000	0.000000	0.000000	0.000000	0.000000	0.000000
69	C5	3pz	0.293501	0.000000	0.000000	0.000000	0.293638	0.000000
70	C5	4xx	0.000000	0.000000	0.000000	0.000000	0.000000	0.000000
71	C5	4yy	0.000000	0.000000	0.000000	0.000000	0.000000	0.000000
72	C5	4zz	0.000000	0.000000	0.000000	0.000000	0.000000	0.000000
73	C5	4xy	0.000000	0.000000	0.000000	0.000000	0.000000	0.000000
74	C5	4xz	-0.012729	0.000000	0.000000	0.000000	-0.012814	0.000000
75	C5	4yz	0.005929	0.000000	0.000000	0.000000	0.006256	0.000000
76	C6	1s	0.000000	0.000000	0.000000	0.000000	0.000000	0.000000
77	C6	2s	0.000000	0.000000	0.000000	0.000000	0.000000	0.000000
78	C6	2px	0.000000	0.000000	0.000000	0.000000	0.000000	0.000000
79	C6	2py	0.000000	0.000000	0.000000	0.000000	0.000000	0.000000
80	C6	2pz	0.392825	0.000000	0.000000	0.000000	0.392611	0.000000
81	C6	3s	0.000000	0.000000	0.000000	0.000000	0.000000	0.000000
82	C6	3px	0.000000	0.000000	0.000000	0.000000	0.000000	0.000000
83	C6	3py	0.000000	0.000000	0.000000	0.000000	0.000000	0.000000
84	C6	3pz	0.293364	0.000000	0.000000	0.000000	0.293496	0.000000
85	C6	4xx	0.000000	0.000000	0.000000	0.000000	0.000000	0.000000
86	C6	4yy	0.000000	0.000000	0.000000	0.000000	0.000000	0.000000
87	C6	4zz	0.000000	0.000000	0.000000	0.000000	0.000000	0.000000
88	C6	4xy	0.000000	0.000000	0.000000	0.000000	0.000000	0.000000
89	C6	4xz	0.006284	0.000000	0.000000	0.000000	0.006613	0.000000
90	C6	4yz	-0.012637	0.000000	0.000000	0.000000	-0.012715	0.000000
91	H7	1s	0.000000	0.000000	0.000000	0.000000	0.000000	0.000000
92	H7	2s	0.000000	0.000000	0.000000	0.000000	0.000000	0.000000
93	H8	1s	0.000000	0.000000	0.000000	0.000000	0.000000	0.000000
94	H8	2s	0.000000	0.000000	0.000000	0.000000	0.000000	0.000000
95	H9	1s	0.000000	0.000000	0.000000	0.000000	0.000000	0.000000
96	H9	2s	0.000000	0.000000	0.000000	0.000000	0.000000	0.000000
97	H10	1s	0.000000	0.000000	0.000000	0.000000	0.000000	0.000000
98	H10	2s	0.000000	0.000000	0.000000	0.000000	0.000000	0.000000
99	H11	1s	0.000000	0.000000	0.000000	0.000000	0.000000	0.000000
100	H11	2s	0.000000	0.000000	0.000000	0.000000	0.000000	0.000000
101	H12	1s	0.000000	0.000000	0.000000	0.000000	0.000000	0.000000
102	H12	2s	0.000000	0.000000	0.000000	0.000000	0.000000	0.000000

6.6. REFERENCES

- 1 Bao, P.; Yu, Z. H. 2006. "Theoretical Studies on the Role of π -Electron Delocalization in Determining the

- Conformation of N-benzylideneaniline with Three Types of LMO Basis Sets." *J. Comput. Chem.*, 27: 809-824.
- 2 Bao, P.; Yu, Z. H. 2007. "Restricted Geometry Optimization: A Different Way to Estimate Stabilization Energies for Aromatic Molecules of Various Types." *J. Phys. Chem. A*, 111: 5304-5313.
- 3 Bao, P.; Yu, Z. H. 2010. "Restricted Geometry Optimization for Estimating Stabilization Energies of Polycyclic Aromatic Hydrocarbons." *J. Phys. Org. Chem.*, 23: 16-29.
- 4 Bao, P.; Yu, Z. H. 2011. "New Procedure to Evaluate Aromaticity at the Density Functional Theory, Hartree-Fock, and Post-Self- Consistent Field Levels." *J. Comput. Chem.*, 32: 248-259.
- 5 Yu, Z. H.; Xuan, Z. Q.; Wang, T. X.; Yu, H. M. 2000. "A Novel Energy Partition for Gaining New Insight into Aromaticity and Conjugation." *J. Phys. Chem. A*, 104: 1736-1747.
- 6 March, J. 1992. *Advanced Organic Chemistry*. New York: John Wiley & Sons.
- 7 <http://en.wikipedia.org/wiki/Hyperconjugation>
- 8 Vollhardt, K. P. C.; Schore, N. E. 1999. *Organic Chemistry, Structure and function*. New York: W. H. Freeman and Company.
- 9 Streitwieser, A.; Heathcock, C. H.; Kosower, E. M. 1992. *Introduction to Organic Chemistry*. New York: Macmillan.
- 10 Marais, D. J.; Sheppard, N.; Stoicheff, B. P. 1962. "An Investigation of the Structure of Butadiene by High Resolution Infra-Red and Raman Spectroscopy." *Tetrahedron*, 17: 163-169.
- 11 Bartell, L. S.; Higginbotham, J. K. 1965. "Electron Diffraction Study of the Structures of Ethane and Deuteroethane." *J. Chem. Phys.* 42: 851-858.
- 12 Conant, J. B.; Kistiakowsky, G. B. 1937. "Energy Changes Involved in the Addition Reactions of Unsaturated Hydrocarbons." *Chem. Rev.*, 20: 181-194.
- 13 Brown, W. H.; Foote, C. S.; Iverson, B. L.; Anslyn, E. V. 2011. *Organic Chemistry*, Enhanced Edition, Brooks/cole. USA: Cengage Learning.
- 14 Paxson, F. L. 1910. *The Last American Frontier*. Safety Harbor, FL: Simon Publications.
- 15 <http://sy.zlgc.org/Upload/20090527162549546.pdf>.
- 16 <https://www.chegg.com/homework-help/questions-and-answers/2-estimate-stabilization-energy-1-3-pentadiene-using-heats-hydrogenation-table-1-table- 1-h-q27252529>
- 17 Rogers, D. W.; Matsunaga, N.; Zavitsas, A. A.; McLafferty, F. J.; Lieberman, J. F. 2003. "The Conjugation Stabilization of 1,3-Butadiyne Is Zero." *Org. Lett.*, 5: 2373-2375.
- 18 Rogers, D. W.; Matsunaga, N.; McLafferty, F. J.; Zavitsas, A. A.; Lieberman, J. F. 2004. "On the Lack of Conjugation Stabilization in Polyynes." *J. Org. Chem.*, 69: 7143-7147.
- 19 Khristov, V. K.; Angelov, K. M.; Petrov, A. A. 1991. "1,3-Alkadienes and their Derivatives in Reactions with Electrophilic Reagents." *Russ. Chem. Rev.*, 60: 39-56.
- 20 Silvestre-Albero, J; Rupprechter, G; Freund, H. J. 2005. "Atmospheric Pressure Studies of Selective 1,3-Butadiene Hydrogenation on Pd Single Crystals: Effect of CO Addition." *J. Catal.*, 235: 52-59.
- 21 Zhong , G.; Chan, B; Radom, L. 2007. "Hydrogenation of Simple Aromatic Molecules: A Computational Study of the Mechanism." *J. Am. Chem. Soc.*, 129: 924-933.
- 22 Allen, F. H.; Kennard, O; Watson, D. G.; Brammer, L.; Orpen, A. G.; Taylor, R. 1987. "Tables of Bond Lengths Determined by X-Ray and Neutron Diffraction. Part 1. Bond Lengths in Organic Compounds." *J. Chem. Soc., Perkin Trans. 2*, 0: S1-S19.
- 23 Bartell, L. S. 1959. "On the Length of the Carbon-Carbon Single Bond." *J. Am. Chem. Soc.*, 81: 3497-3498.
- 24 Bartell, L. S. 1962. "On Inferences of Bond Character from Bond Length; The Important Role of Nonbonded Interactions." *Tetrahedron*, 17: 177-190.
- 25 Bartell, L. S. 1978. "On the Contributions of Resonance, Hybridization and Nonbonded Interactions to the Structure of Butadiene." *Tetrahedron*, 34: 2891-2892.
- 26 Dewar, M. J. S.; Gleicher, G. J. 1965. "Ground States of Conjugated Molecules. III. Classical Polyenes." *J. Am. Chem. Soc.*, 87: 692-696.
- 27 Dewar, M. J. S.; Schmeising, H. N. 1959. "A Re-evaluation of Conjugation and Hyperconjugation: The Effects

- of Changes in Hybridisation on Carbon Bonds." *Tetrahedron*, 5: 166-178.
- 28 Dewar, M. J. S.; Schmeising, H. N. 1960. "Molecular Orbital Calculations on Some Non-Classical Aromatics." *Tetrahedron*, 11: 121-124.
- 29 Somayajulu, G. R. 1959. "Lengths of CC 'Single' Bonds and Radii of Hybrid Orbitals of Carbon." *J. Chem. Phys.*, 31: 919-921.
- 30 Tantillo Dean J. 2018. *Applied Theoretical Organic Chemistry*. New Jersey: World Scientific Publishing Europe Ltd.
- 31 Jarowski, P. D.; Wodrich, M. D.; Wannere, C. S.; Schleyer, P. v. R.; Houk, K. N. 2004. "How Large Is the Conjugative Stabilization of Diynes?" *J. Am. Chem. Soc.*, 126: 15036-15037.
- 32 Kitaura, K.; Morokuma, K. 1976. "A New Energy Decomposition Scheme for Molecular Interactions within the Hartree-Fock Approximation." *Int. J. Quantum Chem.*, 10: 325-340.
- 33 Bader, R. F. W.; Streitwieser, A.; Neuhaus, A.; Laidig, K. E.; Speers, P. 1996. "Electron Delocalization and the Fermi Hole." *J. Am. Chem. Soc.*, 118: 4959-4965.
- 34 Bader, R. F. W.; Tang, T. H.; Popelier, P. L. A. 1996. "The Electron Pair." *J. Phys. Chem.*, 100: 15398-15415.
- 35 Bader, R. F. W.; Stephens, M. E. 1975. "Spatial Localization of the Electronic Pair and Number Distributions in Molecules." *J. Am. Chem. Soc.* 97: 7391-7399.
- 36 Epotis, N.D. 1983. *Lecture Notes in Chemistry*, Vol. 34. New York: Springer-Verlag.
- 37 Epotis, N.D. 1996. *Deciphering the Chemical Code*, New York: VCH Publishers, Inc..
- 38 Shaik, S.; Shurki, A.; Danovich, D.; Hiberty, P. C. 1997. "A Different Story of Benzene." *Theochem.*, 398-399: 155-167.
- 39 Shaik, S.; Shurki, A.; Danovich, D.; Hiberty, P. C. 2001. "A Different Story of π -Delocalizations – The Distortion of π -Electrons and Its Chemical Manifestations." *Chem. Rev.*, 101: 1501-1540.
- 40 Jug; K.; Köster, A. M. 1990. "Influence of σ and π Electrons on Aromaticity." *J. Am. Chem. Soc.*, 112: 6772-6777.
- 41 Behrens, S.; Köster, A. M.; Jug, K. 1994. "Delocalization Energy of an Electrons as an Index for Aromaticity of Polycyclic Hydrocarbons." *J. Org. Chem.*, 59: 2546-2551.
- 42 Köster, A. M.; Calaminici, P.; Geudtner, G.; Gömez-Sandoval, Z. 2005. "Separation of π and σ Energies." *J. Phys. Chem. A*, 109: 1257-1259.
- 43 Jug, K.; Hiberty, P. C.; Shaik, S. 2001. " π - σ Energy Separation in Modern Electronic Theory for Ground States of Conjugated Systems." *Chem. Rev.*, 101: 1477-1500.
- 44 Wiberg, K. B. 2001. "Antiaromaticity in Monocyclic Conjugated Carbon Rings." *Chem. Rev.*, 101: 1317-1332.
- 45 Cyrański, M. K. 2005. "Energetic Aspects of Cyclic π -Electron Delocalization: Evaluation of the Methods of Estimating Aromatic Stabilization Energies." *Chem. Rev.*, 105: 3773-3811.
- 46 Schleyer, P. v. R.; Puhlfhofer, F. 2002. "Recommendations for the Evaluation of Aromatic Stabilization Energies." *Org. Lett.*, 4: 2873-2876.
- 47 Glendening, E. D.; Faust, R.; Vollhardt, K. P. C.; Weinhold, F.; Streitwieser, A. 1993. "The Role of Delocalization in Benzene." *J. Am. Chem. Soc.*, 115: 10952-10957.
- 48 Weinhold, F.; Landis, C. R. 2005. *Valency and Bonding: A Natural Bond Orbital Donor-Acceptor Perspective*. New York: Cambridge University Press.
- 49 Streitwieser, A. 1961. *Molecular Orbital Theory for Organic Chemists*. New York: Wiley.
- 50 Dewar, M. J. S.; Llano, C. De. 1969. "Ground States of Conjugated Molecules. XI. Improved Treatment of Hydrocarbons." *J. Am. Chem. Soc.*, 91: 789-795.
- 51 Hess Jr, B. A.; Schaad, L. J. 1971. "Hückel Molecular Orbital. π Resonance Energies. New Approach." *J. Am. Chem. Soc.*, 93: 305-310.
- 52 Fishtik, I.; Datta, R. 2003. "Aromaticity vs Stoichiometry." *J. Phys. Chem. A*, 107: 10471-10476.
- 53 Howard, S. T. 2003. "An Atoms-in-Molecules Model of Bond Energy Distributions in Polyatomic Molecules."

- Phys. Chem. Chem. Phys., 5: 3113-3119.
- 54 Mo, Y.; Schleyer, P. v. R. 2006. "An Energetic Measure of Aromaticity and Antiaromaticity Based on the Pauling–Wheland Resonance Energies." *Chem. Eur. J.*, 12: 2009-2020.
- 55 George, P. 1975. "Critique of the Resonance Energy Concept with Particular Reference to Nitrogen Heterocycles, Especially Porphyrins." *Chem. Rev.*, 75: 85-111.
- 56 Cohen, N.; Benson, S. W. 1993. "Estimation of Heats of Formation of Organic Compounds by Additivity Methods." *Chem. Rev.*, 93: 2419-2438.
- 57 Matsunaga, N.; Cundari, T. R.; Schmidt, M. W.; Gordon, M. S. 1992. "A Comparative Study of the Bonding in Heteroatom Analogues of Benzene." *Theor. Chim. Acta.*, 83: 57-68.
- 58 Pauling, L.; Sherman, J. 1933. "The Nature of the Chemical Bond. VI. The Calculation from Thermochemical Data of the Energy of Resonance of Molecules Among Several Electronic Structures." *J. Chem. Phys.*, 1: 606-617.
- 59 Dewar, M. J. S.; Harget, A. J.; Trinajstic', N. 1969. "Ground States of Conjugated Molecules. XV. Bond Localization and Resonance Energies in Compounds Containing Nitrogen or Oxygen." *J. Am. Chem. Soc.*, 91: 6321-6325.
- 60 Schaad, L J; Hess, Jr. B. A. 2001. "Dewar Resonance Energy." *Chem. Rev.*, 101: 1465–1476.
- 61 Mo, Y. R.; Lin, M. H.; Wu, W.; Zhang, Q.E. 2000. "The Block-localized Wavefunction Method and its Application." *Acta Chem. Sin.*, 58: 218-221.
- 62 Deniz, A. A.; Peters, K. S.; Snyder, G. J. 1999. "Experimental Determination of the Antiaromaticity of Cyclobutadiene." *Science*, 286: 1119-1122.
- 63 Katritzky, A. R.; Piotr Barczynski, P.; Musumarra, G.; Pisano, D.; Szafranll, M. 1989. "Aromaticity as a Quantitative Concept. 1. A Statistical Demonstration of the Orthogonality of 'Classical' and 'Magnetic' Aromaticity in Five- and Six-Membered Heterocycles." *J. Am. Chem. Soc.*, 111: 7-15.
- 64 Malrieu, J. P; Lepetit,C.; Gicquel, M.;Heully ,J. L.; Fowler, P. W.; and Remi Chauvin, R. 2007. "Evaluating the Cyclic π -Electron Delocalization Energy through a Double Cut of Conjugated Rings." *New J. Chem.*, 31: 1918-1927.
- 65 Maksić, Z. B. 2009. "Comment on "Restricted Geometry Optimization: A Different Way to Estimate Stabilization Energies for Aromatic Molecules of Various Types." *J. Phys. Chem. A*, 113: 788-789.
- 66 The original version of the Maksić's comment manuscript has been posted on the Blog: http://www.sciencenet.cn/m/user_content.aspx?id=207637.
- 67 Cox, J. D.; Pilcher, G. 1970. *Thermochemistry of Organic and Organometallic Compounds*. New York: Academic Press.
- 68 Granovsky, A. A. Available at: <http://classic.chem.msu.su/gran/gamess/index.html>, Accessed 30 July 2009.
- 69 Katritzky, A. R.; Jug, K.; Oniciu, D. C. 2001. "Quantitative Measures of Aromaticity for Mono-, Bi-, and Tricyclic Penta- and Hexaatomic Heteroaromatic Ring Systems and Their Interrelationships." *Chem Rev.*, 101: 1421-1450.
- 70 Roux, M. V.; Jimenez, P.; Davalos, J. Z.; Abboud, J. L. M.; Molina, M. T. 1996. "Structural Effects on the Thermochemical Properties of Cycloalkanones I. Enthalpy of Combustion, Vapour Pressures, and Enthalpy of Sublimation, and Standard Enthalpy of Formation in the Gaseous Phase of Cyclododecanone." *J. Chem. Thermodyn.*, 28: 1029-1035.
- 71 Adedeji, F. A.; Brown, D. L. S.; Connor, J. A.; Leung, M. L.; Paz-Andrade, I. M.; Skinner, H. A. 1975. "Thermochemistry of Arene Chromium Tricarbonyls and the Strengths of Arene-Chromium Bonds." *J. Organomet. Chem.*, 97: 221-228.
- 72 Jimenez, P.; Roux, M. V.; Davalos, J. Z.; Martin-Luengo, M. A.; Abboud, J.-L. M. 1997. "Structural Effects on the Thermochemical Properties of Cycloalkanones II. Enthalpy of Combustion, Vapour Pressures, Enthalpy of Sublimation, and Standard Molar Enthalpy of Formation in the Gaseous Phase of Cyclopentadecanone." *J. Chem. Thermodyn.*, 29: 1281-1288.
- 73 Roux, M. V.; Jiménez , P.; Dávalos, J. Z.; Ribeiro da Silva , M. A. V.; Ribeiro da Silva, M. D. M. C.; Matos,

- M. A. R.; Amaral, L. M. P. F.; Sánchez-Migallón, A.; Cabildo, P.; Claramunt, R.; Elguero, J.; Liebman, J. F. 1999. "Enthalpies of Formation of *N*-Substituted Pyrazoles and Imidazoles." *J. Phys. Chem. A*, 103: 9336-9344.
- 74 Cohen, N.; Benson, S. W. 1993. "Estimation of Heats of Formation of Organic Compounds by Additivity Methods." *Chem. Rev.*, 93: 2419-2438.
- 75 Krygowski, T. M.; Anulewicz, R.; Kruszewski, J. 1983. "Crystallographic Studies and Physicochemical Properties of π -Electron Compounds. III. Stabilization Energy and the Kekul Structure Contributions Derived from Experimental Bond Lengths." *Acta Crystallogr.*, B39: 732-730.
- 76 Krygowski, T. M.; Anulewicz, R.; Wisiorowski, M. 1995. "Derivation of the Kekulé Structure Contributions from Experimental Bond Lengths for pi-Electron Systems with Nn." *Pol. J. Chem.*, 69: 1579-1584.
- 77 Bird, C. W. 1997. "Heteroaromaticity. 10. The Direct Calculation of Resonance Energies of Azines and Azoles from Molecular Dimensions." *Tetrahedron*, 53: 13111-13118.
- 78 Hess Jr, B. A.; Schaad, L. J.; Holyoke Jr, C. W. 1975. "The Aromaticity of Heterocycles Containing the Imine Nitrogen." *Tetrahedron*, 31: 295-298.
- 79 Hess Jr, B. A.; Schaad, L. S. 1973. "Hückel Molecular Orbital pi-Resonance Energies. Heterocycles Containing Divalent Sulfur." *J. Am. Chem. Soc.*, 95: 3907-3912.
- 80 Hess Jr, B. A.; Schaad, L. J. 1971. "Hückel Molecular Orbital pi. Resonance Energies. Benzenoid Hydrocarbons." *J. Am. Chem. Soc.*, 93: 2413-2416.
- 81 Schaad, L. J.; Hess Jr, B. A. 1974. "Hückel Theory and Aromatically." *J. Chem. Educ.*, 51: 640-643.
- 82 Wiberg, K. B.; Nakaji, D.; Breneman, C. M. 1989. "Azines. A Theoretical Study of π -Electron Delocalization." *J. Am. Chem. Soc.*, 111: 4178-4190.
- 83 Minkin, V. I.; Glukhovtsev, M. N.; Simkin, B. Y. 1994. *Aromaticity and Antiaromaticity. Electronic and Structural Aspects*. New York: Wiley.
- 84 Suzuki, M. ; Okada, T.; Taguchi, T.; Hanzawa, Y.; Iitaka, Y. 1992. " Intramolecular Diels-Alder Reactions of Furan Derivatives: Steric and Electronic Effects of Trifluoromethyl Groups." *J. Fluor. Chem.*, 57: 239-243.
- 85 Fraile, J. M.; Garcia, J. I.; Gracia, D.; Mayoral, J. A.; Pires, E. 1996, "First Asymmetric Diels-Alder Reactions of Furan and Chiral Acrylates Usefulness of Acid Heterogeneous Catalysts." *J. Org. Chem.*, 61: 9479-9482
- 86 Harmata, M. 1999. *Advances in Cycloaddition*, Vol. 6. Stamford: JAI Press Inc.
- 87 Joule, J. A.; Smith, G. F. 1972. *Heterocyclic Chemistry*. London: Van Nostrand Reinhold.
- 88 Hammett, L. P. 1935. "Some Relations between Reaction Rates and Equilibrium Constants." *Chem. Rev.*, 17: 125-136.
- 89 Gould, E. S. 1960. *Structure and mechanism in Organic Chemistry*. New York: Holt-Dryden Book-Henry Holt Co..

CHAPTER 7

POLYCYCLIC BENZENOID HYDROCARBONS

ABSTRACT

At the B3LYP/6-31G* level, our 2007 program, optimizing geometry under the restrictions of π -orbital interactions, is applied to the following eight homologous series of PBHs (polycyclic benzenoid hydrocarbons): acenes (**7-1-n**, n = 1 to 6), benzo[a]acenes (**7-2-n**, n = 1 to 5), dibenzo[a,c]acenes (**7-3-n**, n = 1 to 4), chrysene series (**7-4-n** and **7-5-n**, n = 1,2), dibenzo[de,d'e']acenes (**7-6-(n:0)**, n = 1 to 4; **7-6-(n:1)**, n = 1 to 3) and dinaphtho[2.3-a,2.3-c]acenes (**7-8-n**, n = 0, 1), and seven individual molecules such as tri- and tetra-benzoanthracene (**7-7-n**), benzo- and naphtho-pentaphene (**7-8-n**), dibenzopentacene (**7-9** and **7-11**) and tribenzotetracene (**7-10**), and it provides each of the 35 PBHs with two types of localized geometries: (i) the GL geometry where all double bonds are localized; (ii) k different 'GE-m' geometries (m = 1, 2,, k), in which only a specific pair of double bonds are permitted to be conjugated and all other double bonds are localized. The energy effect difference, $([E(\text{Ground}) - E(\text{GL})] - \Sigma [E(\text{GE-m}) - E(\text{GL})])$, is defined as the extra stabilization energy (ESE) of a PBH. The corrected ESE (CESE) is a result from considering π interactions between pairs of nonbonded double bonds in the GL geometry, and the CESEs/ π (kcal/mol* π) for typical series of PBHs are as follows: **7-1-n**: -6.2 (naphthalene) > -4.9 (anthracene) > -4.0 (tetracene) > -3.5 (pentacene) > -3.1 (hexacene) > 2.9 (heptacene); **7-2-n**: -6.3 (phenanthrene) > -5.4 (n = 2) > -4.7 (n = 3) > -4.2 (n = 4) > -3.8 (n = 5); **7-3-n**: -6.4 (Triphenylene) > -5.7 (n = 2) > -5.3 (n = 3) > -4.7 (n = 4). For a PBH, there are multipole candidates for the GL geometry. A necessary and sufficient condition for the determining the reasonable GL geometry is $N_{\text{GL}} = N_{\text{db}} + 1$, which is called the GL sextet rule (N_{db} is the number of fusion double bonds, and N_{GL} is the number of Kekulé benzenoid rings). According to the requirement of the position rule, the alternating order of the peripheral single and double bonds in the reasonable GL geometry should be consistent with that of the longer and shorter peripheral bonds in the ground state of a PBH. Energy rule requires that the molecular energy of a reasonable GL geometry is the highest of all candidates. For the GL geometry of a PBH, the qualified candidate refers to a type of geometry whose structure conforms to the GL sextet rule. The values of the CESE corresponding to the qualified candidate geometries are always close to each other. The position rule and energy rule must obey the GL sextet rule, and can help the GL sextet rule to choose the most reasonable GL geometry from the qualified candidates. For each of the four homologous series (**7-1-n**, **7-2-n**, **7-3-n**, and **7-6-(n:0)**), CESE/ π can be fitted as a linear function of the p band UV absorption frequency $\tilde{\nu}$. For each of the four series of structural isomers with molecular formulas of C₁₈H₁₂, C₂₂H₁₄, C₂₆H₁₆, and C₃₀H₁₈, CESE/ π can also be fitted as a second-order polynomial function of the p band frequency $\tilde{\nu}$, and as the function of the number of GL sextets. It should be emphasized that the CESEs/ π for all PBHs are less in the absolute value than that (-6.5 kcal/mol* π) of benzene and all the energy effects ΔE^{Am} are destabilizing.

yuzh@iccas.ac.cn

Key words: ESEs of polycyclic benzenoid hydrocarbons; GL sextet rule; energy rule; position rule; candidates for GL geometry.

7.0. FOREWORDS

For a PBH (polycyclic benzenoid hydrocarbon), there are multipole candidates for the GL geometry. A necessary and sufficient condition for the rationality of GL geometry is that the number N_{GL} of the benzenoid rings with three double bonds is equal to $N_{db} + 1$, where N_{db} is the number of the fusion double bonds in the GL geometry. The relationship $N_{GL} = N_{db} + 1$ will be called the GL sextet rule in this Chapter. According to the requirement of the position rule, the alternating order of the peripheral single and double bonds in the reasonable GL geometry of a PBH should be consistent with that of the longer and shorter peripheral bonds in the ground state. According to the energy rule, the molecular energy of a reasonable GL geometry is the highest of all candidates. The position rule and the energy rule are not necessary, and they must obey the GL sextet rule. However, these two rules can help us to choose the most reasonable GL geometry from the candidates that meet the GL sextet rule. These are the three rules that this chapter will focus on.

For each of four homologous series (acene, benzo[a]acenes, dibenzo[a,c]acenes, and dibenzo[de,d'e']acenes), the corrected ESE (CESE) per π -electron, $CESE/\pi$, can be fitted as a linear function of the p-band UV absorption frequency $\tilde{\nu}$. For each of the four series of structural isomers whose molecular formulae are respectively $C_{18}H_{12}$, $C_{22}H_{14}$, $C_{26}H_{16}$, and $C_{30}H_{18}$, $CESE/\pi$ can also be fitted as a second-order polynomial function of the p-band frequency $\tilde{\nu}$, and as the function of the number of GL sextets. It should be emphasized that $CESE/\pi$ for all PBHs are less in the absolute value than that ($-6.5 \text{ kcal/mol}^* \pi$) of benzene and all the energy effects ΔE^{Am} are destabilizing. In this Chapter, these linear relationships will be used to demonstrate the rationality of the above three rules.

Polybenzenoid hydrocarbons are a type of compound containing two or more fused benzenoid rings. Two fused rings share two carbon atoms that are bonded by single or double bond, and the (double) bond shared by two fused rings will be named the fusion (double) bond in this chapter. PBHs are the most commonly used as the model systems for the study of aromatic stability. The studies include:

- (i) Expression of the Kekulé valence structures of a PBH.¹
- (ii) The theoretical and experimental estimation of aromatic stabilization energy.

In essence, there is no difference between the resonance energy and the π electron delocalization energy. But for PBHs, there is a difference in the way to estimate these two energy effects. In the literature, the greatest advantage of the estimation of resonance energy is that it usually does not involve the expression of the Kekulé valence structure of PBH. Therefore, for a long period of time in the past, such methods gained attention and development. However, the calculation of π electron delocalization energy is dependent on choosing a reasonable localized geometry from the Kekulé valence structures. Therefore, correctly expressing the Kekulé valence structures of a PBH is a prerequisite for calculating the π -electron delocalization energy. In this Chapter, Kekulé valence structures are called the candidates for the GL geometry.

7.0.1. Estimation of Resonance Energy

Based on the additive principle, resonance energies are obtained from heats of either combustion or hydrogenation. For benzene, for example, the resonance energy was determined as the difference, in the hydrogenation heat, between benzene and three cyclohexenes by Kistiakowsky in 1936.² Afterwards, as reviewed by Cyrański,³ various methods have been reported in the literature to estimate the resonance energy of PBHs. These methods are roughly divided into the following two categories:

- (i) A comparison of the reference state energy calculated using the additive scheme with the experimental

atomization energy of a PBH.⁴

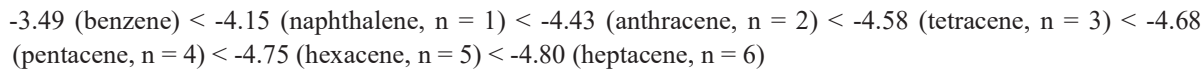
- (ii) Theoretically calculation of resonance energy (aromatic stabilization energy) by isodesmic reactions and homodesmotic reactions.⁵

An early additive bond energy scheme was proposed by Pauling in 1933.⁶ In 1970, a satisfied scheme, taking next-nearest-neighbor interactions into account with a great diversity of functional groups, was adopted by Cox and Pilcher.⁷ Another successful approach based on formation heats is the group additivity method by Cohen and Benson.⁴ A group is defined by Benson⁸ as “a multivalent atom together with all of the atoms bonded to it. Therefore, the group additivity scheme can provide a basis for distinguishing isomers of a PBH, and it is more reasonable than the bond additivity.

At that time, the additivity of the bond and group energies was usually flawless in calculation principle. However, the database used was neither accurate nor can it provide enough types of bonds and groups for various types of PBHs to calculate the atomization heat of the reference states. In addition, the aromatic molecular structure is variable, and the conjugation effect depends not only on the conjugation interaction between the adjacent double bonds, but also on the non-bond interaction between the double bonds. Therefore, it is impossible to reasonably evaluate the aromatic stabilization energy of various types of PBHs using only limited types of the chemical bonds and groups.

According to the idea of isodesmic and homodesmotic reactions, the reaction may be formulated in a very simple way, and the measuring of the aromatic stabilization energy (ASE) can be simplified into the determination of the enthalpy of an appropriate reaction. However, they serve only as a rough estimation of ASE. In the case of benzene, as reviewed by Cyrański,³ the stabilization energy depends upon the structural features of the reference molecules used in a specific reaction, and the range of a series of the values of stabilization energy, the difference between the largest value (-66.9 kcal/mol) and the smallest value (-23.2 kcal/mol), is large, up to -43.8 kcal/mol.

For linear acenes, for example, various methods (such as Cox and Pilcher method, Cohen and Benson method and isodesmic reactions) were used to determine their stabilization energies (SE). Due to that the reference structure(s), used in the isodesmic reactions, is different in the different literatures, and since the energy values of specific bonds such as C_d-C_d are differently specified in different literatures, the values of stabilization energies, obtained from different methods, are very different and are all unreasonable. As an example, the following series of SE3/π (stabilization energy per π electron) were calculated based on increments (C_d-(C_d)H = -6.78 kcal/mol and C_d-(C_d)₂ = -12.3 kcal/mol) for conjugated olefins:⁹



In this series of the SE/π values (in the original literature, the values were expressed as positive), the absolute value increases as the number of fused benzenoid rings increases. But, as shown by the experiments and theoretical calculations,^{10,11} acenes become less “stable” and more reactive with the increasing of the number of rings.

In a word, it seems impossible to use a specific literature method in an attempt to calculate the aromatic stabilization energies of various series of PBHs. Thus, the concept of resonance energies was seriously criticized by George in 1975.¹²

7.0.2. Calculation of Electron Delocalization Energy

Since the introduction of Hückel theory, the importance of the π-electron delocalization for the estimation of the aromatic stabilization energy has been widely discussed. In order to solve the problem of estimating aromatic stabilization energy at the *ab initio* level of theory, and to find answers to the following questions: how much energy is really gained by the π electron delocalization in a conjugated system? and how can this energy gain be defined and

computed within an *ab initio* MO theory? Kollma proposed a method for constructing a localized reference state in 1979.¹³ Although Morokuma developed a method to calculate the energy effects (such as charge transfer energy, exchange energy, polarization energy, etc.) between two molecules by eliminating the Fock matrix elements in 1976,¹⁴ Kollma can still be regarded as a pioneer in calculating π -electron delocalization energy. But from today's perspective, the Kollma's method is still unreasonable. For benzene, for example, the wave function of its localized reference was constructed by replacing the delocalized π MOs of the ground state with the π MOs of three ethylene molecules. In the Kollma's method, the geometry optimization was not involved.

In 1994, Kollma's method was improved by Jug.¹⁵ In the Jug's method implemented using the semi-empirical method SIND01, the molecular energies for the localized systems of several PBHs (such as naphthalene and anthracene) are obtained from the SCF iteration (or from the conditional geometry optimization), but before each SCF iteration, the Fock matrix elements between the double bonds (or groups) are deleted. In terms of computational principle, our 2007 method is exactly the same as the Jug's method, except that our method is capable of running at RHF, MPn and DFT levels. But our most important contribution to the calculation of aromatic stabilization energy is to find new type of energy effect ΔE^{Am} that are additive in the case of acyclic polyenes. In this section, will once again confirm that, so far, our 2007 program, as well as our 2011 program, is only method that can be used to accurately estimate the aromatic stabilization energy of conjugated molecules including the aromatic and anti-aromatic molecules.

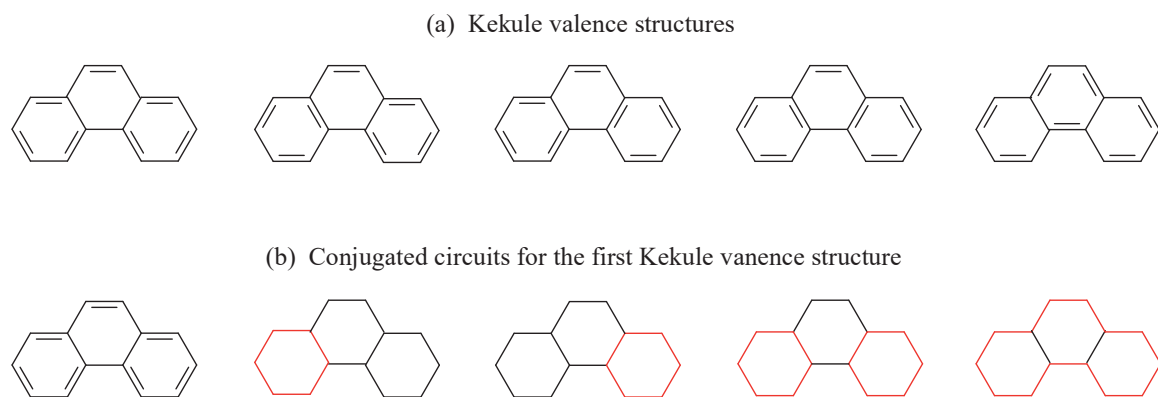


Figure 7-I. (a) the five Kekulé valence structures of phenanthrene; (b) Four conjugated circuits, represented by red lines, for the first Kekulé valence structure.

A GL geometry of an aromatic molecule is actually one of Kekulé valence structures (resonance structures). Taking benzene molecule as an example, the GL geometry is the same as the Kekulé structure in which their π systems are localized on their respective double bonds and there is no conjugation between double bonds. The difference is that benzene has two Kekulé structures. According to the symmetry, two Kekulé structures correspond to the same GL geometry.

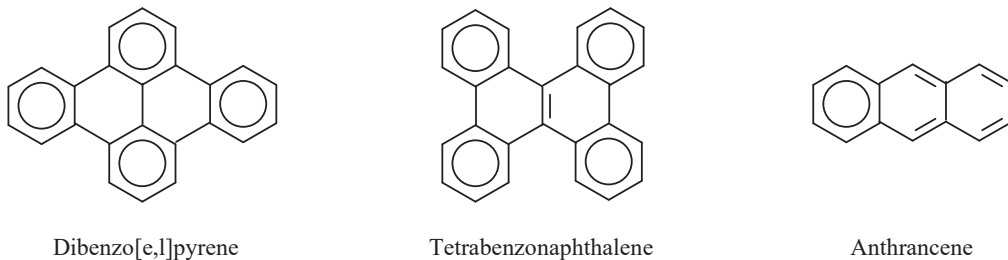
For a PBH, as a rule,¹ the number of Kekulé valence structures is $K+1$, where K is the number of conjugated circuits in each Kekulé valence structure. For phenanthrene, for example, each Kekulé valence structure has four conjugated circuits (Figure 7-Ib), and the number of its Kekulé valence structures is five (Figure 7-Ia). Therefore, the important problem is how to determine a reasonable GL geometry from the candidates (Kekulé valence structures). In 2011, three rules, position rule, energy rule and GL sextet rule, were proposed in our research work to determine the positions of the CC double bonds in the localized geometry (GL geometry) of a PBH.¹⁶

In 2011, a graph method, called the numerical Clar formula, was proposed by Randić and Plavšić in order to determine the positions of double bonds in Kekulé valence structure.¹⁷ The Randić and Plavšić method can provide a theoretical evidence for our position rule. However, the positional rules are only a sufficient condition, not a

necessary condition, and it is only used to determine the positions of the peripheral double bonds in some PBHs. Therefore, the Randić and Plavšić method does not completely solve the problem of how to reasonably determine the GL geometry in the case of PBH.

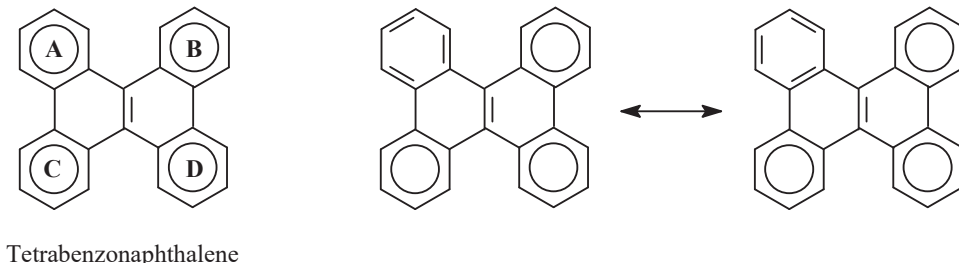
7.0.3. Randić and Plavšić method

According to Clar structures, as shown by Scheme 7-I, PBHs can be divided into three types.¹⁷ In the Clar structure of a PBHs belonging to the first type, there are only aromatic π -sextets (Clar sextet) and empty rings. In the Clar structure of dibenzo[e,l]pyrene, for example, there are four π -sextets and two empty rings. According to Clar's definition, a ring without C=C double bond, such as the two central rings in dibenzo[e,l]pyrene, is defined as the empty ring. A PBH of this type has only one Clar structure. In addition to containing π -sextet and empty rings, a PBH belonging to the second type has one or more benzenoid rings with only one C=C bond. Tetrabenzonaphthalene belongs to the second type. This type of PBHs also has only one Clar structure. A PBH such as anthrancene belongs to the third type, and it has more than one Clar structures. In each of its Clar structures, there are one or more benzenoid rings with a pair of double bonds.



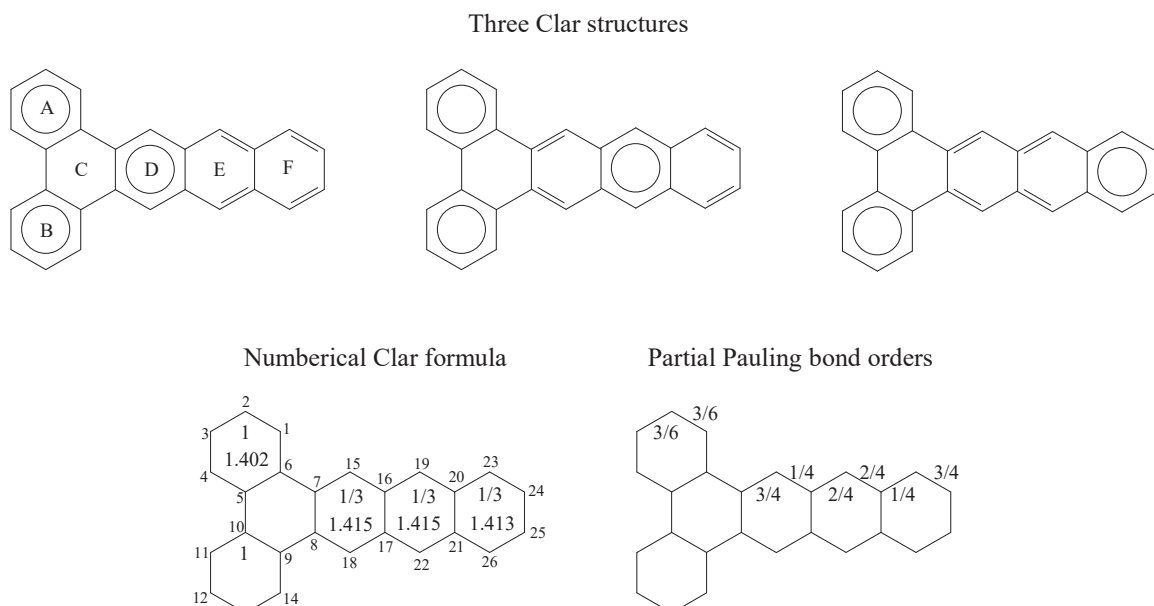
Scheme 7-I

It should be indicated that, for a π -sextet ring itself, the positions of the double bonds are not cared about. For Tetrabenzonaphthalene (Scheme 7-II), for example, the difference between the two resonance structures is in the positions of three double bonds in ring A. For the Kekulé valence structures and for the GL geometry, however, the positions of all double bonds must be determined.



Scheme 7-II

For a PBH belonging to the third type, the Randić and Plavšić method¹⁷ is used to determine the positions of the CC double bonds in some benzenoid rings whose numerical values < 1 in the numerical Clar formula. The Randić and Plavšić method is a multi-step procedure, and the first step is to construct a numerical Clar formula. Then, based on the numerical Clar formula, a canonical Clar structure is picked out from the Clar structures. At last, the positions of double bonds in the benzenoid ring (Kekulé ring) with three double bonds are determined by the partial Pauling bond orders (PPBOs). However, the canonical Clar structure for some PBHs such as acenes is not unique.

**Scheme 7-III**

7.0.3.1. Numerical Clar Formula

For a specific PBH belonging to the third type, the numerical value (π -sextet ring value.), N_{rv} , of a benzenoid ring is defined as the following:

$$N_{rv} = N_{st}/N_c \quad (7-I)$$

where N_c is the number of possible Clar structures, and N_{st} is the number of times a specific ring appears as π -sextet ring in all possible Clar structures. For example, dibenzo[a,c]tetracene has three Clar structures, and each Clar structure has three π -sextets. In three Clar structures, as shown by Scheme 7-III, the number of times ring A appears as π -sextet ring in all possible Clar structures is 3, and its $N_{rv} = 3/3 = 1$. In a similar way, the numerical values, $N_{rv} = 1/3$, of the remaining rings can be determined and are presented in Scheme 7-III. Numerical Clar formula of a PBH refers to a structure formula in which the ring numerical values N_{rv} are presented.

In each benzenoid ring, there are six bonds. The average bond lengths, r_{av} , of benzenoid rings are presented in Scheme 7-III. A comparison of the values of N_{rv} and r_{av} , shows a general rule: a larger numerical value corresponds, generally, to a shorter average bond distance. For rings A and D, the numerical values are 1 and $1/3$, and the corresponding average bond lengths are 1.402 and 1.415 Å.

A Clar structure whose numerical values are the largest of all the structures is called canonical Clar structure. Once the canonical Clar structure is determined, the positions of the double bonds in the other rings with one or two double bonds are definitively determined, we only need to determine the positions of the double bonds in each benzenoid ring (π -sextet ring) with three double bonds, i.e. to calculate PPBOs of the CC bonds in these benzenoid rings. However, for some PBHs such as dibenzo[a,c]tetracene, the canonical Clar structure is not unique. For dibenzo[a,c]tetracene, its three Clar structures are all canonical Clare structure. Therefore, the positions of the double bond in all benzenoid rings need to be determined.

7.0.3.2. Partial Pauling Bond Order

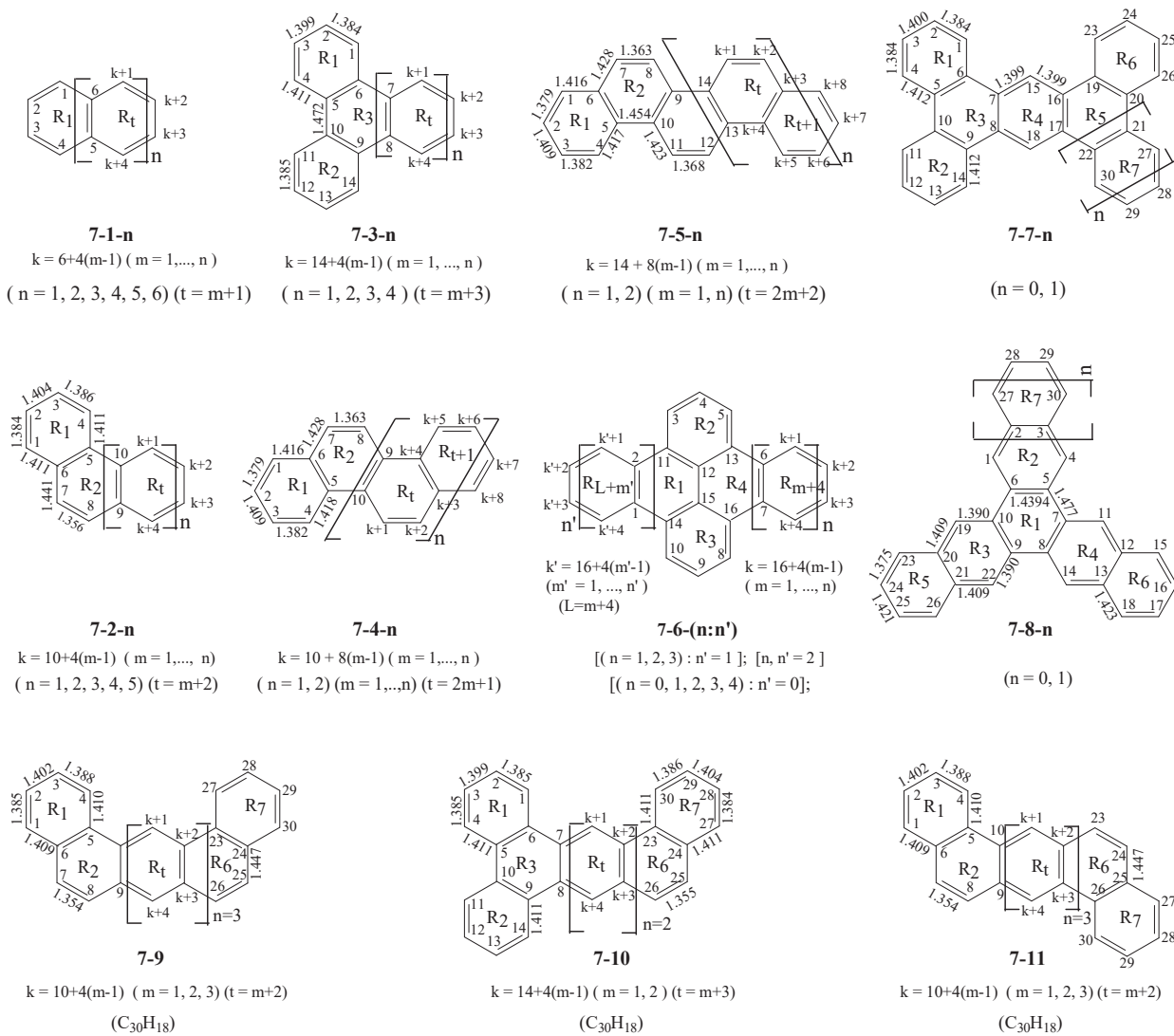


Figure 7-1. Polycyclic benzenoid hydrocarbons (PBHs), and their numbering system of atoms that has nothing to do with IUPAC nomenclature, the bond lengths (\AA) at the ground states of the molecules 7-2-2, 7-3-2, 7-4-2, 7-5-2, 7-7-0, 7-8-0, and three individual molecules 7-9 (dibenzo[1,2,10,11]pentacene), 7-10 (tribenzo[1,2,3,4,7,8]tetracene) and 7-11 (dibenzo[1,2,8,9]-pentacene), and n is the number of chain units.

The partial Pauling bond order, D_p , of a specific peripheral CC bond can be calculated by the following Equation (7-II):

$$D_p = (N_{std} + N_{rdd}) / N_k \quad (7-II)$$

In dibenzo[a,c]tetracene, for example, the benzenoid ring D appears one time as Clar sextet ring (corresponding to two Kekulé valence structures), and it can also appear two times as the benzenoid ring have two double bonds (corresponding to two Kekulé valence structures); in Equation (7-II), therefore, the total number, N_k , of the Kekulé valence structures related the ring D is four; In the two Kekulé valence structures whose ring D is π -sextet ring, the C(7)C(15) bond appears one time as double bond, so $N_{std} = 1$ in Equation (7-II); in the remainder two Kekulé

valence structures, C(7)C(15) bond appears two times as double bond, so $N_{rdd} = 2$ in Equation (7-II). Therefore, for the C(7)C(15) bond in dibenzo[a,c]tetracene, $D_p = (N_{std} + N_{rdd})/4 = 3/4$. Similarly, the partial Pauling bond orders for the peripheral CC bonds are calculated and are presented in Scheme 7-III. For the C(23)-C(24) and C(25)-C(26) double bonds in benzenoid ring F of dibenzo[a,c]tetracene, for example, $N_k = 4$, $N_{std} = 1$, $N_{rdd} = 2$, so $D_p = 3/4$; and for the C(20)-C(23) and C(21)-C(26) bonds, $D_p = 1/4$. Accordingly, the C(23)-C(24) and C(25)-C(26) bonds should be two double bonds in the GL geometry.

In this Chapter, the partial Pauling bond order will be used to support the position rule.

7.1. METHOD

In this Chapter, eight homologous series of PBHs (numbered as **7-1-n** to **7-8-n**) and three individual molecules (numbered as **7-9**, **7-10**, **7-11**) will be used as the research objects (Figure 7-1), and the three rules, position rule, energy rule, and GL sextet rule, will be proposed in order to ensure that a GL geometry can be reasonably picked out from its candidates. For each of these molecules, the numbering system of the atoms differs from that used by standard nomenclature.

All calculations are performed, at B3LYP/6-31G* level, using the PC-Gamess^{18,19} that has been improved in our research group, and were published in 2010.¹⁶

7.1.1. GL Geometry of Phenanthrene

Phenanthrene belongs to the PBH of second type, and has only one Clar structure. According to the definition of the most important Kekulé valence (MIKV) structure (Kekulé valence structure with the maximal number of Kekulé benzenoid ring),^{1,20,21} the C(7)-C(8) bond must be a double bond. However, the calculation of the partial Pauling bond orders cannot help in determining which peripheral CC bonds in the benzene ring R1 are double bond. According to the position rule,¹⁶ when all double bonds in the GL geometry are localized on the positions shown in Figure 7-2-1a, all the double bonds, such as C(1)C(2) and C(3)C(4)bonds, correspond to the shorter peripheral bonds in the ground state geometry. Then the GL geometry can be constructed by the geometry optimization, at B3LYP/6-31G* level, under the following conditional settings (Figure 7-2-1e): before each SCF iteration,

set AO Fork matrix elements $f_{\lambda,\rho} = 0$,
set AO overlap integral matrix elements $s_{\lambda,\rho} = 0$

when

π-type AO $\phi_\lambda \in P$ -th double bond,
π-type AO $\phi_\rho \in Q$ -th double bond
 $P, Q = A, B, C, D, \dots, G; P \neq Q$

In the GL geometry, therefore, the π systems are absolutely localized on their respective double bonds, and the σ system is delocalized over whole molecular framework. The molecular energy difference (adiabatic delocalization energy) $\Delta E^A = E(G) - E(GL) = -11.8$ kcal/mol (Figure 7-2-1), and it is stabilizing.

7.1.2. GE-m Geometries of Phenanthrene

As shown by Figure 7-2-2-a, GE-m geometries are denoted as GE-m(u:v,s:t), and can be viewed as an optimized geometry that is constructed by the local conjugation between a pair of double bonds, $-C(u)=C(v)-$ and

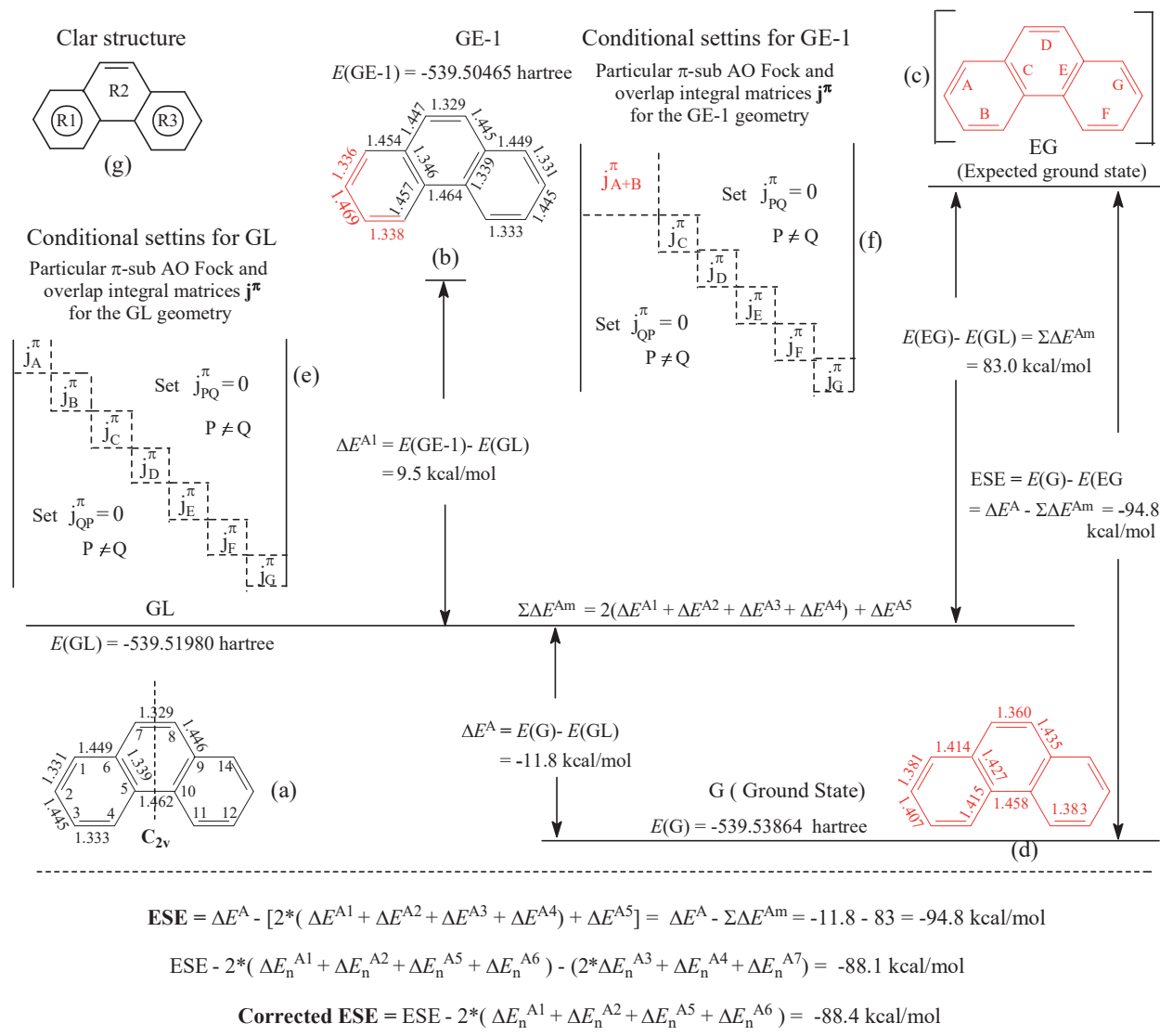


Figure 7-2-1. Procedure for calculating ESE and CESE of phenanthrene (7-2-1), and definitions of the energy differences ΔE^A and ΔE^{Am} , the GL, GE-m, and ground state geometries are obtained from the restricted and full geometry optimizations at the B3LYP/6-31G* level, where the unit of the bond lengths is in angstroms. (e) and (f) Are the conditional settings for optimizing the GL and GE-1 geometries. In the molecular structures, the red and black lines indicate that all the π orbital interactions between the double bonds are set equal to zero, except for those between the red double bonds. (a) The numbering system of the atoms and (c) The numbering system (A, B, C,) of the double bonds.

$-C(s)=C(t)-$, of the GL geometry. For example, GE-1(1:2,3:4) geometry is constructed by the following conditional settings (Figure 7-2-1f): before each SCF iteration,

$$\text{set } f_{\lambda,\rho} = 0 \text{ and } s_{\lambda,\rho} = 0$$

when

π -type AO $\phi_\lambda \in P$ -th double bond,

π -type AO $\phi_\rho \in Q$ -th double bond

$P, Q = (A+B), C, D, \dots, G; P \neq Q$

GE-m(u:v,s:t)	Interacting double bonds	Distance r_{v-s} of single bond (Å)	$E(\text{GE-m})$	ΔE^{Am}
GE-1(1:2,3:4)	C1=C2—C3=C4	C2—C3 $r_{2-3} = 1.469$	-539.50465	9.5
GE-2(1:2,5:6)	C2=C1—C6=C5	C1—C6 $r_{1-6} = 1.472$	-539.50568	8.9
GE-3(3:4,5:6)	C3=C4—C5=C6	C4—C5 $r_{4-5} = 1.477$	-539.50485	9.4
GE-4(5:6,7:8)	C5=C6—C7=C8	C6—C7 $r_{6-7} = 1.468$	-539.50532	9.1
GE-5(5:6,9:10)	C6=C5—C10=C9	C5—C10 $r_{5-10} = 1.486$	-539.50494	9.3

GE _n -m(u:v,s:t) Geometry	Interaction between two nonbonded double bonds	$E(\text{GE}_n\text{-m})$	ΔE_n^{Am}
GE _n -1(1:2,7:8)	GE _n -8(13:14,7:8) C1=C2--- C7=C8	C13=C14--- C7=C8	-539.52202 -1.4
GE _n -2(3:4,7:8)	GE _n -9(11:12,7:8) C3=C4--- C7=C8	C11=C12--- C7=C8	-539.52015 -0.2
GE _n -3(1:2,11:12)	GE _n -10(13:14,3:4) C1=C2 --- C11=C12	C13=C14--- C3=C4	-539.51981 -0.0
GE _n -4(3:4,11:12)		C3=C4--- C11=C12	-539.52021 -0.3
GE _n -5(5:6,11:12)	GE _n -11(9:10,3:4) C5=C6--- C11=C12	C9=C10--- C3=C4	-539.52201 -1.4
GE _n -6(5:6,13:14)	GE _n -12(9:10,1:2) C5=C6--- C13=C14	C9=C10--- C1=C2	-539.52013 -0.2
GE _n -7(1:2,13:14)		C1=C2 --- C13=C14	-539.51980 -0.0

$$\Delta E^{\text{Am}} = E(\text{GE-m}) - E(\text{GL}) \quad \Delta E_n^{\text{Am}} = E(\text{GE}_n\text{-m}) - E(\text{GL})$$

Figure 7-2-2. For phenanthrene (7-2-1), (a) the local π orbital interactions between various pairs of adjacent doubles in the GL geometry; (b) and between pairs of non-bonded double bonds.

In this geometry, the π systems are absolutely localized on the following six groups:

- (i) A locally conjugated group, $-\text{HC}(1)=\text{C}(2)\text{H}-\text{HC}(3)=\text{C}(4)\text{H}-$.
- (ii) Three peripheral double bonds, $-\text{C}(u)\text{H}=\text{HC}(u+1)-$ ($u = 7, 11, 13$).
- (iii) Two fusion double bonds, $-\text{C}(u)=\text{C}(u+1)-$ ($u = 5, 9$).

In each GE-m geometry, the σ system is delocalized over whole molecular framework. In a similar way, other GE-m(u:v,s:t) geometries can be restrictedly optimized, and their molecular energies and the energy effects ($\Delta E^{\text{Am}}(\text{u:v,s:t}) = E(\text{GE-m}) - E(\text{GL})$) are presented in Figure 7-2-2a.

For a PBH, N_{am} is the total number of GE-m(u:v,s:t) geometries, and it depends upon the number of the localized double bonds in the GL geometry. Of all the GE-m geometries, K_{am} is the number of the GE-m(u:v,s:t) geometries with different molecular energies, and it depends on the symmetry of the GL geometry. K_{am} is also the number of the GE-m(u:v,s:t) geometries that must be optimized.

The GL geometry of phenanthrene has the C_{2v} symmetry. In each of the following four pairs of GE-m(u:v,s:t), two geometries have the same molecular energy: GE-1(1:2,3:4) and GE-6(11:12,13:14), GE-2(2:1,6:5) and GE-7(13:14,9:10), GE-3(3:4,5:6) and GE-8(9:10,11:12), and GE-4(5:6,7:8) and GE-9(7:8,9:10). In the actual calculations, therefore, only the following five geometries need to be restrictedly optimized: GE-1(1:2,3:4), GE-2(1:2,5:6), GE-3(3:4,5:6), GE-4(5:6,7:8), GE-4(5:6,9:10). In Figure 7-1-2a, the molecular energies, $E(\text{GE-m})$, of the five GE-m(u:v,s:t), the distance, $r_{v-s}(\text{GE-m})$, of the $\text{C}(v)-\text{C}(s)$ single bond between two conjugated double bonds ($\text{C}(u)=\text{C}(v)$ and $\text{C}(s)=\text{C}(t)$) in each GE-m(u:v,s:t) geometry, and energy effects $\Delta E^{\text{Am}} = [E(\text{GE-m}) - E(\text{GL})]$ are presented.

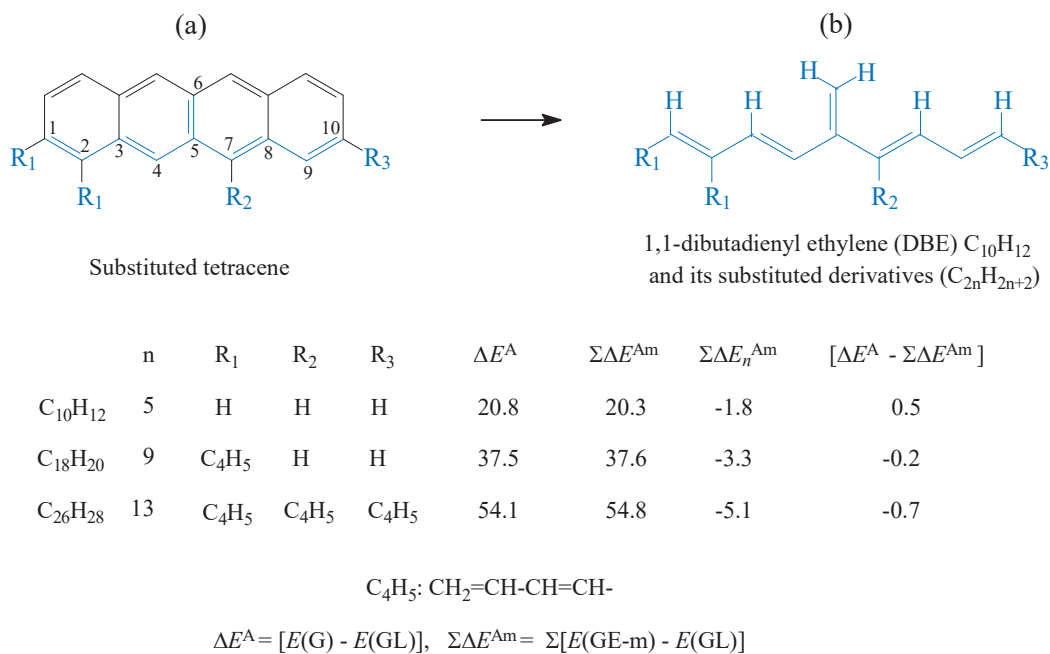


Figure 7-3. For substituted 1,1-dibutadienyl-ethylenes at B3LYP/6-31G* level, the energy effects ΔE^{Am} are additive.

Figure 7-1-2 shows that the energy effect $\Delta E^{Am}(u:v,s:t)$, associated with the local conjugation interaction between two bonded double bonds $-C(s)=C(t)-$ and $-C(u)=C(v)-$ in the GL geometry, is always destabilizing, that is, always $\Delta E^{Am}(u:v,s:t) > 0$. Correspondingly, the sing bond distance $r_{v-s}(GE-m)$ is always longer than that $r_{v-s}(GL)$. For example, $r_{2,3}(GE-1) (1.469 \text{ \AA}) > r_{2,3}(GL) (1.445 \text{ \AA})$, the bond length difference $dr_{2,3} = [r_{2,3}(GE-1) - r_{2,3}(GL)] = 0.024 \text{ \AA}$, and the molecular energy difference $\Delta E^{A1} = [E(GE-1) - E(GL)] = 9.5 \text{ kcal/mol} > 0$.

Similar to the idea to calculate the ESE of benzene, need to confirm that the energy effects ΔE^{Am} are additive in the case of acyclic polyene before calculating the ESE of PBH. Of course, the structure of this type of acyclic polyene should be related to the structures of PBHs.

7.1.3. Substituted 1,1-dibutadienyl-ethylene

In phenanthrene, the $C(5)=C(6)$ double bond is used four times to construct four GE-m($u:v,s:t$) ($m = 2, 3, 4, 5$) geometries (Figure 7-2-2a), and each of the two carbon atoms participates in the formation of two GE-m geometries through bonding, which is different from the double bonds in the GL geometry of benzene in the way to participate in the formation of the GE-m geometry.

For a substituted tetracene in Figure 7-3a, the blue lines in the structural formula represent the structure of substituted 1,1-dibutadienyl-ethylene (substituted DBE, the numbering system of the atoms in Figure 7-3a is different from that used by standard nomenclature). After the groups, represented by the black lines in Figure 7-3a, being replaced with six hydrogen atoms, substituted tetracene is transformed into substituted 1,1-dibutadienyl-ethylene (Figure 7-3b). In the GE-2(3:4,5:6) and GE-3(6:5,7:8) geometries of a substituted 1,1-dibutadienyl-ethylene, two conjugated groups, $-HC(3)=C(4)H-HC(5)=C(6)H_2$ and $H_2C(6)=C(5)H-HC(7)=C(8)H-$, both contain the C(5) atom, which is equivalent to the role of the $C(5)=C(6)$ double bond of the GL geometry of phenanthrene in forming two GE-m geometries.

For three substituted DBEs $C_{10}H_{12}$, $C_{18}H_{20}$ and $C_{26}H_{28}$ (Figure 7-3), $|\Delta E^A - \Delta E^{Am}| \leq 0.7 \text{ kcal/mol}$, and $\Delta E^A \approx \Delta E^{Am}$. The energy effects, ΔE^{Am} , can still be considered additive in the case of substituted 1,1-dibutadienyl-ethylene.

The method for evaluating the ESE of benzene can be applied to PBH.

7.1.4. ESE of Phenanthrene

For phenanthrene, $\Sigma\Delta E^{\text{Am}} = 83.0 \text{ kcal/mol}$ (Figure 7-2-1). If the energy effects ΔE^{Am} are additive, the molecular energy difference, $[E(\text{EG}) - E(\text{GL})]$, between the expected ground state (EG in Figure 7-2-1c) and the GL geometry (Figure 7-2-1a) should be approximately equal to $\Sigma\Delta E^{\text{Am}}$ (83.0 kcal/mol). However, as shown by the data presented in Figure 7-2-1, $\Delta E^{\text{A}} = E(\text{G}) - E(\text{GL}) = -11.8 \text{ kcal/mol}$, and $\Delta E^{\text{A}} - \Sigma\Delta E^{\text{Am}} = [E(\text{G}) - E(\text{GL})] - [E(\text{EG}) - E(\text{GL})] = E(\text{G}) - E(\text{EG}) = (-11.8) - (83.0) = -94.8 \text{ kcal/mol}$. Therefore, -94.8 kcal/mol deviation from the additivity is equal to the molecular energy difference between the real ground state (G) and the expected ground state. Similar to the expected ground state (cyclohexatriene) of benzene, the expected ground state of phenanthrene can also be considered as the virtual reference conjugated molecule of phenanthrene. Thus, $[E(\text{G}) - E(\text{EG})]$ (-94.8 kcal/mol) can be defined as the extra stabilization energy of phenanthrene with respect to its reference conjugated molecule.

Phenanthrene has fourteen π -electrons. The ESE per π -electron, denoted as ESE/π , is equal to $\text{ESE}/14 = 6.77 \text{ kcal/mol}$, and it is greater in absolute value than ESE/π (-6.5 kcal/mol) for benzene, meaning that the ESE of phenanthrene needs to be corrected.

7.1.5. Corrected ESE of Phenanthrene.

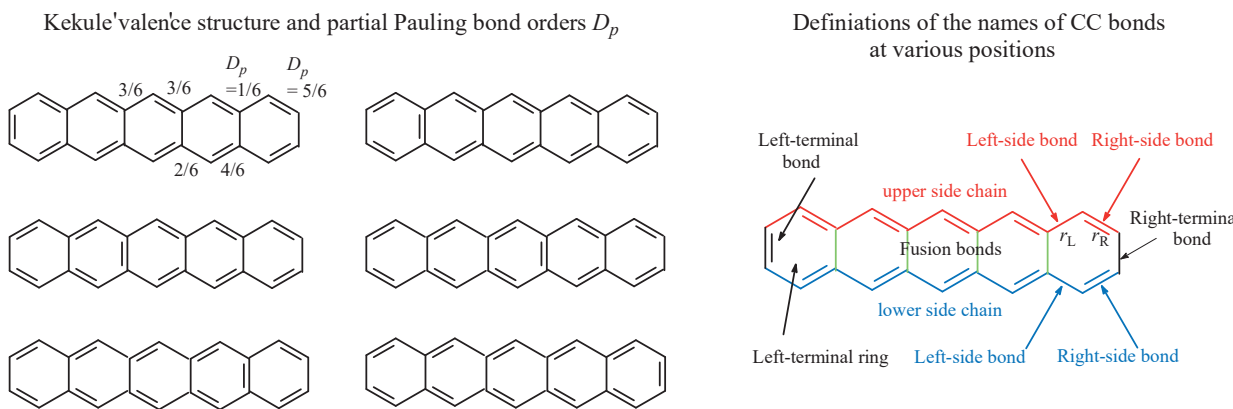
According to Figure 7-2-2b, the π interaction can also occur between a pair of non-bonded double bonds in the GL geometry, thereby forming a locally delocalized geometry denoted as $\text{GE}_{n-m}(s:t,u:v)$. For $\text{GE}_{n-m}(1:2,7:8)$ geometry, for example, it is constructed by the non-bonded interaction between the C(1)=C(2) and C(7)=C(8) double bonds in the GL geometry, and the corresponding energy effect $\Delta E_n^{\text{A}1} = -1.4 \text{ kcal/mol}$. Figure 7-2-2b shows that ΔE_n^{Am} is always stabilizing (always $\Delta E_n^{\text{Am}} < 0$).

For a PBH, $N_{\text{n,m}}$ is the total number of $\text{GE}_{n-m}(u:v,s:t)$ geometries. Of all the GE_{n-m} geometries, $K_{\text{n,m}}$ is the number of the $\text{GE}_{n-m}(u:v,s:t)$ geometries that must be optimized, and it depends on the symmetry of the GL geometry. For Phenanthrene, $N_{\text{n,m}} = 12$, $K_{\text{n,m}} = 7$, and CESE (corrected ESE) = $\Delta E^{\text{A}} - (\Sigma\Delta E^{\text{Am}} + \Sigma\Delta E_n^{\text{Am}}) = \text{ESE} - \Sigma\Delta E_n^{\text{Am}} = -88.1 \text{ kcal/mol}$ (Figure 7-2-1).

The values of ΔE_n^{Am} ($m = 3, 4, 7, 10$) are in the range of 0 to -0.3 kcal/mol. That is to say, when two double bonds do not belong to the two fused benzenoid rings, and they are separated by at least one benzenoid ring, the non-bonded π interaction may be negligible. Therefore, in order to save computation time as much as possible, the corresponding energy effect is considered only when the two non-bonded double bonds belong to two fused benzenoid rings, respectively. In the meantime, the energy effect ΔE_n^{Am} , such as $\Delta E_n^{\text{A}2}(1:2,11:12)$ and $\Delta E_n^{\text{A}7}(1:2,13:14)$, etc., are ignored. For phenanthrene, in this case, $\text{CESE} = -88.4 \text{ kcal/mol}$, and its CESE/π (-6.3 kcal/mol for per π electron) (in absolute value) < CESE/π (-6.5 kcal mol⁻¹/ π) for benzene.

7.2. ACENES

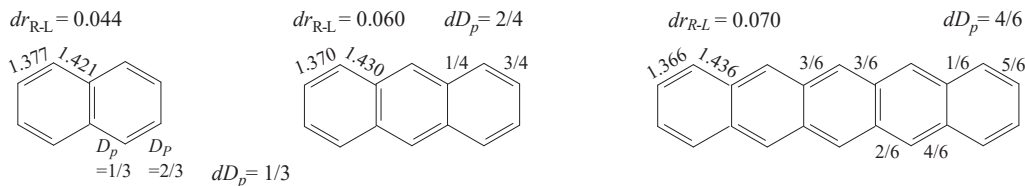
An acene (**7-1-n**) is a type of PBH, and its benzenoid rings are linearly fused. Therefore, an acene has C_{2v} symmetry and its molecular formula can be written as $C_4H_4(C_4H_2)_nC_2H_2$. In this Chapter, acenes include naphthalene ($n = 1$), anthracene ($n = 2$), tetracene ($n = 3$), pentacene ($n = 4$), hexacene ($n = 5$), and heptacene ($n = 6$). For pentacene, for example, there are five conjugated circuits for each Kekulé valence structure. Therefore, the number of Kekulé valence structures should be six (Scheme 7-1). But there are only three candidates for the GL geometry



Scheme 7-1

due to the C_{2v} symmetry. In the first and last Kekulé valence structures, there is only one Kekulé benzenoid ring. In each of other four Kekulé valence structures, there are two Kekulé benzenoid rings, and these two benzenoid rings share a double bond, which is different from the definition of Clar sextet (any double bond in the Clare sextet ring is no longer be considered to belong to other ring(s) fused to the Clar sextet ring). Such Kekulé benzenoid ring will be called the GL sextet in this Chapter. Therefore, the first and last structures are not the most important Kekulé valence structure according to the definition,¹ and these two structures should be excluded from the candidates for the GL geometry. Due to the C_{2v} symmetry, only two most important Kekulé valence structures, the second and third ones in Scheme 7-1, can be considered as the candidates for the GL geometry.

Therefore, the key to calculate the ESE and CESE of a PBH is how to determine a reasonable GL geometry from the candidates. In order to be able to develop the three rules for determining a reasonable GL geometry, various chemical bonds of PBH must first be defined.

Bond length (\AA) and Partial Pauling bond orders D_p of acenes

Scheme 7-2

7.2.1. Generalized Definition of Fusion Bond

In an acene such as pentacene (Scheme 7-1), two groups of the peripheral atoms form two side chains: a red side chain, and a blue side chain. For a green bond between two side chains, due to that it is shared by two benzenoid rings, imitating the IUPAC (International Union of Pure and Applied Chemistry) definition of a fusion atom,²² it is called fusion bond. In this section, for convenience, the definition of fusion bond is generalized to all the bonds between two side chains. Hereafter, the so-called fusion bonds include the following two types of bonds: the terminal CC bond(s) (black), and the green CC bond(s) shared by two benzenoid rings.

In each benzenoid ring such as the right-terminal ring in Scheme 7-1, there are two pairs of the peripheral bonds

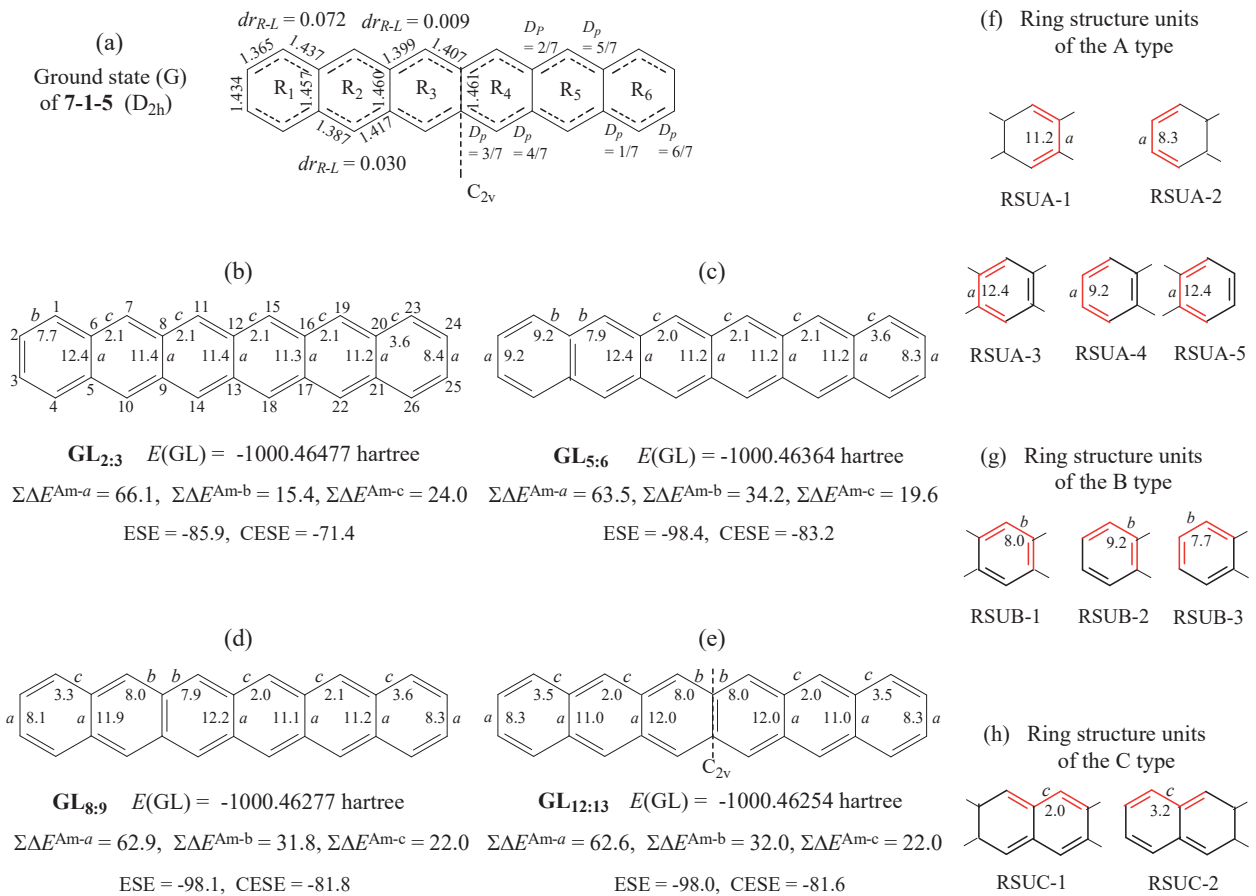


Figure 7-4. Energy Rule and position rule. (a) For the ground state geometry of molecule **7-1-5** (hexacene), the numbering of benzenoid rings, the bond distances and partial Pauling bond orders (PPBO), D_p , of the right-side bond and left-side bond, and their differences dr_{R-L} . (b), (c), (d) and (e) Four candidates $GL_{m:n}$ for the GL geometry. The CESE values obtained from candidates $GL_{m:n}$, and their various components. Here, the characters “*a*”, “*b*”, and “*c*”, at the side of the single bonds, correspond to the energy differences ΔE^{Am-k} ($k = a, b, c$), and the values of ΔE^{Am-k} are presented at the other side of the single bonds. (f), (g) and (h) The types of ring structure units, and their values. The units of all energies, except for that of the molecular energy, are in kcal/mol at B3LYP/6-31G* level. (b) The numbering system of atoms.

belonging to the upper side chain (red) and lower side chain (green), respectively. Each pair of the peripheral bonds can be divided into the left-side (L) bond and right-side (R) bond, and their bond lengths are denoted as r_L and r_R .

For the ground state geometry of an acene, as indicated by Scheme 7-2 and Figure 7-4a, the peripheral bonds have the following characteristics:

- (i) When a benzenoid ring is on the left side of the molecular symmetry axis, the right-side bond is longer than the left-side bond, and the PPBO, D_p , of the former bond is smaller than that of the latter bond; when a benzenoid ring is located at the right-side of symmetry axis, the left- and right-bond features are opposite.
- (ii) For a specific acene, the bond length difference, dr_{R-L} , as well as the PPBO difference dD_p , between the right-side bond and the left-side bond in the left-terminal ring is the largest. As the benzenoid ring approaches the axis of symmetry, dr_{R-L} and dD_p monotonically decreases.
- (iii) In a specific benzenoid ring such as the terminal ring, as the molecular chain length n increases, dr_{R-L} and dD_p also increase.

Table 7-1. For Each of Acenes 7-1-n, Molecular Energies $E(GL_{m:n})$ (hartree) of the Candidates $GL_{m:n}$, ESE, CESE, and CESE per π -Electron (kcal/mol) Calculated Based on Each Candidate $GL_{m:n}$, and Corresponding Energy Effect Sums $\Sigma\Delta E^{Am}$ and $\Sigma\Delta E_n^{Am}$ (kcal/mol), Obtained from Our 2007 Method at B3LYP/6-31G* Level.

* $GL_{m:n}$	N_{GL}	$E(GL_{m:n})$	ΔE^A	ESE	CESE	CESE/ π	$\Sigma\Delta E^{Am}$	$\Sigma\Delta E_n^{Am}$
7-1-1		$C_{10}H_8$						
$GL_{2:3}$	1	-385.87829	-9.1	-52.6	-49.2	-4.9	43.5	-3.4
$\ddot{GL}_{5:6}$	2	-385.87779	-9.4	-65.2	-62.0	-6.2	55.8	-3.2
7-1-2		$C_{14}H_{10}$						
$GL_{2:3}$	1	-539.52490	-3.5	-62.4	-56.1	-4.0	58.9	-6.3
$\ddot{GL}_{5:6}$	2	-539.52404	-4.1	-75.1	-68.2	-4.9	71.0	-6.8
7-1-3		$C_{18}H_{12}$						
$GL_{2:3}$	1	-693.17150	3.6	-70.8	-61.7	-3.4	74.4	-9.1
$GL_{5:6}$	2	-693.17049	2.9	-83.4	-73.7	-4.1	86.3	-9.7
$\ddot{GL}_{8:9}$	2	-693.16998	2.6	-83.2	-72.7	-4.0	85.8	-10.5
7-1-4		$C_{22}H_{14}$						
$GL_{2:3}$	1	-846.81813	11.4	-78.5	-66.7	-3.0	89.9	-11.8
$GL_{5:6}$	2	-846.81704	10.7	-91.1	-78.6	-3.6	101.8	-12.5
$\ddot{GL}_{8:9}$	2	-846.81629	10.3	-90.8	-77.3	-3.5	101.0	-13.4
7-1-5		$C_{26}H_{16}$						
$GL_{2:3}$	1	-1000.46477	19.6	-85.9	-71.4	-2.8	105.5	-14.5
$GL_{5:6}$	2	-1000.46364	18.9	-98.4	-83.2	-3.2	117.4	-15.2
$GL_{8:9}$	2	-1000.46277	18.4	-98.1	-81.8	-3.2	116.4	-16.3
$\ddot{GL}_{12:13}$	2	-1000.46254	18.2	-97.9	-81.5	-3.1	116.2	-16.4

* $GL_{m:n}$ means that, in the candidate $GL_{m:n}$, the C(m)-C(n) fusion bond is a double bond. $E(GL_{m:n})$ is the molecular energy of the $GL_{m:n}$ candidate. N_{GL} is the number of GL sextets (Kekulé benzenoid ring with three double bonds). $\ddot{\cdot}$ the reasonable GL geometry.

In the ground state geometry of hexacene (Figure 7-4a), for example, from the left-terminal ring R_1 to the ring R_3 , the size order of the corresponding dr_{R-L} and dD_P are as follows:

$$0.072 (R_1) > 0.030 (R_2) > 0.009 \text{ \AA} (R_3)$$

$$5/7 (R1) > 3/7 (R2) > 1/7 (R3)$$

From naphthalene (7-1-1) to hexacene (7-1-5), as shown by Scheme 7-2 and Figure 7-4a, the size order of the differences dr_{R-L} and dD_P in their left-end rings (R_1) are as follows:

$$0.044 (\text{naphthalene}) < 0.060 (\text{anthracene}) < 0.067 (\text{tetracene}) < 0.070 (\text{pentacene}) < 0.072 \text{ \AA} (\text{hexacene}).$$

1/3 (naphthalene) < 2/4 (anthracene) < 4/6 (pentacene) < 5/7 (hexacene).

7.2.2. Fusion Double Bond

In every Kekulé valence structure (i. e., every candidate for the GL geometry) of an acene, the number of fused bonds is $n + 2$ (including two end bonds), and only one fused bond is double bond. For an acene, therefore, there are $n+2$ candidates for the GL geometry, where n is the number of chain units $C_4H_4(C_4H_4)_nC_2H_2$. In Table 7-1, the subscript "n:m" in the symbol "GL_{n:m}" indicates that the C(m)-C(n) fusion bond is designated as a CC double bond in a specific candidate GL_{n:m}. In molecule 7-1-5 (hexacene), for example, there are seven fusion bonds (including two end bonds), and the position of a fusion double bond determines the positions of all peripheral double bonds in the GL geometry. According to the C_{2v} symmetry of molecule 7-1-5, 4 fusion bonds can be designated as double bond. Therefore, four candidates for the GL geometry should be optimized and are denoted as GL_{2:3}, GL_{5:6}, GL_{8:9}, GL_{12:13}. In the GL_{5:6} geometry, for example, the C(5)-C(6) bond is designated as a double bond. The size order of the molecular energies $E(GL_{m:n})$ (hartree) for the four candidates is as follow (in the absolute value):

$$-1000.46477 \text{ (GL}_{2:3}\text{)} > -1000.46364 \text{ (GL}_{5:6}\text{)} > -1000.46277 \text{ (GL}_{8:9}\text{)} > -1000.46254 \text{ (GL}_{12:13}\text{)}.$$

For the candidate GL_{2:3} geometry (Figure 7-4b), the two right-side CC bonds of every benzenoid ring are double bond. In the left-terminal benzenoid ring (R_1) of GL_{2:3}, for example, r_{1-2} (1.452 Å, a left-side bond) > r_{1-6} (1.335 Å). That is, for the peripheral bonds in the candidate GL_{2:3} geometry, the alternating order of the single and double bonds (abbreviated as "alternating order") is inconsistent with that of the longer and shorter peripheral bonds in the ground state geometry (Figure 7-4a), and is also inconsistent with the alternating order of the PPBOs in Kekulé valence structure. In the GL_{2:3} geometry, in addition, there is only one benzenoid ring with three double bonds. According to the definition of the most important Kekulé valence structure and based on the difference in the alternating order between the ground state and the GL_{2:3} geometry, therefore, it should not be considered as a candidate for the GL geometry.

In the GL_{12:13} geometry (Figure 7-4e), on the contrary, the alternating order is fully consistent with that of shorter and longer CC bonds in the ground state geometry, and it is also consistent with the alternating order of the PPBOs in Kekulé valence structure. The symmetry (C_{2v}) of GL_{12:13} geometry is also the same as that of ground state.

For any acene, as shown by the data listed in Table 7-1, when a fusion double bond is at (or closest to) the short symmetry axis, the corresponding candidate can be called particular candidate for the GL geometry or the reasonable GL geometry, and its characteristics are as follows:

- (i) Alternating order is fully consistent with that in the ground state geometry and is also consistent with that of the PPBOs in Kekulé valence structure (position rule).
- (ii) Its molecular energy is the highest of all the candidates (energy rule).
- (iii) The number of Kekulé banzenoid rings with three double bonds is 2 (GL sextet rule).

For molecule 7-1-5, for example, the molecular energy (-1000.46254 hartree) of the particular candidate is the highest of the four candidates.

The three characteristics for the particular candidates will be further confirmed and will be named as the following three rules to judge reasonable GL geometry: position rule, energy rule and GL sextet rule.

7.2.3. ESE and CESE

For each of molecules 7-1-n, the reasonable GL geometry is determined by the position and energy rules, and

Table 7-2. For Series of Acenes 7-1-n, ESE/π, CESE and CESE/π, and Contribution, RC_k, Made by k-th ($k = 1, \dots, 7$) Benzenoid Ring, to $\Sigma \Delta E^{\text{Am}}$ at B3LYP/6-31G* Level, and p-band UV Absorption Frequencies $\tilde{\nu} \times 10^{-2} \text{ cm}^{-1}$ (Energy Unit in kcal/mol).

Molecules	*PFDB	ESE/π	CESE	#CESE/π	RC _k (kcal/mol)							$\tilde{\nu}$	
					R1	R2	R3	R4	R5	R6	R7		
7-1-1	C ₁₀ H ₈	5:6	-6.5	-62.0	-6.2	27.9	27.9						350.9
7-1-2	C ₁₄ H ₁₀	5:6	-5.4	-68.2	-4.9	27.7	31.7	11.6					267.0
7-1-3	C ₁₈ H ₁₂	8:9	-4.6	-72.7	-4.0	11.5	31.4	31.4	11.5				212.3
7-1-4	C ₂₂ H ₁₄	8:9	-4.1	-77.3	-3.5	11.4	31.3	30.0	16.5	11.8			171.8
7-1-5	C ₂₆ H ₁₆	12:13	-3.8	-81.5	-3.1	11.7	16.4	29.9	29.9	16.4	11.7		144.3
7-1-6	C ₃₀ H ₁₈	12:13	-2.5	-85.8	-2.9	11.7	16.4	29.9	29.9	15.1	16.7	11.8	

*PFDB: position of fusion double bond. $\tilde{\nu}$: p-band UV absorption frequencies (10^2 cm^{-1}) cited from the following two references: (a) Clar, E.; Schoental, R. 1964. *Polyyclic Hydrocarbons*. London and New York: Academic; (b) Clar, E. 1972. *The Aromatic Sextet*. London: Wiley

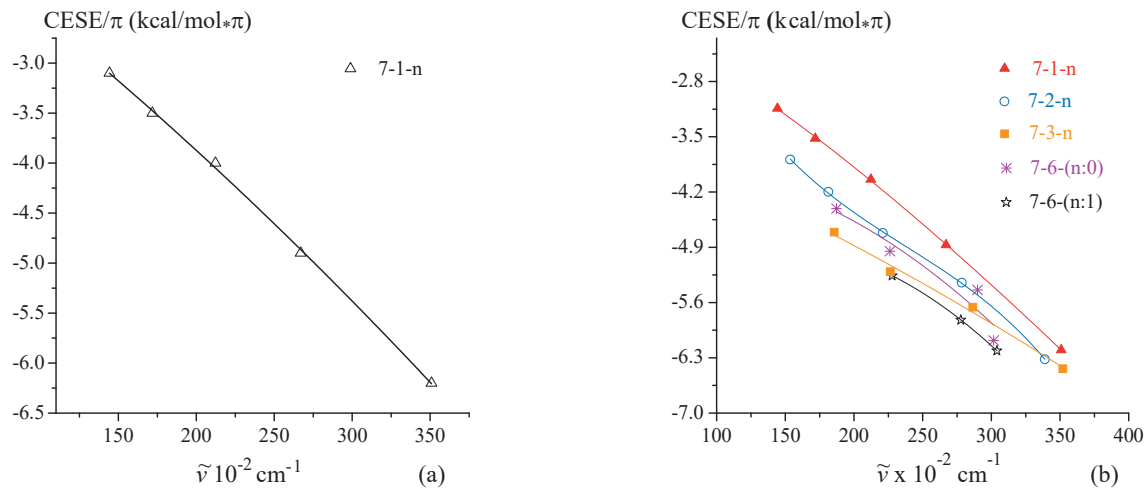


Figure 7-5. (a) For acenes (7-1-n), CESE/π (kcal/mol) can be fitted as a second order polynomial function of p-band UV absorption frequency $\tilde{\nu}$ at B3LYP/6-31G* level. (b) For each series of homologous PBHs, CESE/π is the polynomial function of p band frequency $\tilde{\nu}$ (cm^{-1}) at B3LYP/6-31G*.

then the ESE and CESE are calculated (Table 7-2). As the molecular chain n grows, CESE/π (kcal/mol/π) monotonically decreases, and the size order of CESE/π (absolute values) is as follow:

$$-6.2 \text{ (naphthalene)} > -4.9 \text{ (anthracene)} > -4.0 \text{ (tetracene)} > -3.5 \text{ (pentacene)} > -3.1 \text{ (hexacene)} > 2.9 \text{ (heptacene)}$$

The following two important calculation results should be emphasized and focused:

- (i) CESEs/π of all acenes are smaller than that (6.5 kcal/mol) of benzene.
- (ii) When n > 2, the energy effect ΔE^{A} becomes destabilizing (Table 7-1), which will be further discussed in the next chapter.

In 1971,²³ the correlation between HSRE/ π (Hess and Schaad's resonance energy per π -electron) and the p-band UV (ultraviolet) absorption frequency $\tilde{\nu}$ was first noted by Hess and Schaad. Figure 7-5a shows that for acenes, the CESE/ π (y) can be well fitted as the following second order polynomial function of p-band UV absorption frequency $\tilde{\nu}$ (x) ($cc = 0.9986$):

$$y = -1.32588 - 0.01118x - (7.7859 \cdot 10^{-6})x^2$$

In fact, this second order polynomial function can be approximated as a linear function.

7.2.4. Energy Effect Increments

In order to save time in calculating the ESE of a PBH, an attempt has been made to find the energy effect increments such as bond structure unit and ring structure unit. These increments should be additive, and their values should be approximately independent of a specific molecular structure.

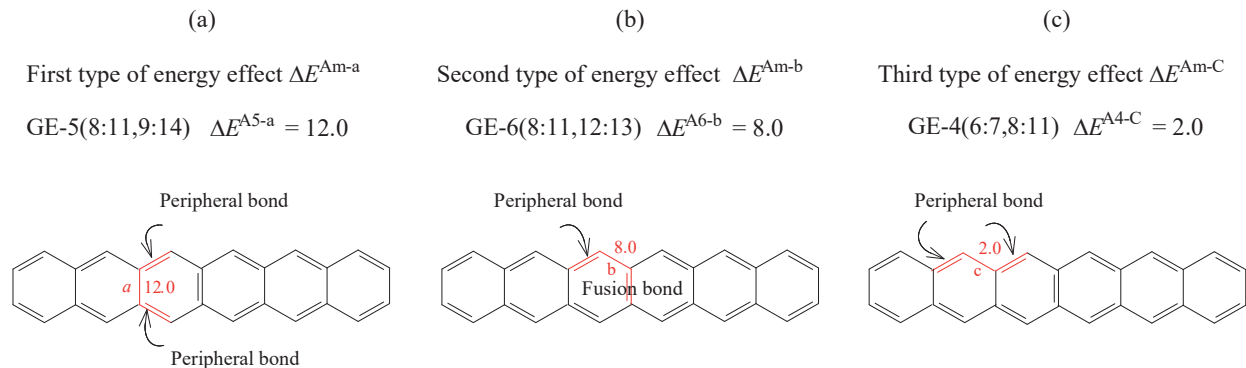


Figure 7-6. Three types of energy effects (kcal/mol) ΔE^{Am-a} , ΔE^{Am-b} , and ΔE^{Am-c} . The numbering system of atoms is shown in Figure 7-4b.

7.2.4.1. Bond Structure Units

ΔE^{Am} is an energy effect associated with the local conjugation interaction between a pair of double bonds in the GL geometry. When two conjugated double bonds are two peripheral bonds belonging to the same benzenoid ring, the corresponding energy effect ΔE^{Am} is grouped to the first type (type A), and it is denoted as ΔE^{Am-a} . In Figure 7-6a, for example, the letter "a" and the value "12.0" are located at the left and right of a red single bond between two red conjugated double bonds, indicating that the corresponding energy effect ΔE^{Am} ($m = 5$) belongs to type A, and its value is 12.0 kcal/mol. In this case, two conjugated double bonds, together with a single bond between them, formed the bond structure unit of the type A (BSUA). According to Figure 7-4, the value of ΔE^{Am-a} is in the range of 8.3 to 12.4 kcal/mol.

When the two conjugated double bonds are, respectively, the peripheral double bond and the fusion double bond, and when these two double bonds belong to the same benzenoid ring (Figure 7-6b), the corresponding energy effect ΔE^{Am} is grouped to the second type (or type B), and it is denoted as ΔE^{Am-b} . In Figure 7-6b, the value "8.0" and the letter "b" are above and below the red single bond between two red conjugated double bonds, indicating that the corresponding energy effect ΔE^{Am} belongs to type B, and its value is 8.0 kcal/mol. In this case, the red lines in Figure 7-6b form a bond structure unit of the type B (BSUB). The value of ΔE^{Am-b} is in the range of 7.7 to 9.2 kcal/mol.

When two conjugated double bonds are two peripheral double bonds belonging, respectively, to two different benzenoid rings fused to each other (Figure 7-6c), the corresponding energy effect ΔE^{Am} is grouped to the third type (or type C), and it is denoted as $\Delta E^{\text{Am-C}}$. In Figure 7-6c, the letter "c" and the value "2.0" indicate that the corresponding energy effect ΔE^{Am} belongs to type C and its value is 2.0 kcal/mol. Thus, the red lines in Figure 7-6c form a bond structure unit of the type C. The value of this type energy effect is in the range of 2.0 to 3.6 kcal/mol.

For the energy effects of the same type, the value of an energy effect also depends upon the position of bond structure unit. Based on the GL geometry of hexacene, as shown in Figure 7-4e, the three energy effects (kcal/mol) of the first type are as follows:

$$\Delta E^{\text{Am-a}}[1:2,3:4] = 8.3, \Delta E^{\text{Am-a}}[6:7,5:10] = 11.0, \Delta E^{\text{Am-a}}[8:11,9:14] = 12.0$$

In the above first BSUA, the two peripheral double bonds are located in the terminal ring R_1 , and the two peripheral double bonds in the last BSUA are located in the middle ring R_3 . In the last structure unit, especially, there is also another double bond in the same benzenoid ring. Therefore, while considering the position of the bond structural unit, the environment of the bonded structural unit should also be considered, which is the concept of the ring structure unit (RSU).

7.2.4.2. Ring Structure Units

As shown in Figure 7-4f, the ring structure unit is a benzenoid ring composed of the red and black lines. The red lines represent a bond structure unit, and the black lines represent the environment. The environment includes the side (peripheral) bonds belonging to other benzenoid rings fused to the ring structure unit.

When a ring structure unit (RSU) contains a first type of bond structure unit, it is referred to as a first type of ring structure unit (RSUA). By analogy, as shown by Figure 7-4g and Figure 7-4h, the second type of ring structure unit (RSUB) and the third type of ring structure unit (RSUC) are defined.

The ring structural units of type A can be divided into two groups, according to whether there is a fused double bond. Thus, as shown by Figure 7-4f, five ring structure units, denoted as RSUA-m, can be divided into two groups. In the first group of RSUA-m ($m = 1, 2$), there is no the fusion double bond in the environmental part. In general, when two ring structures RSUA-m are, respectively, located inside and at the end of the molecular chain, the former's energy effect $\Delta E^{\text{Am-a}}$ is larger than the latter's one $\Delta E^{\text{Am-a}}$. For example, 11.2 kcal/mol (inside RUSA-1) > 8.3 kcal/mol (RUSA-2 at the end), 12.4 kcal/mol (inside RUSA-3) > 9.2 kcal/mol (RSUA-4 at the end). In addition, the energy effect $\Delta E^{\text{Am-a}}$ of the RSUA containing a fusion double bond is greater than that of the RSUA without fusion double bond. For example, 12.4 kcal/mol (RSUA-3 containing a fusion double bond) > 11.2 kcal/mol (RSUA-1 without fusion double bond); 9.2 kcal/mol (RSUA-4 containing a fusion double bond) > 8.3 kcal/mol (RSUA-2 without fusion double bond).

Ring structural units can be grouped more finely and look like Cohen-Benson's group increments, and the establishment of their values may provide a way to simplify the calculation of the extra stabilization energy of PBH.

According to Figure 7-4, the position of a fusion double bond in the candidate $\text{GL}_{m:n}$ geometry does not change the number L_a of BSUAs. For molecule **1-5**, for example, in each of four candidates $\text{GL}_{m:n}$, $L_a = 6$. The size order of the corresponding $\Sigma \Delta E^{\text{Am-a}}$ is as follow:

$$66.1 (\text{GL}_{2:3}) > 63.5 (\text{GL}_{5:6}) > 62.9 (\text{GL}_{8:9}) > 62.6 (\text{GL}_{12:13}) \text{ kcal/mol.}$$

As the double bond moves from the terminal to the molecular center, the value of $\Sigma \Delta E^{\text{Am-a}}$ monotonically decreases. The range of a set of $\Sigma \Delta E^{\text{Am-a}}$ is 3.5 kcal/mol. If the candidate $\text{GL}_{2:3}$ is not considered (it will prove that this candidate geometry should indeed be excluded.), the range of the last three values is 0.9 kcal/mol, indicating that the position of fusion double bond has a slight effect on the value of $\Sigma \Delta E^{\text{Am-a}}$.

Table 7-3-1. For Homologous Series from 7-2-n To 7-5-n, Molecular Energy $E(GL_{m:n})$ (hartree), ESE, CESE, CESE/ π , $\Sigma\Delta E^{Am}$ and $\Sigma\Delta E_n^{Am}$ (kcal/mol), Calculated, on the Basis of a Specific Candidate $GL_{m:n}$, Using Our 2007 Method, at B3LYP/6-31G* Level.

	Molecules	ΔE^A	ESE	CESE	CESE/ π	$\Sigma\Delta E^{Am}$	$\Sigma\Delta E_n^{Am}$	$E(GL_{m:n})$
7-2-n								
7-2-1	C ₁₄ H ₁₀	-11.8	-94.8	-88.4	-6.32	83.0	-6.4	-539.51984
7-2-2	*C ₁₈ H _{12-9:10}	-8.2	-106.3	-96.2	-5.35	98.1	-10.0	-693.16599
7-2-2	C ₁₈ H _{12-12:13}	-7.9	-106.6	-101.7	-5.65	98.7	-5.0	-693.16642
7-2-3	C ₂₂ H _{14-9:10}	-2.0	-115.3	-102.5	-4.66	113.4	-12.9	-846.81229
7-2-3	C ₂₂ H _{14-12:13}	-2.0	-115.5	-103.9	-4.72	113.5	-11.6	-846.81221
7-2-4	C ₂₆ H _{16-9:10}	5.4	-123.4	-107.7	-4.14	128.8	-15.7	-1000.45868
7-2-4	C ₂₆ H _{16-16:17}	5.1	-123.7	-109.2	-4.20	128.8	-14.5	-1000.45818
7-2-5	C ₃₀ H _{18-16:17}	12.8	-131.1	-113.6	-3.79	143.9	-17.4	-1154.10439
7-3-n								
	C ₁₈ H ₁₂	-15.8	-125.7	-115.9	-6.44	109.9	-9.8	-693.15581
7-3-2	C ₂₂ H _{14-7:8}	-12.7	-137.9	-124.5	-5.66	125.2	-13.3	-846.80212
7-3-2	C ₂₂ H _{14-16:17}	-12.5	-139.0	-130.0	-5.91	126.5	-9.0	-846.80246
7-3-3	C ₂₆ H _{16-7:8}	-6.8	-147.2	-131.0	-5.04	140.4	-16.2	-1000.44845
7-3-3	C ₂₆ H _{16-16:17}	-6.9	-148.2	-135.5	-5.21	141.3	-12.7	-1000.44825
7-3-3	C ₂₆ H _{16-20:21}	-6.9	-148.9	-137.1	-5.27	142.0	-11.9	-1000.44823
7-3-4	C ₃₀ H _{18-7:8}	0.5	-155.4	-136.4	-4.55	155.9	-19.0	-1154.09495
7-3-4	C ₃₀ H _{18-16:17}	0.2	-156.3	-140.7	-4.69	156.5	-15.7	-1154.09451
7-3-4	C ₃₀ H _{18-20:21}	-0.2	-156.9	-141.2	-4.71	156.7	-15.6	-1154.09397
7-3-4	C ₃₀ H _{18-24:25}	0.4	-157.0	-142.4	-4.75	157.4	-14.6	-1154.09485
7-4-n, 7-5-n								
7-4-1	C ₁₈ H ₁₂	-13.0	-123.3	-110.6	-6.14	110.2	-12.7	-693.16113
7-4-2	C ₂₆ H ₁₆	-16.1	-181.1	-165.0	-6.34	165.0	-16.1	-1000.44432
7-5-1	C ₂₂ H ₁₄	-14.6	-152.3	-139.4	-6.34	137.7	-12.9	-846.80289
7-5-2	C ₃₀ H ₁₈	-17.6	-210.1	-190.8	-6.36	192.4	-19.2	-1154.08609

*C₁₈H_{12-9:10}, for example, means that, in the candidate $GL_{m:n}$ of molecule 7-2-2, the fusion double bond is localized on the C9-C10 fusion bond.

Table 7-3-2. For Homologous Series From 7-6-(n:n) to 7-7-n, Molecular Energy $E(GL_{m:n})$ (hartree), ESE, CESE, CESE/ π , $\Sigma\Delta E^{am}$ and $\Sigma\Delta E_n^{am}$ (kcal/mol), calculated on Basis of a Specific Candidate $GL_{m:n}$, Using Our 2007 Method, at B3LYP/6-31G* Level.

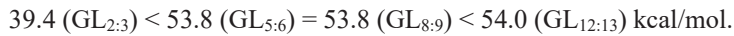
	Molecules	ΔE^A	ESE	CESE	CESE/ π	$\Sigma\Delta E^{Am}$	$\Sigma\Delta E_n^{Am}$	$E(GL_{m:n})$
7-7-n								
7-7-0	C ₂₆ H _{16-7:8}	-15.8	-168.7	-154.3	-5.93	152.9	-14.4	-1000.44428
7-7-0	C ₂₆ H _{16-16:17}	-15.9	-169.5	-157.3	-6.05	153.7	-12.2	-1000.44421
7-7-1	C ₃₀ H ₁₈	-20.3	-201.0	-185.5	-6.18	180.7	-15.5	-1154.08011
7-8-n								
7-8-0	C ₂₆ H _{16-7:8}	-10.1	-150.2	-133.2	-5.12	140.1	-17.0	-1000.44817
7-8-1	C ₃₀ H _{18-7:8}	-7.8	-164.6	-146.3	-4.88	156.8	-18.3	-1154.09391
7-8-1	C ₃₀ H _{18-12:13}	-6.2	-198.5	-195.2	-6.51	192.3	-3.4	-1154.09642
7-6-(n:n')								
	C ₁₆ H ₁₀	-8.4	-99.2	-91.7	-5.73	90.8	-7.6	-615.75973
7-6-(n:0)								
1:0	C ₂₀ H _{12-12:13,6:7}	-13.0	-131.4	-121.7	-6.08	118.4	-9.7	-769.39639
2:0	C ₂₄ H _{14-4:5,6:7}	-9.6	-142.6	-124.8	-5.20	133.0	-17.8	-923.04323
2:0	C ₂₄ H _{14-4:5,18:19}	-9.2	-143.3	-129.9	-5.41	134.1	-13.3	-923.04389
2:0	C ₂₄ H _{14-5:13,6:7}	-9.8	-143.6	-130.6	-5.44	133.8	-13.1	-923.04280
2:0	C ₂₄ H _{14-5:13,18:19}	-9.2	-164.7	-154.7	-6.45	155.5	-10.0	-923.04376
3:0	C ₂₈ H _{16-5:13,6:7}	-3.9	-153.0	-138.7	-4.95	149.1	-14.4	-1076.68918
4:0	C ₃₂ H _{18-5:13,6:7}	3.3	-161.2	-142.6	-4.46	164.6	-18.7	-1230.33571
4:0	C ₃₂ H _{18-5:13,22:23}	3.0	-182.9	-165.9	-5.18	185.9	-17.0	-1230.33519
4:0	C ₃₂ H _{18-4:5,22:23}	3.2	-161.1	-141.2	-4.41	164.3	-19.9	-1230.33546
4:0	C ₃₂ H _{18-4:5,26:27}	3.7	-161.3	-142.4	-4.45	165.0	-18.9	-1230.33633
7-6-(n:1)								
1:1	C ₂₄ H ₁₄	-16.7	-162.1	-149.1	-6.21	145.4	-13.0	-923.03282
2:1	C ₂₈ H _{16-5:13,18:19}	-13.5	-175.2	-162.9	-5.82	161.7	-12.3	-1076.67917
3:1	C₃₂H_{18-4:5,18:19}	-7.9	-184.4	-168.4	-5.26	176.5	-16.0	-1230.32493
7-6-(2:2)								
	C ₃₂ H ₁₈	-10.4	-186.3	-166.1	-5.19	175.9	-20.1	-1230.32532

Table 7-4. For 7 Homologous Series, ESE/π, CESE and CESE/π, and Ring Contributions RC_k Made By the *k*-th (*k* = 1,..., 7) Benzenoid Ring to CESE at B3LYP/6-31G* Level.

Molecules	*PFDB	ESE/π	CESE	CESE/π	RC _k (kcal/mol)						v × 10 ⁻² cm ⁻¹	
		Kcal/mol	R ₁	R ₂	R ₃	R ₄	R ₅	R ₆	R ₇			
series 7-2-n N _{db} = 2												
7-2-1	C ₁₄ H ₁₀	5:6, 9:10	-6.8	-88.4	-6.3	27.8	27.5	27.8				339.0
7-2-2	C ₁₈ H ₁₂	5:6, 9:10	-5.9	-96.2	-5.4	27.6	27.4	31.5	11.6			278.5
7-2-3	C ₂₂ H ₁₄	5:6, 12:13	-5.3	-103.9	-4.7	27.7	11.4	31.5	31.4	11.5		221.0
7-2-4	C ₂₆ H ₁₆	5:6, 16:17	-4.8	-109.2	-4.2	27.8	11.6	16.7	30.1	31.3	11.4	181.5
7-2-5	C ₃₀ H ₁₈	5:6, 16:17	-4.4	-113.6	-3.8	27.8	11.5	16.6	30.0	29.9	16.4	11.7
series 7-3-n N _{db} = 3												
7-3-1	C ₁₈ H ₁₂	5:6, 9:10, 7:8	-7.0	-115.9	-6.4	27.6	27.6	27.0	27.6			352.1
7-3-2	C ₂₂ H ₁₄	5:6, 9:10, 7:8	-6.3	-124.5	-5.7	27.6	27.6	26.9	31.5	11.6		286.5
7-3-3	C ₂₆ H ₁₆	5:6, 9:10, 20:21	-5.7	-137.1	-5.3	27.7	27.7	11.6	17.0	30.4	27.6	226.5
7-3-4	C ₃₀ H ₁₈	5:6, 9:10, 20:21	-5.2	-141.2	-4.7	27.7	27.7	11.5	16.9	30.2	31.3	11.4
N _{db} for molecules 7-4-1, 7-5-1, 7-4-2 and 7-5-2 are 3, 4, 5 and 6, respectively												
7-4-1	C ₁₈ H ₁₂		-6.9	-113.6	-6.3	27.7	27.4	27.4	27.7			313.5
7-5-1	C ₂₂ H ₁₄	Every fusion bond is double bond	-6.9	-139.4	-6.3	27.8	27.4	27.3	27.4	27.8		304.0
7-4-2	C ₂₆ H ₁₆		-7.0	-165.0	-6.3	27.7	27.4	27.3	27.3	27.4	27.7	295.9
7-5-2	C ₃₀ H ₁₈		-7.0	-190.8	-6.4	27.7	27.4	27.3	27.4	27.3	27.4	27.7
N _{db} for molecules 7-7-0 and 7-7-1 are 4 and 5, respectively												
7-7-0	C ₂₆ H ₁₆	5:6, 9:10, 16:17, 19:20	-6.5	-157.3	-6.1	27.7	27.7	11.5	31.8	27.4	27.6	289.9
7-7-1	C ₃₀ H ₁₈	5:6, 9:10, 16:17, 19:20, 21:22	-6.7	-185.5	-6.2	27.5	27.5	27.0	31.8	11.5	27.7	299.9
N _{db} = 3 and 4												
7-8-0	C ₂₆ H ₁₆	5:6, 7:8, 9:10	-5.8	-133.2	-5.1	26.8	27.5	31.4	31.4	11.5	11.5	295.0
7-8-1	C ₃₀ H ₁₈	5:6, 7:8, 9:10	-5.5	-146.3	-4.9	27.0	31.6	31.6	31.6	11.6	11.6	294.1
7-9	C ₃₀ H ₁₈	5:6, 16:17, 23:24	-5.2	-140.7	-4.7	27.8	11.6	16.7	30.1	31.5	11.3	27.7
7-10	C ₃₀ H ₁₈	5:6, 9:10, 20:21, 23:24	-6.0	-165.3	-5.51	27.8	27.2	11.6	17.0	302.	27.2	27.6
7-11	C ₃₀ H ₁₈	5:6, 16:17, 25:26	-5.2	-140.7	-4.7	27.8	11.6	16.7	30.1	31.5	11.3	27.7

* The positions of the fusion double bonds (PFDB). In molecule **2-1**, for example, “5:6,9:10” means that the fusion double bonds are localized on the C(5)-C(6) and C(9)-C(10) bonds. All *p*-band UV absorption frequencies are cited from (a) Clar, E.; Schoental, R. 1964. *Polycyclic Hydrocarbons*. London and New York: Academic; (b) Clar, E. 1972. *The Aromatic Sextet*. London: Wiley

The numbers, L_b and L_c , of BSUBs and BSUCs depend upon the position of a fusion double bond, but the total number ($L_b + L_c$) is a constant. In the candidate $GL_{2:3}$ of molecule **1-5**, for example, $L_b = 2$, $L_c = 10$, and in each of other three candidates $GL_{m:n}$, $L_b = 4$ and $L_c = 8$. As a result, the size order of ($\Sigma\Delta E^{Am-b} + \Sigma\Delta E^{Am-c}$) is as follow:

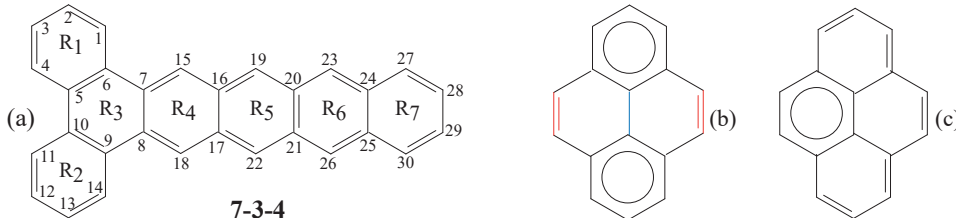


The range of the above four values is 14.6 kcal / mol and is 73 times the range (0.2 kcal / mol) of the last three values. When the $GL_{2:3}$ geometry is excluded from the candidate, the position of fusion double bond has a slight effect on the value of ($\Sigma\Delta E^{Am-b} + \Sigma\Delta E^{Am-c}$).

A fine analysis of ring structure effects further confirms that a fusion double bond should be reasonably located in order to ensure that the positions of the long and short peripheral bonds in the GL geometry should be the same as their positions in the ground state geometry as far as possible.

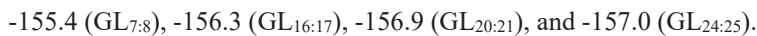
7.3. POSITION RULE AND ENERGY RULE

In the case of acenes such as hexacene, as mentioned above, the value of the sum $\Sigma\Delta E^{Am-a}$, as well as the value of ($\Sigma\Delta E^{Am-b} + \Sigma\Delta E^{Am-c}$), is almost constant when the $GL_{2:3}$ geometry is excluded from the candidate, which further proves the reliability of the position rule.



Scheme 7-3

PBHs, such as **7-2-n**, **7-3-n**, **7-7-n** and **7-8-n**, can be viewed as the benzoacenes. For example, molecule **7-3-2** is named dibenzanthracene. In each of PBHs **7-4-n** and **7-5-n**, all the fusion bonds are double bonds. For each of these six series of PBHs, therefore, the GL geometry can be reasonably determined by the position rule. Then, based on the GL geometry and its candidates $GL_{m:n}$, the ESE and CESE, denoted as $ESE(GL_{m:n})$ and $CESE(GL_{m:n})$, are calculated at B3LYP/6-31G* level, and their values are listed in Table 7-3-1 and Table 7-3-2. An inspection of these two Tables shows the following a general phenomenon: for every PBH, the particular candidate $GL_{k:l}$ has the highest molecular energy of all the candidates $GL_{m:n}$ for the GL geometry, which further confirm the energy rule. It is especially worth noting that for every PBH (**7-2-n**, **7-3n**, and **7-7-n**), the values of $ESE(GL_{m:n})$ are almost equal to each other, where $ESE(GL_{m:n})$ is the ESE calculated based on the $GL_{m:n}$ candidate. For PBH **7-3-4**, for example, its particular GL geometry is the candidate $GL_{20:21}$, and the values of $ESE(GL_{m:n})$ are as follows:



The range of the four values is -1.6 kcal/mol. However, the effect of the position of fusion double bond on the CESE value is larger than on the ESE value. For PBH **7-3-4** (Scheme 7-3a), for example, the values of CESE are as follows:



The range of the four values is -6.0 kcal/mol, but the range of the last three values is -1.7 kcal/mol. For these PBHs, the position rule is still useful to accurately evaluate the CESE of a PBHs. When determining reasonable GL geometry, the judgment conclusions of the position rule and energy rule are consistent. For the homologous series **7-2-n**, **7-3-n**, **7-4-n**, **7-5-n**, **7-7-n**, and **7-8-n** together with three individual molecules **7-9**, **7-10** and **7-11**, their reasonable GL geometries are determined using these two rules, and their ESEs and CESEs, together with the p-band UV absorption frequencies, are listed in Table 7-4. It should be emphasized that CESEs/ π of all PBHs involved in this Chapter are less than the CESE/ π (6.5 kcal/mol) for benzene.

Figure 7-5b shows that, for each of the three homologous series **7-1-n**, **7-2-n**, and **7-3-n**, CESE/ π can be well fitted as a linear (or second order polynomial) function of p-band UV absorption frequency $\tilde{\nu}$, and their correlation coefficients are 0.9995, 0.9993, 0.9769, respectively.

7.4. DIBENZOACENES

In this Chapter, molecules **7-6-(n:0)** (Figure 7-1) is specially referred to as dibenzoacenes, and they include benzo[e]pyrene (**7-6-(1:0)**), naphtho[2,3-e]pyrene (**7-6(2:0)**), dibenzo[de,uv]pentacene (**7-6-(3:0)**), and dibenzo[de,yz]hexacene (**7-6-(4:0)**).

According to the definition of Clar structure, the structure that has the largest number of Clar sextets (aromatic π -sextets) is the Clar structure.²⁴ For pyrene, accordingly, the structure in Scheme 7-3b is a Clar structure, and the red and blue bonds should be, respectively, double bond and single bond in the Kekulé valence structure of pyrene. Then, for each of two Clar sextets in pyrene, the double bonds positions need to be determined. That is, for the GL geometry of molecule **7-6(2:0)** (Figure 7-7), for example, in each of the following two pairs of adjacent fusion bonds: C(11)-C(12) and C(12)-C(13) bonds, and C(14)-C(15) and C(15)-C(16) bonds, which one is double bond needs to be determined.

7.4.1. Naphtho[2,3-e]pyrene

According to the definition of Clar structure, the rings R2 and R3 should be Clar sextet. In the GL geometry of naphtho[2,3-e]pyrene (Figure 7-7), therefore, the C(1)-C(2) and C(12)-C(15) bonds must be, respectively, double bond and single bond. Based on the calculation of partial Pauling bond orders and according to the definition of the most important Kekulé valence structure, the C(21)-C(22) and C(23)-C(24) bonds should be double bond.

In the ground state geometry of naphtho[2,3-e]pyrene (**7-6(2:0)**, Figure 7-7a), the bond length differences, ($r_{2-11} - r_{1-2}$), between two bonds C(2)-C(11) and C(1)-C(2) is 0.077 Å, and the difference, ($r_{18-21} - r_{21-22}$), between two bonds C(18)-C(21) and C(21)-C(22) is 0.051 Å, where, for example, r_{2-11} is the distance of the C(2)-C(11) bond. These two differences are so large that the double bonds in the benzenoid rings R1 and R6 can only be located at the C(1)-C(2) bond and at C(21)-C(22) and C(23)-C(24) bonds according to the position rule. Once these three double bond positions are determined, it is impossible for the C(12)-C(15) fusion bond (the brown color bond in Figure 7-7b) to be double bond, due to the following facts: the distances, $r_{6-13} = r_{7-16} = 1.472$ Å, of the C(6)-C(13) and C(7)-C(16) bonds are the longest of all the CC bonds in the pyrene group. Otherwise, as shown by Figure 7-7b, will lead to the following unreasonable results:

- (i) Two longest bonds, C(6)-C(13) and C(7)-C(16), must be two double bonds.
- (ii) In this Kekulé valence structure, there is only one Clar sextet (R_4) in the pyrene group.

Therefore, as shown by Figure 7-7, the molecule **7-6-(2:0)** can only have the following four candidates for the GL geometry: $GL_{11:12,6:7}$ and $GL_{12:13,6:7}$, $GL_{11:12,18:19}$ and $GL_{12:13,18:19}$, where, for example, the subscript " $_{11:12,6:7}$ " in the symbol " $GL_{11:12,6:7}$ " means that three fusion double bonds are localized on the C(11)-C(12), C(14)-C(15) and

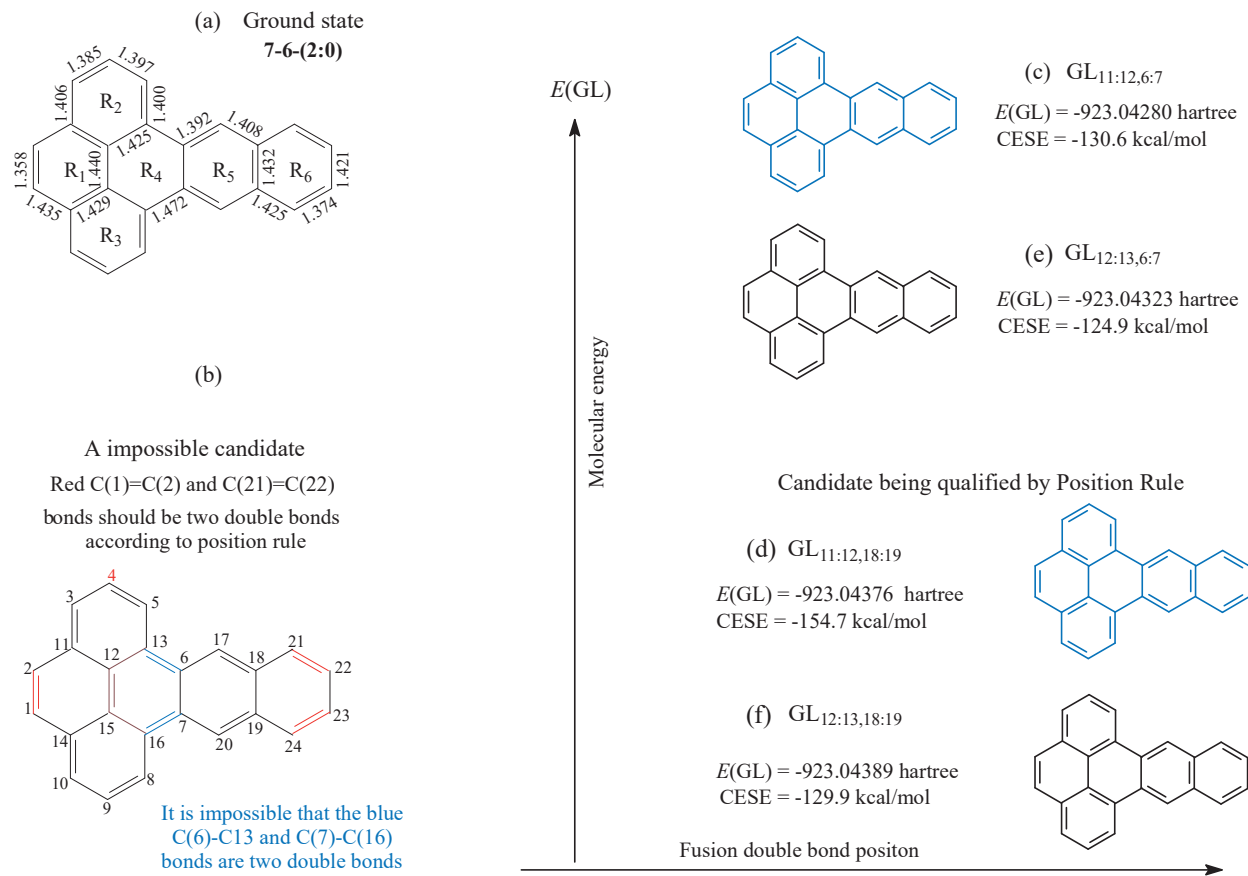


Figure 7-7. The four candidates for GL geometry of naphtho[2,3-e]pyrene (**7-6-(2:0)**) at B3LYP/6-31G* level. The numbering of the atoms is different from the standard nomenclature.

C(6)-C(7) bonds. Based on the four candidates, the values (kcal/mol) of CESE(GL_{m:n,k:l}) for molecule **7-6-(2:0)** are as follows:

-130.6 (GL_{11:12,6:7}), -124.9 (GL_{12:13,6:7}), -154.7 (GL_{11:12,18:19}), -129.9 (GL_{12:13,18:19}).

The range of the above four CESE values is large, up to -29.8 kcal/mol. Therefore, it is necessary to choose a reasonable GL geometry from the candidates.

7.4.1.1. Conflict between Position Rule and Energy Rule

Due to two rings, R₂ and R₃, being symmetric, the positions of the double bonds in the ring R₃ should be symmetrical with the positions of corresponding double bonds in the ring R₁. According to the positions of the fusion double bonds in pyrene group, these four candidates can be divided into two groups, which are represented respectively with blue structures and black structures (Figure 7-7).

At the ground state, $(r_{11-12} - r_{12-13}) = (1.429 - 1.425) = 0.004$ and $(r_{4-5} - r_{3-4}) = (1.397 - 1.385) = 0.012 \text{ \AA}$ (R₁), and $(r_{17-18} - r_{6-17}) = (1.401 - 1.392) = 0.009 \text{ \AA}$ (R₅). According to the position rule, the candidate GL_{11:12,18:19} can be considered as the reasonable GL geometry. But the molecular energies (hartree) for four candidates is as follows: -923.04280 (GL_{11:12,6:7}), -923.04323 (GL_{12:13,6:7}), -923.04376 (GL_{11:12,18:19}), and -923.04389 (GL_{12:13,18:19}). Among the

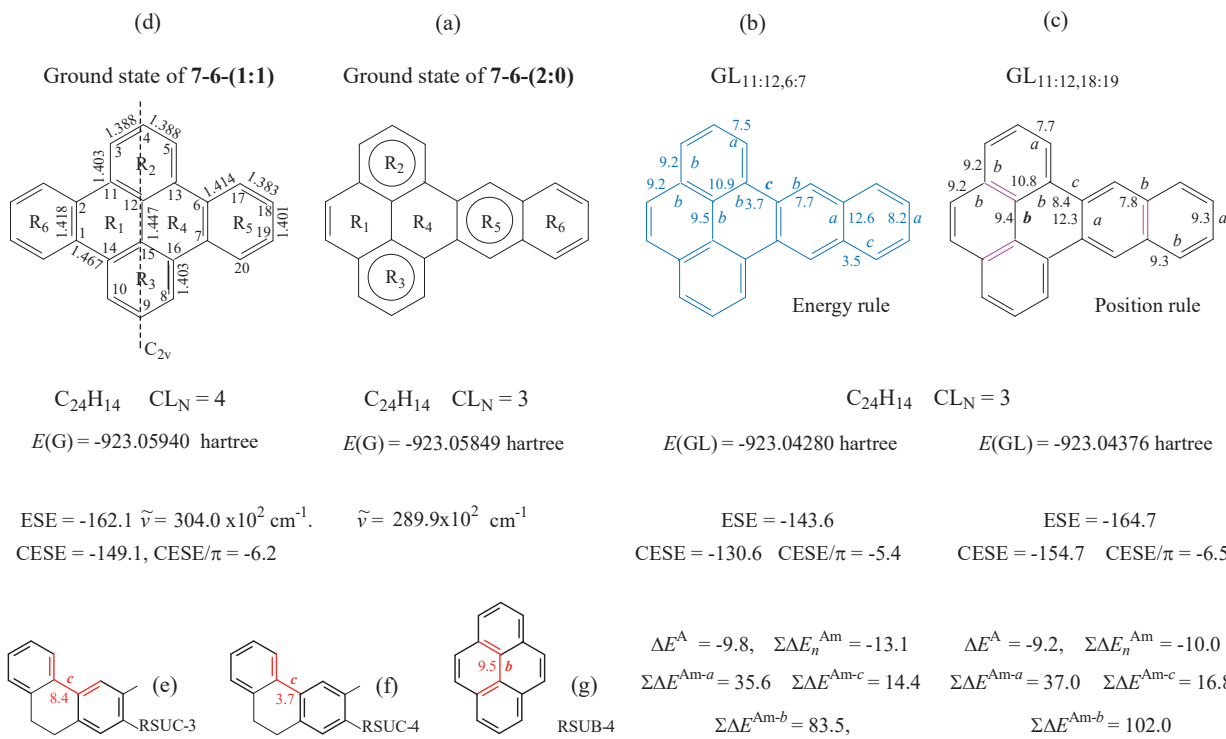


Figure 7-8. The position rule and energy rule conflict with each other. (a) and (d) Are the ground states of molecules 7-6-(2:0) and 7-6-(1:1), and the numbering systems of atoms. (b) and (c) Are two qualified candidates for the GL geometry of molecule 7-6-(2:0). (e), (f) and (g) Are three ring structure units related to the pyrene group. Here, CL_N is the number of Clar's sextets. The units of all energies, except for that of the molecular energy, are in kcal/mol at B3LYP/6-31G* level.

four candidates, the candidate GL_{11:12,18:19} accords with position rule, but it's molecular energy is not the highest. It is candidate GL_{11:12,6:7} that the molecular energy is the highest. So, in the case of molecule 7-6-(2:0), the position rule and energy rule conflict with each other.

According to the position rule and energy rule, the candidates GL_{11:12,k:1} ($k:1 = 6:7, 18:19$), are two main qualified candidates (two blue structures) for the GL geometry (Figure 7-7 and Figure 7-8). There is no difference, in the structure of pyrene group, between the two candidates. Due to the difference, in the position of third fusion double bond, between the two qualified candidates, the difference between CESE(GL_{11:12,18:19}) and CESE(GL_{11:12,6:7}) is large, up to 24.1 kcal/mol.

Based on the two main qualified candidates, as shown by Figure 7-8b and Figure 7-8c, $\Sigma \Delta E^{Am-a}$ are 35.6 (GL_{11:12,6:7}) kcal/mol and 37 (GL_{11:12,18:19}) kcal/mol, and $\Sigma \Delta E^{Am-c}$ are 14.4 (GL_{11:12,18:19}) kcal/mol and 16.8 (GL_{11:12,6:7}) kcal/mol. There is no large difference between each of the two pair values. The difference, in the structure, between the two candidates lies in the position of the C(k)=C(l) fusion double bond, leading to that the numbers of bond structure units of type B are 9 (GL_{11:12,6:7}) and 11 (GL_{11:12,18:19}), respectively. The corresponding $\Sigma \Delta E^{Am-b}$ are, respectively, 83.5 and 102.0 kcal/mol. The difference between them is big, up to 19.5 kcal/mol, and it is about 3/4 times of the corresponding CESE difference (24.1 kcal/mol).

7.4.1.2. CESE/ π and UV Absorption Frequency

In order to provide a reasonable GL geometry for molecule 7-6-(2:0), a reliable method is to use the quantitative relationship between CESE/ π and p-band UV absorption frequency $\tilde{\nu}$. Four series of structural

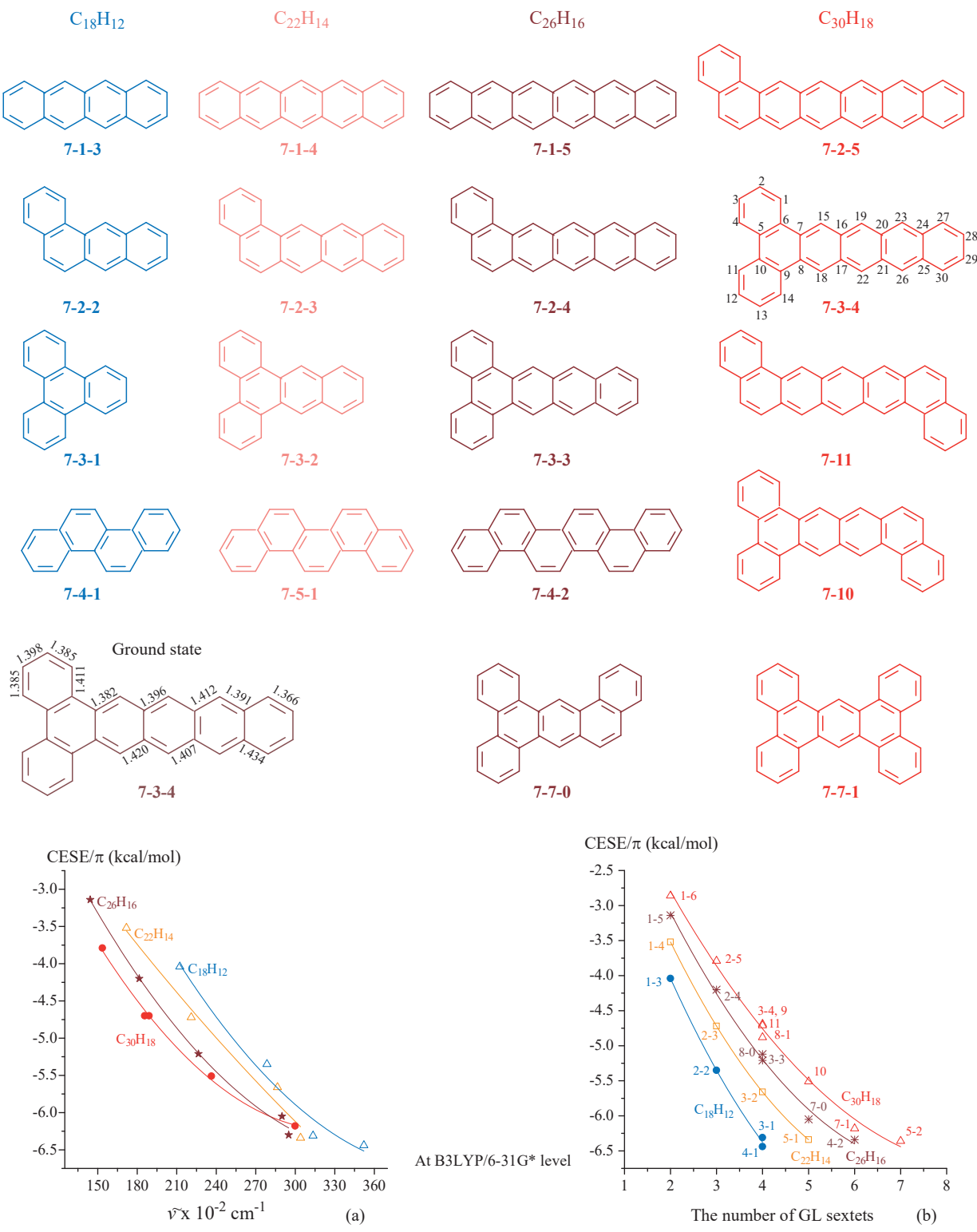


Figure 7-9. CESE/ π can be fitted as a second order polynomial function of (a) *p*-band UV absorption frequency $\tilde{\nu}$ (cm^{-1}). (b) The number of G sextets for each of the following four series of structural isomers: $C_{18}H_{12}$, $C_{22}H_{14}$, $C_{26}H_{16}$ and $C_{30}H_{18}$.

Table 7-5. For Pyrene series, Molecular Energy $E(GL)$ (hartree) of GL Geometry, ESE/ π , CESE and CESE/ π (kcal/mol) at B3LYP/6-31G*, the Number N_{GL} of GL Sextets in the GL Geometry, and p-band UV Absorption Frequencies $\tilde{\nu}$ (cm⁻¹).

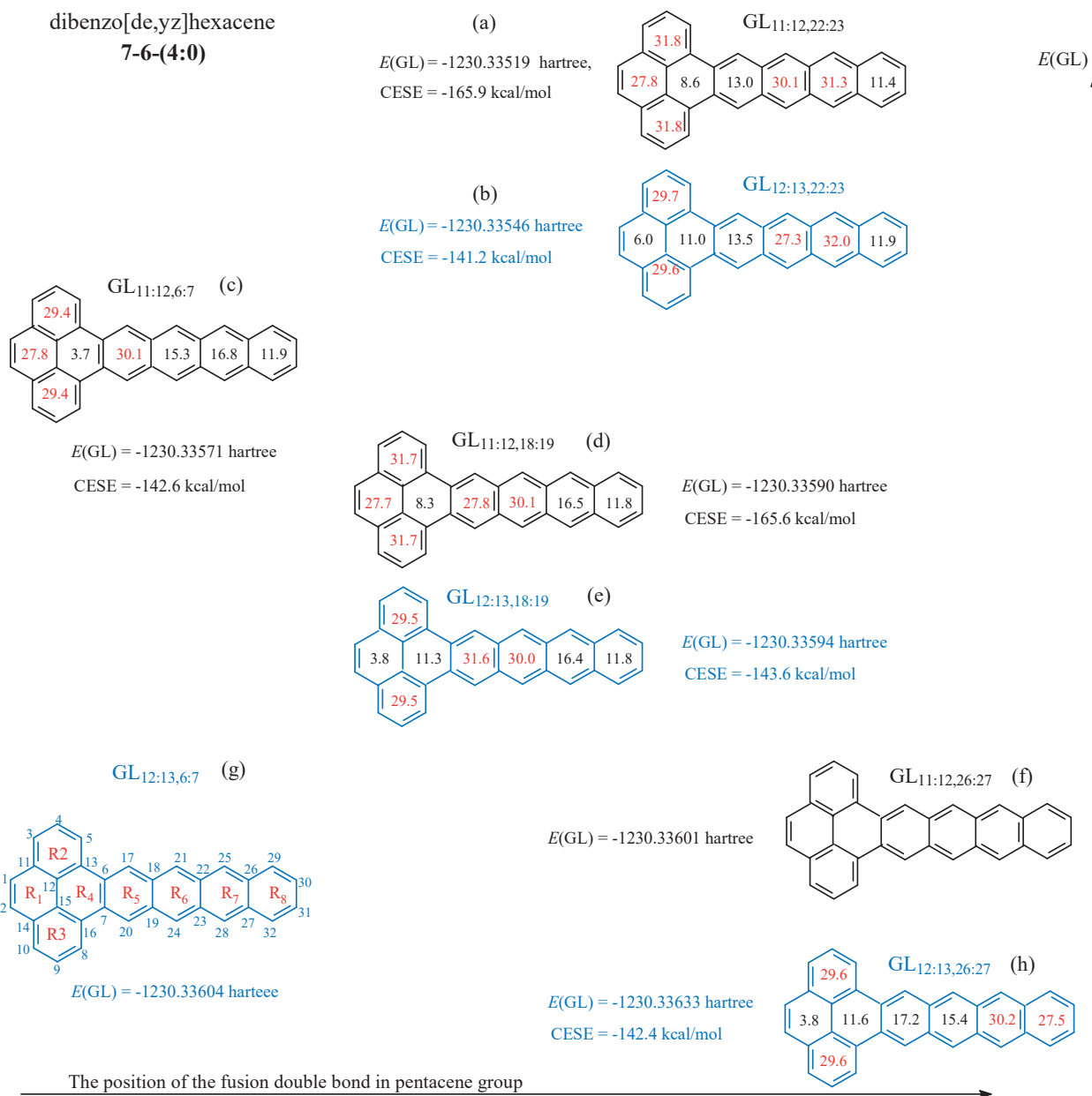
Molecules	PFDB	$E(GL)$	N_{GL}	ΔE^A	ESE/ π	CESE	CESE/ π	$\tilde{\nu} \times 10^{-2}$
n	C ₁₆ H ₁₀ (pyrene)	11:12, 14:15	-615.75973	3	-8.4	-6.2	-91.7	-5.7
7-6-(n:0)								
1	C ₂₀ H ₁₂	11:12, 14:15, 6:7	-769.39639	4	-13.0	-6.6	-120.0	-6.0
2	C ₂₄ H ₁₄	11:12, 14:15, 6:7	-923.04280	4	-9.8	-6.0	-130.6	-5.4
3	C ₂₈ H ₁₆	12:13, 15:16, 18:19	-1076.68968	4	-3.6	-5.5	-135.4	-4.8
4	C ₃₂ H ₁₈	12:13, 15:16, 22:23	-1230.33546	4	3.2	-5.1	-141.2	-4.4
7-6-(n:1)								
1	C ₂₄ H ₁₄	1:2, 11:12, 14:15, 6:7	-923.03282	5	-16.7	-6.8	-149.1	-6.2
2	C ₂₈ H ₁₆	1:2, 12:13, 15:16, 18:19	-1076.67917	5	-13.5	-6.3	-162.9	-5.8
3	C ₃₂ H ₁₈	1:2, 12:13, 15:16, 18:19	-1230.32493	5	-7.9	-5.8	-168.4	-5.3
7-6-(2:2)								
2	C ₃₂ H ₁₈	1:2, 11:12, 14:15, 6:7	-1230.32532	5	-10.4	-5.8	-166.1	-5.2

All *p*-band UV absorption frequencies are cited from (a) Clar, E.; Schoental, R. 1964. *Polycyclic Hydrocarbons*. London and New York: Academic; (b) Clar, E. 1972. *The Aromatic Sextet*. London: Wiley

isomers are presented in Figure 7-9, their molecular formulas are as follows: C₁₈H₁₂, C₂₂H₁₄, C₂₆H₁₆ and C₃₀H₁₈. The corresponding UV absorption frequencies $\tilde{\nu}$ are listed in Table 7-2 and Table 7-4. For each of four series of structural isomers, as shown by the curve lines in Figure 7-9a, CESE/ π can be well fitted as a second order polynomial function of *p*-band UV absorption frequency $\tilde{\nu}$, and their correlation coefficients are 0.976, 0.982, 0.996, and 0.997, respectively. In each series of structural isomers with the same molecular formula and different structures, therefore, the higher the UV absorption frequency $\tilde{\nu}$, the larger the absolute value of corresponding CESE/ π is. For example, the structural isomers with C₃₀H₁₈ formula include molecules **7-2-5**, **7-3-4**, **7-11**, **7-10**, and **7-7-1**, their molecular structures are completely different from each other, but their CESE/ π (y) can be well fitted as the following second polynomial function of *p*-band UV absorption frequency $\tilde{\nu}$ (x) (red curve line in Figure 7-9a):

$$y = 2.23631 - 0.05148x + (7.82336 \times 10^{-5})x^2 \quad (\text{cc} = 0.994)$$

Molecule **7-6-(1:1)** (dibenzo[e,l]pyrene, Figure 7-8d) is a structural isomer of molecule **7-6-(2:0)**, and it has D_{2h} symmetry. Therefore, its GL_{11:12,6:7} geometry is only one candidate for GL geometry. The value of its CESE/ π can be determined without any doubt, and is -6.2 kcal/mol (Table 7-5). The UV absorption frequency (304.0 $\times 10^2$ cm⁻¹) of molecule **7-6-(1:1)** is higher than that (289.9 $\times 10^2$ cm⁻¹) of its isomer **7-6-(2:0)**. Therefore, CESE/ π for **7-6-(1:1)** should be larger in absolute value than for **7-6-(2:0)**. According to Figure 7-8, CESE/ π for molecule **7-6-(2:0)** has two possible values. One value is -5.4 kcal/mol (GL_{11:12,6:7}), and it is less than that (-6.2 kcal/mol) for **7-6-(1:1)**; the other is -6.5 kcal/mol (GL_{11:12,18:19}), and it is larger than that of **7-6-(1:1)**. For molecule **7-6-(2:0)**, therefore, the



Scheme 7-4

GL_{11:12,6:7} candidate should be considered to be a reasonable GL geometry, and the corresponding CESE should be -130.6 kcal/mol. In the case of this molecule, the position rule should obey the energy rule.

A comparison of Figure 7-8b and Figure 7-8c shows an important difference in the structure between two candidates GL_{11:12,6:7} and GL_{11:12,18:19} of molecule **7-6-(2:0)**. In GL_{11:12,18:19}, $N_{db} = 3$, $N_{GL} = 5$, and $N_{GL} = N_{db} + 2$, where N_{GL} is the number of the Kekulé benzenoid rings with three double bonds, and N_{db} is the number of fusion double bonds. But in both two GL geometries (the GL_{11:12,6:7} of **7-6-(2:0)** and the only GL geometry of **7-6-(1:1)**), $N_{db} = 3$ and $N_{GL} = 4$, leading to the discovery of an important relationship (will be called GL sextet rule), namely $N_{GL} = (N_{db} + 1)$. In particular, it is worth mentioning that as the evidence of the rule, among the four candidates of **7-6-(2:0)** (Figure 7-7), the structures of the three candidates (GL_{11:12,6:7}, GL_{12:13,6:7} and GL_{12:13,18:19}) conform to the $N_{GL} = N_{db} + 1$

rule, and the corresponding CESE values (-130.6, -124.9, and -129.9 kcal/mol) are close to each other.

7.4.2. GL Sextet Rule

As mentioned above, the position rule should obey the energy rule when the position rule and energy rule conflict. However, the exception to energy rule has also been found in molecule **7-6-(4:0)**.

7.4.2.1. Dibenzo[hi,uv]hexacene

For molecule **7-6-(4:0)** (dibenzo[de,yz]hexacene), there is no doubt that the C(1)-C(2), C(29)-C(30) and C(31)-C(32) bonds are double bond for the same reasons as for molecule **7-6(2:0)**. According to that, for the two fused bonds, C(11)-C(12) and C(12)-C(13), in the ring R2, either of the two can be selected as a double bond, the eight candidates for the GL geometry can be divided into the following two groups: $GL_{11:12,k:l}$ (black structures) and $GL_{12:13,k:l}$ (blue structures) (Scheme 7-4), where k:l is the position of the fusion double bond in tetracene group and it can be any of the following four positions: C(6)-C(7), C(18)-C(19), C(22)-C(23), and C(26)-C(27).

In Scheme 7-4, the eight candidates are arranged from top to bottom in the order of molecular energy from high to low, and four pairs of candidates are arranged from left to right according to the position of the fusion double bond in the tetracene group. Of the eight candidates, the molecular energy (-1230.33519 hartree) of $GL_{11:12,22:23}$ is the highest. According to the energy rule, it can be considered a reasonable GL geometry. The corresponding $CESE(GL_{11:12,22:23}) = -165.9$ kcal/mol, and it is greater by -24.7 kcal/mol than the $CESE(G_{12:13,22:23})$. It is important to note that, from the candidate $GL_{12:13,22:23}$ having the second highest molecular energy to the candidate $GL_{12:13,26,27}$ with the lowest molecular energy, all CESEs presented in Scheme 7-4, except for the $CESE(GL_{11:12,18:19})$, are in the range of 141.2 to 143.6 kcal/mol. Therefore, the rationality that the $CESE(GL_{11:12,22:23})$ (165.9 kcal/mol) is regarded as the CESE of molecule **7-6-(4:0)** requires strict argument.

Two candidate $GL_{11:12,22:23}$ and $GL_{12:13,22:23}$ for the GL geometry can be considered as two preliminary qualified candidates (Figure 7-10) based on the following three facts (Scheme 7-4):

- (i) $CESE(GL_{12:13,22:23})$ (-141.2 kcal/mol) is almost equal to the CESEs calculated based on other three candidates $GL_{11:12,6:7}$ (black), $GL_{12:13,18:19}$ (blue) and $GL_{12:13,26,27}$ (blue).
- (ii) Molecular energy of the candidate $GL_{12:13,22:23}$ is the second highest.
- (iii) First candidate $GL_{11:12,22:23}$ conforms to the position rule (Figure 7-10b) and energy rule.

Molecule **7-6-(2:2)** (dibenzo(hi,uv)hexacene) (Figure 7-10a), as well as its Clar structures, has D_{2h} symmetry. Based on the calculation of partial Pauling bond orders and according to the position rule, the C(21)-C(22) and C(23)-C(24) bonds should be double bond, which determines that there are two pairs of the following Kekulé valence structures with C_{2v} symmetry (Figure 7-10e): $GL_{k:l,6:7}$ (black), and $GL_{k:l,18:19}$ (blue), where k:l = 11:12, and 12:13). In each pair of the candidates $GL_{k:l,m:n}$, two candidate geometries (k:l = 11:12, and 12:13) are equivalent due to that these two candidates are mirror images of each other. In the case of molecule **7-6-(2:2)**, therefore, the difference in the structure between the candidates depends on the position of the fusion double bond C(m)=C(n). In this case, it had to be considered necessary that $N_{GL} = N_{db} + 1$, so the C(6)-C(7) and C(1)-C(2) bonds in the GL geometry of **7-6-(2:2)** must be double bond. For molecule **7-6-(2:2)**, the GL is unique, and the corresponding CESE is -166.1 kcal/mol.

For molecule **7-6-(4:0)**, as a structural isomer of molecule **7-6-(2:2)**, the CESE values corresponding to its two qualified candidates are -165.9 (k:l = 11:12) and -141.2 (k:l = 12:13) kcal/mol. The p-band UV absorption frequencies of two structural isomers are 187.3×10^2 (**7-6-(4:0)**) and 292.4×10^2 cm^{-1} (**7-6-(2:2)**). According to Figure 7-9a, the first qualified candidate $GL_{11:12,22:23}$ of molecule **7-6-(4:0)** is not a reasonable GL geometry because the corresponding CESE (-165.9) and CESE/ π (-5.2 kcal/mol) are almost equal to those (-166.1 and -5.2 kcal/mol of

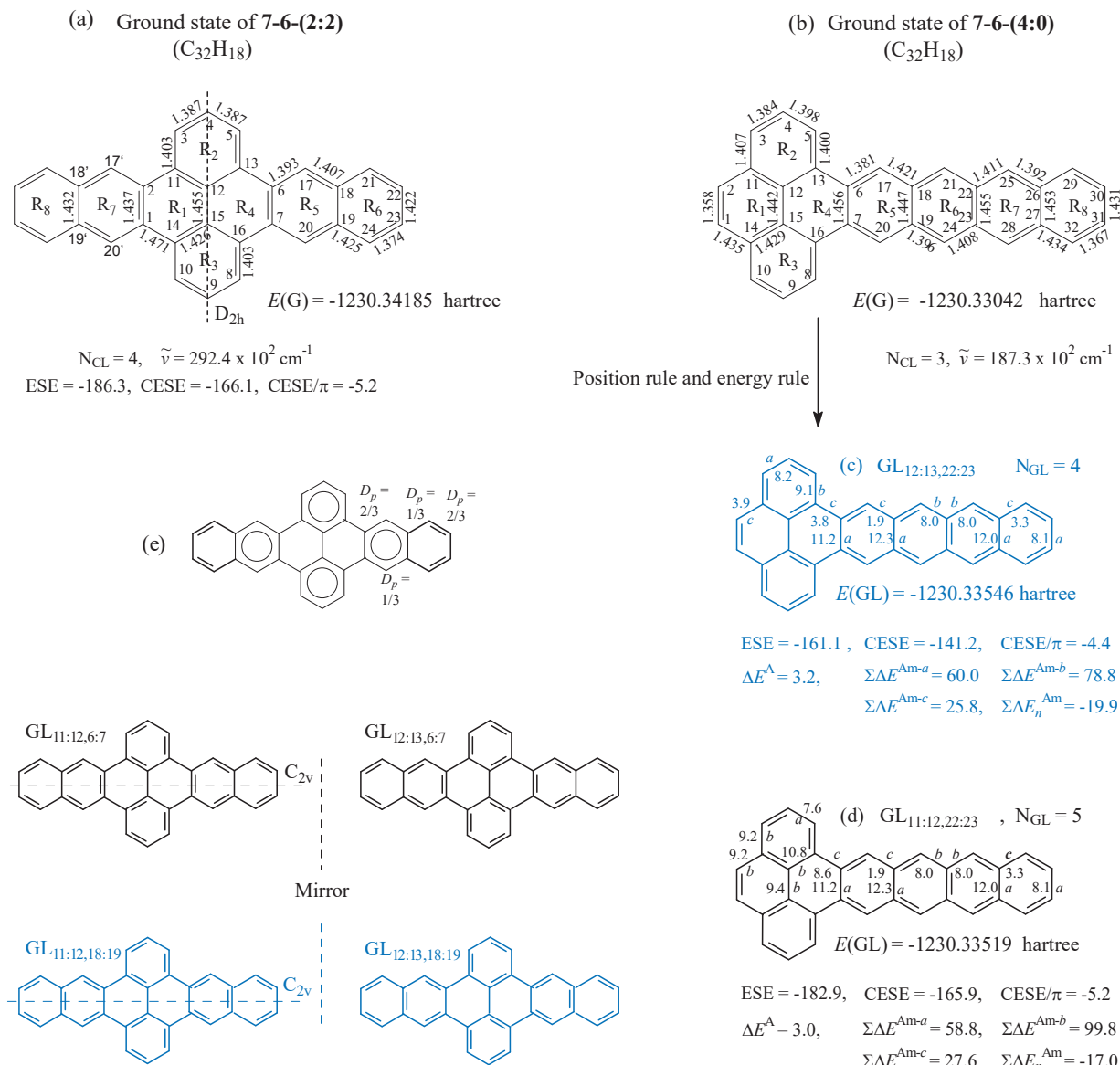


Figure 7-10. GL sextet rule. (a) and (b) are the ground states of two structural isomers 7-6-(2:2) and 7-6-(4:0), and the numbering systems of the atoms. (c) and (d) are the candidates for the GL geometries of molecule 7-6-(4:0), and the energy differences ΔE^{Am-a} , ΔE^{Am-b} , and ΔE^{Am-c} . Here, N_{CL} is the number of Clar's sextets, N_{GL} is the number of GL sextets. The units of all energies, except for that of the molecular energy, are kcal/mol.

the isomer 7-6-(2:2). For the molecule 7-6-(4:0), therefore, the second qualified candidate, GL_{12:13,22:23} geometry, should be a reasonable GL geometry because the corresponding CESE and CESE/ π (141.2 and 4.4 kcal/mol) are less in absolute value than those of its structural isomers 7-6-(2:2).

7.4.2.2. Definition of GL Sextet

According to the definitions of the energy effects ΔE^{Am-a} , ΔE^{Am-b} , and ΔE^{Am-c} , the energy effect sum $\Sigma \Delta E^{Am}$ can

be decomposed into the contribution, RC_k or RC_{k+1} , of each benzenoid ring. The symbol " RC_k " is the contribution of k -th ring to $\Sigma\Delta E^{\text{Am}}$. The k -th ring and $(k+1)$ -th ring are two benzenoid ring fused to each other, the contributions of these two rings are calculated, respectively, by Equations (7-1) and Equation (7-2):

$$\begin{aligned} RC_k = & \Delta E^{\text{Am-a}}(u:v,s:t) + \Delta E^{\text{Am-b}}(u:v,y:z) + \Delta E^{\text{Am-b}}(s:t,y:z) + \\ & + 1/2[\Delta E^{\text{Am-c}}(u:v,w:x) + \Delta E^{\text{Am-c}}(s:t,g:h)] \end{aligned} \quad (7-1)$$

$$\begin{aligned} RC_{k+1} = & \Delta E^{\text{Am-a}}(w:x,g:h) + \Delta E^{\text{Am-b}}(w:x,y:z) + \Delta E^{\text{Am-b}}(g:h,y:z) + \\ & + 1/2[\Delta E^{\text{Am-c}}(u:v,w:x) + \Delta E^{\text{Am-c}}(s:t,g:h)] \end{aligned} \quad (7-2)$$

In the two Equations, the C(y)-C(z) bond, such as the C(12)=C(13), C(15)=C(16) and C(22)=C(23) bonds in Figure 7-10c, is the fusion double bond; the C(u)-C(v) and C(s)-C(t) bonds, such as the C(6)=C(17) and C(7)=C(20) bonds, are two peripheral double bonds belonging to the same ring; the C(u)=C(v) and C(w)=C(x) bonds, such as C(6)=C(17) and C(18)=C(21), are two peripheral double bonds belonging to two benzenoid rings fused to each other.

In Table 7-2 and Table 7-4, the contribution of each ring to $\Sigma\Delta E^{\text{Am}}$ is calculated on the basis of the reasonable GL geometry. For molecule 7-1-5, for example, its candidate $GL_{12:13}$ (Figure 7-4e) has been considered as a reasonable GL geometry. Thus, the following contributions (kcal/mol) can be calculated:

$$\begin{aligned} RC_3 &= \Delta E^{\text{Am-a}}(8:11,9:14) + 2\Delta E^{\text{Am-b}}(8:11,12:13) + 1/2[2\Delta E^{\text{Am-c}}(6:7,8:11)] = 12.0 + 2*8.0 + 2.0 = 30.0 \\ RC_1 &= \Delta E^{\text{Am-a}}(1:2,3:4) + 1/2[2\Delta E^{\text{Am-c}}(1:2,6:7)] = 8.3 + 3.5 = 11.8. \end{aligned}$$

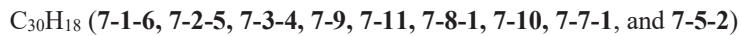
As shown by the data listed in Table 7-2, in any candidate $GL_{m:n}$, when a ring R_k has three double bonds, its RC_k is always larger than 27 kcal/mol. These three double bonds include the fusion double bond shared by two benzenoid ring fused to each other. This type of benzenoid ring is called the particular benzenoid ring. In Figure 7-4c, for example, benzenoids R_1 and R_2 are the two particular benzenoid ring. In each of these two rings, there are three double bonds, and the C(5)=C(6) is shared by the two particular rings R_1 and R_2 . In the GL geometry of molecule 7-3-4 (Figure 7-9), for example, three fusion double bonds are localized on the C(5)-C(6), C(9)-C(10) and C(20)-C(21) bonds, and four particular benzenoid rings and their contributions RC_k (kcal/mol) are as follows:

$$R_1 (RC_1 = 27.7), R_2 (RC_2 = 27.7), R_5 (RC_5 = 30.2), R_6 (RC_6 = 31.3).$$

In this chapter, the π -electronic framework of a particular benzenoid ring is defined as the GL sextet. The definition of GL sextet is different from the definition of Clar's sextet. In the GL geometry of molecule 7-4-2 (Figure 7-9 and Table 7-4), for example, the number, N_{CL} , of Clar's sextets is 3, but the number of GL sextets is 6. Every benzenoid ring in the GL geometry of molecule 7-4-2 is GL sextet ring. In a reasonable GL geometry of a PBH, must $N_{GL} = (N_{db} + 1)$, which is called the GL sextet rule.

As shown by the curve lines in Figure 7-9b, the CESE/ π can be well fitted as a second order polynomial function of N_{GL} (correlation coefficients of 0.998 ($C_{18}H_{12}$), 1.0 ($C_{22}H_{14}$), 0.995 ($C_{26}H_{16}$) and 0.994 ($C_{30}H_{18}$)) for each of the following four series of structural isomers (In Figure 7-9b, for example, molecule "7-1-3" is shortened into "1-3"):

- $C_{18}H_{12}$ (7-1-3, 7-2-2, 7-4-1 and 7-3-1)
- $C_{22}H_{14}$ (7-1-4, 7-2-3, 7-3-2, and 7-5-1)
- $C_{26}H_{16}$ (7-1-5, 7-2-4, 7-8-0, 7-3-3, 7-7-0, and 7-4-2)



For a structural isomer series with molecular formula $\text{C}_{30}\text{H}_{18}$, for example, B3LYP/6-31G* value of CESE/ π can be well fitted as the following second order polynomial function of N_{GL} :

$$\text{CESE}/\pi = -0.17098 - 1.48181 * N_{\text{GL}} + 0.08374 * (N_{\text{GL}})^2 \quad (\text{CC} = 0.992).$$

7.4.2.3. GL Sextet Rule Being Sufficient and Necessary

For molecule **7-6-(4:0)**, as shown in Figure 7-10 and Scheme 7-4, there are three fusion double bonds in any candidate for the GL geometry, but the numbers, N_{GL} , of GL sextets are different for the different candidates. For example, in the candidate $\text{GL}_{11:12,22:23}$ (Figure 7-10d), three fusion double bonds are localized, respectively, on the C(11)–C(12), C(14)–C(15) and C(22)–C(23) bonds. As a result, the number of its GL sextets is five, and the five GL sextets correspond to the R_1 , R_2 , R_3 , R_6 and R_7 rings, which does not accord with the GL sextet rule. Although the candidate $\text{GL}_{11:12,22:23}$ conform to the position rule and energy rule, as having been described, it still can't be chosen as the reasonable GL geometry. For the second qualified candidate $\text{GL}_{12:13,22:23}$, on the contrary, it has four GL sextets, respectively, corresponding to the R_2 and R_3 , R_6 and R_7 rings, which conforms to the GL sextet rule. So, it can be chosen as the reasonable GL geometry. In this case, the CESE and CESE/π of molecular **7-6-(4:0)** are respectively 141.2 and 4.4 kcal/mol, and their absolute values are less than the CESE and (CESE/π) (166.1 and 5.2 kcal/mol) of its structural isomers **7-6-(2:2)**.

Scheme 7-4 shows a very important phenomenon: regardless of whether a candidate meets the position rule and energy rule, as long as it complies with the GL sextet rule, the corresponding CESE and CESE/π are in reasonable range, otherwise the values of the CESE and CESE/π are unreasonable. For the four candidates, including three blue candidates ($\text{GL}_{12:13,22:23}$, $\text{GL}_{12:13,18:19}$ and $\text{GL}_{12:13,26:27}$) and a black candidate ($\text{GL}_{11:12,6:7}$), example, the positions of their fusion double bonds meet $N_{\text{GL}}+1$ rule (GL sextet rule), but their following structure differences should be emphasized:

- (i) Molecular energy of candidate $\text{GL}_{12:13,26:27}$ is the lowest.
- (ii) For the four candidates, the positions of the two fusion double bonds in the pyrene group are different. In the candidates $\text{GL}_{11:12,6:7}$, C(11)=C(12) and C(14)=C(15) are double bonds, but in the other three candidates, the C(12)=C(13) C(15)=C(16) are double bonds.
- (iii) In the three blue candidates, the fusion double bonds in the pyrene group are in the same positions, but the position of the fusion double bond in the tetracene group is different from each other.

Interestingly, the range of the four CESE values is only -2.4 kcal/mol, and the CESE/π values (-4.5 kcal/mol), calculated on the above last three candidates, are almost equal to that (-4.4 kcal/mol) calculated on the reasonable GL geometry ($\text{GL}_{12:13,22:23}$).

An inspection of Table 7-3-1 and Table 7-3-2 confirms that the GL sextet rule are universal and are the sufficient and necessary conditions for judging reasonable GL geometry. For molecule **7-3-4**, for example, its candidates for the GL geometry are as follows: $\text{GL}_{7:8}$, $\text{GL}_{16:17}$, $\text{GL}_{20:21}$ and $\text{GL}_{24:25}$. In each of the four candidates, there are three fusion double bonds and four GL sextets, indicating that these four candidates are compliant with the GL sextet rule. As the results, the values (kcal/mol) of CESEs, calculated based on these four candidates, are close to each other, and the range of a series of the following values is -6.0 kcal/mol

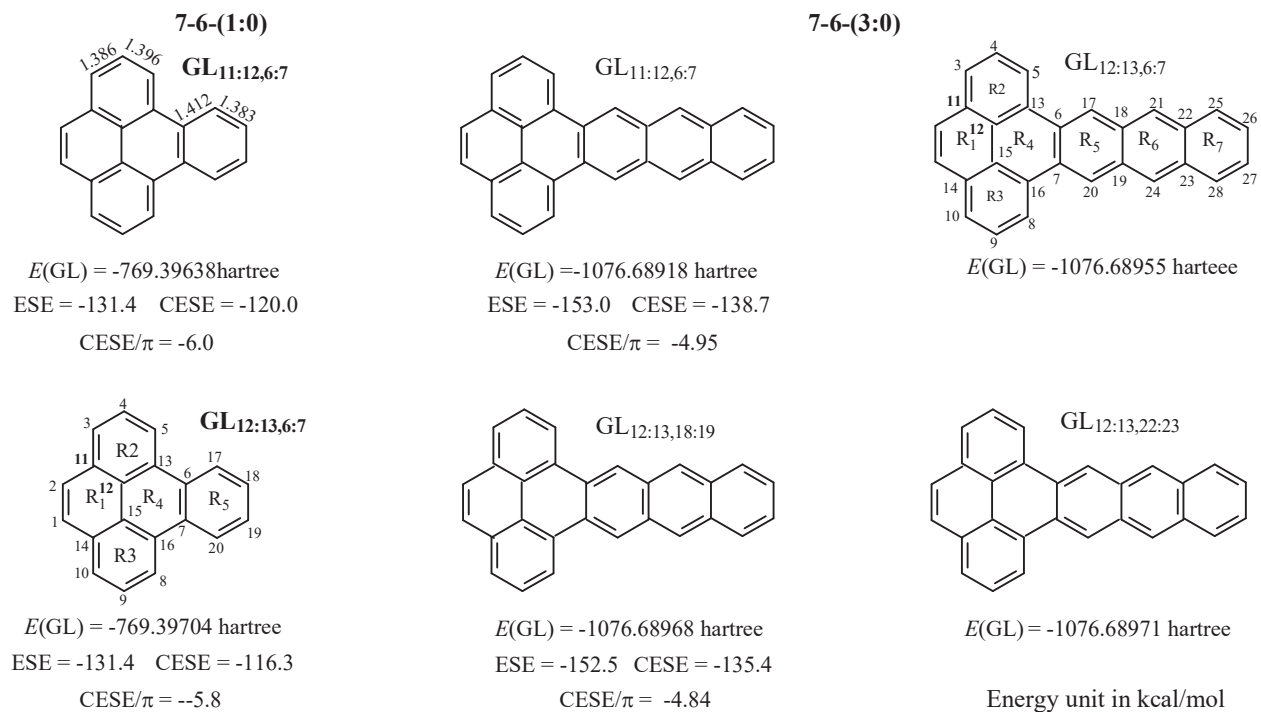


Afterwards, the positional rules and energy rules can help the GL sextet rule to select the most reasonable geometry

from the above four candidates. In the case of molecule **7-3-4**, the candidate GL_{20:21} is the most reasonable GL geometry due to the following facts:

- (i) The alternating order of the peripheral double bond and single bond in the candidate GL_{20:21} is the same as that of the shorter and longer bonds in the ground state geometry (Figure 7-9).
- (ii) The molecule energy (-1154.09397 hartree) of the candidate GL_{20:21} is the highest of the following four molecular energies: -1154.09495 (GL_{7:8}), -1154.09451 (GL_{16:17}), -1154.09397 (GL_{20:21}) and -1154.09485 (GL_{24:25}).

7.4.2.4. Benzo[e]pyrene and Dibenzo[de,uv]pentacene



Scheme 7-5

After establishing the GL sextet rule, for the other two molecules in the series of molecules **7-6-(n:0)** ($n = 1, 2, 3, 4$), the rationality of choosing their GL geometry can be verified.

According to the GL sextet rule, as shown by Scheme 7-5, molecule **7-6-(1:0)** may have two candidates for the GL geometry. The values of ESE, calculated on the two candidate geometries, are the same, and the difference between the two corresponding values of CESE is about -3.7 kcal / mol. Therefore, the position of two fusion double bonds in the pyrene group has a slight effect on the value of CESE, as long as the GL sextet rule is met. Considering the positional rules and energy rules, it is more reasonable for candidate GL_{11:12,6:7} to be chosen as GL geometry.

Dibenzo[de,uv]pentacene, denoted as **7-6-(3:0)**, is the third molecule of the homologues series **7-6-(n:0)**. In line with the positions of three fusion double bonds, molecule **7-6-(3:0)** has three pairs of candidates for the GL geometry, and the molecular energies (hartree) of these candidates are as following:

$$\begin{aligned} &-1076.68918 (\text{GL}_{11:12,6:7}) > -1076.68942 (\text{GL}_{11:12,22:23}) > -1076.68955 (\text{GL}_{11:13,6:7}) > -1076.68961 (\text{GL}_{11:12,18:19}) > \\ &-1076.68968 (\text{GL}_{12:13,18:19}) > -1076.68972 (\text{GL}_{12:13,22:23}) \end{aligned}$$

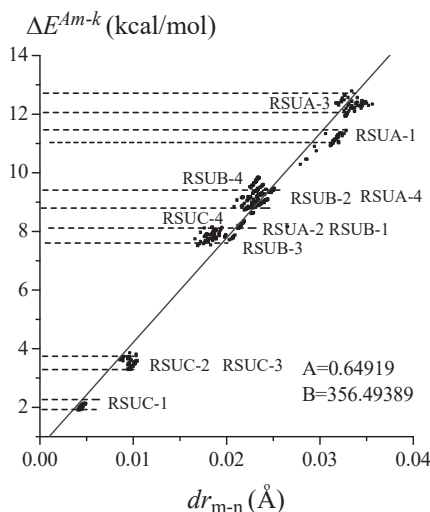


Figure 7-11. Energy effects ΔE^{Am} are fitted as a linear function of the difference, in the distance r_{m-n} of the single bond C(v)-C(s), between the GE-m and GL geometries ($cc = 0.985$). The total number of ring structure units is 621, and these ring structure units are obtained from 58 candidates for the GL geometries of 35 PBHs.

In accordance with the GL sextet rule, as shown by Scheme 7-5, only four $GL_{m:n,kl}$ are the possible candidates for the GL geometry. But according to the energy rule and position rule, the $GL_{11:12,6:7}$ (energy rule) and $GL_{12:13,18:19}$ (position rule) are two qualified candidates, and the corresponding values (-150.0 and -152.5 kcal/mol) of ESE are almost equal to each other. And the difference between CESE($GL_{11:12,6:7}$) and CESE($GL_{12:13,18:19}$) is -3.3 kcal/mol.

To determine which of the two candidates $GL_{11:12,6:7}$ and $GL_{12:13,18:19}$, is the most reasonable, one possible approach might be to use the correlation coefficient between CESE/ π and UV absorption frequency $\tilde{\nu}$ (Figure 7-5b). The actual fittings show that the candidate $GL_{12:13,18:19}$ seems the most reasonable and the corresponding the CESE should be -135.4 kcal/mol.

7.5. CONCLUSIONS

For a PBH, a specific fusion double bond can be localized at multiple positions. Therefore, a PBH can have multiple candidates for the GL geometry. In order to accurately evaluate the ESE by using the restricted geometry optimization (our 2007 method), the position rule, energy rule and GL sextet rule have been suggested. For the GL geometry of PBH, the qualified candidate refers to a type of Kekulé valence structure that conforms to the GL sextet rule. The values of the CESE corresponding to the qualified candidate geometries are always close to each other. The GL sextet rule is sufficient and necessary for determining GL geometry. The position rule and energy rule must obey the GL sextet rule, and can help the GL sextet rule to choose the most reasonable GL geometry from the qualified candidates.

For all of PBHs, their CESEs/ π are less in absolute value than the ESE/ π (6.5 kcal/mol) of benzene. Our 2007 method does be more complex than the literature methods, and more time-consuming. But our 2007 method provides a way to understand the nature of aromaticity, and it also provide a new theory method for reasonably evaluating the aromatic stabilization energy of the PBHs of various types. In particular, this method is purely theoretical and does not require the help of any empirical parameters.

The energy effects, from 630 structural units, can be fitted as a linear function of the distance, in the distance of the single bond, between the GE-m and GL geometries (Figure 7-11). For each type of ring structure units, the

difference between the maximum value and minimum value in a series of energy effects is in the range of 0.5 to 1.0 kcal/mol. Therefore, it is possible that the average value of the energy effects of each type is used as an empirical value (an increment) to simplify the time-consuming calculations (i.e., the restricted geometry optimization).

For each of the four homologous series (**7-1-n**, **7-2-n**, **7-3-n**, and **7-6-(n:0)**), CESE/ π can be fitted as a linear function of the p band UV absorption frequency $\tilde{\nu}$. For each of the four series of structural isomers with molecular formulas of C₁₈H₁₂, C₂₂H₁₄, C₂₆H₁₆, and C₃₀H₁₈, CESE/ π can also be fitted as a second-order polynomial function of the p band frequency $\tilde{\nu}$, and as the function of the number of GL sextets.

It should be emphasized once again that the CESEs/ π for all PBHs are less in the absolute value than that (-6.5 kcal/mol) of benzene and all the energy effects ΔE^{Am} are destabilizing.

7.6. REFERENCES

- 1 Randić, M. 2003. "Aromaticity of Polycyclic Conjugated Hydrocarbons." *Chem. Rev.*, 103: 3449–3605.
- 2 Kistiakowskjy, G. B.; Ruhoff, J. R.; Smith, H. A.; Vaughan, W. E. 1936. "Heats of Organic Reactions. IV. Hydrogenation of Some Dienes and of Benzene." *J. Am. Chem. Soc.*, 58: 146-153.
- 3 Cyrański, M. K. 2005. "Energetic Aspects of Cyclic Pi-Electron Delocalization: Evaluation of the Methods of Estimating Aromatic Stabilization Energies." *Chem. Rev.*, 105: 3773-3811.
- 4 Cohen, N.; Benson', S. W. 1993. "Estimation of Heats of Formation of Organic Compounds by Additivity Methods." *Chem. Rev.*, 93: 2419-2438.
- 5 George, P.; Trachtman, M.; Bock, C. W.; Brett, A. M. 1976. "Momodesnotic Reactions for the Assessment of Stabilization Energies in Benzenoid and Other Conjugated Cyclic Hydrocarbons." *J. Chem. Soc., Perkin Trans. 2*: 1222-1227.
- 6 Pauling, L.; Sherman, J. 1933. "The Nature of the Chemical Bond. VI. The Calculation from Thermochemical Data of the Energy of Resonance of Molecules among Several Electronic Structures." *J. Chem. Phys.*, 1: 606-617.
- 7 Cox, J. D.; Pilcher, G. 1970. *Thermochemistry of Organic and Organometallic Compounds*. London U. K.: Academic.
- 8 Benson, S. W. 1976. *Thermochemical Kinetics*, 2nd ed. New York: Wiley
- 9 Schleyer, P. v. R.; Manoharan, M.; Jiao, H.; Stahl, F. 2001. "The Acenes: Is there a Relationship between Aromatic Stabilization and Reactivity?" *Org. Lett.*, 3: 3643-3646.
- 10 Clar, E. 1964. *Polycyclic Hydrocarbons*, Vols 1, 2. London: Academic Press.
- 11 Aihara, J. I. 1999. "Reduced HOMO–LUMO Gap as an Index of Kinetic Stability for Polycyclic Aromatic Hydrocarbons." *J. Phys. Chem. A*, 103: 7487-7495.
- 12 George, P. 1975. "Critique of the Resonance Energy Concept with Particular Reference to Nitrogen Heterocycles, Especially Porphyrins." *Chem. Rev.*, 75: 85-111.
- 13 Kollmar, H. 1979. "Direct Calculation of Resonance Energies of Conjugated Hydrocarbons with ab Initio MO Methods." *J. Am. Chem. Soc.* 101: 4832-4840.
- 14 Kitaura, K.; Morokuma, K. 1976. "A New Energy Decomposition Scheme for Molecular Interactions within the Hartree-Fock Approximation." *Inter. J. Quantum. Chem.*, 10: 325-340.
- 15 Behrens, S.; Köster, A. M.; Jug, K. 1994. "Delocalization Energy of .pi. Electrons as an Index for Aromaticity of Polycyclic Hydrocarbons Sabine." *J. Org. Chem.*, 59: 2546-2551.
- 16 Bao, P.; Yu, Z. H. 2010. "Restricted Geometry Optimization for Estimating Stabilization Energies of Polycyclic Aromatic Hydrocarbons." *J. Phys. Org. Chem.*, 23: 16–29.
- 17 Randić, M.; Plavšić, D. 2011. "Algebraic Clar Formulas – Numerical Representation of Clar Structural Formula." *Acta Chim. Slov.*, 58: 448–457.

- 18 Granovsky, A. A. Available at: <http://classic.chem.msu.su/gran/gamess/index.html>, Accessed 30 July 2009.
- 19 Schmidt, M. W.; Baldridge, K. K.; Boatz, J. A.; Elbert, S. T.; Gordon, M. S.; Jensen, J. H.; Koseki, S.; Matsunaga, N.; Nguyen, K. A.; Su, S.; Windus, T. L.; Dupuis, M.; Montgomery, J. A. 1993. "General Atomic and Molecular Electronic Structure System." *J. Comput. Chem.*, 14, 1347-1363.
- 20 Fries, K. 1927. "Über Bicyclische Verbindungen und ihren Vergleich mit dem Naphtalin. III. Mitteilung." *Justus Liebigs Ann. Chem.*, 454: 121-324.
- 21 Fries, K.; Walter, R.; Schilling, K. 1935. "Über tricyclische Verbindungen, in denen Naphtalin mit einem Heterocyclus anelliert ist." *Justus Liebigs Ann. Chem.*, 516: 248-285.
- 22 <http://www.chem.qmul.ac.uk/iupac/fusedring/intro.html>.
- 23 Hess, B. A.; Schaad, L. J. 1971. "Hueckel Molecular Orbital .pi. Resonance Energies. New Approach." *J. Am. Chem. Soc.*, 93: 305-310.
- 24 Solà, M. 2013. "Forty Years of Clar's Aromatic π -sextet Rule." *Front. Chem.*, 1: 1-8.

CHAPTER 8

NEW METHOD TO LOCALIZE π -ELECTRONS

ABSTRACT

As an improved version of our 2007 method, our 2011 method can ensure that in the localized geometry such as GL and GE-m, the MO exchange and charge transfer interactions and the two-electron exchange interactions are excluded from between the localized groups (double bonds). As shown by comparison of our 2011 method with Morokuma energy decomposition method and by comparing the calculation results obtained from the five versions of our 2011 method, the source code of modified PC-Gamess, that is, the source code of our 2011 method, is reliable. Due to additional deletion of the particular two-electron exchange integrals, our 2011 method satisfies two basic criteria for judging the rationality of the method of calculating electronic delocalization energy: the electron delocalization energy of cyclobutadiene must be destabilizing, and that of aromatic molecule such as benzene must be stabilizing. For benzene, the range of a set of the ESE (extra stabilization energy) values, obtained from our 2011 method, is -5.3 kcal/mol. For cyclobutadiene, the ranges of the values of the vertical delocalization energy (VDE) and adiabatic delocalization energy (ADE) are 12.0 and 19.3 kcal/mol. The corresponding ranges, obtained from our 2007 method, are -24.4 (ESE), 149.1 (VDE) and 316 (ADE) kcal/mol. The influences of theoretical level and basis set size on the 2011 values of electron delocalization energies are much smaller than on the 2007 values. In particular, the ESE of benzene and the ADE of cyclobutadiene, calculated by our 2011 method at B3LYP/6-31G*, are -36.3 and 53.6 kcal/mol. These two values are almost equal to the corresponding experimental values (-36 and 55 kcal/mol). From the pure correlation functional to the pure exchange functional, the size order of the 6-31G* values of the benzene's ESE (kcal/mol) is as follow: -36.8 (LYP, pure correlation) > -36.3 (B3LYP, hybrid) > -34.5 (BLYP, exchange and correlation) > -32.9 (XPBE96, pure exchange). When the pure correlation density functionals (such as LYP) with the Hartree-Fock exchange is used, the basis set size and theoretical level have the smallest effects on the ESE (and CESE), VDE and ADE, indicating that the DFT type of exchange interaction also has an obvious influence on the structure and molecular energy of localized geometry. Due to that the BLW method can only exclude the MO charge transfer interaction energy from between the localized double bonds through the way to maximize the MO exchange interaction between the double bonds, the VDE (-10.9 kcal/mol) and ADE (-10.3 kcal/ml) of cyclobutadiene, calculated by the BLW method, are stabilizing, indicating the fundamental flaw of the BLW method. Only in the case of allyl cation in which there is no longer the π MO exchange interaction and spatial exchange interaction between the groups $\text{CH}_2=\text{CH}-$ and H_2C^+ , the two ADE values, calculated by our 2011 method and BLW method, are the same. Therefore, the BLW method is only a special case of our 2011 method.

yuzh@iccas.ac.cn

Key words: extra stabilization energy; Benzene; two-electron exchange integrals; vertical delocalization energy; Hartree-Fock exchange; our 2014 method.

8.0. FOREWORDS

“vertical resonance” and “adiabatic resonance energy” are always used in the literature, and they will be written as “vertical delocalization energy” and “adiabatic delocalization energy” in this book. In the literature, the value of a stabilizing energy effect is always written as positive, while the value of the destabilizing energy is always expressed as negative. In our research works including this book, the positive and negative values reported in the literature have been re-written as the negative and positive values.

In the Forewords to Chapter 6, the so-called experimental basis of “conjugation (resonance) stabilization” was questioned. In this chapter, the new version of restricted geometry optimization, our 2011 method, will be detailed (it has been described in our published paper¹), and it will be used (and has been used in our recent paper¹) to continuously question “conjugation stabilization”.

In this Chapter, we will focus on the rationality of our 2011 method. Therefore, it is necessary to introduce the historical roles of cyclobutadiene in judging which method, the MO (molecular orbital) method or the VB (valence bond) method, is more reasonable and in promoting the improvement and development of the MO methods.

8.0.1. Historical Roles of Cyclobutadiene

As a typical anti-aromatic compound, Cyclobutadiene is highly unstable. In the absence of trapping agent, the dimer is produced. This dimerization is an extremely fast reaction and limits the lifetime of cyclobutadiene except at very low temperatures. All synthetic approaches to cyclobutadiene had not been success² until it was trapped in a frozen matrix in 1965³ and until it was observed as a short-lived intermediate in solution.^{4,5} The synthesis of the cyclobutadiene and its derivatives⁶⁻¹⁴ has shown that these species are different from benzene in all respects. From as early as 1970 to 1973,^{15,16} Breslow reported the experimental evidences in support of the highly unstable character of cyclobutadiene. As reviewed by Shaik in 2001,¹⁷ this led Breslow and Dewar to coin the term “antiaromaticity” for π -systems with $4N$ electrons.¹⁸ In 1983,¹⁹ the destabilization resonance energy of 54.7 kcal/mol was calculated by Hess and Schaad. In 1999,²⁰ its anti-aromatic destabilization energy (55 kcal/mol) of cyclobutadiene was experimentally measured by Deniz via photoacoustic calorimetry.

Table 8-I. Vertical Delocalization Energy ΔE^V (kcal/mol) and Adiabatic Delocalization Energy ΔE^A (kcal/mol) of Cyclobutadiene Are Calculated Using Our 2007 Method.

	B3LYP		MP2-RHF*		MP2		Range	
	ΔE^V	ΔE^A						
6-31G*	51.0	64.2	89.4	123.1	96.0	141.9	45.0	77.7
6-311g(2df,p)	59.0	82.8	119.1	240.8	197.7	380.1	138.7	297.3
6-311G**	52.9	66.7	93.5	133.2	109.1	167.8	56.2	101.1
6-311G(2d,2p)	58.0	79.5	113.6	214.1	180.6	317.7	122.6	238.2
DH(2d,2p)	55.3	73.4	105.1	182.0	150.6	266.6	95.3	193.2
TZV	53.4	65.9	89.1	121.8	92.0	122.5	38.6	56.6
Range	8.0	16.6	30.0	117.7	105.7	257.6		
Average	54.9	72.1	101.6	169.2	137.7	232.8		

* The corresponding RHF molecular energies are calculated at the MP2 level of theory.

It is very interesting that resonance energy of cyclobutadiene has been used twice as a benchmark and testing ground to evaluate which method, the VB method or the MO method, gives reasonable results for conjugated molecules. During the first debate, from 1930 to 1950, Wheland's comparisons were even-handed and fair. However, as reviewed by Schaad and Hess in 2001,²¹ Wheland was convinced that cyclobutadiene must exhibit the same additional stability as benzene. So, when he found that the MO calculation did not predict this, he took a viewpoint favoring the VB method over MO method.

During the second argument, from 1980s to 1990s, a qualitative version of VB theory gave stabilizing resonance energy for cyclobutadiene.²²⁻²⁶ This led Shaik to point out: "this was a point of divergence of the MO and VB theories and marked the beginning of the downfall of VB theory".¹⁷ That is to say, the resonance energy of cyclobutadiene can be used to judge whether a calculation method is reasonable or unreasonable. If it is destabilizing, the method may be reasonable, otherwise it must be unreasonable. Accordingly, Bally regrets ground said:²⁷ "there is probably no other single molecule that has fascinated experimental and theoretical chemists so consistently over the past 40 years as has cyclobutadiene".

To our satisfaction, as shown by Table 8-I, the adiabatic delocalization energy and vertical delocalization energy of cyclobutadiene, obtained from our 2007 method, are always destabilizing, independent of the theoretical level and basis set size. Especially at B3LYP/6-31G* level, the values of these two energy effects are 64.2 and 51.0 kcal/mol, and the first one is close to the experimental value of 55 kcal/mol.

8.0.2. 4n+2 Rule

In 1931, Hückel published a paper,²⁸ leading to the famous 4n+2 rule. That is, when the number n of carbon atoms in an [N]annulene (C_nH_n) accords with $N = 4n+2$, the [N]annulene is aromatic, and its resonance energy is stabilizing; when $N = 4n$, it is anti-aromatic, and its resonance energy is destabilizing.

In 2001, as reviewed by Schaad and Hess,²¹ "Hückel's work in the second part of this paper leads to the famous 4n+2 rule for monocyclic conjugated hydrocarbons, though we do not find it explicitly stated here". In 1985,²⁹ however, Ichikawa seemed to attribute the formulation of the (4n+2)/4n rule to Armit and Robinson³⁰. It seems difficult to determine exactly who proposed the 4n+2 rule. For me, however, it is a digression.

The Hückel resonance energy, RE(ann.), of a [N]annulene with 0.5n double bonds is defined by the following Equation:

$$RE(ann) = E(ann) - 0.5nE(CH_2=CH_2)$$

where $E(ann)$ and $E(CH_2=CH_2)$ are the π energies of a [N]annulene and ethylene, and they are calculated using the HMO (Hückel molecular orbital) method. For examples, the resonance energies per π -electron for the benzene and cyclobutadiene are, respectively, 0.333 β and 0.0 β . For [N]annulene (C_nH_n , $n = 4$ to 22), Hückel delocalization energies per π electron, calculated using the Hückel reference structure and the Hückel computational method, are all stabilizing when $n > 4$. That is, as the number N of carbon atoms increases from 4 to 22, the results alternate between aromatic and not-so-aromatic, rather than between aromatic and anti-aromatic. Therefore, the Hückel computational method, together with the Hückel reference structure (ethylene), gave imperfect predictions of aromaticity and anti-aromaticity.²⁸ Afterwards, many efforts were made by Breslow and Mohacsy (1963),³¹ Chung and Dewar (1965),³² Dewar and Schmeising (1959-1960),^{33,34} Dewar and Gleicher (1965),^{35,36} Hess and Schaad (1972),^{37,38} Gutman-Milun-Trinajstić (1977),³⁹ to make the results alternate between aromatic and anti-aromatic. Finally, the Hess-Schaad appears to give roughly correct predictions of aromaticity and anti-aromaticity.

Most of above methods only paid attention to improve the structural parameters of reference state. In that era, due to the limitations of the times, the choice of reference state and the determination of reference molecular structure parameters were empirical and subjective, and the computational methods were also empirical and semi-empirical. The only thing that is preferable is that the resonance energy of cyclobutadiene, calculated by all above methods except for Hückel method, is destabilizing. For example, the resonance energy of cyclobutadiene, obtained

from Hess-Schaad method at Hückel level is 54 kcal/mol (this value was represented as negative in the original article),³⁷ and it is almost equal to our result (the B3LY values listed in Table 8-I).

In short, A reasonable method for calculating π electron delocalization energy (π -EDE) should at least meet the following two basic conditions:

- (i) The calculated electron delocalization energy of an anti-aromatic molecule such as cyclobutadiene must be destabilizing,
- (ii) That of an aromatic molecule such as benzene must be stabilizing.

These two basic conditions are essential. Keep these in mind, this is very important in the subsequent discussion of the rationality of our 2007 and 2011 methods.

8.0.3. Kollma Method and Jug Method

Throughout the development history of the methods for calculating π -EDE, theoretical chemists have been trying to develop a method for constructing a localized state without artificial arbitrariness, or to accurately calculate the molecular energy of localized state, or to do both. For a localized geometry (or state), the accurate calculation of molecular energy refers to the determination of the Fock and coefficient matrices of the localized geometry (or state) itself.

Kollma seems to be first one to attempt to accurately calculate EDE at the *ab initio* level of theory,⁴⁰ but the geometry of localized state is entirely artificial. His calculation (1979) provided the vertical resonance energy of 0.0 kcal/mol for cyclobutadiene. In order to calculate the vertical resonance energy (VRE) of cyclobutadiene, as one of the three methods, Kollma constructed a localized state and calculated the molecular energy of localized state via the following multi-step procedure:

- (i) For cyclobutadiene and its reference state (ethylene), the bond lengths were taken from the following empirical values: C–C, 1.54 Å; C=C, 1.48 Å; C–H, 1.0 Å.
- (ii) Calculating the wave-functions of cyclobutadiene and ethylene with the SCF program at minimal basis level;
- (iii) For cyclobutadiene, the π MOs of the ground state being replaced with the π MOs of two ethylenes, and meanwhile its σ MOs being kept unchanged, to construct the wave-function of the localized state. This step is based on the fact that, at minimal basis level, the AO coefficients of π MOs are independent of the position of the double bonds.
- (iv) Passing the coefficient matrix of localized wave-function and the Fock matrix of the ground state through the energy calculator to get the molecular energy of localized state.

Due the coulomb and exchange (EX) interactions, the localization of the π system should have a large effect on the σ system. For the Kollma's method, however, the structure of the molecule is artificially arbitrary, and the Fock matrix of the localized state borrows the matrix of the ground state. In particular, Kollma method completely ignores the effect of π -localization on the σ system. Accordingly, Kollma still did not solve the problem of how to reasonably construct a localized state (wave-function) without artificial arbitrariness and how to calculate the molecular energy of localized state.

Before our 2007 method, the BLW (Block-Localized Wave function) method (1998 to 2007)⁴¹⁻⁴⁵ and the Jug's method (in 1994)⁴⁶ seem to solve these problems. Jug seems to be the first to optimize the localized geometry of cyclobutadiene via the way to eliminate AO Fock matrix elements between two double bonds, which was implemented using the semiempirical method (SIND01), but he gave 0.0 kcal/mol for the adiabatic delocalization

Table 8-II. Vertical Resonance Energy (hartree) of [N]Annulene Were Obtained from Our 1998 method at RHF/STO-3G Level.

N	Optimization method	R_{long}	R_{short}	ΔE^V
4	HF/6-31G	1.51	1.37	0.0842
8	AM1	1.442	1.335	0.0308
	MP2/6-31G**	1.471	1.351	0.0242
	HF/6-31G**	1.479	1.326	0.0269
10	AM1	1.405	1.352	-0.0285
	HF/6-31G**	1.431	1.356	-0.0216
12	AM1	1.430	1.335	0.0107
14	AM1	1.424	1.339	-0.0063
16	AM1	1.431	1.337	0.0029
16	HF/6-31G**	1.492	1.345	0.0020

energy and vertical delocalization energy of cyclobutadiene.

8.0.4. Fundamental Flaws of BLW Method

It is the same as our methods that the BLW method can provide an optimized geometry for the localized state of conjugated molecule. But, as shown by Figure 6-IV, the vertical resonance energy and adiabatic resonance energy of cyclobutadiene, obtained from the BLW method,⁴¹ are stabilizing. On the contrary, the vertical delocalization energy (44.1 kcal/mol) and adiabatic delocalization energy (53.6 kcal/mol) of cyclobutadiene, obtained from our 2011 method at B3LYP/6-31G* level,¹ are destabilizing; the corresponding values, obtained from our 2007 method at B3LYP/6-31G* level, are also destabilizing (Table 6-I). In fact, as early as in 2000,⁴⁷ the vertical delocalization energies of [N]annulenes were calculated using our 1998 program, and their values (Table 8-II) well accord with predictions of aromaticity and anti-aromaticity. The differences, in the sign of the electron delocalization energy of cyclobutadiene, between the BLW method and our 2011 and 2007 methods mean that there are the fundamental flaws in the BLW method.

The construction of a localized state should include the determination of wave function and the calculation of Fock matrix. The fundamental differences between our method and the BLW method lies in the method of constructing localized state and optimizing localized geometry. In the BLW method, as shown by Equation (8-I) and Equation (8-II),⁴² a localized state, including its wave function, is obtained from the 2 x 2 rotations:

$$\psi_j = \cos(\theta_{ji}) \psi_j^o - \sin(\theta_{ji}) \psi_i^o \quad (8-\text{I})$$

$$\psi_i = \sin(\theta_{ji}) \psi_j^o + \cos(\theta_{ji}) \psi_i^o \quad (8-\text{II})$$

where ψ_i is the unoccupied π MOs of the P-th double bond, and ψ_j is an occupied π MO of the P-th double bond. for any double bond, there is only one occupied π MO. In the Mo's work, however, it did not be mentioned how to

calculate the rotation angle θ_{ji} . According to my knowledge, the rotation angle θ_{ji} in the above two Equations may be obtained from the following procedure: From Equations (8-I) and (8-II), can get Equations (8-III) and (8-IV).

$$F_{jk} = \cos(\theta_{ji}) F_{jk}^o - \sin(\theta_{ji}) F_{ik}^o \quad (8\text{-III})$$

$$F_{ik} = \sin(\theta_{ji}) F_{jk}^o + \cos(\theta_{ji}) F_{ik}^o \quad (8\text{-IV})$$

In the above equations, for example, F_{jk} is a LMO Fock matrix element between the j -th π occupied MO of the P-th double bond and the k -th π occupied MO of the Q-th double bond ($P \neq Q$) (in the BLW method, the LMO Fock matrix elements between various pairs of double bonds are not set equal to zero). From equations (8-III) and (8-IV), the following Equations can be obtained.

$$F_{jk}^2 = (\cos \theta_{ji})^2 (F_{jk}^o)^2 + (\sin \theta_{ji})^2 (F_{ik}^o)^2 - 2(\cos \theta_{ji})(F_{jk}^o)(\sin \theta_{ji})(F_{ik}^o) \quad (8\text{-V})$$

$$F_{ik}^2 = (\sin \theta_{ji})^2 (F_{jk}^o)^2 + (\cos \theta_{ji})^2 (F_{ik}^o)^2 + 2(\cos \theta_{ji})(F_{ik}^o)(\sin \theta_{ji})(F_{jk}^o) \quad (8\text{-VI})$$

Equation (8-V) + Equation (8-VI) has

$$F_{ik}^2 + F_{jk}^2 = (F_{jk}^o)^2 + (F_{ik}^o)^2 \quad (8\text{-VII})$$

Equation (8-VII) and Equation (8-VIII) are similar in form.

$$S_{ik}^2 + S_{jk}^2 = (S_{jk}^o)^2 + (S_{ik}^o)^2 \quad (8\text{-VIII})$$

$$\text{When } d(F_{jk}^2)/d(\theta_{ji}) = 0 \quad (8\text{-IX})$$

$$\tan(2\theta_{ji}) = -2(F_{jk} F_{ik}) / |F_{ik}^2 - F_{jk}^2| \quad (8\text{-X})$$

Equation (8-X) means that the Kost localization procedure⁴⁸, detailed in Chapter 3 and in our papers,⁴⁹ can be used to calculate the rotational angle θ_{ji} when the corresponding LMO overlap integral matrix elements S_{ik} and S_{jk} in Equation (3-11) are replaced with the LMO Fock matrix elements F_{jk} and F_{ik} . Whether using Equation (8-IX) or Equation $d(S_{jk}^2)/d(\theta_{ji}) = 0$ (Equation (3-11)) to calculate the rotation angle θ_{ji} , as the results of the 2 x 2 rotations, the π -MO exchange interaction between the occupied π MO of the P-th double bond and the occupied π MO of the Q-th double bond ($P \neq Q$) is maximized after localization, and meanwhile the π -MO charge transfer (CT) interactions between the unoccupied π MOs of the P-th double and the occupied π MO of the Q-th double bond are minimized. This is to say, as emphasized by Mo himself,⁴² the BLW method can only eliminate the charge transfer interaction between double bonds in the localized geometry. In this case, the molecular energy difference, $E(G) - E(LG)$, between the ground state (G) of a conjugated molecule and its localized state (or geometry) (LG) mainly comes from the charge transfer interactions, partly due to that the exchange interaction in the ground state is weaker than that in the localized geometry. Therefore, regardless of whether the conjugated molecules are aromatic or anti-aromatic, the electron delocalization energy, obtained from the BLW method, is always stabilizing. Indeed, as shown in Figure 6-IV, the vertical resonance energy and adiabatic resonance energy of cyclobutadiene, obtained from the BLW method,

are stabilizing, and their values are -10.9 kcal/mol and -10.3 kcal/mol, respectively (In Mo's work, the values of these two stabilizing energy effects are positive), which is the fundamental difference between our method and the BLW method. According to Shaik's standards, the BLW method must be unreasonable.

Facing the fundamental flaws of BLW method, Mo had to emphasize that π -electron delocalization energy only arises from the charge transfer interaction between double bonds.⁴² However, according to the Morokuma's definition⁵⁰ and Bader's definition⁵¹⁻⁵³, the MO exchange and charge transfer interactions between double bonds, as well as the spatial exchange interaction between the two double bonds, all can cause the π electron delocalization.

8.1. INTRODUCTION

It is different from the BLW method that, in the GL localized geometry and the localized electronic state obtained from our 2007 method, the MO charge transfer and exchange interactions have been excluded from between the double bonds (or localized groups). Correspondingly, as shown by the data listed in Table 8-I, the vertical delocalization energy and adiabatic delocalization energy of cyclobutadiene, obtained from our 2007 method, are always destabilizing. Therefore, only our 2007 method can meet the first basic condition for judging the rationality of the calculation method of electron delocalization energy, not the BLW method.

8.1.1. Our 2007 Method Needing Improvement

However, when using our 2007 method (a method of eliminating matrix elements) to optimize GL geometry and GE-m geometry, the ESE values (kcal/mol) of benzene are as follows:

-39.0 (B3LYP/6-31G*), -40.1 (B3LYP/6-311G**), -41.2 (B3LYP/6-311G (2df,p), -51.2 (MP2/ 6-311G*), -57.3 (MP2/6-311G*), -46.5 (RHF/ 6-31G*), -48.6 (RHF/ 6-311G**).

Accordingly, at the B3LYP level of theory, the effect of basis set size on the ESE value is the smallest, and the B3LYP values of -39.0 kcal/mol is the closest to the experimental value (-36 kcal/ml). At the RHF and MPn ($n = 2, 3$) levels of theory, on the contrary, not only the base set size has a large influence on the value of ESE, and the differences between the corresponding ESE values and the experimental value (-36 kcal/mol) are also big. The use of our 2007 method should be limited at the specific theoretical levels.

For aromatic molecules, especially, the vertical and adiabatic delocalization energies are not always stabilizing, and their size and sign depend upon the theoretical level and basis set size. For example, the following calculation results do not meet the second basic condition for judging the rationality of the calculation method of electron delocalization energy:

- (i) For benzene, as indicated by the data listed in Table 8-1 and Table 6-4, when the vertical destabilization energy ΔE^V and the adiabatic delocalization energy ΔE^A are calculated using our 2007 method at the RHF and MPn ($n = 2, 3$) levels of theory, these two energy effects become destabilizing, and their values also depend on the basis set size.
- (ii) For acenes, as shown by the red curve line in Figure 8-1, the adiabatic delocalization energy ΔE^A becomes destabilizing when $n > 2$.

At the B3LYP level of theory, on the contrary, the vertical destabilization energy ΔE^V and adiabatic delocalization energy ΔE^A are stabilizing, and the influence of basis set size on the B3LYP value is much less than on the RHF and MPn ($n = 2, 3$) values. At the B3LYP, RHF and MPn levels of theory, as shown by the data listed in Table 8-1, the

Table 8-1. Vertical Resonance Energy (kcal/mol), ΔE^V , of Benzene by our 2007 method at B3LYP, RHF and MPn Levels of Theory.

Basis sets	B3LYP	RHF	MP2	MP3
DH(2d, 2p)	-10.1	55.4	242.7	199.0
TVZ	-10.4	45.7	108.0	102.5
6-311G(2d, 2p)	-10.2	57.4	299.4	226.3
6-311G(2df, p)	-5.7	41.9	164.4	154.5
6-311G(d, p)	-16.8	36.0	125.5	120.1
6-311++G(d, p)	-13.9	46.8	152.5	140.3
6-31G(d)	-21.0	26.0	82.8	85.1
6-311G(d)	-16.4	36.8	124.9	120.2
Range	-15.3	29.4	216.6	113.9

Rang: For the series of the values, the difference between the maximum value and minimum value. The data in this Table are not published. If you need to cite these data, please contact the author.

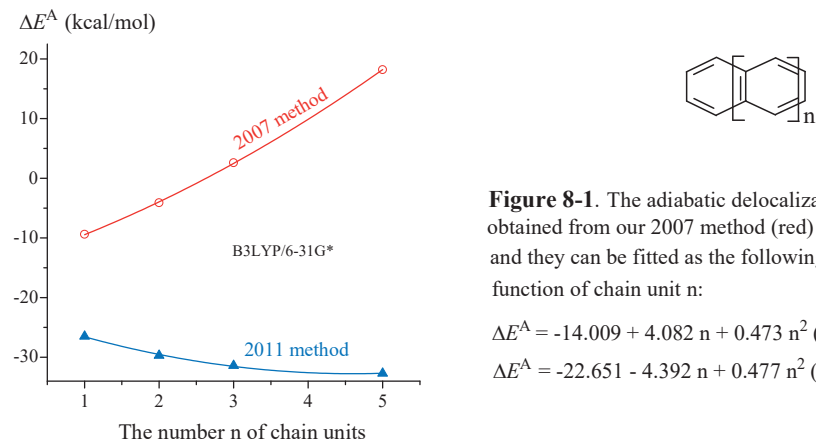


Figure 8-1. The adiabatic delocalization energies ΔE^A of acenes, obtained from our 2007 method (red) and our 2011 method (blue), and they can be fitted as the following second order polynomial function of chain unit n :

$$\Delta E^A = -14.009 + 4.082 n + 0.473 n^2 \text{ (red), and}$$

$$\Delta E^A = -22.651 - 4.392 n + 0.477 n^2 \text{ (blue).}$$

minimum and maximum values (kcal/mol) of vertical delocalization energy for benzene are as follows:

Minimum: -5.7 (B3LYP/6-311G(2df,p)), 26.0 (RHF/6-31G*), 82.8 (MP2/ 6-31G*), 85.1 (MP3 /6-31G*).
Maximum: -21.0 (B3LYP/6-31G*), 57.4 [RHF/6-311G (2d,2p)], 299.4 [MP2/6-311G(2d,2p)], 226.3 (MP3/6-311G(2d,2p)).

A ratio of the MP2 maximum value to the B3LYP minimum value (absolute value), $299.4/|-5.7|$, is large, up to 52.5. Accordingly, our 2007 method needs improvement.

In order to find the way to improve our 2007 method and to demonstrate the fundamental difference between our method and the BLW method, the π - σ energy decomposition should be introduced first, and it will give the following conclusions:

- (i) For planar conjugated molecule, the DSI state constructed by eliminating the LFMO matrix elements is the same as that obtained by eliminating the AO matrix elements.
- (ii) In the DSI state constructed by eliminating the AO matrix elements, the MO exchange and charge transfer interactions both have been excluded from between the localized double bonds.

8.1.2. π - σ Energy Decomposition

π - σ Energy decomposition can be roughly divided into two classes. As described in chapter 4, the first class of methods is to conditionally eliminate the non-diagonal elements of the LMO (localized molecular orbital) matrix, where the matrix refers to the LMO Fock matrix and LMO overlap integral matrix. Using this type of method, four localized electronic states can be constructed, and their molecular energies can be calculated. These four electron states are denoted as DSI, FUD, FUL and DPI (Chapter 4). For a conjugated molecule, for example, the molecular energy difference between the ground state and its DSI state is defined as the vertical delocalization energy. The second class of methods is to decompose the molecular energy of a specific localized electronic state into the π and σ parts and into the CT and EX parts.

In our 1998 method, as detailed in Chapter 4 and our papers,⁵⁴⁻⁵⁶ the LFMO (absolutely Localized fragment molecular orbital) basis set is used to decompose the inter-fragment components of the RHF molecular energy of ground state into the CT and EX contributions. In our 2000 paper,⁴⁷ the π - σ energy decomposition of an electronic state for an aromatic molecule has been detailed. In that paper, however, the π - σ energy decomposition was done at RHF/STO-3G level, and it can only exclude the MO charge transfer and exchange interactions from between the localized double bonds (localized groups) in localized geometry. In this section, the energy decomposition will be performed using our 2011 method at RHF/6-31G* level.

8.1.2.1. Theoretical Basis.

When the electronic states of benzene, such as the ground state and its DSI states (in the DSI state, the π MOs are localized on their respective double bonds, and the σ MO are delocalized on whole molecular framework. The ground state and its DSI state have the same molecular geometry.) are obtained from our 1998 method^{47,54} (including our 2006 method⁵⁶) at the RHF level of theory, total electron energy E_e of an electronic state can be decomposed into the π and σ parts, E_e^π and E_e^σ , using Equation (8-1) and Equation (8-2), and the related data are presented in Figure 8-2c. For the DSI state of benzene at RHF/6-31G* level, for example, $E_e^\pi(\text{DSI}) = -38.08353 \text{ kcal/mol}$, $E_e^\sigma(\text{DSI}) = -396.25280 \text{ kcal/mol}$.

$$E_e^\pi = \sum_{i=1}^{n_\pi} \sum_{j=1}^{n_\pi} (F_{ij}^\pi + H_{ij}^\pi) D_{ij}^\pi \quad (8-1)$$

$$E_e^\sigma = \sum_{i=1}^{n_\sigma} \sum_{j=1}^{n_\sigma} (F_{ij}^\sigma + H_{ij}^\sigma) D_{ij}^\sigma \quad (8-2)$$

In above two equations, for example, when the H_{ij}^π , F_{ij}^π and D_{ij}^π are the matrix elements between π LFMOs at a specific electronic state, E_e^π is the energy of the π system, and $E_e^\pi(G)$ is the E_e^π of the ground state, where **H**, **F**, and **D** are, respectively, LFMO one-electron, Fock and density matrices; n_π is the number of π LFMOs. In this book, a LMO matrix is always represented by a bold uppercase letter such as **H**, and its elements are always represented by Italic uppercase letters, such as H_{ij}^π , with super- and sub-scripts. The corresponding lowercase letters always represent the AO matrix and its elements.

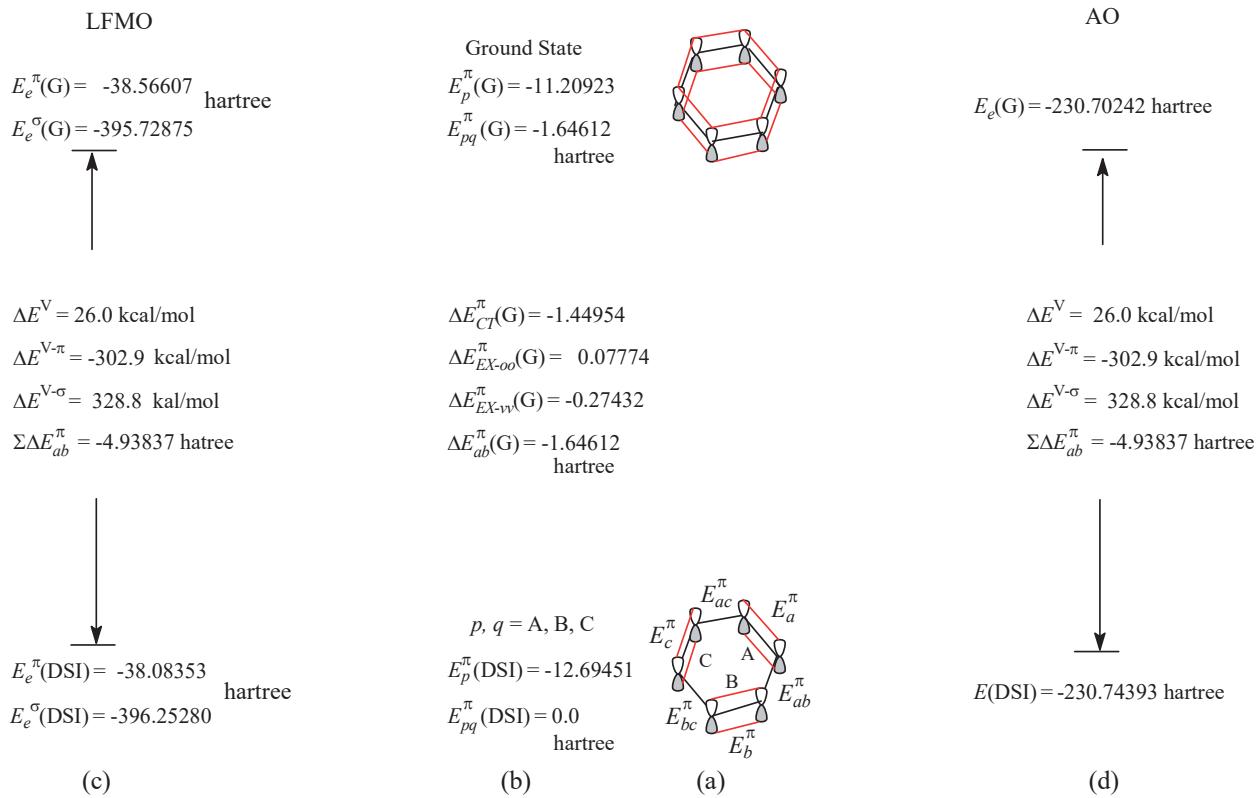


Figure 8-2. For benzene, vertical delocalization energy ΔE^V and its various components are calculated by using our 1998 method and our 2007 method at RHF/6-31G*. The geometry of benzene is optimized at B3LYP/6-311G** level.

Using Equation (8-3), the π energy E_e^π can be further decomposed into the intra-fragment interaction energies E_p^π ($P = A, B, \dots$) and inter-fragment interaction energies E_{pq}^π ($P, Q = A, B, \dots; P \neq Q$).

$$E_e^\pi = \sum_{P=A}^C E_p^\pi + \sum_{P=A}^B \sum_{Q=B, Q \neq P}^C E_{pq}^\pi \quad (8-3)$$

where

$$E_p^\pi = \sum_{i=1, i \in P}^{np} \sum_{j=1, j \in P}^{np} (F_{ij}^\pi + H_{ij}^\pi) D_{ij}^\pi$$

$$E_{pq}^\pi = \sum_{i=1, i \in P}^{np} \sum_{j=1, j \in Q, P \neq Q}^{nq} (F_{ij}^\pi + H_{ij}^\pi) D_{ij}^\pi$$

For the above Equations, n_p and n_q are the numbers of π LFMOs belonging to fragment P and Q. For the ground state of benzene at RHF/6-31G* level, as shown by the data presented in Figure 8-2b, the intra- and inter fragment interaction energies (hartree) are as follows:

$$E_a^\pi(G) = E_b^\pi(G) = E_e^\pi(G) = -11.20923$$

$$E_{ab}^\pi(G) = E_{ac}^\pi(G) = E_{bc}^\pi(G) = -1.64612$$

In the case of the DSI state of benzene, the followings are the corresponding energy effects (hartree):

$$E_a^\pi(\text{DSI}) = E_b^\pi(\text{DSI}) = E_e^\pi(\text{DSI}) = -12.6945.$$

$$E_{ab}^\pi(\text{DSI}) = E_{ac}^\pi(\text{DSI}) = E_{bc}^\pi(\text{DSI}) = 0.$$

Using Equation (8-4), can also continue to decompose $E_{pq}^\pi(G)$ into the charge transfer interaction energy E_{CT}^π and exchange interaction energy E_{EX}^π :

$$E_{pq}^\pi(G) = E_{\text{CT}}^\pi(G) + E_{\text{EX}}^\pi(G) = (E_{\text{CT-ov}}^\pi(G) + E_{\text{CT-vo}}^\pi(G)) + (E_{\text{EX-oo}}^\pi(G) + E_{\text{EX-vv}}^\pi(G)) \quad (8-4)$$

where

$$E_{\text{CT-ov}}^\pi(G) = \sum_P^{\text{all}} \sum_{Q, Q \neq P}^{\text{all}} 2 \left(\sum_{i=1, i \in P}^{\text{occ}} \sum_{j=occ+1, j \in Q}^{\text{unocc}} (F_{ij}^\pi + H_{ij}^\pi) D_{ij}^\pi \right)$$

$$E_{\text{CT-vo}}^\pi(G) = \sum_P^{\text{all}} \sum_{Q, Q \neq P}^{\text{all}} 2 \left(\sum_{i=occ+1, i \in P}^{\text{unocc}} \sum_{j=1, j \in Q}^{\text{occ}} (F_{ij}^\pi + H_{ij}^\pi) D_{ij}^\pi \right)$$

$$E_{\text{EX-oo}}^\pi(G) = \sum_P^{\text{all}} \sum_{Q, Q \neq P}^{\text{all}} 2 \left(\sum_{i=1, i \in P}^{\text{occ}} \sum_{j=1, j \in Q}^{\text{occ}} (F_{ij}^\pi + H_{ij}^\pi) D_{ij}^\pi \right)$$

$$E_{\text{EX-vv}}^\pi(G) = \sum_P^{\text{all}} \sum_{Q, Q \neq P}^{\text{all}} 2 \left(\sum_{i=occ+1, i \in P}^{\text{unocc}} \sum_{j=occ+1, j \in Q}^{\text{unocc}} (F_{ij}^\pi + H_{ij}^\pi) D_{ij}^\pi \right)$$

For the symbol “ $E_{\text{CT-ov}}^\pi(G)$ ”, for example, the subscript “*ov*” means that the charge transfer energy effect $E_{\text{CT-ov}}^\pi(G)$ arises from the interactions between the occupied π LFMOS of fragment P and the unoccupied π LFMOS of fragment Q ($P \neq Q$).

According to the definition and using Equation (8-5), the vertical delocalization energy ΔE^V can be expressed as the sum of all kinds of components.

$$\Delta E^V = E(G) - E(\text{DSI}) = E_e(G) - E_e(\text{DSI}) = (E_e^\pi(G) - E_e^\pi(\text{DSI})) + (E_e^\sigma(G) - E_e^\sigma(\text{DSI})) = \Delta E^{V-\pi} + \Delta E^{V-\sigma} \quad (8-5)$$

where

$$\Delta E^{V-\pi} = \sum_P^{\text{all}} \Delta E_p^{V-\pi} + \sum_{P, Q \neq P}^{\text{all}} \Delta E_{pq}^{V-\pi}$$

$$\Delta E^{V-\sigma} = \sum_P^{\text{all}} \Delta E_p^{V-\sigma} + \sum_{P, Q \neq P}^{\text{all}} \Delta E_{pq}^{V-\sigma}$$

8.1.2.2. Energy Decomposition Examples

For benzene at the RHF/6-31G* level, as shown by Figure 8-2c, $\Delta E^V = 26.0$ kcal/mol, and its two components, $\Delta E^{V-\pi} = -302.7$ kcal/mol, and $\Delta E^{V-\sigma} = 328.8$ kcal/mol. π -electron delocalization can indeed stabilize π system, and meanwhile it destabilizes the σ system when our 1998 program is used to decompose molecular energy. Due to $|\Delta E^{V-\pi}| (-302.7 \text{ kcal/mol}) < \Delta E^{V-\sigma} (328.8 \text{ kcal/mol})$, total energy effect, arising from π -electron delocalization, is destabilizing.

The energy effects $\Delta E^{V-\pi}$ and $\Delta E^{V-\sigma}$ can also be calculated by using our 2007 method, according to the principle of DFT energy decomposition.⁵⁷ For benzene at B3LYP/6-31G* level, the vertical electron delocalization energy $\Delta E^V = -21.2$ kcal/mol, and it is stabilizing, due to that $|\Delta E^{V-\pi} (-235.9 \text{ kcal/mol})| > \Delta E^{V-\sigma} (214.7 \text{ kcal/mol})$. At any level of theory, the π system is always stabilized due to π -electron delocalization, and the σ system is always destabilized. Whether the vertical electron delocalization energy is stabilizing or destabilizing depends upon which one is larger, $\Delta E^{V-\pi}$ or $\Delta E^{V-\sigma}$.

In addition, as shown in Figure 8-2b, the exchange interaction energy $E_{\text{EX-oo}}$ (0.07774 hartree) between the occupied MOs of double bonds is always destabilization, and the charge transfer interaction energy E_{CT} (-1.44954 hartree) is always stabilizing. The calculation results of these two energy effects meet the principles of the two electron stabilization interaction and four electron destabilization interaction.^{58,59} Thus, when the BLW method is used to construct a localized electronic state, the exchange interaction between the occupied π MO of p-th double bond and the occupied π MO of Q-th double bond is maximized, at the same time, the charge transfer interaction energy between two double bonds P and Q ($P \neq Q$) is minimized, leading to that the BLW method must give a stabilizing vertical delocalization energy, whether the molecule is aromatic or anti-aromatic.

8.1.2.3. Decomposition Based on AO Matrices.

When the $\pi-\sigma$ energy decomposition is performed based on the AO matrix elements, as done by our 2007 method and our 2011 method, the F_{ij}^π , S_{ij}^π and D_{ij}^π elements in the Equations mentioned above should be replaced with the AO matrix elements $f^{\pi}_{\lambda\rho}$, $s^{\pi}_{\lambda\rho}$ and $d^{\pi}_{\lambda\rho}$. In this case, the RHF molecular energy can also be decomposed into the π and σ parts using Equations (8-1) to (8-2). But it is a more complex procedure to partition the energy component $E_{pq}^\pi(G)$ into the $E_{\text{CT}}^\pi(G)$ and $E_{\text{EX}}^\pi(G)$ parts. In spite of this, as demonstrated in our 2006 paper⁵⁶ and according to the data presented in Figure 8-2c and Figure 8-2d, for a planar conjugated molecule (or planar conformation) such as benzene, the energy components such as $E_e^\pi(\text{DSI})$ and $E_e^\sigma(\text{DSI})$, obtained by deleting AO matrix elements (our 2007 method), are the same as the corresponding energy components calculated by deleting LFMO matrix elements (our 1998 method and our 2006 method), and certainly the corresponding energy differences, such as $\Delta E^{V-\pi}$ and $\Delta E^{V-\sigma}$, are the same. Therefore, the DSI state obtained from our 2007 method is equivalent to that obtained from our 2006 method. This is to say, in the DSI state obtained from our 2007 method, the MO exchange and charge transfer interactions have been excluded from between the localized double bonds.

8.1.3. Two-electron Exchange Integrals

At the RHF level of theory, AO Fock matrix element can be expressed as Equation (8-6),

$$f_{\lambda\mu} = h_{\lambda\mu} + \sum_{\rho} \sum_{\omega} d_{\rho\omega} [\langle \lambda\mu | \rho\omega \rangle - 1/2 \langle \lambda\rho | \mu\omega \rangle] \quad (8-6)$$

where $h_{\lambda\mu}$ is the element of one-electron matrix \mathbf{h} , $d_{\rho\omega}$ is the element of density matrix \mathbf{d} , and $\langle \lambda\mu | \rho\omega \rangle$ and $\langle \lambda\rho | \mu\omega \rangle$

are, respectively, the two-electron Coulomb and two-electron exchange integrals. For the DSI state of benzene, when the π AO $\phi_\lambda \in P$ -th double bond and the π AO $\phi_\rho \in Q$ -th double bond ($P \neq Q$), the Fock matrix elements $f_{\lambda,\rho}^*$ are set equal to zero. As the results, the AO density matrix elements $d_{\lambda,\rho} = 0$ when the π AOs $\phi_\lambda \in P$ -th double bond and the π AO $\phi_\rho \in Q$ -th double bond and when the AO $\phi_\lambda \in \pi$ system and the AO $\phi_\rho \in \sigma$ system. In this case, therefore, when the π AOs ϕ_λ and $\phi_\mu \in P$ -th double bond, and the π AOs ϕ_ρ and $\phi_\omega \in Q$ -th double bonds ($P \neq Q$), the sum term in Equation (8-6) can expanded into four sum terms according to Equation (8-7).

$$\begin{aligned} & \sum_{\rho}^{\text{all}} \sum_{\omega}^{\text{all}} d_{\rho\omega} [\langle \lambda\mu | \rho\omega \rangle - 1/2 \langle \lambda\rho | \mu\omega \rangle] = \\ &= \sum_{\rho \in A}^{\text{all}} \sum_{\omega \in A}^{\text{all}} d_{\rho\omega} [\langle \lambda\mu | \rho\omega \rangle - 1/2 \langle \lambda\rho | \mu\omega \rangle] + \sum_{\rho \in B}^{\text{all}} \sum_{\omega \in B}^{\text{all}} d_{\rho\omega} [\langle \lambda\mu | \rho\omega \rangle - 1/2 \langle \lambda\rho | \mu\omega \rangle] \\ &+ \sum_{\rho \in C}^{\text{all}} \sum_{\omega \in C}^{\text{all}} d_{\rho\omega} [\langle \lambda\mu | \rho\omega \rangle - 1/2 \langle \lambda\rho | \mu\omega \rangle] + \sum_{\rho \in \sigma}^{\text{all}} \sum_{\omega \in \sigma}^{\text{all}} d_{\rho\omega} [\langle \lambda\mu | \rho\omega \rangle - 1/2 \langle \lambda\rho | \mu\omega \rangle] \end{aligned} \quad (8-7)$$

Throughout each conditional SCF iteration, the two-electron integrals $\langle \lambda\mu | \rho\omega \rangle$ and $\langle \lambda\rho | \mu\omega \rangle$ remain unchanged. In the DSI state, π electron density $d_{\rho\omega}$ in fragment Q still can have an effect on the Fock matrix elements $f_{\lambda,\mu}^*$ of fragment P via two-electron exchange integrals $\langle \lambda\rho | \mu\omega \rangle$, according to Equation (8-7). As indicated by Bader,⁵¹ through electron exchange, Pauli exclusion principle can also cause π -electron delocalization. That is to say, the π -electron localization and the π -MO localization are two different concepts, and the π -MO localization is not enough to ensure π -electrons localization, and it is only necessary condition for π -electron localization. To ensure localization of π -electrons, also must set two-electron exchange integrals $\langle \lambda\rho | \mu\omega \rangle = 0.0$ in addition to conditionally setting $f_{\lambda,\rho}^* = 0$ and $s_{\lambda,\rho} = 0$, when the π AOs ϕ_λ and $\phi_\mu \in P$ -th double bond (group) and the π AOs ϕ_ρ and $\phi_\omega \in Q$ -th double bond (group), $P \neq Q$.

In this book, two-electron exchange interaction, caused by electron exchange, is called the spatial exchange interaction, and the corresponding localization is called electron localization.⁵²

8.1.4. MPn Correlation Energy

The MP2 second order energy correlation $E^{(2)}$ is expressed as Equation (8-8).⁶⁰

$$E^{(2)} = \sum_{b=a+1}^{\infty} \sum_{a=n+1}^{\infty} \sum_{i=j+1}^n \sum_{j=1}^{n-1} [\langle ab | r_{12}^{-1} | ij \rangle - \langle ab | r_{12}^{-1} | ji \rangle]^2 (\varepsilon_i + \varepsilon_j - \varepsilon_a - \varepsilon_b) \quad (8-8)$$

In the Equation, Φ_i , Φ_j , Φ_a and Φ_b are the MOs obtained from the RHF calculation, and ε_i , ε_j , ε_a and ε_b are their energy levels.

In the localized state (such as GL geometry or the DSI state) of benzene, the MO density matrix elements $D_{ij} = 0$ when the π MO $\Phi_i \in P$ -th double bond, and the π MO $\Phi_j \in Q$ -th double bond ($P \neq Q$), which is the result of eliminating the non-diagonal elements F_{ij} of the LFMO Fock matrix or the results of eliminating non-diagonal elements $f_{\lambda,\rho}$ of the AO Fock matrix. According to Equation (8-7), as will be shown in this Chapter, the method for eliminating the non-diagonal elements $h_{\lambda,\rho}$ and related $\langle \lambda\mu | \rho\omega \rangle$ and $\langle \lambda\rho | \mu\omega \rangle$ is equivalent to the method for eliminating non-diagonal elements $f_{\lambda,\rho}$.

In the Gaussian and Gamess software packages, there is a subroutine to transform the AO two-electron integrals $\langle \lambda\mu | \rho\omega \rangle$ and $\langle \lambda\rho | \mu\omega \rangle$ into the MO two-electron integrals such as $\langle ab | ij \rangle$ and $\langle ab | ji \rangle$ in Equation (8-8). For a

Table 8-2. For Benzene, Extra Stabilization Energy (ESE) (kcal/mol) Obtained from Our 2007 Method.

		Pure EX without		Pure Corr.		EX-Corr. without			Hybrid with	
		HF-EX and Corr.		with HF-EX		HF-EX		HF-EX		
		SLATER	XPBE96	CPBE96	LYP	PBE96	SVWN5	BLYP	PBE0	X3LYP
6-31G*	ΔE^A	-19.6	-20.4	39.5	39.0	-20.9	-20.1	-20.5	-8.3	-9.8
	ΔE^{A1}	5.3	4.2	29.7	29.3	4.8	5.5	4.7	10.8	9.9
	ESE	-35.5	-32.9	-49.7	-48.9	-35.4	-36.7	-34.5	-40.8	-39.4
6-311G**	ΔE^A	-15.7	-16.9	48.3	48.8	-17.9	-16.5	-17.1	-4.3	-5.4
	ΔE^{A1}	6.8	5.5	33.3	33.4	6.0	7.0	6.0	12.6	11.7
	ESE	-36.2	-33.4	-51.7	-51.2	-36.0	-37.4	-35.1	-42.0	-40.6
6-311G(2d,2p)	ΔE^A	-11.9	-13.9	80.1	78.8	-14.1	-12.5	-13.7	2.3	0.3
	ΔE^{A1}	7.9	6.4	41.8	41.6	7.1	8.1	7.0	14.7	13.6
	ESE	-35.7	-33.1	-45.3	-46.0	-35.4	-36.8	-34.6	-41.9	-40.5
6-311G(2df,p)	ΔE^A	-9.3	-11.8	95.9	95.0	-11.4	-9.5	-11.2	6.6	4.1
	ΔE^{A1}	9.0	7.3	46.7	46.3	8.2	9.3	8.0	16.6	15.3
	ESE	-36.4	-33.7	-44.1	-43.8	-36.1	-37.5	-35.3	-43.3	-41.8

HF-EX: Hartree-Fock Exchange; EX: exchange; Corr.: correlation.

localized state obtained from our 2007 method, the calculated AO two-electron integrals are always completely retained in each SCF iteration process. Therefore, MO two-electron integrals $\langle ab|r_{12}^{-1}|ij\rangle$ and $\langle ab|r_{12}^{-1}|ji\rangle$ in Equation (8-8), obtained by additionally deleting AO two-electron exchange integrals $\langle\lambda\rho|\mu\omega\rangle$ (will be called our 2011 method), should be different from those obtained by only deleting matrix elements (our 2007 method).

Due to that there is no density element terms in Equation (8-8), the $E^{(2)}$ obtained from our 2011 method is different from that calculated by our 2007 method. For benzene, thus, at the MP2 level of theory, the basis set size has a large effect on the value of the ESE (Table 6-4), and the values of the ESE are all much greater than the B3LYP/6-31G* value of -39.0 kcal/mol when our 2007 method is used.

8.1.5. Evidences for Role of HF-EX.

At the density functional level of theory, the molecular energy can be expressed by Equation (8-9).

$$E_{DFT}(\rho) = E_H + E_J + E_{xc}(\rho) \quad (8-9)$$

where E_H , E_J , and E_{xc} are, respectively, one-electron energy, two-electron Coulomb energy, and exchange-correlation energy.

The four types of density functionals are supported by PC-Gamess package:⁶¹ the pure Exchange density functional without Hartree-Fock Exchange (HF-EX) and correlation, such as SLATER and XPBE96, belongs to the first type; the second type includes the pure Correlation density functionals, such as CPBE96 and LYP, with 100%

Table 8-3. For Benzene, Vertical Delocalization Energy ΔE^V (kcal/mol) Obtained from Our 2007 Method.

	Pure EX without		Pure Corr. with		EX-Corr. without		Hybrid with		
	HF-EX and Corr.		HF-EX		HF-EX		HF-EX		
	SLATER	XPBE96	CPBE96	LYP	PBE96	SVWN5	BLYP	PBE0	X3LYP
6-31G(d)	-28.5	-30.2	25.1	24.7	-31.0	-30.1	-30.8	-18.4	-20.0
6-311G(2d,2p)	-19.9	-22.0	55.6	55.3	-23.2	-22.1	-22.9	-6.8	-8.9
6-311G(2df,p)	-16.2	-18.4	65.0	64.3	-19.3	-18.4	-19.3	-1.9	-4.3
6-311G(d,p)	-24.9	-26.9	33.8	34.3	-28.1	-26.9	-27.7	-14.3	-15.7

HF-EX; the density functionals of third type refer to the exchange-correlation functional, such as PBE96 and BLYP, without HF-EX. The Hybrid density functionals, such as PBE0 and B3LYP, with part of HF-EX belong to the fourth type of density functional.

The ESE of benzene is calculated using our 2007 method at various density functional levels of theory, and its values are listed in Table 8-2. At (CPBE96 and LYP) levels of theory, the 6-31G* values (kcal/mol) of ESE are -49.7 (CPBE96) and -48.9 (LYP), and their absolute values are the greatest of all the 6-31G* values listed in Table 8-2. At (SLATER and XPBE96) levels of theory, the 6-31G* values of ESE (kcal/mol) are -35.5 (SLATER) and -32.9 (XPBE96), and the value of -32.9 are the smallest, in the absolute value, of all the 6-31G* values. The (SLATE, XPBE96, PBE96, SVWN5 and BLYP)/6-31G* values of -35.5, -32.9, -35.4, -36.7 and -34.5 kcal/mol show that, as long as the density functionals do not contain HF-EX, the corresponding ESE values are close to each other, and are close to the experimental value of -36 kcal/mol.

Particularly, as shown by the data in Table 8-2 and Table 8-3, the adiabatic delocalization energy (ΔE^A) and vertical delocalization energy (ΔE^V) are destabilizing when the second type of density functional with 100% HF-EX is used. At 6-31G* level, for example, the values (kcal/mol) of ΔE^A are 39.5 CPBE96) and 39.0 (LYP), and values (kcal/mol) of ΔE^V are 25.1 (CPBE96) and 24.7 (LYP). These energy effects are all destabilizing. When a density functional does not contain the HF-EX term, on the contrary, the corresponding energy effects become stabilizing and the basis set size has a slight effect on the values. At 6-31G* level, for example, the values (kcal/mol) of ΔE^A are -19.6 (SLATER) and -20.1 (SVWN5), the values (kcal/mol) of ΔE^V (kcal/mol) are -28.5 (SLATER) and -30.1 (SVWN5). These energy effects are all stabilizing.

All these mean that the Hartree-Fock exchange plays an important role in determining the sign of energy effects ΔE^A and ΔE^V . In order to ensure that π -electrons are localized, it is necessary to improve our 2007 method. The improved version of our 2007 method will be named our 2011 method. In the localized geometry of benzene obtained from our 2011 method, two-electron exchange integrals, denoted as $\langle \lambda \rho | \mu \omega \rangle$, between two localized double bonds should also be deleted additionally and conditionally.

8.2. OUR 2011 METHOD

Except for the CCSD (single and doubles the coupled cluster) calculation that is performed by using the GAMESS 40 package (US)⁶², all other calculations are performed with the PC-GAMESS 7.0 package⁶³. For the MP2 calculation, all inner orbitals are not frozen. But, for the CISD (configuration interaction singles and doubles) and CCSD calculations, all the inner orbitals are frozen.

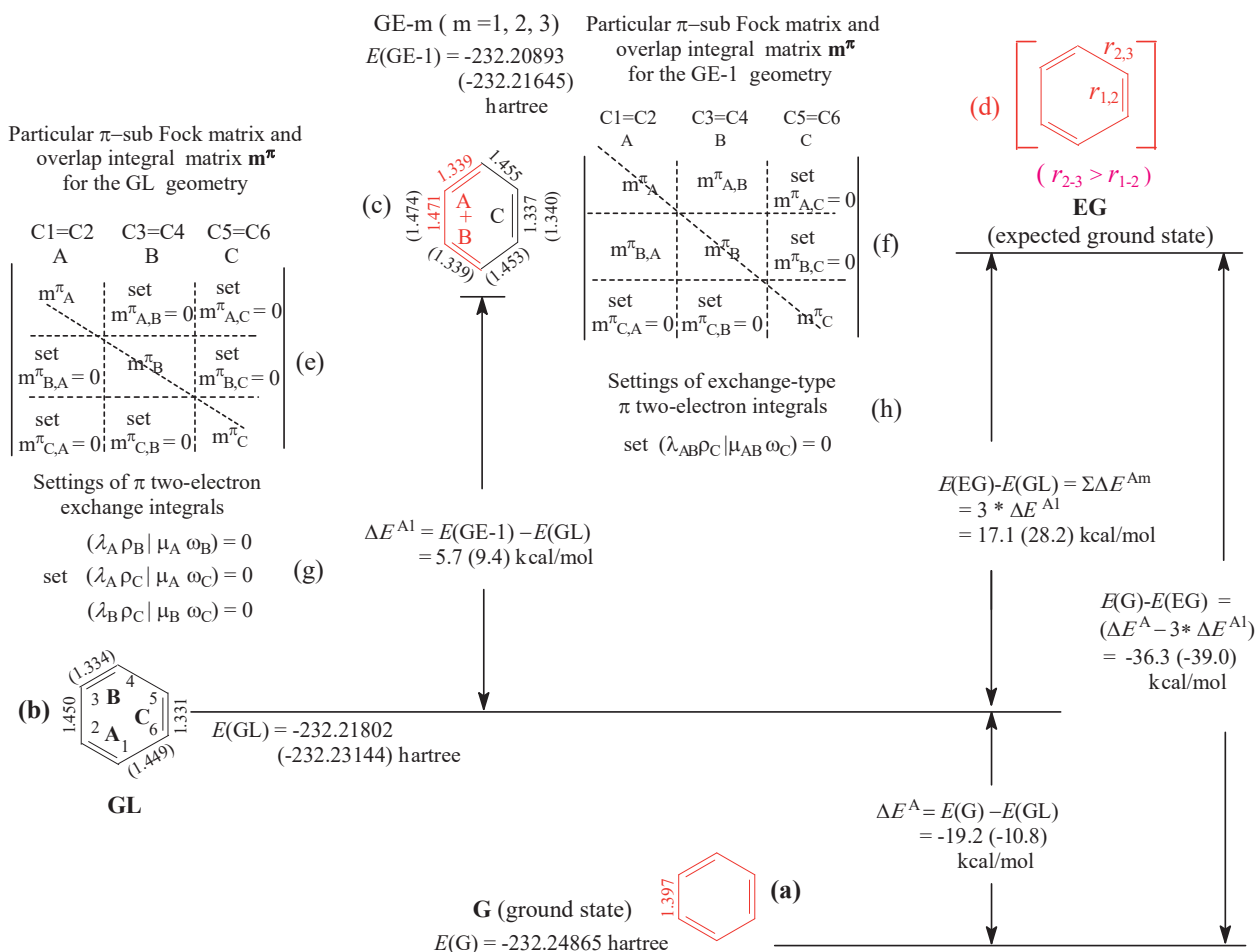


Figure 8-3. Our 2011 method for calculating extra stabilization energy (ESE) of benzene. (a), (b) and (c) The ground state (G) and its GL and GE- m geometries are obtained from the full and restricted geometry optimizations at the B3LYP/6-31G* level, where the unit of bond lengths is in angstroms; (e), (f), (g) and (h) are the conditional settings for the restricted geometry optimization. For a specific geometry, all the π orbital interactions and spatial exchange interaction between the double bonds (or groups) have been set equal to zero, except for the interactions between the red double bonds. The data in parentheses are calculated by using our 2007 method.

8.2.1. Versions of Our 2011 Method

In the process of improving our 2007 method, in order to ensure and confirm the reliability of the source codes of calculation program, three versions of our 2011 method have been written.¹ The first version can only be performed at the RHF and DFT levels of theory. The second version is suitable for the RHF and MPn calculations. The third one is the combination of the above two versions, and it can be used to localize geometry at any level of theory. Finally, the third version is called our 2011 method.

8.2.1.1. First version

At the DFT (density functional theory) level of theory, for example, the GL geometry of benzene is optimized under the following conditional settings:

- (i) Before each SCF iteration, as done in our 2007 method, set $f^{\pi}_{\lambda,\rho} = 0$ and $s^{\pi}_{\lambda,\rho} = 0$ when the π -type AO $\phi_{\lambda} \in$ the P-th double bond, and the π -type AO $\phi_{\rho} \in$ the Q-th double bond, P, Q = A, B, C and P ≠ Q (Figure 8-3e).
- (ii) whenever the calculation of a two-electron exchange integral is finished, set the two-electron exchange integral $\langle \lambda_p \rho_q | \mu_p \omega_q \rangle = 0$ if $p \neq q$ (Figure 8-3g), where, for example, λ_p and ρ_q in the symbol $\langle \lambda_p \rho_q | \mu_p \omega_q \rangle$ mean that a π type of AO $\phi_{\lambda} \in$ fragment P, and a π type of AO $\phi_{\rho} \in$ fragment Q. Hereafter, the two-electron exchange integrals $\langle \lambda_p \rho_q | \mu_p \omega_q \rangle$ are called the particular exchange integrals.

In the GL geometry, as a result of the conditional settings, the π -electrons, as well as the π -MOs, are absolutely localized on their respective C=C double bonds. For the two GL geometries optimized respectively by using our 2007 method and our 2011 method at B3LYP/6-31G* level, the characters of π -MOs, such as the AO coefficients, energy levels (eigenvalues) of molecular orbitals, and Mulliken AO populations (Table 8-4 presented in Appendix), are different. For example, the 19-th MO, as a π MO, is absolutely localized on the C(1)=C(2) double bond, and its energy level is, respectively, -0.2856 hartree (2007) and -0.2794 hartree (2011). In addition, the Mulliken population for the p_z of C(1) atom is 0.52163 (2007) and 0.52832 (2011).

In a similar way, can get a GE-1 geometry, the related conditional settings are shown in Figure 8-3f and Figure 8-3h. In the GE-1 geometry, the π -electrons, as well as the π -MOs, are absolutely localized in the following two groups: -HC(1)=C(2)H-HC(3)=C(4)H-, and -HC(5)=C(6)H-.

8.2.1.2. Second Version

In the second version of our 2011 method, conditional deletion of Fock matrix elements is replaced by conditionally deleting two-electron integrals and one-electron matrix elements ($h_{\lambda,\rho}$). Actual calculations show that, for a planar conjugated molecule, due to the π - and σ -type AOs are orthogonal, so two-electron integrals $\langle \sigma\pi | \sigma\sigma \rangle = 0$, and $\langle \sigma\pi | \pi\pi \rangle = 0$. But, $\langle \sigma\sigma | \pi\pi \rangle \neq 0$, $\langle \sigma\pi | \sigma\pi \rangle \neq 0$. At the RHF and MPn levels of theory, in order to ensure that π -electrons are absolutely localized on their respective double bonds, the GL geometry of benzene can be optimized under the following restrictions:

- (i) Setting $h^{\pi}_{\lambda,\rho} = 0$, $s^{\pi}_{\lambda,\rho} = 0$ when π -type AO $\phi_{\lambda} \in$ the P-th double bond, and π -type AO $\phi_{\rho} \in$ the Q-th double bond ($P \neq Q$).
- (ii) Setting two-electron integrals of 15 types equal to zero. The 15 types of two-electron integrals (the 15 types of integrals) are represented by the red symbols in Figure 8-4.

For the GL geometry of benzene, the above two sets of settings can ensure:

- (i) Fock matrix elements $f^{\pi}_{\lambda,\rho} = 0$ when π -type AO $\phi_{\lambda} \in$ the P-th double bond, and π -type AO $\phi_{\rho} \in$ the Q-th double bond, $P \neq Q$;
- (ii) Particular two-electron exchange integrals between the localized double bonds are equal to zero;
- (iii) At the MPn level of theory, the MO two-electron exchange terms in Equation (8-8) are in line with the principle of differential overlap.

According to Table 8-4 (presented in Appendix), the differences, in the π -MO characters, between the GL(2011) geometry and the GL(2007) geometry are obvious, and they depend upon the level of theory, where the symbols "GL(2011) and GL(2007)" mean that two GL geometries are obtained, respectively, from our 2011 method and our 2007 method. For the GL(2011) and GL(2007) geometries of benzene, for example, the differences $d\varepsilon_{19}$ in the energy level ε_{19} of 19-th MO are as follows:

kl	$\sigma\sigma$	$\pi_P \pi_P$	$\pi_Q \pi_Q$	$\sigma\pi_P$	$\sigma\pi_Q$	$\pi_P \pi_Q$	$\pi_S \pi_T$
ij	$\langle ij kl \rangle$						($S \neq T; S \neq P, Q; T \neq P, Q$)
$\sigma\sigma$	$\langle \sigma\sigma \sigma\sigma \rangle$ $\neq 0$	$\langle \sigma\sigma \pi_P \pi_P \rangle$ $\neq 0$	$\langle \sigma\sigma \pi_Q \pi_Q \rangle$ $\neq 0$	$\langle \sigma\sigma \sigma\pi_P \rangle$ $= 0$	$\langle \sigma\sigma \sigma\pi_Q \rangle$ $= 0$	$\langle \sigma\sigma \pi_P \pi_Q \rangle$ $= 0$ set	$\langle \sigma\sigma \pi_S \pi_T \rangle$ $= 0$ set
$\pi_P \pi_P$	$\langle \pi_P \pi_P \sigma\sigma \rangle$ $\neq 0$	$\langle \pi_P \pi_P \pi_P \pi_P \rangle$ $\neq 0$	$\langle \pi_P \pi_P \pi_Q \pi_Q \rangle$ $\neq 0$	$\langle \pi_P \pi_P \sigma\pi_P \rangle$ $= 0$	$\langle \pi_P \pi_P \sigma\pi_Q \rangle$ $= 0$	$\langle \pi_P \pi_P \pi_P \pi_Q \rangle$ $= 0$ set	$\langle \pi_P \pi_P \pi_S \pi_T \rangle = 0$ $\langle \pi_P \pi_S \pi_P \pi_T \rangle = 0$ set
$\pi_Q \pi_Q$	$\langle \pi_Q \pi_Q \sigma\sigma \rangle$ $\neq 0$	$\langle \pi_Q \pi_Q \pi_P \pi_P \rangle$ $\neq 0$	$\langle \pi_Q \pi_Q \pi_Q \pi_Q \rangle$ $\neq 0$	$\langle \pi_Q \pi_Q \sigma\pi_P \rangle$ $= 0$	$\langle \pi_Q \pi_Q \sigma\pi_Q \rangle$ $= 0$	$\langle \pi_Q \pi_Q \pi_P \pi_Q \rangle$ $= 0$ set	$\langle \pi_Q \pi_Q \pi_S \pi_T \rangle = 0$ $\langle \pi_Q \pi_S \pi_Q \pi_T \rangle = 0$ set
$\sigma\pi_P$	$\langle \sigma\pi_P \sigma\sigma \rangle$ $= 0$	$\langle \sigma\pi_P \pi_P \pi_P \rangle$ $= 0$	$\langle \sigma\pi_P \pi_Q \pi_Q \rangle$ $= 0$	$\langle \sigma\pi_P \sigma\pi_P \rangle$ $\neq 0$	$\langle \sigma\pi_P \sigma\pi_Q \rangle$ $= 0$ set	$\langle \sigma\pi_P \pi_P \pi_Q \rangle$ $= 0$	$\langle \sigma\pi_P \pi_S \pi_T \rangle$ $= 0$
$\sigma\pi_Q$	$\langle \sigma\pi_Q \sigma\sigma \rangle$ $= 0$	$\langle \sigma\pi_Q \pi_P \pi_P \rangle$ $= 0$	$\langle \sigma\pi_Q \pi_Q \pi_Q \rangle$ $= 0$	$\langle \sigma\pi_Q \sigma\pi_P \rangle$ $= 0$ set	$\langle \sigma\pi_Q \sigma\pi_Q \rangle$ $\neq 0$	$\langle \sigma\pi_P \pi_P \pi_Q \rangle$ $= 0$	$\langle \sigma\pi_P \pi_S \pi_T \rangle$ $= 0$
$\pi_P \pi_Q$ ($P \neq Q$)	$\langle \pi_P \pi_Q \sigma\sigma \rangle$ $= 0$ set	$\langle \pi_P \pi_Q \pi_P \pi_P \rangle$ $= 0$ set	$\langle \pi_P \pi_Q \pi_Q \pi_Q \rangle$ $= 0$ set	$\langle \pi_P \pi_Q \sigma\pi_P \rangle$ $= 0$	$\langle \pi_P \pi_Q \sigma\pi_Q \rangle$ $= 0$	$\langle \pi_P \pi_Q \pi_P \pi_Q \rangle$ $= 0$ set	$\langle \pi_P \pi_Q \pi_S \pi_T \rangle$ $= 0$ set

Figure 8-4. For a planar aromatic molecule, two-electron integrals, $\langle \lambda\rho | \mu\omega \rangle$, of 44 types are related to $\pi\text{-}\pi$ interaction. When the restricted geometry optimization is performed at the HF and Post-SCF levels of theory, 15 types of two-electron exchange integrals, the red symbols, are artificially set equal to zero.

$$d\epsilon_{19}(\text{DFT}) = [\epsilon_{19}(2011) - \epsilon_{19}(2007)] = [(-0.2794) - (-0.2856)] = 0.0062$$

$$d\epsilon_{19}(\text{RHF}) = [\epsilon_{19}(2011) - \epsilon_{19}(2007)] = [(-0.3747) - (0.4065)] = 0.0318$$

$$d\epsilon_{19}(\text{RHF})/d\epsilon_{19}(\text{DFT}) = 5$$

where, for example, the symbol “ $\epsilon_{19}(2011)$ ” represents the energy level of 19-th MO in GL(2011) geometry; the symbol “ $d\epsilon_{19}(\text{DFT})$ ” means the difference, in the B3LYP/6-31G* eigenvalue of 19-th MO, between the GL(2011) and GL(2007) geometries.

At the MP2/6-31G*, as shown by Table 8-5, the difference $dE^{(2)}(\text{GL}) = [E^{(2)}(\text{2011}) - E^{(2)}(\text{2007})]$, in the second order energy correction $E^{(2)}$, between the GL(2011) and GL(2007) geometries is 65.1 kcal/mol. It is so large that the adiabatic delocalization energy, $\Delta E^A = [E(\text{G}) - E(\text{GL})]$, is changed from a destabilizing energy effect $\Delta E^A(\text{2007})$ (88.8 kcal/mol) into a stabilizing energy effect $\Delta E^A(\text{2011})$ (-30.1 kcal/mol). Certainly, the change in the sign of ΔE^A should be attributed to the deletion of the two-electron exchange integrals of 15 types.

In addition, as will be shown in this Chapter, at the same density functional level, our 2011 method and our 2007 method may also give benzene different vertical delocalization energy and ESE, including the differences in the size and sign of the values.

8.2.1.3. Third Version

For the third version of our 2011 method, all the conditional settings, used in the first and second versions, are

Table 8-5. For Benzene at MP2/6-31G* Level, Molecular Energies (hartree), $E(\text{RHF})$ and $E(\text{MP2})$, of Ground State and GL Geometry, Second Order Energy Correlation $E^{(2)}$ (hartree), and Energy Effect ΔE^A (kcal/mol).

	Ground	GL(2007)	GL(2011)
$E(\text{RHF})$	-230.70183	-230.76006	-230.67433
$E^{(2)}$	-0.75591	-0.83921	-0.73550
$E(\text{MP2})$	-231.45773	-231.59928	-231.40983
$\Delta E^A(\text{MP2})$		88.8	-30.1

For example, the symbol “GL(2007)” denotes the GL geometry obtained from our 2007 method

included. Therefore, the third version is the combination of the first version and second version, and it can be used to restrictedly optimize GL and GE-m geometries at any level of theory.

8.2.2. Reliable Our 2011 Method

The source codes of PC-Games need to be modified in order to deleting the 15 types of two-electron exchange integrals. Therefore, the rationality and reliability of the modified source codes must be verified. The verification method is to compare the calculation results that are obtained from the different versions of our 2011 method and from the related methods reported in the literatures.

8.2.2.1. Comparison between Program I and Program II

The conditional settings used by above three versions of our 2011 method, together with those used by our 2007 method, are summarized in Figure 8-5. These versions are renamed to “Program IV”, “Program III” and “Program V”. In Figure 8-5, an additional program, called “Program I”, is designed in order to prove that the source code of our 2011 method is reliable. Meanwhile, our 2007 method is renamed to “program II”

For the “program I”, according to Figure 8-5a, the result of $f^{\pi}_{\lambda\rho} = 0$ is achieved by the following conditional settings:

when π -type AO $\phi_\lambda \in$ the P-th double bond, and π -type AO $\phi_\rho \in$ the Q-th double bond ($P \neq Q$)

- (i) setting $h^{\pi}_{\lambda\rho} = 0$.
- (ii) 15 types of two-electron integrals, except for the particular two-electron exchange integrals, are set equal to zero.

Therefore, the “program I” can be considered as a modified version of “Program III” in Figure 8-5c. At the RHF level of theory, “program I” and “program II” (our 2007 method in Figure 8-5b) should be equivalent according to Equation (8-6). At the RHF level of theory, as shown by Table 8-6, the benzene’s ESE(II) (-46.5 kcal/mol), obtained from our 2007 method (“program II” in Figure 8-5), is exactly equal to ESE(I) (-46.5 kcal/mol) from the “program I”.

Because Program II (our 2007 method) completely retains two-electronic integrals, and since all two-electronic integrals represented by the red symbols (all the red two-electron integral), except for the particular two-electronic exchange integrals, have been deleted in Program I, as discussed in Section 8.1.4., Program I should not be equivalent to Program II at the MP2 level of theory. In fact, as shown by the data listed in Table 8-6, the values (-33 kcal/mol) of ESE(I), obtained from the program I, is greatly different from ESE(II) (-51.2 kcal/mol) obtained from the program II (our 2007 method).

Setting matrix elements equal to zero	Additional settings
Particular π -sub h^π matrix for GL geometry	Particular π -sub overlap integrals s^π for GL geometry
(a) Program I (modified program III) 15 types of two-electron integrals are set equal to zero except for following integrals among three localized double bonds. $\langle \lambda_A \rho_B \mu_A \omega_B \rangle \neq 0$ $\langle \lambda_A \rho_C \mu_A \omega_C \rangle \neq 0$ $\langle \lambda_B \rho_C \mu_B \omega_C \rangle \neq 0$	(c) Program III (second version of our 2011 method) 15 types of two-electron exchange integrals are set equal to zero
(b) Program II (Our 2007 method) $\langle \lambda_A \rho_B \mu_A \omega_B \rangle = 0$ $\langle \lambda_A \rho_C \mu_A \omega_C \rangle = 0$ $\langle \lambda_B \rho_C \mu_B \omega_C \rangle = 0$	(d) Program IV (first version of our 2011 method) $\langle \lambda_A \rho_B \mu_A \omega_B \rangle \neq 0$ $\langle \lambda_A \rho_C \mu_A \omega_C \rangle \neq 0$ $\langle \lambda_B \rho_C \mu_B \omega_C \rangle \neq 0$
(e) Program V (combination of programs III and IV) 15 types of two-electron integrals are set equal to zero	

Figure 8-5. The conditional settings, performed in each of the five programs, for optimizing the GL geometry of benzene.

8.2.2.2. Comparison among Programs III, IV and V

At the RHF level of theory, three programs (III, IV and V) should be equivalent according to their conditional settings (Figure 8-5). The data listed Table 8-6 indicate that the ESE value of benzene obtained from these three programs is indeed the same (-34.9 kcal/mol) (The unit of the following ESE values are all in kcal/mol).

At the MP2 level, the programs III and V are equivalent, but these two programs are not equivalent to the program IV because Program IV retains all the red two-electron integrals except for the particular exchange integrals. Therefore, ESE(III) (-35.8) = ESE(V) (-35.8) \neq ESE(IV) (-52.1).

The difference between the Program I and Program III is that, in the Program I, the particular exchange integrals remain unchanged. Correspondingly, at MP2/6-31G*, ESE(I) (-33.0) \neq ESE(III) (-35.8), and at RHF level, ESE(I) (-46.5) \neq ESE(III) (-34.9).

At RHF/6-31G* level, ESE(I) (-46.5) = ESE(II) (-46.5). But, at MP2/6-31G* level, ESE(I) (-33.0) \neq ESE(II) (-51.2), which, together with ESE(II) (-51.2) \approx ESE(IV) (-52.2) and ESE(I) (-33.0) \approx ESE(III) (-35.8), indicates that the influence of the particular exchange integrals on the MP2 value is less than that of 15 types of integrals.

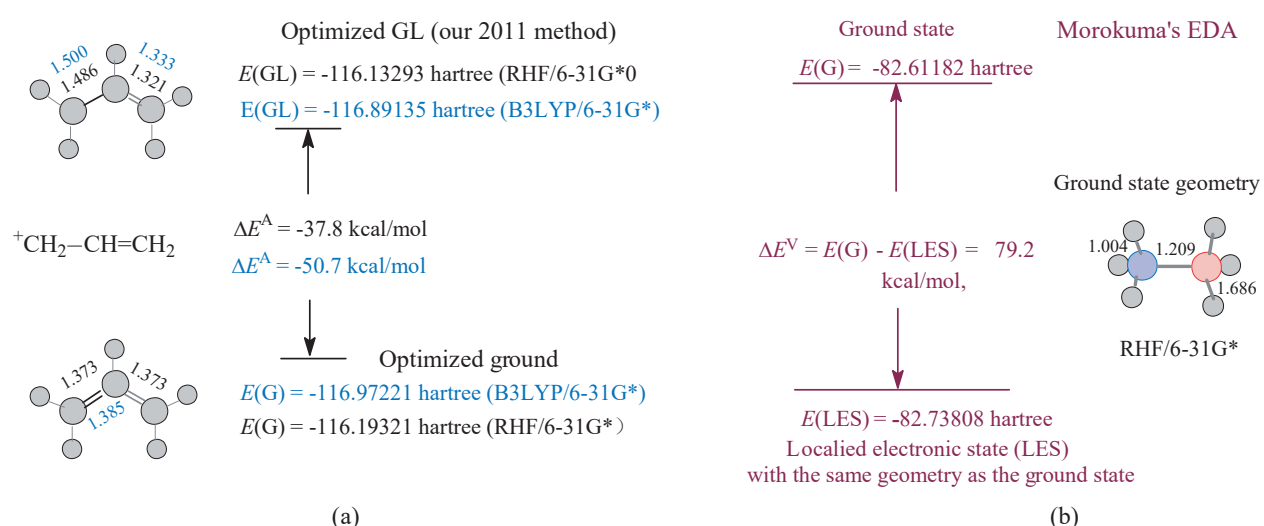
PBE96 is a density functional without HF-EX. At the PBE96 level of theory, therefore, the GL geometry of benzene obtained from our 2011 method should be the same as that obtained from our 2007 method. Therefore, the ESE values of benzene, calculated by the Programs II, IV and V, are all equal to -35.4 kcal/mol (Table 8-6).

The above comparison confirms that the modified source code for executing the conditional setting is reliable.

8.2.2.3. Conjugated Molecules without π MO Exchange

Table 8-6. ESE (kcal/mol) of Benzene, and Energy Differences [$E(G)$ - $E(GL)$] (kcal/mol) for $\text{CH}_2=\text{CH}-\text{H}_2\text{C}^+$ and $\text{CH}_2=\text{CH}-\text{BH}_2$, Obtained from Our Five Programs at 6-31G* Levels.

	ESE			$E(G) - E(GL)$		$E(G) - E(GL)$	
	Benzene			$\text{CH}_2=\text{CH}-\text{H}_2\text{C}^+$		$\text{CH}_2=\text{CH}-\text{BH}_2$	
	RHF	MP2	PBE96	RHF	B3LYP	RHF	B3LYP
I (revised program III)	-46.5	-33.0		-37.8		-7.3	
II (our 2007 method)	-46.5	-51.2	-35.4	-37.8	-50.7	-7.3	-10.9
III (second version)	-34.9	-35.8		-37.8		-7.3	
IV (first version)	-34.9	-52.1	-35.4	-37.8	-50.7	-7.3	-10.9
V (third version)	-34.9	-35.8	-35.4	-37.8	-50.7	-7.3	-10.9



Scheme 8-1

In the ground state geometries of allyl cation $\text{CH}_2=\text{CH}-\text{H}_2\text{C}^+$ and vinylborane $\text{CH}_2=\text{CH}-\text{BH}_2$, there are no the π MO exchange interaction and spatial exchange interaction between the groups $\text{CH}_2=\text{CH}-$ and $-\text{X}$ ($\text{X} = -\text{CH}_2-$, $-\text{BH}_2$). At RHF and B3LYP levels, the five programs in Figure 8-5 should be equivalent to each other when calculating the molecular energy of the GL geometry of these two molecules. For allyl cation (Scheme 8-1a) at RHF/6-31G* level, for example, the values of the energy difference [$E(G) - E(GL)$], obtained from the five programs, are all equal to -37.8 kcal/mol (Table 8-6). The B3LYP/6-31G* values, obtained from the “program II”, “program IV”, and “program V”, are also the same (-50.7 kcal/mol). Accordingly, the two versions of our 2011 method, i. e. “Program III” and program IV, can be combined into “program V” (the third version of our 2011 method).

Because the MP2 energy correlation depends only upon the retention of two-electron integrals, it is unsurprising that for allyl cation at the MP2/6-31G* level, the values of the energy difference [$E(G) - E(GL)$], obtained from our 2007 method and our 2011 method, are different and they are -38.1 and -49.5 kcal/mol, respectively.

All these confirm that the source codes of our new calculation programs are reliability.

8.2.2.4. Comparison with Morokuma's Method

Morokuma's intermolecular energy decomposition analysis (Morokuma's EDA), as a standard program, has been incorporated into PC-Gamess package.

According to the description by Morokuma himself,⁶⁴ the setting's procedure is as follow: before SCF iteration, scanning one- and two-electron integrals, the particular one- and two-electron integrals between the monomers NH₃ and BH₃ are set equal to zero in line with the principle of intermolecular differential overlap. Accordingly, our 2011 method is the same as that of Morokuma's EDA in the calculation principle. Based on that Morokuma's method can only be used at RHF level of theory and can only be used to calculate the intermolecular interaction energy, NH₃BH₃, a donor-acceptor complex, is used as a model molecule to compare our 2011 method with Morokuma's EDA in order to prove that our 2011 method is reasonable, and the calculation result is reliable.

The geometry of the complex NH₃–BH₃ is fully optimized at the RHF/6-31G* level, and its molecular energy $E(G)$ is -82.61182 hartree (Scheme 8-1b). Then, our 2011 method¹ is used to perform a single-point energy calculation, on the optimized geometry of NH₃–BH₃, under the following conditional settings:

- (i) Setting $f_{\lambda,\rho} = 0$, and $s_{\lambda,\rho} = 0$ when (π and σ) AO $\phi_\lambda \in \text{NH}_3$, and (π and σ) AO $\phi_\rho \in \text{BH}_3$
- (ii) Setting all two-electron exchange integrals $\langle \lambda_p \rho_q | \mu_p \omega_q \rangle = 0$ ($p = \text{NH}_3$, $q = \text{BH}_3$),

The conditional single-point energy calculation, performed using our 2011 method, gives NH₃–BH₃ a localized electron state (LES). In this state, all molecular orbitals, as well as all electrons, have been absolutely localized on their respective partners NH₃ and BH₃, and meanwhile the complex geometry is kept unchanged.

For the localized electron state of the complex NH₃–BH₃, as shown by our calculations, the molecular energy $E(\text{LES})$, obtained from our 2011 method, is the same as that obtained from Morokuma's EDA, and it is -82.73808 hartree (Scheme 8-1b), leading to that the energy difference [$E(G) - E(\text{LES})$] between the ground and its localized electron states is 79.2 kcal/mol. The energy difference [$E(G) - E(\text{LES})$] can be considered as an energy effect associated with electron delocalization between the monomers NH₃ and BH₃, and it is destabilizing. It should be emphasized again that this destabilizing energy effect is calculated, respectively, using our 2011 method and Morokuma's EDA, and the two calculated values are the same.

8.2.2.5. Comparison with BLW Method

It has been detailed in Section 8.0.4 that, in the localized geometry obtained from BLW method, only the charge transfer interactions between the localized double bonds are artificially excluded. In contrast, our program excludes all the interactions, including the MO charge transfer and exchange interactions and the spatial exchange interaction, from between the localized double bonds in GL geometry.

In the case of a carbocation such as CH₂=H–H₂C⁺, there are only π -MO charge transfer interactions between the CH₂=H– and –CH₂⁺ groups. Therefore, it is a useful molecule to allow a comparison of our methods (including our 2007 and 2011 methods) with the BLW method.

At (RHF and B3LYP)/6-31G* levels, as shown by the data listed in Table 8-7, the three methods, our 2007 method, our 2011 method and the BLW method, give a same GL geometry for allyl cation. At the RHF/6-31G* level, for example, the distances (1.486 and 1.321 Å) of the CC single bond and CC double bond in the localized geometry, obtained from our methods, are equal to those obtained from BLW method, and the corresponding values of the energy differences [$E(G) - E(\text{GL})$] both are equal to -37.8 kcal/mol. The same conclusion can be obtained from the calculations at B3LYP/6-31G* level.

Therefore, our 2011 method is reliable. The BLW method is just a special case of our 2011 method.

Table 8-7. Molecular Energy $E(GL)$ (Hartree), and Single and Double Bond Distances r_{C-C} and $r_{C=C}$ (\AA) for the GL Geometry of Allyl Cation $\text{CH}_2=\text{CH}-\text{CH}_2^+$, and Energy Difference [$E(G) - E(GL)$] (kcal/mol) between Ground State and GL Geometry, Obtained Respectively from Our 2011 Method and BLW Method.

	RHF/6-31G*				B3LYP/6-31G*			
	$E(GL)$	r_{C-C}	$r_{C=C}$	$E(G) - E(GL)$	$E(GL)$	r_{C-C}	$r_{C=C}$	$E(G) - E(GL)$
^a Our programs	-116.13292	1.486	1.321	-37.8	-116.89135	1.500	1.333	-50.7
^b BLW program	no reported	1.486	1.321	-37.8	no reported	1.500	1.333	-50.7

^a Our programs refer to our 2007 and 2011 methods. ^bThe values obtained from BLW are cited from: (i) Mo, Y. 2004. "Resonance Effect in the Allyl Cation and Anion: A Revisit." *J. Org. Chem.*, 69: 5563-5567; (ii) Mo, Y.; Song, L.; Lin, Y. 2007. "Block-Localized Wave function (BLW) Method at the Density Functional Theory (DFT) Level." *J. Phys. Chem. A*, 111: 8291-8301. For the ground state, the molecular energy are -116.19321 (HF/6-31G*) and -116.97221 (B3LYP/6-31G*) Hartree, and the bond lengths r_{C-C} and $r_{C=C}$ are 1.373 and 1.373 \AA (RHF/6-31G*), and 1.385 and 1.385 \AA (B3LYP/6-31G*).

8.3. EXTRA STABILIZATION ENERGY OF BENZENE

After confirming the reliability of the calculation results obtained from our 2011 method, one of the purposes is of course to demonstrate the rationality of our 2011 method by calculating ESEs of various aromatic molecules, and is to emphasize that the rationality has nothing to do with the theoretical level and basis set size.

Using our 2011 method, it can prove that, for trans-polyene, the energy effects $\Delta E^{\text{Am}} = [E(\text{GE-m}) - E(\text{GL})]$ are still additive. For trans-1,3,5,7-octatetraene at 6-311G(2df,p) level, for example, the values (kcal/mol) of the energy effects, ΔE^{A} , $\sum \Delta E^{\text{Am}}$ and $(\Delta E^{\text{A}} - \sum \Delta E^{\text{Am}} - \sum \Delta E_n^{\text{Am}})$, are as follows:

8.80, 9.78, -1.16 (RHF); 9.35, 9.29, 0.35 (B3LYP); 8.20, 9.46, -1.27 (MP2).

Based on the additivity of the energy effects ΔE^{Am} for polyene, our 2011 method has been used to calculate the ESE (extra stabilization energy) of benzene,¹ and will be used to calculate the ESEs of various aromatic molecules in Chapter 9. These calculations have shown and will confirm that, for the aromatic molecules such as benzene, polycyclic benzenoid hydrocarbon and [N]annulenes ($N = 4n+2$), the vertical delocalization energy ΔE^V and the adiabatic delocalization energy ΔE^{A} are always stabilizing. All these calculations will demonstrate that our 2011 method is more reasonable than our 2007 method. The final purpose of the calculations is to confirm that it is really necessary to exclude the spatial exchange interaction from between the localized double bonds (or localized groups) in localized geometry (or localized electronic state).

In this section, to facilitate the discussion, the symbols " $E^{\circ}(\text{G})$ ", " $E^{\circ}(\text{GL})$ " and " $E^{\circ}(\text{GE-m})$ " with the superscript "o" represent the molecular energies of the following three geometries: ground state geometry (G) of a molecule, and its GL(2007) and GE-m(2007) geometries, where, for example, the symbol "GL(2007)" means that the GL geometry of a conjugated molecule is optimized by using our 2007 method. The corresponding energy differences [$E^{\circ}(\text{G}) - E^{\circ}(\text{GL})$] and [$E^{\circ}(\text{GE-m}) - E^{\circ}(\text{GL})$] are denoted as ΔE_o^{A} and ΔE_o^{Am} with the subscript "o". The symbols " $E(\text{G})$ ", " $E(\text{GL})$ " and " $E(\text{GE-m})$ " without the superscript represent the molecular energies of the G (ground state geometry), GL(2011) and GE-m(2011) geometries. Certainly, $E(\text{G}) = E^{\circ}(\text{G})$, and energy differences [$E(\text{G}) - E(\text{GL})$] = ΔE^{A} and [$E(\text{GE-m}) - E(\text{GL})$] = ΔE^{Am} .

8.3.1. Hartree-Fock Exchange Effects.

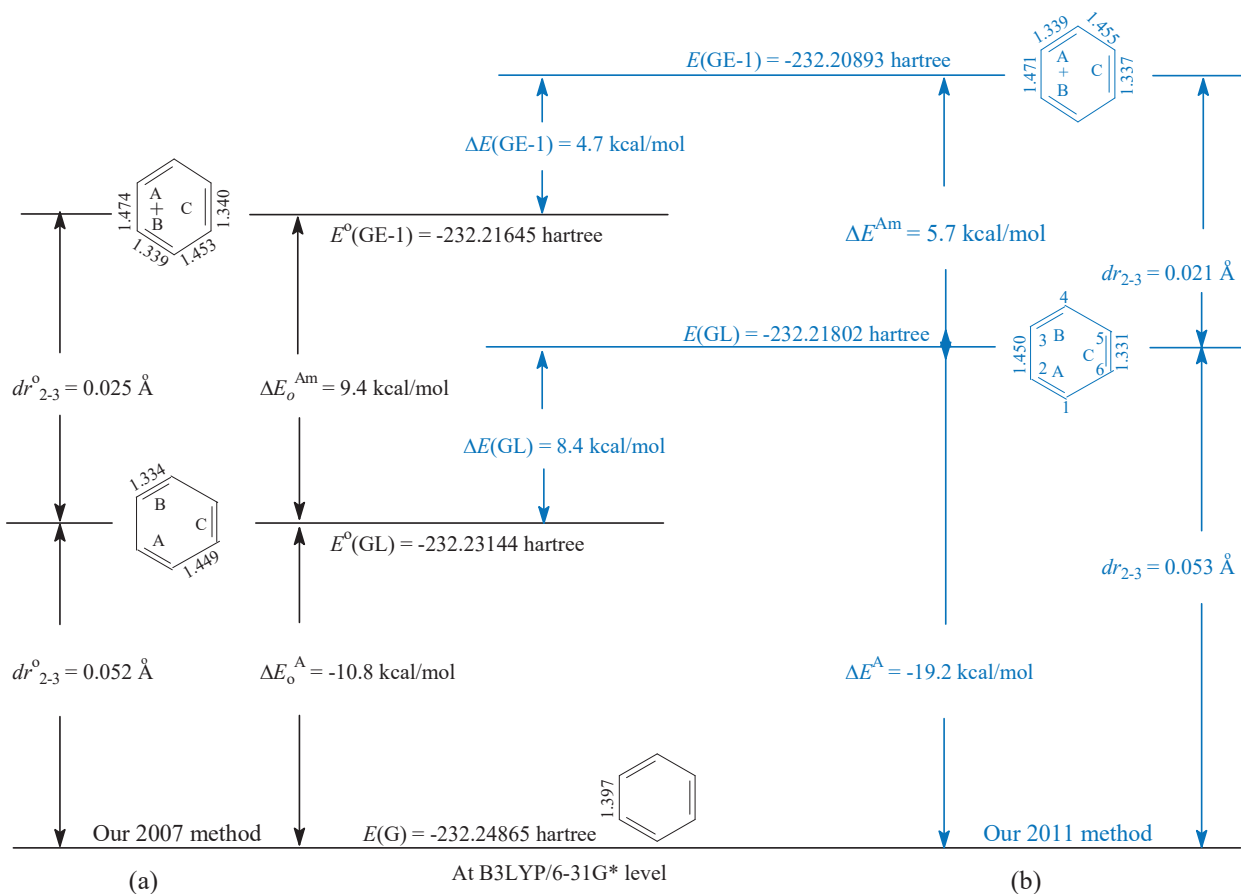


Figure 8-6. Hartree-Fock exchange effects. For benzene, the molecular energies (hartree) of the ground state (G), GL and GE-1 geometries, and molecular energy differences (kcal/mol) and bond length differences (\AA) are obtained from our 2007 (black data) method and from our 2011 method (blue data) at the B3LYP/6-31G* level.

According to Equation (8-6), the particular two-electron exchange integrals, $\langle \lambda \rho | \mu \omega \rangle$, play a stabilizing role when the corresponding density matrix elements $d\rho\omega > 0$. In the GL(2011) and GE-m(2011) geometries, in addition to the π MO charge transfer and exchange interactions, the spatial exchange interaction (particular exchange integrals) have also been excluded from between the localized double bonds (or localized groups). As the results, as shown by Figure 8-6, $|E(\text{GL})| < |E^o(\text{GL})|$, and $|E(\text{GE-1})| < |E^o(\text{GE-1})|$. At B3LYP/6-31G* level, for example, the molecular energies (hartree) of the GL and GE-m geometries, calculated by our 2007 method and our 2011 method, are as follows:

$$\begin{aligned} E(\text{GL}) &= -232.21802, E(\text{GE-1}) = -232.20893 \\ E^o(\text{GL}) &= -232.23144, E^o(\text{GE-1}) = -232.21645 \end{aligned}$$

And can get the following molecular energy differences (kcal/mol):

$$\begin{aligned} |\Delta E^A| &= [E(\text{G}) - E(\text{GL})] = |-19.2| > |\Delta E_o^A| = |-10.8| \\ [E(\text{GL}) - E^o(\text{GL})] (8.4) &> [E(\text{GL-1}) - E^o(\text{GE-1})] (4.7) \\ \Delta E^{\text{Am}} &= [E(\text{GE-m}) - E(\text{GL})] (5.7) < \Delta E_o^{\text{Am}} (9.4). \end{aligned}$$

The trends of these molecular energy changes are consistent with the role of the particular exchange integrals in weakening two-electron Coulomb interaction. The changes in the distances (\AA) of the corresponding C(2)-C(3) single bond are as follows:

$$\begin{aligned} r_{2-3}(\text{GE-1}) & (1.471) > r_{2-3}(\text{GL}) (1.450 \text{ \AA}) \\ r^o_{2-3}(\text{GE-1}) & (1.474 \text{ \AA}) > r^o_{2-3}(\text{GL}) (1.449 \text{ \AA}) \\ dr_{2-3} & = [r_{2-3}(\text{GE-1}) - r_{2-3}(\text{GL})] (0.021 \text{ \AA}) < dr^o_{2-3} (0.025 \text{ \AA}) \end{aligned}$$

The bond distance change, dr^o_{2-3} , resulted from a larger energy effect ΔE^{Am} , is larger than the bond distance change, dr_{2-3} , resulted from a smaller energy effect ΔE^{Am} , where $r_{2-3}(\text{GE-1})$ and $r^o_{2-3}(\text{GE-1})$ are the distance of the C(2)-C(3) singe bond, respectively, in the GE-1(2011) and GE-1(2007) geometries.

8.3.2. More Reasonable Our 2011 Method

Table 6-4 and Table 8-1 indicate that, for benzene, the vertical delocalization energy ΔE_o^V and adiabatic delocalization energy ΔE_o^A , obtained from our 2007 method at the RHF and post-SCF levels of theory, are unreasonable because they are destabilizing. A reasonable calculation method should ensure that the extra stabilization energy of an aromatic molecule is in a reasonable range and the values of its components ΔE^A and ΔE^{Am} are all reasonable. It will be proved in many ways that our 2011 method is more reasonable than our 2007 method. It also will be indicated that the Hartree-Fock exchange (HF-EX) and density functional exchange (DF-EX) both play an important role in ensuring the rationality of the calculation of the extra stabilization energy and its components.

The range of a set of values of a physical quantity such as ESE may help us to understand the influences of the theoretical level and basis set size on a physical quantity, and certainly may be used to say which method, our 2011 method or our 2007 method, is more reasonable. The range, denoted as “Range(ESE,2011)”, is defined as the difference between the greatest and smallest values in a set of the ESE(2011) values calculated by our 2011 method. The similar symbol is “Range(ΔE^A ,2011)”, and so on.

8.3.2.1. ΔE^A (2011) Becoming Always Stabilizing.

For benzene, an inspection of Table 6-4, Table 8-2 and Table 8-8 shows the following facts:

- (i) At the RHF and MP2 levels of theory (Table 6-4), the energy differences (adiabatic delocalization energy) $\Delta E^A(2007)$ is always destabilizing. The larger the basis set size, the more destabilizing the energy difference $\Delta E^A(2007)$. At MP2(Full)/6-311G** level, $\Delta E^A(2007) = 136.1 \text{ kcal/mol}$, and it is the most destabilizing. At PBE96/6-31G* level, $\Delta E^A(2007) = -20.9 \text{ kcal/mol}$, and it is the most stabilizing. The range of all the values of $\Delta E^A(2007)$ listed in Table 6-4 and Table 8-2 is 157 kcal/mol.
- (ii) At the density functional level, the energy effect $\Delta E^A(2007)$ is destabilizing when the functional contains HF-EX component (Table 8-2).
- (iii) On the contrary, as shown by Table 8-8 and Table 8-9, the energy effect $\Delta E^A(2011)$ is always stabilizing without exception, which is the fundamental difference between our 2011 method and 2007 method. At RHF and CPBE96 level, the ranges of $\Delta E^A(2011)$ are -1.9 and -2.0 kcal/mol, and they are the smallest of all the ranges listed in Table 8-8.

According to the literatures cited in this book, the adiabatic delocalization energy and vertical delocalization energy of benzene are stabilizing, no matter how they are calculated, either by using the valence bond method or by using molecular orbital methods at empirical or semi-empirical or non- empirical level. In the case of benzene,

Table 8-8. For Benzene, ESE (kcal/mol) and Its Components (kcal/mol), $\sum\Delta E^{\text{Am}}$ and ΔE^{A} , Obtained from Our 2011 Method.

		6-31G*	6-311 G**	6-311++G (2d,2p)	cc-PVTZ	Range	Average
RHF	$\sum\Delta E^{\text{Am}}$	17.3	17.5	15.7	16.8	0.7	
	ΔE^{A}	-17.6	-16.7	-17.0	-15.7	-1.9	-16.8
	<i>ESE</i>	-34.9	-34.2	-32.7	-32.5	-2.4	-33.6
MP2	$\sum\Delta E^{\text{Am}}$	5.7	7.1	10.9	16.8	11.1	
	ΔE^{A}	-30.1	-28.2	-22.4	-16.7	-13.4	-24.4
	<i>ESE</i>	-35.8	-35.3	-33.3	-33.5	-2.5	-34.5
CISD	$\sum\Delta E^{\text{Am}}$	12.4	13.8				
	ΔE^{A}	-22.0	-20.0			-2.0	-21.0
	<i>ESE</i>	-34.4	-33.8			-0.6	-34.1
CCSD	$\sum\Delta E^{\text{Am}}$	16.7					
	ΔE^{A}	-16.6					
	<i>ESE</i>	-33.3				0.0	-33.3
B3LYP	$\sum\Delta E^{\text{Am}}$	17.1	20.4	24.3	27.3	10.2	
	ΔE^{A}	-19.2	-16.4	-12.5	-10.0	-9.2	-14.5
	<i>ESE</i>	-36.3	-36.8	-36.8	-37.3	-1.0	-36.8
XPBE96	$\sum\Delta E^{\text{Am}}$	12.5	16.5	22.0	23.9	11.4	
	ΔE^{A}	-20.4	-16.9	-12.1	-10.4	-10.0	
	<i>ESE</i>	-32.9	-33.4	-34.1	-34.3	-1.4	-33.7
CPBE96	$\sum\Delta E^{\text{Am}}$	19.1	19.0	17.0	18.5	2.1	
	ΔE^{A}	-18.6	-18.1	-18.3	-16.6	-2.0	-17.9
	<i>ESE</i>	-37.7	-37.1	-35.3	-35.1	-2.6	-36.3
PBE96	$\sum\Delta E^{\text{Am}}$	14.5	18.2	23.2	26.5	12.0	
	ΔE^{A}	-20.9	-17.8	-13.0	-10.2	-10.7	-15.5
	<i>ESE</i>	-35.4	-36.0	-36.2	-36.7	-1.3	-36.1
Range	<i>ESE</i>	-4.8	-3.7	-4.1	-4.8		-2.5
Average	<i>ESE</i>	-35.1	-35.2	-34.7	-34.9		

Table 8-9. For Benzene, ESE (kcal/mol) and Its Components (kcal/mol), $\Sigma\Delta E^{\text{Am}}$ and ΔE^{A} , Obtained from Our 2011 Method.

Basis sets	Energy effects	Pure EX without HF-EX and Corr.		Pure Corr. with HF-EX		EX-Corr. without HF-EX			Hybrid with HF-EX	
		SLATER	XPBE96	CPBE96	LYP	PBE96	SVWN5	BLYP	PBE0	X3LYP
6-31G*	ΔE^{A}	-19.6	-20.4	-18.6	-18.0	-20.9	-20.1	-20.5	-19.3	-19.1
	$\Delta E^{\text{A}1}$	5.3	4.2	6.4	6.3	4.8	5.5	4.7	6.0	5.8
	ESE	-35.5	-32.9	-37.7	-36.8	-35.4	-36.7	-34.5	-37.4	-36.5
6-311G**	ΔE^{A}	-15.7	-16.9	-18.1	-17.2	-17.9	-16.5	-17.1	-17.0	-16.2
	$\Delta E^{\text{A}1}$	6.8	5.5	6.3	6.3	6.0	7.0	6.0	6.9	6.9
	ESE	-36.2	-33.4	-37.1	-36.2	-36.0	-37.4	-35.1	-37.8	-36.9
6-311G(2d,2p)	ΔE^{A}	-11.9	-13.9	-18.2	-17.4	-14.1	-12.5	-13.7	-14.0	-13.4
	$\Delta E^{\text{A}1}$	7.9	6.4	5.7	5.7	7.1	8.1	7.0	7.7	7.6
	ESE	-35.7	-33.1	-35.2	-34.5	-35.4	-36.8	-34.6	-37.0	-36.3
6-311G(2df,p)	ΔE^{A}	-9.3	-11.8	-17.2	-16.4	-11.4	-9.5	-11.2	-11.5	-11.0
	$\Delta E^{\text{A}1}$	9.0	7.3	6.0	5.9	8.2	9.3	8.0	8.7	8.6
	ESE	-36.4	-33.7	-35.2	-34.2	-36.1	-37.5	-35.3	-37.7	-36.9
Range	ΔE^{A}	-10.3	-8.6	-1.4	-1.6	-9.5	-10.6	-9.3	-7.8	-8.1
Range	ESE	-0.9	-0.8	-2.5	-2.6	-0.7	-0.8	-0.8	-0.8	-0.6
Average	ESE	-36.0	-33.3	-36.3	-35.4	-35.7	-37.1	-34.9	-37.5	-36.6

therefore, whether these two energy effects are stabilizing or destabilizing can be used as the second criterion to judge the rationality of a calculation method. Accordingly, our 2011 method is more reasonable than our 2007 method, and the calculation results obtained from our 2011 method should be more reliable than from our 2007 method.

8.3.2.2. Theoretical Level and Basis Set Size Effects

For all the ESE(2011) values listed in the Table 8-8 and Table 8-9, the smallest value is -32.5 kcal/mol (RHF/cc-PVTZ), the biggest one is -37.8 kcal/mol (PBE0/6-311G**), and the range of all the ESE values listed in Table 8-8 and Table 8-9 is -5.3 kcal/mol. Of all the ranges listed in Table 8-8, the B3LYP range (the range at B3LYP level of theory) is -1.0 kcal/mol, and it is the smallest. Especially, the B3LYP/6-31G* ESE of benzene

decreases from -39.0 kcal/mol (obtained from our 2007 method) to -36.3 kcal/mol. The value of -36.3 kcal/mol can be considered equal to the well-known experimental value of -36 kcal/mol.

For all the ESE(2007) values presented in Table 6-4 and Table 8-2, the range is large, up to -24.4 kcal/mol. The ratio, Range(ESE,2007)/Range(ESE,2011) = 4.6. The corresponding ranges of a set of ΔE^A values are -20.8 kcal/mol (from our 2011 method) and 157 kcal/mol (from our 2007 method), and the ratio, 157/-20.8, is about 7.5.

But should also pay attention to the influences of the theoretical level and basis set size on the values of the energy effects ΔE^A and $\Sigma \Delta E^{Am}$. At RHF and CPBE96 levels, there is no any type of two-electron exchange between the localized groups in the GL and GE-m geometries obtained from our 2011 method, so the ranges of ΔE^A and $\Sigma \Delta E^{Am}$ are the smallest of all the ranges listed in Table 8-8. At RHF level, for example, the two ranges are -1.9 and 0.7 kcal/mol. All other pairs of the ranges are larger than this pair of the ranges. At B3LYP level, for example, as the base set changes from 6-31G* to cc-PVTZ, the B3LYP value of $\Sigma \Delta E^{Am}$ (2011) monotonically increases from 17.1 kcal/mol to 27.3 kcal/mol, and the absolute value of ΔE^A (2011) monotonically decreases from -19.2 kcal/mol to -10.0 kcal/mol. The corresponding ranges of $\Sigma \Delta E^{Am}$ and ΔE^A are 10.2 and -9.2 kcal/mol, and the range of ESE is -1.0 kcal/mol. The ratio, B3LYP Range(ΔE^A ,2011) to RHF Range(ΔE^A ,2011), is about 5 although the ratio, B3LYP Range(ESE,2011) to RHF Range(ESE,2011), is about 1/2, indicating that the density functional exchange has also obvious influences on the energy effects $\Sigma \Delta E^{Am}$ and ΔE^A .

Accordingly, the theoretical level and the basis set size have a little influence on the value of ESE(2011) although they have a big influence on the values of the $\Sigma \Delta E^{Am}$ (2011) and ΔE^A (2011). Nevertheless, the theoretical level and basis set size have far less influences on the ESE(2011) and ΔE^A (2011) values than on the ESE(2007) and ΔE^A (2007) values.

8.3.2.3. Density Functionals

For all the ESE(2011) values at the density functional levels of theory (Table 8-9), the range is -4.9 kcal/mol, and for all the ESE(2011) values listed in Table 8-8, the range of -5.5 kcal/mol. These two ranges are approximately equal to each other.

According to all the ESE(2011) values listed in Table 8-9, the average value of ESE is -35.9 kcal/mol. At the RHF and post-SCF levels of theory (Table 8-8), the average value is -33.9 kcal/mol. The former's average value (-35.9 kcal/mol) is closer to the experimental value (-36 kcal/mol) than the latter's average value (-33.9 kcal/mol). In terms of the average value, the density functional is more suitable for the calculation of ESE.

Among the four types of the density functionals, only the density functionals of the second type are the pure correlation functional. Therefore, there is no longer any type of exchange interaction between the localized groups when the localized geometry is optimized by using our 2011 method at the CPE96 and LYP levels of theory. As the results, the ranges (kcal/mol) of the CPE96 and LYP values of ΔE^A are -1.4 and -1.6, and they are the smallest of all the ranges listed in Table 8-9. At the first and third types of density functional levels (such as SLATER and SVWN5) of theory, on the contrary, our 2011 method can't exclude the exchange of the density-functional type (DF-type exchange) from between the localized groups in the localized geometry. At SLATER and SVWN5 levels of theory, the ranges (kcal/mol) of ΔE^A are -10.3 (SLATER) and -10.6 (SVWN5), and they are the biggest of all the ranges listed in Table 8-9.

For all the values of ESE(2011) in Table 8-9, the ranges (kcal/mol) of the CPBE96 and LYP values are -2.5 and -2.6, and they are the largest. At the density functional levels of other three types, the ranges are closer to each other, and they are about -0.7 kcal/mol.

At the specific level, such as CPBE96 and SLATER, of theory, the average value (kcal/mol) of a series of ESEs (Table 8-9) is -36.3 (CPBE96) and -36.0 (SLATER), and they are the closest to the experimental value (-36 kcal/mol). From the pure correlation functional to the pure exchange functional, the size order of ESEs (kcal/mol) at 6-31G* level is as follow:

Table 8-10. Vertical Delocalization Energy ΔE^V (kcal/mol) of Benzene Are Calculated Using Our 2011 Method and 2007 Method.

Basis sets	B3LYP		^a RHF		^a MP2		^a MP3	
	2011	2007	2011	2007	2011	2007	2011	2007
DH(2d,2p)	-24.0	-10.1	-29.0	55.4	-27.3	242.7	-23.7	199.0
TVZ	-22.9	-10.4	-26.5	45.7	-27.8	108.0	-25.4	102.5
6-31G(d)	-31.2	-21.0	-31.9	26.0	-37.1	82.8	-32.6	85.1
6-311G(d)	-28.2	-16.4	-30.3	36.8	-33.9	124.9	-29.5	120.2
6-311G(d,p)	-28.5	-16.8	-30.5	36.0	-34.0	125.5	-29.6	120.1
6311-G(2d,2p)	-24.6	-10.2	-28.8	57.4	-26.3	299.4	-22.9	226.3
6311-G(2df,p)	-21.1	-5.7	-28.1	41.9	-27.4	164.4	-24.1	154.5
6-311++G(d,p)	-26.9	-13.9	-29.6	46.8	-33.3	152.5	-29.0	140.3
Range	-10.1	-15.3	-5.4	31.4	-9.8	216.6	-9.7	141.2
Average	-25.9	-13.1	-29.3	43.3	-33.9	162.5	-29.5	143.5

^aRHF, MP2 and Mp3 values are obtained from the MP3 calculation.

-36.8 (LYP, pure correlation) > -36.3 (B3LYP, hybrid) > -34.5 (BLYP, exchange and correlation) > -32.9 (XPBE96, pure exchange).

As long as the exchange interaction has been excluded from between the localized groups in a localized geometry, no matter whether the exchange is HF-type or DF-type, the corresponding ESE will be more reasonable. The pure correlation density functional and the hybrid density functional seem to be more suitable for calculating the ESE when using our 2011 method.

8.4. VERTICAL DELOCALIZATION ENERGY

For Benzene, as a typical aromatic molecule, its vertical delocalization energy must be stabilizing.¹ An inspection of the data listed in Table 8-10 and Table 8-11 shows the most important fact: the vertical delocalization energy, obtained from our 2011 method, is always stabilizing, which has nothing to do with the theoretical level and basis set size. Based on the comparison of Table 8-10 and Table 8-11, the following facts are worth noting:

- (i) At CPBE96 and LYP levels of theory, the ranges (kcal/mol) are -5.6 and -5.7, respectively. These two ranges are the smallest of all the ranges listed in Table 8-11.
- (ii) At RHF level of theory, the range is -5.4 kcal/mol, and the average values is -29.3 kcal/mol. These two values are almost equal to the corresponding CPBE96 and LYP values;
- (iii) From the pure correlation density functional, through the exchange-correlation density functional, to the pure exchange density functional, the size order of ranges (kcal/mol) is as follow: |-5.6| (CPBE96) < |-10.0| (X3BLYP) < |-11.5| (BLYP) < |-12.3| (SLATER); and the corresponding size order of average values (kcal/mol): |-30.3| > |-26.4| > |-25.2| > |-22.4|.

Table 8-11. Vertical Delocalization Energy (kcal/mol) of Benzene, Obtained from Our 2011 method and our 2007 method.

Basis sets		Pure EX without		Pure Corr.		EX-Corr.		Hybrid		
		HF-EX and Corr.		with HF-EX		without HF-EX		with HF-EX		
		SLATER	XPBE96	CPBE96	LYP	PBE96	SVWN5	BLYP	PBE0	X3LYP
6-31G*	2011	-28.5	-30.2	-32.6	-32.5	-31.0	-30.1	-30.8	-31.4	-31.2
	2007	-28.5	-30.2	25.1	24.7	-31.0	-30.1	-30.8	-18.4	-20.0
6-311G(2d,2p)	2011	-19.9	-22.0	-29.9	-29.5	-23.2	-22.1	-22.9	-25.1	-24.6
	2007	-19.9	-22.0	55.6	55.3	-23.2	-22.1	-22.9	-6.8	-8.9
6-311G(2df,p)	2011	-16.2	-18.4	-27.0	-26.8	-19.3	-18.4	-19.3	-21.6	-21.2
	2007	-16.2	-18.4	65.0	64.3	-19.3	-18.4	-19.3	-1.9	-4.3
6-311G(d,p)	2011	-24.9	-26.9	-31.6	-31.1	-28.1	-26.9	-27.7	-29.1	-28.5
	2007	-24.9	-26.9	33.8	34.3	-28.1	-26.9	-27.7	-14.3	-15.7
Range	2011	-12.3	-11.8	-5.6	-5.7	-11.7	-11.7	-11.5	-9.8	-10.0
	2007	-12.3	-11.8	39.9	39.6	-11.7	-11.7	-11.5	-16.5	-15.7
Average	2011	-22.4	-24.4	-30.3	-30.0	-25.4	-24.4	-25.2	-26.8	-26.4
	2007	-22.4	-24.4	44.9	44.7	-25.4	-24.4	-25.2	-10.4	-12.2

Accordingly, the DF-type exchange has also an influence on the value of ΔE^V . The pure correlation density functional seems to be more suitable for calculating vertical delocalization energy when using our 2011 method.

8.5. CYCLOBUTADIENE

For cyclobutadiene, as shown by the data in Table 8-12 and Table 8-I, the vertical delocalization energy and adiabatic delocalization Energy, obtained from our 2011 method and our 2007 method, are always destabilizing, but the values obtained from our 2011 method are much smaller than the corresponding values from our 2007 method. At 6-31G* level, for example, the values (kcal/mol) of ΔE^V and ΔE^A are as follows:

2017 method: 51.0, 64.2 (B3LYP); 89.4, 123.1 (RHF); 96.0, 141.9 (MP2)

2011 method: 44.2, 53.6 (B3LYP); 48.0, 50.6 (RHF); 40.9, 43.4 (MP2)

At a specific theoretical level, the ranges of a set of values obtained from our 2011 method are smaller than from our 2007 method. At B3LYP level of theory, the ranges (kcal/mol) of ΔE^V and ΔE^A are 8.0 and 16.6 (2007) and 4.6 and 8.1 (2011).

LYP is a pure correlation density functional with HF-EX. When our 2011 method is used to optimize the localized (GL) geometry and to localize the electronic state (DSI state), all the exchanges, including MO exchange, HF-EX and DF-EX, have been excluded from the between localized double bonds. Correspondingly, the ranges of the values of ΔE^V and ΔE^A are 2.9 and 3.6 kcal/mol, and they are the smallest of all the ranges listed in Table 8-11.

Table 8-12. Vertical Resonance Energy ΔE^V (Kcal/Mol) and Adiabatic Delocalization Energy ΔE^A (kcal/mol) for Cyclobutadiene, Obtained from Our 2011 Method.

Basis sets	MP2-RHF		MP2		B3LYP		LYP		Range	
	ΔE^V	ΔE^A								
6-31G*	48.0	50.6	40.9	43.4	44.2	53.6	50.0	51.6	9.1	10.2
6-311G**	47.2	49.8	41.1	43.5	45.2	54.6	49.7	50.5	8.6	11.1
6-311G(2d,2p)	48.9	50.0	47.4	50.2	48.2	61.1	52.4	50.9	5.0	11.1
6-311G(2df,p)	50.1	46.7	49.7	51.1	48.8	62.7	52.9	50.0	4.1	16.0
DH(2d,2p)	47.3	50.7	45.0	46.8	46.4	57.7	51.2	50.3	6.2	10.9
TZV	46.2	55.2	41.0	43.9	45.9	55.1	51.0	53.6	10.0	9.7
Range	2.9	8.5	8.8	7.7	4.6	8.1	2.9	3.6		
Average	47.9	50.5	44.2	46.5	46.5	57.5	51.2	51.2		

ΔE^V (2011) and ΔE^A (2011) are more reasonable than ΔE^V (2007) and ΔE^A (2011). In particular, the (B3LYP and LYP)/6-31G* values (53.6 and 51.6 kcal/mol) of ΔE^A , as well as the averages (57.5 and 51.2 kcal/mol), are almost equal to the experimental value of 55 kcal/mol.

8.6. CONCLUSIONS

Due to additionally deleting the particular exchange integrals between the localized groups (double bonds), our 2011 method satisfies two criteria for judging the rationality of the method of calculating the electronic delocalization energy: the electron delocalization energy of cyclobutadiene must be destabilizing, and that of aromatic molecule such as benzene is stabilizing. The extra stabilization energy (ESE) of benzene and the adiabatic delocalization energy of cyclobutadiene, calculated by our 2011 method at B3LYP/6-31G*, are -36.3 (stabilizing) and 53.6 (destabilizing) kcal/mol, respectively. These two values are almost equal to their corresponding experimental values (kcal/mol) of -36 and 55.

For benzene, the range of a set of the ESE values, obtained from our 2011 method, is -5.3 kcal/mol. For cyclobutadiene, the ranges of the vertical delocalization and adiabatic delocalization energies, from our 2011 method, are 12.0 and 19.3 kcal/mol, respectively. The corresponding ranges, obtained from our 2007 method, are -24.4 (ESE for benzene), 149.1 (ΔE^V) and 316 (ΔE^A) (for cyclobutadiene) kcal/mol. The influences of theoretical level and basis set size on the 2011 values of electron delocalization energies are much smaller than on the 2007 values.

When the pure correlation density functionals (such as PCBE96) with the Hartree-Fock exchange is used, the basis set size and theoretical level have the smallest influence on the energy effects such as the extra stabilization energy (CESE) and vertical delocalization energy, indicating that, for the localized state, the elimination of the exchange interaction of DFT type is also necessary.

Our 2011 method is more reasonable than our 2007 method.

8.7. APPENDIX

Table 8-4. For Benzene, 19-th (Or 21-th) π MO of GL Geometry, and AO Mulliken Populations, Calculated by Using Our 2007 Method and 2011 Method, Respectively, at (B3LYP and RHF)/6-31G* Levels.

			Our 2007 Method				Our 2011 Method			
			B3LYP	RHF	Mulliken		B3LYP	RHF	Mulliken	
			19-th	19-th	B3LYP	RHF	19-th	21-th	B3LYP	RHF
Eigenvalues			-0.2856	-0.4065			-0.2794	-0.3747		
1	C1	s	0.000000	0.000000	1.99193	1.99672	0.000000	0.000000	1.99192	1.99666
2	C1	s	0.000000	0.000000	0.71845	0.67870	0.000000	0.000000	0.71745	0.67424
3	C1	x	0.000000	0.000000	0.75914	0.73913	0.000000	0.000000	0.75800	0.73293
4	C1	y	0.000000	0.000000	0.76675	0.75450	0.000000	0.000000	0.76611	0.75124
5	C1	z	0.388538	0.346221	0.52163	0.45216	0.392529	0.366945	0.52832	0.48612
6	C1	s	0.000000	0.000000	0.50779	0.48633	0.000000	0.000000	0.50808	0.48727
7	C1	x	0.000000	0.000000	0.22947	0.34986	0.000000	0.000000	0.22982	0.35198
8	C1	y	0.000000	0.000000	0.16449	0.16240	0.000000	0.000000	0.16494	0.16464
9	C1	z	0.303490	0.337822	0.47587	0.54360	0.299953	0.320120	0.46901	0.50850
10	C1	xx	0.000000	0.000000	0.01410	0.03226	0.000000	0.000000	0.01415	0.03247
11	C1	yy	0.000000	0.000000	0.00104	0.02153	0.000000	0.000000	0.00106	0.02167
12	C1	zz	0.000000	0.000000	-0.02530	-0.02027	0.000000	0.000000	-0.02516	-0.01942
13	C1	xy	0.000000	0.000000	0.01052	0.01360	0.000000	0.000000	0.01050	0.01343
14	C1	xz	0.012130	0.019063	0.00197	0.00337	0.011694	0.017045	0.00189	0.00297
15	C1	yz	-0.002879	-0.004642	0.00053	0.00087	-0.004184	0.011752	0.00078	0.00241
16	C2	s	0.000000	0.000000	1.99193	1.99672	0.000000	0.000000	1.99192	1.99666
17	C2	s	0.000000	0.000000	0.71845	0.67870	0.000000	0.000000	0.71745	0.67424
18	C2	x	0.000000	0.000000	0.76482	0.75204	0.000000	0.000000	0.76409	0.74832
19	C2	y	0.000000	0.000000	0.76108	0.74159	0.000000	0.000000	0.76002	0.73585
20	C2	z	0.388536	0.346222	0.52163	0.45216	0.392528	0.366945	0.52832	0.48612
21	C2	s	0.000000	0.000000	0.50779	0.48633	0.000000	0.000000	0.50808	0.48727
22	C2	x	0.000000	0.000000	0.16587	0.17743	0.000000	0.000000	0.16617	0.17871
23	C2	y	0.000000	0.000000	0.22809	0.33483	0.000000	0.000000	0.22860	0.33791
24	C2	z	0.303495	0.337822	0.47588	0.54360	0.299958	0.320120	0.46902	0.50850
25	C2	xx	0.000000	0.000000	0.00218	0.02236	0.000000	0.000000	0.00222	0.02258
26	C2	yy	0.000000	0.000000	0.01155	0.03007	0.000000	0.000000	0.01160	0.03031
27	C2	zz	0.000000	0.000000	-0.02530	-0.02027	0.000000	0.000000	-0.02516	-0.01942
28	C2	xy	0.000000	0.000000	0.01192	0.01496	0.000000	0.000000	0.01188	0.01468
29	C2	xz	0.000375	0.000477	-0.00005	-0.00006	-0.000998	0.006914	0.00014	0.00106
30	C2	yz	0.012461	0.019614	0.00255	0.00430	0.012380	0.019515	0.00253	0.00432

31	C3	s	0.000000	0.000000	1.99193	1.99672	0.000000	0.000000	1.99192	1.99666
32	C3	s	0.000000	0.000000	0.71847	0.67870	0.000000	0.000000	0.71746	0.67424
33	C3	x	0.000000	0.000000	0.76241	0.74822	0.000000	0.000000	0.76153	0.74377
34	C3	y	0.000000	0.000000	0.76349	0.74542	0.000000	0.000000	0.76257	0.74041
35	C3	z	0.000000	0.000000	0.52163	0.45216	0.000000	0.000000	0.52832	0.48612
36	C3	s	0.000000	0.000000	0.50774	0.48633	0.000000	0.000000	0.50803	0.48727
37	C3	x	0.000000	0.000000	0.17551	0.21331	0.000000	0.000000	0.17567	0.21387
38	C3	y	0.000000	0.000000	0.21838	0.29895	0.000000	0.000000	0.21902	0.30274
39	C3	z	0.000000	0.000000	0.47586	0.54360	0.000000	0.000000	0.46900	0.50850
40	C3	xx	0.000000	0.000000	0.00410	0.02365	0.000000	0.000000	0.00414	0.02386
41	C3	yy	0.000000	0.000000	0.00731	0.02632	0.000000	0.000000	0.00735	0.02649
42	C3	zz	0.000000	0.000000	-0.02530	-0.02027	0.000000	0.000000	-0.02516	-0.01942
43	C3	xy	0.000000	0.000000	0.01424	0.01742	0.000000	0.000000	0.01421	0.01722
44	C3	xz	0.000000	0.000000	-0.00028	-0.00041	0.000000	0.000000	-0.00018	0.00015
45	C3	yz	0.000000	0.000000	0.00278	0.00465	0.000000	0.000000	0.00285	0.00523
46	C4	s	0.000000	0.000000	1.99193	1.99672	0.000000	0.000000	1.99192	1.99666
47	C4	s	0.000000	0.000000	0.71845	0.67870	0.000000	0.000000	0.71745	0.67424
48	C4	x	0.000000	0.000000	0.75825	0.73875	0.000000	0.000000	0.75707	0.73248
49	C4	y	0.000000	0.000000	0.76764	0.75488	0.000000	0.000000	0.76703	0.75169
50	C4	z	0.000000	0.000000	0.52163	0.45216	0.000000	0.000000	0.52832	0.48612
51	C4	s	0.000000	0.000000	0.50779	0.48633	0.000000	0.000000	0.50808	0.48727
52	C4	x	0.000000	0.000000	0.22217	0.33975	0.000000	0.000000	0.22237	0.34093
53	C4	y	0.000000	0.000000	0.17179	0.17251	0.000000	0.000000	0.17239	0.17568
54	C4	z	0.000000	0.000000	0.47588	0.54360	0.000000	0.000000	0.46901	0.50850
55	C4	xx	0.000000	0.000000	0.01372	0.03176	0.000000	0.000000	0.01376	0.03190
56	C4	yy	0.000000	0.000000	0.00048	0.02091	0.000000	0.000000	0.00048	0.02094
57	C4	zz	0.000000	0.000000	-0.02530	-0.02027	0.000000	0.000000	-0.02516	-0.01942
58	C4	xy	0.000000	0.000000	0.01145	0.01472	0.000000	0.000000	0.01146	0.01473
59	C4	xz	0.000000	0.000000	0.00120	0.00211	0.000000	0.000000	0.00110	0.00155
60	C4	yz	0.000000	0.000000	0.00130	0.00213	0.000000	0.000000	0.00157	0.00383
61	C5	s	0.000000	0.000000	1.99193	1.99672	0.000000	0.000000	1.99192	1.99666
62	C5	s	0.000000	0.000000	0.71845	0.67870	0.000000	0.000000	0.71745	0.67424
63	C5	x	0.000000	0.000000	0.76729	0.75310	0.000000	0.000000	0.76662	0.74956
64	C5	y	0.000000	0.000000	0.75861	0.74053	0.000000	0.000000	0.75748	0.73461
65	C5	z	0.000000	0.000000	0.52163	0.45216	0.000000	0.000000	0.52832	0.48612
66	C5	s	0.000000	0.000000	0.50779	0.48633	0.000000	0.000000	0.50808	0.48727
67	C5	x	0.000000	0.000000	0.18594	0.20522	0.000000	0.000000	0.18663	0.20907

68	C5	y	0.000000	0.000000	0.20802	0.30703	0.000000	0.000000	0.20813	0.30754
69	C5	z	0.000000	0.000000	0.47589	0.54360	0.000000	0.000000	0.46902	0.50850
70	C5	xx	0.000000	0.000000	0.00101	0.02106	0.000000	0.000000	0.00100	0.02106
71	C5	yy	0.000000	0.000000	0.01085	0.02911	0.000000	0.000000	0.01089	0.02922
72	C5	zz	0.000000	0.000000	-0.02530	-0.02027	0.000000	0.000000	-0.02516	-0.01942
73	C5	xy	0.000000	0.000000	0.01380	0.01721	0.000000	0.000000	0.01381	0.01729
74	C5	xz	0.000000	0.000000	0.00206	0.00340	0.000000	0.000000	0.00230	0.00495
75	C5	yz	0.000000	0.000000	0.00044	0.00084	0.000000	0.000000	0.00037	0.00043
76	C6	s	0.000000	0.000000	1.99193	1.99672	0.000000	0.000000	1.99192	1.99666
77	C6	s	0.000000	0.000000	0.71847	0.67870	0.000000	0.000000	0.71746	0.67424
78	C6	x	0.000000	0.000000	0.76577	0.74966	0.000000	0.000000	0.76500	0.74545
79	C6	y	0.000000	0.000000	0.76012	0.74397	0.000000	0.000000	0.75910	0.73871
80	C6	z	0.000000	0.000000	0.52163	0.45216	0.000000	0.000000	0.52832	0.48612
81	C6	s	0.000000	0.000000	0.50774	0.48633	0.000000	0.000000	0.50803	0.48727
82	C6	x	0.000000	0.000000	0.20287	0.25121	0.000000	0.000000	0.20358	0.25528
83	C6	y	0.000000	0.000000	0.19102	0.26105	0.000000	0.000000	0.19111	0.26133
84	C6	z	0.000000	0.000000	0.47586	0.54360	0.000000	0.000000	0.46900	0.50850
85	C6	xx	0.000000	0.000000	0.00330	0.02285	0.000000	0.000000	0.00331	0.02291
86	C6	yy	0.000000	0.000000	0.00716	0.02599	0.000000	0.000000	0.00721	0.02613
87	C6	zz	0.000000	0.000000	-0.02530	-0.02027	0.000000	0.000000	-0.02516	-0.01942
88	C6	xy	0.000000	0.000000	0.01519	0.01855	0.000000	0.000000	0.01518	0.01853
89	C6	xz	0.000000	0.000000	0.00260	0.00431	0.000000	0.000000	0.00277	0.00546
90	C6	yz	0.000000	0.000000	-0.00010	-0.00008	0.000000	0.000000	-0.00010	-0.00008
91	H7	s	0.000000	0.000000	0.53305	0.52358	0.000000	0.000000	0.53327	0.52480
92	H7	s	0.000000	0.000000	0.32860	0.26166	0.000000	0.000000	0.32991	0.26809
93	H8	s	0.000000	0.000000	0.53305	0.52358	0.000000	0.000000	0.53327	0.52480
94	H8	s	0.000000	0.000000	0.32860	0.26166	0.000000	0.000000	0.32990	0.26809
95	H9	s	0.000000	0.000000	0.53306	0.52358	0.000000	0.000000	0.53327	0.52480
96	H9	s	0.000000	0.000000	0.32860	0.26165	0.000000	0.000000	0.32991	0.26809
97	H10	s	0.000000	0.000000	0.53305	0.52358	0.000000	0.000000	0.53327	0.52480
98	H10	s	0.000000	0.000000	0.32860	0.26166	0.000000	0.000000	0.32991	0.26809
99	H11	s	0.000000	0.000000	0.53305	0.52358	0.000000	0.000000	0.53327	0.52480
100	H11	s	0.000000	0.000000	0.32860	0.26166	0.000000	0.000000	0.32991	0.26809
101	H12	s	0.000000	0.000000	0.53305	0.52358	0.000000	0.000000	0.53327	0.52480
102	H12	s	0.000000	0.000000	0.32860	0.26166	0.000000	0.000000	0.32991	0.26809

8.8. REFERENCES

- 1 Bao, P.; Yu, Z. H. 2011. “New Procedure to Evaluate Aromaticity at the Density Functional Theory, Hartree–Fock, and Post-Self- Consistent Field Levels.” *J. Comput. Chem.*, 32: 248-259.
- 2 Cava, M. P.; Mitchell, M. J. 1967. *Cyclobutadiene and Related Compounds*. New York: Academic Press.
- 3 Watts, L.; Fitzpatrick, J. D.; Pettit, D. 1965. “Cyclobutadiene.” *J. Am. Chem. Soc.*, 87: 3253-3254.
- 4 Whitman, D. W.; Carpenter, B. K. 1980. “Experimental Evidence for Nonsquare Cyclobutadiene as a Chemically Significant Intermediate in Solution.” *J. Am. Chem. Soc.*, 102: 4272-4274.
- 5 Whitman, D. W.; Carpenter, B. K. 1982. “Limits on the Activation Parameters for Automerization of Cyclobutadiene-1,2-d2.” *J. Am. Chem. Soc.*, 104: 6473-6474.
- 6 Garratt J. P. 1987. “Benzene and Brethren, the Enigmatic Molecules — 1825–1986.” *Endeavour*, 11: 36-42.
- 7 Garratt, P. J. 1986. *Aromaticity*. New York: Wiley.
- 8 Chapman, O. L.; McIntosh, C. L.; Pacansky, J. 1973. “Photochemical Transformations. XLVIII. Cyclobutadiene.” *J. Am. Chem. Soc.*, 95: 614-617.
- 9 Lin, C. Y.; Kranz, A. 1972. “Matrix Preparation of Cyclobutadiene.” *Chem. Commun.*, 1111-1112.
- 10 Kranz, A.; Lin, C. Y.; Newton, M. D. 1973. “Cyclobutadiene. II. Geometry of the Matrix-Isolated Species.” *J. Am. Chem. Soc.*, 95: 2744-2746.
- 11 Maier, G.; Sauer, W. 1977. “Diradical-Type Behavior of Tri-tert-butylcyclobutadiene.” *Angew. Chem. Int. Ed. Engl.*, 16: 51-52.
- 12 Maier, G. 1974. “The Cyclobutadiene Problem.” *Angew. Chem., Int. Ed. Engl.*, 13: 425-438.
- 13 Kimling, H.; Krebs, A. 1972. “Synthesis of a Cyclobutadiene Stabilized by Steric Effects.” *Angew. Chem. Int. Ed. Engl.*, 11: 932-933.
- 14 Delbaere, L. T. J.; James, M. N. G.; Nakamura, N.; Masamune, S. 1975. “[4]Annulene System. Direct Proof for its Rectangular Geometry.” *J. Am. Chem. Soc.*, 97: 1973-1974.
- 15 Breslow, R.; Washburn, W. J. “Antiaromatic Destabilization of Cyclobutadieno-cyclopentadienyl Anion.” *J. Am. Chem. Soc.*, 92: 427-428.
- 16 Breslow, R.; Grubbs, R.; Muragashi, S. I. 1970. “Electrochemical Evidence for the Anti-aromaticity of Cyclobutadiene.” *J. Am. Chem. Soc.*, 92: 4139-4140.
- 17 Shaik, S.; Shurki, A.; Danovich, D.; Hiberty, P. C. 2001. “A Different Story of π -Delocalization – The Distortion of π -Electrons and Its Chemical Manifestations.” *Chem. Rev.*, 101: 1501-1540.
- 18 Breslow, R. 1973. “Antiaromaticity.” *Acc. Chem. Res.*, 6: 393-398
- 19 Hess, Jr., B. A.; Schaad, L. J. 1983. “Ab Initio Calculation of Resonance Energies. Benzene and Cyclobutadiene.” *J. Am. Chem. Soc.*, 105: 7500-7505.
- 20 Deniz, A. A.; Peters, K. S.; Snyder, G. J. 1999. “Experimental Determination of the Antiaromaticity of Cyclobutadiene.” *Science*, 286: 1119-1122.
- 21 Schaad, L. J.; Hess, Jr. B. A. 2001. “Dewar Resonance Energy.” *Chem. Rev.*, 101: 1465-1476.
- 22 Cooper, D. L. 2002. *Valence Bond Theory*. Amsterdam: Elsevier Science B. V.
- 23 Mo, Y. R.; Wu, W.; Zhang, Q. N. 1994. “Theoretical Resonance Energies of Benzene, Cyclobutadiene, and Butadiene.” *J. Phys. Chem.*, 98: 10048-10053.
- 24 Voter, A. F.; Goddard, W.A. 1986. “Generalized Resonating Valence Bond Description of Cyclobutadiene.” *J. Am. Chem. Soc.*, 108: 2830-2837.
- 25 Dijkstra, F.; van Lenthe, J. H. V.; Havenith, R. W. A.; Jenneskens, L. W. 2003. “Valence Bond Descriptions of Benzene and Cyclobutadiene and their Counterparts with Localized Bonds.” *Int. J. Quantum Chem.*, 91: 566-574.
- 26 Balková, A.; Bartlett, R. J. 1994. “A Multireference Coupled-Cluster Study of the Ground State and Lowest

- Excited States of Cyclobutadiene.” J. Chem. Phys., 101: 8972-8987.
- 27 Bally, T. 2006. “Cyclobutadiene: The Anti-aromatic Paradigm?” Angew. Chem. Int. Ed. Engl., 45: 6616-6619.
- 28 Hückel, E. 1931. “Quantentheoretische Beiträge zum Benzolproblem.” Z. Phys., 70: 204-286.
- 29 Ichikawa, H.; Ebisawa, Y. 1985. “Hartree-Fock MO Theoretical Approach to Aromaticity. Interpretation of Huckel Resonance Energy in Terms of Kinetic Energy of Electrons.” J. Am. Chem. Soc., 107: 1161-1165.
- 30 Armit, J. W.; Robinson, R. 1925. “CCXI. —Polynuclear Heterocyclic Aromatic Types. Part II. Some Anhydronium Bases.” J. Chem. Soc. Trans., 127 1604-1618.
- 31 Breslow R.; Mohacsi, E. 1963. “Studies on d-Orbital Conjugation. III. Non-aromaticity of a Derivative of the 1,3-Dithiepinyl Anion, a Ten π -Electron Conjugated System.” J. Am. Chem. Soc., 85: 431-434.
- 32 Chung, A. L. H.; Dewar, M. J. S. 1965. “Ground States of Conjugated Molecules. I. Semiempirical SCF MO Treatment and Its Application to Aromatic Hydrocarbons.” J. Chem. Phys., 42: 756-766.
- 33 Dewar, M. J. S.; Schmeising, H. N. 1959. “A Re-Evaluation of Conjugation and Hyperconjugation: The Effects of Changes in Hybridisation on Carbon Bonds.” Tetrahedron, 5: 166-178.
- 34 Dewar, M. J. S.; Schmeising, H. N. 1960. “Resonance and conjugation—II Factors Determining Bond Lengths and Heats of Formation.” Tetrahedron, 11: 96-120.
- 35 Dewar, M. J. S.; Gleicher, G. J. 1965. “Ground States of Conjugated Molecules. II. Allowance for Molecular Geometry.” J. Am. Chem. Soc., 87: 685-692.
- 36 Dewar, M. J. S.; Gleicher, G. J. 1965. “Ground States of Conjugated Molecules. III. Classical Polyenes.” J. Am. Chem. Soc., 87: 692-696.
- 37 Hess, B. A., Jr.; Schaad, L. J. 1971. “Hueckel Molecular Orbital .pi. Resonance Energies. New approach.” J. Am. Chem. Soc., 93: 305-310.
- 38 Hess, B. A., Jr.; Schaad, L. J. 1972. “Application of Dewar's Definition Of Resonance Energy to the Hueckel Method.” J. Org. Chem., 37: 4179-4180.
- 39 Gutman, I.; Milun, M.; Trinajstic', N. 1977. “Graph Theory and Molecular Orbitals. 19. Nonparametric Resonance Energies of Arbitrary Conjugated Systems.” J. Am. Chem. Soc., 99: 1692-1704.
- 40 Kollmar, H. 1979. “Direct Calculation of Resonance Energies of Conjugated Hydrocarbons with ab Initio MO Methods.” J. Am. Chem. Soc., 101: 4832-4840.
- 41 Mo, Y.; Schleyer, P. v. R. 2006. “An Energetic Measure of Aromaticity and Antiaromaticity Based on the Pauling-Wheland Resonance Energies.” Chem. Eur. J., 12: 2009-2020.
- 42 Mo, Y. R.; Lin, M. H.; Wu, W.; Zhang, Q. E. 2000. “The Block-Localized Wave function Method and Its Application.” Acta Chin. Sin., 58: 218-221.
- 43 Mo, Y.; Peyerimhoff, S. D. 1998. “Theoretical Analysis of Electronic Delocalization.” J. Chem. Phys., 109: 1687-1697.
- 44 Mo, Y. 2004. “Resonance Effect in the Allyl Cation and Anion: A Revisit.” J. Org. Chem., 69: 5563-5567.
- 45 Mo, Y.; Song, L.; Lin, Y. 2007. “Block-Localized Wavefunction (BLW) Method at the Density Functional Theory (DFT) Level.” J. Phys. Chem., 111: 8291-8301.
- 46 Behrens, S.; Köster, A. M.; Jug, K. 1994. “Delocalization Energy of an Electrons as an Index for Aromaticity of Polycyclic Hydrocarbons.” J. Org. Chem., 59: 2546-2551.
- 47 Yu, Z. H.; Xuan, Z. Q.; Wang, T. X.; Yu, H. M. 2000. “A Novel Energy Partition for Gaining New Insight into Aromaticity and Conjugation.” J. Phys. Chem. A, 104: 1736-1747.
- 48 Kost, D.; Schlegel, H. B.; Mitchell, D. J.; Wolfe, S. 1979. “Molecular Orbitals from Group Orbitals. IX. The Problem of Hybrid Lone Pairs.” Can. J. Chem., 57: 729-732.
- 49 Yu, Z. H. 1994. “Quantitative Perturbational Molecular orbital Analysis of the Conformational preference of Aniline Molecule and Its Intramolecular Force”, *Comput. Chem.*, 18, 95-102
- 50 Kitaura, K.; Morokuma, K. 1976. “A New Energy Decomposition Scheme for Molecular Interactions within the Hartree-Fock Approximation.” Inter. J. Quan-tum Chem., 10: 325-340.
- 51 Bader, R. F. W.; Streitwieser, A.; Neuhaus, A.; Laidig, K. E.; Speers, P. 1996. “Electron Delocalization and the Fermi Hole.” J. Am. Chem. Soc., 118: 4959-4965.

- 52 Bader, R. F. W.; Stephens, M. E. 1975. "Spatial Localization of the Electronic Pair and Number Distributions in Molecules." *J. Am. Chem. Soc.*, 97: 7391-7399.
- 53 Bader, R. F. W.; Johnson, S.; Tang, T. H.; Popelier, P. L. A. 1996. "The Electron Pair." *J. Phys. Chem.*, 100: 15398-15415.
- 54 Yu, Z. H.; Li, L.T.; Fu, W.; Li, L.P. 1998. "Conformations of Stilbene-like Species and New Method of Energy Partition." *J. Phys. Chem. A*, 102: 2016-2028.
- 55 Xu, H.; Yu, Z.H. 2004. "The Driving Forces for Distorting NBA-Like Species away from their Planar Geometries." *J. Mol. Struct. (Theochem)*, 682: 37-46
- 56 Bao, P.; Yu, Z. H. 2006. "Theoretical Studies on the Role of π -Electron Delocalization in Determining the Conformation of N-benzylideneaniline with Three Types of LMO Basis Sets." *J. Comput. Chem.*, 27: 809-824.
- 57 Köster, A. M.; Calaminici, P.; Geudtner, G.; Gómez-Sandoval, Z. 2005. "Separation of σ and π Energies." *J. Phys. Chem. A*, 109: 1257-1259.
- 58 Salem, L. J. 1968. "Intermolecular Orbital Theory of the Interaction between Conjugated Systems. I. General theory." *J. Am. Chem. Soc.*, 90: 543-552.
- 59 Epotis, N. D.; Cherry, W. R.; Shaik, S.; Yates, R.; Bernardi, F. 1977. "Structure Theory of Organic Chemistry." *Top. Curr. Chem.*, 70: 1.
- 60 Levine, I. N. 2004. *Quantum Chemistry*, 5Ed. Beijing: World Publishing Corporation.
- 61 <http://uni-smr.ac.ru/archive/sci-ence/chem/gamess/PCGAMESS%207.1/READMES/read me.dft>.
- 62 Schmidt, M. W.; Baldridge, K. K.; Boatz, J. A.; Elbert, S. T.; Gordon, M. S.; Jensen, J. H.; Koseki, S.; Matsunaga, N.; Nguyen, K. A.; Su, S.; Windus, T. L.; Dupuis, M.; Montgomery, J. A. 1993. "General Atomic and Molecular Electronic Structure System." *J. Comput. Chem.*, 14: 1347-1363.
- 63 Granovsky, A. A. Available at: <http://clasic.chem.msu.su/gran/gamess/in-dex.html>, Accessed 30.
- 64 Morokuma, K.; Kitaura, K. 1981. *Chemical Applications of Electrostatic Potentials*, edited by Politzer, P.; Truhlar, D. G.. New York: Plenum Press.

CHAPTER 9

[N]ANNULENES AND PBHS

ABSTRACT

In the process of deforming benzene from the localized GL geometry to the ground (G) state geometry, the compressing of single bonds and the stretching of double bonds are caused by π -electron delocalization. Finally, the nuclear repulsion between the CC atoms is minimized when the distance of the CC single bonds is equal to that of the CC double bonds, leading to that $\Delta E_e = E_e(G) - E_e(GL) > 0$, $\Delta E_N = E_N(G) - \Delta E_N(GL) < 0$, $|\Delta E_N| > \Delta E_e$, and $\Delta E^A = E(G) - E(GL) = -19.2$ kcal/mol. The minimization of nuclear repulsion minimization plays an important role in the eventual formation of the D_{6h} geometry. But this role is the result of π -electron delocalization. Energy criterion and geometric criterion of the aromaticity are well unified and are mutually causal. This is a new understanding of the essence of aromaticity.

For planar [N]annulenes, the vertical delocalization energy (VRE) and extra stabilization energy (ESE and CESE) are calculated, based on their respective most stable configuration isomers, using our 2011 method at various theoretical levels with different basis sets, and the corresponding B3LYP/6-311G(2df,p) values are the most reasonable.

At B3LYP/6-311G(2df,p) level, the VDEs always alternate between stabilizing and destabilizing as the number of carbon atoms increases. In the meantime, the VDE per π -electron, $\Delta E^V/\pi$, for [4n]annulene quickly becomes constant (about 0.7 kcal/mol*electron) when $N = 16$; the $\Delta E^V/\pi$ for [4n+2]annulene is gradually approaching the limit value of -0.7 kcal/mol*electron when the number of carbon atoms increases from $N = 8$ to $N = 26$.

For [4n+2] annulene, when $N \geq 18$, ΔE^A (about 17 kcal/mol) > 0 , CESE (about -10.0 kcal/mol) < 0 , the ratio $CESE/(\Delta E^{Am} + \Delta E_n^{Am})$ is about 0.35. Accordingly, the large [4n+2]annulene ($N \geq 18$) is no longer a typical aromatic molecule. For [4n]annulene, when $N \geq 16$, the CESEs < 0 (stabilizing), but their values (-0.65 to -2.0 kcal/mol) are so small that the energy effects ΔE^{Am} can be considered additive. In the case of the large [4n]annulene, the sign (stabilizing or destabilizing) of the CESE is no longer worthy of attention. At B3LYP/6-311G(2df,p) level, therefore, [N]annulene can be considered approaching polyene (non-aromatic) when $N \geq 16$, no matter whether it is [4n]annulene or [4n+2]annulene.

For polycyclic benzenoid hydrocarbons, there is no great difference between the CESE values respectively obtained from our 2011 method and from our 2007 method. But, the adiabatic delocalization energy ΔE^A , obtained from our 2011 method, becomes more reasonable than from our 2007 method based on the following two facts: (i) $d[\Delta E^A(2007)]/dn > 0$, and to $d[\Delta E^A(2011)]/dn < 0$; (ii) $\Delta E^A(2011) < 0$ (stabilizing) when structure unit $n < 13$. $\Delta E^A < 0$ should be one of the basic criteria for judging the aromaticity of molecule.

yuzh@iccas.ac.cn

Key words: New concept of aromaticity; benzene; molecular energy decomposition; equalization of CC bonds; minimization of nuclear repulsion; [N]annulene; polyene; extra stabilization energy; vertical localization energy.

9.1. INTRODUCTION

Annulene refers to monocyclic conjugated hydrocarbon with the general formula C_nH_n , and it is denoted as [N]annulene. Cyclobutadiene and benzene can be considered as [4]annulene and [6]annulene.

By 1972, all the annulenes up to [30]annulene, exception for [26]- and [28]annulenes, had been synthesized. In 1911, [8]annulene was synthesized.^{1,2} Inspired by the great difference in the chemical properties between benzene (including the benzene- and furan-like species such as pyridine and pyrrole) and [8]annulene, Hückel published a paper in 1931.³ In this work, Hückel applied Hund-Mulliken-Hückel (HMH) calculation method to [N]annulenes ($N = 4, 6, 8, 10$), and he found that, in an aromatic molecule such as benzene, there is a closed electron group (eine abgeschlossene Elektronengruppe) and in anti-aromatic molecules such as cyclobutadiene and [8]annulene, there is no such a closed electron group. Then, Hückel well interpreted why [8]annulene and cyclobutadiene are more reactivity than benzene, and he expected that [10]annulene, a unknown compound at that time, will be again more aromatic according to the role of closed electron group in inhibiting electron excitation and based on the relationship between the theoretical easiness of electron excitation and the experimental reactivity. As reviewed by Hess and Schaad,⁴ this Hückel's work led to the famous $4n+2$ rule for monocyclic conjugated hydrocarbons. That is to say, the original $4n+2$ rule did not involve the energetic and geometric features of annulenes, and it was only a reactivity criterion. Since then, around the $4n+2$ rule, the core issues of annulene chemistry are as follows:

- (i) How to calculate the π -electron delocalization energy?
- (ii) Is the $4n+2$ rule always truth?
- (iii) What is the driving force for distorting annulene into a structure with alternating single and double bonds?

How to calculate the electron delocalization energy has always been an important issue in physical organic chemistry and quantum chemistry. These methods include the following methods: various empirical and semi-empirical methods based on bond energy additivity, the methods based on homodesmotic reactions, and the methods by eliminating matrix elements. Therefore, how to judge the rationality of the calculation method is often a controversial issue. For instance, as the first two members of [N]annulenes and as two typical representatives of aromatic and antiaromatic molecules, benzene ([6] annulene) and cyclobutadiene ([4] annulene) can be used to verify the rationality of the method of calculating the electronic delocalization energy. Any method that provides stabilizing delocalization energy for cyclobutadiene or provides destabilizing delocalization energy for benzene is always unreasonable. Based on the $4n+2$ rule, therefore, the calculation of resonance energy for higher annulenes was used to verify the rationality of the empirical and semi-empirical methods such as the Hückel method and Hess-Schaad method.⁴ Thus, one of the core contents of this chapter is the calculation of the ESE of the planar annulenes.

The degree of bond length alternation (BLA) (alternation degree) is defined as the bond distance difference between the longer and shorter CC bonds in a cyclic conjugated molecule such as [N]annulene, and it has been used as a geometric criterion to compare the strength of aromaticity.⁵ The small alternation degree indicates aromatic behavior, and the larger alternation degree indicates the absence of aromaticity.

For [N]annulene, the geometric manifestation of aromaticity requires a planar all-cis configuration. As a $[4n+2]$ annulene, for example, [10]annulene is potentially aromatic according to the $4n+2$ rule. But the angle strain and unfavorable steric interactions of internal protons tend to force the molecule into the non-planar cis-trans configuration.⁶⁻¹¹ For a $[4n+2]$ annulene, therefore, it is difficult to experimentally verify the equalization of CC bonds. But it should be possible for the geometry optimization to provide a planar full-cis-configuration for an annulene. For [10]annulene, as indicated by Haddon-Raghavachari in 1982,⁸ all of the Hartree-Fock (HF) treatments favor the bond-alternating structure, but the inclusion of the electron correlation (MP2) in the geometry optimization makes a bond equalization structure preferable. Accordingly, one of the core issues in the field of annulene

chemistry is how big the ring needs to be before the $[4n+2]$ annulene can become a non-aromatic molecule. “How big the ring needs to be” is called the critical size, N_{cr} , of $[4n+2]$ ring. In 1959, Longuet-Higgins and Salem showed $N_{cr} = 8$.¹² Afterwards, further theoretical calculations have been done, and gave the different predictions for the value of N_{cr} . In 1973, Buss thought that $[18]$ annulene should have a marked bond length alternation.¹³ In 1982, Haddon-Raghavachari thought that $[10]$ annulene may be close to the limit of the equalization of the CC bonds of $[4n+2]$ annulene.

The critical value, N_{cr} , of $[4n+2]$ ring has still not been established with certainty,¹⁴ because the structure of $[N]$ annulene depends on the optimization method and basis set size. Computational methods including electron correlation favor more symmetrical geometries, but the results vary. At MNDOC level of theory, as found by Yoshizawa, $[30]$ annulene prefers a bond-alternating D_{3h} geometry over the D_{6h} structure by 4.6 kcal/mol.¹⁵ At B3LYP/6-31G*, this energy difference was only 0.1 kcal/mol.^{16,17} Similarly, as shown by our calculation (Figure 9-1), the geometry optimization at B3LYP and MP2 levels of theory provides a bond equalization structure for the planar full-cis configuration of $[14]$ annulene, but the geometry optimized at RHF level of theory is a distorted D_{7h} symmetry structure with bond length alternation.

Different from the above discussion, Schleyer thought that, for higher $[4n+2]$ annulene (for example, $N = 42, 54$, and 66), bond-alternating form usually becomes progressively more stable.¹⁴

The debate about the critical size of $[4n+2]$ ring may lead to the following question: Is the $[4n+2]$ rule (always) truth?

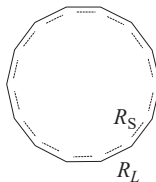
[14]Annulene	RHF	R_L	R_S (Å)	MP2	B3LYP
$R_L \neq R_S$				$R_L = R_S$	$R_L = R_S$
	6-31G*	1.346	1.476	6-31G*	1.417
	6-311G**	1.345	1.477	6-311G**	1.417
	6-311G(2d,2p)	1.342	1.477	6-311G(2d,2p)	1.415
	6-311G(2df,p)	1.341	1.475	6-311G(2df,p)	1.411
					1.408

Figure 9-1. For $[14]$ annulene, the CC bond distances (Å) in the planar full-cis geometry optimized at (RHF, MP2 and B3LYP) levels of theory.

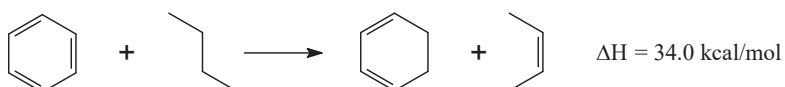
9.1.1. $[4n+2]$ Rule Not Always a Truth

The geometric criterion is not quite satisfactory since the CC bond lengths in all the aromatic compounds except for benzene are not equalized. Therefore, the energy criteria should be applicable in order to test whether the $4n+2$ rule is true or not.

In the early days of the structure theory of organic chemistry, Hückel computational method only considered π electrons and did not involve the geometry structure of a conjugated molecule, so the structure factors related to $[N]$ annulene, including conformation and configuration and ring size, did not need to be explicitly considered. As a result, the empirical Hess-Schaad calculation, a combination of Hückel computation method and Dewar reference structure,^{4,18} gives the resonance energy conforming to the $4n+2$ rule: as the number of carbon atoms increases, the resonance energy of $[N]$ annulene alternates between aromaticity and anti-aromaticity.

On the basis of PPP calculations in 1965, however, Dewar and Gleicher suggested a damping oscillation of resonance energies as the ring size increases, and they found that the $[4n+2]$ annulenes cease to be aromatic when the number of carbon atoms is greater than 22.¹⁹

In 2001, stabilization energy was calculated at B3LYP/6-311+G* level by Wiberg using the following “homisodesmic” reaction:²⁰



Of the [N]annulenes investigated by Wiberg, [18]annulene with $4n+2$ π -electrons can be considered to be planar, and its stabilization energy per π electron is about one third of the stabilization energy of benzene. [16]annulene with $4n$ π -electrons was compared with benzene in the same fashion, and it was found that [16]annulene has almost no antiaromatic character. Therefore, as concluded by Wiberg, the aromatic stabilizing energy of [4n+2]annulene and the antiaromatic destabilizing energy of [4n]annulene are reduced, when the ring size becomes larger.

For [N]annulene, the ISEs (isomerization stabilization energy, kcal/mol), calculated at B3LYP/16-31G*+ZPE on assumed planar structures, are as follows (in the original paper, the stabilizing energy is represented as positive and destabilization energy is done as negative):^{21,22}

[4n]annulene: 35.2 (N = 4), -0.6 (N = 8), 9.0 (N = 12), 6.1 (N = 16), 4.8 (N = 20), 3.1 (N = 24)

[4n+2]annulene: -34.6 (N = 6), -32.6 (N = 10), -26.7 (N = 14), -27.4 (N = 18), -26.3 (N = 22), -24.9 (N = 26), -23.6 (N = 30), -22.9 (N = 42), -22.5 (N = 54).

As the number of carbon atoms increases, the value of the ISE per π -electron of [4n+2]annulene and that of [4n]annulene both approach zero. As long as the ring is large enough, whether it is [4n] or [4n+2] annulene, their energy characteristics are close to nonaromatic.

In 2005, as reviewed by Kertesz,²³ [4n+2]-membered annulenes approach polymer trans-polyene $-(C=C)_n-$, when n increases to infinity.

Therefore, the 4n+2 rule is not always truth.

9.1.2. Driving Force for Distorting Ring

In Hückel era, benzene's CC bond length equalization was attributed to resonance, and the roles of the σ framework and nuclear repulsion are completely ignored. Until the 1980s, such view began to be challenged. In 1987, as emphasized by Shaik, "the π component is, on the one hand, distortive along a localizing mode, and on the other hand, it is stabilized by resonance energy relative to a localized reference." and "electronic delocalization in benzene turns out to be a by-product of the σ -imposed geometric symmetry and not a driving force by itself."²⁴⁻²⁶ Accordingly, the π system in the D_{3h} structure is more stable than the π system in the D_{6h} geometry. In fact, as indicated by Wiberg in 1988,²⁷ it is the Berry's calculations in 1965²⁸ to first suggest that the σ -bonds cause benzene to be a regular hexagon and the π -electrons would prefer a "Kekulé"-like structure. The Berry's suggestion was further amplified by Shaik and Hiberty.

Since 1980's, Epiotis has been questioning the concept of π -delocalization stabilization,²⁹ and in 1996, Epiotis called for expelling "resonance stabilization" concept from the textbooks of Organic Chemistry.³⁰

It should be noted that the definition of Shaik's localization is fundamentally different from ours. The Shaik's localization refers specifically to the molecular structure with alternating single and double bonds. In the Shaik's localization structure, the π MOs are still delocalized on whole molecular framework. In this book, the localized structure refers to such a structure (molecular geometry) or an electronic state whose π MOs and the π electrons are absolutely localized on their respective double bonds (or groups). For a localized geometry obtained from the conditional geometry optimization, its single and double bonds are also alternated. In a localized electronic state of an optimized geometry, however, the single and double bonds may be alternate or equalized, because the localized

electronic state is obtained from the conditional (unconditional) single-point energy calculation on the (conditionally or unconditionally) optimized geometry.

9.2. π - σ ENERGY DECOMPOSITION

In theoretical organic chemistry, π - σ energy decomposition is a basic research tool, and it plays an important role in studying the molecular properties related to π -electron delocalization. In the 1980-1990 period, as reviewed by Shaik in 2001,³¹ the controversy on the π -distortion promoted the development of the π - σ energy decomposition method. Energy decomposition may well reveal how π -electron delocalization drives the molecule distortion.

As outlined in Chapter 8, there are two types of energy decomposition. For the first type, its purpose is to decompose the interaction energy between the groups into the π - π , σ - σ and π - σ parts ($\Delta E^{\pi\pi}$, $\Delta E^{\sigma\sigma}$ and $\Delta E^{\pi\sigma}$), by constructing different localized electronic states. The most typical example is the calculation of vertical delocalization energy. The methods of the second type are used to decompose the molecular energy E of a specific electronic state (or a molecular geometry) into π and σ parts E^π and E^σ . At and only at the RHF level of theory, E^π and E^σ , may also be further decomposed into their intra- and inter-fragment interaction energies denoted as E_p^π and E_p^σ , and E_{pq}^π and E_{pq}^σ . As the most typical example, $\Delta E^V = \Delta E^{V-\pi} + \Delta E^{V-\sigma}$. Therefore, as emphasized again and again in our 2011 paper,³² should pay attention to the difference between the π -electron localization and the π -MO localization, and how to construct a reasonable localized state (geometry) is the core and key issues for our method.

Before 2007, various versions of our method can partition the molecular energy of a specific electronic state (or a specific localized geometry) into π and σ parts only at the RHF level of theory. Our 2007 method and its improved versions can partition the DFT and MPn molecular energies into the π and σ parts.

9.2.1. DFT Molecular Energy

Molecular energy is a sum of the total electronic energy and nuclear repulsion energy. In 1990, Jug and Köster proposed a method of directly decomposing nuclear repulsion energy E_N into the π and σ parts E_N^π and E_N^σ .³³ In 2005, Köster reported a program that can decompose the molecular energy of benzene into π and σ parts at DFT level of theory.³⁴ In 2007, the Köster's principle was introduced into our 2007 method to decompose the molecular energy of a non-planar molecule at the DFT level of theory.^{35,36}

For non-planar molecules such as N-benzylideneaniline, π - σ energy decomposition must be based on the construction of LFMO (absolutely localized fragment molecular orbital) basis set $\{\Psi_m^\pi, \Psi_n^\sigma\}$ (Ψ_n^σ include Ψ_k^δ). For a localized electronic state, the π and σ molecular orbitals, expressed as the linear combination of LFMOs, can be readily distinguished using the LFMO coefficient matrix. In this case, the FUD and the DSI states can be expressed as $\{\Phi_i^\pi, \Phi_j^\sigma\}$ and $\{\Phi_i^{P-\pi}, \Phi_j^\sigma\}$ ($P = A, B, \dots$), respectively, and their π and σ molecular orbitals are completely separated out. Therefore, Equation (9-1) and Equation (9-2) can be used to express the π and σ molecular orbitals, $\{\Phi_i^\pi\}$ and $\{\Phi_j^\sigma\}$, of a localized electronic state.

$$\Phi_i^\pi = \sum_{m=1}^{np} T_{mi}^\pi \Psi_m^\pi + \sum_{n=1}^{ns} T_{ni}^\sigma \Psi_n^\sigma \quad (9-1)$$

$$\Phi_j^\sigma = \sum_{m=1}^{np} T_{mj}^\pi \Psi_m^\pi + \sum_{n=1}^{ns} T_{nj}^\sigma \Psi_n^\sigma \quad (9-2)$$

For π MOs Φ_i^π , $T_{ni}^\sigma = 0$ in Equation (9-1); for σ MOs Φ_j^σ , $T_{mj}^\pi = 0$ in Equation (9-2), np and ns are the numbers of π and σ LFMOs.

Using Equation (9-3), the LFMO coefficients, T_{mi}^π , of the π molecular orbitals Φ_i^π can be transformed into the AO coefficients $t_{\lambda i}^\pi$. In a similar way, as shown by Equation (9-4), the LFMO coefficients, T_{nj}^σ , of the σ molecular orbitals Φ_j^σ can be converted into AO coefficients $t_{\lambda j}^\sigma$.

$$t_{\lambda i} = \sum_{m=1}^{np} a_{\lambda m} T_{mi}^\pi \quad (9-3)$$

$$t_{\lambda j} = \sum_{n=1}^{ns} a_{\lambda n} T_{nj}^\sigma \quad (9-4)$$

In the above Equations, \mathbf{a} is the AO coefficient matrix of the LFMO basis set. Based on Equation (9-3), the AO density matrix, \mathbf{d}^π , of the π molecular orbitals can be obtained from Equation (9-5), and the AO density matrix, \mathbf{d}^σ , of the σ molecular orbitals can be calculated by using Equation (9-6).

$$d_{\mu\omega}^\pi = \sum_{i=1, i \in \pi}^{occ} t_{\mu i} t_{\omega i} \quad (9-5)$$

$$d_{\mu\omega}^\sigma = \sum_{j=1, j \in \sigma}^{occ} t_{\mu j} t_{\omega j} \quad (9-6)$$

where "Occ" denotes that the doubly occupied molecular orbitals Φ_i^π or Φ_j^σ .

The density matrices \mathbf{d}^π and \mathbf{d}^σ are separately passed through the DFT energy calculator to obtain, respectively, the π and σ parts, $E_e^{\pi\pi}$ and $E_e^{\sigma\sigma}$, of total electronic energy E_e . Then cross item $E_e^{\pi\sigma}$ is calculated using the following Equation:

$$E_e^{\pi\sigma} = E_e - (E_e^{\pi\pi} + E_e^{\sigma\sigma})$$

Then the π and σ parts, E_e^π and E_e^σ , of total electronic energy are as follows:

$$E_e^\pi = E_e^{\pi\pi} + (1/2) E_e^{\pi\sigma} \quad (9-7)$$

$$E_e^\sigma = E_e^{\sigma\sigma} + (1/2) E_e^{\pi\sigma} \quad (9-8)$$

According to the Jug's procedure,³³ as shown by Equations (9-9) and (9-10), the nuclear repulsion E_N can be partitioned into the π and σ parts E_N^π and E_N^σ .

$$E_N^\pi = \sum_k \sum_{l>k} [(n_k^\pi n_l^\pi / R_{kl}) + (1/2)(n_k^\pi n_l^\sigma + n_k^\sigma n_l^\pi) / R_{kl}] \quad (9-9)$$

$$E_N^\sigma = \sum_k \sum_{l>k} [(n_k^\sigma n_l^\sigma / R_{kl}) + (1/2)(n_k^\pi n_l^\sigma + n_k^\sigma n_l^\pi) / R_{kl}] \quad (9-10)$$

where R_{kl} is the distance between the k -th and l -th atoms, n_k^π and n_k^σ are the numbers of the π and σ electrons in the k -th atom. At last,

$$E^\pi = E_e^\pi + E_N^\pi \quad (9-11)$$

$$E^\sigma = E_e^\sigma + E_N^\sigma \quad (9-12)$$

9.2.2. MPn Molecular Energy

At MPn (n -th order Møller-Plesset) level of theory, total electronic energy E_e is a sum of Hartree-Fock electronic energy E_{e-HF} and n -th order correlation energies $E^{(n)}$:

$$\begin{aligned} E_e &= E_{e-HF} + E^{(2)} + \dots + E^{(n)} \\ E_{e-HF} &= (\mathbf{h} + \mathbf{f})\mathbf{d} \end{aligned} \quad (9-13)$$

$$E_{HF} = E_{e-HF} + E_N \quad (9-14)$$

where \mathbf{h} , \mathbf{f} and \mathbf{d} are, respectively, one-electron matrix, Fock matrix, and density matrix; E_N is nuclear repulsion.

After distinguishing the π and σ molecular orbitals, set $t_{ij} = 0.0$ when t_{ij} is the AO coefficient of the σ MO Φ_j^σ , and use Equation (9-5) to calculate the density matrix \mathbf{d} . Then, Equation (9-13) gives the Hartree-Fock energy E_{e-HF} , and $E^{\pi\pi}_{e-HF} = E_{e-HF}$.

At MP2 level of theory, pass the coefficient matrix \mathbf{d} through the correlation energy evaluator, where Equation (9-15) is used to calculate the second order correction energy $E^{(2)}$. Due to having set $t_{ij}^\sigma = 0.0$, $E_{\pi\pi}^{(2)} = E^{(2)}$.

$$E^{(2)} = \sum_{b=a+1}^{\infty} \sum_{a=n+1}^{\infty} \sum_{i=j+1}^n \sum_{j=1}^{n-1} [\langle ab | r_{12}^{-1} | ij \rangle - \langle ab | r_{12}^{-1} | ji \rangle]^2 / (\varepsilon_i + \varepsilon_j - \varepsilon_a - \varepsilon_b) \quad (9-15)$$

where ε_i , ε_j , ε_a and ε_b are the energy levels of molecular orbitals.

In a similar way, $E^{\sigma\sigma}_{e-HF}$ and $E_{\sigma\sigma}^{(2)}$ also can be obtained from Equation (9-13) and Equation (9-15). Using Equations (9-7) and (9-8) and using Equations (9-16) and (9-17), the π and σ parts, E_e^π and E_e^σ , of total electronic energy E_e are calculated.

$$E_\pi^{(n)} = E_{\pi\pi}^{(n)} + (1/2) E_{\pi\sigma}^{(n)} \quad (9-16)$$

$$E_\sigma^{(n)} = E_{\sigma\sigma}^{(n)} + (1/2) E_{\pi\sigma}^{(n)} \quad (9-17)$$

At last,

$$E_{MP}^\pi = E_{e-HF}^\pi + \sum_{n=2}^n E_\pi^{(n)} + E_N^\pi \quad (9-18)$$

$$E_{MP}^\sigma = E_{e-HF}^\sigma + \sum_{n=2}^n E_\sigma^{(n)} + E_N^\sigma \quad (9-19)$$

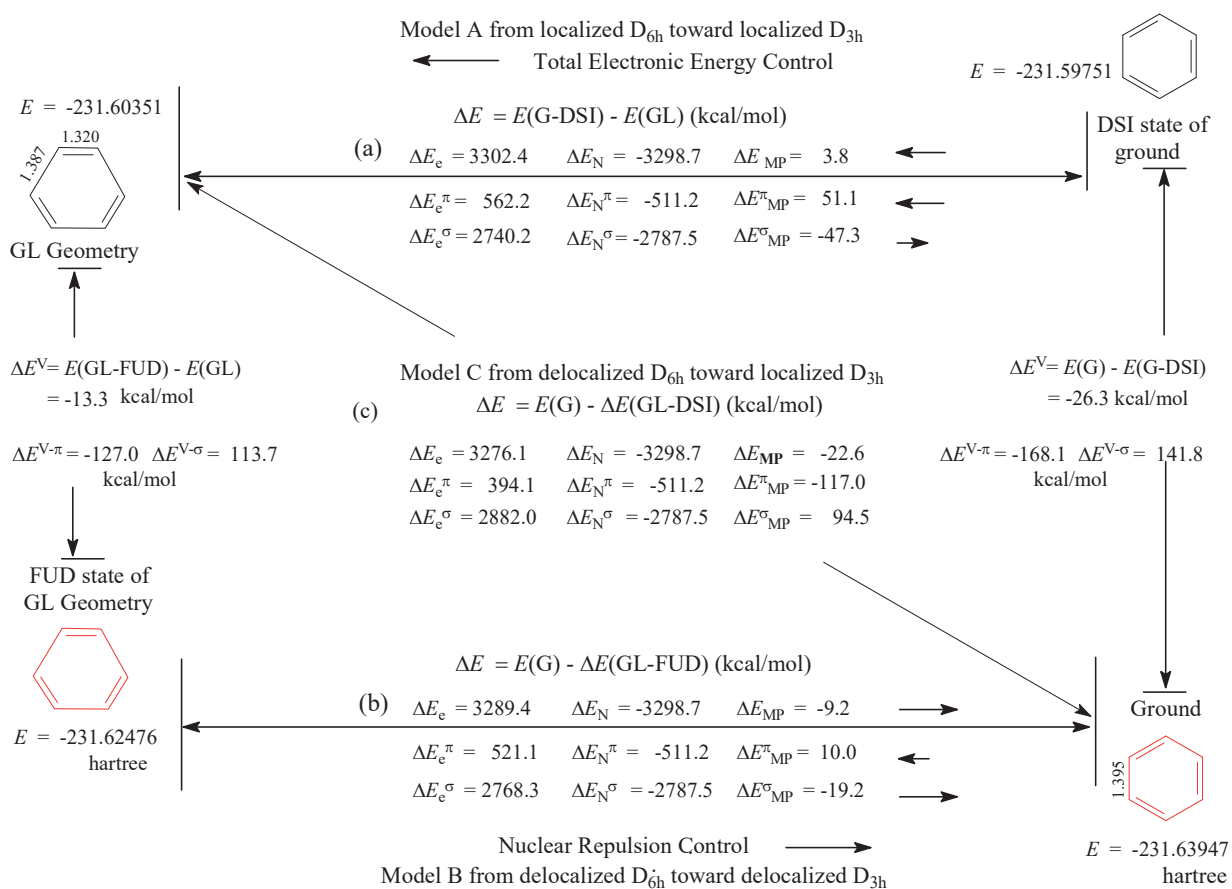


Figure 9-2. Four electronic states of benzene. The molecular energy (hartree) of each state, and its various components, the energy differences (kcal/mol) between each pair of electronic states. The geometry optimization and the energy decompositions are performed at the MP2/6-311G(2d,2p) level by using our 2011 method.

9.3. BENZENE

The definitions of the symbols for the electronic states: DSI: An electronic state in which the π -electrons are localized on their respective double bonds (or groups) and the σ -electrons are delocalized on the whole molecular framework; FUD: A electronic state in which the π - and σ -electrons are delocalized on the whole molecular framework; G-DSI: the DSI state of the optimized ground state geometry, and it is constructed by the conditional single-point energy calculation on the ground state geometry; GL: the localized GL geometry of benzene that is obtained from the restricted geometry optimization; GL-FUD: The FUD state of the optimized GL geometry, and it is constructed by a regular single-point energy calculation on the GL geometry of benzene. In the GL geometry and G-DSI state of benzene, π -electrons are, respectively, localized on the C(1)=C(2), C(3)=C(4), C(5)=C(6) double bonds, and σ -electrons are delocalized on the whole molecular framework. In the G geometry and GL-FUD state of benzene, and σ - and π -electrons are delocalized on the whole molecular framework.

9.3.1. Three Distortion Models

Table 9-1. For Benzene, Ground State (G) and Its Localized DSI State (G-DSI), GL Geometry and Its Delocalized Electronic State (GL-FUD), Various Energy Components (hartree) of Each Electronic State, and Energy Differences (kcal/mol) between Each Pair of Electronic States, Calculated at MP2/6-311G(2d,2p) Level Using Our 2011 Method.

	G E1	G-DSI E2	GL-FUD E3	GL E4	E1 - E2	E3 - E4	E1 - E3	E2 - E4	E1 - E4
$E_{\pi}^{\pi}_{HF}$	-9.21395	-8.94044	-9.23331	-9.02996	-171.6	-127.6	12.1	56.2	-115.5
$E_{\sigma}^{\sigma}_{HF}$	-221.55106	-221.77866	-221.52390	-221.70791	142.8	115.5	-17.0	-44.4	98.4
E_{HF}	-230.76500	-230.71909	-230.75722	-230.73787	-28.8	-12.1	-4.9	11.8	-17.0
$E_{\pi}^{(2)}$	-0.27171	-0.27732	-0.26821	-0.26918	3.5	0.6	-2.2	-5.1	-1.6
$E_{\sigma}^{(2)}$	-0.60275	-0.60110	-0.59933	-0.59646	-1.0	-1.8	-2.1	-2.9	-3.9
$E^{(2)}$	-0.87446	-0.87842	-0.86753	-0.86564	2.5	-1.2	-4.3	-8.0	-5.5
E^{π}_{e-HF}	-38.46624	-38.19273	-39.30019	-39.09684	-171.6	-127.6	523.3	567.3	395.7
E^{σ}_{e-HF}	-395.90287	-396.13045	-400.31788	-400.50189	142.8	115.5	2770.5	2743.1	2885.9
E_{e-HF}	-434.36910	-434.32318	-439.61807	-439.59873	-28.8	-12.1	3293.8	3310.5	3281.6
E_N^{π}	29.25229	29.25229	30.06688	30.06688	0.0	0.0	-511.2	-511.2	-511.2
E_N^{σ}	174.35181	174.35181	178.79398	178.79398	0.0	0.0	-2787.5	-2787.5	-2787.5
E_N	203.60409	203.60409	208.86086	208.86086	0.0	0.0	-3298.7	-3298.7	-3298.7
E_{e-MP}^{π}	-38.73794	-38.47005	-39.56840	-39.36602	-168.1	-127.0	521.1	562.2	394.1
E_{e-MP}^{σ}	-396.50562	-396.73155	-400.91721	-401.09835	141.8	113.7	2768.3	2740.2	2882.0
E_{e-MP}	-435.24356	-435.20160	-440.48561	-440.46437	-26.3	-13.3	3289.4	3302.4	3276.1
E_{MP}^{π}	-9.48566	-9.21776	-9.50152	-9.29914	-168.1	-127.0	10.0	51.1	-117.0
E_{MP}^{σ}	-222.15381	-222.37976	-222.12323	-222.30437	141.8	113.7	-19.2	-47.3	94.5
E_{MP}	-231.63947	-231.59752	-231.62476	-231.60351	-26.3	-13.3	-9.2	3.8	-22.6

The role of the π system in determining the structure of benzene should depend upon the following two different distortion mechanisms:

- (i) During the distortion, the electronic state of π system(s) remains unchanged no matter whether π system is localized or delocalized (Figure 9-2a and Figure 9-2b).
- (ii) Driving force for distorting geometry arises from π electron delocalization. That is, the electronic state of π system(s) changes from the localized state to the delocalized state (Figure 9-2c).

In order to understand the difference, in the role of the π system, between the different distortion mechanisms, the four electronic states, denoted as G (ground), G-DSI, GL-FUD and GL, of benzene are constructed using our

2011 method at MP2/6-311G(2d,2p) level. Various energy components, E_n , of the molecular energy for each electronic state, including the energy component differences, $E_m - E_n$ ($m, n = 1, 2, 3, 4$), between the following three pairs of electronic states: G-DSI and GL, G and GL-FUD, and GL and G (Figure 9-2), are listed in Table 9-1.

Figure 9-2 shows three distortion models A, B, and C. The model C shows the energy effects arising from π -electron delocalization. The model A and model B show the energy changes caused by the geometry distortion during which the π electronic state remains unchanged. For the three distortion models, the nuclear repulsion differences (kcal/mol), including its π and σ parts, between each pair of electronic states are as follows:

$$\begin{aligned}E^{\pi}_N(G\text{-DSI}) - E^{\pi}_N(GL) &= E^{\pi}_N(G) - E^{\pi}_N(GL\text{-FUD}) = E^{\pi}_N(G) - E^{\pi}_N(GL) = -511.2 \\E^{\sigma}_N(G\text{-DSI}) - E^{\sigma}_N(GL) &= E^{\sigma}_N(G) - E^{\sigma}_N(GL\text{-FUD}) = E^{\sigma}_N(G) - E^{\sigma}_N(GL) = -2787.5 \\E_N(G\text{-DSI}) - E_N(GL) &= E_N(G) - E_N(GL\text{-FUD}) = E_N(G) - E_N(GL) = -3298.7\end{aligned}$$

Due to always $\Delta E^{\pi}_N < 0$, $\Delta E^{\sigma}_N < 0$, and $\Delta E_N < 0$, whether the energy differences, $\Delta E^{\pi} = \Delta E^{\pi}_e + \Delta E^{\pi}_N$ and $\Delta E^{\sigma} = \Delta E^{\sigma}_e + \Delta E^{\sigma}_N$, are stabilizing or destabilizing depends on the influences of the π -electron delocalization and geometry distortion on the energy differences ΔE^{π}_e and ΔE^{σ}_e . For the distorted model A (Figure 9-2a) and model B (Figure 9-2b), the followings are the common characteristics:

$$\begin{aligned}\Delta E^{\pi}_e > 0, \Delta E^{\pi}_N < 0, \Delta E^{\pi} > 0 \\ \Delta E^{\sigma}_e > 0, \Delta E^{\sigma}_N < 0, \Delta E^{\sigma} < 0\end{aligned}$$

In the process of the geometry distortion, as long as the π electronic state remains unchanged, regardless of whether the π electrons are delocalized (Model B) or localized (Model A), the π system always prefers the D_{3h} structure due to $\Delta E^{\pi} > 0$, and the σ -framework tends to the D_{6h} structure due to $\Delta E^{\sigma} < 0$.

In the case of distortion model C (distorting localized GL geometry toward the ground state), the energy difference (kcal/mol) are as follows (Figure 9-2c):

$$\begin{aligned}\Delta E^{\pi}_e &= E^{\pi}_e(G) - E^{\pi}_e(GL) = 394.1 > 0 \\ \Delta E^{\sigma}_e &= E^{\sigma}_e(G) - E^{\sigma}_e(GL) = 2882.0 > 0 \\ \Delta E^{\pi}_N &= E^{\pi}_N(G) - E^{\pi}_N(GL) = -511.2 \\ \Delta E^{\sigma}_N &= E^{\sigma}_N(G) - E^{\sigma}_N(GL) = -2787.5\end{aligned}$$

The π and σ parts of total energy effects are:

$$\begin{aligned}\Delta E^{\pi} &= \Delta E^{\pi}_e + \Delta E^{\pi}_N = E^{\pi}(G) - E^{\pi}(GL) = -117.0 < 0 \\ \Delta E^{\sigma} &= \Delta E^{\sigma}_e + \Delta E^{\sigma}_N = E^{\sigma}(G) - E^{\sigma}(GL) = 94.5 > 0\end{aligned}$$

In and only in the case of the distortion model C, as the results of π electro delocalization, $\Delta E^{\pi} < 0$, $\Delta E^{\sigma} > 0$, and $|\Delta E^{\pi}| > \Delta E^{\sigma}$. Only with the help of the stabilizing nuclear repulsion difference, the π system can play decision role in determining the D_{6h} geometry of benzene. In contrast, the σ -framework tends to the localized D_{3h} structure.

9.3.2. BLE Leading to Minimization of Nuclear Repulsion

In order to get insight into the role of nuclear repulsion in determining the geometry of benzene, that is, to understand what is the ultimate driving force for bond length equalization (BLE), as the first step, the energy effects, arising from π -electron delocalization, are decomposed into the intra- and inter-fragment parts. Such

Table 9-2. For Benzene, Total Electronic Energies of (hartree) of Three Electronic States Denoted as G-FUD (G), GL-FUD and GL-DSI (GL), Inter- and Intra-fragment Parts (hartree) of Total Electronic Energy, and Their Differences, $E_m - E_n$ (kcal/mol), between Each Pair of Electronic States, Calculated at RHF Level of Theory by Using Our 2011 Method.

	E_e hartree	Intra-fragment energy components			Inter-fragment energy components		
		E_p^π	E_p^σ	E_p	E_{pq}^π	E_{pq}^σ	E_{pq}
6-31G*							
$E1 = Ex(GL)$	-438.96267	-13.03668	-129.31887	-142.35555	0.00000	-3.96534	-3.96534
$E2 = Ex(GL-FUD)$	-438.97674	-12.09127	-129.05219	-141.14346	-1.00845	-4.17367	-5.18212
$E3 = Ex(G)$	-435.51453	-11.25261	-128.17188	-139.42449	-1.65507	-4.09197	-5.74704
$E2 - E1$	-8.8	593.3	167.3	760.6	-632.8	-130.7	-763.5
$E3 - E1$	2163.7	1119.5	719.7	1839.3	-1038.6	-79.5	-1118.0
6-311G(2d,2p)							
$E1 = Ex(GL)$	-440.83329	-13.10261	-129.68603	-142.78864	0.00000	-4.15580	-4.15580
$E2 = Ex(GL-FUD)$	-440.84386	-11.87961	-129.50445	-141.38406	-1.28209	-4.28179	-5.56389
$E3 = Ex(G)$	-436.16663	-11.04387	-128.09191	-139.13578	-1.86195	-4.39136	-6.25331
$E2 - E1$	-6.6	767.4	113.9	881.4	-804.5	-79.1	-883.6
$E3 - E1$	2928.4	1291.9	1000.3	2292.2	-1168.4	-147.8	-1316.2
6-311G(2df,p)							
$E1 = Ex(GL)$	-441.46130	-13.14378	-130.99678	-144.14056	0.00000	-3.01320	-3.01320
$E2 = Ex(GL-FUD)$	-441.46921	-11.87191	-130.82237	-142.69428	-1.32868	-3.13344	-4.46212
$E3 = Ex(G)$	-436.17158	-11.05590	-129.10457	-140.16048	-1.85762	-3.37259	-5.23021
$E2 - E1$	-5.0	798.1	109.4	907.6	-833.8	-75.5	-909.2
$E3 - E1$	3319.4	1310.2	1187.4	2497.5	-1165.7	-225.5	-1391.2

All the energy effects do not include the nuclear repulsion

energy decomposition can only be implemented at the RHF level of theory. For total electron energy of benzene, the intra- and inter fragment energy components (E_p and E_{pq} , groups P, Q = A, B, C) and their various π and σ parts are listed in Table 9-2.

In Chapter 8, it has been indicated that, at RHF level of theory, the electron delocalization energy calculation and the $\pi-\sigma$ energy decomposition, performed by our 2011 method, are reasonable. In fact, as shown by the data listed in Table 9-2, the basis set size has no effect on the signs of the values although it has obvious effect on the magnitude of the value. In particular, always $\Delta E_p > 0$ and $\Delta E_{pq} < 0$, being in line with the twisting process in which the double bond is elongated and the single bond is compressed.

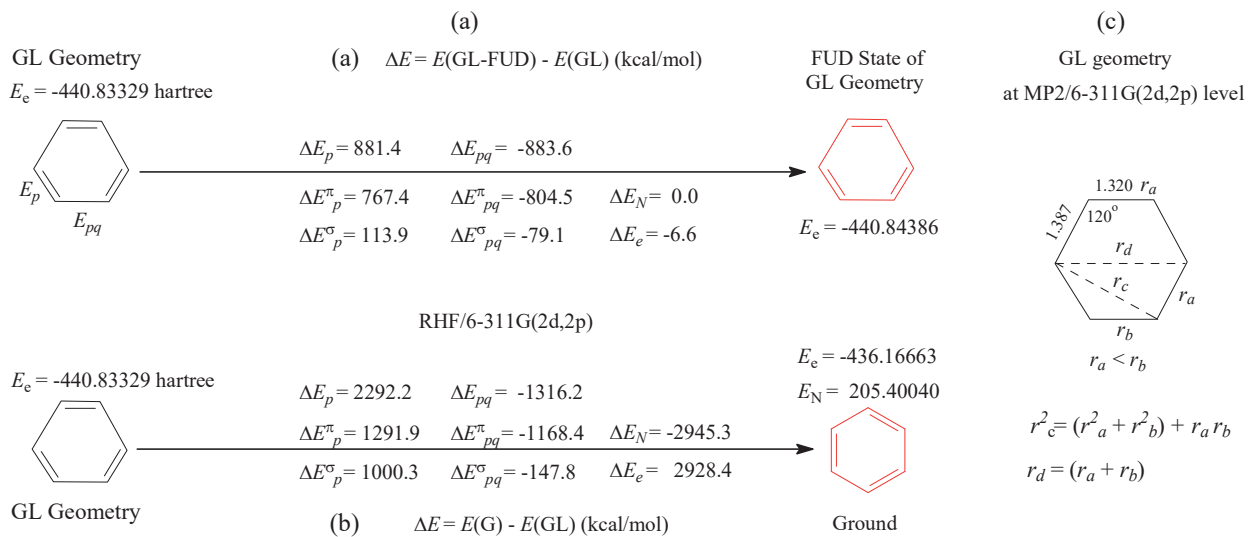


Figure 9-3. Three electronic states of benzene, total electronic energies and their intra- and inter-double bond parts, and their difference between each pair of states, calculated at the RHF/6-311G(2d,2p) level by using our 2011 method.

9.3.2.1. Intra- and Inter-double Bond Interactions

At the RHF/6-311G(2d,2p) level, as shown by Figure 9-3a, the total electronic energy difference ΔE (kcal/mol), i. e. the molecular energy difference, between the GL and its Full delocalized state (GL-FUD) can be partitioned into the intra- and inter-fragment (double bond) parts denoted as ΔE_p and ΔE_{pq} , and the latter's energy parts can be further decomposed into their π and σ parts denoted as ΔE_p^π and ΔE_p^σ , and ΔE_{pq}^π and ΔE_{pq}^σ . The values (kcal/mol) of these energy effects are as follows:

$$\begin{aligned}\Delta E_p &= E_p(\text{GL-FUD}) - E_p(\text{GL}) = 881.4 > 0, \\ \Delta E_p^\pi &= 767.4 > 0, \Delta E_p^\sigma = 113.9 > 0 \\ \Delta E_{pq} &= E_{pq}(\text{GL-FUD}) - E_{pq}(\text{GL}) = -883.6 < 0 \\ \Delta E_{pq}^\pi &= -804.5 < 0, \Delta E_{pq}^\sigma = -79.1 < 0 \\ \Delta E &= E(\text{GL-FUD}) - E(\text{GL}) = 3(\Delta E_{pq} + \Delta E_p) = -6.6 < 0\end{aligned}$$

For the GL geometry, thus, at the moment of the π -electron delocalization (vertical electron delocalization), the intra-double driving force ($\Delta E_p > 0$), resulted from π -delocalization, makes the double bonds lengthened, and at the same time, the inter-double driving force ($\Delta E_{pq} < 0$) shortens the single bonds.

9.3.2.2. Nuclear Repulsion Minimization

According to Figure 9-3c, the total nuclear repulsion between carbon atoms in benzene ring can be written as follow:

$$E_N = 3A(1/r_a + 1/r_b + 1/r_c + 1/r_d)$$

In the above equation, $A = 36ee$, e is proton charge. For the Full delocalized electronic state of the GL geometry, the

CC bond angle is 120° , and it is considered unchanged during the geometric distortion. Thus, the bond distances r_c and r_d can be calculated using the following Equations:

$$\begin{aligned} r_c^2 &= (r_a^2 + r_b^2) - 2r_a r_b \cos(120^\circ) = (r_a^2 + r_b^2) + r_a r_b \\ r_d &= r_a + r_b \end{aligned}$$

The differential equation of E_N can be written as Equation (9-20):

$$dE_N = 3A[\partial(1/r_a)/\partial r_a]dr_a + 3A[\partial(1/r_b)/\partial r_b]dr_b + 3A[d(1/r_c) + d(1/r_d)] \quad (9-20)$$

Due to that the double bonds are lengthened and meanwhile the single bonds are shortened, i.e. $dr_a > 0$ and $dr_b < 0$, and set $dr = dr_a = |dr_b|$. Therefore,

$$\begin{aligned} d(1/r_d)/dr &= 0 \\ d(1/r_c) &= [-0.5(r_a - r_b)/r_c^3]dr \end{aligned}$$

Equation (9-20) can be rewritten as the following:

$$\begin{aligned} dE_N/dr &= 3A(r_a - r_b)[(r_a + r_b)/(r_a^2 r_b^2) - 0.5/r_c^3] \\ d^2 E_N/dr^2 &\approx 3A(2/r_a^3 + 2/r_b^3 - 1/r_c^3) > 0 \text{ due to } r_c > r_a \text{ and } r_c > r_b \end{aligned}$$

At last, we have:

$$dE_N/dr = 0 \text{ when } r_a = r_b$$

When all the CC bond lengths are equalized ($r_a = r_b$), therefore, the nuclear repulsion among the CC bonds in the benzene ring is minimized, leading to the formation of D_{6h} geometry. In this case, the energy differences between the G and GL geometry are as follows (at RHF/6-311G(2d,2f) level):

$$\begin{aligned} \Delta E_N &= E_N(G) - E_N(GL) = -2945.3 \text{ kcal/mol}, \\ \Delta E_e &= E_e(G) - E_e(GL) = 2928.4 \text{ kcal/mol}, \\ |\Delta E_N| &> \Delta E_e, \text{ therefore} \\ \Delta E^A &= E(G) - E(GL) = \Delta E_N + \Delta E_e = -16.9 \text{ kcal/mol} < 0. \end{aligned}$$

For benzene, nuclear repulsion plays a predominated role in eventually determining the D_{6h} geometry, but this driving force results from the influences of π -electron delocalization on the intra- and inter-double interaction energies. The above energy decomposition and discussion unify the energy criterion and geometric criterion of the aromaticity. The geometric criterion and the energy criterion are mutually causal.

9.4. [N]ANNULENES

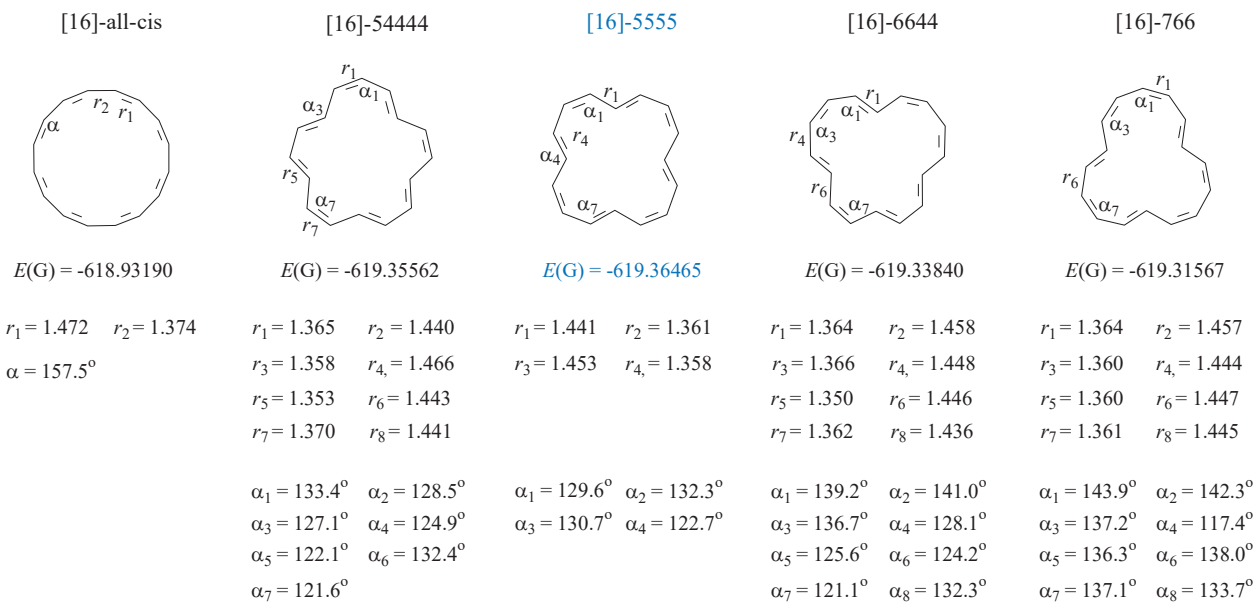


Figure 9-4. The planar configuration isomers of [16]annulene are optimized at B3LYP/6-311G** level, and their molecular energy $E(G)$ (hartree), bond lengths r_n (\AA) and bond angles α_n , the isomer [16]-5555 is the most stable

In this and next sections, we have two main purposes. Firstly, use the vertical delocalization energies of [N]annulenes to demonstrate the rationality of our 2011 program.

In Figure 9-4, the five planar configuration isomers of [16]annulene are obtained from the geometry optimization at B3LYP/6-311G** level. These configuration isomers are, respectively, denoted as [16]-all-cis, [16]-54444, [16]-55555, [16]-66444, and [16]-766. In the [16]-5555 isomer, the largest CC bond angle is about 132° . The range of a set of bond angles is 9.6° , and it is the smallest of all the isomers presented in Figure 9-4. Correspondingly, it is most stable according to the molecular energies of the configuration isomers (Table 9-3 and Figure 9-4).

9.4.1. Meaning of Symbol “[16]-54444”

For the configuration isomer [16]-54444, for example, “[16]” means that [16]-54444 is a configuration isomer of [16]annulene. In the symbol “[16]-54444”, there are the following five Arabic numerals: “5”, “4”, “4”, “4” and “4”. The number of Arabic numerals corresponds to the number of the inner hydrogen atoms and to the number of the pairs of adjacent inner hydrogen atoms (shortened to “inner hydrogen atoms”). All the carbon atoms between two inner hydrogen atoms form a fragment. The arrange order of the five Arabic numerals is the arrange order of the corresponding fragments. the F-th ($F = 1, 2, \dots, n$) Arabic numeral in the symbol “[16]-54444” represents the number, N_{FC} , of carbon atoms in the F-th fragment. For example, the first Arabic numeral is “5”, and it means that, in the first fragment or between the first pair of the inner hydrogen atoms, the number of carbon atoms is 5, that is, $N_{1C} = 5$. Accordingly, in the [16]-54444 isomer, as shown by Figure 9-4, there are five inner hydrogen atoms, and there are five pairs of the inner hydrogen atoms, that is, there are five fragments. In this isomer, the symbols “ N_{FC} ”, including their values (ie. the numbers of the carbon atoms in these fragments), can be written as follows:

$$N_{1C} = 5, N_{2C} = 4, N_{3C} = 4, N_{4C} = 4, \text{ and } N_{5C} = 4.$$

A carbon atom can be shared by two adjacent fragments. When counting the number of carbon atoms in a fragment, the number of carbon atoms in each of two adjacent fragments includes the shared carbon atom.

Table 9-3. Five Planar Configuration Isomers of [16]Annulene, Including Their Molecular Energies (hartree), Are Obtained from the Geometry Optimization at B3LYP/6-311G** Level. Vertical Delocalization Energies (kcal/mol), $\Delta E^V(2011)$, are Calculated, on the B3LYP/6-311G** Optimized Geometries, by Using Our 2011 Program.

Theoretical levels	Basis sets	[16]-5555 -619.36466 ^a	[16]-54444 -619.35562 ^a	[16]-6644 -619.33840 ^a	[16]-766 -619.31568 ^a	[16]-all-cis -618.93190 ^a
B3LYP	6-31G*	-8.4	-1.9	-8.2	-15.1	-33.1
	6-311G(2df,p)	10.1	17.7	10.2	1.9	-22.0
	6-311G**	-3.7	3.7	-3.5	-11.82	-31.9
LYP	6-31G*	12.6	19.1	12.7	5.8	-10.5
	6-311G(2df,p)	20.7	27.9	20.6	12.8	-8.1
RHF	6-311G**	13.7	20.9	13.8	6.2	-12.2
	6-31G*	13.8	20.3	13.9	7.0	-9.4
	6-311G(2df,p)	22.2	29.4	22.1	14.3	-6.6
MP2	6-311G**	15.1	22.3	15.2	7.7	-10.9
	6-31G*	-15.7	-10.2	-15.5	-21.2	-33.9
	6-311G(2df,p)	19.1	25.2	18.9	12.3	-7.1
	6-311G**	-11.1	-5.0	-10.9	-17.0	-32.0

^a Molecular energy (hartree) of a planar isomer optimized at B3LYP/6-311G** level.

When $N_{FC} = 4$, the CC bond angle is about 125° , and the corresponding angle strain should be small. In the second fragment of the isomer [16]54444, for example, $\alpha_4 = 124.9^\circ$, and $\alpha_5 = 122.1^\circ$.

9.4.2. Relationship between Configuration and VDE

[16]annulene is anti-aromatic, according to the $4n+2$ rule, and its vertical delocalization energy (VDE) should be destabilizing. For [16]-all-cis isomer, its molecular energy is the highest of all the planar configuration isomers (Figure 9-4) (may be due to the large CC bond angles (157.5°)), and its vertical delocalization energy $\Delta E^V(2011)$ (the data in the last column of Table 9-3) is always stabilizing without exception.

Based on the comparison of the data listed in Table 9-3, only at the RHF and LYP levels of theory, the vertical delocalization energies $\Delta E^V(2011)$ of other four isomers are destabilizing, but the configuration has an obvious influence on the magnitude of vertical delocalization energy (kcal/mol). At the RHF/6-311G** level, for example, the values of $\Delta E^V(2011)$ are 22.3 ([16]-54444) and 7.7 ([16]-766), and their ratio is about 3.

At 6-311G(2df,p) level, in addition, the vertical delocalization energies of other four isomers are always destabilizing.

In order to reasonably calculate the vertical delocalization energy of an [N]annulene, therefore, it is necessary to determine its most stable (configuration) isomer. For each [N]annulene, the conformations of all its configuration isomers must be planar in order to calculate the vertical delocalization energies using our 2011 method.

Table 9-4. Vertical Delocalization Energy, $\Delta E^V(2011)$ and $\Delta E^V(2007)$ (kcal/mol), of [16]-5555 Isomer, Calculated by Using Our 2011 and 2007 Methods.

Basis sets	Programs	B3LYP	LYP	RHF	MP2 RHF	MP2	Range
6-31G*	2011	-9.1	20.9	19.3	13.0	-16.6	37.5
	2007	9.4	123.5	116.3	117.7	261.9	252.5
6-311G**	2011	-3.7	22.2	20.8	14.5	-11.9	34.2
	2007	13.7	136.4	128.9	131.5	375.4	361.7

The geometry optimization of ground state geometry and the calculation of vertical delocalization energy are performed at the same theoretical level with the same basis set.

The calculation of the vertical delocalization energies (Table 9-4) and the optimization of the ground state geometry are performed at the same theoretical level with the same basis set. Even so, the determination of the most stable isomer still can't ensure that for [16]-5555, the vertical delocalization energy $\Delta E^A(2011)$ is always destabilizing. Emphatically, the vertical delocalization energy $\Delta E^A(2011)$ becomes destabilizing only at the LYP and RHF levels of theory. At these two theoretical levels, all types of the exchange interactions, including the density functional exchange, have been excluded from between double bonds in localized electronic state.

Nonetheless, a comparison of the Range($\Delta E^V, 2011$) and Range($\Delta E^V, 2007$) listed in Table 9-4 show that our 2011 program is more reasonable than our 2007 program although $\Delta E^V(2007)$ is always destabilizing. At the 6-31G* level, for example, Range($\Delta E^V, 2011$) = 37.5 kcal/mol, and Range ($\Delta E^V, 2007$) = 252.5 kcal/mol.

9.4.3. Possible Configuration Isomers of a [N]Annulene

For each of nine [N]annulenes from [10]annulene to [26]annulene, the possible planar configuration isomers are optimized at B3LYP/ 6-311G** level, and then the most stable configuration is determined according to the molecular energies.

For a specific [N]annulene, the determination of the most stable configuration has been a topic of much debate.

9.4.3.1. [10]annulene

[10]annulene was first prepared in 1967.^{37,38} As a potentially aromatic molecule, it should be nearly planar. However, the angle strain and the unfavorable steric interactions of the inner protons tend to force the molecule into non-planar conformation. The different conformations and configurations have been proposed, but it has yet to be characterized unambiguously by X-ray analysis and spectroscopic methods, which may be due to the low energy interconversions between different structures.

In 1969, two structures, all-cis isomer and mono trans isomer, denoted as [10]-all-cis and [10]-10, were assigned by NMR.³⁹ Even at temperatures as low as -100 °C, photochemical interconversions between these two isomers proceed rapidly, and the mono-trans isomer that is near planar, is favorable.^{6,7,40}

The possible structures of [10]annulene were theoretically investigated, but these structures are non-planar.^{7,10,11,41,42} In Figure 9-5, three planar isomers of [10]annulene, denoted as [10]-all-cis, [10]-66, and [10]-10, are optimized at B3LYP/6-311G** level, and their geometrical data are presented. These three planar isomers are unstable, and the last one is the most stable of the three isomers. In the symbol “[10]-10”, there is only one Arabic

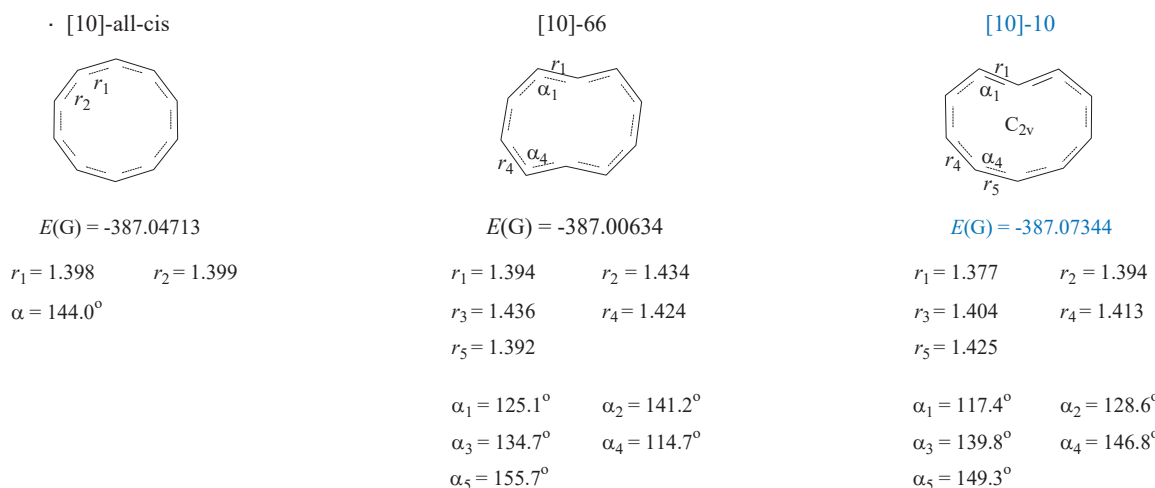


Figure 9-5. The planar isomers of [10]annulene are obtained from geometry optimizations at B3LYP/6-311G**, and the [10]-10 isomer is the most stable.

numerical. Correspondingly, there is only one inner hydrogen atom in the molecule. In this special case, an inner hydrogen atom can be considered as a pair of virtual inner hydrogen atoms, and the number of carbon atoms between this virtual pair of atoms is 10.

For the isomer [10]-all-cis, the CC bond lengths can be considered to be equal, but for the planar isomer [10]-10 that is the most stable, as shown by Figure 9-5, the bond lengths are no longer equal to each other. For example, $r_5 = 1.425 \text{ \AA}$, and $r_1 = 1.377 \text{ \AA}$, and their difference is 0.048 \AA , indicating an interesting fact that the bond length increases monotonically from r_1 to r_5 .

In the case of benzene, the conclusion that the nuclear repulsion is minimized when the CC bond lengths are equalized is based on the setting $dr_a = -dr_b$, where dr_a and dr_b are the changes in the distances of the double bond and single bond. Therefore, as confirmed by the bond lengths in the [10]all-cis and [10]-10 isomers (Figure 9-5), the prerequisite for the equalization of the CC bond lengths is that the configuration of aromatic annulene (such as [10]annulene) must be all-cis configuration.

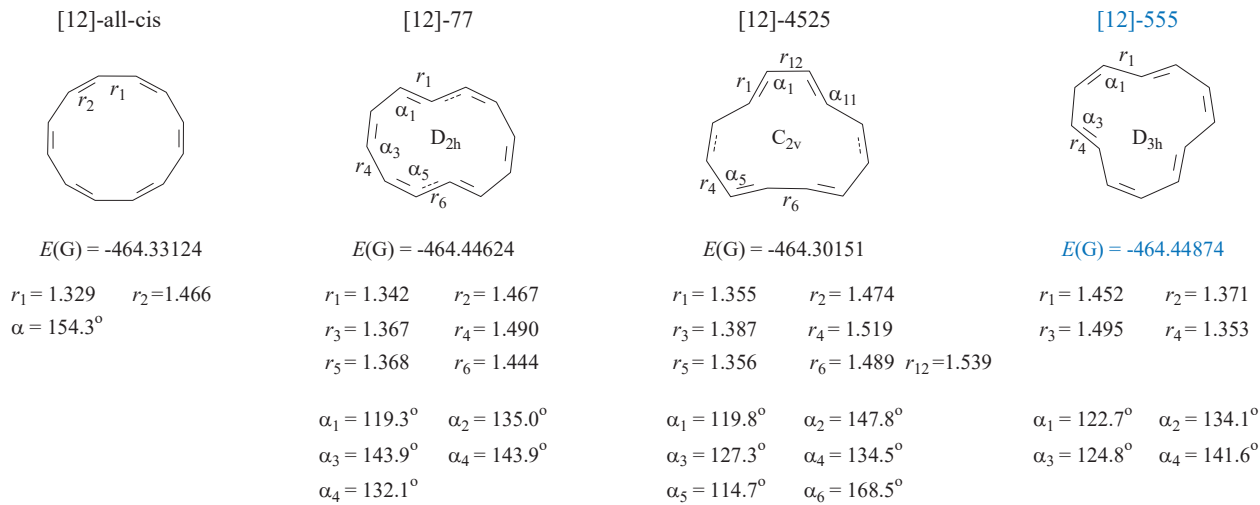


Figure 9-6. The planar isomers of [12]annulene are optimized at B3LYP/6-311G**. The [12]-555 isomer is the most stable.

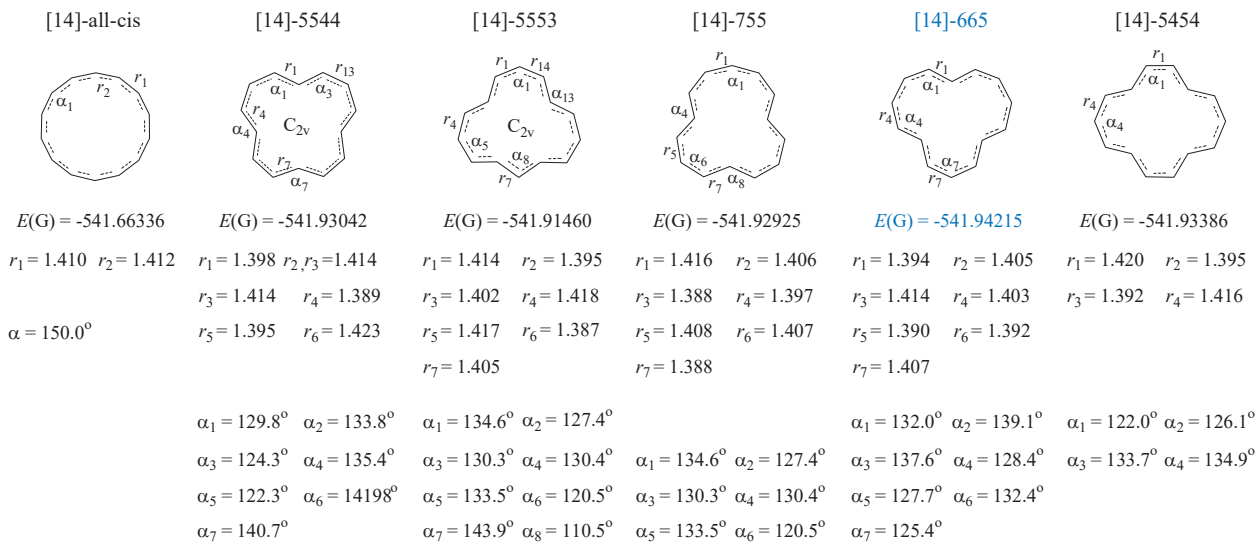


Figure 9-7. The planar isomers of [14]annulene are optimized at B3LYP/6-311G**, and [14]-665 isomer is the most stable.

9.4.3.2. [12]annulene

[12]annulene was first synthesized in 1970,^{43,44} and low-temperature NMR analysis indicates that this molecule, (a tri-trans structure denoted as [12]-555 in this section), is significantly distorted from planarity due to steric hindrance between the inner hydrogen atoms.

Six Möbius structures of [12]annulene were optimized by Castro in 2002, two of six structures are similar to the planar isomers denoted as the [12]-77 and [12]-555 in Figure 9-6.

Its four possible planar isomers in Figure 9-6 are optimized at B3LYP/6-311G** level, and the [12]-555 isomer is the most stable.⁴⁵ The single and double bonds are alternating in any configuration. The Figure 9-6 shows that, in the fragment with 5 carbon atoms, the CC bond angles are the smaller. In the first fragment of [12]-555, the CC bond angles are 122.7, 134.1° and 124.8°. But in the first fragment of [12]-77, there are 7 carbon atoms, and the corresponding CC bond angles are 135.0° and 143.9°.

9.4.3.3. [14]annulene

In 1960, [14]annulene was first synthesized by Sondheimer and Gaoni.⁴⁶ Theoretical calculations suggest that the most stable configuration is [14]-5454.^{47,48} X-ray structure determination confirms this structure.⁴⁹ The nonplanarity is ascribed primarily to nonbonding interactions between the internal protons. Nearly equalized bond lengths (1.40 Å) have been confirmed by calculation as well as X-ray analysis and low-temperature UV studies.

In the case of planar conformation, however, as shown by the molecular energies in Figure 9-7, the [14]-655 isomer, rather than [14]-5454 isomer, is the most stable of the six planar isomers, but the molecular energy difference between two isomers [14]-655 and [14]-5454 is only 5.2 kcal/mol. In the [14]-655 isomer, the CC bond length difference (bond alternation), $\Delta r = 0.017 \text{ \AA}$, are smaller than that, $\Delta r = 0.028 \text{ \AA}$, in the [14]-5454 isomer.

In the all-cis isomer, the CC bond lengths, 1.410 and 1.412 Å, can be considered to be equalized.

9.4.3.4. [18]annulene

[18]Annulene was first synthesized by Sondheimer and co-workers in 1962.⁵⁰ Its structure was first determined by x-ray in 1965,⁵¹ and it was reevaluated in 1995.⁵² The structure of [18]annulene has the D_{6h} symmetry,

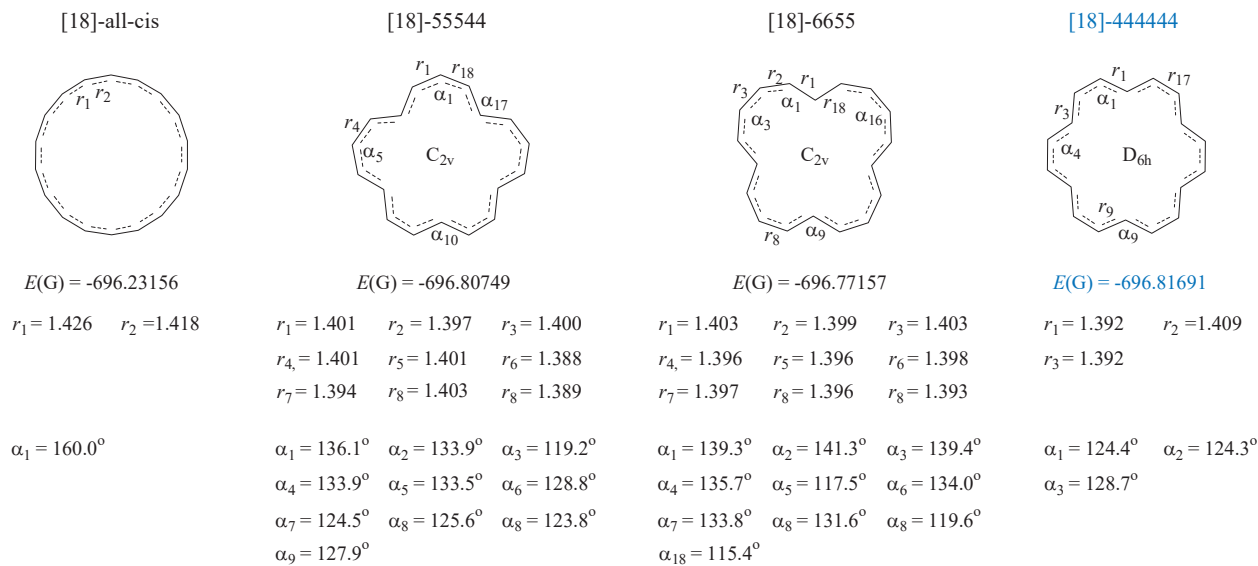


Figure 9-8. The planar isomers of [18]annulene are optimized at B3LYP/6-311G**, and the [18]-444444 isomer is most stable.

and its configuration can be expressed as [18]-444444. Its experimental CC bonds are, respectively, 1.385 and 1.405 Å, which are approximately equal. Density functional and MP2 calculations confirmed that the D_{6h} structure is preferred.^{16,53,54}

The four planar isomers, denoted as [18]-all-cis, [18]-55544, [18]-6655, and [18]-444444, are optimized at B3LYP/6-311G* level, and their geometric data are presented in Figure 9-8. Our calculations confirmed that the planar [18]-444444 isomer with D_{6h} structure is the most stable, and its theoretical CC bond lengths, 1.392 and 1.409 Å, are almost equal to each other.

According to Figure 9-8, in each fragment of [18]-444444, there are four carbon atoms, and the CC bond angle is about 125.0°. In the all-cis isomer, the CC bond lengths are 1.426 and 1.418 Å, and the bond length difference (0.008 Å) is smaller than that (0.017 Å) in [18]-444444 isomer.

9.4.3.5. [20]annulene

In 1971, it was synthesized by Sondheimer and Metcalf, and ^1H NMR data show a mixture of stereoisomers.⁵⁵ The configuration of a stereoisomer in the mixture can be expressed as [20]-5344443 (Figure 9-9), and the non-planar [20]-5344443 isomer can be considered to be the most stable of the three Möbius isomers.⁴⁵

In the case of planar conformation, however, as shown by our calculations, it is the [20]-445445 isomer, rather than [20]-5344443, to be most stable of the 7 possible planar isomers (Figure 9-9). But, [20]-445445 isomer is only -3.0 kcal/mol more stable than [20]-5344443 isomer.

A comparing the CC bond angles in two planar isomers [20]-445445 and [20]-534443 shows the following facts:

- (i) In the first fragment of [20]-445445, there are four carbon atoms, the CC bond angles are about $\alpha_1 = 127.0^\circ$ and $\alpha_{13} = 121^\circ$.
- (ii) In the third fragment of [20]-445445, there are five carbon atoms, the CC bond angles are about $\alpha_5 = 133.0^\circ$ and $\alpha_7 = 121.9^\circ$.
- (iii) In the first fragment of [20]-5344443, there are five carbon atoms, the CC bond angles are about $\alpha_1 = 132.6^\circ$

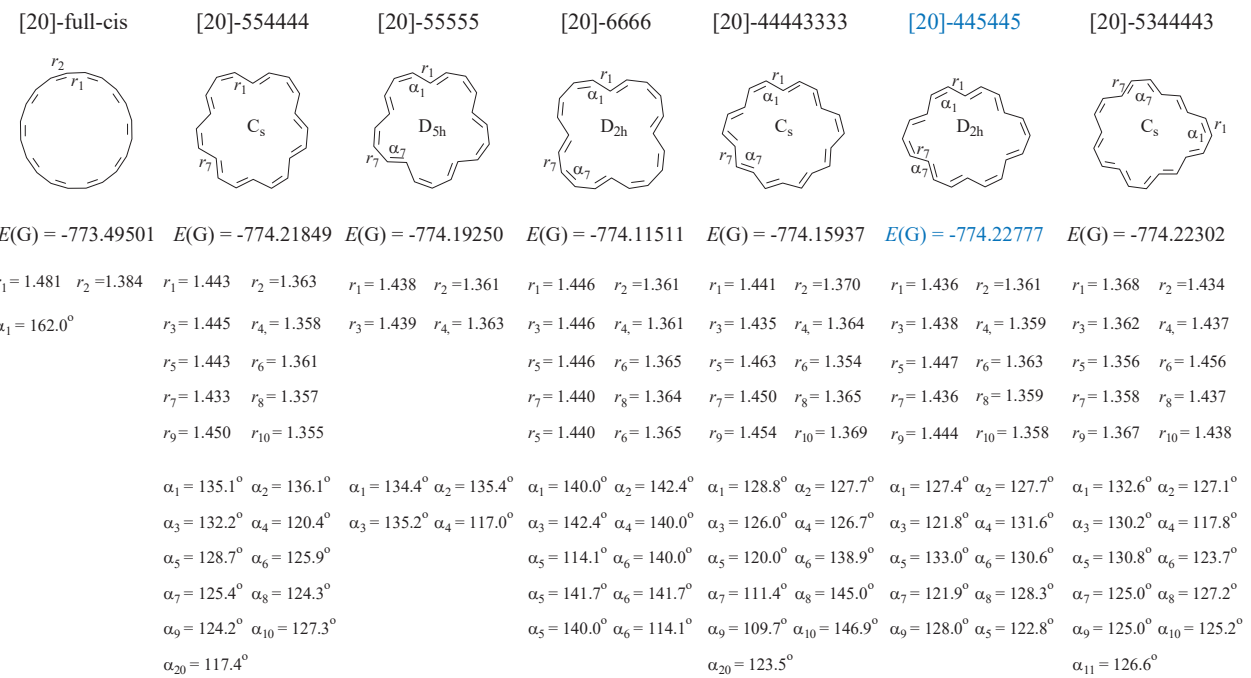


Figure 9-9. The planar isomers of [20]-annulene were obtained from geometry optimizations at B3LYP/6-311G**, and [20]-4-4-5-4-4-5 isomer is the most stable

and $\alpha_2 = 127.1^\circ$.

- (iv) In the second fragment of [20]5344443, there are three carbon atoms, the CC bond angles are $\alpha_4 = 117.8^\circ$ and $\alpha_5 = 130.8^\circ$.
- (v) In the fourth fragment of [20]5344443, there are four carbon atoms, the CC bond angles are $\alpha_9 = 125.0^\circ$ and $\alpha_{11} = 126.6^\circ$.

Accordingly, the following conclusions seems to be reasonable:

- (i) The angle strain in the fragment with four carbon atoms is small.
- (ii) The angle strain in the fragment with three carbon atoms seems to be larger than in the fragment with five carbon atoms.

9.4.3.6. [22]-, [24]- and [26]Annulenes.

The following rules of determining the configuration of an [N]annulene ($N > 20$) can be deduced from the geometry optimization of [N]annulenes ($N \leq 20$):

- (i) When $4 \leq N_{FC} \leq 5$, the angle strain is smaller
- (ii) The number of fragments with $N_{FC} = 4$ should be as many as possible, which means that the number of fragments with $N_{FC} = 5$ must not be greater than 2.

Accordingly, it is speculated that the most stable planar isomers of these three [N]annulenes are, respectively, [22]-5444444, [24]-44444444 and [26]-54445444 (Figure 9-10).

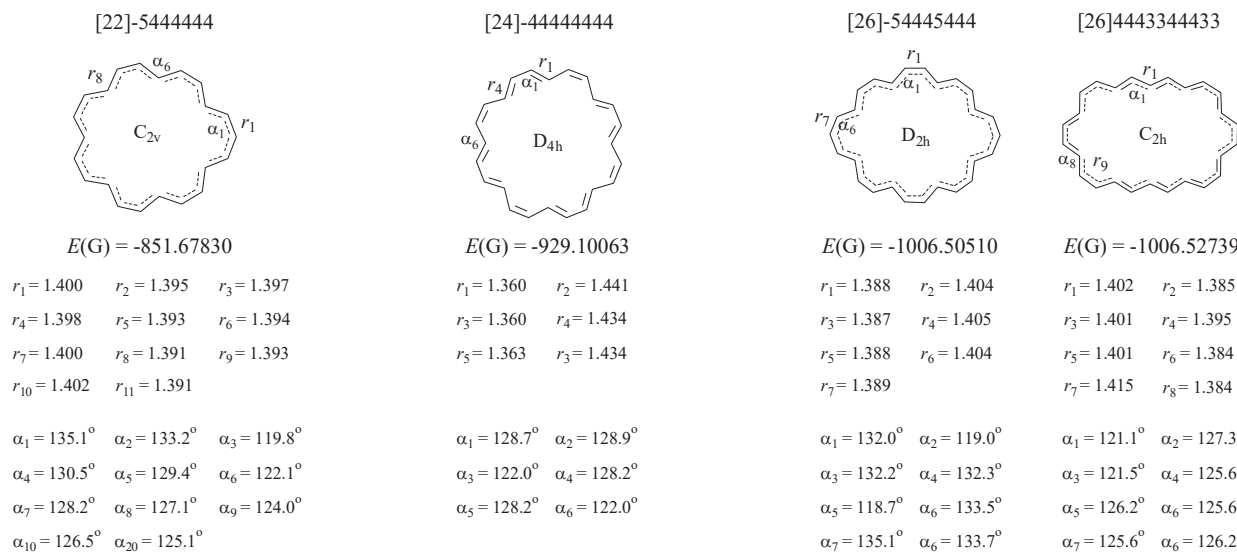


Figure 9-10. For [22]annulene, [24]annulene and [26] annulenes, the speculated most stable planar isomers, and their bond lengths (\AA) and bond angles, obtained from the geometric optimization at B3LYP / 6-311G **

The synthesis of [22]annulene was reported by Sondheim in 1971, and its configuration, expressed as [22]-44434443, is determined by NMR.⁵⁶ The planar conformation (-851.67831 hartree) of [22]-54444444 is -0.4 kcal/mol more stable than that (-851.67268 hartree) of [22]44434443. In the planar conformation of [22]-54444444, the CCC bond angles are in the region of 122 to 135°, and the corresponding angles in the planar conformation of [22]44434443 is in the region of 125 to 128°.

According to ^1H NMR spectroscopy, as reported by Lloyd and coworkers in 2002,⁵⁷ [24]annulene exists as two equilibrating configurations, [24]-44344344 (95%) and [24]-533533533 (5%), in the solution, and these two configurations interconvert extremely rapidly. However, in the case of planar conformation, as shown by the geometry optimizations at B3LYP/6-311G** level, [24]-44444444 (-929.10063 hartree) is -6.6 kcal/mol more stable than [24]-44344344 (-929.09016 hartree). In the planar conformation of [24]-44444444, the CCC bond angles are in the region of 122 to 129°, and the corresponding angles in the planar conformation of [24]44344344 is in the region of 119 to 128°.

In the literature,⁵⁸ the configuration of [26]annulene was expressed as [26]-4443344433. According to the geometry optimizations at B3LYP/6-311G** level (Figure 9-10), the planar conformation of [26]-4443344433 is -14.0 kcal/mol more stable than that of [26]-54445444. A comparison of the CC bond lengths in [26]54445444 and [26]4443344433 shows that the degree of the single and double bond alternation for the former's molecule is slightly smaller than for the latter's molecule. Therefore, the planar conformation of [26]-54445444 will be used to calculate vertical delocalization energy.

9.4.4. Vertical Delocalization Energies

The vertical delocalization energies (VRE) for the planar [N]annulenes are listed in Table 9-5, and they are calculated, on their respective most stable isomers optimized at B3LYP/6-311G** level, using our 2011 method. As shown by the data listed in Table 9-5, the theoretical level and basis set size have the large influences on the sign and size of the vertical delocalization energy value. So far, this problem has only been encountered in the case of [N]annulene, which may arise from the strong π interaction between the nonbonded double bonds. When attempting to theoretically determine the structure of an annulene such as [10]annulene, this type of uncertainty is also

Table 9-5. For Most Stable Planar Isomers of 10 [N]annulenes, Vertical Delocalization Energies ΔE^V (2011) (kcal/mol) Are Calculated, on Their Respective B3LYP/6-311G Optimized Geometries, Using Our 2011 Method. Data (kcal/mol) in Parentheses Are the Vertical Delocalization Energy per π -Electron.**

[N]annulene	Basis sets	RHF	MP2	B3LYP	LYP	Range
[8]-8	6-31G*	14.6 (1.8)	3.6 (0.5)	8.4 (1.1)	14.0 (1.8)	6.2
	6-311G(2d,f,p)	16.6 (2.1)	18.3 (2.3)	14.6 (1.8)	16.0 (2.0)	3.7
	6-311G**	14.6 (1.8)	5.5 (0.7)	9.9 (1.2)	14.0 (1.8)	9.1
[10]-66	6-31G*	-30.8 (-3.1)	-52.9 (-5.3)	-45.1 (-4.5)	-31.8 (-3.2)	-22.1
	6-311G(2d,f,p)	-23.5 (-2.4)	-28.8 (-2.9)	-30.9 (-3.1)	-24.7 (-2.5)	-6.2
	6-311G**	-29.9 (-3.0)	-50.0 (-5.0)	-42.2 (-4.2)	-31.1 (-3.1)	-20.1
[12]-555	6-31G*	11.8 (1.0)	-8.6 (-0.71)	-1.8 (-0.15)	11.0 (0.9)	20.4
	6-311G(2d,f,p)	17.1 (1.4)	14.9 (1.2)	10.4 (0.9)	16.1 (1.3)	6.7
	6-311G**	12.8 (1.1)	-5.9 (-0.5)	1.6 (0.1)	11.9 (1.0)	18.7
[14]-665	6-31G*	-25.3 (-1.8)	-64.2 (-4.6)	-53.2 (-3.8)	-26.7 (-1.9)	-38.9
	6-311G(2d,f,p)	-14.9 (-1.1)	-30.5 (-2.2)	-32.9 (-2.4)	-16.6 (-1.2)	-18.0
	6-311G**	-24.3 (-1.7)	-60.4 (-4.3)	-49.2 (-3.5)	-25.9 (-1.9)	-36.1
[16]-5555	6-31G*	13.8 (0.9)	-15.7 (-1.0)	-8.4 (-0.5)	12.6 (0.8)	29.5
	6-311G(2d,f,p)	22.2 (1.4)	19.1 (1.2)	10.1 (0.6)	20.7 (1.3)	12.1
	6-311G**	15.1 (0.9)	-11.1 (-0.7)	-3.7 (0.2)	13.7 (0.9)	26.2
[18]-444444	6-31G*	-5.3 (-0.3)	-63.4 (-3.5)	-47.7 (-2.7)	-7.1 (-0.4)	-58.1
	6-311G(2d,f,p)	10.7 (0.6)	-16.8 (-0.9)	-17.8 (-1.0)	8.3 (0.5)	-28.5
	6-311G**	-5.3 (-0.3)	-63.4 (-3.5)	-40.5 (-2.3)	-4.5 (-0.3)	-58.9
[20]-445445	6-31G*	18.7 (0.9)	-19.9 (-1.0)	-11.6 (-0.6)	17.1 (0.9)	38.6
	6-311G(2d,f,p)	30.6 (1.5)	25.9 (1.3)	13.7 (0.7)	28.7 (1.4)	16.9
	6-311G**	20.9 (1.0)	-13.2 (-0.7)	-4.9 (-0.2)	19.1 (1.0)	34.1
[22]-5444444	6-31G*	-5.4 (-0.2)	-64.3 (-2.9)	-59.4 (-2.7)	-6.7 (-0.3)	-54.0
	6-311G(2d,f,p)	13.4 (0.6)	-5.6 (-0.3)	-23.4 (-1.1)	11.5 (0.5)	-36.8
	6-311G**	-2.4 (-0.1)	-55.8 (-2.5)	-51.2 (-2.3)	-4.1 (-1.9)	-53.4
[24]-44444444	6-31G*	23.5 (1.0)	-23.9 (-1.0)	-14.9 (-0.6)	21.6 (0.9)	47.4
	6-311G(2d,f,p)	38.9 (1.6)	32.6 (1.4)	17.1 (0.7)	36.5 (1.5)	21.8
	6-311G**	26.7 (1.1)	-15.3 (-0.6)	-6.3 (0.3)	24.5 (1.0)	42.0
[26]-54445444	6-31G*	0.0 (0.0)	-59.0 (-2.3)	-58.8 (-2.3)	-2.5 (-0.1)	-59.0
	6-311G(2d,f,p)	20.2 (0.8)	7.8 (0.3)	-19.1 (-0.7)	17.2 (0.7)	
	6-311G**	3.0 (0.1)	-49.5 (-1.9)	-49.8 (-1.9)	0.2 (0.0)	-52.8

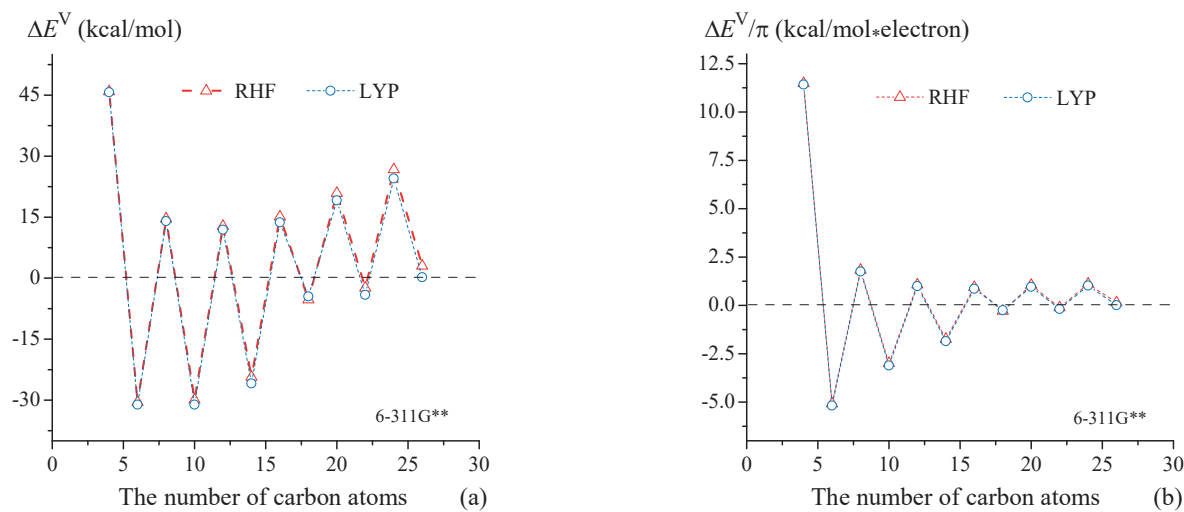


Figure 9-11. For [N]annulenes at (RHF and LYP)/6-311G** level: (a) The vertical delocalization energy. (b) The vertical delocalization energy per π -electron, and they change as the number of carbon atoms increases from $N = 4$ to $N = 26$, which are obtained from the calculations on the B3LYP/6-311G** optimized geometries of their most stable isomers by using our 2011 method.

encountered. As the literature points out, therefore, "Over the past 20 years, computational methods have become more sophisticated but at the same time it has been recognized that these methods need to be used with caution when applied to these complex conjugated systems."⁵⁷

According to Table 9-5, the following general rules are noteworthy:

- (i) When $N \leq 10$ including cyclobutadiene and benzene, the vertical delocalization energy (VDE) is always in accordance with the $4n+2$ rule, that is, for $[4n]$ annulene, $\Delta E^V(2011) > 0$ (destabilizing), and for $[4n+2]$ annulene, $\Delta E^V(2011) < 0$ (stabilizing), which is independent of the theoretical level and basis set size.
- (ii) When $N \leq 16$, the VDE, calculated at 6-311G(2df,p) level, is always in accordance with the $4n+2$ rule, which is independent of the theoretical level.
- (iii) At RHF/(6-31G* and 6-311G*) level, the VDE is in accordance with the $4n+2$ rule when $N < 26$
- (iv) At B3LYP/6-311G(2df,p) level, the VDE always conforms to the $4n+2$ rule, without exception, and VDE of $[4n+2]$ annulene is always stabilizing at B3LYP level.

B3LYP/6-311G(2df,p) will be used to calculate the vertical delocalization energies of the [N]annulenes

9.4.4.1. At (RHF and LYP) Levels of Theory

For $[4n]$ annulene, the vertical delocalization energy is always destabilizing at the (RHF and LYP)/(6-31G*, 6-311G** and 6-311G(2df,p)) levels (Table 9-5), and the vertical delocalization energy per π -electron, denoted as $\Delta E^V(2011)/\pi$, is almost constant since $N = 12$ (Figure 9-11b). For example, the RHF/6-311G** values (kcal/mol*electron) of $\Delta E^V(2011)/\pi$ are as follows: 1.07 ($N = 12$), 0.94 ($N = 16$), 1.05 ($N = 20$), 1.11 ($N = 24$). For $[4n]$ annulene, however, the vertical delocalization energy value themselves monotonically increases (Figure 9-11a). When $N = 24$, the RHF values of the vertical delocalized energy are large, up to the following values (kcal/mol): 23.5 (6-31G*), 26.7 (6-311G**), and 38.9 (6-311G(2df,p)). As the number of carbon atoms increases, $[4n]$ annulene

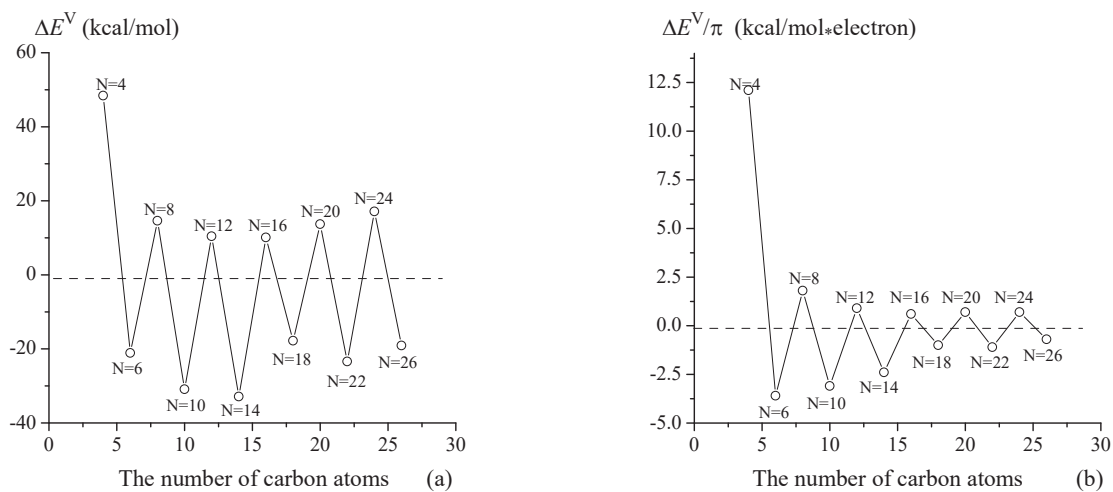


Figure 9-12. For the B3LYP/6-311G** optimized geometry of the most stable isomer of each $[N]$ annulene: (a) The vertical delocalization energy. (b) The vertical delocalization energy per π -electron, and they change as the number of carbon atoms increases from $N = 4$ to $N = 26$, calculated by using our 2011 method at B3LYP/6-311G(2df,p) level.

remains anti-aromatic.

For $[4n+2]$ annulenes, whether the vertical delocalization energy is stabilizing or destabilizing depends upon the number of double bonds, and for a specific $[4n+2]$ annulene, the sign of the vertical delocalization energy depends upon the theoretical level and basis set size. In spite of this, at (RHF and LYP)/(6-31G* and 6-311G**) levels, as the number of carbon atoms increases, $\Delta E^V(2011)$ has the following characters (Table 9-5 and Figure 9-11a):

- (i) For $[4n+2]$ annulene, the vertical delocalization energy is always stabilizing when $N \leq 22$.
- (ii) The value of $\Delta E^V(2011)$ is in the range of -5.4 to 3.0 kcal/mol ($N \geq 18$), and when $N = 24$, $\Delta E^V(2011)$ becomes destabilizing ($\Delta E^V(2011) = 0.0$ or 3.0 kcal/mol).

At RHF/(6-31G* and 6-311G**) levels, in terms of aromatic stabilization energy, the values of -5.4 to 3.0 kcal/mol are so small that $[4n+2]$ annulene can be considered non-aromatic when $N \geq 18$. The RHF/6-311G(2df,p) value of $E^V(2011)$ becomes destabilizing when $N = 4n+2 \geq 18$, but its $E^V(2011)/\pi$ value is in the range of 0.6 to 0.8 kcal/mol*electron. At RHF level, therefore, $[4n+2]$ annulene can be considered ceasing to be aromatic, when $N \geq 18$.

9.4.4.2. At B3LYP/6-311G(2df,p) Level

At B3LYP/6-311G(2df,p) levels, the values of vertical delocalization energy (VDE) have the following interesting characteristics:

- (i) For each $[4n]$ annulene, the B3LYP/6-311G(2df,p) values are the largest of the three B3LYP values listed in Table 9-5. Starting from $N = 16$ (Figure 9-12b), the $\Delta E^V/\pi$ becomes a constant (about 0.7 kcal/mol*electron). But the vertical delocalization energy itself is a monotonically increasing function of the number of carbon atoms. When $N = 24$, $\Delta E^V(2011) = 17.1$ kcal/mol.
- (ii) For each $[4n+2]$ annulene, the absolute B3LYP/6-311g(2df,p) value is the smallest of the three B3LYP values. The VRE/ π is a monotonically increasing function of the number of carbon atoms. When $N \geq 26$, the value of the VRE/ π approaches -0.7 kcal/mol*electron, but the value of the vertical delocalization energy

itself is still large, up to -19.1 kcal/mol.

Therefore, at B3LYP/6-311G(2df,p) level, as shown by the bold data in Table 9-5 and by the curves in Figure 9-12, the vertical delocalization energies always alternate between stabilizing and destabilizing as the number of carbon atoms increases. That is, the energy characters of [N]annulene always alternate between aromaticity and anti-aromaticity. However, when $N \geq 16$, the $\Delta E^V/\pi$ of the [4n]- and [4n+2]annulenes approach their respective constants. For [4n+2] and [4n]annulenes at B3LYP/6-311G(2df,p) level, the $\Delta E^V/\pi$ values (kcal/mol•electron) are as follows:

-1.0 ($N = 18$), -1.1 ($N = 22$), -0.7 ($N = 26$); 0.7 ($N = 16$), 0.7 ($N = 20$), 0.7 ($N = 24$)

Based on the data listed in Table 9-5 and according to the following facts: for the all-cis geometry of [4n+2]annulene (such as [10]annulene) obtained from the geometry optimization at RHF level, the CC bonds obviously alternate between the single and double bond; but for the geometry optimized at B3LYP/6-311G**, the CC bonds can be considered equalized, the B3LYP/6-311G(2df,p) values of the vertical delocalization energy should be the most reasonable.

9.4.5. Extra Stabilization Energy

The vertical delocalization energy is only an energy criterion of aromaticity. It should be the extra stabilization energy (ESE) to quantify the aromaticity and anti-aromaticity of an [N]annulene according to the definitions of the aromaticity and anti-aromaticity. In this section, the extra stabilization energy (ESE) of [N]annulenes will be calculated by using our 2011 method and our 2007 method, and they will be used to discuss the changes in the aromaticity (or antiaromaticity) of [N]annulenes as the number of carbon atoms increases.

For [8]annulene, for example, the localized GL and GE-1 geometries are optimized under the conditional settings detailed in Figure 9-13e to Figure 9-13h. These conditional settings ensure that the MO charge transfer (CT) and exchange (EX) interactions and the spatial exchange interaction are excluded from between the localized double bonds (groups) in the localized geometry. Then the ESE and its components ΔE^A and ΔE^{Am} are calculated at various theoretical levels with four basis sets, and the ESE values are listed in Table 9-6. According to these data, the influences of the theoretical level and basis set size on three energy effects $\Delta E^A(2011)$, $\Delta E^{Al}(2011)$ and ESE(2011) are summarized as follows:

- (i) Similar to the calculation of vertical delocalization energy, at and only at 6-311G(2df,p) level, the sign of three energy effects is independent on the theoretical level, and three energy effects are always destabilizing. The ranges of three sets of the values are 2.8, 1.1 and 5.8 kcal/mol, and they are the smallest of the values calculated at four basis levels.
- (ii) At RHF level of theory, the range of a sets of the ESE values is 1.0 and it is the smallest of the values calculated at four theoretical levels.
- (iii) At (RHF and LYP) levels of theory, the signs of the energy effects are independent on the basis set size, and they are always destabilizing. Correspondingly, the bond distance between two interacting double bonds in GE-1 geometry is longer than that in the GL geometry.

Similar to the calculation of vertical delocalization, it seems to be more reasonable for the ESE to be calculated at the B3LYP/6-311G (2df,p) level. For [16]annulene at 6-31G* level, the values (kcal/mol) of related energy effects, obtained from our 2011 method, are as follows (the values in parentheses come from our 2007 method.):

ΔE^A : 14.76 (125.7) (RHF), 16.39 (LYP), -3.77 (14.2) (B3LYP)
 ESE: -3.77 (34.0) (RHF), -4.05 (LYP), -4.31 (0.1) (B3LYP)

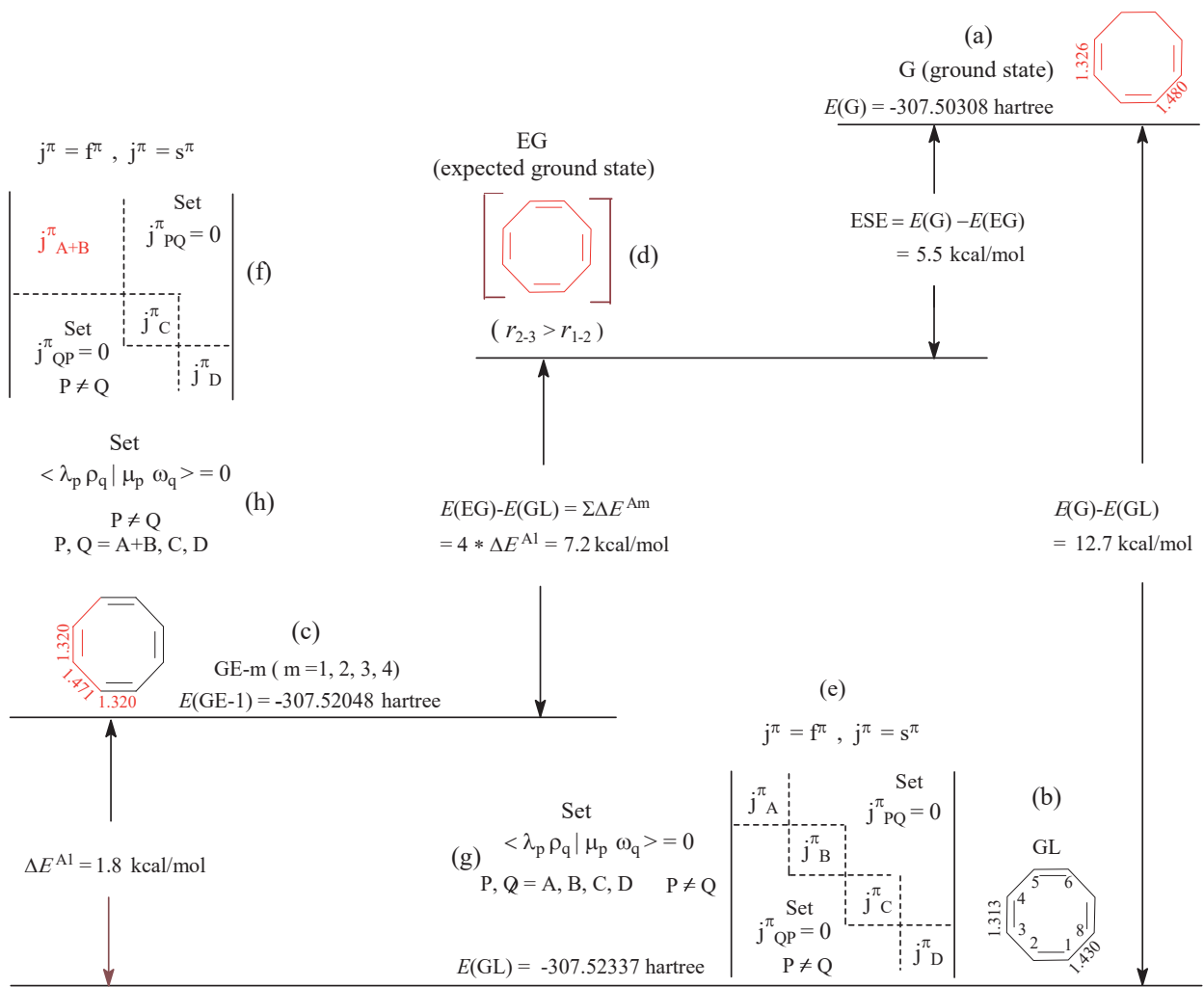


Figure 9-13. The 2011 procedure for calculating ESE of planar [8]annulene (cyclooctatetraene) at RHF/6-31G*. (e), (f), (g) and (h) are the conditional settings for optimizing the GL and GE-1 geometries, where \mathbf{F}^π and \mathbf{S}^π are the particular π -sub Fock matrix and π -sub overlap integral matrix.

CESE: -3.62 (42.9) (RHF), -3.89 (LYP), -3.57 (1.7) (B3LYP).

At 6-311G(2df,p) level, the corresponding values for [16]annulene are as follows:

ΔE^A : 19.16 (RHF), 21.59 (LYP), 15.16 (B3LYP)

ESE: -4.11 (RHF), -4.56 (LYP), -1.84 (B3LYP)

CESE: -4.24 (42.9) (RHF), -4.71 (LYP), -0.65 (B3LYP)

The influence of the theoretical level on the sign of ΔE^A is the same as that on the vertical delocalization energy. For [16]annulene at RHF level of theory, for example, $\Delta E^A > 0$ and $\Delta E^V > 0$, but $\Delta E^A < 0$ and $\Delta E^V < 0$ at B3LYP/6-31G* level. At 6-311G(2df,p) level, always $\Delta E^A > 0$ and $\Delta E^V > 0$. But, the theoretical level has a slight effect on the 6-31G* value of CESE (corrected extra stabilization energy).

Table 9-6. The ESE of [8]annulene (Cyclooctatetraene), and Its Components ΔE^A And ΔE^{A1} (kcal/mol) are Calculated by Using Our 2007 Method and Our 2011 Method.

Basis sets	RHF		MP2		B3LYP		LYP		Range (2011)	
	2011	2007	2011	2007	2011	2007	2011	2007		
6-31G*	ΔE^A	12.7	64.8	1.0	140.8	8.5	16.9	13.7	67.4	12.7
	ΔE^{A1}	1.8	11.3	-1.6	29.1	-0.4	1.2	1.9	11.5	3.5
	ESE	5.5	19.7	7.4	24.5	10.3	12.0	5.9	21.4	4.8
6-311G**	ΔE^A	12.4	70.3	2.7	197.7	10.2	19.8	13.3	73.1	10.6
	ΔE^{A1}	1.7	11.7	-1.3	42.6	-0.1	1.8	1.8	12.0	3.1
	ESE	5.5	23.7	7.7	27.4	10.5	12.5	6.0	25.3	4.5
6-311G(2d,2p)	ΔE^A	11.7		9.4		12.5	24.0	12.7	88.8	3.3
	ΔE^{A1}	1.3		-0.1		0.1	2.2	1.4	9.7	2.3
	ESE	6.5		9.9		12.3	15.1	7.2	50.1	5.8
6-311G(2df,p)	ΔE^A	13.8		15.9		16.0	28.7	15.1	101.3	2.8
	ΔE^{A1}	1.9		1.6		1.0	3.4	2.1	4.5	1.1
	ESE	6.2		9.6		12.0	15.0	6.8	83.2	5.8
Range	ESE	1.0	4.0	2.2	2.9	2.0	3.1	1.3	61.8	
Average	ESE	5.9	21.7	8.7	26.0	11.3	13.7	6.5	45.0	

9.4.5.1. Larger [4n]Annulene Ceasing to Be Anti-aromatic

The calculation of the extra stabilization energy is based on that, in the case of polyenes, the energy effects ΔE^{Am} are additive, that is, $\Delta E^A \approx \Delta E^{Am}$. For larger polyenes, as shown by Table 9-7, only at RHF/6-31G* and B3LYP/6-311G(2df,p)) levels, the energy effects ΔE^{Am} are additive when the calculations are performed using our 2011 method, which is different from the calculation results obtained from our 2007 method. Therefore, the CESEs and the CESE per π electron (CESE/ π) of larger [N]annulenes are calculated at the RHF/6-31G* and B3LYP/6-311G(2df,p) levels, and various energy effects are listed in Table 9-8.

For [4n]annulenes and trans-polyenes at B3LYP/6-311G(2df,p), for example, CESE/ π (y) can be well fitted as the following polynomial functions (Figure 9-14b) of the number n of carbon atoms (x):

$$y = 8.656 - 1.41113x + 0.07487x^2 - 0.0013x^3 \text{ for } [4n]\text{-membered annulenes (cc = 0.9896)}$$

$$y = 0.06563 + 0.00764x - 0.00174x^2 + (4.51003E-5)x^3 \text{ for polyenes (cc = 0.9950)}$$

The red dashed line (polyene) in Figure 9-14b is a linear line that almost overlaps the X axis. For [4n]annulenes, CESE/ π has been changed from a destabilizing energy effect to a stabilizing one since $N = 16$, and the corresponding function line (red solid line with hollow circles) becomes a linear. When $N \geq 16$, this red solid line almost overlaps

Table 9-7. For Trans-polyenes H-(HC=CH)_n-H, the Energy Effects ESE, CESE and CESE/π, and Their Components Are Calculated by Using Our 2011 Method.

		ESE	ESE/π	CESE	CESE/π	ΔE ^A	ΔE ^A /π	ΣΔE ^{Am}	ΣΔE _n ^{Am}
C ₈ H ₁₀	B3LYP/6-311G(2df,p)	0.06	0.01	0.35	0.04	9.35	1.17	9.29	-0.29
	B3LYP/6-31G*	-0.25		-0.15		1.09		1.34	-0.09
C ₈ H ₁₀	RHF/6-31G*	-0.31	-0.04	-0.34	-0.04	7.08	0.98	7.39	0.03
	B3LYP/6-311G(2df,p)	-0.36	-0.04	0.08	0.01	11.45	1.15	11.81	-0.43
C ₁₀ H ₁₂	B3LYP/6-31G*	-0.83		-0.69		0.40		1.23	-0.14
	RHF/6-31G*	-0.55	-0.06	-0.60	-0.06	9.09	0.91	9.64	0.05
C ₁₄ H ₁₆	RHF/6-31G*	-1.09	-0.08	-1.19	-0.08	13.06	0.93	14.15	0.10
	B3LYP/6-311G(2df,p)	-2.03	0.13	-1.15	-0.07	17.30	1.08	19.34	-0.88
C ₁₆ H ₁₈	B3LYP/6-31G*	-3.06		-2.79		-2.14		0.92	-0.27
	RHF/6-31G*	-1.34	-0.08	-1.43	-0.09	15.03	0.94	16.36	0.10
C ₂₀ H ₂₂	B3LYP/6-311G(2df,p)	-3.32	-0.17	-2.18	-0.12	21.07	1.05	24.39	-1.14
	B3LYP/6-31G*	-5.45		-5.85		-3.87		1.58	0.41
C ₂₀ H ₂₂	RHF/6-31G*	-1.82	-0.09	-1.91	-0.10	18.97	0.95	20.79	0.09
	B3LYP/6-311G(2df,p)	-4.63	-0.19	-3.21	-0.13	24.80	1.03	29.43	-1.42
C ₂₄ H ₂₆	B3LYP/6-31G*	-6.35		-5.89		-5.83		0.52	-0.45
	RHF/6-31G*	-2.32	-0.10	-2.40	-0.10	22.91	0.95	25.24	0.07
C ₂₆ H ₂₈	RHF/6-31G*	-2.57	-0.10	-2.63	-0.10	24.88	0.96	27.45	0.05

with the dashed red line near the X axis. For [16]annulene at B3LYP/6-311G(2df,p), for example, CESE/π = -0.04 kcal/(mol*electron), and it is about -0.07 kcal/(mol*electron) for trans-polyene C₁₆H₁₈. Correspondingly, the red solid function line for [4n]annulene in Figure 9-14a is also overlap with the red dashed line (for polyene) when N > 16. In particular, for [4n]annulene at (B3LYP/6-311G(2df,p) and RHF/6-31G*) levels, when N ≥ 16, the absolute ratios of the CESE to the energy effects (ΔE^{Am} + ΔE_n^{Am}) are as follows:

4 % and 20 % (N = 16, B3LYP and RHF), 6 % and 15 %. (N = 20), 6.6 % and 11.8 % (N = 24).

For [4n]annulene at B3LYP/6-311G(2df,p), the energy effects ΣΔE^{Am} can be considered additive when N > 16. At least, [4n]annulene can no longer be considered anti-aromatic when N > 16.

9.4.5.2. Large Annulene Approaching Polyene

For [4n+2]annulenes at B3LYP/6-311G(2df,p), as shown by the red solid line with filled circles in Figure 9-14b,

Table 9-8. For [N]annulenes, the Energy Effects ESE, CESE and CESE/ π , and their Components Are Calculated by Using Our 2011 Method at B3LYP/6-311G(2df,p) and RHF/6-31G* Levels.

Moles		ESE	ESE/ π	CESE	CESE/ π	ΔE^A	$\Delta E^A/\pi$	$\Sigma \Delta E^{Am}$	ΣE_n^{Am}
C_8H_8	B3LYP	12.02	1.50	12.00	1.50	15.98	2.00	3.96	0.02
	RHF	5.49	0.69	5.38	0.67	12.73	1.59	7.25	0.10
$C_{10}H_{10}$	B3LYP	-17.97	-1.80	-17.61	-1.76	-22.41	-2.24	-4.44	-0.36
	RHF	-12.24	-1.22	-12.24	-1.22	-2.11	-0.21	10.13	0.01
$C_{12}H_{12}$	B3LYP	1.67	0.14	2.59	0.22	12.79	1.07	11.12	-0.92
	RHF	-2.41	-0.20	-2.27	-0.19	11.20	0.93	13.62	0.14
$C_{14}H_{14}$	B3LYP	-17.13	-1.22	-16.28	-1.16	-6.89	-0.49	10.23	-0.85
	RHF	-7.62	-0.54	-7.60	-0.54	6.37	0.46	13.98	-0.02
$C_{16}H_{16}$									
$C_{16}H_{16}$ (RHF)		-3.77	-0.24	-3.62	-0.23	14.76	0.92	18.53	-0.14
B3LYP/6-31G*		-4.31	-0.27	-3.57	-0.22	-3.77	-0.24	0.55	-0.75
LYP/6-31G*		-4.05	-0.25	-3.89	-0.24	16.39	1.02	20.44	-0.16
B3LYP/6-311G(2df,p)		-1.84	-0.12	-0.65	-0.04	15.16	0.95	17.00	-1.19
RHF/6-311G(2df,p)		-4.11	-0.26	-4.24	-0.27	19.16	1.20	23.27	0.13.
LYP/6-311G(2df,p)		-4.56	-0.29	-4.71	-0.29	21.59	1.35	26.15	0.15
$C_{18}H_{18}$	B3LYP	-11.89	-0.66	-11.17	-0.62	16.66	0.93	28.55	-0.73
	RHF	-3.66	-0.20	-3.56	-0.20	22.95	1.28	26.61	-0.10
$C_{20}H_{20}$	B3LYP	-3.10	-0.16	-1.51	-0.07	22.11	1.11	25.21	-1.59
	RHF	-3.73	-0.19	-3.69	-0.18	21.18	1.05	24.91	0.04
$C_{22}H_{22}$	B3LYP	-11.19	-0.51	-9.40	-0.42	17.78	0.81	28.97	-1.79
	RHF	-4.04	-0.18	-4.10	-0.19	23.99	1.09	28.03	0.06
$C_{24}H_{24}$	B3LYP	-4.0	-0.17	-2.03	-0.08	28.65	1.19	32.65	-1.97
	RHF	-3.60	-0.15	-3.66	-0.15	27.47	1.14	31.08	0.06
$C_{26}H_{26}$	B3LYP	-10.58	-0.41	-8.62	-0.33	17.37	0.67	27.95	-1.95

CESE/ π (y), $[\Delta E^A - \Sigma \Delta E^{Am} - \Sigma E_n^{Am}] / \pi$, can be well fitted as the following polynomial functions of the number of carbon atoms (x) (cc = 0.9954):

$$y = -3.93492 + 0.24883x - 0.00256x^2 - (6.51042E-5)x^3 \text{ (cc = 0.98962)}$$

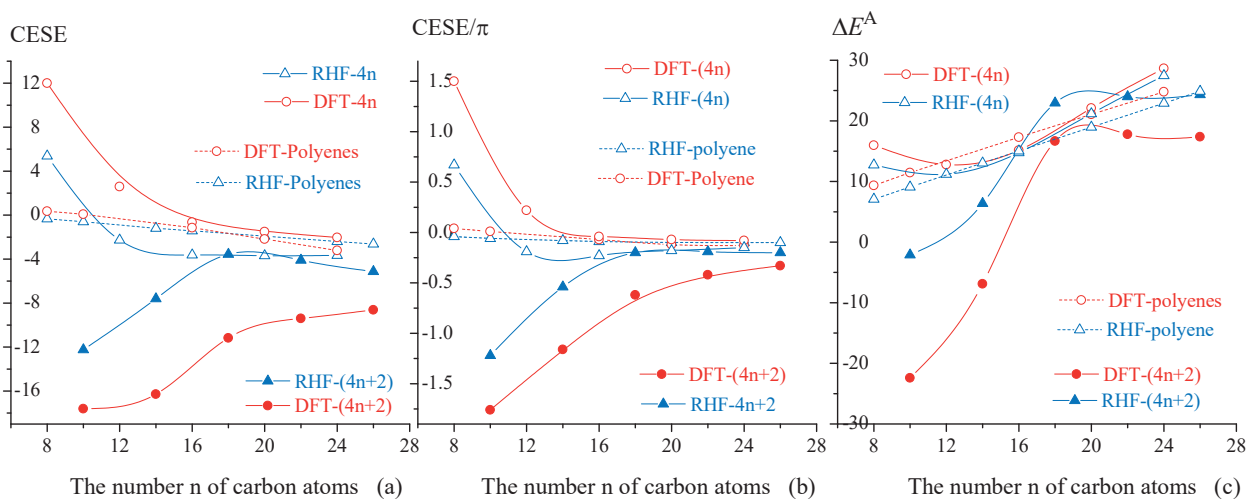


Figure 9-14. For [N]annulenes (solid lines) and trans-polyenes (dashed lines): (a) and (b) The CESE and CESE/π . (c) Adiabatic delocalization energy ΔE^A , these energy effects (kcal/mol and kcal/mol*electron) change as the number of the carbon atoms increases from $N = 4$ to $N = 26$, which are obtained from the geometry optimization at B3LYP/6-311G(2df,p) (red lines) and RHF/6-31G* level (blue lines) using our 2011 program.

According to Figure 9-14a, the red solid line with filled circles ($[4n+2]$ annulenes) approaches to the red dashed line (polyenes) as the number of the carbon atoms increases, but there is still a considerable distance between them (Figure 9-14a). In the meantime, the CESE/π difference the between the $[4n+2]$ annulene and its corresponding trans-polyene is close to a constant (about < -0.4 kcal/mol*electron). Meanwhile, as shown by the red solid line with filled circles in Figure 9-14c, the energy effect ΔE^A for $[4n+2]$ annulene becomes destabilizing and approaches a constant when $N \geq 18$. Therefore, the red lines in Figure 9-14 show the following two interesting facts:

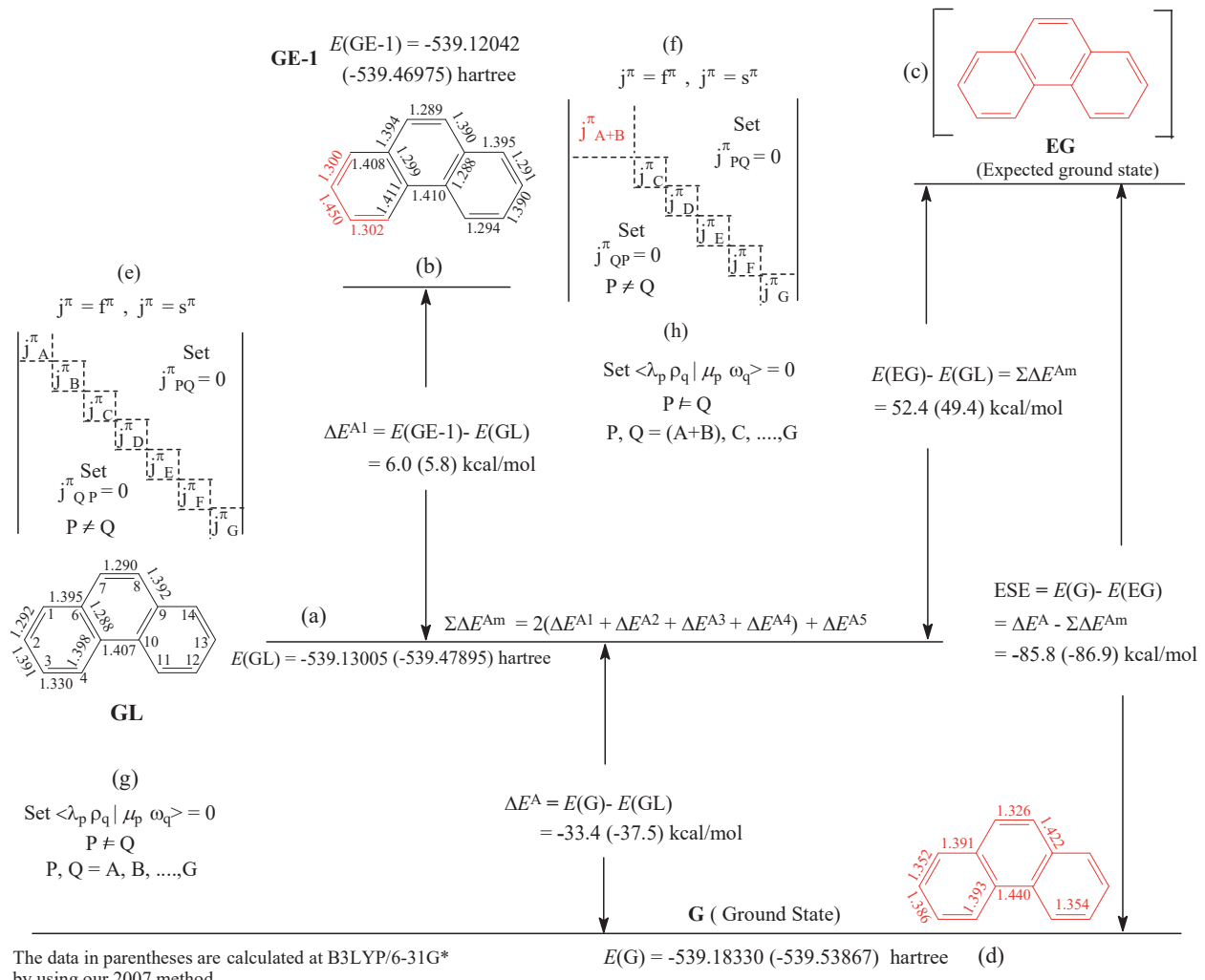
- (i) When $N \geq 18$, $[4n+2]$ annulene is no longer a typical aromatic molecule because its $\Delta E^A > 0$ and the ratio, $\text{CESE}/(\Delta E^{Am} + \Delta E_n^{Am})$, is about 35%, although their CESE value is about -10.0 kcal/mol.
- (ii) For $[4n]$ annulene, when $N \geq 16$, energy effects ΔE^{Am} can be considered additive, meaning that $[4n]$ annulene is no longer anti-aromatic.

At B3LYP/6-311G(2df,p) level, therefore, $[N]$ annulene can be considered approaching polyene (non-aromatic) when $N \geq 16$ no matter whether it is $[4n]$ annulene or $[4n+2]$ annulene. In this case of $[4n]$ annulenes ($N \geq 16$), the $\text{CESEs} < 0$ (stabilizing), but their values (-0.65 to -2.0 kcal/mol) are so small that the sign (stabilizing or destabilizing) of the CESE is no longer worthy of attention.

9.5. PBHS

In this section, the CESEs (corrected ESE) of typical polycyclic benzenoid hydrocarbons will be recalculated using our 2011 program at various levels of theory in order to test the influences of the HF-EX and DF-EX on the energy effects ESE and CESE and on the components ΔE^A , ΔE^{Am} and ΔE_n^{Am} .

9.5.1. Phenanthrene



The data in parentheses are calculated at B3LYP/6-31G* by using our 2007 method.

Figure 9-15. The ESE and CESE of phenanthrene are calculated using our 2011 method at LYP/6-31G*. (e), (f), (g) and (h) Are the conditional settings for optimizing the GL and GE-1 geometries. The data in parentheses calculated by using our 2011 program at B3LYP/6-31G*.

Similar to benzene, as shown by comparing the data in parentheses in Figure 9-15 with the data in Figure 7-2-1, the molecular energies $E(GL)$ and $E(GE-m)$ of the localized geometries GL and GE-m, calculated by using our 2011 method, are higher than the corresponding molecular energies, $E^o(GL)$ and $E^o(GE-m)$, calculated by using our 2007 method. At the B3LYP/6-31G* level, for example, the related molecular energies (hartree) are as follows:

$$E^o(GL) = -539.51984, E^o(GE-1) = -539.50468$$

$$E(GL) = -539.47895, E(GE-1) = -539.46975$$

Therefore

Table 9-9. For Phenanthrene, the Energy Effects (kcal/mol) ESE, CESE and CESE/ π , and the Components (kcal/mol) ΔE^A , ΔE^{Am} and ΔE_n^{Am} are Obtained from Our 2011 method.

		6-31G*	6-31++G**	6-311G(2d,2p)	6-311G**	Range	Average
ESE	CPBE96	-87.6	-87.5	-81.9	-85.7	-5.7	-85.7
	SLATER	-84.6	-84.5	-81.7	-85.2	-4.5	-84.0
	RHF	-81.7	-81.5	-76.5	-81.7	-5.2	-80.3
CESE	CPBE96	-87.0	-86.9	-81.6	-85.5	-5.4	-85.3
	SLATER	-79.0	-78.9	-73.6	-79.9	-6.3	-77.8
	RHF	-81.1	-80.9	-76.2	-81.1	-3.9	-79.8
CESE/ π	CPBE96	-6.2	-6.2	-5.8	-6.1	-0.4	-6.1
	SLATER	-5.7	-5.6	-5.3	-5.7	-0.4	-5.6
	RHF	-5.8	-5.8	-5.5	-5.8	-0.3	-5.7
ΔE^A	CPBE96	-34.5	-34.6	-35.4	-33.9	-1.4	-34.6
	SLATER	-38.8	-29.2	-18.8	-27.2	-11.6	-28.5
	RHF	-33.1	-33.2	-32.5	-33.1	-1.6	-33.0
$\Sigma \Delta E^{Am}$	CPBE96	53.1	52.9	46.5	51.8	-6.6	51.1
	SLATER	45.8	45.2	62.9	57.9	-17.7	53.0
	RHF	48.5	48.3	44.0	48.5	-4.5	47.3
$\Sigma \Delta E_n^{Am}$	CPBE96	-0.6	-0.6	-0.3	-0.2	-0.4	-0.4
	SLATER	-5.6	-5.6	-8.2	-5.3	-2.9	-6.2
	RHF	-0.6	-0.6	-0.2	-0.6	-0.4	-0.5

$$\Delta E^{A1} (5.8 \text{ kcal/mol}) < \Delta E_o^{A1} (9.5 \text{ kcal/mol}), \\ |\Delta E^A (-37.5 \text{ kcal/mol})| > |\Delta E_o^A (-11.8 \text{ kcal/mol})|.$$

The corresponding change in the bond lengths is also self-consistent. For phenanthrene at B3LYP/6-31G* level, as a result, CESE(2011) (-82.1 kcal/mol) is -6.3 kcal/mol less than CESE(2007) (-88.4 kcal/mol). Interestingly, as shown by Table 9-9, the value of $\Sigma \Delta E_n^{Am}$ is almost equal to zero when the calculations are performed at the RHF and CPBE96 levels of theory. At the 6-31G* level, the following size orders (kcal/mol) are also interesting:

- (i) for $\Sigma \Delta E_n^{Am}$, $|-5.6|$ (SLATER, pure exchange) $> |-3.8|$ (B3LYP, hybrid) $> |-0.6|$ (CPBE96, pure correlation) $= |-0.6|$ (RHF).

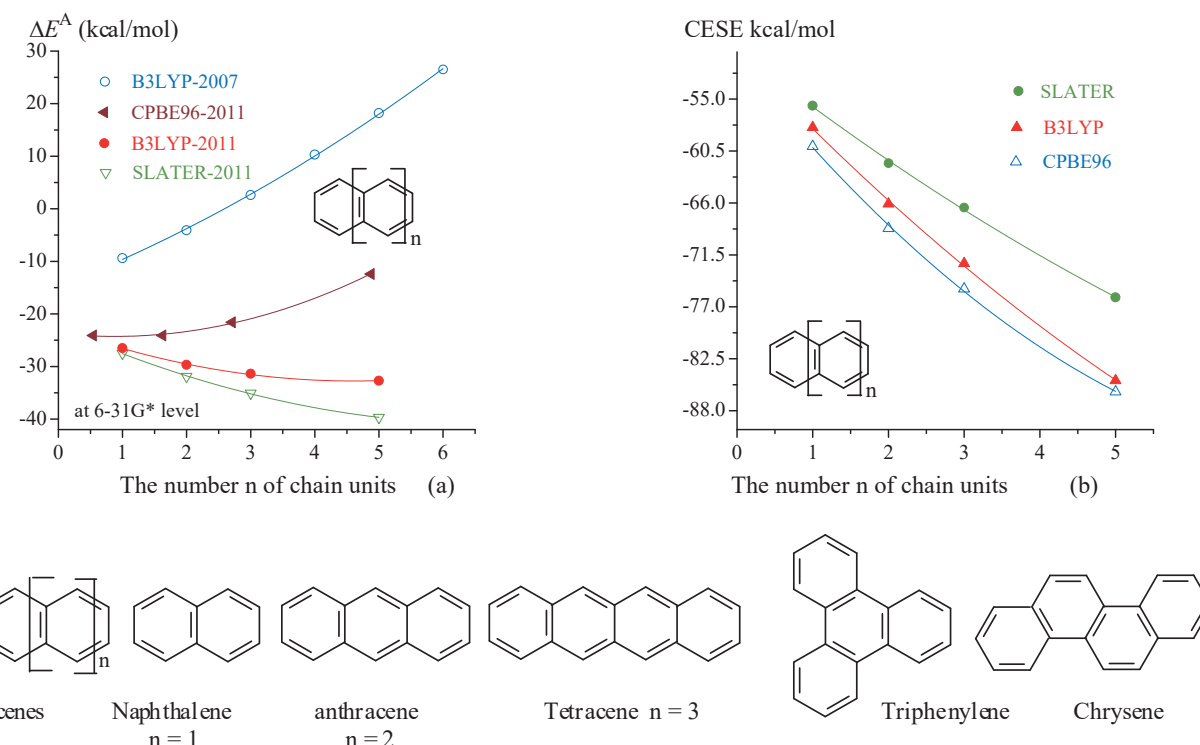


Figure 9-16. (a) For acenes, adiabatic delocalization energy ΔE^A can be fitted as the polynomial function of structure unit n (For example, “B3LYP-2001” in Figure means that ΔE^A is calculated using our 2011 method at B3LYP/6-31G* level); (b) The CESE(2011) versus the number n of structure units at 6-31G* level.

(ii) for ESE, -87.6 (CPBE96) > -86.9 (B3LYP) > -84.6 (SLATER) > -81.7 (RHF).

These two size orders mean that the exchange of DF-type (density functional type) can also affect the value of the ESE and CESE. In order to ensure the localization of π -electrons, had better to use the pure correlation density functionals such as CPBE96 and LYP.

9.5.2. Acenes, Triphenylene and Chrysene

It has been shown that, for benzene, π -electron localization ensures that the adiabatic delocalized energy is always stabilizing. For polycyclic benzenoid hydrocarbons, as will be shown in this section, it is also π -electron localization, rather than MO localization, to be able to ensure that the adiabatic delocalization energy ΔE^A is always stabilizing, which once again demonstrates that our 2011 program is more reasonable than our 2007 program.

9.5.2.1. Adiabatic Delocalization Energy

For acenes, as shown by inspections of the Table 7-1, Table 9-10 and Figure 9-16a, the adiabatic delocalization energies ΔE_o^A , and ΔE^A , calculated using our 2007 method and our 2011 method at B3LYP/6-31G* level, can be well fitted as the following second order polynomial functions of the number n of the chains (structure units):

$$\Delta E_o^A = -14.76 + 4.785 n + 0.3536 n^2 \quad (cc = 0.999)$$

Table 9-10. For Naphthalene (Naphth.), Anthracene (Anthra.), Tetracene (Tetra.), Hexacene (Hexa.), Triphenylene (Triph.) and Chrysene (Chrys.), the ESEs and CESEs (kcal/mol) and Their Components ΔE^A , $\Sigma \Delta E^{Am}$ And $\Sigma \Delta E_n^{Am}$ (kcal/mol) are Calculated Using Our 2007 Method and Our 2011 Method at 6-31G* Level.

Theoretical levels	Energy effects	Our methods	Naphth. n=1	Anthra. n=2	Tetra. n=3	Hexa n=5	Thiph. n=6	Chrys.
B3LYP	ESE	2007	-65.2	-75.1	-83.2	-97.9	-125.7	-123.3
	ESE	2011	-59.5	-69.9	-78.2	-93.9	-115.0	-112.6
	ΔE_o^A	2007	-9.4	-4.1	2.6	18.2	-15.8	-13.0
	ΔE^A	2011	-26.5	-29.7	-31.4	-32.7	-49.8	-47.2
	$\Sigma \Delta E_o^{Am}$	2007	55.8	71.0	85.8	116.2	109.9	110.2
	$\Sigma \Delta E^{Am}$	2011	33.4	40.2	46.8	61.1	65.3	65.4
	CESE	2007	-62.0	-68.2	-72.7	-81.6	-115.9	-110.6
	CESE	2011	-58.0	-66.1	-72.4	-84.8	-109.4	-105.2
	CESE/ π	2007	-6.2	-4.9	-4.0	-3.1	-6.4	-6.4
	CESE/ π	2011	-5.8	-4.7	-4.0	-3.3	-6.1	-5.8
CPBE96	$\Sigma \Delta E_{no}^{Am}$	2007	-3.2	-6.8	-10.5	-16.4	-9.8	-12.7
	$\Sigma \Delta E_n^{Am}$	2011	-1.9	-3.8	-5.8	-9.1	-5.7	-7.5
	ESE	2011	-60.3	-69.4	-76.2	-87.7	-116.6	-113.1
	ΔE^A	2011	-24.1	-24.1	-21.6	-12.4	-46.8	-43.1
	$\Sigma \Delta E^{Am}$	2011	36.2	45.4	54.6	75.3	69.8	69.9
SLATER	CESE	2011	-60.0	-68.7	-75.1	-86.0	-115.7	-111.8
	CESE/ π	2011	-6.0	-4.9	-4.2	-3.3	-6.4	-6.2
	$\Sigma \Delta E_n^{Am}$	2011	-0.3	-0.7	-1.1	-1.7	-0.9	-1.2
	ESE	2011	-58.5	-67.6	-75.5	-90.2	-112.0	-109.9
	ΔE^A	2011	-27.5	-31.9	-35.1	-39.7	-51.2	-49.1

CPBE96: Pure Correlation density function with Hartree-Fock exchange (HF-EX); SLATER: Pure exchange density function without HF-EX and Correlation.

$$\Delta E^A = -22.651 - 4.392n + 0.477 n^2 \text{ (cc = 0.992)}$$

ΔE_o^A is also written as $\Delta E^A(2007)$, and it is stabilizing only when the structure unit $n < 3$ (Figure 9-16a and Table 9-10). But it becomes destabilizing when $n > 2$ due to that always $d(\Delta E_o^A)/dn > 0$, and $d^2(\Delta E_o^A)/dn^2 > 0$. It is different from ΔE_o^A that, as shown by the red curve line in Figure 9-16a, the first order derivative $d[\Delta E^A(2011)]/dn < 0$ when $0 < n < N$, and always $d^2[\Delta E^A(2011)]/dn^2 > 0$. Therefore, when $\Delta E^A(N) = 0.0$, N is called the critical value of n , and it depends upon the theoretical level. At the B3LYP/6-31G*, for example, $d(\Delta E^A)/dn < 0$ ($0 < n < 5$), $d(\Delta E^A)/dn > 0$ ($n > 5$), $\Delta E^A(2011) < 0$ ($0 < n < 13$), and $\Delta E^A(2011)$ becomes destabilizing when $n \geq 13$. When $\Delta E^A(2011)$ becomes destabilizing, the corresponding acene is no longer typical aromatic molecule.

SLATER is a density functional function without HF-EX. At SLATE/6-31G* level, $\Delta E^A(2011) = \Delta E^A(2007)$ and can be fitted as the following polynomial function of the chain unit n (cc = 0.9989, green line in Figure 9-16a):

$$\Delta E^A(2011) = -22.53818 - 5.40636n + 0.39545n^2$$

For the green curve lines in Figure 9-16a, also $d[\Delta E^A(2011)]/dn < 0$, and $d^2[\Delta E^A(2011)]/dn^2 > 0$, which further confirms the rationality of our 2011 method. Therefore, as shown by the data listed in Table 9-10, our 2011 program can ensure that, for polycyclic aromatic hydrocarbon, the adiabatic delocalization energy is always stabilizing.

9.5.2.2. Extra Stabilization Energy ESE(2011).

In the GL geometry of phenanthrene (Figure 9-15), the length of C1=C2 double bond is 1.292 Å at LYP/6-31G* level, and the corresponding bond length is 1.328 Å at the B3LYP/6-31G* level. For the C=C double bond, the standard length is about 1.33 Å,^{59,60} and the experimental length of C=C double bond in fragment -C-CH=CH-C (cis) is about 1.317 Å.⁶¹ Therefore, the B3LYP bond length is more reasonable than the LYP bond length.

At (B3LYP, SLATER and CPBE96)/6-31G* levels, the CESE (y) of the acene can be fitted as the following second order polynomial function of the number n of structure units:

$$y = -49.94364 - 8.50727x + 0.30909x^2 \text{ (cc = 0.998) (B3LYP)}$$

$$y = -50.77273 - 9.94545x + 0.58182x^2 \text{ (cc = 0.998) (CPBE96)}$$

$$y = -49.72455 - 6.30409x + 0.21136x^2 \text{ (cc = 0.998) (SLATER)}$$

For a specific acene, as shown by comparison of the CESE(2011) values listed in Table 9-10, the difference between the B3LYP value and CPBE96 value, [CESE(B3LYP) – CESE(CPBE96)], is about 2 kcal/mol, and it almost keeps constant as the structure unit number n increases (Figure 9-16b). Correspondingly, the vertical distance between the red line and the blue line in Figure 9-16b is almost a constant. But the difference (kcal/mol), [CESE(B3LYP) – CESE(SLATER)], between the green line and red line increases as the structure unit number n increases. For example, the size order of the difference (kcal/mol) is as follow: -2.3 ($n = 1$) < -4.3 ($n = 2$) < -5.9 ($n = 3$) < -8.8 ($n = 5$). Especially, as shown by Table 9-10, the difference [CESE(B3LYP) – CESE(CPBE96)] (kcal/mol) for a specific acene is much less than the CESE difference (kcal/mol) between two adjacent acenes. For anthracene, [CESE(B3LYP) – CESE(CPBE96)] = 2.6, and the CESE difference between anthracene and naphthalene is 8.1 at B3LYP/6-31G* level, and the difference between tetracene and anthracene is 6.3. For tetracene, on the contrary, the difference [CESE(B3LYP) – CESE(SLATER)] (-5.9) is almost equal to the CESE difference (-6.3) between tetracene and anthracene. The pure correlation density functional without DF-type exchange (with HF-EX), such as CPBE96 and LYP, can be reasonably used to calculate the CESE although the LYP bond lengths are not very reasonable, and it can save a lot of computation time because the energy effect sum, $\sum \Delta E_n^{Am}$, can be neglected.

At last, it should be mentioned that, for a specific PBH, the difference between CESE(2011) and CESE(2007) is not large. At B3LYP/6-31G* level, for example, the differences (kcal/mol) are as follows:

-62.0 (2007) and -58.0(2011) (naphtha.), -68.2 and -66.1 (Anthra.), -72.7 and -72.4 (Tetra.), -81.6 and -84.8 (Hexa.), -115.9 and -109.4 (Thiph.), -110.6 and -105.2 (Chrys).

9.6. CONCLUSIONS

In the process of deforming benzene from the localized GL geometry to the ground (G) state geometry, the compressing of single bonds and the stretching of double bonds are caused by the delocalization of π electrons. Finally, the nuclear repulsion E_N among the carbon atoms is minimized when the distance of the double bonds is equal to that of the single bonds, leading to that $\Delta E_e = E_e(G) - E_e(GL) > 0$, $\Delta E_N = E_N(G) - \Delta E_N(GL) < 0$, $|\Delta E_N| > \Delta E_e$, and $\Delta E^A = E(G) - E(GL) = -19.2$ kcal/mol. The minimization of nuclear repulsion plays an important role in the eventual formation of D_{6h} geometry. But this role is the result of π -electron delocalization. The energy criterion and geometric criterion of the aromaticity are well unified and are mutually causal.

For planar [N]annulenes, the vertical delocalization energy (VDE) and extra stabilization energy (ESE and CESE) are calculated, based on their respective most stable configuration isomers, using our 2011 method at various theoretical levels with different basis sets, and the corresponding B3LYP/6-311G(2df,p) values are the most reasonable.

At B3LYP/6-311G(2df,p) level, the VDEs always alternate between stabilizing and destabilizing as the number of carbon atoms increases. In the meantime, the VDE per π -electron, $\Delta E^V/\pi$, for [4n]annulene quickly becomes constant (about 0.7 kcal/mol*electron) when $N = 16$; the $\Delta E^V/\pi$ for [4n+2]annulene is gradually approaching the limit value of -0.7 kcal/mol*electron when the number of carbon atoms increases from $N = 8$ to $N = 26$.

For [4n+2] annulene, when $N \geq 18$, ΔE^A (about 17 kcal/mol) > 0 , CESE is about -10.0 kcal/mol, the ratio $CESE/(\Delta E^{Am} + \Delta E_n^{Am})$ is about 35. Accordingly, the large [4n+2]annulene ($N \geq 18$) is no longer a typical aromatic molecule. For [4n]annulene, when $N \geq 16$, the CESEs < 0 (stabilizing), but their values (-0.65 to -2.0 kcal/mol) are so small that the energy effects ΔE^{Am} can be considered additive. In the case of the large [4n]annulene, the sign (stabilizing or destabilizing) of the CESE is no longer worthy of attention. At B3LYP/6-311G(2df,p) level, therefore, [N]annulene can be considered approaching polyene (non-aromatic) when $N \geq 16$, no matter whether it is [4n]annulene or [4n+2]annulene.

For polycyclic benzenoid hydrocarbons, there is no great difference between the CESE values respectively obtained from our 2011 method and from our 2007 method. But the adiabatic delocalization energy ΔE^A , obtained from our 2011 method, becomes more reasonable than from our 2007 method, the first order derivative of adiabatic delocalization energy ΔE^A is changed from $d[\Delta E^A(2007)]/dn > 0$ to $d[\Delta E^A(2011)]/dn < 0$. Our 2011 method ensures that always $\Delta E^A(2011) < 0$ (stabilizing) when structure unit $n < 13$.

9.7. REFERENCES

- 1 Willstätter, R.; Waser, E. 1911. "Über Cyclo-octatetraen." Chem. Ber., 44: 3423-3445.
- 2 Willstätter, R.; Heidelberger, M. 1913. "Zur Kenntnis des Cyclo-octatetraens (Sechste Mitteilung zur Kenntnis der Cyclooctan-Reihe.)." Chem Ber., 46: 517-527.
- 3 Hückel, E. 1931. "Quantentheoretische Beiträge zum Benzolproblem. I. Die Elektronenkonfiguration des Benzols und verwandter Verbindungen." Z. Phys., 70: 204-286.
- 4 Schaad, L. J.; Hess, Jr. B. A. 2001. "Dewar Resonance Energy." Chem. Rev., 101: 1465-1476.
- 5 Bergmann, E. D.; Pullman, B. Eds. 1971. *Aromaticity, Pseudo-Aromaticity, Anti-Aromaticity*. Jerusalem: Israel Academy of Science and Humanities.

- 6 Spitzer, E. L.; Johnson II, C. A.; Haley, M. M. 2006. "Renaissance of Annulene Chemistry." *Chem. Rev.*, 106, 5344-5386.
- 7 Castro, C.; Karney, W. L.; McShane, C. M.; Pemberton, R. P. 2006. "[10]Annulene: Bond Shifting and Conformational Mechanisms for Automerization." *J. Org. Chem.*, 71: 3001-3006.
- 8 Haddon, R. C.; Raghavachari, K. 1982. "Planar cis-[10]annulene and Azulene Revisited." *J. Am. Chem. Soc.*, 104: 3516-3518.
- 9 Schleyer, P. v. R.; Jiao, H.; Sulzbach, H. M.; Schaefer, H. F. 1996. "Highly Aromatic Planar all-cis-[10]Annulene Derivatives." *J. Am. Chem. Soc.*, 118: 2093-2094.
- 10 Sulzbach, H. M.; Schaefer, H. F.; Klopper, W.; Lüthi, H. P. 1996. "Exploring the Boundary between Aromatic and Olefinic Character: Bad News for Second-Order Perturbation Theory and Density Functional Schemes." *J. Am. Chem. Soc.*, 118: 3519-3520.
- 11 Xie, Y.; Schaefer, III, H. F.; Liang, G.; Bowed, J. P. 1994. "[10] Annulene: The Wealth of Energetically Low-Lying Structural Isomers of the Same (CH)₁₀ Connectivity." *J. Am. Chem. Soc.*, 116: 1442-1449.
- 12 Longuet-Higgins, H. C.; Salem, L. 1959. "The Alternation of Bond Lengths in Long Conjugated Chain Molecules." *Proc. R. Soc. London*, A251: 172-185.
- 13 Buss, V. 1973. "A Simple Model for Analyzing the Extent of Bond Alternation in Annulenes." *Chem. Phys. Lett.*, 22: 191-195.
- 14 Wannere, C. S.; Schleyer, P. v. R. 2003. "How Aromatic Are Large $(4n + 2)\pi$ Annulenes?" *Org. Lett.*, 5: 865-868.
- 15 Yoshizawa, K.; Kato, T.; Yamabe, T. 1996. "Electron Correlation Effects and Possible D_{6h} Structures in Large Cyclic Polyenes." *J. Phys. Chem.*, 100: 5697-5071.
- 16 Choi, C. H.; Kertesz, M. 1998. "Bond Length Alternation and Aromaticity in Large Annulenes." *J. Chem. Phys.*, 108: 6681-6688.
- 17 Choi, C. H.; Kertesz, M. 1997. "Do Localized Structures of [14]- and [18]Annulenes Exist?" *J. Am. Chem. Soc.*, 119: 11994-11995.
- 18 Hess, B. A., Jr.; Schaad, L. J. 1971. "Hückel Molecular Orbital .pi. Resonance Energies. New Approach." *J. Am. Chem. Soc.*, 93: 305-310.
- 19 Dewar, J. M. S.; Gleicher, G. J. 1965. "Ground States of Conjugated Molecules. II. Allowance for Molecular Geometry." *J. Am. Chem. Soc.*, 87: 692-696.
- 20 Wiberg, K. B. 2001. "Antiaromaticity in Monocyclic Conjugated Carbon Rings." *Chem. Rev.*, 101: 1317-1331.
- 21 Wannere, C. S.; Moran, D.; Allinger, N. L.; Hess, B. A.; Schaad, L. J.; Schleyer, P. v. R. 2003. "On the Stability of Large [4n]Annulenes." *Org. Lett.*, 5: 2983-2986.
- 22 Wannere, C. S.; Schleyer, P. v. R. 2003. "How Aromatic Are Large $(4n+2)\pi$ Annulenes?" *Org. Lett.*, 5: 865-868.
- 23 Kertesz, M.; Choi, C. H.; Yang, S. 2005. "Conjugated Polymers and Aromaticity." *Chem. Rev.*, 105, 3448-3481.
- 24 Shaik, S.; Shurki, A.; Danovich, D.; Hiberty, P. C. 2001. "A Different Story of π -Delocalizations – The Distortion of π -Electrons and Its Chemical Manifestations." *Chem. Rev.*, 101: 1501-1540.
- 25 Shaik, S. S.; Hiberty, P. C.; Lefour, J. M.; Ohanessian, G. 1987. "Is Delocalization a Driving Force in Chemistry? Benzene, Allyl Radical, Cyclobutadiene, and Their Isoelectronic Species." *J. Am. Chem. Soc.*, 109: 363-374.
- 26 Hiberty, P. C.; Shaik, S. S.; Lefour, J.-M.; Ohanessian, G. 1985. "Is the Delocalized π System of Benzene a Stable Electronic System?" *J. Org. Chem.*, 50: 4657-4659.
- 27 Wiberg, K. B.; Nakaji, D.; Breneman, C. M. 1989. "Azines. A Theoretical Study of π -Electron Delocalization." *J. Am. Chem. Soc.*, 111: 4178-4190.
- 28 Berry, R. S. 1961. "Zero-Point Vibrations in Benzene." *J. Chem. Phys.*, 35: 2253-2254.
- 29 Epotis, N. D. 1983. "Applications of Molecular Orbital-Valence Bond Theory in Chemistry." *Pure Appl. Chem.*, 55: 229-236.

- 30 Epiotis, N. D. 1996. *Deciphering the Chemical Code*. New York: VCH Publishers, Inc.
- 31 Jug, K.; Philippe C. Hiberty, P.C.; Shaik, S. 2001. "σ-π Energy Separation in Modern Electronic Theory for Ground States of Conjugated Systems." *Chem. Rev.*, 101: 1477-1500.
- 32 Bao, P.; Yu, Z. H. 2011. "New Procedure to Evaluate Aromaticity at the Density Functional Theory, Hartree–Fock, and Post-Self-Consistent Field Levels." *J. Compt. Chem.*, 32: 248-259.
- 33 Jug, K.; Köster, A. M. 1990. "Influence of σ and π Electrons on Aromaticity." *J. Am. Chem. Soc.*, 112: 6772-6777.
- 34 Köster, A.M.; Calaminici, P.; Geudtner, G.; Gómez-Sandoval, Z. 2005. "Separation of σ and π Energies." *J. Phys. Chem. A*, 109: 1257-1259.
- 35 Ma, Y. P.; Bao, P.; Yu, Z. H. 2007. "Substituent Effect on N-Benzylideneanilines by DFT Energy Partition." *Chin. J. Chem.*, 25: 300-306.
- 36 Bao, P. 2007. *Restricted Geometry Optimization: A New Method to Study the Structures of Organic molecules*, Dissertation for Ph. D., Institute of Chemistry, Chinese Academy of Sciences.
- 37 Tamelen, E. E. van.; Burkoth, T. L. 1967. "Cyclodecapentaene." *J. Am. Chem. Soc.*, 89: 151-152.
- 38 Masamune, S.; Chin, C. G.; Hojo, K.; Seidner, R. T. 1967. "Bicyclo [6.2. 0] deca-2, 4, 6, 9-tetraene." *J. Am. Chem. Soc.*, 89: 4804-4805.
- 39 Masamune, S.; Seidner, R. T. 1969. "[10]Annulenes." *J. Chem. Soc. D: Chem. Commun.*, 542-544.
- 40 Cyclodecapentaene", <http://en.wikipedia.org/wiki/Cyclodecapentaene>
- 41 Farnell, L.; Kao, J.; Radom, L.; Schaefer, H. F. 1981. "Structures and stabilities of Isomeric [10]annulenes." *J. Am. Chem. Soc.*, 103: 2147-2151.
- 42 Sulzbach, H. M.; Schleyer, P. v. R.; Jiao, H.; Xie, Y.; Schaefer, H. F. 1995. "A [10]annulene Isomer May Be Aromatic, after all!" *J. Am. Chem. Soc.*, 117: 1369-1373.
- 43 Oth, J. F. M; Röttele, H.; Schröder, G. 1970. "[12]annulene" *Tetrahedron Lett.*, 11: 61-66.
- 44 Oth, J. F. M.; Gilles, J.-M.; Schröder, G. 1970. "Configuration and Conformational Mobility of [12]annulene from NMR Studies at Various Temperatures." *Tetrahedron Lett.*, 11: 67-72.
- 45 Castro, C.; Isborn, C. M.; Karney, W. L.; Mauksch, M.; Schleyer, P. v. R. 2002. "Aromaticity with a Twist: Möbius [4n]Annulenes." *Org. Lett.*, 20: 3431-3434.
- 46 Sondheimer, F.; Gaoni, Y. 1960. "Unsaturated Macroyclic Compounds. XV. Cyclo-tetradecaheptaene." *J. Am. Chem. Soc.*, 82: 5765-5766.
- 47 Baumann, H.; Bünzli, J. 1989. "Photoelectron Spectrum of [14]annulene." *J. Chem. Soc., Faraday Trans.*, 94: 2695-2699.
- 48 Jug, K.; Fasold, E. 1987. "Structure and Aromaticity of 14-annulene and 18-annulene." *J. Am. Chem. Soc.*, 109: 2263-2265.
- 49 Chiang, C. C.; Paul, I. C. 1972. "Crystal and Molecular Structure of [14]annulene." *J. Am. Chem. Soc.*, 94: 4741-4743.
- 50 Sondheimer, F.; Wolovsky, R.; Amiel, Y. 1962. "Unsaturated Macroyclic Compounds. XXIII. The Synthesis of the Fully Conjugated Macroyclic Polyenes Cyclooctadecanonaene ([18]Annulene), Cyclotetracosadodecaene ([24]Annulene), and Cyclotricontapentadecaene ([30]Annulene)." *J. Am. Chem. Soc.*, 84: 274-284.
- 51 Bregman, J.; Hirshfeld, F. L.; Rabinovich, D.; Schmidt, G. M. J. 1965. "The Crystal Structure of [18]Annulene. X-Ray Study." *Acta Crystallogr.*, 19: 227-234.
- 52 Gorter, S.; Rutten-Keulemans, E.; Krever, M.; Romers, C.; Cruickshank, D. W. J. 1995. "[18]Annulene, C₁₈H₁₈, Structure, Disorder and Hückel's 4n + 2 Rule." *Acta Crystallogr.*, B51: 1036- 1045.
- 53 Jiao, H.; Schleyer, P. v. R. 1996. "Is Kekulene Really Superaromatic?" *Angew. Chem. Int. Ed. Engl.*, 35: 2383-2386.
- 54 Baldridge, K. K.; Siegel, J. S. 1997. "Ab Initio Density Functional vs Hartree Fock Predictions for the Structure of [18]Annulene: Evidence for Bond Localization and Diminished Ring Currents in Bicycloannelated [18]Annulenes." *Angew. Chem. Int. Ed. Engl.*, 36: 745-748.
- 55 Metcalf, B. W.; Sondheimer, F. 1971. "Unsaturated Macroyclic Compounds. LXXXVI. [20]Annulene." *J.*

- Am. Chem. Soc., 93: 6675-6677.
- 56 McQuilkin, R. M.; Metcalf, W.; Sondheimer, F. 1971. “[22]annulene.” J. Chem. Soc. D. Chem Commun, 338-339.
- 57 Kennedy, R. D.; Lloyd, D.; McNab, H. 2002. “Annulenes, 1980–2000” J. Chem. Soc., Perkin Trans. 1, 1601–1621.
- 58 <https://pubchem.ncbi.nlm.nih.gov/compound/85784546>
- 59 Berg, J. M.; Tymoczko, J. L.; Stryer, L. 2002. *Biochemistry*. 5th edition. New York: W H Freeman.
- 60 Marriott, S.; Topsom, R. D. 1984. “Standard Bond Lengths for Use in *ab Initio* Molecular Orbital Calculations.” Theochem, 110: 337-340.
- 61 Allen, F. H.; Kennard, O.; Watson, D. G. 1987. “Tables of Bond Lengths Determined by X-Ray and Neutron Diffraction. Part I. Bond Lengths in Organic Compounds.” J. Chem. Soc. Perkin Trans. 2, S1-S19.

CHAPTER 10

STRAINED-AROMATIC MOLECULES – π -DISTORTIVITY

ABSTRACT

19 strained-aromatic molecules (SAM) are divided into two groups: 9 SAM with aromatic small rings (ASRMs) $C_6X_6H_6$ ($X = B, Al, Ga, N, P, As$) and $C_6X_3H_3$ ($X = B, Al, Ga$); 10 SAM with anti-aromatic small ring (AASRMs) C_6X_6 ($X = B, N, P, S$), $C_6X_6H_6$ ($X = C, Si, Ge$) and $C_6X_3H_3$ ($X = N, P, As$). For each SAM, a particular localized geometry (PLG) is restrictedly optimized using our 2011 method. In the PLG, the π -electron interactions are artificially excluded from between the central ring and the annulated small rings. For each group of SAMs, the molecular energy difference, $\Delta E(GP) = E(G) - E(PLG)$, between the ground (G) state geometry and PLG can be fitted as the polynomial function of the difference $d\Delta r(GP) = \Delta r(G) - \Delta r(PLG)$ (for example, $\Delta r(G) = r_{endo}(G) - r_{exo}(G)$ is the bond length difference between the endo- (C(1)-C(2)) and exo-cyclic (C(1)-C(6)) bonds in the G geometry). As shown by the energy decomposition, the π -interaction produces the forces $\Delta F_{12}(GP)$ and $\Delta F_{16}(GP)$ acting on the C(1)-C(2) and C(1)-C(6) bonds, respectively. The $\Delta r_{ij}(GP) = r_{ij}(G) - r_{ij}(PLG)$ ($ij = 12, 16$) is the difference, in the C(i)-C(j) bond distance, between the G and the PLG, and it can be fitted as the polynomial function of $\Delta F_{ij}(GP)$. For 19 molecules, always $\Delta F_{12}(GP) > 0$, and $\Delta r_{12}(GP) > 0$. The endocyclic bonds are always lengthened due to π -interaction.

For 13 SAMs including all AASRMs and 3 ASRMs $C_6X_6H_6$ ($X = N, P, As$) with electron-rich groups, always $\Delta F_{16}(GP) < 0$, $\Delta r_{16}(GP) < 0$, and always $\Delta r(G) > |\Delta r(PLG)| > 0$. Correspondingly, always $\Delta E(GP) > 0$, $d\Delta r(GP) > 0$. For these molecules, therefore, π -interaction is always a driving force for distorting central ring. For 6 ASRMs $C_6X_6H_6$ and $C_6X_3H_3$ ($X = B, Al, Ga$) with electron-deficient group, whether $\Delta r(G) > \Delta r(PLG)$ or $\Delta r(G) < \Delta r(PLG)$ depends on the influences of the secondary effect on the PLG geometry. In summary, π -electron delocalization is distortive and is the main driving force for the distortion of central benzene ring.

The bond length alternation may also be found in the PLG, and it can be fitted as the polynomial function of $\Delta\beta(PLG) = \angle H-XX - \angle C-XX$ (XX: X=X, X-X). As a secondary structure effect, the β angle ($\angle CXX$) difference, $\Delta\beta(PLG)$, can be considered as an angle strain, and it is a main driving force for distorting the central ring of PLG although the value of $\Delta r(PLG)$ is small and $\Delta r(PLG) < \Delta r(G)$ at the most case.

yuzh@iccas.ac.cn

Key words: strained-aromatic molecule; endo- and exo-cyclic bond; conjugation distorting central ring; electron-deficient small ring; electron-sufficient small ring; bond length alternation; π -distortion

10.0. FOREWORDS

As early as 1980 to 1990, as summarized by Shaik at the WATOC conference in Jerusalem during July 8-12, 1996,¹ the π -distortivity was a hot controversial topic. In Chapter 4, using our 1998 method,² we have demonstrated that π - and σ -electron delocalization is the driving forces for distorting NBA-like species away from the planar geometry. In our research works, the driving forces refer to the following destabilizing energy differences (or rather, it should be a first order derivative of the energy difference):

- (i) The molecular energy difference between the full delocalized electron (FUD) state and the σ -electron delocalization (DSI) state. These two electronic states belong to the same optimized geometry, and their molecule energy difference is called the vertical delocalization energy.
- (ii) The molecular energy difference between the DSI state and the FUL (Full localized) state. These two electronic states belong to the same optimized geometry, and their molecular energy difference is called the σ -delocalization energy.

For the Shaik's method, the π -driving force for distorting benzene molecule away from its D_{6h} geometry is the π part of the molecular energy difference between the two distorted geometries. This driving force does not involve the π -electron delocalization. This is a fundamental difference, in discussing π -distortivity, between our method and Shaik's method.

The molecular distortion arising from the electron delocalization can be found in multiple ways. For example, from the GL geometry of a benzene molecule to the D_{6h} geometry of the ground state, the compressing of single bonds and the stretching of double bonds are caused by the delocalization of π electrons, and the final equalization of the CC bond lengths results in the minimization of nuclear repulsion. In the conjugated molecule such as NBA-like species, and in the case of the local conjugation between a pair of the localized double bonds in the GL geometry of the conjugated molecules including aromatic molecules, the destabilizing feature of electron delocalization corresponds to the following distortive characteristics:²⁻¹⁰ the single bond between two double bonds being lengthened due to the conjugation; two conjugated groups being not coplanar.

Conditional settings for optimizing LG		LG	B3LYP	BLYP	LYP	SLATER	RHF	MP2
$h_{\lambda\rho} = 0$		r_{N-B}	0.631	0.633	0.581	0.634	0.582	0.580
$f_{\lambda\rho} = 0$	$AO \phi_\lambda \in NH_3$	r_{N-H2}	0.839	0.833	0.799	0.842	0.770	0.780
$s_{\lambda\rho} = 0$	$AO \phi_\rho \in BH_3$	r_{B-H6}	1.268	1.192	1.163	1.199	1.222	1.215
$<\lambda\rho \mu\sigma>$	$AO \phi_\lambda \text{ and } \phi_\mu \in NH_3$ $AO \phi_\rho \text{ and } \phi_\sigma \in BH_3$	r_{N-H6}	0.990	0.910	1.088	0.917	1.134	1.131
		$H2-N-H3$	118.8°	117.1°	120.0°	118.9°	120.0°	120.0°
		$H6-B-H7$	83.4°	81.4°	106.8°	81.4°	106.2°	106.6°
		$H2-N-B-H6$	-60.0°	-60.0°	-89.6°	-60.0°	-60.0°	-60.0°
		$H4-N-H2-H3$	-158.6°	-146.8°	-174.8°	-145.8°	-178.2°	-177.7°
		$H8-B-H6-H7$	84.1°	82.5°	114.0°	82.5°	112.7°	113.6°
		(c)	(a)			(b)		

Figure 10-I. For the localized geometry (LG) of NH_3BH_3 complex: (a) The configuration and conformation; (b) The bond lengths (\AA), bond angles and dihedral angles at various levels of theory; (c) Conditional settings for optimizing LG geometry. The calculations are performed by using our 2011 method at the 6-311G** level.

In organic chemistry, strained-aromatic molecule is a kind of typical distorted conjugated molecules. In the fields of strained-aromatic molecules, the most controversial issue is the reason for the alternating bond lengths in the central benzene ring. In this chapter, our 2011 method will be used to reveal that, in the central ring of strained aromatic molecules, π -electron delocalization is the main driving force for bond length alternation. Before doing, it is necessary to understand the surprising influences of electron delocalization on the conformation and configuration of the complex NH_3BH_3 : in the localized geometry (LG) of complex optimized using our 2011 method and our 2007 method,⁸ the two partners, NH_3 and BH_3 , are hugged together tightly face to face (Figure 10-Ia) when the electron interactions are excluded from between the two partners. This image is so surprising that it seems necessary to re-examine the distorting role of the electron interactions, including charge transfer (CT) and exchange interaction, between two partners NH_3 and BH_3 in promoting the formation of CT-complex.

10.0.1. Mulliken's Model of Charge Transfer Complex

The charge transfer complex arises from the interactions between electron donor (such as NH_3) and acceptor (such as BH_3). The CT-complex have been an important subject for theoretical and experimental works, and much discussion were done in the books of Briegleb,¹¹ Rose,¹² Andrews and Keefer,¹³ Foster,¹⁴ and Mulliken and Person¹⁵. Early researches, including the recent ones, focused on molecular spectroscopy.¹⁶⁻²⁰ Recently, it has been applied to organic functional materials.²¹

In 1942, Weiss pointed out that a low ionization potential of the electron donor and a high electron affinity of the electron acceptor should favor a stable complex.²² Brackmann (1949) attributed molecular complex (AB) formation to complex resonance between a no-bond structure (A,B) and a structure with a bond (A-B) between the electron donor A and acceptor B.²³ In 1952, Mulliken proposed his model after a selection and combination of Weiss's and Brackmann's ideas and based on the perturbation theory, and he thought that CT interaction plays a decisive role in stabilizing CT complex.²⁴ The Mulliken's model involves resonance between no-bond structures (A,B) and dative structures ($A^+ - B^-$), where A is an electron donor, and B is an electron acceptor. When a CT complex AB is loose, the resonance form (A,B) is the major contribution to the ground state A-B (ψ_G) of the molecular complex, which implies:

$$\Psi_G \approx \Psi_o(A, B) \text{ and } E_G \approx E_o$$

And at the excited state (ψ^*):

$$\Psi^* \approx \Psi_1(A^+ B^-) \text{ and } E^* \approx E_1$$

Accordingly, as Mulliken concluded, "the spectrum associated with the transition may be called an intermolecular charge-transfer spectrum: light absorption causes an electron to jump from B to A". That is to say, light absorption causes color change and eventually leads to the formation of CT complex. However, as Brackmann insisted,²³ it is whole complex itself to determines the color, that is, the light absorption is the result of the formation of CT complex, rather than the cause of the complex formation. Today, the view of Brackmann should be a well-known knowledge. In terms of the controversy about the cause of the color of the complex, however, Brackmann did not address the role of electron delocalization in the formation of complex.

Many literatures²⁵⁻³⁰ indicated that the term "charge-transfer" is not pertinent to the nature of the formation and stability of CT complex, and argued that charge transfer force does not play a dominant role in bonding of the partners. But questioning the role of electron transfer is different from questioning the concept of electronic delocalization stabilization.

10.0.2. Our Energy Decomposition Methods

For any problem involving electron delocalization, there is always a need to establish method for calculating or measuring the electron delocalization energy. As described in the previous chapters of this book, conjugation effect is studied in this way. Certainly, the stabilizing energy of charge-transfer complex should also be done in this way.

In the field of charge transfer complexes, there are the following three types of energy decomposition methods based on the construction of the LMO (localized molecular orbital) basis set, or on the construction of localized geometry (or localized electronic state).

- (i) Morokuma's energy decomposition.³¹
- (ii) BLW method.³²
- (iii) NBO energy decomposition.³³

For examples, the Khalil's method (2008)³⁴ belongs to the second type, and Adeniyi and Ajibade's method (2013)³⁵ belongs to the third type. Our 2011 method belongs to the Morokuma's energy decomposition.

For the second and third types of methods, the fundamental flaws have been detailed in the previous chapters of this book.

10.0.2.1. Construction of LMO Basis Set

In order to understand the roles of the electrostatic (ES), polarization (PL), exchange (EX) and charge transfer (CT) interactions in determining the structure (conformation and configuration) of NH_3BH_3 complex, it is necessary to construct a localized molecular orbital (LMO) basis set.

The MOs Ψ_i of NH_3 monomer is obtained from the single-point energy calculation, on the B3LYP/6-311G** optimized geometry of NH_3 molecule, at RHF/6-31G* level, and it can be expressed as the follow:

$$\Psi_i = \sum_{i=1}^{na} \sum_{\lambda=1}^{na} a_{\lambda i} \phi_{\lambda} \quad (10-\text{I})$$

In Equation (10-I), n_a is the number of atomic orbitals (AOs) ϕ_{λ} , and it is 21 at 6-31G* level. After the single-point energy calculation on the B3LYP/6-311G** optimized geometry of BH_3 molecule, the MOs Ψ_j of BH_3 monomer can be written as follow:

$$\Psi_j = \sum_{j=1}^{nb} \sum_{\rho=1}^{nb} b_{\rho j} \phi_{\rho} \quad (10-\text{II})$$

For the NH_3BH_3 complex, the LMO basis set $\{\Phi_i\}$ can be obtained from the superposition of the MOs Ψ_i and Ψ_j , and it can be written as:

$$\Phi_i = \sum_{i=1}^n \left(\sum_{\lambda=1}^{na} a_{\lambda i} \phi_{\lambda} + \sum_{\rho=na+1}^n b_{\rho i} \phi_{\rho} \right) \quad (10-\text{III})$$

In Equation (10-III), the AO coefficients $b_{\rho i}$ are set equal to zero when the LMO Φ_i belongs to the partner NH_3 , and when Φ_i belongs to the partner BH_3 , set the AO coefficients $a_{\lambda i} = 0$.

It should be emphasized that the Cartesian coordinates of the free molecules NH_3 and BH_3 must be identical to the coordinates of the corresponding partners in the NH_3BH_3 complex, and the Cartesian coordinates of the free molecules and complex must remain unchanged during the single-point energy calculation. In this case, the LMO

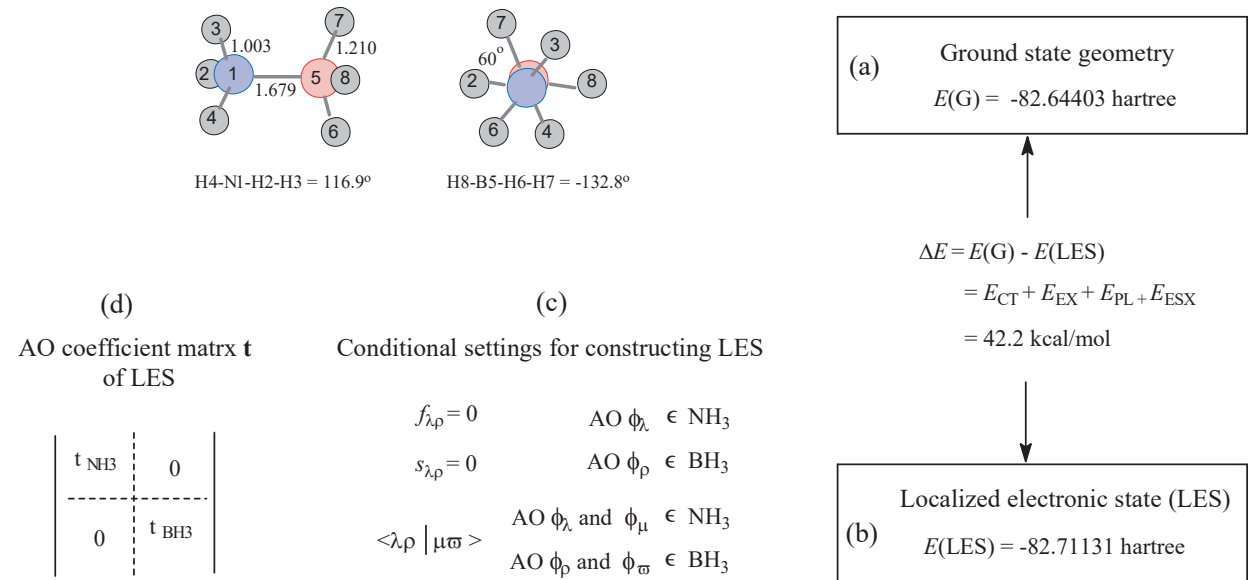


Figure 10-II. The destabilizing energy effect, $\Delta E = [E(\text{G}) - E(\text{LES})]$, of NH_3BH_3 complex is obtained from the single-point energy calculation, on the B3LYP/6-311G** optimized ground state geometry, performed using our 2011 method at the RHF/6-311G** level.

overlap integrals: $\langle \Phi_i | \Phi_i \rangle = 1$, $\langle \Phi_i | \Phi_j \rangle = 0.0$ ($i \neq j$) when Φ_i and Φ_j \in the same partner, and $\langle \Phi_i | \Phi_j \rangle \neq 0.0$ when Φ_i and Φ_j \in the two different partners.

10.0.2.2. Construction of Localized Electronic State

Using our 2011 method at the RHF/6-31G* level, the localized electronic state (LES) of the ground state geometry is constructed by the single-point energy calculation, on the optimized ground state geometry of NH_3BH_3 complex, under the following conditional settings (Figure 10-IIc):

- (i) Set $s_{\lambda\rho} = 0.0$, $h_{\lambda\rho} = 0.0$, and $f_{\lambda\rho} = 0$ when AOs ϕ_λ and ϕ_ρ \in the two different partners, where $s_{\lambda\rho}$, $h_{\lambda\rho}$ and $f_{\lambda\rho}$ are the elements of the AO overlap integral matrix, one-electron matrix and Fock matrix.
- (ii) Set two-electron exchange integrals $\langle \lambda\rho | \mu\omega \rangle = 0$ when the AOs ϕ_λ and $\phi_\mu \in$ the NH_3 partner, and the AOs ϕ_ρ and $\phi_\omega \in$ the BH_3 partner.

In the LES, as shown by the AO coefficient matrix \mathbf{t} in Figure 10-IId, the MOs are absolutely localized on their respective partners. In order to calculate the energy effects denoted as ΔE_x ($x = \text{CT}, \text{EX}, \text{PL}, \text{ESE}$) using Equation (10-IV), the AO coefficient matrix \mathbf{t} of the LES (or the ground state) should be transformed into the LMO coefficient matrix \mathbf{T} using the Equation (10-V):

$$\mathbf{E} = (\mathbf{H} + \mathbf{F}) \mathbf{D} \quad (10-\text{IV})$$

$$\mathbf{T} = \mathbf{a}^{-1} \mathbf{t} \quad (10-\text{V})$$

In the above Equations, the lowercase bold letter "a" is the AO coefficient matrix of LMO basis set $\{\Phi_i\}$, and \mathbf{a}^{-1} is

Table 10-I. For Ground State Geometry and Its Localized Electronic State (LES) of NH_3BH_3 Complex, Various Energy Components E_x of Total Electronic Energy E_e , and Their Differences, $\Delta E_x = E_x(\text{G}) - E_x(\text{LES})$, Obtained from Our 2011 Method at RHF/6-311G** Level (Energy Unit in hartree).

	E_x	$E_x(\text{G})$	$E_x(\text{LES})$	ΔE_x
NH ₃	$E_{\text{ES-O}}$	-77.74498	-70.96762	-6.77736
	$E_{\text{ES-V}}$	-0.05768	-0.17432	0.11664
	E_{PL}	-0.36147	-1.04647	0.68500
(A)	$E_{\text{NH3-e}}$	-78.16413	-72.18840	-5.97573
	$E_{\text{ES-O}}$	-44.11885	-43.58487	-0.53398
	$E_{\text{ES-V}}$	-0.61606	-7.55844	6.94238
(B)	E_{PL}	0.40701	0.07561	0.33140
	$E_{\text{BH3-e}}$	-44.32791	-51.06770	6.73979
	$E_{\text{EX-O}}$	1.49241	0.00000	1.49241
A-B	$E_{\text{EX-V}}$	0.01702	0.00000	0.01702
	$E_{\text{CT-AB}}$	-2.16094	0.00000	-2.16094
	$E_{\text{CT-BA}}$	-0.04529	0.00000	-0.04529
	E_e	-123.18883	-123.25611	0.06728

its reverse matrix, and the bold uppercase letters, **H** and **F**, are the LMO one-electron matrix, LMO Fock matrix, respectively. Then, the LMO density matrix **D** of the LES (or ground state) can be obtained from the LMO coefficient matrix **T**. For the localized electron state (or ground state) of complex, the AO one-electron matrix **h**, AO Fock matrix **f** can be transformed into their corresponding LMO matrices **H** and **F** using the following Equations:

$$\mathbf{H} = \mathbf{a}^* \mathbf{h} \mathbf{a}$$

$$\mathbf{F} = \mathbf{a}^* \mathbf{f} \mathbf{a}$$

10.0.2.3. Energy Decomposition.

The energy difference $\Delta E = E(\text{G}) - E(\text{LES}) = E_e(\text{G}) - E_e(\text{LES})$, where $E(\text{G})$ and $E(\text{LES})$ are the molecular energies of the ground state geometry and its LES. At the RHF/6-31G* level, the molecular energies $E(\text{G})$ and $E(\text{LES})$ are obtained from the single-point energy calculation on the B3LYP/6-311G** optimized ground state geometry. The molecular energy difference ΔE and its various components ΔE_x are listed in Table 10-I. Various energy components are calculated using the following Equations:

$$\Delta E = \Delta E_{\text{ESX}} + \Delta E_{\text{PL}} + \Delta E_{\text{CT}} + \Delta E_{\text{EX}} \quad (10\text{-VI})$$

According to the Morokuma's definitions of interaction energy components,³¹

$$\Delta E_{ESX} = E_{ESX}(G) - E_{ES}(LES) = (E_{ESX-O}(G) + E_{ESX-V}(G)) - (E_{ES-O}(LES) + E_{ES-V}(LES))$$

$$E_{ES-O} = \sum_{\substack{i=1 \\ i \in A}}^{occ} \sum_{\substack{j=1 \\ j \in A}}^{occ} (H_{ij} + F_{ij}) D_{ij} \quad (10\text{-VII})$$

$$E_{ES-V} = \sum_{\substack{i=occ+1 \\ i \in A}}^{na} \sum_{\substack{j=occ+1 \\ j \in A}}^{na} (H_{ij} + F_{ij}) D_{ij}$$

in the above equations, the letter "A" denotes a specific partner (NH_3 or BH_3). In the ground state geometry, the electrostatic energy, calculated by Equation (10-VII), should include the spatial exchange interaction between two partners, and $E_{ES-O}(G)$ should be written as $E_{ESX-O}(G)$. In the LES state constructed by our 2011 method, the two-electron exchange has been excluded from between two partners, so the energy component, calculated by Equation (10-VII), $E_{ESX-O}(LES) = E_{ES-O}(LES)$. Similarly, the E_{PL} , E_{CT} and E_{EX} can be calculated using the following Equations:

$$E_{PL} = \sum_{\substack{i=1 \\ i \in A}}^{occa} \sum_{\substack{j=occ+1 \\ j \in A}}^{na} (H_{ij} + F_{ij}) D_{ij}$$

$$E_{CT-AB} = \sum_{\substack{i=1 \\ i \in A}}^{occa} \sum_{\substack{j=occ_b+1 \\ j \in B}}^{nb} (H_{ij} + F_{ij}) D_{ij}$$

$$E_{CT-BA} = \sum_{\substack{i=occ_a+1 \\ i \in A}}^{na} \sum_{\substack{j=1 \\ j \in B}}^{occ_b} (H_{ij} + F_{ij}) D_{ij}$$

$$E_{EX-O} = \sum_{\substack{i=1 \\ i \in A}}^{occa} \sum_{\substack{j=1 \\ j \in B}}^{occ_b} (H_{ij} + F_{ij}) D_{ij}$$

$$E_{EX-V} = \sum_{\substack{i=occ_a+1 \\ i \in A}}^{na} \sum_{\substack{j=occ_b+1 \\ j \in B}}^{nb} (H_{ij} + F_{ij}) D_{ij}$$

In the above Equations, $occa$ and occ_b are the highest occupied LMOs, respectively, of the partners A (NH_3) and B (BH_3). The energy effect (hartree) ΔE_X ($X = \text{NH}_3, \text{BH}_3$) is the difference, in the energy component ($E_{ESX} + E_{PL}$), between the ground state and its LES, and they are as follows (Table 10-I):

$$\Delta E_{\text{NH}_3} = E_{\text{NH}_3}(G) - E_{\text{NH}_3}(\text{LES}) = -5.97573 > 0 \text{ (stabilizing)}$$

$$\Delta E_{\text{BH}_3} = E_{\text{BH}_3}(G) - E_{\text{BH}_3}(\text{LES}) = 6.73979 < 0 \text{ (destabilizing)}.$$

ΔE_{CT} and ΔE_{EX} are two energy effects (hartree) arising from inter-molecular interactions, and their values are as

follows:

$$\Delta E_{CT-AB} = -2.16094$$

$$\Delta E_{CT-BA} = -0.04529$$

$$\Delta E_{CT} = \Delta E_{CT-AB} + \Delta E_{CT-BA} = -2.20623 \text{ (stabilizing).}$$

$$\Delta E_{EX-O} = 1.49241$$

$$\Delta E_{EX-V} = 0.01702$$

$$\Delta E_{EX} = \Delta E_{EX-O} + \Delta E_{EX-V} = 1.50943 \text{ (destabilizing)}$$

The result that $\text{abs}(\Delta E_{CT-AB}) \gg \text{abs}(\Delta E_{CT-BA})$ is consistent with the direction of charge transfer. For the above energy effects, ΔE_{CT} and ΔE_{NH_3} are stabilizing, but the total stabilization energy effect is, in absolute value, smaller than the total destabilization energy effect. As a result, total energy effect $\Delta E = E(G) - E(LES) = 0.06728 \text{ hartree} = 42.2 \text{ kcal/mol}$, and it is destabilizing.

The energy difference, $\Delta E = E(G) - E(LES)$, between the ground state and its LES state are calculate at (B3LYP, RHF and MP2) levels with different basis sets, and their values (kcal/mol) are as follows:

193.5 (6-31G*), 279.9 (6-311G**), 615.1 (6-311G(2d,2p)), 600.8 (6-311G(2d,fp), 385.7 (6-311++G**) (B3LYP)
 -41.1 (6-31G*), 42.2 (6-311G**), 312.8 (6-311G(2d,2p)), 296 (6-311G(2d,fp)), 127.1 (6-311++G**) (RHF).
 -49.4 (6-31G*), 117.4 (6-311G**), 371.4 (6-311G(2d,2p)), 365.7 (6-311G(2d,fp), 179.0 (6-311++G**) (MP2).

All of the above data, except for the (RHF and MP2)/6-31G* values, indicate that, in the NH_3BH complex, electron delocalization is destabilization.

10.0.3. Thermodynamic Mechanisms of Reaction $NH_3 + BH_3$

To further confirm the destabilization nature of electron delocalization and to discuss its role in determining the structure of complex, the thermodynamic mechanism of the $NH_3 + BH_3$ reaction is shown in Figure 10-II. The thermodynamic mechanism includes the following B3LYP/6-311G** optimized geometries of NH_3BH_3 complex: an artificial geometry, localized geometry (LG), the delocalized electronic (DLE) state of the LG geometry, ground state (G) geometry.

10.0.3.1. Construction of Artificial NH_3BH_3 Geometry.

In order to calculate the BSSE (basis set superposition error) corrected energy of the NH_3 and BH_3 monomers (the geometries of the two monomers and their complex are fully optimized at B3LYP/6-311G** level), as shown by Figure 10-IIIa and Figure 10-IIIb, an artificial geometry of NH_3BH_3 and all the related geometries is obtained from the geometry optimization, at B3LYP/6-311G** level, under the following conditional settings:

- (i) The geometric data of each of the two partners NH_3 and BH_3 are set equal to the geometric data of the corresponding free monomer.
- (ii) The N(1)-B(5) bond length is set equal to that (1.663 Å) in the ground state geometry of NH_3BH_3 complex.
- (iii) The geometrical data of each of two partners, as well as the N(1)-B(5) bond length, remain unchanged during the geometry optimization.

After the geometry optimization, the dihedral angle $H(6)-B(5)-N(1)-H(2) = 60^\circ$, bond angles $H(6)-B(5)-N(1) = 90^\circ$, and $B(5)-N(1)-H(2) = 112.4^\circ$ (Figure 10-IIIb).

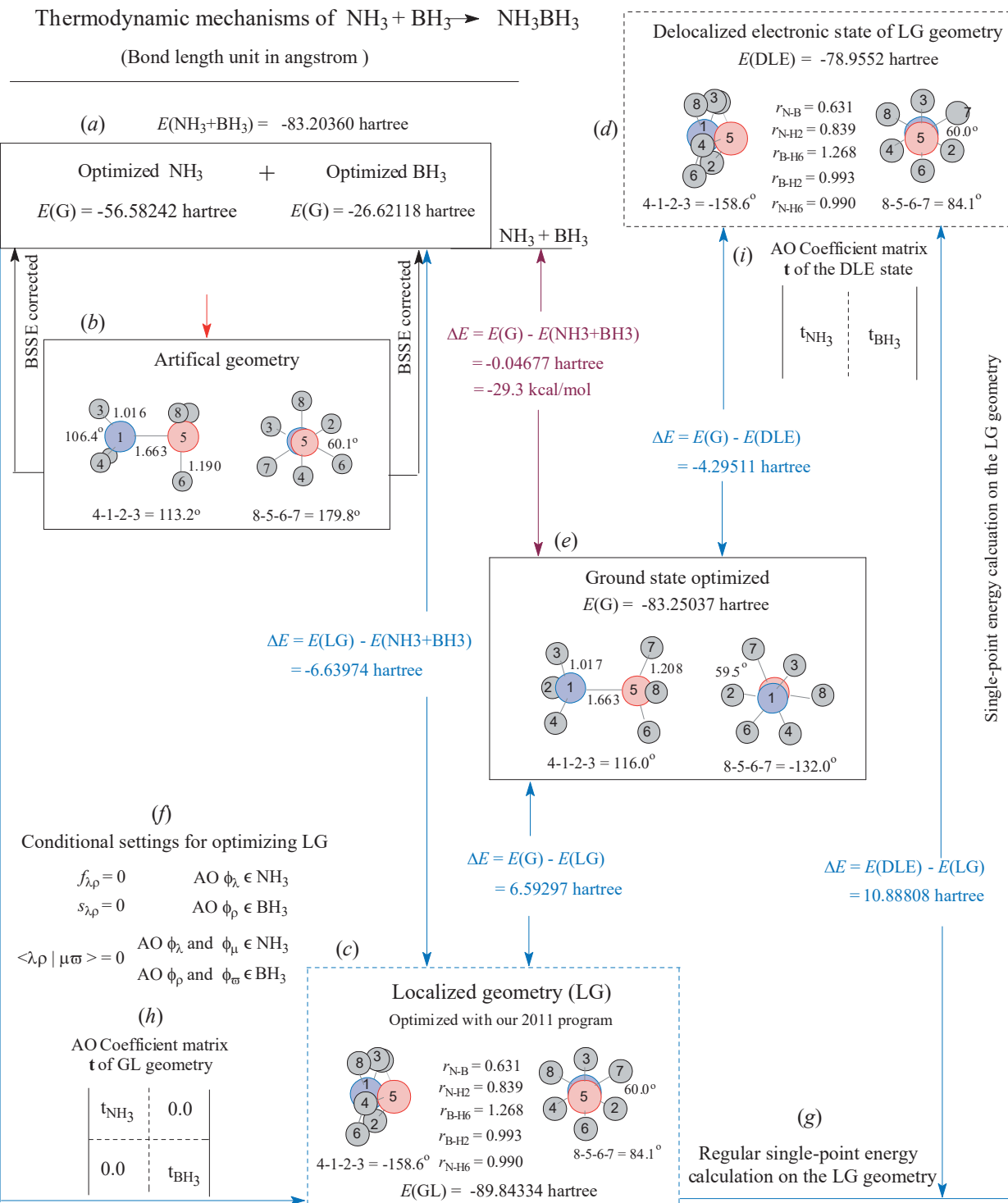


Figure 10-III. The thermodynamic mechanisms of reaction $\text{NH}_3 + \text{BH}_3 = \text{NH}_3\text{BH}_3$. (a) and (b) The BSSE corrected energy of the free molecules NH_3 and BH_3 . (c) The localized geometry (LG) of the complex is conditionally optimized using our 2011 method. (d) The full delocalized electronic state (DLE) of GL geometry is obtained from the regular single-point energy calculation on the LG. (e) The ground state of the complex. All the calculations are performed at the B3LYP/6-311G** level.

The BSSE corrected molecular energies $E(G)$ of the free molecules NH_3 and BH_3 are calculated, on the artificial geometry of NH_3BH_3 complex, using Gaussian 98 package, and they are presented in Figure 10-IIIa.

10.0.3.2. Amazing NH_3BH_3 Localized Geometry

Using our 2011 program at the B3LYP/6-311G** level, as shown by Figure 10-IIIc, the localized geometry (LG) of the complex is obtained from the geometry optimization under the following conditional settings (Figure 10-IIIf):

- (i) Set $s_{\lambda,\rho} = 0.0$, $h_{\lambda,\rho} = 0.0$, and $f_{\lambda,\rho} = 0$ when AOs $\phi_\lambda \in$ the NH_3 partner, and the AOs $\phi_\omega \in$ the BH_3 partner.
- (ii) Set two-electron exchange integrals $\langle \lambda \rho | \mu \omega \rangle = 0$ when the AOs ϕ_λ and $\phi_\mu \in \text{NH}_3$, and the AOs ϕ_ρ and $\phi_\omega \in \text{BH}_3$.

In the LG geometry, therefore, the MO EX and CT interactions, as well as the spatial exchange interaction, have been excluded from between the NH_3 and BH_3 partners (the phrase "the MO EX and CT interactions, as well as the spatial exchange interaction," will be shortened into the phrase "the electron interaction"). In the B3LYP/6-311G** LG geometry (Figure 10-IIIc), the configurations of the two partners have been inverted, the N-B bond length is 0.631 Å, and the distances (1.269 Å) between the boron atom and its three hydrogen atoms (H6, H7 and H8) are even larger than the distances (0.990 Å) between the nitrogen atom and the three hydrogen atoms (H6, H7 and H8) originally belonging to BH_3 partner. The N-B bond distance is so short that two partners hugged tightly together face to face, and 6 hydrogen atoms seem to be bonded to the nitrogen atom, which are very surprising.

In order to understand the influence of theoretical level and basis set size on the distance of N-B bond, the LG geometry is also optimized at (B3LYP, RHF, and MP2) levels with different basis sets, and the distances (Å) of N-B bond are as follows:

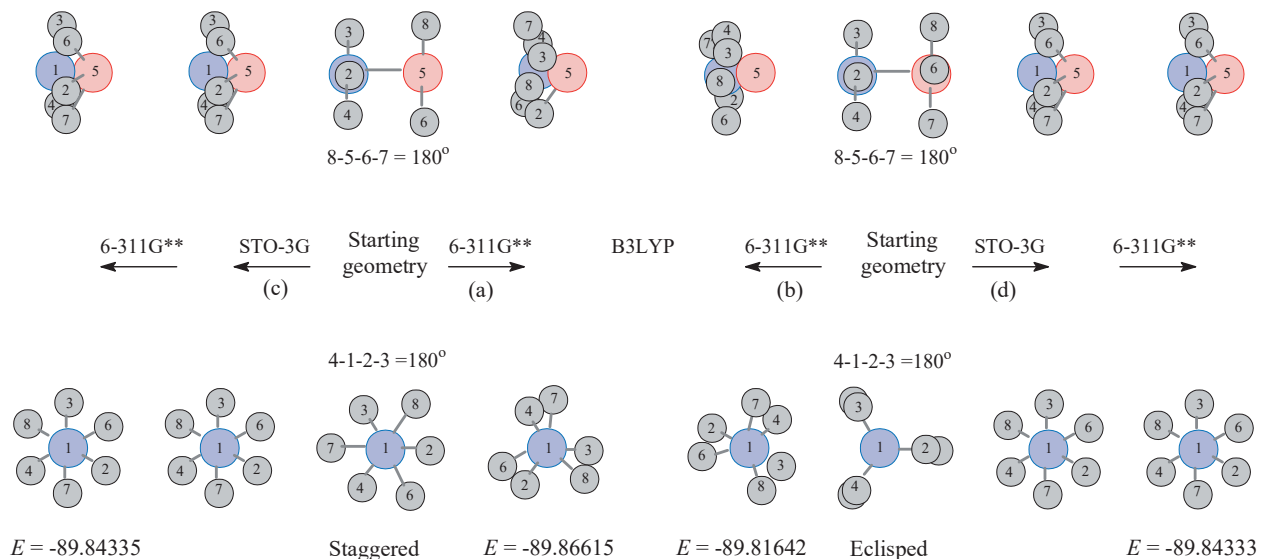
0.583 (6-31G*), 0.631 (6-311G**), 0.536 (6-311G(2d,2p)), 0.564 (6-311G(2df,p)), 0.632 (6-311++G**) (B3LYP).
 0.563 (6-31G*), 0.582 (6-311G**), 0.497 (6-31g(2d)) (RHF)
 0.561 (6-31G*). 0.580 (6-311G**), 0.499 (6-31G(2d)) (MP2)

At the RHF and MP2 level, the distance of N-B bond becomes shorter as the basis set size increases. At 6-31G(2d) level, the RHF and MP2 values (Å) of the distance are 0.497 and 0.499 Å. When the basis set size is larger than 6-31G(2d), the N-B bond is so shorter that the geometry optimization does not converge. Nonetheless, as indicated by the above limited number of distance data, in the case of LG geometry, electron delocalization is always destabilization, and it should be a driving force for distorting the geometry of NH_3BH_3 complex from the LG geometry toward ground state geometry, and meanwhile the N–B bond is lengthened from the shorter distance to the longer distance, which has nothing to do with the theoretical level and the base set size.

Based on the energy decomposition at the RHF/6-311G** level, the energy differences (hartree) between the LG geometry and two free monomers are as follows:

$$\begin{aligned}\Delta E &= E(\text{LG}) - [E(\text{NH}_3) + E(\text{BH}_3)] = \Delta E_{\text{ES}} + \Delta E_{\text{PL}} + \Delta E_{\text{N}} = -5.17614, \\ \Delta E_{\text{ES}} &= -50.4417 \\ \Delta E_{\text{PL}} &= -9.72518 \\ \Delta E_{\text{N}} &= 54.99080\end{aligned}$$

In the LG geometry, the two-electron exchange interaction have been excluded from between two partners. So, there are only the electrostatic (ES) and polarization (PL) interaction, and the electrostatic interaction seems to play a

**Scheme 10-I**

decisive role in promoting the formation of CT-complex. In order to get insight into the role of electrostatic interaction in determining the LG geometry and to confirm that electron delocalization is destabilization, a series of localized geometries $\text{LG}(\text{R})$ with the different distances of the $\text{N}(1)\text{-B}(5)$ bond have to be optimized.

10.0.3.3. A Series of $\text{LG}(\text{R})$ Geometries

A series of localized geometries, denoted as $\text{LG}(\text{R})$, are optimized using our 2011 method under the following conditional settings:

- (i) Distance (R) between the boron and nitrogen atoms is set equal to a specified value, and it remains constant during the geometry optimization.
- (ii) Conditional settings of the electron and MO interactions are the same as those detailed in Figure 10-IIIf.

Due to the face-to-face configuration, the BH_3 partner can't freely rotate about the N-B bond. As a result, the conformation and configuration of a specific localized geometry $\text{LG}(\text{R})$ depend upon the starting geometry. For the $\text{LG}(0.631)$ geometry (the $\text{N}(1)\text{-B}(5)$ bond distance $\text{R} = 0.631 \text{ \AA}$), as shown in Scheme 10-I, the conformations of two starting geometries are staggered and eclipsed conformations, respectively. In these two starting geometries, two partners are planar. Based on these two starting geometries, the following four ways are used to optimize the $\text{LG}(0.631)$ geometry:

- (i) Starting from the staggered geometry (Scheme 10-Ia).
- (ii) Starting from the eclipsed geometry (Scheme 10-Ib);
- (iii) Starting geometry has a staggered conformation. The geometry optimization is performed at the $\text{B3LYP}/\text{STO-3G}$ level, and then the $\text{B3LYP}/\text{STO-3G}$ optimized geometry is used as a starting geometry to optimize the LG geometry at the $\text{B3LYP}/\text{6-311G}^{**}$ level (Scheme 10-Ic);
- (iv) Starting geometry has an eclipsed conformation. The geometry optimization is performed at the $\text{B3LYP}/\text{STO-3G}$ level, and then the $\text{B3LYP}/\text{STO-3G}$ optimized geometry is used as a starting geometry to optimize the LG geometry at the $\text{B3LYP}/\text{6-311G}^{**}$ level (Scheme 10-Id).

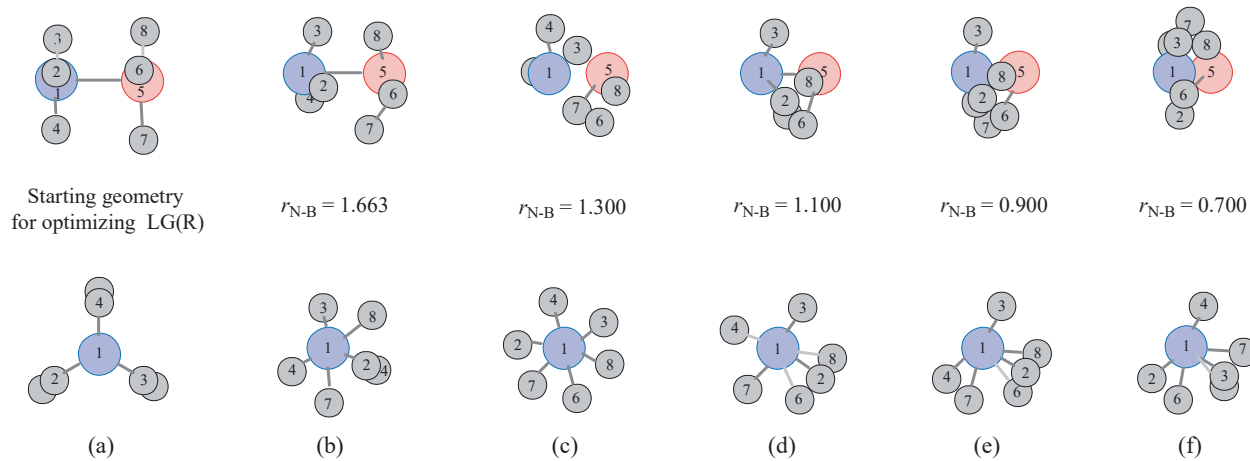


Figure 10-IV. (a) Starting geometry used to optimize LG(R) geometries. (b) - (f) The conformations and configurations of 5 typical LG(R) geometries optimized at B3LYP/6-311G** level (bond length unit in angstrom).

In the case of LG(0.631) geometry, the third and fourth ways seem reasonable, but they can't guarantee the convergence of geometric optimization when $R > 1.0 \text{ \AA}$. In addition, the four ways are also tested by using "NONVDW" input.³⁶ The tests showed that the different ways gave the different molecular energies for a LG(R) geometry when $R \geq 0.7 \text{ \AA}$. In this section, therefore, the eclipsed geometry is used as a starting geometry to optimize a series of LG(R) geometries (second way), and the conformations of typical LG(R) geometries are shown in Figure 10-IV.

10.0.3.4. Electrostatic and Polarization Forces

In the ground state (G) geometry of NH_3BH_3 complex, as shown in Figure 10-IIIe, the two partners adopt back-to-back configuration. Elimination of the electronic interactions between two partners leads to the inversion of the configurations of two partners. In each LG(R) geometry, as a result, two partners take a face-to-face configuration. Figure 10-IV shows the change in the conformation and configuration with the shortening of the N-B bond.

According to the practical calculations, the optimized geometry of LG(R) at the B3LYP/6-311G** level is more reasonable than at the RHF/6-311G** level. For a specific LG(R) geometry, therefore, the energy decomposition is performed, based on the B3LYP/6-311G** optimized geometry, at RHF/6-311G ** level. For the LG(R) geometries, the total electronic energy (E_e) and the molecular energy (E), as well as various energy components, are listed in Table 10-II. The molecular energy $E(R)$ can be fitted as the following third order polynomial function of the N-B bond distance R :

$$E(R) = -81.5350 - 22.14167 R + 23.43934 R^2 - 6.54171 R^3.$$

$$dE(R)/dR = -22.14167 + 46.87868 R - 19.62513 R^2 > 0.$$

The average difference, $\Delta E_e/\Delta R = [E_e(0.631) - E_e(1.663)]/(1.663-0.631) = -32.40740 \text{ hartree}$, can be used to quantify an average attraction between the two partners. It is big enough to overcome the nuclear repulsion (Figure 10-Va). As a result, the total force between the two partners, the first order derivative $dE(R)/dR > 0$, is attraction, and the average total force is $\Delta E/\Delta R = [E(0.631) - E(1.663)]/(1.032) = -4.07960 \text{ hartree}$.

As shown by Figure 10-Vb, the molecular energy difference $\Delta E(R) = E(R) - E(1.663)$ and the components, $\Delta E_X(R) = E_X(R) - E_X(1.663)$ ($X = \text{PL, ES}$), of total electronic energy difference $\Delta E_e(R)$ can be fitted as the following polynomial functions of the distance R of N-B bond, and their correlation coefficients (CC) are greater than 0.999:

Table 10-II. For Each LG(R) Geometry, Molecular Energy $E(R)$, and Its Various Components Are Obtained from Conditional Single-Point Energy Calculation, on B3LYP/6-311G** Optimized LG Geometry, at RHF/6-311G** Level (Energy Unit in hartree).

	R(Å)							
	0.631	0.7	0.8	1.0	1.1	1.3	1.5	1.663
NH ₃ partner								
$E_{\text{ES-O}}(R)$	-88.81933	-87.86500	-86.48765	-83.34844	-81.39781	-78.76079	-77.74966	-76.88799
$E_{\text{ES-V}}(R)$	-5.37840	-4.77906	-4.13891	-4.02595	-4.58243	-5.01572	-5.13624	-4.58261
$E_{\text{PL}}(R)$	-3.89687	-3.21984	-2.20336	-0.70720	-0.48213	-0.55007	-0.68768	-0.63029
$E_{e-\text{NH}_3}(R)$	-98.09459	-95.86390	-92.82992	-88.08159	-86.46237	-84.32657	-83.57358	-82.10090
BH ₃ partner								
$E_{\text{ES-O}}(R)$	-48.67595	-47.32151	-46.17406	-44.51732	-43.87188	-42.54355	-41.68375	-40.57434
$E_{\text{ES-V}}(R)$	-13.84369	-13.86323	-13.84847	-13.46232	-12.79267	-10.66506	-7.66251	-6.97469
$E_{\text{PL}}(R)$	-2.91097	-2.34902	-1.90995	-1.13673	-0.90801	-0.40647	-0.56955	-0.43084
$E_{e-\text{BH}_3}(R)$	-65.43061	-63.53376	-61.93247	-59.11637	-57.57256	-53.61508	-49.91581	-47.97987
Complex								
$E_e(R)$	-163.52521	-159.39767	-154.76239	-147.19796	-144.03492	-137.94167	-133.48939	-130.08077
$E(R)$	-87.82377	-87.80161	-87.56640	-86.80988	-86.27488	-85.02140	-84.11637	-83.61353

$$\Delta E_{\text{PL}}(R) = -10.6473 - 17.6566R + 71.9866R^2 - 59.5992R^3 + 15.03918R^4 < 0$$

$$\Delta E_{\text{ES}}(R) = -94.1412 + 212.1981R - 248.9390R^2 + 146.6860R^3 - 32.0286R^4 < 0$$

$$\Delta E(R) = 1.1188 - 18.3750R + 18.1198R^2 - 3.3307R^3 - 0.7014R^4 < 0$$

For four specific LG(R) geometries denoted as LG(1.663), LG(1.500), LG(1.00), and LG(0.631), the values of the energy differences (hartree) are as follows:

$$\begin{aligned} \Delta E_{\text{PL}}(1.663) &= 0.0, & \Delta E_{\text{ES}}(1.663) &= 0.0 \\ \Delta E_{\text{PL}}(1.500) &= -0.1961, & \Delta E_{\text{ES}}(1.500) &= -3.21253 \\ \Delta E_{\text{PL}}(1.000) &= -0.7828, & \Delta E_{\text{ES}}(1.000) &= -16.3344 \\ \Delta E_{\text{PL}}(0.631) &= -5.74671, & \Delta E_{\text{ES}}(0.631) &= -27.69774 \end{aligned}$$

The followings are the values of the corresponding first order derivatives (hartree/Å):

$$d[\Delta E_{\text{PL}}(1.663)]/dR = 3.96334, \quad d[\Delta E_{\text{ES}}(1.663)]/dR = 12.02161$$

$$d[\Delta E_{\text{PL}}(1.500)]/dR = -0.96221, \quad d[\Delta E_{\text{ES}}(1.500)]/dR = 23.12557$$

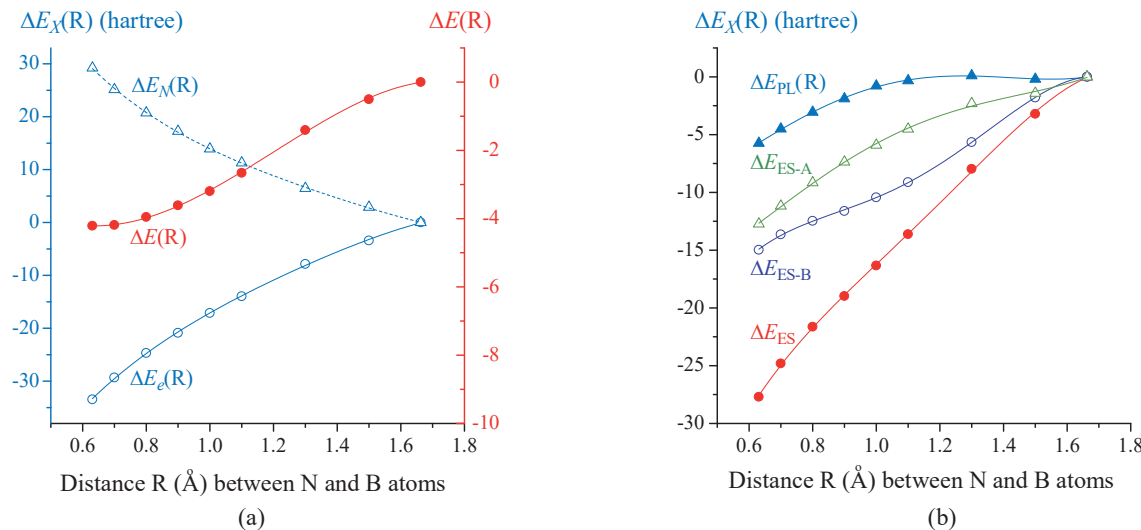


Figure 10-V. For LG(R) geometries: (a) The molecular energy differences $\Delta E(R) = [E(R) - E(1.663)]$, $\Delta E_N(R)$ and $\Delta E_e(R)$; (b) The energy component differences, $\Delta E_X(R) = E_X(R) - E_X(1.663)$ ($X = \text{ES}$, ES-A , ES-B and PL), and their changes as the N-B bond distance R increases, calculated using our 2011 method at RHF/6-311G** level. Each LG(R) geometry is conditionally optimized using our 2011 method at the B3LYP/6-311G** level.

$$\begin{aligned} d[\Delta E_{PL}(1.000)]/dR &= 7.67580, & d[\Delta E_{ES}(1.000)]/dR &= 26.26373 \\ d[\Delta E_{PL}(0.631)]/dR &= 17.11403, & d[\Delta E_{ES}(0.631)]/dR &= 41.06363 \end{aligned}$$

In the region of from $R = 1.500 \text{ \AA}$ to $R = 1.661 \text{ \AA}$, as shown by Figure 10-Vb and by the above calculated values, the electrostatic force and polarization force themselves are not large, but the ratio of $\Delta E_{ES}(1.500)$ to $\Delta E_{PL}(1.500)$ is large, about up to 15, leading to $\Delta E(R) = E(R) - E(1.663) < 0$. However, the $\Delta E_{ES}(R)$, $\Delta E_{PL}(R)$ and $\Delta E(R)$ are the monotonically increasing function of the N-B bond distance R , and $|d[\Delta E_{ES}(R)]/dR| > |d[\Delta E_{PL}(R)]/dR|$, leading to the decreasing of the N-B bond length R . When R is in the region of 1.000 to 0.631 \AA , $(d[\Delta E_{ES}(R)]/dR)/(d[\Delta E_{PL}(R)]/dR)$ is about 3. As a result, $\Delta E_{ES}(0.631)$ itself becomes large, up to -27.69774 hartree although the ratio of $\Delta E_{ES}(0.631)$ to $\Delta E_{PL}(0.631)$ drops to 5. In this region, as Morokuma indicated,³¹ the electrostatic force between two partners is attractive, and it plays a predominant role in determining the LG(R) geometry.

When the electronic interaction between the two monomers is completely eliminated, the two partners are closely hug each other face to face due to the electrostatic interaction between the two partners.

10.0.3.5. Distortion of Electron Delocalization

Before the discussion, it should be mentioned that the LG geometry is different from the LG(R) geometry. At B3LYP/6-311G** level, the LG geometry refers to the LG(0.631) geometry. The LG geometry is optimized, using our 2011 method, under the conditional settings in order to exclude the electron interaction from between two partners, but its geometric optimization is unlimited in the geometric parameters (bond lengths and bond angles).

At the B3LYP/6-311G** level, the delocalized electronic state (DLE) of the LG geometry (Figure 10-IIId) is obtained from the regular single-point energy calculation on the LG geometry, and the molecular energy difference $\Delta E = E(\text{DLE}) - E(\text{LG}) = 10.88808$ hartree, indicating that electron delocalization is strong destabilization. But the molecular energy (-78.95526 hartree) of DLE state is only 4.29511 hartree higher than that (-83.25037 hartree) of the ground state of complex (Figure 10-IIId). The energy difference $\Delta E = E(\text{DLE}) - E(\text{LG})$ are also calculated at

Table 10-III. For the Delocalized Electronic State (DLE) and Localized Electronic State of the LG Geometry, Various Energy Components (hartree) and Their Difference (hartree), $\Delta E_X = E_X(\text{DLE}) - E_X(\text{LG})$, Obtained from the Regular and Conditional Single-Point Energy Calculations, on the B3LYP/6-311G** Optimized LG Geometry, by Using Our 2011 Method at RHF/6-311G** Level.

	x	$E_X(\text{DLE})$	$E_X(\text{LG})$	ΔE_X
NH_3	$E_{\text{ES-O}}$	-98.95107	-89.70958	-9.24149
	$E_{\text{ES-V}}$	-4.01097	-4.82800	0.81703
	E_{PL}	-0.66707	-3.55572	2.88865
	E_{NH3}	-103.62912	-98.09331	-5.53581
BH_3	$E_{\text{ES-O}}$	-54.76992	-48.46146	-6.30846
	$E_{\text{ES-V}}$	-14.18709	-9.41246	-4.77463
	E_{PL}	3.00413	-6.16946	9.17359
	E_{BH3}	-65.95288	-64.04337	-1.90951
Inter-partner	$E_{\text{EX-O}}$	26.35842	0.00000	26.35842
	$E_{\text{EX-V}}$	-5.00641	0.00000	-5.00641
	$E_{\text{CT-AB}}$	-4.28927	0.00000	-4.28927
	$E_{\text{CT-BA}}$	-0.01488	0.00000	-0.01488
Whole complex	E_{ES}	-171.91905	-152.41150	-19.50755
	E_{PL}	2.33706	-9.72518	12.06224
	E_{CT}	-4.30415	0.00000	-4.30415
	E_{EX}	21.35201	0.00000	21.35201
	E_e	-152.53414	-162.13669	9.60255

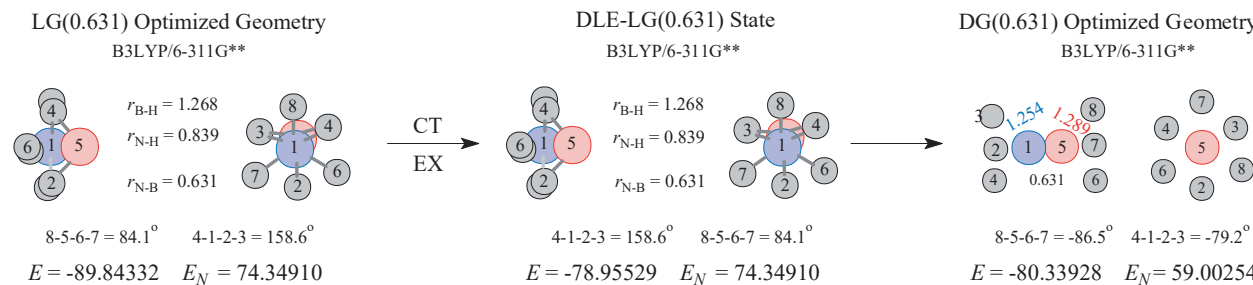
For the DLE state, E_{ES} should be E_{ESX}

(B3LYP, RHF, and MP2) levels with different basis sets, and their values (hartree) are as follows:

12.25672 (6-31G*), 10.88803 (6-311G**), 13.73671 (6311G(2d,2p)), 14.67117 (6-311G(2df,p)), 10.90603 (6-311++G**) (B3LYP)
 11.56264 (6-31G*), 9.93834 (6-311G**), 13.58886 (631G(2d)) (RHF)
 11.60785 (6-31G*), 10.09222 (6-311G**), 13.60910 (6-31G(2d)) (MP2)

All the above energy differences ΔE are strong destabilization, which is independent on the theoretical level and basis set size.

In order to understand the driving force for deforming the LG geometry to the ground state geometry, the delocalized and localized electronic states of the LG geometry are constructed by the regular and conditional single-

**Scheme 10-II**

point energy calculations, on the B3LYP/6-311G** optimized LG geometry, at RHF/6-311G** level, and their energy components are listed in Table 10-III.

At the moment of the electron delocalization (the LG geometry can be considered to remain unchanged), as indicated by the data listed in Table 10-III, the MO exchange and charge transfer interactions between two partners cause the following direct and indirect energy changes $\Delta E_X = \Delta E_X$ (DLE) . ΔE_X (LG) (X = EX, CT, PL, and ESE) (hartree):

$$\Delta E_{\text{EX}} = 21.35201, \text{ and } \Delta E_{\text{CT}} = -4.30415$$

$$\Delta E_{\text{PL}} = 12.06224, \text{ and } \Delta E_{\text{ESX}} = -19.50755$$

$$\Delta E_{\text{EX}} + \Delta E_{\text{PL}} = 33.41425 > 0 \text{ (destabilizing)}$$

$$\Delta E_{\text{CT}} + \Delta E_{\text{ESX}} = -23.81170 < 0 \text{ (stabilizing)}$$

$$\Delta E_{\text{EX}} > \Delta E_{\text{PL}}, \text{ and } \Delta E_{\text{EX}} > |\Delta E_{\text{CT}}|$$

The sum of two destabilizing energy effects ΔE_{EX} and ΔE_{PL} is large enough to overcome the sum of two stabilization energy effects ΔE_{ESX} and ΔE_{CT} . As a result of electron delocalization, total energy effect $\Delta E_e = \Delta E = 9.60255$ hartree, and it is destabilizing. In particular, $\Delta E_{\text{EX}} > \Delta E_{\text{PL}}$ and $\Delta E_{\text{EX}} > |\Delta E_{\text{CT}}|$. The destabilizing ΔE_{EX} is a starting driving force for deforming the LG geometry ($R = 0.631 \text{ \AA}$) into the ground state geometry ($R = 1.663 \text{ \AA}$).

10.0.3.6. Charge Transfer and Exchange Interactions

In order to understand the distortive nature of electron delocalization, a series of the delocalized geometry (DG) with the specified N-B bond distance, denoted as DG(R), is optimized under the following conditional settings: for each DG(R) geometry of NH_3BH_3 complex, the N-B bond length is set equal to a specified value, and it remains unchanged during the geometry optimization. In each DG(R) geometry, electrons are delocalized on the whole complex.

For the LG(0.631) geometry of NH_3BH_3 complex, at the instant of the electron delocalization, as indicated by $\Delta E_e = \Delta E = E_e(\text{DLE}) - E_e(\text{LG})$ (9.60255 hartree) in Table 10-III, the electron interaction between two partners strongly destabilizes the DLE state of LG(0.631). As a result, as shown by Scheme 10-II, the configurations of the two partners in the LG(0.631) geometry is inverted into the configuration of the DG(0.631) geometry to reduce the nuclear repulsion between two partners, and meanwhile the N-H and B-H bonds are lengthened from $r_{\text{N-H}} = 0.839 \text{ \AA}$ and $r_{\text{B-H}} = 1.268 \text{ \AA}$ in the LG(0.631) geometry into $r_{\text{N-H}} = 1.254 \text{ \AA}$ and $r_{\text{B-H}} = 1.289 \text{ \AA}$ in the DG(0.631) geometry.

From the beginning of the DG(0.631) geometry, as shown by Scheme 10-II and Figure 10-VI, the a series of DG(R) geometries has the following characteristics:

- (i) A back-to-back configuration.
- (ii) Staggered conformation;

Delocalized geometry, DG(R), with specified N-B bond distance Å

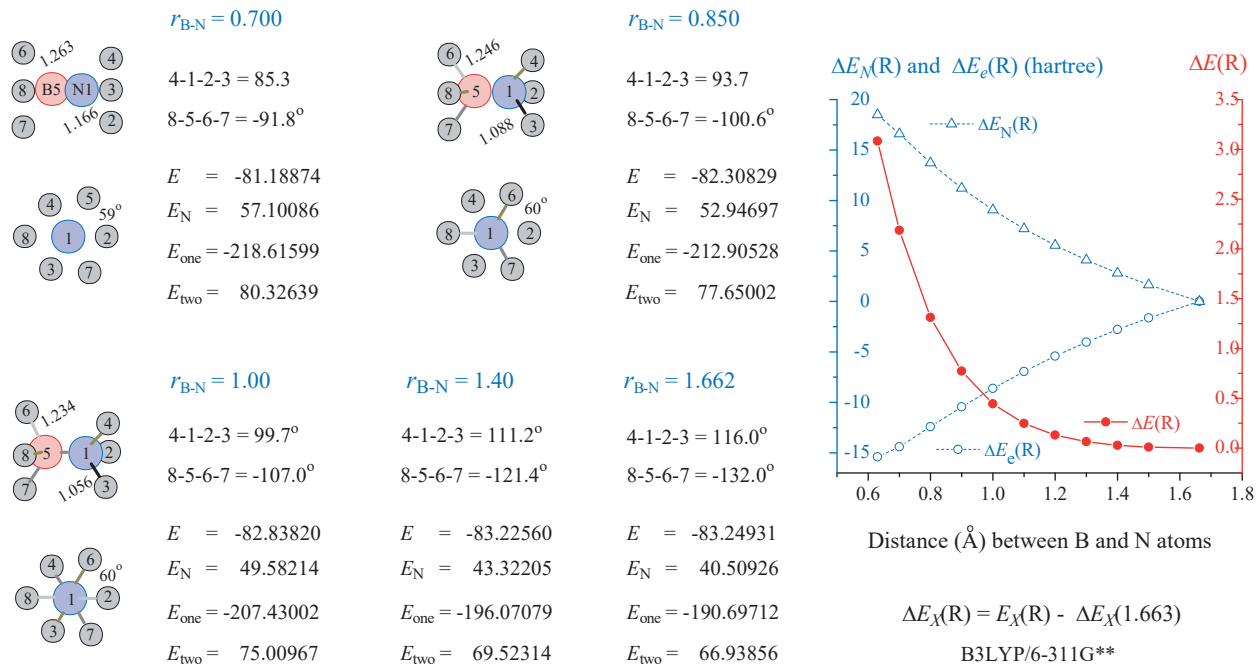


Figure 10-VI. For the DG(R) geometries optimized at B3LYP/6-311G** level, the energy differences (hartree), in the molecular energy, total electron energy and nuclear repulsion, $\Delta E_X(\text{R}) = E_X(\text{R}) - E_X(1.663)$ ($X = e, N$), obtained from the single-point energy calculations at the RHF/6-311G** level.

(iii) Dihedral angles, 4-1-2-3 and 8-5-6-7, are getting larger as the distance of N-B bond increases.

For a pair of DG(R) and LG(R) having the same distance R of N-B bond, as shown by the energy differences between these two geometries, it is the CT and EX interactions between the two partners to cause electrostatic energy and polarization energy change. The exchange and charge transfer energy effects, $\Delta E_{\text{EX}}(\text{R}) = [E_{\text{EX}}(\text{DG}(\text{R})) - E_{\text{EX}}(\text{LG}(\text{R}))]$ and $\Delta E_{\text{CT}}(\text{R}) = [E_{\text{CT}}(\text{DG}(\text{R})) - E_{\text{CT}}(\text{LG}(\text{R}))]$, are called active energy effects. The electrostatic and polarization energy differences, $\Delta E_{\text{ESX}}(\text{R}) = [E_{\text{ESX}}(\text{DG}(\text{R})) - E_{\text{ESX}}(\text{LG}(\text{R}))]$ and $\Delta E_{\text{PL}}(\text{R}) = [E_{\text{PL}}(\text{DG}(\text{R})) - E_{\text{PL}}(\text{LG}(\text{R}))]$, are called the passive energy effects, and they resulted from the influences of the intermolecular (CT and EX) interactions on the electronic energies of the partners themselves, where, for example, $E_{\text{ESX}}(\text{DG}(\text{R}))$ is the ESX energy components of the total electronic energy for the DG(R) geometry. Based on the data listed in Table 10-II and Table 10-IV, however, it is the two passive energy effects, $\Delta E_{\text{ESX}}(\text{R})$ and $\Delta E_{\text{PL}}(\text{R})$, to play a predominate role in determining that the total energy effect, $\Delta E_e(\text{R}) = [E_e(\text{DG}(\text{R})) - E_e(\text{LG}(\text{R}))]$, is destabilizing. For the DG(1.0) geometry, for example, the energy differences (hartree) are as follows:

$$\Delta E_{\text{ESX}}(1.0) + \Delta E_{\text{PL}}(1.0) = 8.90455 + 1.99543 = 10.89998$$

$$\Delta E_{\text{CT}}(1.0) + \Delta E_{\text{EX}}(1.0) = -4.38504 + 8.90163 = 4.51659$$

$$\Delta E_e(1.0) = \Delta E_{\text{CT}}(1.0) + \Delta E_{\text{EX}}(1.0) + \Delta E_{\text{ESX}}(1.0) + \Delta E_{\text{PL}}(1.0) = 15.41657$$

$$\Delta E_N(1.0) = -10.80588$$

Although total inter- and intra-molecular energy effects are destabilizing and although $\Delta E_{\text{CT}}(1.0) + \Delta E_{\text{EX}}(1.0) <$

Table 10-IV. For Each of the B3LYP/6-311G optimized DG(R) Geometries, Molecular Energy (hartree) and Its Various Components (hartree), Obtained from the Singe-point Energy Calculations at RHF/6-311G** Level.

N-B (Å)	E_{ESX}	$E_{\text{ESX-A}}$	$E_{\text{ESX-B}}$	E_{PL}	E_{EX}	E_{CT}	E_{N}	E_e	E
0.630	-150.43687	-86.22550	-64.21137	1.85943	12.19684	-2.18074	59.00071	-138.56134	-79.56063
0.700	-145.19405	-85.12460	-60.06945	1.33956	10.85503	-4.56796	57.11087	-137.56741	-80.45654
0.800	-142.20046	-86.76048	-55.43998	0.65055	12.73550	-6.75175	54.23423	-135.56616	-81.33193
0.900	-141.05564	-87.73682	-53.31882	0.18398	12.27946	-5.01535	51.73662	-133.60755	-81.87093
1.000	-136.44948	-85.30539	-51.14409	0.15150	8.90163	-4.38504	49.58250	-131.78142	-82.19892
1.100	-131.90463	-82.44381	-49.46082	0.20787	5.87945	-4.28925	47.71042	-130.10655	-82.39613
1.200	-128.70032	-80.37119	-48.32913	0.21589	3.99886	-4.09301	46.06582	-128.57857	-82.51275
1.300	-126.53346	-79.07896	-47.45450	0.18390	2.95531	-3.79826	44.61274	-127.19253	-82.57979
1.400	-125.00394	-78.34469	-46.65925	0.13831	2.37185	-3.43977	43.31708	-125.93354	-82.61646
1.500	-123.87194	-77.95942	-45.91252	0.09555	2.00102	-3.01835	42.15901	-124.79373	-82.63472
1.663	-122.48915	-77.65953	-44.82962	0.04594	1.55176	-2.26081	40.50886	-123.15226	-82.64340

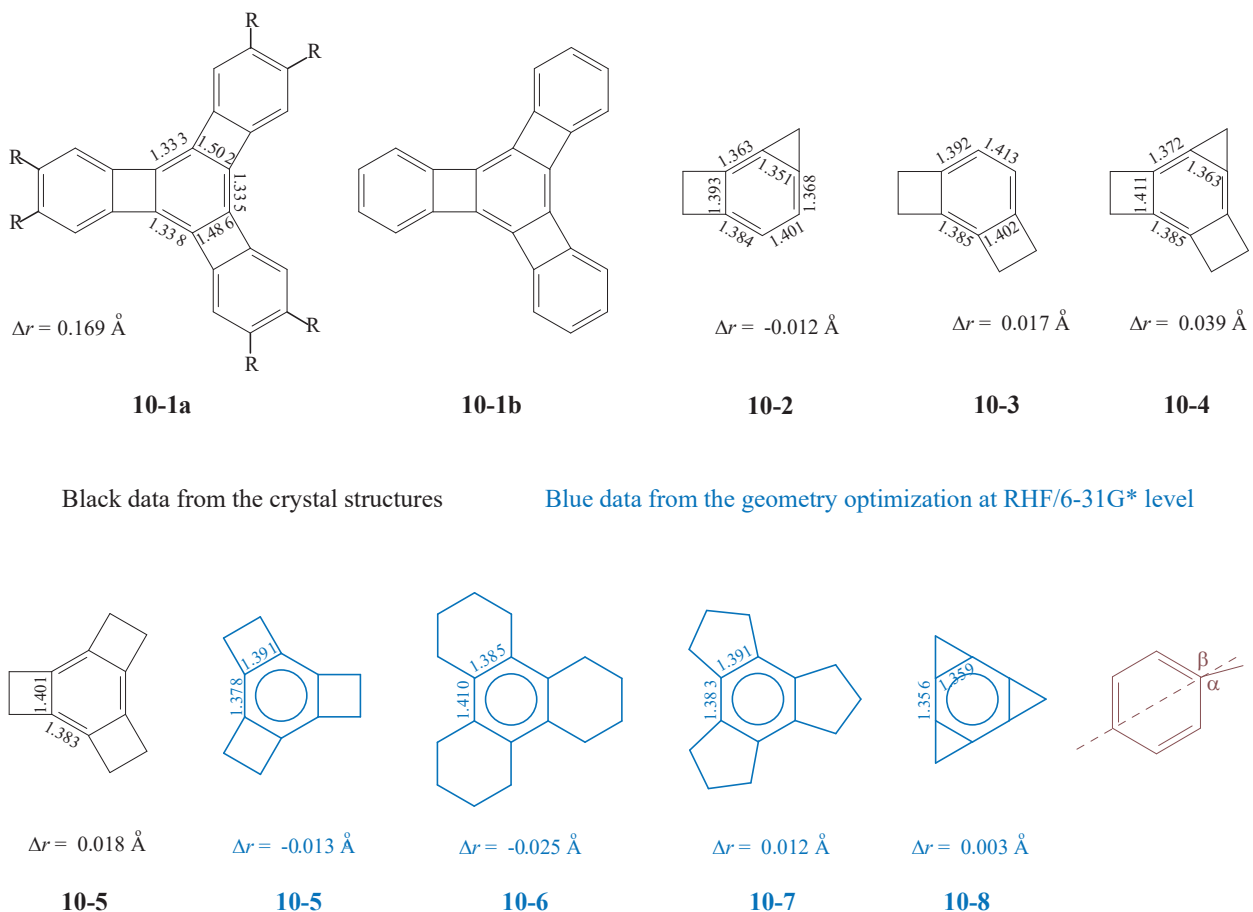
$\Delta E_{\text{ESX}}(1.0) + \Delta E_{\text{PL}}(1.0)$, the CT and EX interactions are the driving force of the electron delocalization, and they play the active role in determining the destabilization of electron delocalization. Any structural factor that is conducive to CT interaction will help stabilize the CT complex. For each DG(R) geometry, the configurations of two partners have been inverted due to the electron delocalization (Figure 10-VI), certainly leading to the decrease of the nuclear repulsion energy, $\Delta E_{\text{N}}(\text{R}) = [E_{\text{N}}(\text{DG}(\text{R})) - E_{\text{N}}(\text{LG}(\text{R}))] < 0$. But, as shown by the data listed in Table 10-II and Table 10-IV, the molecular energy difference, $\Delta E(\text{R}) = \Delta E_{\text{N}}(\text{R}) + \Delta E_e(\text{R})$, is still destabilizing due to $\Delta E_e(\text{R}) > |\Delta E_{\text{N}}(\text{R})|$, and it is getting less destabilizing as the N-B bond distance R increases.

10.0.3.7. Total Energy Effect

Figure 10-VI shows that, for a series of DG geometries, the nuclear repulsion difference, $\Delta E_{\text{N}}(\text{R}) = E_{\text{N}}(\text{R}) - E_{\text{N}}(1.663) > 0$, between the DG(R) and DG(0.630) geometries is a driving force for lengthening the N-B bond, which should be attributed to the destabilizing effect of electron delocalization.

As shown by the thermodynamic mechanisms of reaction $\text{NH}_3 + \text{BH}_3 = \text{NH}_3\text{BH}_3$ (Figure 10-III) (starting from two free molecules NH_3 and BH_3 , through the localized geometry (LG) without the electron interaction between two partners, to the ground state of the complex), due to assuming that there is no electron delocalization between two partners, a stabilizing electrostatic interaction is sufficient to overcome the nuclear repulsion between the two partners, leading to the formation of the localized geometry (LG) in which two partners are hugged tightly together face to face and the N-B bond distance $r_{\text{N-B}} = 0.631 \text{ \AA}$. However, owing to the destabilizing electron delocalization between the two Partners, the total electron energy of the DLE state of LG geometry becomes no longer sufficient to overcome the nuclear repulsion between two partners, eventually leading to the formation of the complex NH_3BH_3 ($r_{\text{N-B}} = 1.663 \text{ \AA}$). At last, the molecular energy difference, $\Delta E = E(\text{G}) - [E(\text{NH}_3) - E(\text{BH}_3)]$, between the complex and the two free molecules (NH_3 and BH_3) is -29.3 kcal/mol. The complexation reaction is exothermic.

10.1. INTRODUCTION



Scheme 10-1

Strained aromatic molecules are a type of molecule in which one to three small rings (three- to five-membered rings) are fused to the central benzene ring (Scheme 10-1). In this chapter, such type of molecules will be successfully used to confirm our viewpoint that π -delocalization is destabilization and is a driving force for bond length alternation in central ring.

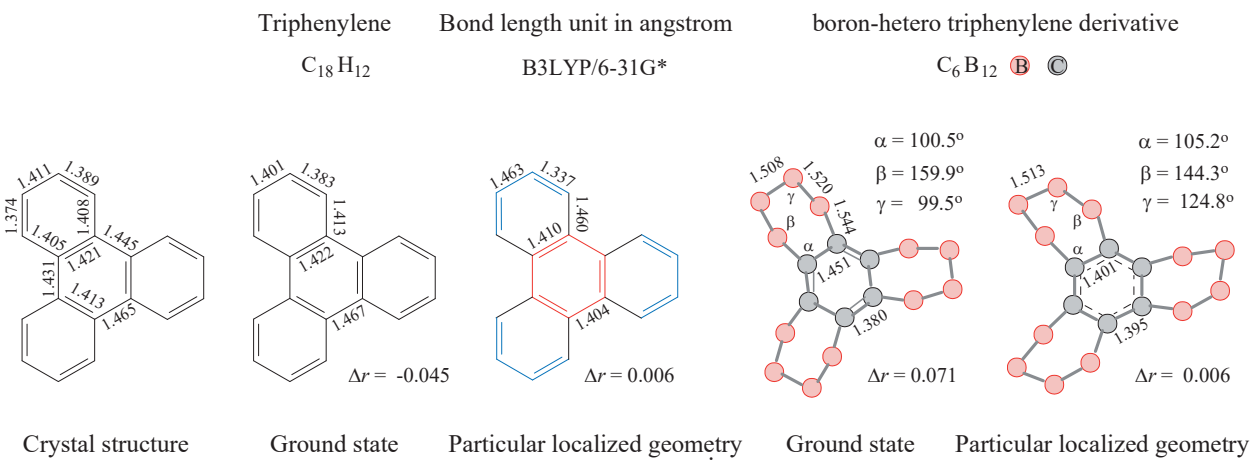
In this type of molecules, a significant bond length alternation is found. The geometrical feature that $r_{\text{endo}} (\text{endocyclic bond length}) > r_{\text{exo}} (\text{exocyclic bond length})$ was proposed, as a theoretical inference, by Mills-Nixon in 1930,³⁷ and it was attributed to bond angle $\alpha <$ bond angle β (the last brown structure in Scheme 10-1). Such a structural effect causing $r_{\text{endo}} > r_{\text{exo}}$ was called Mills-Nixon effect or Mills-Nixon proposal.³⁸

In the literature, whether there is Mills-Nixon effect and which structure effect causes the bond length alternation are the center of controversy, and various theoretical and experimental methods have been (or are being) proposed. However, it seems that these arguments have not reached a consensus so far.

In this Chapter, therefore, the two points will be discussed and emphasized:

- (i) What structural factor causes bond length alternation?.
- (ii) What structural factors determine $r_{\text{endo}} > r_{\text{exo}}?$

In other words, the bond length alternation and the Mills-Nixon effect ($r_{\text{endo}} > r_{\text{exo}}$) are two different concepts, and the bond length alternation does not mean $r_{\text{endo}} > r_{\text{exo}}$ always.



Scheme 10-2

Our 2007 method of restrictedly optimizing geometry was reported in 2007. Based on the calculation results obtained from our 2007 method, as we emphasized,⁷ in strained aromatic molecules, it is π -electron delocalization, rather than the angle strain, to cause the bond length alternation.

In fact, in the conjugated molecules, single and double bond alternation is a common phenomenon. For polycyclic benzenoid hydrocarbon,³⁹ benzenoid rings always have alternating single and double bonds, no matter whether the ring is the center benzenoid ring or the annulated benzene ring. At the ground states of triphenylene and its boron hetero-derivative, for example, the central benzenoid ring have alternating shorter and longer bonds, and their $\Delta r = (r_{\text{endo}} - r_{\text{exo}})$ are -0.045 \AA and 0.071 \AA , respectively (Scheme 10-2).

The crystal structure data of a large number of substituted benzene derivatives have shown that any substituent can cause deformation of benzene ring. In the ortho-disubstituted benzene such as o-dichloro-benzene and 1-nitro-2-chloro-benzene, the bond lengths of benzene ring are always alternating, and the CC bond with the two substituents is the longest, which looks like Mills-Nixon effect. Therefore, the three phenomena, the bond length alternation, the Mills-Nixon effect ($r_{\text{endo}} > r_{\text{exo}}$), and the deformation of benzene ring, are not the unique phenomena that occurs only in strained-aromatic molecules.

In this Chapter, our 2011 method will be used to confirm the conclusion obtained from our 2007 method,⁷ and it will be indicated that in the particular localized geometry, as the secondary structure effects, the strain effect as well as the aromaticity and antiaromaticity of the small rings fused to the central benzenoid ring (hereafter, the phrase "the small rings fused to the central benzenoid ring" will be shortened into "annulated small ring") can only determine which bond, endocyclic bond or exocyclic bond, is longer. In the particular localized geometries of triphenylene and its boron hetero-derivative, for example, the π -MO charge transfer and exchange interactions and spatial π -exchange interaction have been artificially excluded from between the central ring and the annulated benzenoid rings. In this case, as shown by Scheme 10-2, the bond length differences Δr decreases to 0.006 \AA , and the CC bond lengths in the central ring can be considered equal to each other. In benzotricyclobutadiene ($C_{12}H_6$), when the outer peripheral CC double bond of each annulated ring (four-membered ring) is replaced by $B=B$ bond, the resulted molecule (C_6B_6) is called the boron hetero-benzotricyclobutadiene. In this molecule, the angle strain should arise from the sp hybridization of the boron atom, not from the sp^2 hybridization of the carbon atom in central benzene ring, that is, it should be due to the angle C-B-B (about 90°) $\ll 180^\circ$, not due to the angle C-C-B $< 120^\circ$. In this case, the angle strain is no longer the angle strain in the Mills-Nixon sense.

Before the discussion, the phrases, such as "bond localization", should be precisely defined in order to avoid confusion of the basic concepts. In the Kekulé structures (resonance structure) of benzene, for example, the CC bonds alternate between single and double bonds, and the π -electrons are absolutely localized on their respective

double bonds, that is, there is no resonance between the double bonds.⁴⁰ In the literatures related to strained-aromatic molecules, "bond length alternation" is often called "bond localization", and a geometry with alternating bond lengths is called "localized geometry". It should be emphasized that the "bond localization" induced by strain is conceptually different to the "bond localization" used in our works. In the localized geometry obtained from our 2011 method, π -electrons and π -MOs are absolutely localized on their respective groups (or double bonds). Only in this case, the double bond is really localized, and the electronic interaction are artificially excluded from between the localized double bonds. For the ground state of a strained-aromatic molecule, the π -MOs and π -electrons are still delocalized on the whole molecular framework although the bond lengths in central ring are alternating. The "bond localization" should be used with caution. In the phrase "strain-induced bond localization", a reasonable alternative for "bond localization" should be "bond-fixed" (or "fixed-position bond")⁴¹ and "bond fixation"⁴².

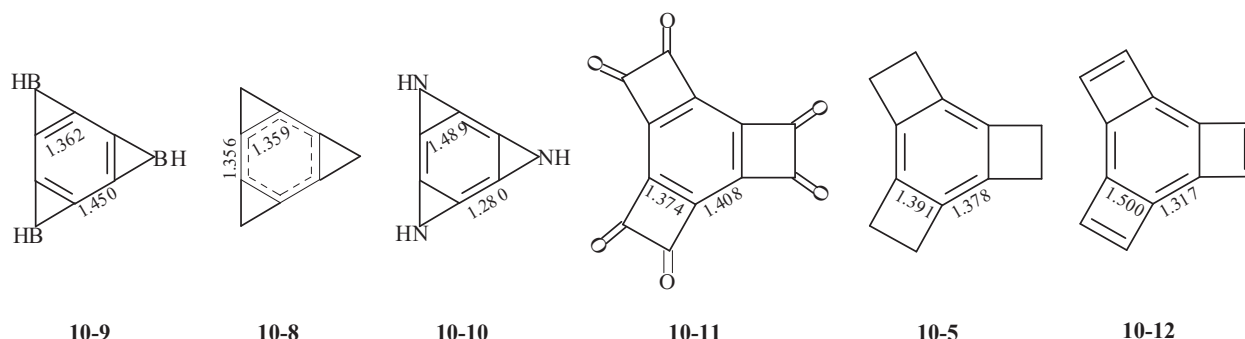
10.1.1. Mills-Nixon Effect.

Over decades, chemists attributed the bond length alternation in various types of benzenoid structures to the Mills-Nixon effect. In the Mills-Nixon era, the view that the structure of benzene acts as a resonance hybrid or tautomeric equilibrium remained controversial⁴³ and the distribution of the carbon valences in benzene were considered to be tetrahedral³⁷ although these arguments and the tetrahedral distribution are now considered ridiculous. Originally, as reviewed by Siegel in 1994,⁴³ Mills-Nixon intended to test for the concept of "rapidly equilibrating Kekulé forms" via pursuing regioselective reactivity of hydroxyindan and tetralin, based on his proposal on the incorrect Kekulé oscillation model of benzene.³⁷ So the Mills-Nixon effect was also known as the directive effect of annulated small rings.⁴⁴ Since then, many experiments and computations were done to investigate the realness of Mills-Nixon effect. However, they often gave the different conclusions.⁴⁵⁻⁵¹

Mills-Nixon effect has become increasingly important, and it was called Mills-Nixon distortion,^{52,53} since Shaik et al. claimed that the π system of benzene prefers a distorted D_{3h} geometry.^{1,54,55} The debate about the Mills-Nixon effect has entered into a new historical stage. Now, the core of the debate becomes which structural effect causes bond length alternation, π - π interaction or angle strain (cyclic strain), and the Mills-Nixon effect itself is no longer so important. In fact, this debate is also the core of my monograph, running through the monograph.

10.1.1.1. Controversy about Mills-Nixon Effect

Before discussing our point of view, it is necessary to briefly review the debate about the Mill-Nixon effect. In 1930, 2-hydroxy-tetrahydronaphthalene and 5-hydroxy-hydridene were used to investigate the regioselectivity of the substitution reaction by Mills-Nixon.³⁷ In each of these two compounds, the outer perimeter, $-(CH_2)_4-$ or $-(CH_2)_3-$, of a ring fused to benzene is composed of the saturated carbon atoms, and the benzene ring was predicted to be cyclohexatriene-like. However, as indicated by Siegel in 1995,⁵⁶ the expectation of Mills-Nixon was based on false assumptions, and the interpretation of the bond length alternation in benzenoid was not supported by the experimental structural proofs. Indeed, as shown by the crystal structural data of the molecules **10-2**, **10-3** and **10-5** (Scheme 10-1),⁵⁷ the considerable bond length alternation in benzene ring is not experimentally recognized. The theoretical conclusion, based on the RHF/6-31G* geometry optimizations of the molecules **10-5** to **10-8** (Scheme 10-1),^{52,53} is similar to the experimental one. Siegel concluded that the significant bond length alternation is not found in these molecules, according to the following endo/exo pairs: 1.391/1.378 (**10-5**), 1.385/1.410 (**10-6**), 1.391/1.383 (**10-7**), 1.359/1.356 (**10-8**). Hence, no significant Mills-Nixon distortion exists in these compounds. But it is worth noting that, in these molecules, the carbon atoms in the annulated small rings are saturated. When the outer perimeter of an annulated small ring is composed of the unsaturated atoms (or heteroatoms), as shown by Scheme 10-3, the bond length alternation is obvious. In this case, the position of the single and double bonds seems to depend upon the number of π -electrons in the annulated small ring, and molecules **10-8** and **10-5** are the useful



Scheme 10-3

reference structure to probe the role of cyclic π effect (aromatic and anti-aromatic) in determining bond length alternation. In molecules **10-10** and **10-12**, the number of π -electrons in their corresponding small rings is 4 if the π -electrons in central ring are evenly delocalized on the benzene ring. Accordingly, as shown by the following endo/exon pairs:^{52,53} 1.489/1.280 (**10-10**) and 1.500/1.317 (**10-12**), the endocyclic bonds had to be longer than exocyclic bonds in order to avoid anti-aromatic destabilization. In molecules **10-9** and **10-11**, if the bond order of endocyclic bonds is greater than that of exocyclic bonds, the small rings are aromatic. In these two molecules, the endocyclic bonds are shorter than the exocyclic bonds according to the following endo/exon pairs:

$$1.362/1.450 (\Delta r = -0.088 \text{ \AA}) \text{ and } 1.324/1.408 (\Delta r = -0.084 \text{ \AA})$$

In the area of Mills-Nixon distortion, a milestone was the synthesis and structural characterization of tris(benzocyclobutadieno)benzene nucleus⁴¹ (**10-1**, Scheme 10-1). In the crystal structure of molecule **10-1**,⁴¹ the central ring is a bond-fixed cyclohexatriene ring, which was ascribed to the extremely strained character of the system. Vollhardt's works, together with Shaik's new point of view, revived the field of bond-fixed aromatic systems (strained-aromatic molecules).

In addition, there are two other ways to explain the bond length alternation: the first other way is the bond localization induced by σ -strain,^{58,59} and the second one, a combination of π and σ effects, was suggested and developed by Shaik.^{1,60,61}

10.1.1.2. Interpretations for Bond Length Alteration

Therefore, during the debate about the Mills-Nixon effect, there are two main points about the origin of bond length alternation: angle strain, and aromaticity-antiaromaticity of annulated small ring.

In order to verify the effect of angle strain, one of the methods is to optimize benzene while keeping CCH angles unchanged. In the work of Stranger,⁵⁹ the optimizations were performed at the RHF/6-31G* and MP2/3-21G levels. In this section, we performed the optimization again at the B3LYP level of theory. According to the calculation results listed in Table 10-1, the angle strain alone is sufficient to induce bond length alternation. For the $\alpha = 90^\circ$ geometry at B3LYP/6-311G(2df,p) level, for example, the bond lengths $r_1 = 1.341 \text{ \AA}$ and $r_2 = 1.522 \text{ \AA}$, and they are almost equal to the distances (1.33 \AA and 1.54 \AA) of the standard $\text{sp}^2\text{-sp}^2$ double and $\text{sp}^3\text{-sp}^3$ single bonds.

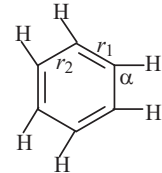
The position-fixed of the double bonds in bent benzene is the most powerful theoretical evidence for strain-induced bond fixation (strain-induced bond localization). Although the NBO and Mulliken population calculations can be used to analyze the reason of the bond length alternation induced by such pure σ -strain, this is not a concern in this section.

There are some facts that can't be explained by the above-mentioned studies. For molecules **10-13** and **10-14**

Table 10-1. The CC Bond Lengths, r_1 and r_2 (\AA), of Bent Benzene. The Geometries of Bent Benzene Are Optimized While Keeping the CCH Angles Unchanged.

α°		r_1	r_2
B3LYP			
90.0	B3LYP/6-31G*	1.348	1.528
90.0	B3LYP/6-311G(2d,2p)	1.342	1.524
90.0	B3LYP/6-311G(2df,p)	1.341	1.522
90.0	RHF/6-31G*	1.329	1.529
90.0	MP3-21G	1.346	1.579
100.0	B3LYP/6-31G*	1.369	1.451
110.0	B3LYP/6-31G*	1.383	1.416
120.0	B3LYP/6-31G*	1.397	1.397

The RHF and MP2 calculations were performed by Stanger in 1991

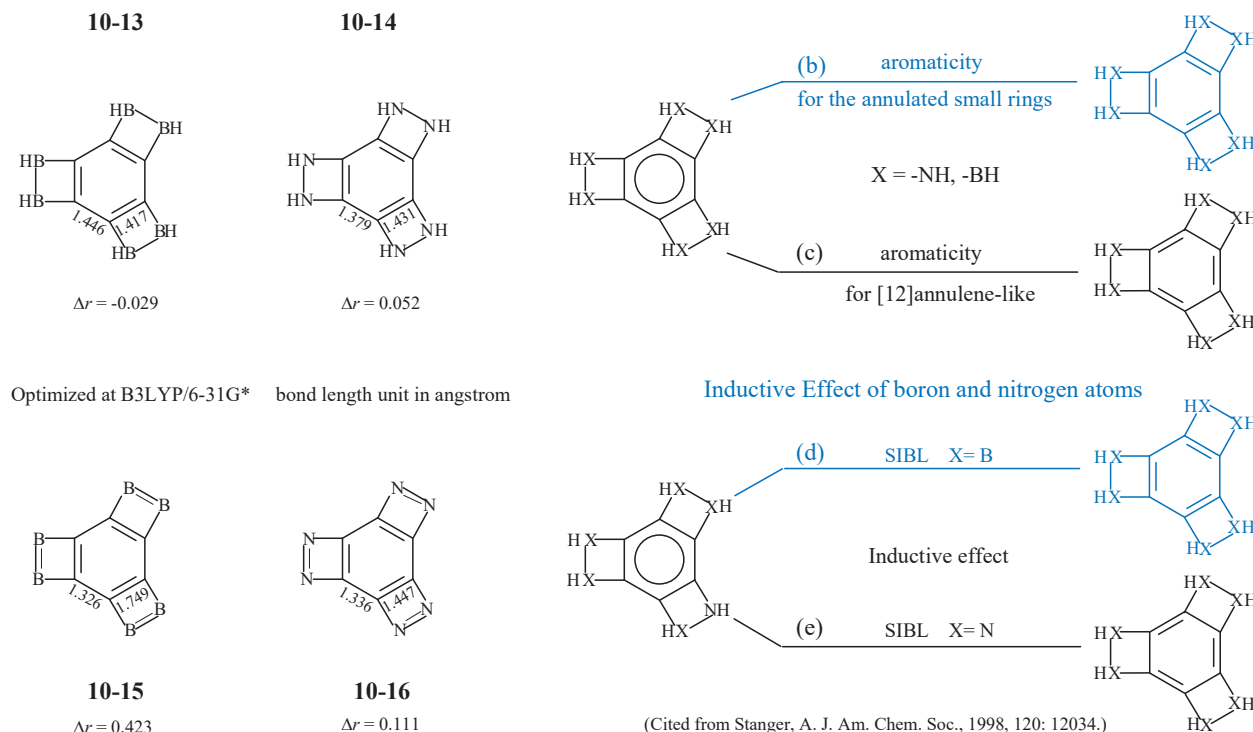


(Scheme 10-4), for example, the small rings are aromatic according to $(4n+2)$ rule, and their bond length difference $\Delta r = (r_{\text{endo}} - r_{\text{exo}})$ should be negative. In fact, as shown by Scheme 10-4,⁵⁸ $\Delta r = (r_{\text{endo}} - r_{\text{exo}}) = 0.052 > 0$ (**10-14**), and $\Delta r = -0.029 < 0$ (**10-13**). In addition, the π systems of molecule **10-15** and **10-16** are isoelectronic, and their small rings all are anti-aromatic. But Δr (0.423 \AA) for molecule **10-15** is greater than that (0.111 \AA) for molecule **10-16**, and the ratio $\Delta r(\mathbf{10-15})/\Delta r(\mathbf{10-16}) \approx 4$.⁵⁸

For the boron- and aza-hetero-tricyclobutabenzenes derivatives, as shown by Scheme 10-4b and Scheme 10-4c, there are the following two ways to count the number of π -electrons: within a small ring, and around the perimeter which looks like triply bridged [12]annulene. In the case of molecule **10-13**, for example, the small rings are aromatic if endocyclic bonds are shorter than the exocyclic bonds (Scheme 10-4b); if the aromaticity of the perimeter is predominant over that of the small rings, the endocyclic bonds should be longer than the exocyclic bonds (Scheme 10-4c).

In 1985, Cremer reported that the heteroatoms building the small ring can influence the curvature of bond via the inductive effect.⁶² The curvature of endocyclic bonds in molecule **10-13** should be larger than that of molecule **10-5** due to the electropositivity of boron atoms, and the curvature of endocyclic bonds in molecule **10-14** should be less than that of molecule **10-5** because nitrogen atom is electronegative. The theoretical results that the bond length difference $\Delta r < 0$ (**10-13**) and $\Delta r > 0$ (**10-14**) seem to mean that the synergy between the inductive effect and the aromatic stabilizing effect determines the geometry of central benzene ring.⁵⁸ For molecule **10-13**, the inductive effect of boron atoms and the aromatic stabilizing effect are consistent, leading to its $\Delta r < 0$ (Scheme 10-4b and Scheme 10-4d). For molecule **10-14**, the inductive effect of nitrogen atoms and the aromatic stabilizing effect of [12]annulene-like is synergistic, resulting in $\Delta r > 0$ (Scheme 10-4c and Scheme 10-4e).

However, as will be argued in the following related sections, first of all, the difference in Δr between molecules **10-15** and **10-16** and between **10-13** and **10-14** should be attributed to π -interaction between the central ring and the X-X (or X=X) bonds in small rings. When the π -interaction is eliminated, as in their particular localized geometries, the CC bonds in the central ring of molecule **10-13** and **10-14** become equalized. Second, it will be found that the great difference in Δr between molecules **10-15** and **10-16** is due to the hybridization differences between the

**Scheme 10-4**

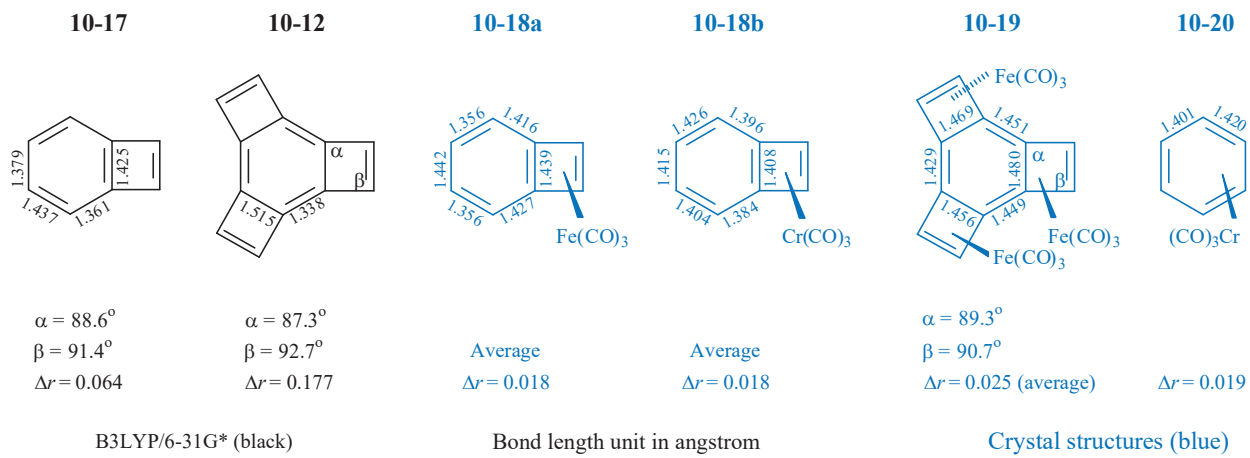
boron and nitrogen atoms. The hybridization difference causes the great difference, in the angle strain ($\angle CXX$, X = B, N), between molecules **10-15** and **10-16**.

10.1.2. Experimental Probe for π -Interaction Role

For strained-aromatic molecules, as described in the above sections, the geometrical structure of central benzene ring is determined mainly by the following three structural factors:

- (i) Aromatic and antiaromatic effect.
- (ii) Inductive effect.
- (iii) Angle strain.

Aromatic and antiaromatic effects involve the π interaction between the central ring and the conjugated group in annulated small ring. To distinguish between these three structural effects, metal complexes **10-18**,⁶³ **10-19**,⁶⁴ and **10-20**⁶⁵ were synthesized, and their crystal structures were determined (Scheme 10-5). In the metal complex, the π -electron density is considered shifting from the ligand to the metal. As the results, the π bonds in ligand are weakened, and the σ system is perturbed only to a small degree.⁶⁴ This type of complexes can be used as a probe to compare the importance of the π and σ systems. The B3LYP/6-31G* optimizations show that the bond lengths in the central benzene ring of molecules **10-12** (Scheme 10-3) and **10-17** (Scheme 10-5) are alternating and the bond length difference, $\Delta r = r_{\text{endo}} - r_{\text{exo}}$, increases from 0.064 Å for molecule **10-17** to 0.177 Å for molecule **10-12** as the number of the annulated small rings increases. In the central ring of the metal complexes **10-18**, as shown by the crystal structure (Scheme 10-5), the bond length difference Δr decreases from 0.064 Å for its free ligand



Scheme 10-5

to 0.018 Å (average value) for the complexes **10-18a** and **10-18b**. And for the central ring of complex **10-19**, the difference Δr decreases greatly from 0.177 Å for its free ligand to 0.025 Å. The difference ($\Delta r(\text{complex}) - \Delta r(\text{ligand})$) (0.152 Å) between the metal complex **10-19** and its free ligand is 3.2 times as large as that (0.047 Å) between the complex **10-18** and its free ligand. The crystal structure of metal complexes, together with the crystal structures of molecules **10-2** to **10-5**, seem to show a fact that the π -interaction between the central ring and the C=C bonds in the small ring plays an important role in causing bond length alternation.

Based on the comparison of the crystal structures of molecules **10-18** and **10-19**, the bond lengths in the central ring become longer as the number of $\text{Fe}(\text{CO})_3$ fragments increases. In the central ring of molecule **10-19**, for example, the bond length is long, up to 1.480 Å. It is almost equal to the distance of CC $\text{sp}^2\text{-sp}^2$ single bond. Accordingly, the metal complex can't ensure that π -electrons are regiospecifically withdrawn from the C=C bonds in the small rings. The design of the experiment is commendable, but the experimental results are not enough to prove that π -interaction is a driving force of bond length alternation.

10.2. ELIMINATING π -INTERACTION

In order to theoretically understand the role of π -interaction between the central ring (fragment A) and the C=C bonds or conjugated groups of annulated small ring (fragment B), it is necessary to construct a particular localized geometry (PLG). In the PLG of benzotricyclobutadiene, for example, the π -MO CT and EX interactions and spatial π interaction have been excluded from between two fragment A and B.

10.2.1. Construction of PLG

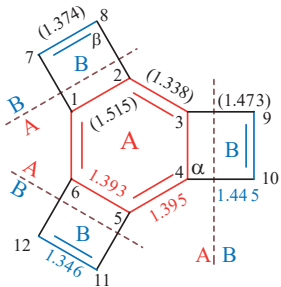
In order to construct a particular localized geometry, as an example, benzotricyclobutadiene (**10-12**) is dissected into two fragments A (red central ring) and B (composed of three blue C=C bonds belonging to their respective annulated small rings) (Figure 10-1a), and then the molecular geometry is optimized under the following conditional settings (Figure 10-1b):

- (i) Setting the Fock and overlap integral matrix elements $f_{\lambda,p} = 0.0$ and $s_{\lambda,p} = 0.0$ when AOs $\phi_\lambda \in$ fragment A,

10-12

When

Settings



$$E(\text{PLG}) = -460.73730 \text{ hartree} \quad (E(\text{G}) = -460.63040 \text{ hartree})$$

(a)

- $\pi \text{ AO } \phi_\lambda \in \text{fragment A}$
 $\pi \text{ AO } \phi_\mu \in \text{fragment A}$
 $\Delta r = -0.002$
 $(\Delta r = 0.177)$

Matrix elements
 $f_{\lambda\rho} = 0, \quad s_{\lambda\rho} = 0$
Hartree-Fock exchanges integrals
 $\langle \lambda\rho | \mu\omega \rangle = 0$

B3LYP/6-31G*

(b)

- $\pi \text{ AO } \phi_\rho \in \text{fragment B}$
 $\pi \text{ AO } \phi_\omega \in \text{fragment B}$

Figure 10-1. For benzotricyclobutadiene, the construction of the particular localized geometry (PLG) at B3LYP/6-31G* level. (a) The way to dissect the molecule into two fragments A (red color) and B (blue color), and bond lengths (\AA) and bond angles α and β in the PLG geometry. (b) Conditional settings for restrictedly optimizing PLG. The data in parentheses are the bond lengths (\AA) and bond angles in the ground state geometry. The black lines between the red and blue fragments mean that all the π MO orbital interactions, as well as the spatial electron interaction, between the fragments A and B have been set equal to zero.

and AO $s \phi_\rho \in$ the fragment B

- (ii) Setting two-electron exchange integrals $\langle \lambda\rho | \mu\omega \rangle = 0.0$ when AO $s \phi_\lambda$ and $\phi_\mu \in$ the fragment A, and AO $s \phi_\rho$ and $\phi_\omega \in$ the fragment B

For the PLG, as shown by the practical calculation, all π -MOs are, absolutely, localized on their respective fragments A and B. For example, the 31-th MO, $\Psi_{31} = \sum a_{\rho,31} \phi_\rho$, is a π -MO, and its AO coefficients $a_{\rho,31} = 0.0$ when the π AO $s \phi_\rho \in$ the fragment B, indicating that the Ψ_{31} is absolutely localized on the central benzene ring. On the other hand, the 35-th MO, $\Psi_{35} = \sum a_{\rho,35} \phi_\rho$, is absolutely localized on fragment B according to that the AO coefficient $a_{\rho,35} = 0.0$ when the π AO $s \phi_\rho \in$ the fragment A.

10.2.2. π -Delocalization Causing BLA

The particular localized geometry of benzotricyclobutadiene (10-12) is optimized at various theoretical levels with different basis sets. The geometrical data, presented in Figure 10-1 and listed in Table 10-2, show the following interesting facts:

- (i) All $\Delta r(\text{PLG}) = r_{\text{endo}}(\text{PLG}) - r_{\text{exo}}(\text{PLG}) < 0$, except for the differences at MP2/(6-31G* and 6-311G**) levels and at (BLYP and B3LYP)/6-311G** level, where, for example, $r_{\text{endo}}(\text{PLG})$ is the distance of the endocyclic CC bond in PLG. Although MP2/(6-31G and 6-311G**) values are two exceptions, their values (0.003 and 0.002 \AA) of $\Delta r(\text{PLG})$ are close to zero.
- (ii) The average and range of a set of $\Delta r(\text{PLG})$ values are -0.011 \AA and -0.036 \AA , respectively. Theoretical level and basis set size have obvious influence on the $\Delta r(\text{PLG})$ value. At the B3LYP level of theory, for example, the largest $|\Delta r(\text{PLG})| < 0.015 \text{ \AA}$. At the MP2 level of theory, $|\Delta r(\text{PLG})|$ is the smallest, but the MP2 calculation takes much CPU time. Therefore, all the calculation will be performed at B3LYP/6-31G* level.
- (iii) The average CC bond distances $\bar{r}_{\text{endo}}(\text{PLG}) = 1.387 \text{ \AA}$ and $\bar{r}_{\text{exo}}(\text{PLG}) = 1.398 \text{ \AA}$. The differences $\bar{r}_{\text{endo}}(\text{PLG})$

Table 10-2. For Particular Localized Geometry (PLG) of Molecule 10-12, the Bond Lengths $r_{i,j}$ (\AA), Bond Angles α and β (Figure 10-1), and Molecular Energy E (hartree), Obtained from the Restricted Geometry Optimization using Our 2011 Method.

	r (benzene)	r_{1-2}	r_{2-3}	Δr	r_{1-7}	r_{7-8}	$\angle\alpha$	$\angle\beta$	$E(\text{PLG})$
		r_{endo}	r_{exo}						
B3LYP/6-31G*	1.397	1.393	1.395	-0.002	1.445	1.346	89.1	90.9	-460.73730
RHF/6-31G*	1.386	1.378	1.389	-0.011	1.461	1.332	89.1	90.9	-457.76313
MP2/6-31G*	1.397	1.400	1.397	0.003	1.460	1.357	89.2	90.8	-459.24701
B3LYP/6-311G**	1.394	1.393	1.393	0.000	1.458	1.347	89.1	90.9	-460.85607
BLYP/6-311G**	1.404	1.406	1.402	0.004	1.467	1.357	89.0	91.0	-460.67659
RHF/6-311G**	1.385	1.375	1.391	-0.016	1.461	1.332	89.2	90.8	-457.85692
MP2/6-311G**	1.398	1.401	1.399	0.002	1.459	1.360	89.2	90.8	-459.46557
B3LYP/6-311G(2d,2p)	1.391	1.384	1.397	-0.013	1.437	1.343	89.2	90.8	-460.89683
BLYP/6-311G(2d,2p)	1.400	1.397	1.405	-0.008	1.443	1.354	89.1	90.0	-460.71687
XPBE96/6-311G(2d,2p)	1.420	1.414	1.424	-0.010	1.465	1.369	89.1	90.9	-457.71375
LYP/6-311G(2d,2p)	1.366	1.350	1.379	-0.029	1.427	1.316	89.3	90.7	-460.55292
RHF/6-311G(2d,2p)	1.382	1.364	1.395	-0.031	1.446	1.329	89.3	90.7	-457.89374
MP2/6-311G(2d,2p)	1.395	1.395	1.398	-0.003	1.440	1.357	89.2	90.8	-459.59354
B3LYP/6-311g(2df,p)	1.390	1.383	1.398	-0.015	1.428	1.343	89.2	90.8	-460.92208
BLYP/6-311g(2df,p)	1.400	1.396	1.406	-0.010	1.433	1.353	89.1	90.9	-460.74266
XPBE96/6-311g(2df,p)	1.419	1.414	1.424	-0.010	1.456	1.368	89.1	90.9	-457.73871
LYP/6-311g(2df,p)	1.366	1.349	1.379	-0.030	1.420	1.315	89.3	90.6	-460.51510
RHF/6-311g(2df,p)	1.382	1.364	1.396	-0.032	1.440	1.328	89.3	90.7	-457.91687
MP2/6-311g(2df,p)	1.391	1.392	1.396	-0.004	1.423	1.353	89.2	90.8	-459.76935
Range	0.056	0.064	0.045	-0.036	0.047	0.054	0.3	0.9	
Average \check{r}	1.393	1.387	1.398	-0.011	1.446	1.345	89.2	90.8	-459.55658

r_{1-2} : Distance of C(1)-C(2) bond. $\Delta r = r_{1-2} - r_{2-3}$. The numbering system of molecule 10-12 is shown in Figure 10-1.

- $\check{r}_b(\text{PLG}) = -0.006 \text{ \AA}$, and $\check{r}_{\text{exo}}(\text{PLG}) - \check{r}_b(\text{PLG}) = 0.005 \text{ \AA}$, where \check{r}_b is the average of a set of the CC bond lengths of benzene. The average CC bond distance of the PLG's center ring is close to that of benzene.

In the PLG of molecule 10-12, accordingly, the equalization of the CC bond lengths in center ring should be attributed to the eliminating of the π -electron interaction between the two fragments A and B.

The geometric data at B3LYP/6-31G* level, presented in Figure 10-1 and listed in Table 10-2, also show the

following differences between the ground state geometry of molecule **10-12** and the particular localized geometry:

- (i) For the optimized PLG, $r_{\text{endo}}(\text{PLG})$ (1.393 Å) $\approx r_{\text{exo}}(\text{PLG})$ (1.395 Å). The average distance (1.394 Å) of the CC bonds in the PLG's center ring is approximately equal to that of the CC bonds (1.397 Å) in benzene molecule.
- (ii) For the ground state geometry, $\Delta r(G) = r_{\text{endo}}(G) - r_{\text{exo}}(G) = 0.177 \text{ \AA} > 0$. But $\Delta r(\text{PLG}) = r_{\text{endo}}(\text{PLG}) - r_{\text{exo}}(\text{PLG}) = -0.002 \text{ \AA} < 0$, where, for example, $r_{\text{endo}}(G)$ and $r_{\text{exo}}(G)$ are the endocyclic- and exocyclic CC bonds in ground state geometry.
- (iii) The molecular energy $E(\text{PLG})$ (-460.73730 hartree) of PLG is lower than that $E(G)$ (-460.63040) of the ground state geometry, and the energy difference $[E(G) - E(\text{PLG})] = 67.1 \text{ kcal/mol}$. The π -interaction between the two fragments A and B is destabilization. Correspondingly, the distance $r_{1-7}(\text{PLG})$ (1.445 Å) $< r_{1-7}(G)$ (1.473 Å), and $r_{7-8}(\text{PLG})$ (1.346 Å) $< r_{7-8}(G)$ (1.374 Å), where, for example, $r_{1-7}(\text{PLG})$ is the distance of the C(1)-C(7) bond in the PLG.
- (iv) The bond angle $\alpha(\text{PLG})$ and $\alpha(G)$ is, respectively, 89.1° and 87.3°. $d\alpha(\text{GP}) = \alpha(G) - \alpha(\text{PLG}) = -1.8^\circ$, and $d\beta(\text{GP}) = 1.8^\circ$. $d\alpha(\text{GP})$ and $d\beta(\text{GP})$ are so small that, in the ground state geometry, it is unreasonable for the obvious bond length alternation ($\Delta r(G) = 0.177 \text{ \AA}$) to be attributed to $\alpha(G) < 120^\circ$ and $\beta(G) < 120^\circ$.

In the ground state geometry of molecule **10-2**, it can be said with certainty that the π -interaction between the central benzene ring and the double bonds in the small rings (rather than the angle strain) plays a decisive role in causing CC the bond length alternation.

10.2.3. Energy Decomposition

To further confirm the decisive role of π -interaction and to demonstrate that the forces acting on the endo- and exo-cyclic CC bonds arise from the π -delocalization, three electronic states should be constructed. An electronic may be localized or delocalized. The particular localized geometry of benzotricyclobutadiene is constructed by conditional geometry optimized at B3LYP/6-31G* level, and its π -electrons are localized on the fragments A and B, respectively. When the regular single-point energy calculation is performed on the particular localized geometry at RHF/6-31G* level, a delocalized electronic (DLE) state is constructed. For molecule **10-12**, the following three electronic states are constructed at RHF/6-31G* level:

- (i) Delocalized electronic state (G) of ground state geometry, and it is constructed by the regular single-point energy calculation on the ground state geometry optimized at B3LYP/6-31G* level.
- (ii) Localized electronic state (PLG) of particular localized geometry, and it is constructed by the conditional single-point energy calculation on the particular localized geometry.
- (iii) Delocalized electronic (DLE) state of the particular localized geometry.

For Each of the three electronic starts. as shown by Figure 10-2, the total electronic energy is decomposed into its components E_{e-ii} and E_{e-ij} using the following Equation:

$$E_{e-ij} = \sum_{k=1}^{ni} \sum_{l=1}^{nj} (f_{kl} + h_{kl}) d_{kl}$$

where AOs $\phi_k \in i$ -th atom, AOs $\phi_l \in j$ -th atom, ni is the number of the AOs belonging to the i-th atom, and nj is the number of the AOs belonging to j-th atom, f_{kl} , h_{kl} and d_{kl} are the elements of the AO Fock (**f**), one-electron (**h**) and density (**d**) matrices. The corresponding nuclear repulsion components E_{N-ij} can be calculated by using the

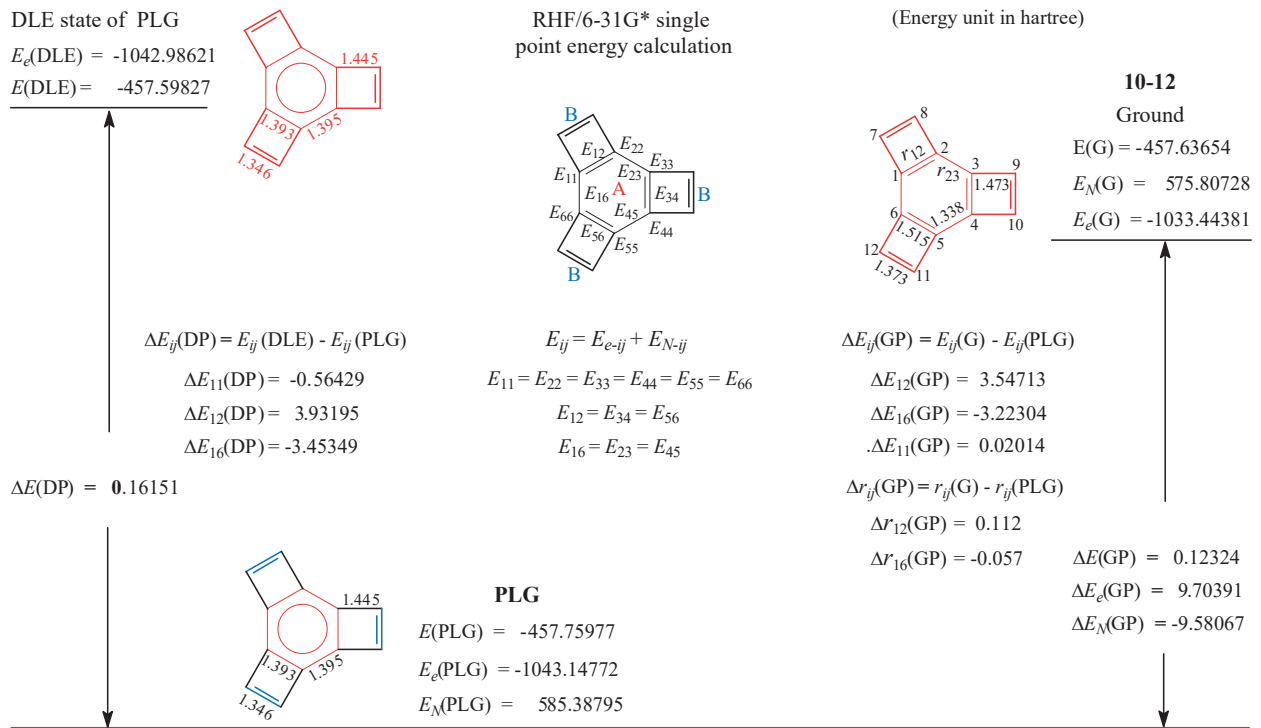


Figure 10-2. For molecule 10-12, ground state (G), PLG and its DLE state are obtained from the regular or conditional single-point energy calculations, on the B3LYP/6-31G* optimized geometries, at RHF/6-31G* level. The intra- and inter-atom contributions, E_{ii} and E_{ij} , to molecular energy, and their difference ΔE_{ii} and ΔE_{ij} between a pair of electronic states. In the PLG structure, the black lines between two fragment A and B mean that all the π -interactions between the central ring (red color) and the C=C bonds (blue color) in small rings have been set equal to zero.

following Equation:

$$E_{N-ij} = (e_i + e_j) / r_{ij}$$

e_i and e_j are the nuclear charges of i -th and j -th atoms, and r_{ij} is the distance between the two atoms. The molecular energy component E_{ij} between the i -th atom and the j -th atom is as follow:

$$E_{ij} = (E_{e-ij} + E_{N-ij})$$

Accordingly, for example, the symbols, used in Figure 10-2, are defined as following energy differences: $\Delta E_{12}(\text{DP}) = E_{12}(\text{DLE}) - E_{12}(\text{PLG})$, where $E_{12}(\text{DLE})$ is the molecular energy component between the 1st and 2nd atoms in the DLE state of PLG; $E_{12}(\text{PLG})$ is the molecular energy component between the 1st and 2nd atoms in the localized electronic state of the PLG geometry. As shown by the data (hartree) presented in Figure 10-2, $\Delta E_{12}(\text{DP}) = 3.93195 > 0$ (destabilizing), and $\Delta E_{16}(\text{DP}) = -3.45349 < 0$ (stabilizing). In instant of π -electron delocalization, endocyclic bonds are subjected to a tensile force, and meanwhile the exocyclic bonds are subjected to a compressive force. Then the endocyclic bonds are lengthened and the exocyclic bonds are shortened until the ground state geometry is reached. Finally, $\Delta E_{12}(\text{GP}) = E_{12}(G) - E_{12}(\text{PLG}) = 3.54713$ hartree > 0 , and $\Delta E_{16}(\text{GP}) = E_{16}(G) - E_{16}(\text{PLG}) = -3.22304$ hartree < 0 . Correspondingly, the C(1)-C(2) bond (endocyclic bond) is lengthened from 1.393

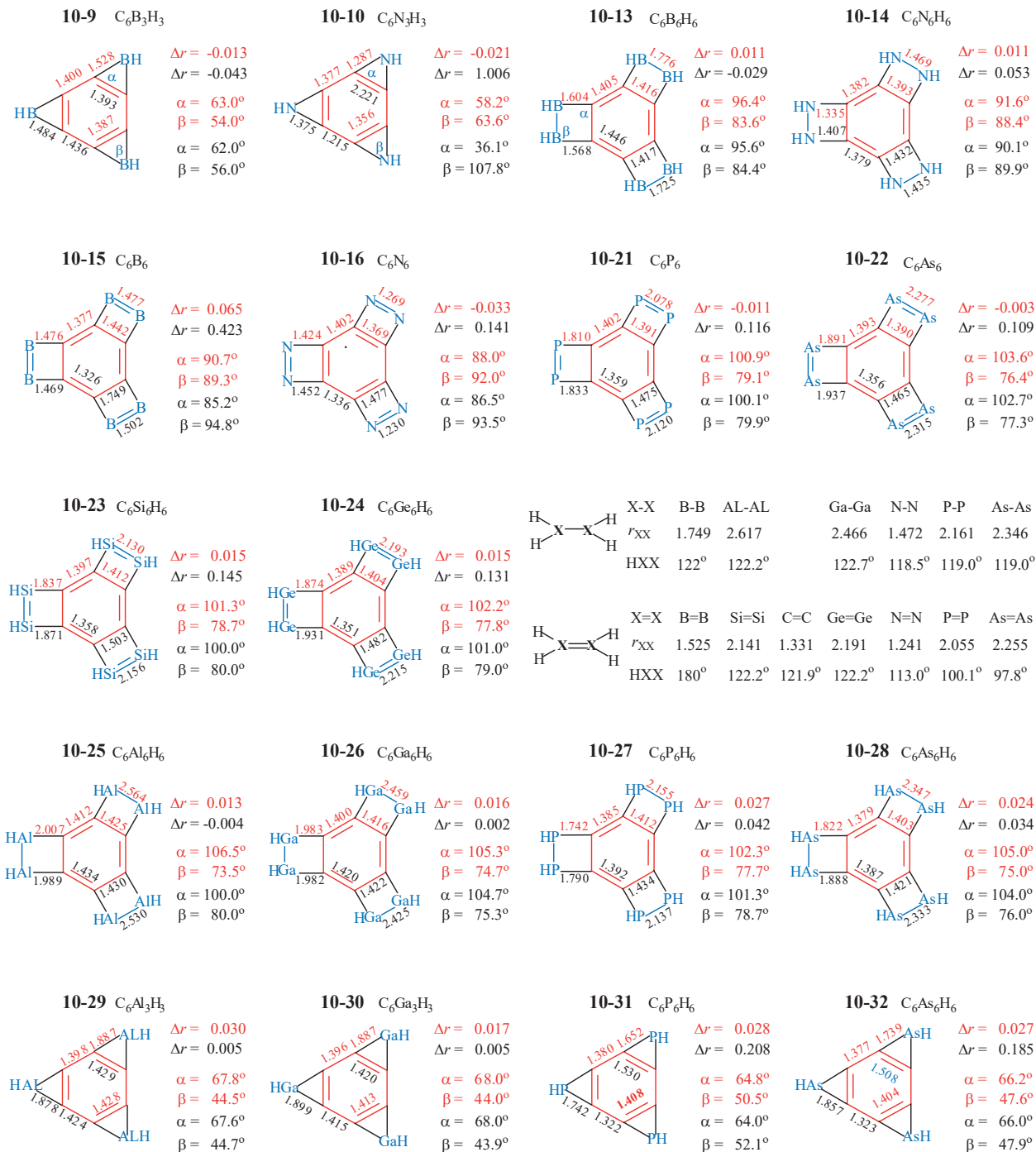


Figure 10-3. For each molecule, the red data are the bond lengths (\AA) and bond angles in the PLG, and they are obtained from our 2011 method at B3LYP/6-31G* level. In the PLG, the π -MO and spatial π -electron interactions between the red fragment and the blue fragment B have been artificially eliminated. The black data are the geometrical data for the ground state geometry.

\AA in the PLG to 1.515 \AA in the ground state geometry, and meanwhile the C(1)-C(6) bond (exocyclic bond) is shortened from 1.395 \AA in the PLG to 1.338 \AA in the ground state geometry.

In PLG of molecule **10-2**, the endo- and exo-cyclic bonds are subjected to different forces due to π -electron delocalization. As the result, the central ring is distorted from the PLG with almost equal CC bond lengths to the ground state geometry with alternating CC bond lengths.

10.3. UNIVERSALITY OF π -DISTORTIVITY

In order to confirm that the above conclusion can be applied to all types of strained-aromatic molecules, the particular localized geometries (PLGs) of 18 molecules are obtained from our 2011 method at B3LYP/6-31G* level. The geometrical data of the PLGs are presented in Figure 10-3, and various energy effect values are listed in Table 10-3. The 18 molecules will be used to discuss the influences of the geometric and electronic structures on the π -distortivity. In the case of strained-aromatic molecules, π -distortivity refers to the differences, in the directions and degree of bond length alternation, between the ground state geometry and its PLG, and it is measured by $d\Delta r(GP) = \Delta r(G) - \Delta r(PLG)$. The geometrical structures include the following structural factors:

- (i) Size of annulated small rings.
- (ii) Types of the hetero-groups in annulated small ring: HX-XH (such as C₆B₆H₆), X=X (such as C₆B₆), and XH (such as C₆B₃H₃).
- (iii) Distances of the X-X, X=X and C-X bonds
- (iv) Bond angles α and β (Figure 10-3).

The electronic structures are as the followings:

- (i) Aromaticity and anti-aromaticity (4n+2 rule) of the annulated small ring.
- (ii) Electronic occupancy (electron-deficiency and electron-richness) of the hetero-groups in the annulated small ring.
- (iii) Inductive effect of the heteroatom in small ring.

10.3.1. Comparison of $\Delta r(PLG)$ and $\Delta r(G)$

There are two ways to confirm the conclusion. The first way is to qualitatively compare $\Delta r(PLG)$ and $\Delta r(G)$. The absolute value of the $\Delta r(G) = r_{endo}(G) - r_{exo}(G)$ is used to quantify the degree of the bond length alternation in the ground state geometry, and the sign of the $\Delta r(G)$ value indicates the direction of the bond lengths alternation. For the PLG, the degree and direction of the bond length alteration are quantified by $\Delta r(PLG) = r_{endo}(PLG) - r_{exo}(PLG)$.

For molecules C₆B₆H₆ and C₆N₆H₆, for example, the following differences are interesting and noteworthy:

- (i) C-X bond length differences, $r_{C-X}(G) - r_{C-X}(PLG)$, are -0.036 Å (X = B) and 0.072 Å (X = N)
- (ii) Differences, $d\Delta r(GP) = \Delta r(G) - \Delta r(PLG)$, are -0.040 Å (B-B) and 0.042 Å (N-N)
- (iii) Differences, $\Delta r(PLG) = r_{endo}(PLG) - r_{exo}(PLG)$, both are 0.11 Å.

For these two molecules, $\Delta r(G)$ (0.053 Å, N-N) > $|\Delta r(G)|$ (-0.029 Å, B-B), and $\Delta r(G)$ (N-N)/ $\Delta r(G)$ (B-B) ≈ 2. In the ground state geometry of these two molecules, the degree and direction of bond length alteration are different. In literature, as discussed in the Introduction section, the differences, in the sign and size of $\Delta r(G)$, between molecules C₆B₆H₆ and C₆N₆H₆ were attributed to the differences, in the inductive effect, between the boron and nitrogen atoms, and to the difference in the way to count the number of π -electrons.⁵⁸ In the PLG of molecule C₆N₆H₆, there is no

Table 10-3. For 19 Strained-Aromatic Molecule ($C_6X_6H_6$, $C_6X_3H_3$, C_6X_6), the Molecular Energy Difference $\Delta E(GP) = [E(G) - E(PLG)]$ (kcal/mol), and Various Differences in the Geometrical Data, Obtained from Our 2011 Method at B3LYP/6-31G* Level (Bond Length Unit in Angstrom).

Mols	$\Delta E(GP)$	$d\Delta r(GP)$	$\Delta r(PLG)$	$\Delta r(G)$	$\Delta\beta(PLG)$	$\Delta\beta(G)$	$\Delta\alpha(PLG)$	$\Delta\alpha(G)$	$r_{XX}(PLG)$	$r_{endo}(PLG)$
$C_6X_6H_6$										
HX-XH										
$C_6B_6H_6$	-82.61	-0.040	0.011	-0.029	38.4	37.6	25.6	26.4	1.776	1.416
$C_6Al_6H_6$	-41.07	-0.017	0.013	-0.004	48.7	48.3	15.5	15.9	2.564	1.425
$C_6Ga_6H_6$	-34.40	-0.014	0.016	0.002	48.0	47.4	16.7	17.3	2.459	1.416
$C_6P_6H_6$	33.10	0.015	0.027	0.042	41.3	40.3	19.7	20.7	2.155	1.412
$C_6As_6H_6$	33.67	0.010	0.024	0.034	44.0	43.0	17.0	18.0	2.347	1.403
$C_6N_6H_6$	61.77	0.042	0.011	0.053	30.1	28.6	30.4	31.9	1.469	1.393
C_6X_6										
X=X										
C_6P_6	38.21	0.127	-0.011	0.116	21.0	20.2	21.1	21.9	2.078	1.391
C_6As_6	40.88	0.112	-0.003	0.109	21.4	20.5	18.4	19.3	2.277	1.390
C_6N_6	63.08	0.174	-0.033	0.141	21.0	19.5	34.0	35.5	1.269	1.369
C_6B_6	40.49	0.358	0.065	0.423	90.7	85.2	31.3	36.8	1.477	1.442
$C_6Si_6H_6$	44.22	0.130	0.015	0.145	43.5	42.2	22.8	22.0	2.156	1.503
$C_6Ge_6H_6$	52.14	0.116	0.015	0.131	44.4	43.2	21.8	23.0	2.215	1.482
HC=CH										
$C_{12}H_6$	67.08	0.179	-0.002	0.177	29.1	27.3	32.9	34.7	1.374	1.515
$C_6X_3H_3$										
XH										
$C_6B_3H_3$	-89.91	-0.030	-0.013	-0.043	66.0	64.0	59.0	60.0	0.000	1.393
$C_6Al_3H_3$	-36.61	-0.025	0.030	0.005	75.5	75.3	54.2	54.4	0.000	1.429
$C_6Ga_3H_3$	-24.94	-0.012	0.017	0.005	76.0	76.1	54.0	54.0	0.000	1.420
$C_6N_3H_3$	48.70	1.027	-0.021	1.006	56.4	12.2	63.8	85.9	0.000	2.221
$C_6As_3H_3$	80.81	0.158	0.027	0.185	72.4	72.1	55.8	56.0	0.000	1.508
$C_6P_3H_3$	81.69	0.180	0.028	0.208	69.7	67.9	57.2	58.0	0.000	1.530

conjugation between the N-N bond and the central benzene ring, and the inductive effect of nitrogen should be stronger than in the ground state geometry because the C-N bond length (1.335 Å) in the PLG is shorter than that (1.407 Å) in the ground state geometry. Accordingly, should $\Delta r(PLG) > \Delta r(G)$ if the inductive effect (electronegative) plays an important role in determining the distance of endocyclic bond. In fact, however, $\Delta r(PLG)$ (0.011 Å) $< \Delta r(G)$ (0.053 Å), and $\Delta r(G)/\Delta r(PLG) \approx 5$. In the PLGs of molecules $C_6B_6H_6$ and $C_6N_6H_6$, especially,

boron is electropositive and nitrogen is electronegative. According to the interpretation by Cremer and Stanger, $\Delta r(\text{PLG})$ ($\text{C}_6\text{N}_6\text{H}_6$) should be different to $|\Delta r(\text{PLG})|$ ($\text{C}_6\text{B}_6\text{H}_6$). However, both $\Delta r(\text{PLG}) = 0.011 \text{ \AA}$.

These facts, together with the theoretical results that for these two molecules, $|\Delta r(\text{G})| > \Delta r(\text{PLG})$, qualitatively confirm the important role of π -delocalization in causing bond length alternation. In Schemes 10-6, six ways for π -electron delocalization to affect bond length alternation are summarized. For most molecules, $|\Delta r(\text{G})| > \Delta r(\text{PLG})$, and for all the molecules, $|\Delta r(\text{G})| \neq |\Delta r(\text{PLG})|$.

But keep in mind, it still does not give the explanation for the great difference, in the size and sign of $\Delta r(\text{G})$, between molecules $\text{C}_6\text{B}_6\text{H}_6$ and $\text{C}_6\text{N}_6\text{H}_6$.

The six ways for π -delocalization to affect $d\Delta r(\text{GP})$

$\pi\text{-delocalization}$ Atoms of carbon family $\Delta E(\text{GP}) > 0$ Atoms of nitrogen family	$\Delta r(\text{PLG}) > 0$ $\Delta r(\text{PLG}) < 0$	$\Delta r(\text{G}) > 0$ $\Delta r(\text{G}) > 0$	$\Delta r(\text{G}) > \Delta r(\text{PLG})$ $\Delta r(\text{G}) > \Delta r(\text{PLG})$	C ₆ X ₆ H ₆ (X = N, P, As, Si, Ge); C ₆ B ₆ C ₆ X ₃ H ₃ (X = P, As);
Atoms of boron family $\Delta E(\text{GP}) < 0$	$\Delta r(\text{PLG}) > 0$	$\Delta r(\text{G}) > 0$ $\Delta r(\text{G}) < 0$	$\Delta r(\text{G}) < \Delta r(\text{PLG})$ $ \Delta r(\text{G}) < \Delta r(\text{PLG})$	C ₆ Ga ₆ H ₆ ; C ₆ X ₃ H ₃ (X = Al, Ga)
	$\Delta r(\text{PLG}) < 0$	$\Delta r(\text{G}) < 0$	$ \Delta r(\text{G}) < \Delta r(\text{PLG})$ $ \Delta r(\text{G}) > \Delta r(\text{PLG})$	C ₆ Al ₆ H ₆ C ₆ B ₆ H ₆
		$ \Delta r(\text{G}) > \Delta r(\text{PLG})$		C ₆ B ₃ H ₃

Scheme 10-6

10.3.2. $d\Delta r(\text{GP})$ versus $\Delta E(\text{GP})$

In order to confirm that the π -electron delocalization plays a decisive role in causing the bond length alternation, and to prove that, for various types of strained-aromatic molecules, the distortions of the central ring all can be attributed to the π -electron delocalization, as the second ways, it is necessary to determine the quantitative relationship between $d\Delta r(\text{GP})$ and $\Delta E(\text{GP})$, where $\Delta E(\text{GP}) = [E(\text{G}) - E(\text{PLG})]$ is the molecular energy difference between the ground state geometry (G) and its PLG geometry.

For 19 molecules listed in Table 10-3, as shown by the red curve line in Figure 10-4a, $d\Delta r(\text{GP})$ (y) can be fitted as the following second order polynomial function of $\Delta E(\text{GP})$ (x) (cc = 0.772):

$$y = 0.0152 + 0.00135x + (8.5266 \cdot 10^{-6})x^2.$$

Two points (blue filled circle), denoted as "NH" and "B=B", lie away from the fitted curve, and they are not included in the curve fitting.

The correlation between the two variables $d\Delta r(\text{GP})$ and $\Delta E(\text{GP})$ merely means that π -electron delocalization plays a decisive role in the change, $d\Delta r(\text{GP})$, of bond length alternation, but it does not mean $|\Delta r(\text{PLG})| < |\Delta r(\text{G})|$ always. For the correlation coefficient (cc), values between 0.7 and 1.0 (-0.7 and -1.0) indicate a strong positive (negative) linear relationship between two variables, according to the definition of the correlation coefficient for linear relationship.⁶⁶ The cc value of 0.772 indicates that there is a quantitative relationship between $d\Delta r(\text{GP})$ and

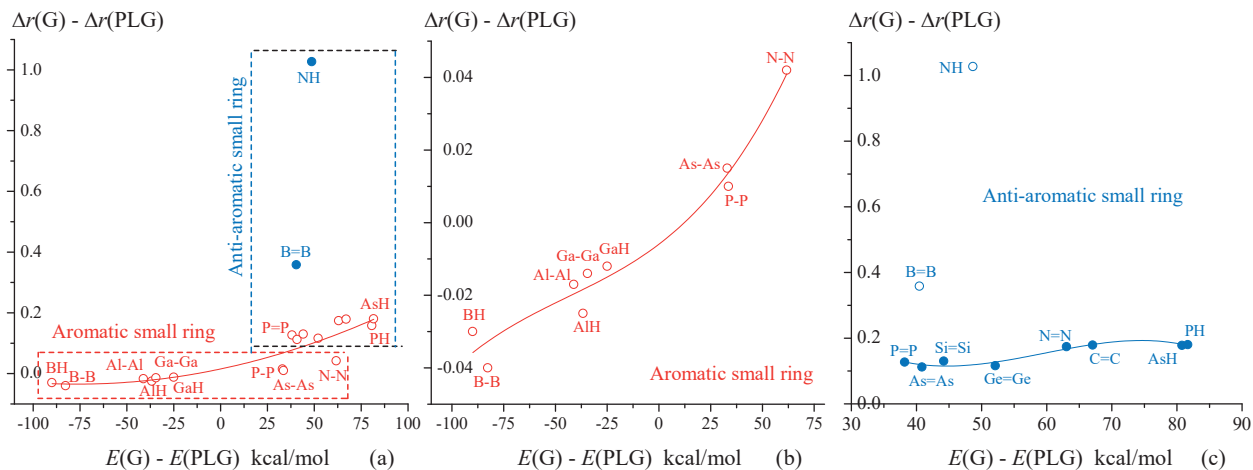


Figure 10-4. $d\Delta r(GP)$ can be fitted as a polynomial function of $\Delta E(GP)$ at B3LYP/6-31G* level. (a) For 17 molecules (red circles). (b) For 9 ASRMs. (c) For 8 AASRMs (blue solid circles). bond length unit in angstrom.

$\Delta E(GP)$, but the correlation between the two variables is not very good. Therefore, 19 molecules should be divided into two groups according to the electronic structures. The 9 molecules, $C_6X_3H_3$ ($X = B, Al, Ga$) and $C_6X_6H_6$ ($B=B, Al-Al, Ga-Ga, N=N, P=P, As=As$), belong to the first group, and their annulated small rings are aromatic according to $4n+2$ rule. Hereafter, these molecules are called “aromatic small ring molecules” (molecules with aromatic small rings) (ASRMs). The second group includes 10 molecules $C_6X_3H_3$ ($X = N, P, As$), C_6X_6 ($B=B, N=N, P=P, As=As$) and $C_6X_6H_6$ ($C=C, Si=Si, Ge=Ge$). These 10 molecules are called “anti-aromatic small ring molecules” (molecules with anti-aromatic small rings) (AASRMs) because their annulated small rings are anti-aromatic. In Figure 10-4a, the points (red hollow circles) corresponding to nine ASRMs are surrounded by a red dotted box, and the points (the eight red hollow circles and the two blue solid circles) corresponding to 10 AASRMs are surrounded by a blue dotted box.

The first order derivative of the fitted function in Figure 10-4a is as follow:

$$dy/dx = 0.00135 + (1.70723 \times 10^{-5})x > 0$$

The fitted function is a monotonically increasing function, that is, a larger energy effect $\Delta E(GP)$ corresponds to a greater difference $d\Delta r(GP)$. When $\Delta E(GP)$ is large enough, always $\Delta r(G) > \Delta r(PLG)$ no matter whether the small ring is aromatic or anti-aromatic. For AASRMs, always $\Delta E(GP) > 0$, $d\Delta r(GP) > 0$, and $\Delta r(G) > 0$ (Table 10-3).

10.3.2.1. Aromatic Small Ring Molecules

For the 9 molecules $C_6X_3H_3$ ($X = B, Al, Ga$) and $C_6X_6H_6$ ($X = B, Al, Ga, N, P, As$), as shown by the red curve line in Figure 10-4b, $d\Delta r(GP)$ (y) can be well fitted as the following third order polynomial function of $\Delta E(GP)$ (x), and cc is large, up to 0.946:

$$y = -0.0059 + (4.3502 \times 10^{-4})x + (3.5842 \times 10^{-6})x^2 + (2.7130 \times 10^{-8})x^3$$

$$dy/dx > 0.$$

Among the 9 molecules, the vertical offsets, 0.007 Å and -0.008 Å, of the points "BH" and "B-B" from the fitted function line are the largest, and those, (0.001, 0.001 and 0.001 Å), of the points "Al-Al", "As-As" and "N-N" are the smallest.

According to the positions of the red circles in Figure 10-4b and to the data listed in Table 10-3, the nine ASRMs can be divided into two sub-groups. The three molecules $C_6X_6H_6$ ($X = N, P, As$) belong to the first sub-group, and the other 6 molecules $C_6X_3H_3$ and $C_6X_6H_6$ ($X = B, Al, Ga$) are grouped into the second sub-group. For the molecules of the first sub-group, the X-X bonds are the electron-rich group. Correspondingly, always $\Delta E(GP) > 0$, $\Delta r(G) > 0$, $\Delta r(PLG) > 0$, and $\Delta r(G) > \Delta r(PLG)$. For $C_6N_6H_6$, for example,

$$\begin{aligned}\Delta E(GP) &= 61.8 \text{ kcal/mol} > 0, \\ \Delta r(G) (0.053 \text{ \AA}) &> \Delta r(PLG) (0.011 \text{ \AA}) \\ d\Delta r(GP) &= 0.042 \text{ \AA} > 0\end{aligned}$$

As the covalent radius increases from 0.75 Å (nitrogen atom), through 1.10 Å (phosphorus), to 1.21 Å (arsenic atom)⁶⁷, the changes in the bond lengths (r_{X-X} and r_{C-X}) and bond angle ($\Delta\beta$) are as follows:

$$\begin{aligned}r_{X-X}(G): 1.435 (\text{N-N}) &< 2.137 (\text{P-P}) < 2.333 (\text{As-As}) \\ r_{X-X}(PLG): 1.469 (\text{N-N}) &< 2.155 (\text{P-P}) < 2.347 (\text{As-As}) \\ r_{C-X}(G): 1.407 (\text{N-N}) &< 1.790 (\text{P-P}) < 1.888 (\text{As-As}) \\ r_{C-X}(PLG): 1.335 (\text{N-N}) &< 1.742 (\text{P-P}) < 1.822 (\text{As-As}) \\ \Delta\beta(G): 28.6 (\text{N-N}) &< 40.3 (\text{P-P}) < 43.0 (\text{As-As}) \\ \Delta\beta(PLG): 30.1 (\text{N-N}) &< 41.3 (\text{P-P}) < 44.0 (\text{As-As})\end{aligned}$$

where, for example, $\beta(\text{As}_2\text{H}_4)$ is the bond angle $\angle \text{H-As-As}$ in the molecule $\text{H}_2\text{As}-\text{AsH}_2$, and $\Delta\beta(PLG) = \beta(\text{X}_2\text{H}_4) - \beta(\text{PLG})$ is the difference, in the Bond angle $\angle \text{HXX}$ ($\angle \text{HAsAs}$), between the H_2XXH_2 molecule and the PLG of a strained-aromatic molecule. Accordingly, $\Delta\beta(G)$ and $\Delta\beta(PLG)$ can be used to measure the angle strain in the ground state geometry and PLG. In the case of molecule $C_6As_6H_6$, $\Delta\beta(PLG)$ (44.0°) and $\Delta\beta(G)$ (43.0°) are large, and the corresponding $\Delta r(PLG)$ and $\Delta r(G)$ are also large, up to 0.024 and 0.034 Å (Table 10-3). In the PLG geometry of molecule $C_6N_6H_6$, $\Delta\beta(PLG)$ (30.1°) is smaller than that (44.0°) for molecule $C_6As_6H_6$, the corresponding $\Delta r(PLG)$ (0.011 \AA) is also smaller than that (0.024 \AA) for molecule $C_6As_6H_6$. The fact that $\Delta r(PLG)(\text{As-As})/\Delta r(PLG)(\text{N-N}) = 2$ seems to mean that the β -angle strain causes the bond length alternation in the PLG of molecule $C_6As_6H_6$. However, the correlation between the two variables $\Delta E(GP)$ and $d\Delta r(GP)$ is well, and the bond length alternation, $\Delta r(G)$ (0.053), in the ground state geometry of molecule $C_6N_6H_6$, is the largest of the three molecules, and $\Delta\beta(G)$ (28.6°) \approx $\Delta\beta(PLG)$ (30.1°). In the ground state geometry, it is π -electron delocalization (rather than β -angle strain) to play an important role in determining the bond length alternation. But, as will be indicated in the last section, the bond length alternation in the PLG is conceptually different from that in the ground state geometry, and it is determined by the secondary structural effect.

For the three ASRMs $C_6X_6H_6$ ($X = N, P, As$), as shown by Figure 10-4a, the three red circles (located at the right side of the red dashed box) are closer to the red circles corresponding to the AASRMs (located at the bottom of the blue dotted box). In term of the ability to distort the central ring, it seems to be more appropriate for the three molecules $C_6X_6H_6$ ($X = N, P, As$) to be grouped into the AASRMs.

For the molecules of the second sub-group, the X-X and XH ($X = B, Al, Ga$) groups are electron-deficient. Correspondingly, as shown by the data in Table 10-3, that always $\Delta E(GP) < 0$ (stabilizing) and always $d\Delta r(GP) < 0$ are the results of the following three possible changes:

$$\begin{aligned}\Delta r(PLG) &> 0, \text{ and } \Delta r(G) < 0 \text{ (B-B, Al-Al)} \\ \Delta r(PLG) &> 0, \text{ and } \Delta r(G) > 0 \text{ (Ga-Ga, AlH, GaH)} \\ \Delta r(PLG) &< 0, \text{ and } \Delta r(G) < 0 \text{ (BH)}\end{aligned}$$

For molecule C₆B₃H₃, for example,

$$\Delta E(\text{GP}) = -89.9 \text{ kcal/mol}$$

$$\Delta r(\text{PLG}) = -0.013 \text{ \AA},$$

$$\Delta r(\text{G}) = -0.043 \text{ \AA}$$

$$d\Delta r(\text{GP}) = -0.030 \text{ \AA}$$

10.3.2.2. Anti-aromatic Small Ring Molecules.

Of ten AASRMs C₆X₃H₃ (X = N, P, As), C₆X₆ (B=B, N=N, P=P, As=As) and C₆X₆H₆ (C=C, Si=Si, Ge=Ge), as shown by the blue curve line in Figure 10-4c, $d\Delta r(\text{GP})$ (y) for 8 molecules can be fitted as the following third order polynomial function of $\Delta E(\text{GP})$ (x) ($cc = 0.7577$):

$$y = 1.1568 - 0.0587x + 0.0011x^2 - (5.9864 \times 10^{-6})x^3$$

For AASRMs, as shown by the data listed in Table 10-3, the basic features, resulting from π -interaction, are always as follows:

$$\Delta E(\text{GP}) > 0, d\Delta r(\text{GP}) > 0.1 \text{ \AA}$$

$$\Delta r(\text{G}) > 0.1 \text{ \AA}, \Delta r(\text{G}) \gg |\Delta r(\text{PLG})|$$

For C₁₂H₆, for example,

$$\Delta E(\text{GP}) = 67.8 \text{ kcal/mol}, d\Delta r(\text{GP}) = 0.179 \text{ \AA}$$

$$\Delta r(\text{G}) = 0.177 \text{ \AA}, \Delta r(\text{G}) \gg |\Delta r(\text{PLG})| (-0.002 \text{ \AA})$$

In the case of AASRM, there is no doubt that the π -interaction not only plays a decisive role in distorting the central ring, but also makes the central ring very distorted

Keeping in mind that the vertical offsets of the points "NH" and "B=B" from the fitted function line are 0.917 \AA and 0.244 \AA , and they are so large that these two points are not included in function fitting. These abnormal vertical offsets will be specially interpreted.

10.3.2.3. Grouping Molecules by Geometric Structures

For AASRM, the correlation coefficient between two variables $d\Delta r(\text{GP})$ and $\Delta E(\text{GP})$ is only 0.7577, and it is not large enough to be able to confirm the correlation between the two variables. In order to determine the correlation between two variables as much as possible, and according to the differences in the geometric structures of the annulated small rings, the 19 strained-aromatic molecules are divided into the following three categories:

- (i) 6 molecules C₆X₆H₆ (X = B, Al, Ga, N, P, As). In each of these molecules, the annulated small ring is an aromatic four-membered ring, and the X-X bond in each annulated small ring is a single bond.
- (ii) 6 molecules C₆X₃H₃ (X = B, Al, Ga, N, P, As) with three-membered ring. These molecules include three ASRMs (X = B, Al, Ga) and three AASRAMs (N, P, As).
- (iii) 7 molecules, C₆X₆ (X = B, N, P, As) and C₆(HX=XH)₃ (X = C, Si, Ge). In each of these molecules, the annulated small ring is an anti-aromatic four-membered ring, and its X=X bond is a double bond.

For the three categories, as shown by Figure 10-5, $d\Delta r(\text{GP})$ (y) can be well fitted as the following polynomial

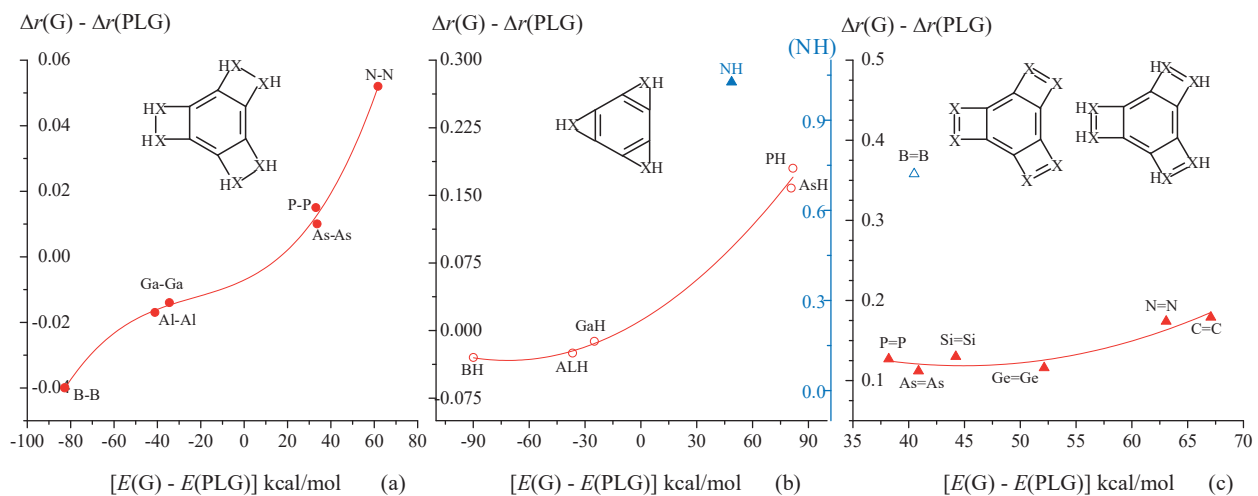


Figure 10-5. For 19 molecules, $d\Delta r(GP)$ can be fitted as the polynomial functions of $\Delta E(GP)$ at B3LYP/6-31G* level (bond length unit in angstrom)

functions of the energy difference $\Delta E(GP)$ (x):

$$\begin{aligned} y &= -0.0071 + (3.1754 \times 10^{-4})x + (5.4848 \times 10^{-6})x^2 \quad (\text{cc} = 0.992) \\ y &= 0.0111 + 0.0012x + (8.6718 \times 10^{-6})x^2 \quad (\text{cc} = 0.991) \\ y &= 0.39024 - 0.01211x + (1.3492 \times 10^{-4})x^2 \quad (\text{cc} = 0.823) \end{aligned}$$

For the molecules of the second category except for molecule $C_6N_3H_3$, the correlation (0.991) between the two variables is still high although the three ASRMs and three AASRMs are included in the same group. When three AASRAMs $C_6X_3H_3$ ($X = N, P, As$) are excluded from the AASRAM group, as shown by curve lines in Figure 10-4c and Figure 10-5c, the correlation coefficient of the two variables is increased from 0.758 to 0.823.

10.3.3. Large Differences between $C_6B_6H_6$ and $C_6N_6H_6$

The annulated small rings in $C_6B_6H_6$ and $C_6N_6H_6$ are aromatic. But the $\Delta E(GP)$ and $d\Delta r(GP)$ values (-82.6 kcal/mol and -0.040 Å) for $C_6B_6H_6$ are greatly different to those (61.8 kcal/mol and 0.042 Å) for $C_6N_6H_6$. Their corresponding points, represented as "B-B" and "N-N" in Figure 10-4b and Figure 10-5a, are located at two different endpoints of the curve. The 4n+2 rule can't interpret why there are such big differences between the two molecules.

10.3.3.1. CT and EX Interactions

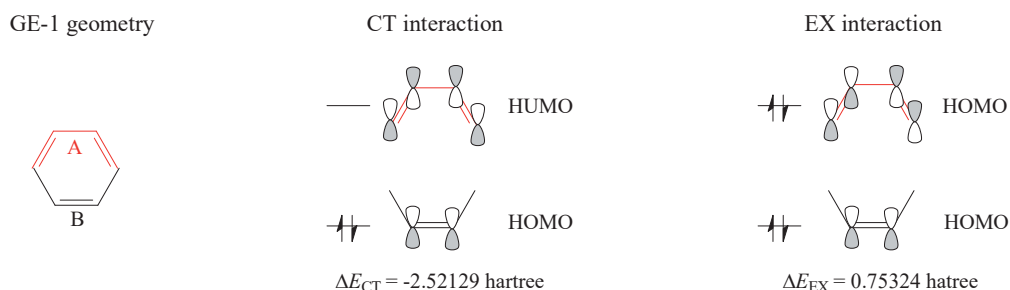


Table 10-4. Various Energy Effects (hartree) Associated with the π -Interaction between the Central Ring and Three X-X (Or XH) Groups, Obtained from Our 2011 Method at RHF/6-31G* Level (Bond Length Unit in Angstrom).

	$\Delta E_{\text{EX}}(\text{DP})$	$\Delta E_{\text{CT}}(\text{DP})$	$\Delta E_{ab}^{\pi}(\text{DP})$	$\Delta E_e(\text{DP})$	$\Delta E_e(\text{GP})$	$\Delta E_N(\text{GP})$	$\Delta E(\text{GP})$	$d\Delta r(\text{GP})$
C ₆ B ₆ H ₆	0.08416	-6.63126	-6.54710	-0.09641	-1.24954	1.14560	-0.10394	-0.040
C ₆ Al ₆ H ₆	0.19449	-7.57708	-7.38259	-0.05437	-1.90757	1.85136	-0.05620	-0.017
C ₆ Ga ₆ H ₆	0.81086	-15.28627	-14.47541	-0.04464	0.19071	-0.23593	-0.04522	-0.014
C ₆ B ₃ H ₃	0.10770	-6.94640	-6.83870	-0.12698	-0.14377	0.00482	-0.13895	-0.030
C ₆ Al ₃ H ₃	0.31374	-7.33943	-7.02568	-0.05563	1.33384	-1.39208	-0.05824	-0.025
C ₆ Ga ₃ H ₃	1.04403	-12.63410	-11.59007	-0.03600	8.55761	-8.59395	-0.03634	-0.012
C ₁₂ H ₆	5.17004	-2.95041	2.21964	0.16151	9.70391	-9.58067	0.12324	0.179
C ₆ N ₆ H ₆	13.83261	-5.35326	8.47935	0.14156	14.73693	-14.62072	0.11621	0.052
C ₆ P ₆ H ₆	13.73165	-6.77135	6.96031	0.07278	19.00713	-18.94144	0.06569	0.015
C ₆ As ₆ H ₆	20.87256	-14.77095	6.10161	0.08005	66.38744	-66.31906	0.06837	0.010

Based on the PMO theory,^{68,69} the $4n+2$ rule is well understood by examining the symmetries of the frontier FMOs (fragment molecular orbitals). For benzene at RHF/6-31G* level, for example, the following large CT interaction energy and small EX interaction energy (hartree) arise from the local π -interaction between ethylenic fragment (fragment A) and butadiene fragment (fragment B) in the GE-1 geometry of benzene: $\Delta E_{\text{CT}} = -2.52129 < 0$ and $\Delta E_{\text{EX}} = 0.75324 > 0$, where, for example, $\Delta E_{\text{CT}} = E_{\text{CT}}(\text{DLE}) - E_{\text{CT}}(\text{GE-1})$ is the difference, in the charge transfer energy effect, between the GE-1 geometry and its DLE state, and $E_{\text{CT}}(\text{GE-1}) = 0.0$. The DLE state of GE-1 geometry is constructed by the standard single-point energy calculation on the GE-1 geometry of benzene. Due to the symmetry matching of fragment molecular orbitals, $|\Delta E_{\text{CT}}| > \Delta E_{\text{EX}}$, and $|\Delta E_{\text{CT}}|/\Delta E_{\text{EX}} > 3$. Total inter-fragment π -interaction energy $\Delta E_{ab}^{\pi} = \Delta E_{\text{CT}} + \Delta E_{\text{EX}} = -1.76806$ hartree < 0 . For benzene, total electronic energy difference, $\Delta E_e = \Delta E$, between the GE-1 geometry and its DLE state is -34.9 kcal/mol and is stabilizing.

In the case of strained-aromatic molecules such as C₆N₆H₆, as indicated by the data listed in Table 10-4, the CT and EX energy effects (hartree) are as follows:

$$\Delta E_{\text{CT}}(\text{DP}) = -5.35326$$

$$\Delta E_{\text{EX}}(\text{DP}) = 13.83261$$

where, for example, $\Delta E_{\text{CT}}(\text{DP}) = E_{\text{CT}}(\text{DLE}) - E_{\text{CT}}(\text{PLG})$ is the difference, in the charge transfer energy effect, between the PLG geometry and its DLE state, and $E_{\text{CT}}(\text{PLG}) = 0.0$ (The definition and construction of the DLE state of PLG are described in Figure 10-2). As a result of $|\Delta E_{\text{CT}}(\text{DP})| < \Delta E_{\text{EX}}(\text{DP})$, the energy effect $\Delta E_{ab}^{\pi}(\text{DP}) = \Delta E_{\text{CT}}(\text{DP}) + \Delta E_{\text{EX}}(\text{DP}) = 8.47935$ hartree > 0 (destabilizing)

10.3.3.2. π Electron-Deficient Groups

The atomic elements B, Al and Ga belong to the boron family of the Periodic Table. When X = B, Al, Ga, the

X-X bonds in $C_6X_6H_6$ and the XH groups in $C_6X_3H_3$ are π -electron-deficient. Correspondingly, as indicated by the data listed in Table 10-4, $\Delta E_{CT}(DP) < 0$, $\Delta E_{EX}(DP) > 0$, and $\Delta E^{\pi}_{ab}(DP) < 0$ due to $|\Delta E_{CT}(DP)| > \Delta E_{EX}(DP)$. For $C_6B_6H_6$, for example, there is no π -electron in each of the B-B bonds, and certainly there is no the occupied-occupied exchange interaction between the central ring and the B-B groups, but there is the charge transfer interaction between these two fragments. In this molecule, the CT and EX energy effects (hartree) are as follows:

$$\Delta E_{CT}(DP) = -6.63126 < 0$$

$$\Delta E_{EX}(DP) = 0.08416 > 0$$

As the result of $|\Delta E_{CT}(DP)|/\Delta E_{EX}(DP) = 78.9$, the following energy effects (hartree) are stabilizing: $\Delta E^{\pi}_{ab}(DP) = -6.54710 < 0$, $\Delta E_e(DP) = -0.09641 < 0$

The atomic element Ga belongs to boron group, and is the element in the fourth period of the Periodic Table. In the Ga-Ga bonds of molecule $C_6Ga_6H_6$, there are π -electrons in the inner fragment molecular orbitals. However, as shown by the data listed in Table 10-4, $\Delta E_{EX}(DP)$ (0.81086 hartree) is still much smaller than $\Delta E_{CT}(DP)$ (-15.28627 hartree), leading to $\Delta E^{\pi}_{ab}(DP) = -14.47541$ hartree < 0 , and $\Delta E_e(DP) = -0.04464$ hartree.

10.3.3.3. π Electron-Rich Groups

On the contrary, when $X = N, P, As$, the X-X groups in molecules $C_6X_6H_6$ are π -electron-rich. In this case, as shown by the data listed in Table 10-4, $\Delta E^{\pi}_{ab}(DP) > 0$ due to $\Delta E_{EX}(DP) > |\Delta E_{CT}(DP)|$. For molecule $C_6N_6H_6$, for example, two lone pairs of π -electrons in each N-N bond greatly increases the exchange interaction between the central ring and the N-N groups, and meanwhile it weakens slightly the charge transfer interaction. As the results, $\Delta E_{EX}(DP)/|\Delta E_{CT}(DP)| = 2.6$, and $\Delta E^{\pi}_{ab}(DP) = 8.47935$ hartree > 0 (destabilizing).

The C=C bonds in $C_6(HC=CH)_3$ can be considered as the boundary between the electron-deficient and electron-rich groups. Starting from molecule $C_6(HC=CH)_3$, has become $\Delta E_{EX}(DP) > |\Delta E_{CT}(DP)|$, and the value (2.21964 hartree) of $\Delta E^{\pi}_{ab}(DP)$ is between the value of the molecule having π electron-deficient group and the value of the molecule having π electron-rich group.

10.3.3.4. $\Delta E(GP)$ versus $\Delta E^{\pi}_{ab}(DP)$

Figure 10-4 and Figure 10-5 indicate that the correlation between two variables $d\Delta r(GP)$ and $\Delta E(GP)$ are good. In order to prove the influence of the differences, in the CT and EX interactions, between the different molecules on the bond length alternation, that is, to understand how the structures of the XX (HX-XH, $X=X$, and XH) bonds determines the bond length alternation, it should be proved that the two variables $\Delta E(GP)$ and $\Delta E^{\pi}_{ab}(DP)$ are quantitatively related.

For eight molecules $C_6X_6H_6$ ($X = N, P, C, B, Al, Ga$) and $C_6X_3H_3$ ($X = B, Al$) (Figure 10-6a) and for eight molecules $C_6X_6H_6$ ($X = N, P, As, B, Al, Ga$) and $C_6X_3H_3$ ($X = Al, Ga$) (Figure 10-6b), interestingly, the energy differences $\Delta E_e(GP)$ and $\Delta E(GP)$ can be well fitted as the following polynomial function of $\Delta E^{\pi}_{ab}(DP)$ (x) :

$$\Delta E_e(GP) = 8.04996 + 1.42303x - 0.00759x^2 - 0.00476x^3 \quad (cc = 0.9207)$$

$$\Delta E(GP) = -0.04879 + 0.00906x + 0.00106x^2 + (2.61591 \times 10^{-5})x^3 \quad (cc = 0.9122)$$

So far, the large differences, in $\Delta r(G)$ and $d\Delta r(GP)$, between the molecules $C_6N_6H_6$ and $C_6B_6H_6$ has been well interpreted. Now, we can say that it is due to the fundamental differences in the CT and EX π -interactions, rather than the difference in the inductive effect, to cause the great differences, in the $d\Delta r(GP)$ and $\Delta r(G)$, between these

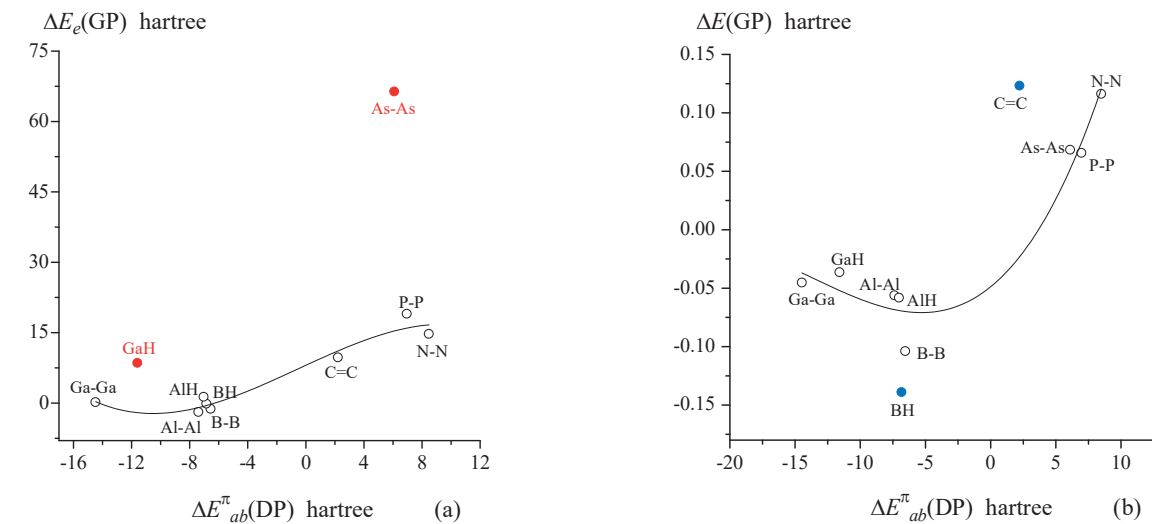


Figure 10-6. $\Delta E_e(\text{GP})$ and $\Delta E(\text{GP})$ can be fitted as polynomial function of $\Delta E_{ab}^\pi(\text{DP})$ at RHF/6-31G* level.

two molecules. Or it is the difference, in the π -electron occupancy, between the B-B and N-N bonds to cause the great difference, in the distortion of central ring, between the two molecules.

For ASRMs, as will be further shown, the π -electron occupancy of heteroatom groups, i. e. electron-richness or electron-deficiency, is a very important electronic structure factor that determines the π -distortion.

10.4. FORCES ACTING ON RING BONDS

For a specific molecule such as benzotricyclobutadiene (**10-12**), the relationship between $\Delta r_{ij}(\text{GP})$ and $\Delta E_{ij}(\text{GP})$ has been qualitatively discussed using the energy decomposition (Figure 10-2). In order to further confirm the role of π -electron delocalization in determining the bond length alternation, the relationship between $\Delta r_{ij}(\text{GP})$ ($ij = 12, 16$) and the forces $\Delta F_{ij}(\text{GP})$ acting on the C(i)-C(j) of central ring should be quantitatively determined, where the $\Delta F_{ij}(\text{GP})$ is defined as an average force acting on the C(i)-C(j) bond by the following Equation:

$$\Delta F_{ij}(\text{GP}) = |\Delta E_{ij}(\text{GP})| / \Delta r_{ij}(\text{GP}) \quad (10-1)$$

In the above Equation, C(1)-C(2) ($ij = 12$) is an endocyclic bond, C(1)-C(6) ($ij = 16$) is an exocyclic bond (seeing the numbering system of atoms in Figure 10-1a), $\Delta r_{ij}(\text{GP}) = r_{ij}(\text{G}) - r_{ij}(\text{PLG})$ is the difference, in the distance of C(i)-C(j) bond ($ij = 12$ or 16), between the ground state (G) geometry and its PLG, and $\Delta E_{ij}(\text{GP}) = E_{ij}(\text{G}) - E_{ij}(\text{PLG})$ is the energy component difference corresponding to $\Delta r_{ij}(\text{GP})$. The energy components, $E_{ij}(\text{G})$ and $E_{ij}(\text{PLG})$, are defined in Figure 10-2.

For each molecule, as shown by the data listed in Table 10-5 and Table 10-6, the sign of the $\Delta E_{ij}(\text{GP})$ value is the same as that of the $\Delta r_{ij}(\text{GP})$ value. In Equation (10-1), therefore, the $\Delta E_{ij}(\text{GP})$ value is an absolute value, and the sign of the $\Delta F_{ij}(\text{GP})$ value is determined by the sign of the $\Delta r_{ij}(\text{GP})$ value. When $\Delta F_{ij}(\text{GP}) > 0$, the CC bond is subject to tensile force, leading to $\Delta r_{ij}(\text{GP}) > 0$. Otherwise, a force acting on the CC bond is a compression force, and $\Delta r_{ij}(\text{GP}) < 0$. Only exception is that, in molecule C₆Ga₃H₃, $\Delta E_{16}(\text{GP}) = -0.11988$ hartree < 0, but $\Delta r_{16}(\text{GP}) =$

Table 10-5. For 19 Strained-Aromatic Molecules, Energy Effect $\Delta E_{12}(\text{GP})$ and Force, $\Delta F_{12}(\text{GP})$ (X) hartree/Å, Acting on C(1)-C(2) Bond due to π -Delocalization, and Their Causing the Change, $\Delta r_{12}(\text{GP})$ (Y), in C(1)-C(2) Bond Length (Å), and the Bond Stiffness G_{12} (hartree/Å²), Obtained from Our 2011 Method at RHF/6-31G* Level.

Mols	$\Delta E_{12}(\text{GP})$	$\Delta F_{12}(\text{GP})$	$\Delta r_{12}(\text{GP})$	G_{12}	$\Delta r_{12}(\text{GP})_T$	dy/dx
ASRMs		$y = 0.01901 - (9.64267\text{E-}5) * x + (1.74744\text{E-}7) * x^2 - (1.01506\text{E-}10) * x^3$				
C ₆ N ₆ H ₆	1.00871	25.86436	0.039	663.18872	0.017	-0.00009
C ₆ P ₆ H ₆	0.79814	36.27954	0.022	3298.14050	0.013	-0.00007
C ₆ As ₆ H ₆	0.62100	34.50000	0.018	1916.66667	0.016	-0.00008
C ₆ B ₃ H ₃	1.01672	169.45333	0.006	28242.22167	0.007	-0.00005
C ₆ Al ₃ H ₃	0.85312	853.12000	0.001	853120.00000	0.001	-0.00002
C ₆ Ga ₃ H ₃	1.76457	252.08143	0.007	36011.63286	0.004	-0.00003
C ₆ B ₆ H ₆	0.50636	506.36000	0.001	506360.00000	0.002	0.00000
C ₆ Al ₆ H ₆	0.83800	167.60000	0.005	33520.00000	0.007	-0.00005
C ₆ Ga ₆ H ₆	1.37344	228.90667	0.006	38151.11167	0.005	-0.00003
AASRMs		$y = 0.47817 - 0.01979 * x + (3.18576\text{E-}4) * x^2 - (1.63426\text{E-}6) * x^3$				
C ₆ N ₃ H ₃	9.40985	10.87844	0.865	12.57623	0.298	-0.01344
C ₆ P ₃ H ₃	4.03401	33.06566	0.122	271.03000	0.113	-0.00408
C ₆ As ₃ H ₃	6.98060	67.12115	0.104	645.39567	0.091	0.00089
C ₆ N ₆	3.50076	32.41444	0.108	300.13370	0.116	-0.00429
C ₆ P ₆	4.64491	55.29655	0.084	658.29226	0.082	0.00045
C ₆ As ₆	7.11664	94.88853	0.075	1265.18040	0.072	-0.00348
C ₆ B ₆	3.20852	10.45121	0.307	34.04303	0.304	-0.01367
C ₁₂ H ₆	3.54713	29.07484	0.122	238.31836	0.132	-0.00541
C ₆ Si ₆ H ₆	3.99324	43.88176	0.091	482.21714	0.085	-0.00127
C ₆ Ge ₆ H ₆	5.66732	72.65795	0.078	931.51218	0.095	0.00062

$\Delta r_{12}(\text{GP})$ are obtained from the geometry optimization at B3LYP/6-31G* level. The energy effects, such as $\Delta E_{12}(\text{GP})$, are obtained from the RHF/6-31G* single-point energy calculation on the B3LYP/6-31G* optimized geometry;

0.019 Å > 0, implying that when covalent radius is large enough, the $1/2[\Delta E_{ii}(\text{GP}) + \Delta E_{jj}(\text{GP})]$ should be a greater part of the force acting on the C(i)-C(j) bond, and it seems that $\Delta F_{ij}(\text{GP})$ should be defined as the following:

$$\Delta F_{ij}(\text{GP}) = [(1/2)\Delta E_{ii}(\text{GP}) + (1/2)\Delta E_{jj}(\text{GP}) + \Delta E_{ij}(\text{GP})]/\Delta r_{ij}(\text{GP})$$

For molecule C₆B₃H₃, for example, the energy components (hartree) are as follows:

Table 10-6. For 19 Strained Aromatic Molecules, $\Delta E_{16}(\text{GP})$ (X) (hartree/Å), $\Delta r_{16}(\text{GP})$ (Y) (Å), and the Bond Stiffness G_{16} (hartree/Å²), the First Order Derivative, dy/dx , of the Fitted Function $y = f(x)$, Obtained From Our 2011 Method at RHF/6-31G* Level.

Mols	$\Delta E_{16}(\text{GP})$	$\Delta F_{16}(\text{GP})$	$\Delta r_{16}(\text{GP})$	G_{16}	$\Delta r_{16}(\text{GP})_T$	dy/dx	$r_{16}(\text{PLG})$
ASRMs		$Y = 0.01748 + (3.60313\text{E-}4) * X + (1.73805\text{E-}6) * X^2 + (2.68928\text{E-}9) * X^3$					
C ₆ N ₆ H ₆	-0.82239	-274.13000	-0.003	91376.66667	-0.006	0.00001	1.382
C ₆ P ₆ H ₆	-1.55530	-222.18571	-0.007	31740.81571	-0.006	-0.00001	1.385
C ₆ As ₆ H ₆	-2.37174	-296.46750	-0.008	37058.43750	-0.007	0.00004	1.379
C ₆ B ₃ H ₃	1.07390	29.83056	0.036	828.62667	0.030	0.00047	1.400
C ₆ Al ₃ H ₃	0.70977	27.29885	0.026	1049.95577	0.029	0.00046	1.398
C ₆ Ga ₃ H ₃	-0.11988	6.30947	0.019	332.07737	0.020	0.00038	1.396
C ₆ B ₆ H ₆	2.19555	53.55000	0.041	1306.09756	0.042	0.00057	1.405
C ₆ Al ₆ H ₆	1.62723	73.96500	0.022	3362.04545	0.055	0.00066	1.412
C ₆ Ga ₆ H ₆	2.08464	104.23200	0.020	5211.60000	0.077	0.00081	1.400
AASRMs		$Y = -0.10784 - 0.00143 * X - (8.40316\text{E-}6) * X^2 - (1.36093\text{E-}8) * X^3$					
C ₆ N ₃ H ₃	-8.49559	-52.44191	-0.162	323.71549	-0.054	0.00220	1.377
C ₆ P ₃ H ₃	-4.59942	-79.30034	-0.058	1367.24724	-0.040	0.00251	1.380
C ₆ As ₃ H ₃	-7.26327	-137.04283	-0.053	2585.71377	-0.035	0.00297	1.377
C ₆ N ₆	-2.31751	-35.11379	-0.066	532.02712	-0.067	0.00197	1.402
C ₆ P ₆	-2.94409	-68.46721	-0.043	1592.26070	-0.045	0.00239	1.402
C ₆ As ₆	-5.17235	-139.79324	-0.037	3778.19568	-0.035	0.00298	1.393
C ₆ B ₆	-0.42223	-8.27902	-0.051	162.33373	-0.097	0.00157	1.377
C ₁₂ H ₆	-3.22305	-56.54474	-0.057	992.01298	-0.051	0.00225	1.395
C ₆ Si ₆ H ₆	-3.02806	-77.64256	-0.039	1990.83487	-0.041	0.00249	1.397
C ₆ Ge ₆ H ₆	-6.04346	-159.03842	-0.038	4185.22158	-0.038	0.00307	1.389

$\Delta r_{16}(\text{GP})$ are obtained from the geometry optimization at B3LYP/6-31G* level. The energy effects, such as $\Delta E_{16}(\text{GP})$, are obtained from the RHF/6-31G* single-point energy calculation on the B3LYP/6-31G* optimized geometry.

$$\Delta E_{11}(\text{GP}) = 0.47505, \Delta E_{66}(\text{GP}) = 0.47605, \Delta E_{16}(\text{GP}) = 1.07390$$

$$\Delta E_{16}(\text{GP}) / (1/2[\Delta E_{11}(\text{GP}) + \Delta E_{66}(\text{GP})]) \approx 2.2$$

For molecule C₆Al₃H₃:

$$\Delta E_{11}(\text{GP}) = 0.49187, \Delta E_{66}(\text{GP}) = 0.49188, \Delta E_{16}(\text{GP}) = 0.70977$$

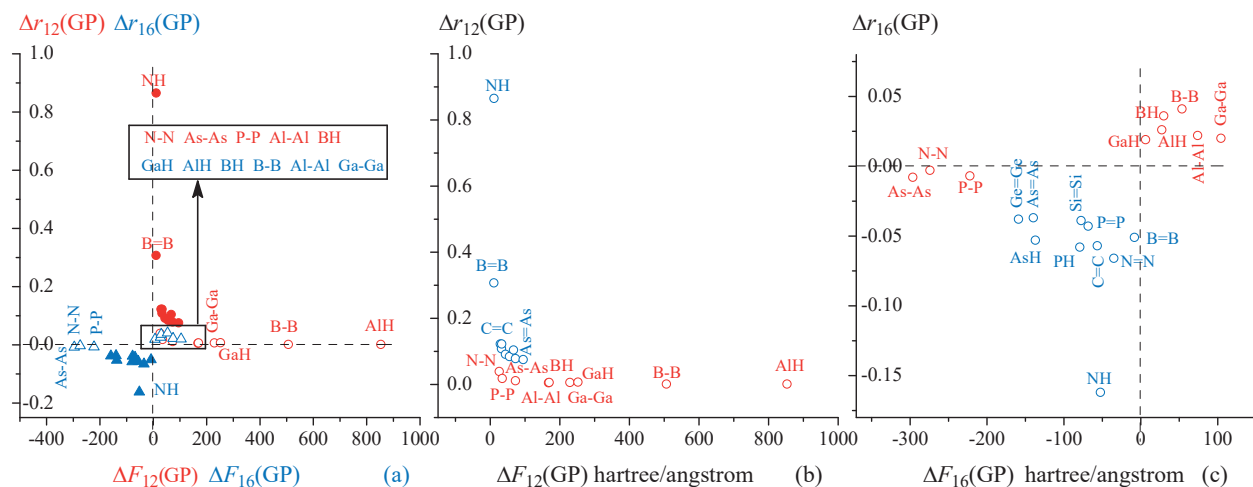


Figure 10-7. For 19 molecules: (a) Scatter plot of $\Delta r_{12}(\text{GP})$ (\AA) versus $\Delta F_{12}(\text{GP})$ (hartree/ \AA) (the red circles), and that of $\Delta r_{16}(\text{GP})$ versus $\Delta F_{16}(\text{GP})$ (the blue triangles). (b) Scatter plot of $\Delta r_{12}(\text{GP})$ (\AA) versus $\Delta F_{12}(\text{GP})$. (c) Scatter plot of $\Delta r_{16}(\text{GP})$ (\AA) versus $\Delta F_{16}(\text{GP})$.

$$\Delta E_{16}(\text{GP})/(1/2[\Delta E_{11}(\text{GP}) + \Delta E_{66}(\text{GP})]) \approx 1.4$$

But for molecule $\text{C}_6\text{Ga}_3\text{H}_3$

$$\Delta E_{11}(\text{GP}) = 1.37224, \Delta E_{66}(\text{GP}) = 1.37351, \Delta E_{16}(\text{GP}) = -0.11988$$

$$\Delta E_{16}(\text{GP})/(1/2[\Delta E_{11}(\text{GP}) + \Delta E_{66}(\text{GP})]) \approx -0.09$$

However, the good correlation between $\Delta F_{ij}(\text{GP})$ and $\Delta r_{ij}(\text{GP})$ will indicate that the simple definition of $\Delta F_{ij}(\text{GP})$ by Equation (10-1) can be considered reasonable.

For $\Delta r_{12}(\text{GP})$ versus $\Delta F_{12}(\text{GP})$, as shown by the scattered red hollow circles (including red solid circles) in Figure 10-7a, always $\Delta F_{12}(\text{GP}) > 0$, and $\Delta r_{12}(\text{GP}) > 0$. The endocyclic bonds are always subject to tensile force due to π -interaction (π -delocalization) between the central and the X-X (or XH groups) bonds, and it always is lengthened. For $\Delta r_{16}(\text{GP})$ versus $\Delta F_{16}(\text{GP})$, as indicated by the blue triangle points in Figure 10-7a, whether the exocyclic bonds are lengthened or shortened due to π -delocalization depends on the specific molecular structure (including the geometrical and electronic structure). For molecule $\text{C}_6\text{N}_6\text{H}_6$ with the electron-rich groups $-\text{NH}-\text{NH}-$, for example,

$$\begin{aligned}\Delta r(\text{PLG}) &= 0.11 \text{ \AA}, \\ \Delta F_{12}(\text{GP}) &= 25.86 \text{ hartree/\AA} \\ \Delta r_{12}(\text{GP}) &= 0.039 \text{ \AA} \\ \Delta F_{16}(\text{GP}) &= -274.13 \text{ hartree/\AA} \\ \Delta r_{16}(\text{GP}) &= -0.003 \text{ \AA} \\ |\Delta F_{16}(\text{GP})|/\Delta F_{12}(\text{GP}) &> 10 \\ \Delta r_{16}(\text{GP})/\Delta r_{12}(\text{GP}) &= 1/13\end{aligned}$$

For molecule $\text{C}_6\text{B}_6\text{H}_6$ with the electron-deficient groups $-\text{B}-\text{B}-$

$$\Delta r(\text{PLG}) = 0.11 \text{ \AA}$$

$$\Delta F_{12}(\text{GP}) = 506.36 \text{ hartree}/\text{\AA},$$

$$\Delta r_{12}(\text{GP}) = 0.001 \text{ \AA}$$

$$\Delta F_{16}(\text{GP}) = 53.55 \text{ hartree}/\text{\AA},$$

$$\Delta r_{16}(\text{GP}) = 0.041 \text{ \AA}$$

$$\Delta F_{16}(\text{GP})/\Delta F_{12}(\text{GP}) \approx 0.1$$

$$\Delta r_{16}(\text{GP})/\Delta r_{12}(\text{GP}) = 41$$

The annulated four-membered rings in molecules $\text{C}_6\text{N}_6\text{H}_6$ and $\text{C}_6\text{B}_6\text{H}_6$ are all aromatic, but the electron occupancies (electron-richness or electron-deficiency) of the N-N and B-B groups are different. The following comparisons well interpret why, in the ground state geometry, the bond length alternation ($\Delta r(\text{G}) = 0.053 \text{ \AA}$) for $\text{C}_6\text{N}_6\text{H}_6$ is so different from that ($\Delta r(\text{G}) = -0.029 \text{ \AA}$) for $\text{C}_6\text{B}_6\text{H}_6$:

- (i) In the PLG of two molecules $\text{C}_6\text{N}_6\text{H}_6$ and $\text{C}_6\text{B}_6\text{H}_6$, both $\Delta r(\text{PLG}) = 0.11 \text{ \AA}$.
- (ii) For endocyclic CC bond, $\Delta r_{12}(\text{GP}) = 0.039 \text{ \AA}$ ($\text{C}_6\text{N}_6\text{H}_6$) > $\Delta r_{12}(\text{GP}) = 0.001 \text{ \AA}$ ($\text{C}_6\text{B}_6\text{H}_6$).
- (iii) For exocyclic CC bond, $\Delta r_{16}(\text{GP}) = -0.003 \text{ \AA}$ ($\text{C}_6\text{N}_6\text{H}_6$) < $\Delta r_{16}(\text{GP}) = 0.041 \text{ \AA}$ ($\text{C}_6\text{B}_6\text{H}_6$).

10.4.1. Endocyclic Bonds

For 19 molecules, as indicated by the data listed in Table 10-5 and as shown by the red cycles located in the region ($x > 0$, $y > 0$) of Figure 10-7a, always $\Delta F_{12}(\text{GP}) > 0$, and $\Delta r_{12}(\text{GP}) > 0$.

For 17 molecules (not include molecules C_6B_6 and $\text{C}_6\text{N}_3\text{H}_3$), as shown by scattered points in Figure 10-7b, the domains of the $\Delta F_{12}(\text{GP})$ for the red (ASRMs) and blue (AASRMs) circles are, respectively, [25.86, 853.12] and [29.07, 94.89]. Therefore, the domain width of $\Delta F_{12}(\text{GP})$ for red circles is 827.26 hartree/ \AA , and it is approximately 12 times that (65.82 hartree/ \AA) for blue circles. On the contrary, the range height (0.038 \AA) of the $\Delta r_{12}(\text{GP})$ for the red circles is close to that (0.047 \AA) for the blue triangles. In order to measure the ability of this CC bond to resist deformation, the stiffness of a specific CC bond, G_{ij} ($ij = 12, 16$), is defined by the following Equation:

$$G_{ij} = \Delta F_{ij}(\text{GP})/\Delta r_{ij}(\text{GP})$$

For C(1)-C(2) bond, as indicated by the data listed in Table 10-5, the stiffness G_{12} of different molecules is rather different. G_{12} (853120.00000 hartree/ \AA^2) of $\text{C}_6\text{Al}_3\text{H}_3$ is the largest among 19 molecules, and that (12.57623 hartree/ \AA^2) of $\text{C}_6\text{N}_3\text{H}_3$ is the smallest. In general, the G_{12} for ASRMs is higher than for AASRMs. For $\text{C}_6\text{As}_6\text{H}_6$ belonging to ASRM, for example, $G_{12} = 1916.66667 \text{ hartree}/\text{\AA}^2$, it is the second lowest of all ASRMs, but it is higher than those for all AASRMs.

10.4.1.1. Aromatic Small Ring Molecules

For eight ASRMs, as shown by the red curve line in Figure 10-8a, $\Delta r_{12}(\text{GP})$ (y) can be fitted as the following third order polynomial function of $\Delta F_{12}(\text{GP})$ (x) ($\text{cc} = 0.8000$):

$$y = 0.01901 - (9.64267 \cdot 10^{-5})x + (1.74744 \cdot 10^{-7})x^2 - (1.01506 \cdot 10^{-10})x^3$$

$$dy/dx = -9.64267 \cdot 10^{-5} + (3.49488 \cdot 10^{-7})x - (3.04518 \cdot 10^{-10})x^2$$

The vertical offset of the point "N-N" is 0.022 \AA , and it is so great that the function curve fitting does not include the point "N-N". From point "As-As" to point "B-B", the first order derivative $dy/dx < 0$, indicating that a smaller change of the force $\Delta F_{12}(\text{GP})$ corresponds to a larger bond length change $\Delta r_{12}(\text{GP})$ (the stiffness is higher).

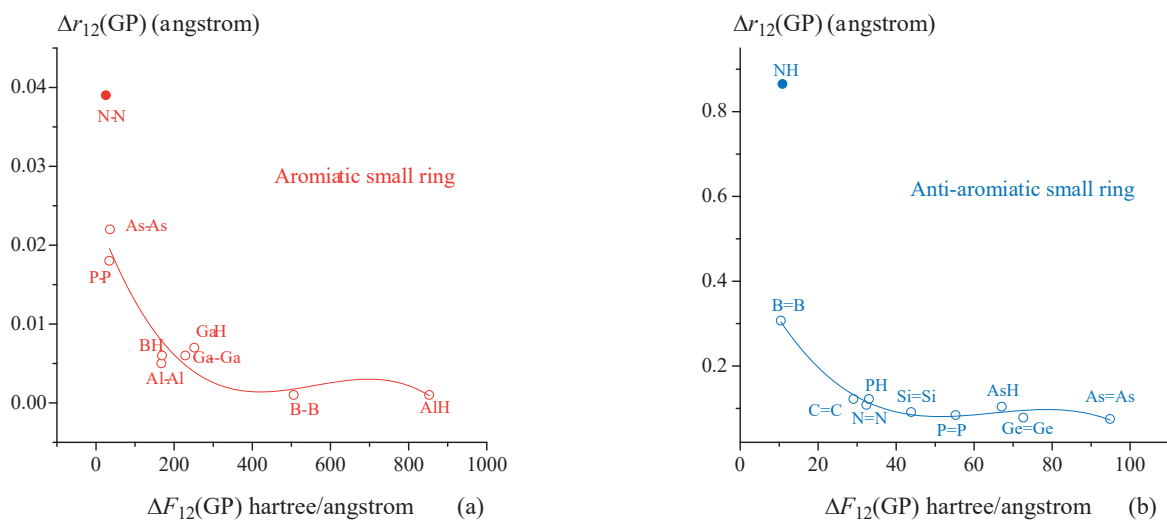


Figure 10-8. At RHF/6-31G* level, $\Delta r_{12}(\text{GP})$ can be fitted as the polynomial function of $\Delta F_{12}(\text{GP})$. (a) For eight ASRMs. (b) For nine AASRMs.

For six ASRMs $C_6X_6H_6$ and $C_6X_3H_3$ ($X = B, Al, Ga$) with electron-deficient groups, the first order derivative dy/dx of the fitted function is almost equal to zero (Table 10-5, Figure 10-8a). From the point "Al-Al" to the point "AlH", the tensile force $\Delta F_{12}(\text{GP})$ acting on an endocyclic bond increases from 167.60 to 853.12 (hartree/Å), but the corresponding $\Delta r_{12}(\text{GP})$ almost keeps unchanged, and $\Delta r_{12}(\text{GP}) < 0.007 \text{ Å}$. For molecule $C_6Al_3H_3$, for example, the endocyclic bond is elongated under the maximum tensile force (853.12 hartree/Å), but the change in length ($\Delta r_{12}(\text{GP}) = 0.001 \text{ Å}$) is minimal.

On the contrary, for a molecule with electron-rich groups, such as $C_6N_6H_6$, $\Delta F_{12}(\text{GP})$ is 25.86 hartree/Å, and it is the smallest among 9 ASRMs, but the corresponding the change in length, $\Delta r_{12}(\text{GP})$ (0.039 Å), is the largest (Table 10-5).

For the ASRMs with the electron-deficient groups, the stiffness of endocyclic bond is much higher than for the ASRMs with the electron-rich groups.

10.4.1.2. Anti-aromatic Small Ring Molecules

For nine AASRMs, as shown by the blue curve line in Figure 10-8b, $\Delta r_{12}(\text{GP})$ (y) can be well fitted as the following third order polynomial function of $\Delta F_{12}(\text{GP})$ (x) ($cc = 0.9705$):

$$y = 0.4782 - 0.0198x + (3.1858 \times 10^{-4})x^2 - (1.6343 \times 10^{-6})x^3.$$

A solid blue circle, denoted as "NH", lies away from the fitted function line, and its offset from the fitted line is 0.567 Å. So, the fit of the function curve does not include this point.

Table 10-5 shows that the first order derivative dy/dx for AASRMs is larger than that for ASRMs. In general, the stiffness of the endocyclic bond in the AASRMs is lower than that in the ASRMs, and the smaller $\Delta F_{12}(\text{GP})$ also corresponds to the larger $\Delta r_{12}(\text{GP})$.

10.4.2. Exocyclic Bonds

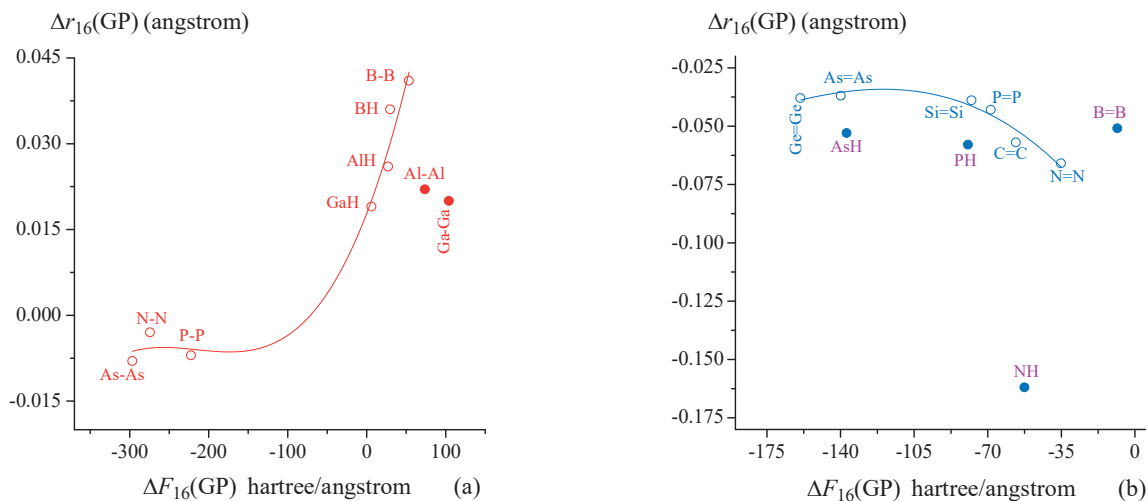


Figure 10-9. $\Delta r_{16}(\text{GP})$ (\AA) can be fitted as the polynomial function of $\Delta F_{16}(\text{GP})$ at RHF/6-31G* level. (a) For nine ASRMs; (b) For six of ten AASRMs

All the blue circles corresponding to 10 AASRMs are located on the area ($x < 0$, $y < 0$) of Figure 10-7c, indicating that always $\Delta F_{16}(\text{GP}) < 0$, $\Delta r_{16}(\text{GP}) < 0$ (Table 10-6). For AASRMs whose heteroatoms belonging to the same family, a larger $\Delta F_{16}(\text{GP})$ not always causes a larger change in $\Delta r_{16}(\text{GP})$, but the stiffness G_{16} increases as the atomic number increases. For nitrogen family, for example, the size order of stiffness G_{16} (hartree/ \AA^2) are as follows:

$$\begin{aligned} 323.71549 (\text{NH}) &< 1367.24724 (\text{PH}) < 2585.71377 (\text{AsH}), \\ 532.02712 (\text{N=N}) &< 1592.26070 (\text{P=P}) < 3778.19568 (\text{As=As}), \\ 0.174 (\text{N=N}) &> 0.127 (\text{P=P}) > 0.112 (\text{As=As}) \quad (d\Delta r(\text{GP})) \end{aligned}$$

These size orders indicate that the influence of π -delocalization on the degree and direction of bond length alternation becomes smaller as the atomic covalent radius increases.

In Figure 10-7c, the area occupied by the blue circles divides the red circles into two groups that are far apart from each other. All the red circles are above the blue circles. A group of red circles on the left correspond to the ASRMs with electron-rich groups, and a group of red circles on the right correspond to the ASRMs with electron-deficient groups. For all the ASRMs (red circles) except for $C_6B_6H_6$, their $\Delta r_{16}(\text{GP})$ are smaller in the absolute value than those for AASRMs (blue solid circles).

For three ASRMs $C_6X_6H_6$ with the electron-rich groups $HX-XH$ ($X = N, P, As$), always $\Delta F_{16}(\text{GP}) < 0$, $\Delta r_{16}(\text{GP}) < 0$. Particularly, the absolute values of $\Delta F_{16}(\text{GP})$ and $\Delta r_{16}(\text{GP})$ are, respectively, the greatest and smallest of 19 molecules. The corresponding stiffness G_{16} is the highest.

For six ASRMs $C_6X_6H_6$ and $C_6X_3H_3$ with the electron-deficient group (-XH- and -HX-XH-, $X = B, Al, Ga$), always $\Delta F_{16}(\text{GP}) > 0$, $\Delta r_{16}(\text{GP}) > 0$

10.4.2.1. Aromatic Small Ring Molecule

For seven ASRMs, as shown by the red curve line in Figure 10-9a, $\Delta r_{16}(\text{GP})$ (y) can be well fitted as the following third order polynomial function of $\Delta F_{16}(\text{GP})$ (x) ($cc = 0.9553$):

$$y = 0.01748 + (3.6031 \times 10^{-4})x + (1.73805 \times 10^{-6})x^2 + (2.68928 \times 10^{-9})x^3$$

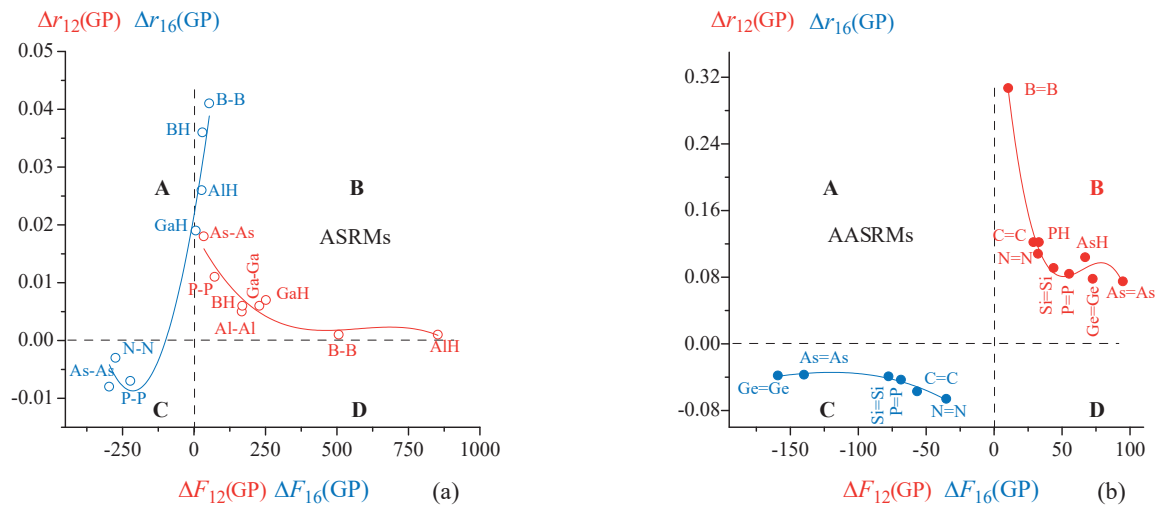


Figure 10-10. $\Delta r_{12}(\text{GP})$ versus $\Delta F_{12}(\text{GP})$ (red circles), and $\Delta r_{16}(\text{GP})$ versus $\Delta F_{16}(\text{GP})$ (blue circles). And their comparisons.

Two molecules, $C_6Al_6H_6$ and $C_6Ga_6H_6$, are not included in the function curve fitting, and their vertical offsets from the functional line are -0.033 and -0.057 Å. Among the seven molecules involved in the function curve fitting, the vertical offset of the data point "BH" is largest, but it is only 0.006 Å.

In Figure 10-10a, the X-Y coordinate plane is divided into 4 regions denoted as A ($X < 0, y > 0$), B ($x > 0, y > 0$), C ($X < 0, y < 0$), and D ($x > 0, y < 0$). The blue and red circles, corresponding to the ASRMs $C_6X_6H_6$ with the electron-rich HX-XH ($X = N, P, As$), are located in regions B and C. For these molecules, therefore, always $\Delta F_{12}(\text{GP}) > 0$, $\Delta r_{12}(\text{GP}) > 0$, and always $\Delta F_{16}(\text{GP}) < 0$, $\Delta r_{16}(\text{GP}) < 0$, and $\Delta r_{12}(\text{GP}) > |\Delta r_{16}(\text{GP})|$. For $C_6N_6H_6$, for example, the forces acting on C(1)-C(6) and C(1)-C(2) bonds are, respectively, compressive force and tensile force, that is, $\Delta F_{16}(\text{GP}) < 0$ and $\Delta F_{12}(\text{GP}) > 0$. The compressive force (-274.13000 hartree/Å) is about 11 times of the tensile force (25.86436 hartree/Å), but $|\Delta r_{16}(\text{GP})|/\Delta r_{12}(\text{GP}) = 1/13$. In this case, the stiffness of C(1)-C(6) bond is much higher than that of C(1)-C(2) bond. As a result, the degree of bond length alternation, $\Delta r = r_{\text{endo}} - r_{\text{exo}}$, increases from $\Delta r(\text{PLG}) = 0.011$ Å to $\Delta r(\text{G}) = 0.053$ Å.

For ASRMs, $C_6X_6H_6$ and $C_6X_3H_3$, with π electron-deficient groups XH-XH or XH ($X = B, Al, Ga$), the corresponding red and blue circles are all located in the region B of Figure 10-10a. For these molecules, always $\Delta F_{12}(\text{GP}) > 0$ and $\Delta r_{12}(\text{GP}) > 0$, and always $\Delta F_{16}(\text{GP}) > 0$ and $\Delta r_{16}(\text{GP}) > 0$, and $\Delta F_{16}(\text{GP}) > \Delta F_{12}(\text{GP})$. But whether $|\Delta r(\text{G})| > |\Delta r(\text{PLG})|$ or $|\Delta r(\text{G})| < |\Delta r(\text{PLG})|$, that is, the size and sign of $d\Delta r(\text{GP})$ depends upon the size and sign of $\Delta r(\text{PLG})$. For $C_6B_3H_3$ for example,

$$\Delta F_{12}(\text{GP}) = 169.45333 \text{ hartree}/\text{\AA} > 0, \Delta r_{12}(\text{GP}) = 0.006 \text{ \AA} > 0$$

$$\Delta F_{16}(\text{GP}) = 29.83056 \text{ hartree}/\text{\AA} > 0, \Delta r_{16}(\text{GP}) = 0.036 \text{ \AA} > 0$$

The force $\Delta F_{12}(\text{GP})$ is 5.7 times $\Delta F_{16}(\text{GP})$, but the corresponding $\Delta r_{12}(\text{GP})$ is 1/6 of $\Delta r_{16}(\text{GP})$. As a result, the stiffness of C(1)-C(2) bond is much higher than of C(1)-C(6), leading to the degree of bond length alternation, $\Delta r = r_{\text{endo}} - r_{\text{exo}}$, increases from $\Delta r(\text{PLG}) = -0.013$ Å to $\Delta r(\text{G}) = -0.043$ Å. In the case of molecule $C_6Al_3H_3$, $\Delta r_{16}(\text{GP})$ (0.026) $>$ $\Delta r_{12}(\text{GP})$ (0.001 Å), but $\Delta r(\text{PLG})$ (0.030 Å) $>$ $\Delta r(\text{G})$ (0.005 Å), and still $\Delta r(\text{G}) > 0$ due to that the positive value (0.030 Å) of $\Delta r(\text{PLG})$ is so large.

In the case of aromatic small ring molecules, in short, the influence of the CC bond distance changes $\Delta r_{16}(\text{GP})$ and $\Delta r_{12}(\text{GP})$ on $\Delta r(\text{G})$ is more complicated, but it does not need to be considered in this section. The main purpose

of this section is to demonstrate the quantitative relationship between two variables $\Delta F_{ij}(\text{GP})$ and $\Delta r_{ij}(\text{GP})$ and finally to confirm the decision role of π -delocalization in causing bond length alternation.

10.4.2.2. Anti-aromatic Small Ring Molecule

For six AASRMs, as shown by the blue hollow circles in Figure 10-9b, $\Delta r_{16}(\text{GP})$ (y) can be fitted as the following third order polynomial function of $\Delta F_{16}(\text{GP})$ (x) ($\text{cc} = 0.844$):

$$y = -0.1078 - 0.0014x - (8.4032 \times 10^{-6})x^2 - (1.3609 \times 10^{-8})x^3$$

The vertical offsets (-0.006 Å) of data point "C=C" is the greatest, and the smallest one is 0.000 Å for "Ge=Ge". Other four molecules $C_6X_3H_3$ ($X = N, P, As$) and C_6B_6 are not included in the function curve fitting, and their vertical offsets from the functional line are as follows: -0.108, -0.018, -0.018, 0.048 Å.

For AASRMs, as shown by Figure 10-10b, always $\Delta F_{16}(\text{GP}) < 0$, $\Delta F_{12}(\text{GP}) > 0$ and $|\Delta F_{16}(\text{GP})| > \Delta F_{12}(\text{GP})$. As the results, always $\Delta r_{16}(\text{GP}) < 0$, and always $\Delta r_{12}(\text{GP}) > 0$, leading to the change in Δr . For molecule C_6N_6 , for example,

$$\Delta F_{16}(\text{GP}) = -35.11379 \text{ hartree}/\text{\AA} < 0, \Delta F_{12}(\text{GP}) = 32.41444 \text{ hartree}/\text{\AA} > 0$$

$$|\Delta F_{16}(\text{GP})| > \Delta F_{12}(\text{GP}),$$

$$\Delta r_{16}(\text{GP}) = -0.066 \text{ \AA}, \Delta r_{12}(\text{GP}) = 0.108 \text{ \AA}$$

$$\Delta r(\text{PLG}) = r_{endo}(\text{PLG}) - r_{exo}(\text{PLG}) = -0.033 \text{ \AA}$$

$$\Delta r(\text{G}) = r_{endo}(\text{G}) - r_{exo}(\text{G}) = 0.141 \text{ \AA}$$

In the case of molecule C_6N_6 , due to the π -interaction between the central ring and the three N=N bonds, the direction of bond length alternation is changed from $r_{endo}(\text{PLG}) - r_{exo}(\text{PLG}) < 0$ to $r_{endo}(\text{G}) - r_{exo}(\text{G}) > 0$, and meanwhile the degree of bond length alternation increases from -0.033 Å to 0.141 Å.

10.5. C_6B_6 AND $C_6N_3H_3$

For most of strained-aromatic molecules, $d\Delta r(\text{GP})$ can be well fitted as a polynomial function of $\Delta E(\text{GP})$, and $\Delta r_{ij}(\text{GP})$ ($ij = 12$ or 16) can be well fitted as a polynomial function of $\Delta F_{ij}(\text{GP})$, which confirms again that π -delocalization plays a decision role in causing the bond length alternation.

However, as shown by an inspection of Table 10-3, C_6B_6 and $C_6N_3H_3$ are two very special molecules. For C_6B_6 , $\Delta r(\text{PLG}) = 0.065 \text{ \AA}$, and it is the greatest of the 19 molecules; for $C_6N_3H_3$, $r_{endo}(\text{G}) = 2.221 \text{ \AA}$, and the C(1)-C(2) bond has actually been broken in the ground state geometry. Accordingly, there should be another structural effect.

10.5.1. Bond Angle

For C_6B_6 , $\Delta r(\text{PLG}) = 0.065 \text{ \AA}$, the bond angle $\angle C-B=B$ in the ground state geometry is 94.8° , and the bond angle $\angle H-B=B$ of HB=BH molecule is 180° (Figure 10-3). $\Delta\beta(\text{G}) = \angle H-B=B - \angle C-B=B = 85.2^\circ$, and it is much larger than for other molecules C_6X_6 ($X = N, P, As$) and $C_6X_6H_6$ ($X = C, Si, Ge$) according to the data listed in Table 10-3. In Figure 10-4c, as a result, the vertical offset of a point "B=B" is 0.244 \AA . It is so great that, in Figure 10-4c, the function fitting does not include this molecule. The practical calculations indicate that it is impossible for the

structures of other two molecules C₆Al₆ and C₆Ga₆ to be obtained from the geometry optimization due to the X=X bond being broken.

For C₆N₃H₃, $\Delta\beta(G) = 120 - 107.8 = 12.2^\circ$, it is much smaller than for other two molecules C₆P₃H₃ and C₆As₃H₃, but its $\Delta\alpha(G)$ (85.9°) is much larger than for the other two molecules. It may be a reason why, in Figure 10-4c, the vertical offset of a point "NH" is abnormally great.

10.5.2. Bond Length

In the ground state geometry of C₆N₃H₃, the bond length $r_{C-N}(G) = 1.375 \text{ \AA}$ and $r_{endo}(G) = 2.221 \text{ \AA}$, if its bond angle $\angle CNC = 50^\circ$ (the average of bond angles $\angle CPC$ and $\angle CASC$ in the molecules C₆P₃H₃ and C₆As₃H₃), should be $r_{C-C} = 1.162 \text{ \AA}$. For the CC bond in the central ring, it is so shorter that the bond angle $\angle CNC$ (β) had to be enlarged in order to lengthen the endocyclic CC bond, resulting in decrease of bond angle α . In the case of molecules C₆P₃H₃ and C₆As₃H₃, the covalent radii (1.10 and 1.21) of the P and As atoms is larger than that (0.75) of nitrogen. In molecules C₆P₃H₃ and C₆As₃H₃, the bond lengths C-P and C-As are, respectively, 1.742 and 1.857 Å, and they are long enough to prevent the endocyclic bond from breaking. Accordingly, the bond length C-X may also play an important role to cause bond length alternation in a special case.

10.6. SECONDARY STRUCTURAL EFFECTS

In the case of PLG geometry, the bond length alternation is also noteworthy. For molecule C₆B₆H₆, for example, there are slight differences, in the bond angles α and β , between the PLG and the ground state (Figure 10-3), but $\Delta r(PLG) = 0.011 \text{ \AA} > 0$, and $\Delta r(G) = -0.029 \text{ \AA} < 0$, which, together with the fact that $\Delta r(PLG)(C_6B_6H_6) = \Delta r(PLG)(C_6N_6H_6) = 0.011 \text{ \AA}$, strongly question the role of the inductive effect of boron and nitrogen atom in causing the bond length alternation. In the PLG geometries of different strained-aromatic molecules in which the π -interaction has been excluded from between the central ring and the XX (or XH) groups, the structural factor that can cause the degrees of bond length alternation to be different is called the secondary structure effect.

Figure 10-11b shows that, for 15 molecules, $\Delta r(PLG)$ (y) can be, approximately, fitted as the following second order polynomial function of $\Delta\beta(PLG)$ (x) ($cc = 0.890$):

$$y = -0.0965 + 0.00638x - (1.21125 \times 10^{-4})x^2 + (7.73961 \times 10^{-7})x^3$$

Although the correlation of the two variables is not very good, the fitted line in Figure 10-11b can still show the following general trend: a larger $\Delta\beta(PLG)$ corresponding to a larger $\Delta r(PLG)$. The four molecules, C₆N₆, C₆P₆, C₆N₃H₃ and C₆B₃H₃, are not included in the function curve fitting, but the three of the four red solid circles, denoted as "N=N", "BH", "NH", also show such a trend.

For 19 molecules, as shown by the scattered blue circles in Figure 10-11a, there is no good correlation between the two variables $\Delta r(PLG)$ and $\Delta\alpha(PLG)$. According to the geometrical structures, the molecules can be divided into the three groups:

- (i) C₆X₃H₃ (X = N, P, As, B, Al, Ga);
- (ii) C₆X₆H₆ (X = B, Al, Ga, N, C, Si, Ge);
- (iii) C₆X₆ (X = N, P, As).

For each of three groups, as shown by the curve lines in Figure 10-11c, $\Delta r(PLG)$ can also be fitted as the polynomial

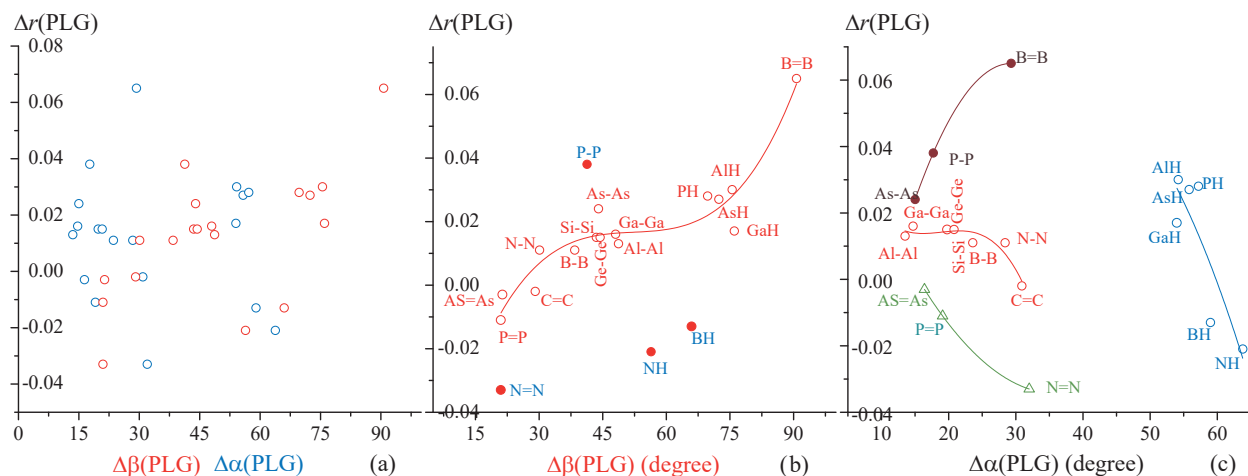
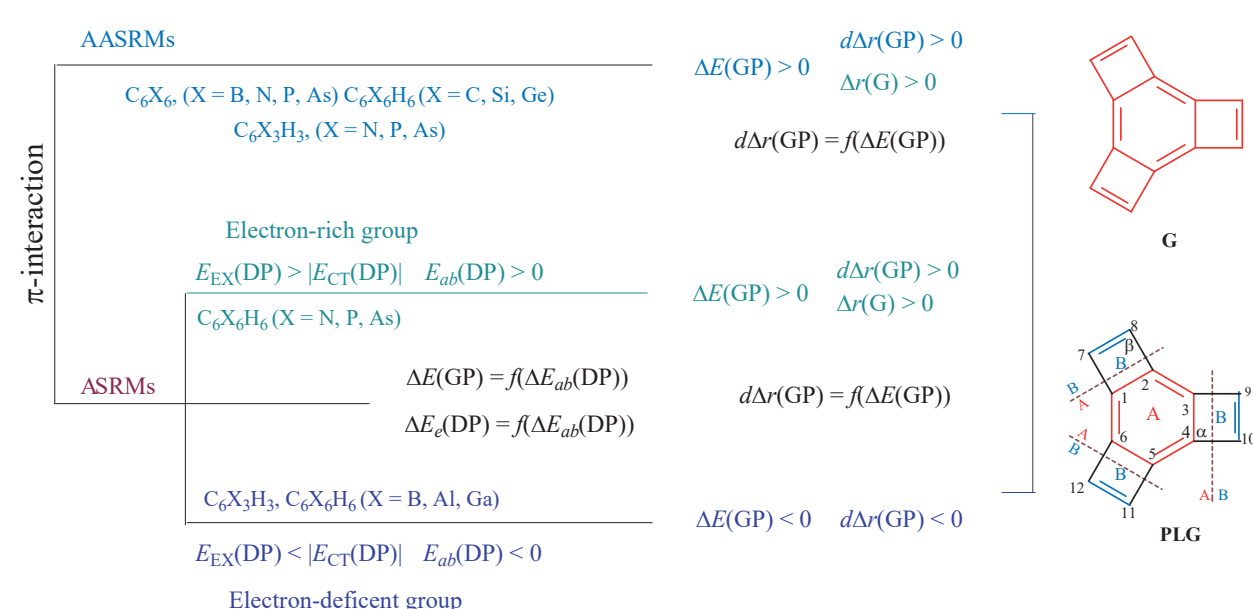


Figure 10-11. (b) For 15 molecules, $\Delta r(\text{PLG})$ (Å) versus $\Delta\beta(\text{PLG})$; (c) for four groups of molecules, $\Delta r(\text{PLG})$ versus $\Delta\alpha(\text{PLG})$

function of $\Delta\alpha(\text{PLG})$, and the correlation coefficients of the first two curve lines are only 0.545, 0.735. But unlike the $\Delta\beta(\text{PLG})$ effect, the three functions show that a larger $\Delta\alpha(\text{PLG})$ corresponds a smaller $\Delta r(\text{PLG})$.

So far, it can be concluded that, due to the difference in the angle β between the strained molecule and its corresponding molecule $\text{H}_2\text{X}-\text{XH}_2$ (or $\text{HX}=\text{XH}$), the angular strain may be a secondary effect that causes the CC bond lengths in the PLG to alternate. In other words, if this secondary effect exists, it can only be generated from $\Delta\beta(\text{PLG})$, and not from $\Delta\alpha(\text{PLG})$.

10.7. CONCLUSIONS



Scheme 10-7

In this Chapter, it has been confirmed again and again that π -delocalization plays a decision role in causing bond length alternation, through the discussion of the following two points:

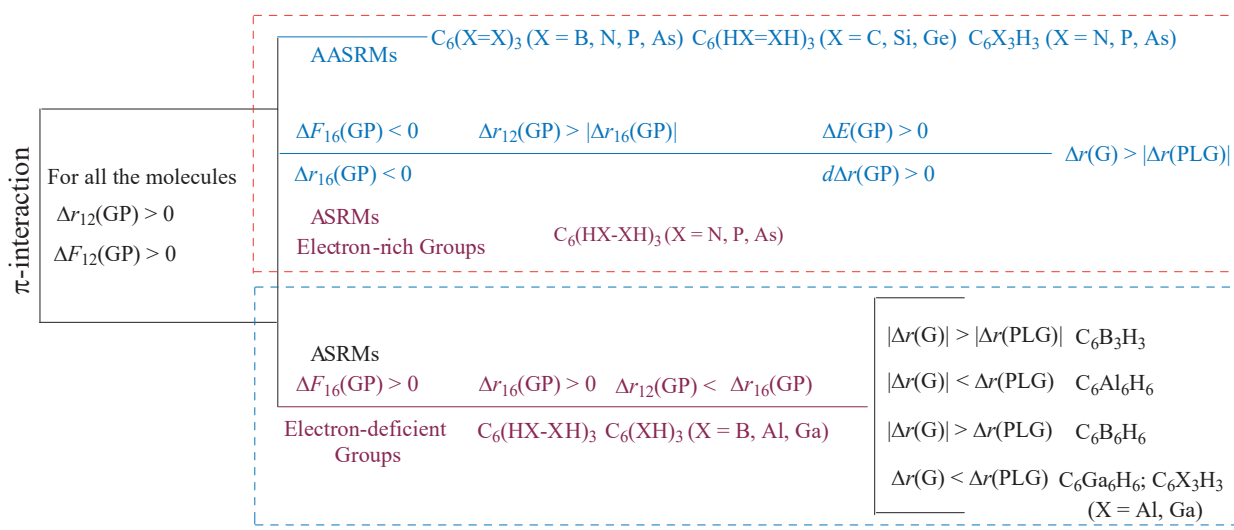
- (i) What structural factor causes bond length alternation?.
- (ii) What factors determine $r_{\text{endo}} > r_{\text{exo}}$ (or $r_{\text{endo}} < r_{\text{exo}}$)?

19 strained-aromatic molecules can be divided into two groups: aromatic small ring molecules, and anti-aromatic small ring molecules. For each of two groups of strained-aromatic molecules, $d\Delta r(\text{GP})$ can be well fitted as the polynomial function of $\Delta E(\text{GP})$. In the central ring of strained-aromatic molecule, the bond length alternation (BLA) should be attributed to the π -interaction (π -interaction between the central ring and the annulated small rings). The influences of the π -interaction (including CT and EX interactions) on the values (degree and direction) of $d\Delta r(\text{GP})$ and $\Delta r(\text{G})$ are summarized in Scheme 10-7. The electron occupancies of the groups (X-X, XH) and the aromaticity-antaromaticity of the annulated small ring determine the values of $d\Delta r(\text{GP})$ and $\Delta r(\text{G})$. For the AASRMs and for the ASRMs with electron-rich groups, always $\Delta E(\text{GP}) > 0$, $d\Delta r(\text{GP}) > 0$, and $\Delta r(\text{G}) > 0$. The influences are simple and straightforward, and there are no exception. For the ASRMs with electron-deficient groups, the influences are complicated.

The π -interaction produces the forces $\Delta F_{ij}(\text{GP})$ acting on the endocyclic and exocyclic bonds, and the $\Delta r_{ij}(\text{GP})$ can be fitted as the polynomial function of $\Delta F_{ij}(\text{GP})$. The influences of the π -interaction on the endo- and exocyclic bonds are summarized in Scheme 10-8. For all molecules, always $\Delta F_{12}(\text{GP}) > 0$, and $\Delta r_{12}(\text{GP}) > 0$. For all AASRMs and for ASRMs with electron-rich group, always $\Delta F_{16}(\text{GP}) < 0$, and $\Delta r_{16}(\text{GP}) < 0$, and $\Delta r(\text{G}) > \Delta r(\text{PLG})$. For these molecules, therefore, π -interaction is always a driving force for causing the single and double bonds in central ring to alternate. As far as the distortivity is concerned, the small ring with an electron-rich group in the three molecules $C_6X_6H_6$ (X = N, P, As) looks like anti-aromatic. For ASRMs with electron-deficient group, the influences are complicated (always $\Delta r(\text{G}) \neq \Delta r(\text{PLG})$), and are summarized in Scheme 10-8.

In summary, all the calculation results, summarized in Scheme 10-7 and Scheme 10-8, indicate that π -electron delocalization is distortive and is the main driving force for the distortion of the central benzene ring.

In the case of particular localized geometries of strained-aromatic molecules, the bond length alternation may also be found, and the distance difference $\Delta r(\text{PLG})$ between the endo- and exo-cyclic bonds in PLG can be fitted as



Scheme 10-8

the polynomial function of $\Delta\beta(\text{PLG})$. Therefore, as a secondary structure effect, $\Delta\beta(\text{PLG})$ can be considered as an angle strain, and it is a main driving force for distorting the central ring of PLG. But, the β angle strain is only a result of the mathematical relationship existing between the side lengths and angle size of a geometric shape (such as triangle and trapezoid).

In the case of strained-aromatic molecules, π -delocalization (interaction) determines the direction and degree of the bond length alternation of the central benzene ring, which is achieved by the following two structural factors:

- (i) The number of π -electrons in the annulated small ring (4n+2 rule).
- (ii) π -electron occupancy (π electron-sufficient and π electron-deficient) of the X-X bonds in the annulated small ring.

10.8. REFERENCES

- 1 Shaik, S.; Danovich, D.; Hiberty, P. C. 1997. "A Different Story of Benzene." *Theochem*, 398-399:155-167.
- 2 Yu, Z. H.; Li, L. T.; Fu, W.; Li, L. P. 1998. "Conformations of Stilbene-like Species and New Method of Energy Partition." *J. Phys. Chem. A*, 102: 2016-2028.
- 3 Yu, Z. H.; Xuan, Z. Q.; Wang, T. X.; Yu, H. M. 2000. "A Novel Energy Partition for Gaining New Insight into Aromaticity and Conjugation." *J. Phys. Chem. A*, 104: 1736-1747.
- 4 Yu, Z. H.; Peng, X. Q. 2001. "New Insight into the Nature of Electron Delocalization: The Driving Forces for Distorting the Geometry of Stilbene-Like Species." *J. Phys. Chem. A*, 105: 8541-8553.
- 5 Xu, H.; Yu, Z. H. 2004. "The Driving Forces for Distorting NBA-Like Species away From Their Planar Geometries." *J. Mol. Struct. (THEOCHEM)*, 682: 37-46.
- 6 Bao, P.; Yu, Z. H. 2006. "Theoretical Studies on the Role of π -Electron Delocalization in Determining the Conformation of N-benzylideneaniline with Three Types of LMO Basis Sets." *J. Comput. Chem.*, 27: 809-824.
- 7 Bao, P.; Yu, Z. H. 2007. "Restricted Geometry Optimization: A Different Way to Estimate Stabilization Energies for Aromatic Molecules of Various Types." *J. Phys. Chem. A*, 111: 5304-5313.
- 8 Bao, P.; Yu, Z. H. 2007. "Restricted Geometry Optimization: A Different Way to Estimate Stabilization Energies for Aromatic Molecules of Various Types." *J. Phys. Chem. A*, 111, Supporting Information.
- 9 Bao, P.; Yu, Z. H. 2011. "New Procedure to Evaluate Aromaticity at the Density Functional Theory, Hartree-Fock, and Post-Self- Consistent Field Levels." *J. Comput. Chem.*, 32: 248-259.
- 10 Yu, Z. H. 1994. "Quantitative Perturbational Molecular orbital Analysis of the Conformational Preference of Aniline Molecule and Its Intramolecular Force." *Computers Chem.*, 18: 95-102.
- 11 Briegleb, G. 1961. *Electronene-Donator-Komplexe*. Berlin: Springer-Verlag.
- 12 Rose, J. 1967. *Molecular Complexes*. London: Pergamon Press.
- 13 Andrews, L. J.; Keefer, R. M. 1964. *Molecular Complexes in Organic Chemistry*. San Francisco: Holden-Day, Inc..
- 14 Foster, R. 1969. *Organic Charge-Transfer Complexes*. London and New York: Academic Press.
- 15 Mulliken, R. S.; Person, W. B. 1969. *Molecular Complexes*. A Lecture and Reprint Volumie. New York: Wiley-Interscience.
- 16 Al-Subi, A. H. 2013. *Photoinduced Electron Transfer in Porphyrin- and Phthalocyanine- Fullerene Dyads in Non-Coordinating and Halide-Coordinating Environments*. Thesis for the degree of Doctor of Science in Technology at Tampere University of Technology.
- 17 Feng, P. L.; Leong, K.; Allendorf, M. D. 2012. "Charge-transfer Guest Interactions in Luminescent MOFs: Implications for Solid-State Temperature and Environmental Sensing." *Dalton Trans.*, 41: 8869-8877.
- 18 Pratibha, B.; Periandy, S.; Govindan, K. 1999. "Spectrophotometric Studies of Charge Transfer Complex

- between *p*-Chloranil and Certain Aromatic Amines at 302." Asian J. Chem., 11, 1205-1210.
- 19 Hashimoto, S.; Hagiwara, N.; Asahi, T.; Masuhara, H. 1999. "Do the Charge-Transfer Complexes of 1,2,4,5-Tetracyanobenzene with Arenes Serve as a Probe for Surveying Chemical Properties Inside the Cavities of Faujasite Zeolites? Time-Resolved and Steady-State Spectroscopic Studies." Langmuir, 15: 3123-3133.
- 20 Kumar, T. V.; Veeraiah, T.; Venkateshwarlu, G. 2000. "Molecular Complexes of Phenols with DDQ." Proc. Indian Acad. Sci. (Chem. Sci.), 112: 119-125.
- 21 Much references can be found from the following Website:
<http://worldwidescience.org/topicpages/c/charge+transfer+interaction.html>
- 22 Weiss, J. 1942. "The Formation and Structure of Some Organic Molecular Compounds." J. Chem. Soc., 245-252.
- 23 Brackmann, W. 1949. "Complexresonance. Preliminary Communication." Rec. Trav. Chim., 68: 147-159
- 24 Mulliken, R. S. 1952. "Molecular Compounds and their Spectra, II." J. Am. Chem. Soc., 74: 811-824.
- 25 Dewar, M. J. S.; Lepley, A. R. 1961. " π -Complexes. I. Charge Transfer Spectra of π -Complexes Formed by Trinitrobenzene with Polycyclic Aromatic Compounds." J. Am. Chem. Soc., 83: 4560-4563.
- 26 Bentley, M. D.; Dewar, M. J. S. 1967. "Some π -Molecular Complexes Showing No Charge Transfer Spectra Formed by P-Toluenesulfonic Esters." Tetrahedron Lett., 8: 5043-5047.
- 27 Hooper, H. O. 1964. "Lack of Charge Transfer in Aromatic Charge-Transfer Complexes." J. Chem. Phys., 41: 599-601.
- 28 Hanna, M. W. 1968. "Bonding in Donor-Acceptor Complexes. I. Electrostatic Contributions to The Ground-State Properties of Benzene-Halogen Complexes." J. Am. Chem. Soc., 90: 285-291.
- 29 Hanna, M. W.; Williams, D. E. 1968. "Bonding in Donor-Acceptor Complexes. II. Electrostatic Contributions to Changes in the Infrared Spectrum of Benzene-Halogen Complexes." J. Am. Chem. Soc., 90: 5358-5362.
- 30 Grozema, F. C.; Zijlstra, R. J.; Swart, M; Duijnen, P. T. v. 1999. "Iodine-Benzene Charge-Transfer Complex: Potential Energy Surface and Transition Probabilities Studied at Several Levels of Theory." Inter. J. Quant. Chem., 75: 709-723.
- 31 Kitaura, K.; Morokuma, K. 1976. "A New Energy Decomposition Scheme for Molecular Interactions within the Hartree-Fock Approximation." Inter. J. Quant. Chem., 10: 325-340.
- 32 Mo, Y. R.; Gao, J. L.; Peyerimhoff, S. D. 2000. "Energy Decomposition Analysis of Intermolecular Interactions Using a Block-Localized Wave Function Approach." J. Chem. Phys., 112: 5530-5538.
- 33 Weinhold, F.; Landis, C. R. 2005. *Valency and bond - A Natural Bond Orbital Donor-Acceptor Perspective*. New York: Cambridge University Press.
- 34 Khaliullin, R. Z.; Bell, A. T.; Head-Gordon, M. 2008. "Analysis of Charge Transfer Effects in Molecular Complexes Based on Absolutely Localized Molecular Orbitals." J. Chem. Phys., 128: 184112- 184128.
- 35 Adeniyi, A. A.; Ajibade, P. A. 2013. "Insights into the Intramolecular Properties of η^6 -Arene-Ru-Based Anticancer Complexes Using Quantum Calculations." J. Chem., 1-14.
- 36 GAMESS Manual, Section 2 - Input Description, Jun 2nd, 1994.
- 37 Mills, W. H; Nixon, I. G. 1930. "CCCXXXII.—Stereocochemical Influences on Aromatic Substitution. Substitution Derivatives of 5-Hydroxy-Hydrindene." J. Chem. Soc., 2510-2524.
- 38 Sutton, L. E.; Pauling, L. 1935. "A Wave-Mechanical Treatment of the Mills-Nixon Effect." Trans. Faraday Soc., 31: 939-945.
- 39 Bao, P.; Yu, Z. H. 2010. "Restricted Geometry Optimization for Estimating Stabilization Energies of Polycyclic Aromatic Hydrocarbons." J. Phys. Org. Chem., 23: 16-29.
- 40 Mo, Y.; Schleyer, P. v. R. 2006. "An Energetic Measure of Aromaticity and Antiaromaticity Based on the Pauling-Wheland Resonance Energies." Chem. Eur. J., 12: 2009-2020.
- 41 Diercks, R.; Vollhardt, K. P. C. 1986. "Tris(benzocyclobutadieno)benzene, the Triangle [4]Phenylene with a Completely Bond-Fixed Cyclohexatriene Ring: Cobalt- Catalyzed Synthesis from Hexaethynyl-benzene and Thermal Ring Opening to 1,2:5,6,9,10-Tribenzo-3,4,7, 8,11, 12-hexa-dehydro[12]annulene." J. Am. Chem. Soc., 108: 3150-3152.

- 42 Mitchell, R. H.; Chen , Y.; Iyer, V. S.; Lau, D. Y. K.; Baldridge, K. K.; Siegel, J. S. 1996. "Bond Fixation in a [14]Annulene: Synthesis, Characterization, and *ab Initio* Computations of Furan Adducts of Dimethyl-dihydropyrene." *J. Am. Chem. Soc.*, 118: 2907-2911.
- 43 Siegel, J. S. 1994. "Mills-Nixon Effect: Wherefore Art Thou?" *Angew. Chem. Int. Ed. Engl.*, 33: 1721-1723.
- 44 Nilsson, J. L.G.; Selander,H.; Sievertsson, H. Skanberg,I.; Svensson, K-G. 1971. "Directive Effects in the Bromination of Bicyclic Phenols Relevance for the Mills-Nixon Effect." *Acta, Chem. Scan.*, 25: 94-100.
- 45 Chung, C. S.; Cooper, M. A.; Manatt, S. L. 1971. "Calculations of Geometries of Organic Molecules Using the CNDO/2 Molecular Orbital Method—II: Structural Predictions for the Benzocycloalkenes, and a Theoretical Rationalization of Their Proton-Proton Spin-Spin Coupling Constants." *Tetrahedron*, 27: 701-709.
- 46 Halton, B.; Halton, M. P. 1973. " SCC-EH Molecular Orbital Calculations of the Election Distribution in Benzo- Cyclopropene and Its Cation, Anion and Radical", *Tetrahedron*, 29: 1717-1720.
- 47 Hiberty, P. C.; Ohanessian, G.; Delbecq, F. 1985. "The Valence-Bond Description of Conjugated Molecules. 40. Theoretical Study of the Mills-Nixon Effect, a Phenomenon of Pi.-Bond Localization in Small Ring Annelated Aromatics." *J. Am. Chem. Soc.*, 107: 3095-3100.
- 48 Dewar, M. J. S.; Holloway, M. K. 1984. "[3]-, [4]-, and [5]-Pericyclyne: through-bond vs. through-space Interactions." *J. Chem. Soc., Chem. Commun.*, 1188-1191.
- 49 Longust-Higgins, H. L.; Coulson, C. A. 1946. "A Theoretical Study of the Mills-Nixon Effect." *Trans. Faraday Soc.*, 42: 756-764.
- 50 Apeloig, Y.; Arad, D. 1986. "Cyclopropabenzenes. Geometry, Electronic Structure, Strain, Reactivity, and the Question of Bond Fixation. a Theoretical Study." *J. Am. Chem. Soc.*, 108: 3241-3247.
- 51 Apeloig, Y.; Arad, D.; Halton, B.; Randell, C. J. 1986. "Studies in the Cyclopropaprene Series: A Theoretical and Experimental Study of the Cyclo-Propabenzynes." *J. Am. Chem. Soc.*, 108: 4932-4937.
- 52 Baldridge, K. K.; Siegel, J. S. 1992. "Bond Alternation in Triannelated Benzenes: Dissection of Cyclic Pi. from Mills-Nixon Effects." *J. Am. Chem. Soc.*, 114: 9583-9587.
- 53 Balaban, A. T.; Oniciu, D. C.; Katritzky, A. R. 2004. "Aromaticity as a Cornerstone of Heterocyclic Chemistry." *Chem. Rev.*, 104: 2777-2812.
- 54 Shaik, S. S.; Hiberty, P. C.; Lefour, J.-M.; Ohanessian, G. 1987. "Is Delocalization a Driving Force in Chemistry? Benzene, Allyl Radical, Cyclobutadiene, and Their Isoelectronic Species." *J. Am. Chem. Soc.*, 109: 363-374.
- 55 Hiberty, P. C.; Shaik, S. S; Lefour, J.-M.; Ohanessian, G. 1985. "Is the Delocalized π System of Benzene a Stable Electronic System?" *J. Org. Chem.*, 50: 4657-4659.
- 56 Bürgi, H-B.; Baldridge, K. K.; Hardcastle, K.; Frank, N. L.; Gantzel, P.; Siegel, J. S.; Ziller, J. 1995. " X-Ray Diffraction Evidence for a Cyclohexatriene Motif in the Molecular Structure of Tris(bicyclo[2.1.1]hexeno)-benzene :Bond Alternation after the Refutation of the Mills- Nixon Theory." *Angew. Chem. Int. Ed. Engl.*, 34: 1454-1456.
- 57 Boese, R.; Blaser, D.; Billups, W. E.; Haley, M. M.; Maulitz, A. H.; Mohler, D. L.; Vollhardt, K. P. C. 1994. "The Effect of Fusion of Angle Strained Rings on Benzene: Crystal Structures of 1,2-Dihydrocyclobuta [a]-cyclopropa[c]-, 1,2,3,4-Tetrahydrocyclo-but[a,c]-, 1,2,3,4-Tetrahydrocyclo-but[a,c]cyclopropa[e]-, and 1,2,3,4,5,6-Hexahydrotricyclobuta[a,c,e]benzene." *Angew. Chem. Int. Ed. Engl.*, 33: 313-317.
- 58 Stanger, A. 1998. "Strain-Induced Bond Localization. The Heteroatom Case." *J. Am. Chem. Soc.*, 120: 12034-12040.
- 59 Stanger, A. 1991. "Is the Mills-Nixon Effect Real?" *J. Am. Chem. Soc.*, 113, 8277-8280.
- 60 Hiberty, P. C.; Danovich, D.; Shurki, A.; Shaik, S. 1995. "Why Does Benzene Possess a D_{6h} Symmetry? A Quasiclassical State Approach for Probing π -Bonding and Delocalization Energies." *J. Am. Chem. Soc.*, 117: 7760-7768.
- 61 Shurki, A.; Shaik, S. 1997. "The Distortive Tendency of Benzene *n*: Electrons: How Is It Related to Structural Observables." *Angew. Chem., Int. Ed. Engl.*, 36: 2205-2208.

- 62 Cremer, D.; Kraka, E. 1985. "Theoretical Determination of Molecular Structure and Conformation. 15. Three-Membered Rings: Bent Bonds, Ring Strain, and Surface Delocalization." *J. Am. Chem. Soc.*, 107: 3800-3810.
- 63 Stanger, A.; Boese, R.; Askenazi, N.; Stellberg, P. 1997. "Evidence for Metal Induced Bond Localization in Cyclobutabenzenes: The Crystal and Molecular Structures of η^6 -Cr(CO)3 and η^4 -Fe(CO)3 Complexes of Cyclobutabenzene." *J. Organomet. Chem.*, 542: 19-24.
- 64 Stanger, A.; Ashkenazi, N.; Boese, R. 1998. "The Competition for Electrons: Aromatic Stabilization in a Six-Membered Ring vs Cyclobutadiene-Iron Complex. The Molecular Structure of Tris(tricarbonyliron)cyclobutadieno)benzene." *J. Org. Chem.*, 63: 247-253.
- 65 Wang, Y.; Angermund, K.; Goddard , R.; Krueger, C. 1987. "Redetermination of the Experimental Electron Deformation Density of (Benzene) Tricarbonylchromium." *J. Am. Chem. Soc.*, 109: 587-589.
- 66 www.dmstat1.com/res/The CorrelationCoefficientDefined.html
- 67 Bondi, A. 1964. "van der Waals Volumes and Radii." *J. Phy. Chem.*, 68: 441-451.
- 68 Dewar, M. J. S. 1969. *The PMO Theory of Organic Chemistry*. New York: McGra-Hill.
- 69 Epotis, N. D.; Cherry, W. R.; Shaik, S.; Yates, R.; Bernardi, F. 1977. "Structure Theory of Organic Chemistry." *Top. Curr. Chem.*, 70: 1-end.

CHAPTER 11

STRAINED-AROMATIC MOLECULES – ESE

ABSTRACT

For benzotricyclobutadiene ($C_{12}H_6$) and 18 strained-aromatic molecules (SAMs), the position rule is used to choose the reasonable GL geometry from two candidates. Based on the good correlation between ESE (energy criterion) and $\Delta r(G)$ (geometric criterion) and according to the consistency principle between these two criteria, the rationality of the position rule is confirmed. For $C_{12}H_6$, the adiabatic delocalization energy $\Delta E^A = E(G) - E(GL) = 38.7$ kcal/mol (destabilizing), $CESE = [\Delta E^A - \Sigma \Delta E^{Am} - \Sigma \Delta E_n^{Am}] = 20.4$ kcal/mol (destabilizing). Therefore, $C_{12}H_6$ is anti-aromatic.

18 SAMs are divided into the following four sets: (i) $C_6X_6H_6$ and $C_6X_3H_3$ ($X = B, Al, Ga$); (ii) $C_6X_6H_6$ ($X = N, P, As, Si, Ge$); (iii) $C_6X_3H_3$ ($X = N, P, As$); (iv) C_6X_6 ($X = B, N, P, As$). The π electron occupancy (electron-deficient or electron-sufficient (rich)) of the X-X (or XH, X=X) groups, the size of annulated small ring, and the period number of the X atom in Periodic Table determine the aromaticity-antiaromaticity of a SAM. For 6 molecules $C_6H_6X_6$ and $C_6X_3H_3$ ($X = B, Al, Ga$) with electron-deficient group, always $\Delta E^A < 0$ (stabilizing), and $|\Delta E^A| > |\Sigma \Delta E^{Am}|$, so that $-36.3 < ESE$ (kcal/mol) < -24.9 (stabilizing). When and only when the X-X (or XH) groups are electron-deficient, the SAMs are aromatic.

For the molecules $C_6H_3X_3$ ($X = N, P, As$) and for the molecules $C_6H_6X_6$ ($X = N, P, As, Si, Ge$), the groups (XH, X-X and HX=XH) are all electron-rich group (or sufficient), but the size of the annulated small ring is different. When the small rings are the three-membered ring, the molecules $C_6H_3X_3$ ($X = N, P, As$) are anti-aromatic due to that $31.2 < ESE$ (kcal/mol) < 66 , and $\Delta E^A > 0$ (destabilizing). For the second set of SAMs, the small rings are the four-membered ring. In this case, the ESE value of these molecule depends on the period number of the X atom. When the period number > 2 , $\Delta E^A > 0$, and $0 < ESE$ (kcal/mol) < 9 , that is, the ESE value is not large enough, and $ESE/\Sigma \Delta E^{Am} > 30\%$ that is a bit big. Hence, the energy effects $\Sigma \Delta E^{Am}$ cannot be considered additive, and it is difficult for the molecules $C_6X_6H_6$ ($X = P, As, Si, Ge$) to be regarded anti-aromatic or non-aromatic.

For molecules C_6X_6 ($X = B, N, P, As$), when period number > 2 , the energy effects $\Sigma \Delta E^{Am}$ are additive, and the molecules C_6P_6 and C_6As_6 are non-aromatic.

For the five molecules ($C_{12}H_6, C_6N_6H_6, C_6N_3H_3, C_6B_6$ and C_6N_6), the ESE values (kcal/mol) are as follows: 20.2, 36.8, 31.2, 38.7 and 14.9. When the X atom belongs to the second period of the Periodic Table, the aromaticity-antiaromaticity of a SAM can be clearly determined. The molecules $C_6B_6H_6$ and $C_6B_3H_3$ are aromatic, and the above five molecules are antiaromatic.

yuzh@iccas.ac.cn

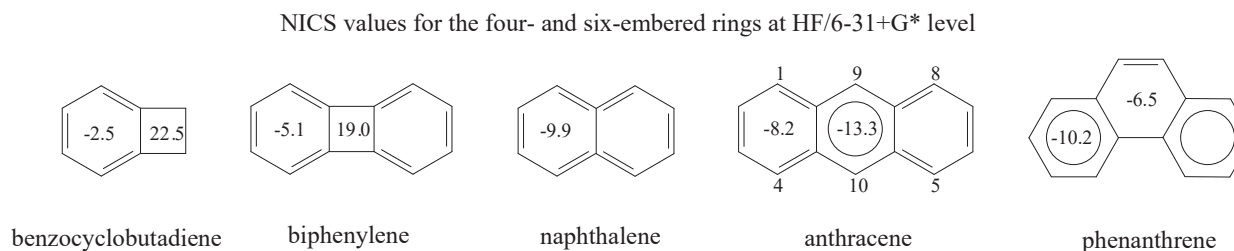
Key words: strained-aromatic molecule; extra stabilization energy; electron-occupancy and aromaticity; energy criterion; geometrical criterion; annulated small ring; period number; position rule; benzotricyclobutadiene.

11.1. INTRODUCTION

For some strained aromatic molecules such as benzotricyclobutadiene, the central ring has alternating bond lengths due to that the four-membered (or three-membered) small rings are fused to central benzene ring. This fact raises the following questions:

- (i) What factor, strain or aromatic-antiaromatic interactions, causes bond length alternation. This question has been discussed in Chapter 10.
- (ii) Does this geometric change lead to loss of aromatic properties? Or how to evaluate the aromaticity of strained-aromatic molecules?
- (iii) The groups X-X (or X=X, XH) annulated to central ring are how to influence the aromaticity of strained-aromatic molecule.

Many aromatic criteria have been reported for the theoretical study of aromaticity. In 1996, Schleyer et al. proposed nucleus-independent chemical shifts (NICS) as a new aromatic-antiaromatic criterion.¹ As an example, they calculated the NICS of strained-aromatic molecules such as benzocyclobutadiene and biphenylene to quantitatively compare the aromaticity of the tension ring. In these two molecules, as shown by the values of NICS presented in Scheme 11-1, the four-membered ring is anti-aromatic; the NICS values (-2.5 and -5.1 ppm) of the six-membered ring in benzocyclobutadiene and diphenylene are smaller than that (-9.7 ppm) of benzene, indicating that, for each of these two molecules, whole molecule is anti-aromatic. Afterwards, this method is generally accepted and widely used. But it has received some criticism.^{2,3}



Scheme 11-1

In some cases, however, the NICS values may conflict with other aromatic criteria. For example, as shown by Scheme 11-1, the NICS values of the six-membered ring in naphthalene, anthracene and phenanthrene are respectively -9.9, -13.3 and -10.2 ppm, and are more negative than that (-9.7 ppm) of benzene so that these rings should be more aromatic than benzene. This contradicts the aromatic geometric criteria. For anthracene, particularly, the central ring (-13.3 ppm) is more aromatic than the terminal ring (-8.2 ppm) according to the NICS values. In fact, anthracene undergoes an electrophilic attack at the 9 position, and the 9 and 10 positions also undergo Diels-Alder reactions, indicating that the central ring is more reactive than the terminal rings. The size order of the NICS values for two six-membered rings in anthracene is contrary to the viewpoint of the characteristic kinetic stability of aromatic compounds. Therefore, a method to calculate the NICS values was suggested by Stanger in 2005.⁴ In this method, the NICS is scanned over distances ranging from 0 to 4.9 Å distances, and the obtained NICS values is divided into in-plane and out of plane contributions.

In 2002, Bachrach designed a series of homodesmotic reactions to calculate the resonance energies (RE) of the following thirty-eight strained-aromatic molecules:⁵ Cyclopropa-, cyclobutana-, and cyclobutena-annulated benzenes, pyridines, and phosphabenzenes. For homodesmotic reactions, as indicated by Bachrach, the magnitude

and sign of the calculated resonance energy depend on the choice of the resonance structure(s) of the strained-aromatic molecule and also on choice of the reference molecule(s). In particular, there are no strict standards for the selection of reference molecules. For a specific strained-aromatic molecule, the sign of the RE values not always the same as the sign of the corresponding NICS value, and the signs of the RE value, obtained from two different homodesmotic reactions, may also be different.

In 2008, the proton transfer reactions, as a type of isodesmic reactions,⁶ were used by Stanger in an attempt to evaluate the aromaticity of strained-aromatic molecules.⁷ When the proton affinity (PA) of a molecule is decreased relative to its open-chain analogue, the molecule is aromatic. Similar to homodesmotic reaction, the proton affinity (PA) of a molecule, calculated by proton transfer reaction, depends upon the choice of reference molecule. Unlike homodesmotic reaction, it does not need to consider the choice of the resonance structures of a conjugated molecule. However, when the theoretical proton affinities of two molecules are derived from two proton transfer reactions with different reference molecules, as emphasized by Stanger, it is meaningless to try to compare the aromaticity of the two molecules using these two proton affinities.

In the field of strained-aromatic molecules, harmonic oscillator model of aromaticity (HOMA), para-delocalization index (PDI), π -electron donor-acceptor parameter (PEDA), and index of deviation from aromaticity (IDA) were also used for theoretical investigation of the aromaticity.^{8,9}

In this Chapter, our 2011 method will be used to calculate the extra stabilization energies of 19 strained aromatic molecules. In this case, the delocalized reference molecule, an expected ground state geometry (EG), is virtual, its structural parameters need not be calculated. The molecular energy difference $E(G) - E(EG)$ between a conjugated molecule and its virtual reference molecule is equal to $\Delta E^A - \Sigma \Delta E^{Am}$. For a strained-aromatic molecule, however, there are two candidates for the GL geometry, so a problem is how to choose a reasonable GL geometry from two candidates.

Compared with the literature methods, the biggest advantage of our 2011 method is that the calculation of delocalization energy does not require the help of any empirical and semi-empirical parameters, because of the discovery of the additivity of energy effects ΔE^{Am} . In our previous work,¹⁰ the position, energy and GL sextet rules were proposed. These three rules ensure that GL geometry is reasonably selected from the possible candidates. In the case of polycyclic benzenoid hydrocarbon, the three rules have been described as follows:

- (i) Position rule: the choice of the positions of the fusion double bonds should ensure as much as possible that the positions of the peripheral double bonds in GL geometry correspond to the positions of the shorter peripheral bonds in the ground state geometry.
- (ii) Energy rule: for a reasonable GL geometry, its molecular energy should be the highest among all possible candidates.
- (iii) GL sextet rule: the number of GL sextets is $N_{db}+1$, where N_{db} is the number of fusion double bonds (the fusion double bond is a double bond shared by two benzenoid rings).

In the case of polycyclic benzenoid hydrocarbon, the GL sextet rule is a necessary and sufficient condition for determining the GL geometry, the other two rules can help the GL sextet rule to choose the most reasonable GL geometry from the qualified candidates.

Fortunately, it will be found that, for the strained-aromatic molecule, the correlation between the ESE (energy criterion) and $\Delta r(G)$ (geometric criterion) is very good. This good correlation can be used to reconfirm the rationality of the position rule.

11.2. BENZOTRICYCLOBUTADIENE

For 19 strained-aromatic molecules, the geometry optimizations are performed at B3LYP/6-31G* using the

Conditional settings for (e)
geometry optimization

When

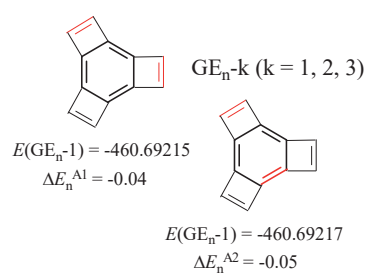
π AOs $\phi_\lambda, \phi_\mu \in P$ -th double bond
 π AOs $\phi_\rho, \phi_\omega \in Q$ -th double bond
 $P \neq Q$

Setting

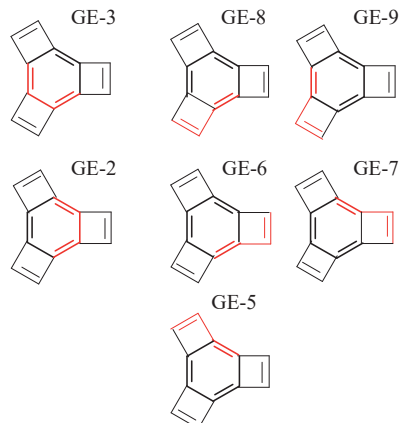
$$f_{\lambda\rho} = 0, \quad s_{\lambda\rho} = 0 \\ \langle \lambda\rho | \mu\omega \rangle = 0$$

GE_{n-k} Geometries (c)

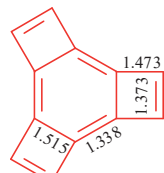
GE_{n-k} ($k = 4, 5, 6$)



GE-m Geometries (b)



(d) G (Ground state)



$$E(G) = -460.63040$$

$$\text{EDSE} = E(G) - E(EG) = 20.16 \text{ kcal/mol}$$

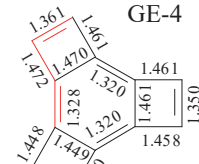
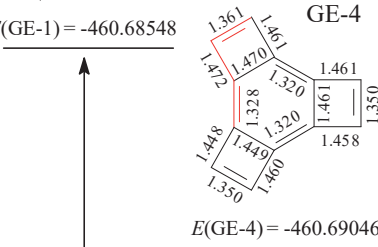
EG (Expected ground state)

$$\Delta E^A = E(G) - E(GL) = 38.71 \text{ kcal/mol}$$

$$E(EG) - E(GL) = \Sigma \Delta E^{Am}$$

$$= 3\Delta E^{A1} + 6\Delta E^{A2}$$

$$= 18.55 \text{ kcal/mol}$$



$$\Delta E^{A2} = E(GE-4) - E(GL) = 1.02 \text{ kcal/mol}$$

$$\Delta E^{A1} = E(GE-1) - E(GL) = 4.15 \text{ kcal/mol}$$

$$\text{EDSE} = \Delta E^A - (\Sigma \Delta E^{Am} + \Sigma \Delta E_n^{Ak}) = E(G) - E(EG) = 20.44 \text{ kcal/mol}$$

The unit of molecular energies E is in hartree
at B3LYP/6-31G*

Figure 11-1. For benzotricyclobutadiene, the procedure of calculating extra destabilization energy (EDSE) and corrected EDSE (CEDSE). (a), (b), (c), and (d) The GL, GE-m ($m=1, 2, \dots, 9$), GE_{n-k} ($k=1, 2, \dots, 6$) geometries, and the ground state; (e) The conditional settings for restricted geometry optimization. All the π orbital interactions and spatial π interaction between the double bonds have been set equal to zero except for the interaction between the double bonds represented by the red lines. The restricted geometry optimizations are performed using our 2011 method at the B3LYP/6-31G* level.

improved PC-Gamess package (our 2011 method).

11.2.1. ESE of Whole Molecule

In order to calculate the ESE of whole molecule, the π MOs of the GL geometry should be localized on their respective double bonds. For benzotricyclobutadiene, there are two candidates, denoted as GL₁₆ and GL₁₂ (Figure 11-1a), for the GL geometry. The symbol "GL₁₆", for example, means that, in the candidate GL₁₆, the double bonds in central ring are artificially localized on the C(1)–C(6), C(4)–C(5) and C(2)–C(3) bonds. The GL geometry, such as GL₁₆ candidate, is obtained from the geometry optimization under the following conditional settings (Figure 11-1e):

- (i) Setting the matrix elements $f_{\lambda,\rho} = 0.0$, $s_{\lambda,\rho} = 0.0$ between the corresponding pairs of double bonds, except for the elements between the C(1)=C(6) and C(2)=C(3).
- (ii) Setting two-electron exchange integrals, (Hartree-Fock two-electron exchange integrals) $\langle \lambda\rho | \mu\omega \rangle = 0.0$, between the corresponding pairs of double bonds, except for the integrals between the C(1)=C(6) and C(2)=C(3).

11.2.1.1. ESE(GL₁₆)

When the GL geometry is conditionally optimized, the fragments P and Q in the central ring refer to the C(1)–C(6), C(2)–C(3) and C(4)–C(5) bonds. In this case, the above conditional settings lead to that the π MOs and π -electrons in the GL geometry are absolutely localized on the following six double bonds: C(1)=C(6), C(2)=C(3), C(4)=C(5), C(7)=C(8), C(9)=C(10) and C(11)=C(12). The positions of the double bonds in the GL₁₆ geometry coincide with the positions of the shorter CC bonds in the ground state geometry. The molecular energy (-460.69208 hartree) of the GL₁₆ geometry is higher than that (-460.71590 hartree) of the GL₁₂ geometry (Figure 11-1a). According to the position and energy rules, the GL₁₆ candidate should be a reasonable GL geometry.

Based on the GL₁₆ geometry, two sets of GE-m geometries (Figure 11-1b) can be obtained from the restricted geometry optimizations. Three geometries of the first set, denoted as GE-m ($m = 1, 2, 3$), are obtained from the local π -interactions between the corresponding pairs of adjacent double bonds in the central ring of GL geometry, and they have the same molecular energy (-460.68548 hartree). Six geometries of the second set, denoted as GE-m ($m = 4, 5, \dots, 9$), resulted from the local π -interactions between the corresponding pairs of double bonds in the GL geometry. In each GE-m geometry ($m = 4, 5, \dots, 9$), one double bond belongs to the central ring, and another double bond belongs to an annulated small ring. These six GE-m geometries have the same molecular energy (-460.69046 hartree). According to the data presented in Figure 11-1, all the local conjugation interactions between the corresponding pairs of double bonds are destabilization and the corresponding single CC bonds are lengthened. For the GE-1 geometry, for example, it is obtained from the geometry optimization under the following conditional settings:

- (i) Setting the matrix elements $f_{\lambda,\rho} = 0.0$, $s_{\lambda,\rho} = 0.0$ when π AO $\phi_\lambda \in P$ -th group, and π AO $\phi_\rho \in Q$ -th group, $P \neq Q$.
- (ii) Setting two-electron exchange integrals (Hartree-Fock exchange integrals) $\langle \lambda\rho | \mu\omega \rangle = 0.0$ when π AOs ϕ_λ and $\phi_\mu \in P$ -th group, and π AOs ϕ_ρ and $\phi_\omega \in Q$ -th group, $P \neq Q$.
- (iii) The fragment P and Q refer to the following five groups: (-C(3)=C(2)–C(1)=C(6)–) and -C(m)=C(m+1)– where $m = 4, 7, 9, 11$.

In the GE-1 geometry, the π -MO and π -electron are respectively localized on the above five groups. As the results of the above conditional settings, $\Delta E^{A1} = E(\text{GE-1}) - E(\text{GL}_{16})$ is the molecular energy difference between the GL₁₆ and

GE-1 geometries, $\Delta E^{A^1} = 4.15$ kcal/mol > 0 (destabilizing); $dr_{12} = r_{12}(\text{GE-1}) - r_{12}(\text{GL})$ is the corresponding difference, in the C(1)-C(2) single bond distance, between the GL₁₆ and GE-1, and $dr_{12} = 1.480 - 1.461 = 0.019 \text{ \AA} > 0$, where, for example, $r_{12}(\text{GE-1})$ is the distance of the C(1)-C(2) single bond between the C(1)=C(6) and C(2)=C(3) double bonds in the GE-1 geometry.

According to the definitions described in Figure 11-1,¹⁰⁻¹² the values (kcal/mol) of the energy effects are as follows:

$$\begin{aligned}\text{ESE} &= \Delta E^A - \Sigma \Delta E^{Am} = 20.2 > 0 \\ \text{CESE} &= \Delta E^A - (\Sigma \Delta E^{Am} + \Sigma \Delta E_n^{Ak}) = 20.4 \\ \Delta E^A &= E(G) - E(GL) = 38.7 > 0 \\ \Sigma \Delta E^{Am} &= \Sigma [E(\text{GE-m}) - E(\text{GL})] = 18.6 > 0 \\ \Sigma \Delta E_n^{Ak} &= \Sigma [E(\text{GE}_n\text{-k}) - E(\text{GL})] = -0.3 < 0\end{aligned}$$

In terms of the size and sign of the energy effect values, these energy effects are different from those for aromatic molecules such as benzene and polycyclic benzenoid hydrocarbons. In this case, total energy effect, ($\Delta E^A - \Sigma \Delta E^{Am}$), had better to be called the extra destabilization energy (EDSE) due to that $\Delta E^A > 0$, and $\Sigma \Delta E^{Am} > 0$, and $\Delta E^A > \Sigma \Delta E^{Am}$, i.e. ΔE^A is more destabilizing than $\Sigma \Delta E^{Am}$.

In the case of benzotricyclobutadiene, “ESE” does not contain the original meaning of “extra stabilization energy”, and it is just seen as a symbol which refers to ($\Delta E^A - \Sigma \Delta E^{Am}$).

11.2.1.2. Our 2011 Method Needing Improvement

In order to understand the influences of the theoretical level and basis set size on the values of the energy effects ESE, CESE, ΔE^A and ΔE^{Am} , the calculations are performed at the B3LYP, RHF and MP2 levels with four different basis sets (6-31G*, 6-311G**, 6-311G(2d,2p) and 6-311G(2df,p)).

At RHF level, as shown by the data listed in Table 11-1, the basis set size has the small influences on these energy values. For each of these five energy effects at a specific level of theory, there is a set of four values (Table 11-1). The range (kcal/mol) of each set of four values, the difference between the maximum value and the minimum value, is as follows:

RHF: 2.1 (ESE), 1.6 (ΔE^A), 1.8 (ΔE^{A^1}), 1.2 (ΔE^{A^4})

The above four RHF ranges are the smallest compared to the corresponding ranges given below:

B3LYP: 3.9 (ESE), 28.6 (ΔE^A), 2.8 (ΔE^{A^1}), 2.8 (ΔE^{A^4})
MP2: 8.3 (ESE), 34.6 (ΔE^A), 1.3 (ΔE^{A^1}), 3.9 (ΔE^{A^4})

At the MP2 level, the range (8.3 kcal / mol) of a set of 4 ESE values is the largest of the corresponding RHF, B3LYP and MP2 values, but as the basis set becomes larger, the difference in ESE between MP2 and B3LYP values at a particular basis level decreases. At the 6-311G(2df,p) level, for example, the MP2 value (24.2 kcal/mol) of ESE is almost equal to the B3LYP value of 24.0 kcal/mol. However, the $\Delta E^{A^1} < 0$ and $\Delta E^{A^4} < 0$ (stabilizing) at MP2/(6-31G* and 6-311G**) levels.

The fact that the RHF and MP2 values, including the size and sign of the values, largely depend upon the theoretical and basis set size means that our 2011 method needs improvement. The improved our 2011 method will be called our 2014 method, and it will be detailed in Chapter 12. In this section, only the values calculated by our 2014 method are listed in Table 11-2. These show the following interesting results:

Table 11-1. For Benzotricyclobutadiene, ESE and CESE (kical/mol), and the Energy Effects, ΔE^A and ΔE^{A^m} (kcal/mol), and the Corresponding Bond Length Differences (\AA), which Are Calculated by Our 2011 Method and Our 2014 Method.

	ESE	CESE	ΔE^A	ΔE^{A^m}	dr_{12}	ΔE^{A4}	dr_{17}	$\Sigma \Delta E_n^{Ak}$	$\Delta r(G)$	$r_{\text{exo}}(G)$
B3LYP Our 2011 Method										
6-31G(d)	20.1	20.4	38.7	4.1	0.019	1.0	0.012	-0.3	0.177	
6-311G(d,p)	20.2	20.6	44.6	5.1	0.019	1.5	0.012	-0.3	0.177	1.334
6-311G(2d,2p)	23.4	23.9	61.2	6.3	0.030	3.1	0.029	-0.5	0.181	1.331
6-311G(2df,p)	24.0	24.8	67.3	6.9	0.036	3.8	0.037	-0.8	0.182	1.330
B3LYP Our 2014 Method										
6-31G(d)	20.3	20.6	39.2	4.2	0.009	1.0	0.002	-0.3		
6-311G(d,p)	20.4	20.8	45.3	5.2	0.008	1.5	0.001	-0.4		
6-311G(2d,2p)	23.7	24.3	62.2	6.5	0.017	3.2	0.015	-0.7		
6-311G(2df,p)	23.8	24.2	68.5	7.2	0.022	3.9	0.021	-0.5		
RHF Our 2011 Method										
6-31G(d)	8.4	8.5	39.6	4.1	0.062	3.2	0.054	0.0	0.183	1.317
6-311G(d,p)	8.2	8.2	38.2	3.8	0.065	3.1	0.055	0.0	0.185	1.316
6-311G(2d,2p)	9.4	8.7	38.7	2.5	0.073	3.6	0.074	0.7	0.186	1.312
6-311G(2df,p)	7.3	6.3	39.8	2.3	0.080	4.3	0.081	1.0	0.186	1.312
RHF Our 2014 Method										
6-31G(d)	9.9	10.0	54.2	7.2	0.015	3.8	0.007	-0.1		
6-311G(d,p)	9.3	9.4	54.8	7.5	0.015	3.8	0.005	-0.1		
6-311G(2d,2p)	11.5	11.8	63.4	8.0	0.018	4.7	0.013	-0.3		
6-311G(2df,p)	11.9	12.1	68.2	8.4	0.022	5.2	0.017	-0.3		
MP2 Our 2011 Method										
6-31G(d)	14.5	14.7	3.9	-1.1	0.048	-1.2	0.051	-0.2	0.165	1.344
6-311G(d,p)	16.8	17.2	7.5	-1.2	0.054	-1.0	0.057	-0.4	0.167	1.345
6-311G(2d,2p)	22.8	22.6	27.7	-0.8	0.063	1.2	0.081	0.2	0.170	1.340
6-311G(2df,p)	21.9	21.3	38.5	0.1	0.075	2.7	0.096	0.6	0.168	1.338
MP2 Our 2014 Method										
6-31G(d)	14.9	15.3	16.8	1.5	0.003	-0.4	0.002	-0.4		
6-311G(d,p)	16.5	17.3	22.4	2.1	0.006	-0.1	0.005	-0.7		
6-311G(2d,2p)	23.3	24.9	51.3	4.1	0.011	2.6	0.015	-1.5		
6-311G(2df,p)	24.2	26.0	66.5	5.8	0.021	4.2	0.026	-1.7		

- (i) The improvement of our 2011 method has little influences on the B3LYP values.
- (ii) For the energy effect ΔE^A at 6-311G(2df,p) level, the MP2 and RHF values (66.5 and 68.2 kcal/mol), obtained from our 2014 method, become almost equal to the B3LYP value of 68.5 kcal/mol.
- (iii) $\Delta E^{A1} > 0$, and $\Delta E^{A4} > 0$ at MP2/(6-311G(2d,2P) and 6-311G(2df,p)) levels. Particularly, at (MP2 and RHF)/6-311G(2df,p) levels, the ΔE^{Am} values become very close to the corresponding B3LYP values.

When our 2011 and 2014 method are used, the 6-311G(2df,p) value of ΔE^A is the most reasonable. Similar calculation results were also obtained in Chapter 9. Only at B3LYP/6-311G(2df, p) level, the energy effects ΔE^{Am} of polyene are additive, and the CESE value of [N]annulene is the most reasonable.

However, the influence of the basis set size is within an acceptable range, according to the following B3LYP values (kcal/mol) of CESE (Table 11-1): 20.4 (6-31G*), 20.6 (6-311G**), 23.9 (6-311G(2d,2p)), 24.8 (6-311G(2df,p)). It can be considered reasonable that the ESE and CESE values, calculated by using our 2011 method at B3LYP/6-31G* level, are used to evaluate the aromaticity (or anti-aromaticity) of strained-aromatic molecule.

When the candidate GL₁₂ is used as the reasonable GL geometry, benzotricyclobutadiene is anti-aromatic, and its CESE is 20.4 kcal/mol.

11.2.1.3. ESE(GL₁₂) of Whole Molecule

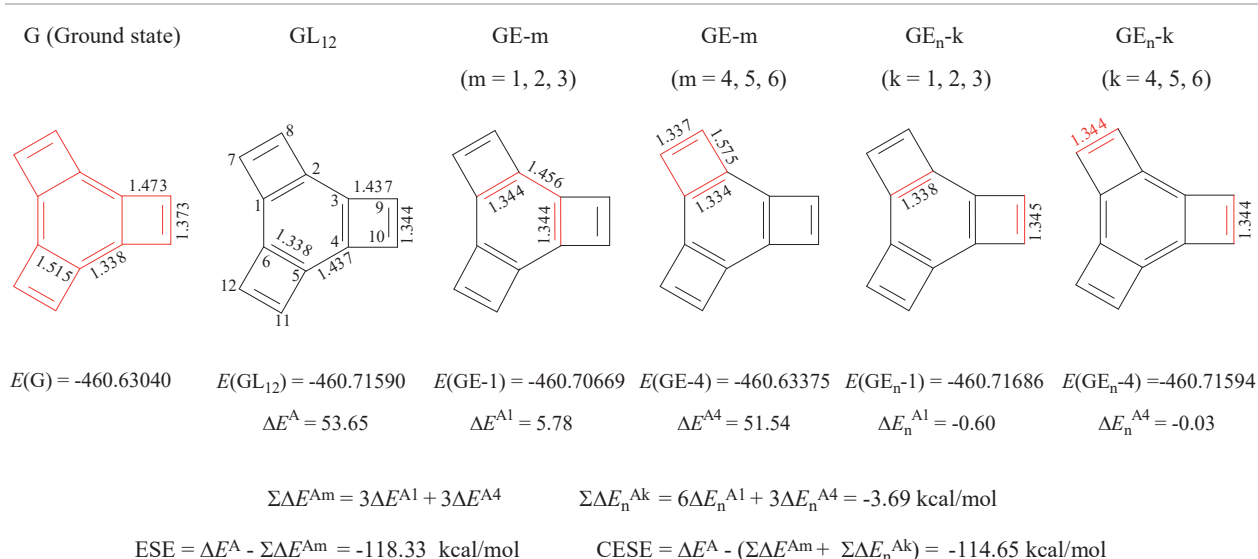


Figure 11-2. For benzotricyclobutadiene, the ESE(GL₁₂) and CESE are calculated, based on the candidate GL₁₂, using our 2011 method at B3LYP/6-31G* level (energy effect unit in kcal/mole, molecular energy unit in hartree).

In the candidate GL₁₂, the π MOs and π -electrons are localized on the following six double bonds: $-C(m)=C(m+1)-$ ($m = 1, 3, 5, 7, 9, 11$). When the candidate GL₁₂ is chosen as the GL geometry, as shown by Figure 11-2, the following results (kcal/mol) are obtained from our 2011 method at B3LYP/6-31G* level:

$$\begin{aligned}\Delta E^A &= 53.7 > 0 \\ \Sigma \Delta E^{Am} &= 172.0 > 0 \\ \Sigma \Delta E_n^{Ak} &= -3.7 < 0 \\ ESE &= -118.3, ESE/\pi = -9.8 \text{ (stabilizing)} \\ CESE &= -114.7, CESE/\pi = -9.6 \text{ (stabilizing)}\end{aligned}$$

In particular, the energy effect ΔE^A , associated with the local π interaction between the two double bonds belonging to a four-membered ring (Figure 11-2), is 51.5 kcal/mol, and it is close to the adiabatic delocalization energy ΔE^A (53.6 kcal/mol) for Cyclobutadiene. It is so large that ΔE^A (53.7 kcal/mol) $< \Sigma \Delta E^{Am}$ (172.0 kcal/mol).

In the case of aromatic molecule such as benzene, $\Delta E^A < 0$, $\Sigma \Delta E^{Am} > 0$. Therefore ESE = $\Delta E^A - \Sigma \Delta E^{Am} < 0$, and it is called extra stabilization energy. For benzotricyclobutadiene, on the contrary, $\Delta E^A > 0$, $\Sigma \Delta E^{Am} > 0$, and $\Sigma \Delta E^A < \Sigma \Delta E^{Am}$. In this case, the ESE value of -118 kcal/mol had better to be called the reduced destabilization energy (RDSE). That is to say, when the GL₁₂ is used as the GL geometry, benzotricyclobutadiene is less destabilized than its virtual reference molecule (expected ground state) due to the π -delocalization, and its reduced destabilization energy ESE = -118.3 kcal/mol.

In terms of the sign of the ESE value, benzotricyclobutadiene seems to be aromatic, and its ESE per π -electron (-9.8 kcal/mol) is larger than that (-6.05 kcal/mol) of benzene, when the candidate GL₁₂ is used as the GL geometry.

11.2.1.4. Rationality of GL₁₆ Candidate.

For the ESE at B3LYP/6-31G* level, based on two different candidates, GL₁₆ and GL₁₂, for the GL geometry, the following two very different values (kcal/mol) are obtained from our 2011 method: 20.2 and -118.3. It is necessary to determine which candidate, or which ESE value, is reasonable.

The followings are the differences, in the molecular structure and ESE value, between triphenylene and benzotricyclobutadiene:

- (i) For benzotricyclobutadiene, the three four-membered rings are anti-aromatic, and corresponding destabilization energy effect $\Delta E^{A4}(GL_{12})$, based on the GL₁₂ geometry, is large, up to 51.5 kcal/mol (Figure 11-2).
- (ii) For triphenylene, the three six-membered rings, fused to central ring, are aromatic. At B3LYP/6-31G* level, $\Delta E^A = -49.8$ kcal/mol < 0 , $\Sigma \Delta E^{Am} = 65.3$ kcal/mol > 0 , and $\Sigma \Delta E_n^{Am} = -5.7$ kcal/mol, leading to ESE = -115.0 kcal/mol and CESE = -109.4 kcal/mol, CESE/ π = -6.055 kcal/mol (Table 9-10).¹⁰

For benzotricyclobutadiene, the CESE(GL₁₂) value (-114.7 kcal/mol), based on the GL₁₂ geometry, is almost equal to the CESE value (-115.9 kcal/mol) of triphenylene, and its CESE/ π (-9.6 kcal/mol*electron) is more negative than that (-6.05 kcal/mol*electron) of benzene, which should be unreasonable.

In benzotricyclobutadiene, in fact, the central benzene ring is indeed a cyclohexatriene, which is consistent with the view of Cava. In 1967, Cava indicated that the low stability of benzotricyclobutadiene is predicted because the bond fixation inhibits the resonance.¹³

For benzotricyclobutadiene, therefore, its reasonable candidate for the GL geometry should be GL₁₆, and the reasonable value of its CESE should be 20.4 kcal/mol (at B3LYP/6-31G* level). Benzotricyclobutadiene is anti-aromatic. The rationality of GL₁₆ will be reconfirmed by the good correlation between ESE and $\Delta r(G)$.

11.2.2. ESE of Central Ring.

To further confirm the rationality of the GL₁₆ candidate, the ESE of central ring is calculated. In benzotricyclobutadiene, the C=C double bonds of annulated small rings, C(7)=C(8), C(9)=C(10) and C(11)=C(12), can be considered as the substituents of benzene. For a substituted benzene, as shown by Figure 11-3a and Figure 11-3g, there are two candidates for the GL geometry according to the positions of the shorter CC bonds in central ring, and the two candidates are denoted as GL₁₆ and GL₁₂. In the GL₁₆ candidate, as shown by Figure 11-3f, the three CC bonds, C(1)-C(6), C(2)-C(3) and C(4)-C(5), are dealt as the shorter CC bonds, and three localized fragments are as the following butadiene fragments: C(1)=C(6)-C(7)=C(8) (fragment A), C(2)=C(3)-C(9)=C(10)

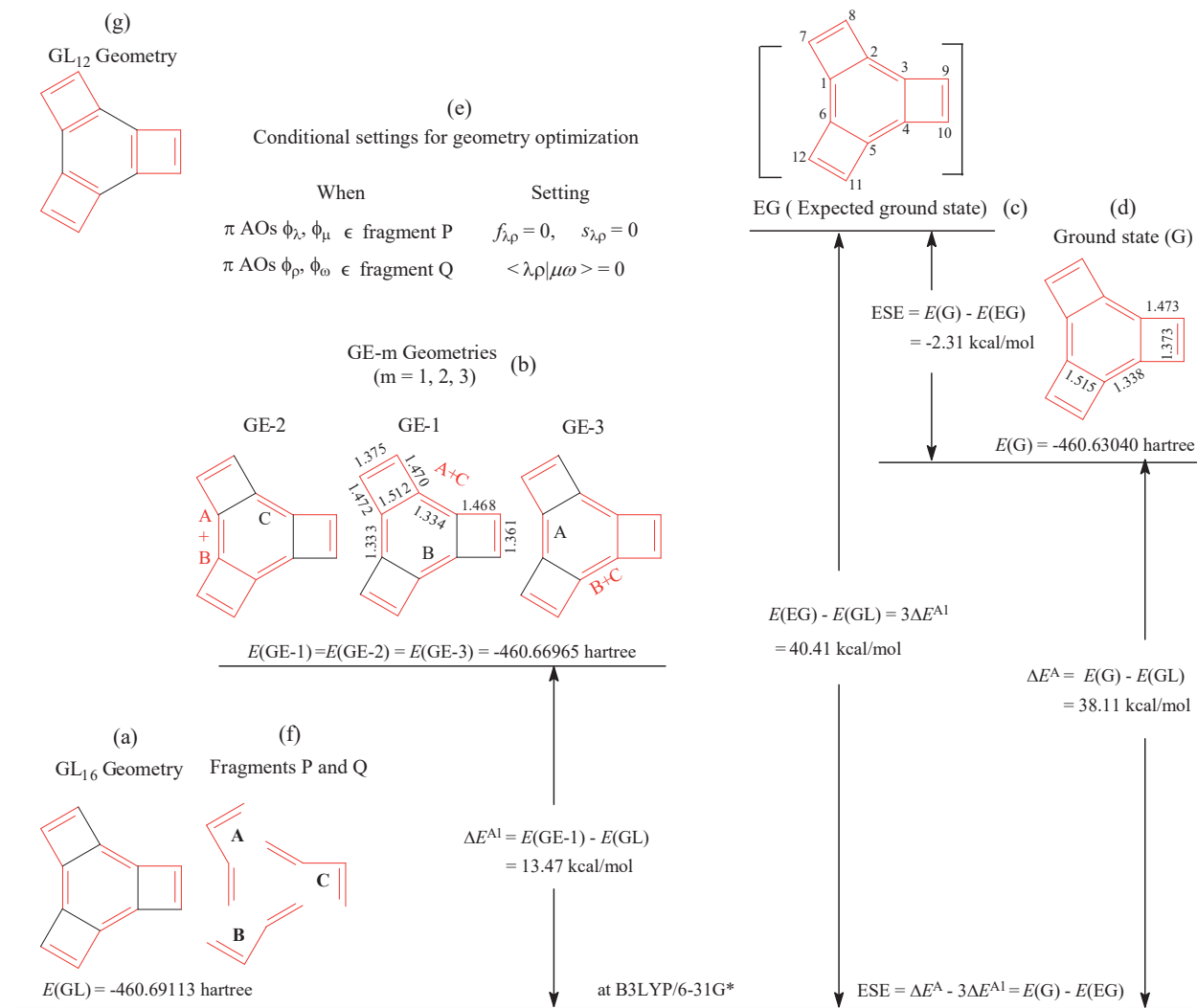
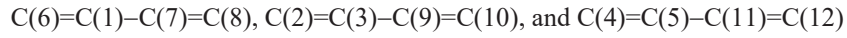


Figure 11-3. The procedure of evaluating the extra stabilization energy for central ring of benzotricyclobutadiene. All the π orbital interactions and the spatial π -electron interactions between the fragments P and Q (P and Q = A, B, C; P \neq Q) have been set equal to zero when the single bonds between the groups P and Q (represented by red lines) are indicated by the black lines. The restricted geometry optimizations are performed using our 2011 method at the B3LYP/6-31G* level.

(fragment C), and C(4)=C(5)=C(11)=C(12) (fragment B). In the candidate GL₁₂, three CC bonds in the central, C(1)-C(2), C(3)-C(4) and C(5)-C(6), are dealt as the double bonds, and the corresponding localized groups are as following cyclobutadiene fragments: C(1)=C(2)=C(7)=C(8), C(3)=C(4)=C(9)=C(10), and C(5)=C(6)=C(11)=C(12).

11.2.2.1. ESE(GL₁₆)

The GL₁₆ candidate for the GL geometry is obtained from the geometry optimization under the conditional settings detailed by Figure 11-3e. In the optimized GL₁₆ geometry, as a result, the π MO and π -electrons are localized on the following three butadiene groups (Figure 11-3a):



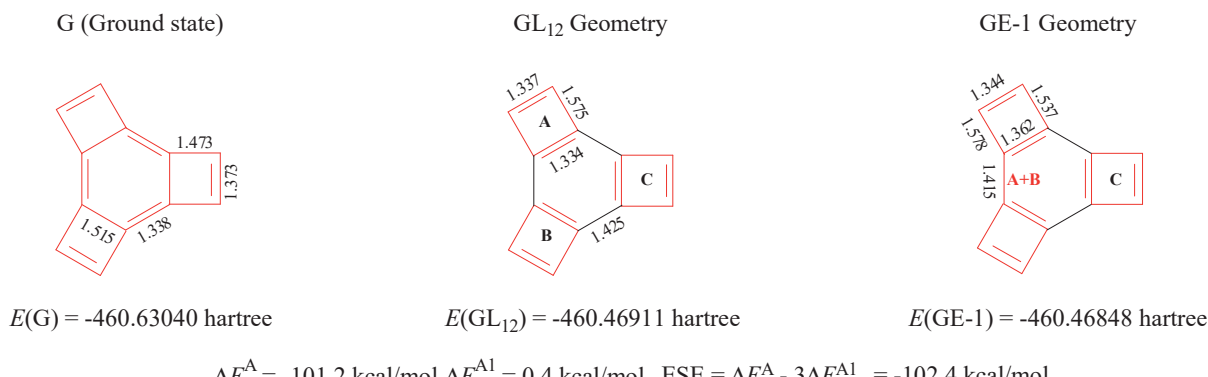


Figure 11-4. For benzotricyclobutadiene, the ESE of the central ring based on the candidate GL₁₂. All the π MO interactions and the spatial π -electron interactions between the groups P and Q ($P \neq Q$) have been set equal to zero when the single bonds between the groups P and Q are represented by the black lines. The restricted geometry optimizations are performed using our 2011 method at the B3LYP/6-31G* level.

In a similar way, three degenerate GE-m ($m = 1, 2, 3$) geometries (Figure 11-3b) can be obtained from the GL₁₂ candidate using our 2011 program. In the GE-1 geometry, for example, the π MO and π -electrons are localized on the fragment (A+C) and fragment B.

For the central ring, as shown by Figure 11-3, the ESE and related energy effects (kcal/mol) are as follows:

$$\Delta E^A = 38.1 > 0$$

$$\Sigma \Delta E^{Am} = 40.4 > 0$$

$$ESE = \Delta E^A - \Sigma \Delta E^{Am} = -2.3 < 0$$

$$|ESE|/\Sigma \Delta E^{Am} = 5.6 \%$$

The value of -2.31 kcal/mol means that $\Delta E^A \approx \Sigma \Delta E^{Am}$, i.e. ΔE^{Am} can be considered additive. The central ring with alternating single (1.515 Å) and double (1.338 Å) bonds looks like substituted cyclohexatriene.

11.2.2.2. ESE(GL₁₂)

When the candidate GL₁₂ is used as a GL geometry, as shown by Figure 11-4, the three localized groups in the GL₁₂ geometry are the cyclobutadiene fragments (represented by red lines). The corresponding energy effects (kcal/mol) are as follows:

$$\Delta E^A = -101.2 > 0$$

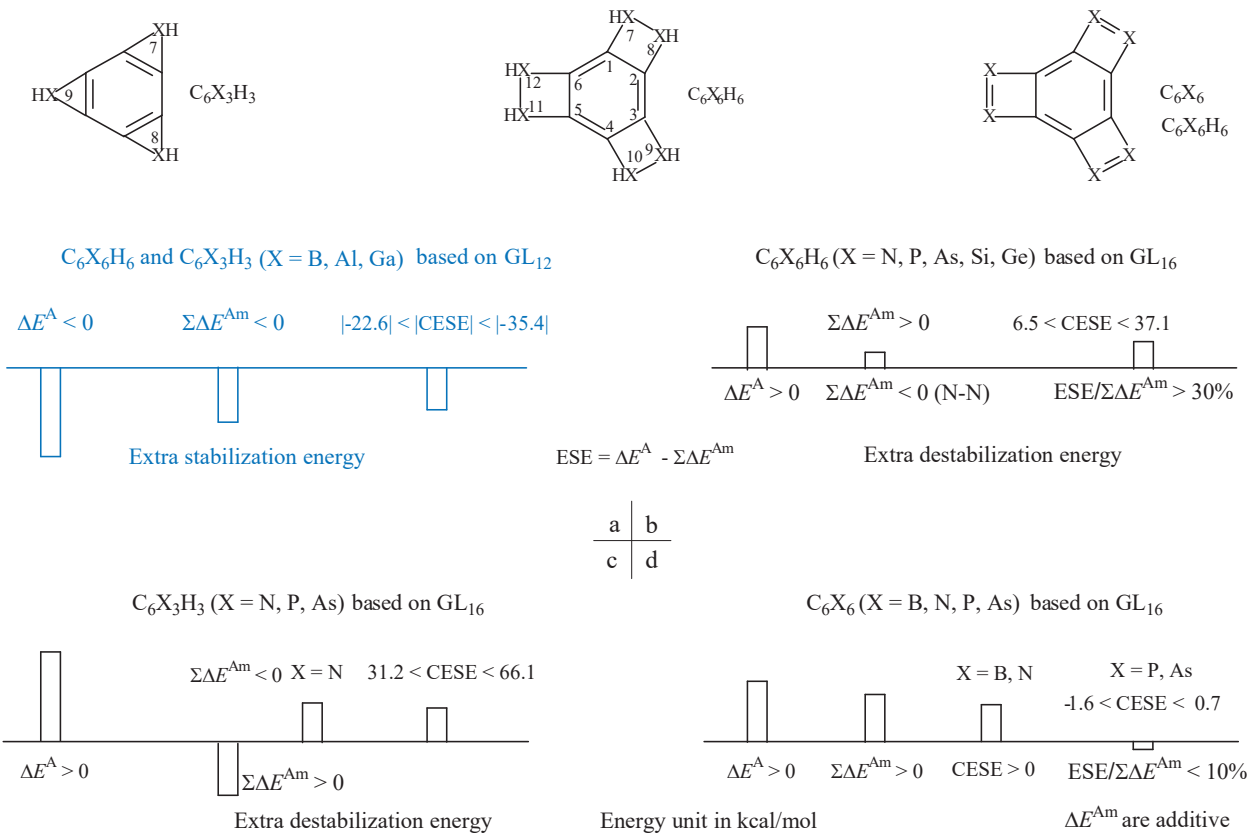
$$\Sigma \Delta E^{Am} = 1.2 > 0$$

$$ESE = \Delta E^A - \Sigma \Delta E^{Am} = -102.4 < 0$$

$$ESE/\pi = -17.1$$

For a distorted benzene ring, it is absolutely impossible that its ESE (-102.4 kcal/mol) is much greater than that (-36.3 kcal/mole¹²) of benzene.

For benzotricyclobutadiene, the CESE of whole molecule and the ESE of central ring are 20.2 kcal/mol and -2.3 kcal/mol, respectively. The entire molecule of benzotricyclobutadiene is anti-aromatic, but its central ring looks like substituted cyclohexatriene and is non-aromatic because the energy effects ΔE^{Am} are additive. All the above calculations confirm that the GL₁₂ candidate is a reasonable GL geometry.



Scheme 11-2

11.3. STRAINED-AROMATIC MOLECULES

The structures of 18 strained-aromatic molecules have been presented in Figure 10-3, and three types of structures are presented in Scheme 11-2. Based on the signs and sizes of the ΔE^A and $\Sigma \Delta E^{Am}$ values, as shown by the data listed in Table 11-2, 18 strained aromatic molecules can be divided into the following four groups (Scheme 11-2): 6 molecules C₆X₆H₆ and C₆X₃H₃ (X = B, Al, Ga); 5 molecules C₆X₆H₆ (X = N, P, As, Si, Ge); 3 molecules C₆X₃H₃ (X = N, P, As); 4 molecules C₆X₆ (X = B, N, P, As). Similar to benzotricyclobutadiene, each molecule has two candidates, GL_{mn} (GL₁₆ and GL₁₂), for the GL geometry. In Table 11-2 to Table 11-4, the red symbol “GL_{mn}” represents a reasonable candidate for the GL geometry.

11.3.1. C₆X₆H₆ and C₆X₃H₃ (X = B, Al, Ga)

The molecules, C₆X₆H₆ and C₆X₃H₃ (X = B, Al, Ga), belong to the first group, and their $\Delta r(G) < 0$ or $\Delta r(G) \approx 0$ (Table 11-2), where $\Delta r(G) = r_{endo}(G) - r_{exo}(G)$ and is the difference between the endocyclic bond length $r_{endo}(G)$ and the exocyclic bond length $r_{exo}(G)$ in the ground state geometry.

When GL₁₆ is used as GL geometry, $\Delta E^{A4}(\text{GL}_{16})$ is an energy effect associated with the local π interaction between the C(1)=C(6) and X(7)=X(8) double bonds (Figure 11-1b). When GL₁₂ is used as GL geometry, $\Delta E^{A4}(\text{GL}_{12})$ arises from the local π interaction between the C(1)=C(2) and X(7)=X(8) double bonds in the GL₁₂.

Table 11-2. For the First Group of Molecules, the Molecular Energy $E(GL)$ (hartree) of the Candidate GL_{mn} , the Extra Stabilization Energy (ESE) and Corrected ESE (kcal/mol), and the Energy Effects (kcal/Mol) ΔE^A , ΔE^{A1} and ΔE^{A4} , which Are Calculated by Our 2011 Method at B3LYP/6-31G* Level.

	GL_{mn}	$E(GL)$	$\Delta r(G)$	ESE	CESE	ΔE^A	ΔE^{A1}	dr_{m-n}	ΔE^{A4}	dr_{1-7}	$\Sigma \Delta E^{Am}$	$\Sigma \Delta E_n^{Ak}$
$C_6B_6H_6$	GL_{12}	-381.00439	-0.029	-28.0	-22.9	-93.3	6.6	0.022	-28.2	-0.039	-65.3	-5.1
	GL_{16}	-380.98243		-41.4	-41.0	-107.1	4.7	0.025	-65.7	-0.049	-65.1	-0.4
$C_6B_3H_3$	GL_{12}	-304.65159	-0.043	-24.9	-22.6	-95.2	6.7	0.022	-30.1	-0.046	-70.3	-2.3
	GL_{16}	-304.59684		-52.9	-52.4	-129.5	2.7	0.022	-14.1	-0.052	-52.9	-0.5
$C_6Al_6H_6$	GL_{12}	-1686.64484	-0.004	-33.2	-27.5	-53.5	6.2	0.025	-13.0	-0.021	-20.4	-5.7
	GL_{16}	-1686.63567		-33.1	-32.2	-59.3	5.3	0.028	-7.0	-0.028	-26.2	-0.9
$C_6Al_3H_3$	GL_{16}	-957.43167	0.005	-36.3	-35.4	-66.2	3.3	0.028	-6.6	-0.023	-29.9	-1.0
	GL_{12}	-957.46529		-30.1	-27.9	-45.1	6.5	0.023	-11.5	-0.006	-15.1	-2.4
$C_6Ga_6H_6$	GL_{16}	-11770.35699	0.002	-34.0	-33.1	-53.5	5.4	0.027	-6.0	-0.011	-19.5	-0.9
	GL_{12}	-11770.36725		-35.9	-29.4	-47.0	6.5	0.024	-10.2	-0.002	-11.2	-6.5
$C_6Ga_3H_3$	GL_{16}	-5999.23174	0.005	-34.0	-33.1	-57.4	3.4	0.025	-5.6	-0.009	-23.4	-0.9
	GL_{12}	-5999.27111		-32.3	-29.7	-32.7	6.5	0.024	-6.7	0.017	-0.4	-2.6

Each molecule has two candidates, GL_{mn} ($mn = 16$ and 12), for the GL geometry. The red symbol, “ GL_{mn} ”, represents a reasonable candidate for the GL geometry.

candidate (Figure 11-2). Due to that the X-X bond (or group XH) in annulated small ring is π electron-deficient group, as shown by data listed in Table 11-2, always $\Delta E^{A4} < 0$ (stabilizing), and $|\Delta E^{A4}| > \Delta E^{A1}$ so that $\Sigma \Delta E^{Am} < 0$, regardless of which candidate is used as the GL geometry. Correspondingly, the single bond C(1)–X(7) in GE-4 geometry is shorter than that in GL geometry. In Table 11-2, always $dr_{1-7} = r_{1-7}(GE-4) - r_{1-7}(GL) < 0$ for this group molecules, and it is the difference, in the distance, r_{1-7} , of C(1)–X(7) bond, between the GE-4 geometry and GL geometry. For $C_6B_6H_6$, for example, when GL_{12} is used as a reasonable GL geometry, $\Delta E^{A1} = 6.6$ kcal/mol, $\Delta E^{A4} = -28.2$ kcal/mol, and $dr_{2-3} = 0.022$ Å, and $dr_{1-7} = -0.039$ Å, where dr_{2-3} is the difference, in the distance of C(2)–C(3) single bond, between the GE-1 and GL_{12} geometries.

For this group, always $\Delta E^A < 0$, $\Sigma \Delta E^{Am} < 0$, and $|\Delta E^A| > |\Sigma \Delta E^{Am}|$ so that ESE < 0 and CESE < 0 (Scheme 11-2a), regardless of which candidate, GL_{12} or GL_{16} , is used as a reasonable GL geometry. In this case, $ESE = (\Delta E^A - \Sigma \Delta E^{Am})$ is still called extra stabilization energy.

In Table 11-2, the red symbols “ GL_{mn} ” indicates that the corresponding GL_{mn} geometry is selected as a reasonable GL geometry according to the position rule. Based on the reasonable GL geometry, the CESE and CESE/ π are always less than those (36.3 kcal/mol and 6.05 kcal/mol $\cdot\pi$) of benzene. When X = Al and Ga, there is no great difference between the two CESE values obtained from two candidates, due to $\Delta r(G) \approx 0.0$ Å.

11.3.2. $C_6X_6H_6$ (X = N, P, As, Si, Ge)

Table 11-3. For the Second Groups of Molecules, the Molecular Energy $E(GL)$ (hartree) of the Candidate GL_{mn} , the Extra Stabilization Energy (ESE) and Corrected ESE (kcal/mol), and the Energy Effects (kcal/mol) ΔE^A , ΔE^{A1} and ΔE^{A4} , which Are Calculated Using Our 2011 Method at B3LYP/6-31G* Level.

	GL_{mn}	$E(GL)$	$\Delta r(G)$	ESE	CESE	ΔE^A	ΔE^{A1}	dr_{m-n}	ΔE^{A4}	dr_{1-7}	$\Sigma \Delta E^{Am}$	$\Sigma \Delta E_n^{Ak}$
HX–XH												
C ₆ N ₆ H ₆	GL ₁₆	-560.39586	0.063	36.8	37.1	34.8	4.0	0.016	-2.3	0.022	-2.0	-0.4
	GL ₁₂	-560.40943		-9.3	2.8	43.4	5.0	0.014	12.5	0.066	53.7	-12.1
C ₆ P ₆ H ₆	GL ₁₆	-2279.87967	0.042	7.5	7.8	10.3	3.8	0.018	-1.5	0.014	2.8	-0.3
	GL ₁₂	-2279.88709		-8.4	2.1	14.9	4.9	0.014	2.9	0.029	23.3	-10.5
C ₆ As ₆ H ₆	GL ₁₆	-13634.46870	0.034	6.1	6.5	11.5	4.2	0.018	-1.2	0.030	5.3	-0.4
	GL ₁₂	-13634.47458		-11.2	3.2	15.2	5.1	0.015	3.7	0.048	26.4	-14.4
HX=XH												
C ₆ Si ₆ H ₆	GL ₁₆	-1968.95823	0.145	6.6	6.8	22.3	4.5	0.022	0.4	0.014	15.7	-0.2
	GL ₁₂	-1968.96903		-83.4	-80.5	29.1	5.6	0.019	31.9	0.132	112.4	-2.8
C ₆ Ge ₆ H ₆	GL ₁₆	-12682.48574	0.131	8.3	8.7	30.1	4.7	0.021	1.3	0.031	21.8	-0.4
	GL ₁₂	-12682.49600		-79.6	-75.7	36.5	5.8	0.019	32.9	0.145	116.1	-3.9

Each molecule has two candidates, GL_{16} and GL_{12} , for the GL geometry. the red symbol, “ GL_{mn} ”, represents a reasonable candidate for the GL geometry.

6 molecules C₆X₆H₆ (X = N, P, As, Si, Ge,), belonging to the second group (Scheme 11-2b), can be further divided into two sub-groups. When X = N, P, As, the molecules belong to the first sub-group, and the X-X single bond is an π electron-sufficient group. When X = Si, Ge, the molecules belong to the second sub-group, and their XX bond is a double bond.

For the first sub-group of molecules, the small ring is aromatic (4n+2 rule), but $\Delta E^{A4}(GL_{12}) > 0$ (destabilizing), and $\Delta E^{A4}(GL_{16}) < 0$ (stabilizing) (Table 11-3). For the second-sub group of molecules, the small ring is anti-aromatic. For these two molecules, as an energy effect associated with π -interaction between the CC bonds in the central ring and the X-X bonds belonging to a hetero-cyclobutadiene fragment, $\Delta E^{A4}(GL_{12}) > 0$, and it is much larger than that for the molecules of the first sub-group. For molecules C₆P₆H₆ and C₆Si₆H₆, for example, the values (kcal/mol) of $\Delta E^{A4}(GL_{12})$ are 2.9 (X = P) and 31.9 (X = Si).

When GL_{16} is used as a reasonable GL geometry according to the position rule, as shown by the red data listed Table 11-3, $\Delta E^A > 0$, $\Sigma \Delta E^{Am} > 0$ (except for C₆N₆H₆), and $\Delta E^A > \Sigma \Delta E^{Am}$ (Scheme 11-2) so that ESE > 0 and CESE > 0. In this case, ESE is an extra destabilization energy.

In terms of the energy and geometrical criteria, the characteristics of these molecules are as follows: (i) $\Delta E^A > 0$, CESE < 9 kcal/mol (except for C₆N₆H₆), which is not big enough. (ii) The ratio ESE/ $\Sigma \Delta E^{Am} > 30\%$, which is bit big; (iii) $0.042 < \Delta r(G) < 0.145$, which is big enough. In this case, the energy effects $\Sigma \Delta E^{Am}$ cannot be considered additive, and it is difficult to define these molecules (except for C₆N₆H₆) as anti-aromatic or non-aromatic.

11.3.3. C₆X₃H₃ (X = N, P, As)

Table 11-4. For the Third and Fourth Groups of Molecules, the Molecular Energy $E(GL)$ (Hartree) of the Candidate GL_m, the Extra Stabilization Energy (ESE) and Corrected ESE (kcal/mol), and the Energy Effects (kcal/mol) ΔE^A , ΔE^{A1} and ΔE^{A4} , which Are Calculated by Our 2011 Method at B3LYP/6-31G* Level.

GL		$E(GL)$	$\Delta r(G)$	ESE	CESE	ΔE^A	ΔE^{A1}	dr_{m-n}	ΔE^{A4}	dr_{1-7}	$\Sigma \Delta E^{Am}$	$\Sigma \Delta E_n^{Ak}$
Third group of strained aromatic molecules												
$C_6N_3H_3$	GL_{16}	-394.45450	1.006	31.2	31.2	79.3	0.3	0.002	8.2	0.040	48.1	-0.1
	GL_{12}	-394.38810		-90.2	-86.7	37.6	5.6	0.014	37.0	1.170	127.7	-3.5
$C_6P_3H_3$	GL_{16}	-1254.03298	0.206	66.0	66.1	45.1	1.7	0.015	-4.3	0.021	-20.9	-0.1
	GL_{12}	-1254.07013		-102.7	-100.6	68.4	5.1	0.014	51.9	0.175	171.1	-2.1
$C_6As_3H_3$	GL_{16}	-6931.29834	0.205	64.5	64.6	44.4	2.0	0.014	-4.3	0.035	-20.1	-0.2
	GL_{12}	-6931.33494		-97.2	-94.0	67.4	5.2	0.014	49.7	0.193	164.6	-3.3
Fourth group of strained aromatic molecules												
C_6B_6	GL_{16}	-377.01677	0.423	38.7	39.1	22.2	3.2	0.037	-4.4	-0.008	-16.5	-0.4
	GL_{12}	-377.01395		10.6	17.9	20.4	5.0	0.012	-1.8	-0.120	9.8	-7.3
C_6N_6	GL_{16}	-556.78032	0.141	14.9	15.0	26.6	3.5	0.015	0.2	0.008	11.7	-0.1
	GL_{12}	-556.82068		-98.6	-96.0	51.9	5.5	0.019	44.7	0.148	150.5	-2.6
C_6P_6	GL_{16}	-2276.64544	0.116	0.4	0.6	11.8	4.6	0.020	-0.4	0.005	11.4	-0.1
	GL_{12}	-2276.66813		-83.9	-81.7	26.0	5.9	0.021	30.8	0.125	110.0	-2.3
C_6As_6	GL_{16}	-13631.34495	0.109	-1.8	-1.6	17.0	5.0	0.021	0.6	0.025	18.8	-0.2
	GL_{12}	-13631.36159		-78.9	-75.5	27.4	6.0	0.021	29.4	0.143	106.3	-3.4

*The reasonable GL geometry

The molecules $C_6X_3H_3$ ($X = N, P, As$) belong to the third group. The size and sign of their ESE and CESE values depend on the choice of the GL geometry. When GL_{16} is used as a reasonable GL geometry according to the position rule, $\Delta E^A > 0$, $\Sigma \Delta E^{Am} < 0$ (except for $C_6N_3H_3$), and $\Delta E^A > |\Sigma \Delta E^{Am}|$ so that ESE > 0 and CESE > 0 (Table 11-4).

When GL_{12} is as a reasonable GL geometry, $\Delta E^{A4}(GL_{12})$ is much larger than the absolute value of $\Delta E^{A4}(GL_{16})$ due to that the XH group is π electron-sufficient. For molecule $C_6N_3H_3$, for example, $\Delta E^{A4}(GL_{12}) = 37.0$ kcal/mol, $\Delta E^{A4}(GL_{16}) = 8.2$ kcal/mol, and $\Delta E^{A4}(GL_{12})/\Delta E^{A4}(GL_{16}) > 4$, leading to that ESE(GL_{12}) = -90.2 kcal/mol.

According to the position rule, however, the candidate GL_{16} can be considered as a reasonable GL geometry. In this case, $(\Delta E^A - \Sigma \Delta E^{Am}) > 0$ should also be called extra destabilization energy (EDSE).

11.3.4. C_6X_6 ($X = B, N, P, As$)

The molecules C_6X_6 ($X = B, N, P, As$) belong to the fourth group. For these four molecules except for C_6B_6 , the size and sign of their ESE and CESE values depend on the choice of the GL geometry (Table 11-4). But, $\Delta E^A > 0$,

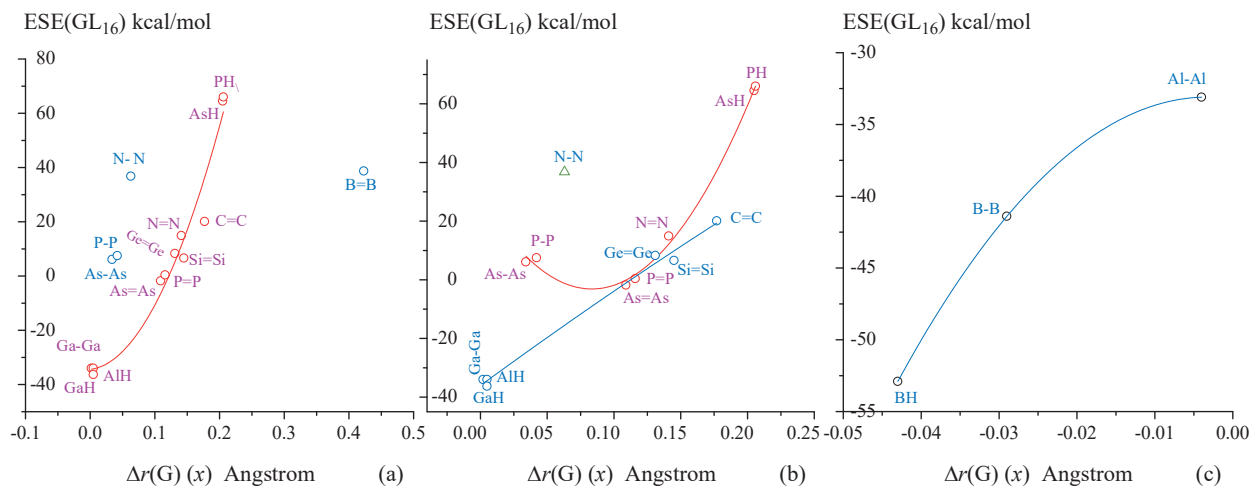


Figure 11-5. At B3LYP/6-31G* level, ESE(GL₁₆) is the polynomial function of $\Delta r(G)$.

$\Sigma \Delta E^{\text{Am}} > 0$ (except for C₆B₆) regardless of which candidate is used as a reasonable GL geometry. When X = P and As, $\Delta E^{\text{A}}(\text{GL}_{16}) \approx \Sigma \Delta E^{\text{Am}}(\text{GL}_{16})$. In this case, the energy effects ΔE^{Am} can be considered additive. As the atomic number of X atom increases, the energy character of molecule changes from anti-aromatic (C₆N₆) to non-aromatic (C₆P₆ and C₆As₆).

When the candidate GL₁₂ is used as the GL geometry, $\Delta E^{\text{A}} > 0$, $\Sigma \Delta E^{\text{Am}} > 0$, and $\Delta E^{\text{A}} < \Sigma \Delta E^{\text{Am}}$ (except for C₆B₆). As the results, ESE(GL₁₂) < 0 and CESE(GL₁₂) < 0. For C₆P₆, for example, ESE(GL₁₆) and ESE(GL₁₂) are, respectively, 0.4 and -83.9 kcal/mol. The position rule should be reasonable.

The molecules C₆N₃H₃ and C₆B₆ have been known as two abnormal molecules in Chapter 10, and their ESEs, including the components ΔE^{A} and $\Sigma \Delta E^{\text{Am}}$, are also abnormal.

11.4. ESE VERSUS $\Delta r(G)$

Since the choice of the GL geometry is based on the position rule, it is necessary to justify the rationality of position rules.

$\Delta r(G) = r_{\text{endo}}(G) - r_{\text{exo}}(G)$, and it is the bond length difference between the endocyclic bond and the exocyclic bond in ground state geometry. In the case of planar conformation, each of 19 strain-aromatic molecules has D_{3h} symmetry. So, $\Delta r(G)$ can be used as a geometric criterion of aromaticity.

According to the sign of $\Delta r(G)$ (Table 10-3), 19 molecules, including benzotricyclobutadiene, can also be divided into two sets. 16 molecules whose $\Delta r(G) > 0$ belong to the first set, and the remaining three molecules, C₆B₆H₆, C₆Al₆H₆ and C₆B₃H₃, are grouped into the second set, and their $\Delta r(G) < 0$.

11.4.1. Molecules with $\Delta r(G) > 0$

For the 16 molecules of the first set, except for two abnormal molecules C₆N₃H₃ and C₆B₆, the molecular energy of the GL₁₆ candidate is generally higher than the molecular energy of the corresponding GL₁₂ candidate (Table 11-2 to Table 11-4). Therefore, the GL₁₆ candidate should be a reasonable GL geometry according to the position and energy rules. However, the rationality of these two rules should be confirmed by another reasonable

Table 11-5. The Correlation of Two Variables $\Delta r(G)$ (\AA) and ESE(GL₁₆) (kcal/mol) Are Examined by the Vertical Offsets from the Fitted Line (Figure 11-5a) At B3LYP/6-31G* Level.

Mols	$\Delta r(G)$	ESE	(ESE) _T	Offset
$\text{ESE(GL}_{16}\text{)} = -34.38341 + 26.15112 * \Delta r(G) + 2110.17302 * \Delta r(G)^2$				
C ₆ Ga ₆ H ₆	0.002	-34.00	-34.32	0.32
C ₆ Ga ₃ H ₃	0.005	-34.00	-34.20	0.20
C ₆ Al ₃ H ₃	0.005	-36.30	-34.20	-2.10
C ₆ As ₆	0.109	-1.80	-6.46	4.66
C ₆ P ₆	0.116	0.40	-2.96	3.36
C ₆ Ge ₆ H ₆	0.131	8.30	5.26	3.04
C ₆ N ₆	0.141	14.90	11.26	3.64
C ₆ Si ₆ H ₆	0.145	6.60	13.77	-7.17
C ₂₄ H ₆	0.177	20.10	36.35	-16.25
C ₆ As ₃ H ₃	0.205	64.50	59.66	4.84
C ₆ P ₃ H ₃	0.206	66.00	60.55	5.45
C ₆ As ₆ H ₆	0.034	6.10	-31.05	37.15
C ₆ P ₆ H ₆	0.042	7.50	-29.56	37.06
C ₆ N ₆ H ₆	0.063	36.80	-24.36	61.16

(ESE)_T: Theoretical ESE value obtained from the fitted function.

method as far as possible. A reasonable approach is to explore the correlation between the geometric criterion ($\Delta r(G)$) and the energetic criterion (ESE).

11.4.1.1. ESE(GL₁₆) versus $\Delta r(G)$

For 11 molecules, C₆X₃H₃ (X = P, As, Al, Ga), C₆X₆H₆ (X = Ga) and C₆X₆ (X = N, P, As, C, Si, Ge), belonging to the first set, as shown by the red cycles in Figure 11-5a, ESE(GL₁₆) (y) can be well fitted as the following second order polynomial function of $\Delta r(G)$ (x) (cc = 0.9567):

$$y = -34.38341 + 26.15112 x + 2110.17302 x^2$$

For three molecules C₆As₆H₆, C₆P₆H₆ and C₆N₆H₆, however, the vertical offsets from the fitted line are, respectively, 37.15, 37.06 and 61.16 kcal/mol (Table 11-5), and they are so large that the corresponding blue circles, denoted as As-As, P-P and N-N in Figure 11-5a, are not involved in the function curve fitting.

Molecules C₆B₆ and C₆N₃H₃ have already been known as the abnormal molecules, and the corresponding data points are not considered in the function line fitting. The remained molecules 14 molecules, C₆X₃H₃ (X = P, As, Al, Ga), C₆X₆H₆ (X = N, P, As, Ga) and C₆X₆ (X = N, P, As, C, Si, Ge), are further divided into two sub-sets according

Table 11-6. The Correlation of Two Variables $\Delta r(G)$ and ESE(GL₁₆) Are Examined by the Vertical Offsets from the Fitted Lines in Figure 11-5b at B3LYP/6-31G* Level.

Mols	$\Delta r(G)$	ESE	dy/dx	(ESE) _T	Offset
$ESE(GL_{16}) = 28.81683 - 766.26262 * \Delta r(G) + 4596.59738 * \Delta r(G)^2$					
C ₆ As ₆ H ₆	0.034	6.10	-453.7	8.08	-1.98
C ₆ P ₆ H ₆	0.042	7.50	-380.1	4.74	2.76
C ₆ As ₆	0.109	-1.80	235.8	-0.09	-1.71
C ₆ P ₆	0.116	0.40	300.1	1.78	-1.38
C ₆ N ₆	0.141	14.90	530.0	12.16	2.74
C ₆ As ₃ H ₃	0.205	64.50	1118.3	64.90	-0.40
C ₆ P ₃ H ₃	0.206	66.00	1118.3	66.03	-0.03
$ESE(GL_{16}) = -36.05609 + 333.33148 * \Delta r(G) - 114.45593 * \Delta r(G)^2$					
C ₆ Ga ₆ H ₆	0.002	-34.00	332.9	-35.39	1.39
C ₆ Ga ₃ H ₃	0.005	-34.00	332.2	-34.39	0.39
C ₆ Al ₃ H ₃	0.005	-36.30	303.3	-34.39	-1.91
C ₆ Ge ₆ H ₆	0.131	8.30	300.1	5.65	2.65
C ₆ Si ₆ H ₆	0.145	6.60	292.8	9.87	-3.27
C ₂₄ H ₆	0.177	20.10	333.3	19.36	0.74

to the Periodic Table family to which the hetero atom belongs. The seven molecules, C₆X₆H₆ and C₆X₃H₃ (X = P, As), and C₆X₆ (X = N, P, As) corresponding to the red cycles in Figure 11-5b, belong to the first sub-set, and their X (N, P, As) atoms belong to the nitrogen family of Periodic Table. The six molecules, C₆X₆H₆ (X = Ga, C, Si, Ge) and C₆X₃H₃ (X = Al, Ga) correspond to the blue cycles in Figure 11-5b, are grouped into the second sub-set, and their X atoms belong to the boron and carbon families of Periodic Table.

For each sub-set of molecules, as shown by the red and blue lines in Figure 11-5b, ESE(GL₁₆) (y) can also be well fitted as the following second order polynomial functions of $\Delta r(G)$ (x):

$$y = 28.81683 - 766.26262x + 4596.59738x^2 \text{ (red line, cc = 0.9932)}$$

$$y = -36.05609 + 333.33148x - 114.45593x^2 \text{ (blue line, cc = 0.9880).}$$

The correlation coefficients of two fitted lines in Figure 11-5b are 0.9932 and 0.9880 and both are larger than that (0.9567) of the red line in Figure 11-5a. For most of these molecules, as shown by comparison of Table 11-5 and Table 11-6, the vertical offsets from the fitted line in Figure 11-5a are larger than the corresponding vertical offsets in Figure 11-5b.

11.4.1.2. ESE(GL₁₂) versus $\Delta r(G)$

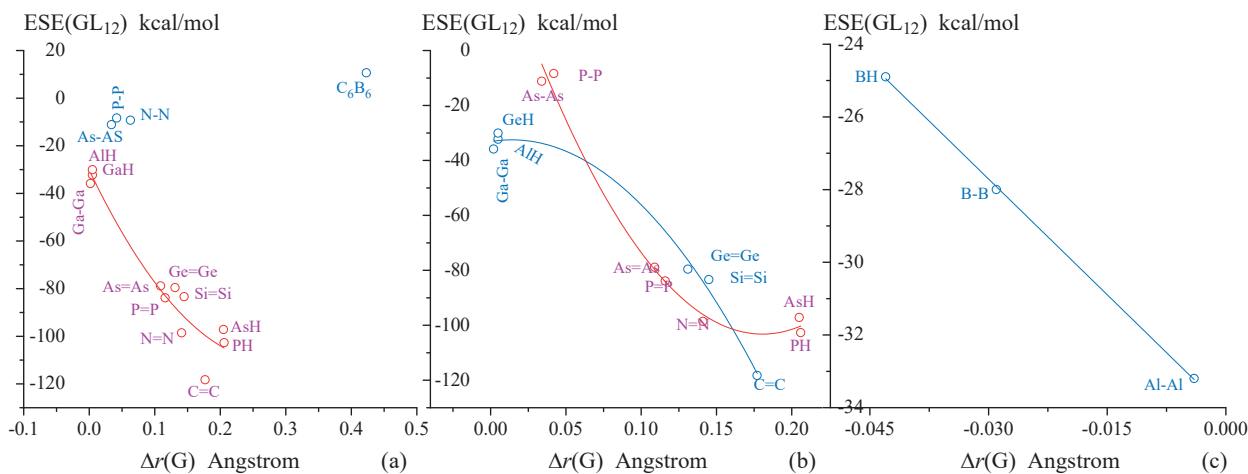


Figure 11-6. ESE(GL₁₂) is the polynomial function of Δr(G) at B3LYP/6-311G* level.

For the 11 molecules, C₆X₃H₃ (X = P, As, Al, Ga), C₆X₆H₆ (X = Ga) and C₆X₆ (X = N, P, As, C, Si, Ge), belonging to the first set, unfortunately, ESE(GL₁₂) (y) can also be well fitted as the following second order polynomial function of Δr(G) (x) (Figure 11-6a):

$$y = -30.22549 - 573.89944x + 1025.67419x^2 \text{ (cc} = 0.9128\text{)}$$

For two sub-sets of the molecules, ESE(GL₁₂) (y) can also be well fitted as the following second order polynomial function of Δr(G) (x) (Figure 11-6b):

$$y = 45.99779 - 1652.83532x + 4577.59109x^2 \text{ (red line, cc} = 0.9834\text{)}$$

$$y = -33.13667 + 89.88494x - 3199.36274x^2 \text{ (blue line, cc} = 0.9889\text{)}$$

The correlation coefficients of the two variables ESE(GL₁₂) and Δr(G) are almost equal to those of the two variables ESE(GL₁₆) and Δr(G). For the red fitted lines in Figure 11-5b and Figure 11-6b, for example, the correlation coefficients are, respectively, 0.9932 and 0.9834.

11.4.1.3. Rationality of ESE(GL₁₆) versus Δr(G)

For aromaticity, ESE is an energy criterion, and Δr(G) is a geometric criterion. For a set of strained-aromatic molecules, these two criteria should be consistent, i. e. the larger Δr(G) should correspond to the less stabilizing ESE or larger destabilizing ESE

For the fitted functions ESE(GL₁₂) = f(Δr(G)) in Figure 11-6a and Figure 11-6b, however, the first order derivative $d\text{ESE(GL}_{12}\text{)}/d\Delta r(\text{G}) < 0$. For the red line in Figure 11-6b, for example, the first order derivative is as follow:

$$d\text{ESE(GL}_{12}\text{)}/d\Delta r(\text{G}) = -1652.83532 + 2 * 4577.59109 * \Delta r(\text{G}) \text{ Å} < 0 \quad (0.034 < \Delta r(\text{G}) \text{ Å} < 0.206)$$

The ESE(GL₁₂) changes from -11.2 kcal/mol (C₆As₃H₃) to -102.7 (C₆P₃H₃) when Δr(G) increases from 0.034 Å to 0.206 Å. A larger Δr(G) generally corresponds to more stabilizing ESE(GL₁₂), that is, the greater the degree, Δr(G), of bond length alternation, the greater the molecular aromaticity. This of course violates the geometric criterion of

Table 11-7. For 18 Strained-Aromatic Molecules, ESEs and Corrected ESEs (kcal/mol) Calculated by Using Our 2011 Method at B3LYP/6-31G* Level.

	GL _{mn}	ESE	CESE	$\Delta r(G)$	ΔE^A	$\Sigma \Delta E^{Am}$	$\Sigma \Delta E_n^{Ak}$
C ₆ B ₆ H ₆	GL ₁₂	-28.0	-22.9	-0.029	-93.3	-65.3	-5.1
C ₆ B ₃ H ₃	GL ₁₂	-24.9	-22.6	-0.043	-95.2	-70.3	-2.3
C ₆ Al ₆ H ₆	GL ₁₂	-33.2	-27.5	-0.004	-53.5	-20.4	-5.7
C ₆ Al ₃ H ₃	GL ₁₆	-36.3	-35.4	0.005	-66.2	-29.9	-1.0
C ₆ Ga ₆ H ₆	GL ₁₆	-34.0	-33.1	0.002	-53.5	-19.5	-0.9
C ₆ Ga ₃ H ₃	GL ₁₆	-34.0	-33.1	0.005	-57.4	-23.4	-0.9
C ₆ N ₆ H ₆	GL ₁₆	36.8	37.1	0.063	34.8	-2.0	-0.4
C ₆ P ₆ H ₆	GL ₁₆	7.5	7.8	0.042	10.3	2.8	-0.3
C ₆ As ₆ H ₆	GL ₁₆	6.1	6.5	0.034	11.5	5.3	-0.4
C ₆ Si ₆ H ₆	GL ₁₆	6.6	6.8	0.145	22.3	15.7	-0.2
C ₆ Ge ₆ H ₆	GL ₁₆	8.3	8.7	0.131	30.1	21.8	-0.4
C ₆ N ₃ H ₃	GL ₁₆	31.2	31.2	1.006	79.3	48.1	-0.1
C ₆ P ₃ H ₃	GL ₁₆	66.0	66.1	0.206	45.1	-20.9	-0.1
C ₆ As ₃ H ₃	GL ₁₆	64.5	64.6	0.205	44.4	-20.1	-0.2
C ₆ B ₆	GL ₁₆	38.7	39.1	0.423	22.2	-16.5	-0.4
C ₆ N ₆	GL ₁₆	14.9	15.0	0.141	26.6	11.7	-0.1
C ₆ P ₆	GL ₁₆	0.4	0.6	0.116	11.8	11.4	-0.1
C ₆ As ₆	GL ₁₆	-1.8	-1.6	0.109	17.0	18.8	-0.2

aromaticity.^{14,15} In fact, the literature indicated that, for [5]paracyclophane, the distortion of benzene fragment reduces its stabilization by about 12 kcal/mol.¹⁶

Conversely, as shown by the dy/dx values listed in Table 11-6, the first order derivative of the function $ESE(GL_{16}) = f(\Delta r(G))$ is usually greater than zero. For the red line in Figure 11-5b, for example, $dESE(GL_{16})/d\Delta r(G) > 0$ when $\Delta r(G) > 0.042 \text{ \AA}$ (C₆P₆H₆ and C₆As₆H₆). For the blue line in Figure 11-5b, always $dESE(GL_{16})/d\Delta r(G) > 0$. For the 11 molecules listed in the Table 11-6, the general trend is that the larger $\Delta r(G)$ corresponds the more destabilizing ESE.

In the case of strained-aromatic molecules with $\Delta r(G) > 0$, the GL₁₆ candidate, determined by the position rule, is a reasonable GL geometry.

11.4.2. Molecules with $\Delta r(G) < 0$

The remaining three molecules are $C_6B_6H_6$, $C_6Al_6H_6$ and $C_6B_3H_3$, and their $\Delta r(G) < 0$ (Table 11-1). For each of these three molecules, there are also two candidates, GL_{12} and GL_{16} , for the GL geometry, and the corresponding $ESE(GL_{12})$ and $ESE(GL_{16})$ both are stabilizing. For the three molecules. The $ESE(GL_{12})$ and $ESE(GL_{16})$ values are as follows:

$$\begin{aligned} GL_{12}: -28.0 \text{ } (C_6B_6H_6), -24.9 \text{ } (C_6B_3H_3), -33.2 \text{ } (C_6Al_6H_6) \\ GL_{16}: -41.4 \text{ } (C_6B_6H_6), -52.9 \text{ } (C_6B_3H_3), -33.1 \text{ } (C_6Al_6H_6) \end{aligned}$$

As shown by Figure 11-5c and Figure 11-6c, $ESE(GL_{16})$ and $ESE(GL_{12})$ can be fitted as the following polynomial functions of $\Delta r(G)$ (x):

$$\begin{aligned} ESE(GL_{16}) &= -33.22774 - 82.13187x - 12549.45055x^2; \\ ESE(GL_{12}) &= -34.0771 - 212.2545x \text{ (cc = 0.9995).} \end{aligned}$$

On the basis of comparison of Figure 11-5c and Figure 11-6c, $ESE(GL_{12})$ becomes less stabilizing and $ESE(GL_{16})$ becomes more stabilizing as the absolute value of $\Delta r(G)$ increases.

For the molecules with $\Delta r(G) < 0$, therefore, the GL_{12} candidate should be chosen as a reasonable GL geometry. The rationality of the position rule is confirmed again.

At last, the ESE and CESE of 18 molecules are listed in Table 11-7.

11.5. CONCLUSIONS

For each of the 19 strained-aromatic molecules (SAMs), the GL geometry has two candidates, and the ESE value depends on the choice of GL geometry. Based on the good correlation between ESE (energy criterion) and $\Delta r(G)$ (geometric criterion) and according to the consistency principle between these two criteria, the rationality of the position rule is confirmed, and it is used to choose the reasonable GL geometry from two candidates.

For benzotricyclobutadiene ($C_{12}H_6$), the adiabatic delocalization energy $\Delta E^A = 38.7$ kcal/mol > 0 , CESE = 20.4 kcal/mol > 0 . Therefore, $C_{12}H_6$ is anti-aromatic. The influences of the theoretical level and basis set size on the ESE value are discussed. At B3LYP level, the influence of basis set size is small. In this Chapter, all the ESE calculations are performed, using our 2011 method, at B3LYP/6-31G** level

18 SAMs are divided into the following four sets: (i) $C_6X_6H_6$ and $C_6X_3H_3$ ($X = B, Al, Ga$); (ii) $C_6X_6H_6$ ($X = N, P, As, Si, Ge$); (iii) $C_6X_3H_3$ ($X = N, P, As$); (iv) C_6X_6 ($X = B, N, P, As$). The π -electron occupancy (electron-deficient or electron-sufficient) of the X-X (or XH, X=X) groups, the size of annulated small ring, and the period number of the X atom in Periodic Table determine the aromaticity-antiaromaticity of a SAM.

For six molecules $C_6H_6X_6$ and $C_6X_3H_3$ ($X = B, Al, Ga$) with electron-deficient groups, $\Delta E^A < 0$, $\Sigma \Delta E^{Am} < 0$, and $|\Delta E^A| > |\Sigma \Delta E^{Am}|$, so that $-35.4 < CESE \text{ (kcal/mol)} < -22.6$ (stabilizing). When and only when the X-X (or XH) groups are electron-deficient, the SAMs are aromatic.

For the molecules $C_6H_3X_3$ ($X = N, P, As$) and for the molecules $C_6H_6X_6$ ($X = N, P, As, Si, Ge$), the groups (XH, X-X and HX=XH) are all electron-rich (or sufficient), but the size of the annulated small ring is different. When the small rings are the three-membered ring, the molecules $C_6H_3X_3$ ($X = N, P, As$) are anti-aromatic due to that $31.2 < ESE \text{ (kcal/mol)} < 66$, and $\Delta E^A > 0$. For the molecules $C_6H_6X_6$ ($X = N, P, As, Si, Ge$), the small rings are the four-membered ring. In this case, the ESE value depends on the period number of the X atom. When the period number > 2 , $0 < ESE \text{ (kcal/mol)} < 9$, that is, The ESE value is not large enough, and $ESE/\Sigma \Delta E^{Am} > 30\%$ that is a bit big. Hence, the energy effects $\Sigma \Delta E^{Am}$ cannot be considered additive, and it is difficult for the molecules $C_6X_6H_6$ ($X = P, As, Si, Ge$) to be regarded anti-aromatic or non-aromatic.

For the last group of molecules C_6X_6 ($X = B, N, P, As$), when the period number of an atom X is greater than 2, the energy effects $\Sigma\Delta E^{Am}$ are additive, and the molecules ($X = P, As$) are non-aromatic.

For the five molecules ($C_{12}H_6$, $C_6N_6H_6$, $C_6N_3H_3$, C_6B_6 and C_6N_6), the ESE values (kcal/mol) are as follows: 20.2, 36.8, 31.2, 38.7 and 14.9. Therefore, when the X atom belongs to the second period of the Periodic Table, the aromaticity-antiaromaticity of a SAM can be clearly determined. The molecules $C_6B_6H_6$ and $C_6B_3H_3$ are aromatic, and the above five molecules are antiaromatic.

11.6. REFERENCES

- 1 Schleyer, P. v. R.; Maerker, C.; Dransfeld, A.; Jiao, H.; Hommes, N. J. R. v. E. 1996. "Nucleus-Independent Chemical Shifts: A Simple and Efficient Aromaticity Probe." *J. Am. Chem. Soc.*, 118: 6317-6318.
- 2 Faglioni, F.; Ligabue, A.; Pelloni, S.; Soncini, A.; Viglione, R. G.; Ferraro, M. B.; Zanasi, R.; Lazzaretti, P. 2005. "Why Downfield Proton Chemical Shifts Are Not Reliable Aromaticity Indicators." *Org. Lett.*, 7: 3457-3460.
- 3 Poater, J.; Sola', M.; Viglione, R. G.; Zanasi, R. 2004. "Local Aromaticity of the Six-Membered Rings in Pyracylene. A Difficult Case for the NICS Indicator of Aromaticity." *J. Org. Chem.*, 69: 7537-7542.
- 4 Stanger, A. 2005. "Nucleus-Independent Chemical Shifts (NICS): Distance Dependence and Revised Criteria for Aromaticity and Antiaromaticity." *Org. Chem.*, 71: 883-893.
- 5 Bachrach, S. M. 2002. "Aromaticity of Annulated Benzene, Pyridine and Phosphabenzene." *J. Organomet. Chem.* 643–644: 39–46.
- 6 Hehre, W. J.; McIver, R. T.; Pople, J. A.; Schleyer, P. v. R. 1974. "Alkyl Substituent Effects on the Stability of Protonated Benzene." *J. Am. Chem. Soc.*, 96: 7162–7163.
- 7 Stanger, A. 2008. "The Different Aromatic Characters of Some Localized Benzene Derivatives." *J. Phys. Chem. A*, 112: 12849–12854.
- 8 Molavian, M. R.; Abdolmaleki, A.; Eskandari, K. 2017. "Strain or Electronic Effects? MP2 and DFT Aromaticity Investigation in Small Ring Annulated Benzene." *Comput. Theor. Chem.*, 1099: 102-108.
- 9 Sakai, S. 2014. "Theoretical Simple Estimation and Accurate Evaluation of Local Aromaticity for Polycyclic Conjugated Hydrocarbons." *J. Phys. Org. Chem.*, 27: 555-564
- 10 Bao, P.; Yu, Z. H. 2010. "Restricted Geometry Optimization for Estimating Stabilization Energies of Polycyclic Aromatic Hydrocarbons." *J. Phys. Org. Chem.*, 23: 16-29.
- 11 Bao, P.; Yu, Z. H. 2007. "Restricted Geometry Optimization: A Different Way to Estimate Stabilization Energies for Aromatic Molecules of Various Types." *J. Phys. Chem. A*, 111: 5304-5313.
- 12 Bao, P.; Yu, Z. H. 2011. "New Procedure to Evaluate Aromaticity at the Density Functional Theory, Hartree-Fock, and Post-Self-Consistent Field Levels." *J. Comput. Chem.*, 32: 248-259.
- 13 Cava, M. P. 1967. *Cyclobutadiene and Related Compounds*. New York: Academic press Inc..
- 14 Bergmann, E. D.; Pullman, B. Eds 1971. *Aromaticity, Pseudo-Aromaticity Anti-Aromaticity*. Jerusalem: Israel Academy of Science and Humanities.
- 15 Katritzky, A. R.; Barczynski, P.; Musumarra, G.; Pisano, D.; Szafran, M. 1989. "Aromaticity as a Quantitative Concept. 1. A Statistical Demonstration of the Orthogonality of 'Classical' and 'Magnetic' Aromaticity in Five- and Six-Membered Heterocycles." *J. Am. Chem. Soc.*, 111: 7-15.
- 16 Rice, J. E.; Lee, T. J.; Remington, R. B.; Allen, W. D.; Clabo, D. A.; Schaefer, H. F. 1987. "[5]Paracyclophane: An Important Example of Ring Strain and Aromaticity in Hydrocarbon Compounds." *J. Am. Chem. Soc.*, 109: 2902-2909.

CHAPTER 12

LOCALIZED GEOMETRY OPTIMIZATION

ABSTRACT

Our 2011 method is improved by additionally deleting the gradients of two-electronic exchange integrals, and the improved version is called our 2014 method. For acyclic polyenes, the additivity of the energy effects $\Delta E^{\text{Am}}(2014)$ becomes better. For a set of the values of adiabatic delocalization energy (kcal/mol) of cyclobutadiene at four theoretical levels using four different basis sets, the range and average values are 16.4 and 57.3 kcal/mol, and the B3LYP/6-31G* value of 54.9 kcal/mol is equal to the experimental value of 55 kcal/mol. For the ESE of benzene, the range (kcal/mol) of a set of the thirty-six values decreases from -5.4 (2011) to -3.0 (2014), and total averages (kcal/mol) are -35.0 (2011) and -37.0 (2014); the B3LYP/6-31G* value (-36.4 kcal/mol) is equal to the experimental value of -36 kcal/mol. For the distance $r_{23}(\text{GL})$ of naked CC single bond in the localized GL geometry of butadiene, the ranges of a set of forty-eight values are 0.067 (2014) Å and 0.117 (2011) Å. All the calculation results mentioned above confirm that our 2014 method is more reasonable than our 2011 method.

For 66 butadiene derivatives, the ranges of the $r_{23}(\text{G})$ values are 0.107 Å. Particularly, $\Delta r_{23}(\text{G}) = r_{23}(\text{G}) - r_{23}(\text{GL})$ can be well fitted as the polynomial function of $\Delta E(\text{G}) = E(\text{G}) - E(\text{GL})$. The ranges of the $\Delta E(\text{G})$ and $\Delta r_{23}(\text{G})$ values are 21.1 kcal/mol and 0.086 Å. The conjugation energy $\Delta E(\text{G})$ indeed determines the bond distance difference $\Delta r_{23}(\text{G})$ between the ground state geometry and its GL geometry. The size and sign of the differences $\Delta E(\text{G})$ and $\Delta r_{23}(\text{G})$ depend on the electron occupancy of substituent(s) and on the position of the element in Periodic Table. For butadiene-like species and XH₂-substituted butadienes (X = B, Al, Ga) with electron-withdrawing group, always $\Delta E(\text{G}) < 0$, and $\Delta r_{23}(\text{G}) < 0$, the ranges of the $\Delta E(\text{G})$ and $\Delta r_{23}(\text{G})$ values are -7.8 kcal/mol -0.041 Å. For halogen- and XH₂-substituted butadienes (X = N, P, As) having electron-releasing groups, always $\Delta E(\text{G}) > 0$ (destabilizing). When halogen atom and X atom (F, N) belong to the second period of Periodic Table, always $\Delta r_{23}(\text{G}) > 0$, and the ranges of the $\Delta r_{23}(\text{G})$, $r_{23}(\text{G})$ and $r_{23}(\text{GL})$ values are 0.037, 0.015 and 0.020 Å, respectively. Otherwise, $\Delta r_{23}(\text{G}) < 0$ (stabilizing), and the corresponding ranges are -0.004, 0.019 Å and 0.022 Å.

For the substituted butadienes with and only with electron-releasing substituent(s), as shown by the energy decomposition, the adjacent conjugation between each double bond and its substituents can obviously affect the distance $r_{23}(\text{GL})$ of naked CC single bond through the σ bonds, and the ranges (Å) of the $\Delta r_{23}(\text{GL})$ values are -0.031 (halogen substituted), -0.034 Å (XH₂-substituted) (X = N, P, As).

yuzh@iccas.ac.cn

Key words: deleting gradient of two-electronic exchange integrals; naked CC single bond between two double bonds; conjugation and adjacent conjugation; electron-withdrawing substituent; electron-releasing substituents; substituted butadiene.

12.1. INTRODUCTION

As a typical and smallest conjugated molecule, trans-1,3-butadiene (butadiene) has long been used to understand and explain the fundamental principles of organic chemistry. The conjugation effect in butadiene involves two basic characteristics, one is the conjugation energy, and the other one is the change in the distance of the CC single bond between two conjugated double bonds. The controversy over the characteristics of the conjugation effect also revolves around these two basic characteristics. This is the last basic issue that this monograph must face.

The conjugation energy (-3.5 kcal/mol) of butadiene was experimentally estimated by the difference, in hydrogenation heat, between 1,3-butadiene and two 1-butene (Kistiakowsky in 1936),^{1,2} and it has long been used as experimental evidence to support the basic concept of π -electron delocalization stabilization.³ (There is a difference, in the way to express the resonance energy value, between our works and the literatures. In the literature such as organic chemistry textbook written by Vollhardt,³ stabilization conjugation energy of butadiene is expressed as a positive value of 3.5 kcal/mol. In this work, it is expressed as a negative value of -3.5 kcal/mol). Based on this so-called experimental basis, the basic concept of conjugation stabilization seems to be unquestionable. But when trans-2-butene and cis-2-butene are used as a reference molecule, as argued by us in Chapter 6, the delocalization energies are, respectively, 1.9 (destabilizing) and -0.1 kcal/mol (stabilizing). Especially, in the case of a selective hydrogenation of butadiene (Silvestre-Albero, et. al. in 2005),⁴ the main product, about 60% yield, is trans-2-butene, and the yields of cis-2-butene and 1-butene are, respectively, 30% and 10% as long as the reaction time is long enough (> 100 min). Accordingly, whether the π -electron delocalization energy is stabilizing or destabilizing depends on the choice of reference molecule. In the case of butadiene, the so-called experimental evidence for the π -delocalization stabilization is only the result of selecting experimental data based on subjective wishes.

Regarding the second basic characteristics of the conjugation effect, the discussion in this chapter will address the following two issues:

- (i) How to reasonably evaluate the distance of the naked sp^m-sp^n single bond.
- (ii) Which structural factor determines the distance of the sp^m-sp^n CC single bond between two conjugated groups.

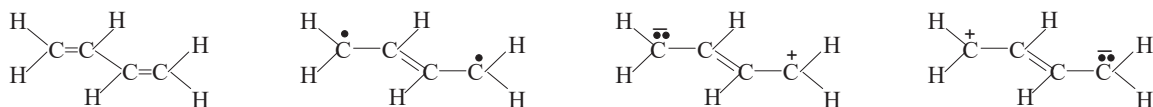
Pauling (1939),⁵⁻⁸ Coulson (1939),⁹⁻¹¹ and Mulliken (1941),^{12,13} as well as Organic chemistry textbooks,³ have introduced the concept of conjugation stabilization, based on the facts that the distance (1.54 Å) of the CC single bond in ethane is longer than any one of the following experimental values of the C-C single bond distance in 1,3-butadiene: 1.467 Å (Trætteberg in 1966),¹⁴ 1.468 Å (Kveseth in 1980),¹⁵ 1.460 Å (Pauling in 1939),^{8,16} 1.467 Å (Caminati in 1988),¹⁷ and 1.454 Å (Craig, in 2006)¹⁸.

In a specific polyene such as butadiene, the structure factors influencing the CC single bond distance include hybridization, conjugation (resonance) effect, hyperconjugation,¹² nonbonded orbital interaction (Epiotis in 1977),¹⁹ inductive effect (Well in 1949),²⁰ van der Waals forces (Bartell in 1960),²¹ polar Effects (Berry in 1959),²² and steric hindrance (Wilson in 1962)²³. The structural effects in butadiene should be significantly different from those in ethane. In the literature, therefore, which structural factor, resonance or hybridization, determines the distance of the C-C single bond in butadiene and whether there is the existence of resonance (conjugation) interaction between the two double bonds were controversial.

12.1.1. Pauling's Resonance Theory

In 1931, Pauling first developed the hybridization theory,²⁴ and he (1939) found that CH bond distance

decreases as the s-character in hybrid increases.⁷ Nevertheless, as the theoretical chemists to extend resonance theory to conjugated molecules (1932), Pauling and his coworkers (1935) clearly expressed their opinion that the distance of the single bond adjacent to double bond depends on the resonance between two or more structures.^{5,6} For butadiene, for example, the CC single bond is 0.08 Å shorter than that of ethane. This shortening was attributed by Pauling to the resonance among the following four electronic structures:⁸



According to the last three resonance structures, the CC single bond between two double bonds has the amount of double bond character. In 1935, the function curve $r = f(x)$, quantitatively describing the dependence of the CC bond distance (r) on the amount (x) of double bond character, was fitted by Pauling, based on the following experimental distance (Å) and amount of double bond character for each of four CC bonds: 1.38 Å and 100% (ethylene), 1.39 Å and 50% (benzene), 1.42 Å and 33.3% (graphite), 1.54 Å and 0 % (diamond, and ethane).⁶ Now, this function can be expressed by us as the following third order polynomial function:

$$r = 1.54 - 0.50105x + 0.46315x^2 - 0.1221x^3$$

With the aid of the fitted function $r = f(x)$, and using the experimental distances of the CX (X = C, N, O) bonds, the corresponding amount of double bond character was assigned by Pauling in 1935⁶ and are listed in the last column of Table 12-1. The first order derivative $dr/dx > 0$, and its value is so large that, as shown by the data listed in Table 12-1, a small increase in the amount of double bond character can result in a significant reduction in the bond length. For diacetylene, for example, the experimental distance of C-C single bond is 1.43 Å (1933), and the corresponding amount of double bond character is 0.29. The amount of double bond character can be used as a criterion of characterizing the strength of resonance, and therefore it can be used to deduce the role of resonance (conjugation) effect in determining the distance of CC single bond.

Table 12-1. Bond Distances (Å) and the Amount of Double Bond Character.

Molecules	Bond	Observed	Amount of Double bond character
Cyclopentadiene	C-C	1.46	0.20 (20 %)
p-Diphenylbenzene	C-C	1.48	0.14
Biphenyl	C-C	1.48	0.14
Cyanogen	C-C	1.43	0.29
Diacetylene	C-C	1.43	0.29
Urea	C-N	1.37	0.28
Thiourea	C-N	1.37	0.38
Cyanuric triazide	C-N	1.38	0.25
Carbon suboxide	C=C	1.30	0.20
	C=O	1.20	0.20

The data are cited from Pauling, L.; Brockway, L. O.; Beach, J. Y. *J. Am. Chem. Soc.* **1935**, 57, 2705.

Table 12-2. Bond Distances Determined by Electron Diffraction.

Molecules	C-C (Å)	C=C (Å)
Ethane	1.55 ± 0.03	
Propane	1.54 ± 0.02	
Isobutane	1.54 ± 0.02	
Neopentane	1.54 ± 0.02	
Cyclopropane	1.53 ± 0.03	
Cyclopentane	1.52 ± 0.03	
Cyclohexane	1.53 ± 0.03	
Allene		1.34 ± 0.02
Ethylene		1.34 ± 0.02
Isobutene	1.54 ± 0.02	
Tetramethyl-ethylene	1.54 ± 0.02	
Mesitylene	1.54 ± 0.01	
Hexamethyl-benzene	1.54 ± 0.01	

The data are cited from Pauling, L.; Brockway, L. O. *J. Am. Chem. Soc.* **1937**, *59*, 1223.

In 1937 and 1939, the structures of 13 non-resonating molecules were experimentally investigated by Pauling in order to support their opinion (Table 12-2). In these molecules, the single bond is only adjacent to a double bond, or it is not between the two conjugated double bonds. As the interesting feature of this type of molecules, the C-C single bonds have the constant distance of $1.54 \pm 0.02 \text{ \AA}$,⁷ and they are unaffected by an adjacent double bond or benzene ring although the hybrid states of the carbon atoms forming C-C single bonds in the different molecules are different. For hexamethyl-benzene, for example, the distance of the CC single bond between methyl group and phenyl ring is 1.54 Å, although this bond is a single bond of $\text{sp}^3\text{-sp}^2$ type. In cyclopropane, the C-C-C bond angles are distorted from $109^\circ 28'$ to 60° , which should lead to the change in the bond distance due to the increase in the strain and s-character. Interestingly, as shown by the data listed in Table 11-2, the carbon-carbon distance (1.53 Å) in cyclopropane is the same as that in the other hydrocarbons.

In each of molecules listed in Table 12-3, the distance of a $\text{sp}^3\text{-sp}$ CC single bond adjacent to a triple bond is in the region of 1.46 Å to 1.49 Å, and the distance of a sp-sp CC single bond between two triple bonds decreases to about 1.38 Å. In diacetylene, for example, the distance of the sp-sp CC single bond is 1.36 Å, and it is shorter than the distance (1.46 Å) of the CC bond between methyl group and triple bond in methylacetylene. In a conjugated molecule such as diacetylene, two conjugated triple bonds can interact through the p_z and p_y orbitals. So, as indicated by Pauling, the conjugation of this system is twice as great as the conjugation between two double bonds in butadiene. Correspondingly, the amount (44%) of double-bond character for diacetylene is about twice that (18%) for butadiene, and the difference (0.18 Å) in the CC single bond length between diacetylene and ethane is also about twice that (0.08 Å) between butadiene and ethane.

Based on the experimental evidences for the role of resonance effect in determining the distance of CC single bonds, Pauling suggested that, for the distance of the CC single bond, the decrease below the normal value of 1.54 Å is due partly to a change in single-bond radii (contribution of about 0.02 Å to the shortening), and mainly due to the

Table 12-3. The CC Single Bond Distances (\AA)

Molecules	sp ³ -sp C-C	triple bond	sp-sp C-C
$\text{CH}_3\text{-C}\equiv\text{CH}$	1.46	1.20	
$\text{CH}_3\text{-C}\equiv\text{C-CH}_3$	1.47	(1.20)	
$\text{CH}_3\text{-C}\equiv\text{C-C}\equiv\text{C-CH}_3$	1.47	1.20	1.38
$\text{HC}\equiv\text{C-C}\equiv\text{CH}$		1.20	1.36
$\text{N}\equiv\text{C-C}\equiv\text{N}$			1.37
$\text{CH}_3\text{-C}\equiv\text{N}$	1.49		

The data are cited from Pauling, L.; Springall, H. D.; Palmer, K. J. *J. Am. Chem. Soc.* **1939**, *61*, 927.

partial double-bond character of the single bond. For butadiene, for example, the decrease in the distance of CC single bond from 1.54 \AA to 1.460 \AA (experimental value determined by Pauling in 1939) was mainly attributed to the resonance between the single and double bonds.

It should be indicated that, in the structures of diacetylene ($\text{HC}\equiv\text{C-C}\equiv\text{CH}$) and cyanogen ($\text{N}\equiv\text{C-C}\equiv\text{N}$) determined by Brockway in 1933,⁶ both CC single bond lengths are 1.43 \AA . In this case, the difference (0.11 \AA), in the CC single bond length, between diacetylene and ethane is only 0.03 \AA greater than that (0.08 \AA) between butadiene and ethane, and the single bond length in diacetylene is also only 0.03 \AA shorter than that in butadiene, which seems not to match the difference, in the number of conjugated double bond pairs, between diacetylene and butadiene. In 1939, Pauling corrected the lengths of the CC single bonds in diacetylene and cyanogen. Their corrected distances are 1.36 and 1.37 \AA , respectively (Table 12-3). As a result, the difference, in the CC single bond distance, between diacetylene and butadiene increases to about 0.1 \AA . This greater difference becomes matched to the difference, in the number of conjugated double bond pairs, between diacetylene and butadiene, and it becomes an evidence of supporting Pauling's opinion.

A similar situation was found in the determination of hexamethylbenzene (HMB) structure. For the CC single bond between methyl group and phenyl ring in HMB, the distance of 1.48 \AA was first determined by x-ray diffraction (Lonsdale in 1929).²⁵ In 1937, the bond length was corrected by Pauling with the value of 1.54 \AA (Table 12-2). In 1939, the structure of HMB was determined once again by x-ray diffraction (Brockway),²⁶ showing the distance of 1.53 \AA .

12.1.2. Coulson's Method

In 1939, Coulson quantitatively correlated the calculated bond order (p) with observed bond length (x). A function curve $x = f(p)$ (Coulson's curve), similar to the Pauling's curve, was fitted in 1939 and 1951 based on the experimental bond distance and calculated bond order for each of the following five molecules: ethane, graphite, benzene, ethylene, and acetylene,^{9,11} and it is almost perfect agreement with the following theoretical formula:

$$x = s - (s - d) / [1 + K(2 - p)/(p - 1)] \quad (12-1)$$

where x is the distance of CC bond, p is total bond order, s and d are the distances (1.540 and 1.330 \AA) of the single and double bonds, and K is constant.

In Coulson's era, the calculation of the bond order needed not the geometrical data. In the Pauling's method, the experimental distance of CC bond was used to calculate the amount of double bond character. Contrary to

Pauling's method, Coulson used the calculated bond order to guess the distance of CC bond.

Coulson intended to demonstrate that the calculation of bond distance is reasonable by Equation (12-1). Once this calculation is proved to be reasonable, the decisive role of the conjugation effect in determining the distance of a single bond can be proved by calculating the bond order of the single bond. For the C=C and C–C bonds in butadiene, for example, the total bond orders of 1.894 and 1.447 were calculated by Coulson. The total bond order of 1.447 is large enough to affirm the important role of the conjugation effect in determining the distance of the CC single bond.

12.1.3. Dewar's Viewpoint of Hybridization

Since the resonance (conjugation) effect was introduced into organic chemistry, the controversy over conjugation effect has not been stopped. Dewar questioned the existence of the resonance interaction between two double bonds in butadiene, and Epiotis clearly proposed his viewpoint of π -delocalization destabilization.²⁷⁻²⁹ Dewar (1958 and 1959)^{30,31} and Brown (1959)³² independently suggested that hybridization of carbon atoms determines the distance of the CC single bond in butadiene. Samayajulu (1959),³³ Lide (1962),³⁴ Bastiansen (1962),³⁵ and Duchesne (1950)^{36,37} expressed the similar opinion.

For three types of conjugated compounds such as Me–Me, Me–C≡C–, and –C≡C–C≡C–, the distances of the CC single bonds are as follows: $1.542 \pm 0.001 \text{ \AA}$ ($\text{sp}^3\text{-sp}^3$), $1.460 \pm 0.003 \text{ \AA}$ ($\text{sp}^3\text{-sp}$), $1.380 \pm 0.002 \text{ \AA}$ (sp-sp). Accordingly, the bond length difference (0.082 \AA) between the $\text{sp}^3\text{-sp}^3$ and $\text{sp}^3\text{-sp}$ CC bonds is the same as the bond length difference (0.080 \AA) between the $\text{sp}^3\text{-sp}$ and sp-sp CC bonds. As Dewar strongly suggested, the decrease in the bond distance is due to the change in covalent radius of carbon with hybridization, and not due to any resonance or delocalization effect.³¹ Interestingly, both Dewar and Pauling used the bond lengths of these three molecules as experimental evidence to support their respective views.

Another evidence for the hybridization effect was from a precision study of cyclooctatetraene by electron diffraction (Bastiansen in 1957).³⁸ Cyclooctatetraene is non-planar, as emphasized by Dewar in 1959,³¹ there is no significant resonance between double bonds. For cyclooctatetraene, the distances of the CC double and single bonds should be close to those of the naked $\text{sp}^2\text{-sp}^2$ double and single bonds. The experimental distance for CC double bond in this molecule is 1.334 \AA , and is the same as the experimental value³⁹ of 1.334 \AA for the double bond in ethylene. But the experimental distance of 1.462 \AA for the single bond is shorter than that for the single bond in butadiene, which seems to support Dewar's suggestion, at least not supports Pauling's point of view. However, in the butadiene and cyclooctatetraene, the distances of the CC single bonds are different in the different reports. For butadiene, for example, the C-C bond distance of 1.460 \AA , experimentally determined by Pauling in 1939, is shorter than that in cyclooctatetraene. In fact, these slight differences are within the experimental error range.

12.1.4. Covalent Radii

The assessment of the relative importance of hybridization and resonance (conjugation) is mainly based on the comparison of the sum of covalent radii and the experimental distance of a CC bond. Pauling neglected the influence of hybridization effect on the covalent radius of carbon atom, and postulated a constant distance for all CC single bonds in 1945.⁴⁰ Then, any deviation from his standard distance was attributed to resonance. This concept has remained in today's standard organic chemistry textbooks and has become a fundamental principle of organic chemistry.³

According to hybridization, the CC bonds were divided by Brown into the following 10 types:

Single bond: $\text{sp}^3\text{-sp}^3$, $\text{sp}^3\text{-sp}^2$, $\text{sp}^3\text{-sp}$, $\text{sp}^2\text{-sp}^2$, $\text{sp}^2\text{-sp}$, sp-sp

Double bond: $\text{sp}^2\text{-sp}^2$, $\text{sp}^2\text{-sp}$; sp-sp

Table 12-4. For CC Bonds, Covalent Radii r_1 and r_2 (\AA), Theoretical Bond Length $d^{\text{cal}} = r_1 + r_2$, and Experimental Bond Length d^{obs} .

	r_1	r_2	d^{cal}	d^{obs}	Molecules
Single bond					
sp ³ -sp ³	0.772	0.772	1.544*	1.545	diamond
Sp ² -sp ²	0.733	0.733	1.466*	1.462	cyclooctatrtraene
sp-sp	0.687	0.687	1.374*	1.377	methyl diacetylene
sp ³ -sp ²	0.772	0.733	1.505	1.501	acetaldehyde
sp ³ -sp	0.772	0.687	1.459	1.460	methylacetylene
sp ² -sp	0.733	0.687	1.420	1.419	phenyl cyanide
Double bond					
sp ² -sp ²	0.668	0.668	1.335*	1.334	cyclooctatrtraene
sp-sp	0.643	0.643	1.285*	1.309	carbon suboxide
sp ² -sp	0.668	0.643	1.311	1.309	allene

* The average of the experimental distances of the CC bonds in various molecules. Data are cited from Brown, M. G., *Trans. Faraday Soc.* **1959**, 55, 694.

Triple bond: sp-sp

In 1959, several hundred structures were classified by Brown under the above combinations of sp^m and sp^n ($m, n = 1, 2, 3$) hybrids, and the covalent radii for CC, CH and CX (X = Cl, Br) bonds were satisfactorily assigned.³² Based on the experimental distances of CC bonds, as shown by Table 12-4, the covalent radius of a sp^n carbon atom was assigned as half distance of $\text{sp}^n\text{-sp}^n$ CC bond. For the $\text{sp}^n\text{-sp}^n$ single CC bonds ($n = 1, 2, 3$), for example, the averages of the experimental distances (\AA) in various molecules are, respectively, 1.374 (sp-sp), 1.466 (sp²-sp²), and 1.544 (sp³-sp³). Therefore, the covalent radii of the corresponding sp^n carbon atoms in CC single bond are 0.687 ($n = 1$), 0.733 ($n = 2$), and 0.772 \AA ($n = 3$). In a similar way, for $\text{sp}^n\text{-sp}^n$ double and triple bonds, the covalent radii (\AA) of the corresponding sp^n carbon atoms were assigned and are listed in Table 12-4. On the basis of the assignments, for example, the theoretical distance, d^{cal} , of a $\text{sp}^m\text{-sp}^n$ CC single bond is the sum of r_1 and r_2 , that is, $d^{\text{cal}} = r_1 + r_2$, where r_1 is the covalent radius of the first (sp^m) carbon atom in the $\text{sp}^m\text{-sp}^n$ CC single bond and r_2 is the covalent radius of the second (sp^n) carbon atom. Particularly, when $r_1 \neq r_2$, d^{cal} is close to the experimental distance d^{obs} . For the sp²-sp CC double bond of allene HC=C=CH , for example, r_1 (0.668 \AA) $\neq r_2$ (0.643 \AA), and $d^{\text{cal}}(1.311 \text{\AA}) \approx d^{\text{obs}}(1.309 \text{\AA})$ (Table 12-4).

For butadiene, the calculated distance (1.466 \AA) of sp²-sp² CC single bond is almost equal to the distance of 1.468 \AA experimentally determined by Kveseth in 1980, but it is 0.006 \AA longer than that (1.460) determined by Pauling in 1939. For a $\text{sp}^m\text{-sp}^n$ CC single bond, the calculated value d^{cal} is close to the experimental value d^{obs} , which seems to support Dewar's viewpoint.

However, as shown by Table 12-5, the carbon atoms in molecule such as butadiene are in a non-integral sp^n hybridization state ($n \neq 1, 2, 3$). The sp^n hybrid and s-character of carbon atoms in butadiene were calculated by us

Table 12-5. For Optimized Geometry of Trans-butadiene $\text{H}_2\text{C}(1)=\text{C}(2)\text{H}-\text{HC}(3)=\text{C}(4)\text{H}_2$, Bond Lengths, Bond Angle $\text{H}(5)-\text{C}(1)-\text{H}(6)$ (α). For Carbon Atom C2 in C(2)–H and C(2)–C(3) Bonds, sp^n Hybrids and s Character Are Obtained from NBO Calculations.

	Bond length Å		Angle α	sp ⁿ for C2 atom		s character % for C2 atom	
	C1-C2	C2-C3		n in C2-H	n in C2-C3	in C2-H	in C2-C3
B3LYP/6-31G*	1.341	1.457	116.6	2.27	2.0	28.3	33.3
B3LYP/6-311G**	1.337	1.456	116.9	2.37	1.93	27.2	34.1
B3LYP/6-311G(2d,2p)	1.333	1.454	116.9	2.34	1.95	27.4	33.9
B3LYP/6-311G(3d,3p)	1.334	1.455	116.9	2.34	1.95	27.4	33.9
B3LYP/6-311G(2df, p)	1.333	1.453	116.8	2.35	1.95	27.3	33.8

using the NBO method, and they are listed in Table 11-5. For the C(2) atom in the C(2)-H bond at B3LYP/6-311G** level, for example, the ratio, p/s, of the p-character to s-characters is 2.37 ($\text{sp}^{2.37}$), and it is different from that ($\text{sp}^{1.93}$) for C(2) atom in the C(2)-C(3) single bond because the bond angle $\angle \text{H}-\text{C}(1)-\text{H} \approx 116.5^\circ \neq 120.0^\circ$, and their s-characters are also different from each other. According to the Equation (12-2), the covalent radii of the carbon atom in the C(2)-H bond should be different from that in the C(2)-C(3) single bond. The CC single bond distance in butadiene cannot serve as the basis for determining the sp^2 radius.

The covalent radius, r_c^{cov} , of a carbon atom was expressed by Mikhailov (1965) as the following linear function of the s-character of its orbital:⁴¹

$$r_c^{\text{cov}} = (0.854 - 0.328s) \quad (12-2)$$

Equation (12-2) was used by Mikhailov to calculate the CC single bond distance in saturated and unsaturated hydrocarbons such as ethane, propane, isobutane, propylene, methylacetylene, and butadiene. For each of these molecules, the calculated distance of the CC single bond differs by 0.004 Å from the corresponding experimental value. For butadiene $\text{H}_2\text{C}(1)=\text{C}(2)\text{H}-\text{HC}(3)=\text{C}(4)\text{H}_2$, for example, the s-characters of C(2) and C(3) atoms both are 0.336, and the calculated distance of C(2)–C(3) bond, by Equation (12-2), is 1.488 Å, and it differs by 0.004 Å from the experimental value of 1.484 Å (the experimental value of 1.484 Å was listed in Table 2 of Mikhailov's article⁴¹). The distances of the CC single bonds in the molecules above mentioned, calculated by Equation (12-2), were used to confirm the theory of hybridization.

However, for the relative importance of resonance and hybridization effects, the conclusions obtained from the covalent radii of carbon atoms are not completely consistent, due to the different calculation method. Coulson found that the covalent radius of the sp carbon in acetylene is 0.735 Å according to the distance of CH bond (seeing ref. 41), which was based on the following two assumptions: (i) A constant radius (0.323 Å) for hydrogen; (ii) for a specific carbon atom of a molecule, the covalent radius in the CH bond is the same as that in the CC bond. For CC sing bond in methylacetylene, therefore, $d^{\text{cal}} = 0.735 (\text{sp}) + 0.772 (\text{sp}^3) = 1.507$ Å, and $d^{\text{obs}} = 1.459$ Å, where the value of 0.772 Å was cited from the Brown's value. In this case, $d^{\text{cal}} - d^{\text{obs}}_{\text{CC}} = 0.048$ Å, and this shortening of the CC single bond was attributed to resonance effect by Mikhailov.⁴¹

12.1.5. Controversy over Resonance Existence

In 1953, Ingold summered up the structure theory of organic chemistry.⁴² Since then, as one of the three basic

structural effects (conjugation effect, inductive effect, and steric hindrance), the resonance (conjugation) effect has been used to understand and explain the relationship between molecular structure and its properties. In the field of organic chemistry, it is the mainstream concept (or fundamental concept) that conjugation effect determines the distance of the single bond between two conjugated double bonds, and the hybridization effect has been excluded from the basic structural effects.

Dewar's argument (Dewar's viewpoint of hybridization) raised question of whether there is clear evidence for the existence of resonance effects in the olefin ground state, and has sparked debate about the relative importance of hybridization and resonance. But it should be indicated that Dewar only questioned the existence of the conjugation effect in olefins rather than questioning the stabilization feature of the conjugation effect. Due to Dewar's questioning, the fact that the distance of the CC single bond in butadiene is shorter than the distance of 1.54 Å cannot be used as the basic experimental evidence of conjugation stabilization, although Dewar's view has not yet been written into standard textbooks of organic chemistry, and although this fact is widely used by standard textbook to stress the concept of conjugation stabilization.

Shortening of the CC single bond in the conjugated system such as butadiene was interpreted by Pauling as the result of the resonance among the four electronic structures, and it is attributed to the conjugation between two double bonds in the standard textbook of organic chemistry. However, this interpretation needs to be supported by the fact that the distance of the C=C double bond increases. For the distances of the double bonds in ethylene and butadiene, the experimental values (Å) are 1.334 (or 1.34) (Bartell in 1957)³⁹ and 1.35 (Pauling in 1939)¹⁶, respectively. In the Pauling's era, the expected change (about 0.01 Å) in the double bond distance is not much greater than any possible experimental error (about ±0.02 Å) of the methods. Early in 1944, therefore, Burawoy advanced his ideas that there is no such thing as Pauling's resonance.⁴³

Burawoy's ideas was supported by Duchesne in 1951. For CL-CN and CL-C≡CH molecules, due to the p-π resonance between CL- and -CN (or C≡C), the bond orders of the C≡N and C≡C bonds should be less than those of the corresponding molecules HC≡N and HC≡CH. In fact, as shown by very precise measurements, the resonance has no influences on the bond distance and force constant.⁴⁴⁻⁴⁷ For molecule CLC≡N, for example, the force constant (18 *10⁵ dynes/cm) of its C≡N group is exactly equal to that of the C≡N group in HCN molecule.³⁶

The structural factors governing the bond lengths are very complex, and it is not possible to clearly understand these structural factors before obtaining an accurate wave function. So Mulliken was not entangled with the way to assign the covalent radii of atoms. By citing the LCAO-MO coefficients and bond orders calculated by various authors, and by using a standard bond order–bond length curve (Coulson in 1951)¹¹, Mulliken assumed that, for butadiene, the 40% shortening of CC single bond can be attributed to π-electron delocalization. Accordingly, Mulliken said:¹³ Dewar is partly right in supposing that the distances of conjugated and hyperconjugated CC single bonds are determined by hybridization rather than by π-resonance.

However, as Dewar suggested, the C-C bond order may be reduced to nearly zero if the interelectronic repulsions and correlation energy can be accurately calculated. For the π bond order of the single bond in butadiene, as shown by our practical calculations, the (RHF and MP2)/6-311G** values of 0.005 and 0.001 (if the σ bond order is 1) are nearly equal to zero, and the B3LYP value is in the region of from 0.09 to 0.138.

12.1.6. Historical Limitations

Due to the limitations of the times, theoretical calculations and experimental methods often fail to ensure the validity of the calculation results and the reliability of the experimental data.

For the CC single bonds in 1,3,5,7-cyclooctatetraene, for example, the experimental distance, determined by Trætteberg in 1966 using the sector electron diffraction method,⁴⁸ is 1.48 Å, rather than 1.462 Å measured by Bastiansen in 1957 using electron diffraction.³⁸ As a result, the CC single bond in 1,3,5,7-cyclooctatetraene is 0.01 Å longer than that (1.467 Å)¹⁴ in butadiene (determined by Trætteberg in 1966). In 1976, therefore, Bogg

complained that the discussion of conjugation was confused for many years by the erroneous experimental results.⁴⁹

In 1988 and 2008, the structure of 1,3,5,7-cyclooctatetraene was obtained by Claus⁵⁰ and by Kumml⁵¹, respectively, from the x-ray diffraction at 129 K and from the combination of femtosecond time-resolved rotational coherence spectroscopy with high-level *ab initio* calculation, and the experimental distances of C-C single bonds are 1.465 Å to 1.473 Å (Claus in 1988) and are 1.47 Å (Kumml in 2008), once again indicating that the C–C bond length in cyclooctatetraene is almost equal to the CC single bond length of 1.468 Å (Kveseth in 1980)¹⁵ for 1,3-butadiene. The experimental distances (Å) of the CC single bond in 1,3,5,7- Cyclooctatetraene are summary as follows:

1.462 (1957), 1.48 (1966), 1.465 to 1.473 (1988), 1.47 (2008)

Due to that it is difficult to separate hybridization and resonance off, an interesting phenomenon was that the distances of the CC single bonds in the conjugated molecules such as diacetylene, methyldiacetylene and methylcyanide were used as the experimental evidences, respectively, by Pauling and Brown to support the two conflicted views. Therefore, as Mulliken stressed in 1962,⁵² there are many structural factors that lead to changes in the molecular structure. Their importance varies from case to case, so it is difficult to pick out the real structural factors and give the correct weight. In this section, I only focus on the controversy of the conjugation effect in the development of organic chemistry, not on method of argumentation and on the evidences provided, because, as Mulliken pointed out in 1962, it is almost impossible for chemists to collect and maintain a large experimental and theoretical evidences.

At last, as indicated by Dewar in 1959,³⁰ "Unless the degree of shortening can be estimated, no conclusions can be drawn from the lengths of single bonds in molecules such as butadiene." Therefore, it is necessary to emphasize again that the following two questions raised at the beginning of this chapter are the core of this chapter.

- (i) How to reasonably evaluate the distance of the naked sp^m-sp^n single bond.
- (ii) Which structural factor determines the distance of the sp^m-sp^n CC single bond between two conjugated groups.

12.2. DEVELOPMENT OF OUR METHOD

The only way to be able to evaluate the influence of the conjugation effect on the distance of single bond between two double bonds is to theoretically determine the distance of naked sp^m-sp^n single bond. In the literature, only our 2011 method has this ability.

For trans-1,3-butadiene, for example, the localized GL geometries can be optimized by Our 2011 method under the conditional settings detailed in Figure 12-1e, and it is denoted as GL(2011). The CC single bond in the GL(2011) geometry can be considered as a naked sp^2-sp^2 CC single bond because two double bonds bonded to the two different carbon atoms of the single bond are not conjugated. In trans-1,3-butadiene at B3LYP/6-31G* level, for example, it is 1.441 Å and is shorter than the distance (1.457 Å) in the ground state geometry of trans-1,3-butadiene. When our 2014 method, as the improved version of our 2011 method, is used, this naked distance will increase to 1.451 Å (Figure 12-1c).

Before emphasizing the need to improve our 2011 method, it is necessary to briefly review the development process from our 2007 method to our 2011 method.

12.2.1. Our 2007 Method

In the GL geometry of butadiene constructed by our 2007 method, as shown by the AO coefficients listed in

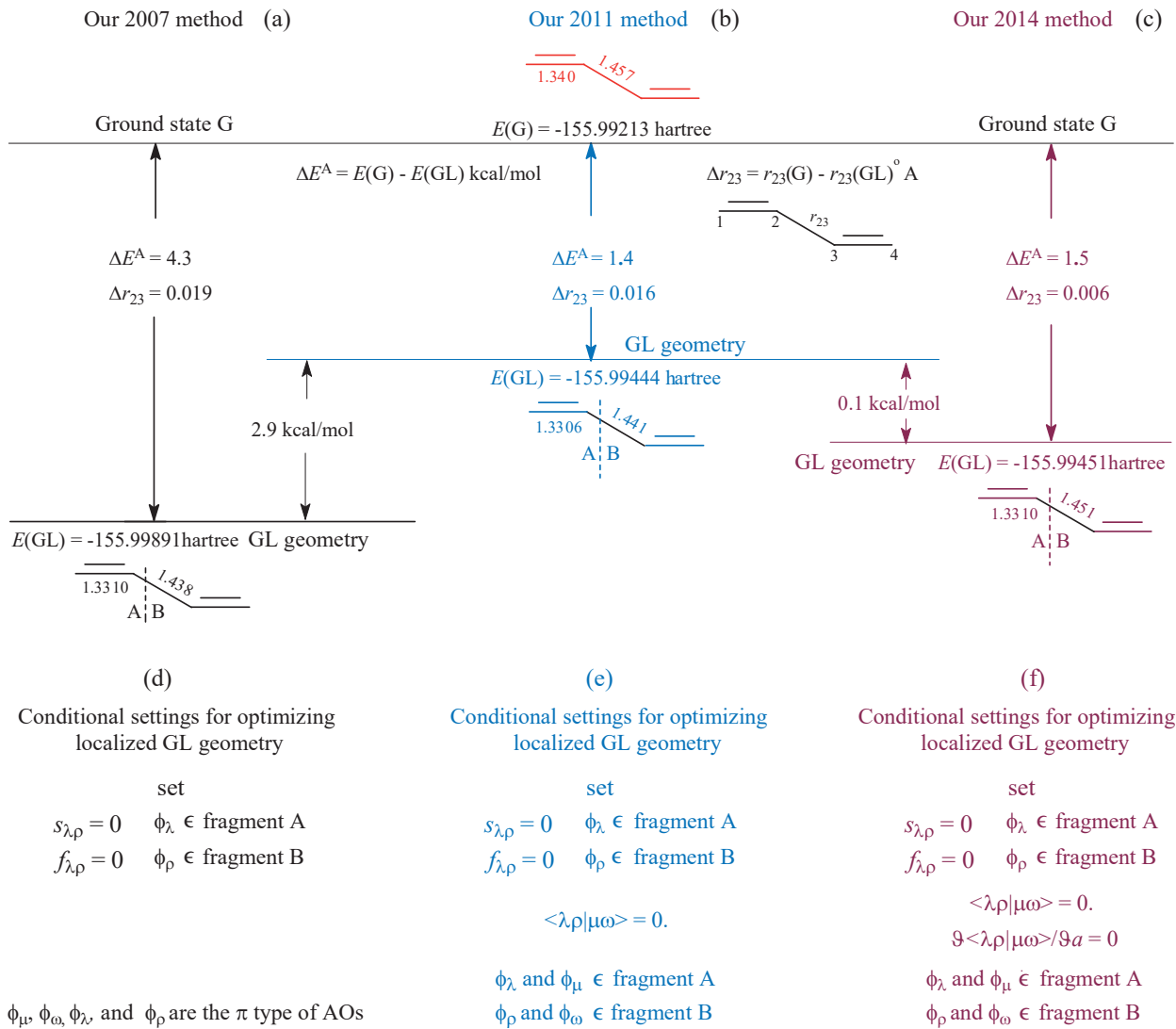


Figure 12-1. For trans-1,3-butadiene at the B3LYP/6-31G* level, the three ways to, restrictedly, optimize the GL geometry. In the GL geometry, the π orbital interaction, the spatial π electron interaction and the exchange gradients between the double bonds have been set equal to zero.

Table 12-6, the π MOs are, absolutely, localized on their respective double bonds. In the meantime, the π -MO charge transfer and exchange interactions have been excluded from between two double bonds (denoted as fragments A and B) due to the following conditional settings (Figure 12-1d): before each SCF iteration, set (AO overlap integral matrix elements) $s_{\lambda,\rho} = 0.0$, and set (AO Fock matrix elements) $f_{\lambda,\rho} = 0.0$, when π AO $\phi_\lambda \in$ fragment A, π AO $\phi_\rho \in$ fragment B. In this case, the GL geometry of butadiene constructed by our 2007 method, denoted GL(2007), is a geometry with localized π -MOs. The construction of GL geometry makes it possible to calculate the energy differences, $\Delta E^A = E(G) - E(GL)$, between the ground state (G) and its GL geometry, and thus it solves a basic problem of how to provide a reference (localized) geometry for the calculation of adiabatic delocalization energy. The energy difference ΔE^A can also be considered as an energy effect arising from the π -MO interaction between the two localized double bonds in the GL geometry of butadiene.

Table 12-6. For Three GL Geometries of Butadiene Obtained from Our 2007, Our 2011 and Our 2014 Methods at B3LYP/6-31G* Level, the Eigenvalues and AO Coefficients of the Two Occupied MOs for Each Geometry.

				GL(2007)		GL(2011)		GL(2014)	
				14-th	15-th	14-th	15-th	14-th	15-th
		Eigenvalues		-0.2770	-0.2769	-0.2753	-0.2752	-0.2750	-0.2750
5	C	1	Z	0.000000	0.393382	0.000000	0.395549	0.000000	0.395884
9	C	1	Z	0.000000	0.259656	0.000000	0.266155	0.000000	0.266850
14	C	1	XZ	0.000000	0.014182	0.000000	0.014481	0.000000	0.014473
15	C	1	YZ	0.000000	-0.005740	0.000000	-0.005886	0.000000	-0.005910
20	C	2	Z	0.000000	0.399931	0.000000	0.401559	0.000000	0.401458
24	C	2	Z	0.000000	0.318070	0.000000	0.308066	0.000000	0.307255
29	C	2	XZ	0.000000	-0.010366	0.000000	-0.011271	0.000000	-0.011569
30	C	2	YZ	0.000000	0.009831	0.000000	0.009249	0.000000	0.008992
35	C	3	Z	0.399951	0.000000	0.401580	0.000000	0.401470	0.000000
39	C	3	Z	0.318045	0.000000	0.308037	0.000000	0.307239	0.000000
44	C	3	XZ	0.010369	0.000000	0.011274	0.000000	0.011572	0.000000
45	C	3	YZ	-0.009841	0.000000	-0.009259	0.000000	-0.008999	0.000000
50	C	4	Z	0.393411	0.000000	0.395578	0.000000	0.395908	0.000000
59	C	4	Z	0.259584	0.000000	0.266085	0.000000	0.266788	0.000000
64	C	4	XZ	-0.014198	0.000000	-0.014496	0.000000	-0.014492	0.000000
65	C	4	YZ	0.005760	0.000000	0.005904	0.000000	0.005931	0.000000

The coefficients of all σ -type AOs are equal to zero, and they are not listed.

Contrary to the expectation of the classical view, the molecular energy difference (adiabatic delocalization energy), $\Delta E^A = [E(G) - E(GL)] = 4.3 \text{ kcal/mol} > 0$, and it is destabilizing (Figure 12-1a). Correspondingly, the distance (1.457 Å) of the C(2)-C(3) single bond in ground state geometry is longer than that (1.438 Å) in the GL(2007) geometry, and the distance difference, $\Delta r_{23} = r_{23}(G) - r_{23}(GL) = 0.019 \text{ Å}$.

The conditional settings also make it possible to construct the GE-m ($m = 1, 2, \dots, k$) geometry. In each GE-m of trans-H-(CH=CH)₇-H (Figure 12-2a), the π -MO interactions between the double bonds have been set equal to zero, except for the interactions between a pair of the red double bonds. In the GE-1 geometry, for example, all the π MO interactions, except for the interaction between two red double bonds C(1)=C(2) and C(3)=C(4), have been set equal to zero. Therefore, the GE-1 geometry can be considered as a locally delocalized geometry resulted from the local π -MO interaction between two localized double bonds C(1)=C(2) and C(3)=C(4) in the GL geometry. The corresponding energy effect $\Delta E^{Am} = [E(GE-m) - E(GL)]$. Therefore, the localized GL geometry can be considered as a localized reference geometry to calculate the π -electron delocalization energies ΔE^A and ΔE^{Am} .

The discovery of additive energy effects is a prerequisite for the calculation of aromatic stabilization energy. Fortunately, the optimization of GE-m geometry led to the discovery of this new type of additive energy effects

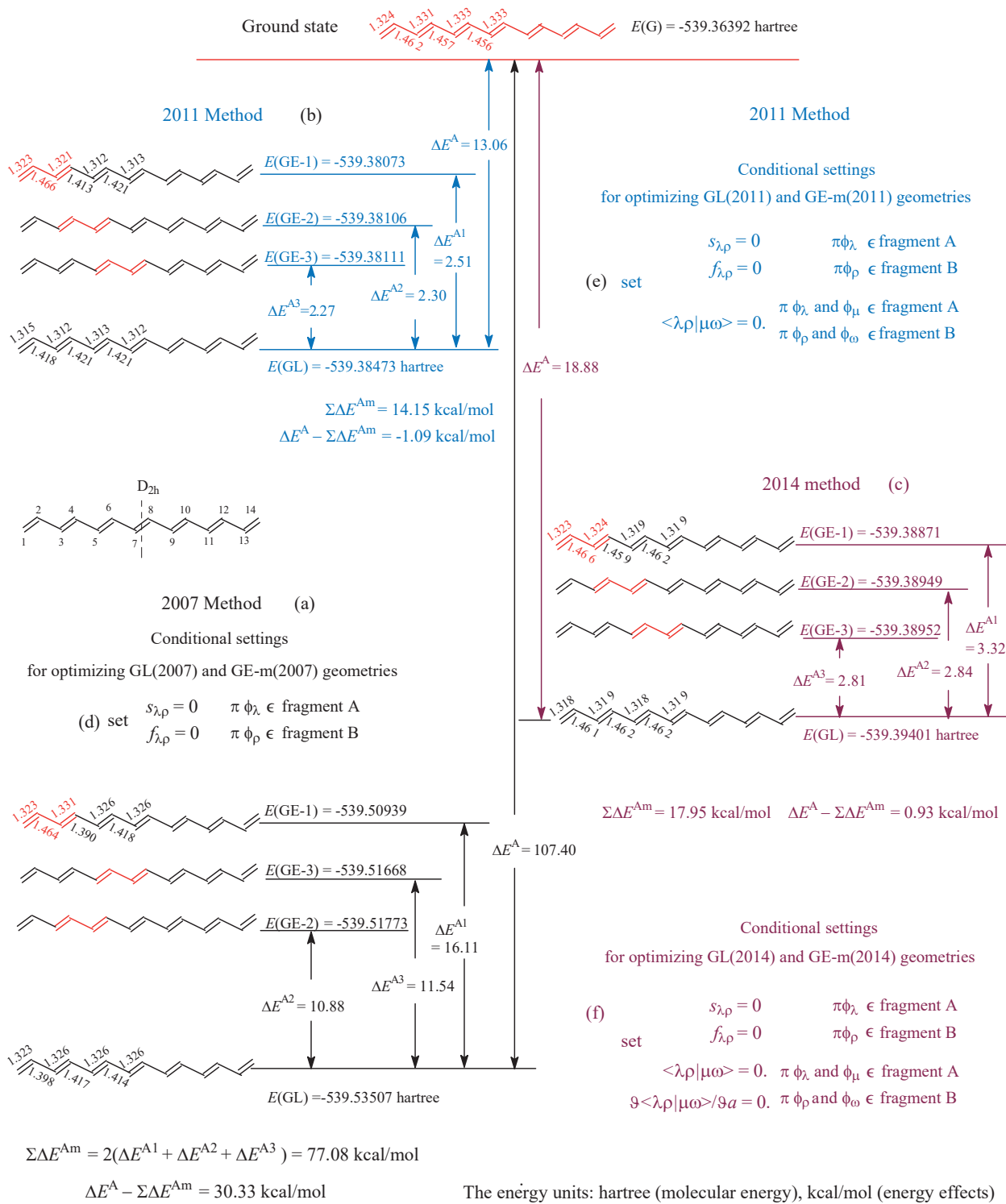


Figure 12-2. For trans-H-(CH=CH)₇-H at RHF/6-31G* level, the influence of the conditional settings on the additivity of energy effects ΔE^{Am} ($m = 1, 2, \dots, 6$). In the molecular structures, the color and black lines indicate that the π interactions between the double bonds have been set equal to zero except for those between two red double bonds.

ΔE^{Am} ($m = 1, 2, \dots, k$). For a planar conjugated molecule, $\Sigma \Delta E^{Am}$ can be considered as the molecular energy difference between the virtual ground state (VG) and GL geometry of conjugated molecule itself, $\Sigma \Delta E^{Am} = [E(VG) - E(GL)]$, so that $\Delta E^A - \Sigma \Delta E^{Am} = [E(G) - E(GL)] - [E(VG) - E(GL)] = E(G) - E(VG)$. In the case of trans-polyene at B3LYP level of theory, $\Sigma \Delta E^{Am} \approx \Delta E^A$, $E(G) \approx E(VG)$, so that energy effects ΔE^{Am} are additive.⁵³ For benzene at B3LYP/6-31G* level, $\Delta E^A - \Sigma \Delta E^{Am} = E(G) - E(VG) = -39$ kcal/mol $\neq 0$. In this case, the virtual ground state is cyclohexatriene. In 2007, the value of -39.0 kcal/mol was defined by us as the extra stabilization energy (ESE) of benzene.⁵³ For benzotricyclobutadiene ($C_{12}H_6$), the central benzene ring is a real cyclohexatriene ring with alternating single (1.515 Å) and double (1.338 Å) bonds. For this substituted central ring, interestingly, the energy effects are as follows (kcal/mol): $\Delta E^A = 38.1$, $\Sigma \Delta E^{Am} = 40.4$, and $\Delta E^A \approx \Sigma \Delta E^{Am}$ (seeing Chapter 11).

The virtual ground state can also be considered as an expected ground state of an aromatic molecule or as a delocalized reference state, and can be used to calculate the extra stabilization energy (ESE) of an aromatic molecule, $ESE = \Delta E^A - \Sigma \Delta E^{Am} = E(G) - E(EG)$. It should be especially emphasized that, as one of the biggest features of our method, the geometrical structure and molecular energy of the virtual delocalized reference state need not to be determined. At B3LYP/6-31G* level, our 2007 method can accurately evaluate the aromatic stabilization energy of various types of aromatic molecules, and it does not require the help of any parameters.

However, the sign and size of the energy effects such as vertical delocalization energy depend on the theoretical level and basis set size. For the vertical delocalization energy ΔE^V of benzene, for example, $\Delta E^V < 0$ (stabilizing) at B3LYP level of theory and at the density functional (without Hartree-Fock exchange) levels of theory, but becomes $\Delta E^V > 0$ (destabilizing) at RHF and MP2 levels of theory and at the density functional (with Hartree-Fock exchange) levels of theory (Table 8-1 and Table 8-3). These differences imply that two-electron exchange integrals, $\langle \lambda \rho | \mu \omega \rangle$, may play an important role in determining the sign and size of the vertical resonance energy.

Our 2007 method is available only at B3LYP theoretical level with small basis sets.

12.2.2. Our 2011 Method

In 1996, Bader indicated that Pauli exclusion principle also controls spatial delocalization of electrons via electron exchange.^{54,55} In the GL(2007) geometry of a conjugated molecule, π -electrons are still not absolutely localized even though all π -MOs have been localized. The localization of π -electron is conceptually different from the localization of π -MOs.

In order to ensure that, in the GL geometry, π -electrons are absolutely localized on their respective double bonds, as have been detailed in Chapter 8 and in our previous work,⁵⁶ the following two-electron exchange integrals (Hartree-Fock exchange, or spatial exchange) should be additionally deleted (Figure 12-1e): when calculating Fock matrix elements $f_{\lambda,\rho}$, set $\langle \lambda \rho | \mu \omega \rangle = 0.0$, where π AOs ϕ_λ and $\phi_\mu \in$ fragment A, and π AOs ϕ_ρ and $\phi_\omega \in$ fragment B. In the GL(2011) geometry of butadiene, therefore, the π two-electron exchange interaction has also been excluded from between two fragments A and B in addition to the π -MO charge transfer and exchange interactions, leading to that the π -MOs and π -electrons are all localized on their respective double bonds. Table 12-6 shows that the AO coefficients of the localized π MOs of GL(2011) geometry are different from those of the GL(2007) geometry.

At B3LYP/6-31G* level, as shown by comparison of Figure 12-1a and Figure 12-1b, the molecular energy $E(GL,2011)$ is 2.9 kcal/mol higher than $E(GL,2007)$, and the distance of the C(2)-C(3) single bond in GL(2011) is 0.003 Å longer than that in GL(2007). Particularly, $\Delta E^A(2011)$ and $\Delta E^A(2007)$ are all destabilizing, but $\Delta E^A(2011)$ (1.4 kcal/mol) $< \Delta E^A(2007)$ (4.3 kcal/mol), and $\Delta r_{23}(2011)$ (0.015 Å) $< \Delta r_{23}(2007)$ (0.018 Å).

Our 2011 method can be used to calculate various types of π -electron delocalization energies at any theoretical levels (seeing Chapter 8), and it no longer has the limitations of Our 2007 method. For benzene, for example, the vertical resonance energy becomes stabilizing at any level of theory, and the ESE(2011) value of -36.3 kcal/mol (at B3LYP/6-31G*) can be considered equal to the experimental value of -36 kcal/mol.

Table 12-7. For Butadiene, the Naked Single C(2)-C(3) Bond Distance $r_{23}(\text{GL})$ in the GL Geometry, the Molecular Energy Difference, $\Delta E^{\text{A}} = E(\text{G}) - E(\text{GL})$ (kcal/mol), and Single Bond Distance Difference, $\Delta r_{23} = r_{23}(\text{G}) - r_{23}(\text{GL})$ (\AA), between the Ground State (G) and the GL Geometry, Obtained from Our 2011 Method.

		6-31G*			6-311G**			6-311G(2d,2p)			6-311G(2df,p)		
		ΔE^{A}	$r_{23}(\text{GL})$	Δr_{23}									
Pure EX without Hartree-Fock exchange and Corr													
1	SLATER	0.6	1.451	0.005	2.0	1.449	0.007	3.5	1.435	0.019	4.3	1.429	0.024
2	XPBE96	-0.1	1.478	0.001	1.0	1.477	0.002	2.2	1.464	0.014	2.9	1.458	0.019
EX-Corr. without HF-EX exchange													
3	PBE96	0.3	1.451	0.003	1.3	1.449	0.005	2.9	1.435	0.017	2.9	1.435	0.017
4	SVWN5	0.9	1.434	0.006	2.1	1.431	0.007	3.8	1.417	0.019	4.6	1.411	0.025
5	BLYP	0.2	1.458	0.002	1.3	1.456	0.004	2.8	1.442	0.016	3.5	1.436	0.022
6	Average*	0.4	1.454	0.003	1.5	1.452	0.005	3.0	1.439	0.017	3.6	1.434	0.021
Pure Corr. with Hartree-Fock exchange													
7	CPBE96	3.0	1.389	0.057	3.0	1.385	0.060	3.0	1.369	0.073	3.3	1.361	0.081
8	LYP	3.0	1.392	0.056	3.1	1.389	0.059	3.2	1.374	0.072	3.5	1.366	0.079
Hybrid with Hartree-Fock exchange													
9	PBE0	1.8	1.434	0.019	2.5	1.431	0.021	3.7	1.416	0.034	4.4	1.409	0.040
10	X3LYP	1.6	1.440	0.016	2.4	1.437	0.018	3.6	1.423	0.031	4.3	1.416	0.037
11	B3LYP	1.4	1.441	0.015	2.3	1.439	0.017	3.5	1.424	0.030	4.2	1.418	0.036
with Hartree-Fock exchange													
12	RHF	2.7	1.410	0.056	2.8	1.407	0.059	2.8	1.393	0.072	3.1	1.385	0.079
13	MP2	-0.5	1.405	0.049	0.1	1.400	0.055	2.2	1.381	0.071	3.6	1.366	0.083
14	Average*	1.9	1.416	0.038	2.3	1.413	0.041	3.1	1.397	0.055	3.8	1.389	0.062
15	Difference*	-1.5	0.038	-0.035	-0.8	0.039	-0.036	-0.1	0.042	-0.038	-0.2	0.045	-0.039
16	Average	1.2	1.432	0.024	2.0	1.429	0.026	3.1	1.414	0.039	3.7	1.408	0.045
17	Range		0.086			0.092			0.095			0.097	

* Each data in row 6 is an average of the data in the first to fifth rows in each corresponding column, and each data in row 14 is an average of the data in the seventh to thirteen rows in each corresponding column. Each data in row 15 is the difference between the two averages in each column. In row 16, each data is the average of all the data in the corresponding column.

However, Table 12-7 shows that the Hartree-Fock exchange still has the effects on the structure and molecular energy of GL(2011) geometry. SLATER and XPBE96 are the density functional without Hartree-Fock exchange, and CPBE96 is a density functional with the Hartree-Fock exchange. In the GL(2011) geometry of butadiene at

6-31G* level, for example, $|r(GL,SLATER) - r(GL,CPBE96)| = 1.451 - 1.389 = 0.062 \text{ \AA}$, but $|r(GL,SLATER) - r(GL,XPBE96)| = |1.451 - 1.478| = 0.027 \text{ \AA}$. In addition, as shown by Table 11-1, the theoretical level and basis set size have the great influences on the values of the energy effects such as ESE, ΔE^A and ΔE^{A1} in the case of strained-aromatic molecules. For benzotricyclobutadiene, for example, the ESE and energy effects (kcal/mol) are as follows:

- 20.1 (ESE), 38.7 (ΔE^A), 4.1 (ΔE^{A1}) at B3LYP/6-31G* level
- 8.4 (ESE), 39.6 (ΔE^A), 4.2 (ΔE^{A1}) at RHF/6-31G* level
- 7.3 (ESE), 39.8 (ΔE^A), 2.3 (ΔE^{A1}) at RHF/6-311G*(2df,p) level.

12.3. OUR 2014 METHOD

For the GL(2011) geometry, the two-electron exchange integrals, $\langle \lambda\rho|\mu\omega \rangle$, in Fock matrix elements $f_{\lambda\rho}$ have been conditionally deleted. However, there are the gradients, $\partial\langle \lambda\rho|\mu\omega \rangle/\partial a$, of two-electron exchange integrals in the following expression (12-3):^{57,58}

$$\begin{aligned} \partial E_e / \partial a = & 2 \sum_{\lambda\mu} d_{\lambda\mu} \{ \partial h_{\lambda\mu} / \partial a + \sum_{\rho\omega}^M d_{\rho\omega} [\partial (\lambda\mu | \rho\omega) / \partial a - \\ & (1/2)\partial (\lambda\rho | \mu\omega) / \partial a] \} - 2 \sum_i^N \sum_{\lambda\mu} c_{\lambda i} c_{\mu i} \varepsilon_i \partial s_{\lambda\mu} / \partial a \end{aligned} \quad (12-3)$$

where a stands for a nuclear coordinate, M is the number of AOs, N is the number of occupied MOs, s is AO overlap integral matrix, d is AO density matrix, c and ε are the AO coefficient matrix and eigenvalue matrix.

Therefore, for example, the optimization of the GL geometry of butadiene should be performed under the following conditional settings (Figure 12-1f):

- (i) When π AOs $\phi_\lambda \in$ fragment A, and π AOs $\phi_\rho \in$ fragment B, setting $s_{\lambda\rho} = 0$, and $f_{\lambda\rho} = 0$ in order to ensure the localization of π MOs.
- (ii) When π AOs ϕ_λ and $\phi_\mu \in$ fragment A, and π AOs ϕ_ρ and $\phi_\omega \in$ fragment B, setting (two-electron exchange integrals) $\langle \lambda\rho|\mu\omega \rangle = 0.0$, in order to ensure the localization of π -electrons.
- (iii) When π AOs ϕ_λ and $\phi_\mu \in$ fragment A, and π AOs ϕ_ρ and $\phi_\omega \in$ fragment B, setting (the gradients of two-electron exchange integrals that hereafter will be shortened to “exchange gradient”) $\partial(\langle \lambda\rho|\mu\omega \rangle)/\partial a = 0.0$, in order to ensure that the structure of the localized GL geometry is the most reasonable.

Our 2011 method was improved by Dr. Bao Peng in 2014. The improved 2011 method is called "Our 2014 method". Table 12-6 shows that, for the three different GL geometries of butadiene, the AO coefficient matrices are different from each other, and the eigenvalue matrices are also different. In particular, among the three GL geometries represented by GL(2007), GL(2011) and GL(2014), only the eigenvalues (-0.2750 and -0.2750 hartree) of two occupied π MOs in the localized GL(2014) geometry are mutual equal, indicating that the GL(2014) geometry is the most reasonable.

According to the conditional settings, our 2007 method can be considered as a method of localizing π MOs, our 2011 method is a method of localizing π electrons, and our 2014 method is to localize geometry although the geometries obtained from our methods are all localized.

12.3.1. More Reasonable than Our 2011 Method

Some of the deficiencies in our 2011 Method and the reasons for its improvement have been highlighted. Of course, it is necessary to discuss the superiority of our 2014 method.

12.3.1.1. Improving Additivity of Energy Effects

It is just due to the additivity of the energy effects ΔE^{Am} that our 2007 and 2011 methods can successfully be used to calculate the aromatic stabilization energy. The rationality of improving our 2011 method should be reflected in several aspects. First of all, of course, conditional deleting of the exchange gradients should increase the additivity of energy effects ΔE^{Am} in the case of polyene.

For 1,3,5,7,9,11,13-tetradecaheptaene at RHF/6-31G* level (Figure 12-2), for example, $\Delta E^{\text{A}}(2007) = 107.4 \text{ kcal/mol}$, and $\Sigma \Delta E^{\text{Am}}(2007) = 2[\Delta E^{\text{A}1}(2007) + \Delta E^{\text{A}2}(2007) + \Delta E^{\text{A}3}(2007)] = 77.1 \text{ kcal/mol}$ (Figure 12-2a), where $\Delta E^{\text{Am}} = E(\text{GE-m}) - E(\text{GL})$ ($m = 1, 2, \dots, 6$). $ESE(2007) = \Delta E^{\text{A}}(2007) - \Sigma \Delta E^{\text{Am}}(2007) = 30.3 \text{ kcal/mol}$. At RHF level of theory, $ESE(2007)$ is so great that the energy effects $\Delta E^{\text{Am}}(2007)$ can't be considered additive when the GL and GE-n geometries are restrictedly optimized using our 2007 method at RHF theoretical level.

Due to conditional deletion of the two-electron exchange integrals, as shown by the data presented in Figure 12-2b, molecular energy (hartree) $|E(\text{GL}, 2011) (-539.38437)| < |E(\text{GL}, 2007) (-539.53507)|$. Correspondingly, the value (kcal/mol) of ΔE^{A} decreases from 107.4 for $\Delta E^{\text{A}}(2007)$ to 13.1 for $\Delta E^{\text{A}}(2011)$. As a result, $ESE(2011) = [\Delta E^{\text{A}}(2011) - \Sigma \Delta E^{\text{An}}(2011)] = -1.1 \text{ kcal/mol}$, and can be considered $\Delta E^{\text{A}}(2011) \approx \Sigma \Delta E^{\text{Am}}(2011)$. At RHF theoretical level, the conditional and additional deletion of two-electron exchange integrals makes the energy effects $\Delta E^{\text{Am}}(2011)$ to become additive.

When the gradients of exchanges integrals are additionally deleted (Figure 12-2c), the molecule energy (hartree) $|E(\text{GL}, 2014) (-539.39401)| > |E(\text{GL}, 2011) (-539.38437)|$, but still $|E(\text{GL}, 2014)| < |E(\text{GL}, 2007) (-539.53507)|$. Finally, $ESE(2014) = [\Delta E^{\text{A}}(2014) - \Sigma \Delta E^{\text{An}}(2014)] = 18.88 - 17.95 = 0.93 \text{ kcal/mol}$, and $ESE(2014) (0.93 \text{ kcal/mol}) < |ESE(2011) (-1.1 \text{ kcal/mol})|$.

In order to compare the additivity of the energy effects $\Delta E^{\text{Am}}(2011)$ and $\Delta E^{\text{Am}}(2014)$, the ratio $R_t(Y)$ ($Y = 2007, 2011$, and 2014) is defined as following:

$$R_t(Y) = |ESE(Y) / \Sigma \Delta E^{\text{Am}}(Y)|$$

$R_t(2014) (0.05) < R_t(2011) (0.08) < R_t(2007) (0.39)$. For polyene at RHF level of theory, it is due to the conditional deletion of the two-electron exchange integrals and their gradients that our method can ensure the additivity of the energy effects ΔE^{Am} . The additivity of energy effects $\Delta E^{\text{Am}}(2014)$ is better than that of $\Delta E^{\text{Am}}(2011)$ although the increase in the additivity is not large.

12.3.1.2. Distance of Naked CC Single Bond in Butadiene

Before discussion, the following symbols are defined in advanced: $r^{\text{NHF}}(\text{GL}, Y)$ is the distance of the naked CC single bond in the GL(Y) ($Y = 2011, 2014$) geometry (of butadiene) optimized at density functional (without HF-exchange) level of theory; $r_{\text{av}}^{\text{NHF}}(\text{GL}, Y)$ is the average of all $r^{\text{NHF}}(\text{GL}, Y)$ values; $r^{\text{HF}}(\text{GL}, Y)$ is distance of the naked CC single bond in the GL(Y) geometry (of butadiene) optimized at density functional (with HF-exchange), RHF and MP2 levels of theory; $r_{\text{av}}^{\text{HF}}(\text{GL}, Y)$ is the average of all $r^{\text{HF}}(\text{GL}, Y)$ values. Hereafter, the CC single bond between two localized double bonds in the GL geometry will be called the naked CC single bond (naked single bond).

For a reasonable calculation method, the differences, in the geometrical data (such as bond distance) and molecular energy, between the molecular geometries optimized at the different theoretical levels using different basis sets should be as small as possible. In order to understand the influences of the exchange gradients $\partial \langle \lambda \rho | \mu \omega \rangle / \partial a$ on the distance, $r(\text{GL})$, of the naked CC single bond in butadiene, the bond distances ($r^{\text{NHF}}(\text{GL}, Y)$ and

Table 12-8. For Butadiene, Naked Single Bond Distance $r(GL)$ (\AA) in the GL Geometry, Molecular Energy Difference, $\Delta E^A = E(G) - E(GL)$ (kcal/mol), and Single Bond Length Difference, $\Delta r = r(G) - r(GL)$ (\AA), between Ground State and Its GL Geometry, Obtained from Our 2014 Method.

		6-31G*			6-311G**			6-311G(2d,2p)			6-311G(2df,p)		
		ΔE^A	$r(GL)$	Δr	ΔE^A	$r(GL)$	Δr	ΔE^A	$r(GL)$	Δr	ΔE^A	$r(GL)$	Δr
Pure EX without Hartree-Fock exchange and Corr.													
1	SLATER	0.6	1.451	0.005	2.0	1.449	0.007	3.5	1.435	0.019	4.3	1.429	0.024
2	XPBE96	-0.1	1.478	0.001	1.0	1.477	0.002	2.2	1.464	0.014	2.9	1.458	0.019
EX-Corr. without HF-EX exchange													
3	PBE96	0.3	1.451	0.003	1.3	1.449	0.005	2.9	1.435	0.017	2.9	1.435	0.017
4	SVWN5	0.9	1.434	0.006	2.1	1.431	0.007	3.8	1.417	0.019	4.6	1.411	0.025
5	BLYP	0.2	1.458	0.002	1.3	1.456	0.004	2.8	1.442	0.016	3.5	1.436	0.022
6	Average	0.4	1.454	0.003	1.5	1.452	0.005	3.0	1.439	0.017	3.6	1.434	0.021
Pure Corr. with Hartree-Fock exchange													
7	CPBE96	4.3	1.434	0.012	4.4	1.433	0.012	4.9	1.425	0.018	5.5	1.421	0.021
8	LYP	4.3	1.437	0.011	4.5	1.436	0.011	5.0	1.428	0.017	5.6	1.424	0.021
Hybrid with Hartree-Fock exchange													
9	PBE0	1.8	1.446	0.007	1.8	1.446	0.007	3.8	1.432	0.018	4.5	1.426	0.023
10	X3LYP	1.6	1.450	0.006	2.5	1.448	0.007	3.7	1.436	0.017	4.4	1.431	0.022
11	B3LYP	1.5	1.451	0.006	2.4	1.449	0.007	3.6	1.437	0.017	4.3	1.432	0.022
with Hartree-Fock exchange													
12	RHF	3.9	1.456	0.011	4.1	1.456	0.011	4.5	1.448	0.016	5.0	1.444	0.020
13	MP2	0.6	1.449	0.005	1.3	1.447	0.008	3.9	1.436	0.016	5.5	1.425	0.024
14	Average	2.6	1.446	0.008	3.0	1.445	0.009	4.2	1.435	0.017	5.0	1.429	0.022
15	Difference	-2.2	0.008	-0.005	-1.5	0.007	-0.004	-1.2	0.004	0.000	-1.4	0.005	-0.001
16	Average	1.7	1.450	0.006	2.4	1.448	0.007	3.7	1.436	0.017	4.4	1.431	0.022
17	Range		0.044			0.046			0.047			0.047	

* Each data in row 6 is an average of the data in the first to fifth rows in each corresponding column, and each data in row 14 is an average of the data in the seventh to thirteen rows in each corresponding column. Each data in row 15 is the difference between the two averages in each column. In row 16, each data is the average of all the data in the corresponding column.

$r^{\text{HF}}(GL,Y)$) and the bond distance averages ($r^{\text{NHF}_{\text{av}}}(GL,Y)$ and $r^{\text{HF}_{\text{av}}}(GL,Y)$) are calculated, and are listed in Table 12-7 (Y = 2011) and Table 12-8 (Y = 2014).

For the GL(2014) geometry, as shown in comparison between Table 12-7 and Table 12-8, the conditional deletion of the exchange gradients reduces the influence of theoretical level on the distance of the naked CC single bond. At 6-31G* level, for example, $[r^{\text{NHF}_{\text{av}}(\text{GL},2014)} - r^{\text{HF}_{\text{av}}(\text{GL},2014)}] = 0.008 \text{ \AA}$, and the range of a set of $r(\text{GL},2014)$ values, the difference between the largest and smallest values, is 0.044 \AA . Correspondingly, $[r^{\text{NHF}_{\text{av}}(\text{GL},2011)} - r^{\text{HF}_{\text{av}}(\text{GL},2011)}] = 0.038 \text{ \AA}$, and the range of a set of $r(\text{GL},2011)$ values is 0.086 \AA (Table 12-7).

Interestingly, Table 12-8 shows that, at a specific basis set level, the total average of all $r(\text{GL},2014)$ values is almost equal to the B3LYP value. At 6-31G* level, for example, total average is 1.450 \AA , and the B3LYP value is 1.451 \AA . Therefore, the B3LYP values can be used as the reference to compare the influences of theoretical level on $r(\text{GL},Y)$ ($Y = 2011, 2014$). In Table 12-8, the 6-31G* values of $r(\text{GL},2014)$ are 1.456 (RHF) and 1.449 (MP2), and 1.451 (B3LYP) \AA , and the differences, in $r(\text{GL},2014)$, between the RHF (and MP2) value and the B3LYP value are 0.005 (RHF) and -0.002 (MP2) \AA , and they are less than the corresponding differences (-0.031 and -0.036 \AA) in $r(\text{GL},2011)$.

Conditional deletion of the exchange gradients can also reduce the influence of basis set size on the distance of single bond. In row 11 of Table 12-8, for example, four values (\AA) of $r(\text{GL},2014)$ are calculated at the B3LYP level using four different basis sets, and are $1.451, 1.449, 1.437$, and 1.432 \AA , respectively. The range of this set of values is 0.019 \AA (B3LYP). At the RHF and MP2 levels of theory, the ranges are 0.012 \AA (RHF), and 0.024 \AA (MP2). Table 12-7 shows that the corresponding ranges are 0.023 (B3LYP), 0.025 (RHF), and 0.039 \AA (MP2).

Remarkably, the adiabatic resonance energy of butadiene is the molecular energy difference, $\Delta E^{\text{A}}(2014) = E(\text{G}) - E(\text{GL},2014)$, between the ground state geometry (G) and the GL(2014) geometry, and always $\Delta E^{\text{A}}(2014) > 0$ (destabilizing). The single bond distance $r(\text{GL},2014)$ in the GL(2014) geometry is always shorter than that in the ground state geometry. At B3LYP/6-31* level, for example, $\Delta E^{\text{A}}(2014) = 1.5 \text{ kcal/mol}$, and it is almost equal to the difference (1.9 kcal/mol)^{1,2} in the hydrogenation heat, between trans-1,3-butadiene and trans-2-butene. Correspondingly, the distance (1.451 \AA) of the single bond in GL(2014) geometry is 0.006 \AA shorter than that (1.457 \AA) in the ground state geometry of butadiene, and it is 0.010 \AA longer than that in the GL(2011) geometry. The distance of 1.451 \AA in the GL(2014) geometry can be regarded as the distance of naked sp^2-sp^2 single bond.

In the case of trans-1,3-butadiene, as Dewar suggested, the conjugation interaction between two double bonds is really very weak. In particular, it should be emphasized that the delocalization (resonance) energy (1.5 kcal/mol), as well as that (1.9 kcal/mol) determined by experiment, is destabilizing, rather than stabilizing.

The influence of basis set size on the distance of naked CC single bond can't be eliminated in any case. As the basis set size increases, the distance $r(\text{GL},2014)$ is, generally, getting shorter. But the distance $r(\text{G},2014)$ in the ground state geometry is almost constant (Table 12-8), and is between two experimental distances 1.454 \AA (Craig, in 2006) and 1.460 \AA (Pauling in 1939). At B3LYP level of theory, for example, the distances (\AA), $r(\text{GL},2014)$ and $r(\text{G},2014)$ are as follows:

$$r(\text{GL}): 1.451 \text{ (6-31G*)}, 1.449 \text{ (6-311G**)}, 1.437 \text{ (6-311G(2d,2p))}, 1.432 \text{ \AA} \text{ (6-311G (2df,p))} .$$

$$r(\text{G}): 1.457 \text{ (6-31G*)}, 1.456 \text{ (6-311G**)}, 1.454 \text{ (6-311G(2d,dp))}, 1.454 \text{ (6-311G(2df,p))}$$

12.3.1.3. Extra Stabilization Energy of Benzene

For Benzene, the theoretical value of the aromatic stabilization energy is often used to test the rationality of a calculation method because its aromatic stabilization energy (-36 kcal/mol) has been experimentally determined (In the literature, the stabilization aromatic energy is expressed as 36 kcal/mol).

In each column of Table 12-9, the values of ESE(2011,B) are calculated at a specific level of theory using various basis sets (B), where $B = 6-31G^*, \dots, 6-311++(2df,p)$, and the average of a set of ESE(2011,B) values is denoted as $ESE_{\text{av}}(2011,T)$ (at a specific level "T"). At a specific basis level ("B"), similarly, $ESE_{\text{av}}(2014,B)$ is the average of a set of the ESE(2014,T) values, where $T = \text{B3LYP}, \text{RHF}, \dots, \text{BLYP}$. At a specific level of theory, the values of $ESE_{\text{av}}(2014,T)$ and $ESE_{\text{av}}(2011,T)$ are listed in the penultimate line of Table 12-9 and are as follows:

Table 12-9. For Benzene, Extra Stabilization Energy (ESE) (kcal/mol), and Energy Effects ΔE^A and ΔE^{A1} (kcal/mol) Are Obtained from Our 2011 and 2014 Methods.

	ΔE^A	RHF		MP2		LYP		B3LYP		SLATER	BLYP	Average(B)	
		2014	2011	2014	2011	2014	2011	2014	2011	2014	2-014	2014	2011
6-31G*	ΔE^A	-13.6	-17.6	-26.7	-30.1	-14.0	-18.0	-19.1	-19.2	-19.6	-20.5		
	ΔE^{A1}	7.9	5.8	3.8	1.9	8.4	6.3	5.8	5.7	5.3	4.7		
	ESE	-37.4	-34.9	-38.2	-35.8	-39.3	-36.8	-36.4	-36.3	-35.5	-34.5	-36.9	-35.6
6-311G**	ΔE^A	-12.2	-16.7	-24.2	-28.0	12.7	-17.2	-16.2	-16.4	-15.7	-17.1		
	ΔE^{A1}	8.3	5.8	4.7	2.4	8.8	6.3	6.9	6.8	6.8	6.0		
	ESE	-37.2	-34.2	-38.2	-35.2	-39.2	-36.2	-36.9	-36.7	-36.2	-35.1	-37.1	-35.6
6-311G(2d,2p)	ΔE^A	-11.0	-16.9	-17.3	-22.6	-11.3	-17.4	-13.3	-13.5	-11.9	-13.7		
	ΔE^{A1}	8.5	5.2	6.6	3.5	9.1	5.7	7.7	7.6	7.9	7.0		
	ESE	-36.6	-32.6	-37.2	-33.1	-38.5	-34.5	-36.3	-36.2	-35.7	-34.6	-36.5	-34.5
6-311G(2df,p)	ΔE^A	-9.2	-15.5	-12.1	-18.4	-9.3	-16.4	-10.8	-11.1	-9.3	-11.2		
	ΔE^{A1}	9.3	5.4	8.6	4.9	9.9	5.9	8.7	8.6	9.0	8.0		
	ESE	-37.0	-31.7	-38.0	-33.0	-39.0	-34.2	-37.0	-36.8	-36.4	-35.3	-37.1	-34.6
6-311++G(2d,2p)	ΔE^A	-10.8	-16.2	-16.8	-22.3	-11.2	-17.4	-12.3	-12.5	-10.3	-12.4		
	ΔE^{A1}	8.7	5.3	6.9	3.6	9.2	5.7	8.2	8.1	8.8	7.7		
	ESE	-37.0	-32.0	-37.6	-33.2	-38.9	-34.6	-37.0	-36.8	-36.6	-35.4	-37.1	-34.8
6-311++G(2df,p)	ΔE^A	-9.1	-16.2	-11.6	-18.2	-9.2	-16.5	-9.9	-10.2	-7.8	-10.0		
	ΔE^{A1}	9.5	5.4	8.9	4.9	10.0	5.9	9.2	9.1	9.8	8.7		
	ESE	-37.4	-32.4	-38.3	-33.0	-39.3	-34.2	-37.6	-37.4	-37.2	-36.0	-36.0	-35.0
Average(T)	ESE	-37.1	-33.0	-37.9	-33.9	-39.0	-35.1	-36.9	-36.7	-36.3	-35.2		
Range(T)	ESE	-0.8	-3.2	-1.1	-2.8	-0.8	-2.6	-1.3	-1.5	-1.7	-1.5		

SLATER and BLYP are the density functional without Hartree-Fock exchange, the values of ESE(2011) are same as the corresponding values of ESE(2014)

Our 2011 method: -33.0 (RHF), -33.9 (MP2), -35.1 (LYP), and -36.7 (B3LYP).

Our 2014 method: -37.1 (RHF), -37.9 (MP2), -39.0 (LYP), and -36.9 (B3LYP)

The difference between the averages, $ESE_{av}(2011,B3LYP) - ESE_{av}(2011,RHF)$, is -3.7 kcal/mol. Accordingly, when the GL and GE-m geometries are optimized using our 2011 method, the theoretical level has an obvious effect on value of $ESE(2011)$ due to the retention of exchange gradients. When the GL and GE-m geometries are optimized using our 2014 method, on the contrary, the difference between the average values, $ESE_{av}(2014,B3LYP) - ESE_{av}(2014,RHF)$, decreases to 0.2 kcal/mol. Conditional deletion of the exchange gradients reduces the influence of theoretical level on the value of ESE .

At the 6-31G* level, the differences, $ESE(2014,RHF) - (-36) = -1.4$ kcal/mol, the difference, $ESE(2014,B3LYP) - (-36) = -0.4$ kcal/mol. The absolute values of these two difference are slightly larger than the corresponding differences ($ESE(2011,RHF) - (-36)$) (1.1 kcal/mol) and ($ESE(2011,B3LYP) - (-36)$) (-0.3 kcal/mol), where -36 kcal/mol is the experimental value of aromatic stabilization energy for benzene. Despite this, a comparison of the ranges indicates that the total influence of basis set size on the value of $ESE(2014)$ is smaller than on the value of $ESE(2011)$. At the RHF level of theory, for example, the range of a set of $ESE(2014,B)$ values, listed in the last line of Table 12-9, is -0.8 kcal/mol, and the range of the corresponding $ESE(2011,B)$ values is -3.2 kcal/mol.

In each row of Table 12-9, the values of $ESE(2014,T)$ are calculated at various levels of theory using a specific basis set. A comparison of the data in the last two columns of Table 12-9 indicates that $(ESE_{av}(2014,B) - (-36))$ kcal/mol $\approx |(ESE_{av}(2011,B) - (-36))$ kcal/mol|. The calculation method has a small influence on the values of $ESE_{av}(2014,B)$ and $(ESE_{av}(2011,B))$, and the ranges for these two averages are -1.1 (2014) and -1.1 (2011) kcal/mol. At 6-31G* level, for example, $ESE_{av}(2014,B) = -36.9$ kcal/mol, and $ESE_{av}(2011,B) = -35.6$. It is difficult to say which value is more reasonable.

For the $ESE(2014)$ of benzene at 6-31G* level, the B3LYP values of -36.4 kcal/mol is almost equal to the experimental value of -36.0 kcal/mol, and the RHF value of -37.4 kcal/mol is very close to the experimental value. For all ESE data listed in Table 12-9, the total averages (kcal/mol) are -35.0 (2011) and -37 (2014), and the average values are in the region of -36 ± 1 .

In a word, at (RHF, MP and B3LYP) levels of theory, our 2014 method is more reasonable than our 2011 method

12.3.1.4. Adiabatic Delocalization Energy of Cyclobutadiene

As emphasized by Shaik,⁵⁹ cyclobutadiene has been used as a touchstone to assess whether a calculation method is reasonable. If the calculated π -electron delocalization energy is stabilizing, the method is certainly unreasonable.

No matter whether ΔE^A is calculated by our 2011 method or by our 2014 method, as shown by the data in Table 12-10, ΔE^A is always destabilizing without exception, and the distance of the CC single bond in the GL geometry is always shorter than that in ground state geometry.

At a specific basis level ("B"), the average of a set of $\Delta E^A(Y,T)$ ($T = RHF, \dots, XPBE96$) values are listed in the last two columns of Table 12-10, and they are denoted as $\Delta E^A_{av}(2014,B)$ and $\Delta E^A_{av}(2011,B)$. At the 6-31G* and 6-311G** levels, for example, the values of $\Delta E^A_{av}(2014,B)$ are 53.1 and 53.8 kcal/mol, and the ranges of a set of $\Delta E^A(2014,T)$ values are 10.23 and 8.54 kcal/mol. The corresponding values of $\Delta E^A_{av}(2011,B)$ are 49.5 and 49.2 kcal/mol, and the ranges are 10.17 and 9.52 kcal/mol. $\Delta E^A_{av}(2014,B)$ are closer to the experimental value of 55 kcal/mol (by Deniz in 1999)⁶⁰ than $\Delta E^A_{av}(2011,B)$, but there are no great difference between the ranges calculated by our 2014 and our 2011 methods.

At 6-311G(2d,2p) and 6-311G(2df,p) levels, on the contrary, the values (54.1 and 55.0 kcal/mol) of $\Delta E^A_{av}(2011,B)$ become closer to the experimental value of 55 kcal/mol than those (60.3 and 62.2 kcal/mol) of $\Delta E^A_{av}(2014,B)$. However, the ranges of set of $\Delta E^A(2011,T)$ values are 13.41 and 16.01 kcal/mol, and the range of the $\Delta E^A(2014,T)$ values are 7.49 and 7.26 kcal/mol.

At a specific theoretical level, the average of the $\Delta E^A(Y,B)$ values are listed in the last row of Table 12-10, and

Table. 12-10. For Cyclobutadiene, Adiabatic Delocalization Energies ΔE^A (kcal/mol), Distances, $r(GL)$ and $r(G)$ (\AA), of CC Single Bond in the GL and Ground State geometries, Calculated Using Our 2011 and 2014 Methods.

	ΔE^A	RHF		MP2		LYP		B3LYP		BLYP	XPBE96	Average ΔE^A	
		2014	2011	2014	2011	2014	2011	2014	2011	2014	2014	2014	2011
6-31G*	ΔE^A	56.06	48.82	49.52	43.38	58.82	51.60	53.82	53.55	51.56	48.59	53.10	49.50
	$r(GL)$	1.456	1.373	1.452	1.374	1.437	1.358	1.454	1.437	1.463	1.483	1.458	1.415
	$r(G)$	1.564		1.566		1.543		1.578		1.593	1.619	1.577	
6-311G**	ΔE^A	55.81	47.73	50.36	43.53	58.60	50.45	54.94	50.45	53.05	50.06	53.80	49.20
	$r(GL)$	1.456	1.368	1.452	1.368	1.436	1.352	1.451	1.352	1.460	1.482	1.456	1.397
	$r(G)$	1.567		1.573		1.544		1.545		1.593	1.620	1.574	
6-311G(2d,2p)	ΔE^A	60.37	47.71	59.70	48.96	63.70	50.96	61.61	61.12	59.92	56.21	60.30	54.10
	$r(GL)$	1.430	1.334	1.434	1.336	1.421	1.319	1.429	1.405	1.434	1.455	1.433	1.381
	$r(G)$	1.565		1.574		1.543		1.577		1.592	1.619	1.578	
6-311G(2df,p)	ΔE^A	61.48	46.69	63.97	51.08	64.97	50.04	63.28	62.70	61.64	57.71	62.20	55.00
	$r(GL)$	1.434	1.320	1.416	1.312	1.414	1.305	1.420	1.395	1.425	1.447	1.426	1.367
	$r(G)$	1.564		1.567		1.542		1.576		1.590	1.617	1.576	
Average ΔE^A		58.40	47.70	55.90	46.70	61.50	50.80	58.40	57.00	56.50	53.10		

they are denoted as $\Delta E_{av}^A(2014,T)$ and $\Delta E_{av}^A(2011,T)$. The value of $\Delta E_{av}^A(2014,T)$ is generally closer to the experimental value of 55 kcal/mol than that of $\Delta E_{av}^A(2011,T)$. At the (RHF and MP2) levels of theory, for example, the values of $\Delta E_{av}^A(2014,T)$ are 58.4 and 55.9 kcal/mol, and the values of $\Delta E_{av}^A(2011,T)$ are 47.7 and 46.7 kcal/mol. $[\Delta E_{av}^A(2014,T) - 55]$ (3.4 and 0.5 kcal/mol) < $[\Delta E_{av}^A(2011,T) - 55]$ (-7.4 and -8.3 kcal/mol). But, at B3LYP level of theory, $\Delta E_{av}^A(2014,T)$ (58.4 kcal/mol) $\approx \Delta E_{av}^A(2011,T)$ (57.0 kcal/mol).

For cyclobutadiene, accordingly, the adiabatic delocalization energy obtained from Our 2014 method is more reasonable than from Our 2011 method.

12.3.1.5. CESE of Polycyclic Benzenoid Hydrocarbons

For polycyclic benzenoid hydrocarbons, the comparison of the rationality of our 2011 method and our 2014 method is mainly focused on the influences of the theoretical level and basis set size on the energy effects such as ESE and ΔE^A .

B3LYP is a hybrid density functional, and it incorporates a portion of the exchange from Hartree–Fock theory and does the exchange and the correlation from other sources. According to the data listed in Table 12-11, at B3LYP/6-31G* level, the conditional deletion of the exchange gradients has a slight influence on CESE and ΔE^A . For naphthalene, for example, CESE(2011) = -58.0 kcal/mol, $\Delta E^A(2011)$ = -26.5 kcal/mol, and CESE(2014) = -58.2

Table 12-11. For Naphthalene (Naphth.), Anthracene (Anthra.), Tetracene (Tetra.), Hexacene (Hexa.), Triphenylene (Triph.), Chrysene (Chrys.), Phenanthrene (Phena.), ESEs and CESEs (kcal/mol) and Energy Effects ΔE^A and $\Sigma\Delta E^{Am}$ (kcal/mol), Obtained from Our 2011 and 2014 Methods at 6-31G* Level.

		Naphth n = 1	Anthra. n = 2	Tetra. n = 3	Hexa. n = 5	Thiph.	Chrys.	Phena.	
B3LYP	ESE	2011	-59.9	-69.9	-78.2	-93.9	-115.0	-112.6	-86.9
		2014	-60.8	-70.1	-78.5	-94.2	-115.4	-113.0	-87.2
	ΔE^A	2011	-26.5	-29.7	-31.4	-32.7	-49.8	-47.2	-37.5
		2014	-26.2	-29.2	-30.8	-31.9	-49.2	-46.6	-37.0
	$\Sigma\Delta E^{Am}$	2011	33.4	40.2	46.8	61.1	65.3	65.4	49.4
		2014	33.9	40.9	47.7	62.4	66.3	66.4	50.1
	CESE	2011	-58.0	-66.1	-72.4	-84.8	-109.4	-105.2	-83.1
		2014	-58.2	-66.2	-72.6	-85.0	-109.7	-105.5	-83.3
CPBE96	ESE	2011	-60.3	-69.4	-76.2	-87.7	-116.6	-113.1	-87.5
		2014	-65.6	-76.7	-83.9	-96.8	-127.4	-123.9	-95.7
	ΔE^A	2011	-24.1	-24.1	-21.6	-12.4	-46.8	-43.1	-34.4
		2014	-15.7	-11.2	-4.4	13.3	-29.9	-26.1	-21.8
	$\Sigma\Delta E^{Am}$	2011	36.2	45.4	54.6	75.3	69.8	69.9	52.9
		2014	50.0	64.8	79.4	110.1	97.5	97.8	73.9
	CESE	2011	-60.0	-68.7	-75.1	-86.0	-115.7	-111.8	-86.9
		2014	-65.1	-75.2	-82.7	-95.3	-125.7	-121.7	-94.6
RHF	ESE	2011	-56.2	-64.6	-70.7	-80.7	-108.5	-105.3	-81.7
		2014	-61.3	-71.0	-78.1	-89.8	-118.8	-115.7	-89.4
	ΔE^A	2011	-23.1	-23.0	-20.5	-11.7	-44.6	-41.3	-33.1
		2014	-14.9	-10.7	-4.1	12.8	-28.3	-24.9	-20.9
	$\Sigma\Delta E^{Am}$	2011	33.2	41.5	50.2	69.0	63.9	64.0	48.5
		2014	46.4	60.2	74.0	106.2	90.4	90.8	68.6
	CESE	2011	-55.9	-63.9	-69.8	-78.9	-107.6	-104.1	-81.7
		2014	-60.6	-70.1	-76.9	-88.3	-117.1	-113.6	-88.3
MP2	ESE	2011	-56.9	-68.9	-79.7	-100.5	-109.5	-106.4	-82.2
		2014	-62.2	-75.6	-87.5	-110.3	-120.5	-117.5	-90.4
	ΔE^A	2011	-48.1	-63.6	-77.6	-104.1	-95.4	-92.2	-70.7
		2014	-41.2	-53.1	-63.6	-83.0	-81.6	-78.2	-60.3
	$\Sigma\Delta E^{Am}$	2011	8.8	5.3	2.1	-3.6	14.0	14.2	11.5
		2014	21.0	22.6	23.9	27.3	38.9	39.2	30.1
	CESE	2011	-55.4	-65.4	-74.4	-90.9	-105.0	-100.4	-79.2
		2014	-60.3	-71.4	-80.9	-99.6	-114.5	-109.6	-86.5

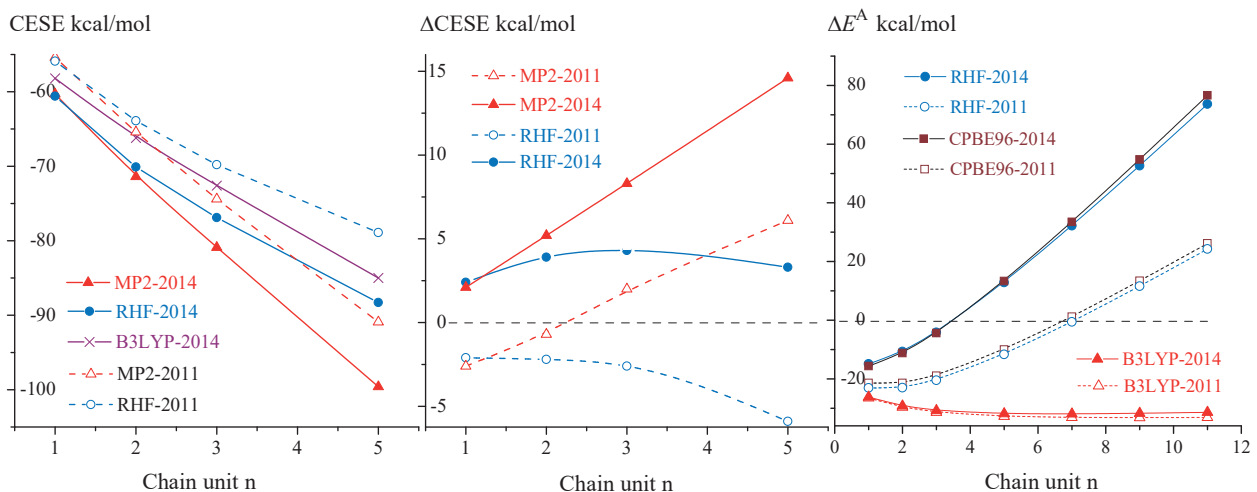


Figure 12-3. For acene series at 6-31G* level: (a) CESE(Y,T) versus the chain unit n; (b) $\Delta\text{CESE}(Y,T)$ versus n, where $\Delta\text{CESE}(Y,T) = \text{CESE}(Y,\text{B3LYP}) - \text{CESE}(Y,T)$ ($T = \text{RHF}, \text{MP2}; Y = 2011, 2014$); (c) ΔE^A versus n.

kcal/mol, $\Delta E^A(2014) = -26.2$ kcal/mol. The differences $\Delta E^A(2014) - \Delta E^A(2011) = 0.3$ kcal/mol, and $\text{CESE}(2014) - \text{CESE}(2011) = -0.2$ kcal/mol, where, for example, the symbol “CESE(2014)” means that the CESE is obtained from our 2014 method.

At (RHF, MP2 and CPBE96) levels of theory, on the contrary, the conditional deletion of exchange gradients has a large influence on the CESE. For phenanthrene at 6-31G* level, for example, the differences (kcal/mol), [$\text{CESE}(2014) - \text{CESE}(2011)$] and [$\Delta E^A(2014) - \Delta E^A(2011)$], are as follows:

-6.6 and 12.2 (RHF), -7.3 and 10.4 (MP2), -7.7 and 12.6 (CPBE96) kcal/mol.

For acene series at RHF level of theory, as shown by two blue lines in Figure 12-3a, the $\text{CESE}(2011)$ and $\text{CESE}(2014)$ are the second order polynomial function of the chain unit n. The two lines, a blue dashed line and a blue solid line, are located on the upper and lower sides of the brown solid line (B3LYP), and $d\text{CESE}(Y)/dn < 0$, and $d^2\text{CESE}(Y)/dn^2 > 0$ ($Y = 2011, 2014$). As the results, as shown by the blue data points in Figure 12-3b, $|\Delta\text{CESE}(2011,\text{RHF})| \approx \Delta\text{CESE}(2014,\text{RHF})$ (2.4 kcal/mol) when $n = 1$ (naphthalene), and $|\Delta\text{CESE}(2011,\text{RHF})| > \Delta\text{CESE}(2014,\text{RHF})$ (3.3 kcal/mol) when $n = 5$ (hexacene), where $\Delta\text{CESE}(Y,T) = \text{CESE}(Y,\text{B3LYP}) - \text{CESE}(Y,T)$. For hexacene, the ratio, $|\Delta\text{CESE}(2014,\text{RHF})/\text{CESE}(2014,\text{B3LYP})|$, is 3.9%. Especially, as shown by the solid blue line in Figure 12-3a and Figure 12-3b, as the chain unit n increases, the $\text{CESE}(2014,\text{RHF})$ value approaches the $\text{CESE}(2014,\text{B3LYP})$ value, but the $\text{CESE}(2011,\text{RHF})$ value gradually moves away from the $\text{CESE}(2014,\text{B3LYP})$ value.

At MP2/6-31G* level, as shown by two red lines in Figure 12-3a, $\text{CESE}(Y)$ ($Y = 2011, 2014$) are the linear function of chain unit n, and the slop of the red solid line is slight greater than that of the red dashed line. As the results, the values of $\Delta\text{CESE}(Y,\text{MP2})$ changes from -2.6 ($Y = 2011$) and 2.1 (2014) kcal/mol for naphthalene to 6.1 ($Y = 2011$) and 14.6 (2014) kcal/mol for hexacene. In the case of polycyclic benzenoid hydrocarbons, the B3LYP and RHF values of $\text{CESE}(2014)$ are reasonable.

In chapter 9, we concerned about the influence of two-electron exchange integrals on $d(\Delta E^A)/dn$. At B3LYP/6-31G* level, the deletion of two-electron exchange integral makes $d(\Delta E^A)/dn$ to change from $d(\Delta E^A)/dn > 0$ to $d(\Delta E^A)/dn < 0$ (Figure 9-16), leading to that $d(\Delta E^A)/dn = 0$ when $n = 13$, and $d(\Delta E^A)/dn > 0$ when $n > 13$. In Figure 12-3c, the solid and dashed red lines overlap. At (RHF and CPBE96)/6-31G* levels, as

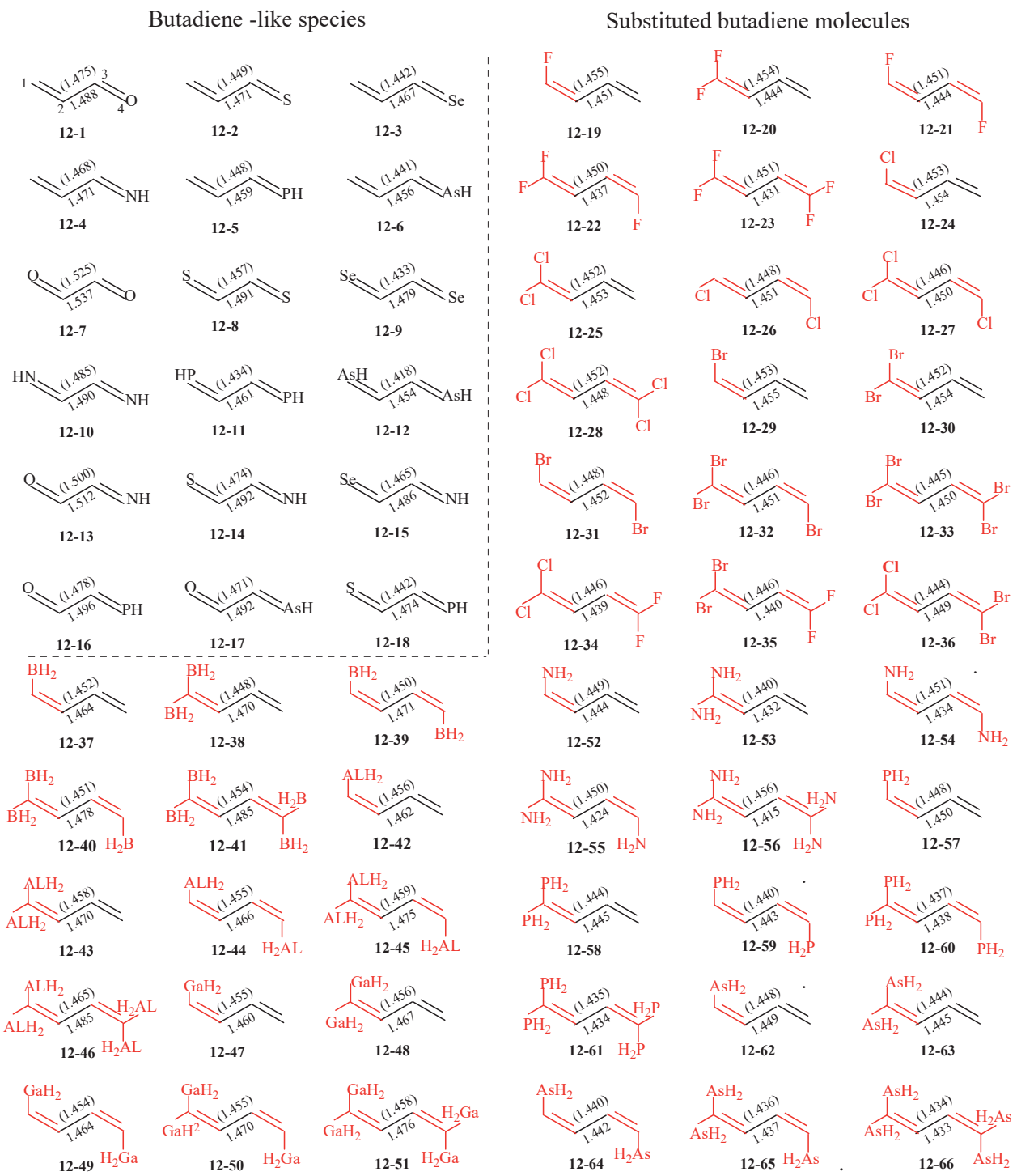


Figure 12-4. For the GL geometry of each of 66 molecules, the structures of two red localized groups, and the distance (\AA) of naked CC single bond between the two red groups. The value in parentheses is the distance of the CC single bond in the ground state geometry. The GL geometries are optimized using our 2014 method at B3LYP/6-31G* level. In the red group, a double bond and its substituent(s) are conjugated, and the black single bond between the two groups (red or black group) means that the two red groups are not conjugated.

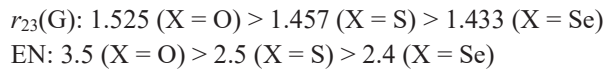
shown by the blue and brown lines in Figure 12-3c, the deletion of exchange gradients has obvious influence on $d\Delta E^A/dn$. At RHF/6-31G* level, for example, $d\Delta E^A(2011)/dn > 0$, and $d\Delta E^A(2014)/dn > 0$, and $d\Delta E^A(2014)/dn > d\Delta E^A(2011)/dn$. At RHF/6-31G* level, ΔE^A tends to become destabilizing.

12.4. BUTADIENE DERIVATIVES

As a reasonable method of optimizing localized geometry, our 2014 method should be able to be used to estimate the distance of the naked CC single bond in butadiene and its substituted derivative. In fact, as shown by Figure 12-1, the distance (1.451 Å) of CC single bond in the GL geometry of butadiene, obtained from our 2014 method, is 0.01 Å longer than the distance obtained from our 2011 method although the molecular energy difference, $E(GL,2014) - E(GL,2011)$, is only -0.1 kcal/mol.

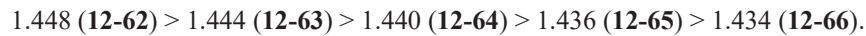
The first object of constructing GL geometry is of course to understand the relationship between the conjugation effect and the change in the CC single bond length. Thus, for 66 butadiene derivatives, the geometries of the ground states are optimized at B3LYP/6-31G* level, and the distance, $r_{23}(G)$, of their CC single bonds are presented in parentheses in Figure 12-4.

May be due to that there are two strongest electron-withdrawing groups –CHO, the distance (1.525 Å) of the CC single bond in the ground state geometry of molecule OHC–CHO is longest, and is close to that (1.54 Å) of sp³-sp³ CC single bond in ethane. In the type of molecules X=CH–HC=Y, the distance (Å) of CC single bond decreases as the electronegativity (EN) of X atom decrease. For molecules X=CH–HC=X (X = O, S, Se), for example, the CC single bond distance $r_{23}(G)$ (Å), the electronegativity (EN) of X atom are as follows:

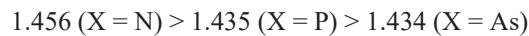


The number of X=CH– groups also have an influence on the distance. For the distance (Å) of CC single bonds in molecules NHCH–CHCH₂ (**12-4**) and NHCH–HCNH (**12-10**), for example, 1.468 (**12-4**) < 1.485 (**12-10**).

The substituent -AsH₂ is an electron-releasing group. For five AsH₂-substituted butadiene molecules (from **12-62** to **12-66**), the distances $r_{23}(G)$ (Å) of the CC single bonds are as follows:



The distance decreases as the number of -AsH₂ groups increases. In the ground state geometry of molecule **12-66** having four -AsH₂ groups, the distance (1.434 Å) is the shortest of the five AsH₂-substituted molecules. For the molecules having 4 electron-releasing groups -XH₂ (X = N, P, As), the electronegativity of electron-releasing groups can also influence the distance $r_{23}(G)$ (Å) according to the following size order:

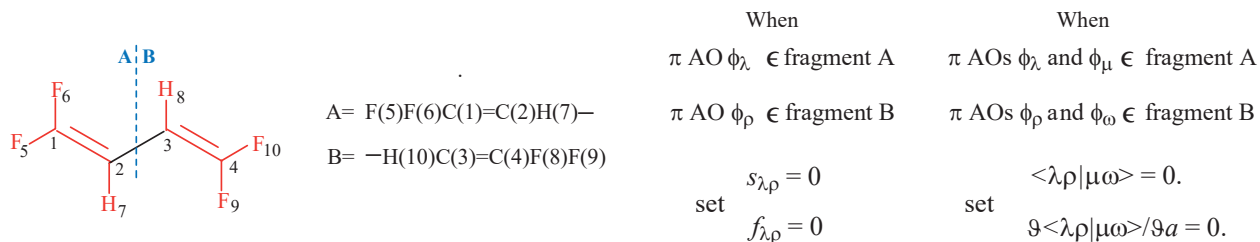


For the CC single bond distance $r_{23}(G)$ in the ground state geometry of 66 molecules presented Figure 12-4, the range, the difference between the longest (1.525 Å) distance and the shortest (1.418 Å) distance, is 0.107 Å. The large range means that, in the ground state geometries of butadiene derivatives, the conjugation between a double bond and its substituent (s) and the conjugation between the two double bonds play an important role in determining the distance of sp²-sp² CC single bond, and the strength of the conjugation effect is governed by the type and number of the substituents and by the type of the double bonds. The conjugation between a double bond and its substituent (s) will be defined as an adjacent conjugation (conjugation adjacent to the CC single bond).

12.4.1. Localized GL Geometries

66 butadiene derivatives, including 18 butadiene-like species $X=C-C=Y$ ($X, Y = O, S, Se, N, P, As$), and 48 substituted butadiene molecules $XX'C=C-C=CY'$ (Figure 12-4), are used as the samples, and their GL geometries are optimized, under the conditional settings detailed in Scheme 12-1, using our 2014 method at B3LYP/6-31G* level. In the GL geometry of $F_2C(1)=C(2)H-$ $HC(3)=C(4)F_2$ (Scheme 12-1), for example, all the π MO interactions, as well as two-electron exchange integrals and exchange gradients, between the group $F_2C(1)=C(2)H-$ (A) and the group $-HC(3)=C(4)F_2$ (B) have been set equal to zero, but in each group (A and B), a double bond and its substituents are conjugated.

In the GL geometry of a butadiene derivative, the two CC double bonds are unconjugated, and the single bond between these two double bonds is called “naked sp^2-sp^2 CC single bond”. Hereafter, the phrase “naked sp^2-sp^2 CC single bond” will be shortened to that “naked single bond” or “naked CC single bond”.



Scheme 12-1

For the GL geometries of 66 molecules, the distances, $r_{23}(GL)$, of naked CC single bond are presented in Figure 12-4, and the longest distance and the shortest distance are presented in Figure 12-5c. Of 66 molecules, glyoxal (**12-7**) has the longest naked single bond, due to that its two $-C=O$ groups are the strongest π and σ electron-withdrawing group. In this molecule, the distance of naked single bond is 1.537 Å, and it can be considered equal to the distance (1.54 Å) of sp^3-sp^3 CC single bond in the ground state geometry of ethane. In the GL geometry of 1,1,4,4-tetraamino-butadiene (**12-56**), on the contrary, four NH_2- groups are the strongest electro-releasing groups. In the GL geometry of molecule **12-56**, as a result, the distance (1.415 Å) of naked single bond is the shortest. For the distances of 66 CC naked single bonds presented in Figure 12-4, the range, the difference between the longest (1.537 Å) distance and the shortest (1.415 Å) distance, is large, up to 0.122 Å.

The construction of localized GL geometry makes it possible to achieve the following two purposes:

- (i) Recognizing the role of the conjugation between two double bonds in determining the distance of CC single.
- (ii) Predicting the structural factors affecting the distance of naked CC single bond, leading to the concept of adjacent conjugation effect and to understand the necessity of constructing GL_n geometry (the construction of the GL_n geometry will be detailed in this section)

12.4.1.1. Conjugation between Two Double Bonds

$\Delta r_{23}(G) = r_{23}(G) - r_{23}(GL)$ is the difference, in the distance of $C(2)-C(3)$ single bond, between the ground state geometry (G) and the GL geometry, and $\Delta E(G) = E(G) - E(GL)$ is the molecular energy difference between the two geometry. Interestingly, for 66 butadiene derivatives, as shown by Figure 12-5a, $\Delta r_{23}(G)$ (y) can be well fitted as a following third order polynomial function of $\Delta E(G)$ (x) ($cc = 0.9836$):

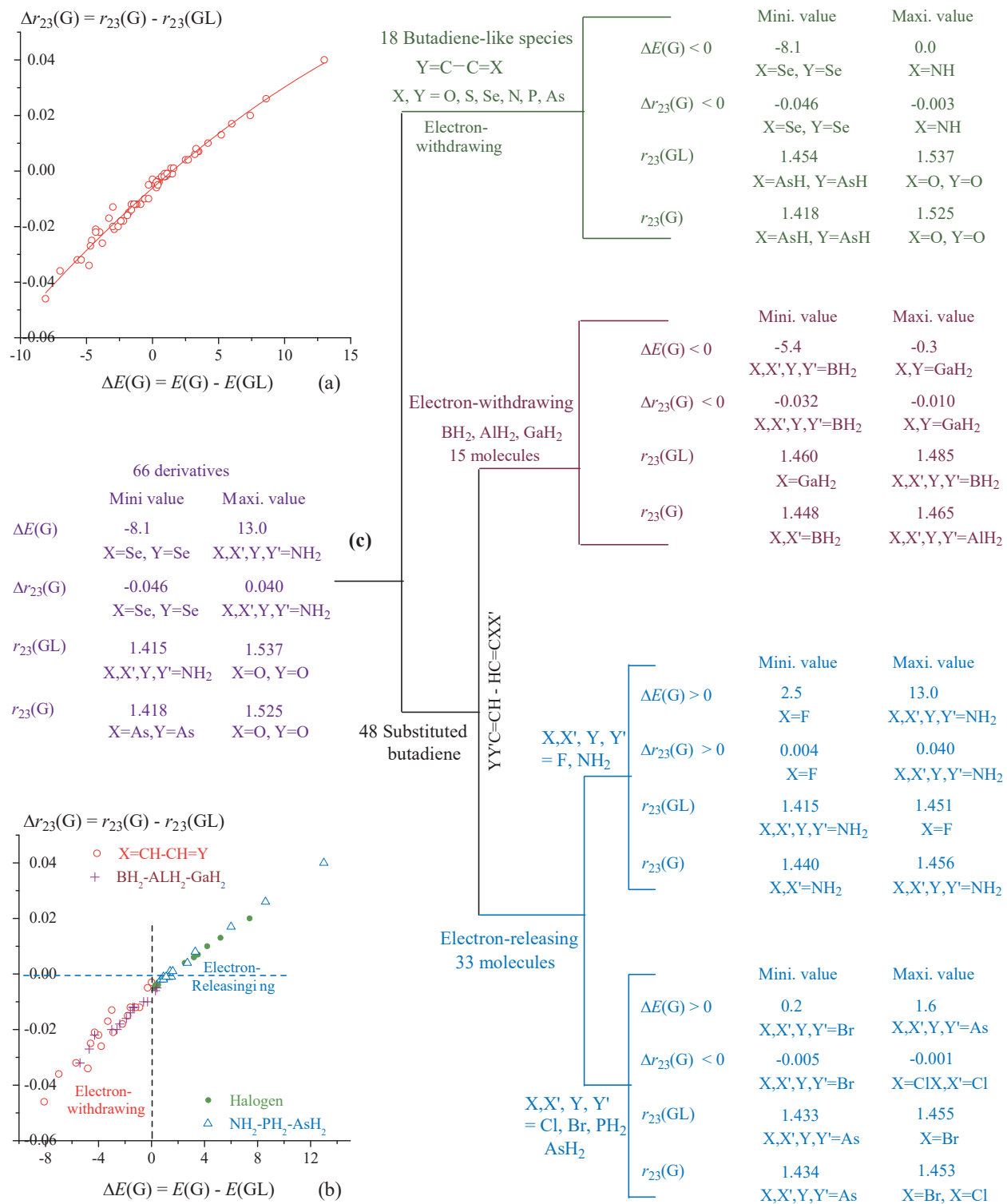


Figure 12-5. For 66 molecules at B3LYP/6-31G* level: (a) $\Delta r_{23}(G)$ (u) can be well fitted as a second order polynomial function of $\Delta E(G)$ (v). (b) The scattered data points (u, v) for various types of butadiene derivatives. (c) Classification of 66 molecules (energy unit in kcal/mol, and distance unit in angstrom).

Table 12-12. For 66 Molecules, Molecular Energy $E(GL)$ (hartree) of GL Geometry, and Molecular Energy Difference $\Delta E(G) = E(G) - E(GL)$ (kcal/mol), and CC Single Bond Distance Difference $\Delta r_{23}(G) = r_{23}(G) - r_{23}(GL)$ (\AA), Calculated by Our 2014 method at B3LYP/6-31G* Level.

MOLES	$E(GL)$	$\Delta E(G)$	$\Delta r_{23}(G)$	MOLES	$E(GL)$	$\Delta E(G)$	$\Delta r_{23}(G)$
CH ₂ CH-CHO	-191.90716	-3.0	-0.013	CL ₂ CCH-CHCF ₂	-1273.65380	3.4	0.007
CH ₂ CH-CHS	-514.86787	-4.0	-0.022	Br ₂ CCH-CHCF ₂	-5496.75058	3.2	0.006
CH ₂ CH-CHSe	-2516.07801	-4.6	-0.025	CL ₂ CCH-CHCBr ₂	-6217.46274	0.3	-0.004
CH ₂ CH-CHNH	-172.03409	0.0	-0.003	BH ₂ HCCH-CHCH ₂	-181.43247	-1.4	-0.012
CH ₂ CH-CHPH	-458.62560	-0.9	-0.012	BH ₂ CCH-CHCH ₂	-206.86770	-4.3	-0.022
CH ₂ CH-CHAsH	-2351.05311	-1.8	-0.015	BH ₂ CCH-CHCHBH ₂	-206.86931	-3.0	-0.020
OCH-CHO	-227.81674	-1.2	-0.012	(BH ₂) ₂ CCH-CHCHBH ₂	-232.30385	-4.7	-0.027
SCH-CHS	-873.73961	-4.8	-0.034	(BH ₂) ₂ CCH-CHC(BH ₂) ₂	-257.73797	-5.4	-0.032
SeCH-CHSe	-4876.16044	-8.1	-0.046	(AlH ₂)HCCH-CHCH ₂	-399.01618	0.3	-0.006
HNCH-CHNH	-188.07205	-0.3	-0.005	(AlH ₂) ₂ CCH-CHCH ₂	-642.03815	-1.3	-0.012
HPCl-CHPH	-761.25595	-3.8	-0.026	(AlH ₂)HCCH-CHCHALH ₂	-642.03731	-0.6	-0.010
HA ₂ CH-CHAsH	-4546.11134	-7.0	-0.036	(AlH ₂) ₂ CCH-CHCHALH ₂	-885.05879	-1.9	-0.016
OCH-CHNH	-207.94416	-1.6	-0.012	(AlH ₂) ₂ CCHCHC(AlH ₂) ₂	-1128.08022	-2.6	-0.020
SCH-CHNH	-530.90533	-2.2	-0.018	GaH ₂ HCCH-CHCH ₂	-2079.61369	0.4	-0.005
SeCH-CHNH	-2532.11581	-2.9	-0.021	(GaH ₂) ₂ CCH-CHCH ₂	-4003.24147	-1.4	-0.012
CHO-CHPH	-494.53781	-3.3	-0.017	GaH ₂ HCCH-CHCHGaH ₂	-4003.23255	-0.3	-0.010
OCH-CHASH	-2386.96561	-4.3	-0.021	(GAH ₂) ₂ CCHCHCHGAH ₂	-5926.86066	-1.6	-0.014
SCH-CHPH	-817.49794	-5.7	-0.032	(GaH ₂) ₂ CCH-CHC(GaH ₂) ₂	-7850.48848	-2.4	-0.018
FHCCH-CHCH ₂	-255.22786	2.5	0.004	NH ₂ HCCH-CHCH ₂	-211.34912	2.7	0.004
F ₂ CCH-CHCH ₂	-354.46810	4.2	0.010	(NH ₂) ₂ CCH-CHCH ₂	-266.70004	3.3	0.008
FHCCH-CHCHF	-354.46150	3.5	0.007	NH ₂ HCCH-CHCH(NH ₂)	-266.70278	6.0	0.017
F ₂ CCH-CHCHF	-453.70156	5.2	0.013	(NH ₂) ₂ HCCH-CHCHNH ₂	-322.05269	8.6	0.026
F ₂ CCH-CHCF ₂	-552.94140	7.4	0.020	(NH ₂) ₂ CCH-CHC(NH ₂) ₂	-377.40176	13.0	0.041
CLHCH-CHCH ₂	-615.59108	1.0	-0.001	(PH ₂)HCCH-CHCH ₂	-497.88963	1.2	-0.001
CL ₂ CCH-CHCH ₂	-1075.18101	1.1	-0.001	(PH ₂) ₂ CCH-CHCH ₂	-839.77508	1.3	-0.001
CLHCH-CHCHCl	-1075.18745	0.5	-0.003	PH ₂ HCCH-CHCHPH ₂	-839.78443	0.7	-0.002
CL ₂ CH-CHCHCl	-1534.77677	0.5	-0.004	(PH ₂) ₂ HCCH-CHCHPH ₂	-1181.66963	0.9	-0.001
CL ₂ CCH-CHCCl ₂	-1994.36579	0.4	-0.004	(PH ₂) ₂ CCH-CHC(PH ₂) ₂	-1523.55459	1.4	0.001
BrHCCH-CHCH ₂	-2727.13898	1.0	-0.002	AsH ₂ HCCH-CHCH ₂	-2390.30458	1.3	-0.001
Br ₂ CCH-CHCH ₂	-5298.28338	0.4	-0.004	(AsH ₂) ₂ CCH-CHCH ₂	-4624.61109	1.5	-0.001
BrHCCH-CHCHBr	-5298.27774	0.9	-0.002	AsH ₂ HCCH-CHCHAsH ₂	-4624.61447	0.9	-0.002
Br ₂ CCH-CHCHBr	-7869.42167	0.3	-0.004	(AsH ₂) ₂ HCCHCHCHAsH ₂	-6858.92099	1.1	-0.001
Br ₂ CCH-CHCBr ₂	-10440.55973	0.2	-0.005	(AsH ₂) ₂ CCH-CHC(AsH ₂) ₂	-9093.22733	1.6	0.001

$$y = -0.00604 + 0.00413x - (6.72248 \times 10^{-5})x^2 + (1.59902 \times 10^{-6})x^3$$

Therefore, the change $\Delta r_{23}(G)$ in the distance of C(2)–C(3) single bond is a result of the conjugation between two localized CC double bonds in the GL geometry.

It should be indicated that the CC single bond length $r_{23}(G)$ in the ground state geometry and the bond length difference $\Delta r_{23}(G)$ are two different physical quantities, they depend on different structural factors. That a molecule has the greatest change $\Delta r_{23}(G)$ in the distance of single bond does not mean that its distance $r_{23}(G)$ must be the longest (or the shortest) of all the molecules. For molecules **12-9** and **12-56**, for example, $\Delta r_{23}(G)$ are -0.46 and 0.041 Å, and are the largest negative value and the largest positive value. But the shortest and longest distances, $r_{23}(G) = 1.418$ Å and $r_{23}(G) = 1.525$ Å, are found in molecules **12-12** and **12-7**.

In the case of the molecules with electron-withdrawing groups, as shown by an inspection of the blue data in Table 12-12, always $\Delta E(G) = E(G) - E(GL) < 0$, (stabilizing), $\Delta r_{23}(G) < 0$, which is consistent with the classic view. The energy effects $\Delta E(G)$ of molecules **12-42** and **12-47** are the two exceptions to the above rule. For molecule **12-9** with two electron-withdrawing groups –C=Se, for example, $\Delta E(G) = -8.1$ kcal/mol < 0, and $\Delta r_{23}(G) = -0.046$ Å < 0. In Table 12-12, these two values are the most negative.

For the molecules with electron-releasing groups, on the contrary, always $\Delta E(G) > 0$ (the black data in Table 12-12), and whether $\Delta r_{23}(G) > 0$ or $\Delta r_{23}(G) < 0$ depends on the position of the element in the Periodic Table. When the X atom, such as F and N, belongs to the second period of the Periodic Table, $\Delta r_{23}(G) > 0$. Otherwise, $\Delta r_{23}(G) < 0$ and $|\Delta r_{23}(G)| < 0.006$. For 1,1,4,4-trtra-amino-butadiene (**12-56**) with four electron-releasing groups –NH₂, especially, $\Delta E(G) = 13.0$ kcal/mol > 0, and it is the greatest positive value. Correspondingly, $\Delta r_{23}(G) = 0.041$ Å, and it is also the greatest.

For 66 butadiene derivatives, the range of a set of $\Delta r_{23}(G)$ values, [0.040 - (-0.046)], is 0.086 Å, and it is so large that it is unreasonable for Dewar to deny the role of conjugation in determining the distance of the CC single bond between two conjugated CC double bonds in the ground state geometry of butadiene derivatives.

12.4.1.2. Mulliken Atomic Overlap Population and Charge

For the distances of the naked single bonds of 66 butadiene derivatives, as mentioned above, the range is 0.122 Å. It is so large that we should investigate the structural factors that determine the distance of naked single bond. The structural factors should include the inductive effect of substituent(s) and the adjacent conjugation between a double bond and its substituent(s). The quantum chemistry calculation provides the following two physical quantities for a molecule: Mulliken atomic overlap population, P_{ij} , between the i -th and j -th atoms; Charges, e_i , on the i -th atom. These two quantities can be used to evaluate the influences of the adjacent conjugation effect and inductive effect on the naked CC single bond in the GL geometry.

According to the Figure 12-6c, 66 butadiene derivatives can be divided into the following four classes:

- (i) 18 butadiene-like species X=CH–HC=Y (X, Y = O, S, Se, HN, HP, HAs, CH₂) (from **12-1** to **12-18**), where the groups “X=C” and “Y=C” are the electron-withdrawing group;
- (ii) 18 halogen-substituted butadienes (X, X' and Y, Y' = F, Cl, Br, H) (from **12-19** to **12-36**), where the halogen groups are π electron-releasing and σ electron-withdrawing;
- (iii) 15 XH₂-substituted butadienes (X = B, Al, Ga, **12-37** to **12-51**), where the substituents XH₂ are electron-deficient, and they are π electron-withdrawing;
- (iv) 15 YH₂-substituted butadienes (Y = N, P, As, **12-52** to **12-66**), and the substituents YH₂ are π electron-releasing.

Figure 12-6 shows the relationship between $r_{23}(\text{GL})$ and $P_{23}(\text{GL})$ and the relationship between $r_{23}(\text{GL})$ and

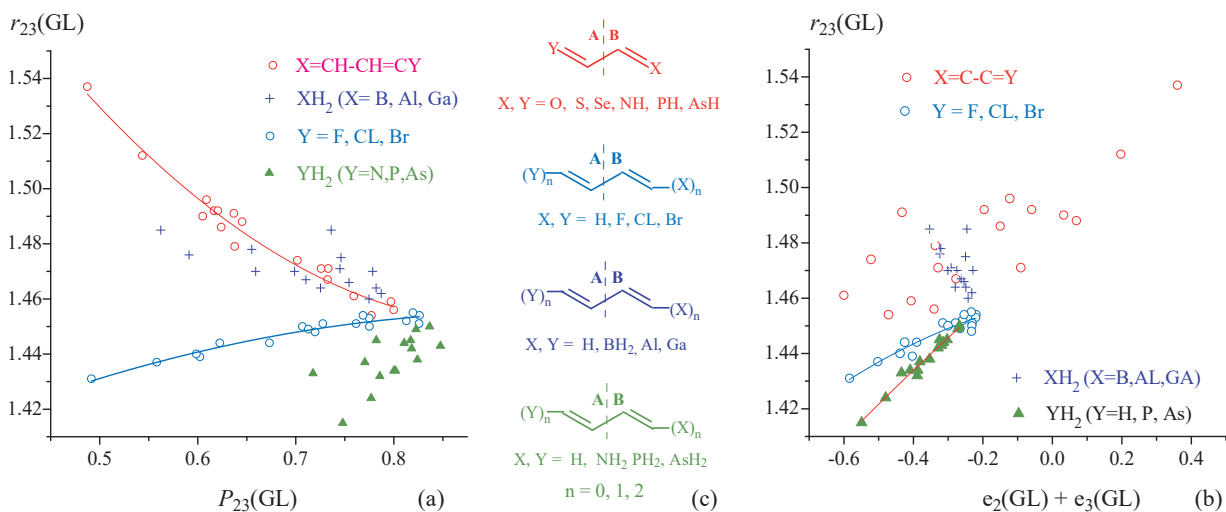


Figure 12-6. At B3LYP/6-31G* level: (a) Polynomial fitting for 18 butadiene-like species (red line) and for 18 halogen-substituted butadienes (blue line). (b) Polynomial fitting for 18 halogen-substituted butadienes (blue line) and for 15 YH_2 -substituted butadienes ($\text{Y}=\text{N, P, As}$, green line). (c) Classification of Butadiene Derivatives.

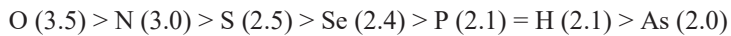
Σe_i . In the GL geometry of each butadiene-like species, there is no conjugation between the $\text{X}=\text{C}-$ and $-\text{C}=\text{Y}$ groups. For a set of $r_{23}(\text{GL})$ values, the largest and smallest values are 1.537 Å ($\text{O}-\text{CH}-\text{CH}=\text{O}$) and 1.454 Å ($\text{HAs}=\text{CH}-\text{HC}=\text{AsH}$), and the range is large, up to 0.083 Å (Table 12-13).

In a planar GL geometry, $P_{23}(\text{GL})$ is contributed only by the σ -type AO coefficients, $c_{\lambda,i}$ and $c_{\rho,i}$, of the C(2) and C(3) atoms, and the charge e_i on the C(i) atom is related to the π - and σ -type AO coefficients of all atoms. Therefore, the charges on the carbon atoms C(2) and C(3) can be used to evaluate the influence of the adjacent conjugation between each CC double and its substituent(s) on the distance of CC single bond, and Mulliken atomic overlap population, $P_{23}(\text{GL})$, can be used to measure the inductive effect of substituent.

For the GL geometries of 18 butadiene-like species, as shown by red curve line in Figure 12-6a, $r_{23}(\text{GL})$ (y) can be well fitted as the following second order polynomial function of $P_{23}(\text{GL})$ (x):

$$y = 1.829 - 0.822x + 0.4460x^2 \quad (\text{cc} = 0.9666).$$

The fitted function, $r_{23}(\text{GL}) = f(P_{23})$, is monotonically decreasing. According to the following size order of electronegativities (Pauling):⁶¹



the electron-withdrawing power of oxygen atom is the greatest, and that of Arsenic atom is the smallest. For $\text{OCH}-\text{CHO}$, $P_{23}(\text{GL})$ (0.4874) is the smallest of all $P_{23}(\text{GL})$ in Table 12-13, and the corresponding $r_{23}(\text{GL})$ (1.537 Å) is the longest; for $\text{CH}_2=\text{CH}-\text{CH}=\text{As}$, $P_{23}(\text{GL})$ (0.7999) is the greatest, and the naked single bond distance (1.456 Å) is almost the shortest. For a set of $r_{23}(\text{GL})$ values and for set of $P_{23}(\text{GL})$ values, the ranges are, respectively, 0.081 Å and 0.3235. The fitted function $r_{23}(\text{GL}) = f(P_{23}(\text{GL}))$ reasonably implies that the inductive effect of the group $\text{CH}=\text{X}$ plays an important role in determining the distance of the naked CC single bond in the GL geometry of butadiene-like species.

According to the scattered red circles ($\Sigma e_i(\text{GL}), r_{23}(\text{GL})$) in Figure 12-6b, although there is no polynomial relationship between $r_{23}(\text{GL})$ and $\Sigma e_i(\text{GL})$, the tendency is that the distance of naked CC single bond becomes longer

Table 12-13. For the GL Geometries of 18 Butadiene-like Species Obtained from Our 2014 Method at B3LYP/6-31G* Level, Naked Single Bond Distances $r_{23}(\text{GL})$, Mulliken Atomic Overlap Population $P_{23}(\text{GL})$, and Charges $e_2(\text{GL})$, $e_3(\text{GL})$ and Their Sum $\Sigma e_i(\text{GL})$.

Molecules	$r_{23}(\text{GL}) \text{ \AA}$	$P_{23}(\text{GL})$	$e_2(\text{GL})$	$e_3(\text{GL})$	$\Sigma e_i(\text{GL})$
Butadiene	1.457	0.82108	-0.10458	-0.10458	-0.2092
$\text{CH}_2\text{CH}-\text{CHO}$	1.488	0.64547	-0.16364	0.23258	0.0689
$\text{CH}_2\text{CH}-\text{CHS}$	1.471	0.73318	-0.10846	-0.22016	-0.3286
$\text{CH}_2\text{CH}-\text{CHSe}$	1.467	0.73256	-0.10122	-0.17680	-0.2780
$\text{CH}_2\text{CH}-\text{CHNH}$	1.471	0.72600	-0.13446	0.04368	-0.0908
$\text{CH}_2\text{CH}-\text{CHPH}$	1.459	0.79721	-0.09619	-0.31057	-0.4068
$\text{CH}_2\text{CH}-\text{CHAsH}$	1.456	0.79999	-0.09047	-0.25036	-0.3408
$\text{CHO}-\text{CHO}$	1.537	0.48742	0.17999	0.17999	0.3600
$\text{CHS}-\text{CHS}$	1.491	0.63694	-0.21630	-0.21629	-0.4326
$\text{CHSe}-\text{CHSe}$	1.479	0.63782	-0.16818	-0.16819	-0.3364
$\text{HNCH}-\text{CHNH}$	1.490	0.60519	0.01630	0.01630	0.0326
$\text{HPCH}-\text{CHPH}$	1.461	0.75934	-0.30025	-0.30025	-0.6005
$\text{HAsCH}-\text{CHAsH}$	1.454	0.77724	-0.23577	-0.23576	-0.4715
$\text{CHO}-\text{CHNH}$	1.512	0.54368	0.20582	-0.00922	0.1966
$\text{CHS}-\text{CHNH}$	1.492	0.62069	-0.23985	0.04347	-0.1964
$\text{CHSe}-\text{CHNH}$	1.486	0.62406	-0.20040	0.05025	-0.1501
$\text{CHO}-\text{CHPH}$	1.496	0.60910	0.23787	-0.36022	-0.1223
$\text{CHO}-\text{CHAsH}$	1.492	0.61681	0.24129	-0.30131	-0.0600
$\text{CHS}-\text{CHPH}$	1.474	0.70167	-0.20689	-0.31487	-0.5218

as $\Sigma e_i(\text{GL})$ changes from negative to positive in the case of butadiene-like species. For example, the size order of $\Sigma e_i(\text{GL})$ and corresponding $r_{23}(\text{GL})$ are as follow:

$$\Sigma e_i(\text{GL}): -0.6005 \text{ (12-11)} < -0.5218 \text{ (12-18)} < 0.0326 \text{ (12-10)} < 0.3600 \text{ (12-7)}$$

$$r_{23}(\text{GL}): 1.461 < 1.474 < 1.490 < 1.537 \text{ \AA}.$$

But when $\Sigma e_i(\text{GL})$ is in the region of -0.6 to 0.0, the size order of naked CC single bond distances is chaotic.

15 halogen-substituted butadienes can be divided into the following three sub-groups: 5 fluoro-substituted, 5 chloro-substituted, and 5 bromo-substituted molecules. In each sub-group, the distance $r_{23}(\text{GL})$ in the mono-substituted molecule is the longest. For fluoro-substituted butadienes, for example, the size orders of $r_{23}(\text{GL})$ (\AA) and $P_{23}(\text{GL})$ are as follows (Table 12-14):

Table 12-14. For the GL Geometries Of 18 Halogen-Substituted Butadienes Optimized by Our 2014 Method at B3LYP/6-31G* Level, Naked Single Bond Distances $r_{23}(\text{GL})$ (Å), Mulliken Atomic Overlap Population $P_{23}(\text{GL})$, and Charges $E_2(\text{GL})$, $E_3(\text{GL})$ and Their Sum $\Sigma E_i(\text{GL})$.

Molecules	$r_{23}(\text{GL})$ Å	$P_{23}(\text{GL})$	$e_2(\text{GL})$	$e_3(\text{GL})$	$\Sigma e_i(\text{GL})$
Trans-1,3-Butadiene	1.457	0.82108	-0.10458	-0.10458	-0.2092
FHCCH-CHCH ₂	1.451	0.72770	-0.20792	-0.10799	-0.3159
F ₂ CCH-CHCH ₂	1.444	0.67334	-0.29052	-0.10032	-0.3908
FHCCH-CHCHF	1.444	0.62262	-0.21242	-0.21242	-0.4248
F ₂ CCH-CHCHF	1.437	0.55824	-0.29649	-0.20642	-0.5029
F ₂ CCH-CHCF ₂	1.431	0.49162	-0.29204	-0.29204	-0.5841
CLHCH-CHCH ₂	1.454	0.82628	-0.10753	-0.11242	-0.2199
CL ₂ CCH-CHCH ₂	1.453	0.77510	-0.10730	-0.11344	-0.2207
CLHCH-CHCHCl	1.451	0.82585	-0.11564	-0.11557	-0.2312
CL ₂ CH-CHCHCl	1.450	0.77517	-0.11581	-0.11597	-0.2318
CL ₂ CCH-CHCCL ₂	1.448	0.71983	-0.11647	-0.11647	-0.2329
BrHCCH-CHCH ₂	1.455	0.81959	-0.12297	-0.11038	-0.2334
Br ₂ CCH-CHCH ₂	1.454	0.76869	-0.14352	-0.11037	-0.2539
BrHCCH-CHCHBr	1.452	0.81295	-0.12897	-0.12893	-0.2579
Br ₂ CCH-CHCHBr	1.451	0.76165	-0.15073	-0.12809	-0.2788
Br ₂ CCH-CHCBr ₂	1.450	0.70688	-0.14997	-0.14997	-0.2999
CL ₂ CCH-CHCF ₂	1.439	0.60231	-0.09782	-0.30495	-0.4028
Br ₂ CCH-CHCF ₂	1.440	0.59877	-0.13566	-0.30230	-0.4380
CL ₂ CCH-CHCBr ₂	1.449	0.71298	-0.11229	-0.15376	-0.2660

$r_{23}(\text{GL})$: 1.451 (1-fluoro-) > 1.444 (1,1-difluoro-) = 1.444 (1,4-difluoro) > 1,437 (1,1,4-trifluoro-) > 1.431 (1,1,4,4-tetra-fluoro-).

$P_{23}(\text{GL})$: 0.7277 > 0.6733 > 0.6226 > 0.5582 > 0.4916.

For 15 halogen-substituted butadienes, as shown by the blue curve line in Figure 12-6a, $r_{23}(\text{GL})$ can be fitted as the second order polynomial functions of $P_{23}(\text{GL})$. But it is different to the red curve line that, for halogen-substituted butadienes, $r_{23}(\text{GL}) = f[P_{23}(\text{GL})]$ is a monotonically increasing function. According to the definition, $P_{23}(\text{GL})$ is the function of the density matrix elements, p_{uv} , between the C(2) and C(3) atoms, the larger $P_{23}(\text{GL})$ should correspond to the shorter naked CC single bond $r_{23}(\text{GL})$.^{6,9,11} Therefore, the polynomial fitting curve $r_{23}(\text{GL}) = f[P_{23}(\text{GL})]$ is meaningless although $cc = 0.9666$.

For 15 halogen-substituted butadienes, the single bond distance $r_{23}(\text{GL})$ (y) can also be fitted as the following second order polynomial function of $\Sigma e_i(\text{GL})$ (x) (a blue line in Figure 12-6b):

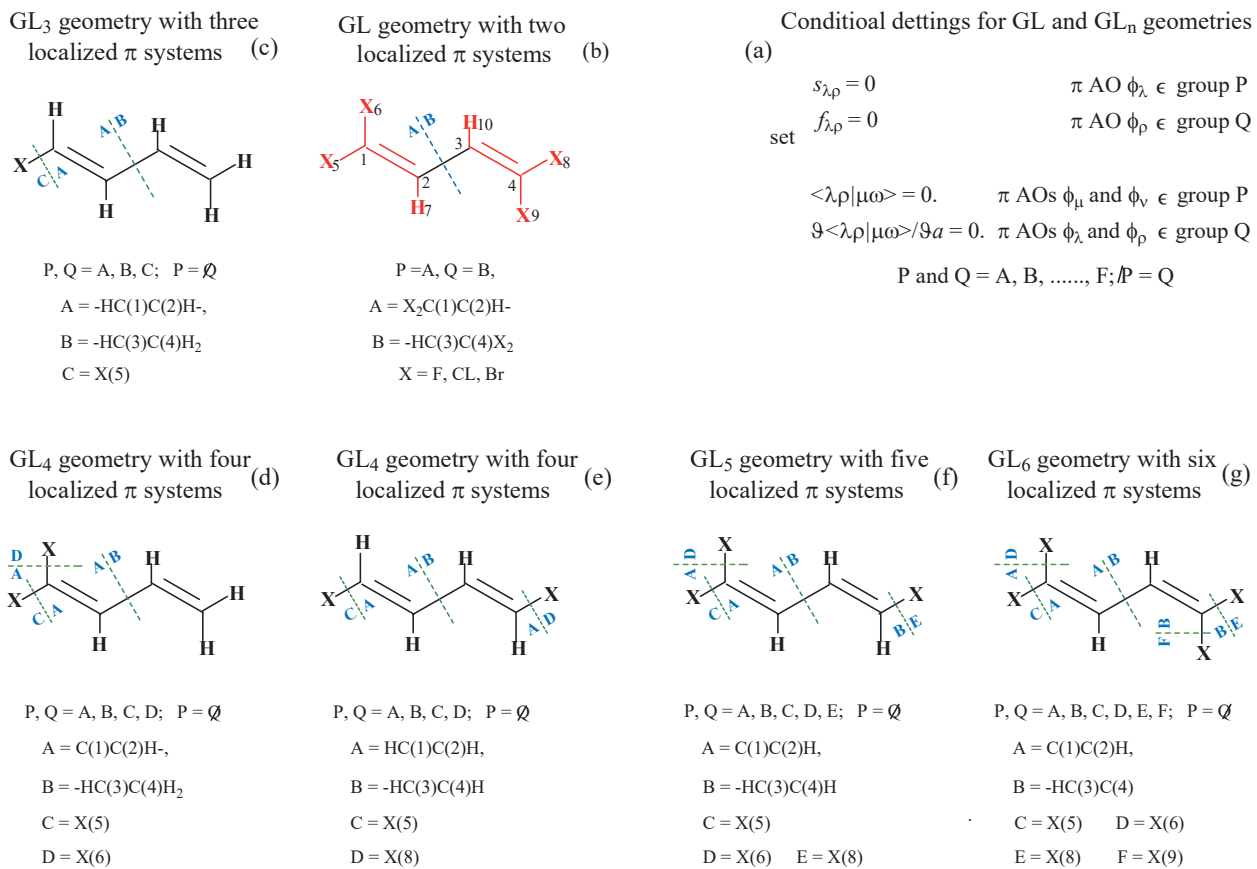


Figure 12-7. For each halogen-substituted butadiene (X = F, Cl, Br), the optimizations of the GL (with two localized π systems) and GL_n geometries (with n localized π systems) are performed, at B3LYP/6-31G* level, using our 2014 method. The subscript 'n' in the symbol GL_n is the number of localized π systems in GL_n geometry.

$$y = 1.46 + 0.0219x - 0.0486x^2 \text{ (cc = 0.885)}$$

The fitted line shows that the distance $r_{23}(\text{GL})$ increases as negative charge decreases and as positive charge increases. The fitted function, $r_{23}(\text{GL}) = f[\Sigma e_l(\text{GL})]$, is reasonable.

In the GL geometry of a halogen-substituted butadiene, the conjugation between the double bond and its halogen substituents increases the charges on C(2) and C(3) atoms, and the inductive effect of halogen atom decreases the value of $P_{23}(\text{GL})$. The fact that the first order derivative $d[r_{23}(\text{GL})]/d[\Sigma e_l(\text{GL})] > 0$ imply that, in the GL geometry of a halogen-substituted, the conjugation between each double bond and its substituent(s) plays an important role in determining the distance of naked single bond, and it is called the adjacent conjugation because this conjugation is adjacent to the naked CC single bond. The influence of the adjacent conjugation on the distance of naked single bond is called the adjacent conjugation effect.

12.4.1.3. Localized GL and GL_n Geometries

In order to understand the adjacent conjugation effect, it is necessary to construct the localized GL_n geometry. For halogen-substituted butadienes, as shown by Figure 12-7, there are two ways to localize the π system. In the first way, as shown by Figure 12-4, Scheme 12-1, and Figure 12-7b, the π system is localized on two groups

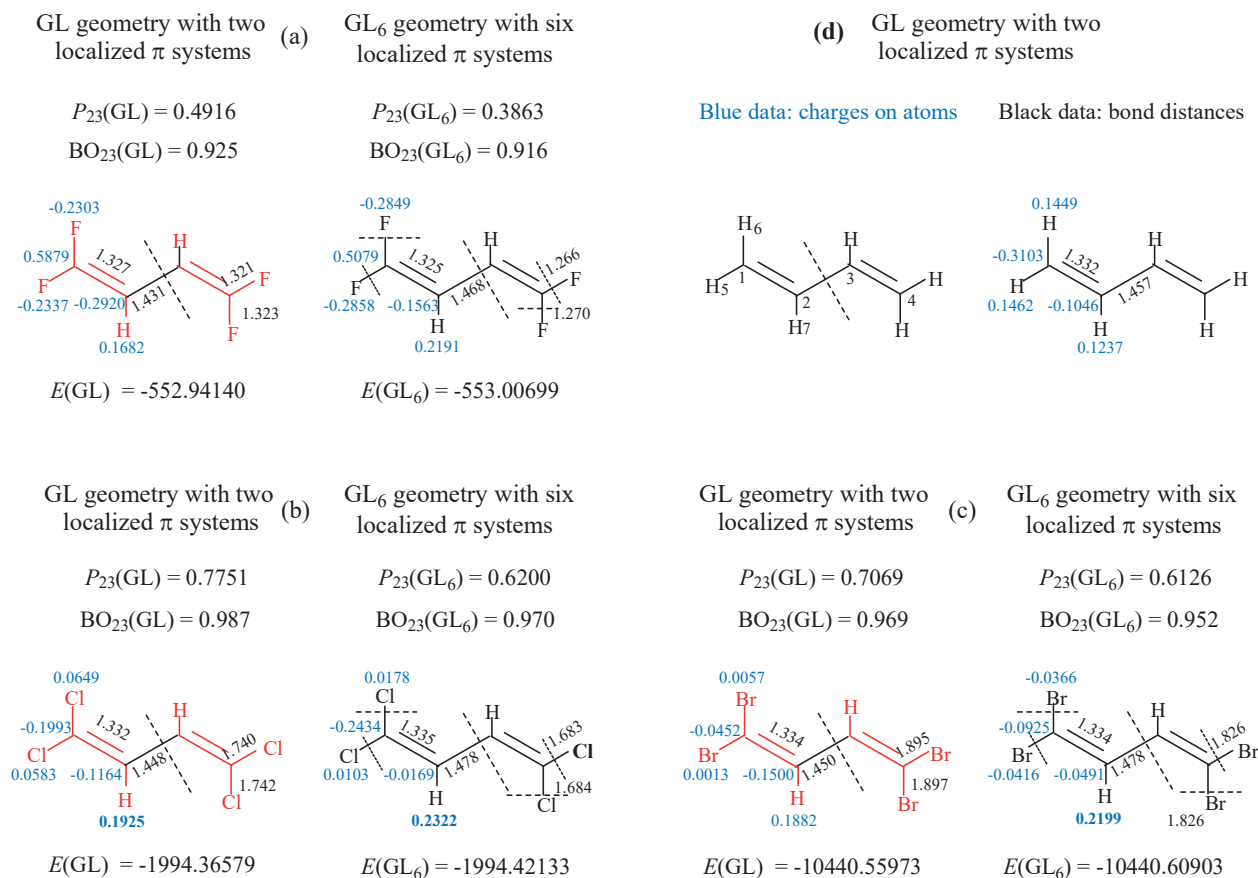


Figure 12-8. For three tetra-halogen-substituted butadienes, two ways to localize the π system. Bond distance (\AA , black data), charges on the atoms (blue data), bond orders, $\text{BO}_{23}(\text{GL})$ and $\text{BO}_{23}(\text{GL}_n)$, of C(2)-C(3) bond , and molecular energies (hartree) for GL and GL_n geometries, obtained from our 2014 method at B3LYP/6-31G* level.

XX'C=CH– and –HC=CYY' (X, X', Y, Y' = F, Cl, Br, H), regardless of the number of substituents, and the localized geometry, obtained from our 2014 method, is denoted as GL or GL(2014). According to the second ways, as shown by Figure 12-7c to Figure 12-7-g, the π systems are localized on n groups, and the localized geometry, obtained from our 2014 method, is denoted as GL_n or GL_n(2014). The subscript “n” in the symbol GL_n is the number of the localized π systems, n = 3, 4, 5, 6. In the GL and GL_n geometry, all the π interactions, including the two-electron exchange integrals and their gradients, have been excluded from between n localized groups.

In the GL and GL₆ geometries of 1,1,4,4-tetra-chloro-butadiene, as shown by the data presented in Figure 12-8b, the charges on atoms are as follows:

$$\begin{aligned} \text{GL: } & -0.1993 (\text{C1}), -0.1164 (\text{C2}), 0.0583 (\text{Cl5}), 0.0649 (\text{Cl6}) \\ \text{GL}_6: & -0.2434 (\text{C1}), -0.0169 (\text{C2}), 0.0103 (\text{Cl5}), 0.0178 (\text{Cl6}). \end{aligned}$$

In the GL₆ geometry, accordingly, the charges (0.0103 and 0.0178) on Cl(5) and Cl(6) atoms are positive, and they are all less than those (0.0583 and 0.0649) in the GL geometry. On the contrary, the charges (-0.0169) on the C(2) atom in the GL₆ geometry is negative, and it is less negative than that (-0.1164) in the GL geometry. Corresponding to the charge change, $\Delta r_{23}(\text{GL}) = r_{23}(\text{GL}) - r_{23}(\text{GL}_n) = -0.030 \text{ \AA}$. For 1,1,4,4-tetrabromo-butadiene, the charges on the bromine atoms change from the negative values in GL₆ geometry to the positive values in the GL

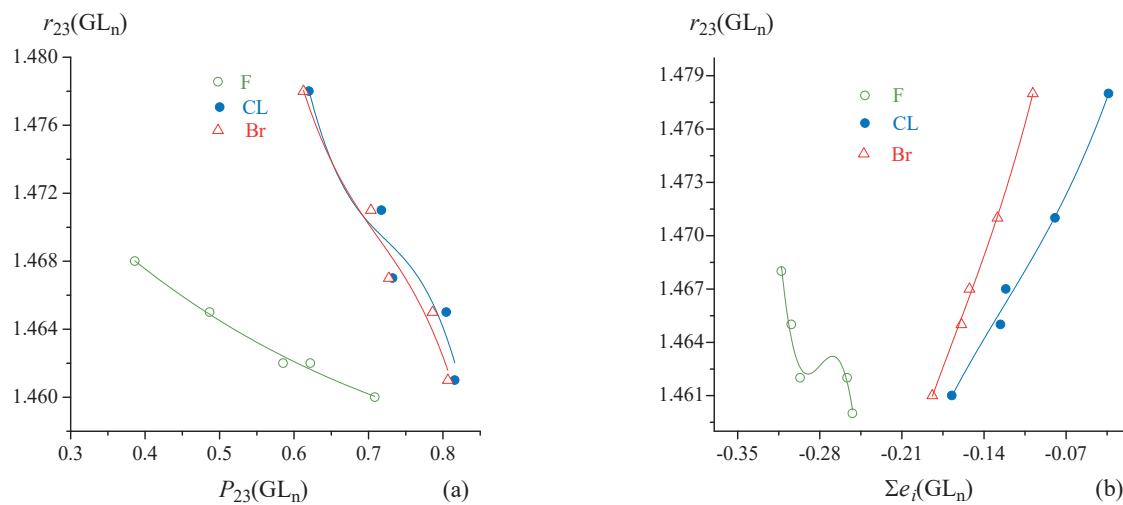


Figure 12-9. For halogen-substituted butadienes at B3LYP/6-31G* level: (a) The polynomial function relationship between $r_{23}(GL_n)$ (Å) and $P_{23}(GL_n)$. (b) Between $r_{23}(GL_n)$ (Å) and $\Sigma e_i(GL_n)$.

geometries, and the corresponding $\Delta r_{23}(GL) = -0.028$ Å (Figure 12-8c).

The fitted function $r_{23}(GL) = f(\Sigma e_i(GL))$ confirms the role of the adjacent conjugate effect in determining the distance of naked C-C single bond. However, the adjacent conjugation effect and the substituent effect are two different subjects. Before exploring the relationship between the adjacent conjugation and the naked CC single bond distance, it is necessary to predict which structural effect, the conjugation effect or inductive effect, determines the distance of the naked CC single bond in the different localized geometries such as GL and GL_n geometries.

Figure 12-9a and Table 12-15 show that, for three sub-groups, the polynomial functions, $r_{23}(GL_n) = f[P_{23}(GL_n)]$, are all monotonically decreasing, and the fitted function is reasonable. In the GL_n geometry, the inductive effect plays an important role in determining the distance $r_{23}(GL_n)$. The fluorine atom has +I effect, and it is so great that the number of fluorine atoms has a smaller effect on $r_{23}(GL_n)$ than the chlorine and bromine atoms have (Figure 12-9a). In addition, the distances (1.683 and 1.826 Å) of C-CL and C-Br bonds in the GL_6 geometries are much longer than that (1.266 Å) of F-C bond in the GL_6 geometry (Figure 12-8). For fluoro-substituted butadienes, therefore, the slope of the green line (Figure 12-9a) is much smaller than those for the red and blue lines.

As shown in Figure 12-9b, the distance $r_{23}(GL_n)$ can also be fitted as the polynomial functions of $\Sigma e_i(GL_n)$. The fitted function for chloro- and bromo-substituted butadienes are monotonically increasing, and the fitted line for fluoro-substituted butadienes (green line in Figure 12-9b) can be considered as a decreasing function. Except for Fluoro-substituted butadienes, therefore, the fitted functions, $r_{23}(GL_n) = f[\Sigma e_i(GL_n)]$, are also reasonable. In the GL_n geometry, there is no adjacent conjugation, and it should be attributed to the inductive effect that the electron charge sum, $\Sigma e_i(GL_n)$, changes as the number of halogen atoms increases. In terms of the influence on $\Sigma e_i(GL_n)$, the inductive effect of fluorine in the GL_n geometry is different from that of chlorine and bromine atoms (Table 12-15).

A comparison of Figures 12-9a and 12-6b shows that from the GL_n geometry to the GL geometry, the structural factor that determines the naked CC single bond distance changes from $P_{23}(GL_n)$ (Figure 12-9a) to $\Sigma e_i(GL)$ (Figure 12-6b) due to the adjacent conjugation.

12.4.2. Adjacent Conjugation and Transmission

There should be no direct relationship between the molecular energy difference $\Delta E(GL) = E(GL) - E(GL_n)$ and the single bond distance difference $\Delta r_{23}(GL) = r_{23}(GL) - r_{23}(GL_n)$, where $\Delta E(GL)$ is the molecular energy difference

Table 12-15. For GL_n ($n = 3, 4, 5, 6$) Geometries of 15 Halogen-Substituted Butadienes, Naked Single Bond Distances $r_{23}(GL_n)$ (\AA), Mulliken Atomic Overlap Population $P_{23}(GL_n)$, Charges $e_2(GL_n)$, $e_3(GL_n)$ and Their Sum $\Sigma e_i(GL_n)$, and Single Bond Distance Difference $\Delta r_{12}(GL) = r_{12}(GL) - r_{12}(GL_n)$ (\AA) and Molecular Energy Difference $\Delta E(GL) = E(GL) - E(GL_n)$ (kcal/mol), Obtained from Our 2014 Method at B3LYP/6-31G* Level.

Molecules	n^*	$r_{23}(GL_n)$	$\Delta r_{23}(GL)$	$\Delta E(GL)$	$P_{23}(GL_n)$	$e_2(GL_n)$	$e_3(GL_n)$	$\Sigma e_i(GL_n)$
FHCCH-CHCH ₂	3	1.460	-0.009	9.9335	0.70865	-0.13246	-0.11961	-0.2521
F ₂ CCH-CHCH ₂	4	1.462	-0.018	22.1511	0.62201	-0.12954	-0.12705	-0.2566
FHCCH-CHCHF	4	1.462	-0.018	19.4967	0.58533	-0.14835	-0.14836	-0.2967
F ₂ CCH-CHCHF	5	1.465	-0.028	30.8860	0.48675	-0.14578	-0.15845	-0.3042
F ₂ CCH-CHCF ₂	6	1.468	-0.037	41.1521	0.38615	-0.15635	-0.15635	-0.3127
CLHCH-CHCH ₂	3	1.461	-0.007	8.1137	0.81589	-0.04761	-0.11976	-0.1674
CL ₂ CCH-CHCH ₂	4	1.467	-0.014	18.9759	0.73244	0.01046	-0.13186	-0.1214
CLHCH-CHCHCl	4	1.465	-0.014	15.5936	0.80452	-0.06296	-0.06299	-0.1259
CL ₂ CH-CHCHCl	5	1.471	-0.021	25.6338	0.71749	-0.00581	-0.07360	-0.0794
CL ₂ CCH-CHCCL ₂	6	1.478	-0.030	34.8456	0.61998	-0.01687	-0.01687	-0.0337
BrHCCH-CHCH ₂	3	1.461	-0.006	7.0030	0.80654	-0.06763	-0.11639	-0.1840
Br ₂ CCH-CHCH ₂	4	1.467	-0.013	13.1150	0.72740	-0.02589	-0.12649	-0.1524
BrHCCH-CHCHBr	4	1.465	-0.013	17.0118	0.78605	-0.07961	-0.07958	-0.1592
Br ₂ CCH-CHCHBr	5	1.471	-0.020	22.5088	0.70331	-0.03986	-0.08859	-0.1285
Br ₂ CCH-CHCBr ₂	6	1.478	-0.028	30.9362	0.61265	-0.04916	-0.04916	-0.0983

between the GL geometry and GL_n geometry, and is an energy effect arising from the adjacent conjugation; $\Delta r_{23}(GL)$ is the difference, in the naked CC single bond, between the GL geometry and the GL_n geometry, and it measures the indirect influence of the adjacent conjugation on the distance of naked CC single bond.

Interestingly, as shown by the functional lines in Figure 12-10a, the distance difference $\Delta r_{23}(GL)$ (y) can be well fitted as the following polynomial function of the molecular energy difference $\Delta E(GL)$ (x):

$$y = -0.00379 - (3.41994E-4)x - (2.18733E-5)x^2 + (2.56138E-7)x^3 \quad (\text{F, cc} = 0.9730)$$

$$y = 0.00116 - 0.00123x + (2.98252E-5)x^2 - (5.84447E-7)x^3 \quad (\text{CL, cc} = 0.9568)$$

$$y = 0.00227 - 0.00146x + (4.12347E-5)x^2 - (8.31537E-7)x^3 \quad (\text{Br, cc} = 0.9211)$$

That is to say, the adjacent conjugation is an indirect driving force for distorting naked CC single bond. But Figure 12-10b and Figure 12-10c show that the adjacent conjugation can cause Mulliken atomic overlap population and charge change $\Delta P_{23}(GL)$ and $\Delta \Sigma e_i(GL)$. In particular, $\Delta r_{23}(GL)$ can be well fitted as the polynomial function of $\Delta P_{23}(GL)$ and the function of $\Delta \Sigma e_i(GL)$, and the corresponding correlation coefficients are as follows: $\Delta P_{23}(GL)$: 0.9965 (F), 0.9960 (CL), 0.9990 (Br); $\Delta \Sigma e_i(GL)$: 0.8934 (F), 0.7858 (CL), 0.8723 (Br). As the results of the adjacent

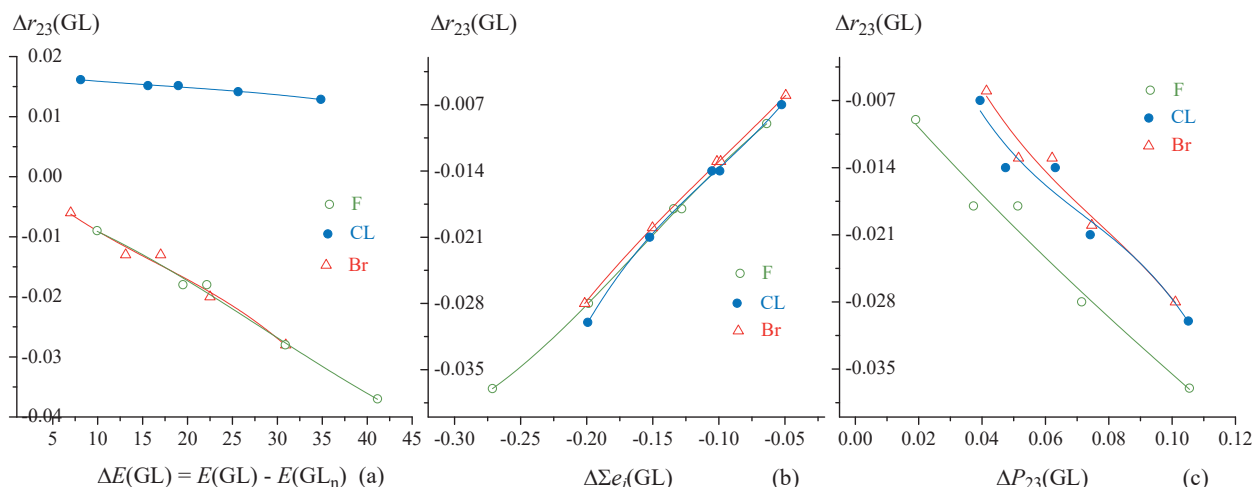


Figure 12-10. For halogen-substituted butadienes at B3LYP-631G* level: (a) $\Delta r_{23}(\text{GL})$ (Å) versus $\Delta E(\text{GL})$ (kcal/mol). (b) $\Delta r_{23}(\text{GL})$ (Å) versus $\Delta \Sigma e_i(\text{GL})$. (c) $\Delta r_{23}(\text{GL})$ (Å) versus $\Delta P_{23}(\text{GL})$.

conjugation, the differences $\Delta P_{23}(\text{GL}) = [P_{23}(\text{GL}) - P_{23}(\text{GL}_n)]$ and $\Delta \Sigma e_i(\text{GL}) = [\Sigma e_i(\text{GL}) - \Sigma e_i(\text{GL}_n)]$ are two direct driving forces for distorting naked CC single bond. To explain the mechanism of the adjacent conjugation affecting the distance of the naked single bonds in the GL geometry, the molecular energy decomposition will be performed at RHF/6-31G* level, based on the following three electronic states:

- The FL_n (full localized) and LD_n (locally delocalized) electronic states belonging to the same GL_n geometry. $E(\text{FL}_n)$ and $E(\text{LD}_n)$ are the molecular energies of these two electronic states.
- The LD_2 (locally delocalized) electronic state of the GL geometry, and $E(\text{LD}_2)$ is its molecular energy.

12.4.2.1. Halogen-substituted Butadienes

For 1,4-difluoro-butadiene, for example, the FL_4 (FL_n , $n=4$) state is constructed by the RHF/6-31G* single-point energy calculation, based on the B3LYP/6-31G* optimized GL_4 geometry, under the same conditional settings as those used to optimize GL_4 geometry. In the FL_4 state of GL_4 geometry, as shown by Figure 12-11a, four π systems are localized on the groups $\text{HC}(1)=\text{C}(2)\text{H}$ (group A), $\text{HC}(3)=\text{C}(4)\text{H}$ (group B), F(5) (group C), and F(10) (group D). The LD_4 electronic state of GL_4 geometry can be considered as the result of the adjacent conjugation, and it is constructed by the RHF/6-31G* single-point energy calculation, based on the B3LYP/6-31G* optimized GL_4 geometry, under the same conditional settings as those used to optimize the GL geometry. In the LD_4 state of GL_4 geometry, as shown by Figure 12-11b, two π systems are localized on two red groups $\text{FHC}(1)=\text{C}(2)\text{H}$ (group A) and $\text{HC}(3)=\text{C}(4)\text{HF}$ (group B). The LD_2 state of GL geometry is obtained from the RHF/6-31G* single-point calculation, based on the B3LYP/6-31G* optimized GL geometry, under the same conditional settings as those used to optimize the GL geometry. In the LD_2 state of the GL geometry (Figure 12-11c), two π systems are localized on the following two red groups: $\text{FHC}(1)=\text{C}(2)\text{H}-$ and $-\text{HC}(3)=\text{C}(4)\text{HF}$.

$\Delta E(\text{LD}_4) = E(\text{LD}_4) - E(\text{FL}_4)$ is the molecular energy difference between the LD_4 and FL_4 states of the GL_n geometry, and it is total energy effect arising from the adjacent conjugation between each CC double bond and its substituents. In the case of halogen-substituted butadienes, always $\Delta E(\text{LD}_4) > 0$ (destabilizing) (Table 12-16). $\Delta E^\pi_{XP}(\text{LD}_4) = E^\pi_{XP}(\text{LD}_4) - E^\pi_{XP}(\text{FL}_4)$ is a π component of $\Delta E(\text{LD}_4)$, and it is an π -energy effect directly arising from the p- π conjugation (adjacent conjugation), and $E^\pi_{XP}(\text{FL}_4) = 0$. $\Sigma \Delta E^\pi_{XP}(\text{LD}_4)$ is a sum of $\Delta E^\pi_{XP}(\text{LD}_4)$, where X = C, D, E, F (substituents); P = A, B (double bonds) (Figure 12-8 and Figure 12-11a). $\Delta E^\sigma_{XP}(\text{LD}_4) = E^\sigma_{XP}(\text{LD}_4) -$

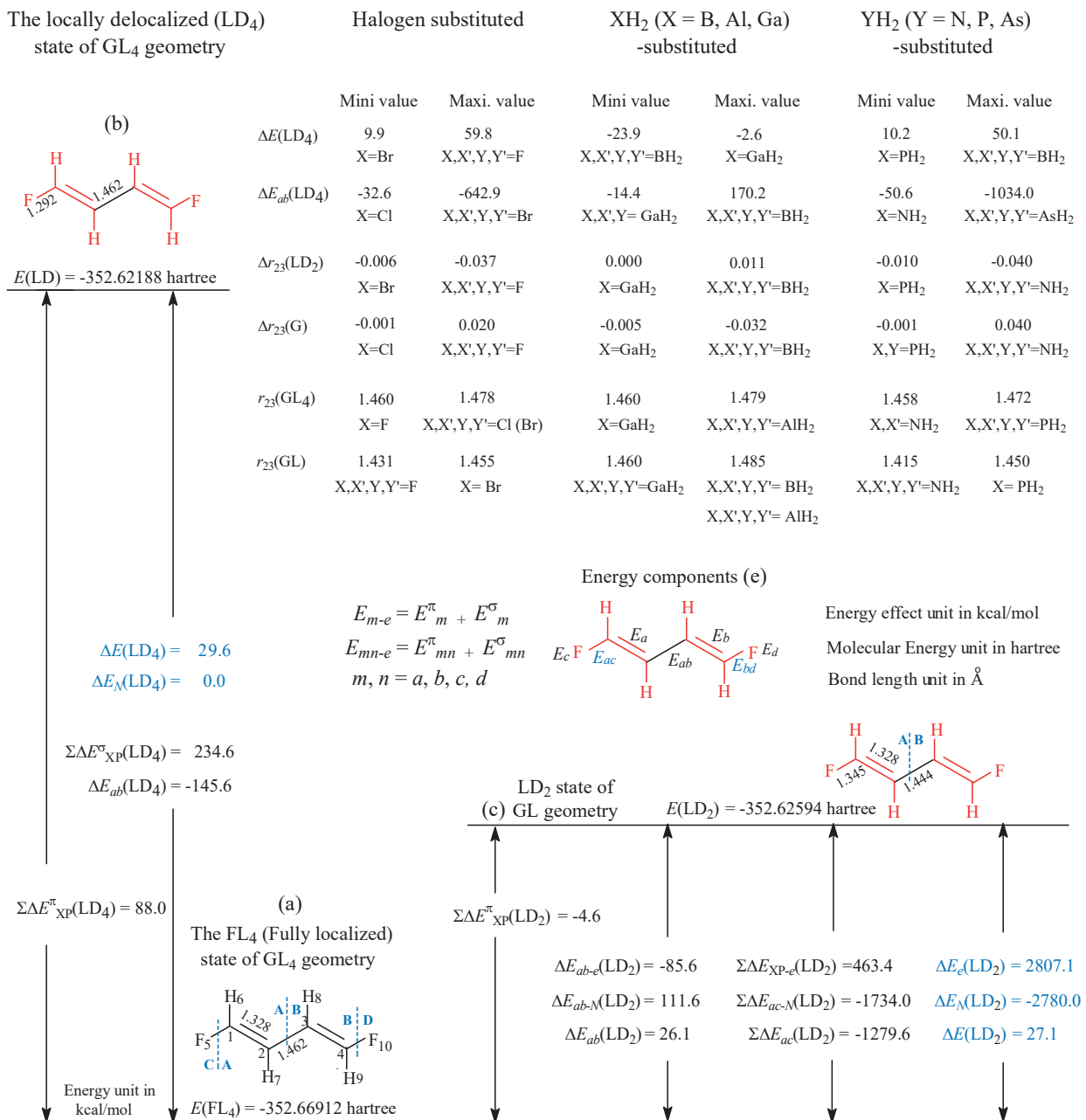


Figure 12-11. The energy decomposition at RHF/6-31G* level, the electronic states, FL₄ and LD₄, of GL₄ geometry, and the LD₂ state of GL geometry, and various energy differences between them. The single black lines between two heavy atoms such as C and F, including the black line between two red double bonds, means that the all the π -interactions have been excluded from between two groups.

$E^{\sigma}_{\text{XP}}(\text{FL}_4)$ is the σ components of $\Delta E_{\text{XP}}(\text{LD}_4)$ (or $\Delta E(\text{LD}_4)$, or $\Delta E_{ab}(\text{LD}_4)$), and it measures the influence of the p- π adjacent conjugation on the σ interaction energy component, E^{σ}_{XP} , between the C=C group (P) and its substituent (X). $E^{\sigma}_{\text{XP}}(\text{FL}_4) \neq 0$, and $\Sigma \Delta E^{\sigma}_{\text{XP}}(\text{LD}_4)$ is s sum of $\Delta E^{\sigma}_{\text{XP}}(\text{LD}_4)$. For most of halogen-substituted butadienes, as shown by Table 12-16, $\Sigma \Delta E^{\sigma}_{\text{XP}}(\text{LD}_4) > 0$ (destabilizing), and always $\Sigma \Delta E^{\sigma}_{\text{XP}}(\text{LD}_4) > 0$.

Table 12-16. For Halogen-Substituted Butadienes, Energy Difference $\Delta E(LD_n)$ and Its Various Components (kcal/mol) Are Obtained from the Single-Point Energy Calculation at RHF/6-31G* Level. The Bond Lengths and Bond Length differences (\AA) Are Obtained from Geometry Optimization at B3LYP/6-31G* Level, all the Calculations Are Performed by Using Our 2014 Method.

	$\Delta E(LD_n)$	$\Sigma \Delta E^{\pi}_{XP}(LD_n)$	$\Sigma \Delta E^{\sigma}_{XP}(LD_n)$	$\Delta E_{ab}(LD_n)$	$\Delta E_{ab}(LD_2)$	$\Delta r_{15}(\text{GL})$	$\Delta r_{23}(\text{GL})$
FHCCHCHCH ₂	15.0	35.8	120.1	-50.6	24.4	0.054	-0.009
F ₂ CCHCHCH ₂	31.4	-141.1	277.2	-164.9	42.8	0.055	-0.018
FHCCHCHCHF	29.6	88.0	234.6	-145.6	26.1	0.053	-0.018
F ₂ CCHCHCHF	45.3	-80.8	401.6	-297.8	18.3	0.054	-0.018
F ₂ CCHCHCF ₂	59.8	-279.0	618.0	-477.6	-6.1	0.055	-0.037
CLHCHCHCH ₂	10.9	257.6	83.0	-32.6	48.5	0.050	-0.007
CL ₂ CCHCHCH ₂	25.0	709.1	233.5	-154.4	10.3	0.061	-0.014
CLHCHCHCHCL	21.0	554.4	144.4	-82.3	92.1	0.048	-0.014
CL ₂ CHCHCHCL	34.1	1046.2	269.2	-241.8	16.9	0.060	-0.021
CL ₂ CCHCHCCL ₂	46.2	1569.4	339.8	-453.3	-123.1	0.057	-0.030
BrHCCHCHCH ₂	9.9	200.5	83.8	-43.8	29.6	0.060	-0.006
Br ₂ CCHCHCH ₂	23.2	624.4	257.7	-191.6	-54.0	0.074	-0.013
BrHCHCHCHBr	18.9	447.2	164.4	-127.9	9.6	0.062	-0.013
Br ₂ CCHCHCHBr	31.4	920.8	348.0	-343.6	-156.7	0.071	-0.020
Br ₂ CCHCHCBr ₂	43.1	1432.0	526.0	-642.9	-417.0	0.069	-0.028

The energy effect components of $\Delta E(LD_4)$ also include the $\Delta E_{ab}(LD_4)$ (Figure 12-11e). $\Delta E_{ab}(LD_4) = E_{ab}(LD_4) - \Delta E_{ab}(\text{FL}_4)$, and it measures the influence of the adjacent conjugation on the interaction energy between two CC double bonds. Always $\Delta E_{ab}(LD_4) < 0$, and it measures the influence of the adjacent conjugation on the interaction energy component, E_{ab} , between two CC double bonds. In the case of 1,4-difluoro-butadiene, for example, $\Delta E_{ab}(LD_4) = E_{ab}(LD_4) - E_{ab}(\text{FL}_4) = -145.6$ kcal/mol. In the moment of the adjacent interaction, and when the change in the structure of GL₄ geometry has not happened, a force acts on the naked CC single bond due to the adjacent conjugation, and it tends to shorten the naked C(2)–C(3) single bond.

With shortening of naked CC single bond, as shown by Figure 12-11c, always $\Delta E_{ab-e}(LD_2) = E_{ab-e}(LD_2) - E_{ab-e}(\text{FL}_4) < 0$, and $\Delta E_{ab-N}(LD_2) > 0$, and should be $d[\Delta E_{ab-e}(LD_2)]/dr_{23} > 0$ and $d\Delta E_{ab-N}(LD_2)/dr_{23} > 0$ before the GL geometry is reached. At last, the naked CC single bond is shortened from 1.462 \AA in GL₄ geometry to 1.444 \AA in GL geometry although two C=C double bonds are kept to be unconjugated. In the meantime, the C(1)-F(5) bond is lengthened from 1.292 \AA to 1.345 \AA .

Figure 12-12a shows that, for each of three types of halogen-substituted butadienes, $\Delta E_{ab}(LD_n)$ (y) can be well fitted as the following polynomial function of $\Sigma \Delta E^{\sigma}_{XP}(LD_n)$ (x):

$$\begin{aligned} y &= -7.49907 - 0.11872x - 0.00233x^2 + (2.08495E-6)x^3 \quad (\text{F, cc} = 0.9936). \\ y &= 81.27851 - 2.10379x + 0.01091x^2 - (2.75595E-5)x^3 \quad (\text{CL, cc} = 0.9908). \\ y &= -5.31772 - 0.37524x - 0.0017x^2 + (2.07431E-7)x^3 \quad (\text{Br, cc} = 0.9860) \end{aligned}$$

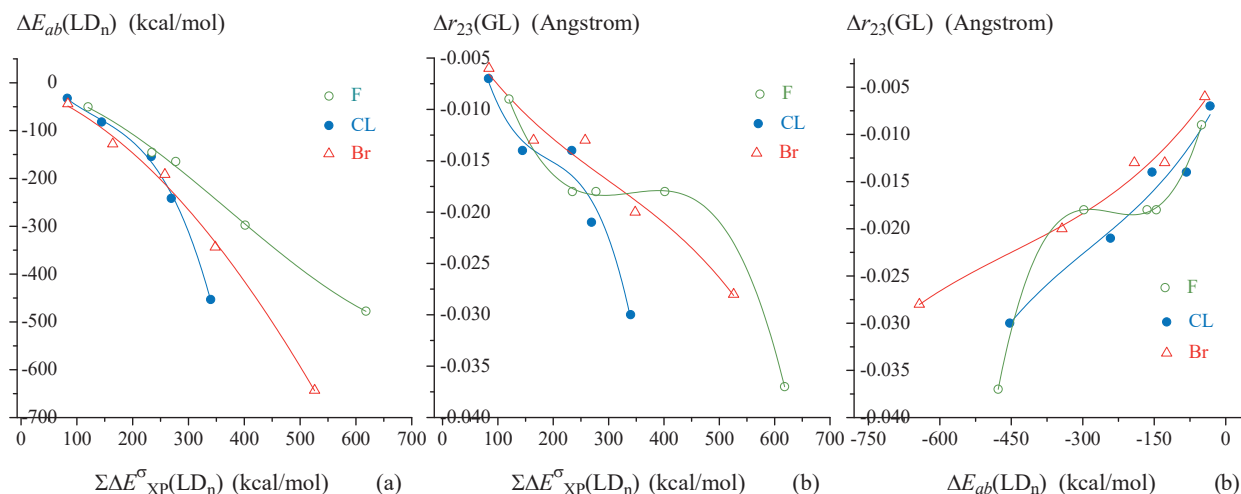


Figure 12-12. For halogen-substituted butadienes at RHF/6-31G* level: polynomial fittings: (a) $\Delta E_{ab}(LD_n)$ versus $\Sigma \Delta E_{XP}^\sigma(LD_n)$; (b) $\Delta r_{23}(GL)$ versus $\Sigma \Delta E_{XP}^\sigma(LD_n)$; (c) $\Delta r_{23}(GL)$ versus $\Delta E_{ab}(LD_n)$.

It is especially interesting that $\Delta r_{23}(GL) = r_{23}(GL) - r_{23}(GL_n)$ (y) can also be fitted as the polynomial function of $\Sigma \Delta E_{XP}^\sigma(LD_n)$ (Figure 12-12b) and $\Delta E_{ab}(LD_n)$ (Figure 12-12c). The functional lines in Figure 12-12c and the data listed in Table 12-16 show a fact: the greater absolute value of $\Delta E_{ab}(LD_n)$ corresponds generally to the greater absolute difference $\Delta r_{23}(GL)$. For 5 chloro-substituted butadienes, for example, the absolute size order of $\Delta E_{ab}(LD_n)$ (kcal/mol) and $\Delta r_{23}(GL)$ (\AA) are as follows:

$$\Delta E_{ab}(LD_n): -32.6 \text{ (1-chloro)} < -82.3 \text{ (1,4-chloro)} < -154.4 \text{ (1,1-chloro)} < -241.8 \text{ (1,1,4-chloro)} < -453.3 \text{ (1,1,4,4-tetra-chloro)}$$

$$\Delta r_{23}(GL): -0.007 < -0.014 = -0.014 < -0.021 < -0.030.$$

The fitted functions, $\Delta r_{23}(GL) = f[\Sigma \Delta E_{XP}^\sigma(LD_n)]$ and $\Delta r_{23}(GL) = f[\Delta E_{ab}(LD_n)]$, suggest an interesting phenomenon that the adjacent conjugation effect can be transmitted to the naked single bond through the σ bond, and such conjugation, taking place within the X-C=C group, may have a significant effect on the distance of the naked single bond adjacent to the conjugated system(s) X-C=C-. In the case of tetra-fluoro-substituted butadiene, $\Delta r_{23}(GL) = r_{23}(GL) - r_{23}(GL_6)$ is the largest, up to -0.037 \AA .

In the classical structure theory of organic chemistry, this type of conjugation effect (adjacent conjugation effect), including its transmission through the σ bonds, cannot be found and understand.

12.4.2.2. Inductive Effect and Conjugation Transmission

Table 12-16 and Figure 12-12 also imply the influence of the electronegativity of the halogen atom on the conjugation effect Transmission. The electronegativity (4.0) of fluorine is greater than that (3.0) of chlorine. Correspondingly, $\Delta r_{23}(GL)$ for fluoro-substituted butadiene is generally more negative than the corresponding $\Delta r_{23}(GL)$ for chloro-substituted butadiene. For Fluoro- and chloro-disubstituted butadienes, for example, the absolute size order of $\Delta r_{23}(GL)$ (\AA) are as follows:

$$-0.009 \text{ (1-fluoro)} < -0.018 \text{ (1,1,-difluoro)} = -0.018 \text{ (1,4-difluoro)} = -0.018 \text{ (1,1,4-trifluoro)} < -0.037 \text{ \AA (1,1,4,4-tetrafluoro)}$$

Table 12-17. For XH_2 -Substituted Butadienes ($\text{X} = \text{B}, \text{Al}, \text{Ga}$), Various Energy Differences (kcal/mol) Arising from π -Interactions between CC Double Bonds and Their Substituents Are Obtained from Single-Point Energy Calculation at RHF/6-32G* Level. Naked Single Bond Distances r_{23} (Å) and Their Differences $\Delta r_{23}(\text{GL}) = r_{23}(\text{GL}) - r_{23}(\text{GL}_n)$ (Å) Are Obtained from Geometry Optimization Using Our 2014 Method.

	ΔE (LD _n)	$\Sigma \Delta E_{\text{XP}}^{\pi}$ (LD _n)	$\Sigma \Delta E_{\text{XP}}^{\sigma}$ (LD _n)	ΔE_{ab} (LD _n)	Δr_{23} (GL)	r_{23} (GL _n)	P_{23} (GL _n)	r_{23} (GL)	P_{23} (GL)
(BH ₂)CCH-CHCH ₂	-6.4	-374.2	-31.9	6.8	0.003	1.461	0.799	1.464	0.782
(BH ₂) ₂ CCH-CHCH ₂	-12.3	-823.6	-25.2	64.3	0.004	1.466	0.731	1.470	0.699
(BH ₂)HCCHCHCH(BH ₂)	-12.6	-781.6	-52.8	17.1	0.006	1.465	0.779	1.471	0.745
(BH ₂) ₂ CCH-CHCH(BH ₂)	-18.3	-1258.6	-38.5	85.2	0.009	1.469	0.708	1.478	0.655
(BH ₂) ₂ CCH-CHC(BH ₂) ₂	-23.9	-1756.5	-12.2	170.2	0.011	1.474	0.638	1.485	0.562
(ALH ₂)CCH-CHCH ₂	-3.4	-359.5	4.8	3.3	0.001	1.461	0.795	1.462	0.787
(ALH ₂) ₂ CCH-CHCH ₂	-6.5	-879.8	18.5	44.4	0.002	1.468	0.791	1.470	0.778
(ALH ₂)HCCHCHCH(ALH ₂)	-6.8	-799.2	13.0	11.7	0.002	1.464	0.772	1.466	0.754
(ALH ₂) ₂ CCH-CHCH(ALH ₂)	-9.9	-1393.5	26.3	63.7	0.004	1.471	0.769	1.475	0.746
(ALH ₂) ₂ CCH-CHC(ALH ₂) ₂	-12.8	-2054.1	36.4	130.7	0.006	1.479	0.765	1.485	0.736
(GAH ₂)CCH-CHCH ₂	-2.6	-579.7	-0.1	-8.6	0.000	1.460	0.778	1.460	0.775
(GAH ₂) ₂ CCH-CHCH ₂	-4.3	-1591.9	-43.7	24.3	0.000	1.467	0.717	1.467	0.710
(GAH ₂)HCCHCHCH(GAH ₂)	-5.2	-1380.8	-2.0	-14.4	0.001	1.463	0.734	1.464	0.725
(GAH ₂) ₂ CCH-CHCH(GAH ₂)	-6.9	-2610.3	-61.1	39.8	0.001	1.469	0.672	1.470	0.659
(GAH ₂) ₂ CCH-CHC(GAH ₂) ₂	-8.4	-3986.9	-137.8	121.8	0.002	1.474	0.609	1.476	0.591

-0.007 (1-chloro) < 1,1-dichloro) -0.014 = -0.014 (1,4-dichloro) < -0.021 (1,1,4-trichloro) < -0.030 Å (1,1,4,4-tetrachloro).

For tetra-halogen substituted butadienens, the absolute size order of $\Delta r_{23}(\text{GL})$ (Å) is as follow:

-0.037 (tetrafluoro) > -0.030 (tetrachloro) > -0.028 (tetrabromo)

Butadienes substituted by the XH_2 group(s) (X atom belongs to the boron or nitrogen family) will further display that the type of substituents can greatly affect the transmission of the adjacent conjugation effect.

12.4.2.3. XH_2 -Substituted Butadienes ($\text{X} = \text{B}, \text{AL}, \text{Ga}$)

For XH_2 -substituted butadienes ($\text{X} = \text{B}, \text{AL}, \text{Ga}$), as shown by the energy differences listed in Table 12-17, always $\Delta E(\text{LD}_n) < 0$, $\Sigma \Delta E_{\text{XP}}^{\pi}(\text{LD}_n) < 0$ (stabilizing), and $|\Sigma \Delta E_{\text{XP}}^{\pi}(\text{LD}_n)| > |\Sigma \Delta E_{\text{XP}}^{\sigma}(\text{LD}_n)|$. Due to that the boron

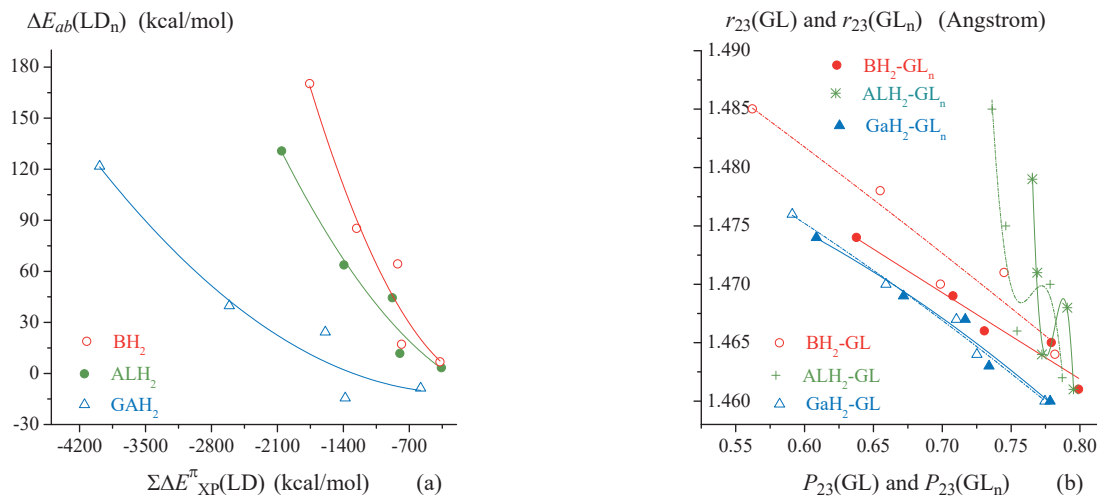


Figure 12-13. For XH_2 -substituted butadienes ($\text{X} = \text{B}, \text{AL}, \text{Ga}$), polynomial fitting of the following two variables: (a) $\Delta E_{ab}(\text{LD}_n)$ and $\Sigma \Delta E^{\pi}_{\text{XP}}(\text{LD}_n)$. (b) $r_{23}(\text{GL})$ and $P_{23}(\text{GL})$ (dashed lines), and $r_{23}(\text{GL}_n)$ and $P_{23}(\text{GL}_n)$ (solid lines). The energy components $\Delta E_{ab}(\text{LD}_n)$ and $\Sigma \Delta E^{\pi}_{\text{XP}}(\text{LD}_n)$ are calculated at RHF/6-31G* level, and the quantities such as r_{23} and P_{23} are obtained from the geometry optimization that is performed using our 2014 method at B3LYP/6-31G* level.

family element, such as B, AL and Ga, is electron-deficient, these energy differences all differ, in the size and sign, from the corresponding the energy differences for halogen-substituted butadienes. In the meantime, becomes $\Delta E_{ab}(\text{LD}_n) > 0$. As a result of the adjacent conjugation, a force acts on the naked CC single bond, and makes $\Delta r_{23}(\text{GL}) > 0$.

Figure 12-13a indicates that, for XH_2 -substituted butadienes ($\text{X} = \text{B}, \text{AL}, \text{Ga}$), $\Delta E_{ab}(\text{LD}_n)$ (y) can be fitted as the polynomial function of $\Sigma \Delta E^{\pi}_{\text{XP}}(\text{LD}_n)$ (x), and their correlation coefficients are as follows: 0.8858 (BH_2), 0.9231 (ALH_2), 0.9037 (GaH_2). May be due to that $\Delta E_{ab}(\text{LD}_n)$ (for XH_2 -substituted) $< |\Delta E_{ab}(\text{LD}_n)|$ (for halogen-substituted), and owing to the role of the nuclear repulsion, $\Delta E_{ab-N}(\text{LD}_2)$, between two double bonds, the differences $\Delta r_{23}(\text{GL})$ are mostly less than 0.006 Å, and they are much smaller in absolute value than those for the corresponding halogen-substituted butadienes. For tetra-substituted butadienes, for example, $\Delta r_{23}(\text{GL})$: $|-0.037| \text{ \AA}$ (tetrafluoro-) $> 0.011 \text{ \AA}$ (tetra- BH_2).

However, as shown by the dashed lines in Figure 12-13b, for each sub-group of XH_2 -substituted butadienes ($\text{X} = \text{B}, \text{AL}, \text{Ga}$), $r_{23}(\text{GL})$ can be fitted as the polynomial function of $P_{23}(\text{GL})$, and the fitted function can be regarded as monotonically decreasing. Accordingly, the type and number of substituents have a significant effect on the distance of the naked CC single bond in the GL geometry. In the GL geometries of five BH_2 -substituted butadienes, for example, the longest and shortest distances (Å) are 1.464 (1-mono- BH_2 -) and 1.485 (1,1,4,4-trtra- BH_2), the range of a set of $r_{23}(\text{GL})$ is 0.021 Å, which should be attributed to the inductive effect of the substituent groups.

In particular, for a specific sub-group of XH_2 -substituted butadienes, as shown by Figure 12-13b, $dr_{23}(\text{GL}_n)/dP_{23}(\text{GL}_n)$ (solid line) $\approx dr_{23}(\text{GL})/dP_{23}(\text{GL})$ (dashed line). In the case of GaH_2 -substituted butadienes, for example, two blue lines are almost overlap each other. These facts confirm that the inductive effect plays a predominate role in determining the distance of naked single bond in the GL and GL_n geometries.

For the 1,3-butadiene substituted by the electron-deficient group(s) XH_2 ($\text{X} = \text{B}, \text{Al}, \text{Ga}$), the adjacent conjugation has a slight influence on the naked single bond in the GL geometry. The type and number of the substituent groups XH_2 can affect the distance of naked single bond through inductive effect.

12.4.2.4. XH_2 -Substituted Butadienes ($\text{X} = \text{N, P, As}$)

Table 12-18. For XH₂-Substituted Butadienes (X = N, P, As), Energy Difference $\Delta E(LD_n)$ Arising from Adjacent Conjugation, and Its Components (kcal/mol), Obtained from the Energy Decomposition at RHF/6-31G* Level, and Naked Single Bond Distances, $r_{23}(GL)$ and $r_{23}(GL_n)$, and Their Differences $\Delta r_{23}(GL)$ (\AA) Are Calculated by the Geometry Optimization That Is Performed Using Our 2014 Method at B3LYP/6-31G* Level.

	ΔE (LD _n)	ΔE_{ab} (LD _n)	Δr_{23} (GL)	r_{23} (GL _n)	P_{23} (GL _n)	r_{23} (GL)	P_{23} (GL)	$\Sigma e_i(GL)$
(NH ₂)CCHCHCH ₂	11.4	-50.6	-0.015	1.459	0.7811	1.444	0.8106	-0.3135
(NH ₂) ₂ CCH-CHCH ₂	23.2	-189.1	-0.026	1.458	0.7415	1.432	0.7857	-0.3887
(NH ₂)HCCHCHCH(NH ₂)	22.9	-144.4	-0.026	1.460	0.7385	1.434	0.8016	-0.4091
(NH ₂) ₂ CCHCHCH(NH ₂)	23.2	-327.5	-0.036	1.460	0.6969	1.424	0.7769	-0.4797
(NH ₂) ₂ CCHCHC(NH ₂) ₂	49.6	-541.2	-0.044	1.459	0.6526	1.415	0.7478	-0.5487
(PH ₂)CCHCHCH ₂	10.2	-70.8	-0.010	1.460	0.8053	1.450	0.8366	-0.2674
(PH ₂) ₂ CCHCHCH ₂	24.8	-230.8	-0.019	1.464	0.7709	1.445	0.8172	-0.3028
(PH ₂)HCCHCHCH(PH ₂)	19.4	-175.2	-0.020	1.463	0.7865	1.443	0.8475	-0.3188
(PH ₂) ₂ CCHCHCH(PH ₂)	33.4	-377.0	-0.029	1.467	0.7479	1.438	0.8241	-0.3533
(PH ₂) ₂ CCHCHC(PH ₂) ₂	47.3	-630.1	-0.038	1.472	0.7071	1.434	0.8001	-0.3875
(ASH ₂)CCHCHCH ₂	10.6	-82.9	-0.010	1.459	0.7932	1.449	0.8227	-0.2714
(ASH ₂) ₂ CCHCHCH ₂	26.4	-312.1	-0.019	1.464	0.7252	1.445	0.7821	-0.3247
(ASH ₂)HCCHCHCH(ASH ₂)	20.0	-243.6	-0.020	1.462	0.7587	1.442	0.8181	-0.3285
(ASH ₂) ₂ CCHCHCH(ASH ₂)	35.2	-578.3	-0.029	1.466	0.6810	1.437	0.7704	-0.3812
(ASH ₂) ₂ CCHCHC(ASH ₂) ₂	50.1	-1034.0	-0.028	1.471	0.5960	1.433	0.7176	-0.4342

Due to that the halogen group X (X = F, Cl, Br) and the XH₂ (X = N, P, As) group are all the electron-releasing group, as shown by the data in Table 12-18, always $\Delta E(LD_n) > 0$, $\Delta E_{ab}(LD_n) < 0$ and $\Delta r_{23}(GL) < 0$. For NH₂-substituted butadienes, for example, the largest and smallest negative values of $\Delta r_{23}(GL)$ are -0.015 and -0.044 \AA , and the range of a set of $\Delta r_{23}(GL)$ values is -0.029 \AA . Similar to halogen-substituted butadienes, $\Delta r_{23}(GL)$ (y) can be well fitted as the following second order polynomial function of $\Delta E_{ab}(LD_n)$ (x) (cc are 0.9504, 0.9126 and 0.8745, respectively (Figure 12-14a):

$$\begin{aligned}y &= -0.00922 + (1.2943E-4)x + (1.92348E-7)x^2 + (1.33149E-10)x^3 \quad (\text{NH}_2) \\y &= -0.00437 + (9.13594E-5)x + (9.10606E-8)x^2 + (4.90097E-11)x^3 \quad (\text{PH}_2) \\y &= -0.00579 + (5.67188E-5)x + (2.37764E-8)x^2 - (9.94756E-12)x^3 \quad (\text{AsH}_2)\end{aligned}$$

In the case of XH₂-substituted Butadienes (X = N, P, As), the adjacent conjugation produces a force acting on the naked single bond adjacent to the C=C-XH₂ group(s), and it can be regarded as a driving force for shortening the naked single bond in the GL geometry. But this is not certain that the adjacent conjugation determines the distance

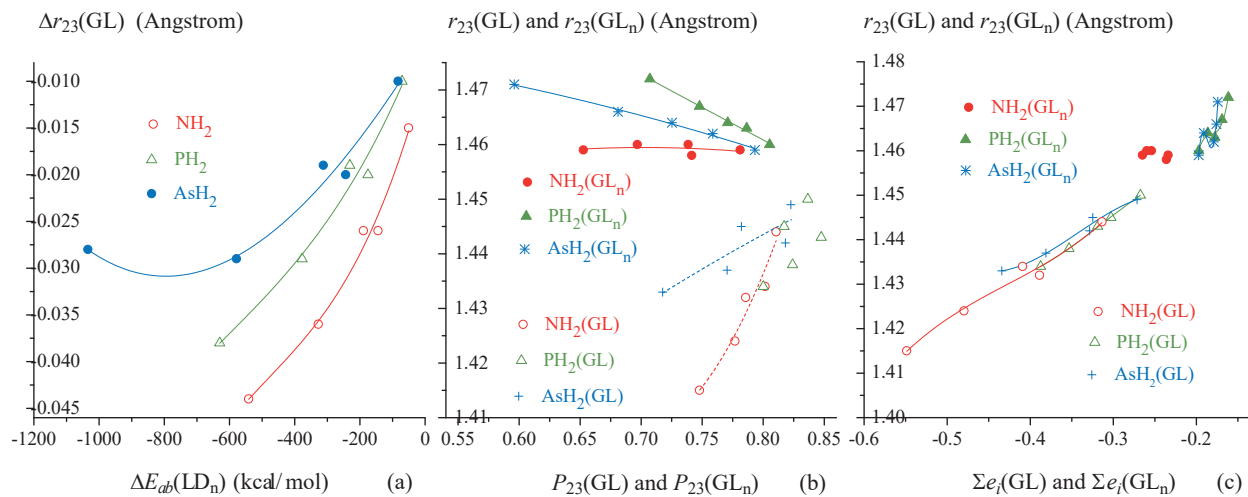


Figure 12-14. For XH_2 -substituted butadienes ($\text{X} = \text{N}, \text{P}, \text{As}$), polynomial fitting of the following two variables: (a) $r_{23}(\text{GL})$ and $\Delta E_{ab}(\text{LD}_n)$. (b) $\Delta r_{23}(\text{GL})$ and P_{23} . (c) r_{23} and Σe_i . The energy effects $\Delta E_{ab}(\text{LD}_n)$ are calculated at RHF/6-31G* level, and the quantities such as Δr_{23} , P_{23} and Σe_i are obtained from the geometry optimization by our 2014 method at B3LYP/6-31G*.

$r_{23}(\text{GL})$ of the naked single bond in the GL geometry.

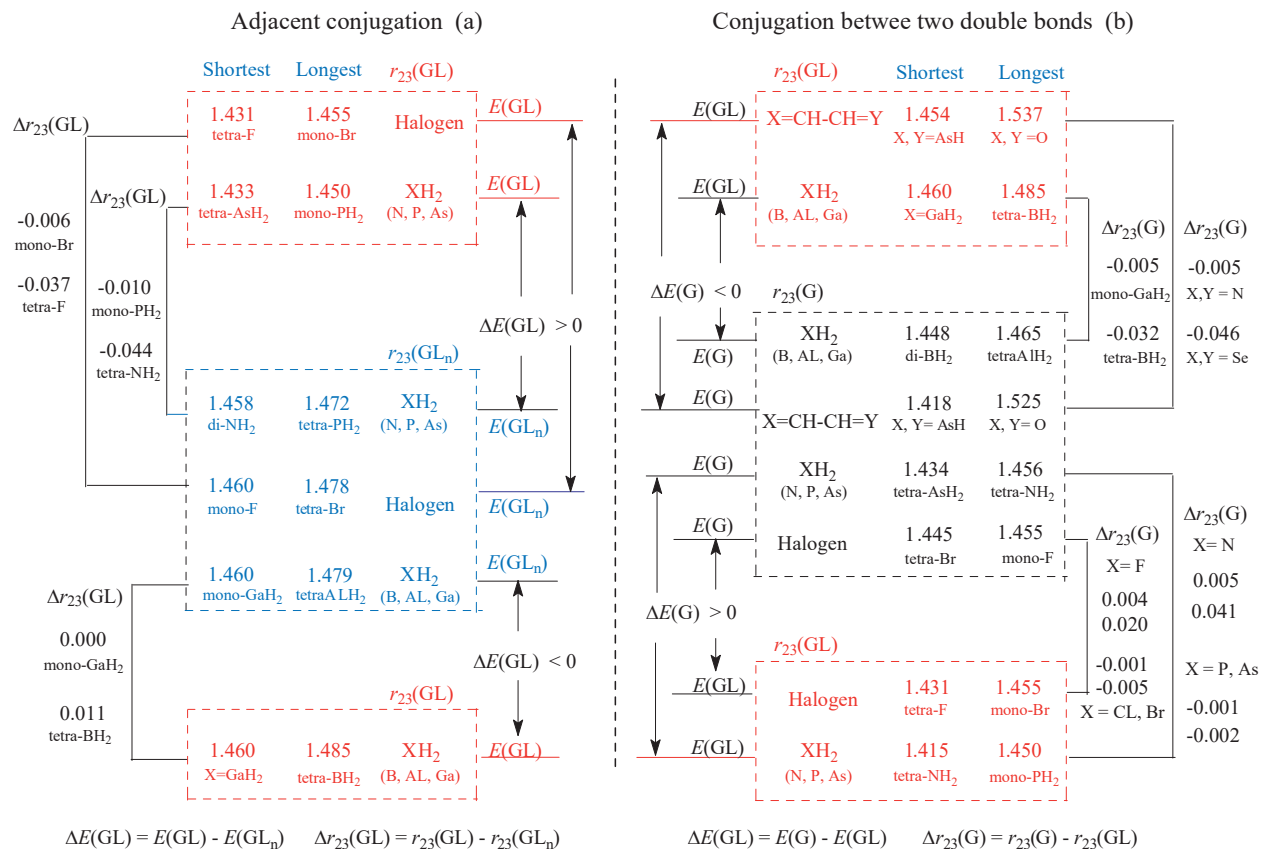
According to the solid lines in Figure 12-14b, the CC single bond distance $r_{23}(\text{GL}_n)$ in the GL_n geometry can be fitted as a polynomial function of $P_{23}(\text{GL}_n)$, and the fitted function is the monotonically decreasing function. In the GL_n geometry, therefore, the groups XH_2 ($\text{N}, \text{P}, \text{As}$) can affect the CC single bond distance through inductive effect. However, as shown by Figure 12-14c, the CC single bond distance $r_{23}(\text{GL})$ in the GL geometry can be fitted as the polynomial function of $\Sigma e_i(\text{GL})$, and it increases as $\Sigma e_i(\text{GL})$ becomes less negative. As a result of adjacent conjugation, the charge sum $\Sigma e_i(\text{GL})$ plays an important role in determining the distance of CC single bond in the GL geometry.

When and only when the substituent is electron-releasing, the adjacent conjugation effect can be transmitted to the naked CC single bond between two CC double bonds, and it has a great effect on the distance of the naked CC single bond.

12.5. CONCLUSIONS

Our 2011 method is improved by additionally deleting the exchange gradients. The improved version is called “our 2014 method”. In the case of acyclic polyene, the additivity of the energy effects $\Delta E^{\text{Am}}(2014)$ calculated by our 2014 method has been further improved. For 1,3,5,7,9,11,13-tetradecaheptaene at RHF/6-31G* level, for example, $R_t(2014) (0.05) < R_t(2011) (0.08) < R_t(2007) (0.39)$. Afterwards, the superiority of our 2014 method to our 2011 is further confirmed by the following calculation results at various theoretical levels using different basis sets: the extra stabilizing energy of benzene; vertical delocalization energy ΔE^{A} of cyclobutadiene; the CC single bond of butadiene; the extra stabilization energy of polycyclic benzenoid hydrocarbons.

For cyclobutadiene, $\Delta E^{\text{A}}(2014)$ and $\Delta E^{\text{A}}(2011)$ are calculated, using our 2014 method and our 2011 method, at (RHF, MP2, LYP, B3LYP, BLYP and XPBE96)/(6-31G*, 6-311G**, 6-311G(2d,2p) and 6-311G(2df,p)) levels, the range (16.4 kcal/mol) of the 24 values of $\Delta E^{\text{A}}(2014)$ is smaller than that (19.3 kcal/mol) of the 24 values of $\Delta E^{\text{A}}(2011)$. The average (57.3 kcal/mol) of the $\Delta E^{\text{A}}(2014)$ values and the average (51.9 kcal/mol) of the $\Delta E^{\text{A}}(2011)$



Scheme 12-2

values are both close to the experimental value (55 kcal/mol). At B3LYP/6-311G** level, the value of 54.9 kcal/mol (from our 2014 method) is equal to the experimental value.

For the ESE of benzene, the B3LYP/6-31G* value is -36.4 (2014) and -36.3 (2011) kcal/mol, and are both equal to the experimental value of -36 kcal/mol. For the thirty-six values calculated at six theoretical levels using six basis sets, the range (kcal/mol) of the ESE values decreases from -5.4 (from our 2011 method) to -3.0 (from 2014 method). The average (kcal/mol) of the thirty-six values is -35.0 (from our 2011 method) and -37.0 (from our 2014 method), respectively. Therefore, the theoretical level and the base set size have a slight influence on the ESE(2014) value.

For the naked CC single bond in the GL geometry of butadiene, the distance $r_{23}(GL)$ are calculated at 12 theoretical levels using four basis sets, the range of a set of forty-eight values is 0.067 (2014) Å and 0.117 (2011) Å, respectively. In the absence of experimental value, the distance obtained from our 2014 method can be considered to be more reasonable than from the 2011 method. At B3LYP/6-31G* level, the conjugation energy $\Delta E^A(2014) = 1.1$ kcal/mol (destabilizing), and it is almost equal to the difference (1.9 kcal/ml) in the hydrogenation heat between the two trans-2-butene and the trans-1,3-butadiene, and the corresponding $\Delta r_{23}(2014) = 0.006$ Å, which is contrary to the classic viewpoint..

For 66 butadiene derivatives at B3LYP/6-31G* level, the longest (1.525 Å) and shortest (1.418 Å) distances $r_{23}(G)$ of the CC single bond are found in the ground state geometries of the molecules O=C-C=O and HAs=C-C=AsH, and the range of a set of $r_{23}(G)$ is large, up to 0.107 Å. Particularly, $\Delta r_{23}(G)$ can be well fitted as the polynomial function of the molecular energy difference (conjugation energy) $\Delta E(G)$. The maximum positive

value and maximum negative value of $\Delta r_{23}(G)$ are 0.040 Å ($(\text{NH}_2)_2\text{C}=\text{CH}-\text{CH}=\text{C}(\text{NH}_2)_2$) and -0.046 Å ($\text{HAs}=\text{C}-\text{C}=\text{AsH}$), that is, the range of a set of the $\Delta r_{23}(G)$ values is 0.086 Å. The bond distance difference, $\Delta r_{23}(G) = r_{23}(G) - r_{23}(\text{GL})$, between the ground state geometry and the GL geometry is indeed caused by the conjugation, $\Delta E(G) = E(G) - E(\text{GL})$, between two localized double bonds (groups) in the GL geometry. Certainly, this change $\Delta r_{23}(G)$ in the distance of sp^2-sp^2 single bond is not the result of referring to the distance of the sp^3-sp^3 single bond in ethane.

The size and sign of the differences $\Delta E(G)$ and $\Delta r_{23}(G)$ depend on the electron occupancy of substituent(s) and on the position of the element in Periodic Table. For butadiene-like species $\text{X}=\text{C}-\text{C}=\text{Y}$ ($\text{X}, \text{Y} = \text{O}, \text{S}, \text{Se}, \text{NH}, \text{PH}, \text{AsH}$) and XH_2 -substituted butadienes ($\text{X} = \text{B}, \text{Al}, \text{Ga}$) with electron-withdrawing group, always $\Delta E(G)$ (stabilizing) < 0 , and $\Delta r_{23}(G) < 0$, the ranges of the $\Delta E(G)$ and $\Delta r_{23}(G)$ values are -7.8 kcal/mol -0.041 Å, which is in line with the structural theory of organic chemistry.

For the halogen- and XH_2 -substituted butadienes ($\text{X} = \text{N}, \text{P}, \text{As}$) having electron-releasing groups, always $\Delta E(G) > 0$ (destabilizing). When halogen atom and X atom (F, N) belong to the second period of Periodic Table, always $\Delta r_{23}(G) > 0$, and the ranges of the $\Delta r_{23}(G)$, $r_{23}(G)$ and $r_{23}(\text{GL})$ values are 0.037, 0.015 and 0.020 Å, respectively. Otherwise, $\Delta r_{23}(G) < 0$, and the corresponding ranges are -0.004, 0.019 Å and 0.022 Å.

For the halogen-substituted, $r_{23}(\text{GL}) = f(\Delta \Sigma e_i)$ in the GL geometry (Figure 12-6c), and $r_{23}(\text{GL}_n) = f(P_{23}(\text{GL}_n))$ in the GL_n geometry (Figure 12-9a). According to this change in the functional relationship, and based on the energy decomposition, the adjacent conjugation between each double bond and its substituent(s) has the large influence on the difference $\Delta r_{23}(\text{GL}) = r_{23}(\text{GL}) - r_{23}(\text{GL}_n)$ through the σ bonds in and only in the case of halogen- and NH_2 -substituted butadiene with electron-releasing groups. The ranges (Å) of the $\Delta r_{23}(\text{GL}) = r_{23}(\text{GL}) - r_{23}(\text{GL}_n)$ values are -0.031 (halogen), -0.034 Å (XH_2) ($\text{X} = \text{B}, \text{Al}, \text{Ga}$).

For XH_2 -substituted butadienes ($\text{X} = \text{B}, \text{Al}, \text{Ga}$) with electron-withdrawing substituents, the adjacent conjugation has a slight influence on the difference of the naked CC single bond distance, according to that the maximum value and minimum value of $\Delta r_{23}(\text{GL})$ are 0.011 and 0.000 Å.

12.6. REFERENCES

- 1 Conant, J. B.; Kistiakowsky, G. B. 1937. "Energy Changes Involved in the Addition Reactions of Unsaturated Hydrocarbons." *Chem. Rev.*, 20: 181-194.
- 2 Kistiakowsky, G. B.; Ruhoff, J. R.; Smith, H. A.; Vaughan, W. E. 1936. "Heats of Organic Reactions. IV. Hydrogenation of Some Dienes and of Benzene." *J. Am. Chem. Soc.*, 58: 146-153.
- 3 Vollhardt, K. P. C., Schore, N. E. 1998. *Organic Chemistry, Structure and Function*. Third Edition, New York: W. H. Freeman and Company.
- 4 Silvestre-Albero, J; Rupprechter, G; Freund, H. J. 2005. "Atmospheric Pressure Studies of Selective 1,3-Butadiene Hydrogenation on Pd Single Crystals: Effect of CO Addition." *J. Catal.*, 235: 52-59.
- 5 Pauling, L. 1932. "Interatomic Distance in Covalent Molecules and Resonance between Two or More Lewis Electronic Structures." *Proc. Natl. Acad. Sci.*, 18: 293-297.
- 6 Pauling, L.; Brockway, L. O.; Beach, J. Y. 1935. "The Dependence of Interatomic Distance on Single Bond-Double Bond Resonance." *J. Am. Chem. Soc.*, 57: 2705-2709.
- 7 Pauling, L.; Brockway, L. O. 1937. "Carbon-Carbon Bond Distances. The Electron Diffraction Investigation of Ethane, Propane, Isobutane, Neopentane, Cyclopropane, Cyclopentane, Cyclohexane, Allene, Ethylene, Isobutene, Tetramethylethylene, Mesitylene, and Hexamethylbenzene. Revised Values of Covalent Radii." *J. Am. Chem. Soc.*, 59: 1223-1236.
- 8 Pauling, L.; Springall, H. D.; Palmer, K. J. 1939. "The Electron Diffraction Investigation of Methylacetylene,

- Dimethylacetylene, Dimethyldiacetylene, Methyl Cyanide, Diacetylene, and Cyanogen." J. Am. Chem. Soc., 61: 927-937.
- 9 Coulson, C. A. 1939. "The Electronic Structure of Some Polyenes and Aromatic Molecules VII. Bonds of Fractional Order by the Molecular Orbital Method." Proc. Roy. Soc. A, 169: 413-428.
- 10 Coulson, C. A. 1952. *Valence*. London: Oxford University Press.
- 11 Coulson, C. A. 1951. "Bond Lengths in Conjugated Molecules: The Present Position." Proc. Roy. Soc. A, 207: 91-100.
- 12 Mulliken, R. S.; Rieke, C. A.; Brown, W. 1941. "Hyperconjugation." J. Am. Chem. Soc., 63: 41-56.
- 13 Mulliken, R. S., 1959. "Bond Lengths and Bond Energies in Conjugation and Hyperconjugation." Tetrahedron, 6: 68-87.
- 14 Haugen, W.; Trætteberg, M. 1966. "The Molecular Structures of 1, 3-Butadiene and 1, 3, 5-trans-Hexatriene." Acta Chem. Scand., 20: 1726-1728.
- 15 Kveseth, K.; Seip, R.; Kohl, D. 1980. "Conformation Analysis. The Structure and Torsional Potential of 1,3-butadiene as Studied by Gas Electron Diffraction." Acta Chem. Scand. A, 34: 31-42.
- 16 Schomaker, V.; Pauling, L. 1939. "The Electron Diffraction Investigation of the Structure of Benzene, Pyridine, Pyrazine, Butadiene-1,3, Cyclopentadiene, Furan, Pyrrole, and Thiophene." J. Am. Chem. Soc., 61: 1769-1780.
- 17 Caminati, W.; Grassi, G.; Bauder, A. 1988. "Microwave Fourier Transform Spectrum of s-Trans-1,3-Butadiene-1, 1-d2." Chem. Phys. Lett., 148: 13-16.
- 18 Craig, N. C.; Groner, P.; McKean, D. C. 2006. "Equilibrium Structures for Butadiene and Ethylene: Compelling Evidence for π -Electron Delocalization in Butadiene." J. Phys. Chem. A, 110: 7461-7469.
- 19 Epiotis, N. D.; Cherry, W. R.; Shaik, S.; Yates, R.; Bernardi, F. 1977. "Structure Theory of Organic Chemistry." Top. Curr. Chem., 70: 1-end.
- 20 Wells, A. F. 1949. "Bond Lengths in Some Inorganic Molecules and Complex Ions." J. Chem. Soc., 55-67.
- 21 Bartell, L. S. 1960. "On the Effects of Intramolecular van der Waals Forces." J. Chem. Phys., 32: 827-831.
- 22 Berry, R. S. 1959. "Conjugation and Polar Effects in Butadiene." J. Chem. Phys., 30: 936-941.
- 23 Wilson, E. B. 1962. "Conjugation, Hybridization, and Steric Hindrance in Relation to Bond Lengths." Tetrahedron, 17: 191-198.
- 24 Pauling, L. 1931. "The Nature of the Chemical Bond. Application of Results Obtained from the Quantum Mechanics and from a Theory of Paramagnetic Susceptibility to the Structure of Molecules." J. Am. Chem. Soc., 53: 1367-1400.
- 25 Lonsdale, K. 1929. "The Structure of the Benzene Ring in C₆(CH₃)₆." Proc. Roy. Soc., A123: 494-515.
- 26 Brockway, L. O.; Robertson, J. M. 1939. "The Crystal Structure of Hexamethyl-benzene and the Length of the Methyl Group Bond to Aromatic Carbon Atoms." J. Chem. Soc., 1324-1332.
- 27 Epiotis, N. D. 1983. "Applications of Molecular Orbital-Valence Bond Theory in Chemistry." Pure Appl. Chem., 55: 229-236.
- 28 Epiotis, N. D. 1983. *Lecture Notes in Chemistry*. New York: Springer-Verlag.
- 29 Epiotis, N. D. 1996. *Deciphering the Chemical Code*. New York: VCH Publishers Inc..
- 30 Dewar, M. J. S.; Schmeising, H. N. 1958. *Report at Conference on Hyperconjugation*. Bloomington, Indiana, June.
- 31 Dewar, M. J. S.; Schmeising, H. N. 1959. "A Re-evaluation of Conjugation and Hyper-conjugation: The Effects of Changes in Hybridisation on Carbon Bond." Tetrahedron, 5:166-178
- 32 Brown, M. G. 1959. "Atom Hybridization and Bond Properties. Some Carbon-containing Bonds." Trans. Faraday Soc., 55: 94-701.
- 33 Somayajulu, G. 1959. "Lengths of CC 'Single' Bonds and Radii of Hybrid Orbitals of Carbon." J. Chem. Phys., 31: 919-921.
- 34 Lide, d. 1962. "A Survey of Carbon-Carbon Bond Lengths." Tetrahedron, 17: 125-134.
- 35 Bastiansen, O.; Trettenberg, M. 1962. "The Nature of Bonds between Carbon Atoms How They Vary with Environment." Tetrahedron, 17: 147-154.

- 36 Duchesne, J. 1951. "The Role of Hybridization and Resonance in Molecular Structure." *J. Chem. Phys.*, 19: 246-247.
- 37 Duchesne, J. 1950. "Covalent Radius and Molecular Structure." *Trans. Faraday Soc.*, 46: 187-190.
- 38 Bastiansen, O.; Hedberg, L.; Hedberg, K. 1957. "Reinvestigation of the Molecular Structure of 1,3,5,7-Cyclooctatetraene by Electron Diffraction." *J. Chem. Phys.*, 27: 1311-1317.
- 39 Bartell, L. S.; Bonham1, R. A. 1957. "Structure of Ethylene." *J. Chem. Phys.*, 27: 1414-1415.
- 40 Pauling, L. 1945. *The Nature of the Chemical Bond*. New York: Cornell University Press.
- 41 Mikhailov, B. M. 1965. "Interatomic Distance in Non-aromatic Hydrocarbon in the Light of Hybridization Theory." *Tetrahedron*, 21: 1277-1285.
- 42 Ingold, C. K. 1953. *Structure and Mechanism in Organic Chemistry*. New York: Cornell University Press.
- 43 Burawoy, A. 1944. "The Constitutive Changes of the Covalent Linkages, Their Nature and Cause." *Trans. Faraday Soc.*, 40: 537-544.
- 44 Dailey, B. P.; Mays, J. M.; Townes, C. H. 1949. "Microwave Rotational Spectra and Structures of GeH₃Cl, SiH₃Cl, and CH₃Cl." *Phys. Rev.*, 76: 136-137.
- 45 Gordy, W. 1948. "Microwave Spectroscopy." *Rev. Modern Phys.*, 20: 668-717.
- 46 Duchesne, J.; Monfils, A. 1949. "A Further Interpretation of Interaction Terms in the Potential Function of Polyatomic Molecules." *J. Chem. Phys.*, 17: 586-587.
- 47 Westenberg, A. A.; Goldstein, J. H.; Wilson Jr. E. B. 1949. "The Microwave Spectrum of Chloroacetylene and Deuterochloro-acetylene." *J. Chem. Phys.*, 17: 1319-1321.
- 48 Trætteberg, M. 1966. "The Molecular Structure of 1,3,5,7-Cyclo-octatetraene." *Acta Chem. Scand.*, 20: 1724-1726.
- 49 Skaarup, S.; Boggs, J. E.; Skancke, P. N. 1976. "Contributions of Resonance, Hybridization and Nonbonded Interaction to the Structure of Butadiene." *Tetrahedron*, 32: 1179-1181.
- 50 Claus, K. H.; Krüger, C. 1988. "Structure of Cyclooctatetraene at 129 K." *Acta Cryst.*, C44: 1632-1634.
- 51 Kummler, D. S.; Lobsiger, S.; Frey, H-M.; Leutwyler, S.; Stanton, J. F. 2008. "Accurate Determination of the Structure of Cyclooctatetraene by Femtosecond Rotational Coherence Spectroscopy and *ab Initio* Calculations." *J. Phys. Chem. A*, 112: 9134-9143.
- 52 Mulliken, R. S. 1962. "Discussion." *Tetrahedron*, 17: 247-266.
- 53 Bao, P.; Yu, Z. H. 2007. "Restricted Geometry Optimization: A Different Way to Estimate Stabilization Energies for Aromatic Molecules of Various Types." *J. Phys. Chem. A*, 111: 5304-5313.
- 54 Bader, R. F. W.; Streitwieser, A.; Neuhaus, A.; Laidig, K. E.; Speers, P. 1996. "Electron Delocalization and the Fermi Hole." *J. Am. Chem. Soc.*, 118: 4959-4965.
- 55 Bader, R. F. W.; Johnson, S.; Tang, T. H.; Popelier, P. L. A. 1996. "The Electron Pair." *J. Phys. Chem.*, 100: 15398-15415.
- 56 Bao, P.; Yu, Z. H. 2011. "New Procedure to Evaluate Aromaticity at the Density Functional Theory, Hartree-Fock, and Post-Self- Consistent Field Levels." *J. Comput. Chem.*, 32: 248-259.
- 57 Yamaguchi, Y.; Osamura, Y.; Goddard, J. D.; Schaefer, H. F. 1994. *A New Dimension to Quantum Chemistry: Analytic Derivative Methods in Ab Initio Molecular Electronic Structure Theory*. Oxford: Oxford University Press.
- 58 Dupuis, M.; King, H. F. 1978. "Molecular Symmetry. II. Gradient of Electronic Energy with Respect to Nuclear Coordinates." *J. Chem. Phys.*, 68: 3998-4004.
- 59 Shaik, S.; Shurki, A.; Danovich, D.; Hiberty, P. C. 2001. "A Different Story of π -Delocalizations – The Distortion of π -Electrons and Its Chemical Manifestations." *Chem. Rev.*, 101: 1501-1540.
- 60 Deniz, A. A.; Peters, K. S.; Snyder, G. J. 1999. "Experimental Determination of the Antiaromaticity of Cyclobutadiene." *Science*, 286: 1119-1122.
- 61 Gould, E. S. 1959. *Mechanism and Structure in Organic Chemistry*. New York: Henry Holt and Company.

INDEX

- Acenes, 219, 243, 314
 anthracene, 219
 CESE, 222, 224
 CESE versus UV frequency, 224
 fusion double bond, 223
 heptacene, 219
 hexacene, 219
 candidates for the GL geometry, 221
 Kekulé valence structure, 220
 ring structure units, 221
 naphthalene, 219
 pentacene, 219
 tetracene, 219
 Active energy effects, 337
 Adiabatic delocalization energy ΔE^A
 alternating between stabilizing and destabilizing, 306, 310
 $d\Delta E^A/dn$ for acenes,
 $d\Delta E^A/dn > 0$ from our 2007 method, 421
 $d\Delta E^A/dn < 0$ from our 2011 method, 421
 definition $\Delta E^A = E(G) - E(GL)$, 178
 destabilizing $\Delta E^A > 0$
 for all anti-aromatic, 275, 307
 for all larger [N]annulene, 310
 for $C_6X_3H_3$ ($X = N, P, As$), 178, 216, 227
 for C_6X_6 ($X = B, N, P, As$), 178, 216, 227
 for $C_6X_6H_6$ ($X = N, P, As, C, Si, Ge$), 178, 216, 227
 for furan-like species, 185
 for polyenes, 309
 ΔE^A versus chain unit number, 314
 ΔE^A versus the number of carbon atoms, 311
 HF-EX effect on ΔE^A , 421
 seeing [N]annulene
 seeing benzene
 seeing cyclobutadiene
 seeing polycyclic benzenoid hydrocarbon
 seeing strained-aromatic molecule
 stabilizing $\Delta E^A < 0$
 for aromatic molecule, 178, 216, 227
 for $C_6X_6H_6$ and $C_6X_3H_3$ ($X = B, Al, Ga$), 178, 216, 227
 Adjacent conjugation, 431, 435, 438, 439, 440, 441, 442
 conjugation effect, 424, 431, 433, 438, 439
 conjugation energy $\Delta E(GL)$, 435
 definition, 423
 effect on adjacent CC single bond, 434
 electron-deficient substituent, 439
 electron-sufficient substituent, 441, 437
 energy decomposition, 436
 force acting on adjacent CC single bond, 437
 $r_{23}(GL_n)$ versus $\Sigma e_i(GL_n)$, 433
 $r_{23}(GL_n)$ versus $P_{23}(GL_n)$, 433
 $\Delta r_{23}(GL_n)$ versus $\Delta E(GL_n)$, 433
 transmission through σ bonds, 433
 Alternating single and double bonds, 283, 339, 340, 341, 342, 345, 348, 351, 355, 360, 366, 368
 degree and direction, 351, 368
 π -distortion, 351
 $d\Delta r(GP)$ versus $\Delta E(GP)$, 353
 experimental probe, 344
 interpretations, 342
 Mills-Nixon effect, 339, 340, 341, 374
 seeing strained-aromatic molecules
 structural factors, 321
 [N]Annulenes, 283, 294
 alternating between aromaticity and anti-aromaticity, 303
 [10]annulene, 283, 297, 298, 302
 [12]annulene, 299
 [14]annulene, 280, 284, 299, 319
 [18]annulene, 284, 285, 299
 [20]annulene, 300
 [22]-, [24]- and [26]annulenes, 301
 approaching polyene, 309
 B3LYP/6-311G(2df,p) value
 CESE/ π , 310
 VDE/ π , 303
 ceasing to be anti-aromatic, 308
 CESE versus number of carbon atoms, 311
 configuration isomer, 295
 configuration and VDE, 296
 extra stabilization energy (ESE), 306
 [8]annulene, 307
 geometry optimization, 296
 4n+2 rule, 304
 basis set size, 304

- theoretical level, 304
- nomenclature of configuration isomer, 295
 - the number of carbon atoms in F-th fragment, 295
 - the number of inner hydrogen atoms, 295
- possible isomers of a [N]annulene, 297
- VDE/ π versus number of carbon atoms, 304
- AO Fock and overlap matrices, 64
 - particular matrix, 89
- Aromatic stabilization energy, 166, 167, 171, 180, 190, 194
- Aromaticity, 165, 169, 204
 - energy and geometric criteria
 - consistency, 396
 - unified and mutually causal, 317
 - energy criterion, 187, 306
- Average bond lengths, 213
- Azobenzene, 21, 22, 24, 48
 - conformation, 22
 - p- π interaction, 24
 - experimental twist angle, 24
 - gas electron diffraction, 24
 - ^1H NMR, 22
 - x-ray diffraction, 22
 - UV absorption, 21
- Benzene, 165, 289
 - adiabatic delocalization energy, 177, 269, 417
 - basis set size effect, 246
 - theoretical level effect, 246
 - bent benzene, 343
 - bond length change, 177, 178
 - bond length equalization, 291
 - CT and EX interaction energies, 357
 - destabilizing energy effect $\Delta E^{\text{A}1}$, 177, 178
 - Dewar resonance energy, 167
 - electronic states, 254, 290
 - energy decomposition
 - DFT energy, 286
 - π - σ energy decomposition, 286
 - inter-double bond interactions, 293
 - intra-double bond interactions, 293
 - MPn energy, 254, 256
 - extra stabilization energy (ESE), 179, 256, 267, 277, 416
 - basis set size effect, 251
 - density functional effect, 258
 - experimental value of -36 kcal/mol, 165
 - 36.3 kcal/mol, 260
- 36.4 kcal/mol, 417
- 39.0 kcal/mol, 177
- theoretical level effect, 251
- two-electron exchange integrals, 256
- hydrogenation heat, 165
- local conjugation, 177, 267
- localized geometry
 - GE-m geometry, 177, 267
 - GL geometry, 177, 267
- molecular deformation
 - force acting on CC bonds, 255, 293
 - force distorting ring, 285
 - σ -framework role, 291
 - nuclear repulsion role, 294
 - π -system role, 291
- nuclear repulsion energy
 - bond length equalization, 293
 - between carbon atoms, 293
 - minimization, 293
- Pauling resonance energy, 167
- reference states, 179
- Shaik's view point, 166
- three distortion models, 289
 - delocalized to delocalized ring
 - localized to delocalized ring
 - localized to localized ring
- vertical delocalization energy
 - basis set size effect, 252
 - density functional effect, 274
 - Hartree-Fock exchange effects, 267
 - from our 2007 method, 252
 - from our 2011 method, 273
 - theoretical level effect, 252
- virtual delocalized cyclohexatriene, 178, 378
- Benzene-like species, 182, 183, 184, 185, 187, 188
 - chemical shift versus $E_{\text{ov}}^{\text{pq}}$, 189
 - ESE, 180
 - pyrazine, 180
 - pyridazine, 180
 - pyridine, 180
 - pyrimidine, 180
 - tetrazine, 180
 - triazine, 180
 - GL and GE-m geometries, 182
 - size order of the ESEs, 84
- Benzo[el]pyrene, 241
 - CESE/ π versus UV absorption frequency, 233
 - conflict between position and energy rules, 232

- naphtho[2,3-e]pyrene, 231
- Benzotricyclobutadiene, 340, 378, 397
 - angle strain, 349
 - anti-aromatic molecule, 380
 - average distance of CC bonds, 348
 - bond length alternation (BLA), 346
 - arising from π -delocalization, 346
 - candidates for GL geometry, 380, 382
 - CESE and ESE
 - for central ring, 383
 - for molecule, 380
 - destabilization π -interaction energy, 348
 - eliminating π -interaction, 345
 - energy decomposition, 348
 - particular localized geometry (PLG), 345
 - construction, 346
 - equalization of CC bond lengths, 347
 - forces acting on CC bonds, 349
 - fragmentation, 345
 - localized π -electrons, 348
 - rationality of GL₁₆ candidate, 384
 - N-Benzylideneaniline (NBA), 19, 20, 25, 35, 44, 49, 58, 85, 90, 116, 123, 137, 141, 148, 153
 - construction of electronic states
 - DSI state, 89
 - FUD state, 90
 - construction of LFMO basis set, 59
 - CT and EX Interactions, 130
 - destabilizing π - σ interaction, 137
 - experimental twist angle of 55°
 - interpretations of non-planar conformation, 24
 - seeing Controversy over large twist angle
 - NBO basis set, 116
 - nine sum terms of Fock matrix element, 120
 - non-bonded σ - σ interaction, 147
 - twisted geometries, 118, 125, 138
 - vertical delocalization energy, 91, 124, 125, 126, 133
 - Bird resonance energy, 180
 - BLW method, 168, 249, 250, 251, 256, 266, 324
 - comparison with our method, 266
 - fundamental differences, 169
 - a special case of our method, 266
 - π -delocalization energy for allyl cation, 267
 - GL geometry for allyl cation, 267
 - a method only used to localize double bonds, 249
 - 2 x 2 rotation, 249
 - fundamental flaws of BLW method, 249
 - maximizing exchange energy, 65, 67, 249,
 - minimizing charge transfer energy, 250
 - an unreasonable method, 249
 - stabilizing ADE for cyclobutadiene, 169
 - Bond
 - bond energy additivity, 180
 - bond length, 369
 - bond length equalization, 291, 298, 317
 - bond localization, 340, 342, 374, 375
 - Bond angle, 368
 - $\angle C-B=B$, 368
 - $\angle C-B-C$, 369
 - $\angle C-X-X$ (X = B, Al, Ga, N, P, As), 350
 - $\angle C-X=X$ (X = B, C, Si, Ge, N, P, As), 350
 - $\angle H-C-C$ in bent benzene, 343
 - pure σ -strain (angle strain), 343
 - Δr (PLG) versus $\Delta\beta$ (PLG), 369
 - secondary structure effect, 369
 - Bond angle deformation, 23
 - for C-X-X (X = B, Al, Ga, N, P, As), 350
 - for C-X=X (X = B, Si, C, N, P, As), 350
 - Bond length alternation (BLA), 283, 346
 - angle strain, 343
 - bent benzene, 343
 - π -driving force, 339
 - experimental probe, 344
 - seeing [N]annulene
 - seeing strained-aromatic molecule
 - two other ways to explain BLA, 342
 - Bond structure unit
 - environment, 226
 - type A, 225
 - type B, 225
 - type C, 226
 - 1,3-Butadiene, 3, 17, 163, 204, 399, 407, 416, 444
 - controversy over
 - conjugation stabilization, 162
 - resonance existence, 405
 - covalent radii, 403
 - distance of naked CC single bond, 414, 416
 - basis set size influence, 415
 - exchange gradient influence, 412, 415
 - theoretical level influence, 415
 - hybridization, 403
 - 1,4-hydrogenation, 164

- hydrogenation heat difference, 162, 416
 destabilizing conjugation energy, 162, 408
 Kistiakowsky experiment, 162
 questioning conjugation stabilization, 162
 unreasonable reference molecule, 162
- hydrogenation heat difference between, 162, 163
 trans-butadiene and two 1-butenes, 162
 trans-butadiene and two cis-2-butenes, 162
 trans-butadiene and two trans-2-butenes, 162
 various experimental distances of CC single bonds, 399
- 1,3-Butadiene derivatives
 seeing 1,3-butadiene-like species
 seeing substituted butadiene
- 1,3-Butadiene-like species, 422, 427
 CC single bond distance, 422
 longest distance, 425
 shortest distance, 425
 charges $e_i(GL)$, 429
 construction of localized GL geometry, 422
 electron-withdrawing group, 425
 Mulliken atomic overlap population $P_{23}(GL)$, 429
 naked CC single bond distance, 422
 inductive effect, 428
 longest distance, 425
 $r_{23}(GL)$ versus $P_{23}(GL)$, 428
 shortest distance, 425
 $\Delta r_{23}(G)$ versus $\Delta E(G)$, 425, 426
 $X=C-C=Y$ ($X, Y = O, S, Se, N, P, As$), 424
- 1,3-Butadiyne, 163
 hydrogenation heat, 163
- CC single bond distance, 399, 407, 414, 423, 430, 437, 440
 sp-sp bond, 402
 sp^2-sp^2 bond, 400
 sp^3-sp bond, 402
 sp^3-sp^2 bond, 401
 corrected distance in diacetylene and cyanogen, 402
 naked CC single bond, 398, 443
 naked sp^m-sp^n CC single bond, 399, 407
 structural factors determining distance
 bond order, 402
 conjugation (resonance), 399
 covalent radii, 403
 hybridization, 399, 403, 405, 406, 407, 445
- experimental distances
 in butadiene, 399
 in cyclooctatetraene, 407
 in diacetylene, 401
- Chain unit 6, 8, 12, 13
- Charge transfer, 80, 101, 113, 323, 336, 340, 358
 π Charge transfer, 188
 charge transfer versus chemical shift, 189
- Charge transfer complex NH_3BH_3 , 323, 372
 amazing localized geometry, 330
 Brackmann's view, 323
 distortivity of electron delocalization, 334
 electronic states, 329
 energy decomposition, 323
 charge transfer energy, 336
 electrostatic energy, 332
 exchange interaction energy, 336
 polarization energy, 332
 Mulliken's model, 323
 thermodynamic mechanisms of reaction $NH_3 + BH_3$, 328
- Chemical shifts, 188
 for benzene-like species, 189
 chemical shift versus charge transfer energy, 189
 closed CT loop, 188
 for furan-like species, 189
- Chrysene, 314
- Conditional SCF-MO calculation, 59, 67
 single-point energy calculations, 137, 151
- cis-Configuration, 54
- Configuration isomers, 295, 296, 297
 of [16]annulene, 296
 configuration and VDE, 296
 meaning of symbol “[16]-54444”
 most stable isomers, 317
 possible configuration isomers, 297
- Conformation, 19, 26, 29, 30, 31, 37, 38, 40, 46
- Conjugation effect, 165, 399, 403, 407, 423, 438, 442
 between central ring and annulated small ring, 353
 conjugation 2, 3, 4, 16
 destabilization, 353
 distortivity seeing driving force between fragments, 91
 local conjugation energy, 173, 379
 stabilization 1, 3, 4, 16, 162
 transmission, 438
 between two double bonds, 424

- Controversy over distance of CC single bond
 amount of double bond character, 400
 Coulson's method, 402
 covalent radii, 403, 444
 Dewar's hybridization, 403
 is there resonance energy? 405
 non-integral sp^n , 404
 Pauling's resonance theory, 399
- Controversy over large twist angle
 crystal force, 22, 23
 interpretation of large twist angle, 22, 24
 Ahmet and Silver, 22
 Bernstein, 22
 Bürgi, 24
 Mootz, 22
 Nakai, 25
 Wiebecke, 22
 seeing N-benzylideneaniline
 seeing NBA-like species
 Skraba's experiments, 26
 Traetteberg viewpoint, 24
 twist angle, 2, 4, 15, 19, 30, 38, 40, 44
- Controversy over Mills-Nixon effect, 341
 angle strain, 339
 definition of Mills-Nixon effect, 339
 factor causing bond length alternation
 factors determining $r_{\text{endo}} > r_{\text{exo}}$
- Crossed-conjugated system 4, 5
- CT and EX interactions, 357
 CT energy effect, 188
 CT state, 82
 CT-1 effect, 25
 CT-2 interaction, 19, 25, 29, 30
- Cyclobutadiene, 167, 168, 188, 206, 246, 249, 274
 adiabatic delocalization energy (kcal/mol), 169,
 246, 249, 282, 314, 398, 419, 442
 -10.3 from BLW method, 169
 55.0 from experiment, 169
 53.6 from our 2011 method, 169
 54.9 from our 2014 method, 443
 construction of localized state, 169, 248
 historical roles, 246
 confirming reasonability of MO theory, 3
 testing rationality of method calculating
 conjugation energy, 442
 most basic conjugated molecule, 168
- DFT molecular energy, 286
 energy decomposition, 286
- Dihedral angle (twist angle)
 azobenzene, 24
 N-benzylideneaniline (NBA), 22
 3-[N-methyl, N-(2-naphthyl)]amino-acrolein,
 15
 5-[N-methyl, N-(2-naphthyl)]amino-penta-2,4-dienal, 15
 3-[N-(2-naphthyl)]amino-acrolein, 16
 5-[N-(2-naphthyl)]amino-penta-2,4-dienal, 16
 NBA-like species, 21
 optimized non-planar butadiene, 164
 seeing NBA-like species
 seeing substituted NBAs
 stilbene, 24
 substituent effect, 25
- Density functionals, 131, 132, 272
 four types of density functionals, 258
 hybrid density functionals, 259
 pure correlation density functionals, 258
 pure exchange density functional, 258
 test HF-EX effect, 259
- Destabilizing $\pi-\sigma$ interaction, 137
 energy decomposition 139
- Dewar resonance energy, 167, 168, 180
- Dibenzoacenes, 231
- Dibenzo[de,uv]pentacene, 241
- 1,2-Difluoroethylene, 54
- π -Distortivity, 196, 322
 bond length alternation (BLA), 346
 seeing strained-aromatic molecules
 single bond distance
 between substituent and phenyl ring, 196
 between two double bonds, 17, 173
 universality, 351
- 1,2-Disubstituted ethylenes, 54
- Divinyl ether-like species, 182
 additive energy effects, 186
 N-(1,3-butadienyl)-formamide, 186
 1,3-butadienyl formimide, 186
 1,3-butadienyl-vinyl ether, 186
 divinyl ether, 186
 N-(iminomethyl)-imidoformamide, 186
 [N-vinyl,N-(2,3-butadienyl)]-amine, 186
 N-vinyl-ethenamine, 186
 N-vinyl-formamide, 186
 vinyl formimide, 186
- Double bond character, 400
 amount of double bond character, 400

- Doubly occupied and vacant MOs, 63
- Driving force and resistance of molecular distortion, 31, 32, 35, 38
- for distorting central ring, 359
 - for distorting molecule 3
 - for distorting NBA-like species, 53
 - distortion of electron delocalization, 334
 - driving force, 162, 166, 168, 190, 195, 322
 - forces acting on ring bonds, 360
 - molecular distortion, 21, 33, 36, 37, 40, 45, 87
- Electron-deficient groups, 396, 440
- electron acceptor, 323
 - π electron-deficient groups, 358
 - electron-withdrawing group, 23, 29, 79, 102
- π Electron delocalization energy, 80, 209
- seeing adiabatic delocalization energy
 - seeing vertical delocalization energy
- Electron localization, 257
- Bader's definition, 251
 - eliminating AO matrix element method, 127
 - eliminating two-electron exchange integrals, 261
 - particular exchange integrals, 261
- π -Electron localization, 286
- Bader's spatial exchange, 251
 - deleting exchange integrals, 131
 - Pauli exclusion principle, 257
- π Electron-rich groups, 359
- Electron-sufficient group, 376, 396
- electron donor, 323
 - electron-releasing group, 23, 30, 43, 44, 104, 423, 427, 441
- Electronic interaction, 332, 334, 341
- influence of π - σ interaction on molecular conformation, 137
 - π - π interaction 24, 85
- Electronic structures, 351, 354
- Endocyclic and exocyclic bonds, 364, 365, 391
- seeing strained-aromatic molecule
- Energy change characteristics, 80
- Energy decomposition, 286, 292, 323, 326, 348, 373
- Energy effect, 55, 58
- increments, 225
- Estimation of resonance energy, 209
- Exchange, 80, 84, 98, 101, 104, 323, 327, 330, 336, 338, 340, 346, 359
- Exchange-correlation functional, 259
- Extra destabilization energy, 174, 177, 190, 306, 316, 379, 381
- Extra stabilization energy (ESE)
- definition, 178
 - ESE versus $\Delta r(G)$, 391
 - for phenanthrene, 219
 - seeing [N]annulene, 309
 - seeing benzene
 - seeing benzene-like species, 180
 - seeing furan-like species, 184
 - seeing polycyclic benzenoid hydrocarbons
 - seeing strained-aromatic molecule.
 - seeing substituted benzene 189
- Fermi correction, 83
- FMO Fock and overlap matrices, 64
- Fock matrix
- LFMO Fork matrix, 89
 - LFMO Fock matrix element, 128
 - nine sum terms, 127
 - particular sum term, 128
 - full matrix, 89
 - NBO Fock matrix, 120
 - NBO Fock matrix element, 127
 - nine sum terms, 127
 - particular AO Fock matrix, 128
 - particular MO Fock matrix, 82
 - transforming particular AO Fock matrix, 128
- Four-electron destabilization interaction, 53
- Fragment molecular orbital (FMO) basis set, 53
- electronic occupancies, 55, 58, 63, 67
 - Kost localization procedure, 65, 250
 - referential hydrogen atom, 60, 67, 71
 - singly occupied FMO, 52, 55, 60, 63, 65, 69, 71
- Fragmentation of a molecule, 59
- cartesian coordinates, 61, 64
 - fragment molecules, 61
 - fragments, 52, 55, 58, 59, 60, 61, 70, 71
- Frontier molecular orbital theory, 4, 54
- Fundamental principles of organic chemistry
- basic causal relationship 3, 16, 24
 - CC single bond (1.36 Å) in diacetylene, 402
 - distorting molecule, 24
 - destabilizing steric hindrance, 24
 - stabilizing p- π interaction, 24
 - stabilizing conjugation energy (-3.5 kcal/mol) of butadiene, 162, 399
 - resistance to molecular distortion, 3, 24
- Pauling's resonance theory, 399
- Furan-like species, 184

- chemical shift versus CT interaction energy, 189
 ESE (reduced destabilization energy), 185
 GL and GE-m geometries, 185
 not appear to be aromatic, 188
 2,5-addition reactions, 188
 $\Delta E^A > 0$, 185
 no CT loop, 189
 size order of ESEs, 187
 Gas electron diffraction, 21, 24
 Geometrical structures, 369
 GL and GE-m geometries of phenanthrene, 215
 GL geometries of 66 butadiene derivatives, 443
 definition, 238
 GL_m geometry, 388
 Gradients of the two-electron exchange integrals,
 conditionally deleting, 442
 influence on energy effects
 CESE for PBHs, 419
 ESE for benzene, 416
 VDE for Cyclobutadiene, 418
 our 2014 method, 413
 seeing butadiene
 seeing substituted butadiene
 Ground state, 116, 118, 127, 137
 Harmonic oscillator stabilization energy, 180
 Hartree-Fock exchange (HF-EX)
 deleting integrals
 seeing our method
 effect on sign of VDE for benzene
 seeing vertical delocalization energy
 effect on twist angle, 30
 effect on VDE value, 98
 effects, 30, 98, 131, 135, 258, 267
 gradient of two-electron exchange integrals, 413
 role of two-electron exchange integrals, 99
 testing HF-EX effect, 259
 two-electron exchange integrals, 83, 96, 99, 131,
 170, 245, 257, 259, 261, 268, 275
 15 types of exchange integrals, 262
 Hexacene, 208, 210, 222, 223, 224
 trans-1,3,5-Hexatriene, 170, 172, 173
 Higher order perturbation, 82
 3H-indoles, 26
 substituted, 26
 UV absorption wave length, 26
 Homodesmotic reaction, 210, 378
 Homologous linear rule 1, 2, 5, 8, 16
 combination law, 4
 homologous factor, 6, 8, 11, 12
 homologous linear lines, 11
 homologous series, 5, 6, 8
 substituent equivalent, 5
 uniqueness, 8
 Hückel resonance energy, 247
 Hydrogen bond, 19, 25, 42
 intra-molecular hydrogen bond, 42
 hydrogen bond energy versus twist angle, 43
 Hydrogenation heats, 163, 164
 for acetylene bonds, 165
 for benzene, 165
 for 1,3-butadiene, 163
 Hydroxy-substituted molecules, 101
 Inductive effect and conjugation transmitting, 438
 $\pi-\sigma$ Interaction
 characteristics, 137
 effect on molecular conformation, 137
 energy decomposition, 253, 286
 seeing NBA-like species
 seeing N-benzylideneaniline
 $\sigma-\sigma$ Interaction energy, 148
 seeing N-benzylideneaniline
 Insight into driving force and resistance, 32
 Intra- and inter-double bond interactions, 293
 Isodesmic reactions, 210, 378
 Kekulé valence structure, 209, 215, 223, 231, 237
 benzenoid ring, 212, 220, 231, 236, 239
 canonical Clar structure, 212
 Clar sextet, 212, 220, 239
 definition of Clar structure, 231
 empty ring, 212
 most important structure, 215
 numerical Clar formula, 211, 212, 213
 numerical value of a benzenoid ring, 213
 partial Pauling bond order, 213, 223
 Randić and Plavšić method, 211, 212
 the number of
 conjugated circuits, 211
 Kekulé valence structures, 211
 possible Clar structures, 213
 times, 213, 214
 Kistiakowsky's method, 164, 165
 Less destabilizing energy, 198
 LFMO basis set, 52, 53, 55, 57, 58, 59, 61, 70, 71
 absolute localization, 62
 calculation of $\text{tg}(2\beta)$ for 2x2 rotation, 67

- complete π and σ separation, 67
- conditional RHF computation, 67
- corrected electron occupancy, 72
- diagram of localizing FMOs, 66
- FMO basis set, 63
- Kost localization procedure, 65, 250
- localized molecular orbital, 84
- overlap integral $S_{l,k-s}$ between two singly occupied FMOs, 66
- Perkins' method, 58
- 2x2 rotation for maximizing $S_{l,k-s}$, 66
- reference hydrogen atom, 61, 63, 64, 65, 67
- sub-LFMO basis set for a fragment, 52, 59, 69
- superposition of sub-basis sets, 70
- LFMO-n basis set, 87
 - reorganization, 89
- Liao-Wu-Liu *ab initio* program, 85
- π -Like molecular orbital 13
- Linear function line 6
- Literature methods to localize MOs
 - BLW method, 168
 - Jug method, 211, 248
 - Kollma method, 211, 248
 - Kost-wolfe method, 63
 - WSW procedure, 55, 59, 60
- LMO, 84, 113
 - basis set, 116
 - interactions between the fragments, 129
- Local conjugation, 174, 177, 180, 182, 184, 186, 190
- Localization degree of LMO, 116, 123, 126, 130, 153, 64, 168, 170, 174, 180, 204
 - an entire LMO basis set, 123
 - individual LMO, 123
- Localized electronic state, 58, 285, 286, 297
 - DEL-PLG, 349
 - DSI (delocalized sigma) state, 85
 - DSI-LFMO state, 116, 118, 125
 - DSI-NBO, 119, 125, 128
 - FUD-GL, 290
 - FUD-NBO, 119, 125, 128
 - FUL (full localized) state, 85, 143
 - G-DSI, 290
 - PDSI (partially delocalized sigma state), 85, 146
- Localized geometry
 - GL and GE-m geometries, 179, 424
 - GL and GL_n geometries, 431
 - LG, 323, 328, 330
 - localized reference geometry, 170
- localized reference molecule, 378
- locally delocalized geometry, 176
- Saik's definition, 20
- Localized GL geometry, 209, 220, 231, 236, 241, 378, 380, 386, 391, 395, 396
 - 66 butadiene derivatives, 443
 - candidates, 208, 220, 223, 231, 237, 240, 384
 - GL sextet rule, 209, 215, 223, 237, 242, 378
 - energy rule, 378, 391
 - particular candidate, 223, 230
 - position rule, 376, 378, 388, 391, 395
 - position rule and energy rule conflict, 237
 - rationality of position rules, 394
 - conditional settings for construction, 173, 260, 410
 - GL₁₆ candidate, 384
 - GL₁₂ geometry, 380, 387, 390
 - GL sextet, 208, 215, 220, 223, 238, 239, 242
 - HF-EX effect seeing Hartree-Fock exchange sufficiency and necessity, 240
- Locally delocalized energy ΔE^{Am}
 - additivity for polyene
 - seeing new type of additive energy effect
 - always $\Delta E^{\text{Am}} > 0$
 - for furan-like species, 185
 - for all hydrocarbon, 227, 228, 309, 389
 - $\Delta E^{\text{Am}} < 0$ for electron-withdrawing U=V (U, V = B, Al, Ga, N, P, As), 395
 - ΔE^{Am} versus dr , 242
 - HF-EX effect, 268
- Matrix transformation and expansion, 81
- Metal complex
 - benzotricyclobutadiene, Cr(CO)₃, 345
 - Fe(CO)₃, 345
 - Cr(CO)₃ complex of benzene, 345
- Method of localizing molecular orbital, 61
- 2-(N-Methylamino)-anthracene
 - synthesis, 7
- MO interaction
 - charge transfer, 250, 251
 - exchange interaction, 250, 251
- π -MO localization, 257, 286
- Molecular energy decomposition, 435
- Molecular orbitals (MO)
 - LCAO MO, 90, 106

- LC-LFMO MO, 90, 106
 LC-NAO, 116, 117
 Morokuma energy decomposition, 80, 266, 324
 MPn calculation
 $\pi\text{-}\sigma$ energy decomposition, 288
 molecular energy, 288
 MPn correlation energy, 257
 second order energy correlation, 257
 Mulliken atomic overlap population, 42, 43, 427
 Mulliken's model of charge transfer complex, 323
 4n+2 rule, 247
 annulene, 283
 closed electron group, 283
 Hückel's work, 283
 seeing strained-aromatic molecules
 not always a truth, 284
 verifying the rationality of calculation method,
 283
 NBA-like species, 141, 322
 N-benzylidene-2-naphthylamine, 28
 N-(4-chlorobenzylidene)-2-pyridinamine, 28
 crystal structures,
 π -delocalization destabilization, 100
 destabilizing interaction
 non-bonded $\sigma\text{-}\sigma$ interaction, 143
 vertical delocalization energy, 92
 N-[(4-dimethylamino)benzylidene]-2-benzo-thiazoleamine, 28
 N-[(4-dimethylamino)benzylidene]-2-pyridin-amine, 28
 N-[(4-dimethylamino)phenyl]-diphenyl-keten-imine, 28
 electronic energy versus twist angle, 35, 38
 Hartree-Fock exchange, 131
 molecular energy versus twist angle, 33
 N-(4-nitrobenzylidene)-2-pyridinamine, 28
 N-(4-nitrobenzylidene)-2-pyrimidinamine, 28
 N-(4-nitrophenyl)-bis(4-methoxyphenyl)-keten-imine, 28
 N-(4-nitrophenyl)-diphenyl-ketenimine, 28
 N-[(4-nitrophenyl)methylene]-2-thiazoleamine,
 28
 N-phenyl-diphenylketenimine, 28
 N-(phenylmethylene)-2-thiazoleamine, 28
 nuclear repulsion versus twist angle, 35, 38
 twist angle, 28
 NBO energy decomposition
 basic flaws, 127
 vertical delocalization energy, 119, 126
 deleting NBO matrix elements,
 NBO basis set, 55, 58, 75, 116, 119, 130, 131,
 153
 first type, 116
 incomplete separation of π and α NBOs, 56
 incorrected electronic occupancies, 58
 low localization degree, 123
 second type, 116
 NBO decomposition analysis, 58, 80, 112, 324
 stabilizing exchange interaction, 130
 there is no four-electron interaction, 84
 two types of energy decomposition, 286
 an unreasonable method, 85
 NBO-II basis set 116, 119, 124, 125
 New type of additive energy effects, 169, 174, 177
 for aza-1,3,5-hexatrienes, 181
 basis set size effect, 309
 definition of ΔE^{Am} , 174
 HF-EX effect, 206, 410
 for trans-1,3,5,7,9,11-dodecahexaene, 176
 for trans-polyene, 174, 309
 for substituted 1,1-dibutadienyl-ethylene, 218
 theoretical level effect, 310, 410
 NH₃BH₃ complex, 323, 328
 amazing localized geometry (LG), 330
 DLE state, 336
 charge transfer and exchange interactions, 336
 construction of artificial geometry, 328
 delocalized geometry, 337
 distortivity of electron delocalization, 334
 electrostatic, 80, 84, 112, 324, 327, 330, 334
 electrostatic and polarization forces, 332
 electrostatic energy, 327
 LG(R) geometries, 331
 thermodynamic mechanism of reaction 328
 Nitro group, 99, 102, 103
 Nitrogen bridge compounds
 abnormal dihedral angle, 15
 abnormal single bond length, 15
 ω -(N-2-anthryl, N-methyl)aminoacrolein 13
 branched-chain, 5, 6, 8
 characteristics of UV absorption spectra, 10
 competing for π -like orbital, 13
 conjugated backbone, 2, 4, 5, 8, 9, 10, 12, 13
 conjugated branches, 2
 conjugation competition, 6, 8, 13

- alternating competition, 12
- (N, N-dimethylamino)(2-acene), 6
- ω -(dimethylamino)acrolein 9
- ω -(dimethylamino)polyenal, 6
- (N, N-dimethyl)formamide, 11
- 2-(methylamino)anthracene, 7
- ω -(N-(2-naphthyl)-amino)polyenal, 15
- ω -[(N-2-naphthyl, N-methyl)amino]acrolein, 10, 13
- Newman projection, 13
- (N-phenyl, N-methyl)formamide, 11
- polyenal group, 10
- questioning fundamental principles, 15
- synthesis, 7
- UV absorption frequencies, 7
 - spectra, 10
- Nitrogen lone-pair 1, 6, 8, 12, 13, 15, 16, 25, 30
- Non-bonded interaction, 24
 - σ -interaction destabilization, 143, 146
 - interaction role, 27
 - interaction theory, 54
- Nucleus-independent chemical shifts, 377
- Opened shell MOs, 63
 - FMOs, 59
 - MOs for fragment B, 63
- Our methods
 - development, 407
 - localized GL and GL_m geometries
 - seeing benzene
 - our 1998 program, 80, 85
 - construction of LFMO basis set, 87
 - deleting LFMO matrix elements, 256
 - our 2007 method, 162, 169, 179, 181, 187, 194, 251, 407, 411
 - deleting AO matrix elements, 173
 - MO localization, 172
 - seeing new type of additive energy effects
 - virtual reference molecule, 177
 - our 2011 method, 259, 260
 - comparison with BLW method, 168, 266
 - comparison with Morokuma's method, 266
 - deleting matrix elements, 260
 - deleting two-electron exchange integrals, 260
 - electron localization, 131
 - versions of our 2011 method, 260
 - our 2014 method, 413
- deleting exchange gradients, 413
- comparison with our 2011 method, 412, 415, 417
- Packing of molecule, 23
- Particular localized geometry (PLG), 321, 340, 345
 - benzotricyclobutadiene, 346
 - boron-hetero triphenylene derivatives, 340
 - 18 strained-aromatic molecules, 350
 - triphenylene, 340
- Passive energy effects, 337
- Pauli exclusion principle, 83
- Pauling resonance energy, 168
- Period number, 396
- Perturbation molecular orbital, 54
- PES scan, 19, 30, 31, 32, 33, 34, 36, 44, 45
 - Relaxed PES scan, 31
- Picking out π -type NBOs, 116
- PMO theory
 - qualitative theory, 54
 - quantitative method, 5
- Polarization, 80, 82, 112, 114, 324, 330, 337
- Polycyclic benzenoid hydrocarbons (PBH), 209
 - acenes, 214
 - benzo[a]acenes, 214
 - benzopentaphene, 214
 - benzo[e]pyrene, 241
 - candidates for GL geometry, 209, 220, 221, 222
 - canonical Clar structure, 212, 213
 - CESE, 216, 224, 219, 227, 229, 235, 419,
 - CESE/ π versus the number of GL sextet, 234
 - CESE/ π versus UV frequency, 224, 234
 - chrysene series, 214
 - classification, 212
 - dibenzo[a,c]acenes, 214
 - dibenzo[de,d'e']acenes, 214
 - dibenzo[de,uv]pentacene, 241
 - dinaphtho[2.3-a,2.3-c]acenes, 214
 - energy effect increments, 225
 - fused benzenoid ring, 209, 210, 226
 - fusion bond, 220, 223, 225, 232
 - fusion double bond, 220, 223
 - homologous series, 215
 - Kekulé valence structures, 211
 - left- and right-bonds, 220
 - naphthopentaphene, 214
 - particular benzenoid ring, 239
 - particular candidate, 223

- peripheral bonds, 209, 215, 220, 225, 230
phenanthrene, 311
 CESE, 219
qualified candidates, 233
 π -sextet, 213
side chain and side bond, 220
structural isomers, 234
tri- and tetra-benzoanthracene, 214
tribenzotetracene, 214
- Polyene
 aza-1,3,5-hexatrienes, 181
 ΔE^{Am} versus dr_{m-n} , 182
CESE and ESE, 309、1,3,5-hexatriene, 173
 GL and GE-m geometry, 173
 energy effects, ΔE^{Am} , 173
trans-1,3,5,7,9-decapentaene, 174
hydrogenation heat, 162
new type of additive energy effect, 174, 414
substituted 1,1-dibutadienyl-ethylene, 218
trans-1,3,5,7-octatetraene, 267
used as reference molecule, 171
- Program of localizing geometry, 170
program of localizing MOs, 63
Proton affinity, 378
Proton transfer reaction, 378
Questionable fundamental principles, 14
 cause of questioning, 14
 conformation of N-benzylideneaniline, 22
 energy preferential crowded conformation, 35
experimental questioning, 27
large distorted NBA-like species, 21
fitted functions
 $dE(\theta)/d\theta < 0$, 33
 $dE_e(\theta)/d\theta > 0$, 35, 36
 $dE_N(\theta)/d\theta > 0$, 35, 36
 $dE_N^{\text{PO}}(\theta)/d\theta > 0$, 36
 $E(\theta)$ versus twist angle θ , 33
 $E_N(\theta)$ versus θ , 35
 $E_N^{\text{PO}}(\theta)$ versus θ , 36
 $E_e(\theta)$ versus θ , 35
between naphthyl and amino groups,
 abnormal bond distance, 15
 abnormal dihedral angle 14, 15
questioning classic views
 CT-2 interaction role, 29
 non-bonded hydrogen interaction, 27
- theoretical questioning, 30
relaxed PES scan, 31
Reduced destabilization energy, 384
 seeing furan-like species
Reference molecule, 164
Reference state (molecule), 170
 two type of reference states, 169
Resistance to molecular distortion, 33, 35, 40, 87, 120, 138, 141
Resonance 2, 17
 energy, 209, 210, 243
Restricted geometry optimization, 161, 169, 204, 206, 170, 177, 190
 seeing our methods
Right-side bond, 221, 223
Ring current, 188
Ring structure units, 226
 first type, 226
 second type, 226
 third type, 226
Sampled conformation
 with the two nonplanar groups, 32
 with the two planar aromatic groups, 31
Scheme of Cox and Pilche, 180
Second basic feature of the conjugation effect, 399
Secondary LMO basis set, 151
Secondary structural effects, 369
Separation of π and σ MOs, 125
 σ AO coefficient method, 65
 degree of separation, 125
 distinguish between the π and σ FMOs, 65
 identifying of π -type AOs, 171
 overlap integral method, 65
 separation degree of the π and σ LMOs, 124
 σ -type atomic orbitals, 61
Shaik's localization structure, 285
Single-point energy calculation 55, 58, 61, 69, 84, 90, 116, 127, 131, 137, 144, 146
Six-membered heterocyclic aromatic compound, 182
Source codes of PC-Gamess, 85
Spatial exchange interaction, 83, 136, 257
Stabilization enthalpy, 165
Stationary point, 92
Steric hindrance 1, 15, 16, 19, 21, 24, 27, 36, 42
 destabilization, 162
 nuclear repulsion between fragments, 162
Stiffness of CC bond, 364

- definition, 363
 endocyclic bond, 361
 exocyclic bond, 362
- Stilbene, 19, 20, 21, 22, 24, 48, 49
 like species, 19, 20, 21
 twist angle
 from gas electron diffraction, 24
 from liquid crystal NMR, 22
 from x-ray diffraction, 22
- UV absorption frequency, 21
- Strained-aromatic molecule, 321, 340, 351, 358, 370
 annulated small ring, 340
 anti-aromatic small ring, 356
 aromatic small ring, 354
 bond length alternation, 350
 angle strain, 342
 Cremer's interpretations, 343
 endocyclic bond, 342
 endo/exo pairs, 341
 exocyclic bond, 342
 hybridization effect, 343
 $r_{\text{endo}} - r_{\text{exo}}$, 343
 Stanger's interpretations, 343
- $\text{C}_6\text{X}_3\text{H}_3$ ($\text{X} = \text{B}, \text{Al}, \text{Ga}, \text{N}, \text{P}, \text{As}$), 356
- C_6X_6 ($\text{X} = \text{B}, \text{N}, \text{P}, \text{As}$), 356
- $\text{C}_6\text{X}_6\text{H}_6$ ($\text{X} = \text{B}, \text{Al}, \text{Ga}, \text{N}, \text{P}, \text{As}$), 354
- $\text{C}_6\text{X}_6\text{H}_6$ ($\text{X} = \text{C}, \text{Si}, \text{Ge}$), 356
 categories, 356
 construction of PLG, 345
 crystal structures, 339
 definition, 339
 $d\Delta r(\text{GP})$ versus $\Delta E(\text{GP})$, 352, 354
 $\Delta E(\text{GP})$ versus $\Delta E^{\pi}_{ab}(\text{DP})$, 359
 extra stabilization energy (ESE)
 central ring, 384
 whole molecule, 383
 metal complexes, 345
 $\Delta r_{12}(\text{GP})$ versus $\Delta F_{12}(\text{GP})$, 363, 365, 367
 $\Delta r_{16}(\text{GP})$ versus $\Delta F_{16}(\text{GP})$, 363, 366, 367
 $\Delta r(\text{PLG})$ versus $\Delta\alpha(\text{PLG})$, 370
 $\Delta r(\text{PLG})$ versus $\Delta\beta(\text{PLG})$, 370
 secondary structural effects, 369
 strain-induced bond fixation, 342
 strain-induced bond localization, 342
- Structural isomers, 209, 234, 235, 239, 240
- Substituent effect, 23, 25, 190
- Substituted benzenes, 189
 aromatic stabilization energies ASE(n), 190
 candidates for the GL geometry, 191
 GL and GE-m geometries, 191
 GL-II geometry, 194
 isomerization reactions, 190
 extra stabilization energy (ESE), 191, 192
 isolated phenyl ring, 193
 multiple substituted benzenes, 192
 size order, 191
 position rule, 192
 pure conjugation effect, 194
 pure inductive effect, 195
 substituent effect, 99
 distortion, 195
 electron-releasing group, 192
 electron-withdrawing group, 192
- Substituted butadiene, 422
 adjacent conjugation, 437, 439, 440, 443
 energy decomposition, 436
 halogen-substituted, 428, 430, 435
 localized geometries
 GL, 424
 GL_n , 431, 432
 $r_{23}(\text{GL})$ versus $P_{23}(\text{GL})$, 428, 430
 $r_{23}(\text{GL}_n)$ versus $\Sigma e_i(\text{GL}_n)$, 433
 $r_{23}(\text{GL}_n)$ versus $P_{23}\text{GL}_n$, 433
 $\Delta r_{23}(\text{G})$ versus ΔEG , 425
 substituted effect, 423, 440
 conjugation transmission, 438
 electron-releasing groups, 423
 inductive effect, 438
 XH_2 -substituted ($\text{X} = \text{B}, \text{Al}, \text{Ga}, \text{N}, \text{P}, \text{As}$), 427
- Substituted N-benzylideneanilines, 22
 characteristics of VDE, 100
 construction of electronic states
 DSI-2 state, 91
 FUD state, 90
 FUL state, 144
 PDSI, 145
 construction of LFMO basis set, 87
 decomposition of π - σ energy, 139
 π -delocalization destabilization, 100
 experimental twist angle, 22
 hydrogen bond, 42
 MO interactions
 σ - s interaction energy, 148
 non-bonded σ - σ interaction, 143

- Nakai's interpretation, 25
- non-bonded interaction, 27
- nuclear repulsion differences, 36
- RHF/STO-3G method, 104
- substituent effect, 25
- Skraba's Experiments, 26
- total electronic energy differences, 36
- vertical delocalization energy (VDE), 91, 100, 104
- Theoretical level and basis set size effects, 271
- Triphenylene, 314
- Two-electron stabilization interaction, 53
- UV absorption, 2
 - absorption peak, 2, 9
 - p-band absorption frequency, 225
 - K-band of strong absorption, 9
 - conjugation competition alternation, 12
 - dibenzo[de,uv]pentacene, 233
 - 2-(dimethylamino)acenes, 7
 - ω -(dimethylamino)polyenal, 7
 - fitted function, 4, 5, 6, 8, 11, 13, 225
 - CESE versus UV frequency, 224, 230, 234
 - frequency versus homologous factor, 11
- 3H-indoles, 26
- nitrogen bridge compounds, 7, 10
- polycyclic benzenoid hydrocarbons, 224, 229
- spectra, 4
- substituted NBAs and substituted 3H-indoles, 26
- wavelength 9, 10
- Vertical delocalization energy (VDE), 79, 87, 119, 125, 130, 135, 246, 273, 302
 - abnormal VDE for [16]5555, 297
 - for [16]annulene, 249
 - for [N]annulene, 249, 303
 - for benzene
 - by our 2007 method, 259
 - by our 2011 method, 273, 274
- configuration effect, 296
- decomposition of VDE, 254
- definition, 87
- destabilizing AO-VDE
 - for cyclobutadiene, 246, 275
 - for NBA by our 2007 method, 126
 - for NBA by our 2011 method, 132, 133, 134
 - for substituted NBA by our 2011 method, 134
- destabilizing LMO-VDE
 - LFMO for NBA, 93, 94
- LFMO for NBA-like species, 98
- LFMO for substituted NBAs, 100
- NBOII for NBA, 125, 126
- HF-EX effect on VDA, 259, 273, 274
- localization degree effect, 126
- stabilizing NBO-VDE, 119
 - VDE versus twist angle, 93
 - VDE versus twist angle for NBA, 119
- vertical resonance, 246, 248, 249, 250
- Woodward–Hoffmann rule 54